

**DETECTION AND ANTIMICROBIAL ACTIVITY OF IMMOBILIZED QUATERNARY
AMMONIUM ANTIMICROBIAL MONOLAYERS ON POROUS AND NON-POROUS
SURFACES**

by

Lukasz Porosa

Bachelor of Science in Applied Chemistry and Biology,

Ryerson University, Toronto, Canada, 2006

Master of Science in Molecular Science,

Ryerson University, Toronto, Canada, 2008

A dissertation presented to Ryerson University

in partial fulfillment of the requirements for the Doctorate of Philosophy

in the Program of Environmental Applied Science and Management

Toronto, Ontario, Canada, 2014

©Lukasz Porosa 2014

AUTHOR'S DECLARATION

I hereby declare that I am the sole author of this dissertation. This is a true copy of the dissertation, including any required final revisions, as accepted by my examiners.

I authorize Ryerson University to lend this dissertation to other institutions or individuals for the purpose of scholarly research

I further authorize Ryerson University to reproduce this dissertation by photocopying or by other means, in total or in part, at the request of other institutions or individuals for the purpose of scholarly research.

I understand that my dissertation may be made electronically available to the public.

DETECTION AND ANTIMICROBIAL ACTIVITY OF IMMOBILIZED QUATERNARY AMMONIUM ANTIMICROBIAL MONOLAYERS ON POROUS AND NON-POROUS SURFACES

PhD, Lukasz Porosa, Environmental and Applied Science, Ryerson University, 2014

ABSTRACT

This research describes the development of novel, environmentally-friendly, non-releasing contact-active thin film coatings by immobilizing the quaternary ammonium (QA) antimicrobial group on a multitude of surfaces. Various chemical anchors based on organosilanes (i.e. textiles, silica, oxide surfaces), organosulfur comprising of thiol (noble metals), organophosphorus comprising of phosphonate and phosphonic acid (i.e. stainless steel (SS), titanium (Ti)), and catechol (Ti, SS) monolayers are employed to attach the QA antimicrobial onto metal surfaces, while benzophenone photoactive crosslinkers containing QA groups are used to coat plastic surfaces (C-H surfaces, i.e. polyethylene (PE), silicone (Si), polyvinylchloride (PVC)). Surfaces treated with covalently attached antimicrobial coatings function by killing microbes on contact, preventing surface attachment, colonization and contamination without releasing the chemical into the environment. The advantages of this method of delivery of the antimicrobial include a lower cost of application, decreased antimicrobial resistance, lower toxicity and increased environmental safety.

Samples prepared by an overnight immersion in an ethanolic solution of phosphorus containing quats followed by an overnight cure at 100°C showed the highest antimicrobial reduction versus electrospray application and no curing. Short chain phosphonic acid quats and the organosilane quat were inactive on titanium. Antimicrobial activity of long chain

phosphonate quats prepared by dip coating and annealing on metal surfaces (Ti, SS, Al) was tested by growth enumeration in the dry state utilizing methods developed in the Wolfaardt lab. All samples showed a 100% reduction (10^6 cells) of viable *Salmonella*, *Arthrobacter*, *S.aureus* and *P.aeruginosa* after 2 hrs of contact time and maintained their activity over 24 hrs versus the uncoated controls. To demonstrate the phosphonate quats were truly immobilized, Ti samples from the first trial were washed in distilled H₂O, dried, and re-innoculated with 10^6 *Arthrobacter* colonies. No visible colonies of *Arthrobacter* remained after 2 hrs of contact time with the Ti surfaces indicating a contact killing mechanism at play.

ACKNOWLEDGEMENTS

First and foremost, I would like to thank my supervisors, Dr. Foucher and Dr. Gideon Wolfaardt for this research opportunity and providing me with what ever I asked for. Secondly, I would like to thank Joe Raich and Bioshield Technologies Canada Ltd. for teaming up with Ryerson University and providing the necessary funding to run this project successfully. Special recognition goes out to my committee/candidacy members Dr. Russ Viirre, Dr. Bryan Koivisto, Dr. Rob Gossage, and Dr. Donal Macartney for their insights, helpful advice and thesis corrections. I would also like to recognize Dr. Michal Bardecki for playing a key role in my acceptance to the EnSciMan program and for supporting Ryerson athletics over the years.

I would also like to thank all of the undergraduate students I had the pleasure to guide and work with over the past four years including Kamlesh Mistry, Shayan Hamzehi, Khaled Hamza, Amanda Mocella, Shayan Hamzehi and Hellen Deng. They were all instrumental in work and help on the Bioshield project over the years. Specifically, I would like to acknowledge the pioneer of the dansyl work, Kamlesh Mistry who contributed along with Grace Luk to collecting UV-VIS/fluorescence spectra. Thanks to Gabriel Wolfaardt who spent countless hours inoculating various bugs on metal and plastic surfaces treated with the QAC antimicrobials in the Wolfaardt and thanks to Alexander Caschera for his assistance with formatting the appendix. As well thanks to all of the graduate students (Aman, Sofija, Shane, Khrystyna, Michelle) who had to put up with me over the years. Most importantly, I would like to thank my patient, loving and supporting parents, Irena Porosa and Mirosław Porosa who started everything and the reason you are reading this today.

DEDICATION

To all my friends and family, especially my parents Mirek and Irena Porosa and my sister Natalia Porosa-Paoli for all the unconditional love and support over the years.

TABLE OF CONTENTS

AUTHOR'S DECLARATION	ii
ABSTRACT	iii
ACKNOWLEDGEMENTS	v
DEDICATION	vi
TABLE OF CONTENTS	vii
LIST OF TABLES	xii
LIST OF FIGURES	xiv
LIST OF ABBREVIATIONS	xxiv
1.0 RATIONALE FOR ANTIMICROBIAL SURFACES	1
1.1 Examples and Preparation of Antimicrobial Surfaces	5
1.2 1st Generation Antimicrobial Coatings: Literature Examples of Contact Active QA Antimicrobial Surfaces	10
1.2.1 Polyhydroxylated Surfaces (Textiles, Silica, Glass)	10
1.2.2 Metal Oxides	17
1.2.3 Plastic Surfaces	25
1.2.3.1 “QAC’s as Additives”	28
1.2.3.2 Thermoset Antimicrobial Coatings: Cross Linked Networks	29
1.2.3.3 “Grafting Onto” and “Grafting From” Plastic Surfaces	31
1.3 2nd Generation Antimicrobial Coatings: Literature Examples of Dual Action Antimicrobial Surfaces	36
1.4 Kill Mechanisms of QAC	38
1.4.1 Mechanism of Killing in Solution.....	39
1.5. Mechanism of Immobilized Contact Active QAC	46
1.5.1 Polymeric Spacer Effect.....	47
1.5.2 Phospholipid Sponge Effect	49
1.6 Antimicrobial Testing	51
1.6.1 Growth Based Enumeration	52

1.6.1.1 Immersion Inoculation.....	52
1.6.1.2 Direct Inoculation.....	53
1.6.1.2.1 Zone of Inhibition.....	53
1.6.1.2.2 Textiles	55
1.6.1.2.3 Hard Surfaces: Metals, Plastics, Glass	55
(a) Aerosol Inoculation.....	55
(b) Industrial Standard Test Methods	57
(c) Wolfaardt's Lab Modification of ISO 22196.....	59
(d) Green's Lab Modification (SLSDSS) of ISO 22196	60
1.6.2 Cell Viability Enumeration	62
1.7 CHEMISTRY OF QUATERNARY AMMONIUM GROUPS AND PHOSPHONIC ACIDS	64
1.7.1 Menshutkin Quaternization Reaction	64
1.7.2 Precursors for the Menshutkin Reaction	67
1.7.3 Stability of Quaternary Ammonium Groups	71
1.7.4 Detection of QAC in Solution and on Surfaces	75
1.8 CHEMISTRY OF ORGANOPHOSPHORUS COMPOUNDS.....	79
1.8.1 Mono and Didealkylation of Phosphonate Esters	79
1.8.2 Synthesis of Phosphonic Acids	85
1.9 RESEARCH GOALS	87
2.0 - RESULTS AND DISCUSSION.....	88
2.1 Synthesis.....	88
2.1.1 Alkoxysilane-Functional Quaternary Ammonium Cations (SiQAC)	88
2.1.2 Organophosphorus Functional Quaternary Ammonium Cations QAC Antimicrobials (PQAC).....	94
2.1.2.1 γ -Monophosphonic Acids QAC Antimicrobials (γ -MPQAC)	94
2.1.2.2 γ -Bisphosphonic Acids QAC Antimicrobials (γ -BPQ) Synthesis	104
2.1.2.3 α -CH Bisphosphonic Acids QAC Antimicrobials (α -CH-BPQA) Synthesis	109
Method 1: Onepot Bis Addition of Dialkylphosphites to Aldehydes.....	110

Method 2: Michael Addition to Diethylvinylphosphonate.....	116
Method 3: C-P Formation.....	118
Method 4: Direct Alkylation.....	120
2.1.2.4 Bisphosphonates via the 3-Component Reaction.....	130
2.1.2.5 α -Aminobisphosphonic acids QAC Antimicrobials (α -ABPQA).....	131
2.1.2.6 β -Aminobisphosphonic Acids QAC Antimicrobials (β -ABPQA).....	143
2.1.2.7 Tridentate Phosphonic Acid QAC Antimicrobials (TPQA)	154
2.1.2.8 Amine Scaffolds for Tetra Phosphonic Acid QAC Antimicrobials.....	159
2.2 Catechol QAC	162
2.3 Organosulfur Based QAC	164
2.4 Benzophenone QAC (Plastic Coating)	167
2.5 Dansyl QAC	170
2.5.1 Fluorescent Antimicrobial Coating Detection.....	170
2.5.2 CO ₂ Detection-Dansyl Amidine.....	177
2.5.3 Unsuccessful Dansyl Reactions	181
2.5.3 Fluorescence Properties of Dansyl QAC	185
2.6 Characterization and Properties	188
2.6.1 X-ray Crystallography.....	188
2.6.2 Antimicrobial Detection / Coating Procedures	195
2.6.2.1 Plastic Surfaces.....	197
2.6.2.3 Metal Surfaces	200
2.6.3 Antimicrobial Activity	201
2.6.3.1 Solution Killing: Minimum Inhibitory Concentration's (MIC's).....	201
2.6.3.2 Contact Killing on Hard Surfaces.....	205
3.0 CONCLUSION	211
4.0 FUTURE WORK	214
5.0 - EXPERIMENTAL PROCEDURES	218
5.1 Materials and Instrumental Methods	218

5.2 General Procedures	219
Method 5.2.1 Sealed Tube Reactions	219
Method 5.2.2 μ W Reactions	220
5.2.3 Purification/Preparation of Common Starting Materials	220
5.2.4 Dow Antimicrobial Synthesis	222
5.3 General Procedure for the Synthesis of (γ –MPQA’s)	222
5.3.1 Abruzov Reaction	222
5.3.2 Menschutkin Quaternization	228
5.3.3 Didealkylation of Phosphonate diesters	237
5.4 General Procedures for the Synthesis of α-CH Bisphosphonic Acids QAC Antimicrobials (α-CH-BPQA)	242
5.4.1 Method 1: Bis Addition of Dialkylphosphites to Aldehydes	242
5.4.1.1 Sequential Addition	242
5.4.1.2 Synthesis of Aldehyde Precursors	244
5.4.2 Method 2: Michael Addition to Diethylvinylphosphonate	246
5.4.3 Method 3: C-P Bond Formation	247
5.4.4 Method 4: Alkylation of Methylenebisphosphonate	248
5.5.0 General Procedure for the 3-Component Reaction	257
5.6.0 General Procedure for the Bis Kabachnik Fields Reaction	258
5.7.0 General Procedure for the Bis Michael Addition of Amines onto Vinylphosphonates	267
5.8.0 Preparation of Tris Phosphonic Acid Derivatives	276
5.9.0 Preparation of Bis Amines Scaffolds for Multidentate Phosphonic Acid Synthesis	280
5.10 Preparation of Catechol QAC	282
5.11 Preparation of Organosulfur QAC	284
5.12 Preparation of Benzophenone QAC	287
5.13 Preparation of Dansyl QAC	290
6.0 APPENDICES	308
List of Appendix Tables	308

List of Appendix Figures.....	308
6.1 X-Ray Data Tables	320
6.2 NMR Spectra.....	368
6.3 MS Spectra.	766
7.0 REFERENCES.....	790

LIST OF TABLES

SECTION 1.0

Table 1.1: Measured persistence of different nosocomial pathogens on inanimate surfaces.	2
Table 1.2: Measured bacterial loads CFU/cm ² in the healthcare and food related surfaces.....	3
Table 1.3: Summary of different surfaces immobilized with antimicrobial organosilanes.	16
Table 1.4: Common medical devices vulnerable to microbial contamination.....	26
Table 1.5: Polymers commonly used for food packaging materials.....	27
Table 1.6: Examples of the benzophenone group utilized to create antimicrobial surfaces.	35
Table 1.7: MIC values for ADBAC and DDAC against increasing <i>S. aureus</i> concentrations after 48 hrs of incubation in TSA medium.....	41
Table 1.8: MIC values of Commercial Disinfectant BAK 50 versus thiol QAC's.....	44
Table 1.9: Antibacterial activity of compound 3 in solution.	53
Table 1.10: Relative rates of the Menshutkin quaternization in various solvents.....	65
Table 1.11: Examples of literature Menshutkin reaction conditions.	66
Table 1.12: Examples of the S _N 2 dequaternization reaction.....	72
Table 1.13: Literature examples of the dealkylation of phosphonate esters with mineral acids.	80
Table 1.14: Literature examples of the dealkylation of phosphonate esters with BBr ₃	84

SECTION 2.0

Table 2.1: Literature/patent procedures describing the preparation of SiQAC 3	89
Table 2.2: ¹ H NMR (CDCl ₃) monitoring of the formation of 3	91
Table 2.3: Optimization of Step 1: Abruzov reaction between trialkyl phosphites (4 , 5A-B) and dibromoalkanes (6 , 7 or 8) or bromoalkanes (9 , 10 or 11).	96

Table 2.4: Optimization of Step 2: Menschutkin reaction between bromoalkylphosphonates 12-14 and tertiary amines 2, 21-25	101
Table 2.5: Optimization of Step 4: Didealkylation of phosphonate diester quats.	103
Table 2.6: Attempted Grignard addition reactions onto 68	117
Table 2.7: Preparation of bisphosphonates 49, 77-78 by Method 3.	119
Table 2.8: Synthesis of α -C-H bisphosphonates by Method 4.....	122
Table 2.9: Optimization of the Kabachnik-Fields reaction.....	133
Table 2.10: Optimization of the Michael addition to β -aminobisphosphonates QAC 131-144	145
Table 2.11: Didealkylation of dansyl phosphonate diesters 211 and 212	174
Table 2.12: MIC plate counts of samples using a 10^{-3} (about 200000 cfu/ml) culture of <i>S.aureus</i>	205
Table 2.13: <i>Arthrobacter</i> reduction by antimicrobial metal surfaces treated with 26 and 34A	207
Table 2.14: <i>P. aeruginosa</i> (PA01) reduction by antimicrobial metal surfaces treated with 26 and 34A	208
Table 2.15: <i>P. aeruginosa</i> (PA01) reduction by antimicrobial Ti surfaces treated with 34A and retested.	209
Table 2.16: Determination of initial bacterial load dried on titanium surfaces from plate counts.	210
Table 2.17: Determination of initial bacterial load dried on SS surfaces from plate counts (raw data).....	210

LIST OF FIGURES

SECTION 1.0

Figure 1.1: Representation of bacterial adhesion and biofilm formation.	4
Figure 1.2: The role of surfaces and antimicrobial surface coatings in the epidemiology of HAI's—beating the “nosocomial infection loop.”	5
Figure 1.3: Example of various types of antimicrobial surfaces prepared in the literature	6
Figure 1.4: Possible anchors to generate self assembled monolayers of small molecules and polymers on various substrates	7
Figure 1.5: Literature examples of different biocide immobilization strategies.....	8
Figure 1.6: Initiators typically used for growing antimicrobial polymers from surfaces “grafting from.”	9
Figure 1.7: Examples of antimicrobial organosilanes described in the literature.	11
Figure 1.8: Typical procedure for immobilizing SiQAC on polyhydroxy surfaces.	13
Figure 1.9: Anchoring of trialkoxysilyl compounds onto polyhydroxide surfaces.	14
Figure 1.10: Comparison of silanization to phosphonic acid monolayer formation on metal oxide surfaces.	18
Figure 1.11: Hydrolytic loss of dansyl-cysteine from a silane based SAM vs a phosphonate based SAM.....	19
Figure 1.12: Mechanism of organophosphorus monolayer formation on metal oxide surfaces..	20
Figure 1.13: IR spectrum of a deposited film of octadecylphosphonic acid..	21
Figure 1.14: Example of literature QAC phosphonic acid antimicrobials..	22
Figure 1.15: Bactericidal QAC prepared by plasma treated stainless steel via grafting to approach.....	23

Figure 1.16: Example of literature QAC catechol antimicrobials.	24
Figure 1.17: Example of a contact active plastic self-finishing coating.	29
Figure 1.18: Monomers and quats used to prepare polymer-QAC antimicrobial plastic coatings.	31
Figure 1.19: Bactericidal QAS polymers and small molecules prepared by plasma treated polypropylene.	32
Figure 1.20: Example of “grafting from” immobilization of biocidal polymers employing the benzophenone surface bound initiator.	33
Figure 1.21: Examples of benzophenone used to prepare antimicrobial surfaces.....	34
Figure 1.22: Example of “grafting from” a plastic surface. Immobilization of biocidal polymers without employing a surface bound initiator.	35
Figure 1.23: Example of a releasing and repelling 2 nd generation dual action antimicrobial surface.	37
Figure 1.24: Example of a dual action and reversible contact killing / hydrophobic antimicrobial surface.	38
Figure 1.25: QAC disinfectants commercially employed.	40
Figure 1.26: Bacterial membrane destruction by QAC disinfectants in solution..	40
Figure 1.27: Scanning electron micrographs of <i>S. aureus</i> strain ATCC 25923 indicating the effect didecyldimethylammonium chloride (DDAC) had on cell morphology.	42
Figure 1.28: The “Cut off Effect:” A hyperbolic trend observed in MIC values of surfactants as a function of the length of the hydrocarbon chain..	43
Figure 1.29: Effect of chain length on antimicrobial activity in solution.....	46
Figure 1.30: Example of the polymeric spacer effect with long chain QAC.....	48

Figure 1.31: Contact-killing via the polymeric spacer mechanism..	48
Figure 1.32: Contact-killing via the phospholipid sponge mechanism..	51
Figure 1.33: ASTM E2149-10.....	52
Figure 1.34: ZOI Agar diffusion method: Antimicrobial releasing plastic film surface on <i>A. Niger</i>	54
Figure 1.35: Standard methods for testing antimicrobials on textiles.....	55
Figure 1.36: Diagram of the aerosol inoculation method: (i) $5-50 \times 10^6$ CFU/mL (inoculum) ..	56
Figure 1.37: Results from the aerosol inoculum method with an immobilized QAS polymer onto a glass slide.....	57
Figure 1.38: Industrial standard method for testing antimicrobials on hard surfaces by growth enumeration.....	59
Figure 1.39: Modified method for testing antimicrobials on hard surfaces by growth enumeration in the dry state testing developed in the Wolfaardt lab.....	60
Figure 1.40: A schematic diagram of the symmertric SSLDS method depicting three distinct antimicrobial agent states.....	61
Figure 1.41: Direct innoculation SLDSS methods. (A) symmetric design, (B) asymmetric design.....	62
Figure 1.42: Diagram of a high-thoughtput biofilm retention assay that measures absorbance or fluorescence from a 96-well plate.....	62
Figure 1.43: Polypropylene microscopy of control ~ 50 cfu/mL (A) vinyl terminated QAC sprayed (10%) 0 cfu/mL (B).....	63
Figure 1.44: SEM images of bacteria incubated with antimicrobial silica nanoparticles.....	64
Figure 1.45: Reactivity of the Menshutkin reaction.....	65

Figure 1.46: Preparation of Menshutkin precursors from primary amines by direct alkylation.	68
Figure 1.47: Preparation of Menshutkin precursors from primary amines.	68
Figure 1.48: Mechanism of the Eschweiler-Clarke <i>N,N</i> -methylation.	69
Figure 1.49: Preparation of Menshutkin precursors from alcohols.	70
Figure 1.50: Side reactions favoured over the Menshutkin reaction.	74
Figure 1.51: Monophasic titration with bromophenol blue.	76
Figure 1.52: Monophasic titration with dichlorofluorescein.	77
Figure 1.53: Biphasic ion pair titration based on bromophenol blue and SiQAC 3 .	77
Figure 1.54: Dansyl linkers previously synthesized in the Foucher lab.	78
Figure 1.55: Examples of reagents used to dealkylate phosphonate esters.	79
Figure 1.56: Mechanism of the didealkylation of phosphonate diesters in mineral acids.	81
Figure 1.57: Mechanism of the didealkylation of dialkylphosphonate esters via silylation and hydrolysis.	82
Figure 1.58: Possible products resulting from the hydrolysis of bistrimethylsilyl phosphonates.	83
Figure 1.59: Mechanism of phosphonic acid dealkylation with BBr ₃ .	85
Figure 1.60: Literature routes describing the preparation of QA phosphonic acids.	86

SECTION 2.0

Figure 2.1: ¹ H NMR (CDCl ₃) spectrum of compound 1 + 2 in at T = 0 (A), and the formation of 3 at T = 48 hrs (B).	92
Figure 2.2: Comparison of trimethoxysilane pricing as of May 2013 (SA: Sigma Aldrich).	93
Figure 2.3: Cyclic oxaphospholane by-products formed during the Abruzov reaction.	99

Figure 2.4: ^1H NMR (CDCl_3) spectra showing successful didealkylation of the ethyl phosphonate ester QAC 26 and isopropyl ester QAC 27 to the corresponding phosphonic acid QAC 34 (D_2O).	104
Figure 2.5 : ^1H NMR (D_2O) spectrum of γ -BPQAC 42	107
Figure 2.6: ^{31}P NMR (CDCl_3) reaction monitoring of compound 45	109
Figure 2.7: Retrosynthesis of α -CH bisphosphonic acid quats.....	109
Figure 2.8: Four retrosynthetic methods for the preparation of α -CH-BPQA's.....	110
Figure 2.9: The Horner-Wadsworth-Emmons rearrangement of 49	113
Figure 2.10: ^1H NMR (CDCl_3) spectrum of QAC aldehyde precursor 66	115
Figure 2.11: ^1H NMR (MeOD) spectrum of cyclic bisphosphonate by-product 97	125
Figure 2.12: ^{31}P NMR (CDCl_3) monitoring for compound 94 and 95 prepared by Method 4..	125
Figure 2.13: ^1H NMR (CDCl_3) spectrum of α -CH-QAC 93 prepared by Method 4.	127
Figure 2.14: ^1H NMR (CDCl_3) spectrum of precursor 102	129
Figure 2.15: ^1H NMR (CDCl_3) spectrum of the undesired product 124 isolated from the Kabachnik-Fields Kabachnik-Fields reaction.....	135
Figure 2.16: Possible mechanistic routes involved in the Kabachnik-Fields reaction.	136
Figure 2.17: Attempted quaternization of triazine 123 with bromoctadecane (^1H NMR (CDCl_3)).	139
Figure 2.18: ^1H NMR (CDCl_3) spectrum of α -ABPQA 121	140
Figure 2.19: ^{31}P NMR (CDCl_3) reaction monitoring of 121 cleavage with HBr and TMSBr ...	141
Figure 2.20: ^{31}P NMR (CDCl_3) reaction monitoring of tetraphosphonate 127	143
Figure 2.21: Reaction monitoring of Michael addition reactions by ^{31}P NMR (D_2O).	148
Figure 2.22: Decomposition of 132 at RT by ^{31}P NMR (CDCl_3)......	149

Figure 2.23: ^1H NMR (CDCl_3) spectrum of β -ABPQA 137	150
Figure 2.24: Preparation of diethylvinylphosphonate 130 (crude mixture by ^{31}P NMR (CDCl_3)).	151
Figure 2.25: ^1H NMR (CDCl_3) of 144 after N_2H_4 deprotection.	153
Figure 2.26: Mechanism of boiling H_2O BOC deprotection.	158
Figure 2.27: ^1H NMR (CDCl_3) of catechol QAC 188 (upper) and 189 (lower).	163
Figure 2.28: ^1H NMR (CDCl_3) spectra of organosulfur QAC 192 and 199	165
Figure 2.29: ^1H , ^{13}C NMR (CDCl_3) spectra of compound 206	169
Figure 2.30: ^1H NMR spectra of 208 (CDCl_3), 209 (CDCl_3), and 217 (D_2O).	175
Figure 2.31: ^1H , ^{13}C NMR (CDCl_3) spectra of dansyl acrylamide 219	177
Figure 2.32: ^1H , ^{13}C NMR (D_2O) spectra of dansyl amine 221 (upper) and dansyl amidine 222 (lower).	180
Figure 2.33: Attempted deprotection of dansyl thioacetate 218 to dansyl thiol 212	181
Figure 2.34: ^1H NMR ($\text{DMSO}-d_6$) spectrum of compound 225	182
Figure 2.35: ESI-TOF MS spectrum of compound 225	183
Figure 2.36: ^{31}P NMR (D_2O) reaction monitoring of the formation of 226 after 3 d. at RT.	184
Figure 2.37: Absorption spectra of dansyl QAC's in MeOH ($\lambda_{\text{ex}} = 525$ nm).	186
Figure 2.38: Absorption spectra of dansyl QAC 213 at different pH's ($\lambda_{\text{ex}} = 525$ nm).	186
Figure 2.39: Fluorescence spectra of dansyl QAC's in MeOH ($\lambda_{\text{ex}} = 360$ nm).	187
Figure 2.40: X-ray crystal structure of 34	189
Figure 2.41: Crystal packing interactions of two molecules of 34	190
Figure 2.42: X-ray crystal structure of 66	191
Figure 2.43: X-ray crystal structure of 19	192

Figure 2.44: X-ray crystal structure of 220	194
Figure 2.45: Coating procedure of QAC antimicrobials onto porous and nonporous surfaces.	196
Figure 2.46: Plastic coating experimental set-up.....	198
Figure 2.47: Bromophenol blue (detection of QAC antimicrobials on plastic surfaces.....	198
Figure 2.48: Fluorescent detection of dansyl QAC's.	199
Figure 2.49: Metal coating experimental set up using 20 mL glass screw cap vial open to air.	200
Figure 2.50: Experimentally determined MIC (CFU/mL) of SiQAC 3 , 34A and 34B	204
Figure 2.51: Colony forming units per mL of <i>Salmonella</i> and <i>S. aureus</i> after 3 hrs of drying on Ti surfaces.....	206
Figure 2.52: Agar growth method showing <i>P. aeruginosa</i> (PA01) reduction by antimicrobial Ti surfaces treated with 34A	209

LIST OF SCHEMES

SECTION 2.0

Scheme 2.1: Preparation of Dow's antimicrobial 3	88
Scheme 2.2: Optimized conditions for the synthesis of γ -monophosphonic acid QAC's.	95
Scheme 2.3: Preparation of γ -Bisphosphonic acid 41	105
Scheme 2.4: Preparation of the potassium salt of 41	106
Scheme 2.5: Attempted preparation of compound 47	108
Scheme 2.6: Preparation of 50 by Method 1.	111
Scheme 2.7: Attempted stepwise preparation of 49	112
Scheme 2.8: Synthesis of bisphosphonates 57-59 from aldehydes.	113
Scheme 2.9: Synthesis of aldehyde precursors 47 , 54-55 used for Method 1.	114
Scheme 2.10: Possible synthetic routes leading to aldehyde QAC 56	115
Scheme 2.11: Preparation of tetraethyl ethene-1,1-diylbis(phosphonate) 73	118
Scheme 2.12: Preparation of THP protected 3-bromopropanol 9	118
Scheme 2.13: Preparation of bisphosphonates by direct alkylation.	120
Scheme 2.14: Intramolecular bisphosphonate alkylation.	124
Scheme 2.15: Preparation of bisphosphonate QAC 96 via alkylation.	126
Scheme 2.16: Attempted preparation of trisphosphonic acid 102 via alkylation of 96	128
Scheme 2.17: Preparation of halo QAC 83 and 102 precursors for Method 4.	129
Scheme 2.18: Attempted preparation of bisphosphonate 106	130
Scheme 2.19: Synthetic route to α -aminobisphosphonate QAC 121 . Optimized conditions for each step.	132
Scheme 2.20: Attempted stepwise preparation of 121	139

Scheme 2.21: Attempted didealkylation of α -aminobisphosphonate QAC 121	141
Scheme 2.22: Tetraphosphonate 127 by C-P alkylation of 113	142
Scheme 2.23: Optimized synthetic route to β -aminobisphosphonate QAC 136	144
Scheme 2.24: Attempted synthetic route to tetraphosphonate QAC 146 from β -amino bis-phosphonate 141	152
Scheme 2.25: Preparation of amine quat 144	153
Scheme 2.26: Attempted synthesis of tris- α -hydroxyphosphonate QAC 161	155
Scheme 2.27: Attempted synthesis of precursors 162 and 164 to tris- β -hydroxyphosphonate QAC's.	156
Scheme 2.28: Attempted synthesis of tris- γ -hydroxyphosphonate QAC 168	157
Scheme 2.29: Preparation of mesyl 158 and tosyl phosphonate 170	158
Scheme 2.30: Preparation of tris-BOC 157 and deprotection in boiling H ₂ O to tris 171	158
Scheme 2.31: Michael addition of NMe ₂ to tris acrylamide 173	159
Scheme 2.32: Attempted preparation of tetradentate β -amino QAC 179	160
Scheme 2.33: Attempted preparation of tetradentate β -amino QAC 183	161
Scheme 2.34: Attempted <i>N,N</i> -dimethylation of dopamine 184	162
Scheme 2.35: Attempted preparation of catechol QAC 190	163
Scheme 2.36: Literature routes to target thiol QAC's 194 and 199	166
Scheme 2.37: Preparation of the benzophenone QAC's 205 and 206	168
Scheme 2.38: Preparation of dansyl dimethyl 208 and halo precursors 209 and 210 for quaternization.	171
Scheme 2.39: Preparation of bifunctional dansyl anchors 211-216 for binding onto porous and non-porous surfaces.	172

Scheme 2.40: Preparation of dansyl acrylamide QAC 219	176
Scheme 2.41: Preparation of dansyl amindine switchable fluorophore 222 and 223	179
Scheme 2.42: Attempted preparation of dansyl DTC 225	182
Scheme 2.43: Attempted preparation of dansyl bis β -phosphonate 226	184

SECTION 4.0

Scheme 4.1: Catalytic Finkelstein / Menschutkin reaction in the preparation of the Dow antimicrobial 3	214
Scheme 4.2: Onepot preparation of α -CH-bisphosphonates from the aldehyde quat precursor, 56	215
Scheme 4.3: Preparation of catechol QAC, 190	215
Scheme 4.4: Preparation of thiol QAC, 199	216
Scheme 4.5: Synthesis of multifunctional QAC antimicrobial polymer coating.	216
Scheme 4.6: Synthesis of multifunctional QAC antimicrobial polymer coating.	217

LIST OF ABBREVIATIONS

Ac	Acetyl
Ar	Aromatic
AMA	Antimicrobial Agent
APA	Amino Phosphonic Acid
ARI	Antimicrobial Resistant Infection
Aq.	Aqueous
ATRP	Atom Transfer Radical Polymerization
BOC	<i>tert</i> -Butyloxycarbonyl
Bn	Benzyl
<i>t</i> -Bu	Tert butyl
Cat	Catalyst
Cbz	Carboxybenzoyl
CDI	1,1'-Carbonyldiimidazole
CFU	Colony Forming Units
d.	Days
DCM	Dichloromethane
Diox.	Dioxane
DIPEA	Diisopropylethylamine
DMAEMA	2-(<i>N,N</i> -dimethylamino)ethyl Methacrylate
DMSO	Dimethylsulfoxide
DTC	Dithiocarbamate
EPA	Environmental Protection Agency
Eq.	Equation
Et	Ethyl
Et ₃ N	Triethylamine
Hrs	Hours
HAI	Hospital Acquired Infection
HMPA	Hexamethylphosphoramide

HCWU	Health Care Workers Uniforms
HRMS	High Resolution Mass Spectrometry
IAI	Implant Associated Infections
<i>i</i> AMA	Immobilized Antimicrobial Agent
<i>i</i> Pr	Isopropanol
LAH	Lithium Aluminum Hydride
LG	Leaving Group
Mon.	Months
Me	Methyl
MIC	Minimum Inhibitory Concentration
MLC	Minimum Lethal Concentration
Mp	Melting Point
Mol	Moles
MS	Mass Spectrometry
NMR	Nuclear Magnetic Resonance
Nu	Nucleophile
Ms	Mesyl
ON	Overnight
PBS	Phosphate buffered saline
PCC	Pyridinium Chlorochromate
PMMA	Poly Methyl Methacrylate
PMRA	Pest Management Regulatory Agency
QA	Quaternary Ammonium
QAC	Quaternary Ammonium Compound
QAM	Quaternary Ammonium Monomer
QUAT	Quaternary Ammonium Cation
QAS	Quaternary Ammonium Salt
RBF	Round Bottom Flask
RT	Room Temperature

RXN	Reaction
SAM	Self-Assembled Monolayer
Si-QAC	3-(trimethoxysilyl)propyldimethyl-Octadecyl Ammonium Chloride
SIP	Surface Initiated Polymerization
Solv.	Solvent
ST	Sealed Tube
THF	Tetrahydrofuran
TLC	Thin Layer Chromatography
TOL	Toluene
PG	Protecting Group
PHT	Phthalimide
TMSCl	Trimethylsilylchloride
TMSBr	Trimethylsilylbromide
TMSI	Trimethylsilyliodide
TMTC	Too Many To Count
Tos	Tosyl
μ W	Microwave
UTI	Urinary Track Infection
Yr.	Year
4-VP	4-Vinylpyridine
Wks.	Weeks

CHAPTER 1 - INTRODUCTION

1.0 RATIONALE FOR ANTIMICROBIAL SURFACES

Common surfaces that are frequently touched are inhabited by a variety of microorganisms such as bacteria, viruses and fungi which can persist on these “touch surfaces” anywhere from a couple of hours up to six months (Table 1.1).¹ If pathogenic bacteria persist in healthcare and food preparation facilities, patients and workers can readily develop and spread nosocomial infections from touch surfaces such as door handles, pens, telephones, health care workers uniforms (HCWU’s), stethoscopes, IV poles, faucets, food and food preparation surfaces (Table 1.2).^{2,3}

The healthcare and food industry are facing an ever growing microbial contamination problem. Contamination of medical devices, healthcare products, H₂O purification systems, food packaging and food storage are becoming a serious threat both in terms of cost and safety.⁴ To date, infection control counter measures which rely on personal hygiene, hand washing, masks and the use of disinfectants on hospital equipment to prevent the spread of infections have been largely unsuccessful. According to the World Health Organization (WHO), nosocomial or hospital-acquired infection (HAI’s) are becoming a national economic burden resulting in prolonged hospitalization and can lead to serious complications and even death.⁵ For example, hospital-acquired infection (HAI’s) from contact with pathogenic microorganisms affect approximately 2 million people and result in more than 100,000 deaths each year in the US.⁶ Such unintended infections require 10-20 d. of additional patient hospitalization, costing the already strained US health-care system between ~\$25,000-\$30,000 per infection and billions of dollars per year.⁶ Another route for bacteria to infect patients is through hospital invasive support

equipment such as intravascular lines and implanted medical devices such as artificial prosthetics, cardiovascular implants and urinary catheters.^{6,7} Implant associated infections (IAI's) occur in more than 1 million patients and cost an estimated \$3 billion in the US per year to treat.⁴ For example, approximately 10-50% of patients with implanted catheters run the risk of developing urinary tract infections (UTI's) translating to an average of \$200,000 per infection in additional healthcare costs. The rise in the frequency and severity of (HAI's) and (IAI's) can be attributed to decreased antibiotic efficacy against drug-resistant strains of pathogens found in surface biofilms.³

Table 1.1: Measured persistence of different nosocomial pathogens on inanimate surfaces.⁸

Type of Bacterium	Duration of Persistence	Type of Virus	Duration of Persistence	Type of fungus	Duration of Persistence
<i>Acinetobacter spp.</i>	3 d. to 5 mon.	Adenovirus	7 d. - 3 mon.	<i>C.albicans</i>	1 - 120 d.
<i>Bordetella pertussi,</i>	3-5 d.	Astrovirus	7 - 90 d.	<i>C.parapsilosis</i>	14 d.
<i>C. difficile</i> (spores)	5 mon.	HIV	7 d.	<i>Torulopsis glabrata</i>	102 - 150 d.
<i>E. coli</i>	1.5 hrs to 16 mon.	Herpes Simplex	4.5 hrs to 8 wks.		
<i>H. influenza</i>	12 d.	Influenza	1 - 2 d.		
<i>M. tuberculosis</i>	1 d. to 4 mon.	Parvovirus	1 yr.		
<i>S. aureus</i> (including MRSA)	7 d. to mon.	Papiloma	7d.		
<i>S. pyogenes</i>	3 d. to 6.5 mon.	Rhino Virus	2 hrs to 7 d.		

Table 1.2: Measured bacterial loads in the healthcare and food related surfaces (colony forming units, CFU/cm²).⁹

Site of Study	Site	Bacterial Load Found
Food	Abattoir surfaces	8 to 1.3×10^4 cfu/cm ²
Food	Food contact surfaces	630 to 1.8×10^9 cfu/cm ²
Food	Meat preparation surfaces	10^5 cfu/cm ²
Food	Refrigerator surfaces	813 to 6×10^8 cfu/cm ²
Food	Vegetable preparation surfaces	$>10^5$ cfu/cm ²
Healthcare	Nurse workstation	< 9 cfu/cm ²
Healthcare	Hospital ward surfaces	2.5 to 40 cfu/cm ² , cleaning reduced to < 2.5 cfu/cm ²
Healthcare	Hospital kitchen surfaces	2-29 cfu/cm ²
Healthcare	Hospital ward floors	< 5 cfu/cm ²
Healthcare	Hospital underward bed	< 25 cfu/cm ²
Healthcare	Stethoscope membrane	In $> 54\%$ of cases > 5 cfu/cm ² , in 18% of cases > 29 cfu/cm ²

Surface biofilms are complex communities of bacteria that offer protection from environmental hazards (eg. biocides). Biofilm formation involves three phases beginning with the initial reversible adhesion of bacteria through polysaccharides and adhesion proteins on the bacterial membrane (phase I). After 2-3 hrs under appropriate conditions, bacteria irreversibly attach to a surface (phase II). Once formed (usually after 24 hrs) the bacterial biofilms secrete a protective peptidoglycan matrix (biofilm) capable of withstanding $1000 \times$ the antibiotic dose of non adherent bacteria (Figure 1.1).¹⁰ As a result, once the infection occurs, it becomes difficult to

treat and strategies that prevent bacterial contamination or destroy adsorbed microorganisms that lead to biofilm formation are actively sought.¹⁰

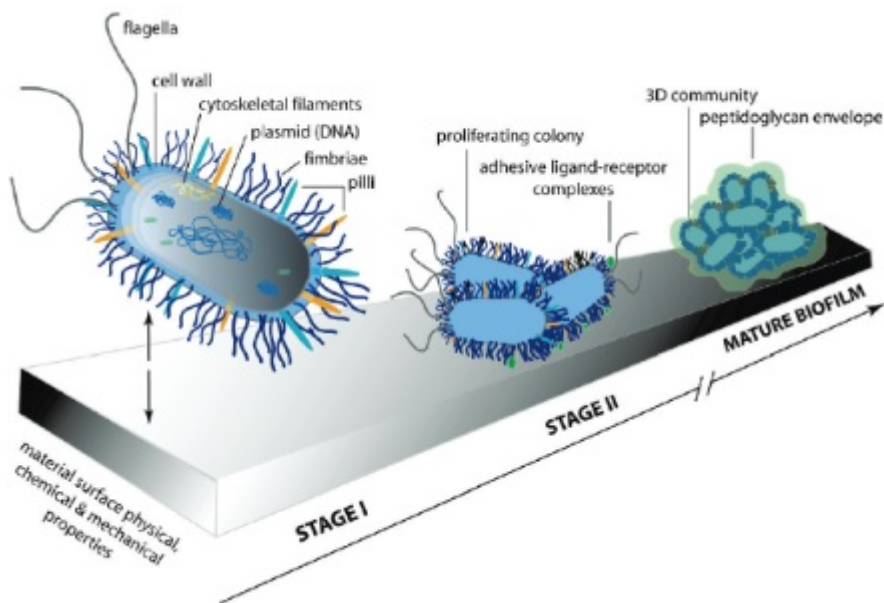


Figure 1.1: Representation of bacterial adhesion and biofilm formation (Used with permission from Ref.¹⁰).

Consumer demand for odor and contamination free hygienic textile products has grown remarkably. Estimates of antimicrobial textile production worldwide were 100,000 tonnes in 2000.¹¹ With an estimated growth of 15% per year in Western Europe, antimicrobial textiles are one of the fastest growing sectors in this industry.¹¹ In addition, managers in the health care/food industries as well as medical device makers are actively seeking to introduce antimicrobial coatings as part of an infection control strategy combined with hygiene and disinfection protocols. In this regard, introducing antimicrobial surfaces that prevent biofilm formation could help reduce the spread of pathogenic bacterial infections from surfaces and implants to patients and healthcare workers, thereby closing the “nosocomial infection loop” (See Figure 1.2).^{8,9}

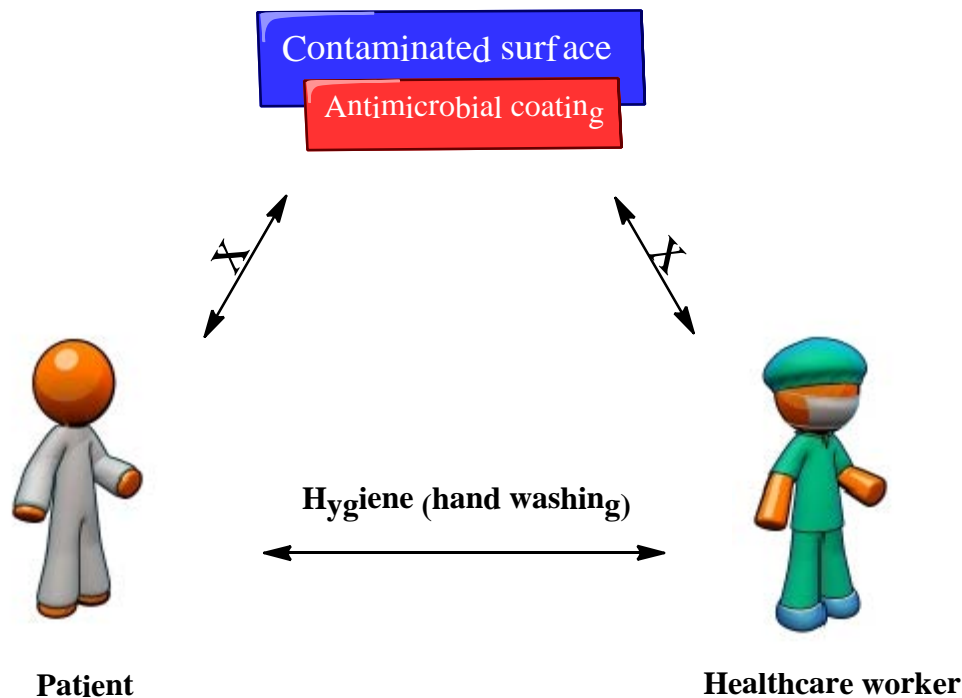


Figure 1.2: The role of surfaces and antimicrobial surface coatings in the epidemiology of HAI's—beating the “nosocomial infection loop.”^{8,9}

1.1 Examples and Preparation of Antimicrobial Surfaces

In order to prevent the formation of biofilms, strategies utilizing antimicrobial surfaces have been employed to make surfaces inhospitable to bacteria.^{12,13} Small molecule monolayers or polymer thin films either “grafted to” or “grown from” a surface have been widely used to prepare antimicrobial surfaces and clothing. Figure 1.3 shows examples of the different approaches that have been used to prepare antimicrobial surfaces or objects. These prior art monolayers or polymer coatings include, for example, non-biofouling coatings which are passive strategies that rely on preventing bacterial adhesion with hydrophobic or zwitterionic thin films, but do not kill the approaching bacteria. A second class of antibacterial thin films kills microbes on contact either by releasing a biocidal agent or immobilizing a biocidal agent. A third class of

antibacterial thin films utilize a combination strategy of including a non-biofouling and biocidal component into the coating (see Section 1.3).^{12,13}

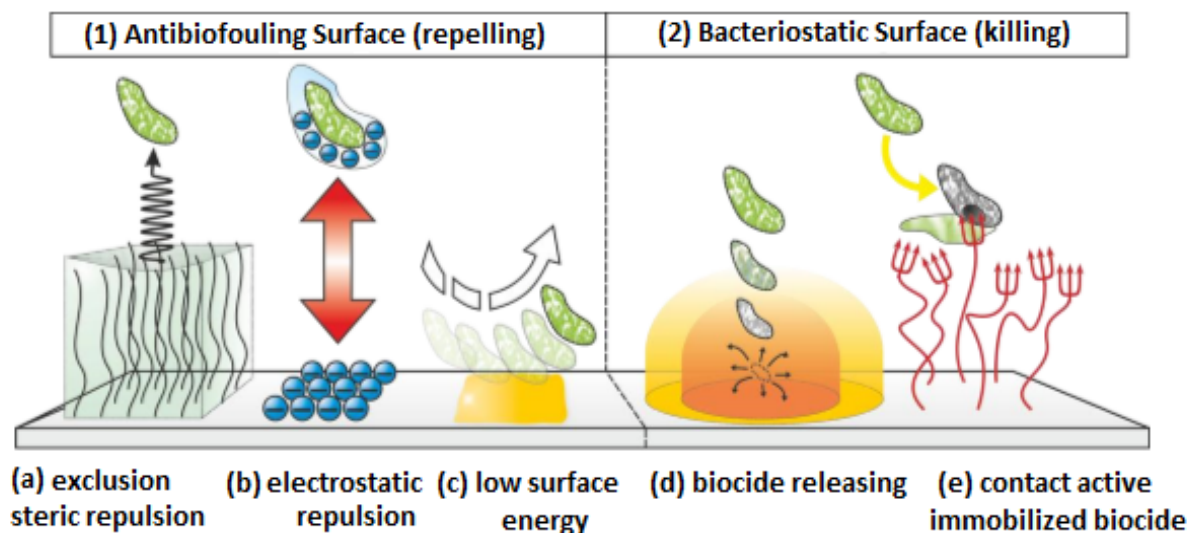


Figure 1.3: Example of various types of antimicrobial surfaces prepared in the literature (Used with permission.^{12,13}

Active releasing antimicrobial coatings based on the leaching of biocides are typically prepared by impregnating biocides in a polymer matrix coating. In this way, the leachable biocide is gradually released from the coating and kills adhered microorganisms via interaction with the cell depending on the biocide mode of action.^{14,15} The most popular leachable biocide is silver ion (Ag^+).^{16,17} Quaternary ammonium compounds, although used in leaching type systems, are largely immobilized onto surfaces as small molecules or polymers that provide contact killing without leaching. The advantages of the non-leaching immobilized approach include longer antimicrobial efficacy, less chance for the development of resistant bacteria and overall is more environmentally friendly.^{3,18,19}

Quaternary ammonium biocides can be immobilized onto various surfaces either as small molecule monolayers with various anchors (Figure 1.4) or as polymers.^{20,21} Grafting of larger molecules onto surfaces such as polymers can be accomplished in one of three ways; (A) physisorption of a polymer to a surface (*grafting to* approach); (B) chemisorption via reaction of anchors in the polymer with complementary functional groups at the substrate surface (*grafting to* approach); (C) growth of polymer brushes via surface-initiated polymerization techniques such as Atom Transfer Radical Polymerization (ATRP) (*grafting from* approach) (Figure 1.5). Grafting from approaches use ATRP polymerization initiators such as 2-bromoisobutryl bromide (BIBB) directly bound to a surface or immobilized through an anchor (Figure 1.6).²² Photochemical linkers have also been used to bind antimicrobials onto textiles and polymers.²³⁻²⁶

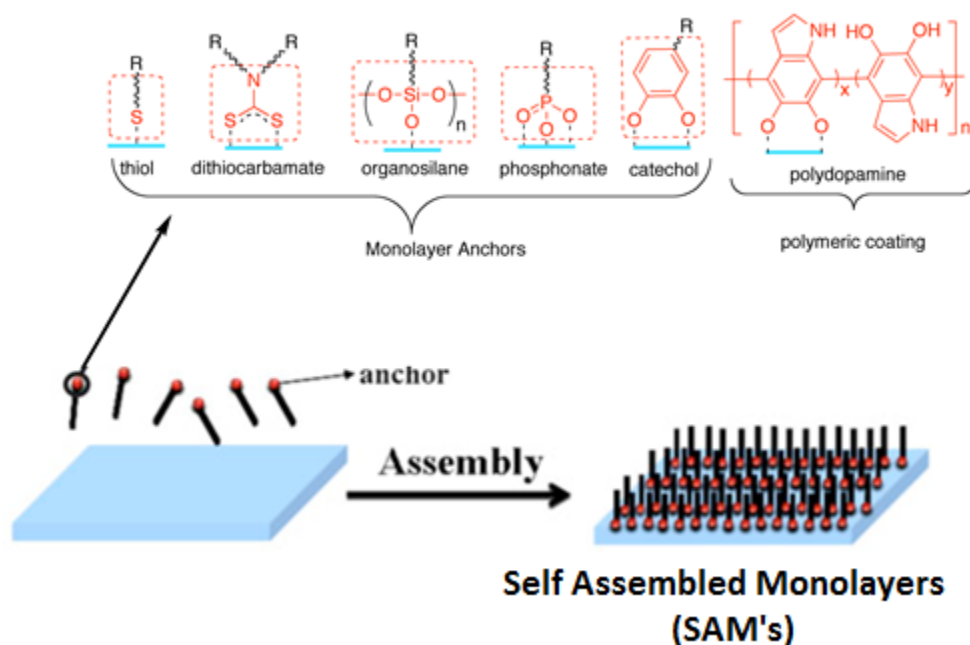


Figure 1.4: Possible anchors to generate self assembled monolayers of small molecules and polymers on various substrates (Adapted from Ref.²⁷).

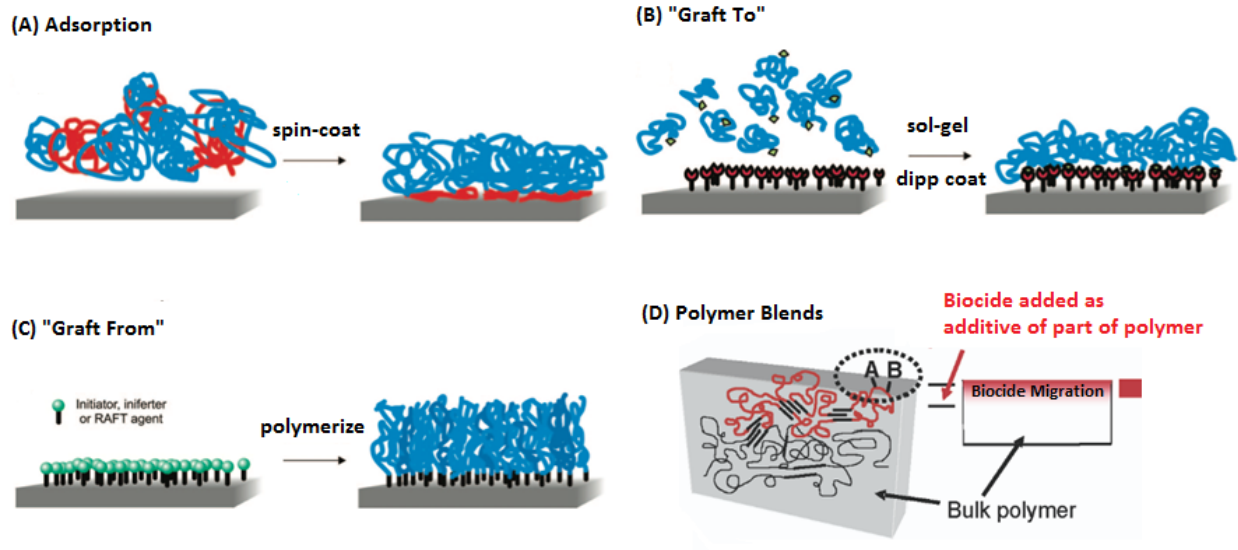


Figure 1.5: Literature examples of different biocide immobilization strategies. (A) Polymeric thin films coating are adsorbed or painted on compatible surfaces, (B) Self Assembling Polymers (SAP's) or Self Assembling Monolayers (SAM's) of small molecules with pending biocides have been employed, (C) biocidal polymers grown from a surface via a pre-immobilized Atom Transfer Radical Polymerization (ATRP) initiator, (D) self-finishing surface where the biocide is added during the polymerization process or is attached to the monomer prior to polymerization (Adapted from Ref.²⁸).

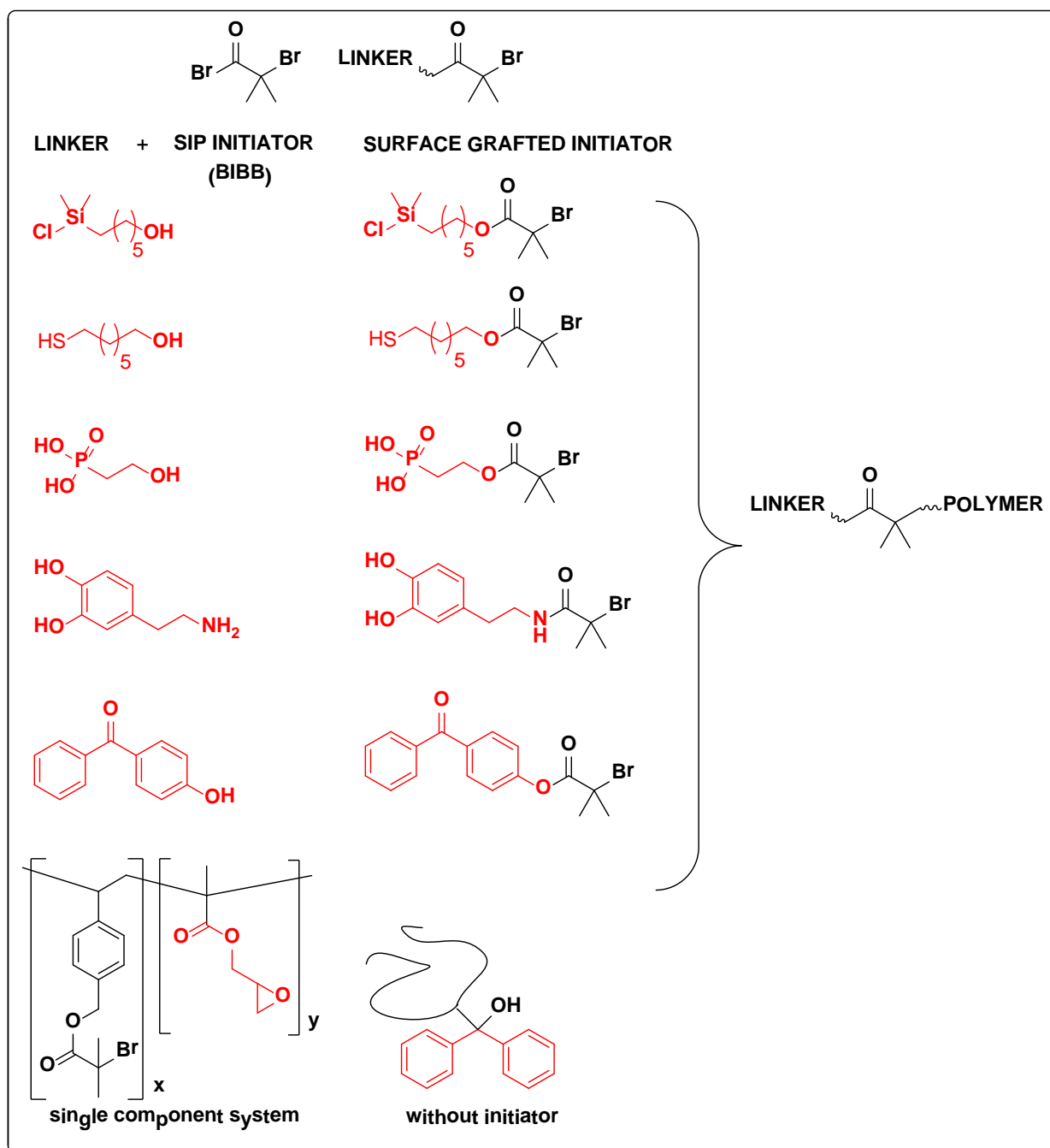


Figure 1.6: Initiators typically used for growing antimicrobial polymers from surfaces “grafting from.”^{29,30,31,32,33,34}

The research proposed is based on developing novel, non-releasing, contact-active monolayer thin film coatings. The following sections will highlight literature examples of

immobilized QA antimicrobials on porous (polyhydroxylated surfaces) and non-porous (metal and plastic) surfaces.

1.2 1st Generation Antimicrobial Coatings: Literature Examples of Contact Active QA Antimicrobial Surfaces

1.2.1 Polyhydroxylated Surfaces (Textiles, Silica, Glass)

Akin to the discovery of the antibiotic penicillin by Alexander Fleming, who noticed after a month long vacation that a petri dish contaminated by a fungus killed the growing bacteria, the first contact active antimicrobial surface coating was also discovered by accident. The first report describing a surface bound antimicrobial capable of killing microorganisms on contact was published in 1972 by Isquith *et al.*, who prepared antimicrobial glass and cotton samples with octadecyldimethyl (3-trimethoxysilylpropyl)-ammonium chloride (ODDMAC or Si-QAC) (see Figure 1.7, Compound **3**).³⁵ The publication was based on Abbott's research at Dow Corning on silicone and silane based compounds for the control of algae.³⁶ When measuring minimum inhibitory concentrations (MIC's) of silane quaternary ammonium compounds in solution, Abbott unexpectedly found that he was getting extremely low values (cfu \approx 0).³⁶ He attributed his observations of false positives to the adsorption of the active compounds on to the wall of his equipment.³⁶ As a result, (3-trimethoxysilylpropyl)dimethylalkyl ammonium chlorides with alkyl chains from 6 to 22 carbons produced the highest algae reductions and were quickly patented by DOW Corning (Figure 1.7, Compounds **1-11**).³⁷

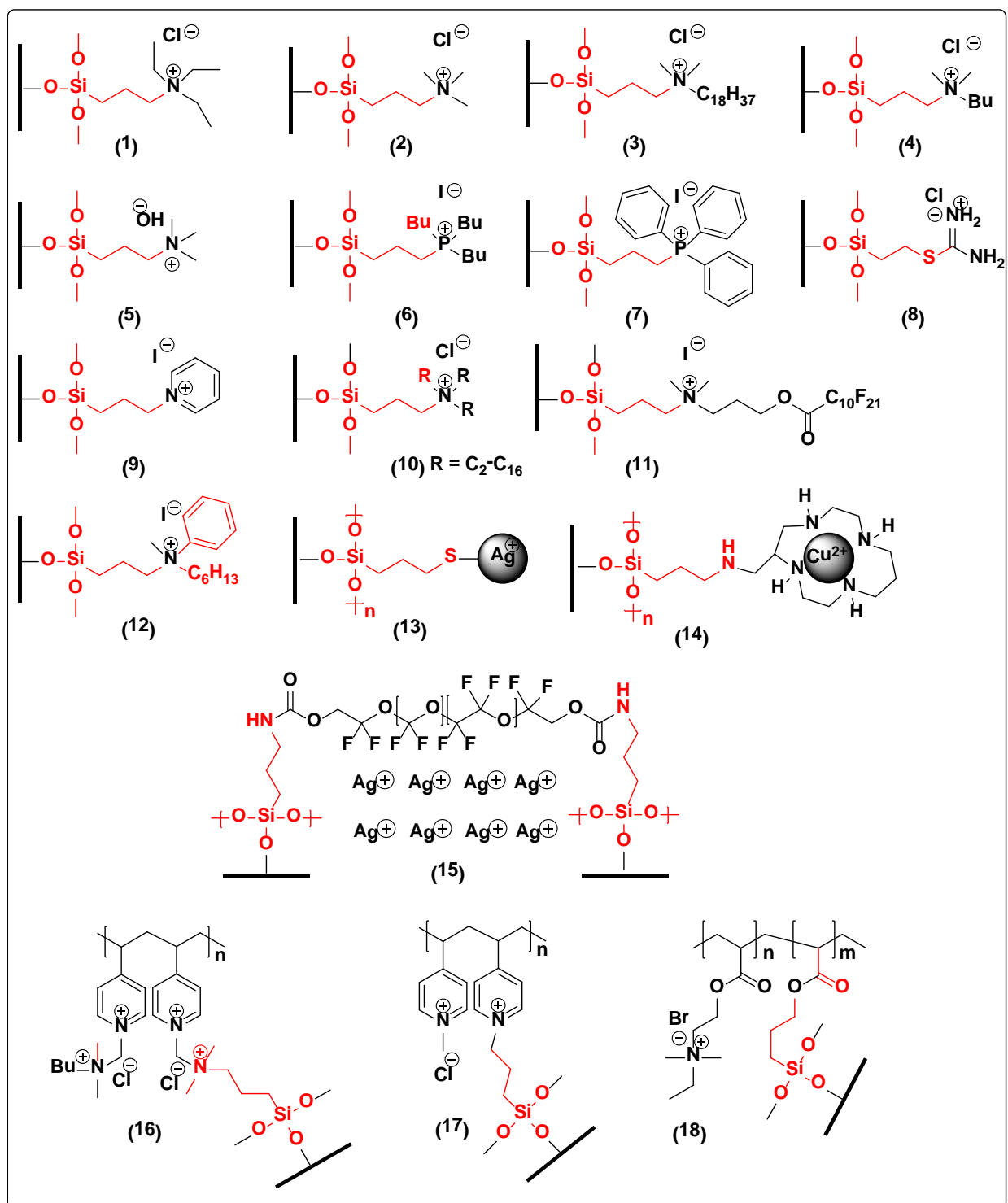


Figure 1.7: Examples of antimicrobial organosilanes described in the literature. (1)³⁸, (2-11)³⁶, (13)³⁹, (14)⁴⁰, (15)^{39, 41}, (16)⁴², (17)⁴³, (18)⁴⁴.

After years of extensive toxicological testing, Dow Corning's antimicrobial quaternary ammonium agent **3**, sold as an antimicrobial finish for textiles, was approved by the EPA in 1977 and received the Industrial Research and Development award as the best new commercialized product that year.³ SiQAC (Figure 1.7, Compound **3**), is commercially prepared from 3-chloropropyl trimethoxysilane (excess ~1.2 eq.) and *N,N*-dimethyloctadecylamine, and available as a 40-72% methanolic solution from the following companies: Aegis (AEM 5772), Piedmont (Ztrex72), Flexipel (Q-1000), and Dow Corning (Q9-6346), (Figure 1.7, Compound **3**).⁴⁵

In the original publication, Si-QAC (72%) was typically applied as a 0.1 wt % solution in H₂O on cleaned glass or cotton followed by annealing at 70°C for 30 min in order to form strong Si-O-Si bonds with free –OH groups on oxide surfaces, e.g glass, ceramics, cellulose, silica. However, for industrial applications the compound was limited by the ready polymerization of neighbouring silanols in H₂O and precipitation of the product upon long term storage (Figure 1.8). In aqueous environments, alkoxy silanes are rapidly hydrolyzed under neutral conditions leading to condensation of neighbouring silanols, resulting in the undesired precipitation or gelling of the product (Figure 1.9). For large scale applications, methanol-based products are undesirable due to their toxicity, flammability and the highly regulated nature of methanol.⁴⁶

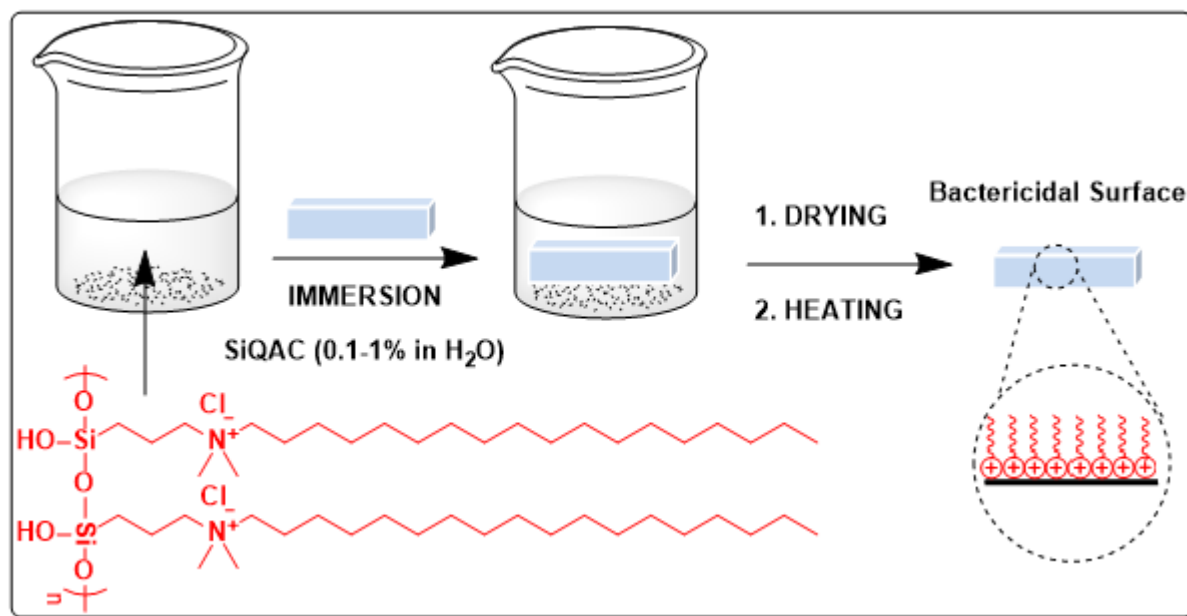


Figure 1.8: Typical procedure for immobilizing SiQAC on polyhydroxy surfaces.³⁸

commercially available from Pureshield as a H₂O soluble solution of the active quat at 5 wt % and sold under different brand names such as AM 500, SiShield 500, BioProtect 500, or Microbe Guard in several countries. The product is currently used commercially as an antimicrobial finish on textiles such as cotton, nylon, polyester and wool.^{11,20}

In the original publication, Isquith claimed that immobilized Si-QAC on different substrates such as siliceous surfaces, natural fibers, man-made fibers, metals and others had broad-spectrum antimicrobial activity.³⁸ However, the publication only demonstrated antimicrobial activity of Si-QAC on glass against *F. faecalis* (gram-positive) and on cotton cloth against *E. coli* (gram-negative). The silane modified surfaces killed > 95% of the *F. faecalis* visible colonies after 30 min measured with the Dow Corning Corporate Test Method 0923 (CTM-0923, See Section 1.6.1.1.1).³⁸

The antibacterial treatment of Si-QAC and related organosilanes onto polyhydroxy surfaces such as textile fabrics, glass and silica nanoparticles (NP's) are well studied in the literature. Table 1.3 summarizes the historical account of various antimicrobial organosilane treated surfaces described in the literature starting from the original publication by Isquith in 1972 until 2013. Examples include different textiles surfaces: polyester fabrics (Entry ii), cotton polyester (Entry vi), microfibrillated cellulose (Entry xi), cotton gauze (Entry xiv), cotton textile (Entry xv) as well as glass (Entries i-ii, iv, xiii, xvii), titanium (Entry xii) and silica NP's (Entry xvi). These treated materials were shown to be antimicrobicidal after treatment with the antimicrobial trialkoxysilane **1**. Other surfaces normally inert to silanization such as silicone rubber and metal oxides were also coated with **1** but required prior surface pre-treatment: sanding (Ti, Entry ix) and plasma treatment (silicone, Entries vii and x) necessary to activate them towards silanization. Similarly, organosilane antimicrobials based on the release of Ag⁺

(Entries xiii and xv) and polymeric QAC's (Entries xv and xvi) were developed after the original silane QAC 3. However the application of the antimicrobial varies in each study as well as the type of bacteria tested and the testing methods.

Table 1.3: Summary of different surfaces immobilized with antimicrobial organosilanes.

Entry	Antimicrobial silane	Immobilized Surface	Year
i ^{38, 48}	1	Siliceous surfaces, man-made fibres, natural fibres, metals, leather, wood, rubber.	1972
ii ⁴⁸	1	Glass, cotton, cellulose, polyester	1973
iii ³⁶	2-16	Cellulose acetate, nylon 6,6, polyester, silica	1982
iv ⁴⁹	1	Glass	1984
v ⁵⁰	1	Polyurethane foam	1985
vi ⁵¹	1	Cotton-polyester fabrics	1988
vii ⁵²	1	Silicone rubber	2002
viii ⁵³	1	Polyethylene terephthalate (PET)	2004
ix ⁵⁴	1	Titanium dental implants	2005
x ⁵⁵	1	Silicone rubber stents	2006
xi ⁵⁶	1	Microfibrillated cellulose	2007
xii ^{42,57, 58}	16,17	Glass, cotton, paper	2008
xiii ⁵⁹	12	Glass	2009
xiv ⁶⁰	1	Cotton gauze	2010
xv ⁶¹	1	Cotton textile	2011
xvi ⁶²	1	SiO ₂ nanoparticles	2011
xvii ⁶³	1	Glass	2011

1.2.2 Metal Oxides

Basic metal oxide surfaces (e.g. Ti, SS) typically contain far fewer surface functional groups (-OH) than are necessary for grafting monolayers and often require surface pretreatment, also known as passivation, in order to increase surface -OH groups compared to the acidic metal oxide surface representative of silica. Passivation is typically achieved by either chemical means^{64, 65} (dipping in Pirhana solution, sanding, or heating over 130°C in air) or physical methods (electrochemical grafting, plasma deposition).⁶⁶

A simpler way to functionalize metal oxide surfaces without the use of expensive and surface altering plasma pre-treatment involves the direct formation of phosphonates and catechol monolayers on metal oxide surfaces. Phosphonate monolayers have been shown to be advantageous over self-assembled monolayers (SAMs) of thiols and silanes in terms of durability, long-term stability and surface coverage, especially on Ti and SS.⁶⁷⁻⁶⁹ Thiol-based SAM's lack substrate specificity (mainly reserved for Au surfaces) and long-term stability needed for biomedical applications, (i.e. implants).⁷⁰ Over time, thiols become oxidized to sulfonates, which lack affinity for Au and become displaced from the surface.⁷¹

In comparison to silane based SAM's on metal oxide surfaces, phosphonate based SAM's are advantageous because they resist hydrolysis under physiological conditions and higher surface coverage can be obtained without a harsh acid surface pretreatment (to increase OH content).⁷² The problem with silanization on the native oxide of titanium is the presence of only 15% surface hydroxyl groups (XPS data).⁶⁹ Silanization consumes surface OH sites and a lack of a neighbouring OH group can promote the cross-linking of nearby silanes to siloxanes. Siloxanes are known to be hydrolytically unstable and are easily hydrolyzed under physiological

conditions.⁶⁹ Once a phosphonic acid molecule coordinates to a metal, proton transfers between the coordinated phosphonate and the metal surface can take place which can create new –OH groups accessible for further monolayer formation and result in bidentate or tridentate coordination (Figure 1.10).⁶⁹

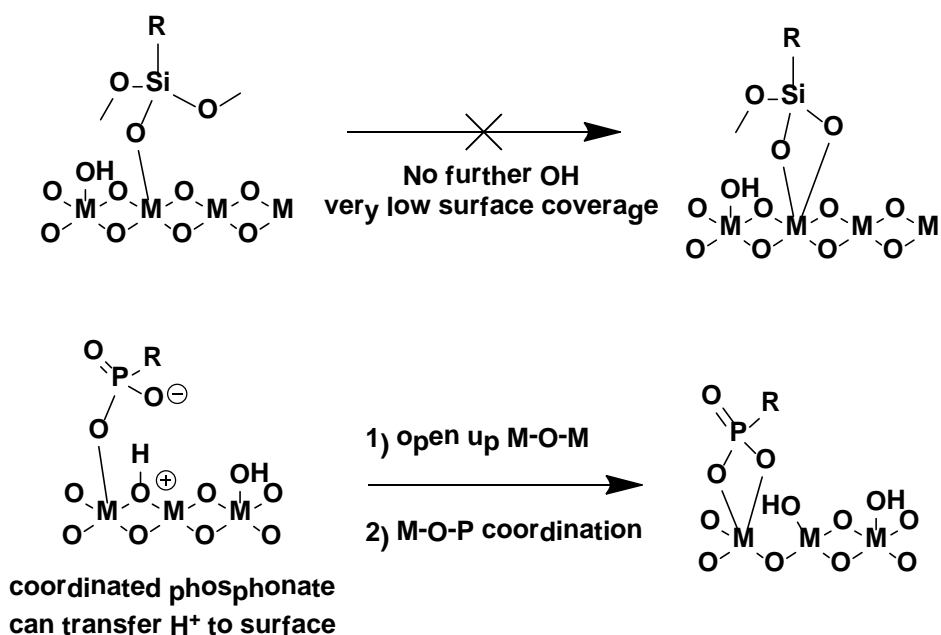


Figure 1.10: Comparison of silanization to phosphonic acid monolayer formation on metal oxide surfaces.⁶⁹

For example, the hydrolytic stability of silane to phosphonate based SAM's was directly compared with the incorporation of a fluorescent dansyl tag.⁷³ The silane-dansyl molecule was assembled on Ti either by (i) attaching the silane linker aminopropyl(triethoxy)silane (APTES) on Ti followed by coupling with a maleimido reagent and capped with the fluorescent tag or (ii) attachment to Ti with preformed (3-triethoxysilylpropyl)-6-*N*-maleimidohexanamide followed by capping with the dansyl tag (Figure 1.11, (ii)). The phosphonic acid-dansyl reporter was prepared from Ti immobilized 11-hydroxyundecylphosphonic acid followed by coupling with the maleimido reagent and capped with the dansyl cysteine (Figure 1.11, (iii)).⁷³ Both surface

loadings and shear strengths of each monolayer were found to be durable enough for biomedical device surface coating. However, as expected, the Si-O-M bonds in the silane based film were completely hydrolyzed after 7 d. in pH 7 buffer, while the phosphonate film remained intact (Figure 1.11).⁷³

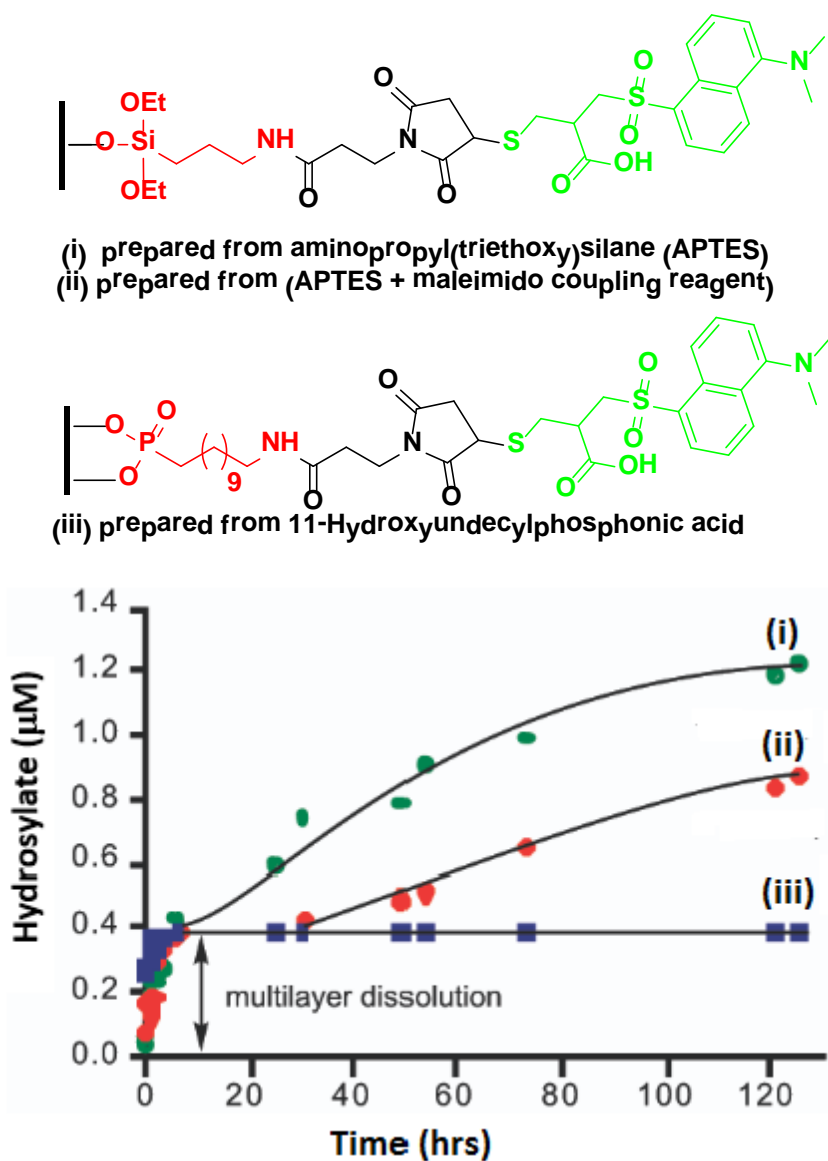


Figure 1.11: Hydrolytic loss of dansyl-cysteine from a silane based SAM vs a phosphonate based SAM (Used with permission from Ref⁷³).

Similar to the formation of silane monolayers on polyhydroxy surfaces, phosphonic acid monolayer formation on metal oxides requires a thermal curing step to drive off H_2O resulting in a strong M-O-P bond.⁷⁴ Both bidentate and tridentate phosphonate coordination modes to metal oxides are possible and depend on the metal surface and the temperature of the annealing step (Figure 1.12). For example, surface coverage of the phosphonate monolayer was enhanced 5-fold by depositing the monolayer with six cycles of spray/heat/rinse versus just one cycle (Figure 1.13 A vs. B). Six cycles of deposited phosphonate films were found to be very durable and resisted desorption by solvent rinsing or by a mechanical peeling test with tape (compared by IR peak intensities, Figure 1.13 B).⁷²

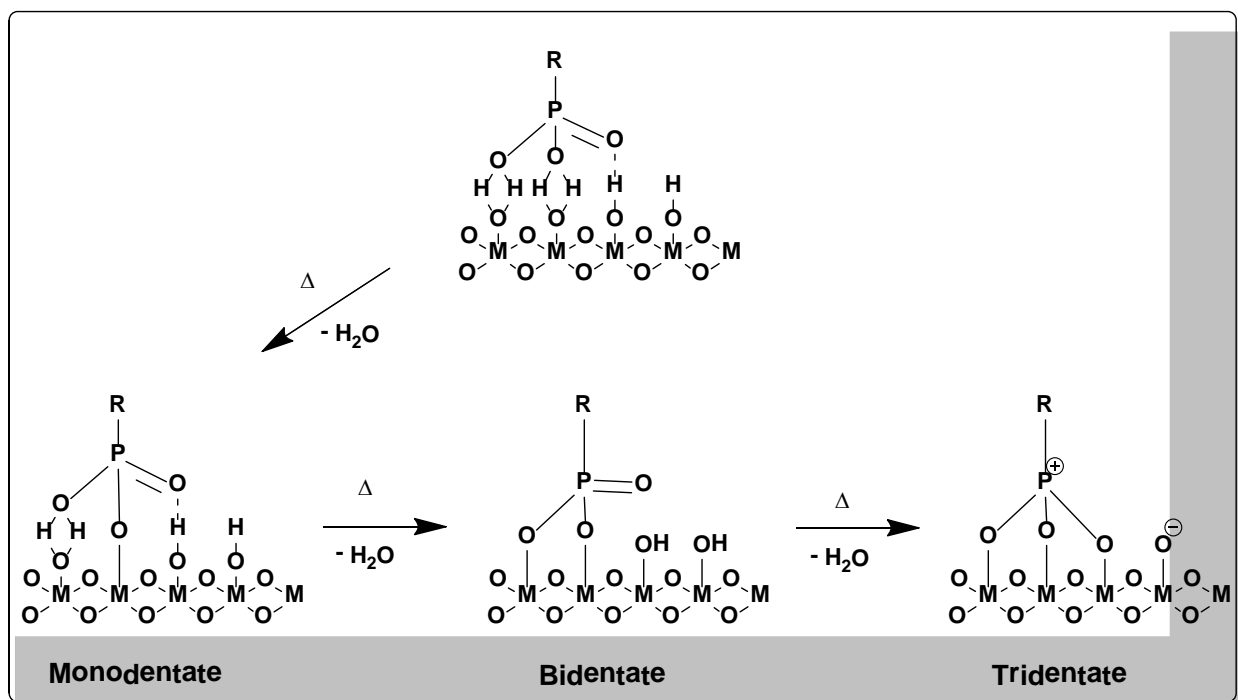


Figure 1.12: Mechanism of organophosphorus monolayer formation on metal oxide surfaces.⁷⁵⁻

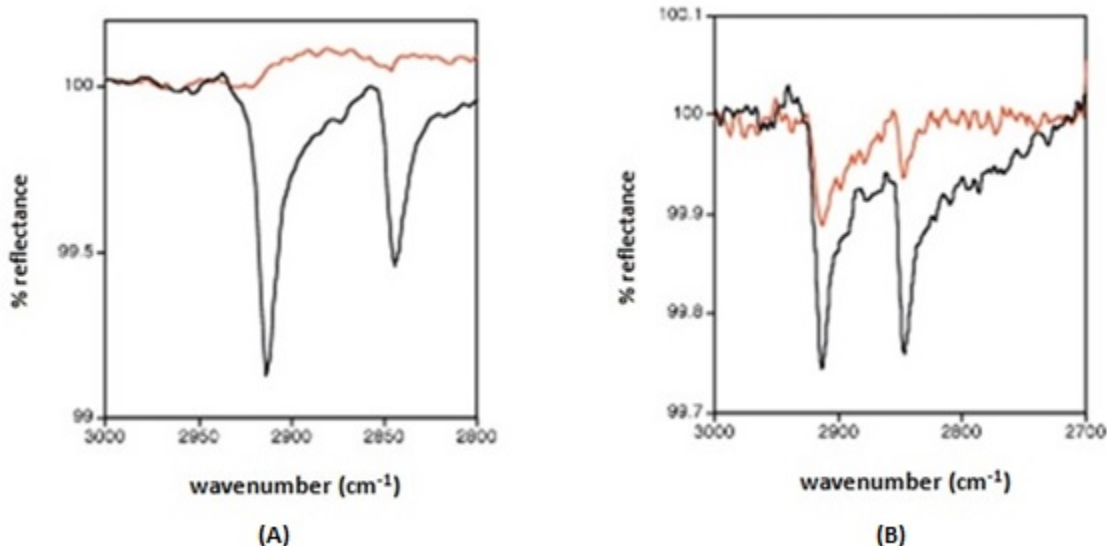


Figure 1.13: IR spectrum of a deposited film of octadecylphosphonic acid. (A) no heat, control, before (lower trace) and after solvent wash (upper trace), (B) monolayer after six cycles of deposition, with heat treatment (lower trace), compared with one cycle (upper trace), after both solvent wash and tape peel tests.⁷²

Both active and passive strategies to prevent biofilm formation have been described with mono- or bisphosphonate monolayers and polymer thin films (Figure 1.14). Examples of active surfaces include contact killing monolayers employing immobilized quaternary ammonium salts (Figure 1.14, **19-21, 23, 24**), and the antibiotics daptomycin and vanomycin (Figure 1.14, **25, 28**). Active surface coatings releasing biocidal NO and Ag⁺ ions have been patented (Figure 1.14, **20, 22**).⁷⁴ Passive strategies were described employing hydrophobic perfluorinated bisphosphonates on stainless steel, silicon, and titanium oxide surfaces for anticorrosion applications.⁷⁴

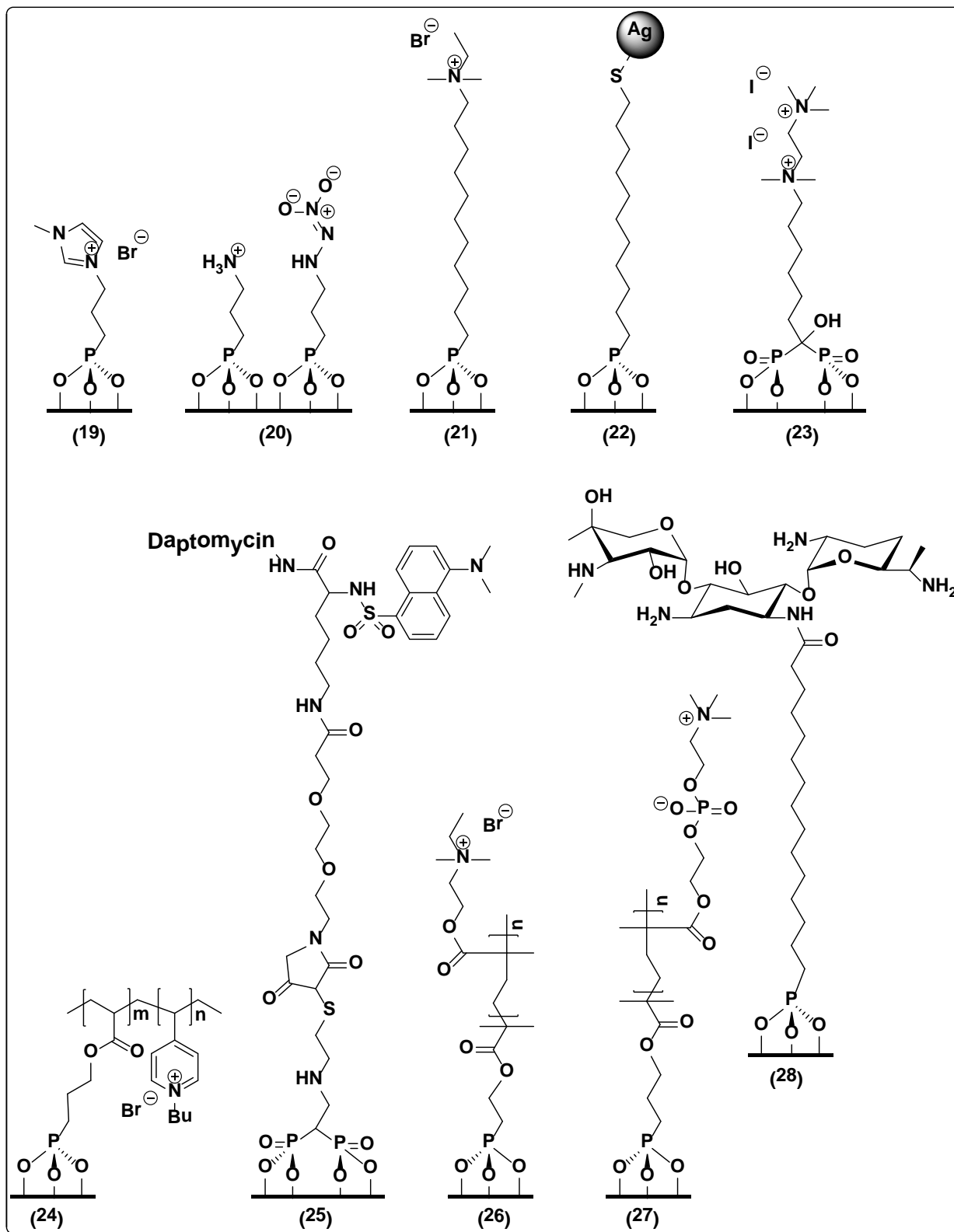


Figure 1.14: Example of literature QAC phosphonic acid antimicrobials. (19-21)⁷⁸⁻⁸⁰, (22)^{79,81}, (23)^{82,83}, (24)⁸⁴, (25)⁸⁵, (26)⁸⁶, (27)⁸⁷.

Another example describes an antimicrobial stainless steel (SS) surface with immobilized QAC's via plasma activation. To prepare the surface, an ethylenediamine low pressure plasma was used to functionalize the SS surface with primary amines. Quats were formed by reacting the plasma-deposited amines with hexyl bromide to generate secondary and tertiary C₁₆ amines which were later quaternized with MeI (Figure 1.15). These QAC modified SS surfaces showed excellent bactericidal properties by killing more than 98% and 99.9% of *K.pneumoniae* and *S.aureus* respectively.⁶⁶

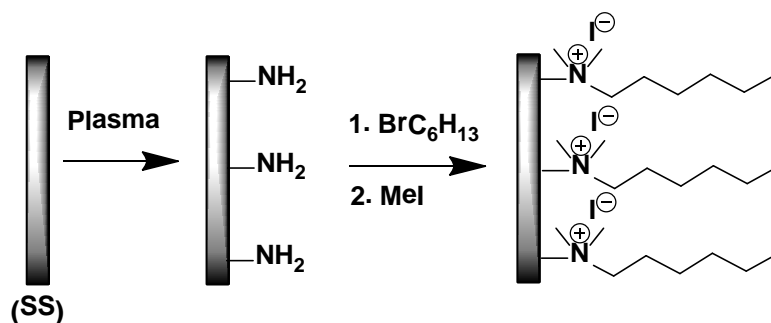


Figure 1.15: Bactericidal QAC prepared by plasma treated stainless steel via grafting to approach (Adapted from Ref.⁶⁶).

Another linker strategy for immobilizing polymer thin films either by “graft to” or “graft from” methods onto a variety of metal oxide surfaces was introduced by the Messersmith group. Inspired by mussel adhesive proteins which contain the catechol group, the Messersmith group functionalized various polymers with this anchor and used it to create both passive and active antimicrobial surfaces for the purposes of biofilm prevention and control.⁸⁸ Since the introduction of the catechol as a versatile linker, other groups created antibacterial metal surfaces by immobilizing polyethylene (PE) based polymers with microbe repelling capabilities (compound **28**), and various biocidal moieties such as antibiotics, antimicrobial peptides and quaternary QAS polymers via catechol groups (Figure 1.16, compounds **18-33**).

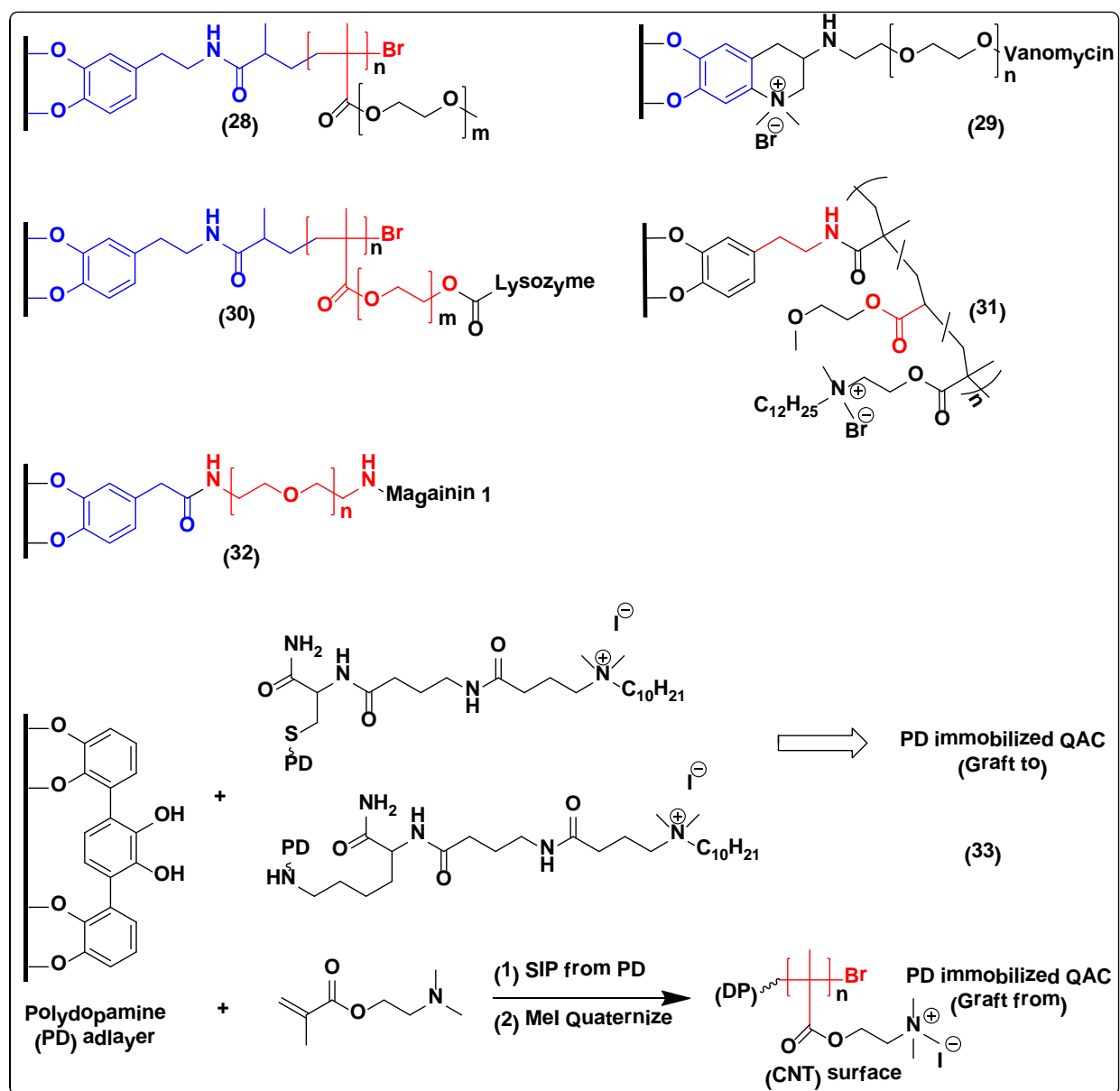


Figure 1.16: Example of literature QAC catechol antimicrobials. (28)^{88, 89}, (29)⁹⁰, (30)⁹¹, (31)⁹², (32)⁹³, (33)⁹⁴

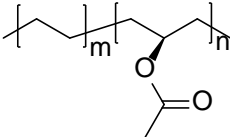
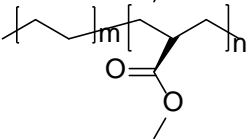
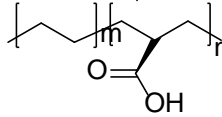
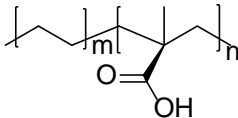
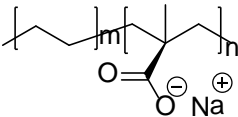
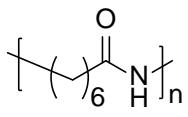
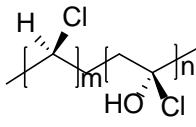
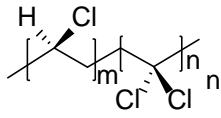
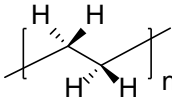
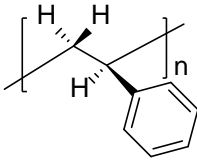
1.2.3 Plastic Surfaces

Common plastic or polymers surfaces widely used in the medical and food industries as medical devices and food packaging materials respectively (Tables 1.4, 1.5) are also very susceptible to biofilm colonization.^{95,96} Unlike polyhydroxy and metal oxide surfaces, plastic surfaces with functional C-H bonds such as polyethylene, polypropylene, and polystyrene or C-OR bonds in the case of polyesters are inert to direct silanization using the anchor chemistries previously described for -OH bearing surfaces / metal oxides, and thus require a different strategy to immobilize an antimicrobial group. The literature contains a limited number of examples of covalently immobilized antimicrobials as a finishing coating on plastics, however many examples are prevalent where the antimicrobial is introduced as an additive or polymerized into the plastic during the manufacturing process. Antimicrobials incorporated into plastics where the active species migrates to the surface during the polymerization process are termed “self-finishing” coatings.¹⁸

Table 1.4: Common medical devices vulnerable to microbial contamination.²⁹

Medical Device	Polymeric Materials
Breast implants	Silicones
Catheters	Silicones, PVC, urethanes, fluoropolymers
Contact lenses	Methacrylates, silicones
Dental implants	Silicones
Heart valves	Polyester, polyoxymethylene,
Hip and knee prostheses	UHMWPE, PMMA
Intraocular lens	Methacrylates, silicones
Left ventricular assist device	Urethanes, carbonates
Pacemakers	Urethane
Renal dialyzers	Polyacrylonitrile

Table 1.5: Polymers commonly used for food packaging materials.^{95, 97}

Polymer	Formula
Ethylene vinyl acetate (EVA)	
Ethylene methyl acetate (EMA)	
Ethylene acrylic acid (EAA)	
Ethylene methacrylic acid (EMAA)	
Ionomer	
Nylon	
Polyvinylidene chloride (PVDC) Polyvinyl chloride copolymer (PVC)	
Ethylene vinyl alcohol (EVOH)	
Polyethylene copolymer (PE)	
Polystyrene (PS)	

1.2.3.1 “QAC’s as Additives”

Wynne prepared polyurethane-QAC antimicrobial coatings by blending a long chain quat with oxyethylene groups into polyurethane.⁹⁸ By increasing the length of the hydrophobic alkyl chain to octyl and decreasing the length of the oxyethylene groups from $n = 4$ to $n = 2$, allowed for increased migration of the QAC to the surface of the polyurethane resin (measured by X-ray photoelectron spectroscopy (XPS)) resulting in a 7-log reduction of *S. aureus* and *E. coli* (Figure 1.17).⁹⁸ Furthermore, the antimicrobial plastics with the highest surface concentration ($n = 8$, $m = 2$) maintained their activity after immersion in H_2O for 7 d., demonstrating they were truly surface bound. HPLC and antimicrobial analysis of the H_2O phase further confirmed that the plastic sample was non-leaching and contact killing. This suggests that the QAC additives are initially mobile and able to surface-concentrate in the uncured polyurethane but become “locked” in place once the resin has cured. Thus, diffusion of the antimicrobial agents out of the film is prevented despite the inherent H_2O solubility of the quat.⁹⁸

The Foucher group successfully incorporated SiQAc into polypropylene (PP) during the injection molding process at 5wt % and obtained significant reduction in biofilm growth, the treated surface stained blue with bromophenol blue indicating presence of the antimicrobial at the surface.⁹⁹

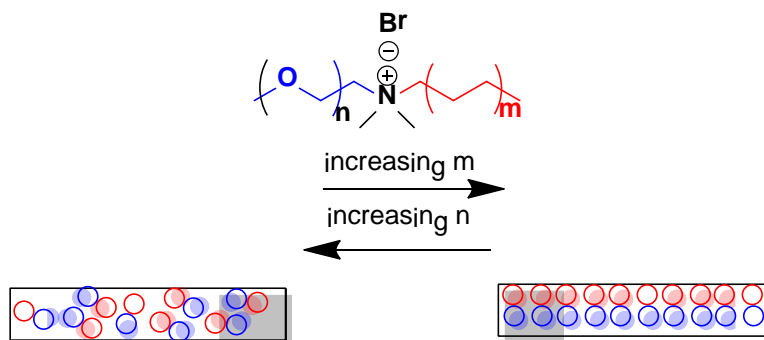


Figure 1.17: Example of a contact active plastic self-finishing coating.⁹⁸

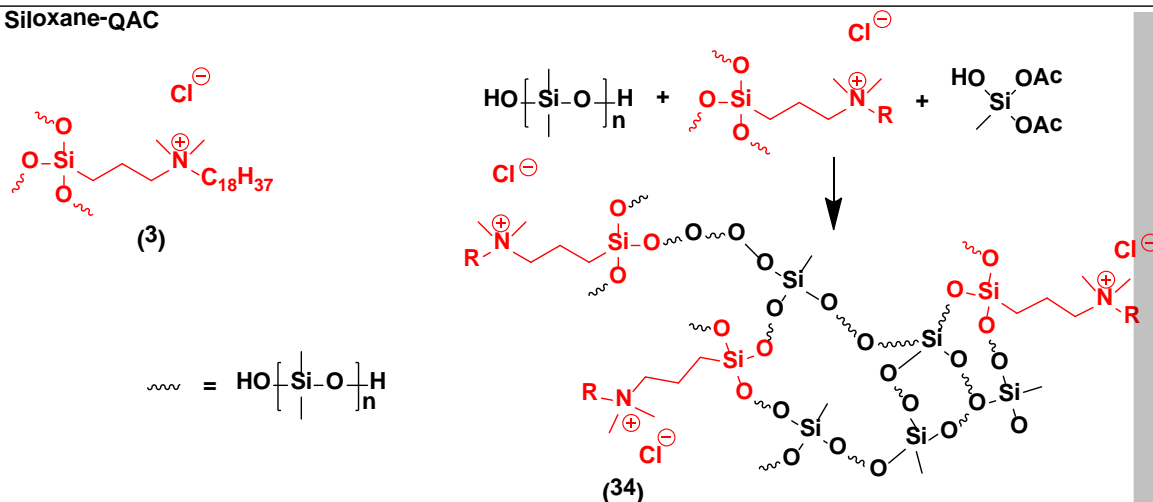
1.2.3.2 Thermoset Antimicrobial Coatings: Cross Linked Networks

Non-leaching antimicrobial-QAC thermoset plastic coatings are prepared by crosslinking the antimicrobial agent with polymerizable functional groups such as siloxanes, polyurethanes, epoxides and acrylates into polymerizable networks (Figure 1.18).

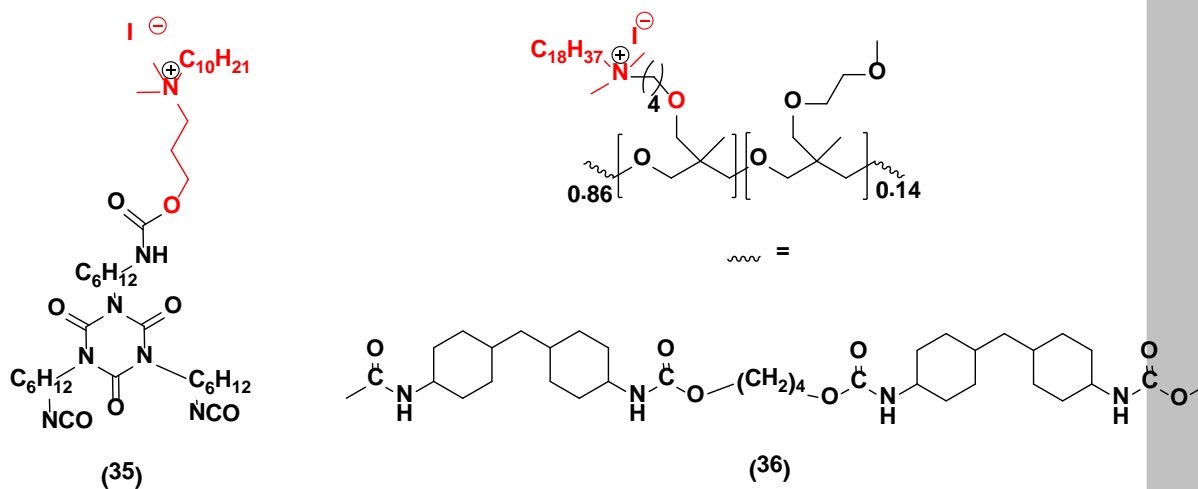
Clarkson first prepared SiQAC-(SE) plastics by incorporating the antimicrobial agent, SiQAC, into silicone elastomer (SE) polymers via crosslinking with the hydroxy groups present in the poly(dimethylsiloxane) polymer. The coating was toxic to the algae, *Amphora coffeaeformis* for up to 20 weeks, but lost activity after 23 weeks in sea H₂O. The toxicity of the SiQAC-SE surfaces was attributed to a slow leaching of residual uncrosslinked SiQAC from the coating. Once all excess uncrosslinked SiQAC was removed by boiling solvent Soxhlet extraction, the polymer lost its anti-algal activity.¹⁰⁰ Structures of crosslinked siloxanes,¹⁰¹ polyurethanes¹⁰², epoxides¹⁰³ and acrylates crosslinked by UV light¹⁰⁴ with the antimicrobial QAC as part of the polymer are shown in Figure 1.18. For example, the polyurethane QAC **35** prepared by a covalently bonded hydroxyl terminated QAC bearing a long perfluorinated tail with a

polyisocyanate cross linker showed a 5 log reduction of *S. aureus* and *E. coli* at low concentrations (0.5 wt %, 0.007 mmol/g) with ISO 22196 and JIS Z 2801 protocols.¹⁰²

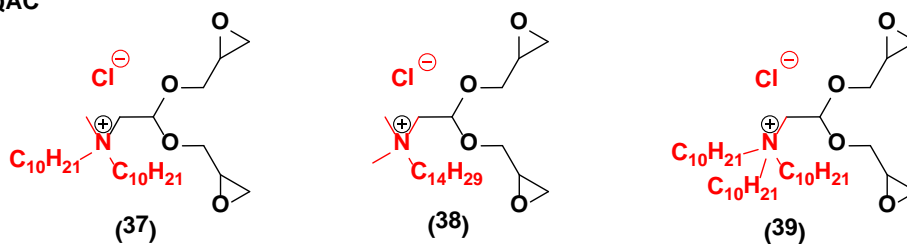
1. Siloxane-QAC



2. Polyurethane-QAC



3. Epoxide-QAC



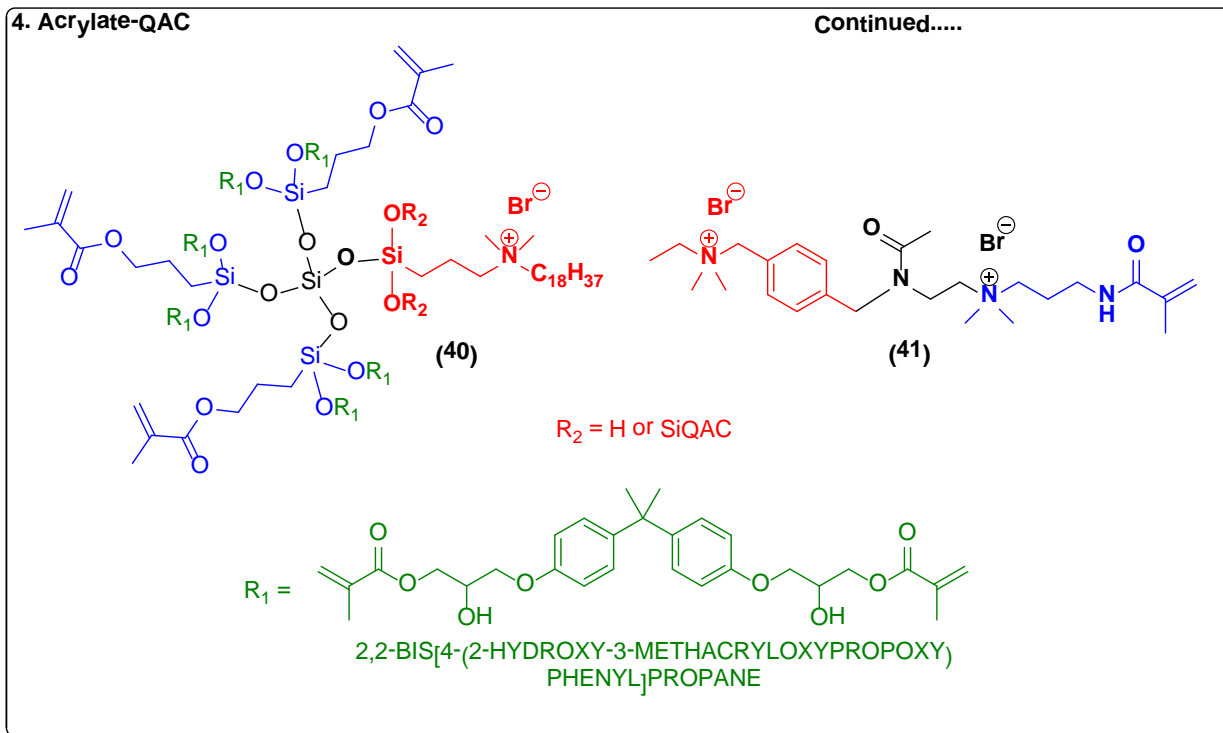


Figure 1.18: Monomers and quats used to prepare polymer-QAC antimicrobial plastic coatings. (34)¹⁰¹, (35-36)¹⁰², (37-39)¹⁰³, (40-41).¹⁰⁴

1.2.3.3 “Grafting Onto” and “Grafting From” Plastic Surfaces

Covalently attached biocides such as QAS onto plastics can be achieved by involving either (i) plasma activation in order to functionalize the C-H surface with reactive groups such as OH or NH₂ onto which biocidal polymers can be grafted to or from (ii) or UV light activation of functional groups known to directly react with inert C-H groups present on the polymer backbone such as benzophenones, vinyls, propargyls. In 2002, Gotenboss described the 1st antimicrobial QA plastic surfaces on an OH terminated silicone rubber after plasma treatment with SiQAC. In 2003, a patent described the plasma activation of polypropylene to either (A)

generate radicals from which QAC monomers were “grafted from” or (B) introduce functional groups onto which QAC polymers were “grafted to” (Figure 1.19).⁵²

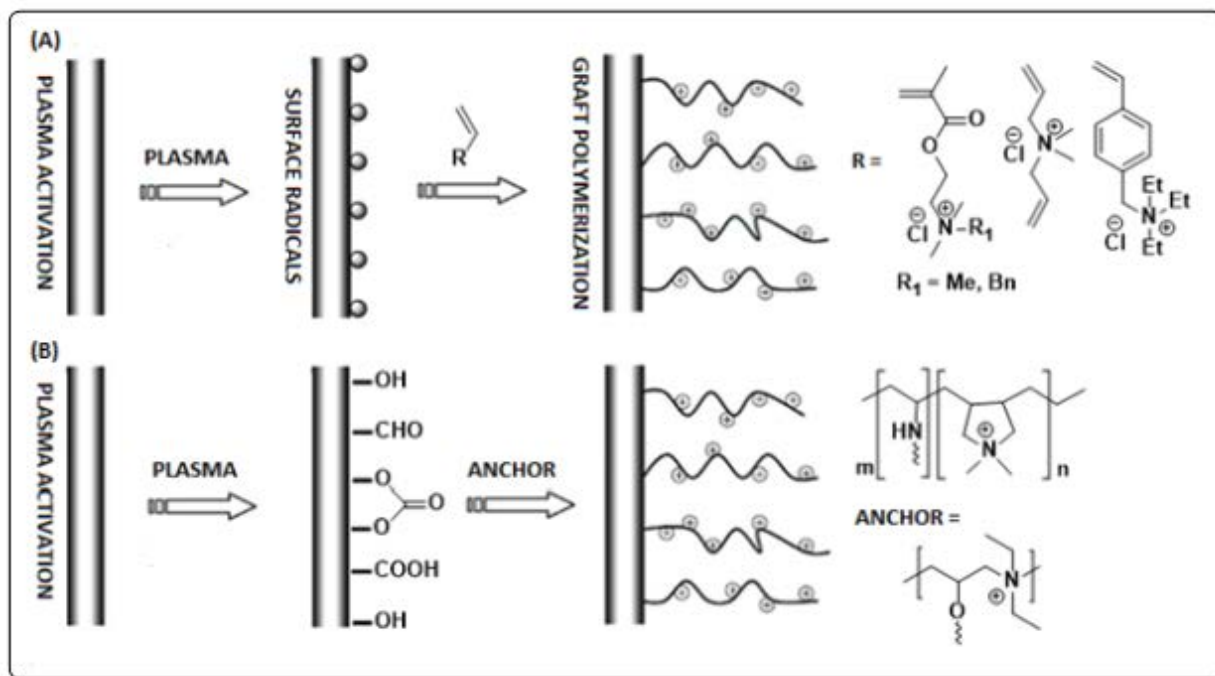


Figure 1.19: Bactericidal QAS polymers and small molecules prepared by plasma treated polypropylene (A) “grafting from” and (B) “grafting to” (Adapted from Ref.³²).

An alternative way to effectively attach polymeric or monomeric antimicrobials to plastics surfaces is with photochemically active groups such as the benzophenone cross-linker. When irradiated with UV light (345-365 nm), the benzophenone group abstracts a hydrogen atom from a polymer (C-H) surface, forming a strong C-C bond (Figure 1.20).²⁴ This linker has recently been used to attach thin polymer films to metal oxide and polyhydroxy surfaces via a phosphonic acid or silane group (Figure 1.20, **42**, **45**). Other examples include “grafting to” of antimicrobial QAC molecules and polymers with benzophenone groups to plastic surfaces with C-H groups under UV light (Figure 1.21, **43**, **44**, **46**, **47**). Dhende was first to covalently attach a quaternized polyethyleneimine (PEI) polymer onto various plastic surfaces²⁵ (Figure 1.21, Table

1.6, compound **43**) while the Foucher group experienced success with a benzophenone terminated C₁₈ quat on PVC and silicone grade medical tubing¹⁰⁵ (Figure 1.21, Table 1.6, compound **44**). The coating was visualized with bromophenol blue and found to be stable up to 3 rinse cycles after destaining with anionic detergents and restaining. Lastly, Yang *et al.*, used benzophenone as a surface initiator and grew polymers from PP surfaces that were later either quaternized or first quaternized and crosslinked (Figures 1.21 and 1.22, Table 1.6, Compound **47**).¹⁰⁶ With the unquaternized surfaces, a surface charge density of $\sim 3.50 \mu\text{mol cm}^{-2}$ was enough to kill both *E. coli* and *S. aureus* cells after 5 min. However, once the polymers were cross-linked, the surface lost its antimicrobial activity which was attributed to the loss of mobility of the immobilized polymeric cations.¹⁰⁶

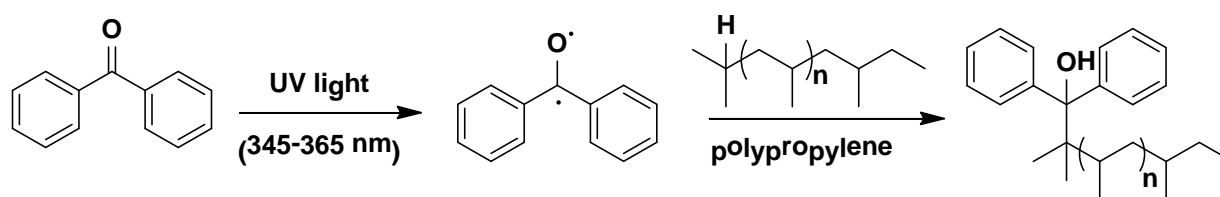


Figure 1.20: Example of “grafting from” immobilization of biocidal polymers employing the benzophenone surface bound initiator.²⁴

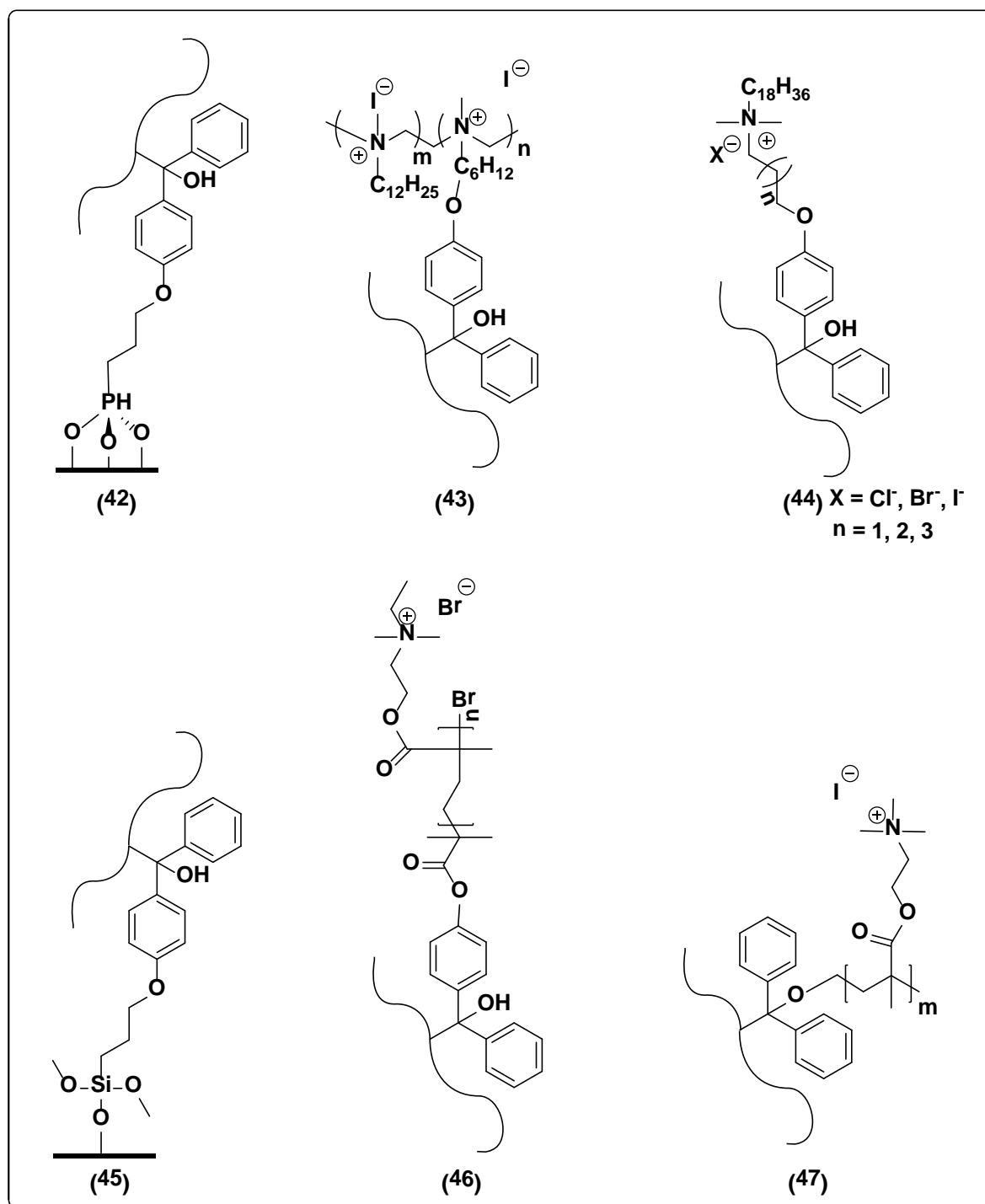


Figure 1.21: Examples of benzophenone used to prepare antimicrobial surfaces. (42)^{23,107}, (43)²⁵, (44)¹⁰⁵, (45)¹⁰⁸, (46)³², (47)¹⁰⁶.

Table 1.6: Examples of the benzophenone group utilized to create antimicrobial surfaces.

Antimicrobial Compound	Surface Tested	Immobilization type	Contact killing (%)
42 ^{23,27}	Ti, Al	Bifunctional-PO ₃ H ₂ SAM on metal with benzophenone polymer cap	N/A
43 ²⁵	PP, PVC, PE	Benzophenone grafting onto (1.5% sprayed, acetone), UV light (365 nm, 180 mW/cm ²) for 15 min	99% <i>E. coli</i> and <i>S.aureus</i> for > 35 nm thickness coating
44 ¹⁰⁵	PP, PVC, Silicone	Benzophenone grafting onto (1-5% sprayed, EtOH), UV light (365 nm, 180 mW/cm ²) for 5 min	99% <i>E. coli</i> reduction on Silicone
45 ¹⁰⁸	Si Wafer	Bifunctional-silane SAM on glass and benzophenone to antimicrobial polymer cap	N/A
46 ³²	PP	Benzophenone to BIBB SIP initiator ester coupling followed by ATRP graft with DMAEMA, quaternized with EtBr	95% <i>S.aureus</i>
47 ¹⁰⁶	PP	Benzophenone adlayer to “grafting from” with acrylate monomers then quaternizing	95% <i>S.aureus</i>

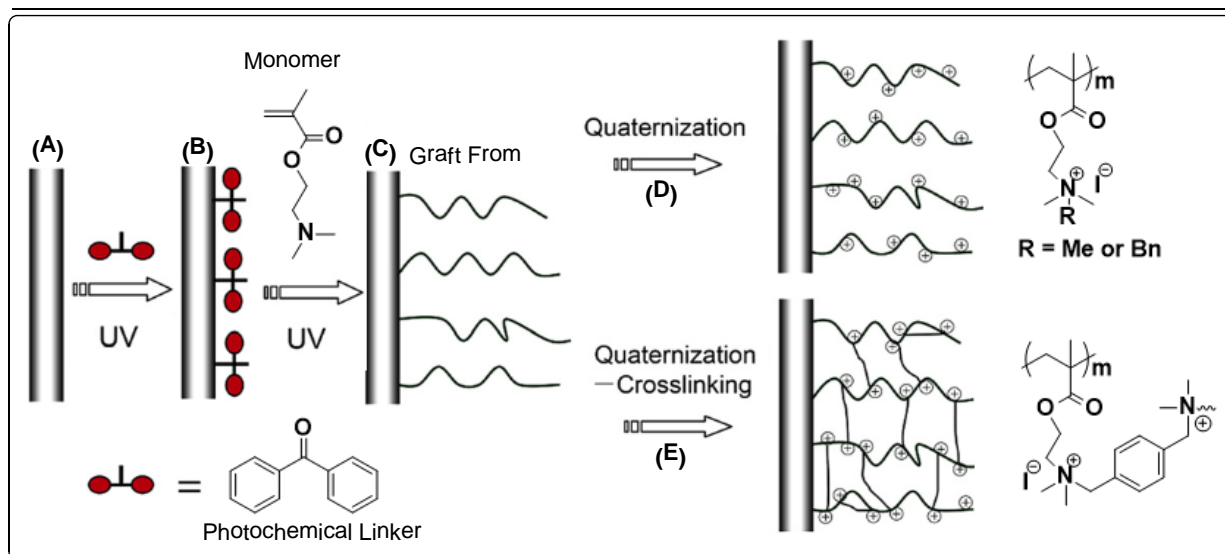


Figure 1.22: Example of “grafting from” a plastic surface. Immobilization of biocidal polymers without employing a surface bound initiator (Adapted from Ref.¹⁰⁶).

1.3 2nd Generation Antimicrobial Coatings: Literature Examples of Dual Action Antimicrobial Surfaces

Since the advent and popularity of contact active QAC antimicrobials, current research has shifted towards combining both passive and active antimicrobial coating strategies on a single surface, giving rise to 2nd generation antimicrobials.¹⁰⁹ These surfaces were designed to improve on the drawbacks of the 1st generation coatings which provide only one level of protection, either a microbe killing or microbe repelling role. 2nd generation coatings provide dual protection against invading bacteria by combining contact-killing with repelling capabilities so dead bacteria are swept or released from the surface after being killed.¹⁰⁹ In theory, these ideal surface coatings are difficult and costly to prepare, with few literature examples (mainly on Au surfaces) known. One example of a dual killing surface with contact killing and biocide releasing (killing) capabilities was prepared by growing cationic chains from Au surfaces followed by impregnation with Ag⁺ ions (Figure 1.23).¹⁰⁹ One apparent problem with solely killing surfaces is the build up and attachment of dead cells or debris that can deactivate the surface if not reactivated by a cleaning step. One solution to this problem was realized with a polymeric coating on Au surfaces that can be hydrolyzed from the quaternary ammonium (killing) to the zwitterionic form (repelling) reversibly (Figure 1.24).¹¹⁰ However, this surface required a manual hydrolysis similar to a cleaning step, otherwise the surface won't automatically switch after a build up of cells is sensed (Figure 1.24). The Foucher group is also interested in biocidal and self-cleaning surface coatings. Synthesis of an azo-benzene QAC with inherent self-cleaning capabilities switching from the *cis* and *trans* configuration under UV light is currently under study.⁹⁹

The 3rd generation of antimicrobial coatings is foreseen to be capable of responding to stimuli so the surface can switch from a killing to a repelling one and vice-versa when necessary and target pathogenic bacteria exclusively. No literature reports of such stimuli responsive “switchable,” “smart,” futuristic surfaces are yet available.

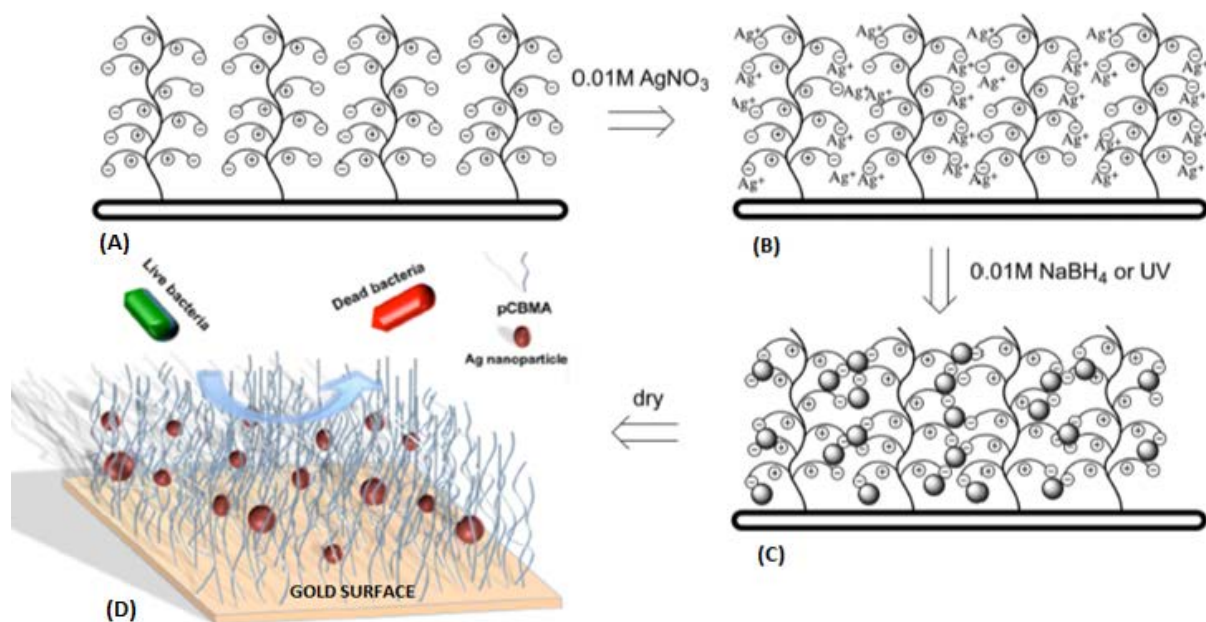


Figure 1.23: Example of a releasing and repelling 2nd generation dual action antimicrobial surface.¹⁰⁹

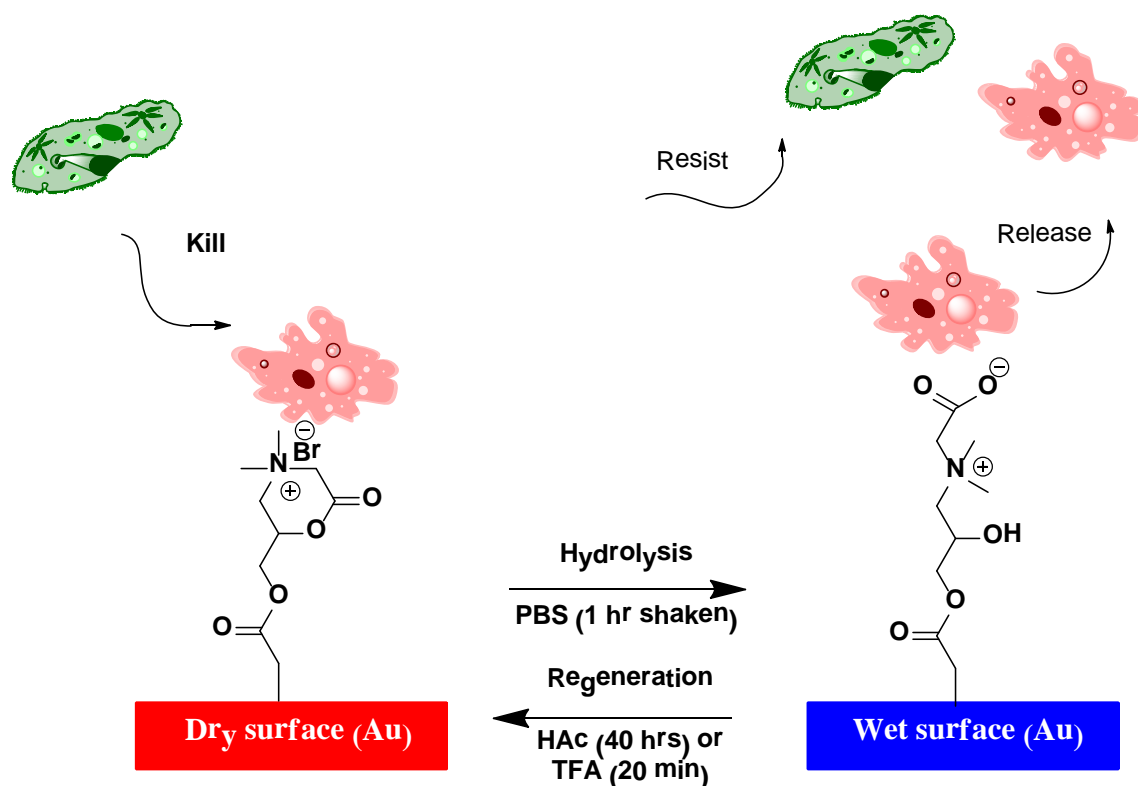


Figure 1.24: Example of a dual action and reversible contact killing / hydrophobic antimicrobial surface.¹¹⁰

1.4 Kill Mechanisms of QAC

The kill mechanism of QAC's in solution or immobilized onto a surface is dependent on a host of factors that influence the compound's antimicrobial activity. Some of the factors include: (i) solution testing vs. surface testing, (ii) concentration/surface coverage, (iii) size (molecular weight), (iv) structural backbone, (v) type of counter ion, (vi) number of positive charges, and (vii) hydrophobicity of *n*-alkyl chains in the backbone of the QAC molecule or polymer.^{13,97,111,112} The bacterial cytoplasmic membrane is commonly targeted by different types of cationic QAC's that eventually result in cell death and is discussed below along with the

structural factors influencing QAC's antimicrobial activity both in solution and on hard surfaces.¹³

1.4.1 Mechanism of Killing in Solution

In solution, long chain monocationic QAC's such as those employed commercially as disinfectants (Figure 1.25) destroy the bacterial cell wall and or cytoplasmic membranes by a two step process (Figure 1.26).^{113,114} First, the positively charged QAC's are initially attracted to the negatively charged bacterial cell after which the QAC's diffuse and firmly bind to the inner cytoplasmic membrane. QAC's form ion-pairs with the head groups of acidic-phospholipids namely phosphatidylethanolamine (70% membrane composition) and in the process displace the Mg^{2+} and Ca^{2+} cations used to stabilize the lipid bilayer (Figure 1.26 b).⁷⁶ Membrane function is further disrupted by the hydrophobic portion of the molecule by denaturing structural membrane proteins and inserting itself into the cytoplasmic membrane (Figure 1.26 c,d). With the QAC concentration approaching the minimum inhibitory concentration (MIC), the membrane begins to lose vital physiological functions such as osmoregularity and begins to leak K^{+} ions and protons.⁷⁶ Eventually, physiologically relevant membrane protein function is inhibited and the cell loses the ability to respire, transport solutes, and resynthesize the cell wall.¹¹³ At high concentrations, the disinfectants form micellar aggregates that completely solubilize membrane phospholipids and proteins causing leakage of the intracellular material, cell lysis and eventually cell death (Figure 1.26 e, f).^{113,115}

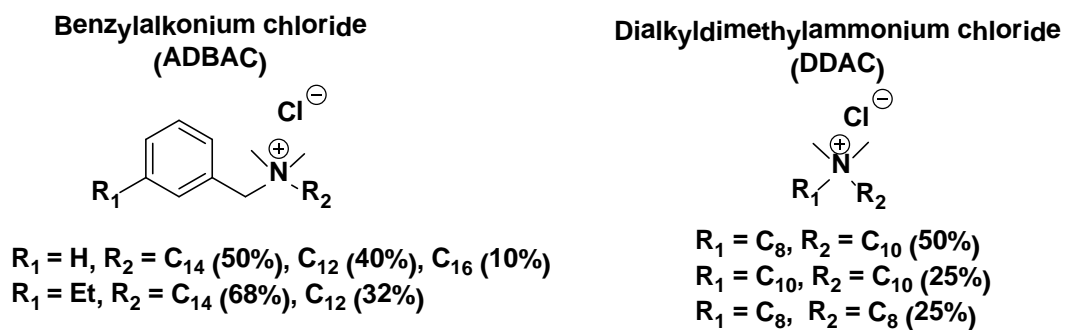


Figure 1.25: QAC disinfectants commercially employed.¹¹⁶

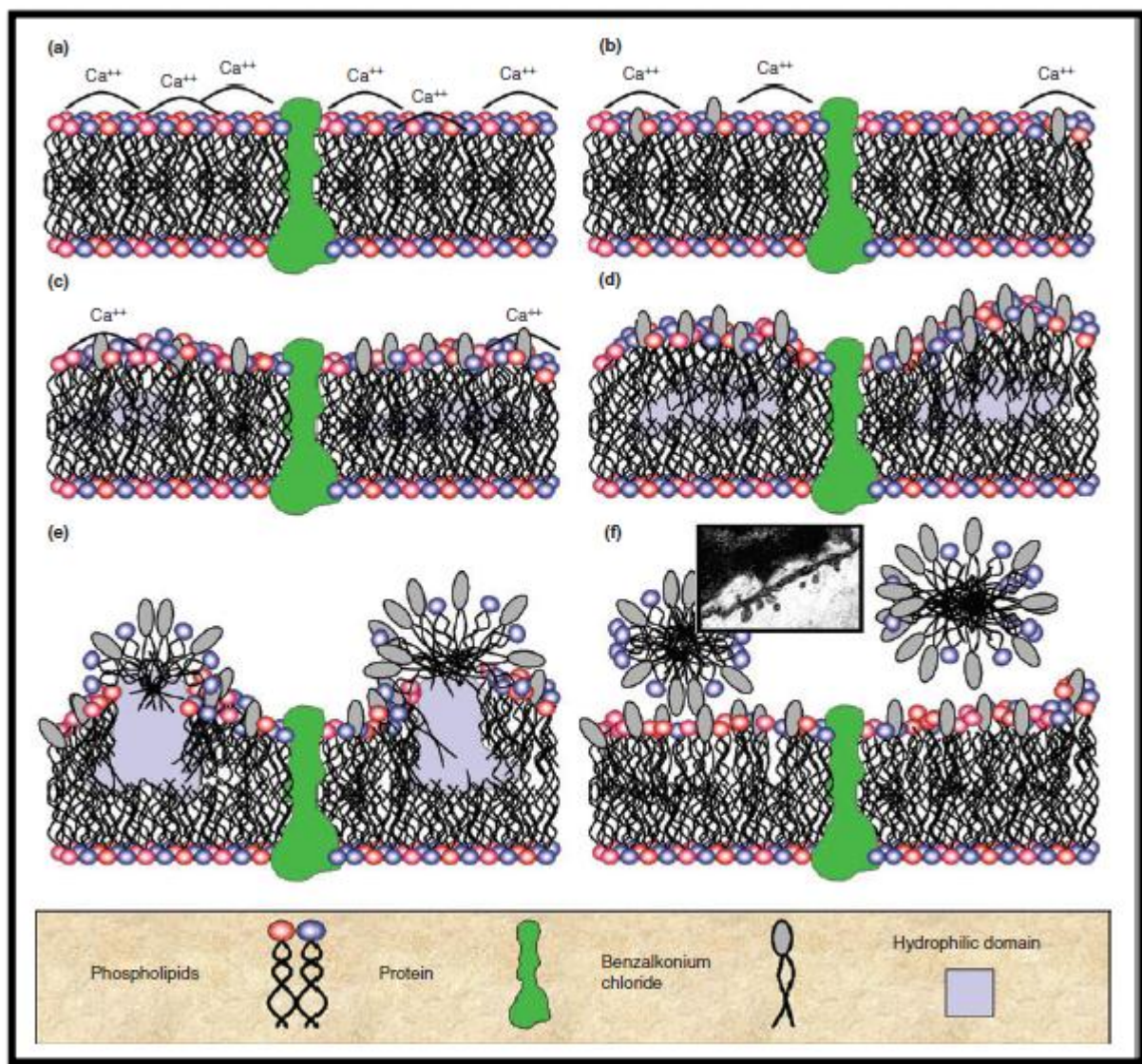


Figure 1.26: Bacterial membrane destruction by QAC disinfectants in solution. (Used with permission from Ref. ¹¹³).

For example, Iannou *et al.*, found that the adherence of alkyldimethylbenzylammonium chloride (ADBAC, Figure 1.25) (a blend of C₁₂, C₁₄ and C₁₆ alkyl homologues) and didecyldimethylammonium chloride (DDAC, Figure 1.25) to *S. aureus* cells occurred through slightly different mechanisms.¹¹⁷ ADBAC formed single monolayer coverage around the *S. aureus* outer membrane, while the DDAC formed a double layer. Both disinfectants eventually caused cell leakage and a total release of the intracellular K⁺ and 260 nm-absorbing proteins. Autolysis concentrations were similar regardless of the monolayers formed at 9 ug/mL (for both disinfectants), along with the depletion of approximately 30% of the internal K⁺ pool.¹¹⁷ The authors attributed the lethality of ADBAC and DDAC to the autolysis of *S. aureus*, however, it was concluded that mechanical lysis also seemed to be involved because cell autolytic enzymes became inhibited at the disinfectant concentrations employed (Table 1.7).¹¹⁷

Table 1.7: MIC values for ADBAC and DDAC against increasing *S. aureus* concentrations after 48 hrs of incubation in TSA medium.¹¹⁷

Biocide	Biocide MIC (μg/mL) for inoculum test conc. (CFU/mL)				
	10 ⁵	10 ⁶	10 ⁷	10 ⁸	10 ⁹
ADBAC	0.6	0.6	0.7	1.0	1.8
DDAC	0.4	0.4	0.4	0.6	1.6

In another example, electron microscopy was used to study the interaction and effects of QAC's on the *S. aureus* membrane. The micrographs (Figure 1.27) clearly showed the different stages of insertion of the QAC into *S. aureus* strain ATCC 25923. On the right, the arrows indicate tiny holes showing nodule formation (ND), indicating the beginning of cellular material leaking out of the cell. Cell deformity and cell leakage (CL) was also evident. Interestingly, after performing elemental analysis on QAS treated and untreated cells, the authors were unable to

detect the QAC chlorine counterion after it was taken up by the cells. It was theorized that the chlorine was pumped out of the cell on its own or together with the QAC from the cell prior to cell lysis.¹¹⁴ Another possibility could be that upon binding to the membrane, the chlorine counterion was displaced from the QAC forming $MgCl_2$ with structural cations within the microbial membrane.

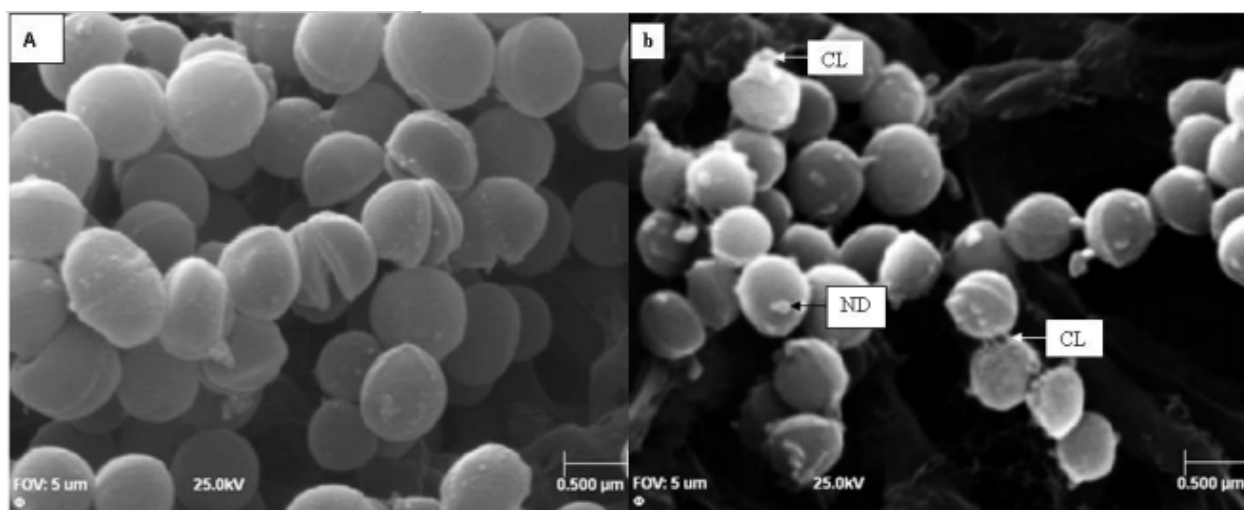


Figure 1.27: Scanning electron micrographs of *S. aureus* strain ATCC 25923 indicating the effect didecyldimethylammonium chloride (DDAC) had on cell morphology, (a) control *S. aureus* cells containing no DDAC displayed normal spherical shapes, (b) cells treated with 20 g/L DDAC for 10 min. The arrows indicated where cell leakage (CL) and nodule formation (ND) was observed when the *S. aureus* cells were incubated with DDAC. (Used with permission from Ref.¹¹⁴).

The antimicrobial activity of the disinfectants discussed thus far are dependent on the length of the hydrophobic chain which follows a parabolic trend of MIC values (Figure 1.28). This phenomenon is called the “cut-off effect” where QAC’s with C_{12} - C_{14} alkyl chain lengths show the highest activity against gram-positive bacteria and yeast, while those with longer alkyl chains (C_{14} - C_{16}) show the highest activity against gram-negative bacteria. Compounds with short alkyl chains ($n < 4$) or very long alkyl chains ($n > 18$) showed the lowest activity.¹¹³ QAC’s

with the highest antimicrobial activity and lowest MIC values are observed when the total alkyl chain length is ($n > 10$). In solution, QAC's with the optimum alkyl chain length ($n > 10$), exist as dimers because the attractive forces of neighbouring hydrophobic tails overcome the repulsive positive charges of neighbouring cations and thus show the highest kill activity. Dimeric-QAC's interact and solubilize bacterial membranes more freely in comparison to the monomeric QAC's. As a result the most effective QAC disinfectants are sold as a mixture of different chain lengths in order to ensure broad spectrum activity against different types of bacteria.¹¹⁶

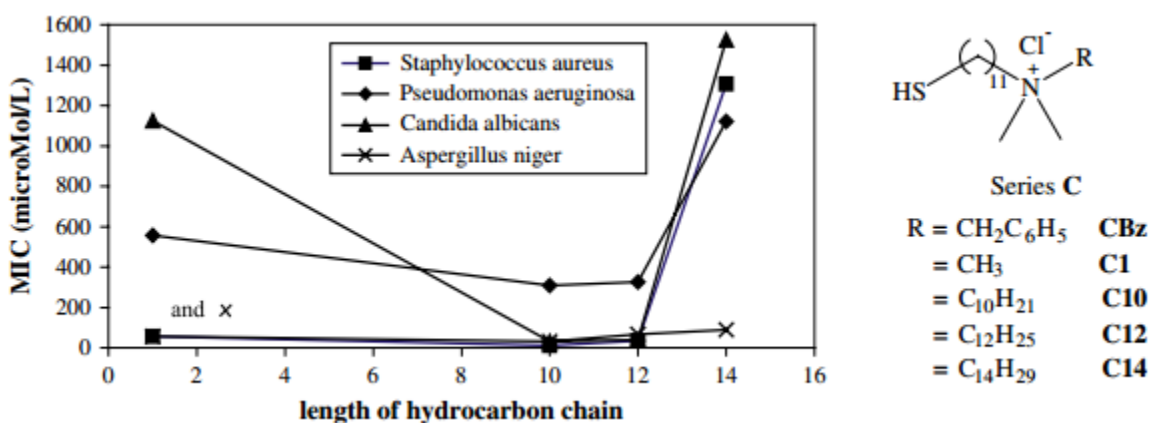


Figure 1.28: The “Cut off Effect:” A hyperbolic trend observed in MIC values of surfactants as a function of the length of the hydrocarbon chain. (Used with permission from Ref.¹¹⁸).

When QAC disinfectants are used at concentrations above bacterial MIC's, developing resistance is unlikely, however, when bacteria are exposed to sub-MIC concentrations various resistant genes are acquired.^{119,120} In fact, gram-negative bacteria such as *E. coli*¹²¹ and *P. aeruginosa*¹²² have acquired QAC efflux pumps capable of removing quats out of the cell. *P. aeruginosa* also contain enzymes capable of metabolizing QAC's as a source of carbon and nitrogen, therefore, the MIC's are much higher (upto 10 ×) for this bacterium (Table 1.8). Further adaptive resistance to QAC's exists in bacteria capable of forming a biofilm, where the biofilm secreted lipopolysaccharide layer can protect the bacteria from coming into contact with the

biocide. Single strain bacterial biofilms resistant to QAC's studied include those of *P.aeruginosa* and *Salmonella Enterica Serovar Enteritidis* ATCC 4931.¹²³ Lastly, gram-positive bacterial membranes are less resistant to QAC's due to the loosely packed peptidoglycan outer layer allowing easier access to their inner cytoplasmic membrane and typically show lower MIC values (Table 1.8, *S. aureus*). Meanwhile, gram-negative bacterial membranes are inherently more resistant because a QAC must first cross the outer membrane with a bilayer phospholipid structure before it can gain access to the inner cytoplasmic membrane.

Table 1.8: MIC values of Commercial Disinfectant BAK 50 versus thiol QAC's.¹¹⁸

Compound	MIC (μmol/L)			
	<i>S.aureus</i>	<i>P.aeruginosa</i>	<i>C.albicans</i>	<i>A.niger</i>
BAK 50	3.2	93	8.36	4.74
R = CH ₂ C ₆ H ₅	56.6	556.9	1124.8	56.6
R = CH ₃	681.6	1055.9	471.6	351.0
R = C ₁₀ H ₂₁	11.6	308.9	31.6	31.6
R = C ₁₂ H ₂₅	34.7	326.2	39.5	67.2
R = C ₁₄ H ₂₉	1306.3	1121.5	1524.6	90.0

When dealing with polymeric QAC's in solution, factors such as polymer size, type of counter ion, the length of the hydrophobic backbone and location of the positive charge along the backbone all have an affect on the antimicrobial activity. Typically, polymeric biocides are designed with the QAC's spread throughout the backbone as repeat units and such polymer

systems show a dependence on molecular weight where a $1.4 - 9.4 \times 10^4$ Da range shows maximum activity. Polymers exceeding the cut-off range are inactive because they are too large to adhere to or enter the bacterial cytoplasm.⁹⁷

QAC-polymers with loosely bound counter anions foster increased antimicrobial activity because the weaker ion pair readily dissociates from the quat, which leads to ion-pair formation with the negatively charged bacterial membrane. On the other hand, strong ion-pair counterion associations with the polymer show decreased antimicrobial activity because the tightly held counter ion will prevent the polymeric quats from associating with the bacteria.¹²⁴

The spacer length or alkyl chain length refers to the length of the carbon chain that composes the polymer backbone. The length of this chain has been investigated to see if it affects the antimicrobial activity of the polymer. Results have generally shown that longer alkyl chains result in higher antimicrobial activity. There are two primary explanations for this effect. Firstly, longer chains have more active sites available for adsorption with the bacteria cell wall and cytoplasmic membrane. Secondly, longer chains aggregate differently than shorter chains, which again may provide a better means for adsorption.¹²⁴

Lastly, with polymeric QAC's, changing the hydrophobic portions can have a drastic effect on the efficacy of the antimicrobial in solution. Tiller's group synthesized a C₁₂ mono quaternary oxazoline polymer with a terminal hydrophobic end group with either 10 or 16 hydrocarbons in length.¹²⁵ Only the hexadecyl polymer demonstrated antimicrobial activity, while the shorter decyl chain prevented the polymer from refolding into the right orientation necessary to lyse the bacterial membrane (Figure 1.29).¹²⁵

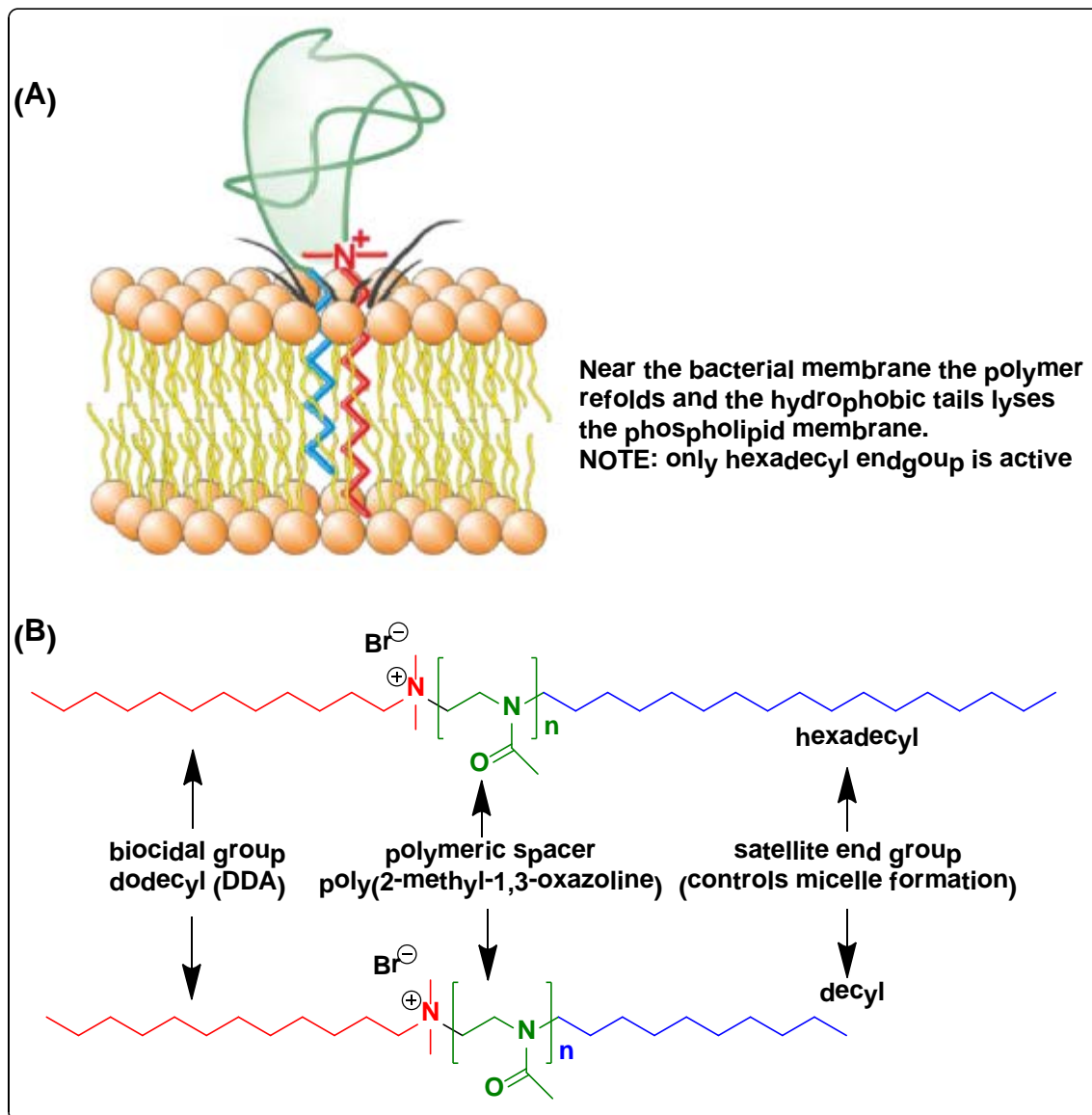


Figure 1.29: Effect of chain length on antimicrobial activity in solution (Adapted from Ref.¹²⁵).

1.5. Mechanism of Immobilized Contact Active QAC

Some authors suggest that surfaces immobilized with QAC compounds kill microbes on contact by disruption of the microbial membranes based on observations with structurally different polycationic polymers. Two contact killing hypotheses were proposed and are based on

disruption of the microbial membranes either by (i) physical means, e.g. membrane penetration/disruption or (ii) electrostatic/ionic interactions with oppositely charged bacterial phospholipids and the polycationic molecules/polymers. Both mechanisms are described below.

1.5.1 Polymeric Spacer Effect

The first contact killing hypothesis was proposed in 2001 by Klivanov *et al.*, after showing that long chain cationic polymers of poly(4-vinyl-*N*-hexyl)pyridinium bromide “grafted-from” or *N*-alkyl PEI adsorbed onto glass slides were highly antimicrobial (Figure 1.30).¹²⁶⁻¹²⁸ Glass surfaces modified with large cationic polymers ranging from 25 kD to 750 kD resulted in instant killing, meanwhile the shorter chain polymers (2 kD) were inactive towards airborne *S. aureus* cells sprayed onto these surfaces (Section 1.6.1.2.3 (a)). Similarly, glass slides immobilized with these antimicrobial polymers were capable of reducing both gram-positive and gram-negative bacteria by a factor of 10^9 cells after immersing these surfaces into bacterial solutions according to live/dead staining. Since bacterial cell walls typically range from 16 to 80 nm, the surface grafted cationic polymer coatings needed to be long and flexible enough to be able to penetrate the cell wall and disrupt the negatively charged inner bacterial membranes, e.g. a polymeric spacer of 50 nm would be required to destroy the *E. coli* cytoplasmic membrane which are ~ 46 nm thick (Figure 1.31).¹²⁶

1.5.2 Phospholipid Sponge Effect

A second membrane disrupting, contact-killing mechanism was proposed after observations that the short chain Si-QAC **3** and other shorter polymer brushes grown from surfaces (less than 10 nm) were also highly antimicrobial. Instead of being long enough to penetrate the cell wall, these surface immobilized shorter chain polycationic antimicrobials were hypothesized to disrupt membranes via ion-exchange between the polycationic biocides and structurally important mobile cations (Ca^{2+} and Mg^{2+}) within the bacterial cytoplasmic membrane (Figure 1.32).¹³⁰ Based on observations with short chain polycationic polymers ‘grafted onto’ glass slides via silane linkers, surfaces with a charge density of QA cations (10^{12} - 10^{16} N^+ positive charges per cm^2) were required for killing after 10 min contact time depending on the type of bacterium. Approximately $\sim 1 \times 10^{10}$ QA or 0.015 pmol N^+ was calculated to be necessary to kill one bacterium, thus a surface with 3.2×10^{14} N^+ / cm^2 would roughly kill $\sim 0.3 \times 10^5$ bacteria/ cm^2 . In all cases, surfaces grafted with more charges/ cm^2 of short chain QAC’s caused faster release of counterions and resulted in higher and faster killing.^{42,131}

In addition, Tiller proposed that highly charged surfaces without polymeric spacers need a certain degree of hydrophobicity around the quat in order to effectively kill microbes on contact. Based on observations with quaternized *N*-butyl or *N*-dodecyl-*N,N*-dimethyldeoxyammonium cellulose polymer surfaces prepared from tosyl cellulose, polymers with only 50% of the tosyl groups (hydrophobic residues) substituted with the non-biocidal short chain (*N*-butyl-quat) were found to be biocidal whereas polymers with the same amount of N^+ charges but with a low degree of substitution of the biocidal longer chain (*N*-dodecyl-quat) were

not biocidal. However, tosyl celluloses fully quaternized with the C₁₂ tail were highly biocidal while the same polymers substituted with the C₄ chain had no antimicrobial activity.^{132, 133}

To further prove that a contact active mechanism was involved, the C₁₂ fully substituted cellulose coatings were deactivated with sodium dodecyl sulfate (SDS, 1g/L, 1 min) and an oppositely charged phospholipid (liposomes with 10% phosphatidylglycerol). As expected, antimicrobial activity against *S. aureus* was lost as these anionic molecules completely blocked the cationic sites on the antimicrobial surface, preventing the removal of bacterial phospholipids. In contrast, the same coating but with a polyethyloxazoline spacer (~100 polymeric units) between the C₁₂ quat and the cellulose backbone was unaffected by the same oppositely charged deactivating treatment and killed all *S. aureus* cell in support of the polymeric spacer mechanism. The authors proposed that in the phospholipid sponge mechanism, the H₂O-insoluble bacterial phospholipids are removed from the bacterial membrane and transverse through small holes in the bacterial cell-wall as micelles in order to reach the oppositely charged antimicrobial coating (Figure 1.32). A hydrophobic portion surrounding the positive charge may be required to further stabilize the newly formed ion-pair, utilizing van der Waals interactions with the hydrophobic tail of the removed lipids.

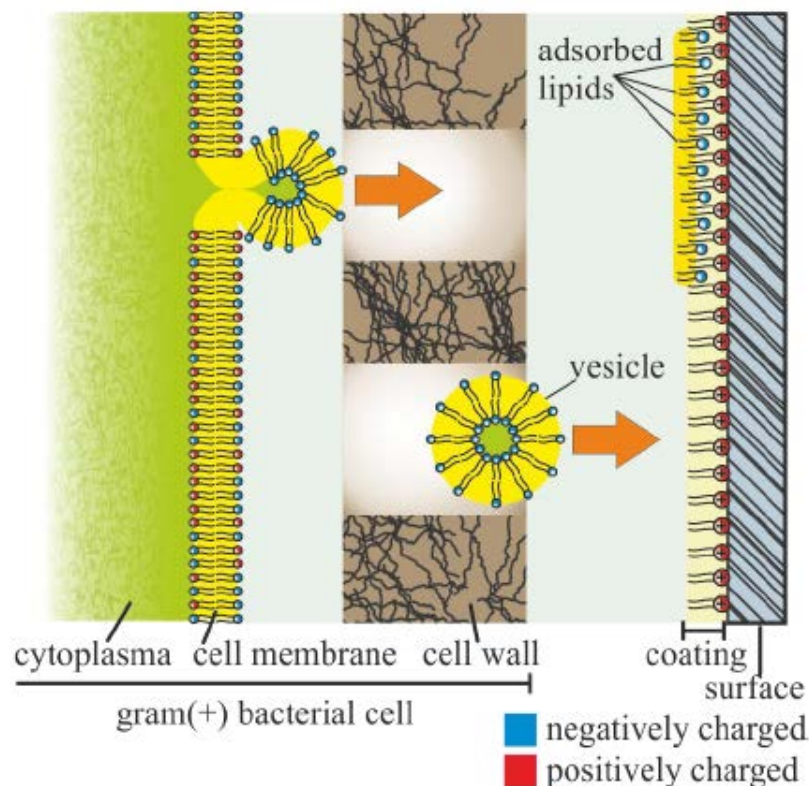


Figure 1.32: Contact-killing via the phospholipid sponge mechanism. (Used with permission from Ref.^{13,133}).

1.6 Antimicrobial Testing

A variety of methods are available for testing non-leaching (immobilized) antimicrobial products or surfaces based on either (i) growth enumeration of recovered bacterial colonies or (ii) cell viability enumeration after coming into contact with the active surface. With growth based methods, each method was tailored to a specific type of surface (textiles, metals, plastics) and differ in the way the bacterial inoculum is applied. Some methods require immersion of a test substrate with inoculum, while others apply the inoculum directly via (i) aerosol spraying and/or (ii) placing a drop of inoculum and allowing it to dry on the surface prior to enumeration. Cell viability enumeration is typically based on fluorescence staining combined with real time

microscopy or assayed with various molecular biology techniques. Both growth and cell viability enumeration methods are discussed below along with their drawbacks and limitations.

1.6.1 Growth Based Enumeration

1.6.1.1 Immersion Inoculation

1.6.1.1.1 ASTM E2149-10

Originally developed by Isquith *et al.*, the Dow Corning Corporate Test Method 0923 (CTM-0923)³⁵ became known as the ASTM E2149-01,¹⁸ the standard test method for determining the antimicrobial activity of immobilized antimicrobial agents under dynamic contact and was later superseded by ASTM E2149-10.¹³⁴ Active surfaces are tested by immersion with inoculum following shaking and removal of samples at different times. Cells are serially diluted and colonies are enumerated on agar plates (Figure 1.33).

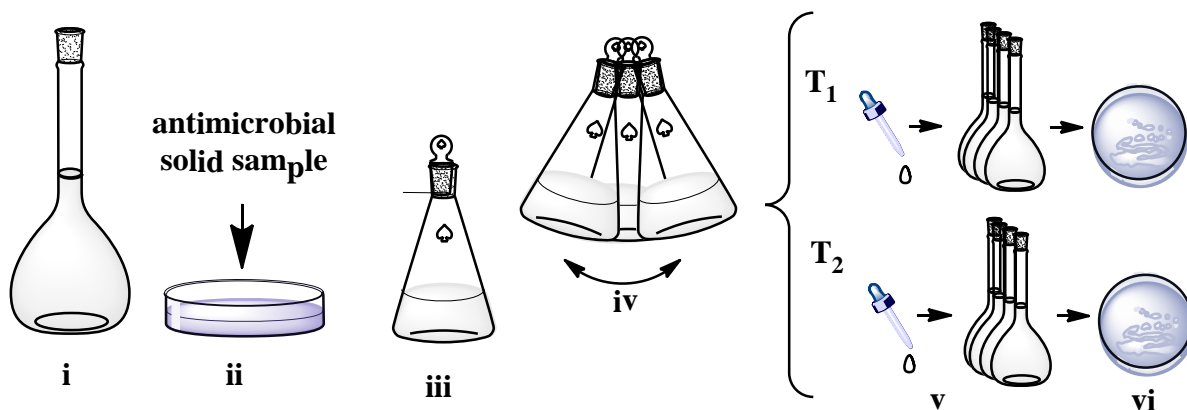


Figure 1.33: ASTM E2149-10: (i) $1.5-3.0 \times 10^5$ CFU/mL (inoculum), (ii) treated surface cut into smaller pieces, (iii) treated surface mixed with 50 mL inoculum, (iv) place on mechanical shaker, (v) periodically remove 1.0 mL samples (T_1 - T_4), (vi) dilute serially + growth on agar, (vii) compare to controls and calculate percent or log 10 reduction of viable cells.¹⁸

Even though the ASTM E2149 method has become the industrial benchmark for testing non-leaching (immobilized) antimicrobial products or surfaces, it has been debated whether it

could clearly distinguish between a contact killing surface and a biocide releasing one.⁶³ The growth based enumeration test method assumes that an overall reduction of living cells (CFU's, colony forming units) is due to contact killing without taking into account that some of the killing could be due to slow leaching of the immobilized antimicrobial over time.⁶³ Since the minimum inhibitory concentration (MIC) and minimum lethal concentrations (MLC) of Si-QAC in solution are very low, it is possible to observe bacterial kill from surface leaching of the active over time. For example, White *et al.*, reported a very low MIC for gram-positive bacteria (MIC = 10 µg/mL, *S. aureus*) and a much higher concentration for gram-negative bacteria (MIC = 100 µg/mL, *E. coli*) and (MIC = 1000 µg/mL, *A. niger*).²⁷ Le Song also reported a similar result (MLC = 84 µg/mL, *E. coli*).²⁴ However, in saline solution, the activity of compound **3** was negligible (see Table 1.9).²⁴

Table 1.9: Antibacterial activity of compound **3** in solution.²⁴

Test medium	Compound	MLC (µg/mL)
Deionized H ₂ O	3	< 84
Artificial sea H ₂ O	3	8000

1.6.1.2 Direct Inoculation

1.6.1.2.1 Zone of Inhibition

In the agar diffusion test, or the Kirby-Bauer disk-diffusion method, the zone of inhibition is often used to determine if an antimicrobial surface releases biocides or if it kills on contact.¹³ An agar plate with a visible zone of dead bacteria around the antimicrobial surface is attributed to the release of the active biocide that exceeds the MIC, meanwhile an uncolonized surface with no such zone is typically considered to kill on contact (Figure 1.34). The size of the

zone depends on factors such as the diffusion kinetics through the nutrient media and the original concentration of the active chemical present. With this test, however, it is difficult to prove if the immobilized surface is truly contact killing solely by the absence of a zone of inhibition. For example, monolayers of immobilized biocides typically contain a very small amount of the active molecule and thus the absence of a zone of inhibition could be mistaken for a non-releasing surface when in fact the concentration of the antimicrobial agent is above the MIC.¹³ On the other hand, interferences such as charged proteins and other growth media nutrients that can deactivate cationic immobilized antimicrobials on the test surface would raise the MIC and result in a smaller or no zone in an eluting surface.¹³

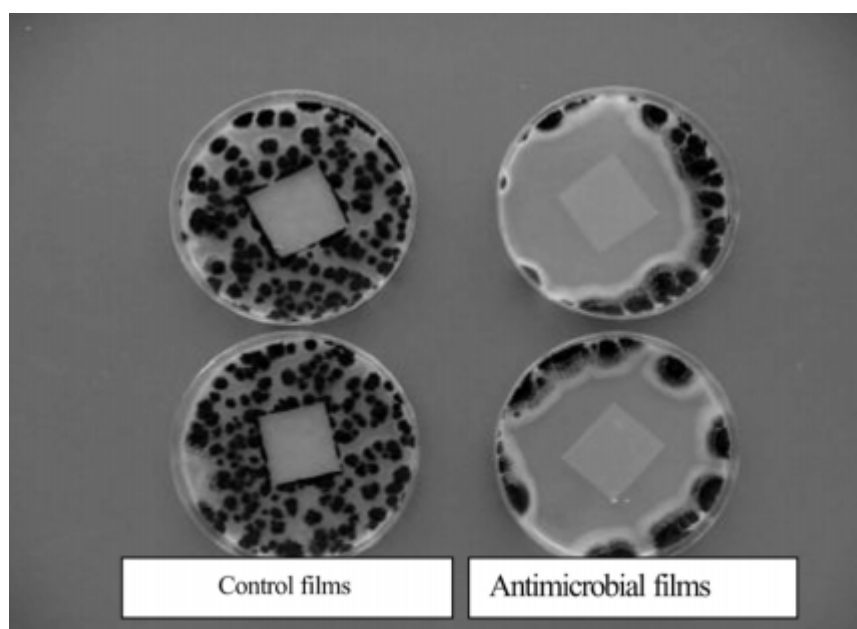


Figure 1.34: ZOI Agar diffusion method: Antimicrobial releasing plastic film surface on *A. niger*. (Used with permission from Ref.⁹⁵)

1.6.1.2.2 Textiles

The AATCC 100-2004 test method or the “padding test” is very similar to the Dow suspension test except only textile samples are tested and no shaking takes place. Circular textile samples are inoculated, incubated and colonies are counted after serial dilutions (Figure 1.35).¹⁸

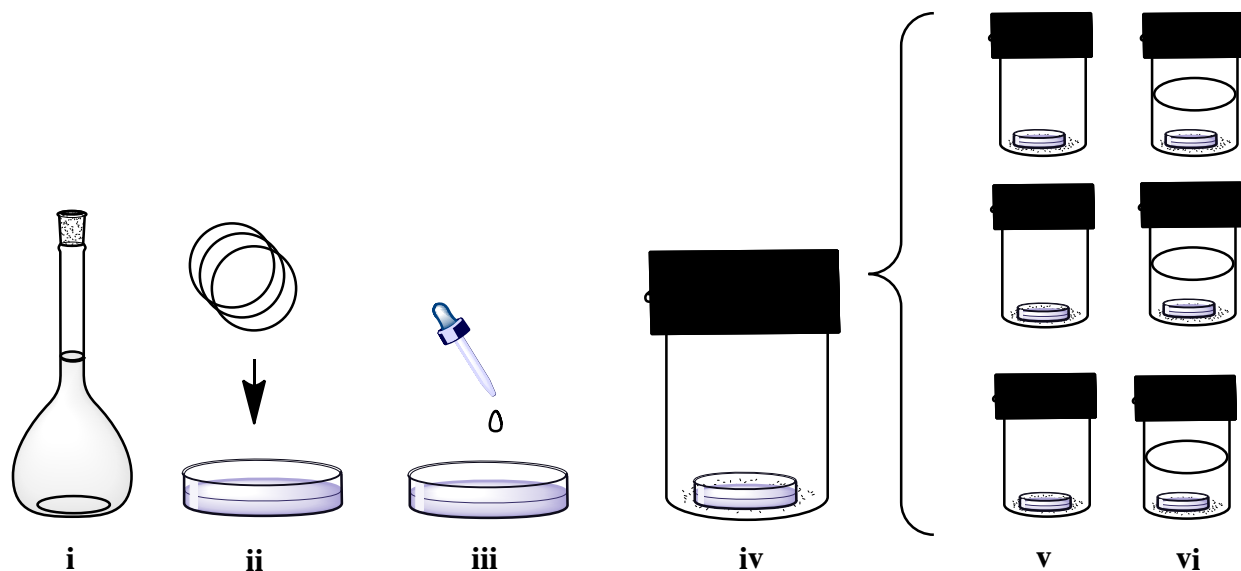


Figure 1.35: Standard methods for testing antimicrobials on textiles. (i) $1-2 \times 10^5$ CFU/mL (inoculum), (ii) place textile in petri dish, (iii) 1 mL inncolumn is added (iv) transfer to jar to prevent evaporation, (v) incubate, (vi) add neutralizer solution, (vii) serial dilutions, incubate and agar plating, (viii) compare to controls and calculate percent of log 10 reduction.¹⁸

1.6.1.2.3 Hard Surfaces: Metals, Plastics, Glass

(a) Aerosol Inoculation

This method, designed to mimic airborne deposition of microorganisms on surfaces, utilizes a readily available TLC sprayer to deposit a bacterial inoculum as a mist on hard surfaces followed by air drying, agar incubation and viable colony counts (Figure 1.36). Simple in design, the drawback of this method is reproducibility in the delivery of the inoculum which makes it difficult to compare to non-aerosol methods.¹⁸ Also the aerosol method does not distinguish

between contact killing or release killing from the surface.⁶³ A literature example described by Klibanov shows the results of the aerosol method of a glass slide with covalently attached cationic antimicrobial PVP polymer (Figure 1.37).¹²⁷

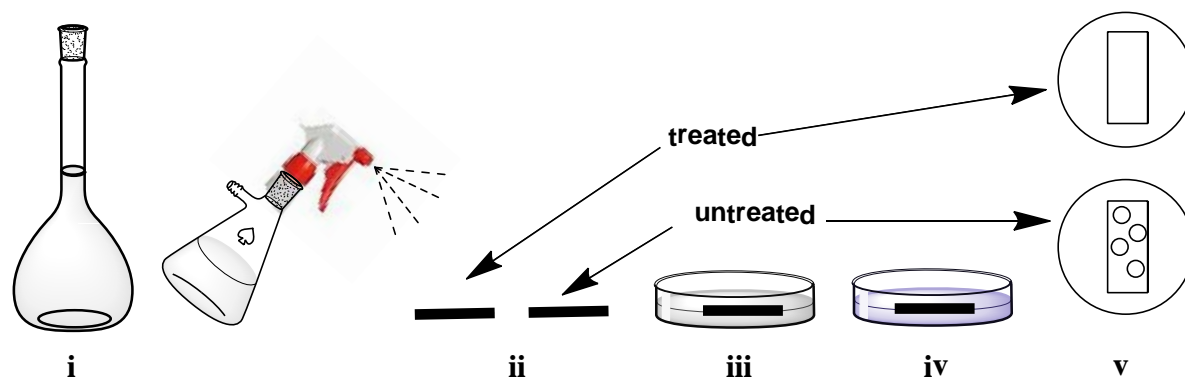


Figure 1.36: Diagram of the aerosol inoculation method: (i) $5-50 \times 10^6$ CFU/mL (inoculum), (ii) inoculum sprayed onto treated and control surfaces and allowed to air dry for 2 min, (iii) cover with agar and incubate 37°C ON, (iv) compare to controls and calculate percent or log 10 reduction.¹⁸

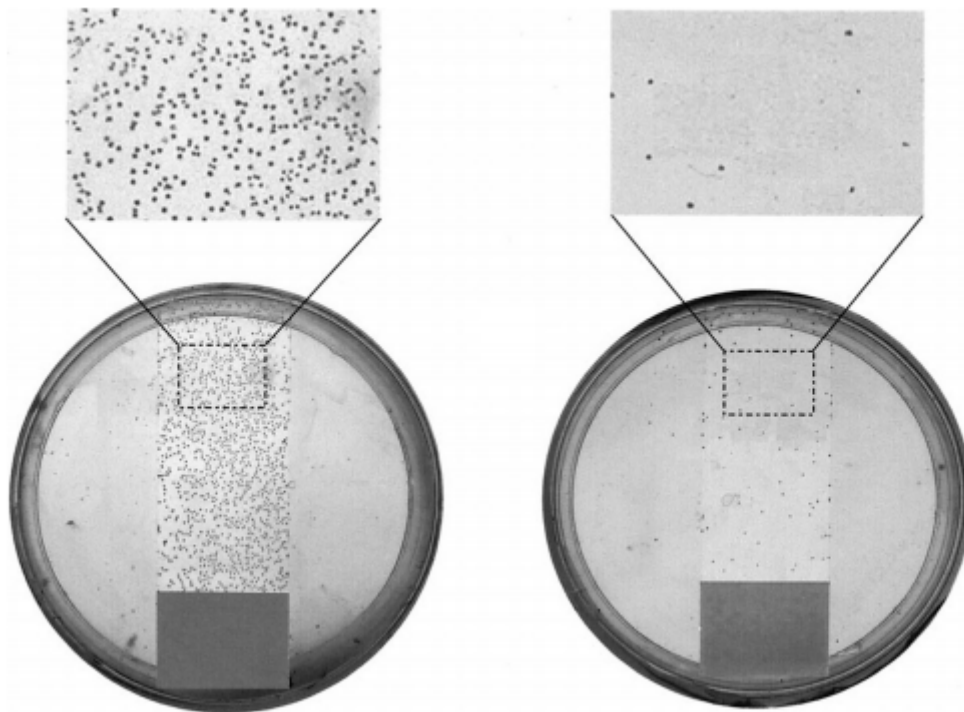


Figure 1.37: Results from the aerosol inoculum method with an immobilized QAS polymer onto a glass slide. Left (control), right (polymer modified slide). (Used with permission from Ref.¹²⁷)

(b) Industrial Standard Test Methods

A variety of standard test methods designed to quantitatively test microbial inhibition via direct inoculation on solid surfaces include the (i) JIS Z 2801, the Japanese standard, developed in 2006 and superseded by (ii) ISO 22196, the international standard method. Other similar standard methods for hard surfaces include (iii) EN ISO 846, plastics-evaluation of the action of microorganisms, (iv) ASTM G21-90, standard practice for determining resistance of synthetic polymeric materials to fungi, and (v) ASTM G22-76, standard practice for determining resistance of synthetic polymeric materials to bacteria.^{18,95}

As with the immersion inoculation method, the test microorganism is cultured, usually by growth in a liquid culture medium. The suspension of test microorganism is standardized by

dilution in a nutritive broth (this affords microorganisms the potential to grow during the test).⁹⁵ Control and test surfaces are inoculated with microorganisms in triplicate, and then the microbial inoculum is covered with a thin, sterile film. Covering the inoculum spreads it, prevents it from evaporating, and ensures close contact with the antimicrobial surface. Microbial concentrations are determined at "time zero" by elution followed by dilution and plating. A control is run to verify that the neutralization/elution method effectively neutralizes the antimicrobial agent in the antimicrobial surface being tested.⁹⁵ Inoculated covered control and antimicrobial test surfaces are allowed to incubate undisturbed in a humid environment for 24 hrs.⁹⁵ After incubation, microbial concentrations on surfaces are determined. The reduction of microorganisms relative to initial concentrations and the control surface is then calculated (Figure 1.38).

The drawback of the ISO 22196 method is that it is not representative of the actual antimicrobial surface contamination scenario. Typically upon landing, microbial contaminants dry very quickly on surfaces, whereas with this method, the use of a cover slip keeps the contact between bacteria and the surface in a wet state typically overnight. In reality, bacteria rarely spend that long of an interaction with the surface in the wet state.¹³⁵ As well, cells adhered to the cover slip are not typically taken into account, inflating log reduction values (LRV's).¹³⁶ This method has recently been modified by the Wolfaardt lab, by forgoing the glass cover slip and allowing the inoculum to dry on the surface prior to analysis and by the Green lab, by using a polypropylene spacer in between the substrate surface and the coverslip in order to distinguish release killing vs. contact killing (discussed below).⁶³

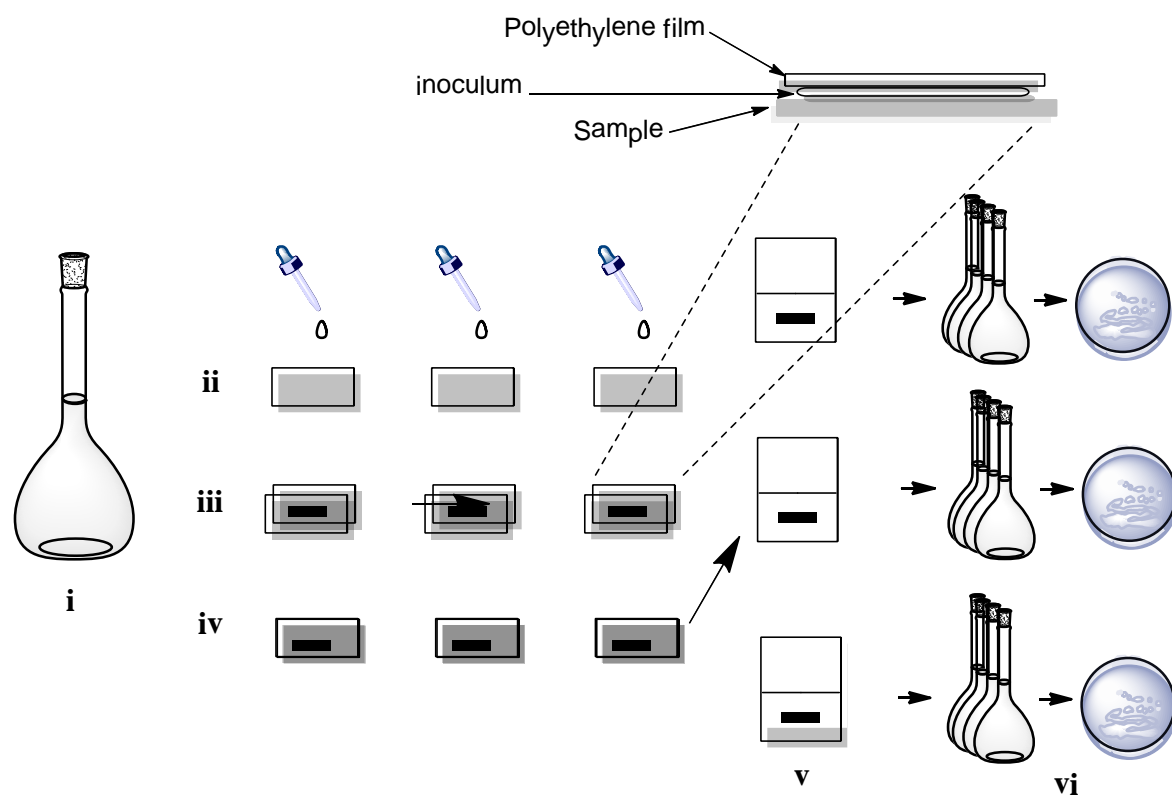


Figure 1.38: Industrial standard method for testing antimicrobials on hard surfaces by growth enumeration, (i) 1×10^6 CFU/mL (inoculum), (ii) 400 μ L inoculum added to each 50 mm \times 50 mm sample, (iii) cover inoculum with 40 mm \times 40 mm sterile polypropylene coverslip, (iv) incubate for 24 hrs, (v) transfer to individual containers with 10 mL neutralizer (vi) serial dilutions, incubate and agar plating, (vii) compare to controls and calculate percent of log 10 reduction.¹⁸

(c) Wolfaardt's Lab Modification of ISO 22196

The Wofaardt method differs from the ISO 22196 method by foregoing the coverslip altogether and allowing a droplet of inoculum to dry in direct contact on the treated surface. Once dried, the surface is shaken with saline to remove unbound cells followed by serial dilution and enumeration on agar as with the other methods (Figure 1.39).¹³⁷

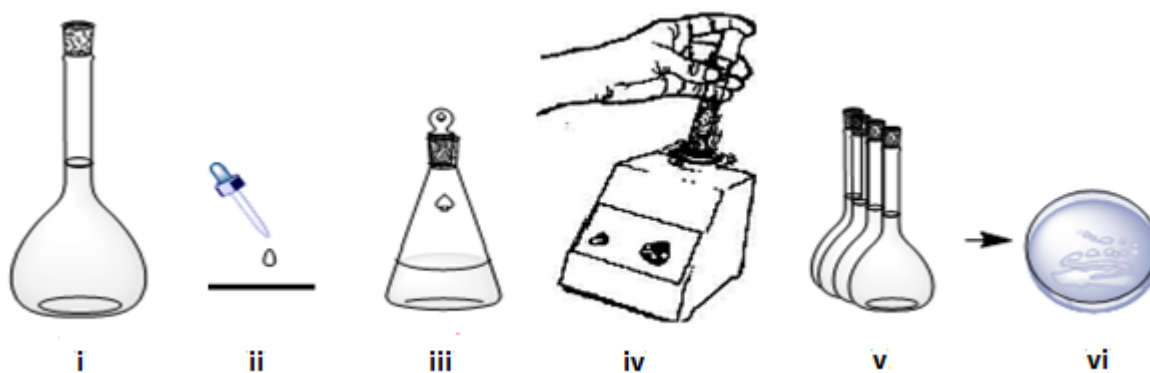


Figure 1.39: Modified method for testing antimicrobials on hard surfaces by growth enumeration in the dry state testing developed in the Wolfaardt lab. (i) 1×10^{10} CFU/mL (inoculum), (ii) 1 mL inoculum added to 1 cm \times 1 cm solid sample and left to dry for appropriate time 2-24 hrs, (iii) sample is added to 0.9% saline solution, (iv) vortex saline solution to remove attached cells, (v) serial dilutions and agar plating, (vi) compare to controls and calculate percent of log 10 reduction.

(d) Green's Lab Modification (SLSDSS) of ISO 22196

Recently Green *et al.*, reported an improved microbiological test method that differentiates between contact killing and release killing from immobilized antimicrobial surfaces. The new method, known as the semi-quantitative surface-separated live–dead staining (SSLDS) technique, is a modification of the traditional live-dead staining technique based on fluorescence microscopy.⁶³ By utilizing 50 mm polystyrene spacers between the treated surface and a control surface, the method can distinguish three outcomes: (A) live or dead cells on the control surface, (B) live or dead cells on the treated surface, (C) live or dead cells leaching (Figure 1.40). Thus in the first outcome (A) the immobilized agent is ineffective and no bacteria are killed (cells stained green), (B) the treated surface agent is firmly immobilized and only kills bacteria at the treated surface (cells are stained red) while cells on the coverslip survive (stain green) (C) the antimicrobial leaches from the treated surface via the spacer and kill cells throughout, all cells are stained red or dead (Figure 1.40).⁶³

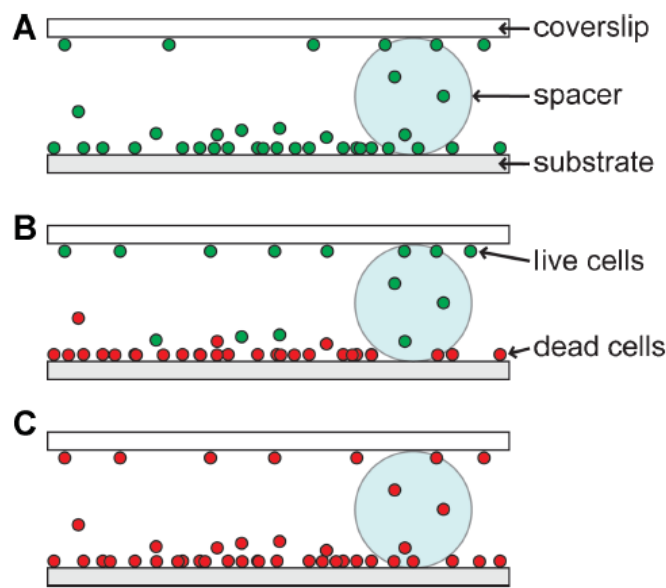


Figure 1.40: A schematic diagram of the symmetric SSLDS method depicting three distinct antimicrobial agent states: (A) no kill, all cells are stained live (green), (B) on cell that come into contact with immobilized antimicrobial are killed (bottom), (C) all cells are killed because of antimicrobial leaching.⁶³

The Green lab modified their SSLDS method further by incorporating an asymmetric direct inoculation design in comparison to their standard symmetric design. The difference between the two designs being in the asymmetric design with both treated active glass surfaces are separated by a spacer, meanwhile the symmetric design uses an untreated control glass (coverslip) on top and an active treated slide with the immobilized antimicrobial agent on the bottom (Figure 1.41). In this way, false positives resulting from non-adherent cells or interaction of the fluorescent dyes with the antimicrobial substrate found in the symmetric SSLDS are minimized. For example, if the bacterial strains fail to adhere to the active surface and after being killed detach to the coverslip, then false conclusions can be drawn that the surface was eluting.¹³⁶

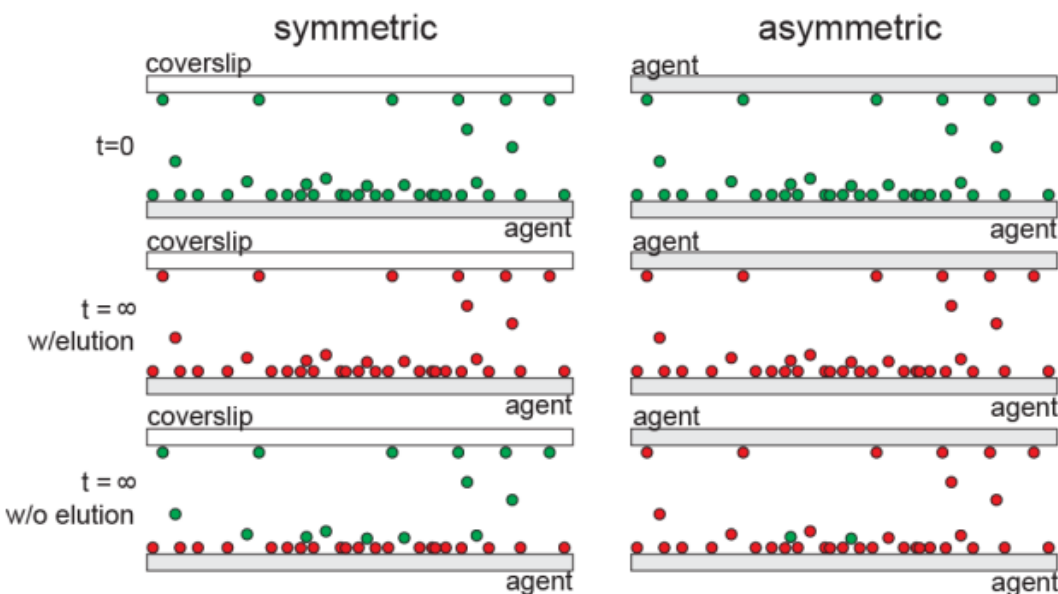


Figure 1.41: Direct inoculation SLDSS methods. (A) symmetric design, (B) asymmetric design.¹³⁶

1.6.2 Cell Viability Enumeration

Cell viability on the surface can be quantified with fluorescence based on live dead staining combined with real time microscopy or assayed with various molecular biology techniques that measure (i) cellular ATP with bioluminescence, or (ii) CO₂ respiration with flow cells or with (iii) redox active indicator dye (2,3-bis-(2-methoxy-4-nitro-5-sulfophenyl)-2H-tetrazolium-5-carboxanilide) (XTT) measured spectrophotometrically (Figure 1.42).

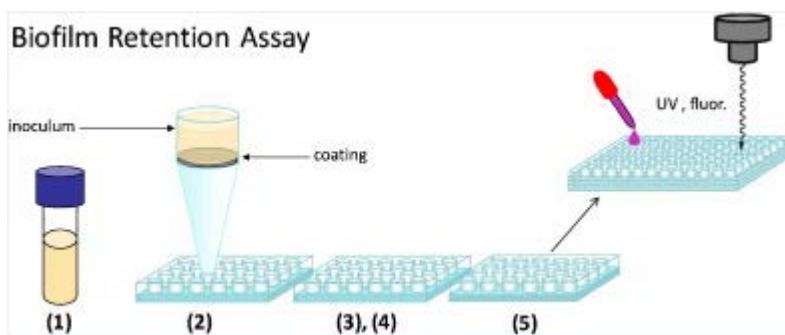


Figure 1.42: Diagram of a high-throughput biofilm retention assay that measures absorbance or fluorescence from a 96-well plate.¹⁸

Microscopy techniques can be employed as tools to test antimicrobial activity on a surface. The Foucher group in collaboration with the Wolfaardt group tested QAC immobilized PP surfaces for bacterial growth. SEM microscopy showed considerable bacterial colonization on the control (left) and virtually no growth on the treated surface indicative of a contact killing surface (Figure 1.43).¹³⁸

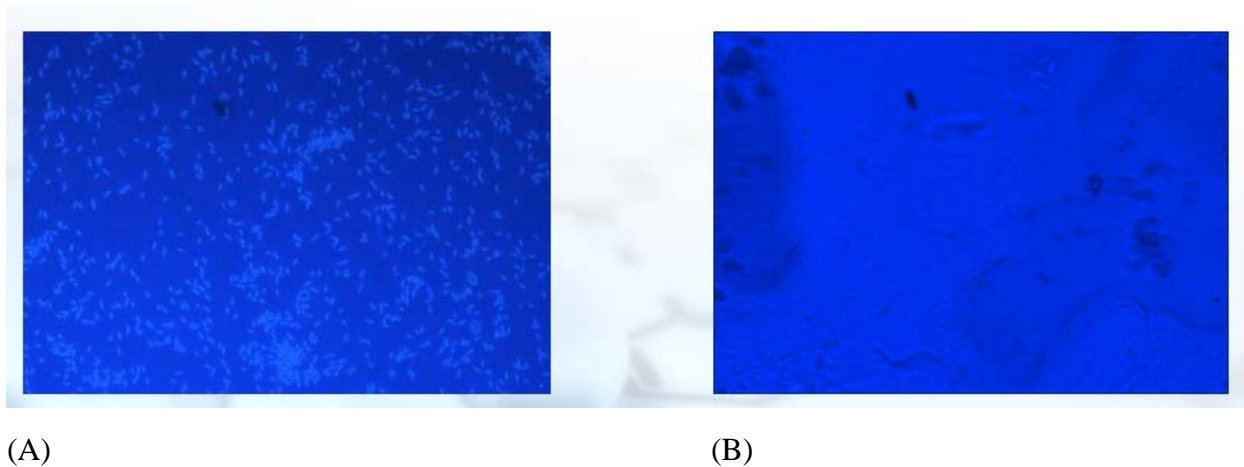


Figure 1.43: Polypropylene microscopy of control ~ 50 cfu/mL (A) vinyl terminated QAC sprayed (10%) 0 cfu/mL (B).¹³⁸

Other groups captured the disruption of gram-positive and gram-negative bacterial membranes with SEM images after incubation with QAC-silica nanoparticles. Both the untreated and non quat treated nanoparticles (NP) showed normal cell morphology, meanwhile the QAS treated NP's showed cell lysis and cell death. (Figure 1.44).

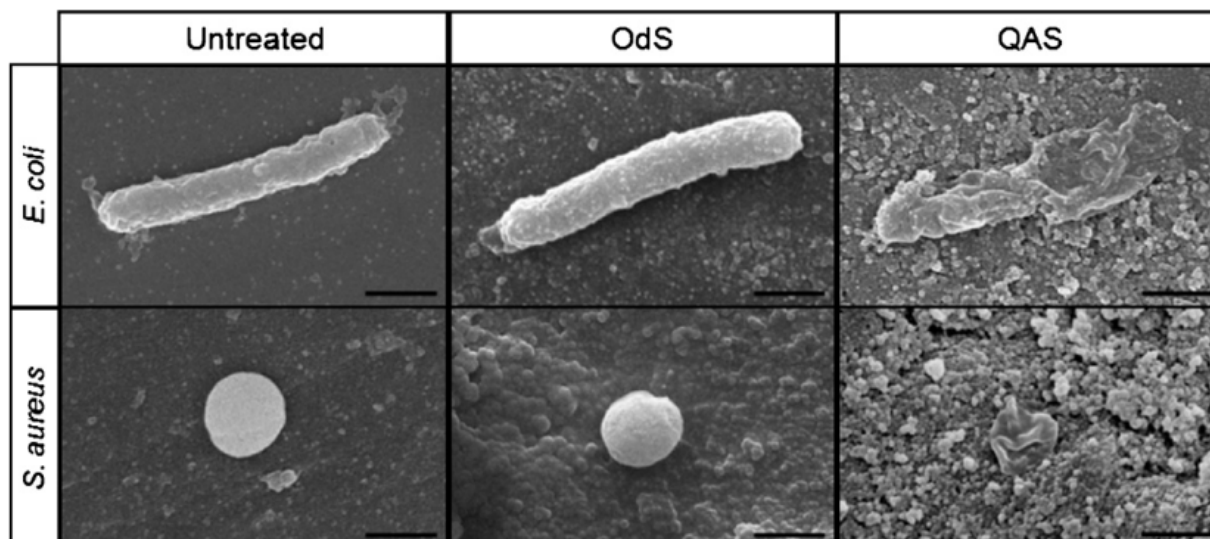


Figure 1.44: SEM images of bacteria incubated with antimicrobial silica nanoparticles. OdS = silica with C₁₈ chain lacking a quat, QAS = SiQAC **3**. (Used with permission from Ref. ⁶²).

1.7 CHEMISTRY OF QUATERNARY AMMONIUM GROUPS AND PHOSPHONIC ACIDS

1.7.1 Menshutkin Quaternization Reaction

Discovered in 1890 by Nicoli Menshutkin, the quaternization or quat formation reaction is widely used industrially for the synthesis of antimicrobials, phase transfer catalysis, pesticides, ionic liquids and natural products.¹³⁹ A typical quaternization reaction involves the reaction between two neutral molecules, a tertiary amine with an alkylhalide or sulfonate. Upon nucleophilic attack, the amine substitutes the alkylhalide or sulfonate leaving group in an S_N2 fashion producing a positively charged quaternary amine with four bonds and a negatively charged counter ion, thus forming an ion pair. In accordance with an S_N2 mechanism, the reaction is accelerated by more nucleophilic amines, increased leaving group ability, increased pressure and elevated temperature (Figure 1.45).¹⁴⁰ Polar solvents also speed up the reaction by stabilizing the charged transition state (Table 1.10).¹⁴¹ With alkyltosyl or mesylates the reaction

is favored at lower temperatures and polar protic solvents in order to avoid the competing elimination reaction.¹⁴²

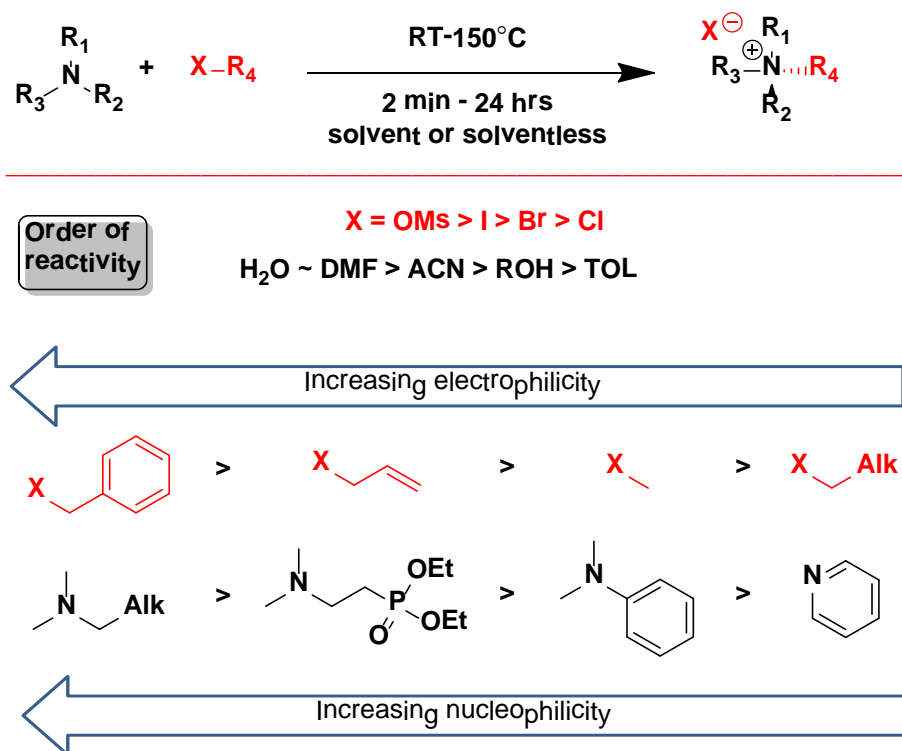


Figure 1.45: Reactivity of the Menshutkin reaction.

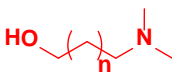
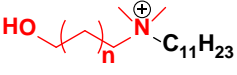
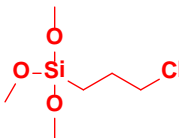
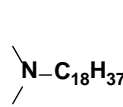
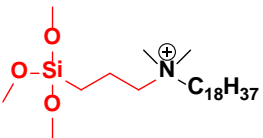
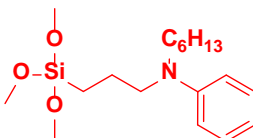
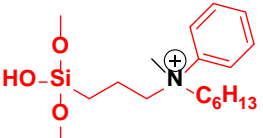
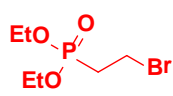
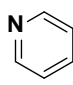
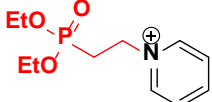
Table 1.10: Relative rates of the Menshutkin quaternization in various solvents (Adapted from Ref.¹⁴³).

Solvent	Relative Rate (s ⁻¹)	Solvent	Relative Rate (s ⁻¹)
CH ₃ (CH ₂) ₄ CH ₃	1	EtOH	200
Et ₂ O	4	MeOH	285
C ₆ H ₆	38	(CH ₃) ₂ CO	340
<i>n</i> -BuOH	70	ACN	375
CHCl ₃	100	CH ₃ NO ₂	500
EtOAc	125	DMF	900

In accordance with the aims of this thesis, the synthesis of quaternary ammonium antimicrobials for surface immobilization will be conducted through the Menshutkin quaternization reaction. Typically, the reaction goes to completion by employing refluxing temperatures in polar solvents from which QAS products crystallize or can be precipitated with the addition of Et₂O or hexanes. Selected literature quaternization examples showing reaction conditions used to prepare surface bound antimicrobials are presented in Table 1.11.

Table 1.11: Examples of literature Menshutkin reaction conditions.

$$\begin{array}{c} R_1 \\ | \\ R_3-N-R_2 \\ + \quad X-R_4 \end{array} \xrightarrow[\text{solvent or solventless}]{\begin{array}{c} \text{RT-150}^\circ\text{C} \\ 2 \text{ min} - 24 \text{ hrs} \end{array}} \begin{array}{c} X^\ominus \quad R_1 \\ | \quad | \\ R_3-N^\oplus \cdots R_4 \\ | \\ R_2 \end{array}$$

Entry	Starting Materials	Product	Solvent	Temp (°C)	Time (hrs)	Yields (%)	
i ^a		Br-C ₁₁ H ₂₃		<i>i</i> Pr:MeOH	80	0.5	na
				<i>i</i> Pr:MeOH	80	12	na
ii ^b				neat	110	48	na ^h
iii ^c		MeI		THF	RT	24	76
iv ^c				H ₂ O	82	48	na ⁱ

Continued....

Entry	Starting Materials	Product	Solvent	Temp (°C)	Time (hrs)	Yields (%)
vi			1.1 <i>t</i> -amyIOH	95	96	na
			1.2 <i>t</i> -amyIOH	60	24	46
vig			1.1 THF	50	6	na
			1.2 EtOH	50	12	na

(i),¹⁰² (ii),³⁸ (iii),⁵⁹ (iv),¹⁴⁴, (v),²⁵ (vi),⁴²; b (diluted directly to 50 wt% in MeOH) c (used directly following hydrolysis with HCl, not shown), f-g (used directly in step 1.2, final yield not reported).

1.7.2 Precursors for the Menshutkin Reaction

Unless commercially available, the precursor amine and alkylhalide or sulfonate often require synthesis. The most direct method for the preparation of *N*-alkyl secondary or tertiary amines is alkylation of a primary amine with an alkylhalide (or sulfonate) known as the “Hoffman alkylation.”¹⁴⁵ Although the method seems simple at first glance, it lacks control due to the possibility of overalkylation (Figure 1.46).^{145,146} When starting with unactivated primary amines the higher substituted *N*-alkyl amine products formed can react with the alkyl halide giving a mixture of primary, secondary, tertiary and QAS that are impossible to separate. In practice, completion only to the secondary amine stage can be achieved by using a large excess (10-100 ×) of the primary amine (Figure 1.46). However the drawbacks are the price of the starting amine used in excess and the extra purification steps required (normally distillation) to

remove the excess amine. The cost of the starting amine limit the scope of the reaction because only inexpensive simple primary amines such as methyl and benzyl amines could realistically be used.¹⁴⁵

Recent developments showed that by adding a small amount of an additive (silica¹⁴⁷, CsOH¹⁴⁸) one can selectively stop the *N*-alkylation reaction at the secondary or tertiary amine without QAS formation. Stopping at the tertiary amine is also possible with microwave (μ W) radiation under aqueous conditions (NaOH/H₂O^{149,150} or NaHCO₃/H₂O¹⁵¹). Additionally, with activated substrates such as allylhalide or CH₃I, a primary amine can be driven to the quaternary amine as the sole product with the addition of a base (Figure 1.46, further discussion below).

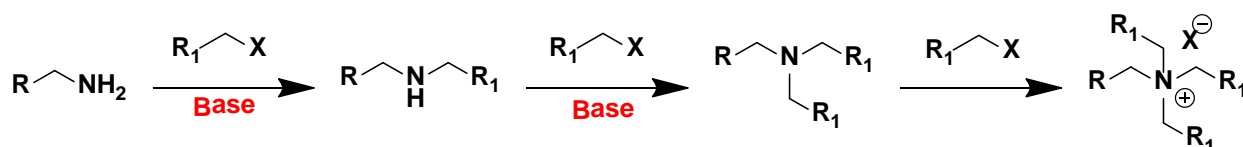


Figure 1.46: Preparation of Menshutkin precursors from primary amines by direct alkylation.

If more control is needed, two alternative reactions can be used to give *N,N*-methylated tertiary amines as the sole products (Figure 1.47).

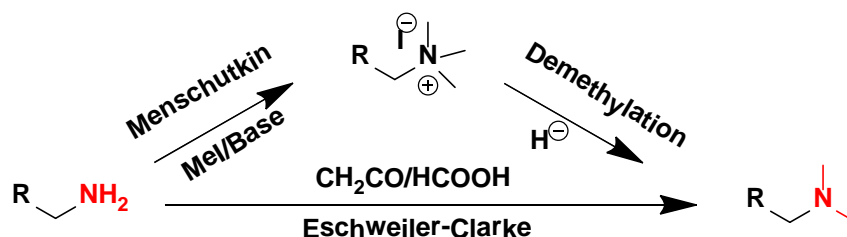


Figure 1.47: Preparation of Menshutkin precursors from primary amines.

N,N-dimethyltertiaryamines are most commonly synthesized by the classic Eschweiler Clarke (EC) reaction from primary or secondary amines using formaldehyde as the source of the methyl groups and formic acid as the reducing agent generating H₂O and CO₂ in the mechanism

(Figure 1.48).¹⁵² Alternative reducing agents include the borohydrides, NaBH_4 ,¹⁵³ $\text{NaBH}(\text{OAc})_3$,^{154,155} NaCNBH_4 ,¹⁵⁶ and zinc reagents, $\text{ZnCl}_2/\text{NaBH}_4/\text{DCM}$ ¹⁵⁷ and $\text{Zn}/\text{AcOH}/\text{H}_2\text{O}$.¹⁵⁸ The advantage of the EC reductive methylation over amine methylations with MeI is that the reaction halts at the tertiary amine without producing quaternary ammonium salt because tertiary amines are inert to further imine formation with formaldehyde. However, the intermediate imine formed in the reaction can sometimes isomerize, and upon hydrolysis, yield the carbonyl derivative of the starting amine plus methylamine.^{152,159} As a result of by-product formation, the EC reaction can give poor yields and can be difficult to purify if mixtures of mono- and dimethylated products are formed. An alternative synthetic strategy to *N,N*-dimethyl tertiary amines can be considered.

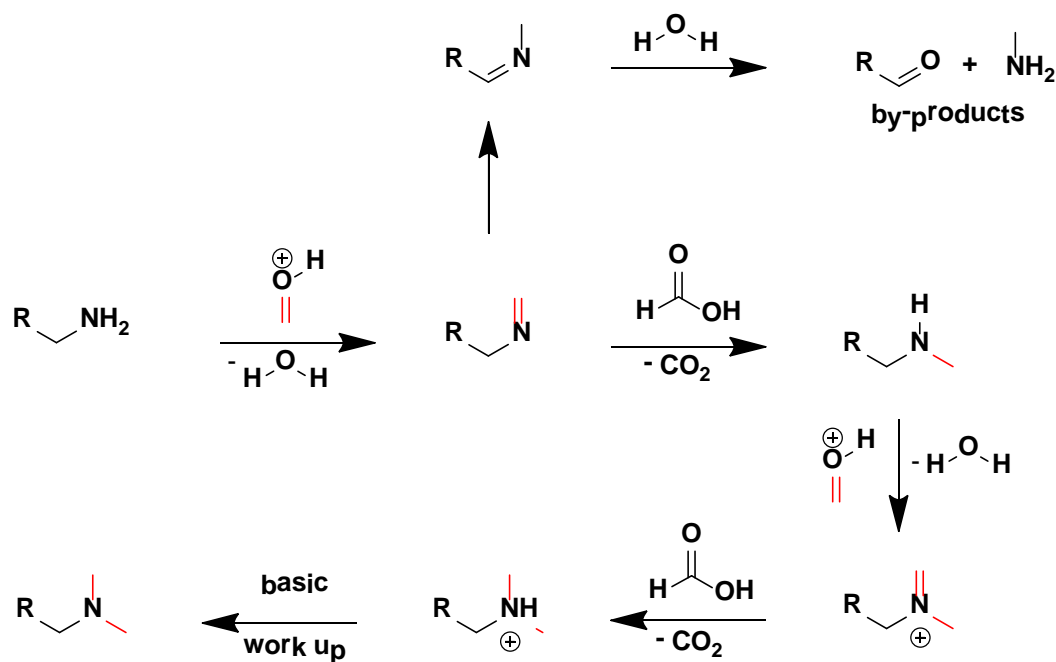


Figure 1.48: Mechanism of the Eschweiler-Clarke *N,N*-methylation.

Combination of the Menshutkin quaternization with demethylation is another route towards *N,N*-dimethyl tertiary amines which avoids epimerization like the EC reaction. For

example the reaction has to be performed sequentially when the demethylating nucleophilic hydride is LAH.¹⁵⁹ The first step performed in MeOH/bicarbonate gives *N,N,N*-trimethylalkyl amines which are isolated and demethylated in THF/LAH (Figure 1.47). A one-pot synthesis of *N,N*-dimethylalkyl amines is achieved by tandem quaternization/demethylation when NaBH₄ was used as the nucleophile.¹⁶⁰ A one-pot procedure involved quaternization of either primary, secondary or tertiary amines with MeI in a polar aprotic solvent (DMF, DMSO, ACN) utilizing a sterically hindered organic base¹⁴³ of greater basicity than the starting amine such as 2,6 lutidine (pK_a ~ 6.77), tri-*n*-butylamine (pK_a ~ 10.89), 1,2,2,6,6-pentamethylpiperidine or PMP (pK_a ~ 11.2), to mop up the HI formed in the reaction. This sequence is followed by demethylation with the addition of NaBH₄ to the reaction without isolation of the trimethylalkylquaternary ammonium salt.¹⁶⁰ Alternatively, alcohols can be used as starting materials to prepare halo and *N,N*-dimethylamine functional groups either directly with the Appel reaction (CBr₄/PPh₃)¹⁶¹ or indirectly by substitution of an activated alcohol either by mesylation (MsCl/NMe₃·HCl, LiBr)¹⁶², or silylation (TMSCl/LiBr)¹⁶³ (Figure 1.49).

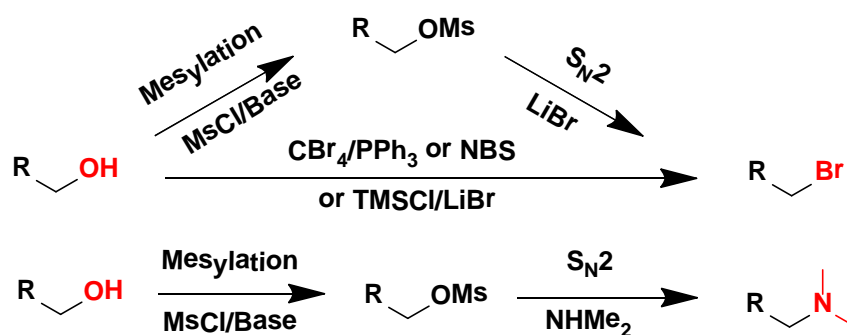


Figure 1.49: Preparation of Menshutkin precursors from alcohols.

1.7.3 Stability of Quaternary Ammonium Groups

Quaternary ammonium salts undergo dequaternization or dealkylation (debenzylation, deallylation, demethylation, dealkylation) by various nucleophiles in an S_N2 fashion producing tertiary amines and transalkylated by-products bound to the nucleophile. By varying the nucleophile and the alkyl leaving groups the substitution can be selective, giving the desired tertiary amine or can occur randomly, providing a mixture of products (Table 1.12).¹⁶⁴ Selective dequaternization of QAS is an effective method used to prepare tertiary amines having different alkyl substituents.^{146,165} Selective dequaternization is only possible when one of the alkyl groups is a better leaving group compared to the other three groups on the quaternary nitrogen. Two examples demonstrate the utility of this discriminating method for the preferential dealkylation. In the first approach, heating a QAC bearing a 2-hydroxyethyl group with hydroxide ion allows for its preferential and clean cleavage. This is because upon heating, only the 2-hydroxyethyl group leaves as ethylene oxide whereas other alkyl groups remain untouched by hydroxide (Table 1.12, Entry i).¹⁴⁶ In the second approach, a QAC attached through a benzyl group to a solid support resin (Merrifield resin) and bearing three different substituents can be preferentially removed from the resin by selective debenzylation over demethylation. This is possible because the alkyl leaving group ability from QAS increases with resonance stabilization and the loss of a benzyl group and allyl group is preferred over the loss of a methyl group which itself is favored over the loss of longer alkyl groups (Table 1.12, Entry iii).¹⁶⁵ Other nucleophiles capable of selective QAC demethylation to the desired tertiary amines include the hydrides; LAH,¹⁵⁹ NaBH₄ (HMPA, DMSO, sulfone)¹⁶⁰, LiBH(Et)₃,¹⁵⁹ LiBH(S-Bu)₃,¹⁵⁹ and also Na/NH₃,¹⁶⁶ OH(CH₂)₂NH₂,¹⁶⁷ LiI,¹⁶⁷ PhS⁻Na⁺,¹⁶⁸ CH₃(CH₂)₂S⁻Li⁺,¹⁶⁹ and piperidine¹⁷⁰ (Table 1.12, Entry iii).

Table 1.12: Examples of the S_N2 dequaternization reaction.

<div>$\begin{array}{c} R_1 \\ \\ R_3^+-N-R_4 \\ \\ R_2 \end{array} + Nu \xrightarrow[\text{Solvent}]{S_N2} \begin{array}{c} R_1 \\ \\ R_3-N \\ \\ R_2 \end{array} + R_4-Nu$</div>						
<div>Order of reactivity</div> <div>$R_4 = \text{epoxide} > \text{Nu-Ph} > \text{Nu-CH=CH}_2 > \text{Nu-Me} > \text{Nu-CH}_2\text{CH}_2\text{Alk}$</div>						
Entry	Starting Material	Nu	Products	Temp (°C)	Time (hrs)	Yield (%)
i ^a		⁻ OH		120 ^e	1	95
ii ^b		⁻ OH		n/a		35
iii ^c		⁻ OH				65
iv ^d				100 ^f	10	85 ^f
v ^d				86 ^g	18	92
				150 ^h	3	68

a¹⁴⁶, b¹⁷¹, c¹⁶⁵, d¹⁷⁰, e (no solvent), f (R = n-Bu (85%), Et (83%)), Me (83%)¹⁶⁵, (no solvent), g (EtOH), h (EtOH = no reaction, DMF).

Otherwise, when a non-selective nucleophile such as OH^- is reacted with a QAC possessing benzyl and methyl substituents, a mixture of products is possible (Table 1.12, Entry ii). For example, heating benzyltrimethylammonium hydroxide gives a mixture of benzyldimethyl amine and MeOH (35%) resulting from an $\text{S}_{\text{N}}2$ attack on one of the methyl groups, while attack on the benzyl carbon results in benzyl alcohol and Et_3N (65%). Elimination products (alkenes and tertiary amines) are not possible in this case because this substrate lacks β -hydrogens necessary for elimination to take place. Of course E2 elimination, favoured by sterically hindered bases can occur only on QAC substrates with β -hydrogens and the leaving group in the trans configuration.¹⁷² On the otherhand, the E1 mechanism is possible only on QAC substrates with sterically hindered α and β -carbons atoms.¹⁷²

Lastly, depending on the nature of the alkyl halide and the basicity of the amine, competing side reactions may take place in favor of the Menshutkin reaction. For example when an electron withdrawing group (eg. ethyl ester) is located two carbons away from the halide atom, the elimination reaction dominates and the thermodynamically favoured ethyl acrylate is formed as the sole product over the quat (Figure 1.50 a). Similarly the presence of acidic functional groups with a lower pK_a than the amine result in protonation of the nucleophilic amine instead of the $\text{S}_{\text{N}}2$ quaternization (Figure 1.50 b). In order to prepare such carboxylic acid quats, the tertiary amine are quaternized with propiolactone followed by acidic work up (Figure 1.50 c).¹⁷³

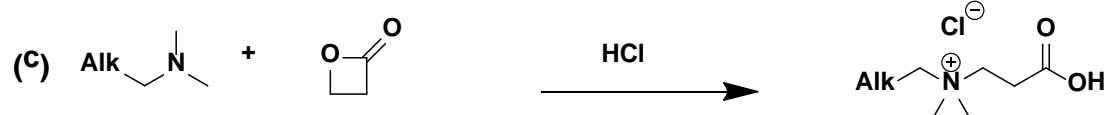
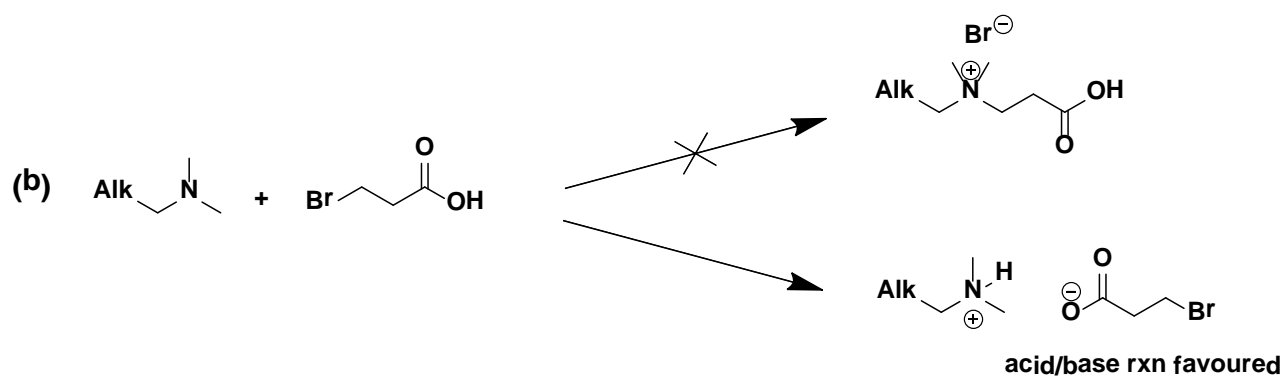
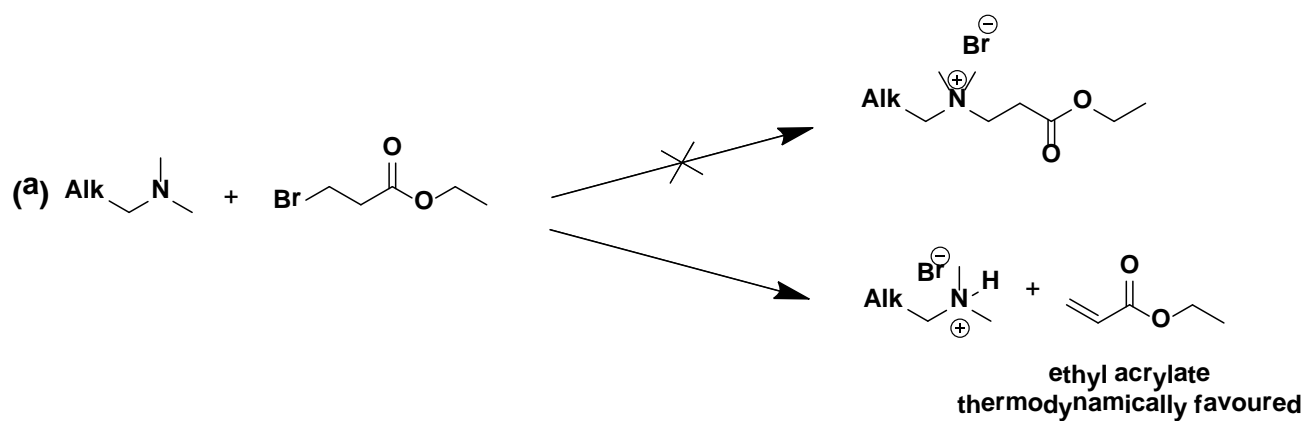
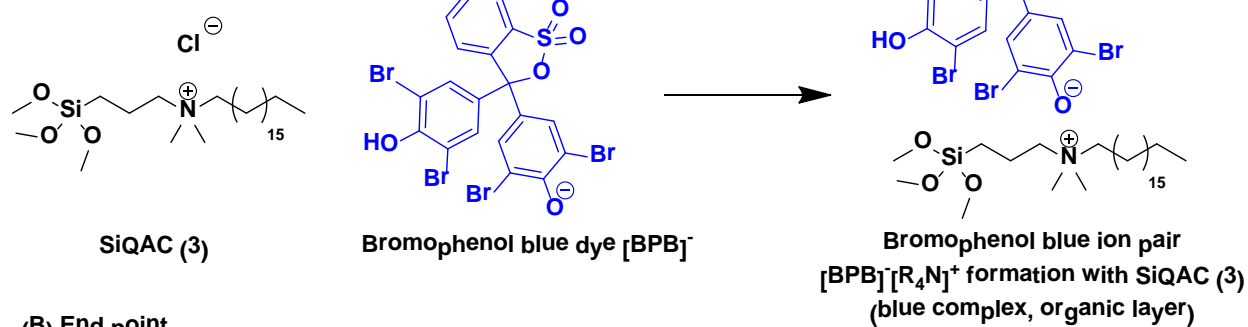


Figure 1.50: Side reactions favoured over the Menshutkin reaction.

1.7.4 Detection of QAC in Solution and on Surfaces

A variety of titration methods employing organic dyes were developed to quantify the amount of quaternary ammonium salts widely employed as antimicrobials in consumer products and pesticides in waste H_2O .^{174,175} The most popular methods employ bromophenol blue and dichlorofluorescein as dyes capable of binding to the quaternary ammonium through an ion pair interaction. Biphasic titrations employed bromophenol blue (Figure 1.51, 1.53) whereas dichlorofluorescein was used in a monophasic titration to determine QAS directly (Figure 1.52).¹⁷⁶ The biphasic titration¹⁷⁶ involves an ion pair complex formation between the active ingredient quaternary ammonium cation and the indicator bromophenol blue anion which is readily soluble in DCM (blue bottom organic phase, Figure 1.53 b). Upon addition of $[\text{BPh}_4]^- \text{Na}^+$ the bromophenol blue anion was displaced from the complex and migrated up into the top aqueous layer turning the organic bottom layer clear at the end point of the titration (Figure 1.53, c).

(A) Start of biphasic titration with bromophenol blue



(B) End point

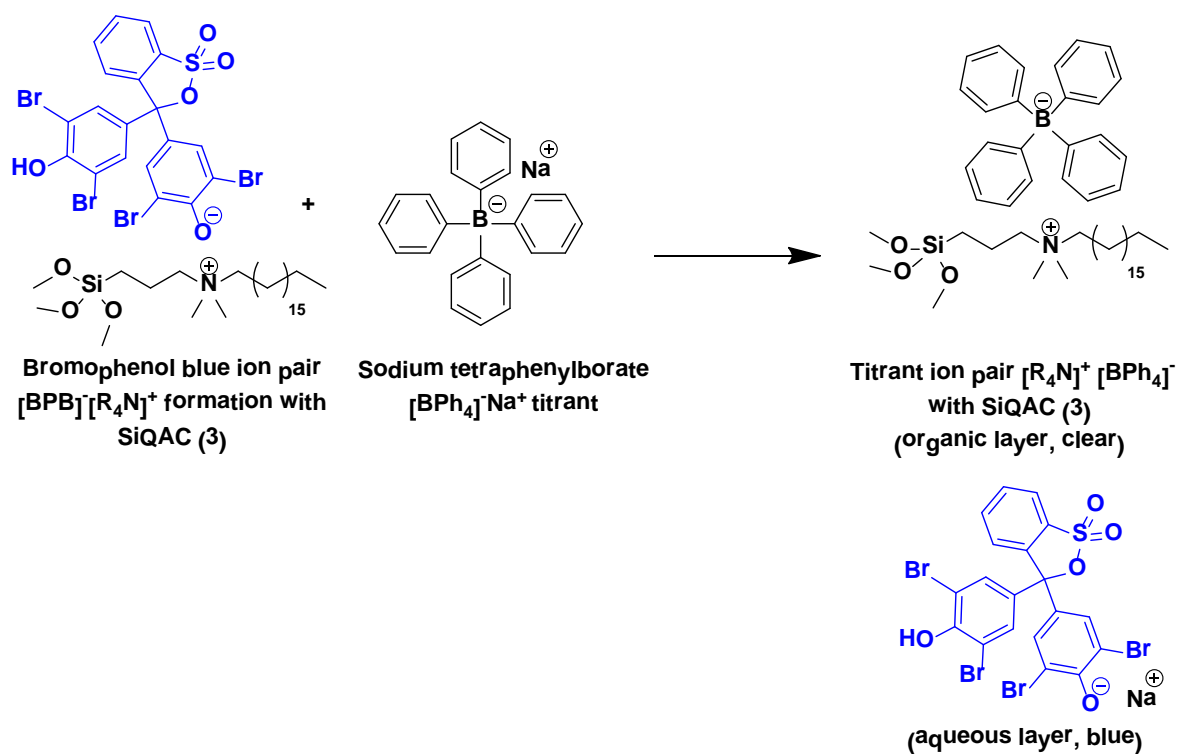


Figure 1.51: Monophasic titration with bromophenol blue.

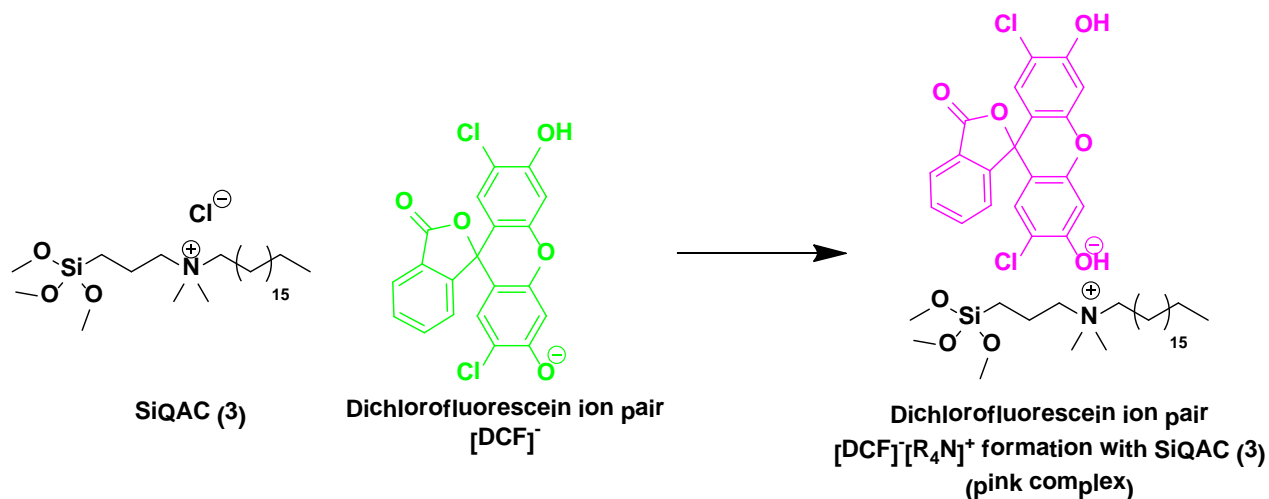


Figure 1.52: Monophasic titration with dichlorofluorescein.

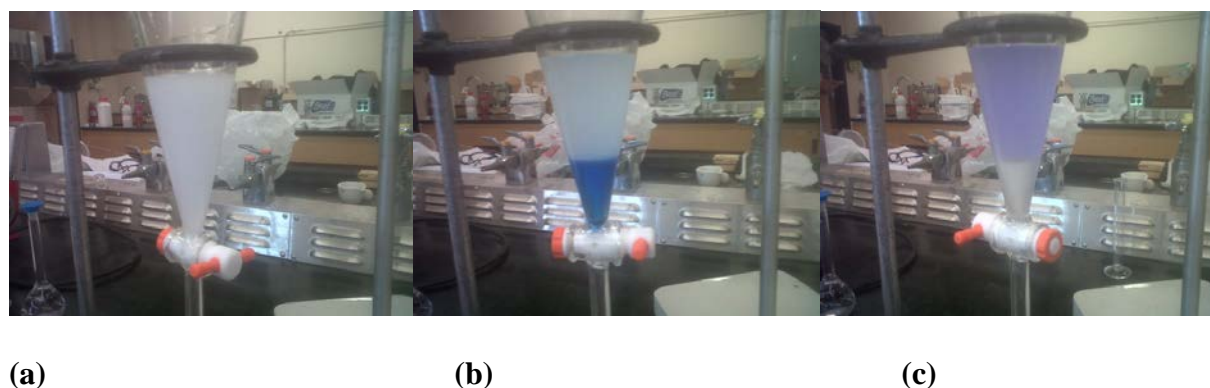


Figure 1.53: Biphasic ion pair titration based on bromophenol blue and SiQAC 3, (a) prior to addition of indicator (b) start of titration, (c) past end point.

The amount of QAS in the test sample employing the titration methods mentioned above is calculated using the following equation: % QUAT = $(V_{\text{tit}} \times N_{\text{tit}} \times M_{\text{QAS}}) / W_{\text{tQAS}}$. where V_{tit} is the volume of titrant, STPB added to the test solution to reach the end-point (in mL), N_{tit} is the normality of titrant (in mol/L), M_{QAS} is the equivalent molecular weight of the QAS, W_{tQAS} is the gross weight of the QAS (in grams).

The bromophenol blue dye has also been used to directly visualize quaternary ammonium compounds coated on fabric surfaces (porous surfaces). This H₂O soluble anionic dye complexes

surface bound quaternary ammonium compounds forming an ion pair which stains the surface a blue colour.² However, the bromophenol blue dye once complexed to the fabric stains the surface, potentially damaging the test material for future use. The same dyes may be utilized to indirectly detect the presence of surface bound quats on non-porous surfaces such as glass, and plastic.

A simple alternative to bromophenol blue for the detection of QAC surface coverage and coating uniformity is fluorescent detection. Thus, treated surfaces would glow fluorescent under exposure to a low power UV lamp, identifying areas of poor adhesion as well as missed areas during application. Additionally, it can also act as a unique product identifier and security feature for treated surfaces when added in trace amounts to functional antimicrobial solutions. Previously in the Foucher group, dansyl tags with organosilane,¹⁷⁷ phosphonate,¹⁷⁷ benzophenone¹⁰⁵ and vinyl¹³⁸ linkers were synthesized (Figure 1.54).

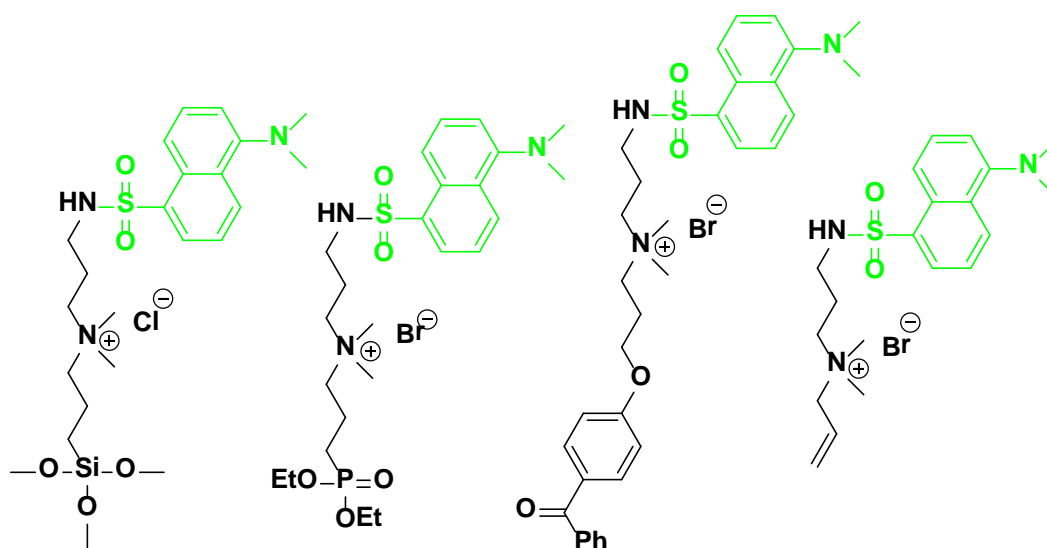


Figure 1.54: Dansyl linkers previously synthesized in the Foucher lab.^{105,138,177}

1.8 CHEMISTRY OF ORGANOPHOSPHORUS COMPOUNDS

1.8.1 Mono and Didealkylation of Phosphonate Esters

Dialkyl phosphonates undergo selective dealkylation with heteroatom nucleophiles such as KOH, NH₄OH, LiI or can be directly didealkylated with mineral acids, silicone or boron reagents (Figure 1.55)

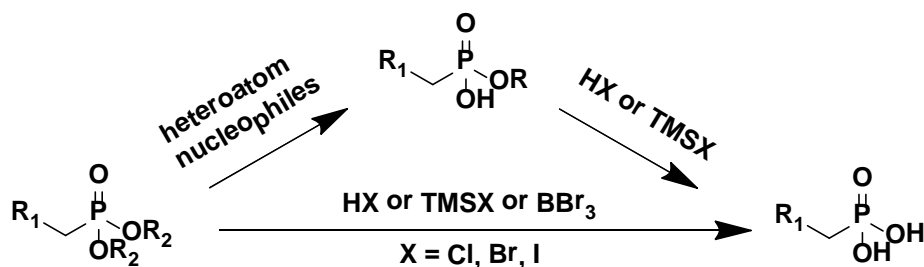


Figure 1.55: Examples of reagents used to dealkylate phosphonate esters.

Mineral acids used to completely dealkylate phosphonate esters include both HCl and HBr, which are added in excess (10-100 ×) and typically require long refluxing conditions (12-24 hrs) especially with the less reactive HCl. Under μW radiation the reaction times are shortened to 30 min with a stoichiometric amount of HCl.^{178,179} Selected literature examples of the dealkylation of phosphonate esters with mineral acids is shown in Table 1.13 and the mechanism of this transformation is shown in Figure 1.56. Since the formation of the carbocation intermediate is the rate determining step, the more stable *i*Pr carbocations and more reactive Br⁻ ions generally give shorter reaction times (Table 1.13).

Table 1.13: Literature examples of the dealkylation of phosphonate esters with mineral acids.

$ \begin{array}{c} \text{R}_1\text{---}\text{P}(=\text{O})(\text{OR}_2)_2 + 2 \text{H---X} \xrightarrow[\substack{\text{or } \mu\text{W} \\ 130\text{--}140^\circ\text{C}, 10\text{--}30 \text{ min}}]{100^\circ\text{C } 8\text{--}24 \text{ hrs}} \text{R}_1\text{---}\text{P}(=\text{O})(\text{OH})_2 + \text{X---R}_2 \\ \text{Order of reactivity} \quad \text{X} = \text{I} > \text{Br} < \text{Cl} \\ \text{R}_2 = i\text{Pr} > n\text{Bu} > \text{Et} < \text{Me} \end{array} $						
Entry	Starting Material	Products	HX (# eq.)	Temp (°C)	Time (hrs)	Yields (%)
i ^a			HCl (20 eq.)	100	24	n/a ^d
			HBr (93 eq.)	100	48	93 ^e
ii ^b			HBr/AcOH	25	20	94
iii ^c			HCl (3 eq.)	100	0.25	79 ^f
iv ^c			HCl (3 eq.)	100	0.1	84 ^f
v ^c			HCl (2 eq.)	140	0.3	78 ^f
vi ^c			HCl (2 eq.)	130	0.1	78 ^f

a,^{178, 179} b,¹⁸⁰ c,¹⁸¹ d, (n = 1), (no yield reported), e, (n = 5,9,13), f, (μW reactions)

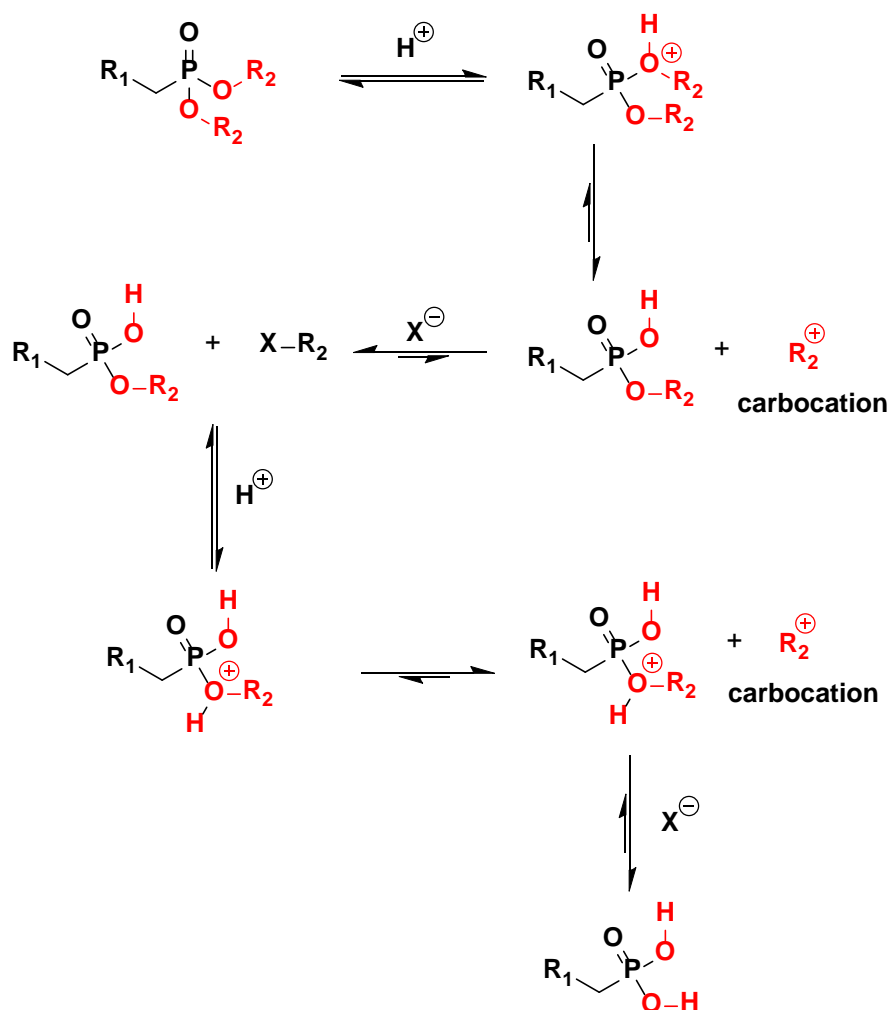


Figure 1.56: Mechanism of the didealkylation of phosphonate diesters in mineral acids.

On the other hand, dealkylation of phosphonate esters with TMSX ($\text{X} = \text{Cl}^-$, Br^- , I^-) occurs via a different mechanism whereby the halide ion acts as both the leaving group and the nucleophile in the reaction (Figure 1.57).¹⁸²⁻¹⁸⁴ In the first step of the mechanism the acidic phosphoryl sp^3 oxygen reversibly attacks the electrophilic silicon of the silylhalide forming a charged phosphonium intermediate while displacing the halide. Irreversible substitution with the nucleophilic halide only occurs with the attack on the phosphonate alkyl group producing one equivalent of an alkyl halide and a mixed trimethylsilylated ester. With TMSI bearing the more nucleophilic iodide ion, the reaction proceeds at a faster rate than TMSBr and occurs predictably

the slowest with TMSCl due to the weakly nucleophilic chloride (typically d. at refluxing temperatures). Another cycle of the mechanism produces dealkylated bis(trimethylsilyl) phosphonate which at this point can be distilled or hydrolysed with H₂O or lower alcohols to the free phosphonic acid.¹⁸⁴ Aqueous hydrolysis always leads to the free phosphonic acids while the use of higher chain alcohols (decanol and above) can result in a mixture of products depending if the nucleophilic attack site is either silicon or phosphorus (Figure 1.58).

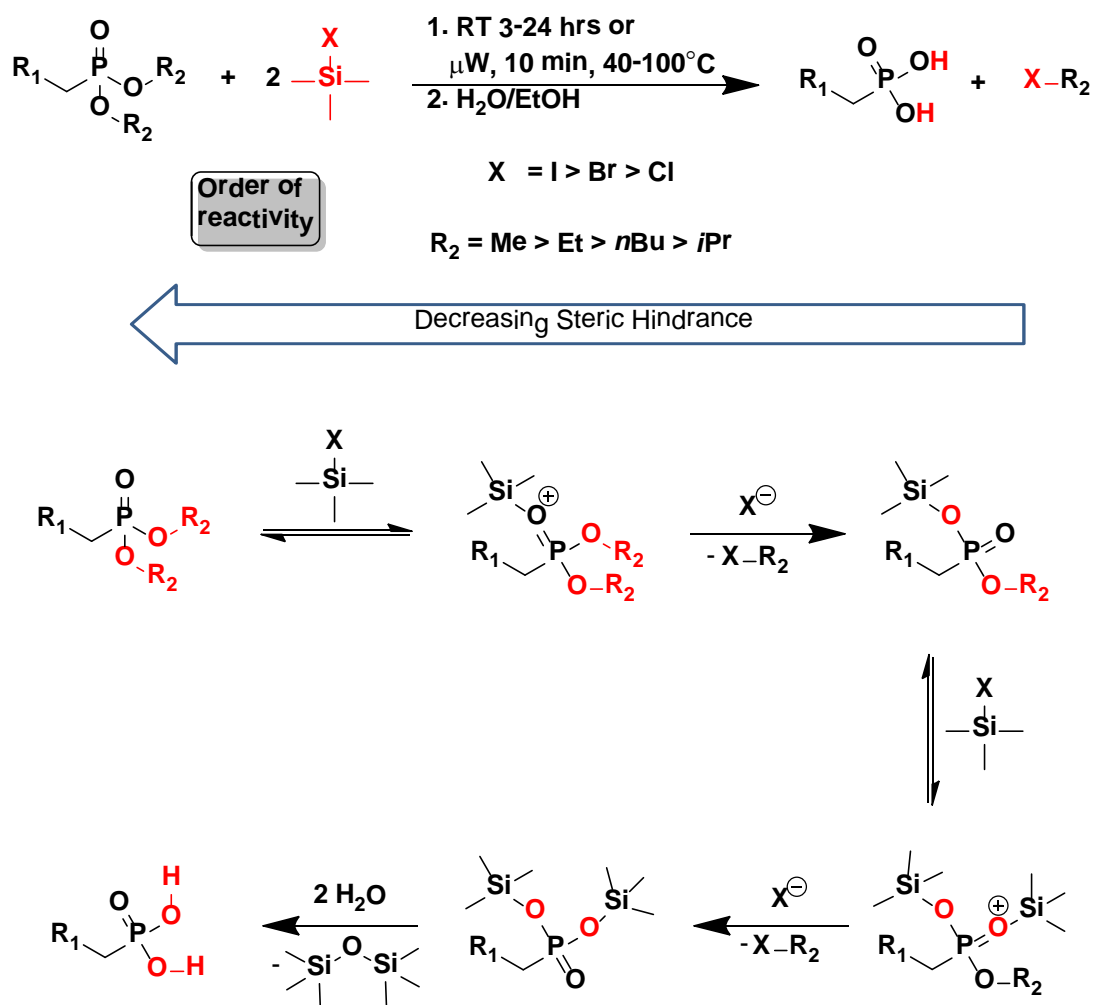


Figure 1.57: Mechanism of the didealkylation of dialkylphosphonate esters via silylation and hydrolysis.

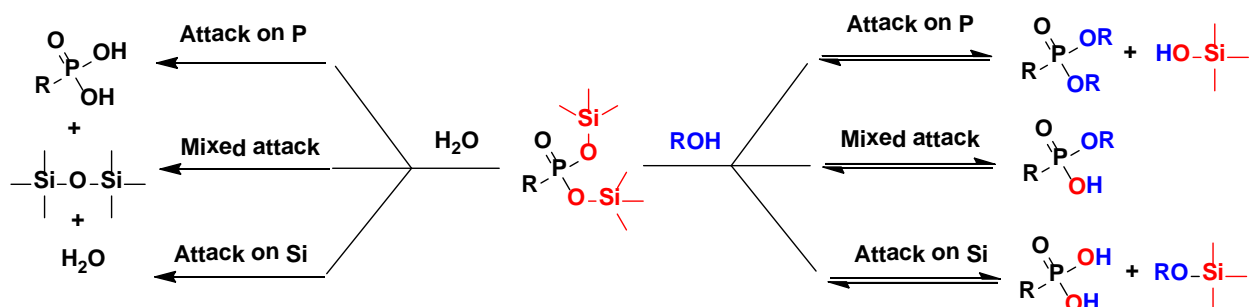
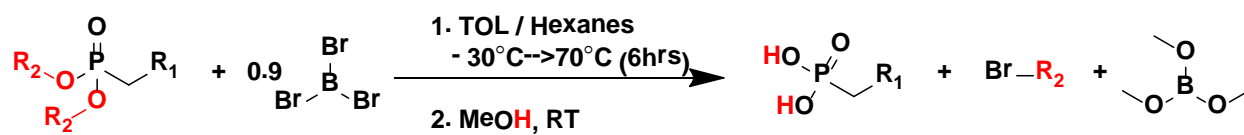


Figure 1.58: Possible products resulting from the hydrolysis of bistrimethylsilyl phosphonates.

Similarly, nucleophilic displacement of alkyl groups from phosphonate esters goes to completion with lithium trialkylborohydrides via a S_N2 mechanism (Table 1.14, Figure 1.59).¹⁸⁵ The advantages of using silicone and boron reagents include milder reaction conditions (RT) and greater function group sensitivity. Additionally, these reagents are compatible with aryl phosphonate esters, carboxylic ester, ethers, halo alkyl, alkyne and alkene functional groups.¹⁸⁶

Table 1.14: Literature examples of the dealkylation of phosphonate esters with BBr₃.



Entry	Starting Material	Products	Yield (%)
i			90 ^a , 95 ^b , 89 ^c , 84 ^d
ii			82
ii			92
iv			77
v			80
vi			80
vii			89

(Redrawn from Ref.¹⁸⁶) a, (R = Me), b, (R = Et), c, (R = *i*Pr), d, (R = *t*-Bu)

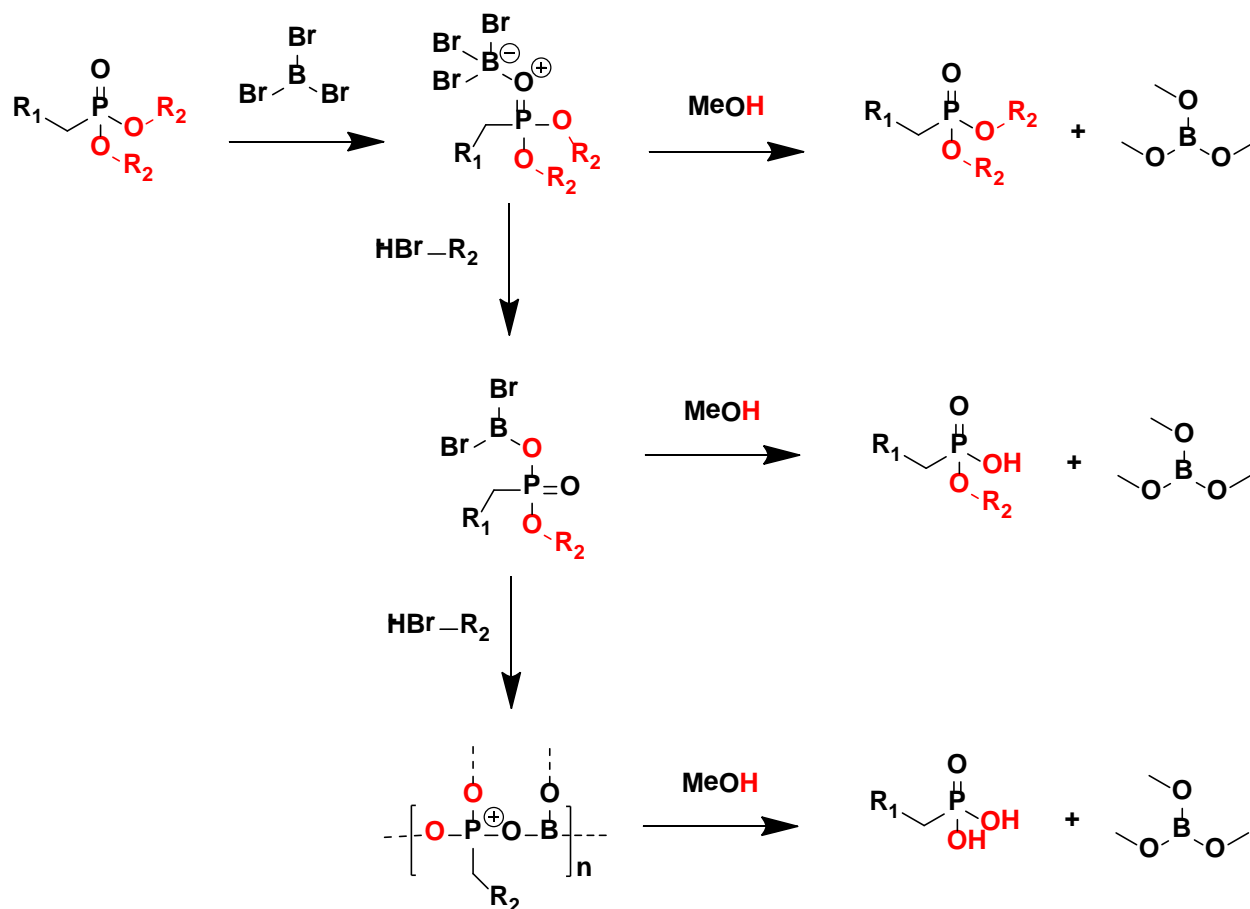


Figure 1.59: Mechanism of phosphonic acid dealkylation with BBr_3 .^{188,189}

1.8.2 Synthesis of Phosphonic Acids

The synthesis of γ -monophosphonic acid QAC's with hydrophobic tails typically from 12 to 18 carbons long are known in the literature. Two syntheses describe the preparation of a C_{18} γ -monophosphonic acid QAC (Figure 1.60), one starting with the bromophosphonate (Route a) while the other with the bromoQAC (Route b), and both are obtained from an Abruzov reaction. Quaternary ammonium phosphonate compounds prepared by Route b were patented in 1955 for use as synthetic detergents.^{190,191} In the reported synthesis, the final product could only be isolated as Na salt of the phosphobetaine after hydrolysis of the phosphonate ester with HCl followed by treatment with NaHCO_3 (Figure 1.60, a). Route b was used by Germanaud who

isolated the quats as betaines after purification on an anion exchange resin (Figure 1.60,b).¹⁹² The products synthesized by this method were not spectroscopically characterized in the patents and were used as is, while Germanaud's purification is costly and doesn't isolate the product as a phosphonic acid.¹⁹² The free phosphonic acid with a C₁₈ was never reported (Figure 1.60, d), however the preparation of the C₁₂ analog by method c starting from 3-bromophosphonic acid is known.¹⁹³ Purification called for extraction of the H₂O soluble C₁₂ betaine into CHCl₃, and no mention of emulsions was reported.¹⁹³

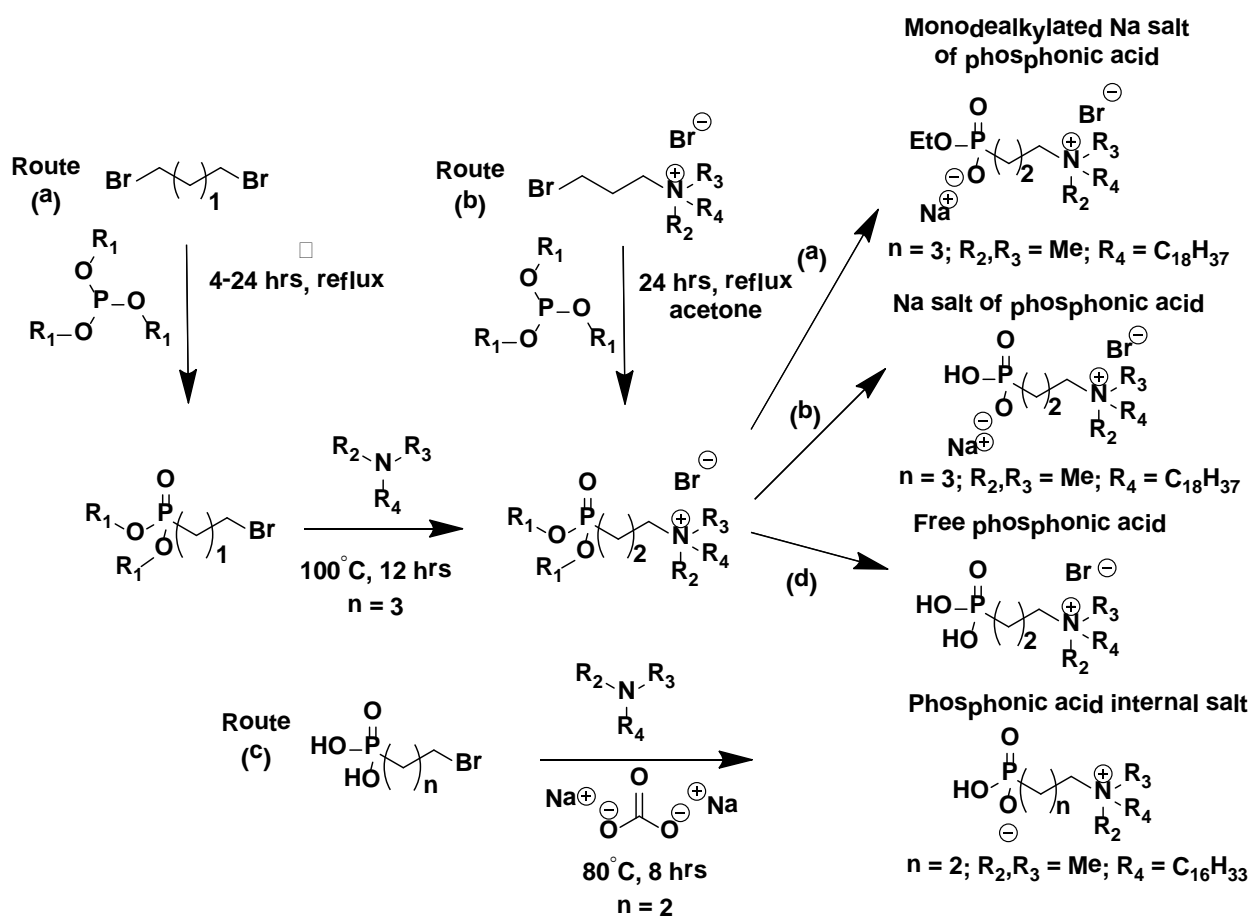


Figure 1.60: Literature routes describing the preparation of QA phosphonic acids.¹⁸⁹⁻¹⁹²

1.9 RESEARCH GOALS

The initial aims of this research were to prepare the EPA approved Dow antimicrobial (3-(trimethoxysilyl)-propyldimethyloctadecyl ammonium chloride)³⁷ or (SiQAC, **3**) and to improve on the original synthesis by altering the reaction parameters and by employing μ W heating.

The primary research goals were to synthesize cost-effective and commercially viable QAC antimicrobials capable of adhering to surfaces other than porous ones (i.e. Ti, SS, plastics) for use in the health care and food handling facilities to help curb the spread of nonsomical infection spread by direct contact with “touch surfaces” colonized by pathogenic bacteria. These new antimicrobials are expected to (i) possess broad spectrum antimicrobial activity, (ii) maintain activity / stability on the treated surface over extended periods of time (months) and (iii) kill microbes on contact without leaching of the chemical into the environment (prevent development of bacterial resistance).

It was hypothesized that the replacement of the trimethoxysilane (SiOMe_3) anchor present in Dow’s commercial antimicrobial with a phosphonate (PO_3R_2), phosphonic acid (PO_3H_2), catechol or thiol end group would dramatically improve adhesion to non-porous surfaces, specifically metals, while retaining the broad spectrum antimicrobial activity of the quaternary ammonium compound. Therefore, a variety of novel and synthetically unknown compounds were targeted comprising of either a mono- (**34-37**), bis-(**42**, **47**, **96**, **126**, **141**), tris-(**161**, **168**) or tetra-multidentate phosphonic acids (**146**, **179**, **183**), catechol (**190**) or thiol (**194** and **199**) end group connected to a long chain quaternary ammonium group. Additionally, the synthesis of a new photoactive benzophenone-silane QAC **206** for coating onto non-porous surfaces, specifically plastic surfaces (C-H surfaces, i.e. polyethylene, silicones) is described.

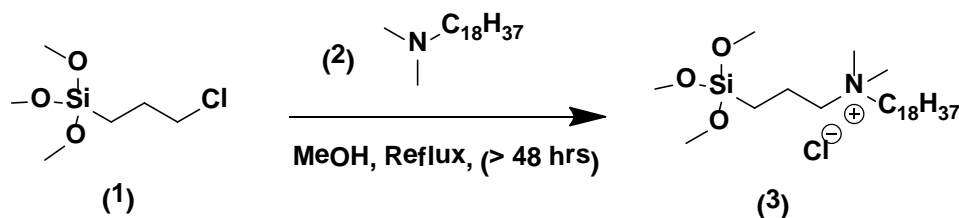
Following synthesis, antimicrobial properties in solution and of monophosphonates **26** and **34A** on metal surfaces (SS, Ti, Al) as well as their detection with dansyl QAC fluorophores and or bromophenol blue was investigated.

2.0 - RESULTS AND DISCUSSION

2.1 Synthesis

2.1.1 Alkoxysilane-Functional Quaternary Ammonium Cations (SiQAC)

The Dow antimicrobial (SiQAC, **3**), synthesized according to published procedures³⁷ suffers from poor purity and a lower than anticipated level of the active antimicrobial in the concentrate formula (< 72 wt %). Commercially, compound **3** is prepared from 3-chloropropyl trimethoxysilane **1** (excess ~1.2 eq.) and *N,N*-dimethyloctadecylamine **2** (Scheme 2.1) as a concentrate in methanol by the following companies: Aegis (AEM 5772); Piedmont (Ztrex72); Flexipel (Q-1000), and Dow Corning (Q9-6346).⁴⁵ Industrially, the final concentrate is used “as is” without a purification step to remove any unreacted starting materials, and as a result, a varying amount of active quat is often produced (Table 2.1, Entry i). The composition of the concentrate on average ranges from ~ 72 wt % for the the active quat **3**, ~ 15 wt % of unreacted **1**, 1-5 wt % of **2**, and ~ 13 wt % MeOH (Table 2.1, Entry i).



Scheme 2.1: Preparation of Dow’s antimicrobial **3**.

Literature (Table 2.2, Entries ii, iii, and v) and patent procedures (Table 2.2, Entries i and iv) describe the preparation of **3** with typically long reaction times (> 24 hrs) but fail to provide

any spectral (NMR) characterization data for the product. Klaus observed complete conversion of starting materials to **3** only after 3 to 4 d. in MeOH without reporting any spectral data (Table 2, Entry ii).¹⁹⁴ Similarly, Chisholm performed the reaction under solventless conditions at 110°C for 48 hrs in a sealed tube and directly prepared a 50 wt % MeOH solution without initial characterization (Table 2.1, Entry iii).¹⁹⁵ In a recent patent, Ludwig reacted **1** with a variety of commercially available products containing alkyl amine mixtures with varying carbon chain lengths (C₁₀, C₁₂, C₁₄, C₁₆, C₁₈ in different ratios) under neat conditions and reported a 100% conversion at 90°C after 48 hrs with a commercial starting material consisting mostly of **2** (Table 2.1, Entry iv).⁴⁵ Instead of NMR, completion of the reaction was determined by diluting aliquots of the reaction mixture first in propylene glycol (1:1, 2 g total) followed by H₂O (1000 mL of pH 3, 500 ppm final dilution) at different time intervals and titrating for the Cl⁻ ion content (CHEMetrics, Inc., Calverton, Va).⁴⁵ Lastly, Huang reported the synthesis of **3** using μ W radiation in a 89% yield at 150°C for 1.5 hrs in MeOH (Table 2.1, Entry v).¹⁹⁶

Table 2.1: Literature/patent procedures describing the preparation of SiQAC **3**.

					Composition of reaction (rxn) mixture (%)			
Entry	Solvent	Time (hrs)	Temp (°C)	Ratio (1):(2)	1	2	3	MeOH
i ³⁷	MeOH	n/a	n/a	1.2:1	15	1-5	72	13
ii ¹⁹⁷	MeOH*	72-96	110	1:1	n/a	n/a	n/a	n/a
iii ¹⁹⁵	Neat	48	110	1:0.95	n/a	n/a	n/a	50
iv ⁴⁵	Neat	48	90	1:1	0	0	100	Neat
v ¹⁹⁶	MeOH	1.5	150	-	-	-	89	-

* = 5 bar pressure, - = not reported.

Due to the added costs and difficulties associated with distillation¹⁹⁷ and column chromatography necessary to purifying the final product, driving the reaction to completion employing solventless conditions and or μ W heating would (i) save on energy costs, (ii) avoid the shipment of the concentrate with flammable organic solvents and (iii) reduce the environmental impact of the toxic unreacted impurities (**1**, **2**) in the concentrate and (iv) potentially require less stabilizer.

Microwave (μ W) heating was investigated in the synthesis of **3** according to Scheme 2.1 in order to improve the yield (72 %, commercially) by altering the reaction time, temperature and solvent choice. Results from both sealed tube (ST) and μ W reactions employing solvent and neat conditions are summarized in Table 2.2. Complete conversion to **3** employing a 1:1 or a 1:0.95 ratio of **1**:**2** was never observed even after 48 hrs reflux in MeOH (Table 2.2, Entry v) or 72 hrs at 110°C under neat conditions (Table 2.2, Entry iii). These results clearly contrast those reported by Ludwig (Table 2.1, Entry ii), where complete conversion was observed at 90°C after 3 d. Monitoring the reaction by ¹H NMR is advantageous over the titration method for free Cl⁻ content used by Ludwig and clearly shows that the reaction never achieves completion. At best, a 76-80% yield is obtained only after prolonged heating times (> 48 hrs).

Additional μ W reactions (4 mmol scale) were attempted in hopes of obtaining a further conversion to quat **3** by employing higher temperatures and shorter reaction times. Performing the reaction neat in the μ W (Table 2.2, Entry vi) resulted in only a 10% conversion after 45 min at 150°C whereas under similar reaction conditions, but with MeOH, the reaction reached 58% conversion (Table 2.2, Entry vii). These results support those obtained by Huang who observed an 89% conversion after 90 min at 150°C in MeOH under μ W heating (Table 2.1, Entry v).¹⁹⁶ Another μ W experiment employing the higher boiling *i*PrOH instead of MeOH, at 165°C for 60

min (Table 2.2, Entry xiii), also failed to drive the quaternization to completion with product conversion reaching only 64%.

Table 2.2: ^1H NMR (CDCl_3) monitoring of the formation of **3**.

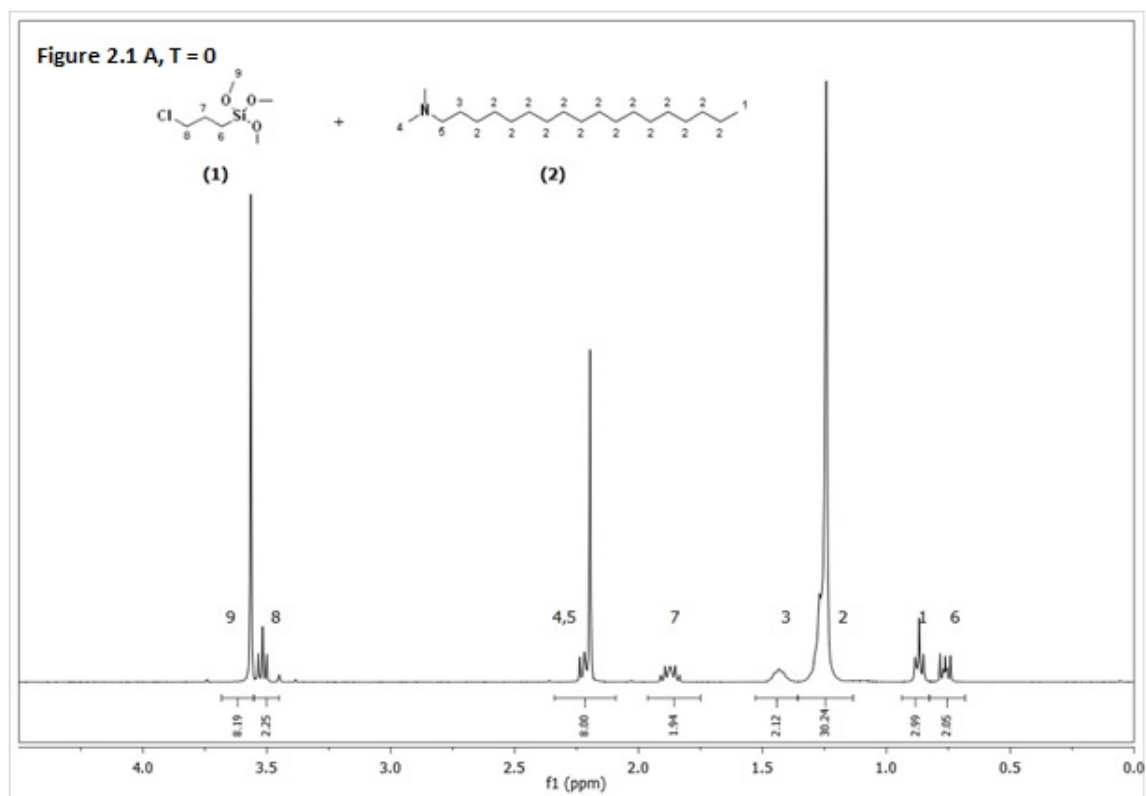
(% Conversion (limiting reagent) by ^1H NMR (CDCl_3))					
Entry	Solvent	Time (hrs)	Temp ($^\circ\text{C}$)	Ratio (1):(2)	PRD. (3 %)
i	Neat	24	110	1:0.95	~ 30
ii	Neat	48	110	1:0.95	~ 53
iii	Neat	72	110	1:0.95	~ 80
iv	MeOH	24	Reflux	1:1	~ 45
v	MeOH	48	Reflux	1:1	~ 76
vi	Neat	0.45	150 $^\mu\text{W}$	1:1	~ 10
vii	MeOH	0.45	150 $^\mu\text{W}$	1:1	~ 58
viii	<i>i</i> PrOH	0.6	165 $^\mu\text{W}$	1:0.95	64

n/a : not attempted.

Progress of the formation of **3** was monitored with ^1H NMR (CDCl_3) by observing the disappearance of the overlapping dimethylamino and amino $-\text{CH}_2$ protons [$-\text{CH}_2-\text{N}(\text{CH}_3)_2$] at ~ 2.2 ppm from the limiting starting amine **2** and the appearance of two new upfield resonance at ~ 3.5 ppm [$-\text{CH}_2-\text{N}^+(\text{CH}_3)_2$] and ~ 3.3 ppm [$(-\text{N}^+-\text{CH}_3)_2$] resulting from the quaternized product (Figure 2.1).¹⁰¹ Percent conversion was calculated from ^1H NMR (CDCl_3) integrations of the *N,N*-dimethyl peaks from the limiting starting amine **2** and the quat dimethyl peak in the product **3** according to the following formula:

$$\% \text{ Conversion} = (x/6)/((x/6) + (y/8))$$

where y = the disappearance of the (-N(CH₃)₂) SM. **2** peak ~ 2.3 ppm, and x = the formation of [(-N⁺-(CH₃)₂) PRD. **3** peak at ~ 3.3 ppm (See, Figure 2.1 A and B, Appendix 1.2, Figure A18, A19). For example, % conversion (2.48/6)/[(2.48/6) + (2.97/8)] = 53% (Table 2.2, Entry ii).



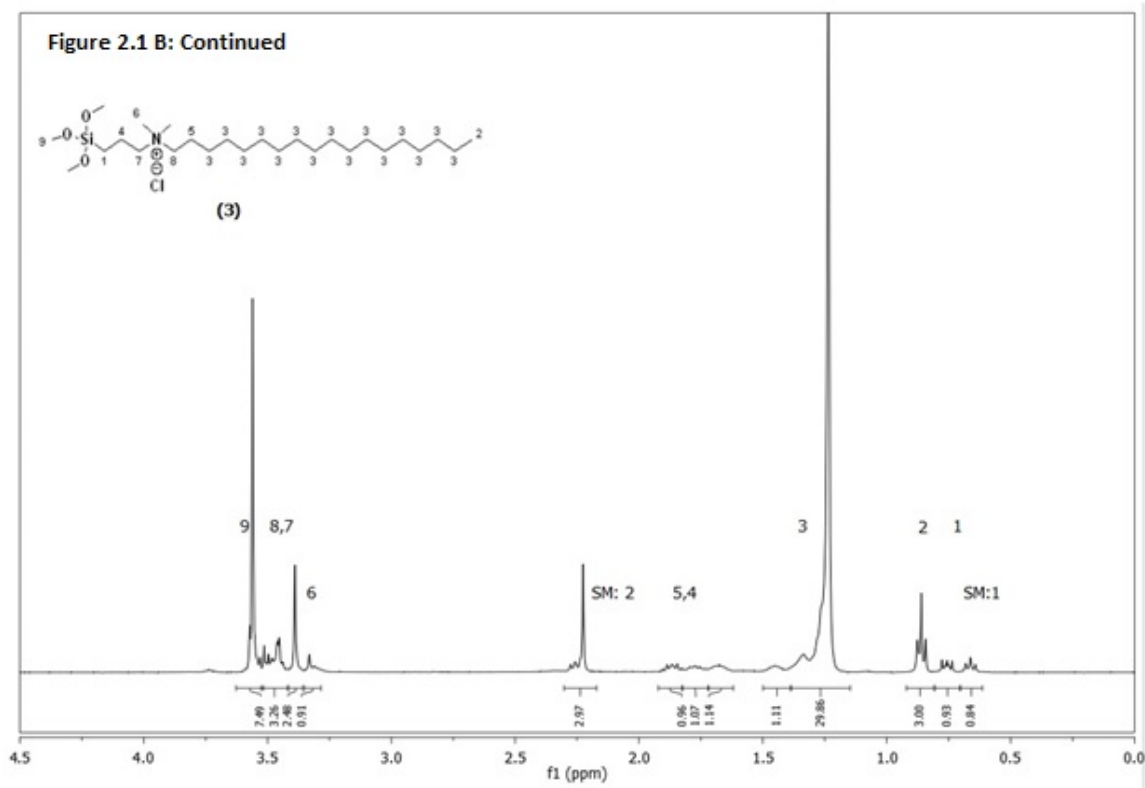


Figure 2.1: ¹H NMR (CDCl₃) spectra of compound **1** + **2** in at T = 0 (A), and the formation of **3** at T = 48 hrs (B).

Another option to save on energy during manufacturing is replacing the cheap but unreactive **1** with more reactive silanes (Figure 2.2). Employing other trimethoxysilanes like the bromo or iodo derivative would significantly speed up the Menshutkin reaction, however due to their high costs (> 100 × more expensive) versus the chloro derivative, this option is commercially unrealistic (Figure 2.2).

\$0.25 / 1 mL SA \$0.05 / 1 mL Gelest	\$61.4 / 1 mL SA \$5.7 / 1 mL Gelest	\$5.38 / 1 mL SA \$2.16 / 1 mL Gelest	\$6.86 / 1 mL SA \$3.58 / 1 mL Gelest

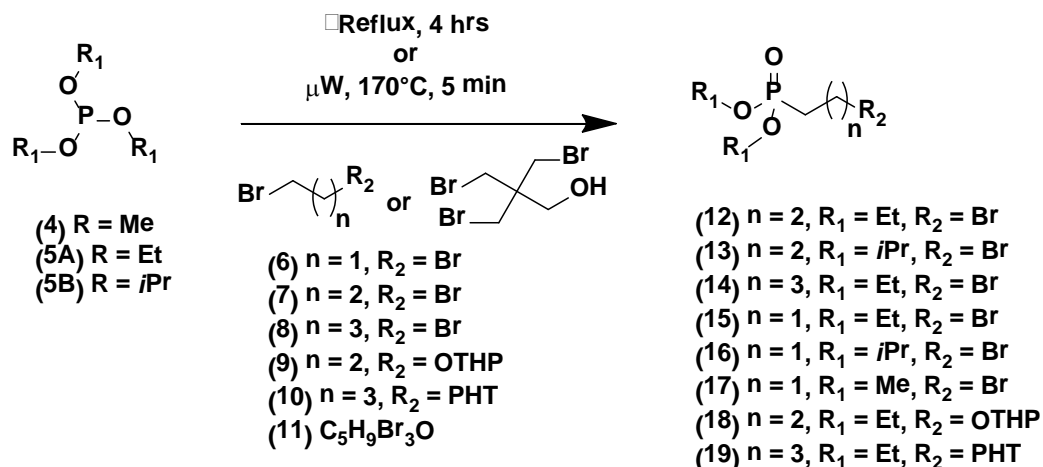
Figure 2.2: Comparison of trimethoxysilane pricing as of May 2013 (SA: Sigma Aldrich).

2.1.2 Organophosphorus Functional Quaternary Ammonium Cations QAC Antimicrobials (PQAC)

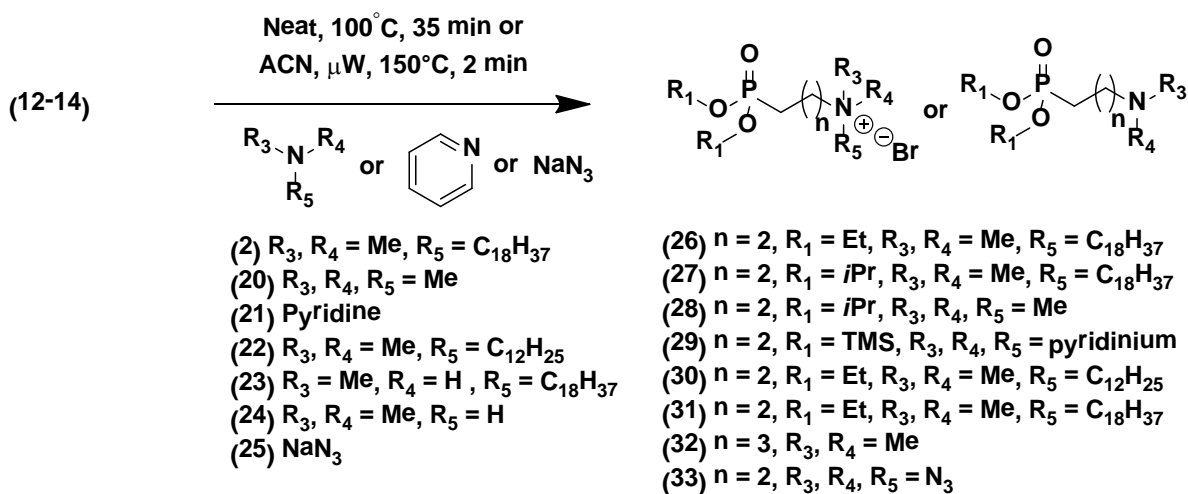
2.1.2.1 γ -Monophosphonic Acids QAC Antimicrobials (γ -MPQAC)

A series of γ -monophosphonic acid QAC's (γ -MPQAC) derivatives **34-37** for binding onto Ti, SS and Al were prepared in three steps (Scheme 2.2). First, the Abruzov reaction between trialkyl phosphites (**4**, **5A-B**) and dibromoalkanes **6-16** or haloalkanes **18-19** produced the phosphonate esters **12-19** in 50-93 % yield (Tables 2.3, Entries i-xix). Compounds **12-14** were quaternized with various tertiary amines **2-24** by the Menshutkin reaction to produced QAC phosphonate esters **26-32**, while compounds **12-13** were alkylated with HNMe₂ and NaN₃ to give precursors **32** and **33** for use in Section 2.1.3.2, Method 3. Didealkylation of **26-30** with either HX (X = Cl or Br) or TMSBr afforded the desired antimicrobial phosphonic acid derivatives **34-37**. All three steps were optimized with μ W heating which resulted in shorter reaction times at higher temperatures and improved yields (Tables 2.3 - 2.5, Scheme 2.2).

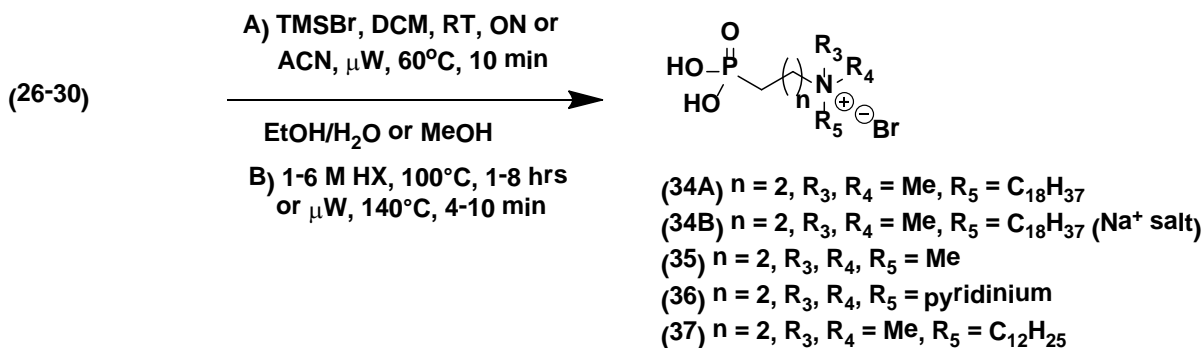
Step 1 - Abruzov Reaction



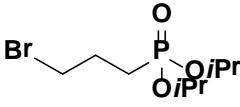
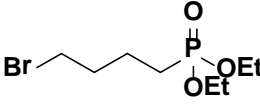
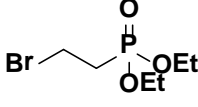
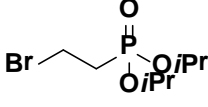
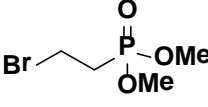
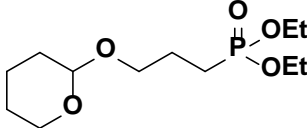
Step 2 - Alkylation, Quaternary Amine Formation (Menschutkin Reaction)

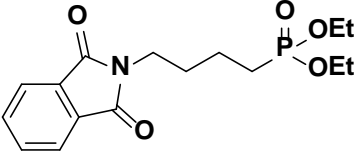
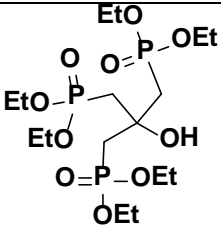


Step 3 - Phosphonate Ester Didealkylation



Scheme 2.2: Optimized conditions for the synthesis of γ -monophosphonic acid QAC's.

Entry	Compound	Time	Temp. (°C)	Ratio of reactants	PRD.	BY- PRD. A %	BY- PRD. B %
iv	 (13)	3 hrs	Reflux	(5B + 7) / <u>1:4</u>	79	21	0
v		3.4 hrs	Reflux	(5B + 7) / <u>1:4</u>	80	14	0
vi		2 min	170	(5B + 7) / <u>1:1.2</u>	48	17	0
vii		5 min	170	(5B + 7) / <u>1:1.2</u>	74 ^D	10 ^D	0
viii	 (14)	20 hrs	Reflux	(5A + 8) / <u>1:4</u>	50	15	35
xi		5 min	190	(5A + 8) / <u>1:2</u>	72 ^D	10 ^D	0
x		5 min	170	(5A + 8) / <u>1:1.2</u>	70.4	19	0
xi		5 min	170	(5A + 8) / <u>1:2</u>	74	2	10
xii	 (15)	2.2 hrs	Reflux	(5A + 6) / <u>1:4</u>	67	15.4	0
xiii		4.3 hrs	Reflux	(5A + 6) / <u>1:4</u>	71.6	15.4	0
xiv		36 hrs	110 ^{TOL}	(5A + 6) / <u>1:4</u>	54	14	0
xv	 (16)	12 hrs	Reflux	(5B + 6) / <u>1:4</u>	81	10	0
xvi	 (17)	12 hrs	Reflux	(4 + 6) / <u>1:2</u>	65	0	0
xvii	 (18)	6 hrs	Reflux	(5B + 9) / <u>3:1</u>	90 ^D	n/a	n/a

Entry	Compound	Time	Temp. (°C)	Ratio of reactants	PRD.	BY- PRD. A %	BY- PRD. B %
xviii	 (19)	20 hrs	Reflux	(5B + 10) / <u>3:1</u>	90 ^{RC}	n/d	n/d
xx	 (20)	0.2 hrs	160 ^μ W	(5B + 11) / <u>6:1</u>	0	n/a	n/a
xxi		24 hrs	Reflux	(5B + 11) / <u>6:1</u>	0	n/a	n/a

Unless indicated, the crude reaction composition was checked by ¹H and ³¹P NMR (CDCl₃) after the time indicated. D = distilled product, RC = recrystallized product. By-product (A) is a result of dialkylation, by-product (B) is a result of intramolecular alkylation.

Compounds **12-16** were formed in ~70 % yield on average, with the rest of the mass corresponding to phosphorus by-products identified by ¹H and ³¹P NMR (CDCl₃) including the higher boiling 5- and 6-membered cyclized oxaphospholanes (Table 2.3, by-product A) as well as the corresponding bisphosphonates (Table 2.3, by-product B). The thermodynamically favourable cyclic 5- and 6-membered by-products (Table 2.3, Entries i-x) were a likely result of intramolecular attack by oxygen of the phosphoryl group of the electrophilic C₃ and C₄ carbon atoms, respectively. The driving force is likely to be the energy gain in the formation of 5- and 6-membered rings (Figure 2.3).¹⁹⁸

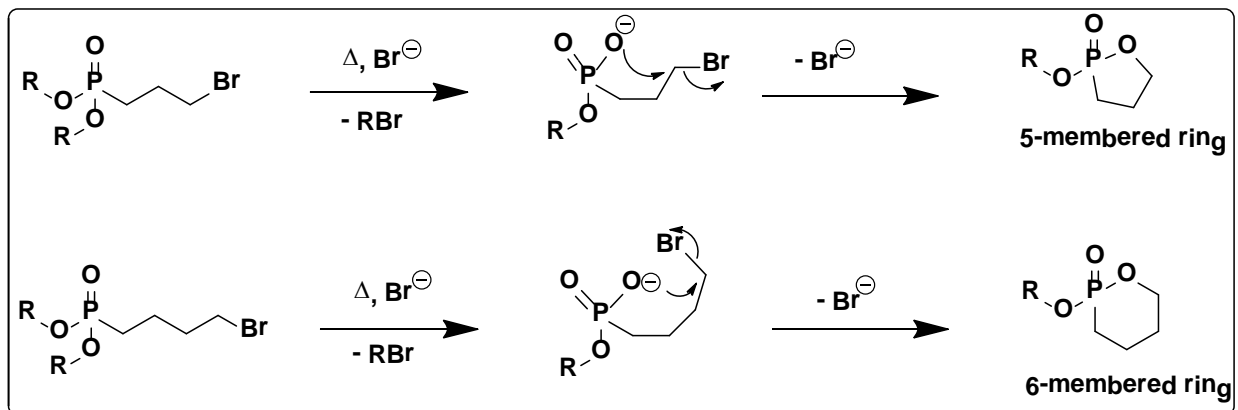


Figure 2.3: Cyclic oxaphospholane by-products formed during the Abruzov reaction.

Most of the lower boiling by-products which include ethyl or isopropyl bromides, and triethyl or triisopropyl phosphates were removed by distillation from the mixture while traces of the corresponding bisphosphonates (by-product B) co-distilled with the product (Table 2.3, Entries i, ii, vi, viii). With compound **14**, a new ^{31}P NMR (CDCl_3) resonance was observed at 24 ppm and was attributed to the cyclic by-product, A, due to intramolecular cyclization. Compound **14** was also difficult to separate with distillation as it codistilled with the by-product upon purification. Both by-products (A and B) were readily removed in the subsequent Menshutkin reaction either by an aqueous extraction of the short chain phosphonate QAC's **28-29** or after precipitation of the longer chain phosphonates QAC's **26-27**.

Compounds **15-17** were prepared as precursors for dialkyl vinylphosphonates (Section 2.1.2.6). Compound **15** was used directly after distillation without characterization by NMR. Compounds **18** and **19** (Table 2.3, Entries xvi, xvii, xviii) were prepared in high yield employing an excess of $\text{P}(\text{OEt})_3$ (3 eq.), (Section 2.1.2.3, Method 3). A crystal structure of compound **19** was obtained after distillation to remove excess $\text{P}(\text{OEt})_3$ and re-crystallization from EtOAc (Section 2.6.1).

Preparation of compound **20** was attempted under μ W heating followed by distillation which resulted in thermal decomposition of the reactants and products that led to the formation of multiple peaks observed by ^{31}P NMR. Another attempt to prepare compound **20** was performed under reflux conditions with purification on column chromatography. After 24 hrs of reflux, the ^{31}P NMR spectrum (CDCl_3) of the crude reaction mixture revealed mainly unreacted $\text{P}(\text{OEt})_3$, likely as a result of steric hindrance. Chromatography on a short pad of silica eluted mostly $\text{P}(\text{OEt})_3$ which was subsequently converted to $\text{HP}(\text{OEt})_2$ on the column (Table 2.3, Entries xx and xxi).

The second step involving the Meshchutkin reaction was optimized (Table 2.4, Compounds **12-14**). With the bromo leaving group, the Menshutkin reaction was more rapid compared to the chloro derivative (48-72 hrs, reflux, compound **3**, Figure 1.45). Employing a sealed screw cap glass vial in refluxing ACN, the reaction was complete in 3-4 hrs (Table 2.4, Entries ii, iv, ix) while under μ W heating at 150°C the reaction was complete in 2-10 min (Table 2.4, Entries iii, v, vi, vii, viii). Compound **28** was prepared from $\text{NMe}_3\cdot\text{HCl}$ by neutralizing the amine in ethanol/ NaOH followed by the Abruzov reaction with **13** directly in the μ W without filtering off NaCl . Compound **29** was reacted for 10 min to ensure complete conversion of the weaker nucleophilic pyridine and then dealkylated directly in the same vial with either TMSBr/ACN or $\text{HBr}/\text{H}_2\text{O}$ (Table 2.4). ACN was the preferred solvent for the quaternization by enhancing the rate and in most cases the products solidified directly from the reaction mixture or with the addition of Et_2O . Compounds **32** and **38** were prepared by nucleophilic substitution of **14** by NHMe_2 and **12** by NaN_3 for use in Section 2.1.3.2, Method 3.

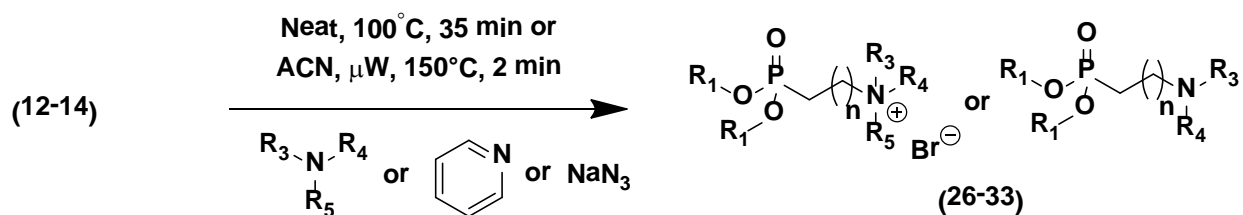
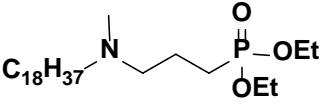
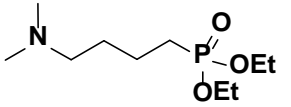
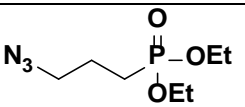


Table 2.4: Optimization of Step 2: Menshutkin reaction between bromoalkylphosphonates 12-14 and tertiary amines 2, 21-25.

Rxn. Comp. (%) by $^1\text{H } ^{31}\text{P}$ NMR (CDCl_3)							
Entry	Compound	Solvent	Time	Temp ($^\circ\text{C}$)	Ratio of reactants	SM. %	PRD. %
i	 (26)	Neat	30 hrs	100	(12 + 2) / <u>1:1</u>	n/d	67 ^{RC}
ii		ACN	2 hrs	Reflu _x	(12 + 2) / <u>1:1</u>	10	90
iii μW		ACN	2 min	150	(12 + 2) / <u>1:1</u>	4	96
iv	 (27)	ACN	2 hrs	Reflu _x	(13 + 2) / <u>1:1</u>	10	90
v μW		ACN	2 min	150	(13 + 2) / <u>1:1</u>	3	97
vi μW	 (28)	EtOH	2 min	150	(13 + 20) / <u>1:1.1</u>	n/d	68 ^{RC}
vii μW		EtOH	3 min	150	(13 + 20) / <u>1:1.4</u>	6	94
viii μW	 (29)	ACN	10 min	150	(13 + 21) / <u>1:1</u>	Ester not isolated (one-pot reaction see 4-3)	
ix	 (30)	ACN	4 hrs	Reflu _x	(13 + 22) / <u>1:1.2</u>	Excess	95*

Entry	Compound	Solvent	Time	Temp (°C)	Ratio of reactants	SM. %	PRD. %
x	 (31)	ACN	24 hrs	60	(12 + 23) / <u>1:1.1</u>	n/a	90
xi ^{μW}	 (32)	EtOH	5 min	110	(13 + 24) / <u>1:2</u>	0	100
xii	 (33)	Acetone	12 hrs	Reflux	(13 + 22) / <u>1:1.2</u>	0	100

Didealkylation of compound **26-29** was first explored with TMSBr and then optimized with HCl and HBr (Table 2.5, Entries i-xi). With anhydrous TMSBr the reaction was performed in DCM overnight and complete conversion was observed, however *in situ* generation of the reagent from TMSCl/NaI in ACN failed to give the dealkylated product (Table 2.5, Entry ii). This can be attributed to poor solubility of quat **26** in ACN vs DCM. Next, the phosphonate quats were successfully dealkylated in H₂O with a two fold excess of HCl or HBr. Since the formation of the carbocation intermediate is the rate determining step in the mineral acid didealkylation of phosphonate esters (see Figure 1.53), the more stable *i*Pr carbocations and the more reactive Br⁻ ions proceeded faster compared to Et esters (Table 2.5, Entry iv vs Entry v and Entry vi vs Entry vii) and HBr was faster than HCl (Table 2.5, Entry iv vs Entry vi and Entry v vs Entry vii). ^{μW} heating was also optimized with compounds **27** and **28** with complete conversion observed within 6-10 min at 140-150°C (Table 2.5, Entries ix and xi).

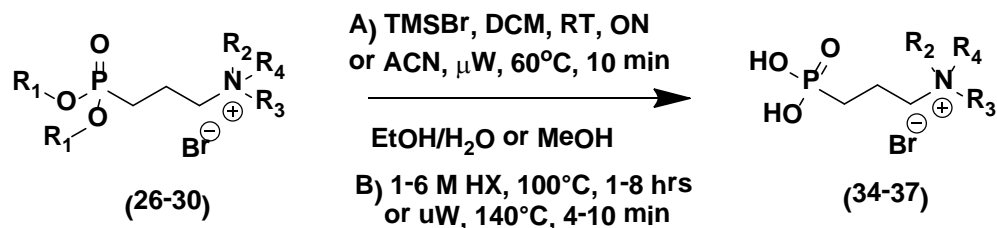


Table 2.5: Optimization of Step 4: Didealkylation of phosphonate diester quats.

Rxn. Comp. (%) by ³¹ P NMR (CDCl ₃)							
Entry	Compound	Reagent (R)	Time	Temp (°C)	Ratio of Reagent (R) : SM	SM %	PRD %
i	 (34)	TMSBr	24 hrs	RT	(R + 26) / <u>3:1</u>	0	100
ii		TMSCl/ NaI	24 hrs	RT	(R + 26) / <u>4:1</u>	n/a	n/a
iii		HCl	6 hrs	Reflux	(R + 26) / <u>4:1</u>	60	40
iv		HCl	20 hrs	Reflux	(R + 26) / <u>4:1</u>	0	100
v		HCl	2 hrs	Reflux	(R + 27) / <u>4:1</u>	0	100
vi		HBr	3 hrs	Reflux	(R + 26) / <u>4:1</u>	0	100
vii		HBr	1 hr	Reflux	(R + 27) / <u>4:1</u>	0	100
viii	 (35)	HBr	3 min	140 μ W	(R + 28) / <u>4:1</u>	20	80
ix		HBr	6 min	140 μ W	(R + 28) / <u>4:1</u>	0	100
x*	 (36)	TMSBr	10 min	60 μ W	(R + 29) / <u>2.5:1</u>	0	100
xi*		HBr	10 min	150 μ W	(R + 29) / <u>4:1</u>	0	100
xii	 (37)	n/a	n/a	n/a	(R + 30) / <u>4:1</u>	n/a	n/a

* One pot rxn.

The long chain C₁₈ phosphonic acid quat, **34**, previously only isolated as the Na salt of the phosphobetaine or as an internal salt after purification on an expensive anion exchange resin (see Figure 1.57) was successfully recrystallized from EtOAc:EtOH and X-ray quality crystals were obtained (Figure 2.4, and Figure 2.40).

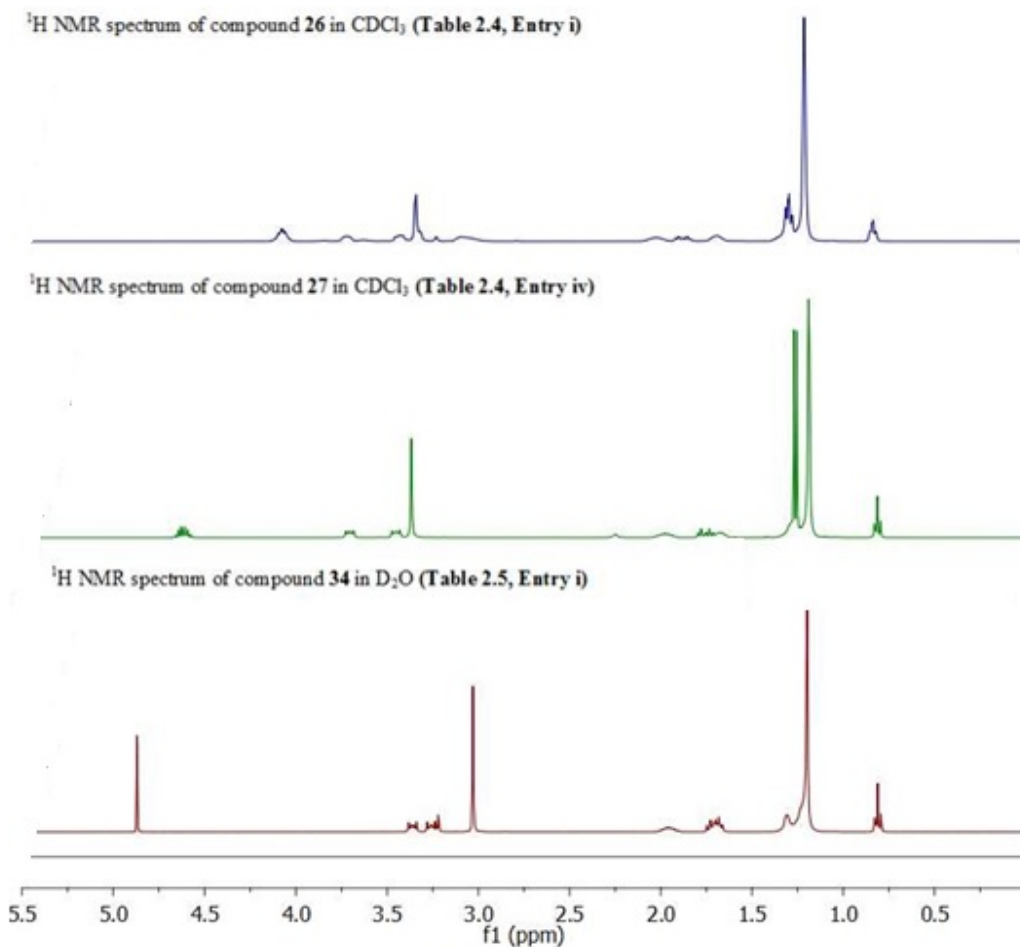
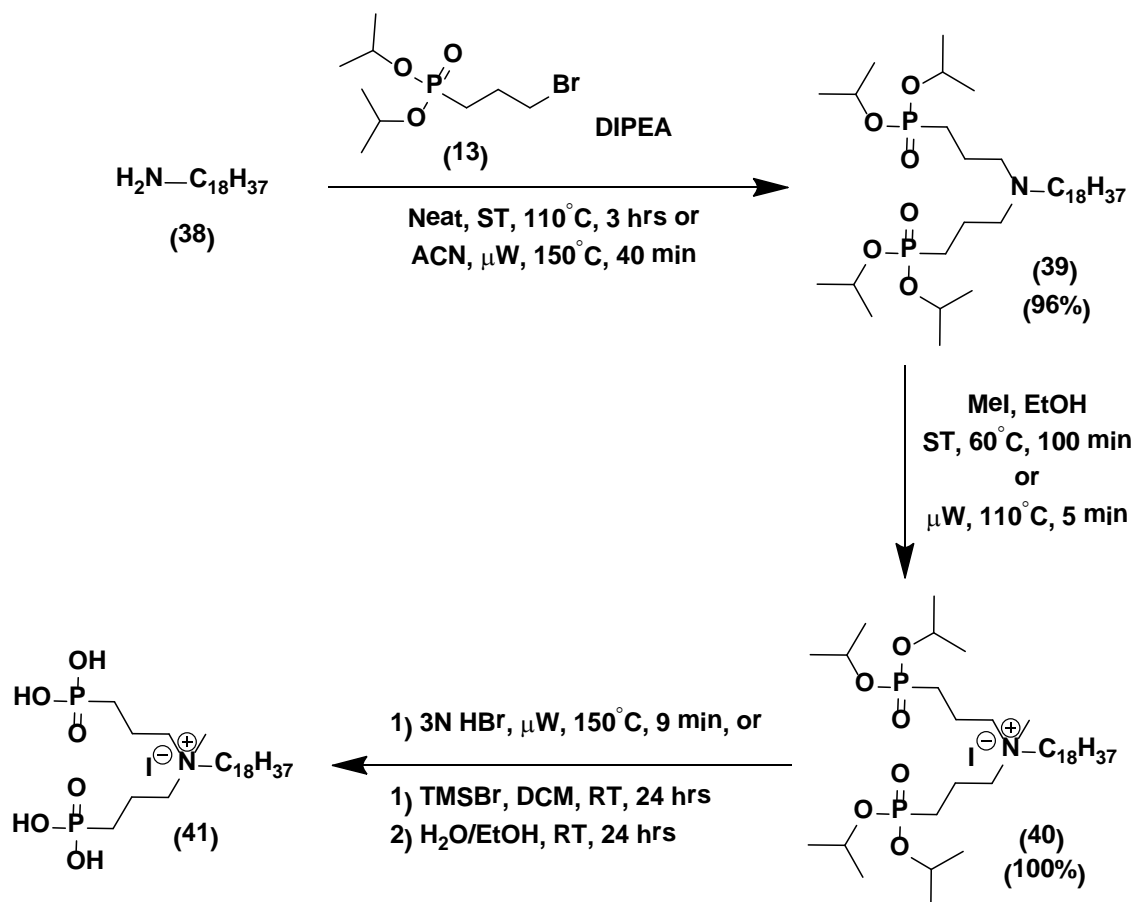


Figure 2.4: ¹H NMR (CDCl₃) spectra showing successful didealkylation of the ethyl phosphonate ester QAC **26** and isopropyl ester QAC **27** to the corresponding phosphonic acid QAC **34** (D₂O).

2.1.2.2 γ -Bisphosphonic Acids QAC Antimicrobials (γ -BPQ) Synthesis

Bisalkylation of the commercially available octadecylamine **38** with **13** employing Hunig's base afforded the desired *i*Pr-bisphosphonate **39** in good yield with conventional

(solventless) or μ W heating (ACN). Trialkylbromophosphonates (where alkyl = Me, Et, *i*Pr) may be used interchangeably in this reaction, however **13** was used instead of **12** due to easier cleavage with HBr during the last step of the synthesis. Any trace amounts of unreacted starting materials in the crude sample of **39** had no effect on the quaternization reaction with MeI (1.2 eq.), resulting in quantitative conversion to **40**. These by-products may be purified at any stage in the preparation of **41** (Scheme 2.3). The last dealkylation step to obtain **41** proved to be a challenge due to insolubility of the bisphosphonic acid product.

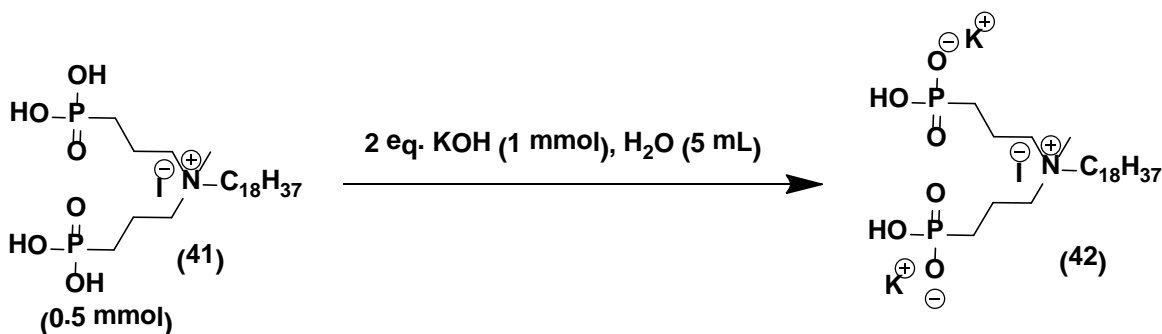


Scheme 2.3: Preparation of γ -Bisphosphonic acid **41**.

Initially the reaction was attempted with μ W heating, however it was difficult to monitor due to solidification of the product in the NMR tube (D₂O). Other deuterated solvents such as

CDCl₃ or DMSO also failed to show any ³¹P signals of the crude reaction mixture. After evaporation of the crude product to an orange paste, the residue was treated with DCM/TMSBr at RT overnight in an attempt to isolate a crystalline compound after TMS ester hydrolysis. Once again, after extensive solubility analysis, the residue remained practically insoluble in every solvent including the NMR solvents mentioned above.

Compound **41** is insoluble in H₂O due the presence of two phosphonic acid groups and the hydrophobic C₁₈ tail and the quat contributes to its insolubility in most polar solvents. Only after treatment with 2 eq. KOH to make the potassium salt of the bisphosphonic acid, **42**, was it possible to solubilize the compound in D₂O and obtain a clean NMR (Scheme 2.4, Figure 2.5).



Scheme 2.4: Preparation of the potassium salt of **41**.

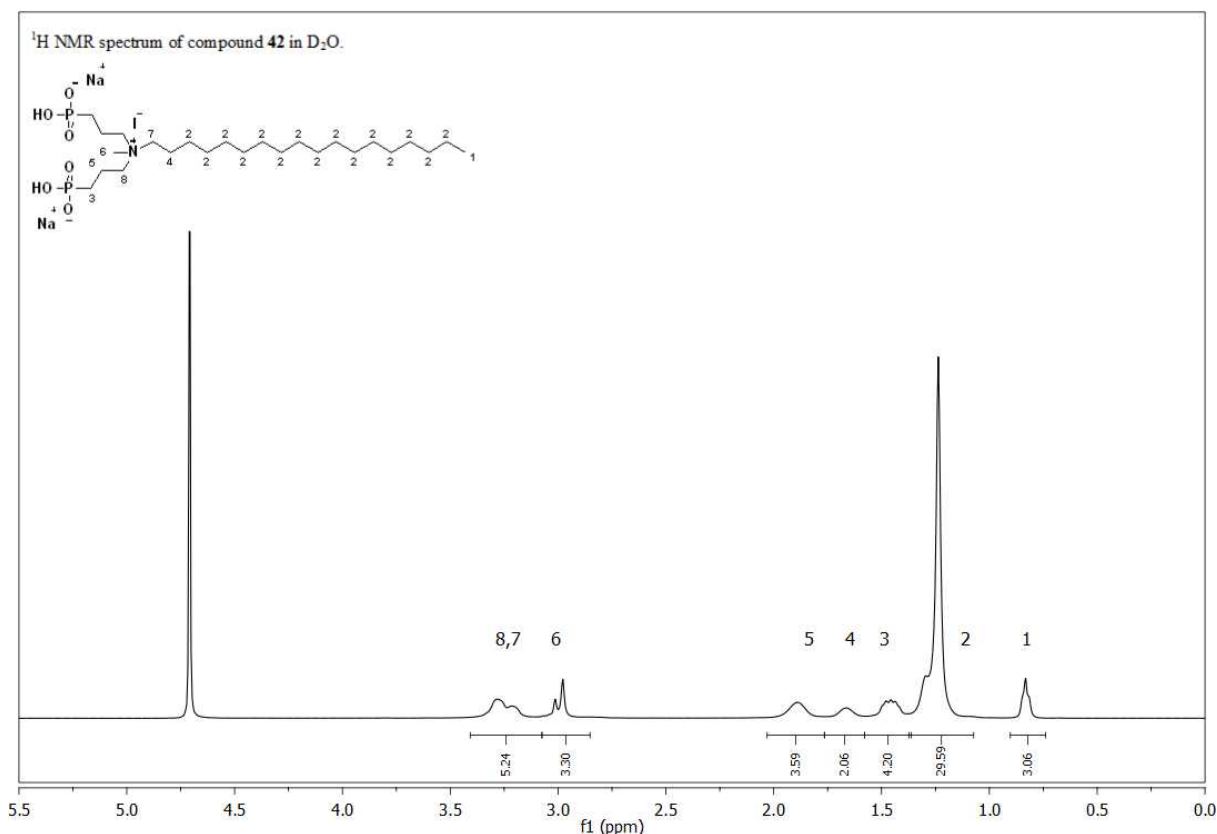
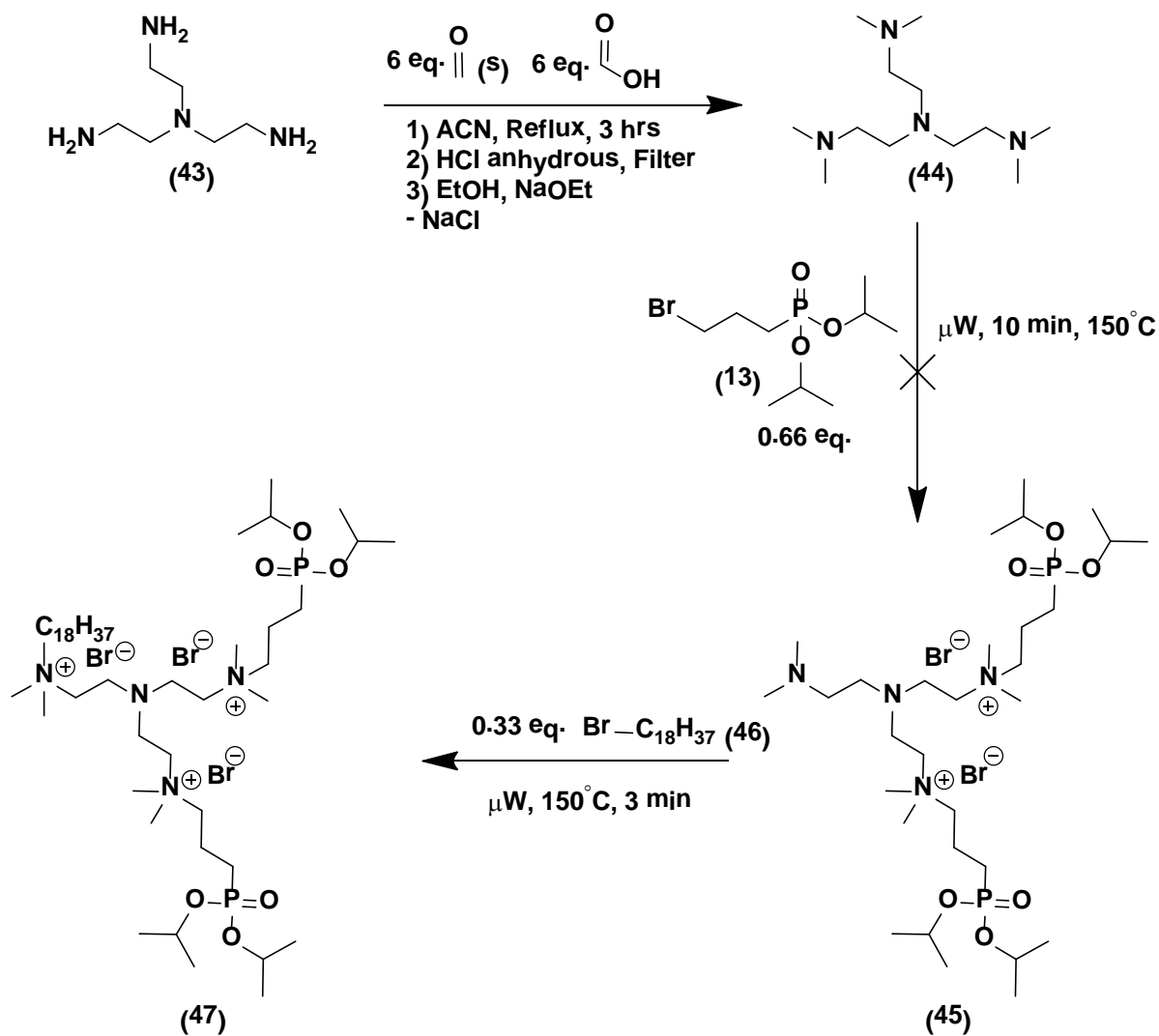


Figure 2.5 : ¹H NMR (D₂O) spectrum of γ -BPQAC **42**.

An alternative (γ -BPQ) synthesis was attempted starting with *N*¹,*N*¹-bis(2-aminoethyl)ethane-1,2-diamine scaffold based on Yoshimura's work with a tridodecyl quaternized star-shaped precursor **44** (Scheme 2.5).¹⁹⁹ Precursor **44** was prepared by a modified procedure starting with paraformaldehyde instead of formalin and heated in ACN, employing anhydrous HCl and NaOEt instead of HCl(aq) and NaOH to obtain the free base amine (see Experimental, Section 5.3.3). Attempted synthesis of **45** by quaternizing with 0.33 eq. bromooctadecane followed by 0.66 eq. of **13** or vice-versa failed to give the desired quaternized product peak (³¹P NMR δ ~ 29 ppm, Scheme 2.5, Figure 2.6). Instead, an unidentified upfield peak from the starting material **13** was observed (³¹P NMR δ ~ 30 ppm, Figure 2.6), in a 1:1 ratio with unreacted **13** (Figure 2.6). Since the reaction was performed without filtering off NaCl after

44 was freebased with NaOEt prior to adding **13**, any excess base could have reacted with **13**. No further experimentation was attempted with this scaffold.



Scheme 2.5: Attempted preparation of compound **47**.

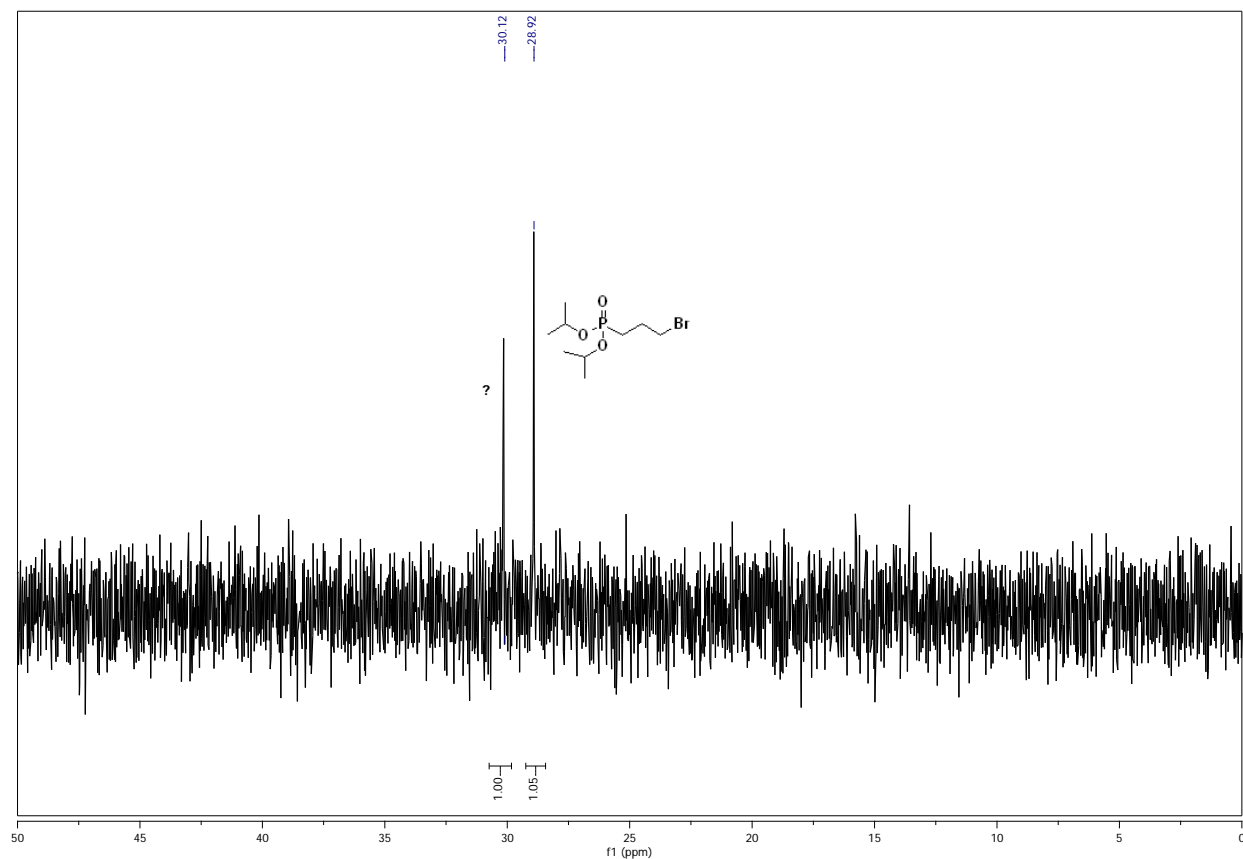


Figure 2.6: ^{31}P NMR (CDCl_3) reaction monitoring of compound **45**.

2.1.2.3 α -CH Bisphosphonic Acids QAC Antimicrobials (α -CH-BPQA) Synthesis

α -CH Bisphosphonic acid quats envisioned coming from alkylated methylenebis (phosphonate) (Figure 2.7) were also patentable synthetic targets of various small molecule multidentate phosphonic acid antimicrobials.

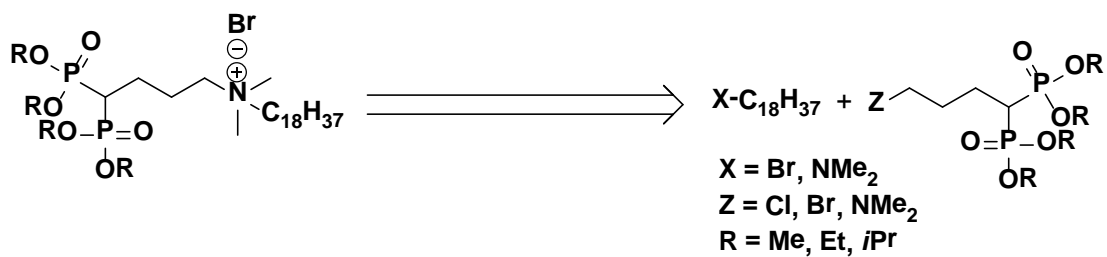


Figure 2.7: Retrosynthesis of α -CH bisphosphonic acid quats.

Four methods were identified in the literature for the preparation of halo or *N,N*-dimethyl substituted methylene bisphosphonate precursors for the Menshutkin reaction. Surprisingly, none of these have been used to make QAC's (Figure 2.8). The following starting materials can be used to prepared alkylated methylene bisphosphonates: (i) aldehydes, (ii) monophosphonates, (iii) dialkylvinylphosphonate (iv) methylene bisphosphonates. Each of the four methods are individually discussed in the following sections.

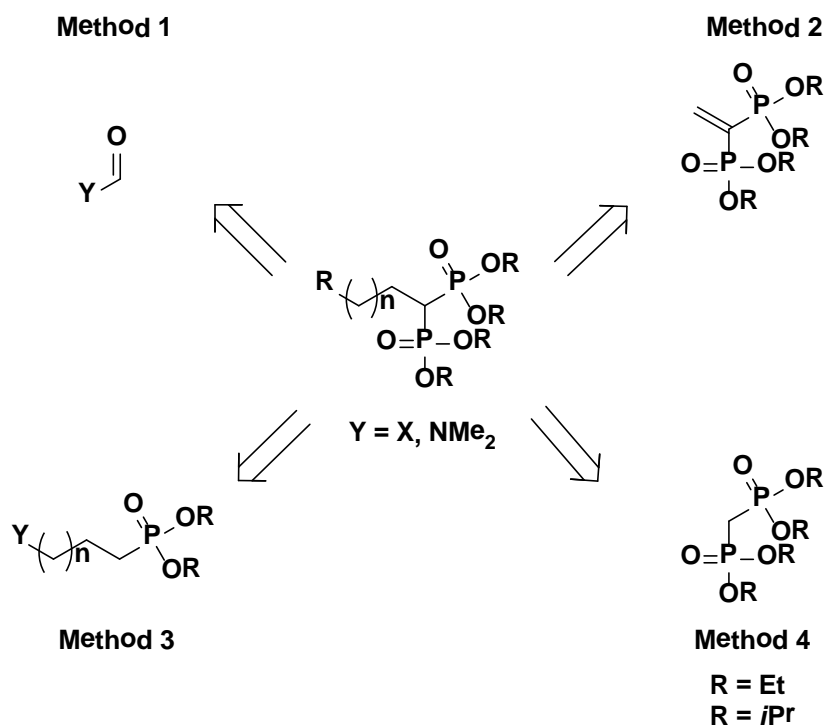
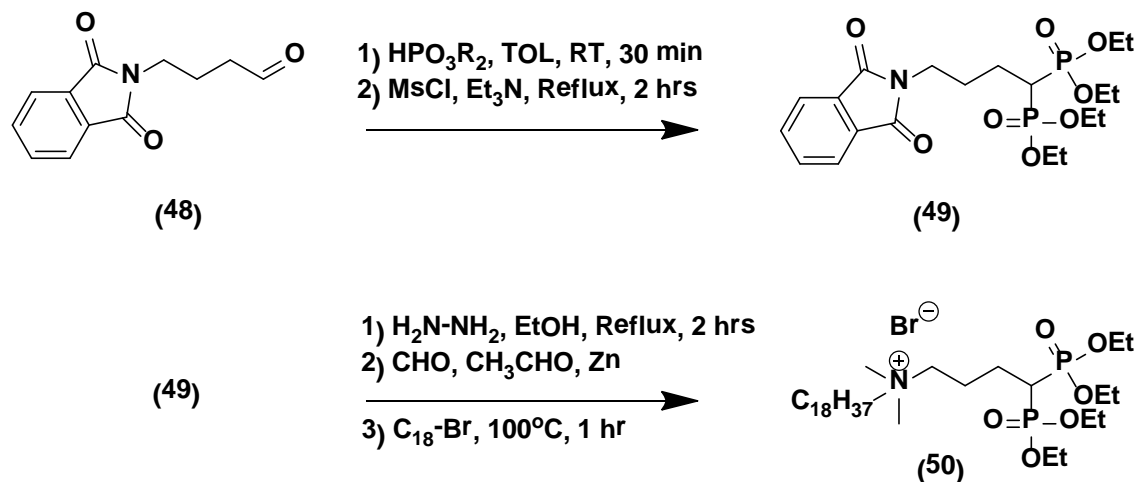


Figure 2.8: Four retrosynthetic methods for the preparation of α -CH-BPQA's.

Method 1: Onepot Bis Addition of Dialkylphosphites to Aldehydes

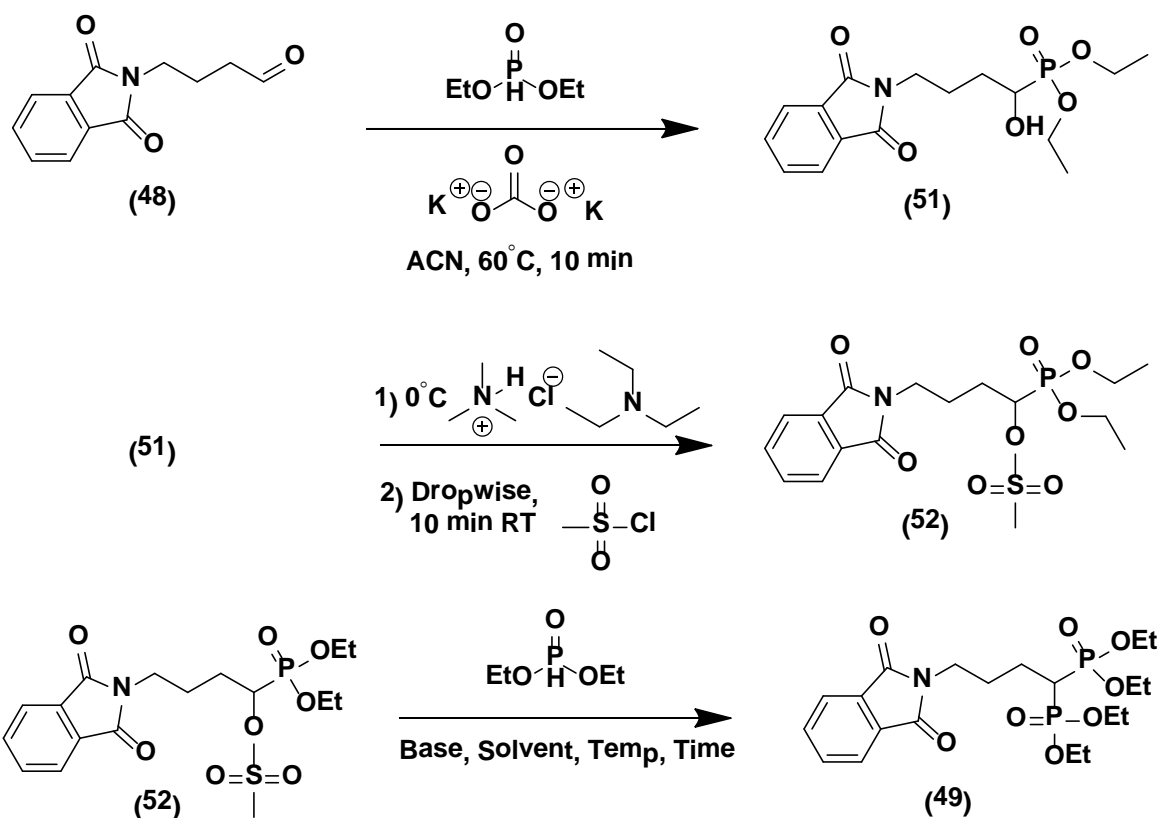
The most cost effective reaction to prepare the α -CH bisphosphonate scaffold involves the one pot addition reaction of 1 eq. of $\text{HP}(\text{OEt})_2$ to an aldehyde followed by mesylation of the *in situ* formed α -hydroxyl phosphonate and subsequent substitution by another equivalent of

nucleophilic diethylphosphite (Scheme 2.6). The only drawback here is the extra step required to prepare the commercially unavailable aldehydes.



Scheme 2.6: Preparation of **50** by Method 1.

Using Method 1, bisphosphonic quat **50** was targeted from the phthalimide protected aldehyde **48** after hydrazine deprotection of **49** followed by *N,N*-methylation and quaternization (Scheme 2.6). However, the first reaction in the sequence failed to give the desired product (^{31}P NMR ~ 24 ppm) by the one-pot method. Instead, the one pot reaction was performed sequentially isolating each intermediate according to Scheme 2.7.



Scheme 2.7: Attempted stepwise preparation of **49**.

Synthesis of the bisphosphonate **49** from **52** was unsuccessful, leading to a mixture of products (^{31}P NMR, CDCl_3). All base/solvent combinations including $\text{K}_2\text{CO}_3/\text{EtOH}$, $\text{Cs}_2\text{CO}_3/\text{ACN}$, $\text{Cs}_2\text{CO}_3/\text{ACN}$, pyridine/TOL also failed to give the desired ^{31}P resonance at $\delta \sim 23\text{--}24$ ppm, with unidentified peaks at 17.7 ppm and 0.7 ppm always observed.

A closer investigation of the literature revealed that the phthalimide protecting group is incompatible with Method 1, leading instead to heterocyclic products.²⁰⁰ Deprotonation of the newly formed bisphosphonate by the one pot reaction creates a nucleophilic carbanion that undergoes an intramolecular Horner-Wadsworth-Emmons reaction between the formed imide and the β -functionalized phosphonate (Figure 2.9).

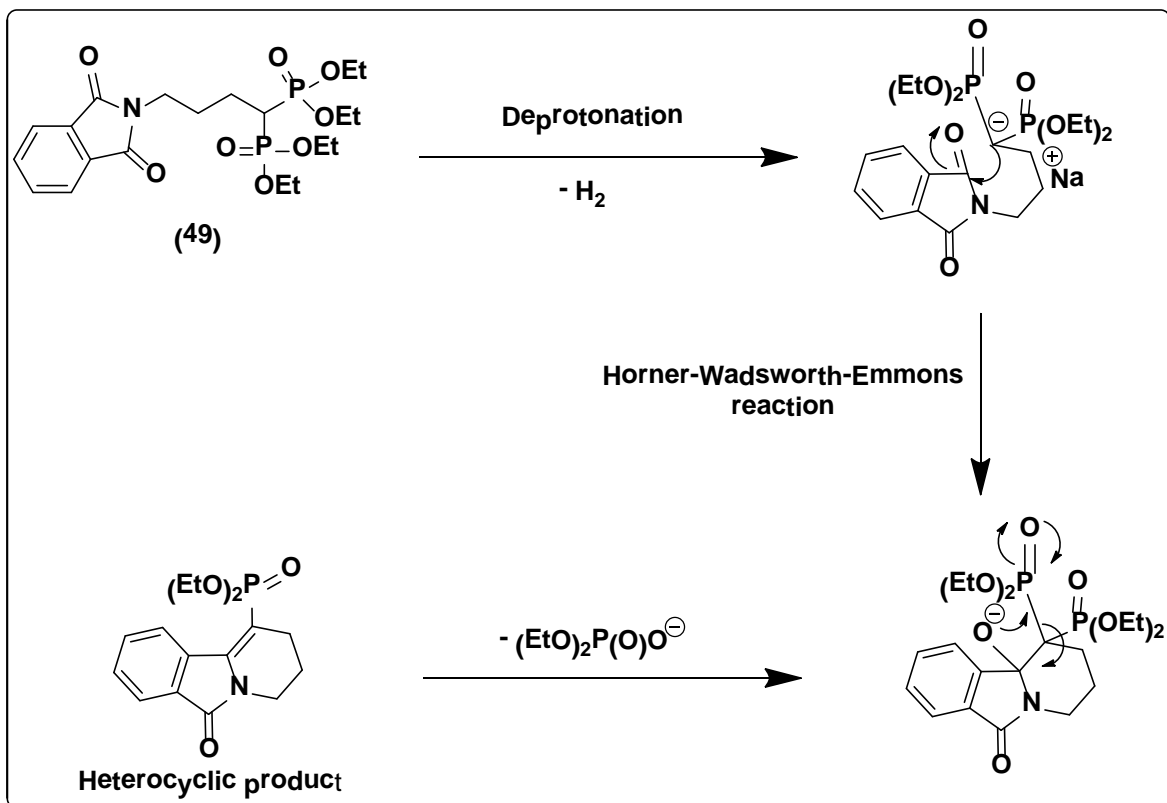
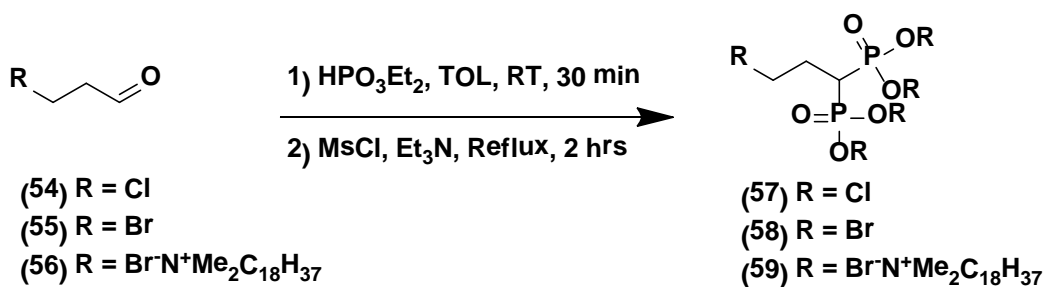


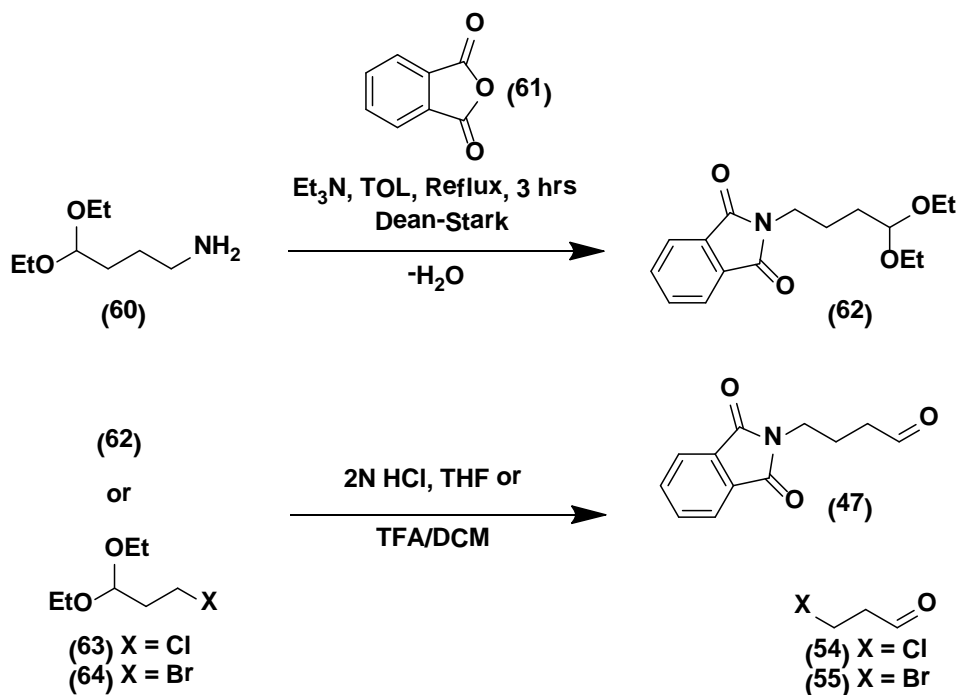
Figure 2.9: The Horner-Wadsworth-Emmons rearrangement of **49**.²⁰⁰

Due to the rearrangement observed with precursor **49**, it was hypothesized that switching to a different aldehyde would allow the one pot reaction to proceed without heterocycle formation. Synthesis of various halo substituted **54** and **55** and the quat aldehyde **56** was attempted, but were problematic to isolate by recrystallization (Scheme 2.8).

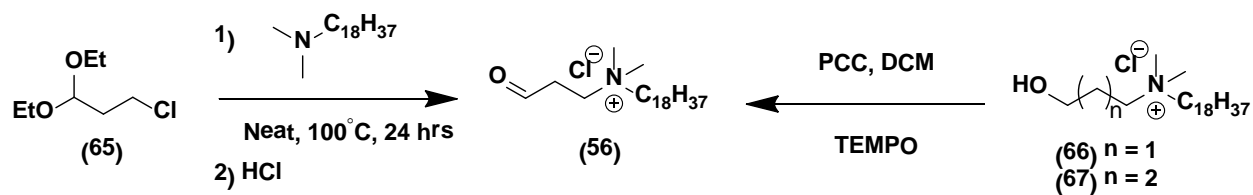


Scheme 2.8: Synthesis of bisphosphonates **57-59** from aldehydes.

Synthesis of QAC aldehyde **56** was first attempted by quaternizing the commercially available acetal **65** with **2**. The desired product was obtained along with an unidentified inseparable impurity by ^1H NMR (CDCl_3) after numerous attempts at recrystallization. No further reaction with this compound was pursued. The second way to obtain **56** is the oxidation of the quat alcohols **66** or **67** prepared in high yield (98%) and purity (Figure 2.10, Section 2.6.1, see crystal structure). Compounds **66** and **67** remain to be oxidized with pyridinium chlorochromate (PCC) as shown in Scheme 2.10. Preparation of the chloro and bromo aldehydes precursors **54** and **55** was attempted by employing refluxing HCl or TFA/DCM with loss of the volatile product aldehydes upon distillation (Scheme 2.10). Additionally, a potential problem with Method 1 is the possibility of the unwanted substitution of the halo group with nucleophilic $\text{HP}(\text{OEt})_2$. Instead, Methods 2-4 were explored in order to prepare α -CH-BPQA's.



Scheme 2.9: Synthesis of aldehyde precursors **47**, **54-55** used for Method 1.



Scheme 2.10: Possible synthetic routes leading to aldehyde QAC 56.

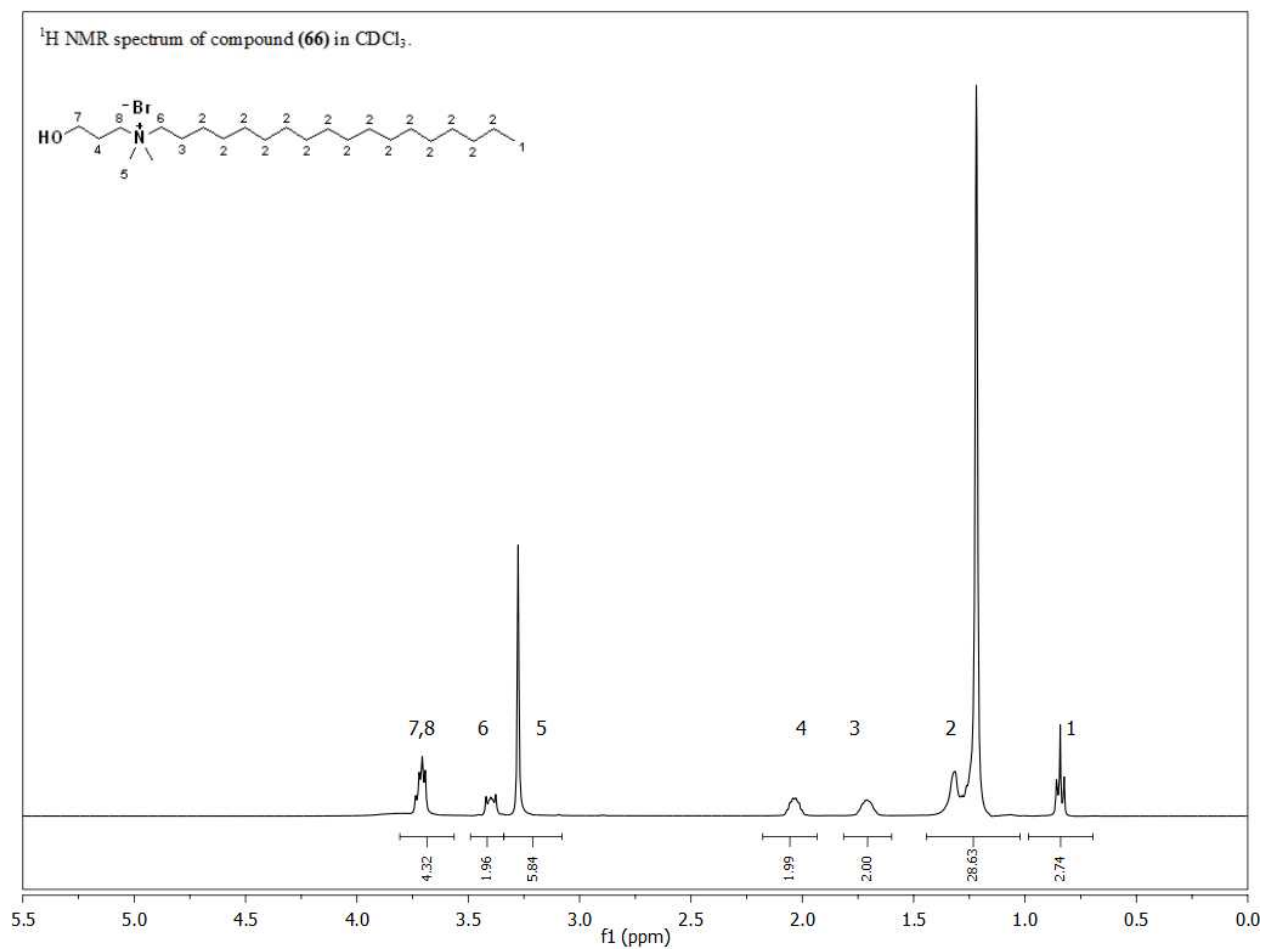


Figure 2.10: ¹H NMR (CDCl₃) spectrum of QAC aldehyde precursor 66.

Method 2: Michael Addition to Diethylvinylphosphonate

THP protected bisphosphonate intermediate **71** and **72** are known literature compounds prepared by Method 2 (see Experimental, Section 5.4.2). However numerous attempts to obtain these compounds via the Michael addition of the Grignard to **68** failed to give the desired product according to Table 2.6. In all cases, the reaction did not proceed (Table 2.6, Entries i and ii) or resulted in a mixture of products by ^{31}P NMR (CDCl_3) after EtOAc extraction (Table 2.6, Entry iii). The failure of Method 2 can be attributed to an incomplete conversion of the alkyl halide to the Grignard nucleophile or its decomposition after it was prepared. A variety of ways to prepare the Grignard reagent were investigated. First, overnight sonication of Mg metal in Et_2O was tested, however, the next day incomplete consumption of the metal remained (Table 2.6, Entry i). Activation of Mg by refluxing for 2 hrs followed by stirring at RT ON resulted in consumption of Mg and a cloudy solution was obtained (Table 2.6, Entry ii). In another trial, Mg was stirred at RT ON before adding it to **68** (Table 2.6, Entry iii). In all cases, no Michael addition products were detected by ^{31}P NMR (CDCl_3).

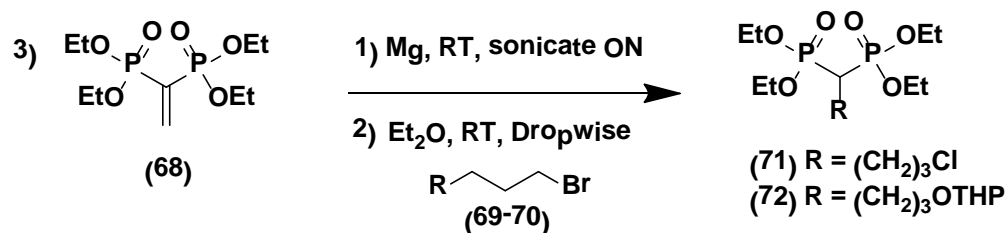
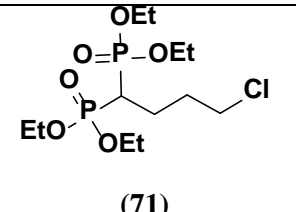
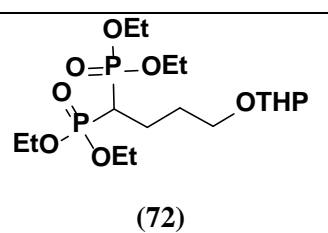
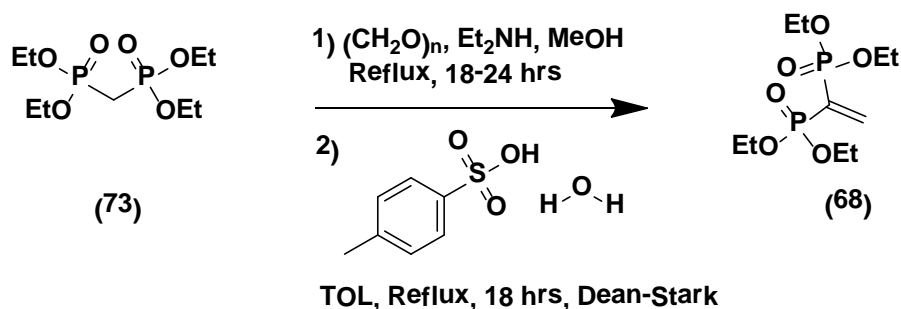


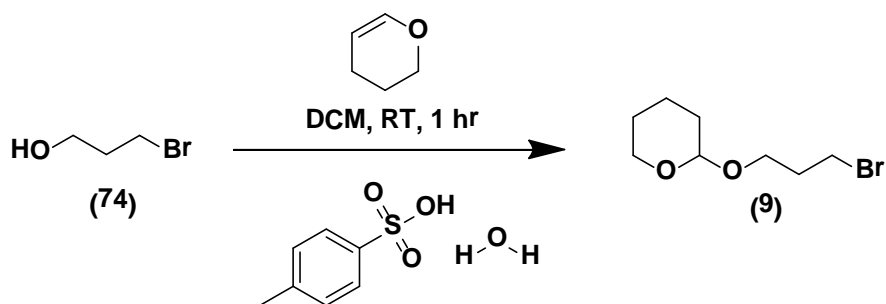
Table 2.6: Attempted Grignard addition reactions onto **68**.

Rxn. Comp. (%) by (³¹ P) NMR (CDCl ₃)							
Entry	Prdt. No.	Solvent (0.5M)	Time (hrs)	Temp. (°C)	PRD %	SM %	Other %
i	 (71)	Et ₂ O	24	0-RT	64	0	36
ii	 (72)	THF	1	-10	100	0	0
iii		THF	2	0-RT	0.07	13	86.9

Precursors for the Michael addition were prepared by literature procedures (see Experimental, Section 5.4.2). Compound **68** was prepared from the commercially available tetraethyl methyl bisphosphonate **73** and purified by distillation according to Scheme 2.11, while **74** was protected with tetrahydropyran and purified by column chromatography (Scheme 2.12). After performing the THP protection numerous times it was found that the reaction was complete after 1hr without added catalyst.



Scheme 2.11: Preparation of tetraethyl ethene-1,1-diylbisphosphonate **73**.



Scheme 2.12: Preparation of THP protected 3-bromopropanol **9**.

Method 3: C-P Formation

Method 3 was attempted in order to prepare the amine protected **49** and **77-78** according to Table 2.7. Compound **77** was only successfully prepared on a small scale (< 1 g) when LDA was made *in situ* from *n*-BuLi/diisopropylamine (Table 2.7, Entry iii) in ~ 60% yield and purified by column chromatography. Unfortunately LDA failed to deprotonate the phthalimide protected monophosphonate **19** at -78 °C due to solubility issues (Table 2.7, Entry iv). When the same reaction was performed at -10°C, a mixture of two unknown products by ^{31}P NMR (CDCl_3) were observed at $\delta = 31.43$ ppm (30%) and $\delta = -13.13$ ppm (70%) respectively, but not the desired bisphosphonate **49** ($\delta_{\text{expected}} \sim 24$ ppm) (Table 2.7, Entry v). Lastly the *N,N*-dimethyl phosphonate **32** also could not be deprotonated due to insolubility in THF (Table 2.7, Entry vi). For large scale preparation of **77**, Method 4 was investigated and is discussed below.

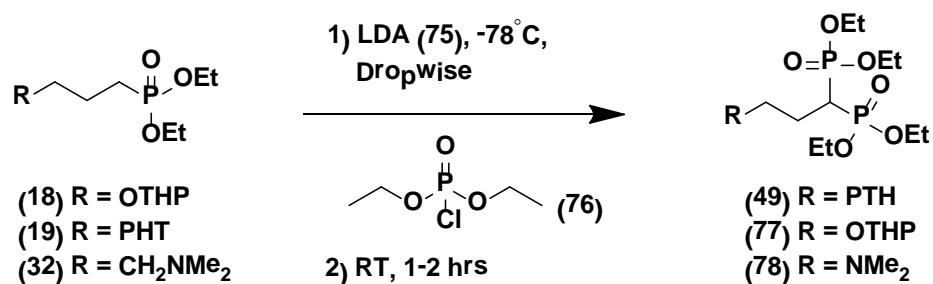


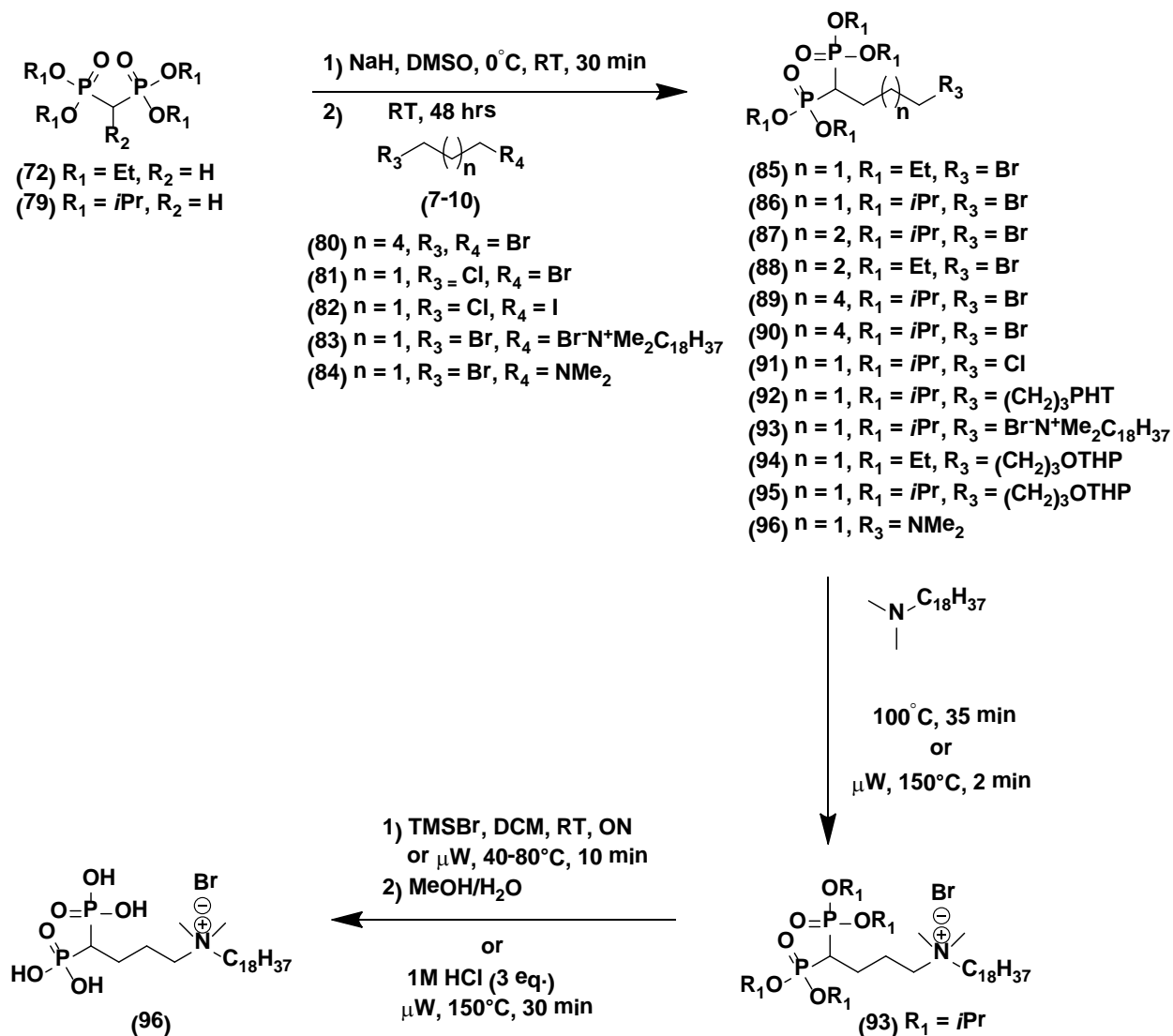
Table 2.7: Preparation of bisphosphonates **49**, **77-78** by Method 3.

Rxn. Comp. (%) by ¹ H, ³¹ P NMR (CDCl ₃)						
Entry	Reactant	Base	Time (hrs)	Temp. (°C)	PRD. %	³¹ P NMR (ppm)
i	 (77)	NaHMDS	2	-78	0	n/a
ii		LDA	2	-78	10	24.14
iii		<i>n</i> -BuLi / DIA	2	-78	60	23.78
iv	 (49)	LDA	2	-78	0	n/a
v		LDA	2	-10	0*	n/a
vi	 (78)	n/a (SM (32) insoluble in THF)				

Precursors **18** and **19** were prepared by the Abruzov reaction in one step while **32** was prepared in two steps utilizing the Abruzov reaction followed by alkylation with dimethylamine (see Table 2.3, Section 2.1.2.1). A pure sample of **32**, a new compound, was isolated by column chromatography (note: compound turns dark on storage at RT).

Method 4: Direct Alkylation

In contrast to Methods 1-3, all of the starting materials used in Method 4 are commercially available and were employed to prepare the bisphosphonate QAC **93** on a large scale after a lengthy optimization of the first alkylation step according to Scheme 2.13.



Scheme 2.13: Preparation of bisphosphonates by direct alkylation.

The direct alkylation of **72** or **79** to **85-96** was explored with different alkyl halides employing different solvents and bases (Table 2.8). Reaction progress was monitored by ³¹P

NMR (CDCl₃) by observing the consumption of **72** OEt (δ = 19.27 ppm), and **79** OiPr (δ = 18.06 ppm, Table 2.8). In all cases, the alkylation was incomplete and resulted in a mixture containing the desired product along with unreacted starting material, often requiring a difficult column chromatography purification (Table 2.8, Entries xiv, xv, xvi).

The choice of alkylhalide proved to be the most critical step in the reaction. Alkylation with the bromopropyl QAC (Table 2.8, Entry xviii) that could directly lead to the desired product in one step, failed to react (³¹P NMR) while the *N,N*-dimethyl **84** intermediate, also failed to alkylate. Next, dihalo precursors of various chain lengths C₃-C₆ were employed (Table 2.8, **7** (C₃), **8** (C₄), **80** (C₆)) resulting in low yields. When NaH/DMSO (Table 2.8, Entries iii, xviii, xix, xxii) was employed with the dihalo compounds, higher yields were obtained versus THF while the *n*-BuLi/THF reaction resulted in a complicated mixture of products (Table 2.8, Entry iv). When an excess of NaH in DMSO was used, compound **88** was unexpectedly dialkylated due to an intramolecular reaction (Scheme 2.14, Table 2.8, Entry xvii, Figure 2.11).

As a result, a protective group strategy employing compound **10** was used as the alkyl halide to prepare **93** on a large scale (Figure 2.12). Compound **95**, a known compound, was previously synthesized in the literature by Method 4 with NaH/THF in low yield (30%). As a result both NaH/THF and NaH/DMSO combinations were tested in an attempt to improve the yield. Even though the NaH/DMSO conditions were higher yielding (Table 2.8, Entry xxvi), it was difficult to remove the solvent fully during extraction or distillation. Instead, when THF was dried (4°A MS) ON (Table 2.8, Entry xxiii) a 60% yield was obtained and the unreacted starting material **79** was carried throughout a lengthy deprotection/mesylation/substitution procedure to convert the alcohol to either a bromo **87** or *N,N*-dimethyl group **96** (Scheme 2.16).

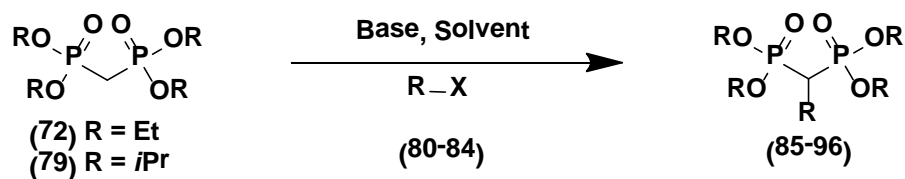
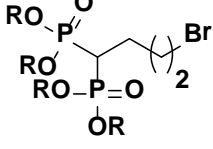
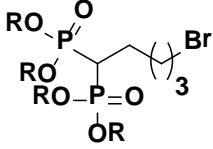
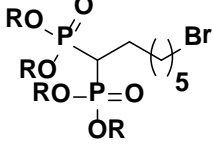
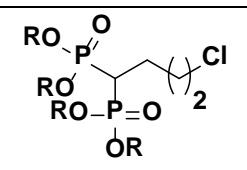
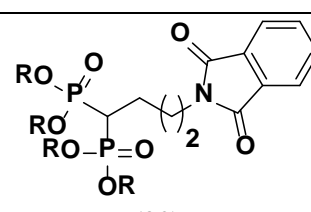
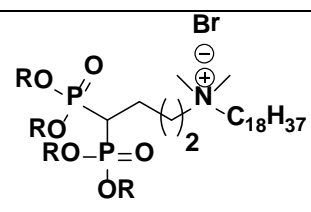
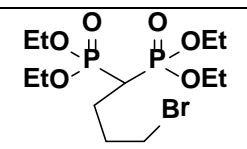
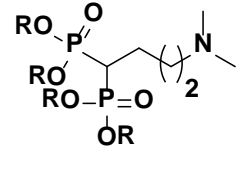
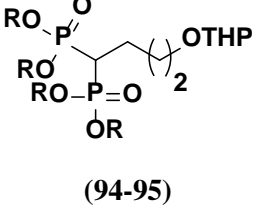


Table 2.8: Synthesis of α -C-H bisphosphonates by Method 4.

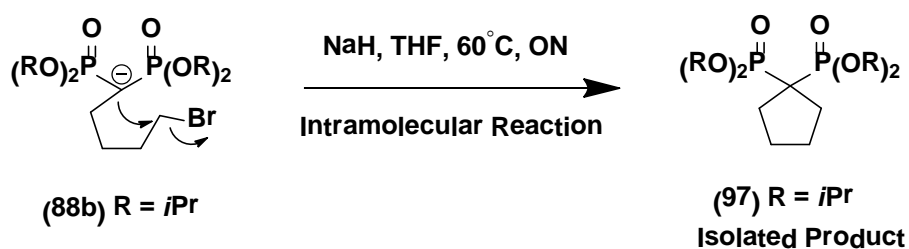
Entry	R-X	Base	Solv.	Time (hrs)	T (°C)	Ratio of reactants	PRD %	PRD. ^{31}P ppm (CDCl ₃)
i	 <p>(85-86)</p>	NaH	THF	48	RT	(72 + 7)/ <u>1:4</u>	3	25.63
ii		NaH	DMF	12	RT	(72 + 7)/ <u>1:4</u>	1	25.67
iii		NaH	DMSO	24	RT	(72 + 7)/ <u>1:4</u>	22	25.69
iv*		BuLi	THF	24	RT	(72 + 7)/ <u>1:4</u>	0	n/a
v		BuLi	THF	24	RT	(79 + 7)/ <u>1:4</u>	0	n/a
vi		Cs ₂ CO ₃	ACN	0.1	150	(72 + 7)/ <u>1:4</u>	5	26.01
vii*		Cs ₂ CO ₃	ACN	0.1	150	(72 + 7)/ <u>1:4</u>	n/a	n/a
viii		NaHMDS	DMF	24	RT	(72 + 7)/ <u>1:4</u>	20	25.80
ix		NaHMDS	THF	24	60	(72 + 7)/ <u>1:4</u>	31	25.64
x	 <p>(87-88)</p>	NaH	DMSO	48	RT	(79 + 8)/ <u>1:1.1</u>	68	26.73
xi		NaH	DMSO	48	RT	(79 + 8)/ <u>1:1.1</u>	54	26.79
xii	 <p>(89-90)</p>	NaH	THF	48	RT	(79 + 80)/ <u>1:4</u>	52	20.46

Entry	R-X	Base	Solv.	Time (hrs)	T (°C)	Ratio of reactants	PRD %	PRD. ³¹ P ppm (CDCl ₃)
xiii	 (91)	NaH	THF	24	60	(79 + 81)/ <u>1:4</u>	0	n/a
xiv		NaH	Diox.	24	60	(79 + 81)/ <u>1:4</u>	0	n/a
xv*		NaH	THF	24	70	(79 + 82)/ <u>1:1.1</u>	n/a	n/a
xvi	 (92)	NaH	DMSO	48	RT	(79 + 10)/ <u>1:1.1</u>	0	n/a
xvii		NaH	Diox.	24	80	(79 + 10)/ <u>1:1.1</u>	8	24.98
xviii	 (93)	NaH	DMSO	24	80	(79 + 83)/ <u>1:1.1</u>	24	21.07
xix	 (88a)	NaH	DMSO	24	RT	(72 + 7) / <u>1:1.5</u>	99	28.50
xx	 (96)	NaH	DMSO	24	70	(72 + 84) / <u>1:1</u>	0	n/a

* multiple peaks ,** PCT (phase transfer catalyst).

Rxn. Comp. (%) by ^{31}P NMR (CDCl_3)								
Entry	R-X	Base	Solv.	Time (hrs)	T ($^{\circ}\text{C}$)	Ratio of reactants	PRD %	PRD. ^{31}P ppm (CDCl_3)
xxi	 <p>(94-95)</p>	NaH	THF	48	60	(79 + 9)/ <u>1:1</u>	47	23.94
xxii		NaH	THF	72	RT	(72 + 9)/ <u>1:1.1</u>	n/a	n/a
xxiii		NaH	THF	48	70	(79 + 9)/ <u>1:1</u>	60	n/a
xxiv *		Cs_2CO_3	ACN	48	90	(79 + 9)/ <u>1:2</u>	23	23.78
xxv		Cs_2CO_3	ACN	72	90	(79 + 9)/ <u>1:1</u>	44	23.75
xxvi		NaH	DMS O	RT	24	(79 + 9)/ <u>1:5</u>	62	23.71
xxvii		NaH^{eq}	DMS O	RT	96	(79 + 9)/ <u>1:1</u>	92	23.66

* multiple peaks, ** PCT (phase transfer catalyst).



Scheme 2.14: Intramolecular bisphosphonate alkylation.

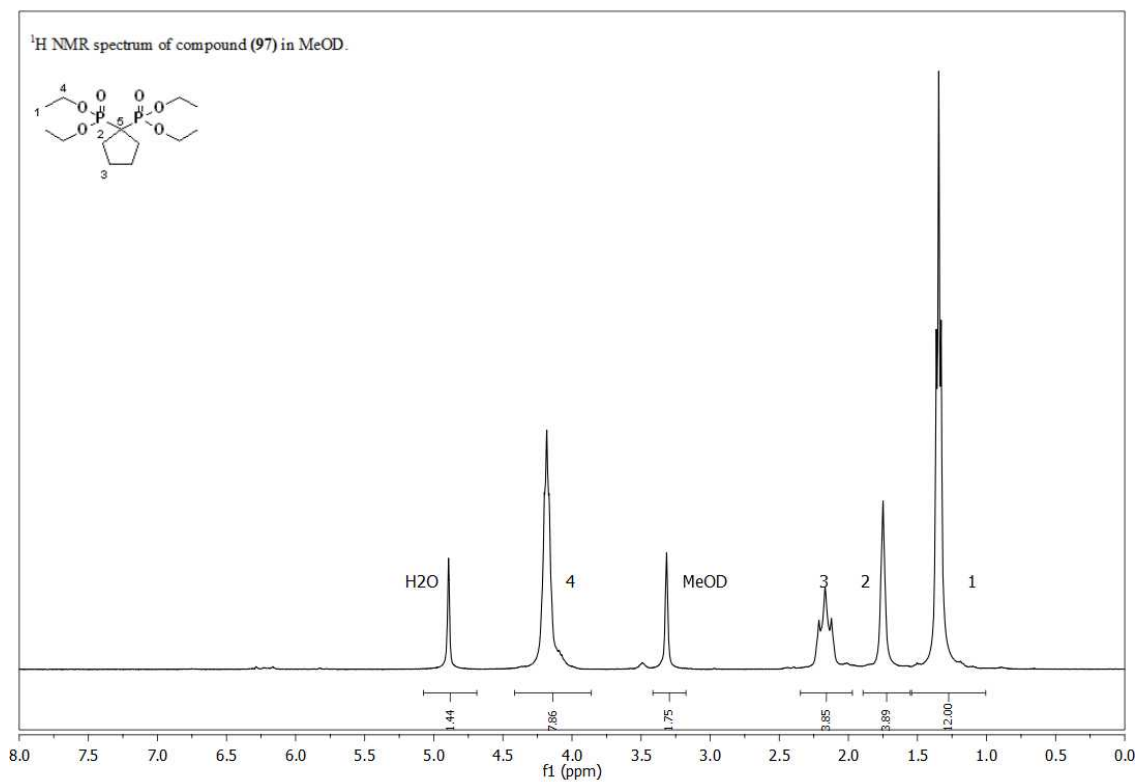


Figure 2.11: ¹H NMR (MeOD) spectrum of cyclic bisphosphonate by-product **97**.

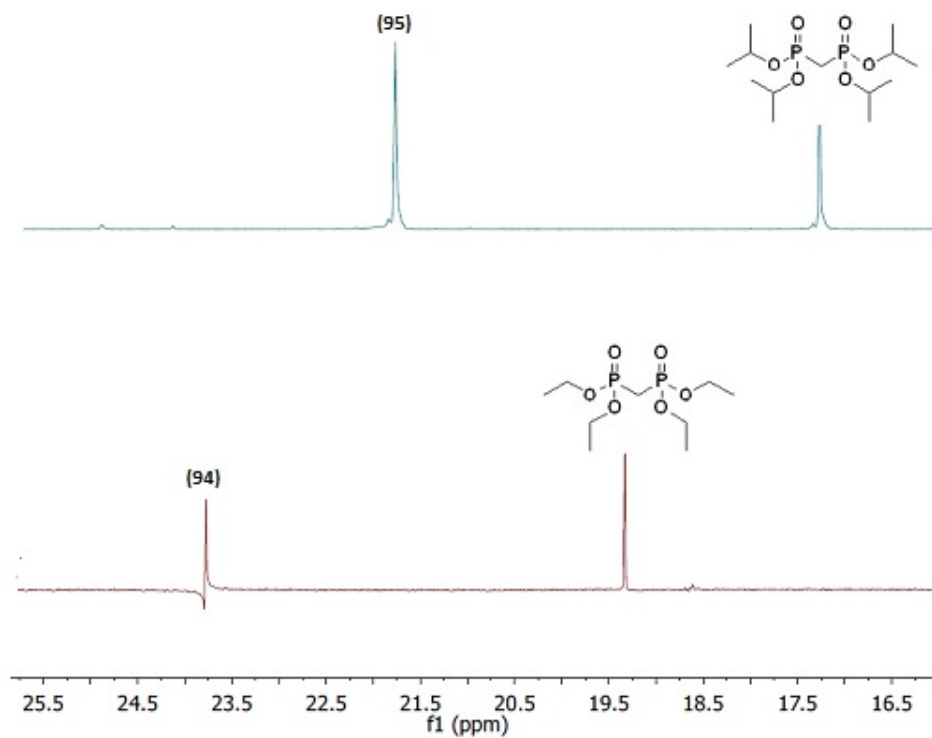
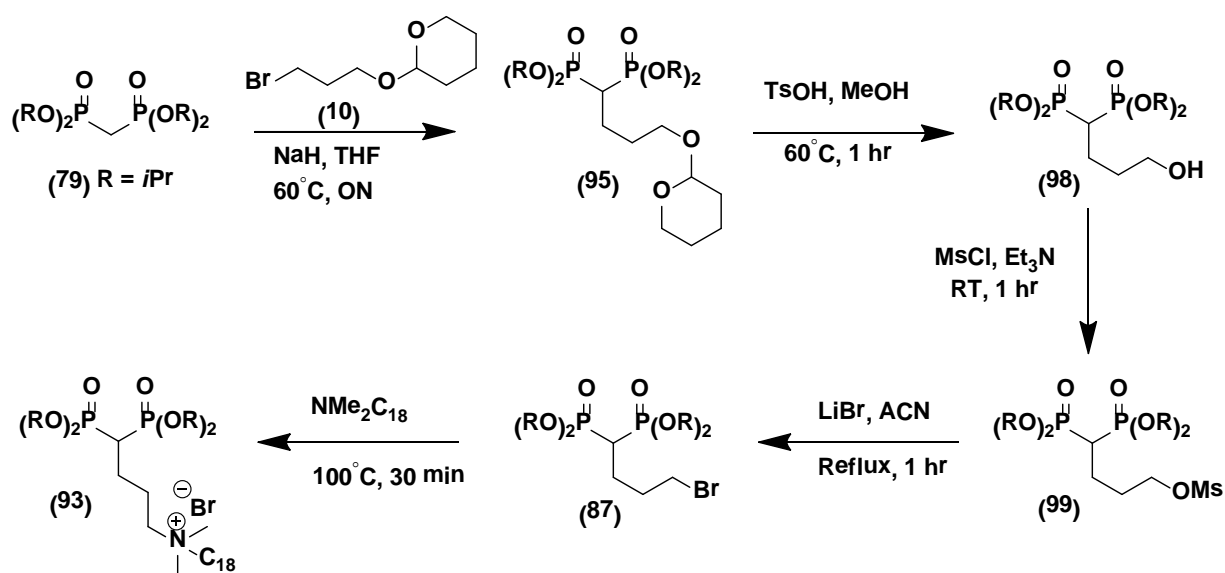


Figure 2.12: ³¹P NMR (CDCl₃) monitoring for compound **94** and **95** prepared by Method 4.



Scheme 2.15: Preparation of bisphosphonate QAC **96** via alkylation.

Quaternization of **87** (Scheme 2.15) gave the desired bisphosphonate quat **93** (Figure 2.13), however, dealkylation with HBr (μW , 8 min) could not be monitored due to precipitation of the product **97** in the NMR tube (D_2O) as well as several other deuterated solvents (CDCl_3 , DMSO), failing to show any ^{31}P NMR signals of the crude reaction mixture.

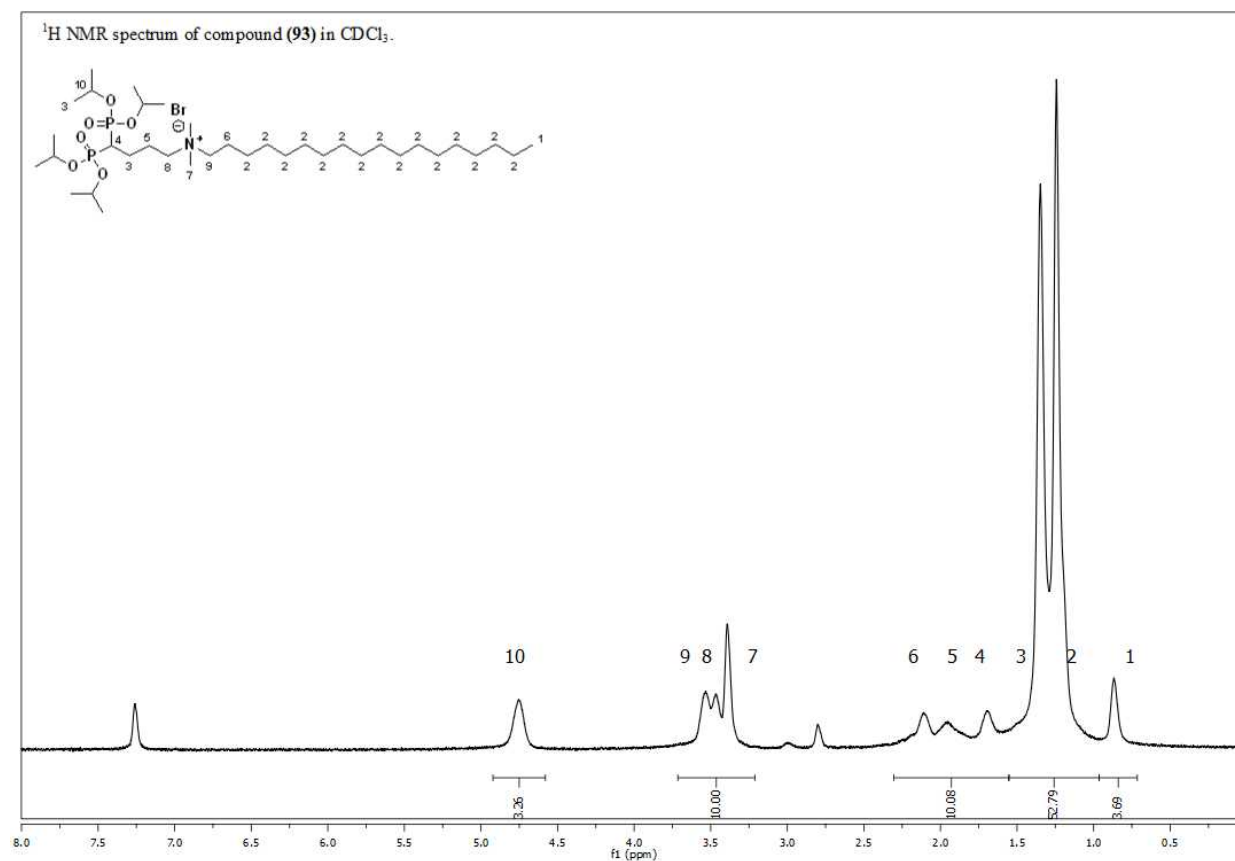
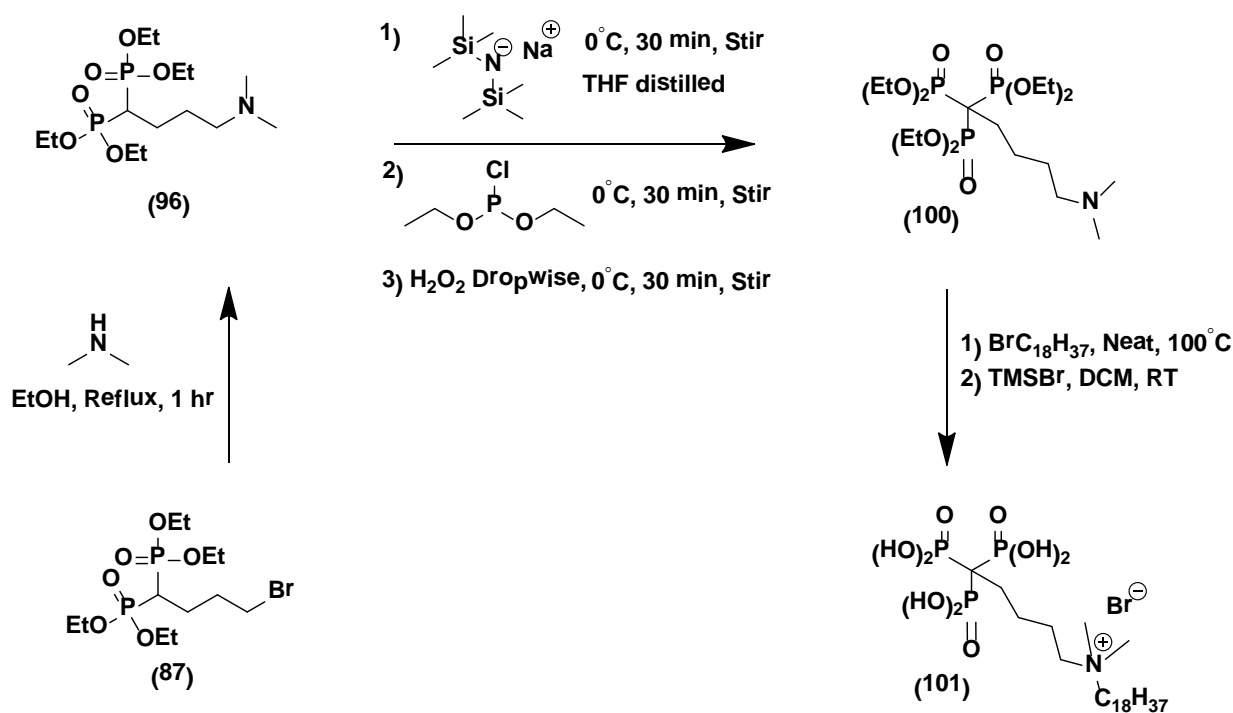


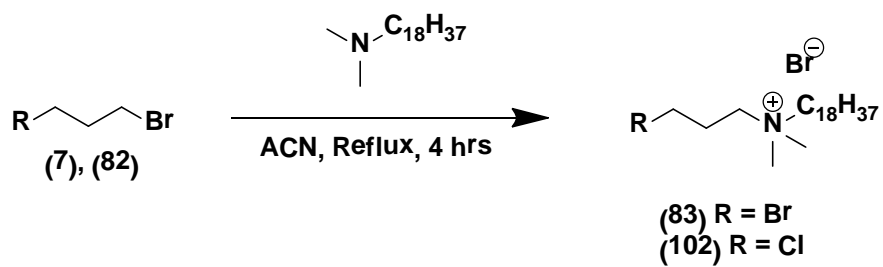
Figure 2.13: ¹H NMR (CDCl₃) spectrum of α -CH-QAC **93** prepared by Method 4.

The rest of compound **87** was used to make the dimethyl derivative **96** in order to prepare trisphosphonate **101** via alkylation with NaHMDS/DECP (Scheme 2.16).



Scheme 2.16: Attempted preparation of trisphosphonic acid **101** via alkylation of **96**.²⁰¹

Halo QAC's **83** (bromo) and **102** (chloro) were synthesized by the Menshutkin reaction as precursors for alkylation of **79** in order to directly obtain the target bisphosphonate QAC **93** in one step with Method 4 (Scheme 2.17 and Scheme 2.13). Alkylation with bromo precursor **83** resulted in only a 24 % conversion by NMR spectroscopy (^1H , ^{31}P , CDCl_3) (Table 2.8, Entry xviii). Purifying the product from the quat mixture was never attempted. The less reactive chloro precursor was made and characterized by NMR spectroscopy (^1H , ^{31}P , CDCl_3 , Figure 2.14) but never employed in the alkylation reaction with **79** due the low product conversion with the bromo precursor.



Scheme 2.17: Preparation of halo QAC **83** and **102** precursors for Method 4.

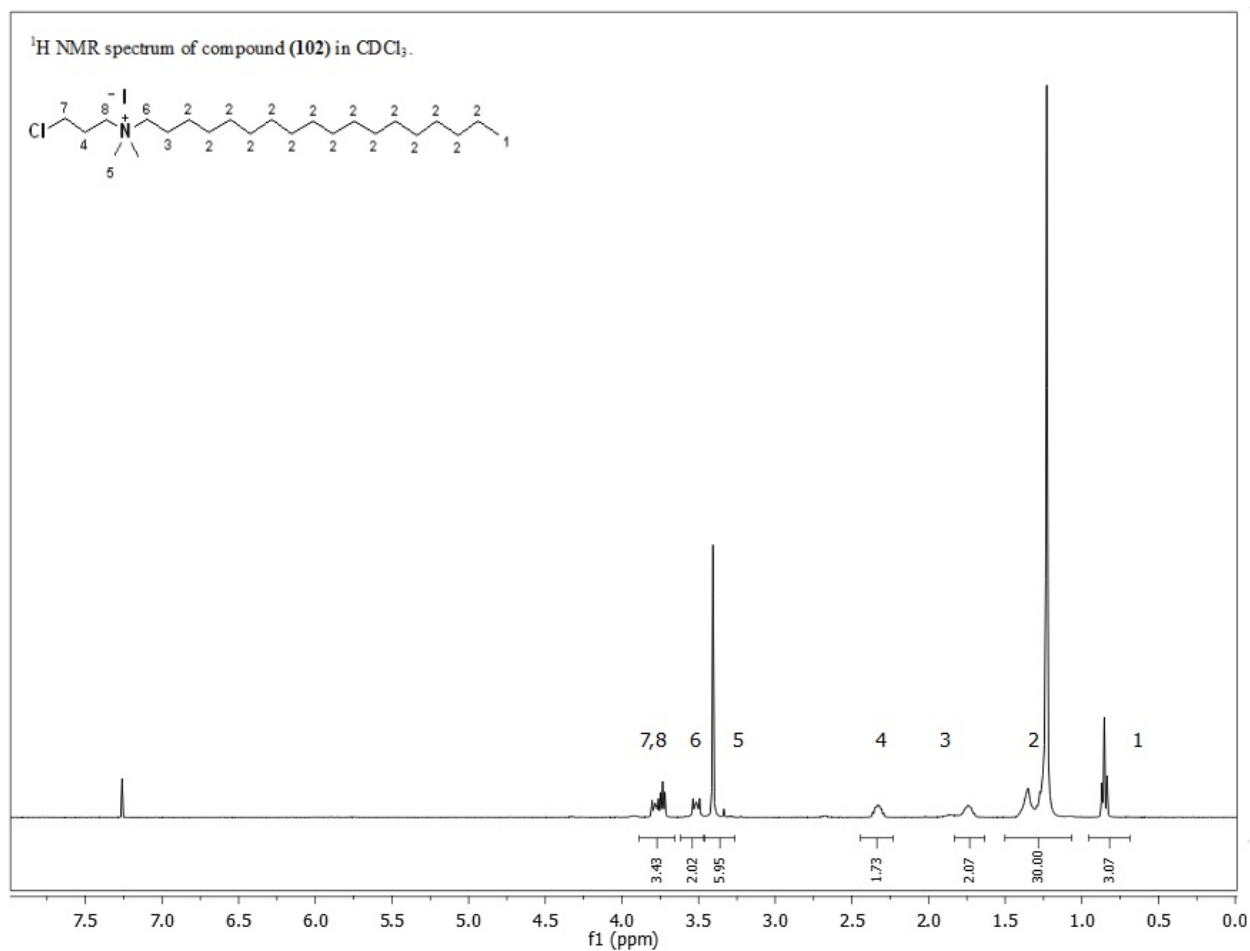
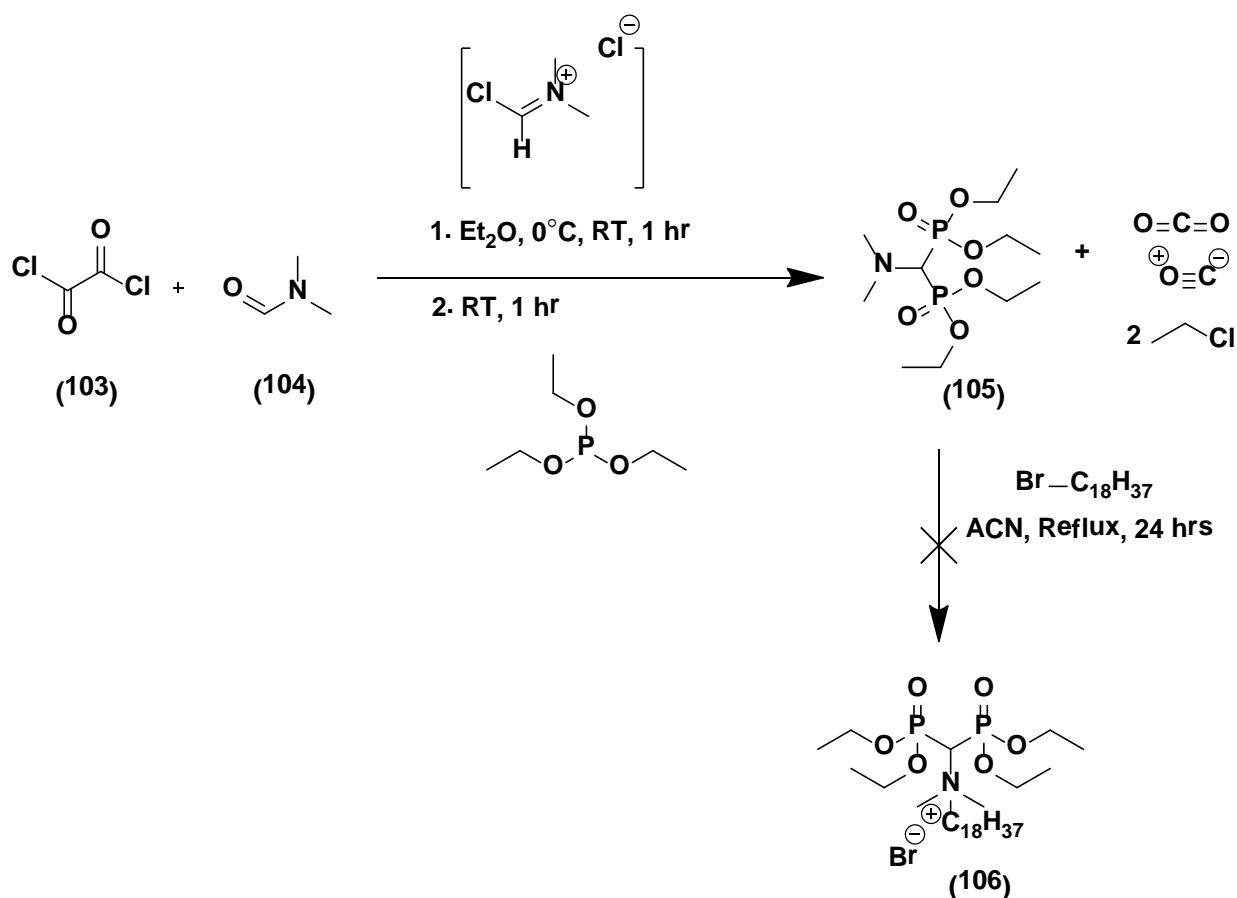


Figure 2.14: ¹H NMR (CDCl₃) spectrum of precursor **102**.

2.1.2.4 Bisphosphonates via the 3-Component Reaction

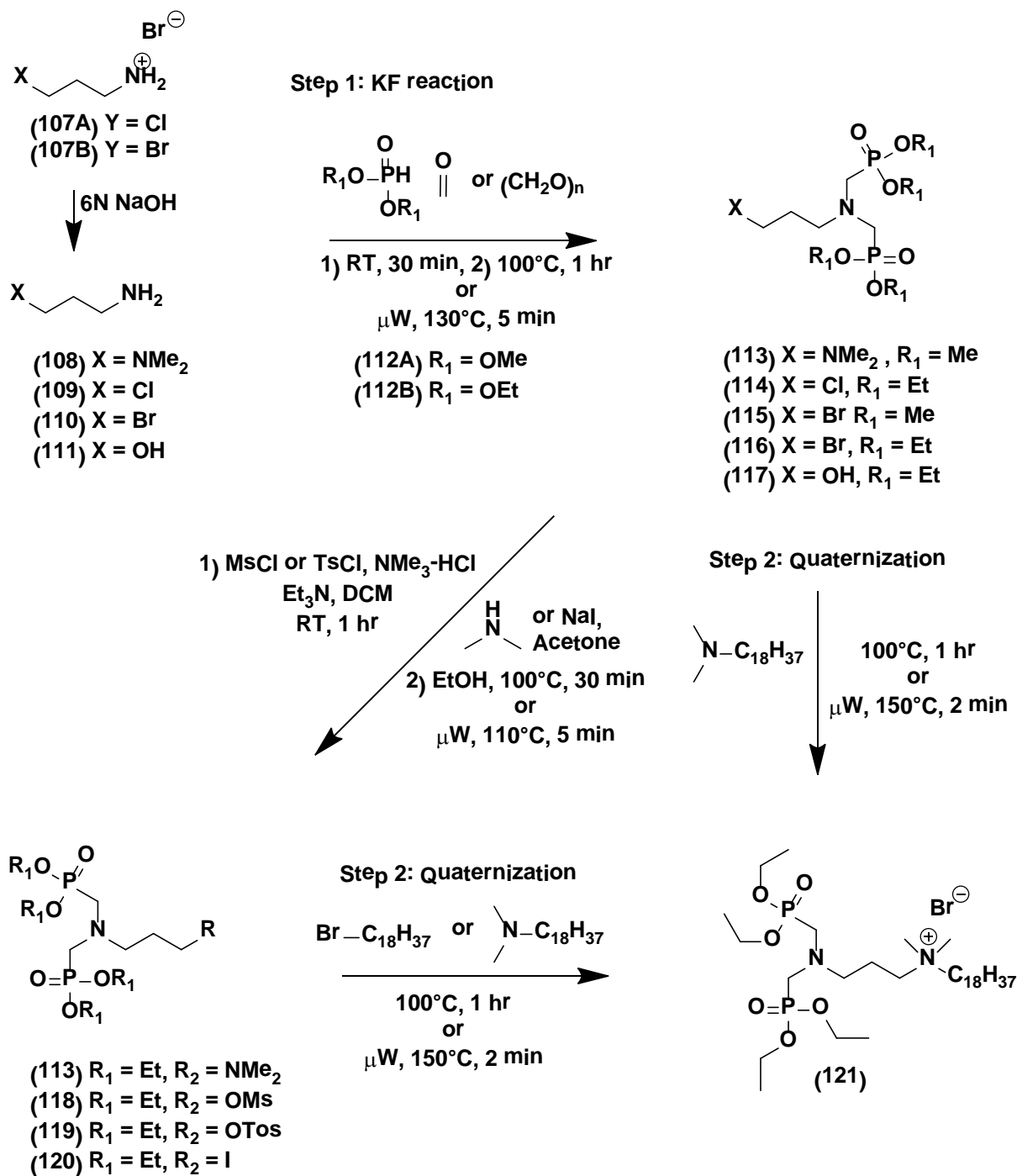
A 3-component reaction was used to prepare precursor **105** in 75% yield (Experimental, Section 5.5.0) according to known procedures and quaternized with bromooctadecane (Scheme 2.18).²⁰² No useful NMR data was obtained for compound **106** due to difficulties with purification. It remains doubtful whether **105**, a weak and hindered nucleophile due to the presence of two electron withdrawing phosphonate ester groups could be quaternized.



Scheme 2.18: Attempted preparation of bisphosphonate **106**.

2.1.2.5 α -Aminobisphosphonic acids QAC Antimicrobials (α -ABPQA)

α -Aminobisphosphonic acid QAC's were synthesized either directly via the three component Kabachnik-Fields reactions between formaldehyde, a primary amine and dialkyl phosphite (Scheme 2.19) or sequentially by isolating the imine intermediate (Scheme 2.20). The synthesis required a three step process starting with the Kabachnik-Fields reaction to generate novel bifunctional molecules with the α -bisphosphonates anchored at one end and either a *N,N*-dimethylamino **113** or halo **114-117**, **120** end group required for the quaternization reaction. The third and final step required didealkylation of the QAC bisphosphonate **121** to the free phosphonic acid **126** (Scheme 2.21). Initially *N*¹,*N*¹-dimethylpropane-1,3-diamine **108** seemed like the most logical choice of starting material for the Kabachnik-Fields reaction in order to obtain compound **113**. Compound **108** is an inexpensive commercially available liquid and required no additional steps to free the primary amine as was the case with the halo precursors **109**, **110** and sold as the HCl and HBr salts, respectively.



Scheme 2.19: Synthetic route to α -aminobisphosphonate QAC **121**. Optimized conditions for each step.

As a result, optimization of the Kabachnik-Fields reaction was first explored with **108** (Table 2.10, Entries i-iv) as well as with the triazine intermediate **123** (Table 2.10, Entry v). In

all cases, the expected α -bisphosphonate **113** product peak at $\delta \sim 26$ -24 ppm (^{31}P NMR, CDCl_3) was observed while monitoring the reaction, however it was incorrectly assigned as compound **113**. After minimal mass was recovered in the organic layer after extraction, the reaction was directly purified by column chromatography and the peak at ~ 26 ppm was attributed to compound **124** after a further ^1H NMR (CDCl_3) analysis (Figure 2.15).

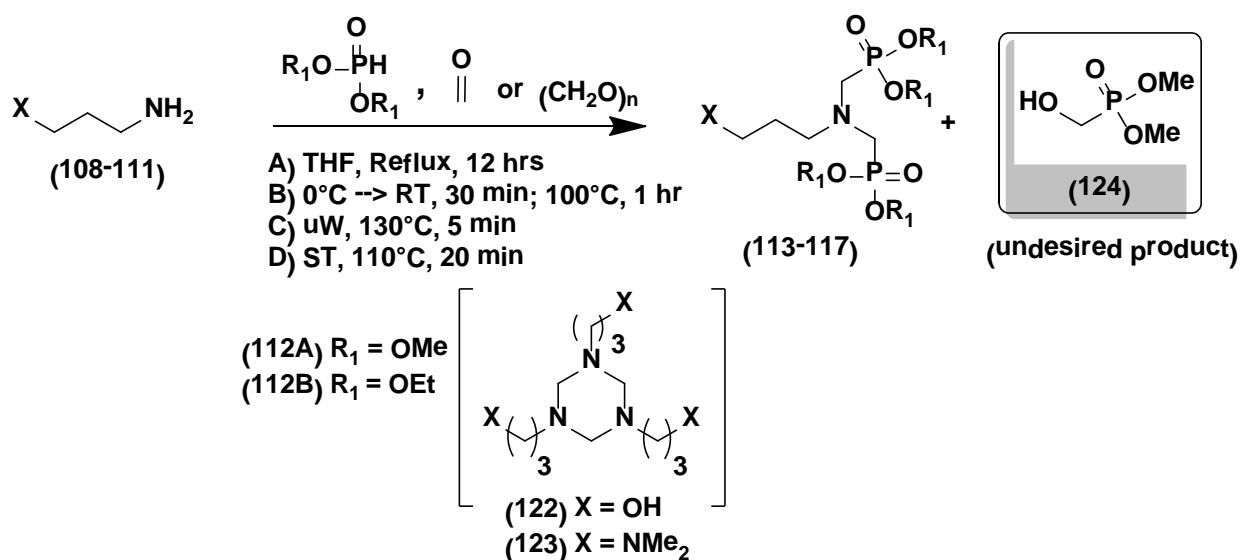


Table 2.9: Optimization of the Kabachnik-Fields reaction.

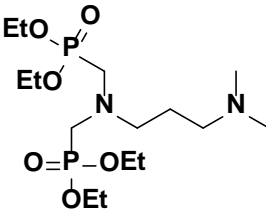
Rxn. Comp. (%) by (^{31}P) ppm NMR (CDCl_3)								
Entry	Reactant	SM	Base	Temp. ($^\circ\text{C}$)	Time	Solv.	PRD %	PRD ^{31}P ppm
i	 (113)	112A + 108	n/a	RT	24 hrs	H_2O	70	26.85
ii		112A + 108	n/a	RT	5 min	THF	36	26.42
iii		112A + 108	n/a	80	4 hrs	THF	66	26.61
iv		112A + 108	n/a	80	20 hrs	THF	76	26.61
v		112A + 108	n/a	Reflux	3 hrs	ACN	50	25.01

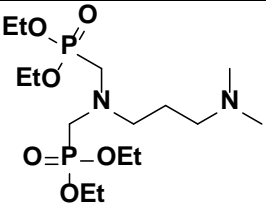
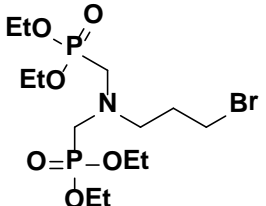
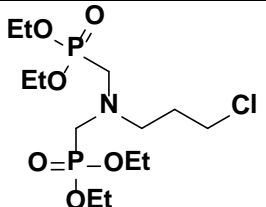
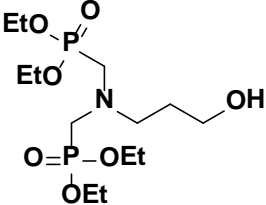
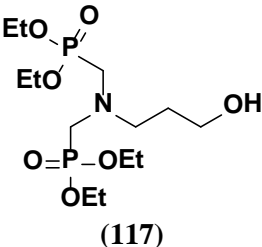
Table 2.9 continued					Rxn. Comp. (%) by (³¹ P) ppm NMR (CDCl ₃)			
Entry	Reactant	SM	Base	Temp. (°C)	Time	Solv.	PRD .%	PRD ³¹ P ppm
vi	 (113)	112B + 108	NMe ₂	Reflux	30 min	EtOH	62	24.89
vii		112B + 108	NMe ₂	110	5 min	EtOH	65	24.52
viii	 (115-116)	112A + 110	Et ₃ N	70	20 hrs	THF	94	8.32
ix		112B + 110	NaOH	100	1 hr	H ₂ O	1	n/a
x		112B + 110	NaOH	100	1 hr	H ₂ O	21	24.69
xi		112B + 110	NaOH	100	1 hr	H ₂ O	53	24.69
xii ^{uW}		112B + 110	NaOH	130	5 min	Neat	40	24.68
xiii	 (114)	112B + 109	NaOH	100	1 hr	H ₂ O	46	24.65
xiv		112B + 109	KOH	100	1 hr	H ₂ O	48	24.40
xv	 (117)	112B + 111	n/a	80	4 hrs	THF	63	27.42
xvi		112B + 111	n/a	80	20 hrs	THF	85	26.60

Table 2.9 continued					Rxn. Comp. (%) by (^{31}P) ppm NMR (CDCl_3)			
Entry	Reactant	SM	Base	Temp. ($^{\circ}\text{C}$)	Time	Solv.	PRD %	PRD ^{31}P ppm
xvii*	 (117)	112B + 111	n/a	Reflux	20 hrs	ACN	80	25.00
xviii μW		112B + 111	n/a	130	5 min	Neat	73	24.83
19		112B + 111	n/a	110	0.5 hr	Neat	85	24.84

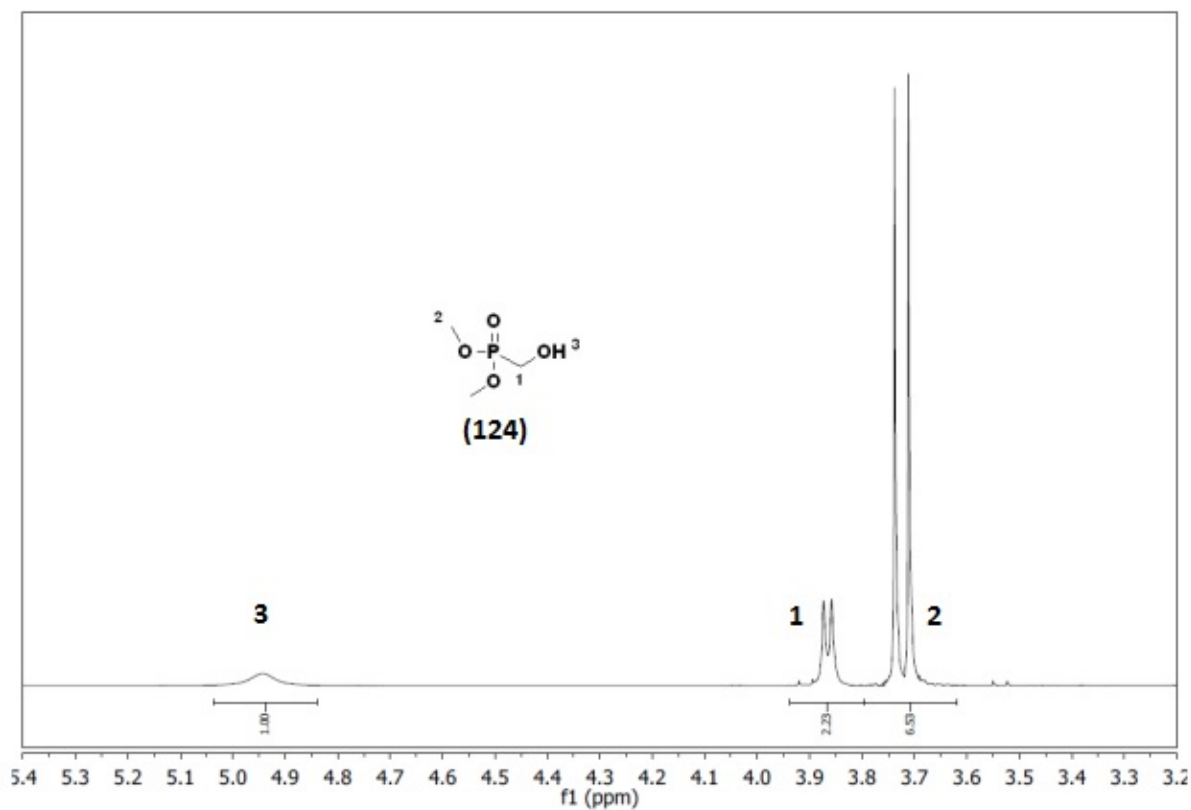


Figure 2.15: ^1H NMR (CDCl_3) spectrum of the undesired product **124** isolated from the Kabachnik-Fields reaction.

Based on the Kabachnik-Fields mechanism (Figure 2.16), the basic *N,N*-dimethylamine appears to play a catalytic role in driving the Abramov addition of dialkylphosphite to C=O bond forming α -hydroxy phosphonate (Route B) over the Pudovik addition of dialkylphosphite to the imine (Figure 2.16, Route A). In fact, the literature preparation of **124** requires a catalytic amount of base (see Section 2.1.2.7). In contrast, when starting materials without a basic group such as the halo or OH derivatives were used, the Kabachnik-Fields reaction mechanism is favoured (Figure 2.16, Route A) and the bisphosphonates, **114-117** were obtained when 2 eq. of the dialkylphosphite was employed.

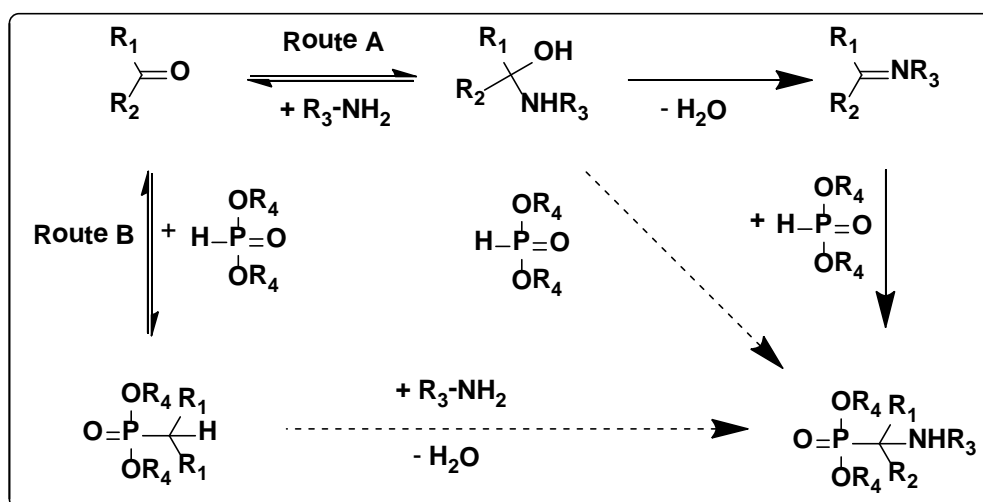


Figure 2.16: Possible mechanistic routes involved in the Kabachnik-Fields reaction.²⁰³

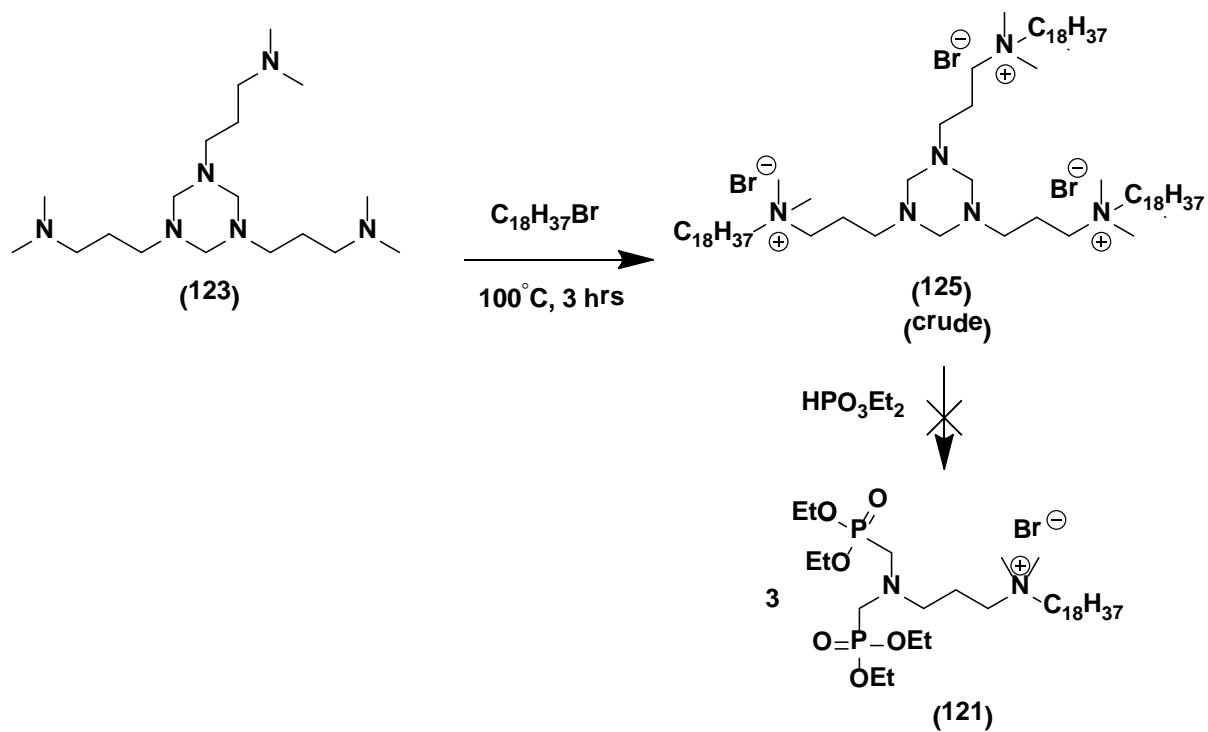
Next, the halo starting materials **107A** and **107B** (Scheme 2.19) were investigated in the Kabachnik-Fields reaction. As mentioned earlier, both the bromo **107A** and chloro **107B** sold as the HCl and HBr salts respectively, required an extra step to free base the amine salt prior to addition of formaldehyde and dialkylphosphonate. When Et₃N or NaOH (1 eq.) were stirred with **107A** for 20 min prior to the addition of formaldehyde and dialkylphosphonate in the same pot, the desired bisphosphonate was never observed (Table 2.9, Entries viii and ix). Instead of the desired bisphosphonate product with a ³¹P NMR (D₂O) peak at ~ 24 ppm, a major downfield ³¹P

NMR peak at $\delta \sim 8$ ppm was observed with complete consumption of $\text{HPO}(\text{OMe})_2$ (^{31}P , $\delta = 14.7$ ppm). In order for the reaction to proceed, **109** and **110** required a tedious extraction from 6N NaOH or KOH with isolation of the separated free bases as yellow oils that had to be used directly otherwise self-polymerization took place (Table 2.9, Entries x-xiv). No solvent was added during the extraction because when DCM, CHCl_3 , or EtOAc were employed for the free based halo derivatives, which preferred the aqueous phase over the organic phase ($\sim 5\%$ extraction efficiency by weight). As a result, the oily extracts of the free based compounds were contaminated with $\sim 40\%$ H_2O (^1H NMR), resulting in only $\sim 50\%$ overall extraction yield starting from the amine salts (Table 2.9, Entries xx-xiv, note low product yields, 21-53%). Lastly, $\text{Et}_3\text{N}/\text{ACN}$ was employed in order to deprotonate the starting materials *in situ* without the need to extract and thus improve the yield, however the resulting triethylamine salt failed to precipitate from the solution and could not be removed prior to the Kabachnik-Fields reaction.

Due to problems with starting materials **108-110** in the Kabachnik-Fields reaction described above, the reaction was screened with the amino alcohol **111** used in the literature to make **117** in refluxing THF (Experimental, Section 5.6.0). Under reflux conditions, the aminoalcohol **111** (Table 2.9, Entries xv and xvi, THF) or the triazine **122** (Table 2.9, Entry xv, ACN) worked well in the Kabachnik-Fields reaction with solid paraformaldehyde, resulting in yields over 70% by ^{31}P NMR (CDCl_3). Similarly, μW heating under neat conditions gave a 74% yield when reaction parameters were optimized to 5 min at 130°C (Table 2.9, Entry xxviii). This is the first μW synthesis of **117**, while synthesis of α -bisphosphonates with only alkyl chains (starting with 3-aminopropanol), has been previously reported with the Kabachnik-Fields reaction under μW heating (60 min, 100°C).^{204,205} After success under solventless conditions in the μW , a sealed tube experiment was thus performed with the alcohol starting material under

neat conditions for 30 min at 110°C which resulted in a 85% yield after column chromatography (Table 2.9, Entry xix). With the successful preparation of **117**, the conversion to either a bromo, iodo (Experimental, Section 5.6.0) or NMe₂ (Table 2.9, Entries vi and vii) required two extra steps, activation via mesyl or TsCl followed by the S_N2 reaction. All sulfonyl chloride reactions resulted in higher yields and faster conversion times when the catalyst NMe₃·HCl¹⁶² was employed (30 min vs 24 hrs for non-catalyzed reaction).

When the amine starting materials **108** or **111** were reacted solely with formaldehyde without addition of HP(OEt)₂, the corresponding imines were formed respectively. However at RT, the imine compounds were in equilibrium with the trimer compounds **122** and **123** as observed by ¹H NMR (CDCl₃, Scheme 2.20).²⁰⁶ Trimer **123** was purified by an aqueous wash and subjected to quaternization with bromooctadecane. However, purification of the final product failed to give clean samples for characterization by ¹H NMR spectroscopy (Figure 2.17). Instead, compound **121** was prepared from **115** and quaternized with bromooctadecane. Compound **115** was prepared via a longer route by activating the alcohol **111** via the mesyl **118** or tosyl **119** group refluxing in excess HNMe₂ (Scheme 2.19, Step 1-2). Pure **121** was finally obtained after column chromatography eluting with EtOH(NaBr_{sat}):ACN (1:3) (Figure 2.18).



Scheme 2.20: Attempted stepwise preparation of **121**.

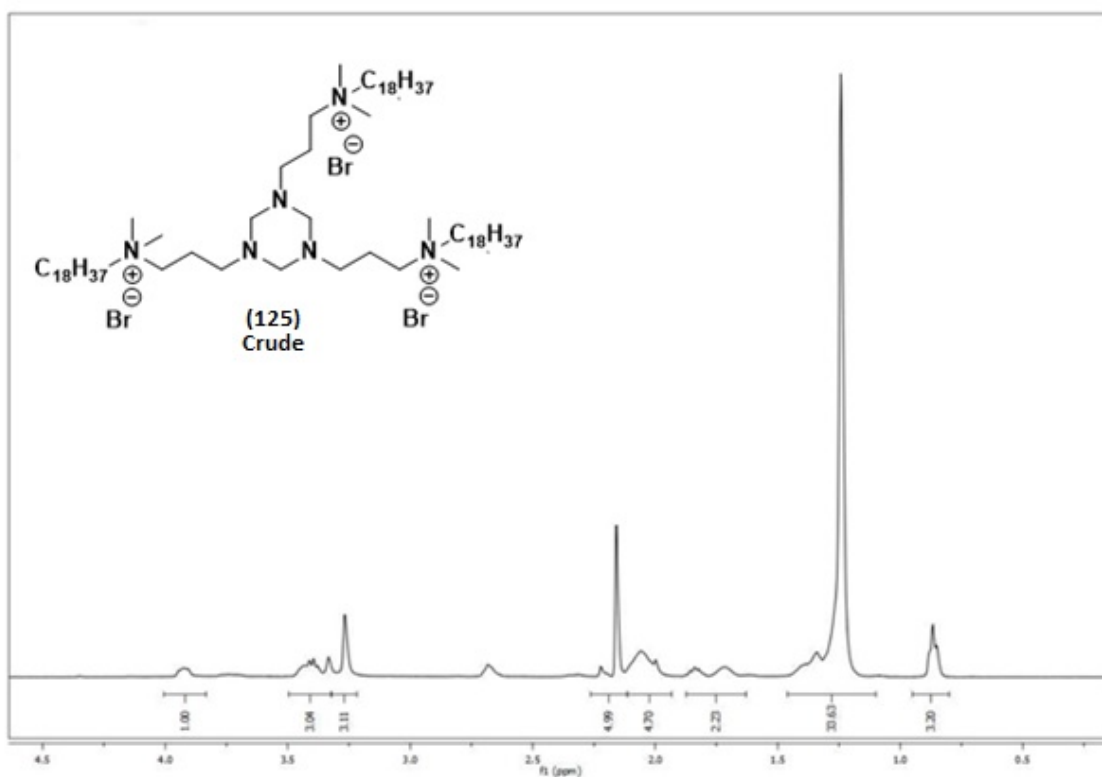


Figure 2.17: Attempted quaternization of triazine **123** with bromooctadecane (^1H NMR (CDCl_3)).

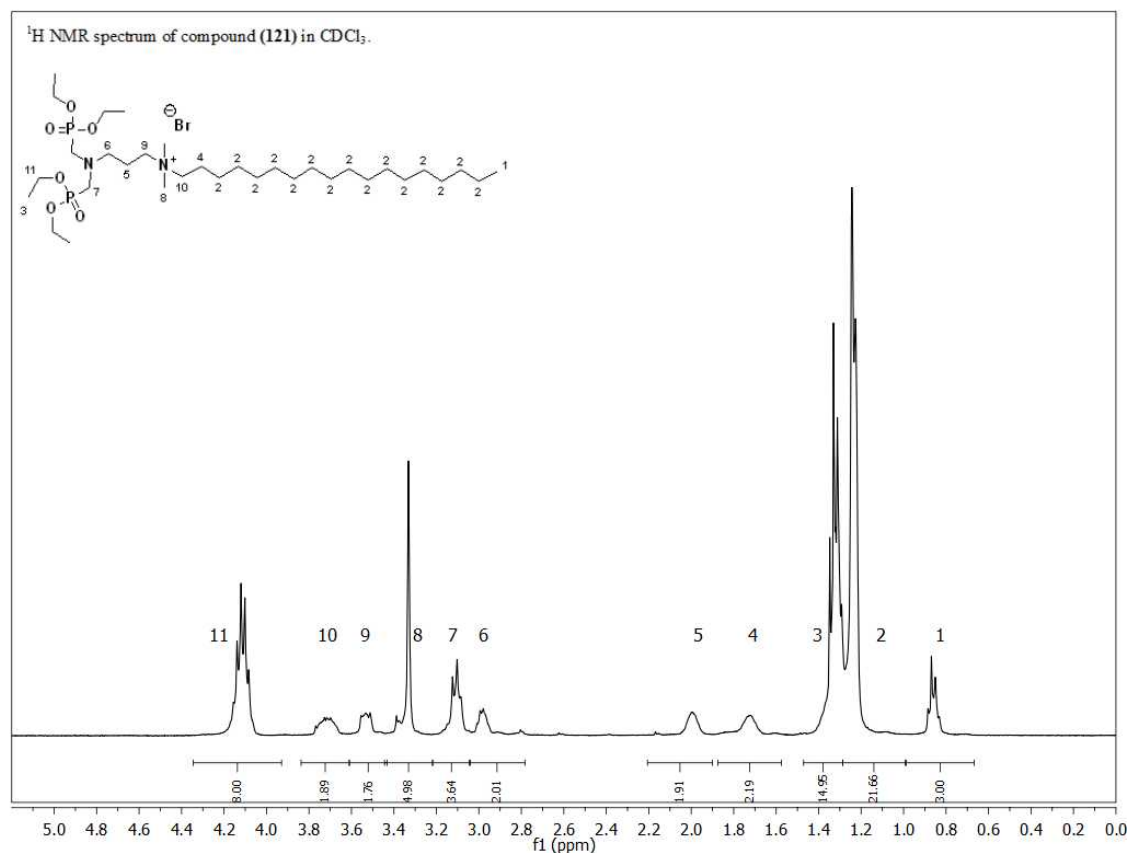
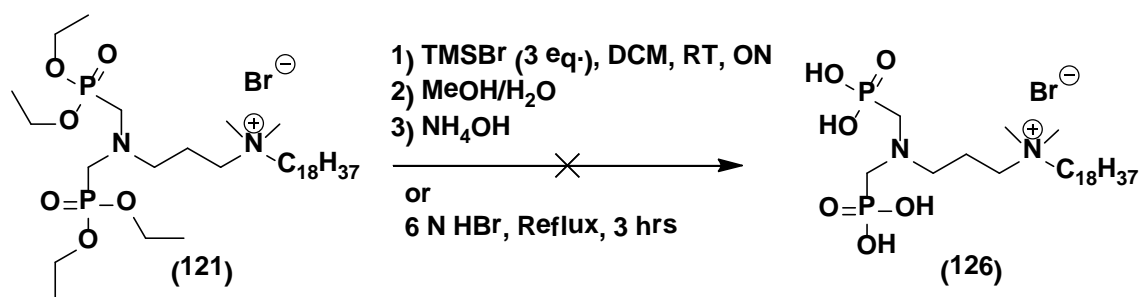


Figure 2.18: ¹H NMR (CDCl₃) spectrum of α -ABPQA **121**.

Dealkylation of ester **121** to the desired α -bisphosphonic acid **126** was unsuccessful with both HBr and TMSBr (Scheme 2.21, Figure 2.19, a and b) and resulted in a mixture of products by ³¹P NMR (D₂O). The TMSBr reaction seemed promising at first by ³¹P NMR with a major peak at ~ 10 ppm attributed to the TMS ester (Figure 2.19, b). However, after hydrolysis with H₂O and evaporation of volatiles, the product was insoluble in both D₂O and CDCl₃. After treatment of **126** with 1 eq. of NaOH to make the sodium salt, decomposition was observed with three unidentified ³¹P NMR (D₂O) signals at δ ~ 21, 16 and 6.5 ppm resulting in an inseparable mixture of products (Figure 2.19, c). According to Guerrero, instead of the phosphonic acid, phosphonate esters may also bind to metal oxide surfaces with the loss of an ethyl group.²⁰⁷



Scheme 2.21: Attempted didealkylation of α -aminobisphosphonate QAC **121**.

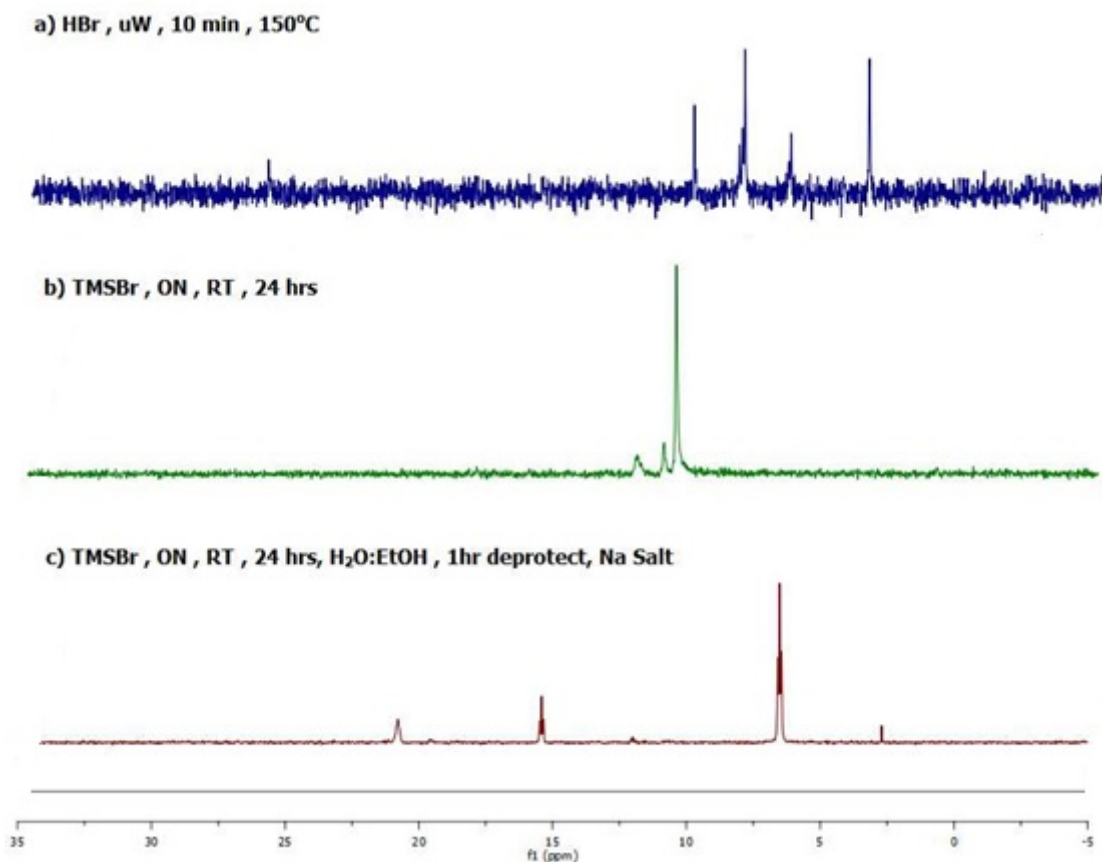
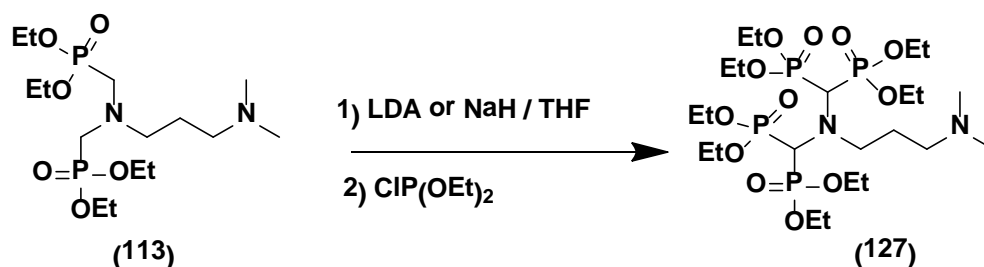


Figure 2.19: ³¹P NMR (CDCl₃) reaction monitoring of **121** cleavage with HBr and TMSBr.

Synthesis of tetraphosphonate **127** was attempted from α -bisphosphonate **113** after deprotonation with a strong base (LDA or NaH) and substitution with $\text{ClP}(\text{OEt})_2$ (Scheme 2.22). Monitoring the reaction with LDA as base at -10°C after 10 min by ^{31}P NMR spectroscopy (CDCl_3) showed no product **127** formation (Figure 2.20 a). Employing the same conditions as above but allowing the reaction to stir for 60 min at RT and extracting into EtOAc recovered mainly unreacted SM **113**. Switching to NaH made no difference and no reaction took place (Figure 2.20 c). Allowing the deprotonation to occur at -78°C with LDA prior to the addition of $\text{ClP}(\text{OEt})_2$ seemed promising with consumption of **113** by ^{31}P NMR spectroscopy (Figure 2.20 e), however after extraction into EtOAc and column chromatography of the reaction mixture no product corresponding to **127** was eluted.



Scheme 2.22: Tetraphosphonate **127** by C-P alkylation of **113**.

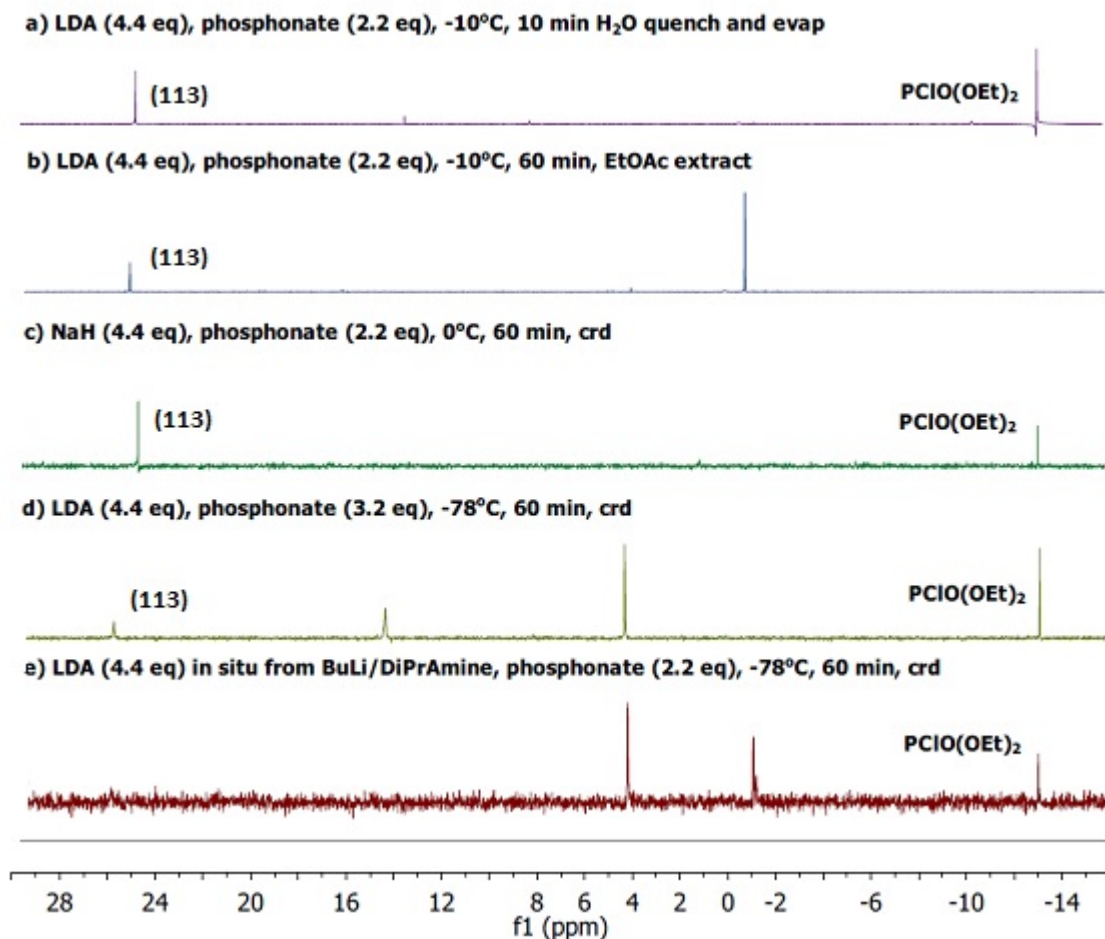
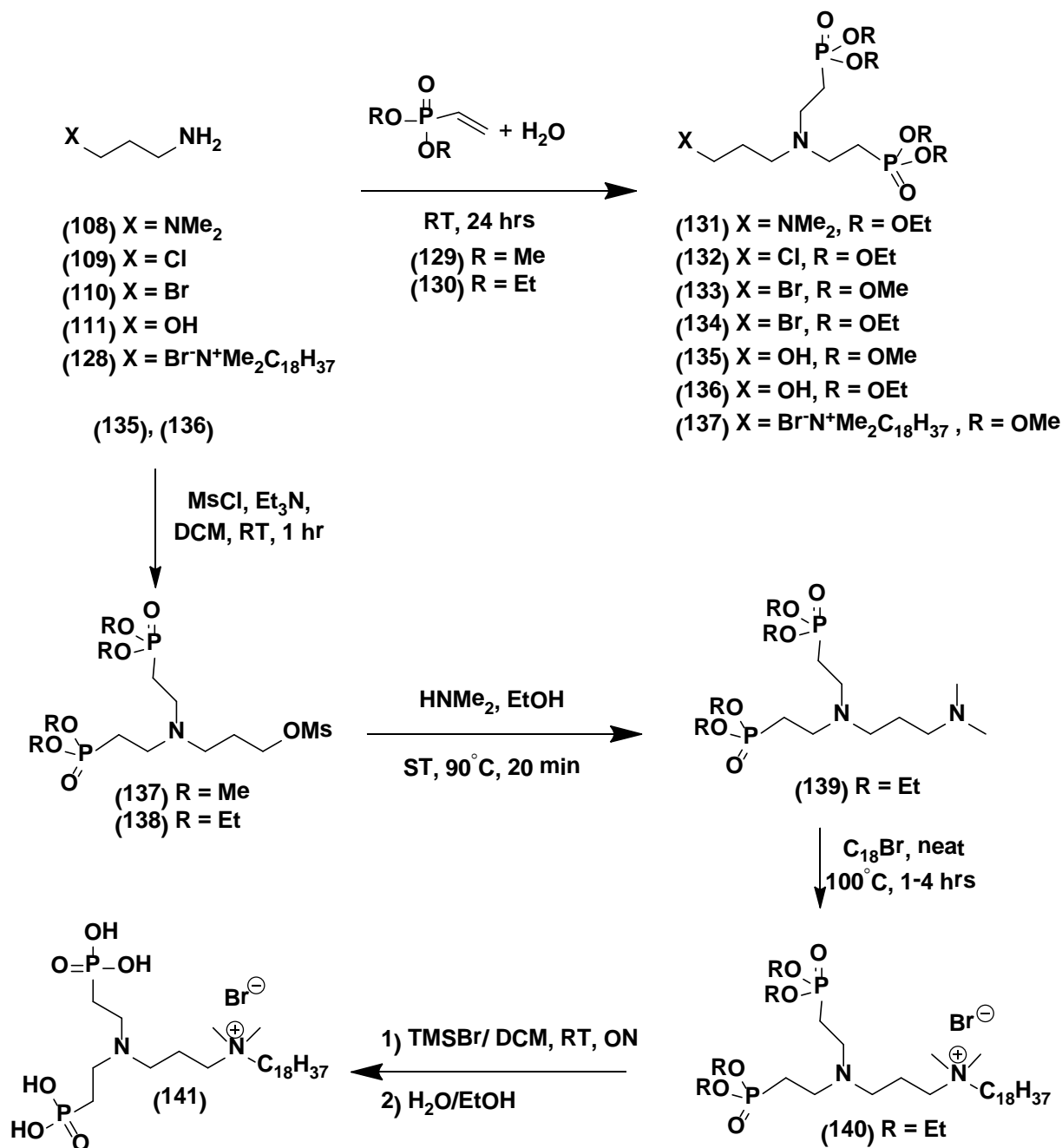


Figure 2.20: ³¹P NMR (CDCl₃) reaction monitoring of tetraphosphonate **127**.

2.1.2.6 β-Aminobisphosphonic Acids QAC Antimicrobials (β-ABPQA)

Inspired by Matveeva's work²⁰⁸ on the H₂O based synthesis of β-aminobisphosphonates, the reaction was explored with various bi-functional amines in order to prepare precursor halo or dimethylamino substituted β-aminobisphosphonates necessary for quaternization (Scheme 2.23, Table 2.10). Similarly to α-aminobisphosphonates (Section 2.1.2.5), the most direct way to prepare *N,N*-dimethyl or halo β-aminobisphosphonates is the addition of vinyl phosphonate to amines **108-110**. The reaction progress was monitored by NMR (³¹P, D₂O) and reaction

completeness was ascertained with the consumption of dialkylphosphite **129** ($\delta = 19.97$ to 23.71 ppm) and **130** ($\delta = 18.10$ ppm to 20.85 ppm, Table 2.10).



Scheme 2.23: Optimized synthetic route to β -aminobisphosphonate QAC **141**.

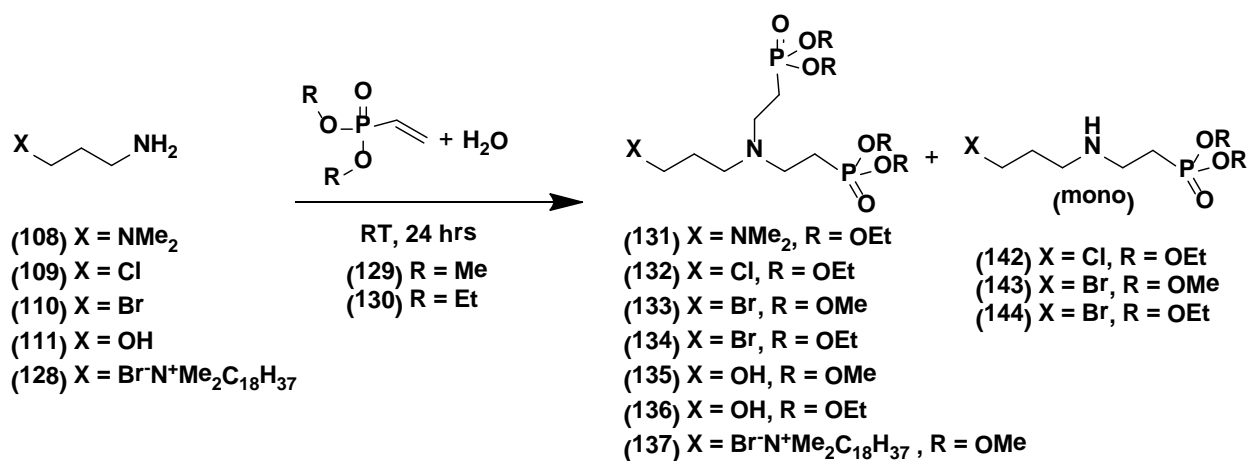


Table 2.10: Optimization of the Michael addition to β-aminobisphosphonates QAC **131-144**.

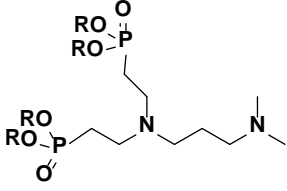
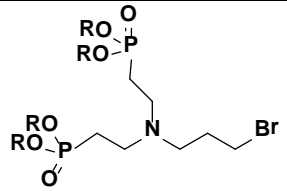
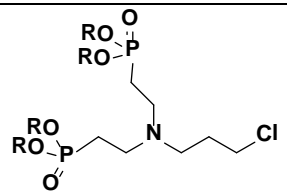
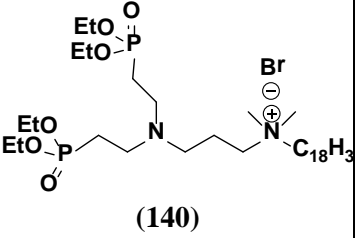
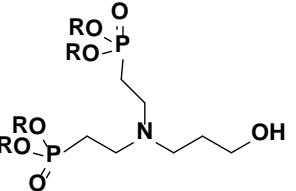
Rxn. Comp. (%) by (³¹ P NMR, D ₂ O)							
Entry	Reactant	SM	Base	Time (hrs)	Temp . (°C)	SM (%/ppm)	PRD. (%/ppm)
i	 (131)	129 + 108	n/a	3	100	0	n/a
ii		129 + 108	n/a	24	RT	36/23.52	55/36.18
iii		129 + 108	n/a	48	RT	30/23.47	59/36.14
iv	 (133-134)	129 + 110	NaOH	3	RT	40/23.56	5/36.16
v		129 + 110	NaOH	24	RT	20*/23.51	10/36.16
vi*		130 + 110	NaOH	24	RT	23.51	n/a
vii	 (132)	130 + 109	DIPEA	64	RT	21*/20.85	31/33.36
viii		130 + 109	NaOMe	48	RT	17/20.85	50/33.40

Table 2.10 continued					Rxn. Comp. (%) by (^{31}P NMR, D_2O)		
Entry	Reactant	SM	Base	Time (hrs)	Temp. ($^{\circ}\text{C}$)	SM (%/ppm)	PRD. (%/ppm)
ix	 <p>(140)</p>	130 + 128	n/a	48	RT	51/23.68	49/35.41
x**	 <p>(135-136)</p>	129 + 111	n/a	24	RT	1/23.71	100/36.39
xi**		129 + 111	n/a	24	RT	1/24.54	100/36.50
xii**		130 + 111	n/a	24	RT	10/20.82	90/30.00

* excess NaOH used (1.2 eq.), ** excess **129-130** was used. n/a: multiple peaks were observed and none of which corresponded to the product.

In most cases the addition to amines **108-110** and the quat amine **128** resulted in a mixture containing the product with unreacted starting material (Table 2.10, Entries i-ix) or in the case of the halo amines with a mixture of mono- and bis- β -aminophosphonates identified by ^{31}P NMR (Figure 2.21 and Table 2.10, Entries iv, v, vii, viii). The added base used (Table 2.10, Entries iv-viii) to freebase the amine salts **107A**, **107B** hindered the bis Michael addition to vinylphosphonate. Even when the based/amine salt was added in a 0.9/1 ratio, the reaction still resulted in an inseparable mixture of mono and bisphosphonates along with unreacted SM in the following ratios: (Figure 2.21 and Table 2.10, Entry v (1.0:0.12:0.32), Entry vii (1.0:0.65:0.43), Entry viii (0.66:1.0:0.34). Surprisingly, the quat amine **128** having no basic functionalities gave a low yield of product **140** with considerable unreacted starting material (~1:1 ratio) and was left unpurified (Figure 2.21 and Table 2.10, Entry ix). As a result bis β -aminobisphosphonates were

successfully prepared by employing a longer indirect method that involving 3-amino-1-propanol **111**. When the reaction was performed with **111** and either dimethyl- or diethylvinylphosphonate (Table 2.10, Entries x-xii) a clean reaction was observed with complete consumption of the starting material. Excess vinylphosphonate was removed by column chromatography to give pure **135** or **136** (Figure 2.21 and Table 2.10, Entries x-xii).

Further functional group transformations were necessary to activate the alcohol **111** into a better leaving group through mesylation followed by substitution with excess dimethylamine and quaternization to give **140** (Scheme 2.23). The mesyl chloride **137** intermediate decomposed over time at RT and was reacted directly (Figure 2.22). Finally, quaternization with bromooctadecane gave quat **140** that was isolated after column chromatography along with 10% of impurities (27.6 and 26.8 ppm by ^{31}P NMR, CDCl_3), (Figure 2.23, Experimental, Section 5.7.0). No dealkylation of **140** to the phosphonic acid **141** was attempted at this time.

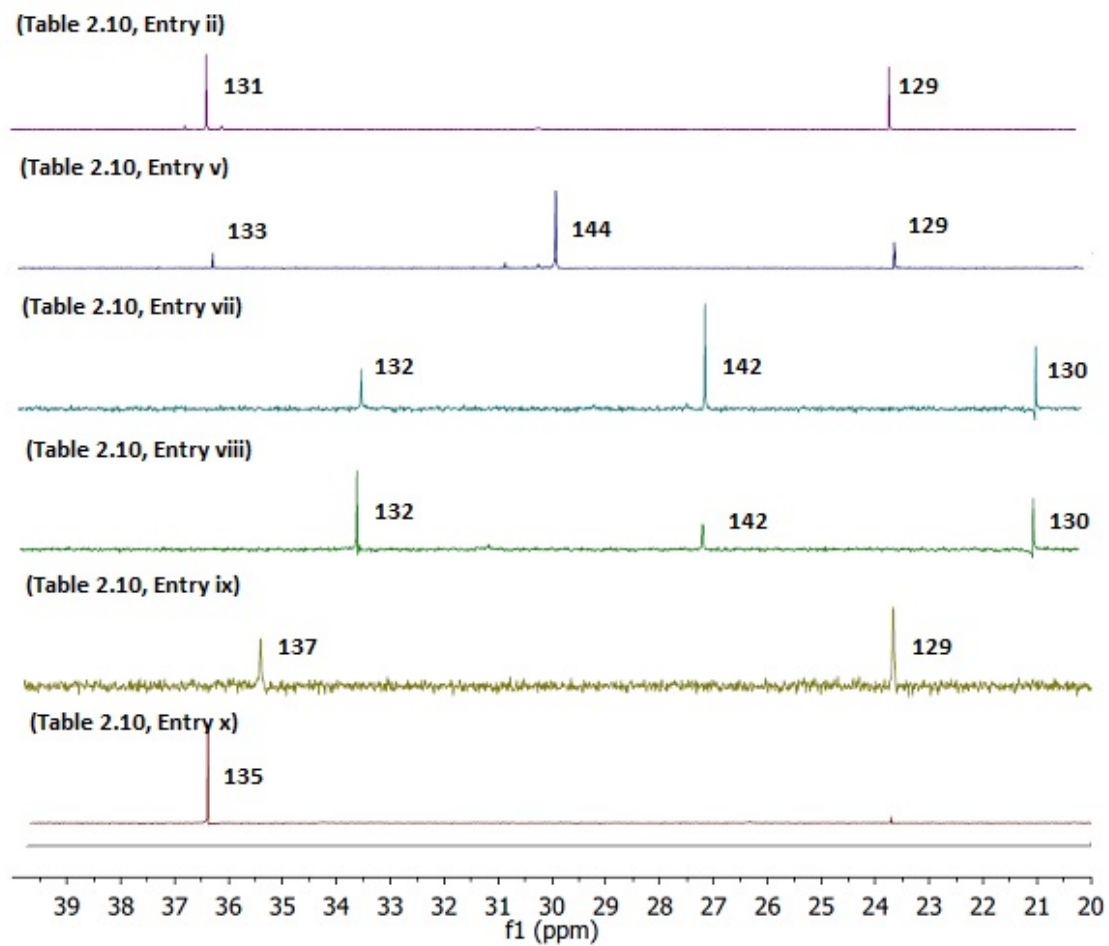


Figure 2.21: Reaction monitoring of Michael addition reactions by ^{31}P NMR (D_2O).

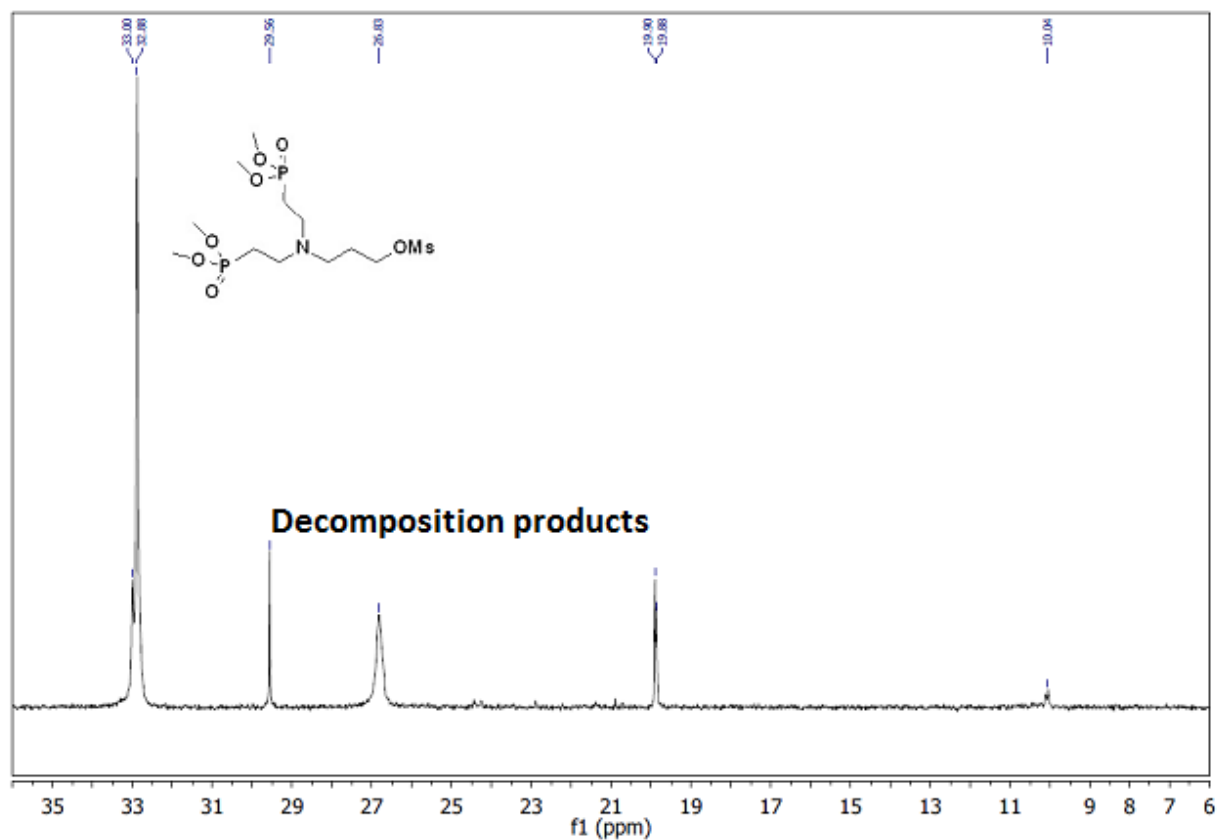


Figure 2.22: Decomposition of **132** at RT by ^{31}P NMR (CDCl_3).

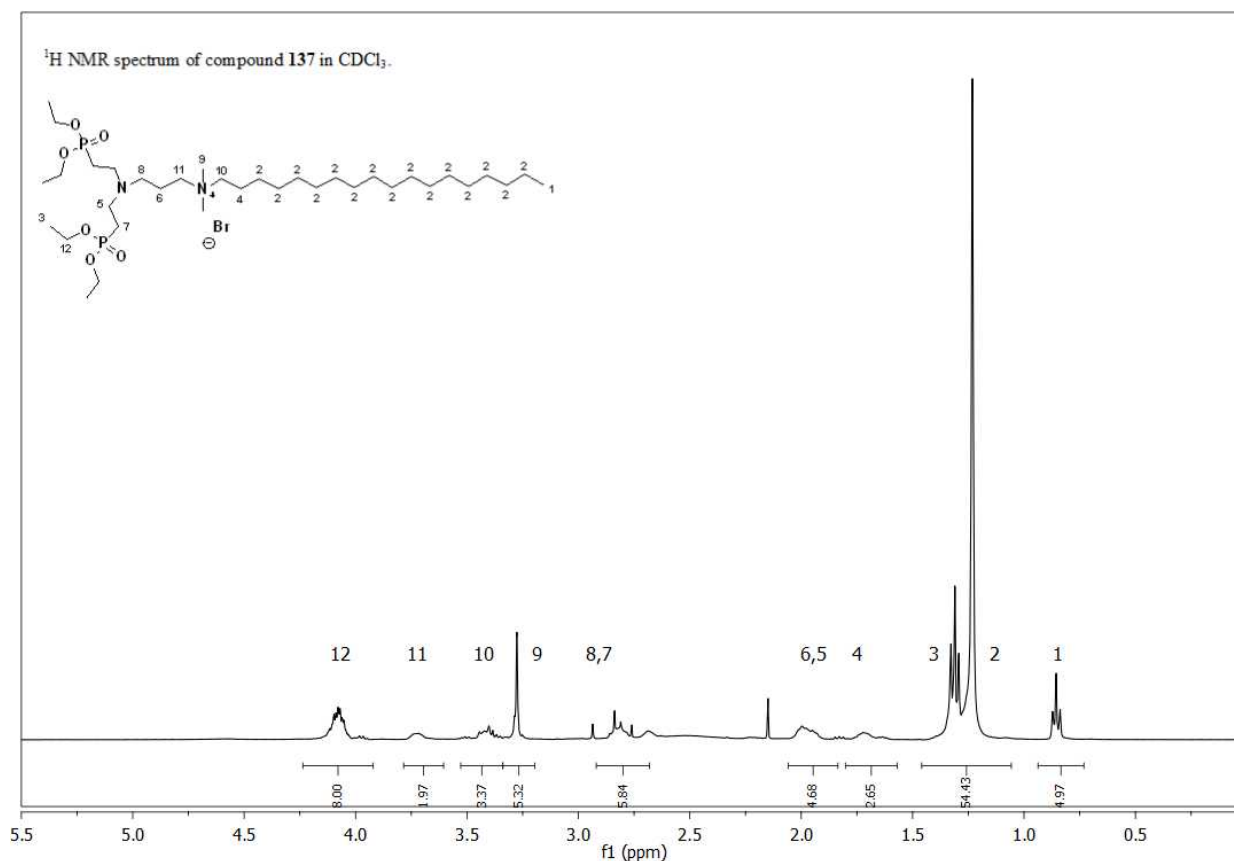


Figure 2.23: ¹H NMR (CDCl₃) spectrum of β-ABPQA **140**.

The commercially available starting material vinyl phosphonates **129-130** were quite expensive to purchase (~ \$213/5mL, 95% for R₁ = Et, S-A) and as a result, all of the optimization reactions were performed on a very small scale (~ 1 mmol). Preparation of **130** was attempted from **15** and KOH in EtOH following literature procedures (Section 2.1.2.1).²⁰⁹ However, the major product was difficult to purify by distillation from unreacted **15** and the by-product, diethyl (2-hydroxyethyl)phosphonate, resulting from the competing elimination reaction (Figure 2.24).

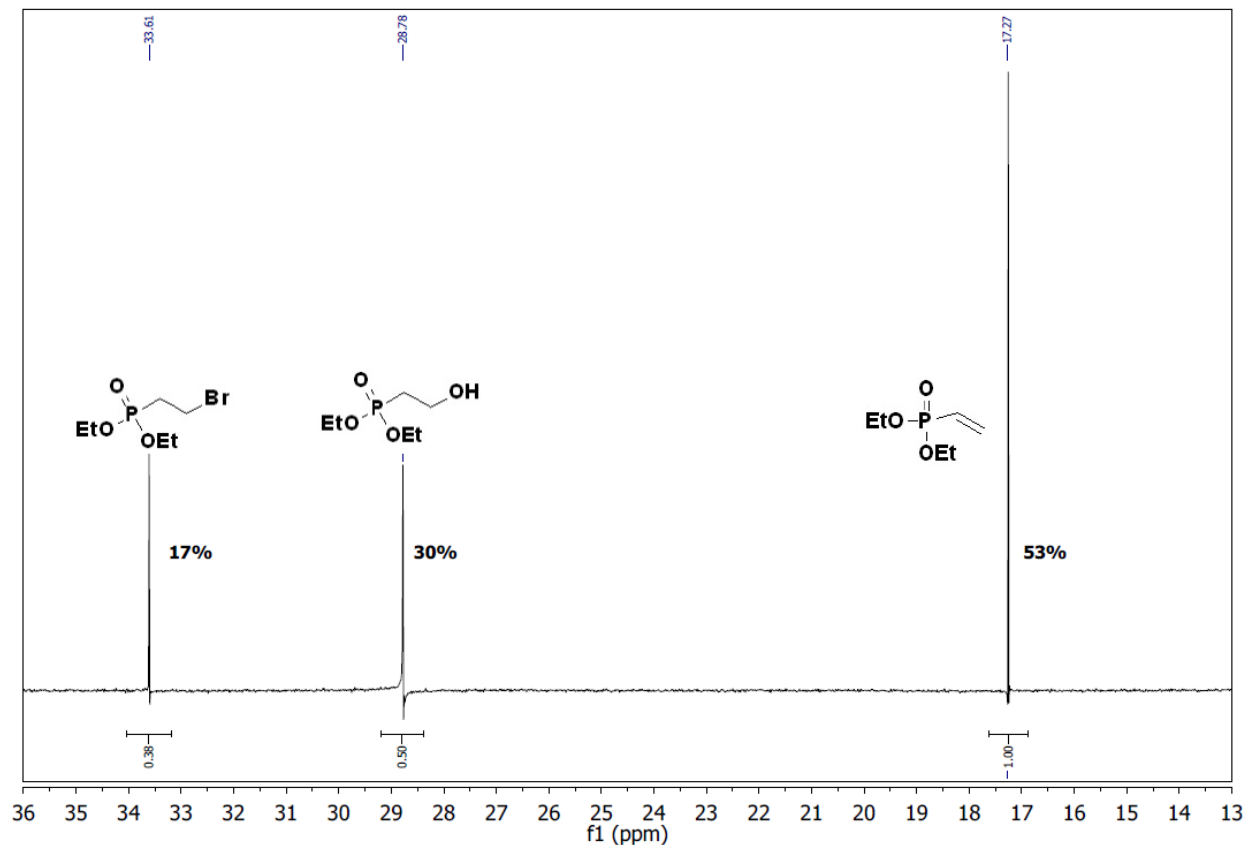
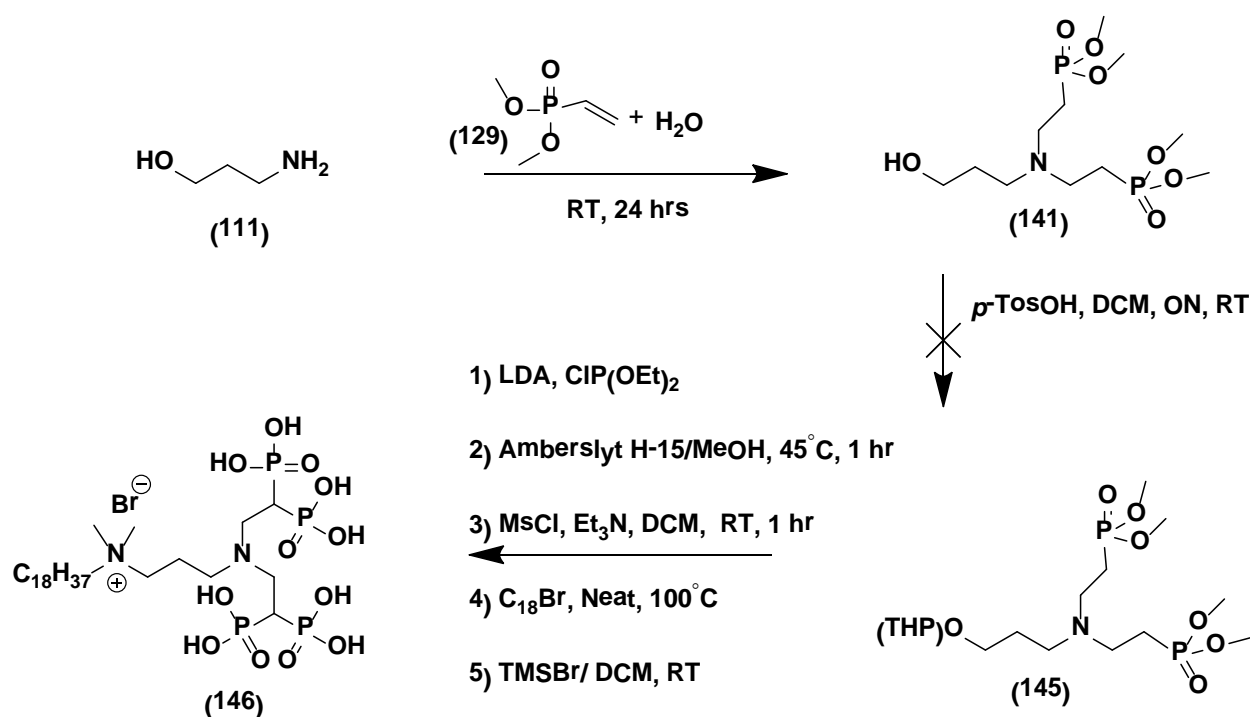


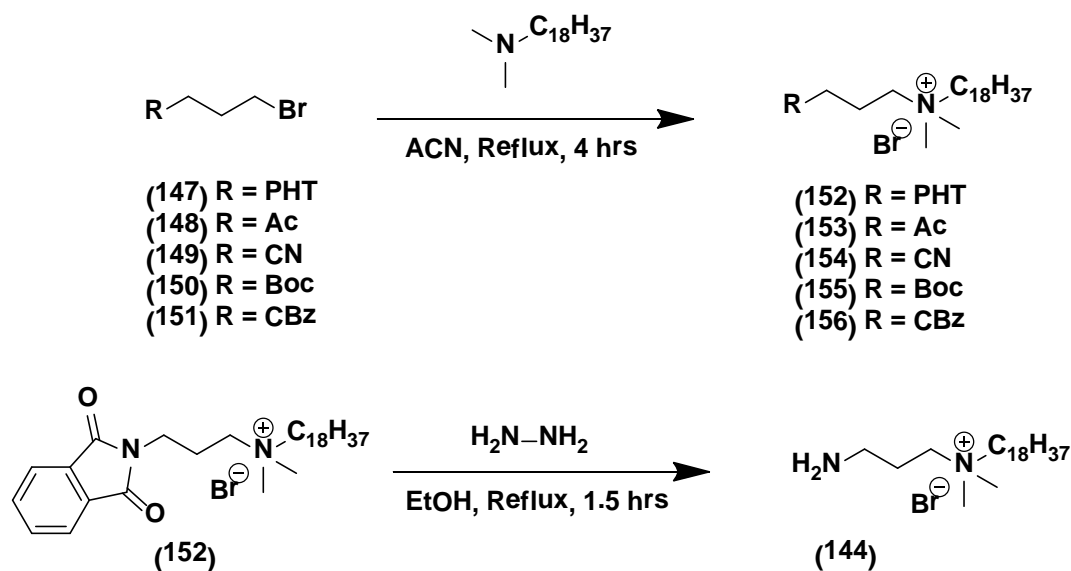
Figure 2.24: Preparation of diethylvinylphosphonate **130** (crude mixture by ^{31}P NMR (CDCl_3)).

Preparation of tetraphosphonates starting from β -aminobisphosphonate **141** according to (Scheme 2.24) was also targeted but abandoned. It was difficult to isolate the THP protected **145** intermediate even after employing an excess of *p*-TosOH catalyst. As a result no further reactions leading to **146** were possible.



Scheme 2.24: Attempted synthetic route to tetraphosphonate QAC **146** from β -amino bisphosphonate **141**.

The amine QAC precursor **144** utilized in the Michael addition was prepared via the Menshutkin reaction from amine protected alkylhalides **147-151** and *N,N*-dimethyloctadecyl amine in good yields. However, only the CBz **156** and PHT **152** protecting groups were successfully deprotected to the free quat amine **144** with H₂/PdC and excess hydrazine hydrate respectively (Scheme 2.25). There is only one literature report describing the preparation of **144** from the amide **153** after basic hydrolysis. However in our hands, extraction of **144** into CHCl₃ upon purification was problematic and led to inseparable emulsions and low product recovery. Figure 2.25 shows the ¹H NMR spectrum (D₂O) of **144** prepared from hydrazine cleavage of **152**.



Scheme 2.25: Preparation of amine quat **144**.

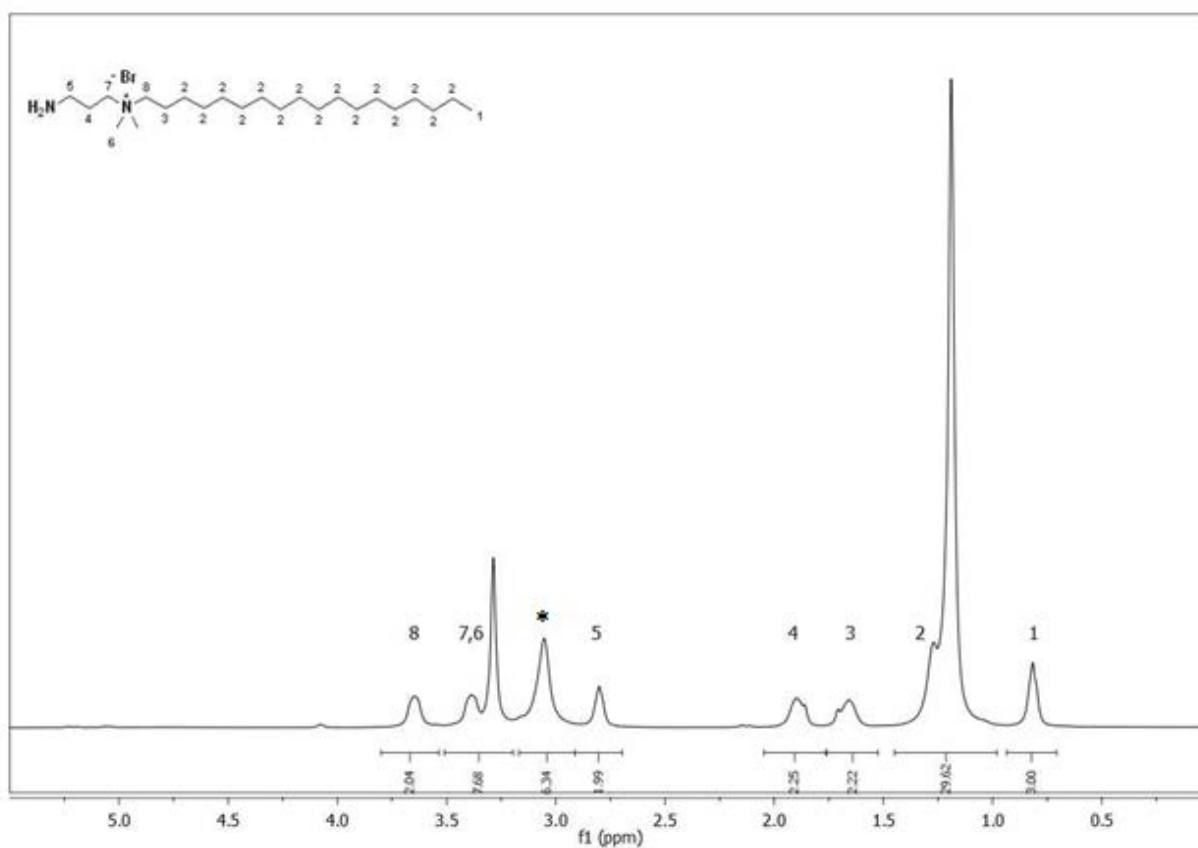
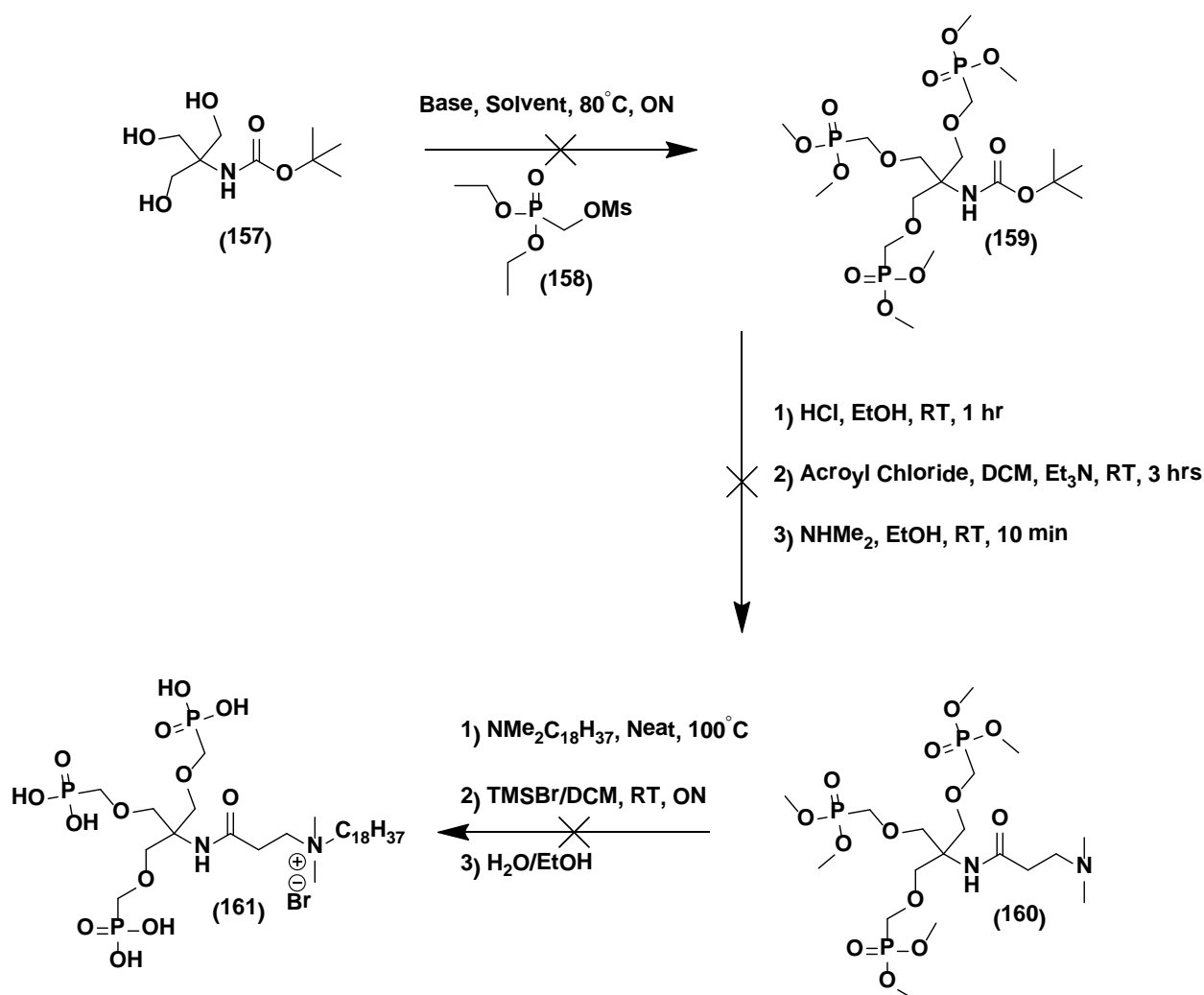


Figure 2.25: ¹H NMR (CDCl₃) spectrum of **144** after N₂H₄ deprotection (* unidentified impurity).

2.1.2.7 Tridentate Phosphonic Acid QAC Antimicrobials (TPQA)

Synthesis of novel multidentate tris- α -hydroxy phosphonic acid, tris- β -hydroxy phosphonic acid and or tris- γ -hydroxy phosphonic acid QAC was explored with the inexpensive and commercially available polyhydroxy 2-amino-2-hydroxymethyl-propane-1,3-diol (tris) scaffold. Prior to installing the phosphonate group from the hydroxyl groups, the primary amine from tris was BOC protected as **157** and used to prepare tris- α -hydroxy phosphonic acid (Scheme 2.26), tris- β -hydroxy phosphonic acid (Scheme 2.27 a) and tris- γ -hydroxy phosphonic acid QAC (Scheme 2.28). Meanwhile, the tris-*N,N*-dimethylacrylamide **163** was also tried in an attempt to prepare tris- β -hydroxy phosphonic acid but was unsuccessful (Scheme 2.27 b).

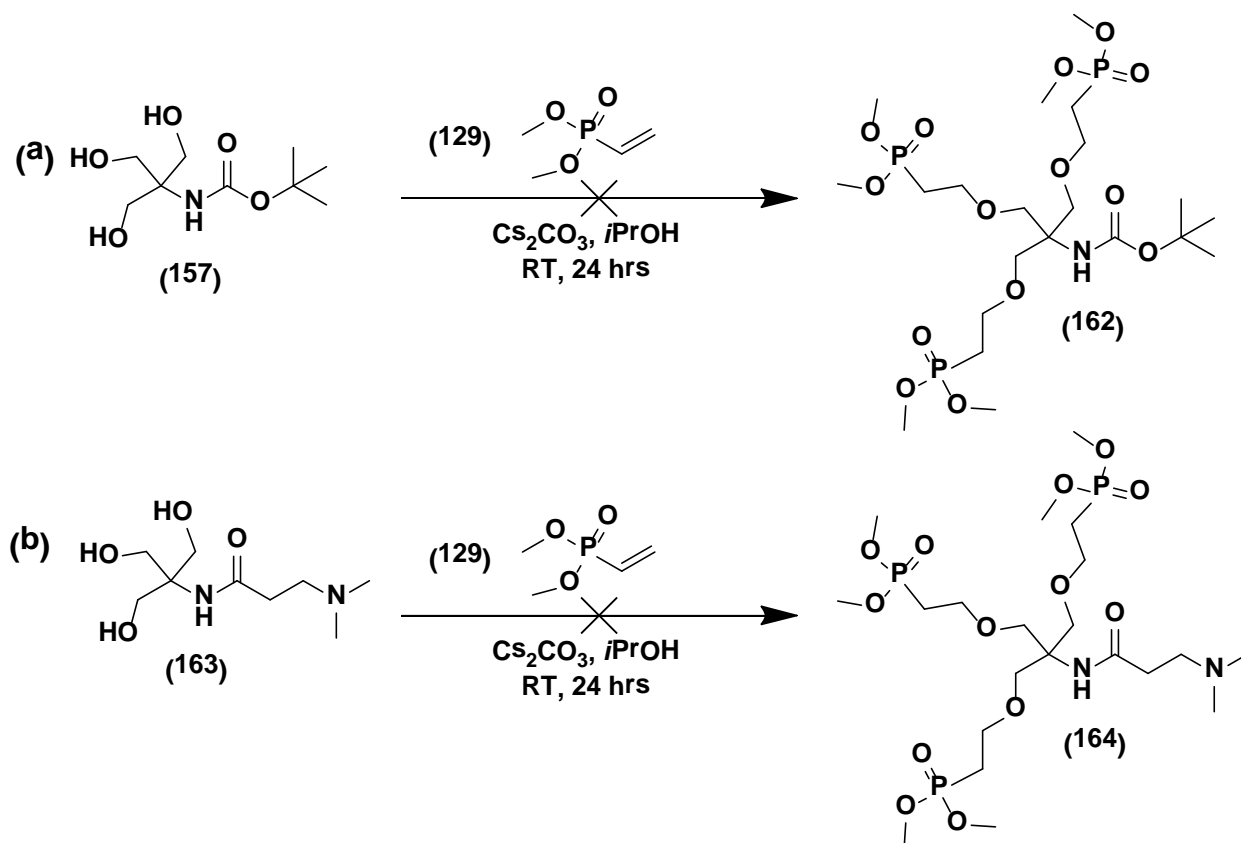
First, in the preparation of tris- α -hydroxy phosphonic acid **161**, the hydroxyl groups from tris-BOC were subjected to nucleophilic substitution with mesylphosphonate **158** according to the first step in Scheme 2.26. Unfortunately, the first step failed and none of the three nucleophilic OH's substituted the mesylphosphonate **158** with the following solvent/base combinations: NaH/DMF, KO*t*-Bu/DMF, KO*t*-Bu/*t*-BuOH. It is possible that steric hindrance along with the presence of multiple nucleophiles and insolubility of tris-BOC in *t*-BuOH played a negative role on the reaction outcome.



Scheme 2.26: Proposed synthesis of tris- α -hydroxyphosphonate QAC **161**.

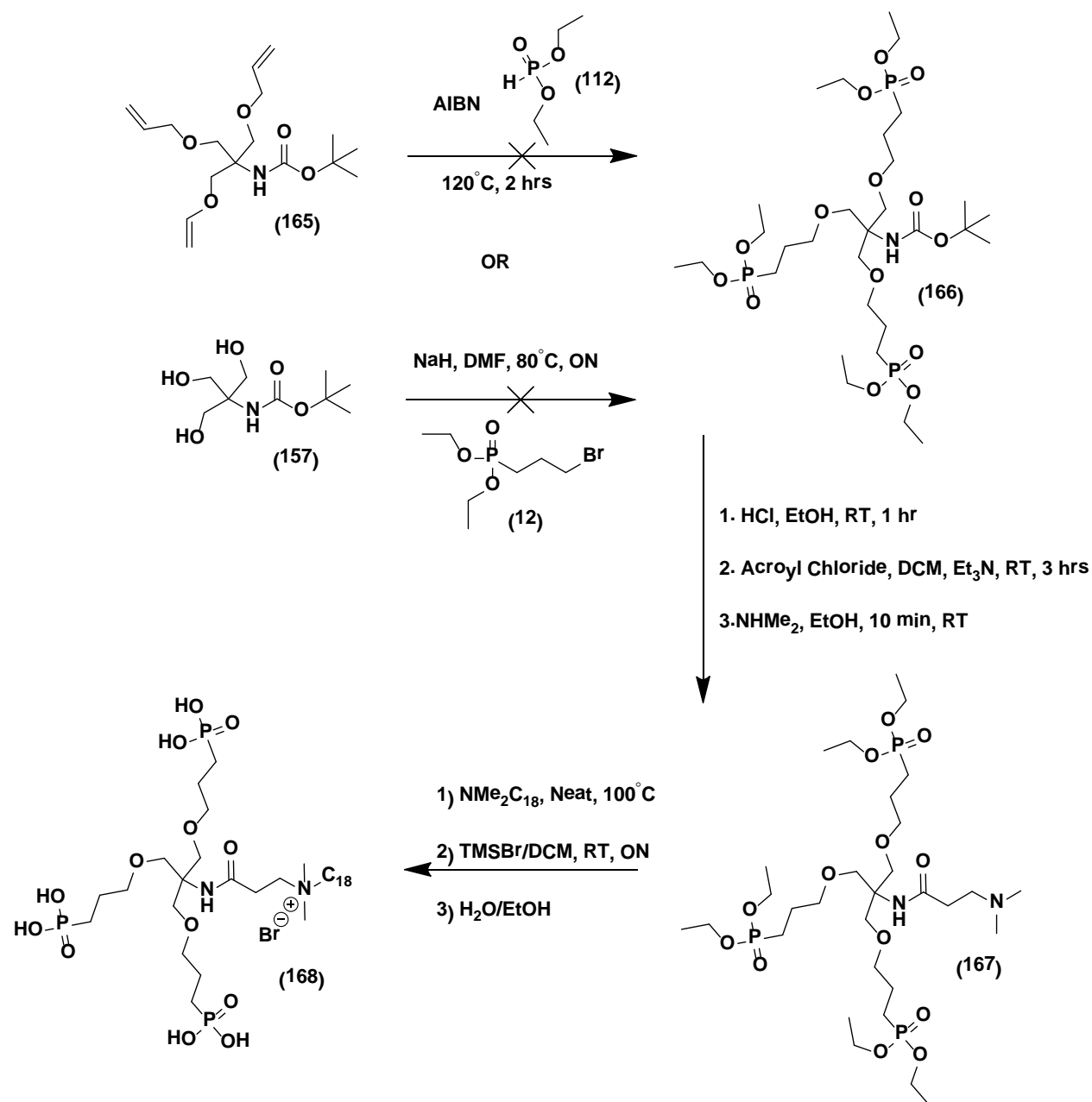
Next, tris- β -hydroxyphosphonate QAC's **162** and **164** were targeted via the *oxa*-Michael addition of the three hydroxy groups from both tris-BOC **157** and tris *N,N*-dimethylacrylamide **163** onto dimethylvinyl phosphonate according to Scheme 2.27. As was the case with tri- α -hydroxyphosphonate QAC, both starting materials were inert in this reaction and no addition products were observed by TLC and NMR (^{31}P , ^1H , D_2O). Once again insolubility and steric factors were likely the result of the failed addition reaction. In order to increase solubility and decrease the steric strain of the three hydroxyl groups in close proximity to each other the

synthesis of tri- γ -hydroxyphosphonate QAC was explored in DMF and a longer carbon spacer (C_3) was used between the phosphonate and oxygen atoms.



Scheme 2.27: Attempted synthesis of precursors **162** and **164** to tris- β -hydroxyphosphonate QAC's.

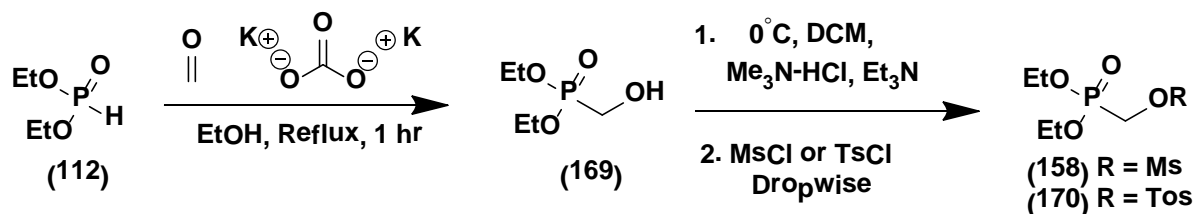
The conversion of BOC protected trivinyl derivative **165** and tris-BOC **157** to tri- γ -hydroxyphosphonate was attempted according to Scheme 2.28. However, like the case with the preparation of tri- α -hydroxyphosphonate and tri- β -hydroxyphosphonate QAC's, the first step of the reaction also failed to add the desired phosphonate groups onto these starting materials. As a result, no further reactions with these starting materials was pursued.



Scheme 2.28: Attempted synthesis of tris- γ -hydroxyphosphonate QAC **168**.

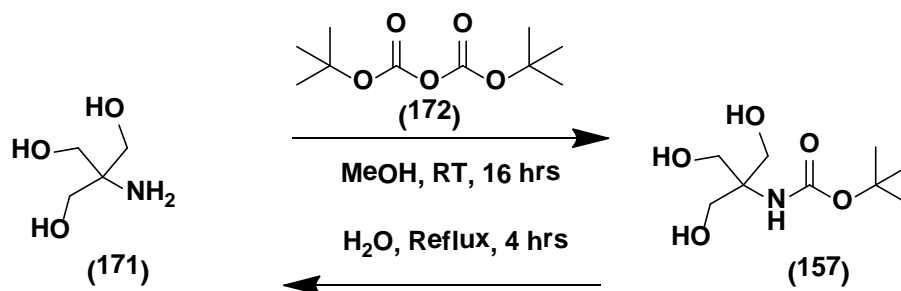
Commercially unavailable mesyl phosphonate **158** utilized in the proposed synthesis of tris- α -hydroxyphosphonate QAC's **161** and **168** (Scheme 2.26) was prepared in > 90% yield in two steps via the addition of dialkylphosphite to paraformaldehyde forming α -hydroxy phosphonate **158** followed by sulfonation with catalytic $\text{Me}_3\text{N}\cdot\text{HCl}$ (Scheme 2.29). The tosyl

phosphonate **170** was also prepared in an analogous fashion, but never utilized in any of the reactions involving the tris scaffold.



Scheme 2.29: Preparation of mesyl **158** and tosyl phosphonate **170**.

BOC protection of the commercially available tris **171** followed by recrystallization from EtOAc gave precursor **157** in good yield (Scheme 2.30). A neutral BOC deprotection procedure that could be applied to any of the envisioned tris-BOC phosphonate intermediates **159**, **162**, **166** was identified using boiling H_2O that was successfully used in deprotecting **157** to the free amine (Scheme 2.30). According to Wang *et al.*, at elevated temperatures H_2O plays the role of a dual acid/base catalyst resulting in the free neutral amine whereas the BOC group breaks down to the easily removable by products, *t*-BuOH and CO_2 (Figure 2.26).²¹⁰



Scheme 2.30: Preparation of tris-BOC **157** and deprotection in boiling H_2O to tris **171**.

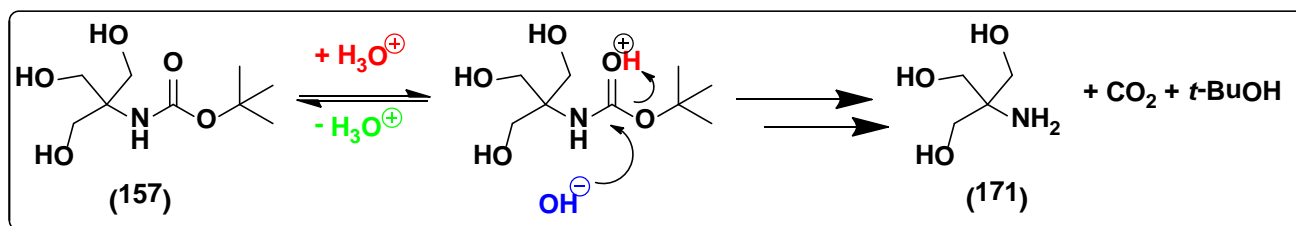
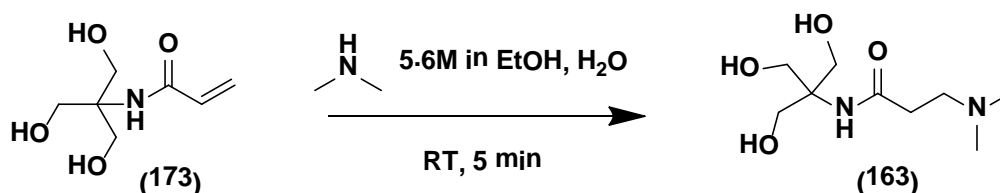


Figure 2.26: Mechanism of boiling H_2O BOC deprotection.²¹⁰

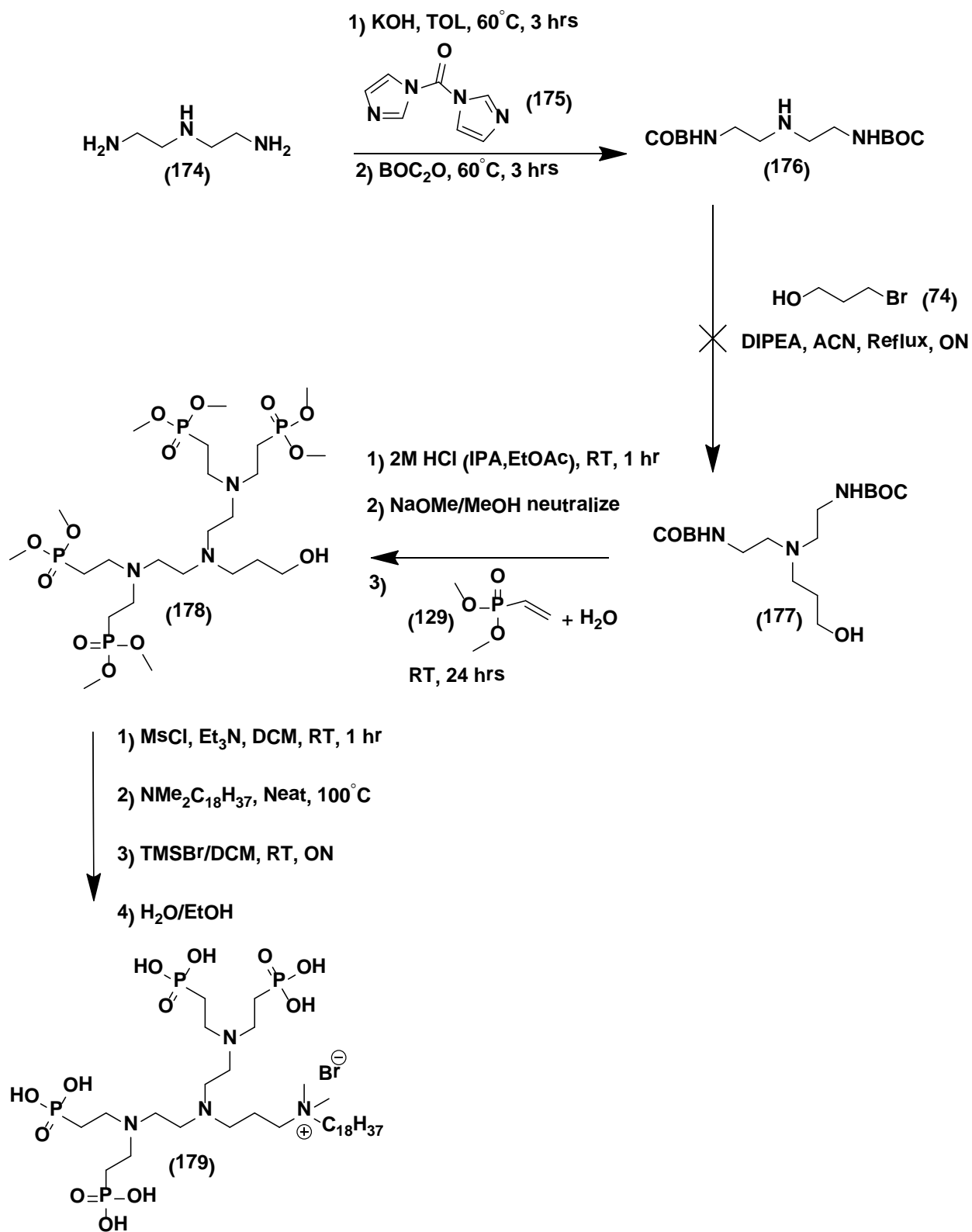
Lastly, precursor **163**, a new compound was prepared from the commercially available tris acrylamine **173**, and was synthesized via the rapid Michael addition with dimethyl amine (5 min by TLC) according to Scheme 2.31. Quaternization of **163** was attempted with $\text{BrC}_{18}\text{H}_{37}$ in DMF, but no clean NMR could be obtained at this time.



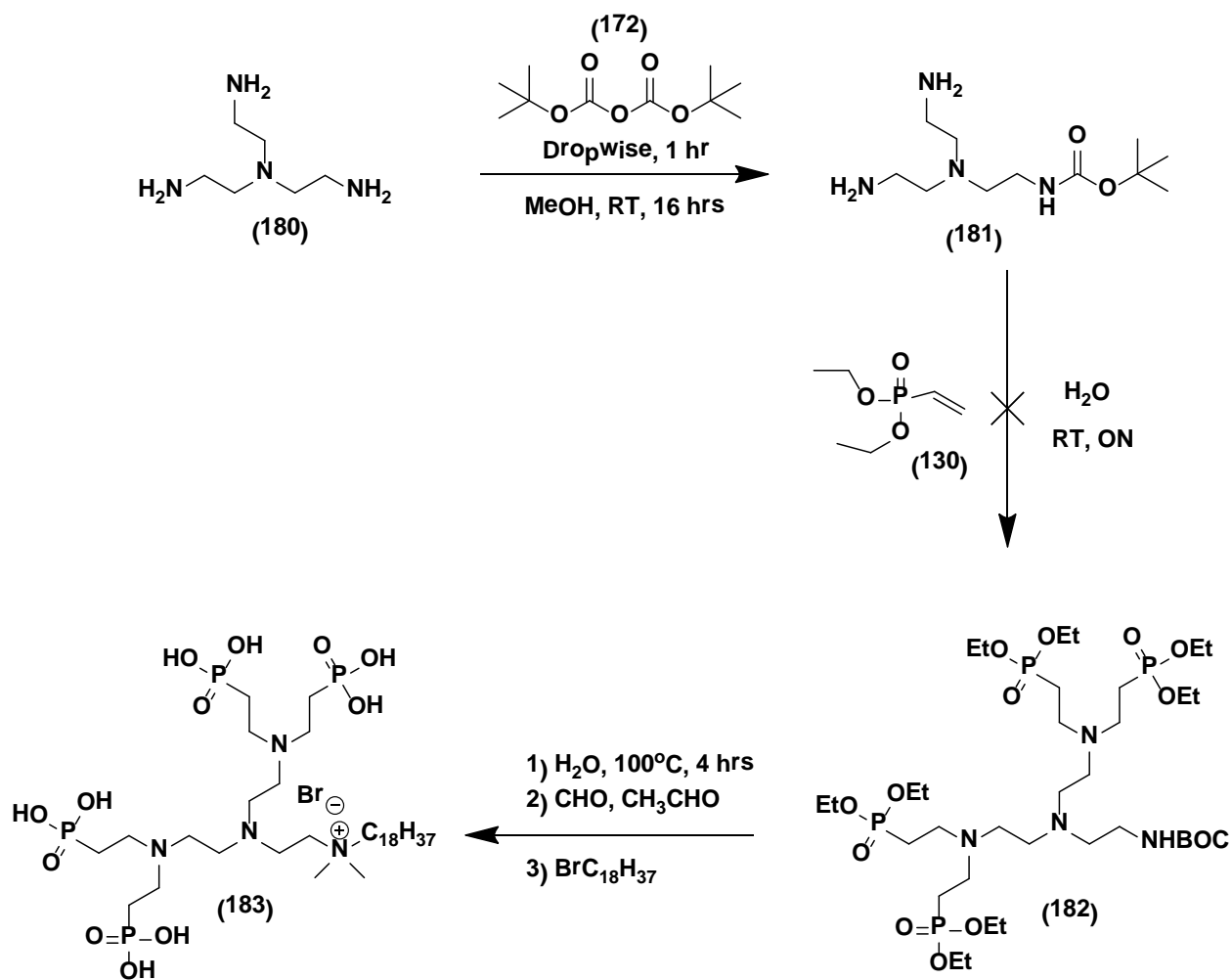
Scheme 2.31: Michael addition of HNMe_2 to tris acrylamide **173**.²¹¹

2.1.2.8 Amine Scaffolds for Tetra Phosphonic Acid QAC Antimicrobials

Synthesis of tetradentate β -amino phosphonate QAC **179** and **183** were targeted via the Michael addition of two free primary amines onto **129** after selective BOC protection of commercially available triamine building blocks **174** and **180** according to Schemes 2.32 and 2.33. Compound **177** decomposed upon BOC deprotection, meanwhile compound **181** was insoluble in H_2O . Since the Phospha-Micheal reaction requires H_2O to work, the addition of 50% EtOH to dissolve the starting material hampered the reaction and only SM was recovered after 72 hrs at RT by ^{31}P NMR. No further reactions were carried out with these polyamine scaffolds.



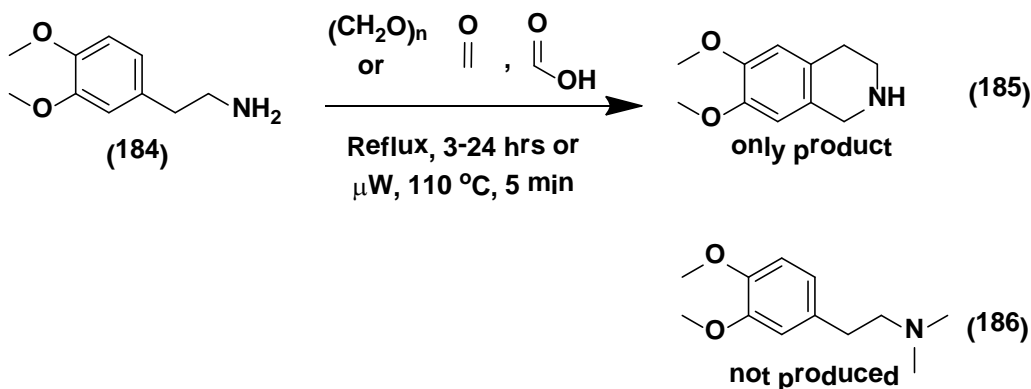
Scheme 2.32: Attempted preparation of tetradentate β -amino QAC **179**.



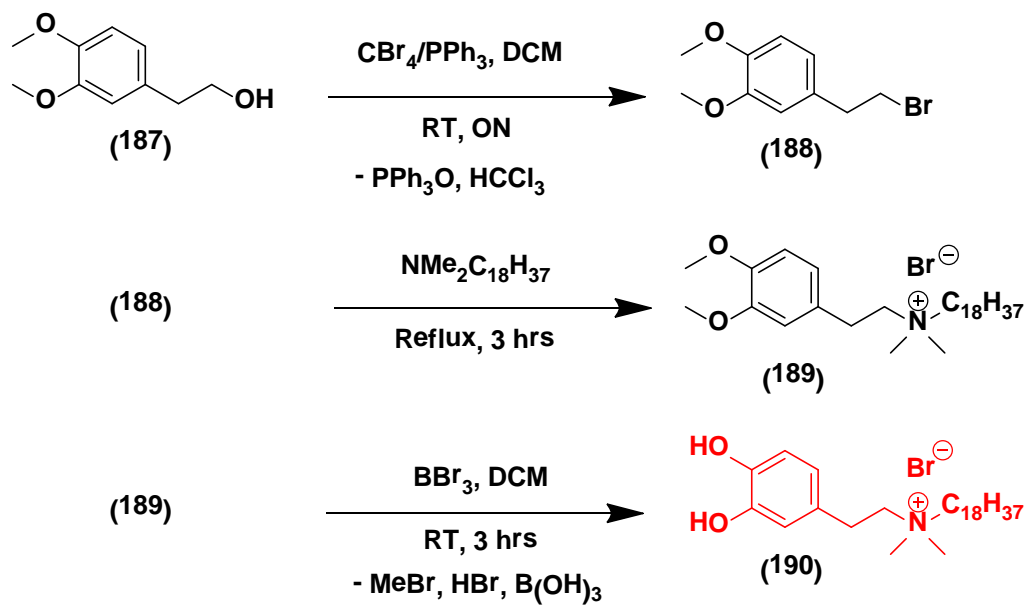
Scheme 2.33: Attempted preparation of tetradentate β -amino QAC **183**.

2.2 Catechol QAC

Research efforts have also focused on trying to design new types of quats from amino acids (AA) with functional linkers for attachment onto metal oxide surfaces. Since AA's are readily available in bulk at low cost and very biodegradable, QAC's based on AA's and their derivatives were envisioned as cheaper and more environmentally friendly source of antimicrobials in addition to the phosphonate QAC's. The target AA-QAC was anticipated from the dopamine amino acid analogue (L-DOPA) for binding to Ti and SS according to Scheme 2.34. Dopamine derivative **184** was the target starting material, but after problems with *N,N*-dimethylation of the primary amine resulting in only the tetrahydroisoquinolinone product **185** due to intramolecular cyclization (Scheme 2.34)²¹¹, it was decided to start from the commercially available OH derivative **187** and convert it to an alkyl halide **188** via the Appel reaction (Scheme 2.35). Thus, the bromo derivative **188** was quaternized with bromooctadecane but failed to crystallize as pure **189** and was analyzed as a mixture by NMR spectroscopy (¹H, ³¹P NMR (CDCl₃), Figure 2.27). No attempt at this time was made at removing the benzyl ethers groups to the target surface active catechol QAC **190**.



Scheme 2.34: Attempted *N,N*-dimethylation of dopamine **184**.²¹²



Scheme 2.35: Attempted preparation of catechol QAC 190.

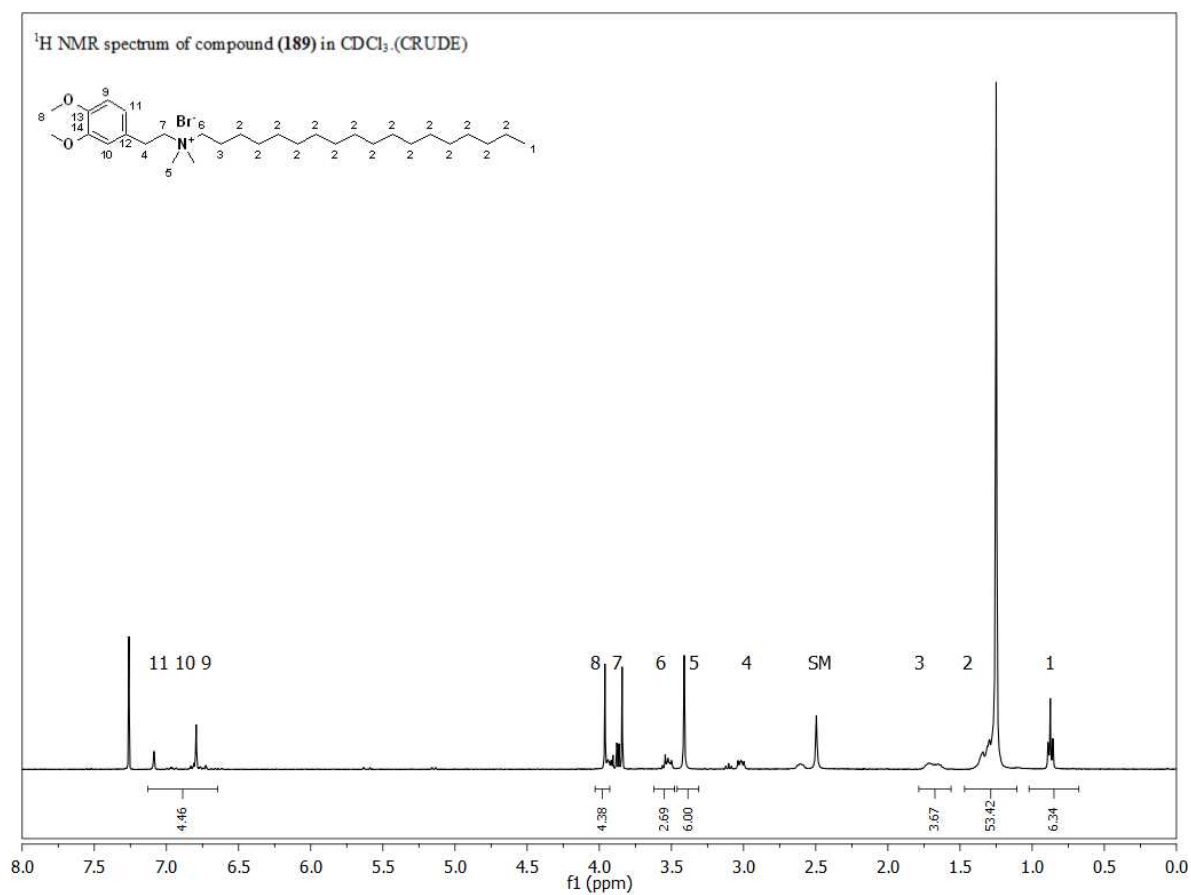


Figure 2.27: ¹H NMR (CDCl₃) spectrum of catechol QAC 189.

2.3 Organosulfur Based QAC

The thiol group represents another functional group suitable for anchoring antimicrobials onto metals. Replacement of the methoxysilane (SiOMe_3) of the commercially available Dow silane antimicrobial with a thiol (S-H) group anchors this QAC to select metal surfaces. The thiol quat forms self-assembled monolayers specifically on Au, Ag, Cu and other suitable metal surfaces while retaining the antimicrobial activity of the quaternary ammonium compound.

The possible synthetic routes identified in the literature for the preparation of the thiol-QAC largely involve commercially unavailable starting precursors (Scheme 2.36, Route iii) or require multiple preparative steps (Scheme 2.36, Route ia, ii). All of the routes feature a common nucleophilic substitution reaction between an alkylhalide (R-X) and a nitrogen nucleophile.

Due to commercial availability of 3-chloropropyl thioacetate **191** and the disulfide **197** routes ib and iv were chosen to prepare the target thiol QAC's **194** and **199**. In the thioacetate route, 3-chloropropylthioacetate was quaternized with **2** in high yield (90%) followed by cleavage with KOH/MeOH to give **194** in a 83% yield (Scheme 2.36, Route ia, Figure 2.28). Numerous attempts at obtaining a crystal structure of **194** were unsuccessful.

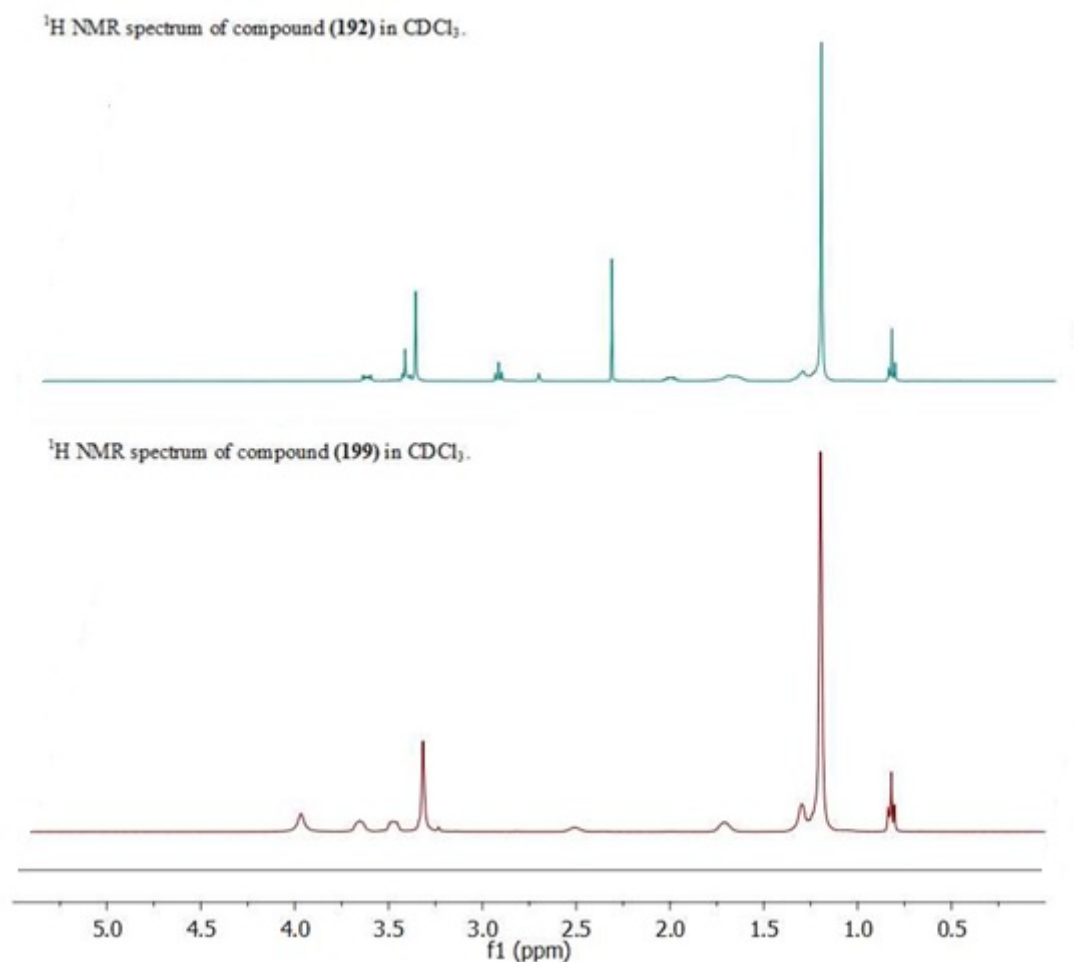
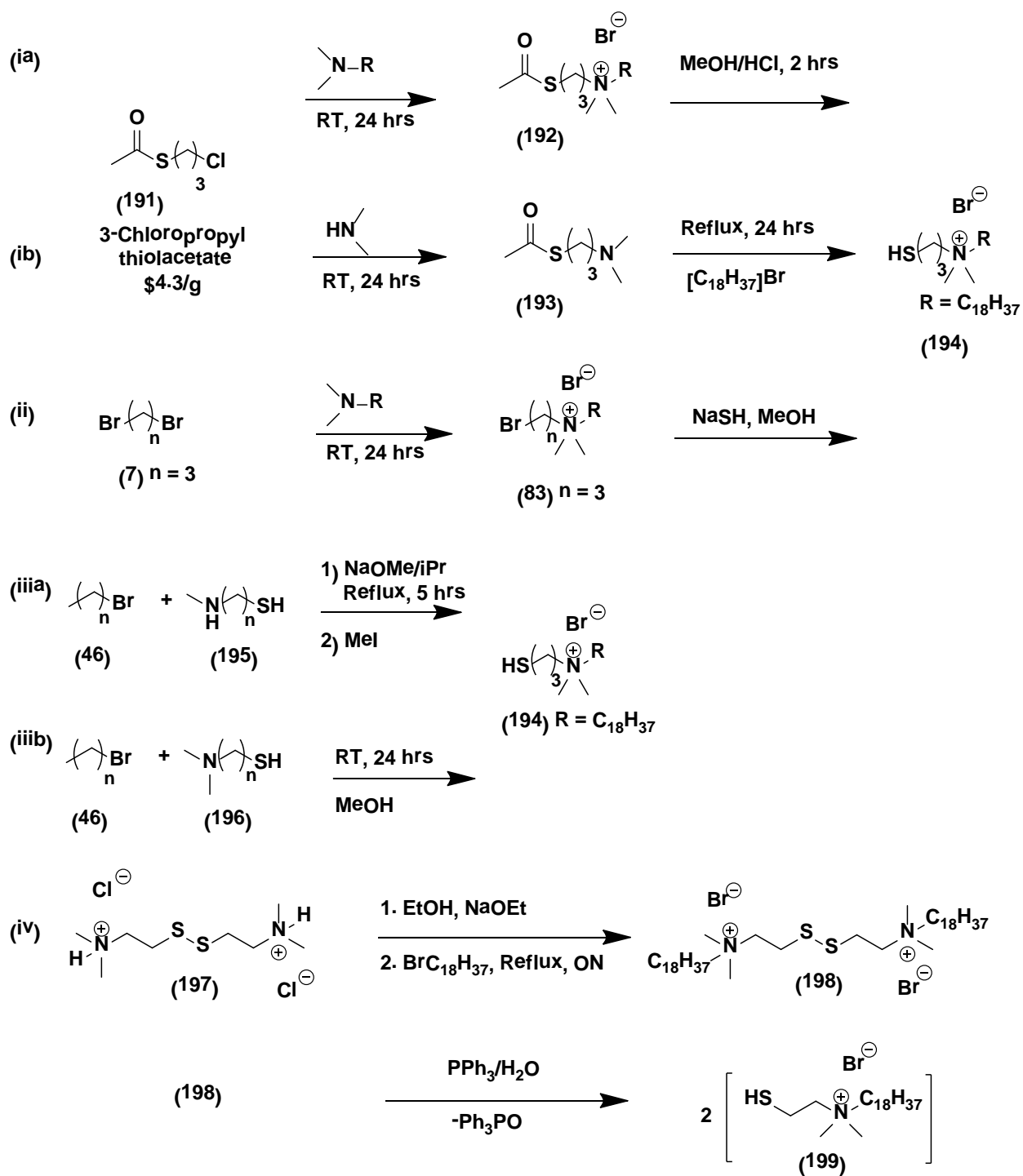


Figure 2.28: ¹H NMR (CDCl₃) spectra of organosulfur QAC **192** (upper) and **199** (lower).

Alternatively, the C₂ thiol quat **199** was prepared from the commercially available disulfide. Deprotonation of **197** with NaOMe in EtOH and the subsequent filtering of NaCl yields the free base which was then quaternized *in situ* with 2 eq. bromooctadecane to **198** in a 80% yield. Cleavage of the disulfide bond was attempted with HCl/Zn and NaBH₄/EtOH, but the final product could not be spectroscopically characterized due to difficulties with purification and reformation of the disulfide in open air. The use of triphenyl phosphine to cleave the disulfide **198** was planned, but not pursued at this time (Scheme 2.36, Route iv).



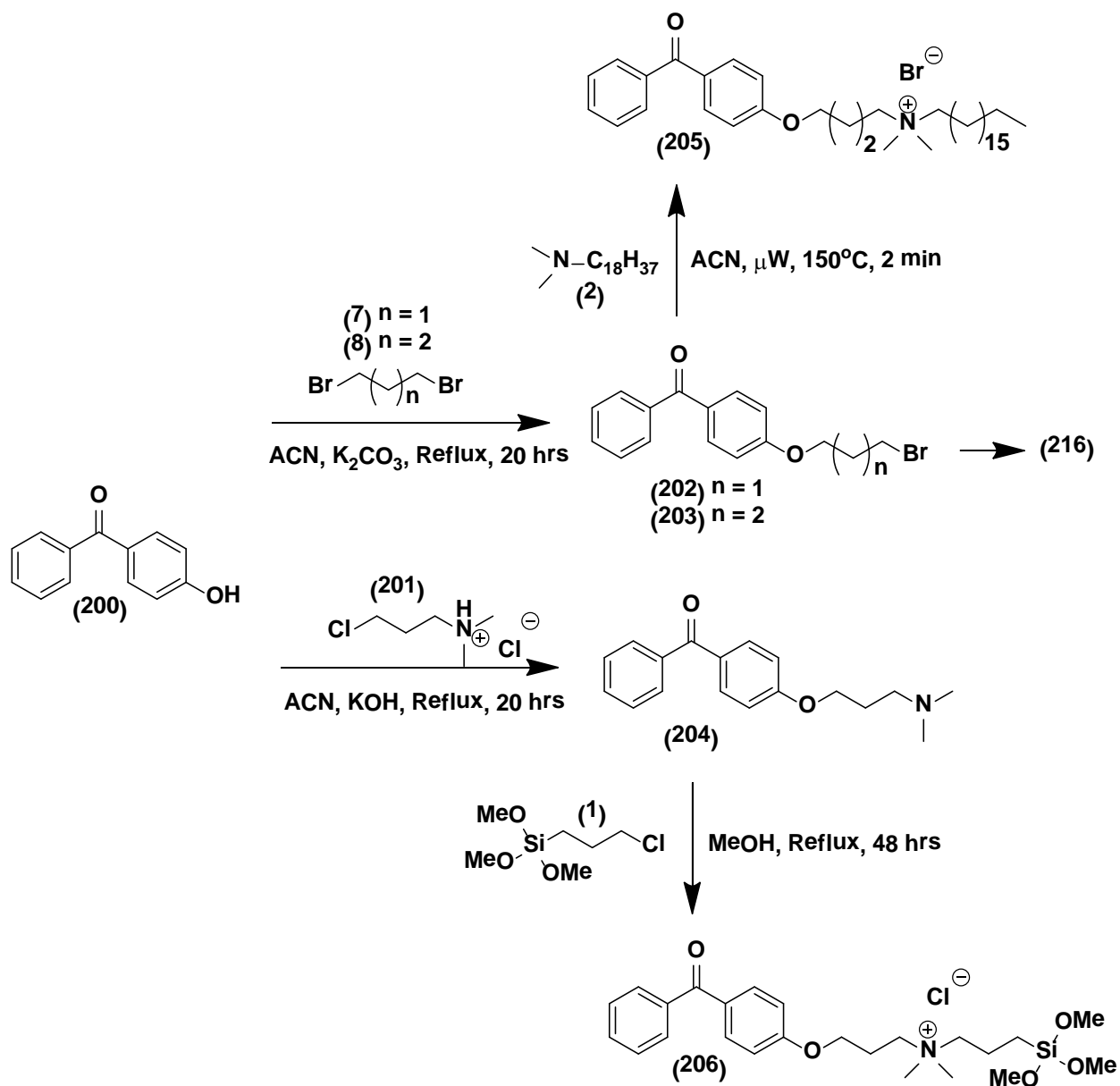
Scheme 2.36: Literature routes to target thiol QAC's **194**²¹³ and **198**²¹⁴.

Previous literature describing the first thiol QAC's SAM failed to prepare a stable coating. An ethanolic solution of the thiol was coated onto Au. However, no surface antimicrobial data was reported, only MIC's in solution were reported.^{118,215} Further work with thiol SAM's was discontinued with greater effort focused on the preparation of organophosphonate QAC's (Section 2.1.2.1-2.1.2.6).

2.4 Benzophenone QAC (Plastic Coating)

Based on previous work in our lab on benzophenone QAC **205**¹⁰⁵, the reaction conditions were optimized under μ W heating by shortening the reaction time to 2 min at 150°C compared to 24 hrs reflux (Scheme 2.37). Dansyl benzophenone **214** was also synthesized for fluorescence testing onto plastics.

In addition a novel benzophenone QAC with a silane linker **206** was synthesized and tested on polypropylene and nylon (Section 2.6.2.1). Post quaternization, compound **206** showed the characteristic upfield ¹H resonances (δ = 3.47 ppm, CDCl₃) due to the two methyl groups on the quaternary amine and the characteristic silane resonance (δ = 3.59 ppm) due to the silane methyl groups –SiOMe₃ (Figure 2.29). ¹³C NMR spectrum revealed that compound **206** was contaminated with a trace of unreacted SM that was difficult to separate from the mixture.



Scheme 2.37: Preparation of the benzophenone QAC's **205** and **206**.

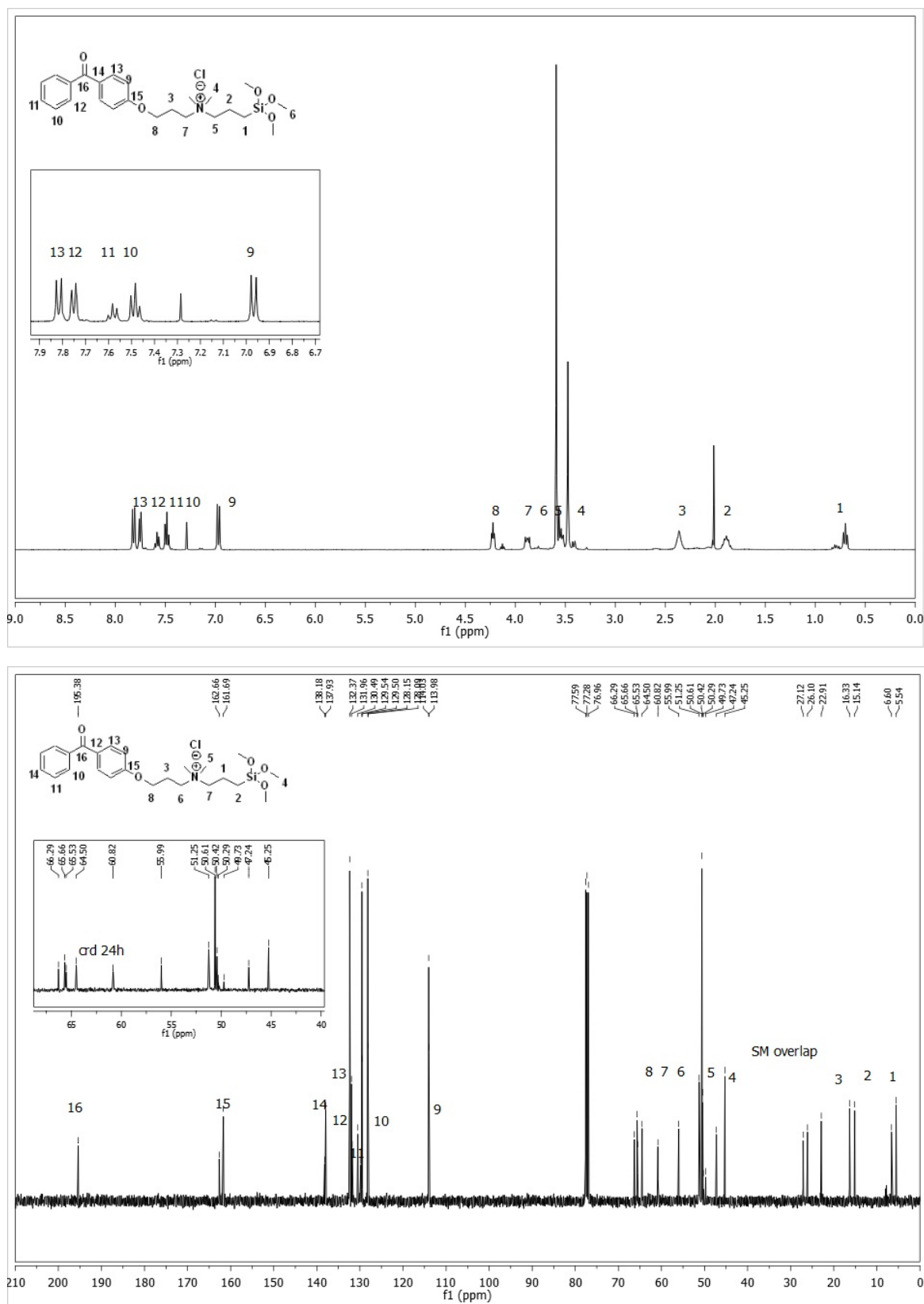
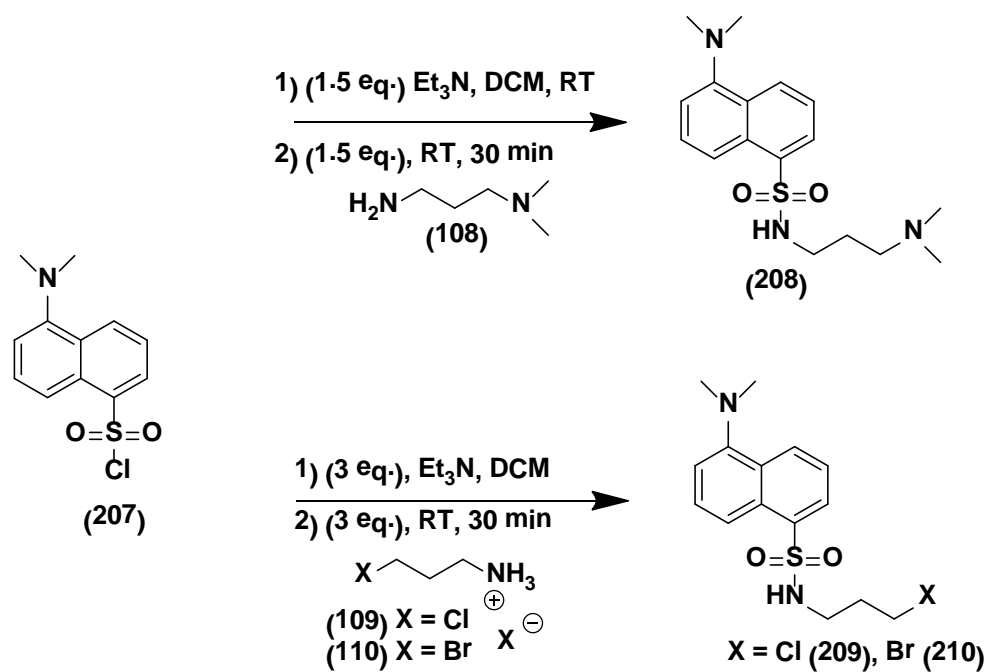


Figure 2.29: ¹H (upper), ¹³C (lower) NMR (CDCl₃) spectra of compound **206**.

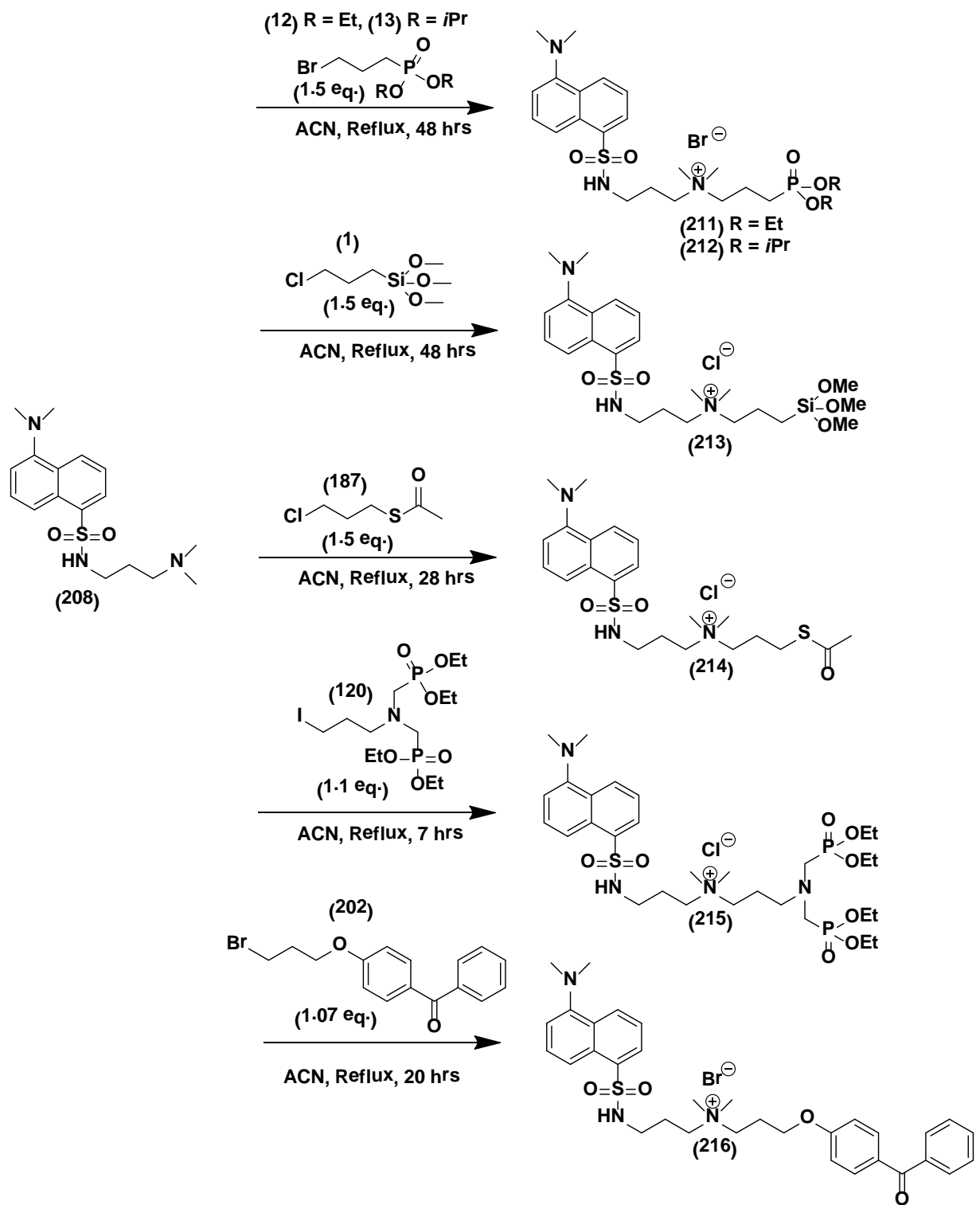
2.5 Dansyl QAC

2.5.1 Fluorescent Antimicrobial Coating Detection

Fluorescence detection of antimicrobial QAC is advantageous over traditional dye based methods (i.e. bromophenol blue) because it allows for easy detection of the Si-QAC once applied by simply irradiating the treated surface with a UV lamp without destructive or permanent binding type testing. Accordingly, three fluorescent dansyl QAC derivatives were synthesized from previously developed procedures in our lab and used in product testing onto different surfaces (see Section 2.7.2).^{105,177} The compounds, dansylphosphonate **211-212** (metals), dansylsilane **213** (non-porous surfaces), dansyl benzophenone **216** (plastic surfaces) previously synthesized in our lab were prepared on a larger scale via the Menschutkin reaction between dansyl dimethyl obtained from dansyl chloride (Scheme 2.38) and the appropriate alkyl halide (Scheme 2.39). New dansyl derivatives reported herein were prepared in the same fashion and include dansyl isopropyl phosphonate **212**, dansyl thioacetate **214** and dansyl α -bisphosphonate **215** (Scheme 2.39). All dansyl compounds **211-216**, **217** and **219** comprising of a dansyl group and a quaternary amine salt, represent a novel class of H₂O soluble fluorescent reporters.



Scheme 2.38: Preparation of dansyl dimethyl **208** and halo precursors **209** and **210** for quaternization.



Scheme 2.39: Preparation of bifunctional dansyl anchors **211-216** for binding onto porous and non-porous surfaces.

Didealkylation of dansyl QAC diethyl and diisopropyl phosphonate esters **211** and **212** respectively was accomplished in the absence of previous literature describing the dealkylation of such compounds. Herein are presented optimized dealkylation conditions with the appropriate reagents according to Table 2.11. Both TMSBr in DCM (Table 2.11, Entry i) and HX (aq) reagents (Table 2.11, Entries iv-viii) were successful at generating the free phosphonic acid in quantitative yield while leaving the quat group intact. However, *in situ* generation of TMSBr from TMSCl/LiBr was incompatible with these compounds due to poor solubility of the quat group in ACN (Table 2.11, Entry ii).

Of the mineral acids employed under both (ST) (Table 2.11, Entries iv-v and vii-viii) and μ W heating (Table 2.11, Entry vi), it was necessary to use aqueous HBr as anhydrous HBr (20% in EtOH) tested initially with these compounds was significantly slower at cleaving the phosphonate ethyl ester and never reached completion even after prolonged heating (Table 2.11, Entry iii). In aqueous HBr (Table 2.11, Entry iv), the reaction was complete after 2 hrs whereas after 24 hrs of heating in ethanolic HBr (Table 2.11, Entry iii) the reaction was only 71% completed.

HBr (aq) (Table 2.11, Entries iv and vii) as expected resulted in faster dealkylation compared to HCl (Table 2.11, Entries vi-vii) and the *i*Pr leaving group (Table 2.11, Entries vii and viii) also resulted in faster dealkylation versus the Et group (Table 2.11, Entries iv and v). Both the HBr and the *i*Pr leaving groups produced more stable intermediates during the course of the reaction and these are supported by the observations in Table 2.11. Compound **217** is the first example of a fluorescent dansyl QA phosphonic acid compound connected through a quaternary ammonium group with excellent solubility in aqueous solution (Figure 2.30).

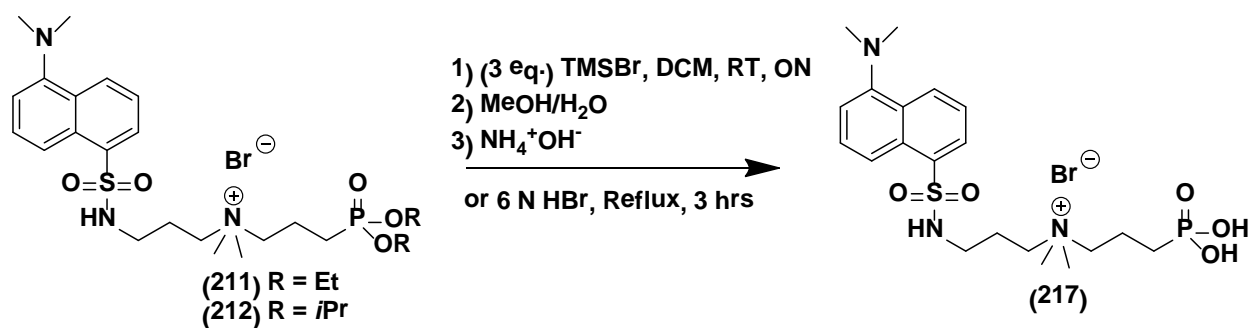


Table 2.11: Didealkylation of dansyl phosphonate diesters **211** and **212**.

						Rxn. Comp. (%) by ³¹ P NMR (D ₂ O)	
Entry	R	Reagent	Solvent	Time (hrs)	Temp. (°C)	SM	PRD.
i	Et	TMSBr	DCM	24	RT	0	100
ii	Et	TMSCl/LiBr	ACN	24	RT	n/a	n/a
iii	Et	20% HBr	EtOH	24	Reflux	29	71
iv*	Et	HBr	H ₂ O	2	Reflux	0	100
v	Et	HCl	H ₂ O	12	Reflux	0	100
vi	Et	HCl	H ₂ O	0.3	150	0	100
vii*	<i>i</i> Pr	HBr	H ₂ O	1	Reflux	0	100
viii	<i>i</i> Pr	HCl	H ₂ O	2	Reflux	0	100

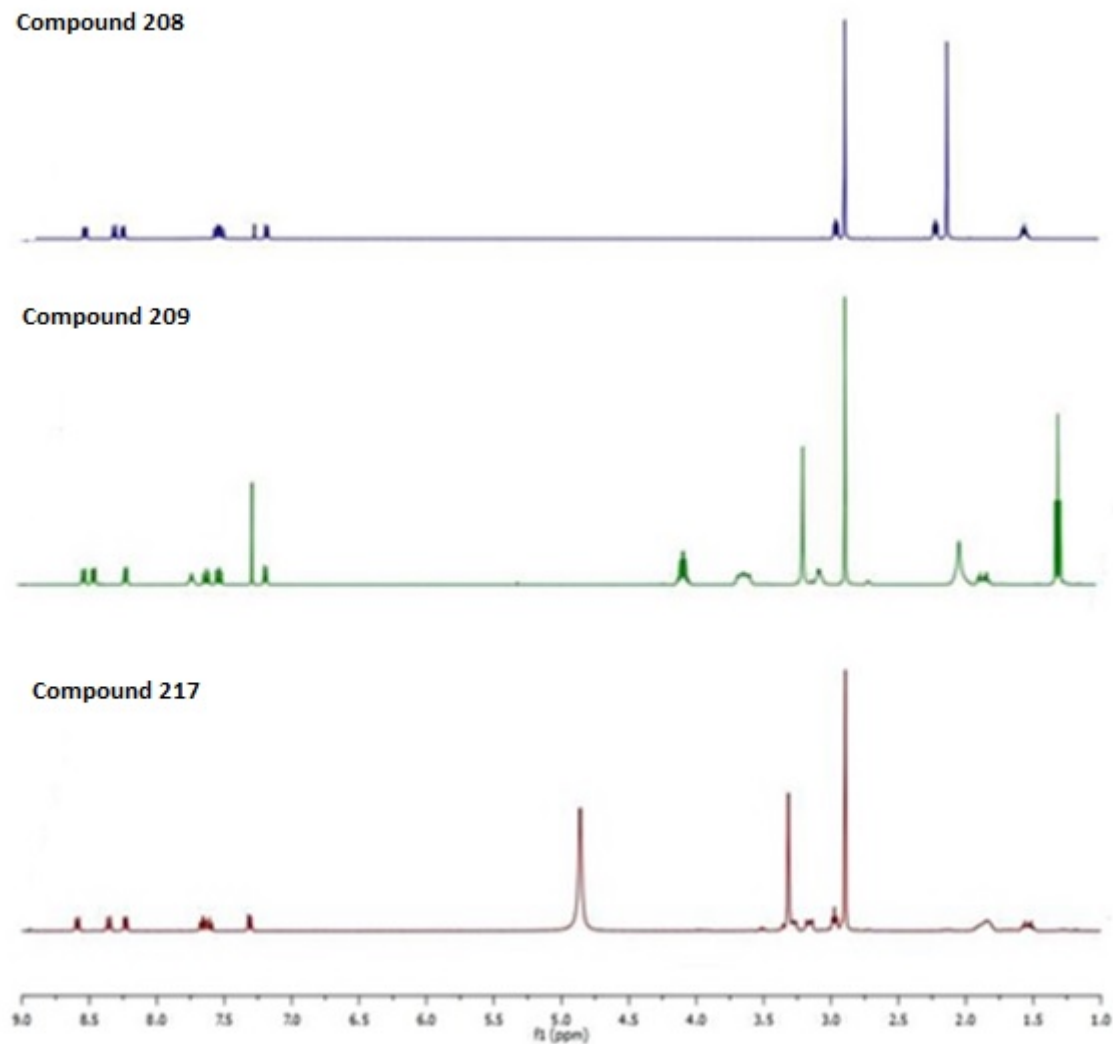
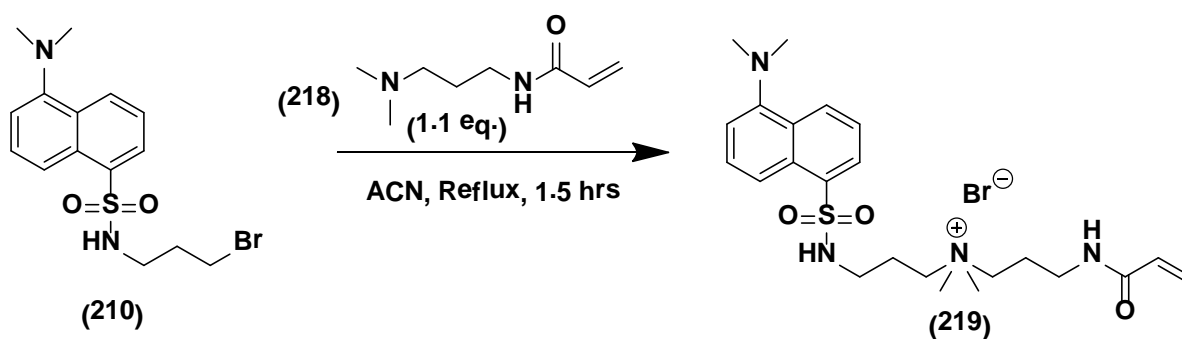


Figure 2.30: ^1H NMR spectra of **208** (CDCl_3), **209** (CDCl_3), and **217** (D_2O).

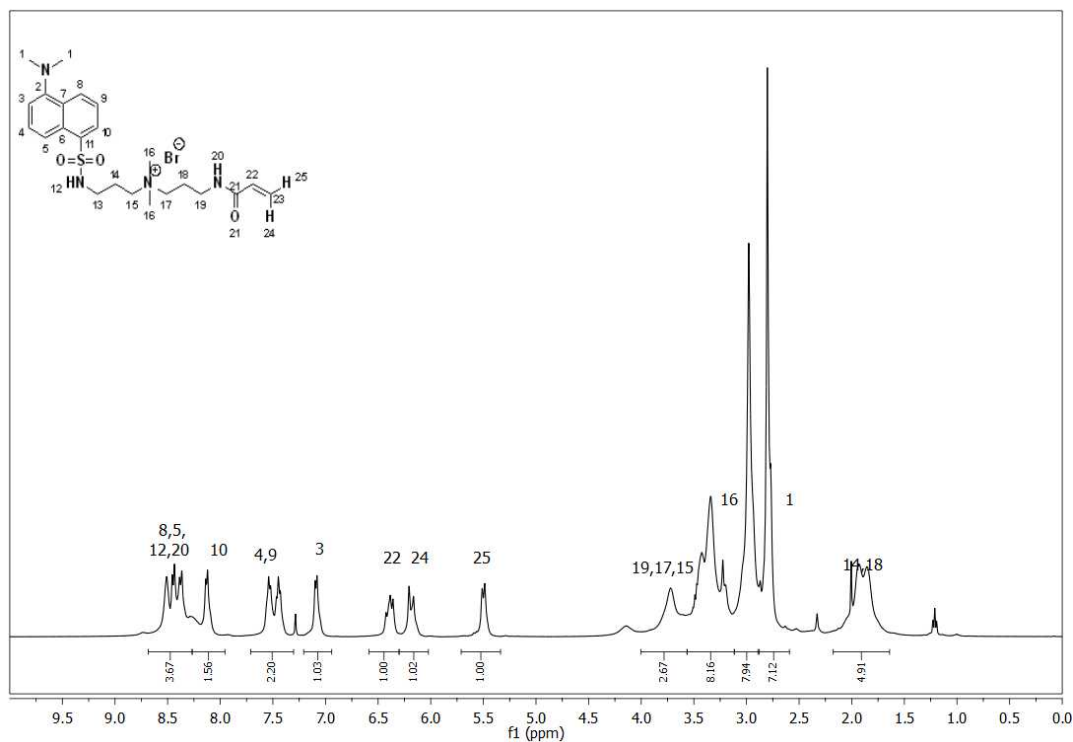
The thioacetate protected dansyl derivative **214** for binding onto noble metals was also successfully prepared from **208** and the commercially available 3-chloropropylthioacetate. NMR analysis (^1H , ^{13}C , CDCl_3) spectrum for **214** revealed characteristic hydrogen (^1H , $\delta = 2.28$ ppm) and carbon resonances (^{13}C , $\delta = 195.80$ and $\delta = 30.77$ ppm) typical for the thioacetate group.

Dansyl acrylamide, **219**, was prepared in an analogous fashion to compounds **209-214** by the Menshutkin reaction except by employing the dansyl bromo precursor **210** instead of dansyl

dimethyl **208** and quaternized with the commercially available *N,N*-dimethylacrylamide derivative **218** (Scheme 2.40). Compound **219** was characterized by (¹H, ¹³C) NMR spectroscopy and showed typical proton resonances corresponding to the acrylamide protons at $\delta \approx 6.38$ and 6.20 ppm. The ¹³C NMR spectrum revealed the expected ketone carbon resonance at $\delta \approx 166.5$ ppm and two new resonances $\delta \approx 130.3$ and 126.1 ppm due to the vinyl carbons (Figure 2.31). Compound **219** may find use as a solid fluorescent marker additive during the injection molding of plastics.



Scheme 2.40: Preparation of dansyl acrylamide QAC **219**.



Scheme 2.24 Continued.....

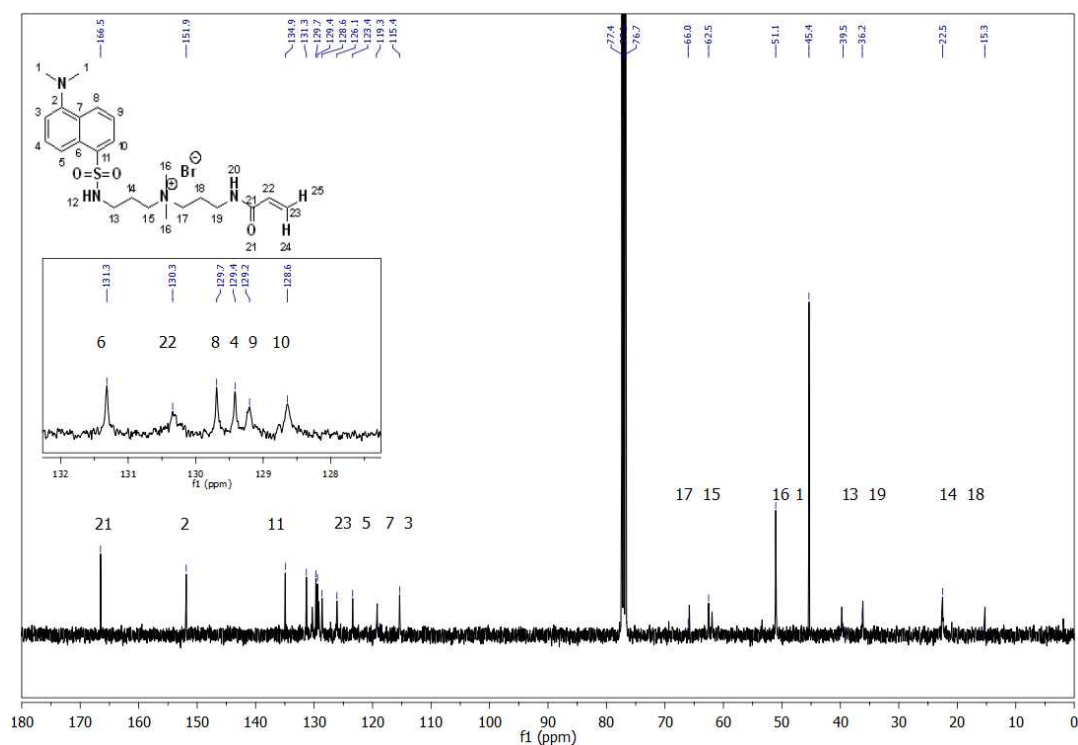


Figure 2.31: ^1H (upper), ^{13}C (lower) NMR (CDCl_3) spectra of dansyl acrylamide **219**.

2.5.2 CO_2 Detection-Dansyl Amidine

Synthesis of amidine containing dansyl fluorophore **222** was achieved from dansyl amine **221** which was synthesized via the Menshutkin reaction similarly to dansyl QAC's **209-214** described above (Scheme 2.41). The amidine group in **222** was attached according to a procedure from Jessup *et al.*, by employing EtOH instead of THF.²¹⁶ In a typical amidine synthesis, the condensation of a primary amine with N,N-dimethylacetamide dimethyl acetal yields a mixture of acetamidine and imidate ester depending on the temperature, solvent, and structure of the primary amine. It was possible to suppress the formation of the imidate ester by performing the reaction in the presence of excess dimethyl amine, yielding acetamidine as the exclusive product. The synthesized primary amine **221** (obtained from hydrazine deprotection of **220**) was used to

prepare amidine **222** in good yield after high vacuum purification. NMR analysis (^1H , ^{13}C , CDCl_3) spectrum for **222** revealed characteristic amidine hydrogen (^1H , $\delta = 2.47$, $\delta = 1.83$ ppm) and carbon resonances (^{13}C , $\delta = 174.11$, $\delta = 50.29$ and $\delta = 22.05$ ppm, Figure 2.32).

In the presence of CO_2 , fluorophore **222** underwent a reversible phase change to **223** that could act as a fluorescence reporter for bacterial respiration. It was thought the reversible phase change to **223** would cause fluorescence quenching that would be directly proportional to the rate of CO_2 produced by bacterial biofilms. However, no such change was observed with UV-light after 60 min of CO_2 bubbling at RT. A H_2O soluble fluorophore capable of reporting biofilm CO_2 production remains a challenge at this point.

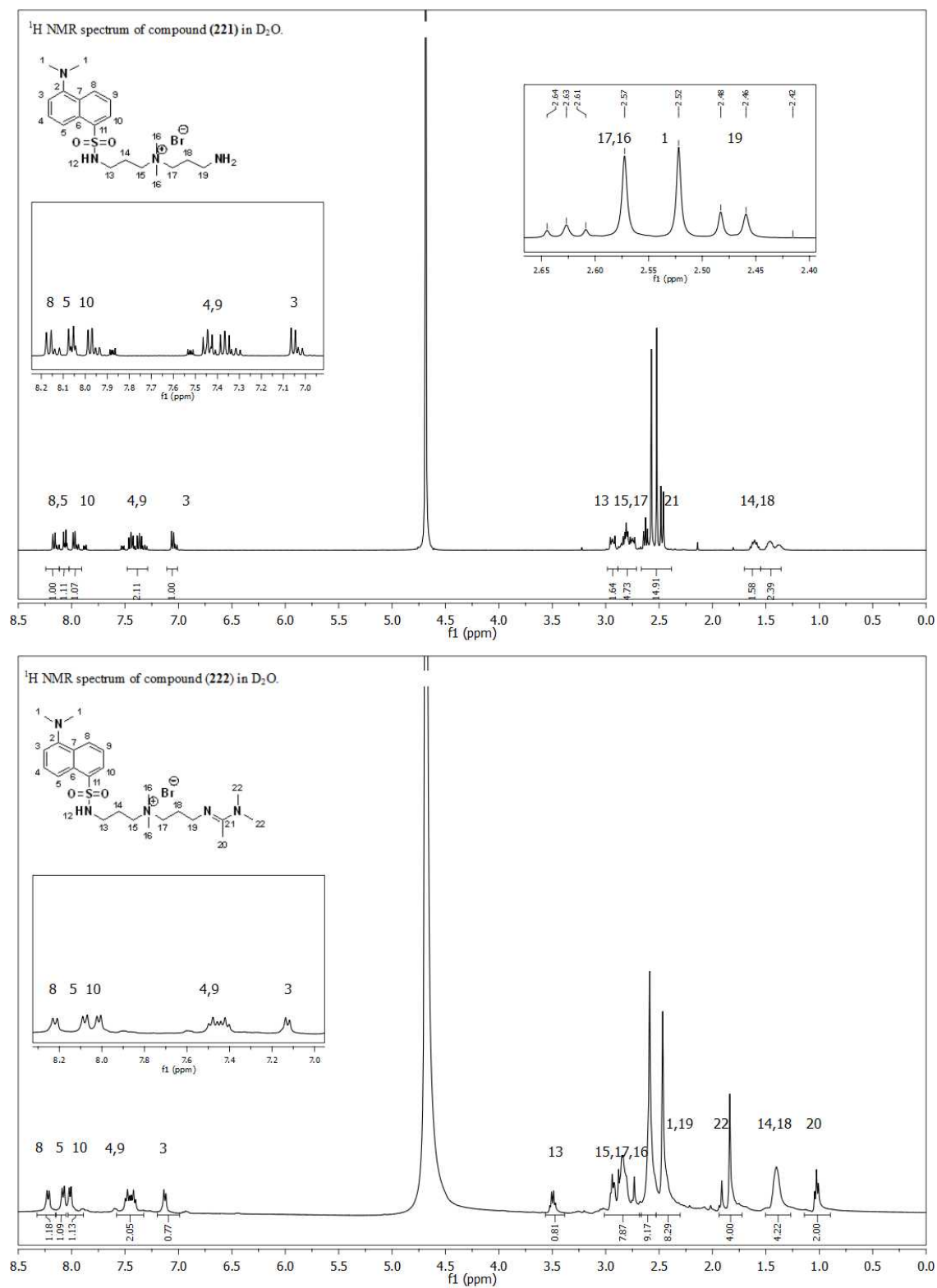


Figure 2.32: ¹H NMR (D₂O) spectra of dansyl amine **221** (upper) and dansyl amidine **222** (lower).

2.5.3 Unsuccessful Dansyl Reactions

Attempted deprotection of dansyl thiolacetate **214** to the free thiol **224** with KOH was unsuccessful and the reaction turned from a light yellow to green and finally to a deep purple colour after stirring at RT for 60 min (Figure 2.33). ^1H NMR (D_2O) analysis of the crude mixture showed a complicated spectrum due to decomposition of the free thiol and disulfide formation. No further attempts to make the free thiol derivative were carried out.

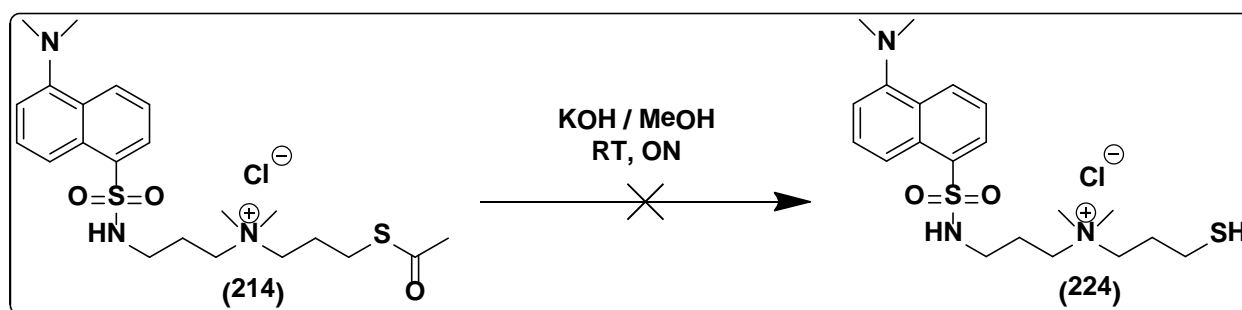
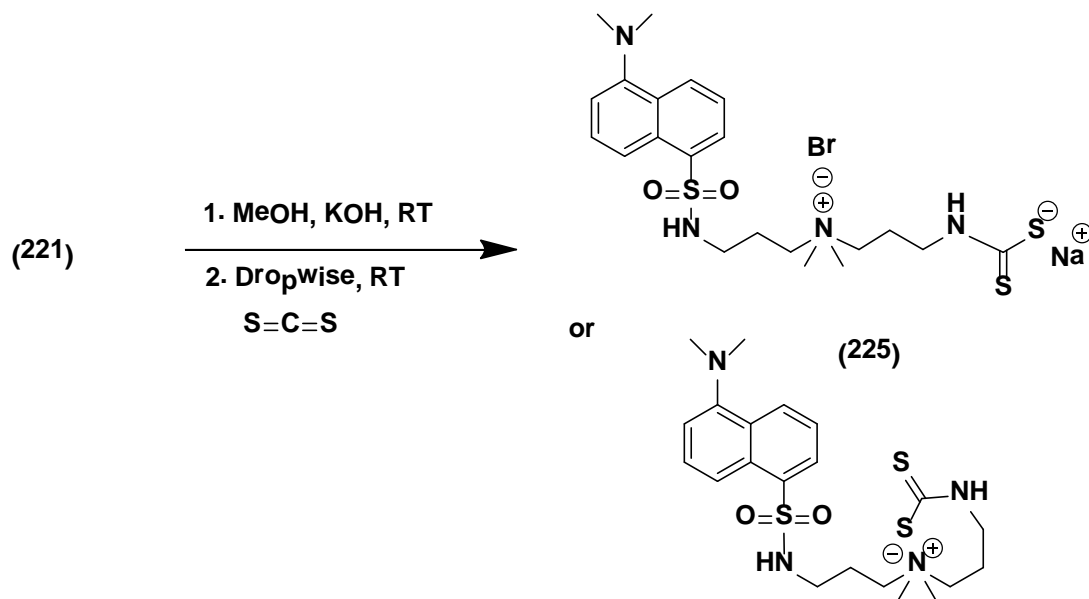


Figure 2.33: Attempted deprotection of dansyl thioacetate **218** to dansyl thiol **212**.

In addition to thiol fluorophore QAC **224**, a dithiocarbamate (DTC) anchored QAC was also targeted as an improved anchor for binding onto metals such as Au, Ag and Cu. The DTC N-C-S₂ group forms a resonance structure that allows bidentate coordination to noble metals versus only monodentate coordination for thiol groups. Thus the DTC binding group forms a stronger and more stable monolayer on Au versus the thiol anchor. To the best of my knowledge, no QAC's dithiocarbamate exist in the literature.

The synthesis of fluorophore **225** was attempted via the dropwise addition of CS₂ to a stirred solution of **221** in methanolic KOH. A precipitate was observed after a few minutes and spectroscopically characterized (Experimental, Section 5.13). From the NMR evidence it was inconclusive whether **225** exists as the bis salt or the internal salt (Figure 2.34, Scheme 2.42).

Additionally characterization of **225** by HRMS spectrometry (ESI-TOF) accounted for a mass of (m/z : 469.1760, $C_{21}H_{33}N_4O_2S_3$) indicative of the internal salt (Figure 2.35).



Scheme 2.42: Attempted preparation of dansyl DTC **225**.

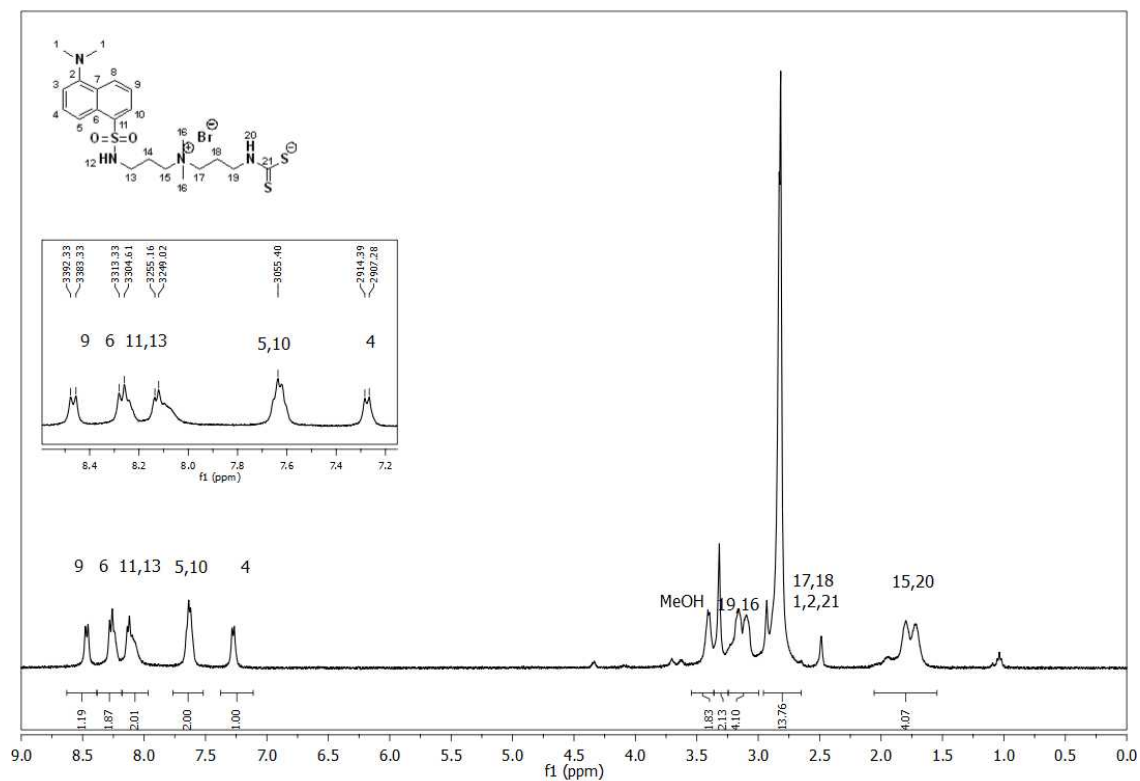


Figure 2.34: ^1H NMR (DMSO-d_6) spectrum of compound **225**.

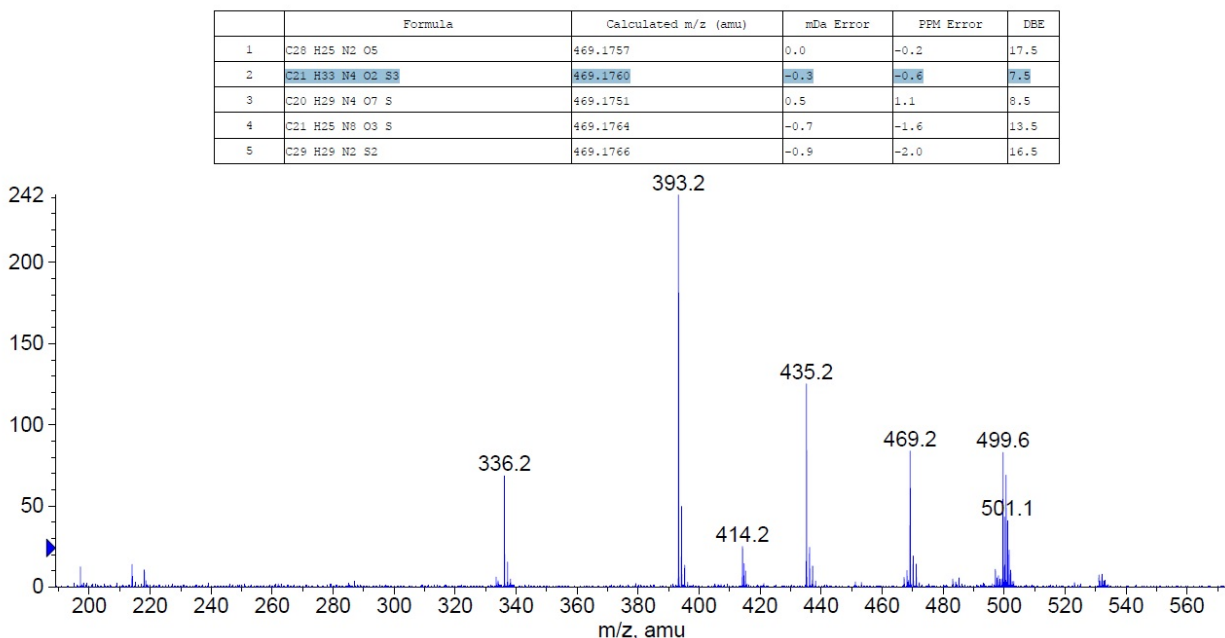
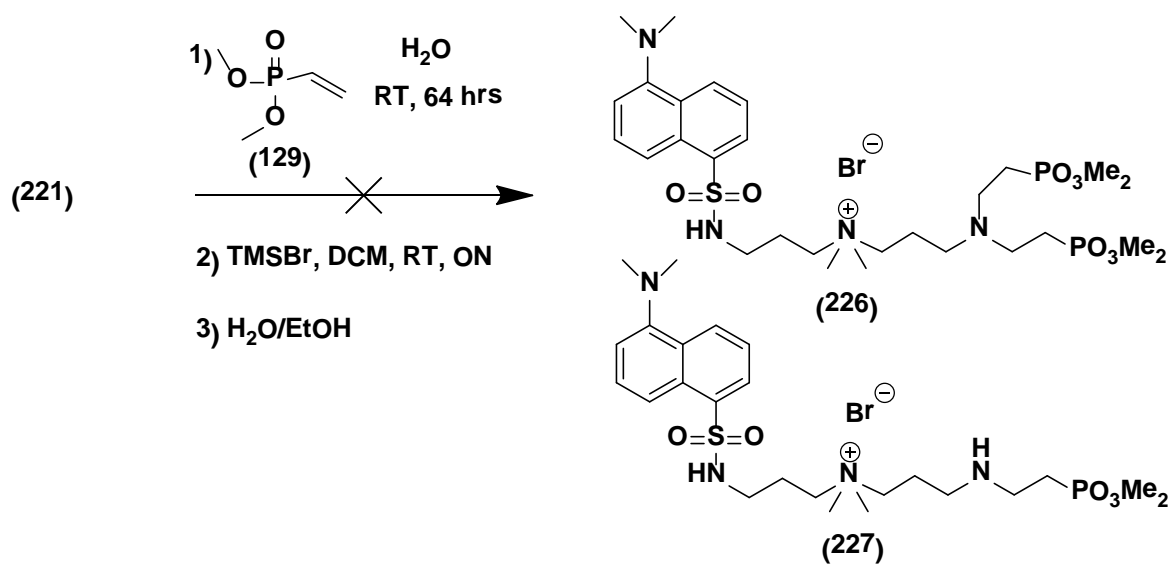


Figure 2.35: ESI-TOF MS spectrum of compound **225**.

Lastly, the synthesis of bis β -amino phosphonate fluorophore **226** was undertaken from the amine quat **221** (Scheme 2.43), however the reaction resulted in a mixture of unreacted starting material, the monophosphonate, and the desired product in a (0.51:0.71:1.0) ratio by ^{31}P NMR spectroscopy (CDCl_3) after 3 d. Purification of the crude reaction mixture of quats was unsuccessful by column chromatography (Figure 2.36).



Scheme 2.43: Attempted preparation of dansyl bis β -phosphonate **226**.

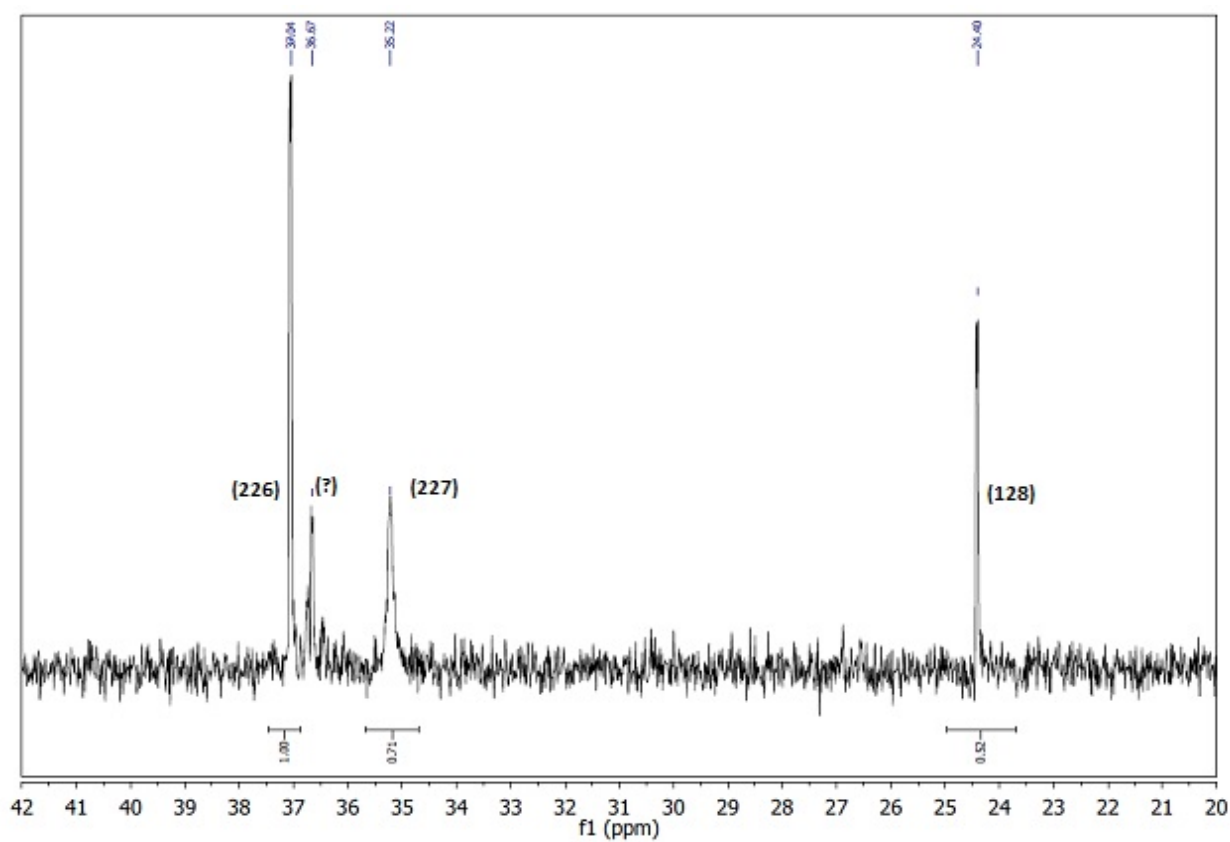


Figure 2.36: ³¹P NMR (D₂O) reaction monitoring of the formation of **226** after 3 d. at RT.

2.5.3 Fluorescence Properties of Dansyl QAC

As expected, all dansyl QAC derivatives analyzed in MeOH exhibited similar fluorescence emission ($\lambda_{\text{emission}} = 525 \text{ nm}$) and absorption spectra ($\lambda_{\text{absorption}} = 340 \text{ nm}$) characteristic of the green-yellow dansyl tag ($\lambda_{\text{emission}} = 525 \text{ nm}$, $\lambda_{\text{absorption}} = 360 \text{ nm}$). Only compound **216** exhibited a different major absorption wavelength at $\sim 300 \text{ nm}$ due to the benzophenone group (Figure 2.37). However, in aqueous environments at low pH (0.1 N HCl) fluorescence quenching of the dansyl fluorophore **213** was observed due to protonation of the aromatic *N,N*-dimethylamine (Figure 2.38). At pH 7 (phosphate buffer) no deviation from the characteristic dansyl fluorescence spectra occurred, only a slight decrease in intensity was observed at the same concentration versus analysis in MeOH. At high pH (0.1 N NaOH) absorption was shifted to $\sim 310 \text{ nm}$ which produced a lower intensity emission at 325 nm when excited at 340 nm (Figure 2.39). Noticable fluorescence quenching was also observed with derivative **220** likely due to π stacking interactions of the phthalimide group and the aromatic amine from the dansyl group (Figure 2.39).

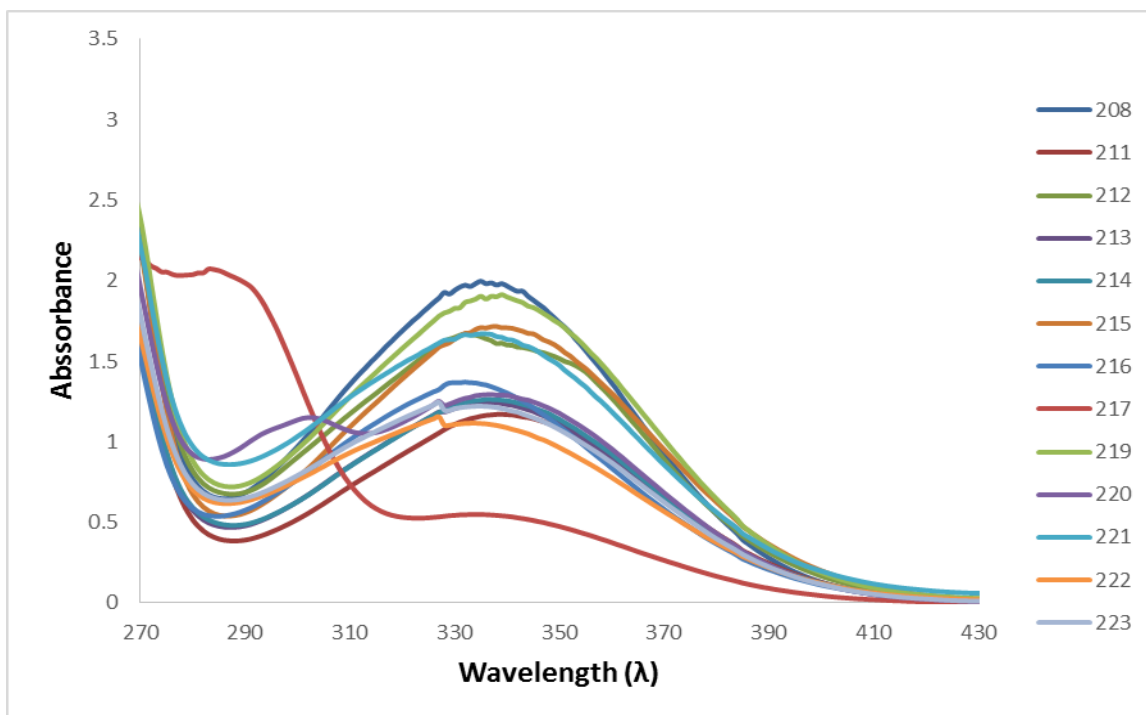


Figure 2.37: Absorption spectra of dansyl QAC's ($\sim 1 \times 10^{-3}$ M) in MeOH ($\lambda_{\text{ex}} = 330$ nm).

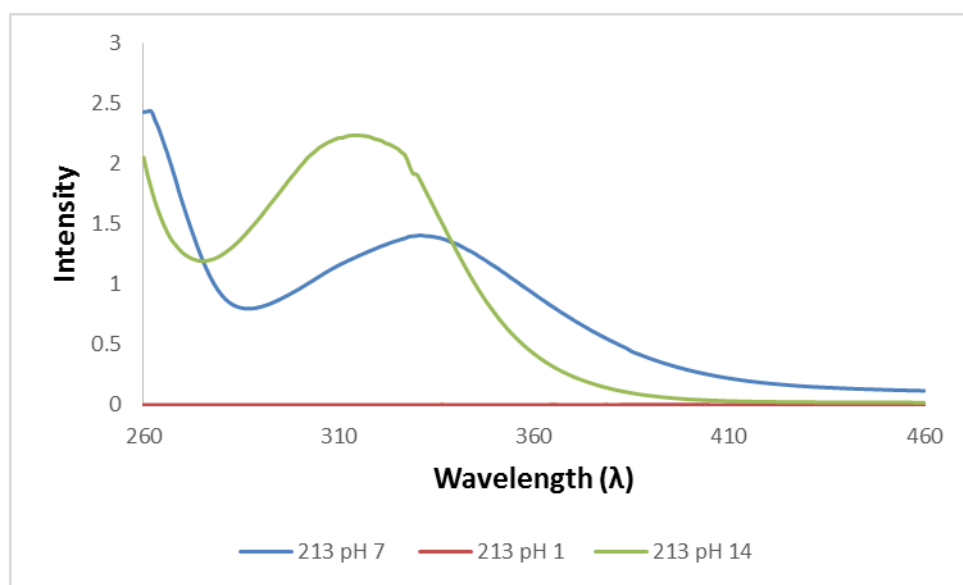


Figure 2.38: Absorption spectra of dansyl QAC **213** ($\sim 1 \times 10^{-3}$ M) at different pH's ($\lambda_{\text{ex}} = 330$ nm).

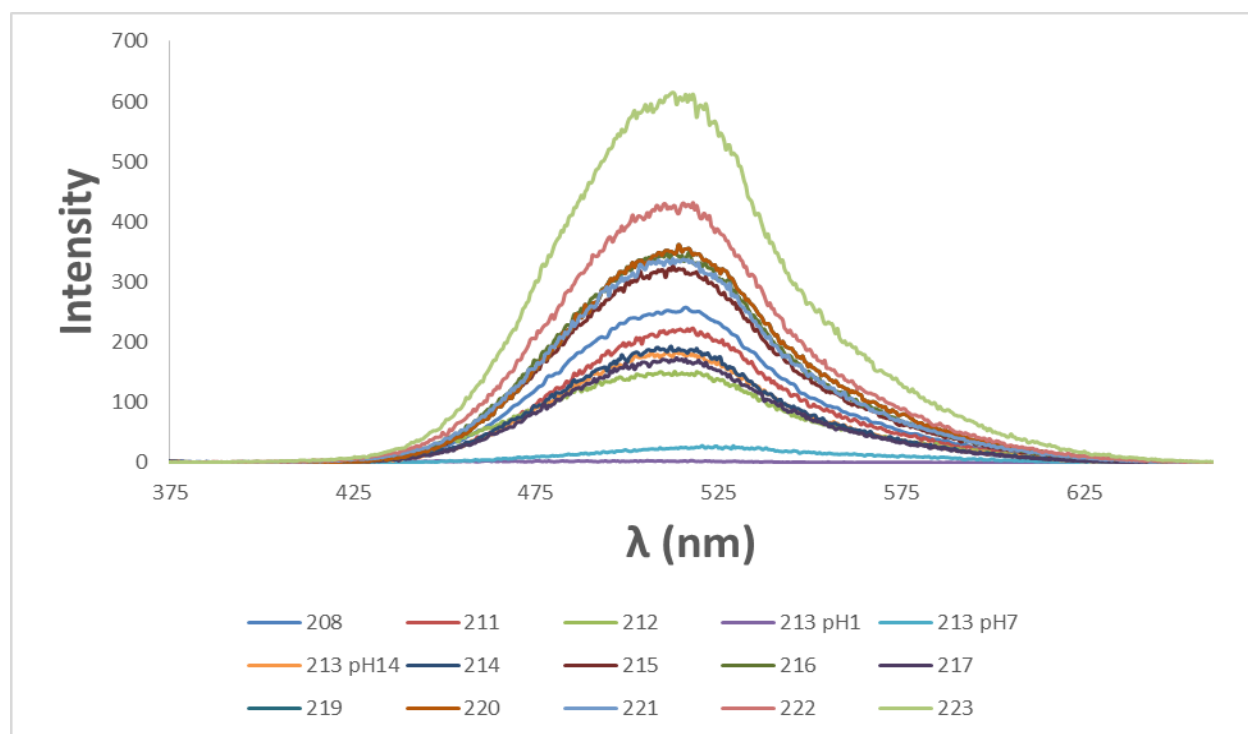


Figure 2.39: Fluorescence spectra of dansyl QAC's ($\sim 1 \times 10^{-3}$ M) in MeOH ($\lambda_{\text{ex}} = 525$ nm).

2.6 Characterization and Properties

2.6.1 X-ray Crystallography

Four novel crystal structures of **34**, **19**, **66** and **220** were obtained during the course of this research and are depicted in Figures 2.24, 2.25, 2.26, 2.27. The phosphonic acid quat **34** was re-crystallized using a 80% EtOH/EtOAc mixture, resulting in the isolation of long crystals growing vertically from the solution, representative of the long C₁₈ chain (Figure 2.40). A hydrogen donor and acceptor group found at the end of both **34** and **66** was necessary in the formation of X-ray quality crystals of these long chain molecules (Figure 2.41). Structures with C₁₈ tails are difficult to crystallize and are rare in the literature.

In addition to **34**, a crystal structure of the C₁₈ QAC intermediate **66** was obtained with a hydroxyl terminal end group instead of a phosphonic acid (Figure 2.42). This compound was re-crystallized from ACN by slow evaporation of the solvent at RT, resulting in the isolation of fine, white, prismatic crystals. Compound **66** had been previously reported in the literature, but a crystal structure of this long chain QAC was unknown.

Crystals of both **34** and **66** exhibited average carbon-nitrogen bond lengths typical for an ammonium salt (1.499 Å).²¹⁷ From the data obtained (see supplementary information) the bond lengths for N(1)-C(23), N(1)-C(22), N(1)-C(4), and N(1)-C(3) were 1.486(8) Å, 1.505(7) Å, 1.522(8) Å, and 1.523(8) Å respectively. These bond lengths agree with the above mentioned C-N_{QAC} average bond lengths and along with other characterization data (Section 6.0, Appendix 1.1) support the identity of **34** and **66**.

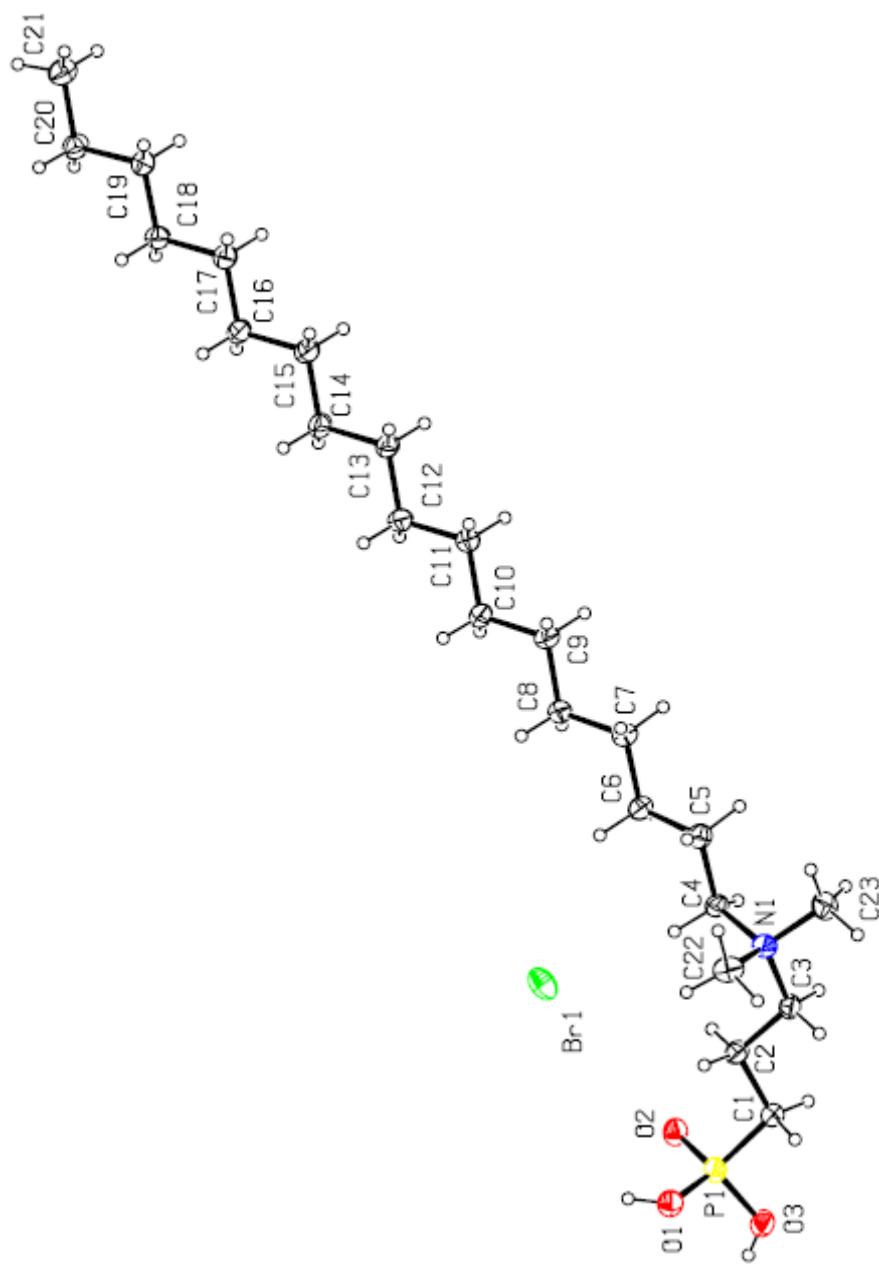


Figure 2.40: X-ray crystal structure of **34**.

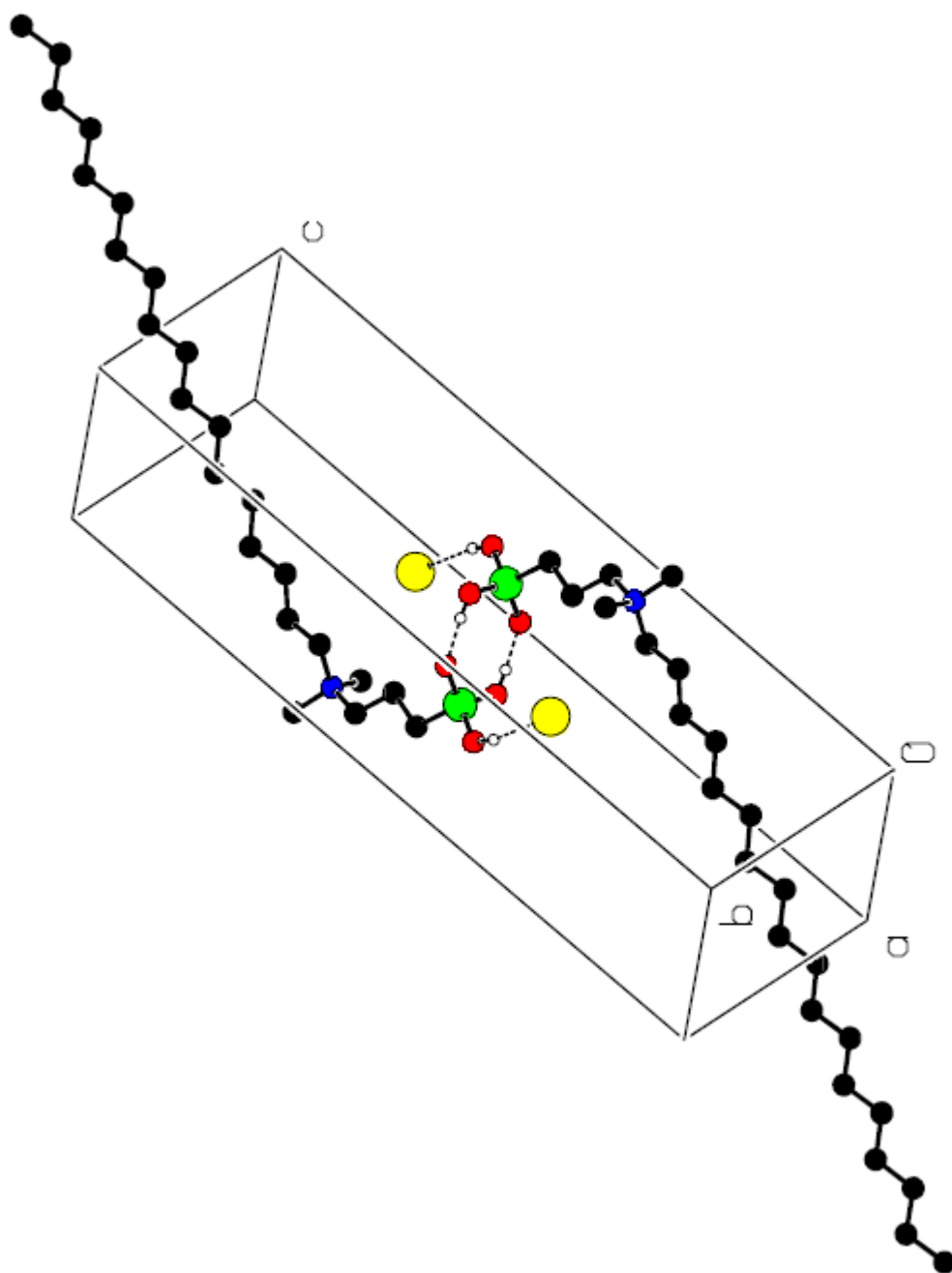


Figure 2.41: Crystal packing interactions of two molecules of **34**.

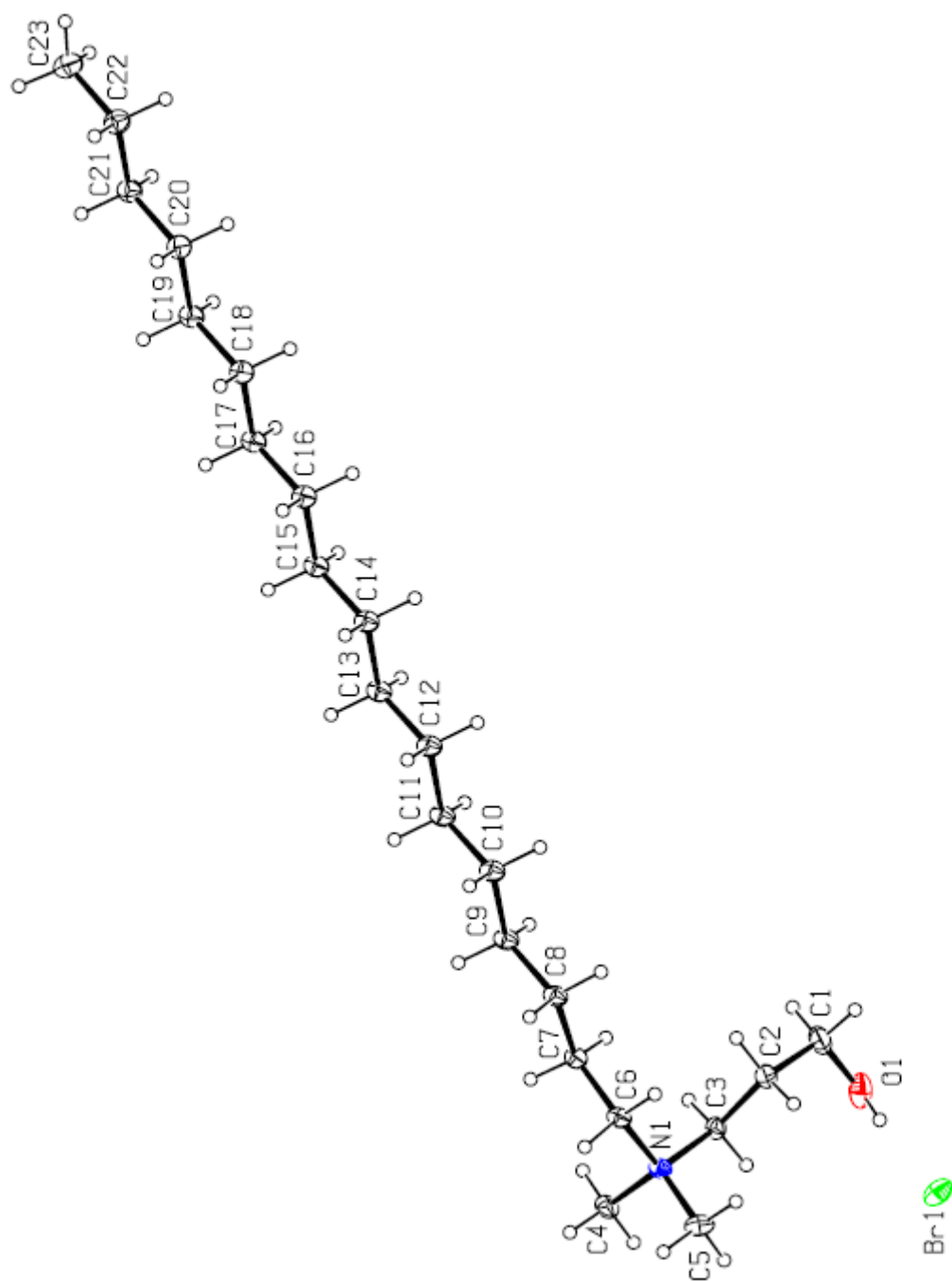


Figure 2.42: X-ray crystal structure of **66**.

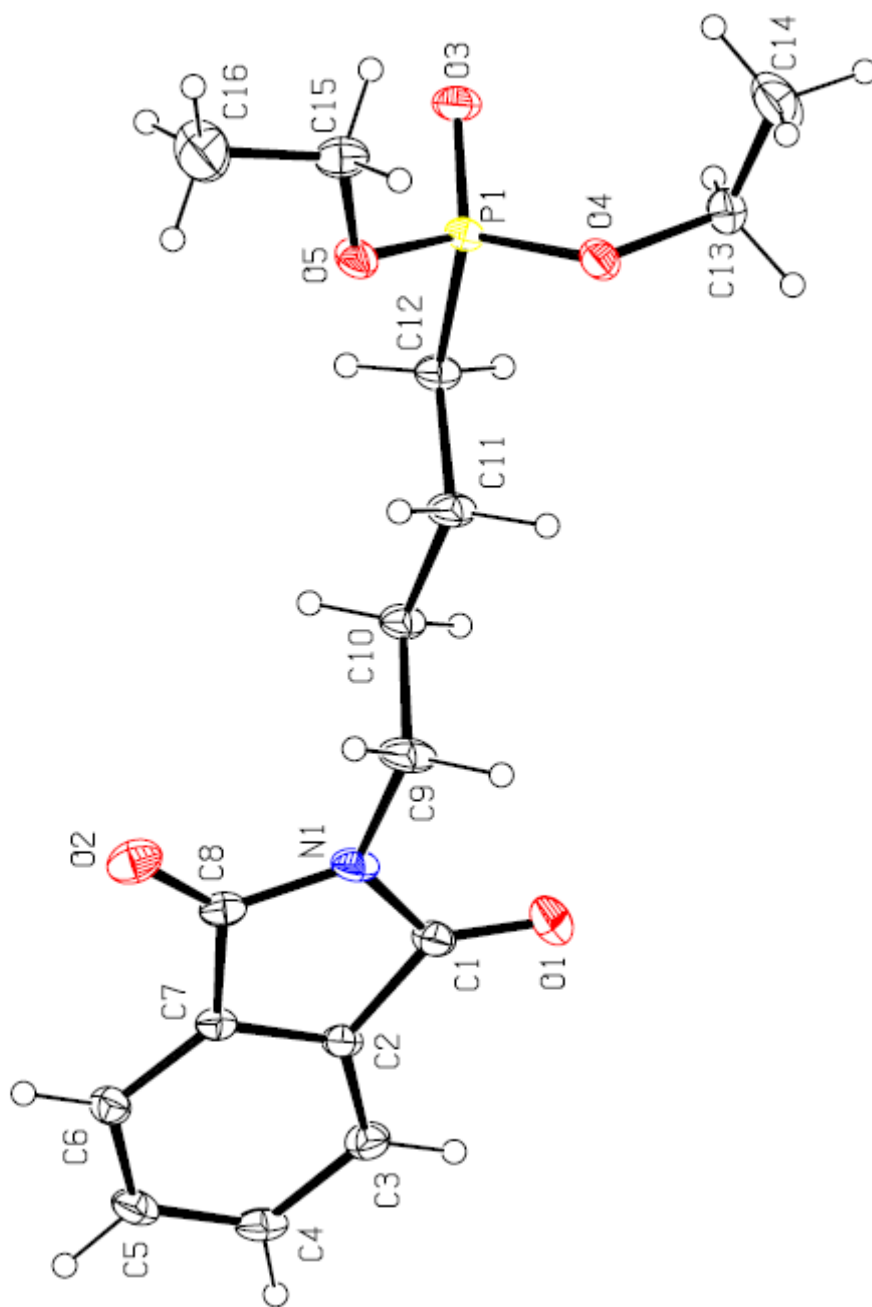


Figure 2.43: X-ray crystal structure of **19**.

Two intermediate compounds **19** and **220** containing phthalimide protecting groups were crystallized and X-ray structures were obtained. The diethylphosphonate intermediate, **19**, was

crystallized from EtOAc at -20°C, forming square, clear crystals (Figure 2.43). The dansyl phthalimide QAC intermediate **220** was crystallized inside an NMR tube from D₂O at RT, forming star shaped, clear crystals. From the crystal structure, a close interaction of the phthalimide group near the dansyl group can be observed (Figure 2.44). This interaction supports the fluorescence quenching data for this compound due to π - π stacking of the two aromatic rings. The bond lengths and bond angles for all of these compounds are provided (Section 6.0, Appendix 1.1).

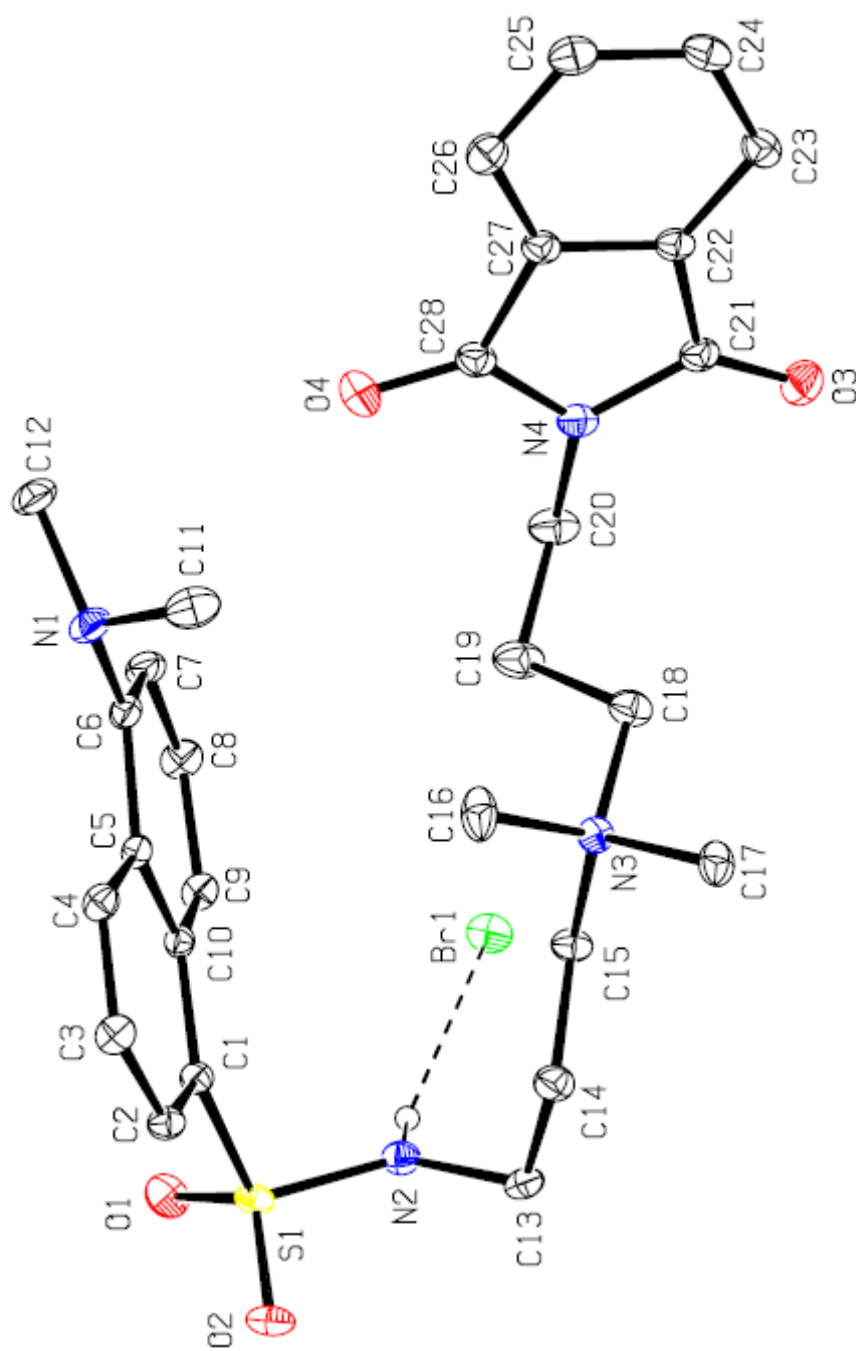


Figure 2.44: X-ray crystal structure of **220**.

2.6.2 Antimicrobial Detection / Coating Procedures

Both non-fluorescent and fluorescent dansyl quats were attached to porous (cotton, SiO₂) and non-porous (metals, plastics) by dip coating a given surface in the appropriate compound according to Figure 2.45. The dansyl QAC compounds were visualized under UV light while non-fluorescent QAC's were visualized with bromophenol blue. Coating procedures with examples on plastics and metals are described below.

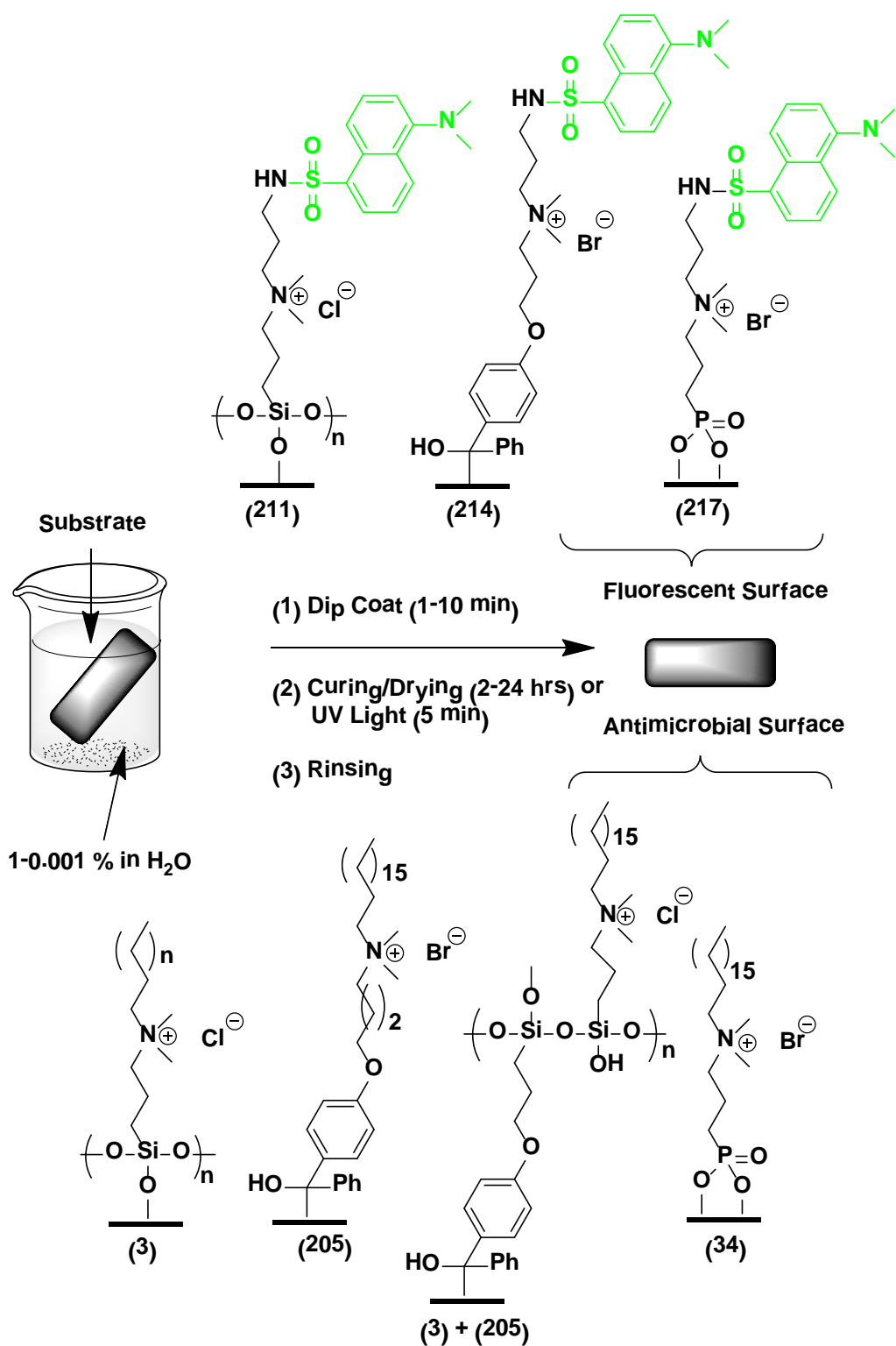


Figure 2.45: Coating procedure of QAC antimicrobials onto porous and nonporous surfaces.

2.6.2.1 Plastic Surfaces

Grafting of non-fluorescent benzophenone compounds **205** and **3** + **205** onto polypropylene (PP) and silicone was performed as follows: plastic samples were cut into rectangles (3.5×2.5 cm), rinsed with H₂O and MeOH and air dried prior to their use. The clean substrates were dipped into a 0.01% (w/v) solution of **214** and irradiated with UV (5 min) and any unbound material was rinsed from the substrates using H₂O prior to visualization with bromophenol blue (Figure 2.46). Both PP and silicone surfaces stained a deep blue colour indicating the presence of quats on these plastic surfaces, while the controls remained unstained (Figure 2.47).

Dansyl fluorescent compounds were successfully visualized without the bromophenol blue dye. Medical grade silicone tubing coated with **214**, silica NP's treated with **211**, PP coated with **214**, and SS coated with **217** all fluoresced green, indicating their presence on these surfaces when imaged under UV light (Figure 2.48).

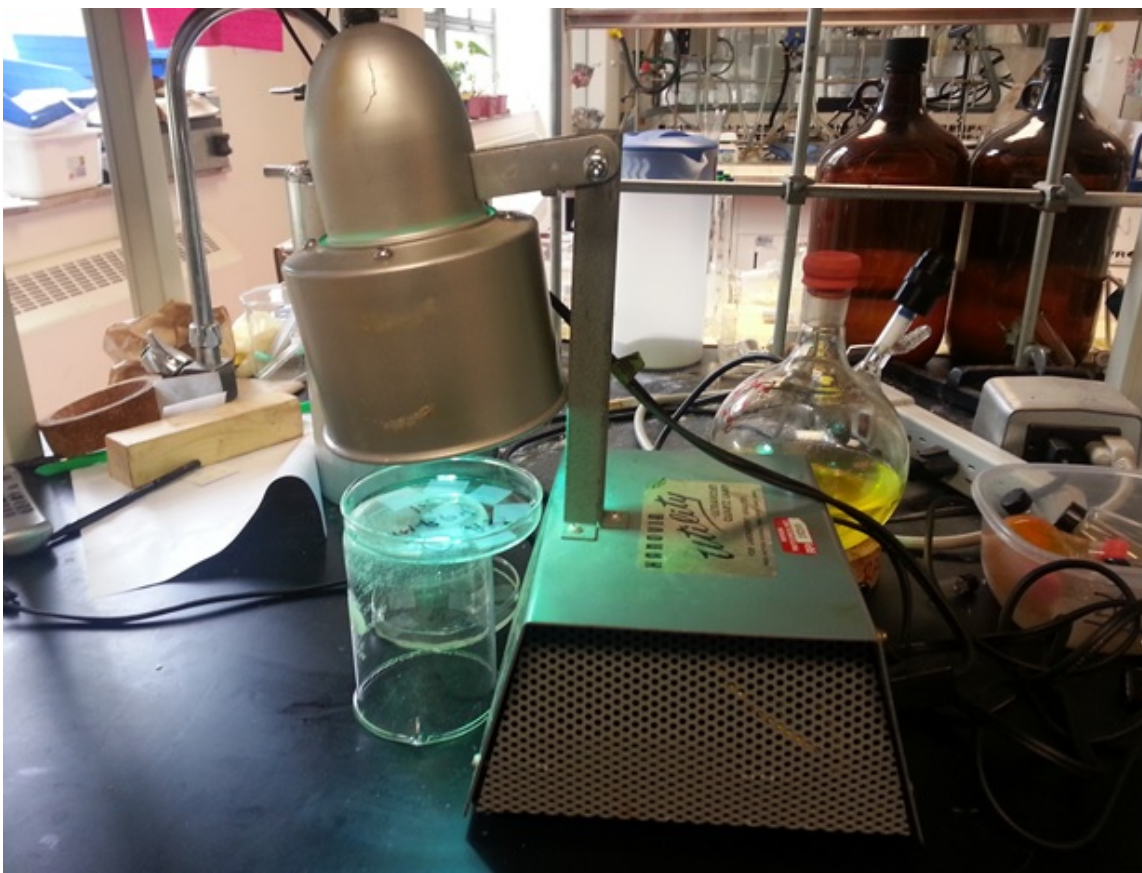


Figure 2.46: Plastic coating experimental set-up.

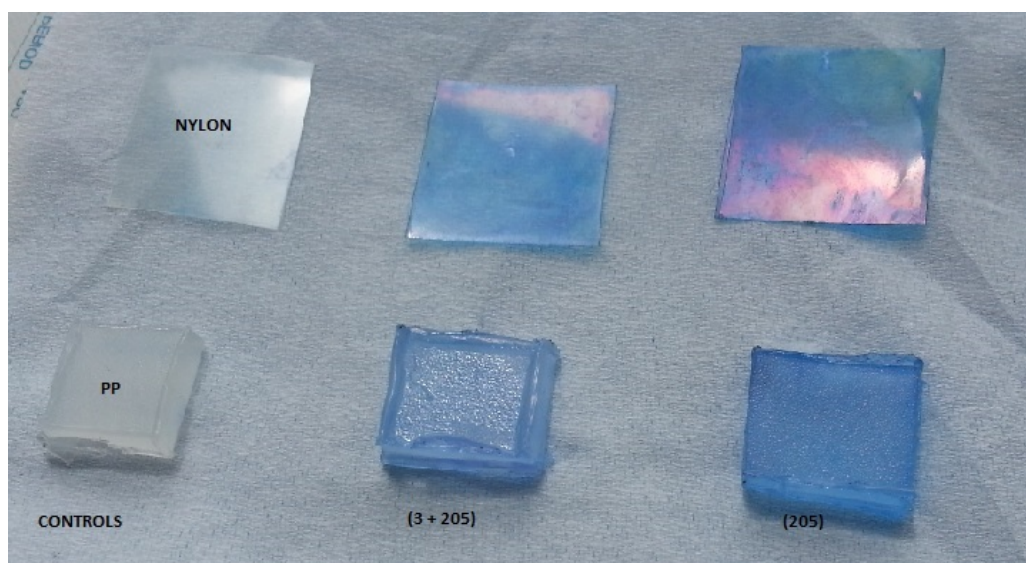


Figure 2.47: Bromophenol blue (0.01 M) detection of QAC antimicrobials on plastic surfaces.

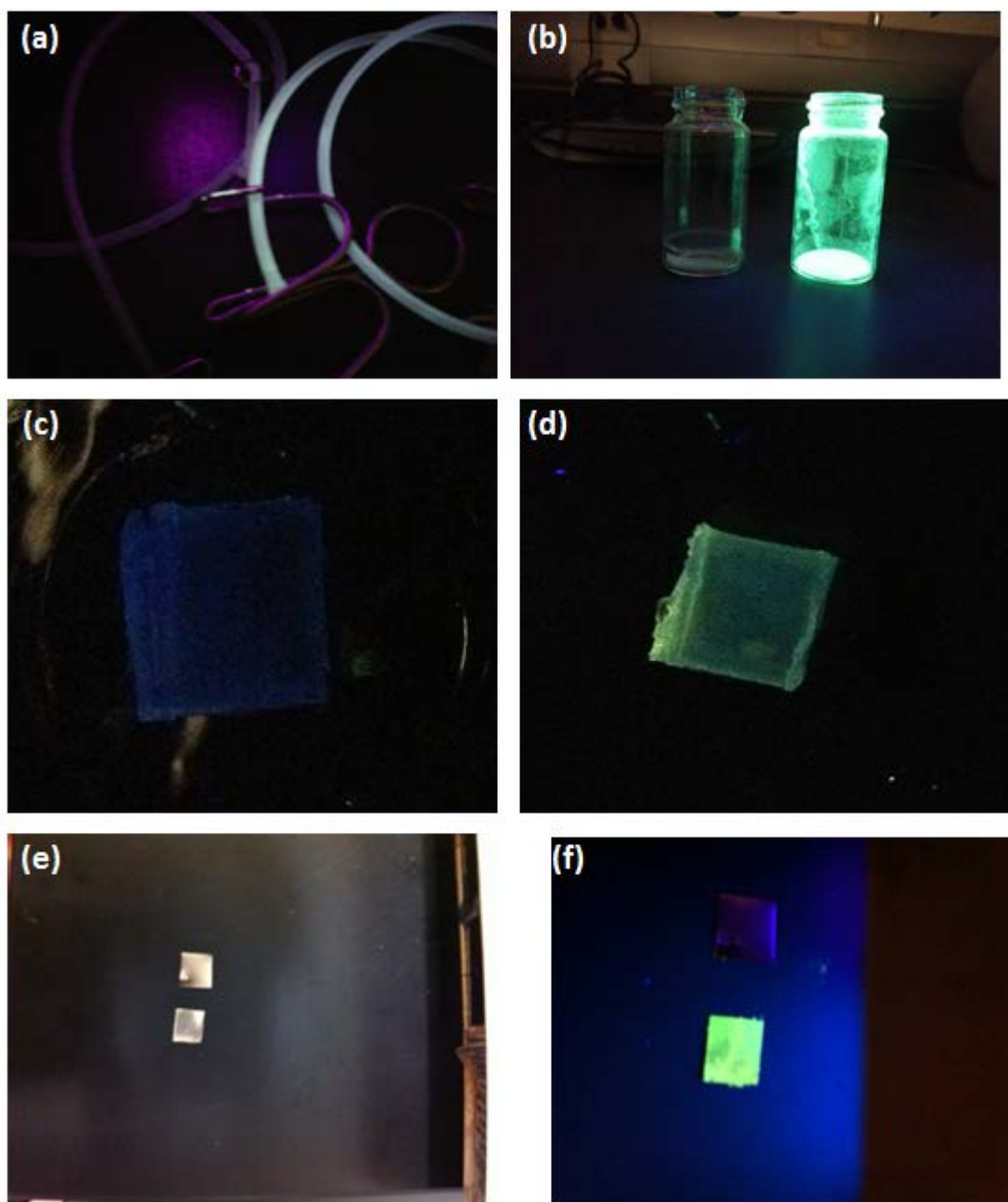


Figure 2.48: Fluorescent detection of dansyl QAC's. (a) Medical grade silicone tubing coated with control (left) and with **214** (right), imaged under UV light, (b) silica NP's treated with **211**, PP plastic coated (c) control and (d) **214**, (e) SS coated with control (upper) and **217** (lower) imaged under ambient light, (f) same image as (e) but imaged in the dark under UV light (TLC lamp).

2.6.2.3 Metal Surfaces

Preparation of self-assembled monolayers of compound **211** on cotton and silica NP's were prepared by dip coating the samples in 0.01% (w/v) H₂O or MeOH solution of **211** ON or until the solvent evaporated, followed by heating (100 °C, 24 hrs) and drying (Figure 2.49). Note a faster procedure was developed by placing the vials into an oven (100 °C) and letting the solvent evaporate (~ 30-60 min) followed by a rinsing step (MeOH) and a short oven cure (100 °C, 1 hr). Samples prepared in both ways were found to possess the same antimicrobial activity while uncured samples were inactive.



Figure 2.49: Metal coating experimental set up using 20 mL glass screw cap vial open to air.

2.6.3 Antimicrobial Activity

2.6.3.1 Solution Killing: Minimum Inhibitory Concentration's (MIC's)

Minimum inhibitory concentration (MIC) experiments were performed according to standard procedures²¹⁸ with both gram-positive and gram-negative bacterial strains: *S. aureus*, *Listeria*, *Salmonella*, and *E. coli*. Solutions of long chain QAC antimicrobials (0.01g/mL or 1%) were dissolved in H₂O, inoculated with the test organism and serially diluted from 10⁻¹-10⁻³, representing a dilution range from (0.01g/mL to 0.00001g/mL), followed by plate counts to determine the MIC values (Figure 2.50).

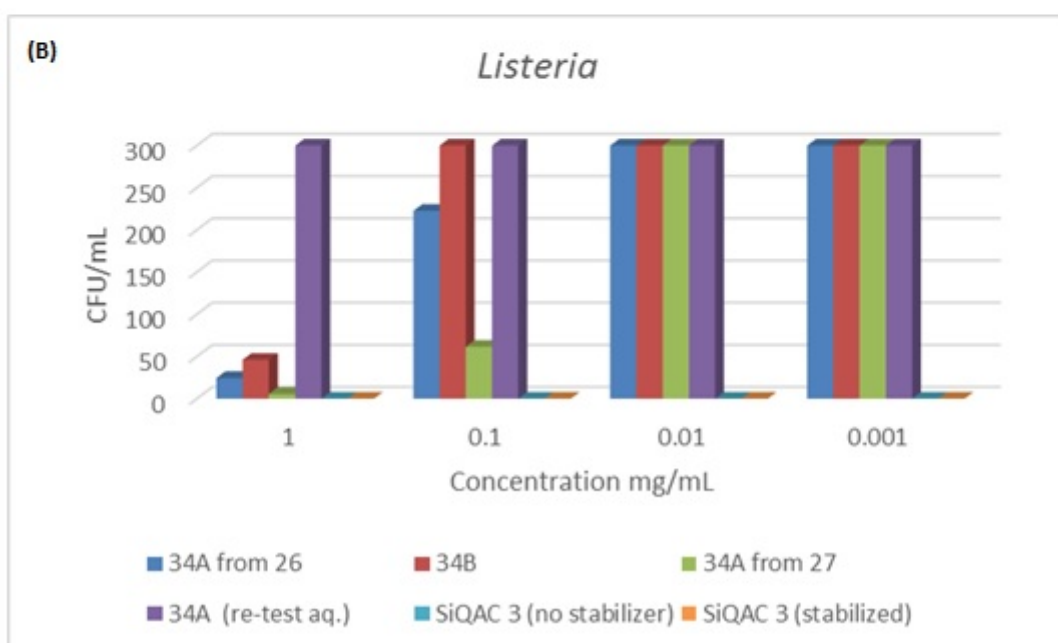
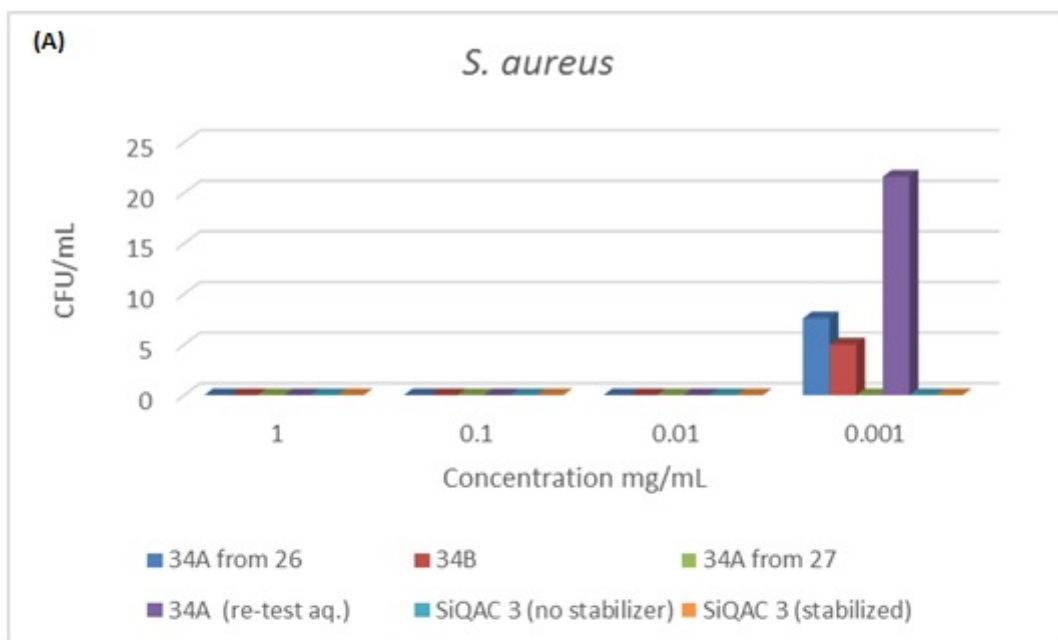
Samples 1-3 were prepared with (1%) solutions of the C₁₈ phosphonic acid QAC **34A** obtained from hydrolysis of the phosphonate ester **26** or **27**. Sample 1 is compound **34A** obtained by TMSBr dealkylation of the ethyl ester (Et, TMSBr), sample 2 is the sodium salt **34B** (Na salt) which is freely soluble in H₂O and sample 3 is compound **34A** obtained by HCl dealkylation of the *i*Pr ester **27** (*i*-Pr, HCl). Sample 4 which was initially a (1%) solution of **34A** used for ON dip coating experiments with Ti metal, is the residual liquid (unknown concentration) after the metal coupon was removed for antimicrobial analysis.

Samples 1-3 prepared with 1% starting solutions of **34A** exhibited similar MIC values but demonstrated 100 × higher efficacy with *Listeria* and *Salmonella* and 10 × higher efficacy against *E. coli* compared to the silane QAC **3** (sample 5 and 6) (Figure 2.50). All compounds were inhibitory towards the gram-positive *S.aureus* bacterium, susceptible to QAC compounds in solution (Figure 2.34). The phosphonate ester **26** (1% in H₂O) was also tested for inhibition

against *S. aureus* and was found to be highly inhibitory even at 100 µg/mL concentrations (Table 2.12).

As expected, sample 4, the retested aqueous phase containing residual **34A** performed poorly with *Listeria*, *Salmonella*, and *E. coli* and no inhibition was observed at the starting concentration. This can be explained by the fact the phosphonic acid molecules in solution formed monolayers on the surface to Ti metal thereby decreasing the concentration 10-100 fold. So in fact the starting concentration was closer to a 0.001 – 0.0001 g/mL which after further dilution was no longer inhibitory (Figure 2.50).

A stock solution (1%) of the silane quat **3** prepared from the 5% stabilized solution in H₂O (SiQAC **3** (stabilized)) or prepared from the 72% concentrate in MeOH and diluted to 1% in H₂O (SiQAC **3** (no stabilizer)) worked extremely well (Figure 2.50). All bacterial strains tested with these samples were inhibited at concentrations up 100 µg/mL which is in close agreement with literature MIC values (84 µg/mL).⁶¹



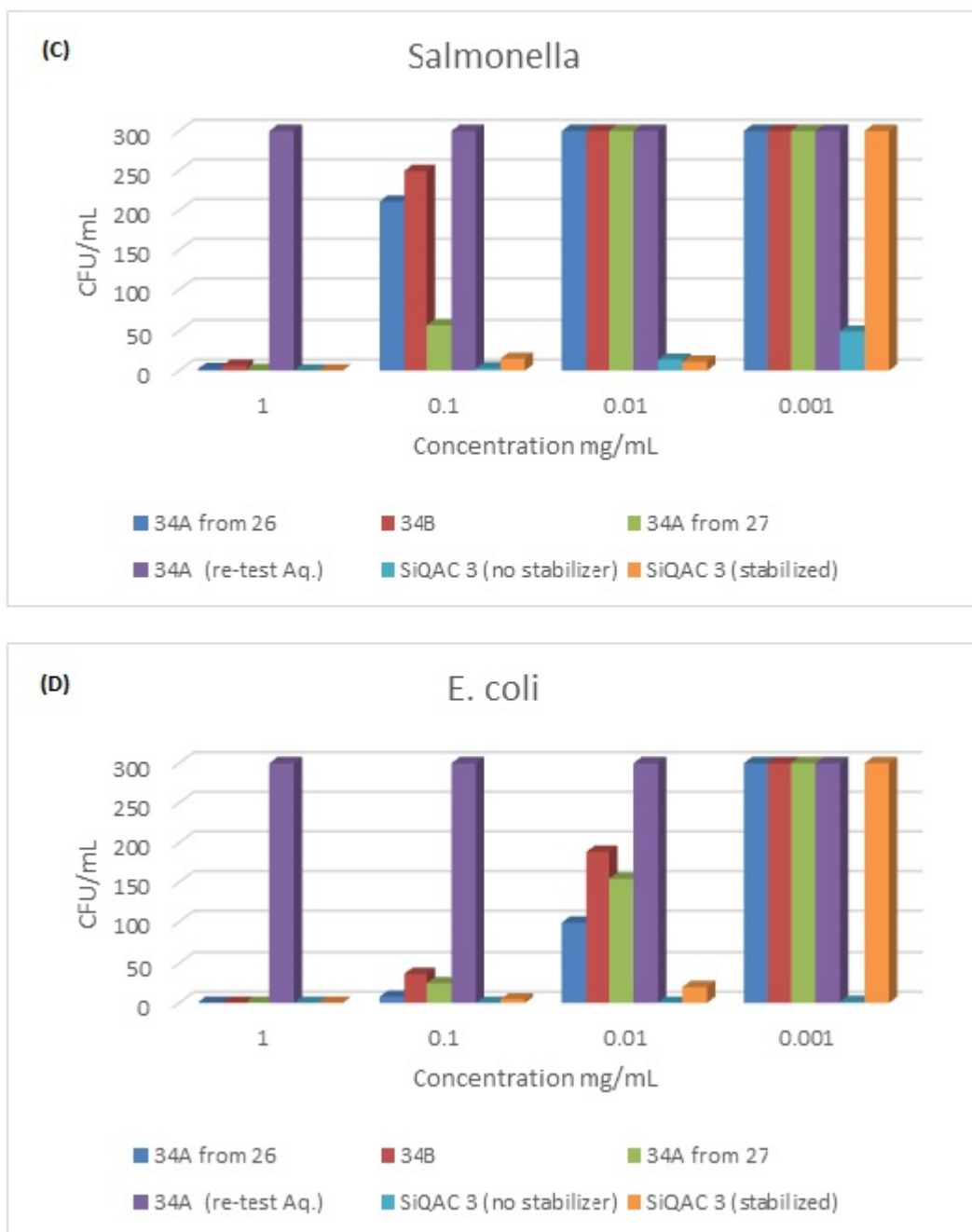


Figure 2.50: Experimentally determined MIC (CFU/mL) of SiQAC 3, 34A and 34B. MIC plate counts of samples were performed using a 10^{-3} (about 200000 cfu/ml) culture of *S. aureus* (A), *Listeria* (B), *Salmonella* (C), *E. coli* (D). Solutions of QAC samples were prepared in H₂O starting at 1mg/mL or 1% and diluted up 10^3 .

Table 2.12: MIC plate counts of samples using a 10^{-3} (about 200000 cfu/mL) culture of *S.aureus*.

QAC	0.01 g/mL	0.001g/mL	0.0001g/mL	0.00001g/mL
(26)	No Growth	No Growth	No Growth	No Growth

2.6.3.2 Contact Killing on Hard Surfaces

Antimicrobial activity of phosphonate QAC coatings and the silane QAC **3** for comparison purposes were prepared on metal surfaces (Ti, SS, Al) and tested by growth enumeration in the dry state testing method developed in the Wolfaardt lab against various strains of bacteria. Initially, 1% solutions of compound **34A** were electrosprayed in triplicate onto (Ti, SS, Al) and cured overnight at 120°C. However, no significant bacterial reduction was observed and the electrosprayed metal coupons were indistinguishable to the unsprayed controls (results not shown). Ti samples prepared by an overnight immersion in an aqueous or ethanolic solution of compound **34A** followed by an overnight cure at 100°C showed promising results versus uncured samples. Ti samples were coated with compound **34A** obtained by either TMSBr dealkylation of the ethyl ester (Et, TMSBr) or of the *i*Pr ester by the HCl method (*i*Pr, HCl). In both cases the ^{31}P NMR spectrum were identical, however, **34A** prepared by the TMSBr method was only slightly soluble in H₂O and was tested in ethanol, while **34A** prepared by the HCl method was tested in H₂O at 10 mg/mL. *S. aureus* and *Salmonella* inoculated antimicrobial Ti surfaces were sampled after 3 hrs of drying and showed 99-100% reduction in viable bacteria versus the controls and uncured surfaces (Figure 2.51).

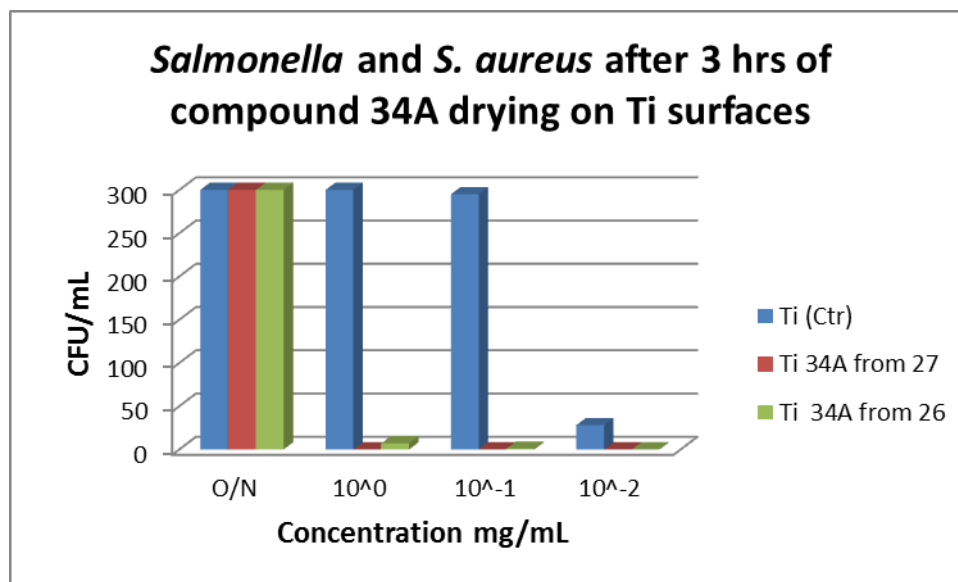


Figure 2.51: Colony forming units per mL of *Salmonella* and *S. aureus* after 3 hrs of drying on Ti surfaces. O/N is the initial concentration (10^5 cells/mL). 300 is the maximum cfu/mL. Blue rectangles = control untreated Ti, Red rectangles = compound **34A** coated Ti (obtained from dealkylation of the *i*Pr ester with HCl), Green = compound **34A** coated Ti (obtained from dealkylation of the ethyl ester with TMSBr)

After success with compound **34A** on Ti, other organophosphorus QAC's including the ester **26**, trimethylammnoium **35**, pyridinium **36** as well as the silane quat SiQAC **3** on Ti were evaluated against a strain of *P.aeruginosa* (PAO1) known for its robust survival on dry surfaces. Only compounds **26** and **34A** showed a significant reduction of bacterial colonies after 4 hrs of sampling while the shorter chain phosphonic acid QAC's **35**, **36** and the silane QAC **3** were indistinguishable from control samples (results not shown). As a result, no further sampling was performed on these surfaces. Instead the active compounds **26** and **34A** were used to coat other metals SS, Al along with Ti and these surfaces were tested with other bacterial strains.

Contact killing was observed immediately with compounds **26** and **34A** on all surfaces tested (Ti, SS, Al). After 2 hrs these antimicrobial coatings had killed all of the cells initially dried on each surface (10^6 bacterial cells, Table 2.13 for *Arthrobacter*, Table 2.14 for PAO1).

Control samples without such coatings showed some bacterial reduction but only after extended periods of time. Typically, 24 hrs were required to reduce the bacterial surface population from 10^6 cells to 10^5 - 10^3 depending on the surface of the controls (Table 2.13). Aluminum control surfaces showed the largest reduction of PAO1 by a factor of 10^3 after 24 hrs while their survival was highest on SS with 10^5 cells remaining after 24 hrs. Such reductions are typical over time on surfaces with limited nutrients necessary for bacterial survival and reproduction. From these observations, the phospholipid sponge mechanism is believed to be responsible for the rapid contact killing with the longer chain QAC's. These monolayer forming organophosphorus antimicrobials required both a quat and a long hydrophobic tail to effectively remove bacterial phospholipids when in close proximity to the cells whereas QAC's without a long hydrophobic chain such as **35** and **36** were completely inactive even though they contained the same number of ammonium (N^+) charges on the surface.

Table 2.13: *Arthrobacter* reduction by antimicrobial metal surfaces treated with **26** and **34A**.

<i>Arthrobacter</i> (CFU/mL)					
Entry	Sample	0 hrs	2 hrs	4 hrs	24 hrs
I	Ti (Ctr)	10^6	10^4	10^2	10^2
Ii	Ti (26)	10^6	0	0	0
Iii	Ti (34A)	10^6	0	0	0
Iv	SS (Ctr)	10^6	10^4	10^2	10^2
V	SS (26)	10^6	0	0	0
Vi	SS (34A)	10^6	0	0	0

Table 2.14: *P. aeruginosa* (PA01) reduction by antimicrobial metal surfaces treated with **26** and **34A**.

<i>P.aeruginosa</i> PA01 (CFU/mL)					
Entry	Sample	0 hrs	2 hrs	4 hrs	24 hrs
I	Ti (Ctr)	10 ⁶	10 ⁶	10 ⁵	10 ⁴
Ii	Ti (26)	10 ⁶	0	0	0
Iii	Ti (34A)	10 ⁶	0	0	0
Iv	Ti (34A)	10 ⁶	0	0	0
V	SS (Ctr)	10 ⁶	10 ⁶	10 ⁵	10 ⁵
Vi	SS (26)	10 ⁶	0	0	0
Vii	SS (34A)	10 ⁶	0	0	0
Viii	Al (Ctr)	10 ⁶	10 ⁶	10 ⁴	10 ³
Ix	Al (26)	10 ⁶	0	0	0
X	Al (34A)	10 ⁶	0	0	0

Surfaces treated with compound **34A** (Table 2.13, Entries i-iii) were further tested to determine if antimicrobial activity was retained. Samples stored in saline for 24 hrs from the first antimicrobial trial were removed, dried, washed in distilled H₂O, dried, re-innoculated and then retested. All samples from the second trial showed similar *Anthrobacter* colony reductions (10⁶ to 0) indicating the molecule was truly immobilized (Table 2.15). The effectiveness of the antimicrobial Ti treated with **34A** to withstand *Anthrobacter* colonization was also demonstrated on agar. The control samples were fully colonized by the bacterium, while the antimicrobial treated Ti sample, effectively killed *Anthrobacter* on contact and no colonies were observed around the metal coupons (Figure 2.52).

Table 2.15: *P. aeruginosa* (PA01) reduction by antimicrobial Ti surfaces treated with **34A** and retested.

<i>P. aeruginosa</i> (PA01) (CFU/mL)				
Entry	Sample	0 hrs	2 hrs	4 hrs
i	Ti (Ctr)	10^6	10^4	10^2
ii	Ti (34A)	10^6	0	0
iii	Ti (34A)	10^6	0	0
iv	Ti (34A)	10^6	0	0

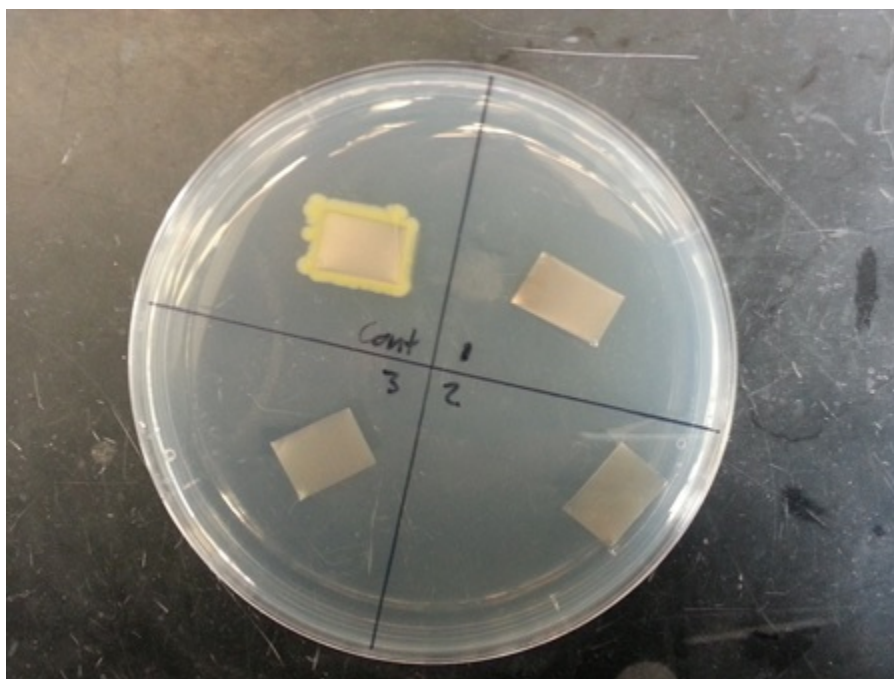


Figure 2.52: Agar growth method showing *P. aeruginosa* (PA01) reduction by antimicrobial Ti surfaces treated with **34A**. (Cont = control, 1, 2, 3 = compound **34A**).

The amount of bacteria initially dried on the metal surfaces tested was determined by serial dilutions and agar plate counts until a countable amount of colonies was observed. For example after six dilutions of the original stock of bacteria applied to Ti and SS, 58 colonies were counted at the beginning of sampling ($T = 0$) which corresponds to a concentration of $\sim 10^6$ cells (Table 2.16, 2.17).

Table 2.16: Determination of initial bacterial load dried on titanium surfaces from plate counts (raw data). Tmtc = too many to count.

<i>Arthrobacter</i> (Titanium) (CFU/mL)								
Control	10^0	10^{-1}	10^{-2}	10^{-3}	10^{-4}	10^{-5}	10^{-6}	10^{-7}
0 hrs	tmtc	tmtc	tmtc	tmtc	tmtc	tmtc	58	5
4 hrs	tmtc	285	24	0	0	0	0	0
24 hrs	tmtc	tmtc	35	3	0	0	0	0

Table 2.17: Determination of initial bacterial load dried on SS surfaces from plate counts (raw data).

<i>Arthrobacter</i> (Stainless Steel) (CFU/mL)								
Control	10^0	10^{-1}	10^{-2}	10^{-3}	10^{-4}	10^{-5}	10^{-6}	10^{-7}
0 hrs	Tmtc	tmtc	tmtc	tmtc	tmtc	tmtc	40	2
4 hrs	Tmtc	tmtc	32	5	0	0	0	0
24 hrs	Tmtc	tmtc	34	4	0	0	0	0

3.0 CONCLUSION

Water soluble quats with anchors specific for forming monolayers onto porous ($[(C_{18}H_{37}-NH-(CH_2)_3-NMe_2-R^+][Cl^-]$ (**3**; anchor = $-Si(OMe)_3$) and non-porous metal oxide (Ti, SS, Al) ($[(C_{18}H_{37}-NH-(CH_2)_3-NMe_2-R^+][Cl^-]$ (**26**; anchor = $-PO(OEt)_2$, **34**; $-PO(OH)_2$) and plastic surfaces (silicones, PP) ($[(C_{18}H_{37}-NH-(CH_2)_4-NMe_2-R^+][Br^-]$ (**205**; anchor = $-benzophenone$), ($[benzophenone-NH-(CH_2)_3-NMe_2-R^+][X^-]$ (**206**; $R = -Si(OMe)_3$, $X^- = Cl^-$) were synthesized by the Menshutkin reaction and used to prepare antimicrobial coating on these surfaces. New compounds were successfully characterized by NMR spectroscopy (1H , ^{13}C , ^{29}Si , and ^{31}P where required), HRMS spectroscopy and in a few instances by X-ray crystallography (**34**, **66**, **19**, **220**).

Improvements in the synthesis of the organosilane QA antimicrobial dimethyloctadecyl[3-(trimethoxysilyl)propyl]ammonium chloride **3**, approved by the Environmental Protection Agency (EPA) and the Pest Management Regulatory Agency (PMRA) was performed both under solventless (72 hrs, $100^\circ C$, 80%) and solvent (MeOH, 48 hrs, 76%) conditions in a sealed tube (ST), as well as with μW radiation in MeOH (45 min, $150^\circ C$, 58%). In all cases, the reaction never reached full conversion even after prolonged heating.

Various monodentate organophosphorus phosphonates and phosphonic acid QAC's **34-37** with short and long chains were successfully synthesized and used to prepare antimicrobial surfaces on Ti, SS and Al. The didealkylation of phosphoate QAC's was explored for the first time under μW heating and proved to be extremely effective and rapid with the following reagents; TMSBr (ACN, 10 min, $60^\circ C$) , HCl (3 M, 30 min, $150^\circ C$) or HBr (3 N, 10 min, $150^\circ C$). Three bisphosphonate QAC's **93**, **121** and **140** were also prepared but their dealkylation to the corresponding phosphonic acids **96**, **126**, **141** was unsuccessful using either HBr or

TMSBr due to insolubility of the formed products in H₂O and organic solvents. Other multidentate phosphonic acid quats were targeted (**161**, **168**, **179**, **183**) but their synthesis was unsuccessful based on the synthetic schemes attempted. Novel thiol and catechol QAC's **194** and **189** were synthesized, both of which require further testing on metal surfaces.

Various new quaternary ammonium dansyl containing compounds with both alkoxysilane **213**, phosphonate **211-212**, **217**, thiolacetate **214**, acrylamide **219**, were similarly prepared and evaluated as potential fluorescent probes in antimicrobial coatings. Physical attachment of dansyl silane **213** to SiO₂ nanoparticles (NP's) and cotton surfaces after immersion in solutions containing the fluorescent dye was verified by exposure to UV light and by complexation with bromophenol blue that rendered the surfaces visibly blue in colour. Plastic surfaces (PP, silicon medical tubing) were UV cured with dansyl benzophenone **216** and resulted in the physical attachment of the dye visualized by UV light. Dansyl phosphonic acid, **217**, was attached to a stainless steel surface by exposure to an aqueous solution containing this dye, followed by a thermal cure (100°C, ON) resulting in the formation of a self-assembled fluorescent monolayer. Synthesis of a C₁₈ benzophenone QAC **205** was improved with μ W heating by lowering the reaction time to 2 min vs. an ON reflux in ACN. A new benzophenone QAC with a silane linker **206** was made and successfully visualized with bromophenol blue on PP and silicone surfaces with bromophenol blue. Antimicrobial activity of **205** and **206** on plastic surfaces remains to be tested. A dansyl amidine probe **222** prepared from dansyl amine **221** was expected to find use in the detection of microbial respiration CO₂, however, no change in fluorescence was observed after exposure to CO₂.

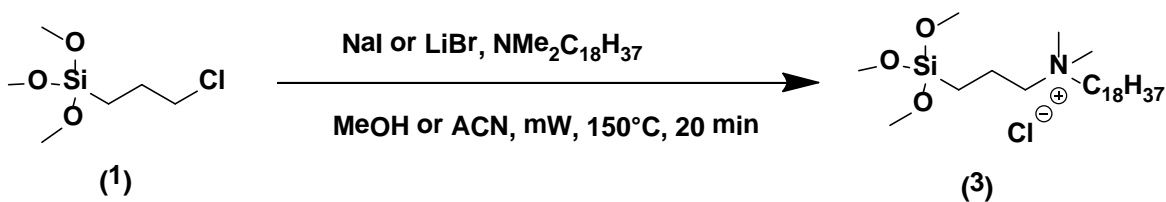
Presence of non-fluorescent antimicrobial QAC coatings on surfaces was successfully detected using the bromophenol blue test. Antimicrobial activity was tested in solution by MIC

determinations and in the solid state (metal surfaces only, Ti, SS, Al) by growth enumeration in the dry state. SiQAC **3** was found to be the most biocidal in solution with an MIC of $\sim 100 \mu\text{g/g}$ which is in close agreement to the literature value of $80 \mu\text{g/g}$. Compounds **26** and **34** on the other hand were more biocidal on metal oxide surfaces and were capable of reducing initial concentrations of *Salmonella*, *Arthrobacter*, *S. aureus* and *P. aeruginosa* by a factor of 10^6 (100%) after a contact time of 2 hrs and maintained their activity after 24 hrs. Re-testing the same active antimicrobial Ti surfaces after 3 weeks with another challenge of bacteria was performed and was also successful. Identical reductions in *Arthrobacter* colonies after a contact time of 2 hrs were observed 10^6 cells \rightarrow 0 cells (100%). These antimicrobial surfaces are believed to kill bacteria on contact because their MIC's are higher in solution compared to compound **3** and the monolayer concentrations of **26** and **34** are too small to effectively kill 10^6 cells if these surfaces released the antimicrobial upon testing.

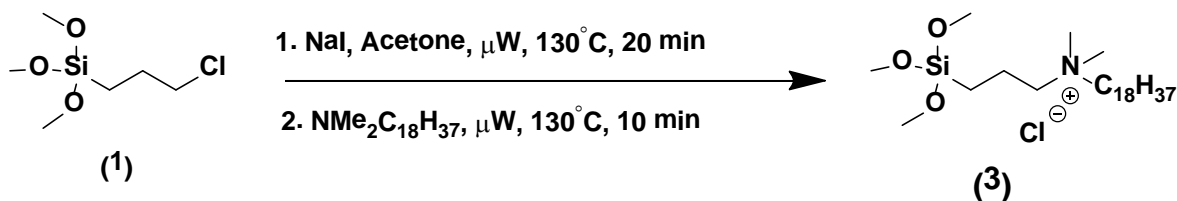
4.0 FUTURE WORK

Another possibility to improving the commercial synthesis of the Dow antimicrobial (SiQAC, **3**) which utilizes the unreactive chlorosilane **1** (see Section 2.1.1), would entail the addition of a catalytic or stoichiometric amount of NaI or LiBr for a onepot Finkelstein / Menshutkin reaction. This would lead to the *in situ* formation of the more reactive iodo or bromosilane and would allow for shorter reaction times and complete conversion to the quat, previously impossible with the chlorosilane (Scheme 4.1 A). Alternatively the Finkelstein/Menschutkin reaction could be performed sequentially with isolation of the iodosilane and the quaternization with dimethyloctadecylamine (Scheme 4.1 B).

(A) One Pot



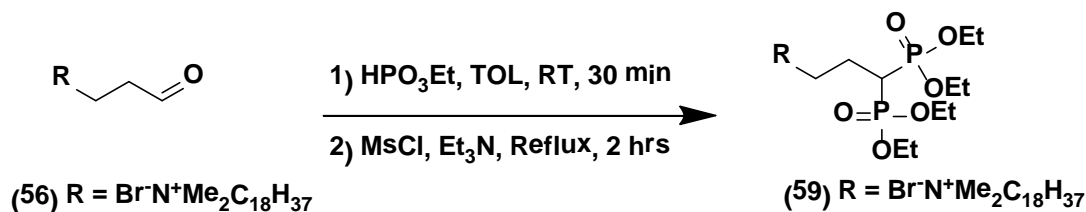
(B) Sequential



Scheme 4.1: Catalytic Finkelstein / Menshutkin reaction in the preparation of the Dow antimicrobial **3**.

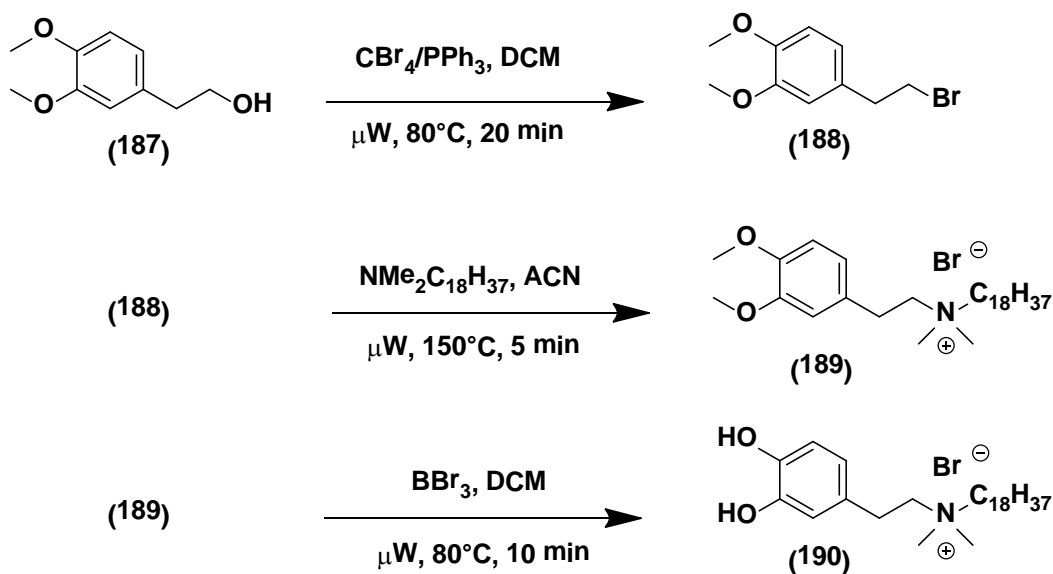
The onepot bis addition of dialkylphosphites to aldehydes (see Section 2.1.2.3) needs to be further explored with the aldehyde quat precursor, **56**, obtained by oxidation of the quat

alcohol with PCC/DCM (see Section 2.1.2.3). Precursor **56** would be an ideal starting material in preparing the target bisphosphonate, **59**, in high yielding single pot reaction (Scheme 4.2).

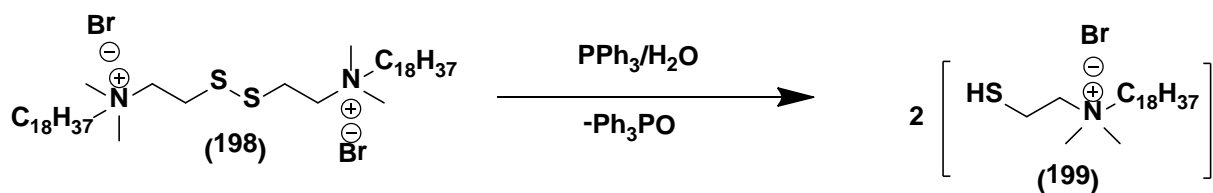


Scheme 4.2 .Onepot preparation of α -CH-bisphosphonates from the aldehyde quat precursor, **56**.

The syntheses of catechol and disulfide QAC's **190** and **199** respectively remains to be finished (see Section 2.3 and 2.4). The final deprotection of catechol QAC **189** remains to be attempted with either BBr₃/DMC or HBr under microwave irradiation (Scheme 4.3). Likewise the final cleavage of the disulfide QAC with PPh₃/H₂O remains to be performed to obtain the target thiol QAC **199** (Scheme 4.4).

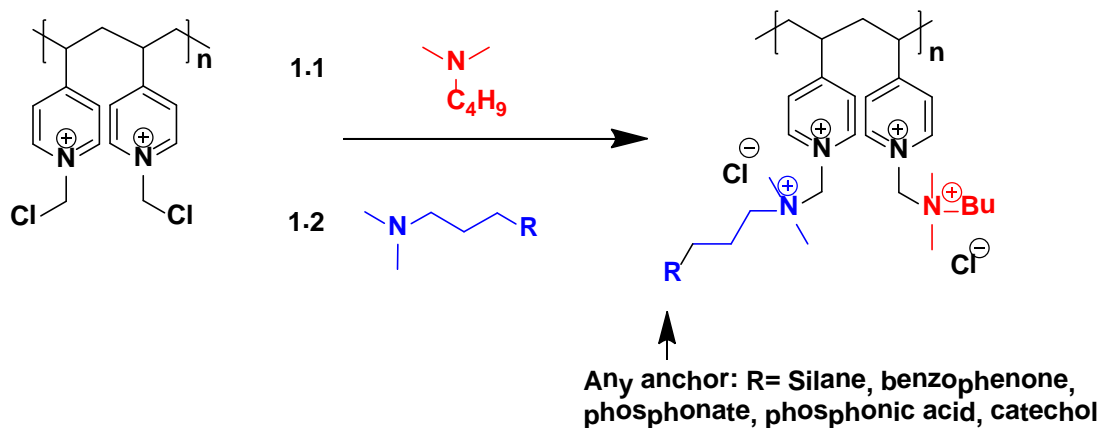


Scheme 4.3: Preparation of catechol QAC, **190**.

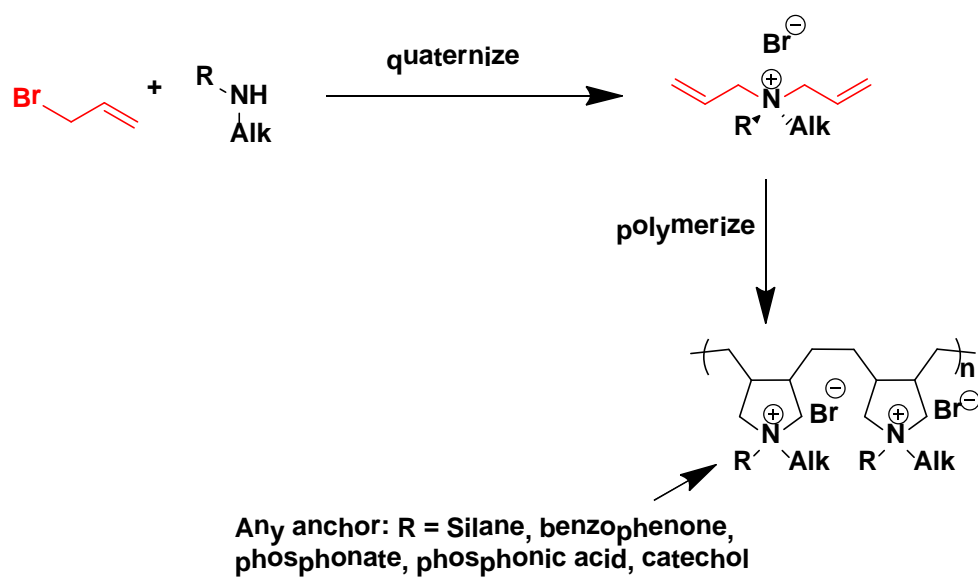


Scheme 4.4: Preparation of thiol QAC, **199**.

The next generation of QA antimicrobials would be capable of binding to every possible surface (eg. both porous and non-porous: metal and plastic surfaces). Synthesis of a universal surface antimicrobial with multiple functional anchors is attractive with the commercially available polymer (Scheme 4.5). Different anchor groups including: silane, phosphonate, catechol and benzophenone groups could potentially be quaternized onto the polymer backbone. Dual cleavage of the catechol, and phosphonate groups may be achieved with BBr_3 if desired. Alternatively, a series of diallyl monomers with different anchors can be co-polymerized to create multifunctional polymer coatings (Scheme 4.6).



Scheme 4.5: Synthesis of multifunctional QAC antimicrobial polymer coating.



Scheme 4.6: Synthesis of multifunctional QAC antimicrobial polymer coating.

5.0 - EXPERIMENTAL PROCEDURES

5.1 Materials and Instrumental Methods

The majority of reagents and solvents were obtained from Sigma-Aldrich (S-A) or Alfa Aesar (A-A) and used as received. Reagents that were purified by vacuum distillation prior to use and include *N,N*-dimethyloctadecylamine (89%), octadecylamine, triethyl and triisopropyl phosphites. Bromooctadecane was purified by column chromatography eluting with 10% acetone/hexanes.

The following anhydrous solvents, ACN (99.8%), 1,4-dioxane, DMF, DMSO, TOL and non-anhydrous solvents, MeOH, EtOH (95%), *i*PrOH, EtOAc and hexanes were purchased from Aldrich and used as received. Anhydrous DCM and THF were obtained from a mBraun solvent purification system by passage of the wet solvent through a bed of activated molecular sieves under an atmosphere of dry nitrogen.

Nuclear magnetic resonance (NMR) experiments were recorded on a 400 MHz Bruker Avance II Spectrometer (Ryerson University) using deuterated chloroform (CDCl_3) as the solvent unless otherwise indicated. ^1H and ^{13}C NMR spectra were referenced to the residual CDCl_3 (7.26 ppm and 77.0 ppm) solvent signal while ^{31}P spectrum were referenced externally to H_3PO_4 (0 ppm). Proton chemical shift assignments are given in δ (ppm) and were interpreted with the aid of 2-D COSY spectra (Section 6, Appendix 1.2), while carbon chemical shift assignments are given in δ (ppm) and were interpreted with the aid of 2-D HSQC spectra (Section 6, Appendix 1.2).

μW reactions were performed in sealed glass reaction tubes utilizing the Biotage® Initiator μW Synthesizer (2.45 GHz) at the Ryerson University Analytical Centre (RUAC). UV-

VIS and fluorescence measurements were recorded on a Perkin Elmer Spectrophotometer (Lambda 20) at the Ryerson University Analytical Centre (RUAC).

High resolution mass spectra (HRMS) were recorded by direct analysis in real time by DART-TOF or by electrospray time-of-flight (ESI-TOF) at the Advanced Instrumentation for Molecular Structure (AIMS) laboratory at the University of Toronto. X-ray crystal structure analysis was performed with a Bruker-Nonius Kappa-CCD diffractometer at the University of Toronto X-ray facilities.

Thin Layer Chromatography (TLC) was carried out on Silica gel 60 aluminum backed plates and visualized with a UV lamp or staining with (KMnO₄ or ninhydrin). Melting points were measured using a Fischer Scientific melting point apparatus. All prepared intermediates and compounds were stored in glass vials at RT while the dansyl derivatives were stored in the dark at RT.

5.2 General Procedures

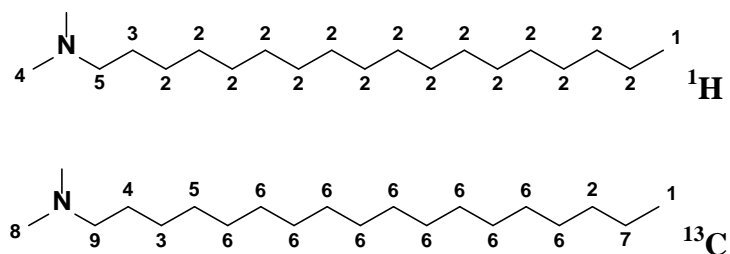
Method 5.2.1 Sealed Tube Reactions

The appropriate reactants were placed, along with a magnetic stirring bar, into a 20 mL glass scintillation vial and sealed with a screw cap. The reaction mixture was heated using an oil or sand bath at the indicated time and temperature. The reaction was transferred to a round bottom flask, and volatiles removed on a rotary evaporator and the crude material purified either by distillation, Dry Column Vacuum Chromatography (DCVC) on silica gel or crystallization as indicated. In the case of dansyl derivatives, Et₂O was added directly to the reaction mixture followed by decanting (repeat Et₂O wash \times 2) and drying under high vacuum.

Method 5.2.2 μ W Reactions

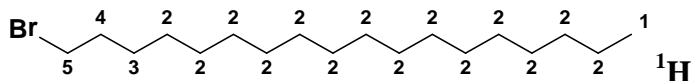
The appropriate reactants were placed, along with a magnetic stirring bar, into the appropriate size glass reaction tube (5 mL or 20 mL supplied from Biotage) and sealed with a septum/aluminum cap. The reaction mixture was heated in the Biotage® Initiator μ W Synthesizer at the indicated time and temperature. Reaction mixtures were transferred to a round bottom flask and removed on a rotary evaporator and the crude material purified either by distillation, crystallization or Dry Column Vacuum Chromatography (DCVC) on silica gel as indicated.

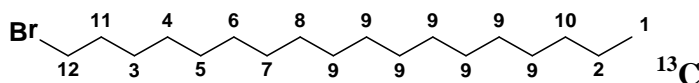
5.2.3 Purification/Preparation of Common Starting Materials



N,N-dimethyloctadecan-1-amine (2):

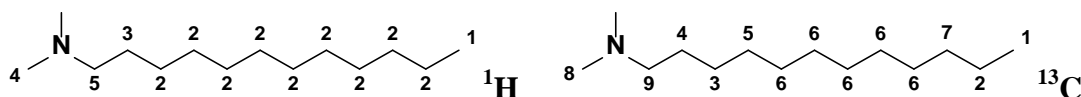
This amine was purified by vacuum distillation (150°C, 0.5 mmHg) using a shortpath distillation head attached to a Schlenk line utilizing a silicon oil bath (200°C) and isolated as a clear, colourless liquid that solidified at RT. ^1H NMR (400 MHz, CDCl_3 , δ): 2.24-2.14 (m, 8H, (H4, H5 overlap)), 1.45-1.36 (m, 2H, H3) 1.22 (brs, 30H, H2 overlap), 0.84 (t, $J = 7.1$ Hz, 3H, H1) ppm; ^{13}C NMR (100 MHz, CDCl_3 , δ): 60.0 (C9), 45.5 (C8), 31.9 (C7), 29.7-29.6 (C6 overlap), 29.3 (C5), 27.8 (C4), 27.5 (C3), 22.7 (C2), 14.1 (C1) ppm.





1-Bromooctadecane (46):

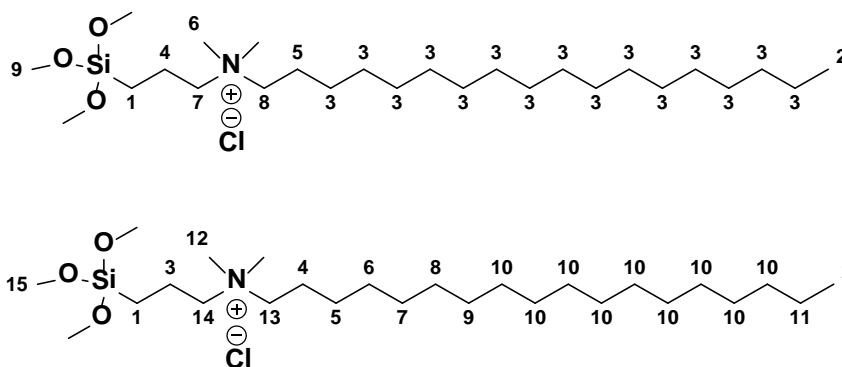
This starting material from Aldrich (brown solid, 97%) was packed onto silica (20g / (~ 20 mL SM) and purified by dry column chromatography (4.5 cm \times 5.0 cm frit, 50 g silica) eluting with 10% acetone/hexanes (150 mL) to afford ~ 9 g of a clear oil that solidified at RT. (Note: the brown coloured impurities remained on column under these conditions but will elute in 50% acetone/hexanes). ^1H NMR (400 MHz, CDCl_3 , δ): 2.21-2.14 (m, 2H, H5), 1.88-1.81 (m, 2H, H4), 1.46-1.38 (m, 2H, H3), 1.24 (brs, 28H, H2), 0.86 (t, $J = 7.0$ Hz, 3H, H1) ppm; ^{13}C NMR (100 MHz, CDCl_3 , δ): 33.9 (C12), 32.8 (C11), 31.9 (C10), 29.7-29.6 (C8, C9 overlap), 29.5 (C7), 29.4 (C6), 29.3 (C5), 28.7 (C4), 28.2 (C3), 22.7 (C2), 14.1 (C1) ppm.



N,N-dimethyldodecan-1-amine (22):¹⁹³

This compound was prepared by Method 5.2.2 with the EC reaction. ^1H NMR (400 MHz, CDCl_3 , δ): 2.21-2.14 (m, 8H, (H4 + H5 overlap)), 1.44-1.36 (m, 2H, H3) 1.21 (brs, 30H, H2 overlap), 0.84 (t, $J = 7.0$ Hz, 3H, H1) ppm; ^{13}C NMR (100 MHz, CDCl_3 , δ): 60.0 (C9), 45.5 (C8), 31.9 (C7), 29.7-29.6 (C6 overlap), 29.3 (C5), 27.8 (C4), 27.5 (C3), 22.7 (C2), 14.1 (C1) ppm. (Agrees well with literature NMR values).¹⁹³

5.2.4 Dow Antimicrobial Synthesis



N,N-dimethyl-*N*-(3-(trimethoxysilyl)propyl)nonadecan-1-ammonium chloride (**3**):^{194, 219}

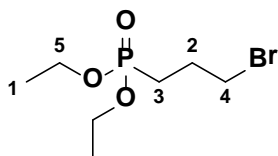
See (Table 2.2, Entry iii). This compound was synthesized according to Method 5.2.1 by heating 3-chloropropyltrimethoxysilane **1** (0.814 g, 4.1 mmol, 1.05 eq.) and *N,N*-dimethyloctadecyl-1-amine (DMOA) **2** (1.190 g, 4 mmol, 1.0 eq.) neat for 72 hrs at 110°C. Crude yield: ~ 80% by ¹H NMR spectroscopy (Section 6, Appendix 1.2, Figure A19). ¹H NMR (400 MHz, CDCl₃, δ): 3.33 (s, 9H, H₉), 3.32-3.08 (m, 10H, (H₈ + H₇ + H₆ overlap)), 1.67-1.41 (m, 4H, (H₅ + H₄ overlap)), 1.01 (s, 30H, H₃), 0.63 (t, *J* = 7.0 Hz, 2H, H₂), 0.44 (t, *J* = 7.4 Hz, 2H, H₁) ppm; ¹³C NMR (100 MHz, CDCl₃, δ): 65.56 (C₁₅), 64.14 (C₁₄), 50.61 (C₁₃), 31.69 (C₁₁), 29.5-29.35 (C₁₀ overlap), 29.26 (C₉), 29.18 (C₈), 29.12 (C₇), 29.03 (C₆), 22.44 (C₅), 16.26 (C₄), 15.02 (C₃), 13.85 (C₂), 5.40 (C₁) ppm. (No NMR values reported in the literature).

5.3 General Procedure for the Synthesis of (γ –MPQA's)

5.3.1 Abruzov Reaction

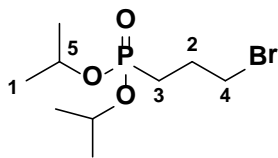
According to general procedures^{220,221} for the Abruzov reaction, to a flame dried round bottom flask equipped with a reflux condenser connected to an inert atmosphere manifold, were added the appropriate reagents according to (Table 2.3). The flask was evacuated (2 min), backfilled

with N₂ (g) and the reaction mixture refluxed for the appropriate time according to (Table 2.3) using an oil bath (175°C). The solution was then cooled to RT and excess dibromoalkane, trialkylphosphite and lower boiling by-products were removed by vacuum distillation (100°C, 1×10⁻² mm Hg) using a shortpath distillation head attached to a Schlenk line. Compounds (**2-1-2-7**) were vacuum distilled as clear, colourless liquids, while compound **2-8** was recrystallized from EtOAc as a brittle crystalline solid. This reaction was also performed under μ W radiation according to Method 5.2.2 and Table 2.3.



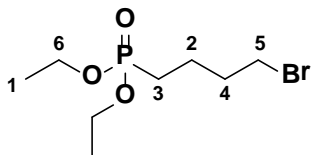
Diethyl (3-bromopropyl)phosphonate (**12**):²²⁰

See (Table 2.3, Entry iii). This compound was synthesized according to Method 5.2.1 by refluxing 1,3-dibromopropane (40 mL, 394 mmol, 4.0 eq.) and P(OEt)₃ (13 mL, 75.8 mmol, 1.0 eq.) for 6 hrs. Yield: 79% (15.54 g). TLC (10% MeOH:EtOAc, KMnO₄ stain), R_f = 0.65; ¹H NMR (400 MHz, CDCl₃, δ): 4.12-4.00 (m, 4H, H5), 3.43 (t, 2H, J = 4.3 Hz, H4), 2.16-2.05 (m, 2H, H3), 1.90-1.81 (m, 2H, H2), 1.28 (t, J = 7.0 Hz, 6H, H1) ppm; ¹³C NMR (100 MHz, CDCl₃, δ): 61.6 (d, $^2J_{C-P}$ = 6.5 Hz, (C5)), 33.71 (d, $^3J_{C-P}$ = 18.6 Hz, (C4)), 25.92 (d, $^2J_{C-P}$ = 4.4 Hz, (C2)), 23.64 (d, $^1J_{C-P}$ = 142.5 Hz, (C3)), 16.4 (d, $^2J_{C-P}$ = 6.2 Hz, (C1)) ppm; ³¹P NMR (121.45 MHz, CDCl₃, δ): 30.2 ppm. (Agrees well with literature NMR values).²²⁰



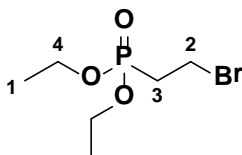
Diisopropyl (3-bromopropyl)phosphonate (13):²²²

See (Table 2.3, Entry vii). This compound was synthesized according to Method 5.2.2 by μ W heating 1,3-dibromopropane (5.48 mL, 53.9 mmol, 1.1 eq.) and $\text{P}(\text{OiPr})_3$ (11.16 mL, 49 mmol, 1.0 eq.) for 5 min at 170°C. The title compound **13** was isolated as a mixture after distillation with tetraisopropyl propane-1,3-diylbis(phosphonate) by-product A and 1-isopropoxyphospholane 1-oxide by-product B in a 0.05:0.05:1 mass ratio determined by ^{31}P NMR spectroscopy. Of the 10.45 g isolated, approximately (5%, 0.522 g) was the bisphosphonate and the other (5%, 0.522 g) was the cyclic 5-membered ring oxaphospholane. Yield: 64% (9.45 g). TLC (10% MeOH, EtOAc, KMnO_4 stain), $R_f = 0.7$; ^1H NMR (400 MHz, CDCl_3 , δ): 4.70-4.61 (m, 2H, H5), 3.42 (t, 2H, $J = 6.5$ Hz, H4), 2.15-2.04 (m, 2H, H3), 1.85-1.75 (m, 2H, H2), 1.27 (d, $J = 7.21$ Hz, 12H, H1) ppm; ^{13}C NMR (100 MHz, CDCl_3 , δ): 70.12 (d, $^2J_{\text{C-P}} = 6.51$ Hz, (C5)), 33.70 (d, $^3J_{\text{C-P}} = 20.38$ Hz, (C4)), 26.19 (d, $^1J_{\text{C-P}} = 4.32$ Hz, (C2)), 25.76 (d, $^2J_{\text{C-P}} = 25.76$ Hz, (C3)), 24.01 (t, $^2J_{\text{C-P}} = 3.44$ Hz, (C1)) ppm; ^{31}P NMR (121.45 MHz, CDCl_3 , δ): 28.34 ppm. (Agrees well with literature NMR values).²²²

**Diethyl (4-bromobutyl)phosphonate (14):**²²³

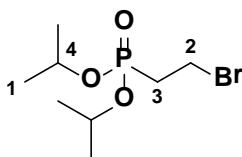
See (Table 2.3, Entry ix). This compound was synthesized according to Method 5.2.2 by μ W heating 1,4-dibromobutane (0.88 mL, 8.69 mmol, 1.1 eq.) and $\text{P}(\text{OEt})_3$ (1.32 mL, 7.9 mmol, 1.0 eq.) for 5 min at 190°C. Isolated as a mixture with the bisphosphonate tetraethyl butane-1,4-diylbis(phosphonate) and $\text{P}(\text{OEt})_3$ in a 0.1:0.29:1 mass ratio determined by ^{31}P NMR. Of the 1.32

g isolated, approximately (~ 10%, 0.132 g) was the bisphosphonate by-product B and (~ 29%, 0.27 g) was by-product A. Yield: 63% (0.95 g). TLC (10% MeOH:EtOAc, KMnO₄ stain), R_f = 0.65; ¹H NMR (400 MHz, CDCl₃, δ): 4.10-3.93 (m, 4H, H6), 3.38-3.29 (m, 2H, H5), 1.91-1.80 (m, 2H, H4), 1.75-1.60 (m, 4H, (H2, H3)), 1.30-1.20 (m, 6H, H1) ppm; ³¹P NMR (121.45 MHz, CDCl₃, δ): 31.23 ppm. (Agrees well with literature NMR values).²²³



Diethyl (2-bromoethyl)phosphonate (**15**):²²¹

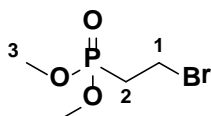
See (Table 2.3, Entry xiii). This compound was synthesized according to Method 5.2.1 by refluxing 1,2-dibromoethane (40 mL, 394 mmol, 4.0 eq.) and P(OEt)₃ (13 mL, 75.8 mmol, 1.0 eq.) for 4.3 hrs. The title compound **15** was purified by distillation and used directly without ¹H and ¹³C NMR characterization in the synthesis of diethyl vinyl phosphonate **130**.



Diisopropyl (2-bromoethyl)phosphonate (**16**):²²⁴

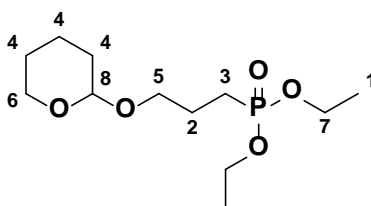
See (Table 2.3, Entry xv). This compound was synthesized according to Method 5.2.1 by refluxing 1,2-dibromoethane (49.6 mL, 576 mmol, 4.0 eq.) and P(OiPr)₃ (32.8 mL, 144 mmol, 1.0 eq.) for 12 hrs. The title compound was isolated as a mixture after distillation with tetraisopropyl ethane-1,2-diylbis(phosphonate) by-product B and by-product A in a 0.09:0.1:1 mass ratio determined by ³¹P NMR spectroscopy. Of the 24.82 g isolated, approximately (~ 10%,

2.36 g) was identified as bisphosphonate and the other (~ 10%, 2.36 g) was the by-product A. Yield: 64% (20.10 g). TLC (10% MeOH, EtOAc, KMnO₄ stain), R_f = 0.7; **¹H NMR** (400 MHz, CDCl₃, δ): 4.68-4.58 (m, 2H, H4), 3.43 (q, *J* = 8.8 Hz, 2H, H3), 3.31-2.20 (m, 2H, H2), 1.24 (d, *J* = 6.2 Hz, 12H, H1) ppm; **¹³C NMR** (100 MHz, CDCl₃, δ): 70.61 (d, ²*J*_{C-P} = 6.70 Hz, (C4)), 32.05 (d, ²*J*_{C-P} = 134.80 Hz, (C2)), 24.10 (s, C3), 23.90 (t, ²*J*_{C-P} = 3.0 Hz, (C1)) ppm; **³¹P NMR** (121.45 MHz, CDCl₃, δ): 28.34 ppm. (Agrees well with literature NMR values).²²⁴



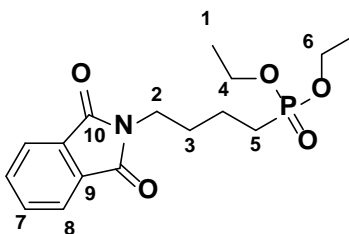
Dimethyl (2-bromoethyl)phosphonate (17):²²⁵

See (Table 2.3, Entry xvi). This compound was synthesized according to Method 5.2.1 by refluxing 1,2-dibromoethane (24.12 mL, 280 mmol, 4.0 eq.) and P(OMe)₃ (11.05 mL, 70 mmol, 1.0 eq.) for 12 hrs. Yield: 65% (10 g). TLC (10% MeOH, EtOAc, KMnO₄ stain), R_f = 0.7; **¹H NMR** (400 MHz, CDCl₃, δ): 3.60-3.46 (m, 6H, H3), 1.30-1.26 (m, 2H, H2), 1.25-1.21 (m, 2H, H1), ppm; **¹³C NMR** (100 MHz, CDCl₃, δ): 51.9 (d, ²*J*_{C-P} = 6.6 Hz, (C3)), 10.2 (C1), 8.8 (C2) ppm; **³¹P NMR** (121.45 MHz, CDCl₃, δ): 33.10 ppm. (Agrees well with literature NMR values).²²⁵



Diethyl (3-((tetrahydro-2H-pyran-2-yl)oxy)propyl)phosphonate (18):²²⁶

To a 20 mL conical round bottom flask was added the THP protected bromopropylalcohol **10** (4.55 g, ~ 20 mmol) followed by excess $\text{P}(\text{OEt})_3$ (10.0 mL, 60.0 mmol, 3.0 eq.). The reaction was heated at reflux (175°C) overnight. Excess $\text{P}(\text{OEt})_3$ was vacuum distilled at reduced pressure providing the pure product as a clear, viscous oil. Yield 89% (5.0 g). ^1H NMR (400 MHz, CDCl_3 , δ): 4.57 (t, $J = 3.54$ Hz, 1H, H8), 4.17-4.04 (m, 4H, H7), 3.86-3.72 (m, 2H, H6), 3.52-3.40 (m, 2H, H5), 1.93-1.77 (m, 4H, H3 + H4), 1.73-1.67 (m, 4H, H2), 1.31 (t, $J = 7.04$ Hz, 6H, H1) ppm; ^{13}C NMR (100 MHz, CDCl_3 , δ): 98.90 (C8), 67.50 (d, $^3J_{\text{C-P}} = 6.5$ Hz, (C5)), 62.3 (C6), 61.45 (d, $^2J_{\text{C-P}} = 3.7$ Hz, (C7)), 32.90 (C4), 30.65 (d, $^3J_{\text{C-P}} = 9.9$ Hz, (C5)), 25.43 (C4), 23.15 (d, $^2J_{\text{C-P}} = 3.7$ Hz, (C3)), 19.45 (d, $^2J_{\text{C-P}} = 2.3$ Hz, (C2)) 16.45 (d, $^3J_{\text{C-P}} = 5.9$ Hz, (C1)) ppm; ^{31}P NMR (121.45 MHz, CDCl_3 , δ): 32.32 ppm. (Agrees well with literature NMR values).²²⁶



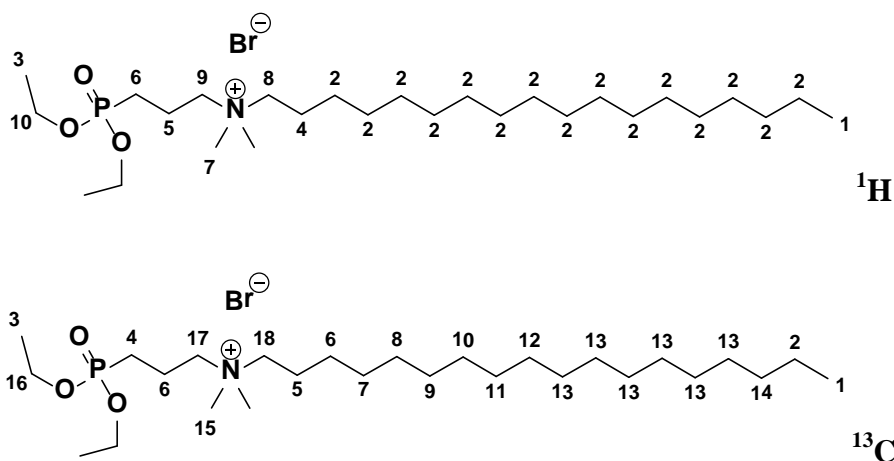
Diethyl (4-(1,3-dioxoisindolin-2-yl)butyl) phosphonate (19):²²⁷

To a flame dried 50 mL round bottom flask equipped with a reflux condenser was added *N*-(4-bromobutyl)-phthalimide (5g, 17.7 mmol, 1.0 eq.) followed by $\text{P}(\text{OEt})_3$ (18.24 mL, 106.3 mmol, 6 eq.) and the mixture was refluxed overnight (175°C) using a sand bath. The reaction was then cooled to RT and excess $\text{P}(\text{OEt})_3$ was vacuum distilled using a shortpath distillation head attached to a Schlenk line. Once all of the excess $\text{P}(\text{OEt})_3$ was removed, the title compound was placed under high vacuum (~ 30 min) until it solidified. Further recrystallization from EtOAc (5

mL) at -20°C provided pure product. Colourless crystals. Yield: 90% (5.43 g). TLC (5% MeOH: EtOAc), $R_f = 0.90$, $M_p = 80-81^{\circ}\text{C}$; $^1\text{H NMR}$ (400 MHz, CDCl_3 , δ): 7.82- 7.77 (m, 2H, H8), 7.70-7.66 (m, 2H, H7), 4.11-3.98 (m, 4H, H6), 3.66 (m, $J = 7.0$ Hz, 2H, H5), 1.81-1.71 (m, 4H, (H4, H3)), 1.67-1.56 (m, 2H, H2), 1.27 (t, $J = 7.1$ Hz, H1) ppm; $^{13}\text{C NMR}$ (100 MHz, CDCl_3 , δ): 168.29 (C10), 133.91 (C9), 132.06 (C7), 123.18 (C8), 61.48 (d, $^2J_{\text{C-P}} = 6.5$ Hz, (C6)), 37.23 (d, $^1J_{\text{C-P}} = 1.33$ Hz, (C5)), 29.25 (d, $^2J_{\text{C-P}} = 16.77$ Hz (C4)), 24.44 (C2), 19.81 (d, $^3J_{\text{C-P}} = 5.01$ Hz, (C3)), 16.42 (d, $^3J_{\text{C-P}} = 6.01$ Hz, (C1)) ppm; $^{31}\text{P NMR}$ (121.45 MHz, CDCl_3 , δ): 31.48 ppm. **HRMS-DART** (m/z): $[\text{M}^+]$ calculated for $\text{C}_{16}\text{H}_{23}\text{NO}_5\text{P}$, 340.1308; found, 340.1317. (Agrees well with literature NMR values).²²⁷

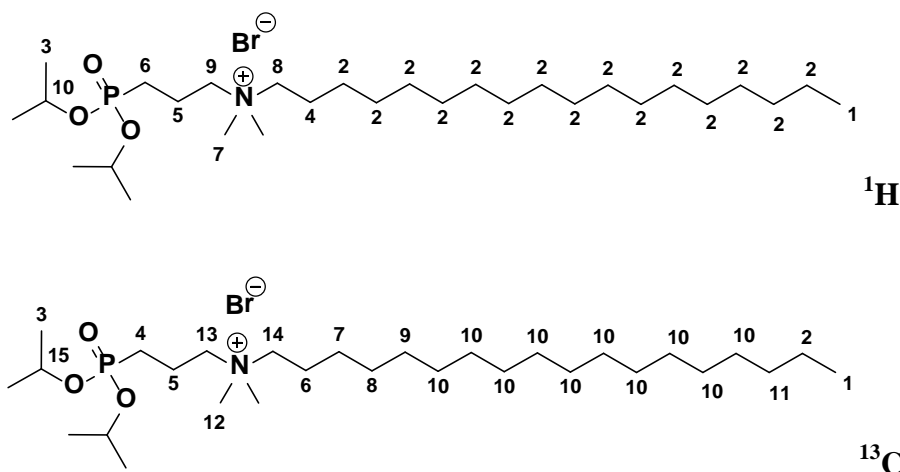
5.3.2 Menshutkin Quaternization

General Procedure for the Menshutkin Quaternization. The appropriate tertiary amine and alkyl halide (1-2 eq.) were mixed with ACN or EtOH (0.5 M) employing Method 5.2.1 or Method 5.2.2 and heated for the appropriate length of time (Table 2.4) until ^{31}P NMR spectroscopy showed the consumption of the starting phosphonates. The vial was allowed to cool to RT and the crude product was purified either by extraction (aq. phase isolated after washing with Et_2O for H_2O soluble compound only), centrifugation with a non-polar solvent, recrystallization, or dry packed onto silica and purified via dry column chromatography (4.5 cm \times 5.0 cm frit, 40 g silica), eluting with 6% NaBr in MeOH/ACN (20:80). This method was also successfully used to make compounds **26-33**, **40** (Scheme 2.2).



***N*-(3-diethoxyphosphorylpropyl)-*N,N*-dimethyloctadecan-1-ammonium bromide (**26**):**^{192,228}

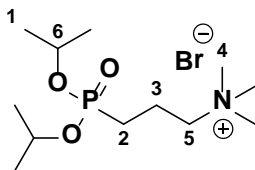
This compound was prepared by the Menshutkin reaction using Method 5.2.1, dimethyl (3-bromopropyl)phosphonate **12** (1.264g, 4.88 mmol) and *N,N*-dimethyloctadecylamine (DMOA) (1.71 g, 5.1 mmol, 1.1 eq.) were reacted neat for 35 min at 100°C until the mixture solidified. The mixture was then cooled to RT, centrifuged from hexanes (15 mL), and recrystallized from 20 mL EtOAc / hexanes (1:5) to afford **26**. Yield: 67% (1.82 g). Mp = 54-55 °C; ^1H NMR (400 MHz, CDCl_3 , δ): 4.09-4.01 (m, 2H, H10), 3.66-3.22 (m, 2H, H9) 3.43-3.38 (m, 2H, H8), 3.31 (s, 6H, H7), 2.03 (brs, 2H, H6), 1.84-1.80 (m, 2H, H5), 1.67 (brs, 2H, H4), 1.33-1.25 (m, 6H, H3), 1.19 (brs, 30H, H2), 0.83-0.79 (m, 3H, H1) ppm; ^{13}C NMR (100 MHz, CDCl_3 , δ): 64.25 (C18), 63.09 (d, $^3J_{\text{C-P}} = 6.54$ Hz, (C17)), 62.14 (d, $^2J_{\text{C-P}} = 6.54$ Hz, (C16)), 51.25 (C15), 31.86 (C14), 29.66-29.58 (C13 overlap), 29.55 (C12), 29.44 (C11), 29.38 (C10), 29.29 (C9), 29.19 (C8), 26.25 (C7), 22.69 (C6), 22.62 (C5), 16.49 (C4), 16.45 (C3), 16.39 (C2), 14.05 (C1) ppm; ^{31}P NMR (121.45 MHz, CDCl_3 , δ): 29.54 ppm. HRMS-DART (m/z): $[\text{M}^+] - \text{Br}^-$ calculated for $\text{C}_{27}\text{H}_{59}\text{NO}_3\text{P}$, 476.4227; found, 476.4240. (Agrees well with literature NMR values).^{192,228}



***N*-(3-(diisopropoxyphosphoryl)propyl)-*N,N*-dimethyloctadecan-1-ammonium bromide**

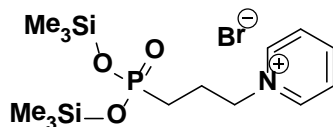
(27):

See (Table 2.4, entry iv). This compound was prepared by the Menshutkin reaction using Method 5.2.1. Diisopropyl (3-bromopropyl)phosphonate **13** (0.964g, 3.36 mmol) and DMOA (1g, 3.36 mmol, 1.0 eq.) were refluxed in ACN for 3 hrs. The mixture was then cooled to RT, poured into 20 mL of Et₂O, and placed into a freezer (-20°C) for 60 min to precipitate **27** as a white waxy solid. Yield: 89% (2.53 g). Mp = 54-55°C; ¹H NMR (400 MHz, CDCl₃, δ): 4.68-4.60 (m, 2H, H10), 3.78-3.67 (m, 2H, H9) 3.50-3.42 (m, 2H, H8), 3.39 (s, 6H, H7), 2.05-1.92 (m, 2H, H5), 1.83-1.62 (m, 4H, H4 + H6), 1.28 (d, ²*J* = 6.20 Hz, 12H, H3) 1.21 (brs, 30H, H2), 0.84 (t, *J* = 7.03 Hz, 3H, H1) ppm; ¹³C NMR (100 MHz, CDCl₃, δ): 70.65 (d, ²*J*_{C-P} = 6.54 Hz, (C15)), 64.09 (C14), 62.85 (d, ³*J*_{C-P} = 6.54 Hz, (C13)), 51.55 (C12), 31.84 (C11), 29.66-29.55 (C10 overlap), 29.40 (C9), 29.29 (C8), 29.18 (C7), 22.41 (d, ²*J*_{C-P} = Hz, (C6)), 23.95 (d, ¹*J*_{C-P} = Hz, (C5)), 22.61 (C4), 22.42 (C3), 16.70 (C2), 14.06 (C1) ppm; ³¹P NMR (121.45 MHz, CDCl₃, δ): 27.08 ppm. HRMS-DART (m/z): [M⁺] - Br⁻ calculated for C₂₉H₆₃NO₃P, 504.4540; found, 504.4546.



3-(diisopropoxyphosphoryl)-*N,N,N*-trimethylpropan-1-ammonium bromide (28):

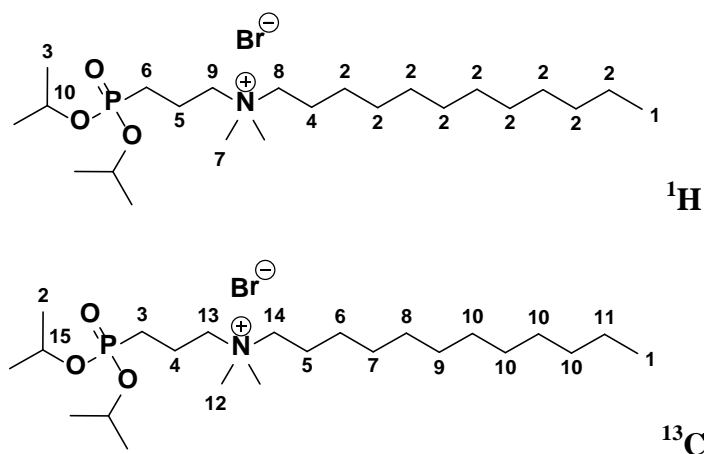
See (Table 2.4, Entry vi). $\text{NMe}_3 \cdot \text{HCl}$ (0.5g, 1.5 eq., 5.2 mmol) and NaOH (0.196 g, 1.4 eq., 4.9 mmol) were placed, with a magnetic stirring bar, into a 20 mL glass reaction tube and sealed. EtOH (18 mL) was injected via a syringe and the mixture was stirred for 2 min at RT to free base the $\text{NMe}_3 \cdot \text{HCl}$. Next diisopropyl (3-bromopropyl)phosphonate **13** (1.0 g, 3.48 mmol) was introduced via syringe and the reaction mixture was heated in the μW at 150 °C (3 min). Volatiles were removed on a rotary evaporator and the crude material purified by dissolving the mixture in CHCl_3 (30 mL), filtering off salts through a short pad of Celite and extracting the title compound into 30 mL of H_2O . H_2O was co-evaporated from ACN (100 mL), and the final product was further dried under high vacuum (~ 1 hr). Compound **28** was isolated as a clear, colourless oil. Yield: 80% (0.96 g). ^1H NMR (400 MHz, CDCl_3 , δ): 4.69-4.53 (m, 2H, H6), 3.83-3.70 (m, 2H, H5) 3.51-3.36 (brs, 9H, H4), 2.10-1.93 (m, 2H, H3), 1.83-1.67 (m, 2H, H2), 1.36-1.20 (m, 12H, H1) ppm; ^{31}P NMR (121.45 MHz, CDCl_3 , δ): 26.77 ppm.



Bis(trimethylsilyl)-3-propylphosphonatepyridin-1-ium bromide (29):

See (Table 2.4, Entry viii). This compound was prepared in a one pot reaction on a 1.74 mmol scale by reacting pyridine (0.137g, 1.74 mmol) with diisopropyl (3-bromopropyl)phosphonate **13**

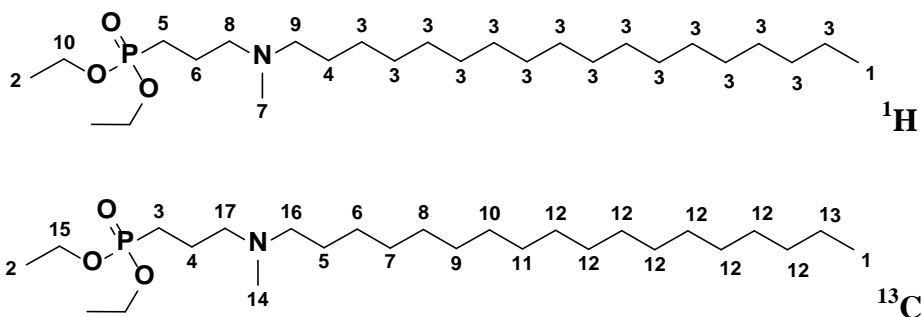
(0.5 g, 1.74 mmol) in ACN (1.5 mL) under μ W heating (150°C, 10 min). Next TMSBr (0.6 mL, ~2.5 eq.) was syringed into the same vial and heated in the μ W (60 °C, 10 min) to obtain a complete conversion of the TMS ester. ^{31}P NMR (121.45 MHz, CDCl_3 , δ): 10.60 ppm. This reactive intermediate was hydrolyzed directly with H_2O to compound **36** (Table 2.5, Entry ix).



***N*-(3-(diisopropoxyphosphoryl)propyl)-*N,N*-dimethyldodecan-1-ammonium bromide (**30**):**

See (Table 2.4, Entry ix). This compound was prepared by the Menshutkin reaction using Method 5.2.1: diisopropyl (3-bromopropyl)phosphonate **13** (1.13 g, 4.11 mmol, 1.15 eq.) and dimethyldodecylamine DMDA **22** (0.665 g, 3.58 mmol, 1.0 eq.) were refluxed in ACN for 4 hrs. The mixture was then cooled to RT, poured into 20 mL of Et_2O , and placed into a freezer (-20°C) for 24 hrs. No precipitation of the title compound was observed so volatiles were evaporated and the crude mixture containing 28% excess diisopropyl (3-bromopropyl)phosphonate **13** (δ = 28.31 ppm, ^{31}P NMR) was partitioned between 30 mL of H_2O and 30 mL DCM and left to settle overnight. In the absence of a clear separation, the volatiles were evaporated and the crude material was chromatographed eluting with acetone / MeOH (9:1) resulting in a mixed fraction and as a result **30** was analyzed impure with left over starting material **13**. Purification by further column chromatography was unsuccessful. Crude yield: 95% (1.70 g). ^1H NMR (400 MHz,

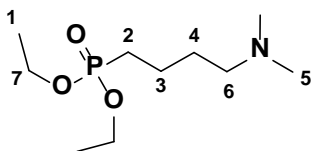
CDCl₃, δ): 4.72-4.61 (m, 2H, H10), 3.79-3.73 (m, 2H, H9) 3.52-3.36 (m, 2H, H8), 3.40 (s, 6H, H7), 2.17-1.94 (m, 2H, H6), 1.88-1.67 (m, 4H, H4 + H5), 1.36-1.17 (m, 30H, (H2 + H3 overlap)), 0.86 (t, $J = 7.03$ Hz, 3H, H1) ppm; ¹³C NMR (100 MHz, CDCl₃, δ): 70.77 (d, $^2J_{C-P} = 6.70$ Hz, (C15)), 70.19 (C14), 64.33 (C13), 51.27 (C12), 31.87 (C11), 29.60-29.50 (C10), 29.42 (C9), 29.38 (C8), 29.29 (C7), 29.20 (C6), 26.28 (C5), 24.01 (d, $^2J_{C-P} = 4.29$ Hz, (C4)), 22.69 (d, $^1J_{C-P} = 8.99$ Hz, (C3)), 16.79 (d, $J = 4.78$ Hz, (C2)), 14.08 (C1) ppm; ³¹P NMR (121.45 MHz, CDCl₃, δ): 27.04 ppm.



Diethyl (3-(methyl(octadecyl)amino)propyl)phosphonate (**31**):

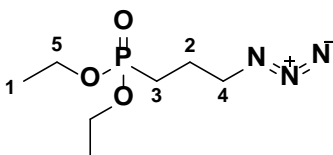
A solution of *N*-methyloctadecylamine (0.284 g, 1 mmol), *N,N*-diisopropylethylamine (0.26 mL, 1.5 mmol, 1.5 eq.), diethyl (3-bromopropyl)phosphonate **12** (0.2 mL, 1.1mol, 1.1eq.) in 10 mL ACN were heated (24 hrs). After completion of the reaction (monitored by TLC) the reaction mixture was evaporated to dryness under reduced pressure. The residue was dissolved in DCM (40 mL) and washed with H₂O (5 mL). The organic layer was dry packed onto Celite and purified by (DVCC) pre-eluting with acetone (150 mL) and eluting with 30% IPA/acetone (300 mL). The solvent was removed under reduced pressure to yield **31** as a white waxy solid. Yield: 90% (0.363 g). Mp = 36°C; ¹H NMR (400 MHz, CDCl₃, δ): 3.50-3.40 (m, 4H, H10), 2.09 (t, $J = 6.2$ Hz, 2H, H9), 2.00 (t, $J = 7.8$ Hz, 2H, H8), 1.81(s, 3H, H7), 1.25-1.14 (m, 4H, (H5 + H6

overlap)), 0.97-0.87 (m, 2H, H4), 0.71-0.60 (m, 34H, (H2 + H3 overlap)), 0.24 (t, $J = 6.1$ Hz, 3H, H1) ppm; ^{13}C NMR (100 MHz, CDCl_3 , δ): 61.92 (d, $^3J_{\text{C-P}} = 43.40$ Hz, (C17)), 56.86 (C16), 56.60 (d, $^2J_{\text{C-P}} = 17.22$ Hz, (C15)), 40.21 (C14), 31.69 (C13), 29.44-29.36 (C12 overlap), 29.31 (C11), 29.27 (C10), 29.11 (C9), 26.84 (C8), 25.46 (C7), 23.87 (C6), 22.36 (C4), 21.91 (d $^2J_{\text{C-P}} = 21.91$ Hz, (C5)), 18.64 (d, $^1J_{\text{C-P}} = 4.41$ Hz, (C3)), 15.35 (d, $^3J_{\text{C-P}} = 6.04$ Hz, (C2)), 13.09 (C1) ppm; ^{31}P NMR (121.45 MHz, CDCl_3 , δ): 32.34 ppm.



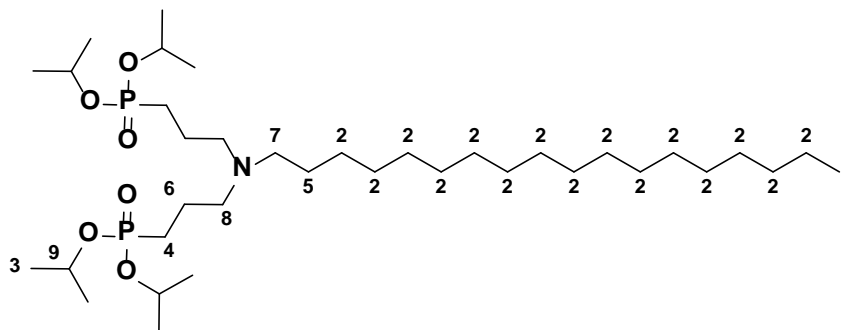
Diethyl (4-(dimethylamino)butyl)phosphonate (32):¹⁵³

A mixture of diethyl (4-bromobutyl)phosphonate **14** (5.0 g, 18.3 mmol) with NHMe_2 (5.6 M in EtOH, 10 mL, excess) was placed, with a magnetic stirring bar, into a 20 mL glass reaction tube and sealed. The reaction mixture was placed in the μW at 110 °C (5 min). Volatiles were removed on a rotary evaporator and the crude material purified by DCVC (50 g silica, 3.5 cm \times 5.5 cm) eluting first with 150 mL (10% MeOH/acetone) collecting 250 mL (10% MeOH/ 10% NH_4^+OH^- / 80% acetone) and evaporated to a yellow oil. Yield: 81% (3.55 g); TLC (20% NH_4^+OH^- /acetone), $R_f = 0.50$; ^1H NMR (400 MHz, CDCl_3 , δ): 4.06-3.92 (m, 4H, H7), 2.85 (t, 2H, $J = 7.96$ Hz, H6), 2.62 (s, 6H, H5), 1.83-1.53 (m, 6H, (H4 + H3 + H2 overlap)), 1.22 (t, 6H, $J = 7.04$ Hz, H1) ppm; ^{13}C NMR (100 MHz, CDCl_3 , δ): 61.71 (d, $^2J_{\text{C-P}} = 6.60$ Hz, (C7)), 57.68 (C6), 43.58 (C5), 25.68 (t, $^1J_{\text{C-P}} = 14.07$ Hz, (C2)), 24.13 (C4), 19.90 (d, $^2J_{\text{C-P}} = 4.60$ Hz, (C3)), 16.41 (d, $^3J_{\text{C-P}} = 6.22$ Hz, (C1)) ppm; ^{31}P NMR (121.45 MHz, CDCl_3 , δ): 30.94 ppm. (Agrees well with literature NMR values).¹⁵³



Diethyl (3-azidopropyl)phosphonate (33):²²⁹

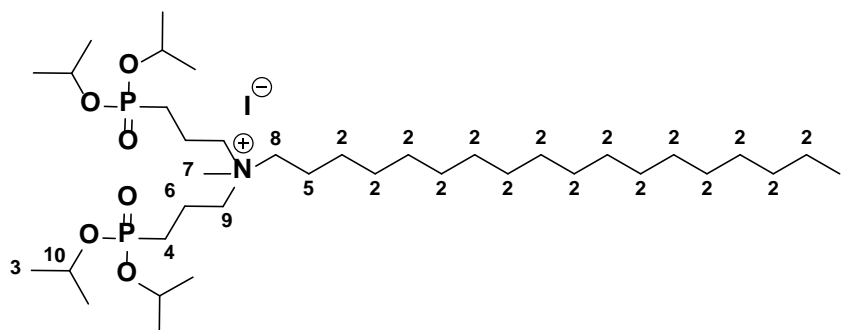
To a stirred solution of diethyl (3-bromopropyl)phosphonate **12** (1 mL, 5.2 mmol) in acetone (20 mL) was added NaN₃ (0.68, 10.4 mmol, 2 eq.) and the mixture was refluxed for 12 hrs. After cooling to RT, the mixture was filtered through Celite, washing with acetone and evaporated *in vacuo* to give the title compound as a yellow oil. Yield: 98% (1.13 g); TLC (60% acetone/hexanes), R_f = 0.50; ¹H NMR (400 MHz, CDCl₃, δ): 4.16-4.02 (m, 4H, H5), 3.37 (t, 2H, *J* = 6.52 Hz, H4), 1.92-1.74 (m, 4H, (H3 + H2 overlap)), 1.31 (t, 2H, *J* = 7.06 Hz, H1) ppm; ¹³C NMR (100 MHz, CDCl₃, δ): 61.64 (d, ²*J*_{C-P} = 6.59 Hz, (C5)), 51.45 (d, ³*J*_{C-P} = 16.29 Hz (C4)), 22.86 (d, ¹*J*_{C-P} = 4.98 Hz, (C3)), 22.40 (d, ²*J*_{C-P} = 143.06 Hz, (C2)), 16.43 (d, ²*J*_{C-P} = 5.91 Hz, (C1)) ppm; ³¹P NMR (121.45 MHz, CDCl₃, δ): 30.75 ppm. (Agrees well with literature NMR values).²²⁹



Tetraisopropyl ((octadecylazanediyl)bis(propane-3,1-diyl))bis(phosphonate) (39):

A solution of octadecylamine (1.0 g, 3.7 mmol), *N,N*-diisopropylethylamine (0.26 mL, 10 mmol, 2.7 eq.), diethyl (3-bromopropyl)phosphonate **12** (2.34, 8.16 mol, 2.2 eq.) were placed in a 20

mL vial, sealed and heated at 110°C (3 hrs). After completion of the reaction (monitored by ^{31}P NMR) the reaction was cooled to RT and the orange residue dissolved in DCM (60 mL) and washed with H_2O (60 mL). The organic layer was dry packed onto Celite and purified by (DVCC) pre-eluting with 30% acetone/hexanes (150 mL) and eluting with 10% MeOH/acetone (160 mL). The solvent was removed under reduced pressure to yield the title compound as a yellow oil. Note: this compound may be used without further purification in the next reaction. Yield: 96% (2.43 g). ^1H NMR (400 MHz, CDCl_3 , δ): 4.70-4.59 (m, 4H, H₉), 2.44-2.28 (m, 6H, (H₈ + H₇ overlap)), 1.71-1.59 (m, 10H, (H₆ + H₅ + H₄ overlap)), 1.42-1.14 (m, 54H, (H₃ + H₂ overlap)), 0.83(t, J = 5.4 Hz, 3H, H₁) ppm; ^{31}P NMR (121.45 MHz, CDCl_3 , δ): 30.09 ppm.

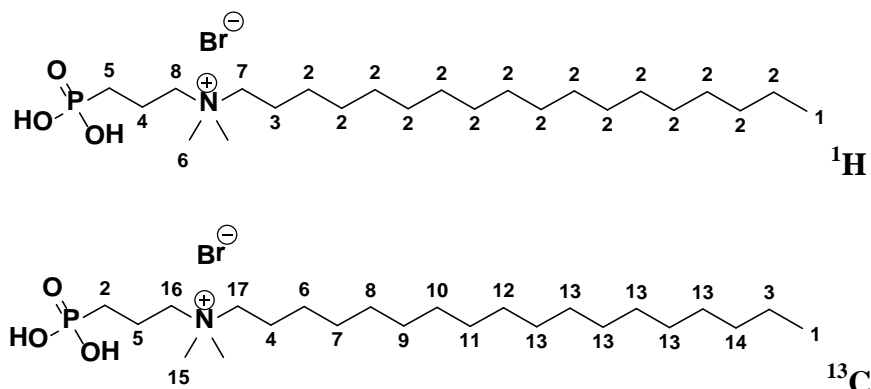


***N,N*-bis(3-(diisopropoxyphosphoryl)propyl)-*N*-methyloctadecan-1-ammonium iodide (40):**

To a solution of **39** (4.0 g, 5.8 mmol) in IPA (3 mL) was added MeI (0.45 mL, 7 mmol, 1.2 eq.), in a 20 mL glass reaction tube and sealed. The reaction mixture was heated in the μW at 110 °C (5 min). Volatiles were removed on a rotary evaporator and the crude material purified by DCVC (100 g silica, 4.5 cm \times 5.5 cm) pre-eluting first with 200 mL (10% MeOH/acetone) and collecting 300 mL (50% MeOH/ acetone). Yield: 74% (3.55 g); TLC (50% MeOH/ acetone), R_f = 0.30; ^1H NMR (400 MHz, CDCl_3 , δ): 4.72-4.59 (m, 4H, H₁₀), 3.80-3.62 (m, 4H, H₉), 3.40-3.32 (m, 4H, H₈), 3.28 (s, 3H, H₇), 2.11-1.96 (m, 4H, H₆), 1.87-1.68 (m, 6H, (H₄ + H₅

overlap)), 1.40-1.15 (m, 54H, (H3 + H2 overlap)), 0.84 (t, $J = 6.9$ Hz, 3H, H1) ppm; ^{31}P NMR (121.45 MHz, CDCl_3 , δ): 27.20 ppm.

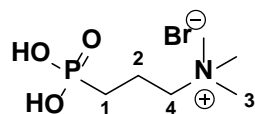
5.3.3 Didealkylation of Phosphonate diesters.



N,N-dimethyl-*N*-(3-phosphonopropyl)octadecan-1-ammonium bromide (34):^{230,231}

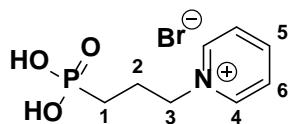
Inside a flame dried and evacuated 20 mL screw cap vial *N*-(3-(diethoxyphosphoryl)propyl)-*N,N*-dimethyloctadecan-1-ammonium bromide **26** (0.27 g, 0.46 mmol) was dissolved in anhydrous DCM (5 mL). To the clear stirred solution was added TMSBr (0.25 mL, 1.9 mmol, 4.0 eq.) through a rubber septum via syringe and the reaction was stirred at RT overnight. Completion of the reaction was followed by ^{31}P NMR spectroscopy after which the reaction was quenched with EtOH (10 mL) and stirred for 1 hr followed by addition of H₂O (1 mL). Volatiles were removed with a rotary evaporator connected to a high vacuum Schlenk line and the crude product was centrifuged with Et₂O (2 × 10 mL) to remove brown coloured impurities isolating **4-1** as a white solid. Yield: 94% (0.942 g). A small portion of the title compound was recrystallized as clear, long needles from EtOAc/IPA for MS and X-ray analysis. Mp = 118-120 °C; ^1H NMR (400 MHz, MeOD, δ): 3.38-3.33 (m, 2H, H8), 3.28-3.23 (m, 2H, H7), 3.02 (s, 6H, H6), 2.02-1.90 (m, 2H, H5), 1.75-1.65 (m, 4H, H4, H3), 1.20 (brs, 30H, H3), 0.82 (t, $J = 6.9$ Hz, 3H, H1),

ppm; ^{13}C NMR (CDCl_3 , 100 MHz, δ): 64.24 (C17), 63.54 (d, $^1J_{\text{C-P}} = 16.5$ Hz, C16), 49.94 (C15), 31.68 (C14), 29.45-29.37 (C13 overlap), 29.37 (C12), 29.35 (C11), 29.27 (C10), 29.20 (C9), 29.08 (C8), 29.86 (C7), 26.02 (C6), 23.15 (d, $^2J_{\text{C-P}} = 141.29$ Hz, C5), 22.34 (C4), 22.17 (C3), 16.47 (d, $^1J_{\text{C-P}} = 4.07$ Hz, C2), 13.08 (C1) ppm; ^{31}P NMR (121.45 MHz, CDCl_3 , δ): 26.92 ppm; **HRMS-DART** (m/z): $[\text{M}^+] - \text{Br}^-$ calculated for $\text{C}_{23}\text{H}_{51}\text{NO}_3\text{P}$, 420.3601; found, 420.3608. (No NMR values reported in the literature).^{230,231}



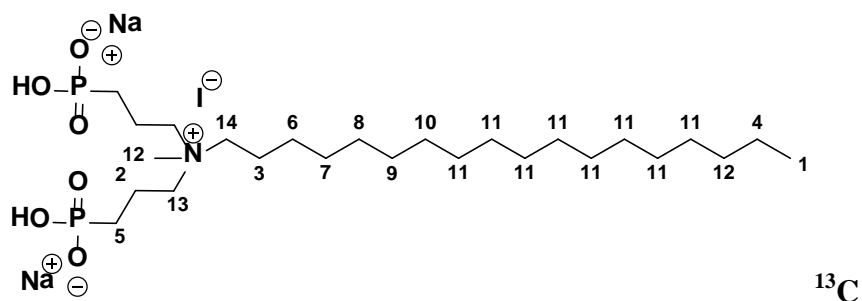
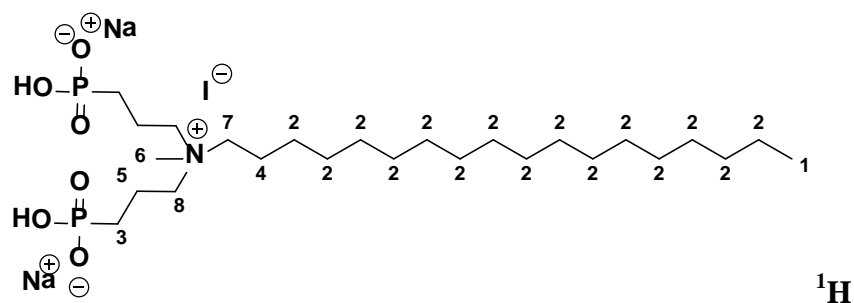
***N,N,N*-trimethyl-3-phosphonopropan-1-ammonium bromide (35):**

Table 2.4 (Entry xiii). A mixture of diisopropyl (3-bromopropyl)phosphonate **28** (0.96g, 2.78 mmol) and HBr (6 M, 1.85 mL, 4 eq.) was placed, with a magnetic stirring bar, into a 5 mL glass reaction tube and sealed. The reaction mixture was heated in the μW at 140 °C (10 min). Volatiles were removed on a rotary evaporator and the crude material was purified by recrystallization from MeOH/IPA (1:1, 20 mL) by slow evaporation of solvent ON and recovered as white crystals. Yield 80% (0.582 g); ^1H NMR (400 MHz, CDCl_3 , δ): 3.35-3.29 (m, 2H, H4) 3.04 (s, 9H, H3), 2.03-1.91 (m, 2H, H2), 1.77-1.66 (m, 2H, H1) ppm; ^{13}C NMR (100 MHz, CDCl_3 , δ): 66.24 (dt, $^3J_{\text{C-P}} = 2.92$ Hz, C4), 52.92 (t, $^4J_{\text{C-P}} = 3.93$ Hz, C3), 22.6 (d, $^1J_{\text{C-P}} = 137.50$ Hz, C1), 16.69 (d, $^2J_{\text{C-P}} = 3.55$ Hz, C2) ppm; ^{31}P NMR (121.45 MHz, CDCl_3 , δ): 26.77 ppm.



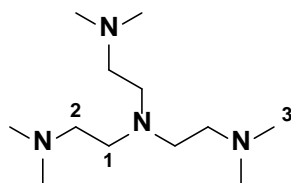
3-phosphonopropan-1-pyridin-1-ium bromide (36):

This compound was made by a one pot reaction in either ACN/TMSBr or H₂O/HBr. (See **13** for procedure, Table 2.4 (Entry xi)). A mixture of **13** (0.5g, 1.74 mmol) and HBr (2 M, 3.1 mL, 4 eq.) was placed, with a magnetic stirring bar, into a 5 mL glass reaction tube and sealed. The reaction mixture was heated in the μ W at (150 °C, 10 min). The aqueous phase was neutralized with NH₄⁺OH⁻ (2 mL) in 20 mL H₂O and washed with CHCl₃ (10 mL) followed by evaporation of the organic phase (100 mL ACN co-evap) to a solid which was purified by recrystallization from MeOH/IPA (2:1, 30 mL) by slow evaporation of solvent ON and recovered as white crystals. Yield 90% (0.441 g); ¹H NMR (400 MHz, CDCl₃, δ): 8.78 (t, *J* = 5.52 Hz, 2H, H6), 8.48 (t, *J* = 7.0 Hz, 1H, H5), 7.99 (t, *J* = 5.60 Hz, 2H, H4), 4.80-4.60 (m, 2H, H3 overlap w D₂O), 2.27-2.14 (m, 2H, H2), 1.77-1.66 (m, 2H, H1) ppm; ¹³C NMR (100 MHz, CDCl₃, δ): 147.20 (C5), 144.78 (C6), 128.33 (C4), 61.35 (d, ³*J*_{C-P} = 18.35 Hz, (C3)), 25.04 (d, ²*J*_{C-P} = 4.38 Hz, (C2)), 23.21 (d, ¹*J*_{C-P} = 139.29 Hz, (C1)) ppm; ³¹P NMR (121.45 MHz, CDCl₃, δ): 26.99 ppm. HRMS-DART (m/z): [M⁺] - Br⁻ calculated for C₈H₁₃NO₃P, 202.0628; found, 202.0624.



Sodium ((methyl(octadecyl)ammonio)bis(propane-3,1-diyl))bis(hydrogenphosphonate) iodide (42):

A mixture of **41** (3.288 g, 4.82 mmol) and HBr (2 M, 8.4 mL, 3.5 eq.) were placed, with a magnetic stirring bar, into a 10 mL glass reaction tube and sealed. The reaction mixture was heated in the μW at 150 °C (10 min). Volatiles were removed on a rotary evaporator and the crude material was purified by adding NaOH (2eq. in 10 mL H_2O) to make the monosodium salt of the bisphosphonic acid. Evaporation of H_2O gave the title compound as a white solid. Yield: 90% (3.15 g); ^1H NMR (400 MHz, D_2O , δ): 3.34-3.16 (m, 4H, (H8 + H7 overlap)), 2.97 (s, 3H, H6), 1.97-1.83 (m, 2H, H5), 1.71-1.61 (m, 2H, H4), 1.50-1.40 (C3), 1.23 (brs, 30H, H2), 0.83 (t, $J = 5.6$ Hz, 3H, H1), ppm; ^{13}C NMR (D_2O , 100 MHz, δ): 62.52 (C15), 61.85 (d, $^3J_{\text{C-P}} = 19.94$ Hz, C14), 47.96 (C13), 32.00 (C12), 30.20-29.85 (C11 overlap), 29.81 (C10), 29.65 (C9), 29.49 (C8), 29.21 (C7), 26.26 (C6), 25.02 (d, $^1J_{\text{C-P}} = 132.27$ Hz, C5), 22.68 (C4), 22.01 (C3), 17.24 (C2), 13.96 (C1) ppm; ^{31}P NMR (121.45 MHz, D_2O , δ): 21.11 ppm.



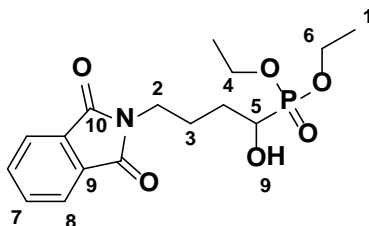
***N*¹,*N*¹-bis(2-(dimethylamino)ethyl)-*N*²,*N*²-dimethylethane-1,2-diamine (44):**¹⁹⁹

This compound was made by a modification of the literature procedure¹⁹⁹ by employing paraformaldehyde and anhydrous HCl. ACN (200 mL) was added to a 500 mL RBF containing tris(2-aminoethyl)amine (7.3115 g, 50 mmol) and paraformaldehyde (10 g, 333 mmol, 6.66 eq.) followed by formic acid (17 mL, 295 mmol, 5.9 eq.) at RT, and the mixture was refluxed for 3 hrs. The mixture was then cooled to RT, placed on ice and anhydrous HCl (2 N in EtOH/IPA, 100 mL) was added, and a white precipitate was isolated. The residual solid was diluted with MeOH (200 mL), filtered through a Buchner funnel and washed twice with MeOH (2 × 100 mL) to give tris (*N,N*-dimethyl-2-aminoethyl)amine hydrochloride as a yellow/white solid (12 g, 70%). Next, tris (*N,N*-dimethyl-2-aminoethyl)- amine hydrochloride (2.0 g, 6.89 mmol) was added slowly to 50 mL of an ethanolic solution containing NaOEt (1.4g, 20.67 mmol), and stirred at RT for 1 hr. The mixture was filtered through Celite, evaporated in vacuo, CHCl₃ was added to the residue, and the solution was filtered to remove more of the inorganic precipitate (NaCl). The evaporation of the solvent on a Schlenk line gave the title compound as a brown liquid. Yield: 65% (7.49 g); ¹H NMR (400 MHz, CDCl₃, δ): 3.28-3.19 (m, 6H, H3), 2.98-2.85 (m, 6H, H2), 2.81 (s, 18H, H1) ppm. ¹³C NMR (100 MHz, CDCl₃, δ): 53.89 (C3), 47.24 (C2), 43.16 (C1) ppm. (Agrees well with literature NMR values).¹⁹⁹

5.4 General Procedures for the Synthesis of α -CH Bisphosphonic Acids QAC Antimicrobials (α -CH-BPQA)

5.4.1 Method 1: Bis Addition of Dialkylphosphites to Aldehydes

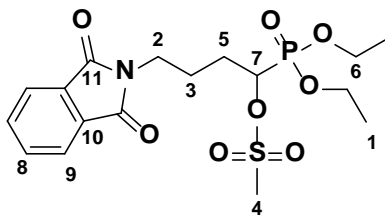
5.4.1.1 Sequential Addition



Diethyl (4-(1,3-dioxoisindolin-2-yl)-1-hydroxybutyl) phosphonate (**51**):

A 25 mL round bottom flask, equipped with a magnetic stir bar and a condenser was charged with the aldehyde **48** (2.28 g, 10.5 mmol), diethylphosphonate (1.52 g, 11.0 mmol, 1.05 eq.), K_2CO_3 (0.073 g, 0.53 mmol, 0.05 eq.) and ACN (5 mL). The heterogeneous solution was stirred at 60°C for 15 min at which point TLC showed disappearance of the starting aldehyde (60% EtOAc in hexanes, 10 mL). The reaction was cooled to 0°C, filtered and evaporated. The resulting yellow oil solidified under high vacuum (10 min) and was recrystallized from hot EtOAc (5 mL) after cooling for 20 min at 0°C. Yield 69.1% (2.578 g); TLC (60% EtOAc in hexanes), R_f = 0.2; Mp = 91-94°C; $^1\text{H NMR}$ (400 MHz, CDCl_3 , δ): 7.83-7.79 (m, 4H, H8), 7.71-7.64 (m, 4H, H7), 4.18-4.07 (m, 4H, H6), 3.89 (quintet, J = 4.59 Hz, 1H, H5), 3.77-3.66 (m, 2H, H4), 2.05-1.95 (m, 2H, H3), 1.87-1.68 (m, 2H, H2), 1.29 (t, J = 7.08 Hz, 6H, H1) ppm; $^{13}\text{C NMR}$ (100 MHz, CDCl_3 , δ): 168.37 (C10), 133.90 (C9), 132.10 (C7), 123.18 (C8), 68.12 (C5), 62.65 (q^2 , $J_{\text{C-P}}$ = 7.3 Hz, C6), 37.52 (C2), 28.43 (d, $^1J_{\text{C-P}}$ = 1.45 Hz, C5), 25.02 (C3), 24.96 (C4),

16.46 (d, $^3J_{\text{C-P}} = 5.20$ Hz, C1) ppm; ^{31}P NMR (121.45 MHz, CDCl_3 , δ): 24.64 ppm. **ESI-TOF** (m/z): $[\text{M}^+]$ calculated for $\text{C}_{16}\text{H}_{22}\text{NO}_6\text{P}$, found, 434.1.

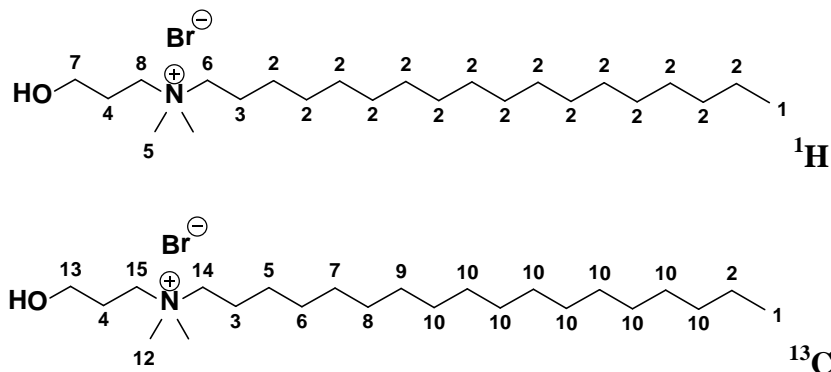


Example 14 - 1-(diethoxyphosphoryl)-4-(1,3-dioxoisindolin-2-yl) butyl methanesulfonate (52):

To a flame dried and evacuated 50 mL round bottom flask, equipped with a magnetic stir bar was added sequentially $\text{NMe}_3 \cdot \text{HCl}$ (0.062g, 0.62 mmol, 0.20 eq.), DCM (2 mL), Et_3N (0.65 mL, 4.63 mmol, 1.5 eq.) and **51** (1.097 g, 3.09 mmol) and the solution was cooled to 0°C in an ice bath. To the chilled stirred solution was added, dropwise, mesyl chloride (0.25 mL, 3.70 mmol, 1.2 eq.) in anhydrous DCM (2 mL) and the cloudy yellow mixture was stirred for 20 min at RT at which point TLC showed disappearance of the starting amine (10% MeOH in EtOAc, 10 mL). The reaction was diluted with H_2O (1×10 mL) and extracted with DCM (2×5 mL total), the combined organic layers were dried over MgSO_4 , filtered and evaporated to give a yellow oil. The crude product (1.409 g) containing traces of DCM and excess mesyl chloride by ^1H NMR, was placed under high vacuum at 60°C for 1 hr. Yield 93% (1.201 g); TLC (10% MeOH in EtOAc), $R_f = 0.5$; ^1H NMR (400 MHz, CDCl_3 , δ): 7.85-7.81 (m, 2H, H9), 7.73-7.70 (m, 2H, H8), 4.94-4.88 (m, 1H, H7), 4.20-4.15 (m, 4H, H6), 3.77-3.70 (m, 2H, H5), 3.15 (s, 3H, H4), 1.95-1.82 (m, 4H, H2, H3), 1.41-1.25 (m, 6H, H1) ppm; ^{13}C NMR (100 MHz, CDCl_3 , δ): 168.26 (C11), 133.98 (C10), 132.08 (C9), 123.22 (C8), 74.79 (C7), 63.31 (q, $^2J_{\text{C-P}} = 7.3$ Hz, C6),

52.56 (C2) , 39.11 (C4), 27.58 (C3), 24.45 (d, $^2J_{\text{C-P}} = 11.67$ Hz C5), 16.45 ($^2J_{\text{C-P}} = 5.20$ Hz, C1) ppm; ^{31}P NMR (121.45 MHz, CDCl_3 , δ): 17.63 ppm.

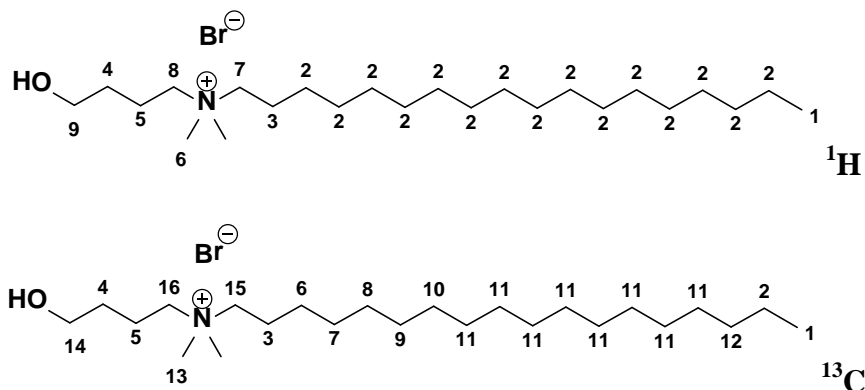
5.4.1.2 Synthesis of Aldehyde Precursors



N-(3-hydroxypropyl)-*N,N*-dimethyloctadecan-1-ammonium (66):²³²

This compound was prepared by the Menshutkin reaction using Method 5.2.1: 3-(dimethylamino)propan-1-ol (0.515 g, 5 mmol) and 1-bromooctadecane (1.667 g, 5 mmol, 1.0 eq.) were reacted at 100°C neat for 1 hr until the mixture solidified. The mixture was then dissolved in MeOH (40 mL) and hot filtered from charcoal. Volatiles were removed on a rotary evaporator and the crude was recrystallized from MeOH/ACN (1:3, 40 mL) by slow evaporation over a few d. as a brittle crystalline solid. A small sample was used to obtain a crystal structure. Yield: 90% (1.962 g). Mp = $93\text{--}95^\circ\text{C}$; ^1H NMR (400 MHz, CDCl_3 , δ): 3.74–3.68 (m, 4H, (H8 + H7 overlap)), 3.43–3.37 (m, 2H, H6), 3.27 (s, 6H, H5), 2.07–1.99 (m, 2H, H4), 1.75–1.67 (m, 2H, H3), 1.21 (brs, 30H, H2), 0.84 (t, $J = 7.0$ Hz, 3H, H1) ppm; ^{13}C NMR (100 MHz, CDCl_3 , δ): 64.59 (C15), 62.65 (C14), 58.20 (C13), 51.24 (C12), 31.89 (C11), 29.73–29.60 (C10 overlap), 29.51 (C9), 29.45 (C8), 29.33 (C7), 29.24 (C6), 26.33 (C5), 25.98 (C4), 22.82 (C3), 22.66 (C2),

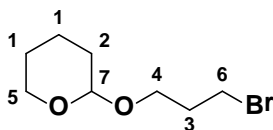
14.09 (C1) ppm. **HRMS-DART** (m/z): $[M^+] - Br$ calculated for $C_{23}H_{50}NO$, 356.3886; found, 356.3891. (Agrees well with literature NMR values).²³²



***N*-(4-hydroxybutyl)-*N,N*-dimethyloctadecan-1-ammonium bromide (67):**

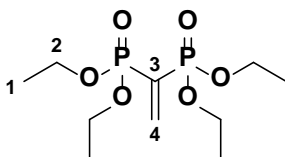
This compound was prepared by the Menshutkin reaction using method 5.2.1, 4-(dimethylamino)butan-1-ol (0.586 g, 9.8 mmol) and 1-bromooctadecane (1.667 g, 9.8 mmol, 1.0 eq.) were reacted at 110°C neat for 20 min until the mixture solidified. The mixture was then dissolved in EtOH (20 mL) and hot filtered from charcoal. Volatiles were removed on a rotary evaporator and the crude was recrystallized from acetone (20 mL) by slow evaporation after 20 min as fine white crystalline needles. Yield: 63% (2.8 g). Mp = 94°C; ¹H NMR (400 MHz, MeOD, δ): 3.64 (t, *J* = 6.13 Hz, 2H, H₉), 3.39-3.31 (m, 4H, (H₇ + H₈ overlap)), 3.11 (s, 6H, H₆), 1.89-1.80 (m, 4H, (H₅ + H₄ overlap)), 1.64-1.57 (m, 2H, H₃), 1.30 (brs, 30H, H₂), 0.91 (t, *J* = 7.0 Hz, 3H, H₁) ppm; ¹³C NMR (100 MHz, MeOD, δ): 63.99 (C₁₆), 63.70 (C₁₅), 60.43 (C₁₄), 49.86 (C₁₃), 31.69 (C₁₂), 29.42-29.35 (C₁₁ overlap), 29.28 (C₁₀), 29.20 (C₉), 29.10 (C₈), 28.87 (C₇), 28.68 (C₆), 26.03 (C₅), 22.36 (C₄), 22.18 (C₃), 18.98 (C₂), 13.10 (C₁) ppm.

5.4.2 Method 2: Michael Addition to Diethylvinylphosphonate



2-(3-bromopropoxy)tetrahydro-2H-pyran (9):²³³

To a stirred solution inside a 125 mL round bottom flask containing 3-bromo-1-propanol (6.95 g, 50 mmol, 1 eq.) in DCM (25 mL) was added 3,4-dihydropyran (5.93 mL, 65 mmol, 1.3 eq.). The mixture was stirred overnight at RT at which point TLC showed disappearance of 3-bromo-1-propanol (20% EtOAc in hexanes, 10 mL, KMnO₄). The reaction was evaporated and the crude material was purified by flash chromatography on silica gel (20 g silica, 1.5 cm i.d) eluting with 10% EtOAc: hexanes (100 mL) to obtain the title compound as a clear oil. Yield: 86.4% (9.637 g); TLC (20% EtOAc in hexanes), R_f = 0.85; ¹H NMR (400 MHz, CDCl₃, δ): 4.59 (t, 1H, J = 3.52 Hz, H7), 3.90-3.81 (m, 2H, H6), 3.55-3.47 (m, 4H, (H4, H5)), 2.16-2.08 (m, 2H, H3), 1.90-1.64 (m, 2H, H2), 1.57-1.50 (m, 4H, H1) ppm; ¹³C NMR (100 MHz, CDCl₃, δ): 98.90 (C7), 64.88 (C6), 62.26 (C5), 32.90 (C3), 30.59 (d, ² J = 6.04 Hz, C4), 25.41 (C2), 19.48 (C1) ppm. (Agrees well with literature NMR values).²³³

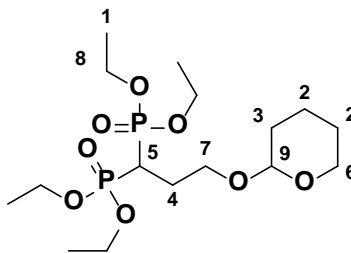


Tetraethyl ethene-1,1-diylbis(phosphonate) (68):²³⁴

A 50 mL round bottom flask was charged with paraformaldehyde (6.3 g, 200 mmol, 4.0 eq.) and HNEt₂ (5.2 mL, 50 mmol, 1 eq.) in MeOH (125 mL) and the mixture was stirred under reflux until a clear solution was obtained (~ 5 min). Tetraethylmethylene bisphosphonate was added via

syringe (12.4 mL, 50 mmol, 1.0 eq.) and the solution was refluxed overnight (24 hrs). The clear solution was concentrated in vacuo and then re-evaporated from TOL (2×10 mL) completely removing residual MeOH to give the intermediate methyl ether as a clear oil. The residue was dissolved in TOL (100 mL), treated with p-toluenesulphonic acid (38 mg, 0.02 mmol), and refluxed through a Dean-Stark trap overnight. The orange solution was concentrated in vacuo, dissolved in CHCl_3 (50 mL), washed with H_2O (2×10 mL), dried over MgSO_4 , and concentrated in vacuo. A portion of the orange oil (6 g) was further distilled under high vacuum. Yield: 90% (5.40 g); TLC (EtOAc), $R_f = 0.2$; $^1\text{H NMR}$ (400 MHz, CDCl_3 , δ): 7.02-6.86 (m, H3, 2H), 4.10-4.05 (m, H2, 8H), 1.34-1.21 (m, H1, 12H) ppm; $^{13}\text{C NMR}$ (100 MHz, CDCl_3 , δ): 149.04 (m, C4), 133.77-129.71 (m, C3), 62.54 (t, $^2J_{\text{C-P}} = 2.88$ Hz, C2), 16.17 (t, $^3J_{\text{C-P}} = 3.15$ Hz, C1) ppm; $^{31}\text{P NMR}$ (121.45 MHz, CDCl_3 , δ): 21.0 ppm. (Agrees well with literature NMR values).²³⁴

5.4.3 Method 3: C-P Bond Formation

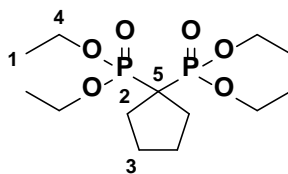


Tetraisopropyl (3-(((tetrahydro-2H-pyran-2-yl)oxy)propane-1,1-diyl)bis(phosphonate) (77)
).²³⁵

To a solution of freshly prepared LDA ($n\text{-BuLi}$ (1.6 M in hexane, 4.93 mL, 7.88 mmol) and $\text{HN}(i\text{Pr})_2$ (1.12 mL, 7.97 mmol) in anhydrous THF (10 mL) -78°C) was added **18** (1.10 g, 3.94 mmol) in THF (5 mL). After 0.5 h, diethyl chlorophosphate (0.84 mL, 4.73 mmol) was added

dropwise via syringe, and the mixture stirred for 1 hr at -78 °C and 30 min at RT. The reaction was quenched with $\text{NH}_4\text{Cl}_{\text{sat}}$ (10 mL) and extracted with EtOAc (1×10 mL). The organic layer separated, dried over MgSO_4 , evaporated *in vacuo* and the crude product (in a 0.8:0.2 ratio with excess unreacted diethyl chlorophosphate) was loaded onto silica (10 g, EtOAc, 15 mL) and purified by column chromatography on silica gel (50 g) pre-eluting with EtOAc (1×50 mL) to remove unextracted diethyl chlorophosphate. The column was eluted with MeOH:EtOAc (20%, 60 mL) to afford the title compound as a light yellow oil. Yield: 74% (0.741 g); TLC (10% MeOH:EtOAc), $R_f = 0.30$; ^1H NMR (400 MHz, CDCl_3 , δ): 4.59-4.55 (m, 1H, H9), 4.22-4.06 (m, 2H, H8), 3.90-3.77 (m, 2H, H7), 3.62-3.42 (m, 2H, H6), 2.66-2.48 (m, 1H, H5), 2.26-2.09 (m, 2H, H4), 1.82-1.61 (m, 2H, H3), 1.58-1.42 (m, 4H, H2), 1.33 (t, $J = 7.03$ Hz, 12H, H1); ^{13}C NMR (100 MHz, CDCl_3 , δ): 98.57 (C9), 65.13 (C7), 62.63-63.39 (m, C8), 62.19 (C6), 32.81 (t, $^1J_{\text{C-P}} = 134.7$ Hz, (C6)), 30.59 (C3), 25.40 (C4), 19.46 (C2), 16.34 (t, $^3J_{\text{C-P}} = 2.81$ Hz, (C2)) ppm; ^{31}P NMR (121.45 MHz, CDCl_3 , δ): 23.77 ppm. (Agrees well with literature NMR values).²³⁵

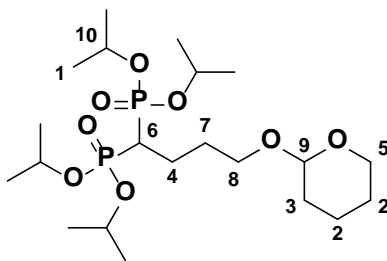
5.4.4 Method 4: Alkylation of Methylenebisphosphonate



Tetraethyl cyclopentane-1,1-diylbis(phosphonate) (97):²³⁶

To a stirred solution (250 mL Schlenk flask, under argon) of tetraethyl methylenediphosphonate (7.45 mL, 30 mmol, 1.0 eq.) in DMSO (60 mL) at 0°C was added excess solid NaH (60% dispersion in mineral oil, 2.4 g, 60 mmol, 2.0 eq.) portionwise. The reaction was brought to RT and stirred (30 min), washed with more DMSO (60 mL) and evacuated and

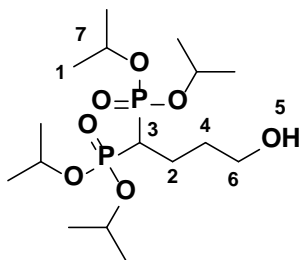
backfilled with Ar (2 cycles). When hydrogen gas evolution ceased and the mixture cleared (~ 40 min later), 1,4-dibromobutane (5.37 mL, 45.0 mmol, 1.5 eq.) was added and the resulting yellow orange mixture was stirred overnight at RT. The solution was then cooled to RT, neutralized with NH_4^+Cl^- sat:H₂O (1:3, 400 mL) and extracted with EtOAc (1 × 400 mL, 1 × 300 mL). The organic phases were washed with brine (1 × 50 mL), dried over MgSO_4 , filtered and concentrated in vacuo. The crude product (only one peak by ^{31}P NMR at 28.50 ppm) was loaded onto silica (40 g, 30 mL EtOAc) and purified by column chromatography (100 g) pre-eluting with EtOAc (2 × 60 mL) to remove any unextracted DMSO. The column was eluted with 10% MeOH/acetone (200 mL) to afford the title compound as a light yellow oil. Yield: 78% (10.0 g); TLC (20% MeOH in acetone), R_f = 0.60; ^1H NMR (400 MHz, CDCl_3 , δ): 4.18 (t, J = 6.61 Hz, 8H, H4), 2.16 (t, J = 18.17 Hz, 4H, H3), 1.80-1.70 (m, 4H, H2), 1.34 (t, 12H, J = 6.97 Hz, H1) ppm; ^{13}C NMR (100 MHz, CDCl_3 , δ): 63.00 (t, 2J = 2.81 Hz, (C5, C4 overlap)), 30.96 (t, 3J = 4.14 Hz, C3), 26.48 (t, 2J = 4.28 Hz, C2), 15.37 (t, 3J = 2.67 Hz, C1) ppm; ^{31}P NMR (121.45 MHz, CDCl_3 , δ): 28.40. (Agrees well with literature NMR values).²³⁶



Tetraisopropyl (4-((tetrahydro-2H-pyran-2-yl)oxy)butane-1,1-diyl) bis (phosphonate) (95):²³⁷

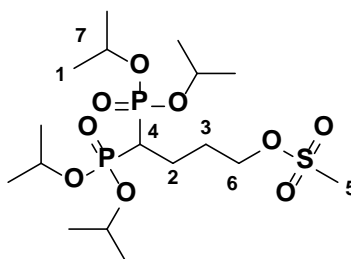
To a stirred suspension (250 mL Schlenk flask, under Ar) of NaH (60% dispersion in mineral oil, 1.76 g, 60 mmol, 2.0 eq.) in anhydrous THF (100 mL, pre-dried ON over MS) was added

dropwise (canula) tetraisopropyl methyldiene bisphosphonate (14 mL, 44 mmol, 1.0 eq.) in THF (20 mL) at 0°C. The reaction was brought to RT and stirred (30 min), and evacuated and backfilled with Ar (2 cycles). When hydrogen gas evolution ceased and the mixture cleared, 2-(3-bromopropoxy)tetrahydro-2H-pyran (5.976 g, 43 mmol, 0.98 eq.) in THF (20 mL) was added dropwise by canula and the resulting clear mixture was refluxed (72 hrs). The solution was then cooled to RT, neutralized with $\text{NH}_4^+\text{Cl}^-\text{sat}:\text{H}_2\text{O}$ (1:1, 100 mL) and extracted with EtOAc (1×150 mL). The organic phases were washed with brine (1 × 50 mL), dried over MgSO_4 , filtered and concentrated in vacuo. The crude product (in a 0.62:0.38 ratio with unreacted tetraisopropyl methyldienebisphosphonate) was loaded onto silica (40 g, 10% acetone/hexanes, 30 mL) and purified by column chromatography on silica gel (100 g) pre-eluting with 10% acetone/hexanes (2 × 100 mL) to remove unextracted (3-bromopropoxy)tetrahydro-2H-pyran. The column was eluted with acetone (200 mL) to afford the title compound in a 0.62:0.38 ratio with unreacted tetraisopropyl methyldienebisphosphonate by (^{31}P NMR) as a light yellow oil (14.78 g). Yield 49.5% (9.163 g); TLC (acetone), R_f = 0.50; ^1H NMR (400 MHz, CDCl_3 , δ): 4.85-4.65 (m, 4H, H10), 4.59-4.50 (m, 1H, H9), 3.86-3.60 (m, 2H, H8), 3.50-3.20 (m, 2H, H7), 2.27-2.06 (m, 1H, H6), 2.08-1.71 (m, 4H, (H5, H4)), 1.70-1.40 (m, 6H, (H3 + H2)), 1.30 (s, 24H, H1); ^{13}C NMR (100 MHz, CDCl_3 , δ): 98.51 (C9), 70.96 (C10), 66.57 (C8), 62.09 (C5), 38.21 (C6), 30.62 (C7), 29.01 (C3), 25.45 (C4), 23.85 (C1), 19.22 (C2) ppm; ^{31}P NMR (121.45 MHz, CDCl_3 , δ): 21.83 ppm. (Agrees well with literature NMR values).²³⁷



Tetraisopropyl (3-hydroxybutane-1,1-diyl)bis(phosphonate) (98):^{237,238}

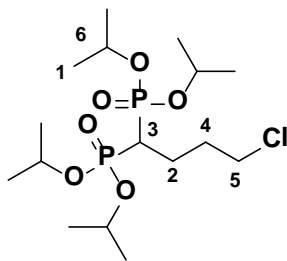
To a stirred solution of the crude product **95** (10 g, 14.4 mmol) in MeOH (50 mL) was added Amberlite IR-120 (0.5 g). The reaction mixture was heated to 50°C ON, filtered (Celite), and concentrated in vacuo. The crude product containing the unreacted tetraisopropyl methylenebisphosphonate (38% by weight, 3.8g, ³¹P NMR, δ = 17.36 ppm) was used directly in the next reaction without purification. Yield: 100% (5.791 g); TLC (15% MeOH/EtOAc), R_f = 0.35; ¹H NMR (400 MHz, CDCl₃, δ): 4.80-4.65 (m, 4H, H7), 3.60 (m, 2H, H6), 3.11 (s, 1H, H5), 2.25-1.70 (m, 5H, (H4 + H3 + H2 overlap)), 1.29 (s, 32H, H1); ¹³C NMR (100 MHz, CDCl₃, δ): 71.13 (C7), 61.19 (C6), 37.25 (t, ¹J = 138.0 Hz, C3), 31.98 (t, ²J = 5.64 Hz, C2), 23.88 (d, ³J = 2.52 Hz, C1), 21.63 (t, ³J = 5.33 Hz, C4) ppm; ³¹P NMR (121.45 MHz, CDCl₃, δ): 22.33 ppm. (Agrees well with literature NMR values).^{237,238}



4,4-bis(diisopropoxyphosphoryl)butyl methanesulfonate (99):

To a flame dried and evacuated 125 mL round bottom flask, equipped with a magnetic stir bar was added sequentially NMe₃·HCl (1.5g, 1.44 mmol, 0.1 eq.), DCM (20 mL), Et₃N (17.43 mL, 21.6 mmol, 1.5 eq.) the crude alcohol **98** (5.791 g, 14.4 mmol, 1.0 eq.) and the solution cooled to 0°C (ice bath). To the chilled, stirred solution was added, dropwise, MsCl (1.22 mL, 15.8 mmol, 1.1 eq.) followed by rinsing the addition funnel with anhydrous DCM (5 mL) and the cloudy yellow mixture was stirred for 30 min at RT at which point TLC showed disappearance of the

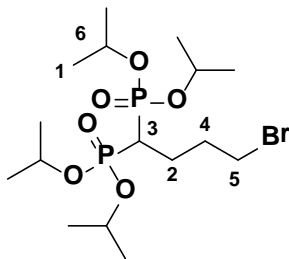
starting alcohol (15% MeOH in EtOAc, 10 mL). The reaction was diluted with H₂O (1 × 100 mL) and extracted with DCM (100 mL total), the organic layer was re-washed with brine (1 × 50 mL), dried over MgSO₄, filtered and evaporated to give a light yellow oil. The crude product (10.72 g) containing the unreacted tetraisopropyl methylenebisphosphonate (38% by weight, 3.80 g, ³¹P NMR, δ = 17.36 ppm) was used directly in the next reaction without purification. Yield 100 % (6.919 g); TLC (15% MeOH/EtOAc), R_f = 0.45; ¹H NMR (400 MHz, CDCl₃, δ): 4.83-4.60 (m, 4H, H7), 4.24-4.17 (m, 2H, H6), 2.98 (m, 3H, H5), 2.40-2.25 (m, 1H, H4), 2.11-1.86 (m, 4H, (H3 + H2)), 1.46-1.14 (m, 24H, H1) ppm; ¹³C NMR (100 MHz, CDCl₃, δ): 71.09 (C7), 69.50 (C6), 37.42 (d, ³J = 2.81 Hz, C4), 36.46 (C5), 28.36 (C3), 24.06 (C1), 22.29 (C2) ppm; ³¹P NMR (121.45 MHz, CDCl₃, δ): 20.95 ppm.



Tetraisopropyl (4-chlorobutane-1,1-diyl)bis(phosphonate) (91):

To a stirred solution (250 mL Schlenk flask, under argon) of tetraisopropyl methylenedibisphosphonate (9.0 mL, 25 mmol, 1 eq.) in DMSO (40 mL) at 0°C was added solid NaH (60% dispersion in mineral oil, 1.05 g, 26.4 mmol, 1.05 eq.) portionwise. The reaction was brought to RT and then stirred at 60°C (10 min), washed with additional DMSO (50 mL), evacuated and backfilled with Ar (2 cycles). When hydrogen gas evolution ceased and the mixture cleared (30 min later), 3-bromo-1-chloropropane (2.47 mL, 25.0 mmol, 1 eq.) was added and the resulting yellow mixture was stirred overnight at RT. The solution was then cooled to RT, neutralized with NH₄⁺Cl⁻ (300 mL) and extracted with ethyl acetate (300 mL). The organic

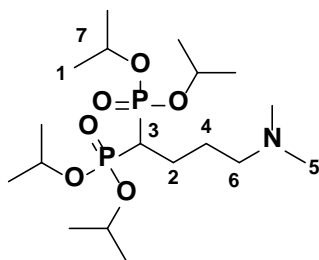
phase was washed with brine (1 × 300 mL), dried over MgSO₄, filtered and concentrated *in vacuo*. The crude product (~7.712 g, after high vac, 3 hrs) was loaded onto silica (40 g, 30 mL hexanes) and purified by column chromatography on silica gel (100 g) pre-eluting with hexanes (200 mL), followed by 30% EtOAc/hexanes (100 mL) to remove any unextracted DMSO. The column was eluted with 50% acetone/hexanes (50 mL) to afford the title compound, a colourless oil (1.0 g) while the rest of the crude product was recovered by eluting with acetone (200 mL) as a yellow oil (5.305 g) that was comprised of a mixture of the title compound with unreacted tetraisopropyl methylenedibisphosphonate in a 0.38:0.62 ratio by ³¹P NMR spectroscopy. Yield: 25.1% (3.02 g); TLC (70% acetone in hexanes), R_f = 0.45; ¹H NMR (400 MHz, CDCl₃, δ): 4.56-4.40 (m, 4H, H6), 3.10-3.00 (m, 2H, H5), 2.38-2.20 (m, 4H, (H4 + H3 overlap)), 1.99-1.85 (m, 2H, H2), 1.11 (s, 24H, H1) ppm; ¹³C NMR (100 MHz, CDCl₃, δ): 78.07 (C5), 71.72 (t, ²J = 3.46 Hz, C6), 24.56 (C3), 22.98 (d, ³J = 22.38 Hz, C1), 16.77 (C4) ppm; ³¹P NMR (121.45 MHz, CDCl₃, δ): 24.34 ppm.



Tetraisopropyl (4-bromobutane-1,1-diyl)bis(phosphonate) (87):

To a stirred solution of the crude product **99** (3.459 g, 7.2 mmol) in ACN (25 mL) was added LiBr (1.25 g, 14.4 mmol, 2.0 eq.) and the reaction was refluxed (1.5 hrs). The solution was then cooled to RT, quenched with H₂O (50 mL), extracted with ethyl acetate (100 mL), dried over MgSO₄, filtered and concentrated *in vacuo*. The crude product containing the unreacted

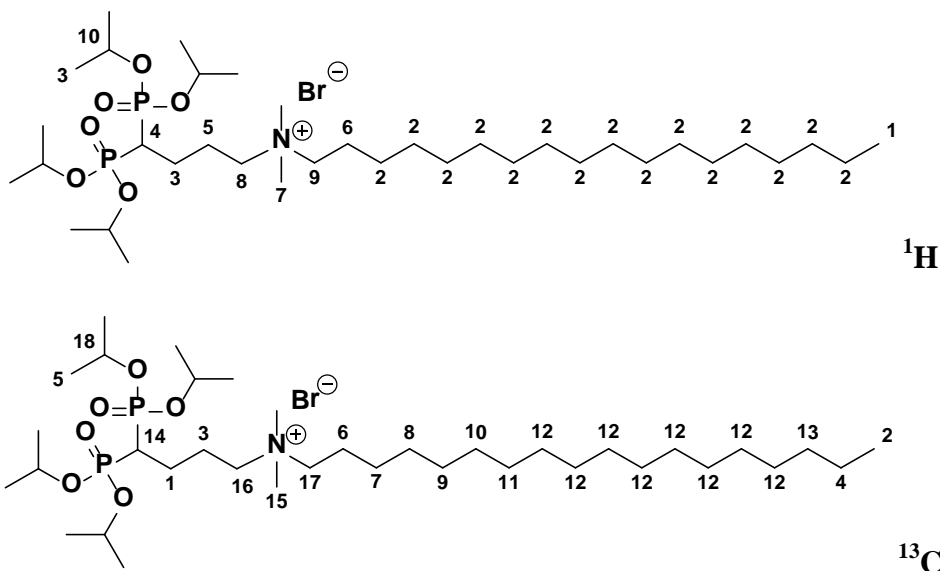
tetraisopropyl methylenebisphosphonate (38% by weight, 1.9 g, ^{31}P NMR (CDCl_3) = 17.36 ppm) was used directly in the next reaction without purification and recovered as an orange oil. Yield: 100 % (3.35 g); TLC (15% MeOH/EtOAc), R_f = 0.45; ^1H NMR (400 MHz, CDCl_3 , δ): 4.82-4.62 (m, 4H, H6), 3.41-3.28 (m, 2H, H5), 2.31 (t, J = Hz, 3H, H5), 2.19-1.86 (m, 4H, (H3 + H2 overlap)), 1.29 (s, 24H, H1) ppm; ^{31}P NMR (121.45 MHz, CDCl_3 , δ): 21.36 ppm.



Tetraisopropyl (4-(dimethylamino)butane-1,1-diyl)bis(phosphonate) (96):

To a 20 mL glass screw cap vial equipped with a magnetic stir bar was added the crude product **87** (3.459 g, 7.2 mmol), NHMe_2 (5.6 M in EtOH, 3.8 mL, excess) and stirred at reflux sealed for 1.5 hrs, at which point the TLC plate showed disappearance of the starting material (1% NH_4^+OH^- in acetone, 10 mL, R_f = 0.95). The reaction was cooled to RT, evaporated, filtered (Celite), washed with EtOAc and loaded onto silica (40 g, 30 mL EtOAc). The title compound was purified by column chromatography on silica gel (100 g) pre-eluting with 10% MeOH/EtOAc (50 mL), and eluted with (10% $\text{NH}_4\text{OH}/\text{ACN}$, 100 mL). The eluted fraction was separated from H_2O by coevaporation from ACN, stirring in CHCl_3 (10 mL) for 5 min, filtering (Celite) and drying under high vacuum (60 min) and recovered as a yellow oil. Yield: 64% (2.0 g); TLC (1% NH_4^+OH^- in Acetone, 10 mL) or (20% MeOH (6% NaBr): ACN, R_f = 0.40; ^1H NMR (400 MHz, CDCl_3 , δ): 4.82-4.65 (m, 4H, H7), 2.29-2.07 (m, 2H, H6), 2.17 (s, 6H, H5), 1.91-1.62 (m, 6H, (H4 + H3 + H2 overlap)), 1.29 (s, 24H, H1) ppm; ^{13}C NMR (100 MHz,

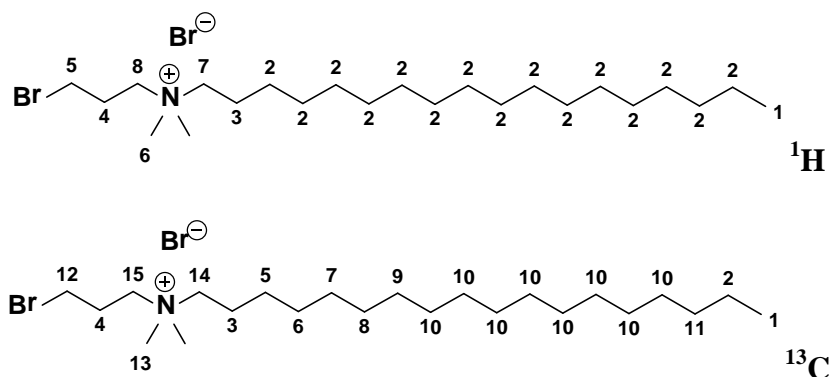
CDCl₃, δ): 70.87 (q, 2J = Hz, C7), 59.50 (C6), 45.34 (C5), 38.36 (d, 1J = Hz, C3), 27.06 (t, 2J = Hz, C2), 24.19 (C4), 23.90 (t, 3J = Hz, C1) ppm **³¹P NMR** (121.45 MHz, CDCl₃, δ): 24.34 ppm.



***N*-(4,4-bis(diisopropoxyphosphoryl)butyl)-*N,N*-dimethyloctadecan-1-ammonium (93):**

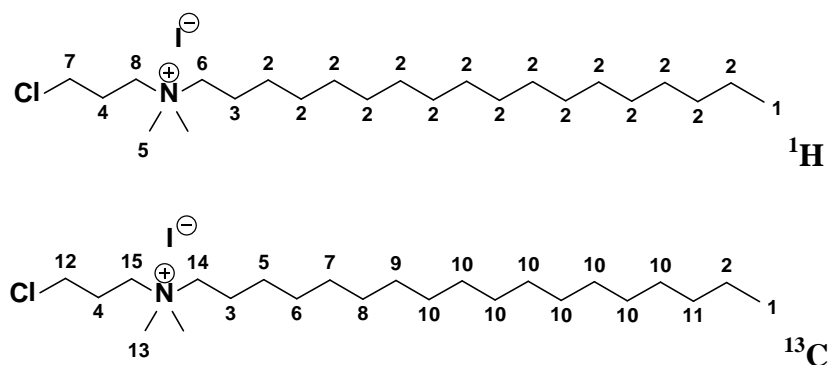
This compound was prepared by the Menshutkin reaction using Method 5.2.1: **87** (2.28 g, 5.57 mmol) and DMOA (1.65 g, 5.57 mmol, 1.0 eq.) in ACN (10 mL) were refluxed for 4 hrs. The mixture was then cooled to RT, poured into 20 mL of Et₂O, and placed into a freezer (-20°C) ON. The title compound did not solidify so the crude product was loaded onto silica (40 g, 30 mL acetone) and purified by column chromatography on silica gel (100 g) pre-eluting with acetone (100 mL), and eluted with 20% (6% NaBr in MeOH): ACN (150 mL) to give the title compound as a yellow oil. Yield: 50% (2.12 g); **¹H NMR** (400 MHz, CDCl₃, δ): 3.82-3.71 (m, 4H, (H8 + H7 overlap)), 3.56-3.49 (m, 2H, H6), 3.40 (s, 6H, H5), 2.36-2.28 (m, 2H, H4), 1.80-1.69 (m, 2H, H3), 1.23 (brs, 30H, H2), 0.85 (t, J = 7.0 Hz, 3H, H1) ppm; **¹³C NMR** (100 MHz, CDCl₃, δ): 65.88 (C15), 61.55 (C14), 52.14 (C13), 41.14 (C12), 31.90 (C11), 29.71-29.62 (C10

overlap), 29.46 (C9), 29.34 (C8), 29.18 (C7), 26.15 (C6), 26.14 (C5), 22.75 (C4), 22.66 (C3), 22.66 (C2), 14.10 (C1) ppm.



N-(4-hydroxybutyl)-N,N-dimethyloctadecan-1-ammonium bromide (83):²³⁹

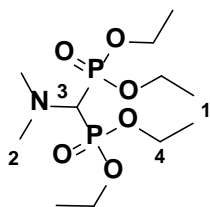
This compound was prepared by the Menshutkin reaction using Method 5.2.1: 1,3-dibromopropane (4.079 mL, 44 mmol, 4 eq.) and DMOA (2.9 g, 9.8 mmol, 1.0 eq.) in ACN:EtOH (6:1, 70 mL) were refluxed for 3 hrs. The mixture was then cooled to RT, poured into 30 mL of Et₂O, and placed into a freezer (-20°C) for 10 min to precipitate the title compound as a white solid. Yield: 50% (2.95 g). Mp = 93-95°C; ^1H NMR (400 MHz, CDCl₃, δ): 3.84-3.77 (m, 4H, H8), 3.53-3.44 (m, 2H, H7), 3.36 (s, 6H, H6), 2.33-2.19 (m, 4H, (H5 + H4 overlap)), 1.80-1.71 (m, 2H, H3), 1.23 (brs, 30H, H2), 0.86 (t, J = 7.0 Hz, 3H, H1) ppm; ^{13}C NMR (100 MHz, CDCl₃, δ): 66.47 (C15), 60.90 (C14), 51.29 (C13), 34.54 (C12), 31.92 (C11), 29.95-29.62 (C10 overlap), 29.55 (C9), 29.48 (C8), 29.36 (C7), 29.29 (C6), 26.32 (C5), 22.95 (C4), 22.68 (C3), 20.88 (C2), 14.12 (C1) ppm. (Agrees well with literature NMR values).²³⁹



***N*-(3-chloropropyl)-*N*,*N*-dimethyloctadecan-1-ammonium iodide (102):**²⁴⁰

This compound was prepared by the Menshutkin reaction using Method 5.2.1: 3-chloro-1-iodo propane (2.019 g, 9.8 mmol) and DMOA (2.9 g, 9.8 mmol, 1.0 eq.) in ACN (10 mL) were refluxed for 1.5 hrs. The mixture was then cooled to RT, poured into 20 mL of Et₂O, and placed into a freezer (-20°C) for 10 min to precipitate the title compound as a white solid. Yield: 69% (3.1 g). Mp = 91°C; ¹H NMR (400 MHz, CDCl₃, δ): 3.82-3.71 (m, 4H, (H8 + H7 overlap)), 3.56-3.49 (m, 2H, H6), 3.40 (s, 6H, H5), 2.36-2.28 (m, 2H, H4), 1.80-1.69 (m, 2H, H3), 1.23 (brs, 30H, H2), 0.85 (t, *J* = 7.0 Hz, 3H, H1) ppm; ¹³C NMR (100 MHz, CDCl₃, δ): 65.88 (C15), 61.55 (C14), 52.14 (C13), 41.14 (C12), 31.90 (C11), 29.71-29.62 (C10 overlap), 29.46 (C9), 29.34 (C8), 29.18 (C7), 26.15 (C6), 26.14 (C5), 22.75 (C4), 22.66 (C3), 22.66 (C2), 14.10 (C1) ppm. (Agrees well with literature NMR values).²⁴⁰

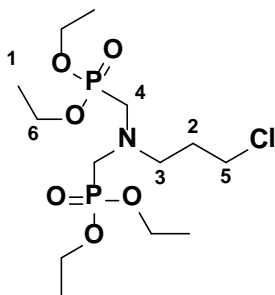
5.5.0 General Procedure for the 3-Component Reaction



Tetraethyl dimethylaminomethylenediphosphonate (105):²⁰²

To a chilled solution of DMF (3.87 mL, 50 mmol) in DCM (75 mL) was added dropwise with stirring a solution of oxalyl chloride (25 mL, 2M in DCM, 50 mmol). Following addition, the mixture was allowed to warm to RT and stirred for 1 hr. P(OEt)₃ (18.77 mL, 109.5 mmol, 2.19 eq.) was then added dropwise with stirring. After 1 hr the mixture was concentrated under reduced pressure to a yellow oil. Yield: 75.5% (12.42 g). **¹H NMR** (400 MHz, CDCl₃, δ): 4.21-4.14 (m, 8H, H4), 3.22 (dt, 1H, ¹J = 24.98 Hz, ²J = 24.98 Hz, H3), 2.58 (s, 6H, H2), 3.18 (dt, 12H, ¹J = 7.07 Hz, ²J = 7.06 Hz, 1H) ppm; **¹³C NMR** (100 MHz, CDCl₃, δ): 62.70 (t, ¹J_{C-P} = 3.05 Hz, C3), 62.40 (t, ²J_{C-P} = 3.61 Hz, C4), 44.11 (t, ³J_{C-P} = 4.71 Hz, C2), 16.39 (q, ³J_{C-P} = 3.01 Hz, C1) ppm; **³¹P NMR** (121.45 MHz, CDCl₃, δ): 19.15 ppm. (Agrees well with literature NMR values).²⁰²

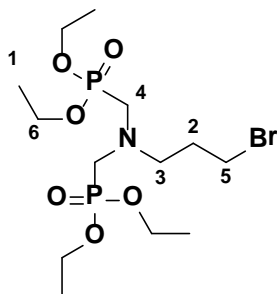
5.6.0 General Procedure for the Bis Kabachnik Fields Reaction



Tetraethyl (((3-chloropropyl)azanediyl)bis(methylene))bis(phosphonate) (114):

To a 20 mL glass screw cap vial, equipped with a magnetic stir bar was added diethylphosphite (2.86 g, 20.74 mmol, 2.0 eq.). The vial was placed on ice to cool. In a separate beaker, 3-aminopropyl-1-chloride hydrochloride (2.0 g, 11.4 mmol) was treated with NaOH (~12 N, 2.0 g in 5 mL) and stirred at 0°C until a yellow oil appeared (~ 5 min). The mixture was then extracted without solvent, adding the upper yellow layer of the free base 3-aminopropyl-1-

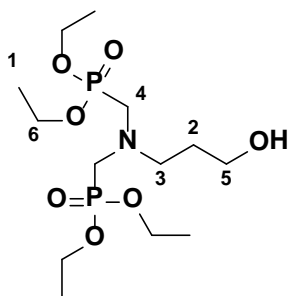
chloride to the vial containing diethylphosphite cooled to 0-5 °C (ice bath). To the chilled solution was added formalin, dropwise, via syringe (37%, 2.15 mL, 25.79 mmol, 2.5 eq.) over 10 min maintaining the reaction temp under 10°C. The mixture was then warmed, with stirring, to RT for 10 min, then heated to 100°C for 30 min. Excess formaldehyde and H₂O were removed via rotary evaporator and the crude material purified by DCVC (20 g silica, 3.5 cm × 4.5 cm) eluting with 80 mL EtOAc and collecting 50 mL (20% MeOH/EtOAc). Yield: 50% (2.03 g); TLC (10% MeOH in EtOAc), R_f = 0.70; ¹H NMR (400 MHz, CDCl₃, δ): 4.18-4.09 (m, 8H, H6), 3.62 (t, 2H, *J* = 6.6 Hz, H5), 3.17 (d, 4H, *J* = 8.6 Hz, H4), 2.97 (t, 2H, *J* = 6.6 Hz, H3), 2.00 (m, 2H, H2), 1.33 (t, 12H, *J* = 7.1 Hz, H1); ¹³C NMR (100 MHz, CDCl₃, δ): 61.84 (m, C6), 53.93 (t, ³*J*_{C-P} = 7.44 Hz, (C5)), 50.18 (dd, ¹*J*_{C-P} = 6.08 Hz, ¹*J*_{C-P} = 6.00 Hz, (C4)), 42.47 (C3), 30.77 (C2), 16.45 (t, ³*J*_{C-P} = 2.94 Hz, (C1)); ³¹P NMR (121.45 MHz, CDCl₃, δ): 24.40 ppm.



Tetraethyl (((3-bromopropyl)azanediyl)bis(methylene))bis(phosphonate) (116):

To a 20 mL glass screw cap vial, equipped with a magnetic stir bar was added diethylphosphite (2.77 mL, 21.56 mmol, 2.2 eq.) and the vial was placed on ice meanwhile 3-aminopropyl-1-bromide hydrobromide (~2.5 g, ~11 mmol) was treated with KOH (6 N, 6 g in 20 mL) and stirred at 0°C until a yellow oil appeared (~5 min). The mixture was then extracted without solvent, collecting the upper yellow layer of the free base aminopropyl-1-bromide (incompletely

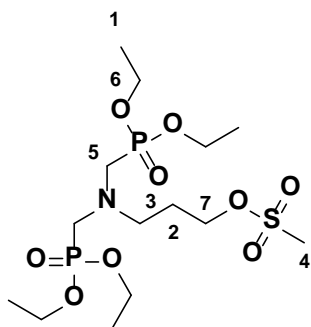
dry by NMR, 50% H₂O present). The amine (1.350 g, 9.78 mmol) was added to the vial containing diethylphosphite and cooled at 0-5 °C (ice bath). To the chilled, stirred solution was added formalin, dropwise (37%, 2.12 mL, 25.43 mmol, 2.6 eq.) over 10 min while maintaining the reaction temp under 10°C, then warming the mixture to RT for 30 min, and finally to 100 °C for 1hr. The reaction was diluted with 0.2N NaOH (~ 300 mg in 40 mL) and extracted with CHCl₃ (1 × 30 mL, 1 × 10 mL), the organic layer was separated, washed with brine (1 × 20 mL) and dried over anhydrous MgSO₄ filtered and concentrated to afford a yellow oil. The title compound was in poor yield, however analysis by ¹H NMR spectroscopy revealed >98% purity and required no further purification. Yield: 20.9 % (0.76 g); TLC (5% MeOH in EtOAc), R_f = 0.48; ¹H NMR (400 MHz, CDCl₃, δ): 4.17-4.07 (m, 8H, H6), 3.47 (t, 2H, *J* = 6.7 Hz, H5), 3.14 (d, 4H, *J* = 8.5 Hz, H4), 2.93 (t, 2H, *J* = 6.6 Hz, H3), 2.00 (q, 2H, *J* = 6.58 Hz, H2), 1.31 (t, 12H, *J* = 7.1 Hz, H1); ¹³C NMR (100 MHz, CDCl₃, δ): 61.9 (t, ²*J*_{C-P} = 3.36 Hz, C6), 55.08 (C3), 49.43 (C4), 31.09 (C5), 30.96 (C2), 16.49 (t, ³*J*_{C-P} = 2.94 Hz, C1); ³¹P NMR (121.45 MHz, CDCl₃, δ): 24.60 ppm.



Tetraethyl (((3-hydroxypropyl)azanediyl)bis(methylene))bis(phosphonate) (117):²⁴¹⁻²⁴³

To a 20 mL glass screw cap vial, equipped with a magnetic stir bar was added diethylphosphite (2.86 g, 20.74 mmol, 2.0 eq.) and 3-amino-1-propanol (0.768 g, 10.24 mmol,) and the mixture cooled to 0-5 °C (ice bath). To the chilled solution was added formalin, dropwise, via syringe

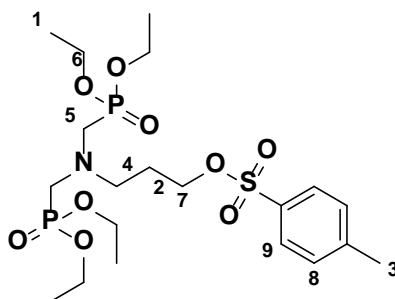
(37%, 2.15 mL, 25.79 mmol, 2.5 eq.) over 10 min maintaining the reaction temp under 10°C. The mixture was warmed, with stirring, to RT for 30 min, then heated to 100°C for 60 min. Excess formaldehyde and H₂O were removed via rotary evaporator and the crude material purified by DCVC (20 g silica, 3.5 cm × 4.5 cm) eluting with 100 mL EtOAc (20% MeOH/EtOAc) to give a light yellow oil after evaporation of solvent. Yield: 50% (2.03 g); TLC (10% MeOH in EtOAc), R_f = 0.50; ¹H NMR (400 MHz, CDCl₃, δ): 4.18-4.09 (m, 8H, H6), 3.62 (t, 2H, *J* = 6.6 Hz, H5), 3.17 (d, 4H, *J* = 8.6 Hz, H4), 2.97 (t, 2H, *J* = 6.6 Hz, H3), 1.61 (m, 2H, H2), 1.32 (t, 12H, *J* = 7.1 Hz, H1) ppm; ¹³C NMR (100 MHz, CDCl₃, δ): 62.06 (t, ²*J*_{C-P} = 3.61 Hz, C6), 59.04 (C5), 53.44 (t, ³*J*_{C-P} = 7.46 Hz, C3), 50.66 (dd, ¹*J*_{C-P} = 9.14 Hz, C4), 29.78 (C2), 16.43 (t, ³*J*_{C-P} = 2.93 Hz, C1) ppm; ³¹P NMR (121.45 MHz, CDCl₃, δ): 25.0 ppm. (Agrees well with literature NMR values).²⁴¹⁻²⁴³



3-(bis((diethoxyphosphoryl)methyl)amino)propyl methanesulfonate (**118**):

To a flame dried and evacuated 125 mL round bottom flask, equipped with a magnetic stir bar was added sequentially NMe₃·HCl (1.50 g, 5 mmol, 0.1 eq.), DCM (50 mL), Et₃N (17.43 mL, 75 mmol, 1.5 eq.), **117** (18.76 g, 50 mmol, 1.0 eq.) and the solution cooled to 0°C in an ice bath. To the chilled, stirred solution was added, dropwise, mesyl chloride (4.5 mL, 58.1 mmol, 1.16 eq.) followed by rinsing the addition funnel with anhydrous DCM (15 mL) and the cloudy yellow

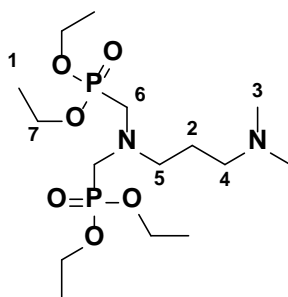
mixture was stirred for 30 min at RT at which point TLC showed disappearance of the starting amine (5% MeOH in EtOAc, 10 mL). The reaction was diluted with H₂O (1 × 75 mL) and extracted with DCM (100 mL total), the organic layer was re-washed with H₂O (2 × 75 mL), dried over MgSO₄, filtered and evaporated to give a light orange oil. The crude material was used without further purification. Yield: 74% (13.39 g); TLC (30% MeOH in EtOAc), R_f = 0.45; ¹H NMR (400 MHz, CDCl₃, δ): 4.33 (t, 12H, *J* = 6.44 Hz, 2H, H7), 4.16-4.06 (m, 8H, H6), 3.12 (d, 4H, *J* = 8.57 Hz, H5), 3.01 (s, 3H, H4), 2.97 (t, 2H, *J* = 6.57 Hz, H3), 1.94-1.85 (m, 2H, H2), 1.31 (t, 12H, *J* = 7.05 Hz, H1); ¹³C NMR (100 MHz, CDCl₃, δ): 67.90 (C7), 61.84 (t, ²*J*_{C-P} = 3.50 Hz, C6), 52.50 (t, ³*J*_{C-P} = 7.61 Hz, C3) 52.54, 49.30 (dd, ¹*J*_{C-P} = 6.57 Hz, C5), 37.07 (C4), 27.21 (C2), 16.39 (t, ³*J*_{C-P} = 2.81 Hz, C1) ppm; ³¹P NMR (121.45 MHz, CDCl₃, δ): 24.50 ppm.



3-bis(((diethoxyphosphoryl)methyl)amino)propyl 4-methylbenzenesulfonate (**119**):

To a flame dried and evacuated 25 mL round bottom flask, equipped with a magnetic stir bar was added sequentially NMe₃·HCl (0.045g, 0.24 mmol, 0.24 eq.), DCM (1 mL), Et₃N (0.58 mL, 2.5 mmol, 2.5 eq.), **117** (0.375g, 1 mmol) and the solution cooled to 0°C in an ice bath. To the chilled, stirred solution was added, dropwise, TsCl (0.286 mg, 1.5 mmol, 1.5 eq.) in anhydrous DCM (2 mL) and the cloudy yellow mixture was stirred for 1 hr at RT at which point TLC showed disappearance of the starting amine (5% MeOH in EtOAc, 10 mL). The reaction was diluted with H₂O (1 × 15 mL) and extracted with DCM (10 mL total), the aqueous layer was re-

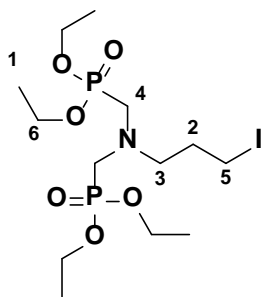
extracted with EtOAc (15 mL) and the combined organic layers were dried over MgSO₄, filtered and evaporated to give a yellow oil. The crude material was purified by flash chromatography on silica gel (20 g silica, 1.5 cm i.d) with gradient elution: 100% EtOAc (35 mL) then 5% MeOH:EtOAc (90 mL) to obtain the title compound as a yellow oil. Yield: 56.7% (0.300 g); TLC (5% MeOH in EtOAc), R_f = 0.42; ¹H NMR (400 MHz, CDCl₃, δ): 7.76 (d, 2H, *J* = 8.24 Hz, H9), 7.32 (d, 2H, *J* = 8.04 Hz, H8), 4.13-4.05 (m, 10H, (H7, H6)), 3.08 (d, 4H, *J* = 8.40 Hz, H5), 2.83 (t, 2H, *J* = 6.70 Hz, H4), 2.42 (s, 3H, H3), 1.81 (t, 2H, *J* = 6.65 Hz, H2), 1.30 (t, 12H, *J* = 7.08 Hz, H1) ; ¹³C NMR (100 MHz, CDCl₃, δ): 44.67 (C11), 133.19 (C10), 129.81 (C8), 127.83 (C9), 68.50 (C7), 61.86 (t, ²*J*_{C-P} = 3.19 Hz, C6), 52.67 (dd, ¹*J*_{C-P} = 6.02 Hz, C5), 52.67 (C4), 27.22 (C2), 21.57 (C3), 16.46 (t, ³*J*_{C-P} = 2.78 Hz, C1) ppm; ³¹P NMR (121.45 MHz, CDCl₃, δ): 24.56 ppm.



Tetraethyl (((3-(dimethylamino)propyl)azanediyl)bis(methylene)) bis(phosphonate) (113):

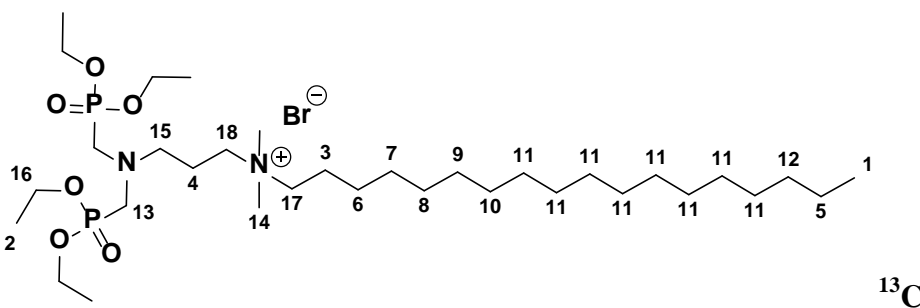
To a 20 mL glass screw cap vial equipped with a magnetic stir bar containing the bromo amino bisphosphonate (0.954 g, 1.8 mmol) was added NHMe₂ (5.6 M in EtOH, 2.5 mL, excess) followed by H₂O (0.5 mL) and the clear mixture was stirred at reflux sealed for 1.5 hr, at which point TLC showed disappearance of the starting material (1% NH₄⁺OH⁻ in Acetone, 10 mL, R_f = 0.95). The cooled yellow reaction diluted with H₂O (1 × 20 mL, pH was 11) and extracted with CHCl₃ (2 × 30 mL), dried over MgSO₄, filtered and evaporated to give an orange oil. The title

compound was isolated > 98% purity (^1H and ^{31}P NMR) and required no further purification. Yield 62% (0.446 g); TLC (1% NH_4^+OH^- in Acetone, 10 mL) or (20% MeOH (6% NaBr)): ACN, $R_f = 0.47$; ^1H NMR (400 MHz, CDCl_3 , δ): 4.15-4.06 (m, 8H, H7), 3.11 (d, 4H, $J = 8.9$ Hz, H6), 2.80 (t, 2H, $J = 6.8$ Hz, H5), 2.27 (t, 2H, $J = 7.5$ Hz, H4), 2.18 (s, 6H, H3), 1.61 (p, 2H, $J = 7.15$ Hz, H2), 1.28 (t, 12H, $J = 7.0$ Hz, H1) ppm; ^{13}C NMR (100 MHz, CDCl_3 , δ): 61.8 (t, $^2J_{\text{C-P}} = 3.3$ Hz, C7), 57.24 (C4), 55.03 (C5), 50.92 (dd, $^1J_{\text{C-P}} = 7.1$ Hz, C6), 49.36 (dd, $^1J_{\text{C-P}} = 6.7$ Hz, C6), 45.48 (C3), 25.65 (C2), 16.48 (t, $^3J_{\text{C-P}} = 2.8$ Hz, C1) ppm; ^{31}P NMR (121.45 MHz, CDCl_3 , δ): 24.89 ppm. **HRMS-DART** (m/z): $[\text{MH}^+]$ calculated for $\text{C}_{15}\text{H}_{36}\text{N}_2\text{O}_6\text{P}_2$, 403.2126; found, 403.2135.

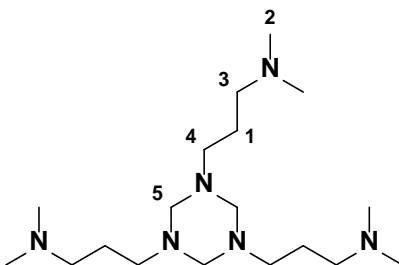


Tetraethyl (((3-iodopropyl)azanediyl)bis(methylene))bis(phosphonate) (120):

A mixture of diethyl (4-bromobutyl)phosphonate (1.0 g, 2.21 mmol, 1.0 eq.) and NaI (0.69 g, 4.6 mmol, 2.08 eq.) in acetone (3 mL) were placed, with a magnetic stirring bar, into a 5 mL μW glass reaction tube and sealed. The reaction mixture was heated in the μW at 100 $^\circ\text{C}$ (5 min). The yellow solid was transferred to a 100 mL RBF washing with acetone (50 mL). Volatiles were removed on a rotary evaporator and the crude material was diluted with brine (10 mL) and extracted with CHCl_3 (1×10 mL). The organic layer was separated, dried over anhydrous MgSO_4 filtered, concentrated and recovered as a yellow oil without further purification. Yield: 75% (0.80 g); TLC (10% NH_4^+OH^- / acetone), $R_f = 0.85$; ^1H NMR (400 MHz, CDCl_3 , δ): 4.20-



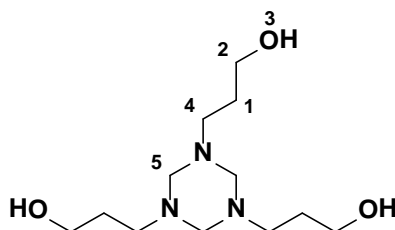
same eluent (1st 40 mL removed upper R_f impurity, compound **121** was obtained in the next 7 fractions totaling (95 mL)) as a yellow oil after filtering off NaBr (Celite), washing with CHCl₃. Yield: 46.1% (0.162 g). TLC (20% MeOH (NaBr 6%): ACN), R_f = 0.5 ; ¹H NMR (400 MHz, CDCl₃, δ) 4.15-4.08 (m, 8H, H11), 3.72-3.69 (m, 2H, H10), 3.55-3.51 (m, 2H, H9), 3.33 (s, 6H, H8), 3.12-3.08 (m, 4H, H7), 2.99-2.97 (m, 2H, H6), 2.0-1.98 (m, 2H, H5), 1.74-1.71 (m, 2H, H4), 1.24-1.20 (br m, 42H, (H2 + H3 overlap)), 0.88-0.83 (m, 3H, H1) ppm; ¹³C NMR (100 MHz, CDCl₃, δ): 65.19-61.96 (C19-C16 overlap, from HSQC: 65.19 (C18), 62.52 (C17), 61.96 (C16)), 53.64 (C15), 50.86 (C14), 50.5 (d, C13), 31.90 (C12), 29.68-29.60 (C11 overlap), 29.57 (C10), 29.47 (C9), 29.39 (C8), 29.34 (C7), 29.26 (C6) 26.12 (C5), 22.83 (C4), 22.66 (C3), 16.58-16.50 (m, ³J_{C-P} = unresolved, C2), 14.10 (C1) ppm; ³¹P NMR (121.45 MHz, CDCl₃, δ) 24.40 ppm. **HRMS-DART** (m/z): [M⁺] – Br[–] calculated for C₃₃H₇₃N₂O₆P₂, 655.4937; found, 655.4938.



3,3',3''-(1,3,5-triazinane-1,3,5-triyl)tris(*N,N*-dimethylpropan-1-amine) (123**):**²⁴⁴⁻²⁴⁵

To a 125 mL round bottom flask, paraformaldehyde (1.652 g, 55 mmol, 1.1 eq.) was added to a solution of *N,N*-dimethylpropane-1,3-diamine (6.29 mL, 50 mmol) in TOL (15 mL). The reaction was refluxed using a Dean-Stark trap for 1.5 hrs. TOL was evaporated and a portion of the residue (1.96 g) was partitioned between CHCl₃ (15 mL) and H₂O (5 mL). The organic layer was separated, dried with MgSO₄ and concentrated to give a clear oil. Yield: 66% (1.307 g).

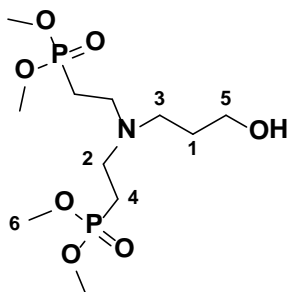
TLC (20% MeOH in EtOAc, 10 mL), $R_f = 0.05$; $^1\text{H NMR}$ (400 MHz, CDCl_3 , δ): 3.29 (brs, 6H, H5), 2.40 (t, 6H, $J = 7.5$ Hz, H4), 2.25 (t, 6H, $J = 7.5$ Hz, H3), 2.18 (s, 18H, H2), 1.59 (p, 6H, $J = 7.5$ Hz, H1) ppm; $^{13}\text{C NMR}$ (100 MHz, CDCl_3 , δ): 74.65 (C5), 57.83 (C3), 50.78 (C4), 45.54 (C2), 25.88 (C1) ppm. (Agrees well with literature NMR values).²⁴⁴⁻²⁴⁵



3,3',3''-(1,3,5-triazinane-1,3,5-triyl)tris(propan-1-ol) (122):^{40,246}

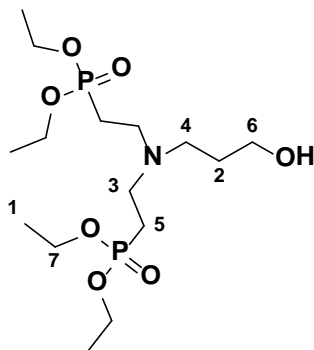
To a 125 mL round bottom flask, formalin (0.813 mL, 10 mmol) was added to a solution of 3-amino-1-propanol (0.751 g, 10 mmol) in ACN (10 mL). The reaction was stirred at RT overnight. Evaporation of volatiles followed by DCVC (20 g silica, 3.5 cm \times 4.5 cm) eluting with 5% NH_4^+OH^- in acetone (50 mL) then collecting (150 mL), provided pure product as a clear oil. Yield: 92% (0.8 g). TLC (5% NH_4^+OH^- in acetone, 10 mL), $R_f = 0.3$; $^1\text{H NMR}$ (400 MHz, CDCl_3 , δ): 4.37 (s, 6H, H5), 3.84 (t, 6H, $J = 7.0$ Hz, H4), 3.71 (s, 3H, H3), 2.97 (t, 6H, $J = 5.6$ Hz, H2), 1.60 (q, 6H, $J = 5.40$ Hz, H1) ppm; $^{13}\text{C NMR}$ (100 MHz, CDCl_3 , δ): 83.06 (C4), 68.12 (C3), 47.78 (C2), 22.45 (C1) ppm. (Agrees well with literature NMR values).^{40,246}

5.7.0 General Procedure for the Bis Michael Addition of Amines onto Vinylphosphonates



Tetramethyl (((3-hydroxypropyl)azanediyl)bis(ethane-2,1-diyl))bis(phosphonate) (135):

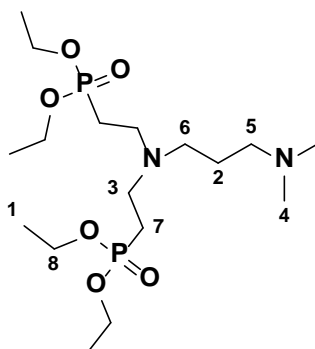
To a 25 mL round bottom flask equipped with a magnetic stir bar, was added a stirred solution of the primary amine (0.448 g, 5.9 mmol) in distilled H₂O (5 mL) at RT. Two equivalents of diethyl vinylphosphonate (1.637 g, 12.03 mmol, 2.01 eq.) was then added and the reaction stirred at RT ON. The reaction was transferred to a 125 mL round bottom flask along with 30 mL ACN and evaporated to a clear oil (2.14 g, containing ~ 7% starting material by ³¹P NMR). The crude material was purified by DCVC (20 g silica, 3.5 cm × 4.5 cm) eluting with 30% MeOH:EtOAc (30 mL fractions, 240 mL). Fractions (2-7) containing were filtered (Celite) and evaporated to obtain the title compound as a yellow oil. Yield: 95% (1.968 g); TLC (30% MeOH:EtOAc), R_f = 0.33; ¹H NMR (400 MHz, CDCl₃, δ): 3.73 (d, *J* = 11.0 Hz, 12H, H6), 3.74-3.70 (m, 2H, H5), 2.82-2.74 (m, 4H, H4), 2.60 (t, 2H, *J* = 6.0 Hz, H3), 1.98-1.88 (m, 4H, H2), 1.71-1.64 (m, 2 H, Hz, H1) ppm; ¹³C NMR (100 MHz, CDCl₃, δ): 61.54 (C5), 52.65 (d, ²*J*_{C-P} = 6.61 Hz, C6), 50.69 (C3), 46.26 (C4), 28.69 (C1), 21.84 (d, ²*J*_{C-P} = 138.47 Hz, C1) ppm. ³¹P NMR (121.45 MHz, CDCl₃, δ): 32.66 ppm.



Tetraethyl (((3-hydroxypropyl)azanediyl)bis(ethane-2,1-diyl))bis(phosphonate) (136):²⁴⁷

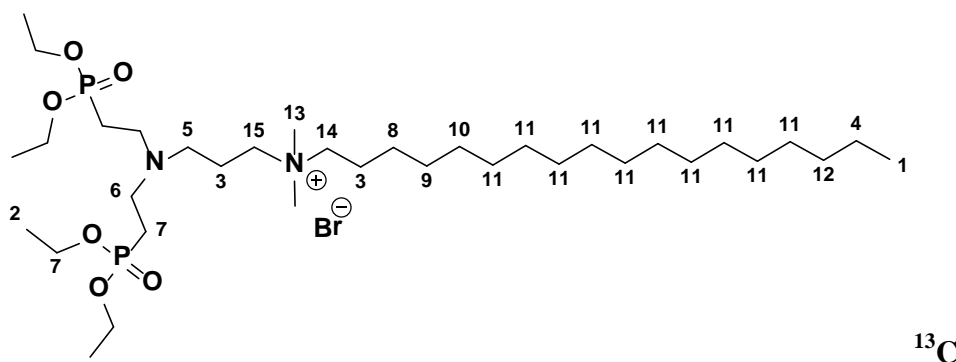
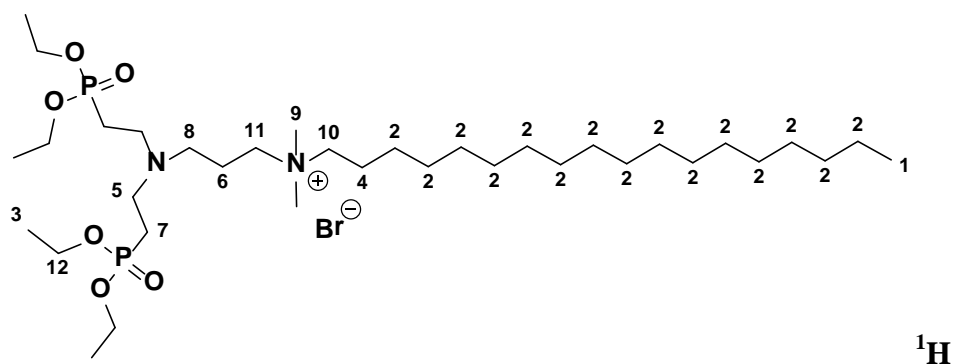
To a 125 mL round bottom flask equipped with a magnetic stir bar, was added a stirred solution of the primary amine (1.016 g, 13.5 mmol) in distilled H₂O (15 mL) at RT. Two equivalents of

diethyl vinylphosphonate (4.44 g, 27.0 mmol, 2.00 eq.) was then added and the reaction stirred at RT ON. H₂O was co-evaporated from ACN (80 mL) and evaporated to a yellow oil (containing ~ 14% starting material by ³¹P NMR). The crude material was purified by DCVC (50 g silica, 3.5 cm × 4.5 cm) pre-eluting with acetone (50 mL) and then eluting with 35% EtOH:Acetone (150 mL) to obtain the title compound as a yellow oil. Yield: 50% (2.722 g); TLC (30% EtOH:Acetone), R_f = 0.40; ¹H NMR (400 MHz, CDCl₃, δ): 4.16-4.03 (m, 8H, H7), 3.75-3.67 (m, 3H, H6), 2.83-2.75 (m, 4H, H5), 2.64-2.59 (m, 2H, H4), 1.97-1.86 (m, 4H, H3), 1.68 (q, 2H, *J* = 5.58 Hz, H2), 1.31 (t, 12 H, *J* = 7.06 Hz, H1) ppm; ³¹P NMR (121.45 MHz, CDCl₃, δ): 30.00 ppm.²⁴⁷



Tetraethyl (((3-(dimethylamino)propyl)azanediyl)bis(ethane-2,1-diyl)) bis (phosphonate) (139):

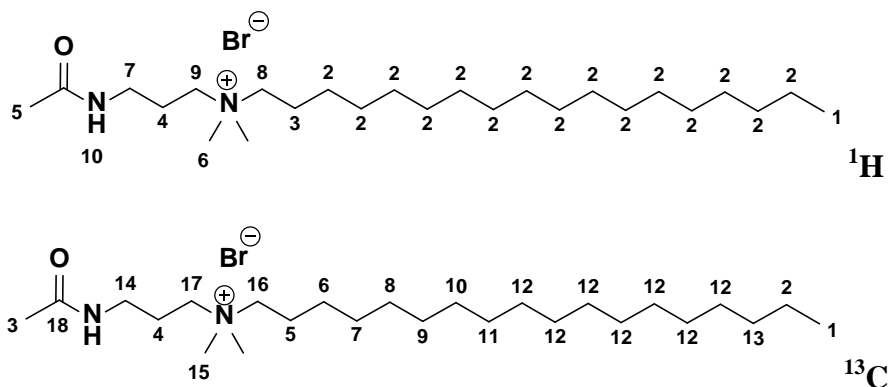
Synthesized from alcohol via mesylate and dimethylamine, see Tetraethyl (((3-(dimethylamino)propyl)azanediyl)bis(methylene))bis(phosphonate) **113** procedure; ¹H NMR (400 MHz, CDCl₃, δ): 4.11-3.99 (m, 8 H, H8), 2.76-2.69 (m, 4H, H7), 2.40 (t, 2H, *J* = 7.12 Hz, H6), 2.22 (t, H5, *J* = 7.14 Hz, H5), 2.16 (s, 6H, H4), 1.91-1.81 (m, 4H, H3), 1.60-1.53 (m, H2, 2H), 1.28 (t, H1, *J* = 7.04 Hz) ppm; ³¹P NMR (121.45 MHz, CDCl₃, δ): 30.57 ppm.



***N*-(3-(bis(2-(diethoxyphosphoryl)ethyl)amino)propyl)-*N,N*-dimethyloctadecan-1-ammonium bromide (140):**

To a flame dried and evacuated 20 mL screw cap vial, equipped with a magnetic stir bar was added a mixture of **139** (0.181 g, 0.42 mmol) and bromooctadecane (0.140 g, 0.42 mmol, 1.0 eq.) was sealed and heated to 100°C on a sand bath. After 1 hr, TLC showed the disappearance of the starting amine (5% MeOH in EtOAc, 10 mL). The mixture was drypacked onto silica and the crude material was purified by DCVC (20 g silica, 3.5 cm × 4.5 cm) pre-washed with 2 × 40 mL 20% MeOH (NaBr 6%): ACN then eluting with the same eluent (50 mL), evaporating, redissolving with CHCl₃ and filtering off NaBr through a pad of Celite, washing with CHCl₃ to provide a yellow wax. Yield: 44% (0.15 g). TLC (20% MeOH (NaBr 6%): ACN), *R*_f = 0.3; ¹H NMR (400 MHz, CDCl₃, δ) 4.14-4.04 (m, 8H, H12), 3.72-3.67 (m, 2H, H11), 3.47-3.36 (m, 2H, H10), 3.27 (s, 6H, H9), 2.85-2.76 (m, 4H, H8), 2.05-1.09 (m, 4H, (H6 + H5)), 1.75-1.65 (m, 2H,

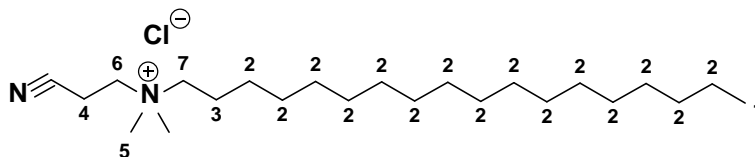
H4), 1.31 (t, $J = 7.03$ Hz, 6H, H3), 1.23 (brs, 30 H, H2), 0.86 (t, $J = 6.94$ Hz, 3H, H1) ppm; ^{13}C NMR (100 MHz, CDCl_3 , δ): 67.49 (C15), 61.93 (C14), 61.78 (C13), 31.89 (C12), 29.68 (C11 overlap), 29.63 (C10), 29.49 (C9), 29.42 (C8), 29.33 (C7), 29.26 (C6), 26.29 (C5), 25.60 (C4), 22.66 (C3), 16.48 (d, $^3J_{\text{C-P}} = 6.03$ Hz, C2), 14.08 (C1) ppm; ^{31}P NMR (121.45 MHz, CDCl_3 , δ) 24.40 ppm.



***N*-(3-acetamidopropyl)-*N,N*-dimethyloctadecan-1-ammonium (153):**²⁴⁸

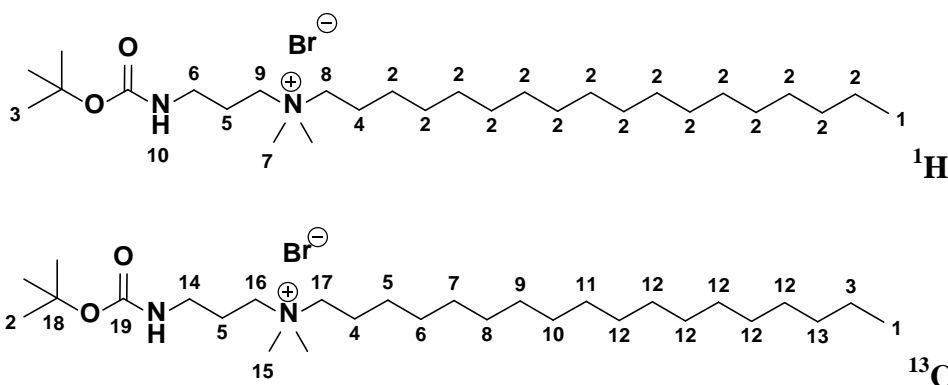
This compound was prepared by the Menshutkin reaction using Method 5.2.1: *N*-(3-(dimethylamino)propyl)acetamide **148** (0.285 g, 1.97 mmol) and 1-bromooctadecane (0.664 g, 1.99 mmol, 1.01 eq.) were reacted at 100°C neat for 4 hrs until the mixture solidified. The mixture was then dissolved in MeOH (10 mL) and hot filtered from charcoal. Volatiles were removed on a rotary evaporator and the crude was recrystallized from acetone (15 mL) by placing the solution on ice (15 min) as a white solid. Yield: 74% (0.720 g). Mp = 93-95°C; ^1H NMR (400 MHz, CDCl_3 , δ): 7.98 (t, $J = 7.98$ Hz, 1H, H10), 3.84-3.78 (m, 2H, H9), 3.39-3.32 (m, 4H, (H7 + H8 overlap)), 3.26 (s, 6H, H5), 2.10-2.00 (m, 2H, H5), 2.04 (s, 3H, H4), 1.75-1.65 (m, 2H, H3), 1.22 (brs, 30H, H2), 0.84 (t, $J = 6.79$ Hz, 3H, H1) ppm; ^{13}C NMR (100 MHz, CDCl_3 , δ): 171.60 (C18), 64.97 (C17), 63.00 (C16), 51.13 (C15), 36.22 (C14), 32.00 (C13),

This compound was prepared by dissolving **152** (10.80 g, 14.16 mmol) in EtOH (80 mL) and deprotecting with hydrazine hydrate (5.5 mL, 5 eq.) under reflux 1.5 hrs. The mixture was then cooled to RT, diluted with CHCl₃/ACN (1:1, 100 mL) and filtered through Celite. Volatiles were removed *in vacuo* and the crude product (8.647 g, yellow gum) was again diluted with CHCl₃/ACN (1:1, 100 mL) and placed in the freezer (-20°C, 30 min) to further precipitate the pthalylhydrazide impurity (white solid) and filtered through Celite. Volatiles were evaporated and the sample was placed under high vacuum (1 hr) to obtain the title compound as a yellow/white waxy solid. Yield: 87% (5.361 g); ¹H NMR (400 MHz, CDCl₃, δ): 3.75-3.66 (m, 2H, H8), 3.48-3.39 (m, 2H, H7), 3.33 (s, 6H, H6), 2.29-2.82 (m, 2H, H5), 2.01-1.87 (m, 2H, H4), 1.79-1.67 (m, 2H, H3), 1.24 (brs, 30H, H2), 0.86 (t, *J* = 7.06 Hz, 3H, H1) ppm; ¹³C NMR (100 MHz, CDCl₃, δ): 64.15 (C11), 62.27 (C10), 51.02 (C9), 38.28 (C8), 31.55 (C7), 29.40-27.31 (C6 overlap), 26.32 (C5), 25.84 (C4), 22.54 (C3), 22.44 (C2), 13.86 (C1) ppm.²⁴⁸



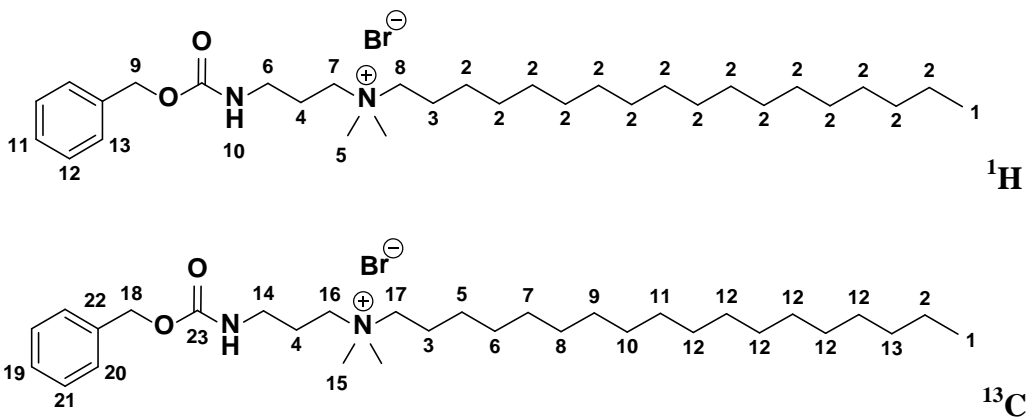
N-(2-cyanoethyl)-N,N-dimethyloctadecan-1-ammonium (154):

This compound was prepared by the Menshutkin reaction using Method 5.2.1: 3-chloropropanenitrile **149** (1.429 g, 18.9 mmol) and DMOA (6.258 g, 18.7 mmol, ~ 1.0 eq.) were reacted at 100°C neat for 5 min until the mixture solidified. To the solid mixture was added MeOH (10 mL) and heating was continued for another 30 min. Volatiles were removed on a rotary evaporator and the crude product was recrystallized from acetone (200 mL) by placing the solution on ice (15 min) recovered a waxy white solid. Yield: 88% (6.0 g). Mp = 54-55°C; ¹H NMR (400 MHz, CDCl₃, δ): 3.72-3.67 (m, 2H, H7), 3.56 (s, 6H, H6), 2.09-1.98 (m, 2H, H5), 1.86-1.76 (m, 2H, H4), 1.42-1.32 (s, 2H, H2), 1.24 (brs, 30H, H2), 0.87 (t, *J* = 6.68 Hz, 3H, H1) ppm.



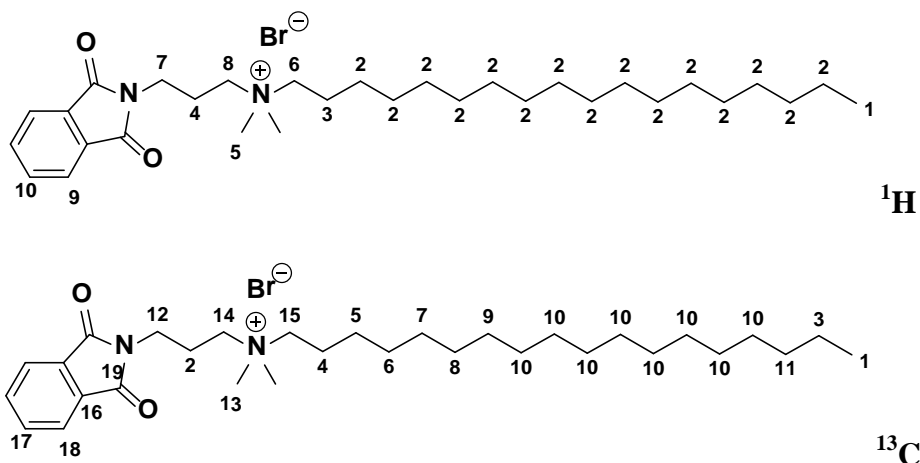
N-(3-((tert-butoxycarbonyl)amino)propyl)-N,N-dimethyloctadecan-1-ammonium (155):²⁴⁹

This compound was prepared by the Menshutkin reaction using Method 5.2.1: tert-butyl (3-bromopropyl)carbamate **150** (1.421 g, 5.96 mmol) and DMOA (2.4649 g, 7.37 mmol, ~1.23 eq.) were reacted at 100°C neat for 35 min until the mixture solidified. The crude reaction was recrystallized from acetone (20 mL) by placing the solution on ice (10 min) and recovered as an off white waxy solid. The final product was isolated as a mixture with the starting material DMOA in a 0.63:0.37 ratio by ^1H NMR and used without further purification. Yield: 70% (2.243 g). Mp = 98-100°C; ^1H NMR (400 MHz, CDCl_3 , δ): 5.8 (s, 1H, H10), 3.65-3.56 (m, 2H, H9), 3.44-3.33 (m, 2H, H8), 3.28 (s, 6H, H7), 3.25-3.17 (m, 2H, H6), 2.07-1.95 (m, 2H, H5), 1.74-1.60 (m, 2H, H4), 1.38 (s, 12H, H3), 1.23 (brs, 30H, H2), 0.83 (t, $J = 7.02$ Hz, 3H, H1) ppm; ^{13}C NMR (100 MHz, CDCl_3 , δ): 156.92 (C23), 136.77 (C22), 128.49 (C21), 128.07 (C20), 128.0 (C19), 66.52 (C18), 64.50 (C17), 62.33 (C16), 51.07 (C15), 37.88 (C14), 31.90 (C13), 29.80-29.74 (C12 overlap), 29.65 (C11), 29.59 (C10), 29.47 (C9), 29.40 (C8), 29.34 (C7), 29.19 (C6), 26.25 (C5), 23.19 (C4), 22.73 (C3), 22.67 (C2), 14.11 (C1) ppm. (Agrees well with literature NMR values).²⁴⁹



***N*-(3-(((benzyloxy)carbonyl)amino)propyl)-*N,N*-dimethyloctadecan-1-ammonium (156):**

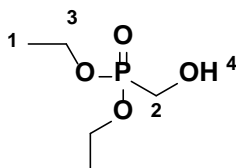
This compound was prepared by the Menshutkin reaction using Method 5.2.1: benzyl (3-bromopropyl)carbamate **151** (0.991 g, 3.64 mmol) and DMOA (1.21 g, 3.62 mmol, ~1.0 eq.) were reacted at 100°C neat for 35 min until the mixture solidified. The mixture was then cooled to RT, poured into 20 mL of Et₂O, and placed into a freezer (-20°C) for 60 min to precipitate the title compound as a white waxy solid. Yield: 70% (1.52 g). Mp = 98-100°C; ¹H NMR (400 MHz, CDCl₃, δ): 7.32-7.27 (m, 3H, H11-13), 6.51 (t, *J* = 6.51 Hz, H10), 5.06 (s, 2H, H9), 3.65-3.56 (m, 2H, H8), 3.35-3.25 (m, 4H, (H6, H7)), 3.18 (s, 6H, H5), 2.05-1.95 (m, 2H, H4), 1.65-1.50 (m, 2H, H3), 1.23 (brs, 30H, H2), 0.86 (t, *J* = 6.69 Hz, 3H, H1) ppm; ¹³C NMR (100 MHz, CDCl₃, δ): 156.92 (C23), 136.77 (C22), 128.49 (C21), 128.07 (C20), 128.0 (C19), 66.52 (C18), 64.50 (C17), 62.33 (C16), 51.07 (C15), 37.88 (C14), 31.90 (C13), 29.80-29.74 (C12 overlap), 29.65 (C11), 29.59 (C10), 29.47 (C9), 29.40 (C8), 29.34 (C7), 29.19 (C6), 26.25 (C5), 23.19 (C4), 22.73 (C3), 22.67 (C2), 14.11 (C1) ppm.



***N*-(3-(1,3-dioxisoindolin-2-yl)propyl)-*N,N*-dimethyloctadecan-1-ammonium bromide (152):**

This compound was prepared by the Menshutkin reaction using Method 5.2.2: 3-bromopropylphthalimide **10** (8.00 g, 29.38 mmol, 1.0 eq.) and DMOA (8.80 g, 29.38 mmol, 1.0 eq.) in ACN (80 mL) were refluxed for 4.2 hrs. The mixture was then cooled to RT, poured into 100 mL of Et₂O, and left at RT for 30 min to precipitate the title compound as a white solid. Yield: 84% (14.172 g). Mp = 100-105°C; ¹H NMR (400 MHz, CDCl₃, δ): 7.82-7.76 (m, 2H, H10), 7.72-7.64 (m, 2H, H9), 3.81 (t, *J* = 6.62 Hz, 2H, H8), 3.76-3.64 (m, 2H, H7), 3.53-3.46 (m, 2H, H6), 3.41 (s, 6H, H5), 2.24-2.13 (m, 2H, H4), 1.75-1.58 (m, 2H, H3), 1.22 (brs, 30H, H2), 0.84 (m, *J* = 6.8 Hz, 3H, H1) ppm; ¹³C NMR (100 MHz, CDCl₃, δ): 168.23 (C19), 134.29 (C18), 131.78 (C17), 123.50 (C16), 64.32 (C15), 61.32 (C14), 51.41 (C13), 34.92 (C12), 31.90 (C11), 29.75-29.65 (C10 overlap), 29.58 (C9), 29.47 (C8), 29.34 (C7), 29.21 (C6), 26.22 (C5), 23.80 (C4), 22.66 (C3), 22.48 (C2), 14.10 (C1) ppm.

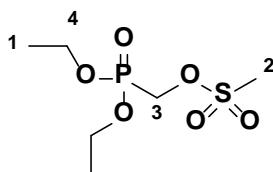
5.8.0 Preparation of Tris Phosphonic Acid Derivatives



Diethyl (hydroxymethyl)phosphonate (**169**):²⁵⁰

Into a Schlenk flask (250 mL flask), equipped with a condenser and a magnetic stirrer, was introduced diethylhydrogenphosphonate HP(O)(OEt)₂ (20 g, 144.8 mmol), paraformaldehyde (5.2 g, 1.2 eq.), EtOH (30 mL) and powdered K₂CO₃ (1 g, 0.05 eq.) and the mixture was refluxed for 60 min. At the end of the reaction, the solution was evaporated and filtered through a short pad of Celite from acetone (50 mL). The solvent was removed under vacuum to obtain the title compound as a clear liquid which may be distilled (bp = 95°C, ~ 5 × 10⁻² mbar) but was used

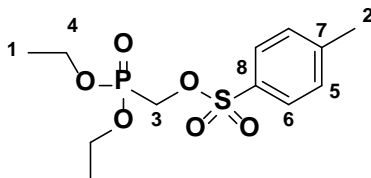
without any further purification. Yield: 94% (22.84 g). $^1\text{H NMR}$ (400 MHz, CDCl_3 , δ): 4.87 (s, 1H, H4); 4.14 (t, $^2J = 5.8$ Hz, 4H, H3); 3.57 (d, $^2J = 5.9$ Hz, 2H, H2); 1.29 (t, $^3J = 7.0$ Hz, 6H, H1) ppm; $^{13}\text{C NMR}$ (100 MHz, CDCl_3 , δ): 62.45 (d, $^1J = 6.7$ Hz, C3), 56.90 (d, $^1J = 162.6$ Hz, C2), 16.35 (d, $^1J = 5.6$ Hz, C1) ppm; $^{31}\text{P NMR}$ (121.45 MHz, CDCl_3 , δ): 24.72 ppm. (Agrees well with literature NMR values).²⁵⁰



(Diethoxyphosphoryl)methyl methanesulfonate (158):²⁵⁰

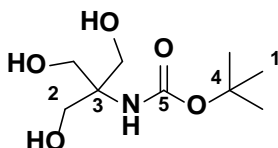
To a flame dried and evacuated 125 mL round bottom flask, equipped with a magnetic stir bar was added sequentially $\text{NMe}_3\cdot\text{HCl}$ (2.41g, 12.68 mmol, 0.20 eq.), DCM (100 mL), Et_3N (13.26 mL, 95.1 mmol, 1.5 eq.) and the alcohol **169** (10.60 g, 63.4 mmol, 1.0 eq.) and the solution was cooled to 0°C in an ice bath. To the chilled stirred solution was added, dropwise, mesyl chloride (~8.5 mL, 69.74 mmol, 1.1 eq.) in anhydrous DCM (2 mL) and the cloudy yellow mixture was stirred for 30 min at RT at which point TLC showed disappearance of the starting alcohol (10% MeOH in EtOAc, 10 mL). The reaction was diluted with H_2O (1×80 mL) and extracted. The organic layer was washed with brine (60 mL) and dried over MgSO_4 , filtered and evaporated to give a yellow oil. The crude product was packed onto silica and purified by dry column chromatography (4.5 cm \times 5.0 cm frit, 40 g silica) pre-eluting with EtOAc/Hexanes (60%, 150 mL) then eluting with EtOAc/MeOH (25%, 200 mL) to afford the title compound as a yellow oil. Yield: 99% (15.50g). $^1\text{H NMR}$ (400 MHz, CDCl_3 , δ): 4.36 (d, $^2J = 7.9$ Hz 4H, H4); 4.20-4.11 (m, 2H, H3); 3.07 (s, 3H, H2); 1.31 (t, $^3J = 7.1$ Hz, 6H, H1) ppm; $^{13}\text{C NMR}$ (100 MHz,

CDCl₃, δ): 63.45 (d, $^1J = 6.4$ Hz, C3), 61.0 (d, $^2J = 169.5$ Hz, C4), 37.80 (C2), 16.35 (d, $^1J = 5.7$ Hz, C1) ppm; **³¹P NMR** (121.45 MHz, CDCl₃, δ): 15.65 ppm. (Agrees well with literature NMR values).²⁵⁰



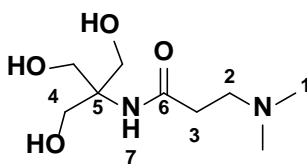
(Diethoxyphosphoryl)methyl 4-methylbenzenesulfonate (170):²⁵¹

To a chilled and stirred solution of the alcohol **169** (0.168 g, 1 mmol), NMe₃·HCl (0.040 g, 0.21 mmol, 0.21 eq.), Et₃N (0.21 mL, 1.5 mmol, 1.5 eq.) in ACN (1 mL) inside a flame dried and evacuated 25 mL round bottom flask was added TsCl (0.210 g, 1.1 mmol, 1.1 eq.) in ACN (1 mL) at 0 °C. The clear and cloudy mixture was stirred for 1 hr at RT at which point TLC showed disappearance of the starting amine (5% MeOH in EtOAc, 10 mL). The reaction was diluted with H₂O (2 mL) and extracted with EtOAc (2 × 5 mL), the organic layer was washed with brine (2 mL), dried over MgSO₄, filtered and evaporated to give a clear oil. The crude material was purified by flash chromatography on silica gel (20 g silica, 1.5 cm i.d) with gradient elution: 100% EtOAc (35 mL) then 5% MeOH:EtOAc (90 mL) to obtain the title compound as a yellow oil. Yield 93% (0.30 g); TLC (5% MeOH in EtOAc), R_f = 0.42; **¹H NMR** (400 MHz, CDCl₃, δ): 7.73 (t, $J = 8.0$ Hz, 4H, H6); 7.29 (t, $J = 3.8$ Hz, 4H, H5); 4.14-4.02 (m, 6H, (H3 + H4 overlap)); 3.39 (s, 3H, H2); 1.23 (t, $J = 7.1$ Hz, 6H, H1) ppm; **¹³C NMR** (100 MHz, CDCl₃, δ): 145.52 (C8), 131.64 (C7), 129.99 (C6), 129.99 (C5), 128.13 (C6), 63.31 (d, $^1J = 36.53$ Hz, C3), 61.28 (d, $^2J = 168.91$ Hz, C4), 21.60 (C2), 16.25 (d, $^1J = 5.81$ Hz, C1) ppm; **³¹P NMR** (121.45 MHz, CDCl₃, δ): 15.12 ppm. (Agrees well with literature NMR values).²⁵¹



Tert-butyl (1,3-dihydroxy-2-(hydroxymethyl)propan-2-yl)carbamate (157):²⁵²

To a solution of 2-amino-2-(hydroxymethyl)propane-1,3-diol (tris) **171** (6.057 g; 50 mmol) dissolved in MeOH (180 mL) was added a solution of Boc₂O (11.350 g; 52 mmol) in MeOH (40 mL) over 30 min and the reaction mixture was stirred at RT overnight. Volatiles were evaporated to dryness, and the title compound recrystallized from EtOAc (100 mL) as white cotton like needles. Yield 94% (10.00 g); ¹H NMR (400 MHz, D₂O, δ): 3.65 (s, 9H, H₂); 1.38 (s, 6H, H₁) ppm; ¹³C NMR (100 MHz, DMSO, δ): 155.25 (C₅), 78.10 (C₄), 60.54 (C₂), 60.43 (C₃), 28.39 (C₁) ppm. (Agrees well with literature NMR values).²⁵²

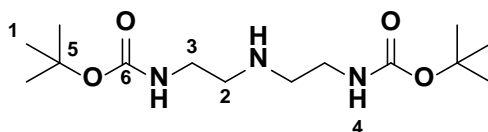


N-(1,3-dihydroxy-2-(hydroxymethyl)propan-2-yl)-3-(dimethylamino)propanamide (163):

To a solution of *N*-[tri(hydroxy- methyl)methyl]acrylamide **173** (1.051g, 6 mmol, 1.0 eq.) in H₂O (3 mL) was added HNMe₂ (2 mL, 5.6 M in EtOH, ~ 2 eq.) at RT and the reaction was stirred for 5 min at which point TLC (EtOAc:MeOH: 1:1, 20 mL) showed consumption of the starting amine. The reaction was separated from H₂O by coevaporation from ACN, stirring in CHCl₃ (10 mL) for 5 min with decanting followed by drying under high vacuum (60 min) and recovered as a white solid. Yield 100% (1.321 g); TLC (50% MeOH in EtOAc), R_f = 0.05; ¹H NMR (400 MHz, D₂O, δ): 3.76 (s, 6H, H₄); 2.67 (t, *J* = 7.03 Hz, 2H, H₃); 2.48 (t, *J* = 3.46 Hz, 2H, H₂); 2.23

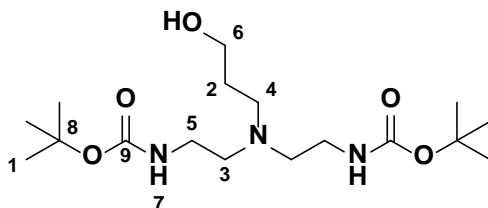
(s, 6H, H1) ppm; ^{13}C NMR (100 MHz, CDCl_3 , δ): 175.0 (C6), 62.95 (C5), 60.27 (C4), 54.12 (C3), 43.59 (C1), 33.38 (C2) ppm. **HRMS-DART** (m/z): $[\text{M}^+]$ calculated for $\text{C}_9\text{H}_{20}\text{N}_2\text{O}_4$, 221.15013; found, 221.14964.

5.9.0 Preparation of Bis Amines Scaffolds for Multidentate Phosphonic Acid Synthesis



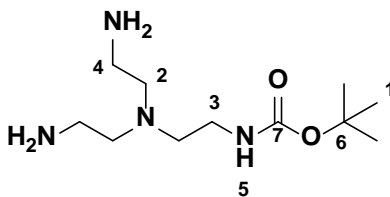
Di-tert-butyl (azanediybis(ethane-2,1-diyl))dicarbamate (176):²⁵³

To a stirred solution of 1,1'-carbonyldiimidazole (CDI) (12.97 g, 80 mmol, 2 eq.), KOH (0.112 g, 2 mmol) and *t*-BuOH (7.65 mL, 80 mmol, 2 eq.) in anhydrous TOL (300 mL) preheated to 60°C for 3 hrs was added *N*-(2-aminoethyl)ethane-1,2-diamine dropwise (4.34 mL, 40 mmol, 1.0 eq.) via a syringe. The reaction was further stirred at 60°C for another 3 hrs and then cooled to RT and rotovaped to remove volatiles. The residue was dissolved in DCM (100 mL) and washed with H_2O (3×50 mL), dried with MgSO_4 , evaporated and placed under high vacuum for 4 hrs to give a thick light yellow oil. Yield: 62% (7.51 g). ^1H NMR (400 MHz, CDCl_3 , δ): 4.10-3.93 (m, 4H, H6), 3.38-3.29 (m, 2H, H5), 1.91-1.80 (m, 2H, H4), 1.75-1.60 (m, 4H, (H2 + H3)), 1.30-1.20 (m, 6H, H1) ppm. (Agrees well with literature NMR values).²⁵³



Di-tert-butyl (((3-hydroxypropyl)azanediyl)bis(ethane-2,1-diyl))dicarbamate (177):

A solution of the secondary amine **176** (7.511 g, 24.7 mol), *N,N*-diisopropylethylamine (5.17 mL, 37.13 mmol, 1.2 eq.), 3-bromo-1-propanol **74** (2.46 mL, 27.23 mmol, 1.1eq.) in 100 mL ACN were refluxed (24 hrs). After completion of the reaction (monitored by TLC) the reaction mixture was evaporated to dryness under reduced pressure. The residue was dissolved in DCM (200 mL) and washed with H₂O (200 mL) followed by another extraction with DCM (200 mL) and a brine wash (100 mL) of the organic phases. Volatiles were removed under reduced pressure and the yellow liquid was placed under high vacuum (15 min) to give a yellow thick oil that solidified in the freezer (-20°C). The collected organic fractions were dried over MgSO₄ and the solvent was removed under reduced pressure to yield the crude product as a yellow oil. Yield: 81% (6.0 g). ¹H NMR (400 MHz, CDCl₃, δ): 5.06 (s, 2H, H7), 3.70 (t, *J* = 5.57 Hz, 2H, H6), 3.22-3.15 (m, 4H, H5), 2.61 (t, *J* = 6.14 Hz, 2H, H4), 2.52 (t, *J* = 6.02 Hz, 4H, H3), 1.61 (m, 2H, H2), 1.42 (s, 18H, H1) ppm; ¹³C NMR (100 MHz, CDCl₃, δ): 156.301 (C8), 79.15 (C7), 61.97 (C6), 53.94 (C3), 52.70 (C4), 38.20 (C5), 30.45 (C2), 28.38 (C1) ppm.

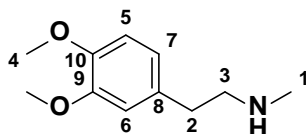


Tert-butyl (2-(bis(2-aminoethyl)amino)ethyl)carbamate (181):²⁵⁴

To a stirred solution of tris(2-aminoethyl)amine (36.5 g, 249 mmol) in dioxane (200 mL) was added Boc₂O dropwise (6.91 mL, 30 mmol, 0.12 eq.) over 15 min, followed by rinsing the addition funnel with dioxane (10 mL). The reaction was stirred at RT overnight (~20 hrs) and then dioxane was removed under reduced pressure. The residue was dissolved in H₂O (80 mL) and repeatedly extracted with DCM (5 × 100 mL) followed by a brine wash (80 mL). Volatiles

were removed under reduced pressure and the yellow liquid was placed under high vacuum (15 min) to give a yellow thick oil that solidified in the freezer (-20°C). Note the NMR spectrum recorded the final product was contaminated with dioxane even after high vacuum. Yield: 81% (6.0g). **¹H NMR** (400 MHz, CDCl₃, δ): 5.21 (s, 1H, H₆), 3.16-3.07 (m, 4H, H₄), 2.71 (t, *J* = 6.15 Hz, 2H, H₃), 2.53-2.46 (m, 6H, H₂), 1.40 (s, 18H, H₁) ppm; **¹³C NMR** (100 MHz, CDCl₃, δ): 156.30 (C₇), 79.13 (C₆), 57.31 (C₂), 54.07 (C₃), 54.07 (C₃), 39.15 (C₄), 28.40 (C₁) ppm. (Agrees well with literature NMR values).²⁵⁴

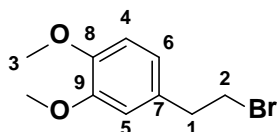
5.10 Preparation of Catechol QAC



2-(3,4-dimethoxyphenyl)-N-methylethanamine (185):²⁵⁵

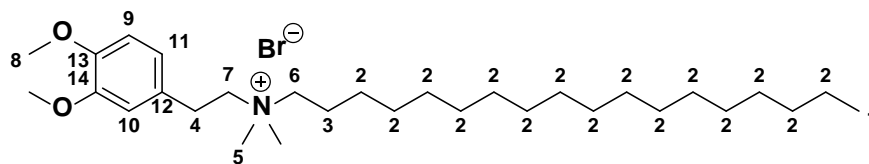
This compound was prepared by the Eschweiler-Clarke reaction using Method 5.2.1: To a refluxing solution of 2-(3,4-dimethoxyphenyl)ethanamine (3.0 g, 16.5 mmol, 1.0 eq.) in MeOH (5 mL) was added by syringe formalin (4.5 mL, 44.8 mmol, 2.7 eq.), formic acid (5.5 mL, 105.05 mmol, 6.3 eq.) and the mixture was left to reflux overnight. MeOH was evaporated *in vacuo* and the reaction pH was brought to pH = 14 with KOH (5.7 g in 50 mL H₂O) at which point a white solid precipitated out on ice and was filtered to afford the crude monomethylated amine as a yellow white solid. This compound was contaminated with the starting material dopamine in ~ 8% by ¹H NMR spectroscopy. Yield: 66% (2.30 g); **¹H NMR** (400 MHz, CDCl₃, δ): 6.73-6.65 (m, 1H, H₅), 6.52 (s, 1H, H₆), 6.43 (s, 1H, H₇), 3.75 (d, *J* = 6.5 Hz, 9H, H₄), 2.75 (t, *J* = 5.8 Hz, 2 H, H₃), 2.57 (t, *J* = 6.0 Hz, 2 H, H₂), 2.35 (s, 3H, H₁) ppm. **¹³C NMR** (100 MHz, CDCl₃, δ): 147.48 (C₉), 147.17 (C₁₀), 126.52 (C₈), 125.67 (C₇), 111.40 (C₆), 109.35

(C5), 55.81 (d, $J = 4.15$ Hz, C4), 52.88 (C1), 45.94 (C2), 28.72 (C3) ppm. (Agrees well with literature NMR values).²⁵⁵



4-(2-bromoethyl)-1,2-dimethoxybenzene (188):²⁵⁶

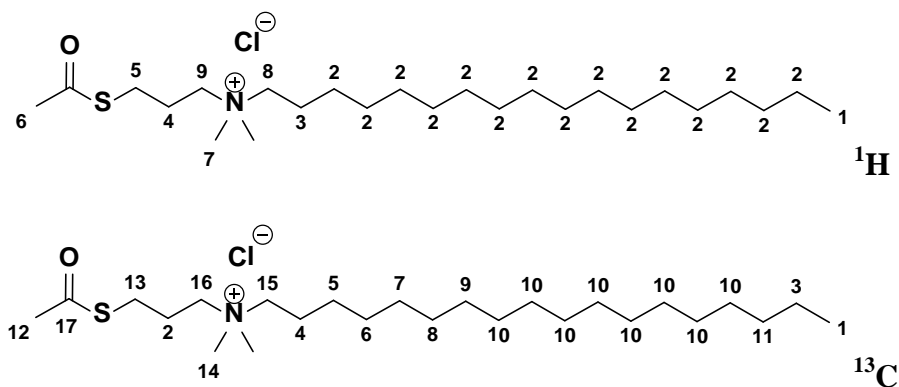
To a solution of 2-(3,4-dimethoxyphenyl)ethanol (0.51 g, 2.8 mmol) and CBr_4 (1.083, 3.2 mmol, 1.14 eq.) dissolved in DCM (10 mL) was added a solution of PPh_3 (0.907g, 3.45 mmol, 1.23 eq.) in DCM (10 mL) over a 30 min period. The reaction was stirred at RT overnight. The crude product was packed onto silica and purified by dry column chromatography (4.5 cm \times 5.0 cm frit, 40 g silica) pre-eluting with hexanes (150 mL) then with 5% EtOAc/Hexanes (100 mL) to remove excess of CBr_4 and then eluting with 10% EtOAc/Hexanes (150 mL) to yield the product as a viscous oil, which solidified under high vacuum as a white/yellow solid. TLC (10% EtOAc/hexanes), $R_f = 0.3$; Yield: 56% (0.64 g). Mp. 57 °C; $^1\text{H NMR}$ (400 MHz, CDCl_3 , δ): 6.85-6.70 (m, 3H, (H4 + H5 + H6), 3.87 (d, $J = 6.4$ Hz, 6H, H3), 3.53 (t, $J = 7.6$ Hz, 2H, H2), 3.09 (t, $J = 7.7$ Hz, 2H, H1) ppm. $^{13}\text{C NMR}$ (100 MHz, CDCl_3 , δ): 148.96 (C9), 147.98 (C8), 131.51 (C7), 120.68 (C6), 111.89 (C5), 111.28 (C4), 55.90 (C3), 39.07 (C2), 33.25 (C1) ppm. (Agrees well with literature NMR values).²⁵⁶



N-(3,4-dimethoxyphenethyl)-N,N-dimethyloctadecan-1-ammonium bromide (189):

To a stirred solution of **188** (0.540 g, 2.2 mmol), in ACN (5 mL) was added DMOA (0.6640 g, 2.43 mmol, 1.1 eq.), and the mixture was refluxed (3 hrs). The reaction was cooled to RT and placed in the fridge (60 min) until a white precipitate appeared. The solid was filtered and dried to give the title compound as an impure mixture with *N,N*-dimethyloctadecylamine (white/yellow solid) and was not purified any further. TLC (10% NH_4^+OH^- /acetone), $R_f = 0.4$; Yield: 56% (0.82 g); ^1H NMR (400 MHz, CDCl_3 , δ): 7.12-7.05 (m, 1 H, H11), 6.86-6.77 (m, 2H, (H10, H9)), 3.96 (s, 6H, H9), 3.93-3.86 (m, 2H, H7), 3.57-3.47 (m, 2H, H6), 3.41 (s, 6H, H5), 3.05-2.98 (m, 2H, H4), 1.76-1.59 (m, 2H, H3), 1.24 (brs, 30H, H2), 0.87 (t, $J = 7.0$ Hz, 3H, H1) ppm.

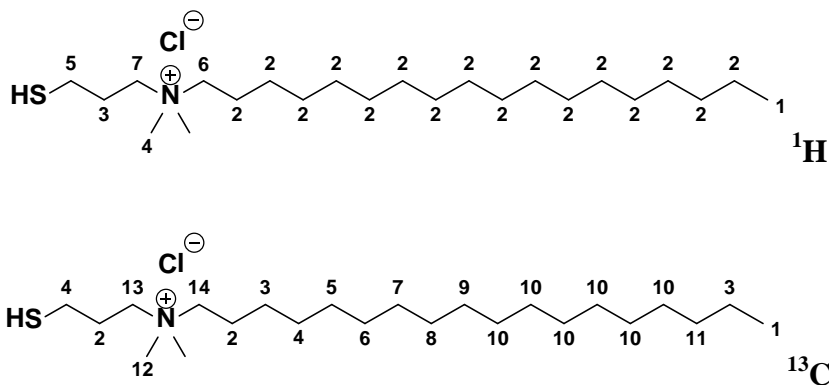
5.11 Preparation of Organosulfur QAC



N-(3-(acetylthio)propyl)-*N,N*-dimethyloctadecan-1-ammonium bromide (192):

This compound was prepared by the Menshutkin reaction using Method 5.2.1: 3-chloropropylthioacetate (7 mL, 53 mmol, 90% from SA) and DMOA (~17 g, 51 mmol, 89% from FLUKA 1.1 eq.) were reacted neat for 24 hrs at 120°C. The hot gummy mixture was dissolved in acetone: Et_2O (1:1, 70 mL) and after 5 min at RT the white solid was filtered. A small portion was further centrifuged from Et_2O (15 mL), and recrystallized from 6 mL acetone

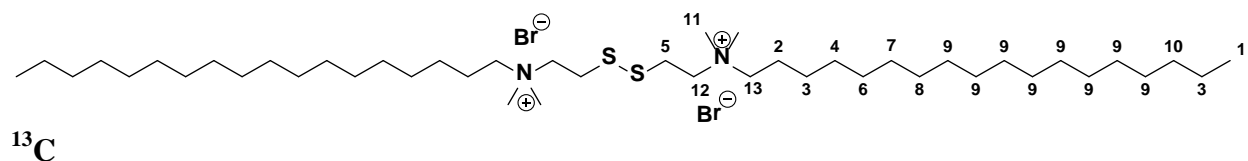
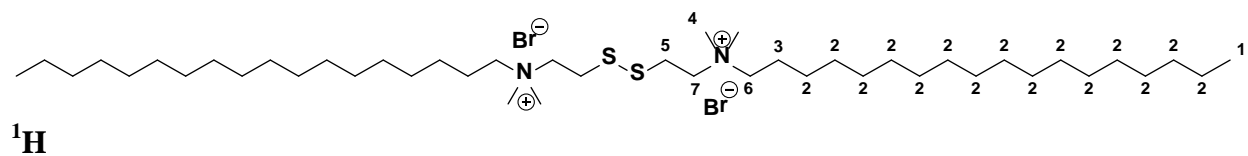
(5 min on ice) to afford the title compound as a white solid. Yield: 70% (16.27 g). Mp = 54-55°C; ^1H NMR (400 MHz, CDCl_3 , δ): 3.69–3.64 (m, 2H, H9), 3.49-3.44 (m, 2H, H8), 3.40 (s, 6H, H7), 2.36 (s, 3H, H6), 2.09-2.01 (m, 2H, H5), 1.78-1.64 (m, 4H, (H3, H4)), 1.24 (brs, 30H, H2), 0.87 (t, J = 6.9 Hz, 3H, H1) ppm; ^{13}C NMR (100 MHz, CDCl_3 , δ): 195.71 (C17), 71.17 (C16), 69.07 (C15), 55.36 (C14), 45.78 (C13), 30.71 (C12), 29.69 (C11), 29.71-29.68 (C10), 29.56 (C9), 29.35 (C8), 29.32 (C7), 29.19 (C6), 26.21 (C6), 25.72 (C4), 23.42 (C3), 22.68 (C2), 14.11 (C1) ppm.



***N*-(3-mercaptopropyl)-*N,N*-dimethyloctadecan-1-ammonium chloride (194):²¹³**

To a flame dried and evacuated 20 mL screw cap vial was added *N*-(3-(acetylthio)propyl)-*N,N*-dimethyloctadecan-1-ammonium chloride (0.490g, 1 mmol) followed by HBr by pasteur pipette (1 mL, 8.88 M) and 5 mL MeOH. The mixture was purged with nitrogen and placed in a 100 °C sand bath for 12 hrs. The mixture was then cooled to RT and concentrated to remove H_2O and methanol, re-dissolved in 5 mL MeOH and stirred with activated charcoal for 3 hrs at RT. The mixture was filtered through Celite (washed with 2 \times 10 mL MeOH), concentrated and recrystallized from CHCl_3 /pentanes to afford a white solid. Yield 83% (0.339 g). Mp = 58-60°C; ^1H NMR (400 MHz, CDCl_3 , δ): 3.85-3.41 (m, 2H, H7), 3.75-3.54 (m, 2H, H6), 3.52-3.40 (m, 2H, H5), 3.31 (s, 6H, H4), 1.82-1.60 (m, 2H, H3), 1.19 (brs, 30H, H2), 0.82 (t, J = 6.9 Hz, 3H, H1)

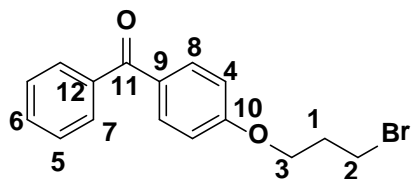
H1) ppm; ^{13}C NMR (100 MHz, CDCl_3 , δ): 65.79 (C14), 60.58 (C13), 51.35 (C12), 31.89 (C11), 29.80-29.85 (C10), 29.71 (C9), 29.65 (C8), 29.61 (C7), 29.39 (C6), 29.34 (C5), 26.38 (C4), 22.95 (C3), 22.64 (C2), 14.06 (C1) ppm. HRMS-DART (m/z): $[\text{M}^+] - \text{Cl}^-$ calculated for $\text{C}_{24}\text{H}_{52}\text{NS}$, 386.3814; found, 386.3821. (Agrees well with literature NMR values).²¹³



2,2'-disulfanediylbis *N,N*-dimethyloctadecan-1-ammonium bromide (198):²¹⁴

This compound was prepared by first stirring 2,2'-disulfanediylbis(*N,N*-dimethylethanaminium) HCl (0.896 g, 3.18 mmol) with NaOEt (0.433 g, 6.37 mmol, 2 eq.) in EtOH (10 mL) for 20 min at RT to free base the bisamine. Next the mixture was filtered through Celite and bromooctadecane was added (2.30 g, 6.9 mmol, 2.2 eq.) followed by reflux overnight. The mixture was hot filtered from charcoal. Volatiles were removed on a rotary evaporator and the crude was recrystallized from acetone (60 mL) by slow evaporation overnight at RT as a white solid. Yield: 70% (1.11 g). Mp = 98-100°C; ^1H NMR (400 MHz, CDCl_3 , δ): 3.90-3.77 (m, 2H, H7), 3.64-3.44 (m, 4H, (H6, H5)), 3.37 (s, 6H, H4), 1.82-1.62 (m, 2H, H3), 1.23 (brs, 30H, H2), 0.85 (t, $J = 6.9$ Hz, 3H, H1) ppm; ^{13}C NMR (100 MHz, CDCl_3 , δ): 64.64 (C13), 62.13 (C12), 51.59 (C11), 31.92 (C10), 29.80-29.70 (C9), 29.67 (C8), 29.58 (C7), 29.42 (C6), 29.36 (C5), 26.35 (C5), 22.96 (C3), 22.67 (C2), 14.10 (C1) ppm. (Agrees well with literature NMR values).²¹⁴

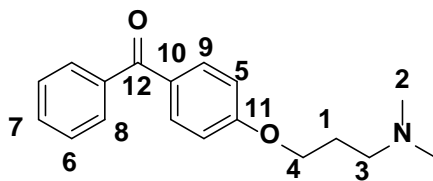
5.12 Preparation of Benzophenone QAC



4-O-(4-bromobutyl)benzophenone (202):¹⁰⁵

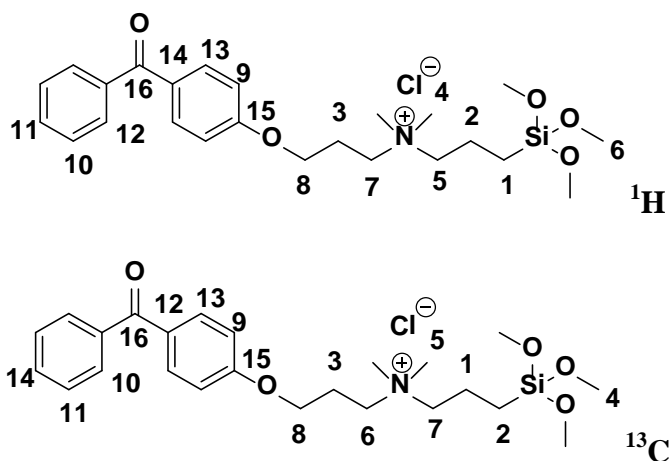
A 50 mL round bottom flask was charged with 1,3-dibromopropane (~ 4 mL, 40 mmol, 4 eq.), K_2CO_3 (2.76 g, 20 mmol, 2 eq.) and ACN (10 mL). A solution of 4-hydroxybenzophenone (1.989 g, 10 mmol) in ACN (4 mL) was prepared and added dropwise to the previous mixture under reflux. The resultant yellow mixture was heated at reflux until a colourless solution was obtained or until TLC showed the disappearance of starting material 4-hydroxybenzophenone (~20 hrs). The excess KBr salt was filtered through Celite and washed with acetone (10 mL). The solution was evaporated under reduced pressure to give the crude product. The crude product was packed onto silica and purified by dry column chromatography (4.5 cm \times 5.0 cm frit, 40 g silica) pre-eluting with 5% EtOAc/Hexanes (150 mL) then eluting with 100% acetone (200 mL) to afford 2.7 g of the desired product contaminated with trace of starting material. The resulting yellow oil was recrystallized from hexanes/EtOAc (8:2) to yield clear, colourless crystals. Yield: 90% (2.3 g). TLC (50% acetone/hexanes, KMnO_4 stain), R_f = 0.8, Mp = 52-53°C. ^1H NMR (400 MHz, CDCl_3 , δ): 7.83 (d, 2H, J = 8.7 Hz, H1), 7.77 (d, 2H, J = 8.3 Hz, H7), 7.58 (t, 1H, J = 7.4 Hz, H3), 7.48 (t, 2H, J = 7.7 Hz, H2), 6.98 (d, 2H, J = 8.7 Hz, H8), 4.20 (t, 2H, J = 5.8 Hz, H10), 3.63 (t, 2H, J = 6.3 Hz, H12), 2.37 (q, 2H, J = 6.0 Hz, H11) ppm; ^{13}C NMR (100 MHz, CDCl_3 , δ): 195.51 (C5), 162.30 (C9), 138.23 (C4), 132.58 (C3), 131.94 (C7), 130.36 (C6), 129.74 (C1), 128.21 (C2), 114.04 (C8), 65.53 (C10), 32.13 (C12), 29.74 (C11)

ppm. **HRMS-DART** (m/z): $[MH^+]$ calculated for $C_{16}H_{15}BrO_2$, 319.0334; found, 319.0329. (Agrees well with literature NMR values).¹⁰⁵



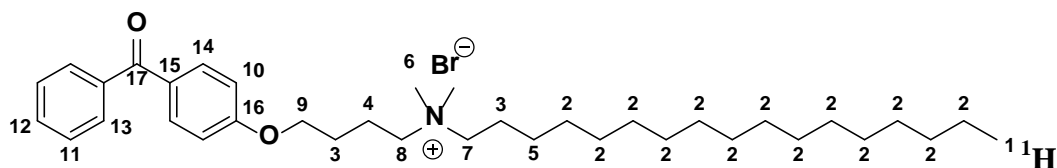
(4-(3-(dimethylamino)propoxy)phenyl)(phenyl)methanone (204):²⁵⁷

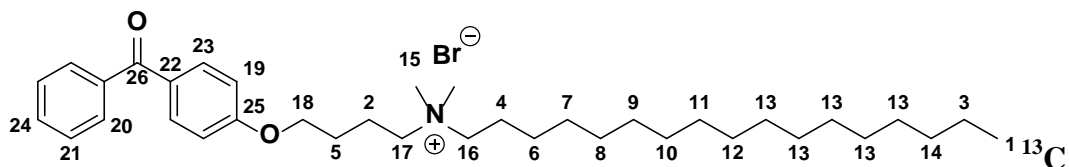
In a 50 mL round bottom flask, powdered KOH was added (0.8 g, 20 mmol, 2 eq.) to a stirred solution of 4-hydroxybenzophenone (1.98 g, 10 mmol) in ACN (4 mL) and the mixture was brought to reflux for 15 min. Dimethylaminopropionylchloride HCl (1.58 g, 10 mmol) was added to the hot mixture in one portion turning the reaction initially from a yellow colour to a clear colour and after a few seconds, back to yellow. The mixture was refluxed ON. The mixture was cooled to RT, evaporated under reduced pressure, packed onto silica and purified by dry column chromatography (4.5 cm \times 5.0 cm frit, 40 g silica) pre-eluting with 100% acetone (100 mL) then eluting with 10% Et_3N /acetone (150 mL) to afford of the desired product as a yellow oil. Yield: 50% (1.426 g). TLC (30% MeOH/acetone), R_f = 0.3; **1H NMR** (400 MHz, $CDCl_3$, δ): 7.77 (d, J = 8.8, 2H, H9), 7.72 (d, J = 7.0, 2H, H8), 7.52 (t, J = 7.4, 1H, H7), 7.43 (t, J = 7.6, 2H, H6), 6.93 (d, J = 8.8, 2H, H5), 4.07 (t, J = 6.4 Hz, 2H, H4), 2.43 (t, J = 7.0 Hz, 2H, H3), 2.23 (s, 6H, H2) 1.97 (m, 2H, H1) ppm; **^{13}C NMR** (100 MHz, $CDCl_3$, δ): 195.4 (C12), 162.7 (C11), 138.3 (C7), 132.5 (C9), 131.8 (C10), 129.7 (C6), 128.1 (C8), 114.0 (C5), 66.4 (C4), 56.2 (C3), 45.5 (C2), 27.4 (C1) ppm. (Agrees well with literature NMR values).²⁵⁷



3-(4-benzoylphenoxy)-N,N-dimethyl-N-(3-(trimethoxysilyl)propyl)propan-1-ammonium chloride (206).

This compound was prepared according to Method 5.2.1 employing compound **204** (1.426 g, 5 mmol) and 3-chloropropyltrimethoxysilane **1** (1.7075g, 5.1 mmol, 1.1 eq.) in MeOH (2.5 mL) for 48 hrs. To purify, Et₂O (2 × 15 mL) was added directly to the reaction mixture and the mixture was triturated followed by drying under high vacuum to give a yellow oil. Yield: 67% (1.76 g); **¹H NMR** (400 MHz, CDCl₃, δ): 7.81 (d, *J* = 8.74, 2H, H13), 7.74 (d, *J* = 7.37, 2H, H12), 7.58 (t, *J* = 7.37, 1H, H11), 7.48 (t, *J* = 7.77, 2H, H10), 6.87 (d, *J* = 8.79, 2H, H9), 4.22 (t, *J* = 5.33 Hz, 2H, H8), 3.93-3.82 (m, 2H, H7), 3.59 (s, 9H, H6), 3.53-3.57 (m, 2H, H5), 3.47 (m, 6H, H4), 2.43-2.28 (m, 2H, H3), 1.95-1.82 (m, 2H, H2), 0.69 (t, *J* = 7.0 Hz, 2H, H1) ppm; **¹³C NMR** (100 MHz, CDCl₃, δ): 195.38 (C16), 161.69 (C15), 137.92 (C14), 132.37 (C13), 130.48 (C12), 129.53 (C11), 128.15 (C10), 114.12 (C9), 64.28 (C8), 60.71 (C7), 55.99 (C6), 50.42 (C5), 45.25 (C4), 22.91 (C3), 15.14 (C2), 5.54 (C1) ppm.

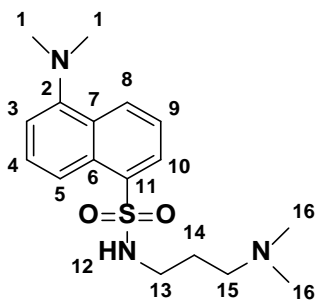




***N*-(4-(4-benzoylphenoxy)butyl)-*N,N*-dimethylheptadecan-1-ammonium bromide (205):**²⁵⁸

This compound was prepared by the Menshutkin reaction using Method 5.2.2: 4-O-(4-bromobutyl)benzophenone (0.333 g, 1 mmol) and DMOA (0.238 g, 1.0 mmol, 1.0 eq.) in ACN (0.5 mL) were heated at 150 °C (2 min). The title compound was placed on ice for 5 min and precipitated from the reaction vial upon cooling as a white solid. Yield: 65% (0.40 g). Mp = 84-87°C; ¹H NMR (400 MHz, CDCl₃, δ): 7.77 (d, *J* = 3.28, 2H, H14), 7.71 (d, *J* = 6.94, 2H, H13), 7.55 (t, *J* = 7.25, 1H, H12), 7.44 (t, *J* = 7.7, 2H, H11), 6.93 (t, *J* = 8.82, 2H, H10), 4.15-4.08 (m, 2H, H9), 3.78-3.69 (m, 2H, H8), 3.51-3.43 (m, 2H, H7), 3.38 (s, 6H, H6), 1.99-1.87 (m, 4H, (H6,H5)), 1.78-1.58 (m, 2H, H3), 1.21 (brs, 30H, H2), 0.84 (t, *J* = 7.07 Hz, 3H, H1) ppm; ¹³C NMR (100 MHz, CDCl₃, δ): 195.47 (C26), 162.15 (C15), 138.07 (C24), 132.55 (C23), 131.99 (C22), 129.68 (C21), 128.18 (C20), 114.08 (C19), 67.10 (C18), 67.11 (C17), 66.97 (C16), 51.19 (C15), 31.88 (C14), 29.67 (C13), 29.62 (C12), 29.57 (C11), 29.45 (C10), 29.38 (C9), 29.32 (C8), 29.20 (C7), 27.73 (C6), 26.27 (C5), 25.81 (C4), 22.65 (C3), 19.75 (C2), 14.09 (C1) ppm. (Agrees well with literature NMR values).²⁵⁸

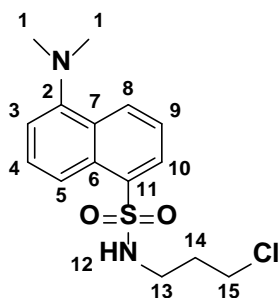
5.13 Preparation of Dansyl QAC



5-(dimethylamino)-N-(3-(dimethylamino)propyl)naphthalene-1-sulfonamide (208):^{177,259}

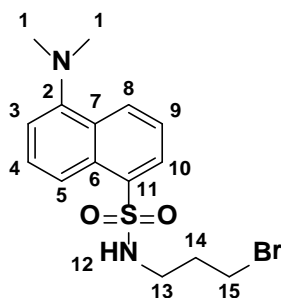
To a flame dried 500 mL round bottom flask with a reflux condenser connected to an inert atmosphere manifold anhydrous DCM (300 mL) was added followed by dansyl chloride (10.0 g, 37.07 mmol), Et₃N (~ 8 mL, 55.61 mmol). While the solution was stirring at RT, 3-(dimethylamino)propylamine (7.0 ml, 55.61 mmol) was added drop wise via syringe resulting in a colour change from orange to lime-green. After stirring for 1 hr, HCl (g) was bubbled through the solution until pH 2 was reached. The resulting mixture was evaporated to dryness, then re-dissolved in saturated brine H₂O (100 mL) and basified to pH 11 with 6 N NaOH (15 mL) at 0 °C until white-yellow precipitate was observed. The mixture was refrigerated overnight enhancing further precipitation of product. The precipitate was filtered washing with H₂O and the filtrate was extracted with DCM (500 mL) and evaporated to dryness to afford a white solid. Yield: 97% (12.1 g). (Recrystallized using 80% EtOH/H₂O). Mp = 122–124°C; TLC (5% NH₄⁺OH:Acetone), UV-Vis (MeOH, 1 × 10⁻³ M), λ_{Abs max} = 516 nm, ε = 447 M⁻¹ cm⁻¹. ¹H NMR (400 MHz, CDCl₃, δ): 8.52 (d, 1H, *J* = 8.5 Hz, H8), 8.31 (d, 1H, *J* = 8.6 Hz, H5), 8.23 (dd, 1H, ¹*J* = 1.2 Hz, ²*J* = 7.3 Hz, H10), 7.58 – 7.50 (m, 2H, H4, H9), 7.17 (d, 1H, *J* = 7.5: H3), 2.94 (t, 2H, *J* = 5.5 Hz, H13), 2.88 (s, 6H, H1), 2.21 (t, 2H, *J* = 5.5 Hz, H15), 2.12 (s, 6H, H16), 1.58-1.52 (m, 2H, H14) ppm; ¹³C NMR (100 MHz, CDCl₃, δ): 151.90 (C2), 134.77 (C11), 129.98 (C6), 128.89 (C8), 129.71 (C4), 129.65 (C9), 128.07 (C10), 123.17 (C5), 119.03 (C7), 115.00 (C3), 59.58 (C15), 45.42 (C1, C16), 44.54 (C13), 24.61 (C14) ppm. **HRMS-DART** (m/z): [M⁺] calculated for C₁₇H₂₆N₃O₂S₁, 336.1736; found, 336.1745.

(This compound has also been prepared on a 25 g, 92.6 mmol scale). (Agrees well with literature NMR values).^{177,259}



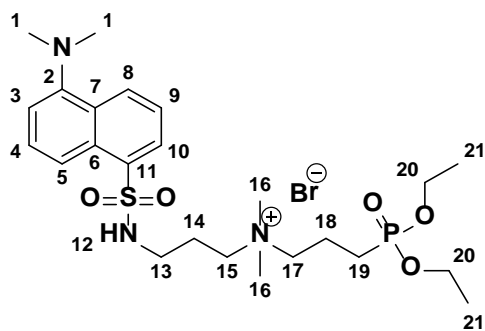
***N*-(3-chloropropyl)-5-(dimethylamino)naphthalene-1-sulfonamide (209):**²⁶⁰

A flame dried 100 mL round bottom flask was charged with DCM (30 mL), Et₃N (~ 1.6 mL, 11.1 mmol, 3.0 eq.) and 3-chloropropan-1-aminium chloride (1.0 g, 5.56 mmol, 1.5 eq.). The reaction was stirred at RT until the amine salt dissolved, afterwhich the dansyl chloride (1.0 g, 3.7 mmol) was added in one portion resulting in a colour change from dark yellow to lime-green. After stirring for 30 min the reaction was quenched with H₂O (50 mL) and the organic layer was extracted, washed with brine (30 mL), dried with MgSO₄ and evaporated to dryness to afford a brown orange solid that was used without any further purification. Yield: 95% (1.15 g). TLC (5% NH₄⁺OH:Acetone), R_f = 0.85 : ¹H NMR (400 MHz, MeOD, δ): 8.66-8.58 (m, 1H, H8), 8.33 (d, *J* = 7.9 Hz, 1H, H5), 8.26 (d, *J* = 6.4 Hz, 1H, H10), 7.39 (q, 2H, *J* = 7.57 Hz, 2H, (H4 + H9)), 7.29-7.21 (m, 1H, H3), 3.34-3.28 (m, 2H, H13), 3.11-3.03 (m, 2H, H15), 2.94 (s, 6H, H1), 1.95 (t, *J* = 6.1 Hz, 2H, H14) ppm; ¹³C NMR (100 MHz, MeOD, δ): 151.9 (C3), 135.5 (C12), 129.8 – 127.7 (m, (C5, C7, C9, C10, C11 overlap)), 122.9 (C6), 119.0 (C8), 115.0 (C4), 44.4 (C1, C2), 44.1 (C16), 39.5 (C14), 32.3 (C15) ppm. (Agrees well with literature NMR values).²⁶⁰



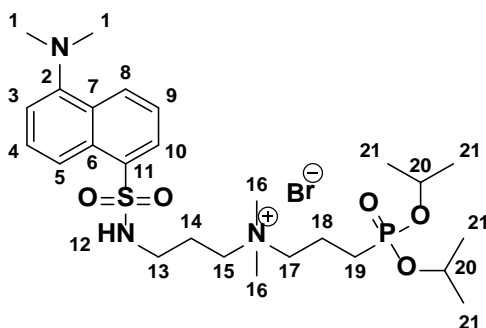
***N*-(3-bromopropyl)-5-(dimethylamino)naphthalene-1-sulfonamide (210):**²⁶¹

A flame dried 250 mL round bottom flask was charged with DCM (50 mL), Et₃N (~ 1.6 mL, 11.1 mmol, 3.0 eq.) and 3-bromopropan-1-aminium bromide (0.9 g, 4.1 mmol, 1.1 eq.). The reaction was stirred at RT to dissolve the amine salt, afterwhich the dansyl chloride (1.0 g, 3.7 mmol) was added in one portion resulting in a colour change from orange to lime-green. After stirring for 40 min the reaction was quenched with H₂O (50 mL) and the organic layer was extracted, washed with brine (30 mL), dried with MgSO₄ and evaporated to dryness to afford a brown orange solid that was used without any further purification. Yield: 95% (1.30 g). TLC (10% IPA:Acetone), R_f = 0.80 : ¹H NMR (400 MHz, MeOD, δ): 8.61 (d, *J* = 8.2 Hz, 1H, H8), 8.32 (d, *J* = 7.9 Hz, 1H, H5), 8.26 (d, *J* = 6.4 Hz, 1H, H10), 7.57 (q, 2H, *J* = 8.4 Hz, 2H, (H4 + H9)), 7.30-7.21 (m, 1H, H3), 3.30 (t, *J* = 3.3 Hz, 2H, H13), 3.13-3.02 (m, 2H, H15), 2.90 (s, 6H, H1), 1.94 (t, *J* = 6.2 Hz, 2H, H14) ppm. (Agrees well with literature NMR values).²⁶¹



3-(diethoxyphosphoryl)-N-(3-(5-(dimethylamino)naphthalene-1-sulfonamido)propyl)-N,N-dimethylpropan-1-ammonium bromide (211):¹⁷⁷

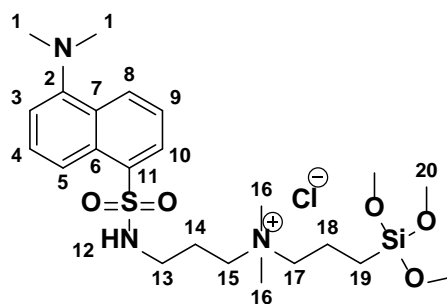
This compound was prepared according to Method 5.2.1: To a stirred solution of compound **208** (2.057 g, 6.13 mmol, 1.0 eq.) in refluxing ACN (15 mL) was added diethyl(3-bromopropyl)phosphonate **12** (~ 2.4 g, 9.2 mmol, 1.5 eq.) via syringe, and the vial was capped and refluxed for 20 hrs. To purify, Et₂O (2 × 40 mL) was added directly to the reaction mixture and the mixture was triturated with decanting to remove any unreacted starting material followed by drying under high vacuum and recovered as a yellow solid. Yield: 90% (3.64 g). UV-Vis (MeOH, 1 × 10⁻³ M), λ_{Abs max} = 334 nm, ε = 505 M⁻¹ cm⁻¹. ¹H NMR (400 MHz, CDCl₃, δ): 8.51 (d, 1H, *J* = 8.3 Hz, H8), 8.43 (d, 1H, *J* = 8.6 Hz, H5), 8.20 (dd, 1H, ¹*J* = 1.0 Hz, ²*J* = 7.3 Hz, H10), 7.71 (s, 1H, H12), 7.59 (t, 1H, *J* = 8.4 Hz, H9), 7.50 (t, 1H, *J* = 7.3 Hz, H4), 7.16 (d, 1H, *J* = 7.4 Hz, H3), 4.11–4.02 (m, 4H, H20), 3.67–3.56 (m, 4H, H15, H17), 3.17 (s, 6H, H16), 3.10–2.99 (m, 2H, H13), 2.86 (s, 6H, H1), 2.10–1.95 (m, 4H, H14, H18), 1.89–1.77 (m, 2H, H19), 1.28 (t, 6H, *J* = 7.1 Hz, H21) ppm; ¹³C NMR (100 MHz, CDCl₃, δ): 151.79 (C2), 134.62 (C11), 130.29 (C4), 129.79 (C6), 129.47 (C8), 129.34 (C9), 128.60 (C10), 123.28 (C5), 119.28 (C7), 115.30 (C3), 62.23–62.16 (overlap, C15, C17, C20), 51.31 (C16), 45.43 (C1), 39.73 (C13), 24.75–22.83 (C14, C18, C19), 16.45 (d, ²*J* = 6.0 Hz, C21) ppm; ³¹P NMR (121.45 MHz, CDCl₃, δ): 29.29 ppm. HRMS-DART (*m/z*): [M⁺ - Br⁻] calculated for C₂₄H₄₁BrN₃O₅P₁S₁, 514.2504; found, 514.2519. (Agrees well with literature NMR values).¹⁷⁷



3-(diisopoxyphosphoryl)-N-(3-(5-(dimethylamino)naphthalene-1-sulfonamido)propyl)-N,N-dimethylpropan-1-ammonium (212):

This compound was prepared according to Method 5.2.1: To a stirred solution of compound **208** (0.5 g, 1.5 mmol) in refluxing ACN (3 mL) was added diisopropyl(3-bromopropyl)phosphonate **13** (0.46 g, 1.6 mmol) via syringe, and the vial was capped and refluxed for 7 hrs. To purify, Et₂O (2 × 15 mL) was added directly to the reaction mixture and the mixture was triturated with decanting to remove any unreacted starting material followed by drying under high vacuum and recovered as a yellow solid. Yield: 70% (0.653 g). UV-Vis (MeOH, 1×10^{-3} M), $\lambda_{\text{Abs max}} = 340$ nm, $\epsilon = 519 \text{ M}^{-1} \text{ cm}^{-1}$. **¹H NMR** (400 MHz, CDCl₃, δ): 8.50 (d, 1H, $J = 8.3$ Hz, H8), 8.43 (d, 1H, $J = 8.6$ Hz, H5), 8.22 (dd, 1H, $^1J = 1.0$ Hz, $^2J = 7.3$ Hz, H10), 7.75 (s, 1H, H12), 7.59 (t, 1H, $J = 8.4$ Hz, H9), 7.49 (t, 1H, $J = 7.3$ Hz, H4), 7.15 (d, 1H, $J = 7.4$ Hz, H3), 4.68–4.56 (m, 2H, H20), 3.66–3.49 (m, 4H, H15, H17), 3.16 (s, 6H, H16), 3.09–2.97 (m, 2H, H13), 2.85 (s, 6H, H1), 2.05–1.90 (m, 4H, H14, H18), 1.80–1.69 (m, 2H, H19), 1.26 (t, 12H, $J = 7.1$ Hz, H21) ppm; **¹³C NMR** (100 MHz, CDCl₃, δ): 151.79 (C2), 134.62 (C11), 130.31 (C4), 129.87 (C6), 129.49 (C8), 129.31 (C9), 128.64 (C10), 123.28 (C5), 119.28 (C7), 115.30 (C3), 70.69 (C20), 62.23–62.16 (overlap, C15, C17), 51.19 (C16), 45.42 (C1), 41.80 (C13), 39.60 (C21), 33.76 (C19), 24.08 (C14, C18) ppm; **³¹P NMR** (121.45 MHz, CDCl₃, δ):

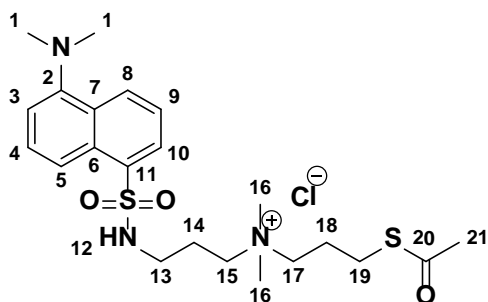
27.32 ppm. **HRMS-ESI-TOF** (m/z): $[M^+ - Br^-]$ calculated for $C_{26}H_{45}BrN_3O_5P_1S_1$, 542.2813; found, 542.2815.



3-(5-(dimethylamino)naphthalene-1-sulfonamido)-*N,N*-dimethyl-*N*-(3-(trimethoxysilyl)propyl)propan-1-ammonium chloride (213):¹⁷⁷

To a flame dried 25 mL round bottom flask with a reflux condenser connected to an inert atmosphere manifold, ACN (20 mL) was added followed by 5-(dimethylamino)-*N*-(3-(dimethylamino)propyl)naphthalene-1-sulfonamide **208** (3.35 g, 10 mmol). While stirring, (3-chloropropyl)trimethoxysilane **1** (~ 5 mL, 25 mmol) was added via an inert syringe. The solution was stirred for 48 hrs at 110°C, and the solution turned to yellow-brownish oil. The oil precipitated in cold (1:1) DCM : Et₂O mixture, forming two layers; a gummy layer and a white liquid layer. The white liquid layer was separated inside a 10 mL syringe and collected in a second 25 mL round bottom flask; the gummy layer left behind was dissolved using DCM and collected in a 25 mL round bottom flask. Excess DCM was evaporated using rotary evaporator resulting in a light yellow powder. Yield: 72.0% (3.849 g). Mp = 85-87°C. UV-Vis (MeOH, 1×10^{-3} M), $\lambda_{Abs\ max} = 340\ nm$, $\epsilon = 413\ M^{-1}\ cm^{-1}$. **¹H NMR** (400 MHz, CDCl₃, δ): 8.48 (d, 2H, $J = 8.6\ Hz$, H8, H5), 8.37 (s, 1H, H12), 8.19 (d, 1H, $J = 7.3\ Hz$, H10), 7.59 (t, 1H, $J = 7.9\ Hz$, H4), 7.49 (t, 1H, $J = 8.2\ Hz$, H9), 7.13 (d, 1H, $J = 7.6\ Hz$, H3), 3.57-3.52 (m, 2H, H17), 3.49 (s, 9H, H20), 3.27-3.20 (m, 2H, H15), 3.10 (s, 6H, H16), 3.08–3.03 (m, 2H, H13), 2.84 (s, 6H, H1),

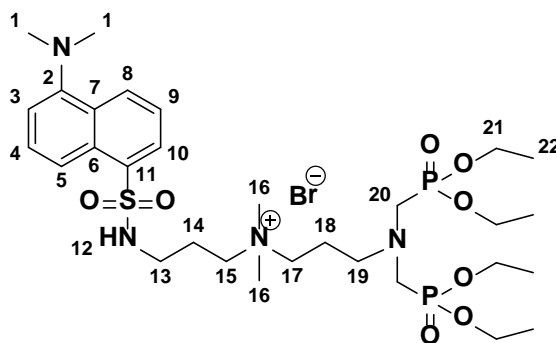
2.01-1.90 (m, 2H, H14), 1.71–1.60 (m, 2H, H18), 0.54 (t, 2H, $J = 7.8$ Hz, H19) ppm; ^{13}C NMR (100 MHz, CDCl_3 , δ): 151.70 (C2), 135.06 (C11), 130.18 (C4), 129.75 (C6), 129.58 (C8), 128.93 (C9), 128.53 (C10), 123.35 (C5), 119.45 (C7), 115.14 (C3), 65.62 (C15), 62.27 (C17), 50.79 (C16), 50.68 (C20), 45.40 (C1), 39.81 (C13), 26.00 (C14), 16.16 (C18), 5.35 (C19) ppm; ^{29}Si NMR (79.4 MHz, CD_3OD , δ): -68.86 ppm. **HRMS-DART** (m/z): $[\text{M}^+ - \text{Cl}^-, - \text{CH}_3]$, calculated for $\text{C}_{23}\text{H}_{40}\text{ClN}_3\text{O}_5\text{SSi}$, 484.2314; found 484.2315. (Agrees well with literature NMR values).¹⁷⁷



3-(acetylthio)-N-(3-(5-(dimethylamino)naphthalene-1-sulfonamido)propyl)-N,N-dimethylpropan-1-ammonium chloride (214):

This compound was prepared according to Method 5.2.1: To a stirred solution of compound **208** (1.0 g, 2.98 mmol) in refluxing EtOH (4 mL) was added 3-chloropropylthioacetate (90%) (0.65 mL, 4.9 mmol, 1.5 eq.) via syringe, and the vial was capped and refluxed for 24 hrs. To purify, Et₂O (2x 15 mL) was added directly to the reaction mixture and the mixture was triturated with decanting to remove any unreacted starting material followed by drying under high vacuum recovered a yellow powder. Yield: 63% (1.10 g). Mp = 35-40°C; $\epsilon = 439 \text{ M}^{-1} \text{ cm}^{-1}$. UV-VIS (MeOH, $1 \times 10^{-3} \text{ M}$), $\lambda_{\text{Abs max}} = 334 \text{ nm}$, $\epsilon = 439 \text{ M}^{-1} \text{ cm}^{-1}$. ^1H NMR (400 MHz, CDCl_3 , δ): 8.49 (d, 1H, $J = 8.4$ Hz, H8), 8.43 (d, 1H, $J = 8.5$ Hz, H5), 8.18 (d, 1H, $J = 7.3$ Hz, H10), 7.57 (t, 1H, $J = 8.0$ Hz, H4), 7.49 (t, 1H, $J = 8.2$ Hz, H9), 7.15 (d, 1H, $J = 7.5$ Hz, H3), 3.57-3.48 (m, 2H,

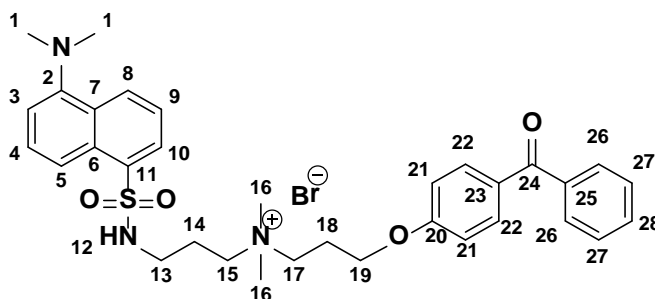
H15), 3.40-3.32 (m, 2H, H17), 3.10 (s, 6H, H16), 3.05-2.98 (m, 2H, H13), 2.86 (s, 6H, H1), 2.83-2.77 (m, 2H, H19), 2.28 (s, 3H, H21), 2.03-1.85 (m, 4H, H14, H18) ppm; ^{13}C NMR (100 MHz, CDCl_3 , δ): 195.80 (C21), 149.79 (C2), 134.73 (C11), 130.34 (C4), 129.67 (C6), 129.43 (C8), 128.32 (C9), 128.71 (C10), 124.64 (C5), 123.52 (C7), 115.45 (C3), 62.92 (C15), 62.73 (C17), 55.14 (C16), 45.32 (C1), 42.90 (C13), 30.77 (C21), 25.57 (C19), 23.16 (C18), 23.00 (C14) ppm. **HRMS-ESI-TOF** (m/z): [$\text{M}^+ - \text{Cl}^-$] calculated for $\text{C}_{22}\text{H}_{34}\text{ClN}_3\text{O}_3\text{S}_2$, 452.2036; found, 452.2037.



3-(bis((diethoxyphosphoryl)methyl)amino)-N-(3-(5-(dimethylamino)naphthalene-1-sulfonamido)propyl)-N,N-dimethylpropan-1-ammonium bromide (215):

This compound was prepared according to Method 5.2.1: To a stirred solution of compound **208** (0.658 g, 1.35 mmol) in refluxing ACN (3 mL) was added compound **120** (0.658 g, 1.35 mmol), and the vial was capped and refluxed for 7 hrs. To purify, Et_2O (2×15 mL) was added directly to the reaction mixture and the mixture was triturated with decanting to remove any unreacted starting material followed by drying under high vacuum to give a yellow powder. Yield: 60% (0.626 g). Mp = 35 – 36°C, UV-Vis (MeOH, 1×10^{-3} M), $\lambda_{\text{Abs max}} = 340$ nm, $\epsilon = 526 \text{ M}^{-1} \text{ cm}^{-1}$. ^1H NMR (400 MHz, CDCl_3 , δ): 8.48-8.38 (m, 2H, H8), 8.37-8.29 (m, 1H, H5), 8.19-8.12 (m, 1H, H10), 7.72 (s, 1H, H12), 7.56-7.38 (m, 2H, H4, H9), 7.15 (m, 1H, H2), 4.16-3.97 (m, 8H, H21),

3.62-3.25 (m, 4H, H15, H17), 3.05-2.85 (s, 6H, H16), 3.10-2.91 (m, 8H, H19, H20, H13), 2.81 (s, 6H, H1), 1.99-1.75 (m, 4H, H14, H18), 1.25 (t, 12H, $J = 7.0$ Hz, H22) ppm; ^{13}C NMR (100 MHz, CDCl_3 , δ): 151.85 (C2), 135.16 (C11), 130.18 (C6), 129.76 (C8), 129.47 (C4), 129.12 (C9), 128.38 (C10), 123.34 (C5), 119.34 (C7), 115.19 (C3), 62.74 (C15), 62.24 (t, $^2J_{\text{C-P}} = 3.5$ Hz, C21), 61.84 (C17), 53.78 (C19), 51.65 (C16), 50.49 (C20), 45.38 (C1), 39.61 (C13), 22.79 (C14), 21.22 (C18), 16.51 (d, $^2J_{\text{C-P}} = 2.5$ Hz, C22) ppm; ^{31}P NMR (121.45 MHz, CDCl_3 , δ): 24.42 ppm. **HRMS-ESI-TOF** (m/z): $[\text{MH}^+ - \text{I}]$ calculated for $\text{C}_{30}\text{H}_{55}\text{IN}_4\text{O}_8\text{P}_2\text{S}_1$, 693.3210; found, 693.3213.

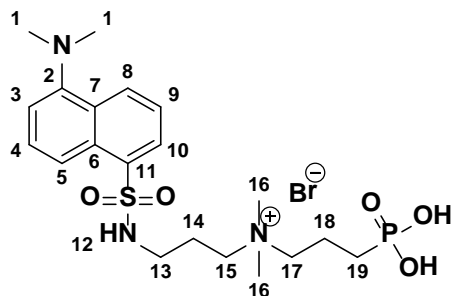


3-(4-benzoylphenoxy)-N-(3-(5-(dimethylamino)naphthalene-1-sulfonamido)propyl)-N,N-dimethylpropan-1-ammonium bromide (216):¹⁰⁵

This compound was prepared according to Method 5.2.1: To a stirred solution of compound **208** (0.5 g, 1.5 mmol) in refluxing ACN (4 mL) was added (4-(3-bromopropoxy)phenyl)(phenyl)methanone (0.72 g, 2.25 mmol, 1.5 eq.) via syringe, and the vial was capped and refluxed for 24 hrs. To purify, Et_2O (2×15 mL) was added directly to the reaction mixture and the mixture was triturated with decanting to remove any unreacted starting material followed by drying under high vacuum to a yellow powder. Yield: 93% (0.91 g). Mp = 75-76°C; UV-VIS (MeOH, 1×10^{-3} M), $\lambda_{\text{Abs max}} = 335$ nm, $\epsilon_1 = 524 \text{ M}^{-1} \text{ cm}^{-1}$, $\lambda_{\text{Abs max}} = 288$ nm, $\epsilon_2 = 327 \text{ M}^{-1} \text{ cm}^{-1}$. ^1H NMR (400 MHz,

CDCl₃, δ): 8.49-8.43 (m, 2H, H5, H10), 8.18 (d, 1H, J = 7.3 Hz, H8), 7.76-7.68 (m, 5H, H28, H22, H12, H9), 7.59-7.52 (m, 2H, H27), 7.47-7.42 (m, 3H, H26, H4), 7.07 (d, 1H, J = 7.6 Hz, H3), 6.82 (d, 2H, J = 8.8 Hz, H21), 4.00 (t, 2H, J = 5.4 Hz, H19), 3.73-3.69 (m, 2H, H15), 3.62-3.59 (m, 2H, H17), 3.22 (s, 6H, H16), 3.11-3.03 (m, 2H, H13), 2.81 (s, 6H, H1), 2.29-2.09 (m, 2H, H14), 2.05-1.95 (m, 2H, H18) ppm; ¹³C NMR (100 MHz, CDCl₃, δ): 195.47 (C24), 161.69 (C20), 151.86 (C2), 137.99 (C11), 134.86 (C25), 132.42 (C6), 132.06 (C28), 130.51 (C23), 130.37 (C8), 129.71 (C22), 129.44 (C26), 129.23 (C4), 129.20 (C9), 128.71 (C10), 128.25 (C27), 123.36 (C5), 119.39 (C7), 115.30 (C3), 114.15 (C21), 65.82 (C17), 64.50 (C15), 62.50 (C19), 51.37 (C16), 45.34 (C1), 39.87 (C13), 22.90 (C18), 15.26 (C14) ppm. **HRMS-ESI-TOF** (m/z): [M⁺ - Br⁻] calculated for C₃₃H₄₀BrN₃O₄S, 574.2749; found, 574.2734.

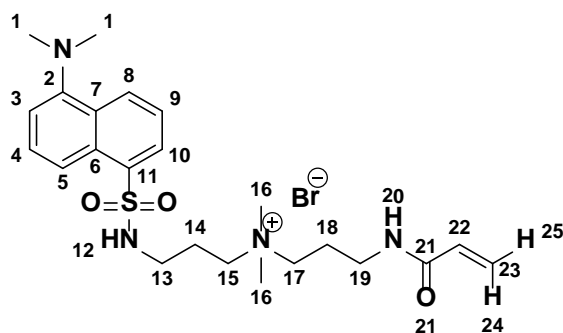
(Agrees well with literature NMR values).¹⁰⁵



3-(5-(dimethylamino)naphthalene-1-sulfonamido)-*N,N*-dimethyl-*N*-(3-phosphonopropyl)propan-1-ammonium bromide (217):

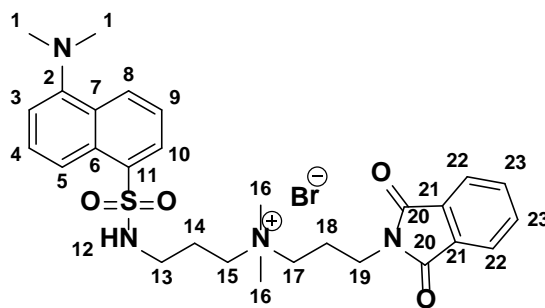
Inside a flame dried and evacuated 20 mL screw cap vial *N*-(3-(diethoxyphosphoryl)propyl)-*N,N*-dimethyloctadecan-1-ammonium bromide (0.35g, 0.58 mmol) was dissolved in anhydrous DCM (5 mL). To the clear stirred solution was added TMSBr (0.23 mL, 1.76 mmol, 3.0 eq.) through a rubber septum via syringe and the reaction was stirred at RT overnight. Completion of

the reaction was followed by ^{31}P NMR spectroscopy after which the reaction was quenched with EtOH (10 mL) and stirred for 1hr followed by addition of H_2O (1 mL). Volatiles were removed with a rotary evaporator connected to a high vacuum Schlenk line and the crude product was triturated with Et_2O (2×10 mL) to remove brown colored impurities. Further purification entailed extraction with $\text{NH}_4^+\text{OH}:\text{H}_2\text{O}$ (1:10, 10 mL) and washing with Et_2O (1×5 mL). The aqueous fluorescent layer was evaporated from ACN (1×50 mL) to give the pure product as beige solid. Yield: 79% (0.25g). Mp = 165-168°C; $\epsilon = 449 \text{ M}^{-1} \text{ cm}^{-1}$. UV-Vis (MeOH, 1×10^{-3} M), $\lambda_{\text{Abs max}} = 342 \text{ nm}$, $\epsilon = 449 \text{ M}^{-1} \text{ cm}^{-1}$. ^1H NMR (400 MHz, D_2O , δ): 8.58 (d, 1H, $J = 8.5$ Hz, H8), 8.35 (d, 1H, $J = 8.5$ Hz, H5), 8.23 (d, 1H, $J = 7.0$ Hz, H10), 7.70–7.58 (m, 2H, H4, H9), 7.31 (d, 1H, $J = 7.5$ Hz, H3), 3.32 (s, 6H, H16), 3.30-3.22 (m, 2H, H17 overlap), 3.19-3.11 (m, 2H, H15), 2.97 (t, 2H, $J = 6.0$ Hz, H13), 2.89 (s, 6H, H1), 1.93-1.86 (m, 4H, H14, H18), 1.57-1.49 (m, 2H, H19) ppm; ^{13}C NMR (100 MHz, D_2O , δ): 133.80 (C2), 131.15 (C11), 130.15 (C6), 129.76 (C8), 128.99 (C4), 128.61 (C9), 128.40 (C10), 124.54 (C5), 119.81 (C7), 116.59, (C3), 64.32 (d, $^3J_{\text{C-P}} = 18.8$ Hz, C17), 61.33 (C15), 53.99 (C16), 45.08 (C1), 39.04 (C13), 24.77 (d, $^1J_{\text{C-P}} = 136.1$ Hz, C19), 21.96 (C14), 16.85 (d, $^2J_{\text{C-P}} = 3.2$, C18) ppm; ^{31}P NMR (121.45 MHz, D_2O , δ): 20.99 ppm. **HRMS-ESI-TOF** (m/z): $[\text{M}^+ - \text{Br}^-]$ calculated for $\text{C}_{20}\text{H}_{33}\text{BrN}_3\text{O}_5\text{P}_1\text{S}_1$, 458.1873; found, 458.1868.



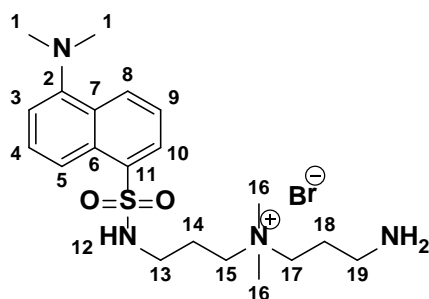
3-acrylamido-*N*-(3-(5-(dimethylamino)naphthalene-1-sulfonamido)propyl)-*N,N*-dimethylpropan-1-ammonium bromide (219):

This compound was prepared according to Method 5.2.1: To a stirred solution of compound **210** (1 g, 2.9 mmol, 1.0 eq.) in refluxing ACN (4 mL) was added *N*-(3-(dimethylamino)propyl)acrylamide (0.5 g, 3.2 mmol, 2.14 eq.) and the vial was capped and refluxed for 24 hrs. To purify, Et₂O (2 × 15 mL) was added directly to the reaction mixture and the mixture was triturated with decanting to remove any unreacted starting material followed by drying under high vacuum and recovered as a yellow solid. Yield: 90% (1.16 g). Mp = 34 – 36°C; ¹H NMR (400 MHz, CDCl₃, δ): 8.61-8.26 (m, 2H, 4 H, (H8, H5, H12, H20)), 8.31 (d, *J* = 8.13 Hz, 1H, H10), 7.54 (t, *J* = 7.3 Hz, 1H, H4), 7.45 (t, *J* = 7.3 Hz, 1H, H5), 7.09 (d, *J* = 7.0 Hz, 1H, H3), 6.38 (t, *J* = 10.3 Hz, 1H, H22), 6.18 (d, *J* = 16.6 Hz, 1H, H24), 5.50 (d, *J* = 9.9 Hz, 1H, H25), 3.60-3.12 (m, 6H, (H19, H17, H15)), 2.97 (s, 6H, H16), 2.80 (s, 6H, H1), 2.12-1.69 (m, 4H, (H14, H18)) ppm; ¹³C NMR (100 MHz, CDCl₃, δ): 166.5 (C21), 151.9 (C2), 134.9 (C11), 131.3 (C6), 130.2 (C22), 129.7 (C8), 129.4 (C4), 129.2 (C9), 128.6 (C10), 126.1 (C23), 123.4 (C5), 119.2 (C7), 115.2 (C3), 66.0 (C17), 62.5 (C15), 51.1 (C16), 45.4 (C1), 39.5 (C13), 36.2 (C19), 22.5 (C14), 15.3 (C18) ppm.



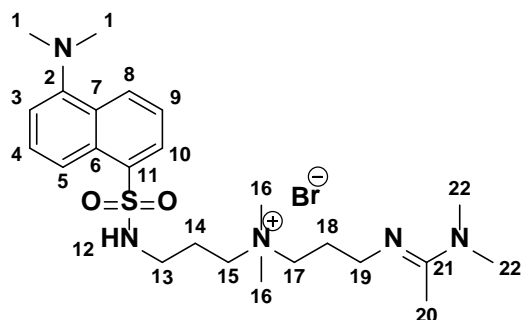
3-(5-(dimethylamino)naphthalene-1-sulfonamido)-*N*-(3-(1,3-dioxoisindolin-2-yl)propyl)-*N,N*-dimethylpropan-1-ammonium bromide (220):

This compound was prepared according to Method 5.2.1 (500 mL glass bottle): A stirred solution of compound **208** (9.02 g, 26.88 mmol, 1.0 eq.) and 3-bromopropylphthalimide **10** (8.716 g, 32.5 mmol, 1.2 eq.) in EtOH (50 mL) was sealed and refluxed for 16 hrs. To purify, Et₂O (1 × 300 mL) was added directly to the reaction mixture and the mixture was triturated with decanting to remove any unreacted starting material followed by another rinse with Et₂O:acetone (3:1, 150 mL). The bottle was placed under high vacuum (60 min) to give a light yellow powder. X-ray quality crystals were obtained by recrystallization from boiling EtOH:H₂O (4:1, 100 mL), cooled to RT and placed at -20°C (2 hrs) or formed ON at RT in an NMR tube (D₂O). Star shaped, colourless crystals were recovered. Yield: 43% (7.0 g). Mp = 123-125°C; ¹H NMR (400 MHz, CDCl₃, δ): 8.44 (d, *J* = 8.3 Hz, 1H, H8), 8.26 (d, *J* = 8.6 Hz, 1H, H5), 8.10 (d, *J* = 6.9 Hz, 1H, H10), 7.86 (t, *J* = 8.4 Hz, 4H, (H22 + H23)), 7.66-7.56 (m, 2H, (H9, H4)), 7.24-7.20 (d, *J* = 7.2 Hz, 1H, H3), 3.69-3.51 (m, 2H, H19), 3.37-3.24 (m, 2H, H17), 3.23-3.09 (m, 2H, H15), 2.87 (s, 6H, H16), 2.79 (s, 6H, (H1, (H2 + H14 overlap))), 2.02-1.85 (m, 2H, H14), 1.81-1.66 (m, 2H, H18) ppm; ¹³C NMR (100 MHz, CDCl₃, δ): 168.4 (C20), 151.89 (C2), 134.88 (C23), 130.07 (C6), 129.47 (C8), 129.38 (C4), 128.98 (C9), 128.49 (C10), 124.16 (C5), 123.54 (C8), 119.48 (C7), 115.23 (C3), 61.76 (C17), 61.59 (C15), 50.26 (C16), 45.50 (C1), 39.50 (C13), 35.14 (C19), 23.01 (C18), 22.12 (C14) ppm.



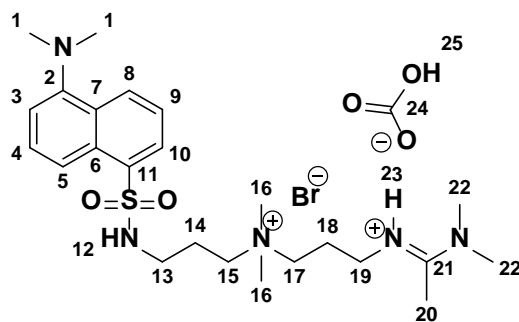
3-amino-N-(3-(5-(dimethylamino)naphthalene-1-sulfonamido)propyl)-N,N-dimethylpropan-1-ammonium bromide (221):

This compound was prepared by dissolving **220** (6.655 g, 11 mmol) in EtOH (50 mL) and deprotecting with hydrazine hydrate (5.0 mL, 44 mmol, 4 eq.) under reflux 2 hrs. The mixture was then cooled to RT, diluted with Et₂O (100 mL) and filtered through Celite. Volatiles were removed *in vacuo* and the crude product (8.647 g, yellow gum) was again diluted with Et₂O (100 mL) and triturated followed by decanting and placed under high vacuum (1 hr) to obtain the title compound as a yellow/white puffy solid. Yield: 99% (5.2 g); Mp = 35-40°C; ¹H NMR (400 MHz, D₂O, δ): 8.17 (d, *J* = 8.61 Hz, 1H, H8), 8.07 (d, *J* = 8.68 Hz, 1H, H5), 8.04 (dd, ¹*J* = 0.95 Hz, ²*J* = 7.35 Hz, 1H, H10), 7.45 (t, *J* = 7.79 Hz, 1H, H4), 7.36 (t, *J* = 7.49 Hz, 2H, H9), 7.05 (d, *J* = 7.05 Hz, 1H, H3), 2.97-2.86 (m, 2H, H13), 2.83-2.57 (m, 2H, H15), 2.63 (t, *J* = 2.63 Hz, 2H, H17), 2.57 (s, 6H, H16), 2.52 (s, 6H, H1), 2.47 (d, *J* = 2.47 Hz, 2H, H19), 1.66-1.54 (m, 2H, H14), 1.49-1.40 (m, 2H, H18) ppm; ¹³C NMR (100 MHz, D₂O, δ): 150.90 (C2), 138.82 (C11), 130.12 (C6), 129.70 (C8), 129.89 (C4), 128.75 (C9), 128.65 (C10), 124.02 (C5), 118.80 (C7), 115.85 (C3), 61.53-61.24 (C15, C17), 50.53 (C16), 44.76 (C1), 39.09 (C13), 33.85 (C19), 22.75 (C18), 22.13 (C14) ppm. **DART** (m/z): [M⁺-Br] calculated for C₂₀H₃₃N₄O₂S, found, 407.3.



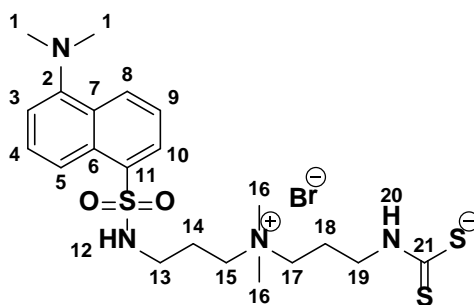
(E)-3-((1-(dimethylamino)ethylidene)amino)-N-(3-(5-(dimethylamino)naphthalene-1-sulfonamido)propyl)-N,N-dimethylpropan-1-ammonium bromide (222):

To a stirred solution (20 ml ST) of dansylamine **221** (0.5 g, 1.06 mmol) and HNMe₂ (1.0 mL of 5.6 M in EtOH, 5.6 mmol) in EtOH (1 mL) was added *N,N*-dimethylacetamide dimethyl acetal (0.2 g, 1.5 mmol) dropwise via a syringe. The reaction mixture was sealed, wrapped in aluminum foil stirred ON at RT in the dark. Volatile EtOH and Me₂NH were evaporated *in vacuo* followed by placing the vial under high vacuum (50°C, 8 hrs) and recovered as a light orange solid. Yield: 99% (0.57 g). **¹H NMR** (400 MHz, D₂O, δ): 8.22 (d, *J* = 8.2 Hz, 1H, H8), 8.08 (d, *J* = 8.5 Hz, 1H, H5), 8.01 (d, *J* = 7.1 Hz, 1H, H10), 7.52-7.38 (m, 2H, (H4 + H9)), 7.12 (d, *J* = 7.36 Hz, 1H, H3), 2.97-2.70 (m, 6H, (H15 + H17 + H13)), 2.58 (s, 4H, H16), 2.47 (s, 8H, (H1 + H22)), 1.83 (s, 3H, H20), 1.50-1.27 (m, 4H, (H14 + H19)), 1.03 (t, *J* = 6.97 Hz, 2H, H19) ppm; **¹³C NMR** (100 MHz, D₂O, δ): 174.11 (C21), 150.85 (C2), 134.05 (C11), 130.07 (C7), 129.72 (C9), 128.87 (C10), 128.73 (C5), 128.61 (C3), 124.10 (C6), 118.88 (C8), 115.91 (C4), 61.73 (C18), 61.10 (C15), 57.34 (C16), 50.29 (C22), 44.77 (C1), 39.11 (C13), 35.84 (C20), 22.01 (C18), 21.80 (C14), 16.70 (C19) ppm. **ESI-TOF** (m/z): [M⁺] calculated for C₂₄H₄₀N₅O₂P, found, 435.2



(E)-N¹-(1-(dimethylamino)ethylidene)-N³-(3-(5-(dimethylamino)naphthalene-1-sulfonamido)propyl)-N³,N³-dimethylpropane-1,3-diammonium bromide hydrogencarbonate (223):

This compound was prepared by dissolving **222** in D₂O and bubbling CO₂ directly into the solution for 60 min. ¹H NMR (400 MHz, D₂O, δ): 8.26 (d, *J* = 8.56 Hz, 1H, H8), 8.12 (d, *J* = 8.64 Hz, 1H, H5), 8.01 (d, *J* = 7.28 Hz, 1H, H10), 7.52 (t, *J* = 8.24 Hz, 1H, H4), 7.46 (t, *J* = 8.02 Hz, 1H, H9), 7.15(d, *J* = 7.68 Hz, 1H, H3), 3.00 (t, *J* = 6.80 Hz, 2H, H19), 2.93-2.89 (m, 6H, (H15 + H17)), 2.71-2.70 (m, 2H, H13), 2.62 (s, 6H, H1), 2.54 (s, 6H, H22), 1.90 (s, 3H, H20), 1.51-1.44 (m, 4H, (H14 + H18)) ppm; ¹³C NMR (100 MHz, D₂O, δ): 174.17 (C21), 151.00 (C2), 133.98 (C11), 130.23 (C6), 129.81 (C8), 128.98 (C4), 128.81 (C9), 128.26 (C10), 124.13 (C5), 118.42 (C7), 115.95 (C3), 61.62 (C17), 61.10 (C16), 50.38 (C16, C22), 44.83 (C1), 38.96 (C13), 35.92 (C19), 22.05 (C20), 21.90 (C14), 21.86 (C18) ppm.



(3-((3-(5-(dimethylamino)naphthalene-1-sulfonamido)propyl) dimethylammonio) propyl) carbamodithioate (225):

To a stirred solution of flourophore **221** (0.5g, 1.05 mmol) in methanolic KOH (5 mL, 65 mg, 1.15 mmol, 1.1 eq.) was added CS₂ (0.1 mL, 1.65 mmol, 1.57 eq.) dropwise via a syringe. A precipitate was observed after a few min and the reaction was further stirred for an additional 5

min until an oily precipitate formed around the stir bar and stopped stirring. The mixture was then diluted with EtOH (10 mL) and decanted. The yellow sticky solid left behind was again diluted with Et₂O (10 mL), triturated followed by decanting and placed under high vacuum (1 hr) to obtain the title compound as a yellow/white powder. This compound was insoluble in CDCl₃, D₂O and MeOD. Yield: 81% (0.4 g); Mp = 220°C; **¹H NMR** (400 MHz, DMSO, δ): 8.46 (d, *J* = 8.46 Hz, 1H, H8), 8.27 (d, *J* = 8.72 Hz, 2H, H5), 8.16-8.03 (m, 2H, (H10 + H12)), 7.69-7.57 (m, 2H, (H4 + H9)), 7.27 (d, *J* = 7.11 Hz, 1H, H3), 3.26-3.03 (m, 2H, (H15 + H17)), 2.81 (brs, 14H, (H1 + H16 + H20)), 1.85-1.65 (m, 4H, (H14 + H19)), ppm; **¹³C NMR** (100 MHz, DMSO, δ): 216.09 (C21), 152.10 (C2), 136.07 (C11), 130.30 (C6), 129.66 (C8), 129.56 (C4), 129.20 (C9), 128.78 (C10), 124.36 (C5), 119.47 (C7), 115.92 (C3), 62.23 (C17), 61.24 (C15), 50.67 (C16), 45.71 (C1), 22.97 (C19), 22.37 (C14), 19.20 (C18) ppm. **ESI-TOF** (m/z): [M⁺] calculated for C₂₁H₃₂N₄O₂S₃, found, 393.2.

6.0 Appendix

List of Appendix Tables

Table A 1. Crystal data and structure refinement for 34	319
Table A 2. Atomic coordinates and equivalent isotropic displacement parameters for 34	320
Table A 3. Bond lengths [Å] and angles [°] for 34	321
Table A 4. Anisotropic displacement parameters for 34	328
Table A 5. Hydrogen coordinates and isotropic displacement parameters	329
Table A 6. Hydrogen bonds for 34	331
Table A 7. Crystal data and structure refinement for 66	331
Table A 8. Atomic coordinates and equivalent isotropic displacement parameters for 66	332
Table A 9. Bond lengths [Å] and angles [°] for 66	332
Table A 10. Anisotropic displacement parameters for 66	340
Table A 11. Hydrogen coordinates and isotropic displacement parameters for 66	341
Table A 12. Torsion angles [°] for 66	342
Table A 13. Hydrogen bonds for 66	343
Table A 14. Crystal data and structure refinement for 19	343
Table A 15. Atomic coordinates and equivalent isotropic displacement parameters for 19	344
Table A 16. Bond lengths [Å] and angles [°] for 19	345
Table A 17. Anisotropic displacement parameters for 19	349
Table A 18. Hydrogen coordinates and isotropic displacement parameters for 19	350
Table A 19. Torsion angles [°] for 19	351
Table A 20. Crystal data and structure refinement for 220	353
Table A 21. Atomic coordinates and equivalent isotropic displacement parameters for 220	354
Table A 22. Bond lengths and angles [°] for 220	355
Table A 23. Anisotropic displacement parameters for 222	361
Table A 24. Hydrogen coordinates and isotropic displacement parameters for 220	363
Table A 25. Torsion angles for 220	364
Table A 26. Hydrogen bonds for 220	366

List of Appendix Figures

Figure A 1. ¹ H NMR spectrum of compound 2 in CDCl ₃	368
Figure A 2. ¹³ C NMR spectrum of compound 2 in CDCl ₃	369
Figure A 3. COSY 2D NMR spectrum of compound 2 in CDCl ₃	370
Figure A 4. ¹ H NMR spectrum of purified 46 in CDCl ₃	371
Figure A 5. ¹³ C NMR spectrum of purified 46 in CDCl ₃	372
Figure A 6. COSY 2D NMR spectrum of purified 46 in CDCl ₃	373
Figure A 7. HSQC 2D NMR spectrum of purified 46 in CDCl ₃	374
Figure A 8. ¹ H NMR spectrum of compound 22 in CDCl ₃	375
Figure A 9. ¹³ C NMR spectrum of compound 22 in CDCl ₃	376

Figure A 10.	HSQC 2D NMR spectrum of compound 22 in CDCl ₃	377
Figure A 11.	¹ H NMR spectrum of compound 1+2 in CDCl ₃	378
Figure A 12.	¹³ C NMR spectrum of compound 1 in CDCl ₃	379
Figure A 13.	¹ H NMR spectrum of compound 3 in CDCl ₃ (Table 2.1, entry i).....	380
Figure A 14.	¹³ C NMR spectrum of compound 3 in CDCl ₃ (Table 2.1, entry i).....	381
Figure A 15.	COSY 2D NMR spectrum of compound 3 in CDCl ₃ (Table 2.1, entry i)	382
Figure A 16.	HSQC 2D NMR spectrum of compound 3 in CDCl ₃ (Table 2.1, entry i)	383
Figure A 17.	¹ H stacked NMR spectra of compound 3 in CDCl ₃ (Table 2.1, entry i-iii)	384
Figure A 18.	¹ H stacked NMR spectra of compound 3 in CDCl ₃ (Table 2.1, entry iv-v, viii)	385
Figure A 19.	¹ H NMR spectrum of compound 3 in CDCl ₃ (Table 2.2, entry iii)	386
Figure A 20.	¹³ C NMR spectrum of compound 3 in CDCl ₃ (Table 2.2, entry iii)	387
Figure A 21.	¹ H NMR spectrum of compound 12 in CDCl ₃ (Table 2.3, entry iii)	388
Figure A 22.	¹³ C NMR spectrum of compound 12 in CDCl ₃ (Table 2.3, entry iii)	389
Figure A 23.	COSY 2D NMR spectrum of compound 12 in CDCl ₃ (Table 2.3, entry iii)	390
Figure A 24.	HSQC 2D NMR spectrum of compound 12 in CDCl ₃ (Table 2.3, entry iii)	391
Figure A 25.	³¹ P NMR spectrum of compound 12 in CDCl ₃ (Table 2.3, entry iii).....	392
Figure A 26.	¹ H NMR spectrum of compound 13 in CDCl ₃ (Table 2.3, entry vii).....	393
Figure A 27.	¹³ C NMR spectrum of compound 13 in CDCl ₃ (Table 2.3, entry vii)	394
Figure A 28.	COSY 2D NMR spectrum of compound 13 in CDCl ₃ (Table 2.3, entry vii)	395
Figure A 29.	HSQC 2D NMR spectrum of compound 13 in CDCl ₃ (Table 2.3, entry vii)	396
Figure A 30.	³¹ P NMR spectrum of compound 13 in CDCl ₃ (Table 2.3, entry vii).....	397
Figure A 31.	¹ H NMR spectrum of compound 14 in CDCl ₃ (Table 2.3, entry ix).....	398
Figure A 32.	¹³ C NMR spectrum of compound 14 in CDCl ₃ (Table 2.3, entry ix).....	399
Figure A 33.	COSY 2D NMR spectrum of compound 14 in CDCl ₃ (Table 2.3, entry ix)	400
Figure A 34.	HSQC 2D NMR spectrum of compound 14 in CDCl ₃ (Table 2.3, entry ix)	401
Figure A 35.	³¹ P NMR spectrum of compound 14 in CDCl ₃ (Table 2.3, entry ix)	402
Figure A 36.	¹ H NMR spectrum of compound 16 in CDCl ₃ (Table 2.3, entry xv).....	403
Figure A 37.	¹³ C NMR spectrum of compound 16 in CDCl ₃ (Table 2.3, entry xv).....	404
Figure A 38.	COSY 2D NMR spectrum of compound 16 in CDCl ₃ (Table 2.3, entry xv)	405
Figure A 39.	HSQC 2D NMR spectrum of compound 16 in CDCl ₃ (Table 2.3, entry xv)	406
Figure A 40.	³¹ P NMR spectrum of compound 16 in CDCl ₃ (Table 4.3, entry xv)	407
Figure A 41.	¹ H NMR spectrum of compound 17 in CDCl ₃ (Table 2.3, entry xvi).....	408
Figure A 42.	¹³ C NMR spectrum of compound 17 in CDCl ₃ (Table 2.3, entry xvi).....	409
Figure A 43.	COSY 2D NMR spectrum of compound 17 in CDCl ₃ (Table 2.3, entry xvi)	410
Figure A 44.	HSQC 2D NMR spectrum of compound 17 in CDCl ₃ (Table 2.3, entry xvi)	411
Figure A 45.	³¹ P NMR spectrum of compound 17 in CDCl ₃ (Table 2.3, entry xvi)	412
Figure A 46.	¹ H NMR spectrum of compound 18 in CDCl ₃ (Table 2.3, entry xvii).....	413
Figure A 47.	¹³ C NMR spectrum of compound 18 in CDCl ₃ (Table 2.3, entry xvii)	414
Figure A 48.	COSY 2D NMR spectrum of compound 18 in CDCl ₃ (Table 2.3, entry xvii) ...	415
Figure A 49.	³¹ P NMR spectrum of compound 18 in CDCl ₃ (Table 4.3, entry xvii).....	416

Figure A 50. ^1H NMR spectrum of compound 19 in CDCl_3 (Table 2.3, entry xviii)	417
Figure A 51. ^{13}C NMR spectrum of compound 19 in CDCl_3 (Table 2.3, entry xviii)	418
Figure A 52. COSY 2D NMR spectrum of compound 19 in CDCl_3 (Table 2.3, entry xviii) ..	419
Figure A 53. HSQC 2D NMR spectrum of compound 19 in CDCl_3 (Table 2.3, entry xviii) ..	420
Figure A 54. ^{31}P NMR spectrum of compound 19 in CDCl_3 (Table 2.3, entry xviii)	421
Figure A 55. ^1H NMR spectrum of compound 26 in CDCl_3 (Table 2.4, entry i)	422
Figure A 56. ^{13}C NMR spectrum of compound 26 in CDCl_3 (Table 2.4, entry i)	423
Figure A 57. COSY 2D NMR spectrum of compound 26 in CDCl_3 (Table 2.4, entry i)	424
Figure A 58. HSQC 2D NMR spectrum of compound 26 in CDCl_3 (Table 2.4, entry i)	425
Figure A 59. ^{31}P NMR spectrum of compound 26 in CDCl_3 (Table 2.4, entry i)	426
Figure A 60. ^1H NMR spectrum of compound 27 in CDCl_3 (Table 4.4, entry iv)	427
Figure A 61. ^{13}C NMR spectrum of compound 27 in CDCl_3 (Table 2.4, entry iv)	428
Figure A 62. COSY 2D NMR spectrum of compound 27 in CDCl_3 (Table 2.4, entry iv)	429
Figure A 63. ^{31}P NMR spectrum of compound 27 in CDCl_3 (Table 2.4, entry iv)	430
Figure A 64. ^1H NMR spectrum of compound 28 in CDCl_3 (Table 2.4, entry vii)	431
Figure A 65. ^{13}C NMR spectrum of compound 28 in CDCl_3 (Table 2.4, entry vii)	432
Figure A 66. COSY 2D NMR spectrum of compound 28 in CDCl_3 (Table 2.4, entry vii)	433
Figure A 67. ^{31}P NMR spectrum of compound 28 in CDCl_3 (Table 2.4, entry vii)	434
Figure A 68. ^{31}P NMR spectrum of compound 29 in CDCl_3 (Table 2.4, entry viii)	435
Figure A 69. ^1H NMR spectrum of compound 30 in CDCl_3 (Table 2.4, entry ix)	436
Figure A 70. ^{13}C NMR spectrum of compound 30 in CDCl_3 (Table 2.4, entry ix)	437
Figure A 71. COSY 2D NMR spectrum of compound 30 in CDCl_3 (Table 4.4, entry ix)	438
Figure A 72. HSQC 2D NMR spectrum of compound 30 in CDCl_3 (Table 2.4, entry ix)	439
Figure A 73. ^{31}P NMR spectrum of compound 30 in CDCl_3 (Table 2.4, entry ix)	440
Figure A 74. ^1H NMR spectrum of compound 31 in CDCl_3 (Table 2.4, entry x)	441
Figure A 75. ^{13}C NMR spectrum of compound 31 in CDCl_3 (Table 2.4, entry x)	442
Figure A 76. COSY 2D NMR spectrum of compound 31 in CDCl_3 (Table 2.4, entry x)	443
Figure A 77. HSQC 2D NMR spectrum of compound 31 in CDCl_3 (Table 4.4, entry x)	444
Figure A 78. ^{31}P NMR spectrum of compound 31 in CDCl_3 (Table 2.4, entry x)	445
Figure A 79. ^1H NMR spectrum of compound 32 in CDCl_3 (Table 2.4, entry xi)	446
Figure A 80. ^{13}C NMR spectrum of compound 32 in CDCl_3 (Table 2.4, entry xi)	447
Figure A 81. HSQC 2D NMR spectrum of compound 32 in CDCl_3 (Table 2.4, entry xi)	448
Figure A 82. ^{31}P NMR spectrum of compound 32 in CDCl_3 (Table 2.4, entry xi)	449
Figure A 83. ^1H NMR spectrum of compound 33 in CDCl_3 (Table 2.4, entry xii)	450
Figure A 84. ^{13}C NMR spectrum of compound 33 in CDCl_3 (Table 2.4, entry xii)	451
Figure A 85. COSY 2D NMR spectrum of compound 33 in CDCl_3 (Table 2.4, entry xii)	452
Figure A 86. HSQC 2D NMR spectrum of compound 33 in CDCl_3 (Table 2.4, entry xii)	453
Figure A 87. ^{31}P NMR spectrum of compound 33 in CDCl_3 (Table 2.4, entry xii)	454
Figure A 88. ^1H NMR spectrum of compound 39 in CDCl_3	455
Figure A 89. COSY 2D NMR spectrum of compound 39 in CDCl_3	456

Figure A 90. ^{31}P NMR spectrum of compound 39 in CDCl_3	457
Figure A 91. ^1H NMR spectrum of compound 40 in CDCl_3	458
Figure A 92. ^{31}P NMR spectrum of compound 40 in CDCl_3 (BEFORE COLUMN)	459
Figure A 93. ^{31}P NMR spectrum of compound 40 in CDCl_3 (AFTER COLUMN)	460
Figure A 94. ^1H NMR spectrum of compound 34 in MeOD (Table 2.5, entry i)	461
Figure A 95. ^{13}C NMR spectrum of compound 34 in MeOD (Table 2.5, entry i)	462
Figure A 96. ^1H NMR spectrum of compound 34 in MeOD (Table 2.5, entry i)	463
Figure A 97. ^1H NMR spectrum of compound 34 in MeOD (Table 2.5, entry i)	464
Figure A 98. ^{31}P NMR spectrum of compound 34 in MeOD (Table 2.5, entry i).....	465
Figure A 99. ^1H NMR spectrum of compound 35 in D_2O (Table 4.5, entry ix)	466
Figure A 100. ^{13}C NMR spectrum of compound 35 in D_2O (Table 2.5, entry ix)	467
Figure A 101. HSQC spectrum of compound 35 in D_2O (Table 2.5, entry xi)	468
Figure A 102. COSY spectrum of compound 35 in D_2O (Table 2.5, entry ix)	469
Figure A 103. ^{31}P spectrum of compound 35 in D_2O (Table 2.5, entry ix).....	470
Figure A 104. ^1H NMR spectrum of compound 35 in D_2O (Table 2.5, entry ix)	471
Figure A 105. ^{13}C NMR spectrum of compound 36 in D_2O (Table 2.5, entry x)	472
Figure A 106. ^1H NMR spectrum of compound 36 in D_2O (Table 2.5, entry x)	473
Figure A 107. HSQC NMR spectrum of compound 36 in D_2O (Table 2.5, entry x)	474
Figure A 108. ^{31}P NMR spectrum of compound 36 in D_2O (Table 2.5, entry x).....	475
Figure A 109. ^1H NMR spectrum of compound 42 in D_2O	476
Figure A 110. ^{13}C NMR spectrum of compound 42 in D_2O	477
Figure A 111. COSY 2D NMR spectrum of compound 42 in D_2O	478
Figure A 112. HSQC 2D NMR spectrum of compound 42 in D_2O	479
Figure A 113. ^{31}P NMR spectrum of compound 42 in D_2O	480
Figure A 114. ^1H NMR spectrum of compound 44 in D_2O	481
Figure A 115. ^{13}C NMR spectrum of compound 44 in D_2O	482
Figure A 116. COSY 2D NMR spectrum of compound 44 in D_2O	483
Figure A 117. HSQC 2D NMR spectrum of compound 44 in D_2O	484
Figure A 118. ^1H NMR spectrum of compound (51) in CDCl_3	485
Figure A 119. ^{13}C NMR spectrum of compound (51) in CDCl_3	486
Figure A 120. COSY 2D NMR spectrum of compound (51) in CDCl_3	487
Figure A 121. HSQC 2D NMR spectrum of compound (51) in CDCl_3	488
Figure A 122. ^{31}P NMR spectrum of compound (51) in CDCl_3	489
Figure A 123. ^1H NMR spectrum of compound (52) in CDCl_3	490
Figure A 124. ^{13}C NMR spectrum of compound (52) in CDCl_3	491
Figure A 125. COSY 2D NMR spectrum of compound (52) in CDCl_3	492
Figure A 126. ^{31}P NMR spectrum of compound (52) in CDCl_3	493
Figure A 127. ^1H NMR spectrum of compound (66) in CDCl_3	494
Figure A 128. ^{13}C NMR spectrum of compound (66) in CDCl_3	495
Figure A 129. COSY 2D NMR spectrum of compound (66) in CDCl_3	496

Figure A 130. HSQC 2D NMR spectrum of compound (66) in CDCl ₃ .	497
Figure A 131. ¹ H NMR spectrum of compound (67) in MeOD.	498
Figure A 132. ¹³ C NMR spectrum of compound (67) in MeOD.	499
Figure A 133. COSY 2D NMR spectrum of compound (67) in MeOD.	500
Figure A 134. HSQC 2D NMR spectrum of compound (67) in MeOD.	501
Figure A 135. ¹ H NMR spectrum of compound (9) in CDCl ₃ .	502
Figure A 136. ¹³ C NMR spectrum of compound (9) in CDCl ₃ .	503
Figure A 137. COSY 2D NMR spectrum of compound (9) in CDCl ₃ .	504
Figure A 138. HSQC 2D NMR spectrum of compound (9) in CDCl ₃ .	505
Figure A 139. ¹ H NMR spectrum of compound (68) in CDCl ₃ .	506
Figure A 140. ¹³ C NMR spectrum of compound (68) in CDCl ₃ .	507
Figure A 141. HSQC 2D NMR spectrum of compound (68) in CDCl ₃ .	508
Figure A 142. ³¹ P NMR spectrum of compound (68) in CDCl ₃ .	509
Figure A 143. ¹ H NMR spectrum of compound (105) in CDCl ₃ .	510
Figure A 144. ¹³ C NMR spectrum of compound (105) in CDCl ₃ .	511
Figure A 145. COSY 2D NMR spectrum of compound (105) in CDCl ₃ .	512
Figure A 146. HSQC 2D NMR spectrum of compound (105) in CDCl ₃ .	513
Figure A 147. ³¹ P NMR spectrum of compound (105) in CDCl ₃ .	514
Figure A 148. ¹ H NMR spectrum of compound (77) in CDCl ₃ .	515
Figure A 149. ¹³ C NMR spectrum of compound (77) in CDCl ₃ .	516
Figure A 150. HSQC 2D NMR spectrum of compound (77) in CDCl ₃ .	517
Figure A 151. ³¹ P NMR spectrum of compound (77) in CDCl ₃ .	518
Figure A 152. ¹ H NMR spectrum of compound (97) in MeOD.	519
Figure A 153. ¹³ C NMR spectrum of compound (97) in MeOD.	520
Figure A 154. COSY 2D NMR spectrum of compound (97) in MeOD.	521
Figure A 155. HSQC 2D NMR spectrum of compound (97) in MeOD.	522
Figure A 156. ³¹ P NMR spectrum of compound (97) in MeOD.	523
Figure A 157. ¹ H NMR spectrum of compound (95) in CDCl ₃ .	524
Figure A 158. ¹³ C NMR spectrum of compound (95) in CDCl ₃ .	525
Figure A 159. COSY 2D NMR spectrum of compound (95) in CDCl ₃ .	526
Figure A 160. ³¹ P NMR spectrum of compound (95) in CDCl ₃ .	527
Figure A 161. ¹ H NMR spectrum of compound (98) in CDCl ₃ .	528
Figure A 162. ¹³ C NMR spectrum of compound (98) in CDCl ₃ .	529
Figure A 163. COSY 2D NMR spectrum of compound (98) in CDCl ₃ .	530
Figure A 164. HSQC 2D NMR spectrum of compound (98) in CDCl ₃ .	531
Figure A 165. ³¹ P NMR spectrum of compound (98) in CDCl ₃ .	532
Figure A 166. ¹ H NMR spectrum of compound (99) in CDCl ₃ .	533
Figure A 167. ¹³ C NMR spectrum of compound (99) in CDCl ₃ .	534
Figure A 168. COSY 2D NMR spectrum of compound (99) in CDCl ₃ .	535
Figure A 169. HSQC 2D NMR spectrum of compound (99) in CDCl ₃ .	536

Figure A 170. ^{31}P NMR spectrum of compound (99) in CDCl_3 .	537
Figure A 171. ^1H NMR spectrum of compound (91) in MeOD.	538
Figure A 172. ^{13}C NMR spectrum of compound (91) in MeOD.	539
Figure A 173. COSY 2D NMR spectrum of compound (91) in MeOD.	540
Figure A 174. HSQC 2D NMR spectrum of compound (91) in MeOD.	541
Figure A 175. ^{31}P NMR spectrum of compound (91) in MeOD. (CRUDE)	542
Figure A 176. ^{31}P NMR spectrum of compound (91) in MeOD. (COLUMNED FRACTION)	543
Figure A 177. ^1H NMR spectrum of compound (87) in CDCl_3 .	544
Figure A 178. ^{31}P NMR spectrum of compound (87) in CDCl_3 .	545
Figure A 179. ^1H NMR spectrum of compound (87) in CDCl_3 .	546
Figure A 180. ^{13}C NMR spectrum of compound (87) in CDCl_3 .	547
Figure A 181. COSY 2D NMR spectrum of compound (96) in CDCl_3 .	548
Figure A 182. HSQC 2D NMR spectrum of compound (96) in CDCl_3 .	549
Figure A 183. ^{31}P NMR spectrum of compound (96) in CDCl_3 .	550
Figure A 184. ^1H NMR spectrum of compound (93) in CDCl_3 .	551
Figure A 185. COSY 2D NMR spectrum of compound (93) in CDCl_3 .	552
Figure A 186. HSQC 2D NMR spectrum of compound (93) in CDCl_3 .	553
Figure A 187. ^{31}P NMR spectrum of compound (93) in CDCl_3 .	554
Figure A 188. ^1H NMR spectrum of compound (83) in CDCl_3 .	555
Figure A 189. ^{13}C NMR spectrum of compound (83) in CDCl_3 .	556
Figure A 190. COSY 2D NMR spectrum of compound (83) in CDCl_3 .	557
Figure A 191. HSQC 2D NMR spectrum of compound (83) in CDCl_3 .	558
Figure A 192. ^1H NMR spectrum of compound (102) in CDCl_3 .	559
Figure A 193. ^{13}C NMR spectrum of compound (102) in CDCl_3 .	560
Figure A 194. COSY 2D NMR spectrum of compound (102) in CDCl_3 .	561
Figure A 195. HSQC 2D NMR spectrum of compound (102) in CDCl_3 .	562
Figure A 196. ^1H NMR spectrum of compound (202) in CDCl_3 .	563
Figure A 197. ^{13}C NMR spectrum of compound (202) in CDCl_3 .	564
Figure A 198. ^1H NMR spectrum of compound (204) in CDCl_3 .	565
Figure A 199. ^{13}C NMR spectrum of compound (204) in CDCl_3 .	566
Figure A 200. ^1H NMR spectrum of compound (206) in CDCl_3 .	567
Figure A 201. ^{13}C NMR spectrum of compound (206) in CDCl_3 .	568
Figure A 202. ^1H NMR spectrum of compound (205) in CDCl_3 .	569
Figure A 203. ^{13}C NMR spectrum of compound (205) in CDCl_3 .	570
Figure A 204. ^{13}C NMR spectrum of compound (114) in CDCl_3 .	571
Figure A 205. COSY 2D NMR spectrum of compound (114) in CDCl_3 .	572
Figure A 206. HSQC 2D NMR spectrum of compound (114) in CDCl_3 .	573
Figure A 207. ^{31}P NMR spectrum of compound (114) in CDCl_3 .	574
Figure A 208. ^1H NMR spectrum of compound (116) in CDCl_3 .	575
Figure A 209. ^{13}C NMR spectrum of compound (116) in CDCl_3 .	576

Figure A 210.	COSY 2D NMR spectrum of compound (116) in CDCl ₃ .	577
Figure A 211.	HSQC 2D NMR spectrum of compound (116) in CDCl ₃ .	578
Figure A 212.	³¹ P NMR spectrum of compound (116) in CDCl ₃ .	579
Figure A 213.	¹ H NMR spectrum of compound (117) in CDCl ₃ .	580
Figure A 214.	¹³ C NMR spectrum of compound (117) in CDCl ₃ .	581
Figure A 215.	COSY 2D NMR spectrum of compound (117) in CDCl ₃ .	582
Figure A 216.	HSQC 2D NMR spectrum of compound (117) in CDCl ₃ .	583
Figure A 217.	³¹ P NMR spectrum of compound (117) in CDCl ₃ .	584
Figure A 218.	¹ H NMR spectrum of compound (118) in CDCl ₃ .	585
Figure A 219.	¹³ C NMR spectrum of compound (118) in CDCl ₃ .	586
Figure A 220.	COSY 2D NMR spectrum of compound (118) in CDCl ₃ .	587
Figure A 221.	HSQC 2D NMR spectrum of compound (118) in CDCl ₃ .	588
Figure A 222.	³¹ P NMR spectrum of compound (118) in CDCl ₃ .	589
Figure A 223.	¹ H NMR spectrum of compound (119) in CDCl ₃ .	590
Figure A 224.	¹³ C NMR spectrum of compound (119) in CDCl ₃ .	591
Figure A 225.	COSY 2D NMR spectrum of compound (119) in CDCl ₃ .	592
Figure A 226.	HSQC 2D NMR spectrum of compound (119) in CDCl ₃ .	593
Figure A 227.	³¹ P NMR spectrum of compound (119) in CDCl ₃ .	594
Figure A 228.	¹ H NMR spectrum of compound (113) in CDCl ₃ .	595
Figure A 229.	¹³ C NMR spectrum of compound (113) in CDCl ₃ .	596
Figure A 230.	COSY 2D NMR spectrum of compound (113) in CDCl ₃ .	597
Figure A 231.	HSQC 2D NMR spectrum of compound (113) in CDCl ₃ .	598
Figure A 232.	³¹ P NMR spectrum of compound (113) in CDCl ₃ .	599
Figure A 233.	¹ H NMR spectrum of compound (120) in CDCl ₃ .	600
Figure A 234.	³¹ P NMR spectrum of compound (120) in CDCl ₃ .	601
Figure A 235.	¹ H NMR spectrum of compound (121) in CDCl ₃ .	602
Figure A 236.	¹³ C NMR spectrum of compound (121) in CDCl ₃ .	603
Figure A 237.	COSY 2D NMR spectrum of compound (121) in CDCl ₃ .	604
Figure A 238.	HSQC 2D NMR spectrum of compound (121) in CDCl ₃ .	605
Figure A 239.	³¹ P NMR spectrum of compound (121) in CDCl ₃ .	606
Figure A 240.	¹ H NMR spectrum of compound (123) in CDCl ₃ .	607
Figure A 241.	¹³ C NMR spectrum of compound (123) in CDCl ₃ .	608
Figure A 242.	HSQC 2D NMR spectrum of compound (123) in CDCl ₃ .	609
Figure A 243.	¹ H NMR spectrum of compound (122) in CDCl ₃ .	610
Figure A 244.	¹³ C NMR spectrum of compound (122) in CDCl ₃ .	611
Figure A 245.	COSY 2D NMR spectrum of compound (122) in CDCl ₃ .	612
Figure A 246.	HSQC 2D NMR spectrum of compound (122) in CDCl ₃ .	613
Figure A 247.	¹ H NMR spectrum of compound (135) in CDCl ₃ .	614
Figure A 248.	¹³ C NMR spectrum of compound (135) in CDCl ₃ .	615
Figure A 249.	HSQC 2D NMR spectrum of compound (135) in CDCl ₃ .	616

Figure A 250.	^{31}P NMR spectrum of compound (135) in CDCl_3	617
Figure A 251.	^1H NMR spectrum of compound (136) in CDCl_3	618
Figure A 252.	^{31}P NMR spectrum of compound (136) in CDCl_3	619
Figure A 253.	^1H NMR spectrum of compound (131) in CDCl_3	620
Figure A 254.	^{31}P NMR spectrum of compound (131) in CDCl_3	621
Figure A 255.	^1H NMR spectrum of compound (140) in CDCl_3	622
Figure A 256.	^{13}C NMR spectrum of compound (140) in CDCl_3	623
Figure A 257.	COSY 2D NMR spectrum of compound (140) in CDCl_3	624
Figure A 258.	HSQC 2D NMR spectrum of compound (140) in CDCl_3	625
Figure A 259.	^1H NMR spectrum of compound (153) in CDCl_3	626
Figure A 260.	^{13}C NMR spectrum of compound (153) in CDCl_3	627
Figure A 261.	^{13}C NMR spectrum of compound (153) in CDCl_3	628
Figure A 262.	^1H NMR spectrum of compound (154) in CDCl_3	629
Figure A 263.	COSY 2D NMR spectrum of compound (154) in CDCl_3	630
Figure A 264.	^1H NMR spectrum of compound (155) in CDCl_3	631
Figure A 265.	COSY 2D NMR spectrum of compound (155) in CDCl_3	632
Figure A 266.	^{13}H NMR spectrum of compound (155) in CDCl_3	633
Figure A 267.	^1H NMR spectrum of compound (156) in CDCl_3	634
Figure A 268.	^{13}C NMR spectrum of compound (156) in CDCl_3	635
Figure A 269.	^1H NMR spectrum of compound (152) in CDCl_3	636
Figure A 270.	^{13}C NMR spectrum of compound (152) in CDCl_3	637
Figure A 271.	COSY 2D NMR spectrum of compound (152) in CDCl_3	638
Figure A 272.	HSQC 2D NMR spectrum of compound (152) in CDCl_3	639
Figure A 273.	^1H NMR spectrum of compound (144) from (152) in CDCl_3	640
Figure A 274.	^1H NMR spectrum of compound (144) from (156) in CDCl_3	641
Figure A 275.	^{13}C NMR spectrum of compound (144) from (152) in CDCl_3	642
Figure A 276.	COSY 2D NMR spectrum of compound (144) from (152) in CDCl_3	643
Figure A 277.	HSQC 2D spectrum of compound (144) from (152) in CDCl_3	644
Figure A 278.	^1H NMR spectrum of compound (169) in CDCl_3	645
Figure A 279.	^{13}C NMR spectrum of compound (169) in CDCl_3	646
Figure A 280.	COSY 2D NMR spectrum of compound (169) in CDCl_3	647
Figure A 281.	HSQC 2D NMR spectrum of compound (169) in CDCl_3	648
Figure A 282.	^{31}P NMR spectrum of compound (169) in CDCl_3	649
Figure A 283.	^1H NMR spectrum of compound (158) in CDCl_3	650
Figure A 284.	^{13}C NMR spectrum of compound (158) in CDCl_3	651
Figure A 285.	COSY 2D NMR spectrum of compound (158) in CDCl_3	652
Figure A 286.	HSQC 2D NMR spectrum of compound (158) in CDCl_3	653
Figure A 287.	^{31}P NMR spectrum of compound (158) in CDCl_3	654
Figure A 288.	^1H NMR spectrum of compound (170) in CDCl_3	655
Figure A 289.	^{13}C NMR spectrum of compound (170) in CDCl_3	656

Figure A 290.	COSY 2D NMR spectrum of compound (170) in CDCl ₃ .	657
Figure A 291.	HSQC 2D NMR spectrum of compound (170) in CDCl ₃ .	658
Figure A 292.	³¹ P NMR spectrum of compound (170) in CDCl ₃ .	659
Figure A 293.	¹ H NMR spectrum of compound (157) in D ₂ O.	660
Figure A 294.	¹³ C NMR spectrum of compound (157) in D ₂ O.	661
Figure A 295.	¹³ C NMR spectrum of compound (157) in DMSO-d ₆ .	662
Figure A 296.	HSQC 2D NMR spectrum of compound (157) in CDCl ₃ .	663
Figure A 297.	¹ H NMR spectrum of compound (163) in D ₂ O.	664
Figure A 298.	¹³ C NMR spectrum of compound (163) in D ₂ O.	665
Figure A 299.	COSY 2D NMR spectrum of compound (163) in CDCl ₃ .	666
Figure A 300.	HSQC 2D NMR spectrum of compound (163) in CDCl ₃ .	667
Figure A 301.	¹ H NMR spectrum of compound (176) in CDCl ₃ .	668
Figure A 302.	COSY 2D NMR spectrum of compound (176) in CDCl ₃ .	669
Figure A 303.	¹ H NMR spectrum of compound (177) in CDCl ₃ .	670
Figure A 304.	¹³ C NMR spectrum of compound (177) in CDCl ₃ .	671
Figure A 305.	COSY 2D NMR spectrum of compound (177) in CDCl ₃ .	672
Figure A 306.	HSQC 2D NMR spectrum of compound (177) in CDCl ₃ .	673
Figure A 307.	¹ H NMR spectrum of compound (181) in CDCl ₃ .	674
Figure A 308.	¹³ C NMR spectrum of compound (181) in CDCl ₃ .	675
Figure A 309.	COSY 2D NMR spectrum of compound (181) in CDCl ₃ .	676
Figure A 310.	HSQC 2D NMR spectrum of compound (181) in CDCl ₃ .	677
Figure A 311.	¹ H NMR spectrum of compound (185) in CDCl ₃ . (CRUDE)	678
Figure A 312.	¹³ C NMR spectrum of compound (185) in CDCl ₃ . (CRUDE)	679
Figure A 313.	COSY 2D NMR spectrum of compound (185) in CDCl ₃ .	680
Figure A 314.	HSQC 2D NMR spectrum of compound (185) in CDCl ₃ .	681
Figure A 315.	¹ H NMR spectrum of compound (188) in CDCl ₃ .	682
Figure A 316.	¹³ C NMR spectrum of compound (188) in CDCl ₃ .	683
Figure A 317.	COSY 2D NMR spectrum of compound (188) in CDCl ₃ .	684
Figure A 318.	HSQC 2D NMR spectrum of compound (188) in CDCl ₃ .	685
Figure A 319.	¹ H NMR spectrum of compound (189) in CDCl ₃ . (CRUDE)	686
Figure A 320.	¹ H NMR spectrum of compound (192) in CDCl ₃ .	687
Figure A 321.	¹³ C NMR spectrum of compound (192) in CDCl ₃ .	688
Figure A 322.	COSY 2D NMR spectrum of compound (192) in CDCl ₃ .	689
Figure A 323.	¹ H NMR spectrum of compound (194) in CDCl ₃ .	690
Figure A 324.	¹ H NMR spectrum of compound (194) in CDCl ₃ .	691
Figure A 325.	COSY 2D NMR spectrum of compound (194) in CDCl ₃ .	692
Figure A 326.	HSQC 2D NMR spectrum of compound (194) in CDCl ₃ .	693
Figure A 327.	¹ H NMR spectrum of compound (198) in CDCl ₃ .	694
Figure A 328.	¹³ C NMR spectrum of compound (198) in CDCl ₃ .	695
Figure A 329.	COSY 2D NMR spectrum of compound (198) in CDCl ₃ .	696

Figure A 330. HSQC 2D NMR spectrum of compound (198) in CDCl ₃ .	697
Figure A 331. ¹ H NMR spectrum of compound (202) in CDCl ₃ .	698
Figure A 332. ¹³ C NMR spectrum of compound (202) in CDCl ₃ .	699
Figure A 333. ¹ H NMR spectrum of compound (204) in CDCl ₃ .	700
Figure A 334. ¹³ C NMR spectrum of compound (204) in CDCl ₃ .	701
Figure A 335. ¹ H NMR spectrum of compound (205) in CDCl ₃ .	702
Figure A 336. ¹³ C NMR spectrum of compound (205) in CDCl ₃ .	703
Figure A 337. ¹ H NMR spectrum of compound (206) in CDCl ₃ .	704
Figure A 338. ¹³ C NMR spectrum of compound (206) in CDCl ₃ .	705
Figure A 339. ¹ H NMR spectrum of compound (208) in CDCl ₃ .	706
Figure A 340. ¹³ C NMR spectrum of compound (208) in CDCl ₃ .	707
Figure A 341. COSY 2D NMR spectrum of compound (208) in CDCl ₃ .	708
Figure A 342. HSQC 2D NMR spectrum of compound (208) in CDCl ₃ .	709
Figure A 343. ¹ H NMR spectrum of compound (209) in MeOD.	710
Figure A 344. ¹³ C NMR spectrum of compound (209) in MeOD.	711
Figure A 345. COSY 2D NMR spectrum of compound (209) in MeOD.	712
Figure A 346. HSQC 2D NMR spectrum of compound (209) in MeOD.	713
Figure A 347. ¹ H NMR spectrum of compound (210) in MeOD.	714
Figure A 348. COSY 2D NMR spectrum of compound (210) in MeOD.	715
Figure A 349. ¹ H NMR spectrum of compound (211) in CDCl ₃ .	716
Figure A 350. ¹³ C NMR spectrum of compound (211) in CDCl ₃ .	717
Figure A 351. COSY 2D NMR spectrum of compound (211) in CDCl ₃ .	718
Figure A 352. HSQC 2D NMR spectrum of compound (211) in CDCl ₃ .	719
Figure A 353. ³¹ P NMR spectrum of compound (211) in CDCl ₃ .	720
Figure A 354. ¹ H NMR spectrum of compound (212) in CDCl ₃ .	721
Figure A 355. ¹³ C NMR spectrum of compound (212) in CDCl ₃ .	722
Figure A 356. HSQC 2D NMR spectrum of compound (212) in CDCl ₃ .	723
Figure A 357. ³¹ P NMR spectrum of compound (212) in CDCl ₃ .	724
Figure A 358. ¹ H NMR spectrum of compound (213) in CDCl ₃ .	725
Figure A 359. ¹³ C NMR spectrum of compound (213) in CDCl ₃ .	726
Figure A 360. COSY 2D NMR spectrum of compound (213) in CDCl ₃ .	727
Figure A 361. HSQC 2D NMR spectrum of compound (213) in CDCl ₃ .	728
Figure A 362. ¹ H NMR spectrum of compound (214) in CDCl ₃ .	729
Figure A 363. ¹³ C NMR spectrum of compound (214) in CDCl ₃ .	730
Figure A 364. COSY 2D NMR spectrum of compound (214) in CDCl ₃ .	731
Figure A 365. HSQC 2D NMR spectrum of compound (214) in CDCl ₃ .	732
Figure A 366. ¹ H NMR spectrum of compound (215) in CDCl ₃ .	733
Figure A 367. ¹³ C NMR spectrum of compound (215) in CDCl ₃ .	734
Figure A 368. COSY 2D NMR spectrum of compound (215) in CDCl ₃ .	735
Figure A 369. HSQC 2D NMR spectrum of compound (215) in CDCl ₃ .	736

Figure A 370.	^{31}P NMR spectrum of compound (215) in CDCl_3	737
Figure A 371.	^1H NMR spectrum of compound (216) in CDCl_3	738
Figure A 372.	^{13}C NMR spectrum of compound (216) in CDCl_3	739
Figure A 373.	COSY 2D NMR spectrum of compound (216) in CDCl_3	740
Figure A 374.	HSQC 2D NMR spectrum of compound (216) in CDCl_3	741
Figure A 375.	^1H NMR spectrum of compound (217) in D_2O	742
Figure A 376.	^{13}C NMR spectrum of compound (217) in D_2O	743
Figure A 377.	COSY 2D NMR spectrum of compound (217) in D_2O	744
Figure A 378.	HSQC 2D NMR spectrum of compound (217) in D_2O	745
Figure A 379.	^{31}P NMR spectrum of compound in (217) D_2O	746
Figure A 380.	^1H NMR spectrum of compound (219) in CDCl_3	747
Figure A 381.	^{13}C NMR spectrum of compound (219) in CDCl_3	748
Figure A 382.	COSY 2D NMR spectrum of compound (219) in CDCl_3	749
Figure A 383.	^1H NMR spectrum of compound (220) in DMSO-d_6	750
Figure A 384.	^{13}C NMR spectrum of compound (220) in DMSO-d_6	751
Figure A 385.	HSQC 2D NMR spectrum of compound (220) in DMSO-d_6	752
Figure A 386.	^1H NMR spectrum of compound (221) in D_2O	753
Figure A 387.	^{13}C NMR spectrum of compound (221) in D_2O	754
Figure A 388.	COSY 2D NMR spectrum of compound (221) in D_2O	755
Figure A 389.	HSQC 2D NMR spectrum of compound (221) in D_2O	756
Figure A 390.	^1H NMR spectrum of compound (222) in D_2O	757
Figure A 391.	^{13}C NMR spectrum of compound (222) in D_2O	758
Figure A 392.	COSY 2D NMR spectrum of compound (222) in D_2O	759
Figure A 393.	HSQC 2D NMR spectrum of compound (222) in D_2O	760
Figure A 394.	^1H NMR spectrum of compound (223) in D_2O	761
Figure A 395.	^{13}C NMR spectrum of compound (223) in D_2O	762
Figure A 396.	HSQC 2D NMR spectrum of compound (223) in D_2O	763
Figure A 397.	^1H NMR spectrum of compound (225) in DMSO-d_6	764
Figure A 398.	^{13}C NMR spectrum of compound (225) in DMSO-d_6	765
Figure A 399.	ESI-TOF spectrum of compound 19	766
Figure A 400.	ESI-TOF spectrum of compound 26	767
Figure A 401.	HRMS ESI-TOF spectrum of compound 27	768
Figure A 402.	ESI-TOF spectrum of compound 34	769
Figure A 403.	HRMS ESI-TOF spectrum of compound 36	770
Figure A 404.	ESI-TOF spectrum of compound 51	771
Figure A 405.	ESI-TOF spectrum of compound 66	772
Figure A 406.	.DART-HRMS spectrum of compound 113	773
Figure A 407.	ESI-TOF spectrum of compound 121	774
Figure A 408.	DART spectrum of compound 163	775
Figure A 409.	HRMS-DART spectrum of compound 163	776

Figure A 410. ESI-TOF spectrum of compound 194	777
Figure A 411. ESI-TOF spectrum of compound 205	778
Figure A 412. DART spectrum of compound 208	779
Figure A 413. HRMS-DART spectrum of compound 208	780
Figure A 414. DART spectrum of compound 211	781
Figure A 415. HRMS-DART spectrum of compound 211	782
Figure A 416. ESI-TOF spectrum of compound 212	783
Figure A 417. HRMS-DART spectrum of compound 213	784
Figure A 418. HRMS-DART spectrum of compound 213	785
Figure A 419. ESI-TOF spectrum of compound 217	786
Figure A 420. DART spectrum of compound 221	787
Figure A 421. ESI-TOF spectrum of compound 222	788
Figure A 422. ESI-TOF spectrum of compound 225	789

6.1 Appendix 1.1 – X-Ray Data

Table A 1. Crystal data and structure refinement for **34**.

Identification code	k1180	
Empirical formula	C ₂₃ H ₅₁ Br N O ₃ P	
Formula weight	500.53	
Temperature	150(1) K	
Wavelength	0.71073 Å	
Crystal system	Triclinic	
Space group	P -1	
Unit cell dimensions	a = 6.5523(5) Å	α = 87.242(4)°.
	b = 7.3545(4) Å	β = 89.564(3)°.
	c = 28.873(2) Å	γ = 77.409(4)°.
Volume	1356.32(16) Å ³	
Z	2	
Density (calculated)	1.226 Mg/m ³	
Absorption coefficient	1.596 mm ⁻¹	
F(000)	540	
Crystal size	0.50 x 0.50 x 0.02 mm ³	
Theta range for data collection	2.83 to 25.00°.	
Index ranges	-7 ≤ h ≤ 7, -8 ≤ k ≤ 8, -34 ≤ l ≤ 34	
Reflections collected	12148	
Independent reflections	4737 [R(int) = 0.1147]	
Completeness to theta = 25.00°	99.1 %	
Absorption correction	Semi-empirical from equivalents	
Max. and min. transmission	0.992 and 0.706	
Refinement method	Full-matrix least-squares on F ²	
Data / restraints / parameters	4737 / 0 / 265	
Goodness-of-fit on F ²	1.079	
Final R indices [I > 2σ(I)]	R1 = 0.0767, wR2 = 0.1501	
R indices (all data)	R1 = 0.1429, wR2 = 0.1819	
Largest diff. peak and hole	0.500 and -0.610 e.Å ⁻³	

Table A 2. Atomic coordinates ($\times 10^4$) and equivalent isotropic displacement parameters ($\text{\AA}^2 \times 10^3$) for **34**.

	x	y	z	U(eq)
Br(1)	6398(1)	3573(1)	6468(1)	56(1)
P(1)	6397(3)	7024(2)	4707(1)	40(1)
O(1)	7347(7)	4952(6)	4696(2)	44(1)
O(2)	4221(7)	7436(6)	4912(2)	45(1)
O(3)	6408(7)	7948(6)	4210(2)	49(1)
N(1)	9810(8)	8204(7)	6300(2)	37(1)
C(1)	8069(10)	8120(8)	5022(2)	38(2)
C(2)	8050(11)	7605(9)	5546(2)	39(2)
C(3)	9370(10)	8708(8)	5787(2)	38(2)
C(4)	7742(10)	8344(9)	6553(2)	36(2)
C(5)	7936(10)	8286(9)	7081(2)	40(2)
C(6)	5862(11)	8014(9)	7289(2)	42(2)
C(7)	5683(11)	8235(9)	7807(2)	42(2)
C(8)	3732(11)	7685(9)	8010(2)	42(2)
C(9)	3324(11)	8125(9)	8512(2)	44(2)
C(10)	1422(11)	7501(9)	8712(2)	44(2)
C(11)	907(11)	8011(9)	9210(2)	43(2)
C(12)	-985(11)	7345(9)	9403(2)	44(2)
C(13)	-1505(11)	7846(9)	9896(2)	42(2)
C(14)	-3389(11)	7170(10)	10092(2)	45(2)
C(15)	-3944(11)	7691(9)	10584(2)	44(2)
C(16)	-5802(11)	6978(10)	10779(2)	44(2)
C(17)	-6376(11)	7491(9)	11272(2)	43(2)
C(18)	-8234(11)	6791(10)	11463(2)	44(2)
C(19)	-8853(11)	7298(9)	11952(2)	43(2)
C(20)	-10742(11)	6602(10)	12125(2)	45(2)
C(21)	-11409(12)	7187(10)	12608(2)	52(2)
C(22)	11117(11)	6252(9)	6355(2)	46(2)
C(23)	11004(10)	9534(9)	6473(3)	48(2)

Table A 3. Bond lengths [Å] and angles [°] for **34**.

P(1)-O(2)	1.514(5)
P(1)-O(1)	1.517(4)
P(1)-O(3)	1.559(5)
P(1)-C(1)	1.773(7)
O(1)-H(1O)	0.8400
O(3)-H(3O)	0.8402
N(1)-C(23)	1.486(8)
N(1)-C(22)	1.505(7)
N(1)-C(4)	1.522(8)
N(1)-C(3)	1.523(8)
C(1)-C(2)	1.544(8)
C(1)-H(1A)	0.9900
C(1)-H(1B)	0.9900
C(2)-C(3)	1.503(9)
C(2)-H(2A)	0.9900
C(2)-H(2B)	0.9900
C(3)-H(3A)	0.9900
C(3)-H(3B)	0.9900
C(4)-C(5)	1.528(9)
C(4)-H(4A)	0.9900
C(4)-H(4B)	0.9900
C(5)-C(6)	1.530(9)
C(5)-H(5A)	0.9900
C(5)-H(5B)	0.9900
C(6)-C(7)	1.513(9)
C(6)-H(6A)	0.9900
C(6)-H(6B)	0.9900
C(7)-C(8)	1.527(9)
C(7)-H(7A)	0.9900
C(7)-H(7B)	0.9900
C(8)-C(9)	1.511(9)
C(8)-H(8A)	0.9900
C(8)-H(8B)	0.9900

C(9)-C(10)	1.520(9)
C(9)-H(9A)	0.9900
C(9)-H(9B)	0.9900
C(10)-C(11)	1.520(9)
C(10)-H(10A)	0.9900
C(10)-H(10B)	0.9900
C(11)-C(12)	1.522(9)
C(11)-H(11A)	0.9900
C(11)-H(11B)	0.9900
C(12)-C(13)	1.504(9)
C(12)-H(12A)	0.9900
C(12)-H(12B)	0.9900
C(13)-C(14)	1.523(9)
C(13)-H(13A)	0.9900
C(13)-H(13B)	0.9900
C(14)-C(15)	1.512(9)
C(14)-H(14A)	0.9900
C(14)-H(14B)	0.9900
C(15)-C(16)	1.522(9)
C(15)-H(15A)	0.9900
C(15)-H(15B)	0.9900
C(16)-C(17)	1.513(9)
C(16)-H(16A)	0.9900
C(16)-H(16B)	0.9900
C(17)-C(18)	1.512(9)
C(17)-H(17A)	0.9900
C(17)-H(17B)	0.9900
C(18)-C(19)	1.507(9)
C(18)-H(18A)	0.9900
C(18)-H(18B)	0.9900
C(19)-C(20)	1.511(9)
C(19)-H(19A)	0.9900
C(19)-H(19B)	0.9900
C(20)-C(21)	1.515(9)
C(20)-H(20A)	0.9900

C(20)-H(20B)	0.9900
C(21)-H(21A)	0.9800
C(21)-H(21B)	0.9800
C(21)-H(21C)	0.9800
C(22)-H(22A)	0.9800
C(22)-H(22B)	0.9800
C(22)-H(22C)	0.9800
C(23)-H(23A)	0.9800
C(23)-H(23B)	0.9800
C(23)-H(23C)	0.9800

O(2)-P(1)-O(1)	112.9(3)
O(2)-P(1)-O(3)	111.1(3)
O(1)-P(1)-O(3)	109.7(3)
O(2)-P(1)-C(1)	110.2(3)
O(1)-P(1)-C(1)	109.4(3)
O(3)-P(1)-C(1)	103.0(3)
P(1)-O(1)-H(1O)	121.5
P(1)-O(3)-H(3O)	123.6
C(23)-N(1)-C(22)	109.3(5)
C(23)-N(1)-C(4)	111.5(5)
C(22)-N(1)-C(4)	110.4(5)
C(23)-N(1)-C(3)	107.3(5)
C(22)-N(1)-C(3)	109.4(5)
C(4)-N(1)-C(3)	108.9(5)
C(2)-C(1)-P(1)	111.8(4)
C(2)-C(1)-H(1A)	109.2
P(1)-C(1)-H(1A)	109.2
C(2)-C(1)-H(1B)	109.2
P(1)-C(1)-H(1B)	109.2
H(1A)-C(1)-H(1B)	107.9
C(3)-C(2)-C(1)	108.0(5)
C(3)-C(2)-H(2A)	110.1
C(1)-C(2)-H(2A)	110.1
C(3)-C(2)-H(2B)	110.1

C(1)-C(2)-H(2B)	110.1
H(2A)-C(2)-H(2B)	108.4
C(2)-C(3)-N(1)	116.3(5)
C(2)-C(3)-H(3A)	108.2
N(1)-C(3)-H(3A)	108.2
C(2)-C(3)-H(3B)	108.2
N(1)-C(3)-H(3B)	108.2
H(3A)-C(3)-H(3B)	107.4
N(1)-C(4)-C(5)	114.0(5)
N(1)-C(4)-H(4A)	108.8
C(5)-C(4)-H(4A)	108.8
N(1)-C(4)-H(4B)	108.8
C(5)-C(4)-H(4B)	108.8
H(4A)-C(4)-H(4B)	107.6
C(4)-C(5)-C(6)	108.1(5)
C(4)-C(5)-H(5A)	110.1
C(6)-C(5)-H(5A)	110.1
C(4)-C(5)-H(5B)	110.1
C(6)-C(5)-H(5B)	110.1
H(5A)-C(5)-H(5B)	108.4
C(7)-C(6)-C(5)	114.4(6)
C(7)-C(6)-H(6A)	108.7
C(5)-C(6)-H(6A)	108.7
C(7)-C(6)-H(6B)	108.7
C(5)-C(6)-H(6B)	108.7
H(6A)-C(6)-H(6B)	107.6
C(6)-C(7)-C(8)	112.6(6)
C(6)-C(7)-H(7A)	109.1
C(8)-C(7)-H(7A)	109.1
C(6)-C(7)-H(7B)	109.1
C(8)-C(7)-H(7B)	109.1
H(7A)-C(7)-H(7B)	107.8
C(9)-C(8)-C(7)	114.6(6)
C(9)-C(8)-H(8A)	108.6
C(7)-C(8)-H(8A)	108.6

C(9)-C(8)-H(8B)	108.6
C(7)-C(8)-H(8B)	108.6
H(8A)-C(8)-H(8B)	107.6
C(8)-C(9)-C(10)	113.7(6)
C(8)-C(9)-H(9A)	108.8
C(10)-C(9)-H(9A)	108.8
C(8)-C(9)-H(9B)	108.8
C(10)-C(9)-H(9B)	108.8
H(9A)-C(9)-H(9B)	107.7
C(9)-C(10)-C(11)	114.9(6)
C(9)-C(10)-H(10A)	108.5
C(11)-C(10)-H(10A)	108.5
C(9)-C(10)-H(10B)	108.5
C(11)-C(10)-H(10B)	108.5
H(10A)-C(10)-H(10B)	107.5
C(10)-C(11)-C(12)	113.8(6)
C(10)-C(11)-H(11A)	108.8
C(12)-C(11)-H(11A)	108.8
C(10)-C(11)-H(11B)	108.8
C(12)-C(11)-H(11B)	108.8
H(11A)-C(11)-H(11B)	107.7
C(13)-C(12)-C(11)	114.1(6)
C(13)-C(12)-H(12A)	108.7
C(11)-C(12)-H(12A)	108.7
C(13)-C(12)-H(12B)	108.7
C(11)-C(12)-H(12B)	108.7
H(12A)-C(12)-H(12B)	107.6
C(12)-C(13)-C(14)	114.2(6)
C(12)-C(13)-H(13A)	108.7
C(14)-C(13)-H(13A)	108.7
C(12)-C(13)-H(13B)	108.7
C(14)-C(13)-H(13B)	108.7
H(13A)-C(13)-H(13B)	107.6
C(15)-C(14)-C(13)	114.6(6)
C(15)-C(14)-H(14A)	108.6

C(13)-C(14)-H(14A)	108.6
C(15)-C(14)-H(14B)	108.6
C(13)-C(14)-H(14B)	108.6
H(14A)-C(14)-H(14B)	107.6
C(14)-C(15)-C(16)	114.2(6)
C(14)-C(15)-H(15A)	108.7
C(16)-C(15)-H(15A)	108.7
C(14)-C(15)-H(15B)	108.7
C(16)-C(15)-H(15B)	108.7
H(15A)-C(15)-H(15B)	107.6
C(17)-C(16)-C(15)	114.8(6)
C(17)-C(16)-H(16A)	108.6
C(15)-C(16)-H(16A)	108.6
C(17)-C(16)-H(16B)	108.6
C(15)-C(16)-H(16B)	108.6
H(16A)-C(16)-H(16B)	107.5
C(18)-C(17)-C(16)	114.5(6)
C(18)-C(17)-H(17A)	108.6
C(16)-C(17)-H(17A)	108.6
C(18)-C(17)-H(17B)	108.6
C(16)-C(17)-H(17B)	108.6
H(17A)-C(17)-H(17B)	107.6
C(19)-C(18)-C(17)	115.7(6)
C(19)-C(18)-H(18A)	108.4
C(17)-C(18)-H(18A)	108.4
C(19)-C(18)-H(18B)	108.4
C(17)-C(18)-H(18B)	108.4
H(18A)-C(18)-H(18B)	107.4
C(18)-C(19)-C(20)	113.8(6)
C(18)-C(19)-H(19A)	108.8
C(20)-C(19)-H(19A)	108.8
C(18)-C(19)-H(19B)	108.8
C(20)-C(19)-H(19B)	108.8
H(19A)-C(19)-H(19B)	107.7
C(19)-C(20)-C(21)	113.4(6)

C(19)-C(20)-H(20A)	108.9
C(21)-C(20)-H(20A)	108.9
C(19)-C(20)-H(20B)	108.9
C(21)-C(20)-H(20B)	108.9
H(20A)-C(20)-H(20B)	107.7
C(20)-C(21)-H(21A)	109.5
C(20)-C(21)-H(21B)	109.5
H(21A)-C(21)-H(21B)	109.5
C(20)-C(21)-H(21C)	109.5
H(21A)-C(21)-H(21C)	109.5
H(21B)-C(21)-H(21C)	109.5
N(1)-C(22)-H(22A)	109.5
N(1)-C(22)-H(22B)	109.5
H(22A)-C(22)-H(22B)	109.5
N(1)-C(22)-H(22C)	109.5
H(22A)-C(22)-H(22C)	109.5
H(22B)-C(22)-H(22C)	109.5
N(1)-C(23)-H(23A)	109.5
N(1)-C(23)-H(23B)	109.5
H(23A)-C(23)-H(23B)	109.5
N(1)-C(23)-H(23C)	109.5
H(23A)-C(23)-H(23C)	109.5
H(23B)-C(23)-H(23C)	109.5

Symmetry transformations used to generate equivalent atoms:

Table A 4. Anisotropic displacement parameters ($\text{\AA}^2 \times 10^3$) for **34**. The anisotropic displacement factor exponent takes the form: $-2p^2[h^2 a^{*2}U^{11} + \dots + 2 h k a^* b^* U^{12}]$

	U ¹¹	U ²²	U ³³	U ²³	U ¹³	U ¹²
Br(1)	47(1)	43(1)	77(1)	-9(1)	-14(1)	-7(1)
P(1)	38(1)	37(1)	44(1)	0(1)	4(1)	-9(1)
O(1)	39(3)	40(2)	52(3)	-4(2)	8(2)	-5(2)
O(2)	36(3)	39(2)	58(3)	-4(2)	10(2)	-7(2)
O(3)	60(3)	54(3)	39(3)	7(2)	-4(2)	-25(2)
N(1)	36(3)	36(3)	38(4)	-3(2)	-1(3)	-4(2)
C(1)	42(4)	38(4)	36(4)	-2(3)	4(3)	-11(3)
C(2)	39(4)	45(4)	32(4)	2(3)	1(3)	-12(3)
C(3)	41(4)	34(3)	40(4)	2(3)	4(3)	-11(3)
C(4)	30(4)	42(4)	35(4)	-6(3)	6(3)	-9(3)
C(5)	34(4)	44(4)	42(5)	-3(3)	3(3)	-9(3)
C(6)	45(5)	45(4)	34(4)	0(3)	5(3)	-11(3)
C(7)	46(5)	47(4)	35(4)	-4(3)	6(3)	-12(3)
C(8)	45(4)	46(4)	38(4)	-8(3)	7(3)	-17(3)
C(9)	50(5)	50(4)	32(4)	-2(3)	2(3)	-16(3)
C(10)	48(5)	51(4)	36(4)	-2(3)	6(3)	-21(3)
C(11)	46(5)	48(4)	39(4)	-7(3)	5(3)	-18(3)
C(12)	46(5)	52(4)	37(4)	-8(3)	6(3)	-16(3)
C(13)	41(4)	55(4)	36(4)	-5(3)	5(3)	-22(3)
C(14)	45(5)	57(4)	39(4)	-2(3)	3(3)	-25(4)
C(15)	47(5)	52(4)	36(4)	-1(3)	3(3)	-16(3)
C(16)	47(5)	53(4)	35(4)	0(3)	4(3)	-19(3)
C(17)	41(4)	49(4)	42(5)	-5(3)	5(3)	-16(3)
C(18)	46(5)	55(4)	36(4)	-8(3)	3(3)	-19(3)
C(19)	43(4)	46(4)	42(5)	-4(3)	7(3)	-16(3)
C(20)	40(4)	59(4)	39(5)	-1(3)	0(3)	-15(3)
C(21)	52(5)	60(5)	42(5)	0(4)	1(4)	-12(4)
C(22)	39(4)	46(4)	44(5)	-1(3)	-2(4)	9(3)
C(23)	30(4)	56(4)	58(5)	-8(4)	1(4)	-14(3)

Table A 5. Hydrogen coordinates ($\times 10^4$) and isotropic displacement parameters ($\text{\AA}^2 \times 10^3$)
for **34**.

	x	y	z	U(eq)
H(1O)	6719	4152	4808	66
H(3O)	5700	7712	3988	74
H(1A)	9514	7739	4903	46
H(1B)	7617	9490	4971	46
H(2A)	6600	7907	5665	46
H(2B)	8622	6253	5604	46
H(3A)	8671	10044	5754	46
H(3B)	10726	8555	5623	46
H(4A)	7109	7304	6465	43
H(4B)	6779	9525	6450	43
H(5A)	8245	9466	7182	48
H(5B)	9089	7244	7187	48
H(6A)	4706	8927	7134	50
H(6B)	5683	6751	7221	50
H(7A)	5646	9550	7873	51
H(7B)	6937	7451	7961	51
H(8A)	2504	8337	7824	50
H(8B)	3869	6329	7980	50
H(9A)	3127	9488	8541	52
H(9B)	4569	7511	8698	52
H(10A)	1656	6129	8696	52
H(10B)	195	8060	8515	52
H(11A)	645	9384	9227	52
H(11B)	2135	7466	9408	52
H(12A)	-2212	7889	9205	53
H(12B)	-721	5972	9387	53
H(13A)	-1777	9219	9912	51
H(13B)	-275	7309	10094	51
H(14A)	-4613	7691	9890	54

H(14B)	-3107	5795	10079	54
H(15A)	-4255	9067	10596	53
H(15B)	-2712	7191	10785	53
H(16A)	-7030	7477	10578	53
H(16B)	-5487	5602	10767	53
H(17A)	-5152	6983	11475	51
H(17B)	-6681	8867	11285	51
H(18A)	-9448	7288	11257	53
H(18B)	-7919	5415	11451	53
H(19A)	-9151	8672	11967	51
H(19B)	-7658	6775	12161	51
H(20A)	-10424	5223	12123	54
H(20B)	-11923	7080	11908	54
H(21A)	-12606	6661	12704	77
H(21B)	-11806	8551	12610	77
H(21C)	-10245	6728	12825	77
H(22A)	12343	6131	6152	69
H(22B)	10284	5361	6269	69
H(22C)	11577	5991	6678	69
H(23A)	12217	9546	6274	71
H(23B)	11479	9146	6791	71
H(23C)	10102	10787	6470	71

Table A 6. Hydrogen bonds for **34** [Å and °].

D-H...A	d(D-H)	d(H...A)	d(D...A)	<(DHA)
O(1)-H(1O)...O(2)#1	0.84	1.62	2.449(6)	171.1
O(3)-H(3O)...Br(1)#1	0.84	2.29	3.102(5)	163.7

Symmetry transformations used to generate equivalent atoms:

#1 -x+1,-y+1,-z+1

Table A 7. Crystal data and structure refinement for **66**.

Identification code	cu_d12327_0m		
Empirical formula	C23 H50 Br N O		
Formula weight	436.55		
Temperature	147(2) K		
Wavelength	1.54178 Å		
Crystal system	Triclinic		
Space group	P -1		
Unit cell dimensions	a = 7.3945(3) Å	a= 87.482(2)°.	
	b = 8.2701(4) Å	b= 81.558(2)°.	
	c = 22.9009(10) Å	g = 65.369(2)°.	
Volume	1259.01(10) Å ³		
Z	2		
Density (calculated)	1.152 Mg/m ³		
Absorption coefficient	2.284 mm ⁻¹		
F(000)	476		
Crystal size	0.36 x 0.22 x 0.05 mm ³		
Theta range for data collection	5.89 to 66.36°.		
Index ranges	-7<=h<=8, -9<=k<=8, -27<=l<=26		
Reflections collected	12902		
Independent reflections	4231 [R(int) = 0.0240]		
Completeness to theta = 66.36°	95.8 %		
Absorption correction	Semi-empirical from equivalents		

Max. and min. transmission	0.8944 and 0.6183
Refinement method	Full-matrix least-squares on F ²
Data / restraints / parameters	4231 / 0 / 242
Goodness-of-fit on F ²	1.080
Final R indices [I>2sigma(I)]	R1 = 0.0354, wR2 = 0.0934
R indices (all data)	R1 = 0.0360, wR2 = 0.0940
Largest diff. peak and hole	1.438 and -0.602 e.Å ⁻³

Table A 8. Atomic coordinates ($\times 10^4$) and equivalent isotropic displacement parameters ($\text{\AA}^2 \times 10^3$) for **66**.

	x	y	z	U(eq)
Br(1)	3802(1)	3378(1)	911(1)	41(1)
O(1)	8589(3)	2020(2)	773(1)	46(1)
N(1)	7166(3)	7645(2)	825(1)	25(1)
C(1)	8881(4)	2712(3)	1284(1)	41(1)
C(2)	7749(4)	4721(3)	1355(1)	32(1)
C(3)	8252(3)	5628(3)	806(1)	25(1)
C(4)	8091(4)	8338(3)	302(1)	31(1)
C(5)	4997(3)	8186(3)	770(1)	35(1)
C(6)	7301(3)	8457(3)	1388(1)	26(1)
C(7)	9429(3)	8037(3)	1490(1)	26(1)
C(8)	9506(3)	8391(3)	2134(1)	27(1)
C(9)	11601(3)	8136(3)	2228(1)	28(1)
C(10)	11856(3)	8220(3)	2873(1)	29(1)
C(11)	13958(3)	7976(3)	2951(1)	29(1)
C(12)	14259(3)	8008(3)	3595(1)	29(1)
C(13)	16358(3)	7773(3)	3674(1)	29(1)
C(14)	16653(3)	7797(3)	4317(1)	29(1)
C(15)	18749(3)	7567(3)	4400(1)	29(1)
C(16)	19033(3)	7591(3)	5044(1)	29(1)
C(17)	21121(3)	7367(3)	5131(1)	30(1)
C(18)	21393(3)	7395(3)	5777(1)	30(1)

C(19)	23479(3)	7169(3)	5869(1)	30(1)
C(20)	23740(3)	7210(3)	6515(1)	31(1)
C(21)	25829(3)	6966(3)	6609(1)	32(1)
C(22)	26087(4)	7012(3)	7255(1)	35(1)
C(23)	28183(4)	6750(4)	7345(1)	43(1)

Table A 9. Bond lengths [Å] and angles [°] for **66**.

O(1)-C(1)	1.408(3)
O(1)-H(1O)	0.82(4)
N(1)-C(5)	1.499(3)
N(1)-C(4)	1.503(3)
N(1)-C(6)	1.513(3)
N(1)-C(3)	1.520(3)
C(1)-C(2)	1.521(3)
C(1)-H(1A)	0.9900
C(1)-H(1B)	0.9900
C(2)-C(3)	1.515(3)
C(2)-H(2A)	0.9900
C(2)-H(2B)	0.9900
C(3)-H(3A)	0.9900
C(3)-H(3B)	0.9900
C(4)-H(4A)	0.9800
C(4)-H(4B)	0.9800
C(4)-H(4C)	0.9800
C(5)-H(5A)	0.9800
C(5)-H(5B)	0.9800
C(5)-H(5C)	0.9800
C(6)-C(7)	1.516(3)
C(6)-H(6A)	0.9900
C(6)-H(6B)	0.9900
C(7)-C(8)	1.528(3)
C(7)-H(7A)	0.9900
C(7)-H(7B)	0.9900

C(8)-C(9)	1.521(3)
C(8)-H(8A)	0.9900
C(8)-H(8B)	0.9900
C(9)-C(10)	1.524(3)
C(9)-H(9A)	0.9900
C(9)-H(9B)	0.9900
C(10)-C(11)	1.519(3)
C(10)-H(10A)	0.9900
C(10)-H(10B)	0.9900
C(11)-C(12)	1.526(3)
C(11)-H(11A)	0.9900
C(11)-H(11B)	0.9900
C(12)-C(13)	1.519(3)
C(12)-H(12A)	0.9900
C(12)-H(12B)	0.9900
C(13)-C(14)	1.522(3)
C(13)-H(13A)	0.9900
C(13)-H(13B)	0.9900
C(14)-C(15)	1.522(3)
C(14)-H(14A)	0.9900
C(14)-H(14B)	0.9900
C(15)-C(16)	1.521(3)
C(15)-H(15A)	0.9900
C(15)-H(15B)	0.9900
C(16)-C(17)	1.519(3)
C(16)-H(16A)	0.9900
C(16)-H(16B)	0.9900
C(17)-C(18)	1.523(3)
C(17)-H(17A)	0.9900
C(17)-H(17B)	0.9900
C(18)-C(19)	1.520(3)
C(18)-H(18A)	0.9900
C(18)-H(18B)	0.9900
C(19)-C(20)	1.524(3)
C(19)-H(19A)	0.9900

C(19)-H(19B)	0.9900
C(20)-C(21)	1.519(3)
C(20)-H(20A)	0.9900
C(20)-H(20B)	0.9900
C(21)-C(22)	1.522(3)
C(21)-H(21A)	0.9900
C(21)-H(21B)	0.9900
C(22)-C(23)	1.517(3)
C(22)-H(22A)	0.9900
C(22)-H(22B)	0.9900
C(23)-H(23A)	0.9800
C(23)-H(23B)	0.9800
C(23)-H(23C)	0.9800

C(1)-O(1)-H(1O)	107(3)
C(5)-N(1)-C(4)	108.15(17)
C(5)-N(1)-C(6)	108.90(16)
C(4)-N(1)-C(6)	109.80(16)
C(5)-N(1)-C(3)	109.48(17)
C(4)-N(1)-C(3)	107.72(15)
C(6)-N(1)-C(3)	112.69(15)
O(1)-C(1)-C(2)	113.7(2)
O(1)-C(1)-H(1A)	108.8
C(2)-C(1)-H(1A)	108.8
O(1)-C(1)-H(1B)	108.8
C(2)-C(1)-H(1B)	108.8
H(1A)-C(1)-H(1B)	107.7
C(3)-C(2)-C(1)	110.38(19)
C(3)-C(2)-H(2A)	109.6
C(1)-C(2)-H(2A)	109.6
C(3)-C(2)-H(2B)	109.6
C(1)-C(2)-H(2B)	109.6
H(2A)-C(2)-H(2B)	108.1
C(2)-C(3)-N(1)	114.73(17)
C(2)-C(3)-H(3A)	108.6

N(1)-C(3)-H(3A)	108.6
C(2)-C(3)-H(3B)	108.6
N(1)-C(3)-H(3B)	108.6
H(3A)-C(3)-H(3B)	107.6
N(1)-C(4)-H(4A)	109.5
N(1)-C(4)-H(4B)	109.5
H(4A)-C(4)-H(4B)	109.5
N(1)-C(4)-H(4C)	109.5
H(4A)-C(4)-H(4C)	109.5
H(4B)-C(4)-H(4C)	109.5
N(1)-C(5)-H(5A)	109.5
N(1)-C(5)-H(5B)	109.5
H(5A)-C(5)-H(5B)	109.5
N(1)-C(5)-H(5C)	109.5
H(5A)-C(5)-H(5C)	109.5
H(5B)-C(5)-H(5C)	109.5
N(1)-C(6)-C(7)	114.18(16)
N(1)-C(6)-H(6A)	108.7
C(7)-C(6)-H(6A)	108.7
N(1)-C(6)-H(6B)	108.7
C(7)-C(6)-H(6B)	108.7
H(6A)-C(6)-H(6B)	107.6
C(6)-C(7)-C(8)	111.27(17)
C(6)-C(7)-H(7A)	109.4
C(8)-C(7)-H(7A)	109.4
C(6)-C(7)-H(7B)	109.4
C(8)-C(7)-H(7B)	109.4
H(7A)-C(7)-H(7B)	108.0
C(9)-C(8)-C(7)	111.58(17)
C(9)-C(8)-H(8A)	109.3
C(7)-C(8)-H(8A)	109.3
C(9)-C(8)-H(8B)	109.3
C(7)-C(8)-H(8B)	109.3
H(8A)-C(8)-H(8B)	108.0
C(8)-C(9)-C(10)	114.25(17)

C(8)-C(9)-H(9A)	108.7
C(10)-C(9)-H(9A)	108.7
C(8)-C(9)-H(9B)	108.7
C(10)-C(9)-H(9B)	108.7
H(9A)-C(9)-H(9B)	107.6
C(11)-C(10)-C(9)	112.93(17)
C(11)-C(10)-H(10A)	109.0
C(9)-C(10)-H(10A)	109.0
C(11)-C(10)-H(10B)	109.0
C(9)-C(10)-H(10B)	109.0
H(10A)-C(10)-H(10B)	107.8
C(10)-C(11)-C(12)	113.76(17)
C(10)-C(11)-H(11A)	108.8
C(12)-C(11)-H(11A)	108.8
C(10)-C(11)-H(11B)	108.8
C(12)-C(11)-H(11B)	108.8
H(11A)-C(11)-H(11B)	107.7
C(13)-C(12)-C(11)	113.80(17)
C(13)-C(12)-H(12A)	108.8
C(11)-C(12)-H(12A)	108.8
C(13)-C(12)-H(12B)	108.8
C(11)-C(12)-H(12B)	108.8
H(12A)-C(12)-H(12B)	107.7
C(12)-C(13)-C(14)	113.56(17)
C(12)-C(13)-H(13A)	108.9
C(14)-C(13)-H(13A)	108.9
C(12)-C(13)-H(13B)	108.9
C(14)-C(13)-H(13B)	108.9
H(13A)-C(13)-H(13B)	107.7
C(15)-C(14)-C(13)	113.98(18)
C(15)-C(14)-H(14A)	108.8
C(13)-C(14)-H(14A)	108.8
C(15)-C(14)-H(14B)	108.8
C(13)-C(14)-H(14B)	108.8
H(14A)-C(14)-H(14B)	107.7

C(16)-C(15)-C(14)	113.69(18)
C(16)-C(15)-H(15A)	108.8
C(14)-C(15)-H(15A)	108.8
C(16)-C(15)-H(15B)	108.8
C(14)-C(15)-H(15B)	108.8
H(15A)-C(15)-H(15B)	107.7
C(17)-C(16)-C(15)	113.99(18)
C(17)-C(16)-H(16A)	108.8
C(15)-C(16)-H(16A)	108.8
C(17)-C(16)-H(16B)	108.8
C(15)-C(16)-H(16B)	108.8
H(16A)-C(16)-H(16B)	107.7
C(16)-C(17)-C(18)	113.69(18)
C(16)-C(17)-H(17A)	108.8
C(18)-C(17)-H(17A)	108.8
C(16)-C(17)-H(17B)	108.8
C(18)-C(17)-H(17B)	108.8
H(17A)-C(17)-H(17B)	107.7
C(19)-C(18)-C(17)	114.13(18)
C(19)-C(18)-H(18A)	108.7
C(17)-C(18)-H(18A)	108.7
C(19)-C(18)-H(18B)	108.7
C(17)-C(18)-H(18B)	108.7
H(18A)-C(18)-H(18B)	107.6
C(18)-C(19)-C(20)	113.93(18)
C(18)-C(19)-H(19A)	108.8
C(20)-C(19)-H(19A)	108.8
C(18)-C(19)-H(19B)	108.8
C(20)-C(19)-H(19B)	108.8
H(19A)-C(19)-H(19B)	107.7
C(21)-C(20)-C(19)	114.07(18)
C(21)-C(20)-H(20A)	108.7
C(19)-C(20)-H(20A)	108.7
C(21)-C(20)-H(20B)	108.7
C(19)-C(20)-H(20B)	108.7

H(20A)-C(20)-H(20B)	107.6
C(20)-C(21)-C(22)	114.05(19)
C(20)-C(21)-H(21A)	108.7
C(22)-C(21)-H(21A)	108.7
C(20)-C(21)-H(21B)	108.7
C(22)-C(21)-H(21B)	108.7
H(21A)-C(21)-H(21B)	107.6
C(23)-C(22)-C(21)	113.7(2)
C(23)-C(22)-H(22A)	108.8
C(21)-C(22)-H(22A)	108.8
C(23)-C(22)-H(22B)	108.8
C(21)-C(22)-H(22B)	108.8
H(22A)-C(22)-H(22B)	107.7
C(22)-C(23)-H(23A)	109.5
C(22)-C(23)-H(23B)	109.5
H(23A)-C(23)-H(23B)	109.5
C(22)-C(23)-H(23C)	109.5
H(23A)-C(23)-H(23C)	109.5
H(23B)-C(23)-H(23C)	109.5

Symmetry transformations used to generate equivalent atoms:

Table A 10. Anisotropic displacement parameters ($\text{\AA}^2 \times 10^3$) for **66**. The anisotropic displacement factor exponent takes the form: $-2p^2[h^2 a^{*2}U^{11} + \dots + 2 h k a^* b^* U^{12}]$

	U11	U22	U33	U23	U13	U12
Br(1)	28(1)	43(1)	48(1)	-13(1)	-9(1)	-9(1)
O(1)	38(1)	32(1)	66(1)	-10(1)	6(1)	-18(1)
N(1)	28(1)	23(1)	20(1)	0(1)	-3(1)	-7(1)
C(1)	39(1)	29(1)	56(2)	10(1)	-7(1)	-16(1)
C(2)	36(1)	29(1)	33(1)	3(1)	-5(1)	-16(1)
C(3)	26(1)	20(1)	28(1)	-2(1)	-3(1)	-9(1)
C(4)	47(1)	31(1)	19(1)	2(1)	-4(1)	-18(1)
C(5)	27(1)	40(1)	32(1)	1(1)	-9(1)	-6(1)
C(6)	32(1)	22(1)	18(1)	-2(1)	-4(1)	-5(1)
C(7)	33(1)	22(1)	20(1)	-2(1)	-3(1)	-9(1)
C(8)	34(1)	25(1)	19(1)	0(1)	-4(1)	-8(1)
C(9)	33(1)	27(1)	20(1)	-1(1)	-4(1)	-7(1)
C(10)	33(1)	29(1)	21(1)	-1(1)	-4(1)	-9(1)
C(11)	33(1)	28(1)	20(1)	0(1)	-3(1)	-8(1)
C(12)	33(1)	30(1)	21(1)	-1(1)	-4(1)	-9(1)
C(13)	32(1)	27(1)	23(1)	-1(1)	-3(1)	-7(1)
C(14)	32(1)	28(1)	23(1)	-2(1)	-3(1)	-9(1)
C(15)	32(1)	26(1)	23(1)	-1(1)	-3(1)	-7(1)
C(16)	31(1)	28(1)	25(1)	-3(1)	-3(1)	-8(1)
C(17)	31(1)	27(1)	26(1)	-1(1)	-4(1)	-7(1)
C(18)	31(1)	27(1)	27(1)	-2(1)	-3(1)	-8(1)
C(19)	30(1)	28(1)	29(1)	-1(1)	-4(1)	-7(1)
C(20)	31(1)	28(1)	30(1)	-4(1)	-4(1)	-9(1)
C(21)	30(1)	28(1)	32(1)	-1(1)	-5(1)	-8(1)
C(22)	34(1)	35(1)	34(1)	-3(1)	-6(1)	-12(1)
C(23)	39(1)	47(1)	44(1)	0(1)	-14(1)	-15(1)

Table A 11. Hydrogen coordinates ($\times 10^4$) and isotropic displacement parameters ($\text{\AA}^2 \times 10^3$) for **66**.

	x	y	z	U(eq)
H(1A)	10334	2389	1272	49
H(1B)	8444	2149	1634	49
H(2A)	6285	5047	1426	38
H(2B)	8118	5131	1701	38
H(3A)	7921	5172	462	30
H(3B)	9718	5293	742	30
H(4A)	7437	9641	308	47
H(4B)	7909	7879	-63	47
H(4C)	9529	7944	318	47
H(5A)	4300	9488	778	53
H(5B)	4378	7707	1100	53
H(5C)	4894	7718	397	53
H(6A)	6639	8024	1727	32
H(6B)	6548	9764	1377	32
H(7A)	9956	8777	1230	31
H(7B)	10297	6772	1386	31
H(8A)	8541	9624	2249	33
H(8B)	9097	7571	2390	33
H(9A)	11925	9065	2010	34
H(9B)	12582	6967	2056	34
H(10A)	10874	9385	3047	35
H(10B)	11552	7282	3091	35
H(11A)	14245	8933	2740	35
H(11B)	14939	6826	2766	35
H(12A)	13274	9156	3780	35
H(12B)	13977	7049	3805	35
H(13A)	16639	8736	3465	35
H(13B)	17345	6627	3487	35
H(14A)	15661	8940	4503	35

H(14B)	16374	6832	4524	35
H(15A)	19742	6424	4214	35
H(15B)	19029	8533	4194	35
H(16A)	18036	8733	5230	35
H(16B)	18756	6624	5250	35
H(17A)	21400	8333	4925	36
H(17B)	22119	6224	4946	36
H(18A)	20395	8539	5961	36
H(18B)	21109	6431	5983	36
H(19A)	23768	8128	5661	37
H(19B)	24478	6021	5687	37
H(20A)	22750	8363	6696	37
H(20B)	23437	6259	6724	37
H(21A)	26134	7916	6400	38
H(21B)	26819	5812	6430	38
H(22A)	25108	8172	7433	42
H(22B)	25771	6070	7465	42
H(23A)	28269	6718	7769	65
H(23B)	28465	7736	7168	65
H(23C)	29169	5625	7156	65
H(10)	7360(60)	2390(50)	778(17)	70(11)

Table A 12. Torsion angles [°] for **66**.

O(1)-C(1)-C(2)-C(3)	-54.0(3)
C(1)-C(2)-C(3)-N(1)	178.88(18)
C(5)-N(1)-C(3)-C(2)	-72.3(2)
C(4)-N(1)-C(3)-C(2)	170.31(18)
C(6)-N(1)-C(3)-C(2)	49.0(2)
C(5)-N(1)-C(6)-C(7)	-178.89(17)
C(4)-N(1)-C(6)-C(7)	-60.6(2)
C(3)-N(1)-C(6)-C(7)	59.4(2)
N(1)-C(6)-C(7)-C(8)	-162.72(16)
C(6)-C(7)-C(8)-C(9)	-174.78(17)

C(7)-C(8)-C(9)-C(10)	-172.08(17)
C(8)-C(9)-C(10)-C(11)	-179.50(17)
C(9)-C(10)-C(11)-C(12)	-178.52(18)
C(10)-C(11)-C(12)-C(13)	-179.76(18)
C(11)-C(12)-C(13)-C(14)	-179.72(18)
C(12)-C(13)-C(14)-C(15)	-179.82(18)
C(13)-C(14)-C(15)-C(16)	-179.94(18)
C(14)-C(15)-C(16)-C(17)	-179.86(18)
C(15)-C(16)-C(17)-C(18)	179.90(18)
C(16)-C(17)-C(18)-C(19)	179.89(18)
C(17)-C(18)-C(19)-C(20)	179.61(18)
C(18)-C(19)-C(20)-C(21)	179.43(18)
C(19)-C(20)-C(21)-C(22)	179.86(19)
C(20)-C(21)-C(22)-C(23)	179.4(2)

Symmetry transformations used to generate equivalent atoms:

Table A 13. Hydrogen bonds for **66** [\AA and $^\circ$].

D-H...A	d(D-H)	d(H...A)	d(D...A)	$\angle(\text{DHA})$
O(1)-H(1O)...Br(1)	0.82(4)	2.39(4)	3.206(2)	173(4)

Symmetry transformations used to generate equivalent atoms:

Table A 14. Crystal data and structure refinement for **19**.

Identification code	d12321	
Empirical formula	$\text{C}_{16} \text{H}_{22} \text{N O}_5 \text{P}$	
Formula weight	339.32	
Temperature	150(2) K	
Wavelength	1.54178 \AA	
Crystal system	Monoclinic	
Space group	P 21/n	
Unit cell dimensions	$a = 12.9548(6) \text{\AA}$	$\alpha = 90^\circ$.

	$b = 8.0163(4) \text{ \AA}$	$\beta = 91.100(2)^\circ$.
	$c = 16.5747(8) \text{ \AA}$	$\gamma = 90^\circ$.
Volume	$1720.96(14) \text{ \AA}^3$	
Z	4	
Density (calculated)	1.310 Mg/m^3	
Absorption coefficient	1.633 mm^{-1}	
F(000)	720	
Crystal size	$0.32 \times 0.12 \times 0.09 \text{ mm}^3$	
Theta range for data collection	4.29 to 66.38° .	
Index ranges	$-15 \leq h \leq 15$, $-9 \leq k \leq 4$, $-19 \leq l \leq 19$	
Reflections collected	11311	
Independent reflections	2936 [$R(\text{int}) = 0.0258$]	
Completeness to $\theta = 66.38^\circ$	96.8 %	
Absorption correction	Semi-empirical from equivalents	
Max. and min. transmission	0.7528 and 0.6679	
Refinement method	Full-matrix least-squares on F^2	
Data / restraints / parameters	2936 / 0 / 210	
Goodness-of-fit on F^2	1.059	
Final R indices [$I > 2\sigma(I)$]	$R1 = 0.0386$, $wR2 = 0.0996$	
R indices (all data)	$R1 = 0.0398$, $wR2 = 0.1007$	
Largest diff. peak and hole	0.570 and $-0.438 \text{ e.\AA}^{-3}$	

Table A 15. Atomic coordinates ($\times 10^4$) and equivalent isotropic displacement parameters ($\text{\AA}^2 \times 10^3$) for **19**. $U(\text{eq})$ is defined as one third of the trace of the orthogonalized U_{ij} tensor.

	x	y	z	$U(\text{eq})$
P(1)	5032(1)	2830(1)	1022(1)	25(1)
O(1)	-396(1)	5618(2)	1055(1)	48(1)
O(2)	1813(1)	9911(2)	1635(1)	40(1)
O(3)	5702(1)	2250(2)	375(1)	34(1)
O(4)	4675(1)	1417(2)	1618(1)	30(1)
O(5)	5542(1)	4128(2)	1622(1)	32(1)
N(1)	894(1)	7480(2)	1408(1)	30(1)

C(1)	-83(1)	7026(2)	1120(1)	31(1)
C(2)	-626(1)	8625(2)	933(1)	25(1)
C(3)	-1613(1)	8909(2)	636(1)	31(1)
C(4)	-1919(1)	10561(2)	534(1)	32(1)
C(5)	-1250(2)	11859(2)	718(1)	32(1)
C(6)	-252(1)	11566(2)	1011(1)	29(1)
C(7)	39(1)	9925(2)	1116(1)	24(1)
C(8)	1032(1)	9201(2)	1418(1)	27(1)
C(9)	1673(2)	6275(3)	1682(1)	38(1)
C(10)	2339(1)	5647(2)	1004(1)	29(1)
C(11)	3170(1)	4463(2)	1327(1)	32(1)
C(12)	3907(1)	3914(2)	671(1)	28(1)
C(13)	4434(2)	-244(2)	1316(1)	36(1)
C(14)	5232(2)	-1432(3)	1619(2)	61(1)
C(15)	6535(1)	3712(3)	1986(1)	37(1)
C(16)	7137(2)	5228(3)	2104(2)	74(1)

Table A 16. Bond lengths [\AA] and angles [$^\circ$] for **19**.

P(1)-O(3)	1.4687(13)
P(1)-O(5)	1.5765(13)
P(1)-O(4)	1.5782(12)
P(1)-C(12)	1.7837(17)
O(1)-C(1)	1.204(2)
O(2)-C(8)	1.210(2)
O(4)-C(13)	1.454(2)
O(5)-C(15)	1.450(2)
N(1)-C(8)	1.390(2)
N(1)-C(1)	1.393(2)
N(1)-C(9)	1.463(2)
C(1)-C(2)	1.492(2)
C(2)-C(3)	1.381(2)
C(2)-C(7)	1.381(2)
C(3)-C(4)	1.392(3)

C(3)-H(3A)	0.9500
C(4)-C(5)	1.384(3)
C(4)-H(4A)	0.9500
C(5)-C(6)	1.392(3)
C(5)-H(5A)	0.9500
C(6)-C(7)	1.379(2)
C(6)-H(6A)	0.9500
C(7)-C(8)	1.489(2)
C(9)-C(10)	1.515(2)
C(9)-H(9A)	0.9900
C(9)-H(9B)	0.9900
C(10)-C(11)	1.524(2)
C(10)-H(10A)	0.9900
C(10)-H(10B)	0.9900
C(11)-C(12)	1.525(2)
C(11)-H(11A)	0.9900
C(11)-H(11B)	0.9900
C(12)-H(12A)	0.9900
C(12)-H(12B)	0.9900
C(13)-C(14)	1.486(3)
C(13)-H(13A)	0.9900
C(13)-H(13B)	0.9900
C(14)-H(14A)	0.9800
C(14)-H(14B)	0.9800
C(14)-H(14C)	0.9800
C(15)-C(16)	1.455(3)
C(15)-H(15A)	0.9900
C(15)-H(15B)	0.9900
C(16)-H(16A)	0.9800
C(16)-H(16B)	0.9800
C(16)-H(16C)	0.9800
O(3)-P(1)-O(5)	115.03(7)
O(3)-P(1)-O(4)	114.48(7)
O(5)-P(1)-O(4)	101.70(7)
O(3)-P(1)-C(12)	114.03(8)

O(5)-P(1)-C(12)	102.37(8)
O(4)-P(1)-C(12)	107.84(8)
C(13)-O(4)-P(1)	120.34(11)
C(15)-O(5)-P(1)	118.00(11)
C(8)-N(1)-C(1)	112.26(14)
C(8)-N(1)-C(9)	124.31(16)
C(1)-N(1)-C(9)	123.41(16)
O(1)-C(1)-N(1)	125.33(17)
O(1)-C(1)-C(2)	129.12(17)
N(1)-C(1)-C(2)	105.54(15)
C(3)-C(2)-C(7)	121.56(16)
C(3)-C(2)-C(1)	130.18(17)
C(7)-C(2)-C(1)	108.26(15)
C(2)-C(3)-C(4)	117.36(17)
C(2)-C(3)-H(3A)	121.3
C(4)-C(3)-H(3A)	121.3
C(5)-C(4)-C(3)	120.86(16)
C(5)-C(4)-H(4A)	119.6
C(3)-C(4)-H(4A)	119.6
C(4)-C(5)-C(6)	121.55(17)
C(4)-C(5)-H(5A)	119.2
C(6)-C(5)-H(5A)	119.2
C(7)-C(6)-C(5)	117.08(17)
C(7)-C(6)-H(6A)	121.5
C(5)-C(6)-H(6A)	121.5
C(6)-C(7)-C(2)	121.59(16)
C(6)-C(7)-C(8)	130.32(16)
C(2)-C(7)-C(8)	108.09(15)
O(2)-C(8)-N(1)	125.22(16)
O(2)-C(8)-C(7)	128.94(17)
N(1)-C(8)-C(7)	105.84(15)
N(1)-C(9)-C(10)	112.86(14)
N(1)-C(9)-H(9A)	109.0
C(10)-C(9)-H(9A)	109.0
N(1)-C(9)-H(9B)	109.0

C(10)-C(9)-H(9B)	109.0
H(9A)-C(9)-H(9B)	107.8
C(9)-C(10)-C(11)	110.82(14)
C(9)-C(10)-H(10A)	109.5
C(11)-C(10)-H(10A)	109.5
C(9)-C(10)-H(10B)	109.5
C(11)-C(10)-H(10B)	109.5
H(10A)-C(10)-H(10B)	108.1
C(10)-C(11)-C(12)	112.22(14)
C(10)-C(11)-H(11A)	109.2
C(12)-C(11)-H(11A)	109.2
C(10)-C(11)-H(11B)	109.2
C(12)-C(11)-H(11B)	109.2
H(11A)-C(11)-H(11B)	107.9
C(11)-C(12)-P(1)	115.29(12)
C(11)-C(12)-H(12A)	108.5
P(1)-C(12)-H(12A)	108.5
C(11)-C(12)-H(12B)	108.5
P(1)-C(12)-H(12B)	108.5
H(12A)-C(12)-H(12B)	107.5
O(4)-C(13)-C(14)	109.08(16)
O(4)-C(13)-H(13A)	109.9
C(14)-C(13)-H(13A)	109.9
O(4)-C(13)-H(13B)	109.9
C(14)-C(13)-H(13B)	109.9
H(13A)-C(13)-H(13B)	108.3
C(13)-C(14)-H(14A)	109.5
C(13)-C(14)-H(14B)	109.5
H(14A)-C(14)-H(14B)	109.5
C(13)-C(14)-H(14C)	109.5
H(14A)-C(14)-H(14C)	109.5
H(14B)-C(14)-H(14C)	109.5
O(5)-C(15)-C(16)	109.45(18)
O(5)-C(15)-H(15A)	109.8
C(16)-C(15)-H(15A)	109.8

O(5)-C(15)-H(15B)	109.8
C(16)-C(15)-H(15B)	109.8
H(15A)-C(15)-H(15B)	108.2
C(15)-C(16)-H(16A)	109.5
C(15)-C(16)-H(16B)	109.5
H(16A)-C(16)-H(16B)	109.5
C(15)-C(16)-H(16C)	109.5
H(16A)-C(16)-H(16C)	109.5
H(16B)-C(16)-H(16C)	109.5

Symmetry transformations used to generate equivalent atoms:

Table A 17. Anisotropic displacement parameters ($\text{\AA}^2 \times 10^3$) for **19**. The anisotropic displacement factor exponent takes the form: $-2p^2[h^2 a^{*2} U^{11} + \dots + 2 h k a^* b^* U^{12}]$

	U ¹¹	U ²²	U ³³	U ²³	U ¹³	U ¹²
P(1)	22(1)	23(1)	30(1)	0(1)	1(1)	6(1)
O(1)	47(1)	24(1)	71(1)	2(1)	4(1)	4(1)
O(2)	25(1)	55(1)	38(1)	-3(1)	-5(1)	0(1)
O(3)	29(1)	36(1)	38(1)	0(1)	7(1)	10(1)
O(4)	35(1)	23(1)	33(1)	0(1)	3(1)	4(1)
O(5)	26(1)	26(1)	44(1)	-3(1)	-7(1)	5(1)
N(1)	26(1)	33(1)	31(1)	5(1)	2(1)	13(1)
C(1)	29(1)	28(1)	36(1)	2(1)	6(1)	8(1)
C(2)	23(1)	26(1)	27(1)	0(1)	4(1)	5(1)
C(3)	23(1)	36(1)	35(1)	-1(1)	1(1)	2(1)
C(4)	24(1)	44(1)	30(1)	3(1)	2(1)	13(1)
C(5)	36(1)	29(1)	32(1)	4(1)	6(1)	14(1)
C(6)	32(1)	26(1)	30(1)	-1(1)	5(1)	3(1)
C(7)	22(1)	28(1)	22(1)	0(1)	4(1)	4(1)
C(8)	24(1)	37(1)	21(1)	0(1)	3(1)	6(1)
C(9)	34(1)	46(1)	33(1)	10(1)	4(1)	23(1)
C(10)	26(1)	32(1)	28(1)	5(1)	1(1)	10(1)
C(11)	27(1)	37(1)	31(1)	8(1)	4(1)	13(1)

C(12)	24(1)	33(1)	28(1)	1(1)	0(1)	7(1)
C(13)	35(1)	27(1)	46(1)	-4(1)	2(1)	-4(1)
C(14)	67(2)	30(1)	86(2)	1(1)	-6(1)	10(1)
C(15)	26(1)	48(1)	36(1)	-1(1)	-5(1)	8(1)
C(16)	40(1)	50(2)	132(3)	-12(2)	-24(2)	-3(1)

Table A 18. Hydrogen coordinates ($\times 10^4$) and isotropic displacement parameters ($\text{\AA}^2 \times 10^{-3}$) for **19**.

	x	y	z	U(eq)
H(3A)	-2066	8012	506	37
H(4A)	-2596	10801	336	39
H(5A)	-1477	12976	643	39
H(6A)	208	12458	1133	35
H(9A)	1324	5315	1934	45
H(9B)	2122	6804	2099	45
H(10A)	2668	6605	735	35
H(10B)	1900	5059	600	35
H(11A)	2836	3467	1559	38
H(11B)	3568	5025	1764	38
H(12A)	4128	4914	370	34
H(12B)	3525	3184	287	34
H(13A)	4421	-238	718	43
H(13B)	3745	-592	1501	43
H(14A)	5056	-2563	1438	91
H(14B)	5259	-1401	2210	91
H(14C)	5906	-1116	1409	91
H(15A)	6909	2934	1632	44
H(15B)	6434	3156	2512	44
H(16A)	7791	4956	2380	112
H(16B)	6748	6018	2432	112

Table A 19. Torsion angles [°] for **19**.

O(3)-P(1)-O(4)-C(13)	-37.34(15)
O(5)-P(1)-O(4)-C(13)	-162.02(12)
C(12)-P(1)-O(4)-C(13)	90.73(14)
O(3)-P(1)-O(5)-C(15)	-51.29(15)
O(4)-P(1)-O(5)-C(15)	73.03(14)
C(12)-P(1)-O(5)-C(15)	-175.52(13)
C(8)-N(1)-C(1)-O(1)	-179.67(18)
C(9)-N(1)-C(1)-O(1)	-0.8(3)
C(8)-N(1)-C(1)-C(2)	-0.44(19)
C(9)-N(1)-C(1)-C(2)	178.46(15)
O(1)-C(1)-C(2)-C(3)	-0.4(3)
N(1)-C(1)-C(2)-C(3)	-179.58(17)
O(1)-C(1)-C(2)-C(7)	179.2(2)
N(1)-C(1)-C(2)-C(7)	-0.04(18)
C(7)-C(2)-C(3)-C(4)	-0.7(3)
C(1)-C(2)-C(3)-C(4)	178.83(17)
C(2)-C(3)-C(4)-C(5)	0.6(3)
C(3)-C(4)-C(5)-C(6)	-0.1(3)
C(4)-C(5)-C(6)-C(7)	-0.5(3)
C(5)-C(6)-C(7)-C(2)	0.5(2)
C(5)-C(6)-C(7)-C(8)	-179.45(16)
C(3)-C(2)-C(7)-C(6)	0.1(3)
C(1)-C(2)-C(7)-C(6)	-179.48(15)
C(3)-C(2)-C(7)-C(8)	-179.95(15)
C(1)-C(2)-C(7)-C(8)	0.46(18)
C(1)-N(1)-C(8)-O(2)	-179.32(16)
C(9)-N(1)-C(8)-O(2)	1.8(3)
C(1)-N(1)-C(8)-C(7)	0.71(19)
C(9)-N(1)-C(8)-C(7)	-178.17(14)
C(6)-C(7)-C(8)-O(2)	-0.7(3)

C(2)-C(7)-C(8)-O(2)	179.32(17)
C(6)-C(7)-C(8)-N(1)	179.22(17)
C(2)-C(7)-C(8)-N(1)	-0.71(18)
C(8)-N(1)-C(9)-C(10)	-93.4(2)
C(1)-N(1)-C(9)-C(10)	87.8(2)
N(1)-C(9)-C(10)-C(11)	177.22(17)
C(9)-C(10)-C(11)-C(12)	-175.49(16)
C(10)-C(11)-C(12)-P(1)	169.45(13)
O(3)-P(1)-C(12)-C(11)	177.35(13)
O(5)-P(1)-C(12)-C(11)	-57.76(15)
O(4)-P(1)-C(12)-C(11)	49.02(16)
P(1)-O(4)-C(13)-C(14)	111.31(18)
P(1)-O(5)-C(15)-C(16)	146.77(19)

Symmetry transformations used to generate equivalent atoms:

Table A 20. Crystal data and structure refinement for **220**.

Identification code	d1317	
Empirical formula	C ₂₈ H ₃₅ Br N ₄ O ₄ S	
Formula weight	603.57	
Temperature	147(2) K	
Wavelength	0.71073 Å	
Crystal system	Triclinic	
Space group	P -1	
Unit cell dimensions	a = 8.4368(14) Å	α = 103.268(4)°.
	b = 11.2944(19) Å	β = 93.320(4)°.
	c = 16.383(3) Å	γ = 109.880(4)°.
Volume	1413.1(4) Å ³	
Z	2	
Density (calculated)	1.419 Mg/m ³	
Absorption coefficient	1.569 mm ⁻¹	
F(000)	628	
Crystal size	0.48 x 0.22 x 0.18 mm ³	
Theta range for data collection	1.29 to 27.55°.	
Index ranges	-10 ≤ h ≤ 10, -10 ≤ k ≤ 14, -21 ≤ l ≤ 19	
Reflections collected	23597	
Independent reflections	6441 [R(int) = 0.0272]	
Completeness to theta = 27.55°	99.0 %	
Absorption correction	Semi-empirical from equivalents	
Max. and min. transmission	0.7456 and 0.6341	
Refinement method	Full-matrix least-squares on F ²	
Data / restraints / parameters	6441 / 0 / 345	
Goodness-of-fit on F ²	1.063	
Final R indices [I > 2σ(I)]	R1 = 0.0272, wR2 = 0.0728	
R indices (all data)	R1 = 0.0304, wR2 = 0.0744	
Largest diff. peak and hole	0.959 and -0.336 e.Å ⁻³	

Table A 21. Atomic coordinates ($\times 10^4$) and equivalent isotropic displacement parameters ($\text{\AA}^2 \times 10^3$) for **220**. U(eq) is defined as one third of the trace of the orthogonalized U_{ij} tensor.

	x	y	z	U(eq)
Br(1)	2188(1)	3861(1)	3729(1)	27(1)
S(1)	3811(1)	6885(1)	2219(1)	20(1)
O(1)	2067(1)	6168(1)	1839(1)	30(1)
O(2)	4506(2)	8277(1)	2356(1)	28(1)
O(3)	8054(2)	1106(1)	4611(1)	34(1)
O(4)	7236(2)	800(1)	1778(1)	36(1)
N(1)	7134(2)	2839(1)	206(1)	26(1)
N(2)	3995(2)	6607(1)	3134(1)	22(1)
N(3)	8227(2)	5296(1)	3634(1)	20(1)
N(4)	7394(2)	1154(1)	3232(1)	24(1)
C(1)	5114(2)	6259(1)	1571(1)	19(1)
C(2)	6334(2)	7135(2)	1266(1)	22(1)
C(3)	7375(2)	6708(2)	725(1)	25(1)
C(4)	7226(2)	5431(2)	524(1)	22(1)
C(5)	6030(2)	4511(1)	856(1)	18(1)
C(6)	5916(2)	3173(2)	667(1)	21(1)
C(7)	4602(2)	2278(2)	916(1)	26(1)
C(8)	3426(2)	2666(2)	1376(1)	26(1)
C(9)	3556(2)	3942(2)	1604(1)	22(1)
C(10)	4877(2)	4903(1)	1358(1)	18(1)
C(11)	8873(2)	3366(2)	668(1)	36(1)
C(12)	6664(3)	1462(2)	-225(1)	33(1)
C(13)	5422(2)	7415(2)	3809(1)	27(1)
C(14)	7060(2)	7128(2)	3723(1)	26(1)
C(15)	6733(2)	5734(2)	3753(1)	22(1)
C(16)	8737(2)	5276(2)	2781(1)	36(1)
C(17)	9745(2)	6169(2)	4284(1)	28(1)
C(18)	7741(2)	3948(2)	3807(1)	28(1)
C(19)	6248(2)	2904(2)	3194(1)	35(1)
C(20)	5946(2)	1570(2)	3342(1)	31(1)

C(21)	8292(2)	916(2)	3876(1)	24(1)
C(22)	9505(2)	363(1)	3470(1)	22(1)
C(23)	10692(2)	-51(2)	3816(1)	26(1)
C(24)	11596(2)	-594(2)	3260(1)	30(1)
C(25)	11340(2)	-696(2)	2402(1)	32(1)
C(26)	10162(2)	-259(2)	2060(1)	29(1)
C(27)	9251(2)	260(2)	2613(1)	23(1)
C(28)	7873(2)	753(2)	2444(1)	25(1)

Table A 22. Bond lengths [Å] and angles [°] for **220**.

S(1)-O(1)	1.4354(12)
S(1)-O(2)	1.4360(12)
S(1)-N(2)	1.6106(14)
S(1)-C(1)	1.7763(15)
O(3)-C(21)	1.214(2)
O(4)-C(28)	1.208(2)
N(1)-C(6)	1.411(2)
N(1)-C(12)	1.456(2)
N(1)-C(11)	1.467(2)
N(2)-C(13)	1.462(2)
N(2)-H(2N)	0.8800
N(3)-C(16)	1.484(2)
N(3)-C(17)	1.499(2)
N(3)-C(15)	1.5101(18)
N(3)-C(18)	1.534(2)
N(4)-C(21)	1.391(2)
N(4)-C(28)	1.398(2)
N(4)-C(20)	1.457(2)
C(1)-C(2)	1.372(2)
C(1)-C(10)	1.431(2)
C(2)-C(3)	1.404(2)
C(2)-H(2A)	0.9500
C(3)-C(4)	1.363(2)

C(3)-H(3A)	0.9500
C(4)-C(5)	1.416(2)
C(4)-H(4A)	0.9500
C(5)-C(10)	1.427(2)
C(5)-C(6)	1.439(2)
C(6)-C(7)	1.377(2)
C(7)-C(8)	1.405(2)
C(7)-H(7A)	0.9500
C(8)-C(9)	1.367(2)
C(8)-H(8A)	0.9500
C(9)-C(10)	1.418(2)
C(9)-H(9A)	0.9500
C(11)-H(11A)	0.9800
C(11)-H(11B)	0.9800
C(11)-H(11C)	0.9800
C(12)-H(12A)	0.9800
C(12)-H(12B)	0.9800
C(12)-H(12C)	0.9800
C(13)-C(14)	1.530(2)
C(13)-H(13A)	0.9900
C(13)-H(13B)	0.9900
C(14)-C(15)	1.516(2)
C(14)-H(14A)	0.9900
C(14)-H(14B)	0.9900
C(15)-H(15A)	0.9900
C(15)-H(15B)	0.9900
C(16)-H(16A)	0.9800
C(16)-H(16B)	0.9800
C(16)-H(16C)	0.9800
C(17)-H(17A)	0.9800
C(17)-H(17B)	0.9800
C(17)-H(17C)	0.9800
C(18)-C(19)	1.512(2)
C(18)-H(18A)	0.9900
C(18)-H(18B)	0.9900

C(19)-C(20)	1.519(2)
C(19)-H(19A)	0.9900
C(19)-H(19B)	0.9900
C(20)-H(20A)	0.9900
C(20)-H(20B)	0.9900
C(21)-C(22)	1.484(2)
C(22)-C(27)	1.381(2)
C(22)-C(23)	1.385(2)
C(23)-C(24)	1.389(2)
C(23)-H(23A)	0.9500
C(24)-C(25)	1.383(3)
C(24)-H(24A)	0.9500
C(25)-C(26)	1.393(2)
C(25)-H(25A)	0.9500
C(26)-C(27)	1.378(2)
C(26)-H(26A)	0.9500
C(27)-C(28)	1.487(2)
O(1)-S(1)-O(2)	119.72(7)
O(1)-S(1)-N(2)	106.44(7)
O(2)-S(1)-N(2)	106.73(7)
O(1)-S(1)-C(1)	107.91(7)
O(2)-S(1)-C(1)	106.14(7)
N(2)-S(1)-C(1)	109.69(7)
C(6)-N(1)-C(12)	116.00(14)
C(6)-N(1)-C(11)	115.17(13)
C(12)-N(1)-C(11)	110.27(14)
C(13)-N(2)-S(1)	123.19(11)
C(13)-N(2)-H(2N)	118.4
S(1)-N(2)-H(2N)	118.4
C(16)-N(3)-C(17)	108.20(13)
C(16)-N(3)-C(15)	112.47(13)
C(17)-N(3)-C(15)	111.09(12)
C(16)-N(3)-C(18)	111.72(14)
C(17)-N(3)-C(18)	105.45(12)
C(15)-N(3)-C(18)	107.70(11)

C(21)-N(4)-C(28)	111.74(13)
C(21)-N(4)-C(20)	123.86(15)
C(28)-N(4)-C(20)	123.70(14)
C(2)-C(1)-C(10)	121.51(14)
C(2)-C(1)-S(1)	116.72(11)
C(10)-C(1)-S(1)	121.75(11)
C(1)-C(2)-C(3)	120.15(14)
C(1)-C(2)-H(2A)	119.9
C(3)-C(2)-H(2A)	119.9
C(4)-C(3)-C(2)	120.37(14)
C(4)-C(3)-H(3A)	119.8
C(2)-C(3)-H(3A)	119.8
C(3)-C(4)-C(5)	120.96(14)
C(3)-C(4)-H(4A)	119.5
C(5)-C(4)-H(4A)	119.5
C(4)-C(5)-C(10)	119.58(13)
C(4)-C(5)-C(6)	120.87(13)
C(10)-C(5)-C(6)	119.50(13)
C(7)-C(6)-N(1)	123.29(14)
C(7)-C(6)-C(5)	118.87(14)
N(1)-C(6)-C(5)	117.80(13)
C(6)-C(7)-C(8)	120.89(14)
C(6)-C(7)-H(7A)	119.6
C(8)-C(7)-H(7A)	119.6
C(9)-C(8)-C(7)	121.53(15)
C(9)-C(8)-H(8A)	119.2
C(7)-C(8)-H(8A)	119.2
C(8)-C(9)-C(10)	119.92(14)
C(8)-C(9)-H(9A)	120.0
C(10)-C(9)-H(9A)	120.0
C(9)-C(10)-C(5)	119.06(13)
C(9)-C(10)-C(1)	123.77(14)
C(5)-C(10)-C(1)	117.15(13)
N(1)-C(11)-H(11A)	109.5
N(1)-C(11)-H(11B)	109.5

H(11A)-C(11)-H(11B)	109.5
N(1)-C(11)-H(11C)	109.5
H(11A)-C(11)-H(11C)	109.5
H(11B)-C(11)-H(11C)	109.5
N(1)-C(12)-H(12A)	109.5
N(1)-C(12)-H(12B)	109.5
H(12A)-C(12)-H(12B)	109.5
N(1)-C(12)-H(12C)	109.5
H(12A)-C(12)-H(12C)	109.5
H(12B)-C(12)-H(12C)	109.5
N(2)-C(13)-C(14)	115.10(13)
N(2)-C(13)-H(13A)	108.5
C(14)-C(13)-H(13A)	108.5
N(2)-C(13)-H(13B)	108.5
C(14)-C(13)-H(13B)	108.5
H(13A)-C(13)-H(13B)	107.5
C(15)-C(14)-C(13)	109.60(13)
C(15)-C(14)-H(14A)	109.8
C(13)-C(14)-H(14A)	109.8
C(15)-C(14)-H(14B)	109.8
C(13)-C(14)-H(14B)	109.8
H(14A)-C(14)-H(14B)	108.2
N(3)-C(15)-C(14)	115.29(12)
N(3)-C(15)-H(15A)	108.5
C(14)-C(15)-H(15A)	108.5
N(3)-C(15)-H(15B)	108.5
C(14)-C(15)-H(15B)	108.5
H(15A)-C(15)-H(15B)	107.5
N(3)-C(16)-H(16A)	109.5
N(3)-C(16)-H(16B)	109.5
H(16A)-C(16)-H(16B)	109.5
N(3)-C(16)-H(16C)	109.5
H(16A)-C(16)-H(16C)	109.5
H(16B)-C(16)-H(16C)	109.5
N(3)-C(17)-H(17A)	109.5

N(3)-C(17)-H(17B)	109.5
H(17A)-C(17)-H(17B)	109.5
N(3)-C(17)-H(17C)	109.5
H(17A)-C(17)-H(17C)	109.5
H(17B)-C(17)-H(17C)	109.5
C(19)-C(18)-N(3)	113.79(14)
C(19)-C(18)-H(18A)	108.8
N(3)-C(18)-H(18A)	108.8
C(19)-C(18)-H(18B)	108.8
N(3)-C(18)-H(18B)	108.8
H(18A)-C(18)-H(18B)	107.7
C(18)-C(19)-C(20)	111.13(15)
C(18)-C(19)-H(19A)	109.4
C(20)-C(19)-H(19A)	109.4
C(18)-C(19)-H(19B)	109.4
C(20)-C(19)-H(19B)	109.4
H(19A)-C(19)-H(19B)	108.0
N(4)-C(20)-C(19)	113.48(14)
N(4)-C(20)-H(20A)	108.9
C(19)-C(20)-H(20A)	108.9
N(4)-C(20)-H(20B)	108.9
C(19)-C(20)-H(20B)	108.9
H(20A)-C(20)-H(20B)	107.7
O(3)-C(21)-N(4)	125.03(15)
O(3)-C(21)-C(22)	128.86(15)
N(4)-C(21)-C(22)	106.07(14)
C(27)-C(22)-C(23)	121.48(15)
C(27)-C(22)-C(21)	108.16(13)
C(23)-C(22)-C(21)	130.33(15)
C(22)-C(23)-C(24)	117.00(16)
C(22)-C(23)-H(23A)	121.5
C(24)-C(23)-H(23A)	121.5
C(25)-C(24)-C(23)	121.38(15)
C(25)-C(24)-H(24A)	119.3
C(23)-C(24)-H(24A)	119.3

C(24)-C(25)-C(26)	121.31(16)
C(24)-C(25)-H(25A)	119.3
C(26)-C(25)-H(25A)	119.3
C(27)-C(26)-C(25)	117.04(16)
C(27)-C(26)-H(26A)	121.5
C(25)-C(26)-H(26A)	121.5
C(26)-C(27)-C(22)	121.78(15)
C(26)-C(27)-C(28)	129.97(16)
C(22)-C(27)-C(28)	108.23(14)
O(4)-C(28)-N(4)	124.86(15)
O(4)-C(28)-C(27)	129.38(16)
N(4)-C(28)-C(27)	105.75(14)

Symmetry transformations used to generate equivalent atoms:

Table A 23. Anisotropic displacement parameters ($\text{\AA}^2 \times 10^3$) for **222**. The anisotropic displacement factor exponent takes the form: $-2p^2[h^2 a^*2U^{11} + \dots + 2 h k a^* b^* U^{12}]$

	U ¹¹	U ²²	U ³³	U ²³	U ¹³	U ¹²
Br(1)	23(1)	28(1)	34(1)	13(1)	13(1)	10(1)
S(1)	18(1)	20(1)	27(1)	8(1)	6(1)	10(1)
O(1)	18(1)	36(1)	36(1)	11(1)	2(1)	11(1)
O(2)	31(1)	21(1)	39(1)	12(1)	13(1)	15(1)
O(3)	39(1)	37(1)	27(1)	5(1)	8(1)	16(1)
O(4)	38(1)	41(1)	33(1)	14(1)	-1(1)	18(1)
N(1)	34(1)	22(1)	23(1)	2(1)	11(1)	12(1)
N(2)	23(1)	21(1)	24(1)	7(1)	7(1)	9(1)
N(3)	15(1)	22(1)	23(1)	5(1)	2(1)	6(1)
N(4)	22(1)	19(1)	31(1)	5(1)	2(1)	8(1)
C(1)	17(1)	20(1)	20(1)	4(1)	2(1)	8(1)
C(2)	23(1)	17(1)	25(1)	5(1)	3(1)	6(1)
C(3)	24(1)	22(1)	25(1)	8(1)	9(1)	4(1)
C(4)	23(1)	23(1)	20(1)	5(1)	7(1)	7(1)
C(5)	20(1)	18(1)	15(1)	3(1)	2(1)	5(1)

C(6)	25(1)	20(1)	16(1)	3(1)	3(1)	8(1)
C(7)	34(1)	17(1)	25(1)	4(1)	6(1)	8(1)
C(8)	27(1)	20(1)	28(1)	8(1)	9(1)	3(1)
C(9)	21(1)	21(1)	22(1)	5(1)	6(1)	5(1)
C(10)	18(1)	18(1)	16(1)	4(1)	0(1)	5(1)
C(11)	29(1)	33(1)	48(1)	7(1)	16(1)	13(1)
C(12)	50(1)	25(1)	25(1)	2(1)	13(1)	18(1)
C(13)	33(1)	20(1)	27(1)	-1(1)	0(1)	13(1)
C(14)	23(1)	19(1)	32(1)	6(1)	-1(1)	5(1)
C(15)	17(1)	20(1)	30(1)	7(1)	5(1)	8(1)
C(16)	32(1)	61(1)	20(1)	10(1)	7(1)	23(1)
C(17)	20(1)	35(1)	25(1)	6(1)	-2(1)	9(1)
C(18)	25(1)	26(1)	35(1)	9(1)	4(1)	11(1)
C(19)	24(1)	27(1)	52(1)	6(1)	-2(1)	12(1)
C(20)	19(1)	23(1)	48(1)	6(1)	3(1)	8(1)
C(21)	24(1)	17(1)	29(1)	3(1)	1(1)	5(1)
C(22)	21(1)	15(1)	28(1)	6(1)	3(1)	4(1)
C(23)	25(1)	25(1)	30(1)	10(1)	2(1)	8(1)
C(24)	23(1)	27(1)	45(1)	14(1)	6(1)	11(1)
C(25)	28(1)	30(1)	40(1)	7(1)	10(1)	14(1)
C(26)	29(1)	28(1)	28(1)	6(1)	6(1)	9(1)
C(27)	22(1)	17(1)	28(1)	6(1)	1(1)	5(1)
C(28)	24(1)	19(1)	31(1)	7(1)	1(1)	7(1)

Table A 24. Hydrogen coordinates ($\times 10^4$) and isotropic displacement parameters ($\text{\AA}^2 \times 10^3$) for **220**.

	x	y	z	U(eq)
H(2N)	3199	5936	3233	67(8)
H(2A)	6476	8033	1421	27
H(3A)	8188	7313	498	29
H(4A)	7936	5155	156	27
H(7A)	4489	1386	774	31
H(8A)	2520	2027	1531	32
H(9A)	2763	4185	1927	26
H(11A)	9169	4290	960	54
H(11B)	9671	3279	267	54
H(11C)	8941	2880	1085	54
H(12A)	5499	1121	-529	50
H(12B)	6727	977	193	50
H(12C)	7451	1361	-629	50
H(13A)	5064	7294	4358	32
H(13B)	5676	8343	3823	32
H(14A)	7446	7252	3179	31
H(14B)	7968	7739	4190	31
H(15A)	6379	5637	4308	27
H(15B)	5768	5143	3307	27
H(16A)	9041	6151	2694	54
H(16B)	7786	4659	2348	54
H(16C)	9722	5004	2739	54
H(17A)	10124	7052	4206	42
H(17B)	10670	5830	4218	42
H(17C)	9434	6195	4854	42
H(18A)	8740	3676	3777	33
H(18B)	7460	4018	4390	33
H(19A)	6473	2882	2605	42
H(19B)	5211	3118	3265	42

H(20A)	5683	1591	3925	37
H(20B)	4940	917	2944	37
H(23A)	10880	32	4408	32
H(24A)	12407	-903	3474	36
H(25A)	11979	-1071	2038	39
H(26A)	9995	-316	1472	35

Table A 25. Torsion angles [°] for **220**.

O(1)-S(1)-N(2)-C(13)	-162.99(12)
O(2)-S(1)-N(2)-C(13)	-34.05(13)
C(1)-S(1)-N(2)-C(13)	80.51(13)
O(1)-S(1)-C(1)-C(2)	123.02(12)
O(2)-S(1)-C(1)-C(2)	-6.47(14)
N(2)-S(1)-C(1)-C(2)	-121.42(12)
O(1)-S(1)-C(1)-C(10)	-55.43(14)
O(2)-S(1)-C(1)-C(10)	175.08(12)
N(2)-S(1)-C(1)-C(10)	60.13(14)
C(10)-C(1)-C(2)-C(3)	0.7(2)
S(1)-C(1)-C(2)-C(3)	-177.76(12)
C(1)-C(2)-C(3)-C(4)	-2.5(2)
C(2)-C(3)-C(4)-C(5)	-0.2(2)
C(3)-C(4)-C(5)-C(10)	4.6(2)
C(3)-C(4)-C(5)-C(6)	-177.81(15)
C(12)-N(1)-C(6)-C(7)	18.4(2)
C(11)-N(1)-C(6)-C(7)	-112.54(18)
C(12)-N(1)-C(6)-C(5)	-159.28(14)
C(11)-N(1)-C(6)-C(5)	69.78(19)
C(4)-C(5)-C(6)-C(7)	-172.13(15)
C(10)-C(5)-C(6)-C(7)	5.4(2)
C(4)-C(5)-C(6)-N(1)	5.6(2)
C(10)-C(5)-C(6)-N(1)	-176.78(13)
N(1)-C(6)-C(7)-C(8)	179.85(15)

C(5)-C(6)-C(7)-C(8)	-2.5(2)
C(6)-C(7)-C(8)-C(9)	-1.0(3)
C(7)-C(8)-C(9)-C(10)	1.5(2)
C(8)-C(9)-C(10)-C(5)	1.5(2)
C(8)-C(9)-C(10)-C(1)	-179.79(15)
C(4)-C(5)-C(10)-C(9)	172.67(14)
C(6)-C(5)-C(10)-C(9)	-4.9(2)
C(4)-C(5)-C(10)-C(1)	-6.2(2)
C(6)-C(5)-C(10)-C(1)	176.25(13)
C(2)-C(1)-C(10)-C(9)	-175.17(15)
S(1)-C(1)-C(10)-C(9)	3.2(2)
C(2)-C(1)-C(10)-C(5)	3.6(2)
S(1)-C(1)-C(10)-C(5)	-178.03(11)
S(1)-N(2)-C(13)-C(14)	-80.18(16)
N(2)-C(13)-C(14)-C(15)	-61.73(19)
C(16)-N(3)-C(15)-C(14)	-64.16(18)
C(17)-N(3)-C(15)-C(14)	57.29(18)
C(18)-N(3)-C(15)-C(14)	172.30(14)
C(13)-C(14)-C(15)-N(3)	177.27(13)
C(16)-N(3)-C(18)-C(19)	-60.96(18)
C(17)-N(3)-C(18)-C(19)	-178.28(14)
C(15)-N(3)-C(18)-C(19)	63.03(18)
N(3)-C(18)-C(19)-C(20)	174.26(14)
C(21)-N(4)-C(20)-C(19)	117.72(18)
C(28)-N(4)-C(20)-C(19)	-72.7(2)
C(18)-C(19)-C(20)-N(4)	-60.4(2)
C(28)-N(4)-C(21)-O(3)	-175.77(15)
C(20)-N(4)-C(21)-O(3)	-5.1(3)
C(28)-N(4)-C(21)-C(22)	2.47(17)
C(20)-N(4)-C(21)-C(22)	173.17(13)
O(3)-C(21)-C(22)-C(27)	176.46(16)
N(4)-C(21)-C(22)-C(27)	-1.69(17)
O(3)-C(21)-C(22)-C(23)	-1.5(3)
N(4)-C(21)-C(22)-C(23)	-179.65(16)
C(27)-C(22)-C(23)-C(24)	-1.0(2)

C(21)-C(22)-C(23)-C(24)	176.70(15)
C(22)-C(23)-C(24)-C(25)	1.0(2)
C(23)-C(24)-C(25)-C(26)	-0.1(3)
C(24)-C(25)-C(26)-C(27)	-0.9(3)
C(25)-C(26)-C(27)-C(22)	0.9(2)
C(25)-C(26)-C(27)-C(28)	-177.21(16)
C(23)-C(22)-C(27)-C(26)	0.0(2)
C(21)-C(22)-C(27)-C(26)	-178.13(15)
C(23)-C(22)-C(27)-C(28)	178.53(14)
C(21)-C(22)-C(27)-C(28)	0.36(17)
C(21)-N(4)-C(28)-O(4)	176.72(16)
C(20)-N(4)-C(28)-O(4)	6.0(3)
C(21)-N(4)-C(28)-C(27)	-2.26(17)
C(20)-N(4)-C(28)-C(27)	-172.97(14)
C(26)-C(27)-C(28)-O(4)	0.5(3)
C(22)-C(27)-C(28)-O(4)	-177.81(17)
C(26)-C(27)-C(28)-N(4)	179.43(16)
C(22)-C(27)-C(28)-N(4)	1.10(17)

Symmetry transformations used to generate equivalent atoms:

Table A 26. Hydrogen bonds for **220** [\AA and $^\circ$].

D-H...A	d(D-H)	d(H...A)	d(D...A)	$\angle(\text{DHA})$
N(2)-H(2N)...Br(1)	0.88	2.54	3.3518(14)	152.9

Symmetry transformations used to generate equivalent atoms:

6.2 Appendix 1.2 – NMR Spectra

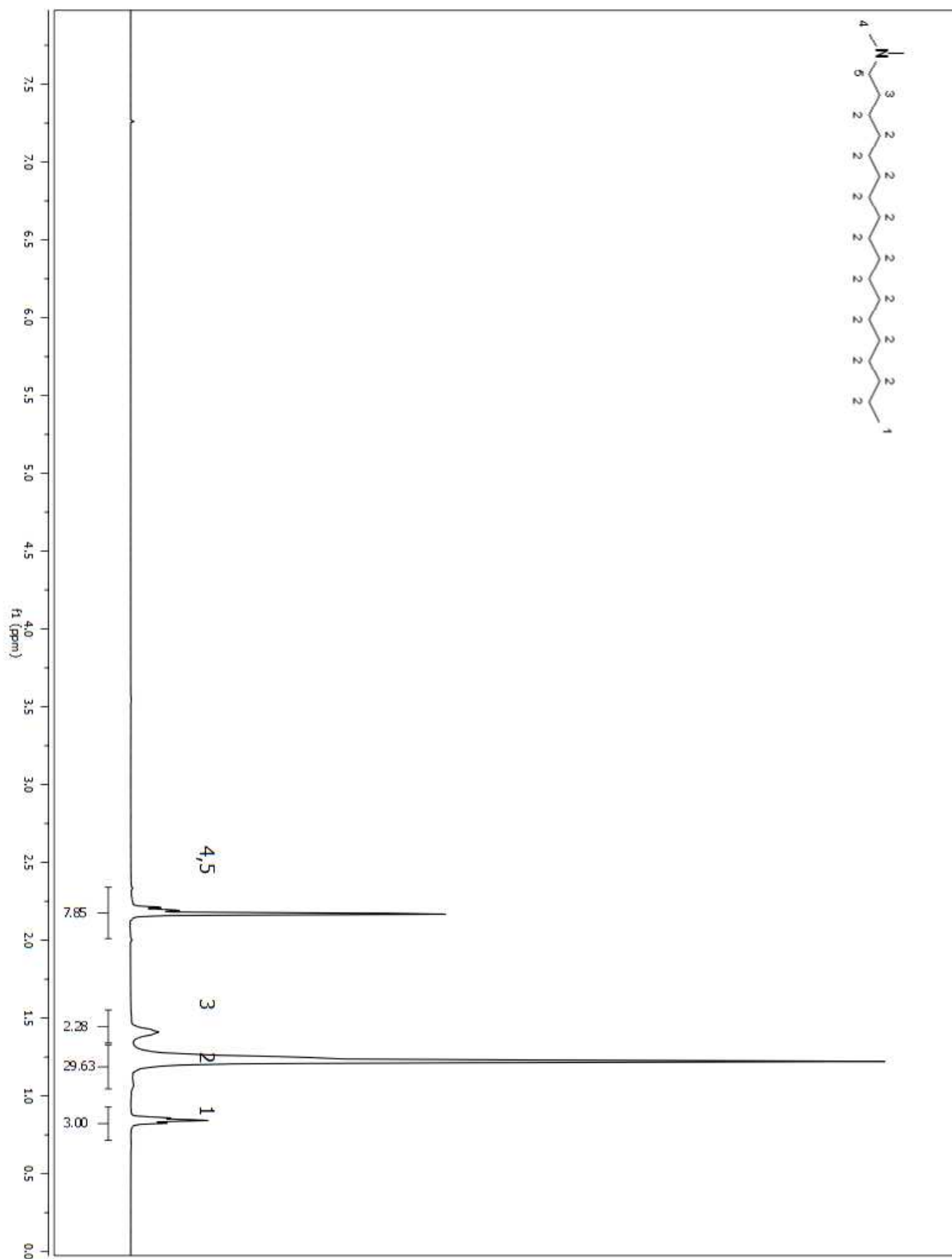


Figure A 1. ^1H NMR spectrum of compound **2** in CDCl_3

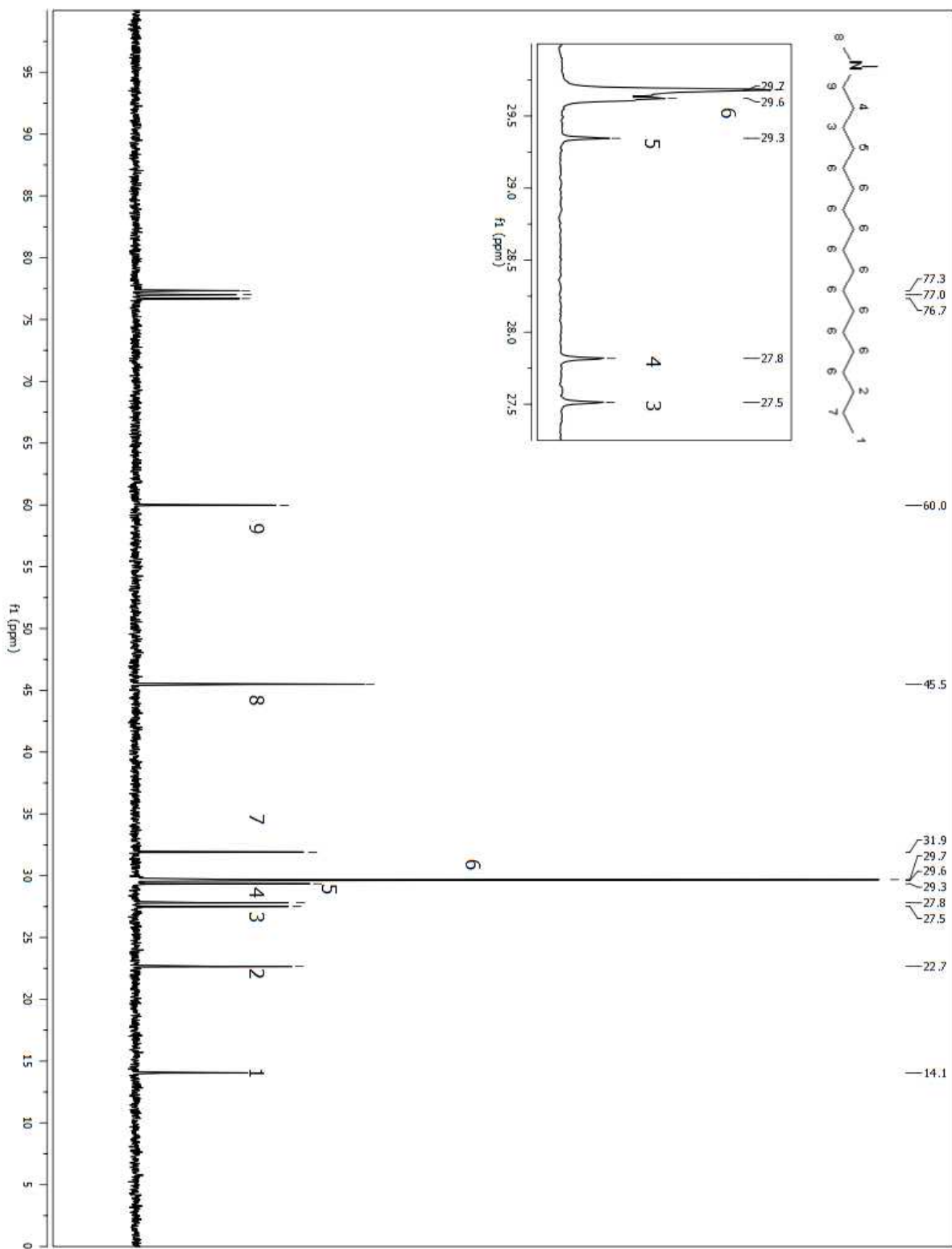


Figure A 2. ^{13}C NMR spectrum of compound **2** in CDCl_3

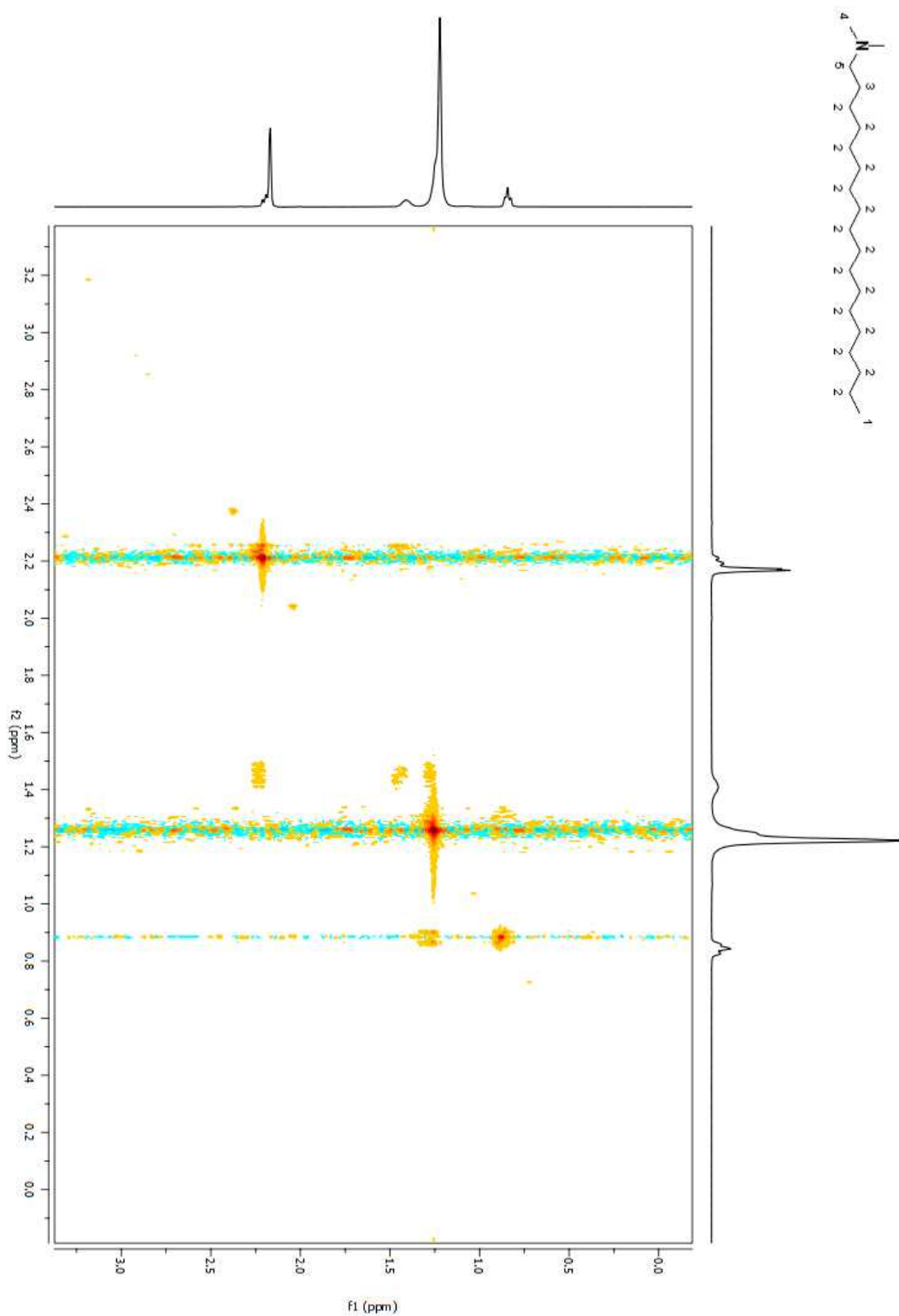


Figure A 3. COSY 2D NMR spectrum of compound **2** in CDCl_3

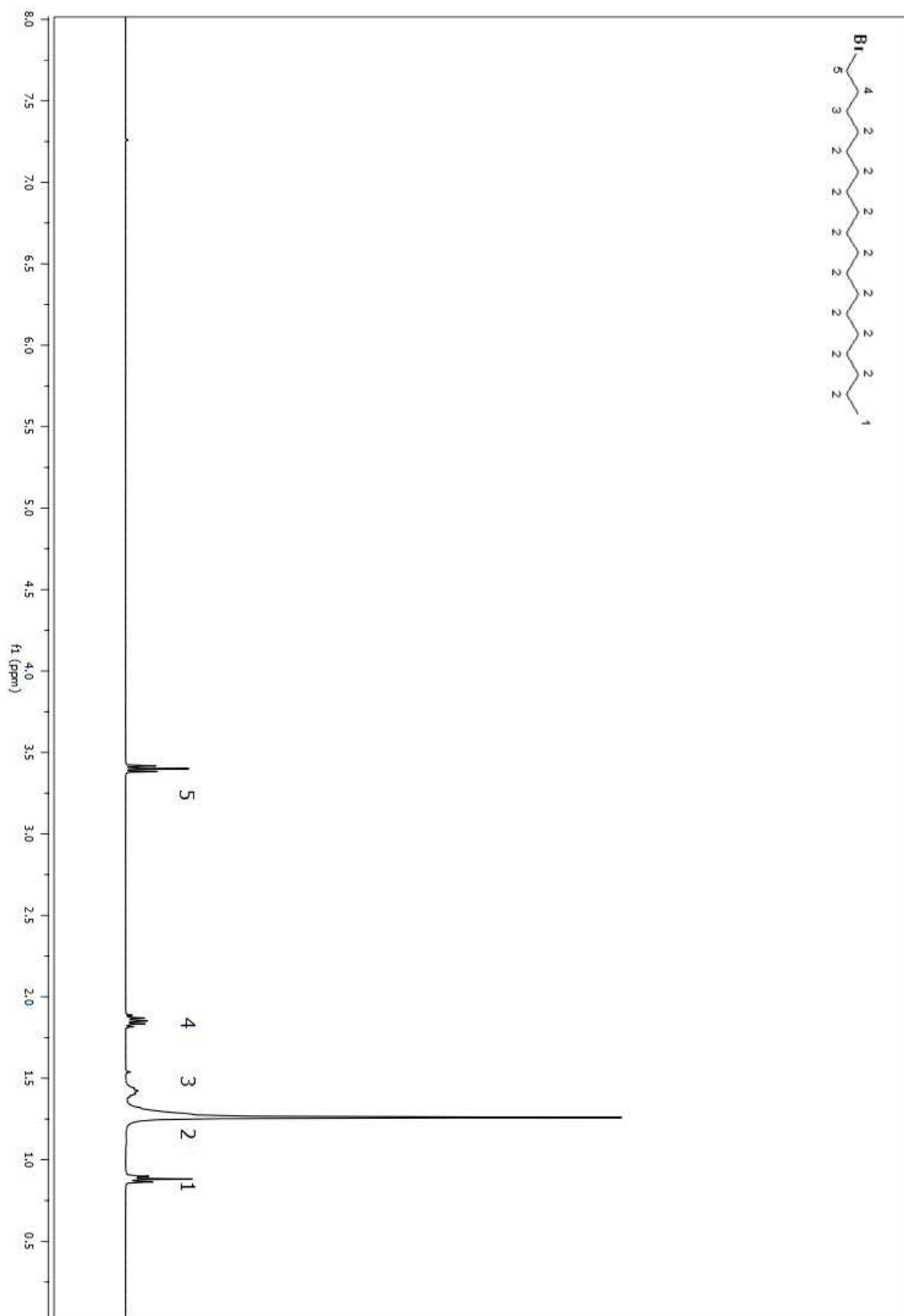


Figure A 4. ^1H NMR spectrum of purified **46** in CDCl_3

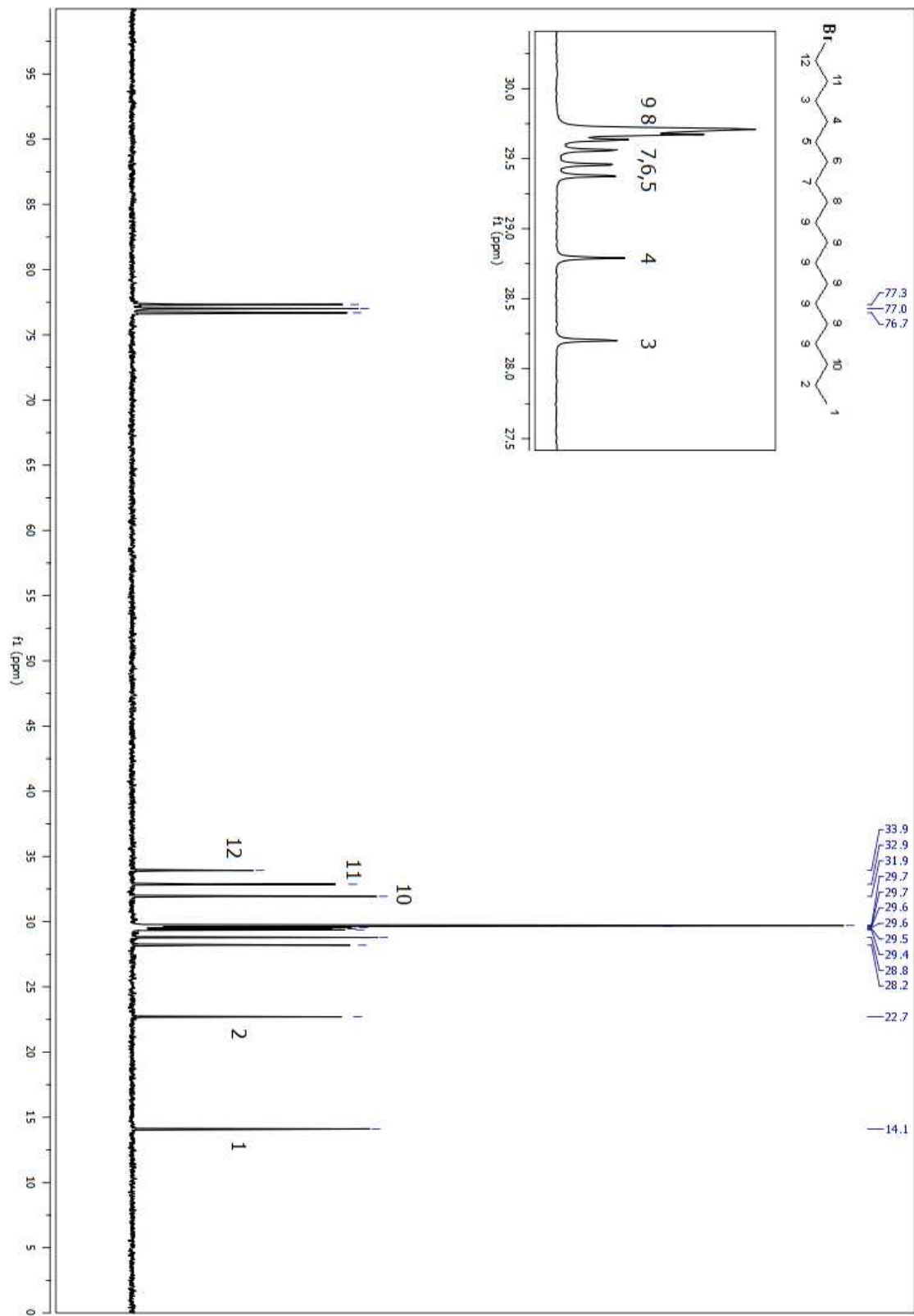


Figure A 5. ^{13}C NMR spectrum of purified **46** in CDCl_3

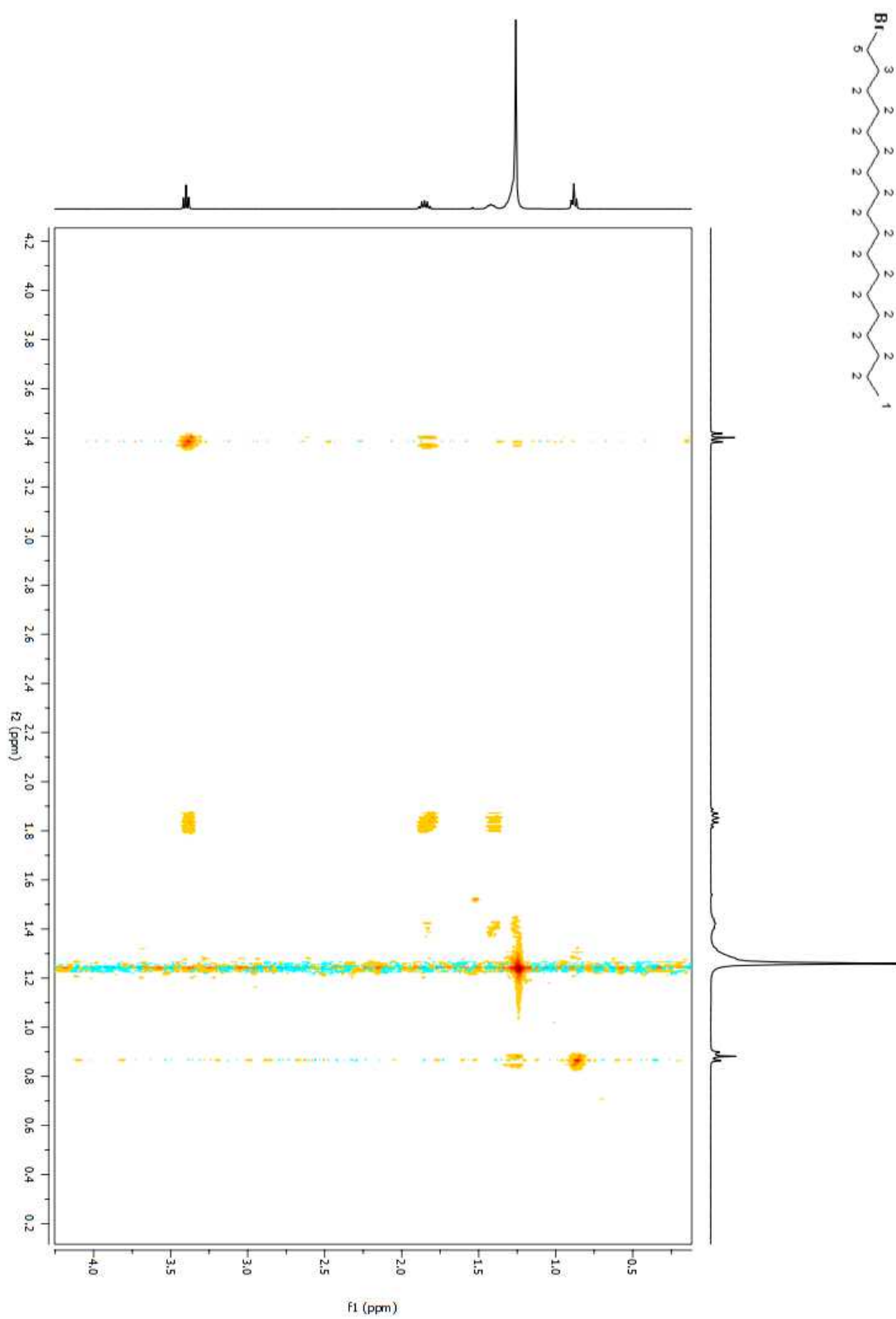


Figure A 6. COSY 2D NMR spectrum of purified **46** in CDCl_3

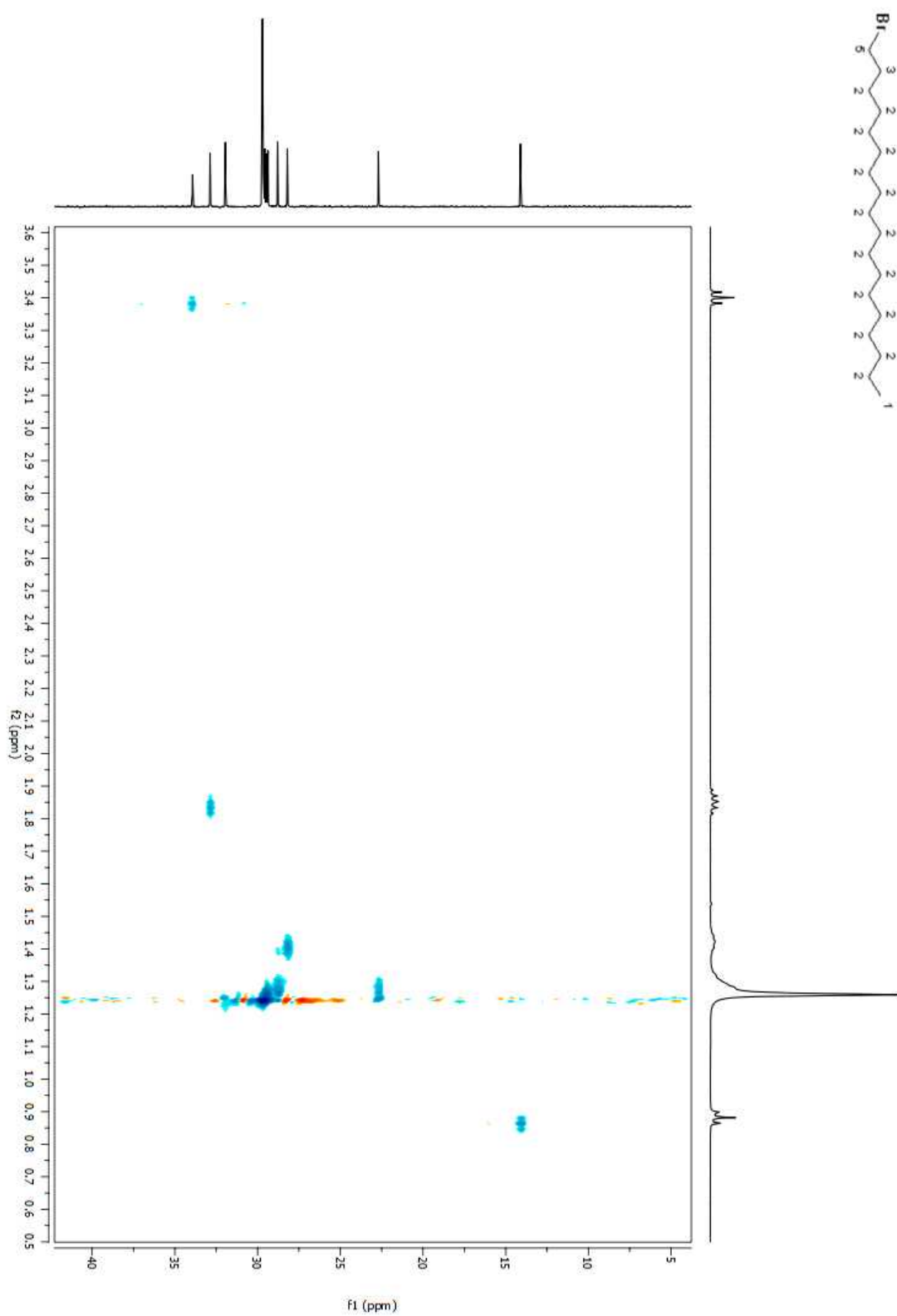


Figure A 7. HSQC 2D NMR spectrum of purified **46** in CDCl_3

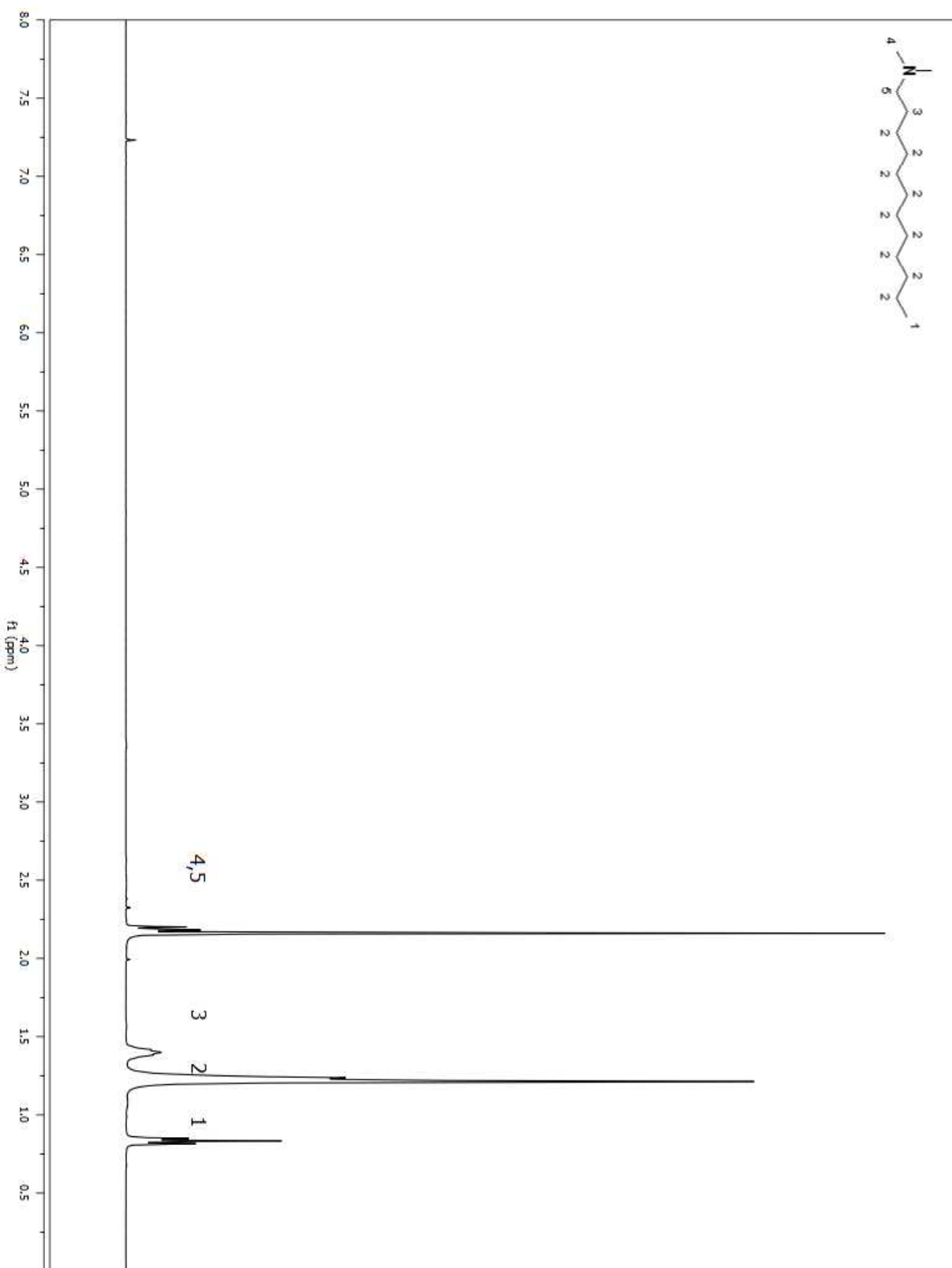


Figure A 8. ^1H NMR spectrum of compound **22** in CDCl_3

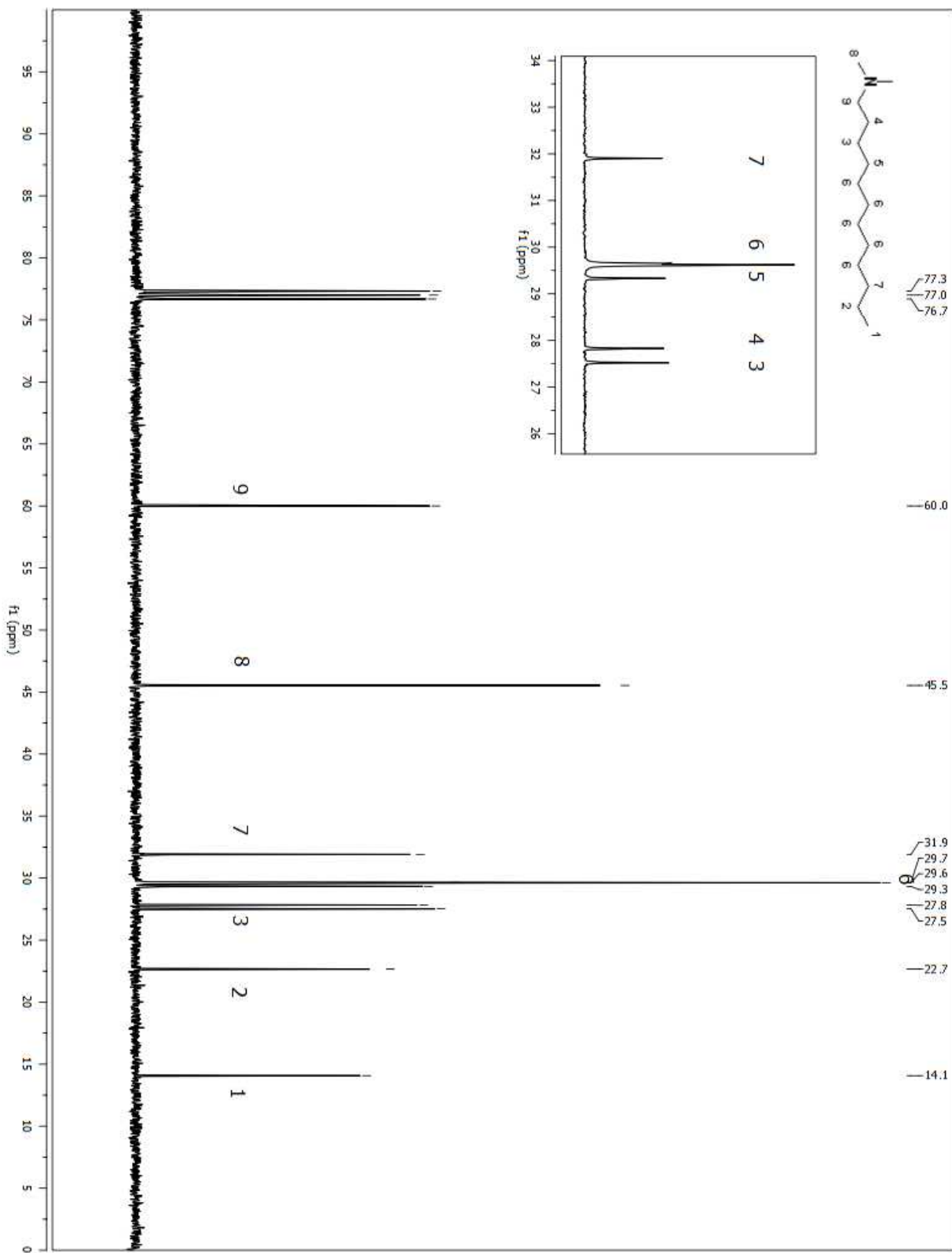


Figure A 9. ^{13}C NMR spectrum of compound **22** in CDCl_3

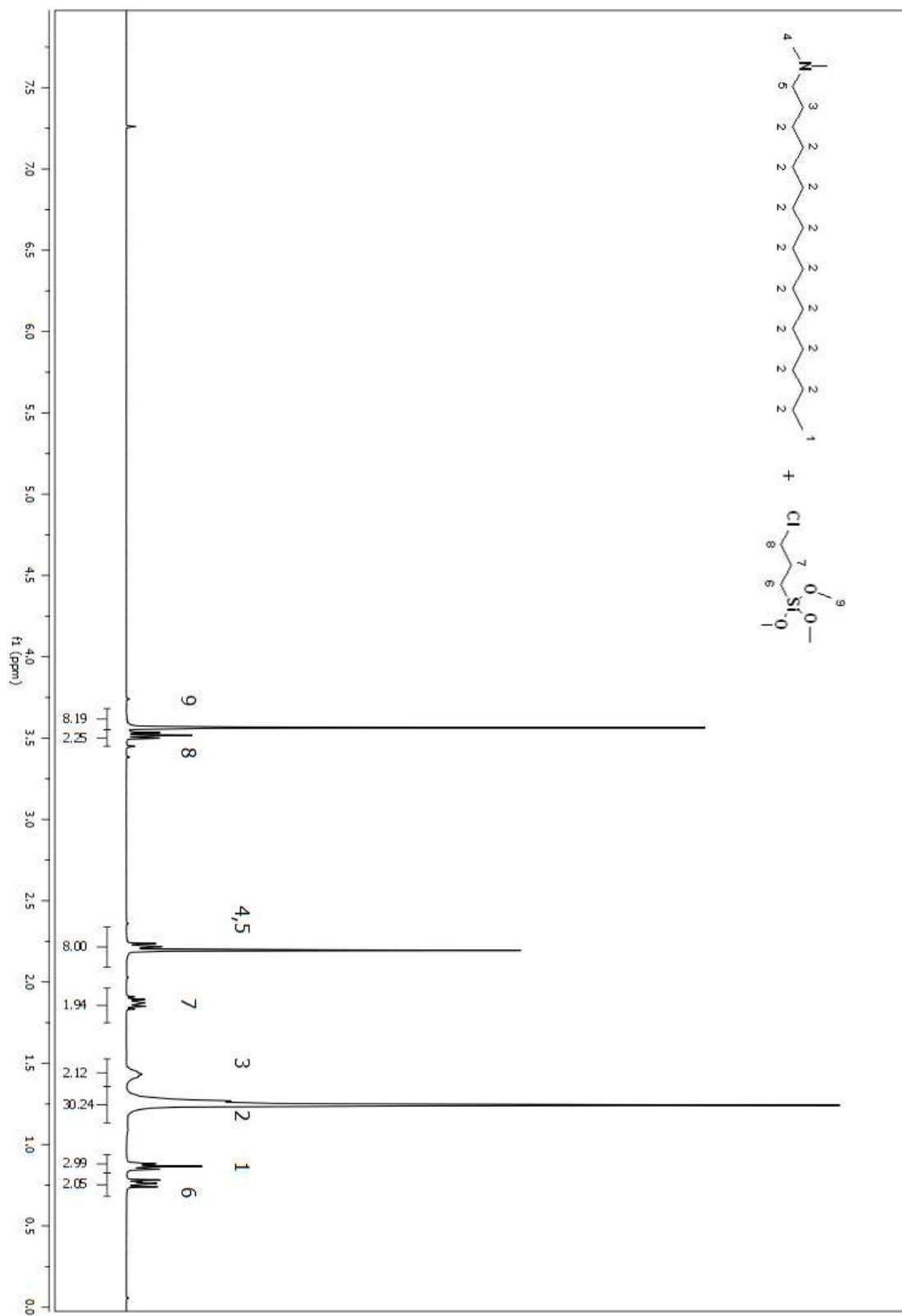


Figure A 11. ^1H NMR spectrum of compound 1+2 in CDCl_3

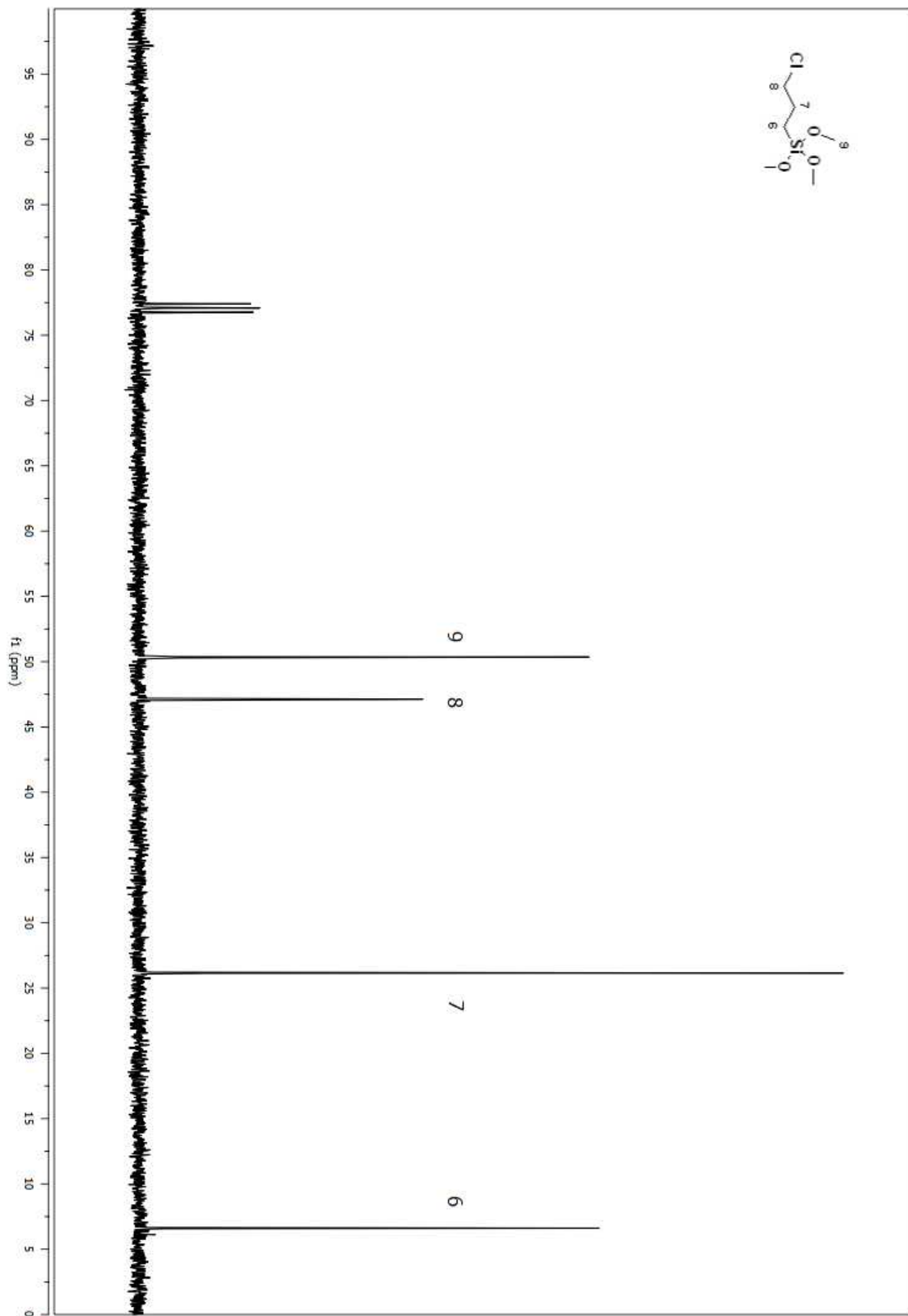


Figure A 12. ^{13}C NMR spectrum of compound **1** in CDCl_3
379

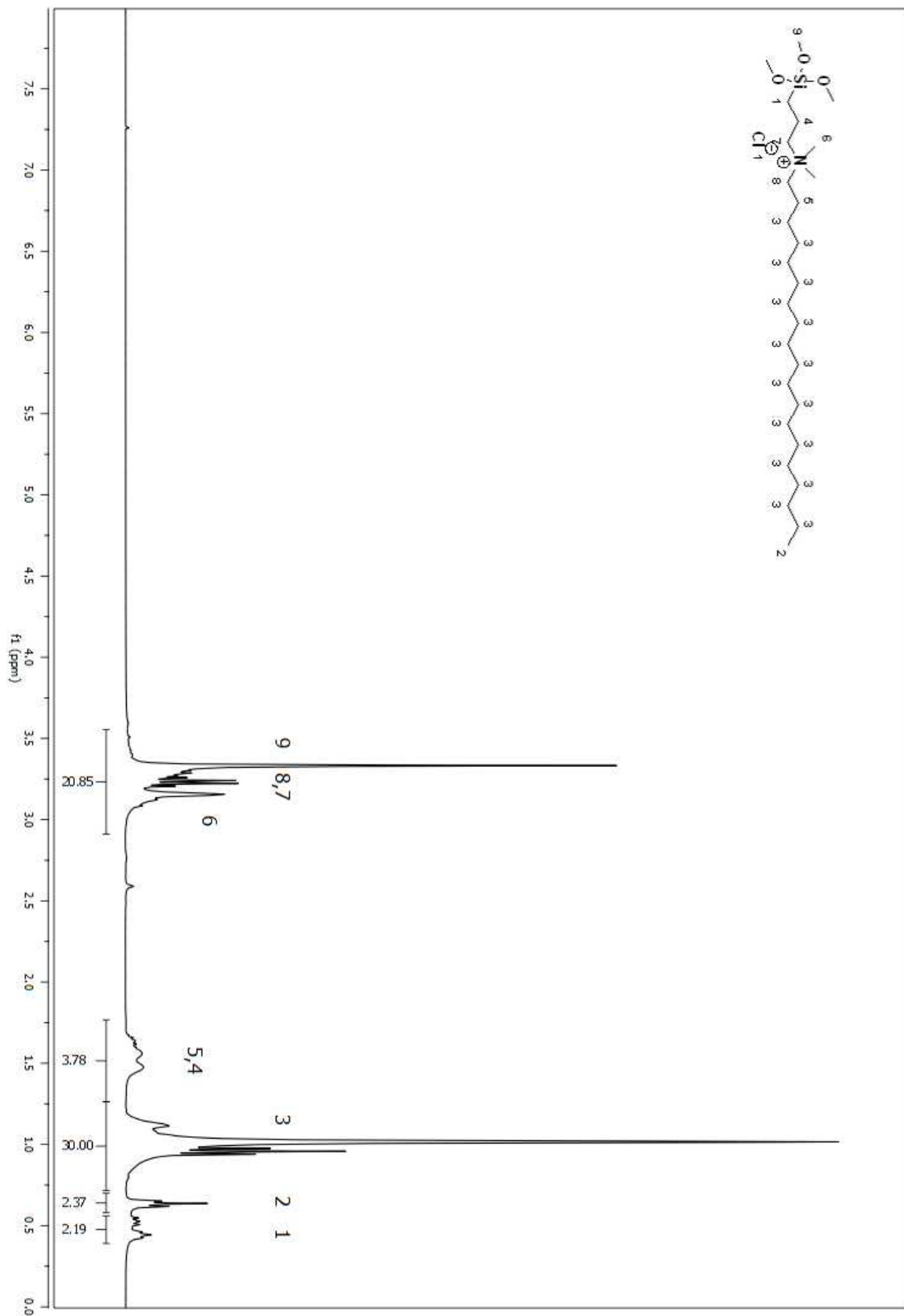


Figure A 13. ^1H NMR spectrum of compound **3** in CDCl_3 (Table 2.1, entry i)

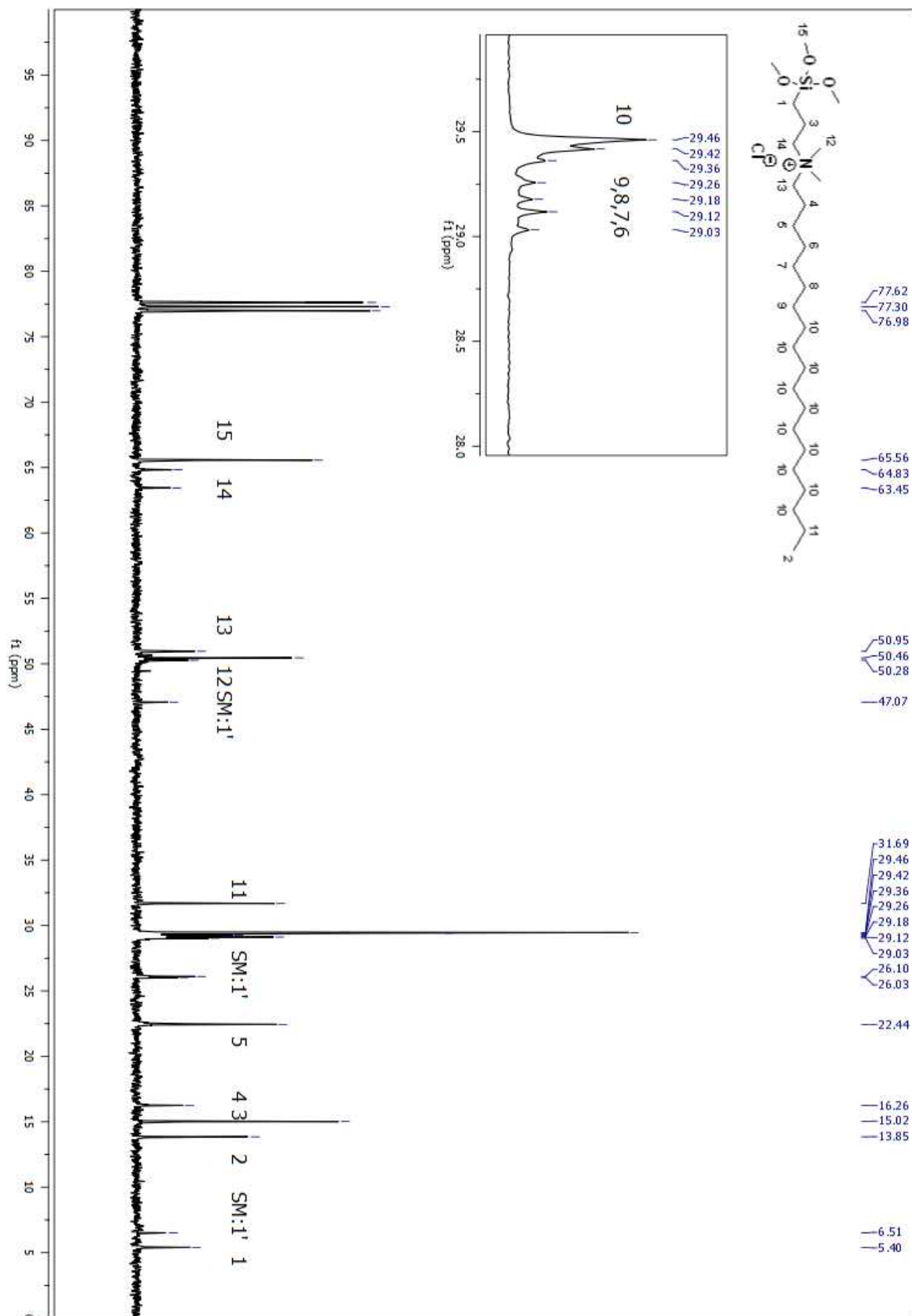


Figure A 14. ^{13}C NMR spectrum of compound **3** in CDCl_3 (Table 2.1, entry i)

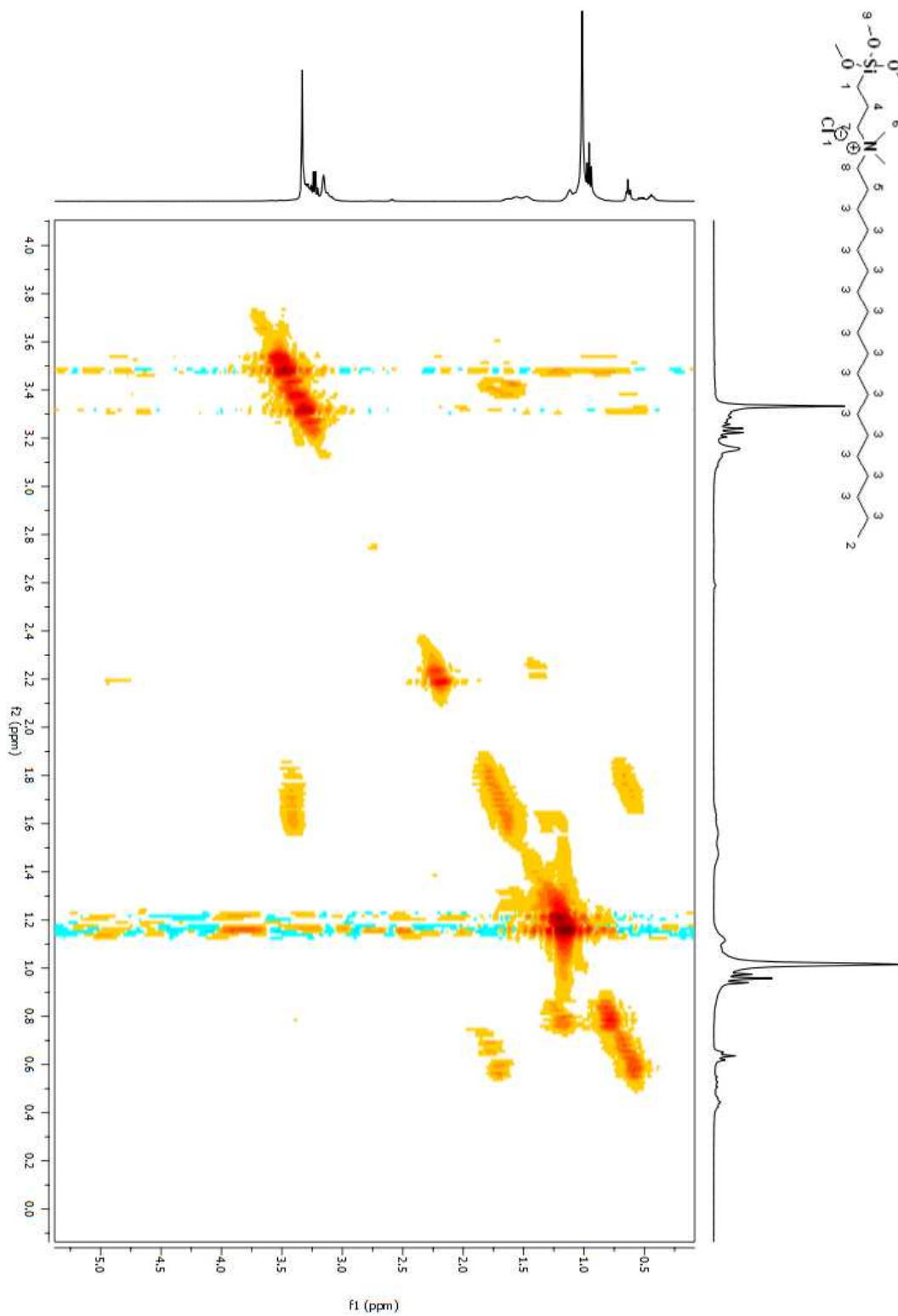


Figure A 15. COSY 2D NMR spectrum of compound **3** in CDCl₃ (Table 2.1, entry i)

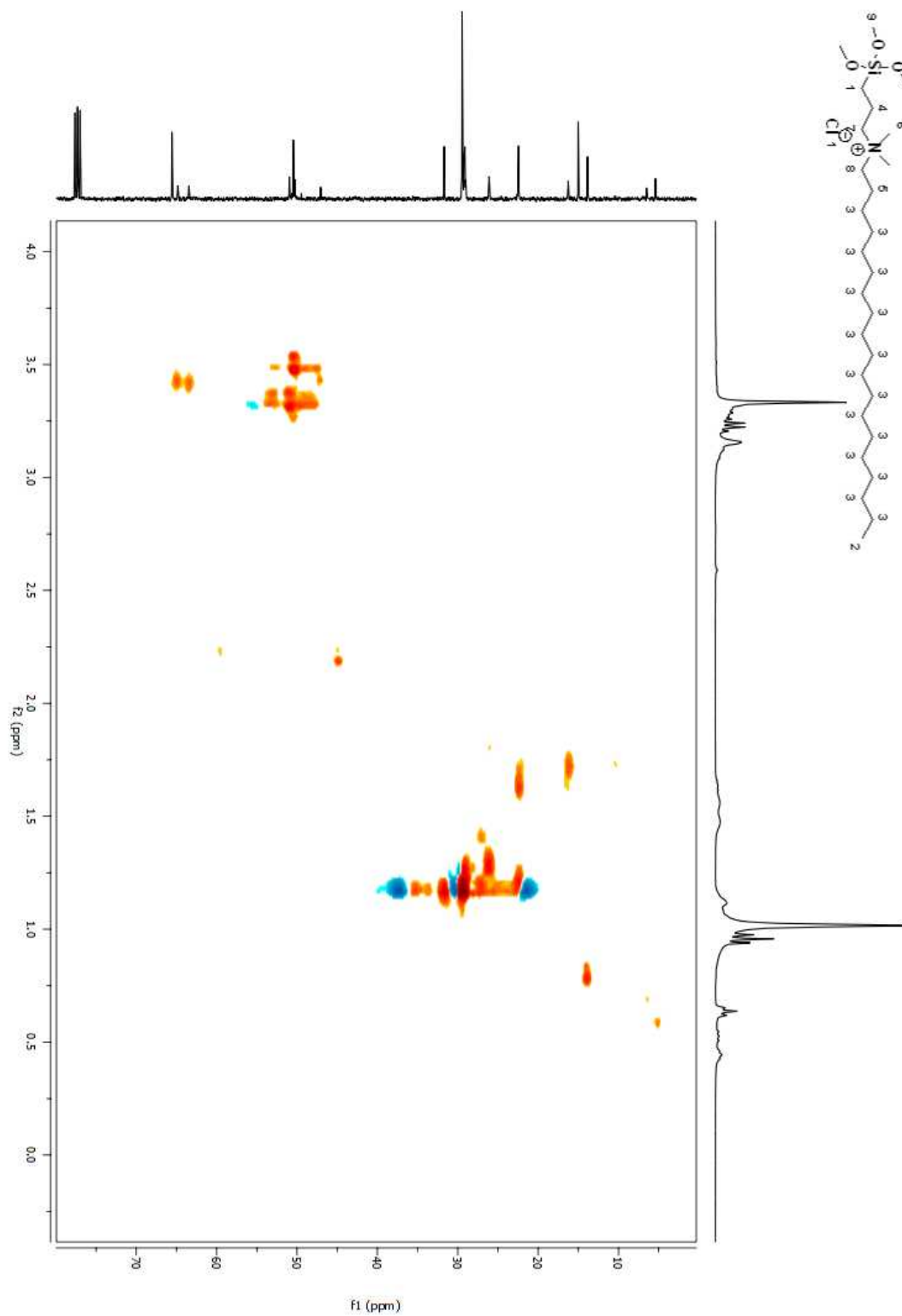


Figure A 16. HSQC 2D NMR spectrum of compound **3** in CDCl₃ (Table 2.1, entry i)

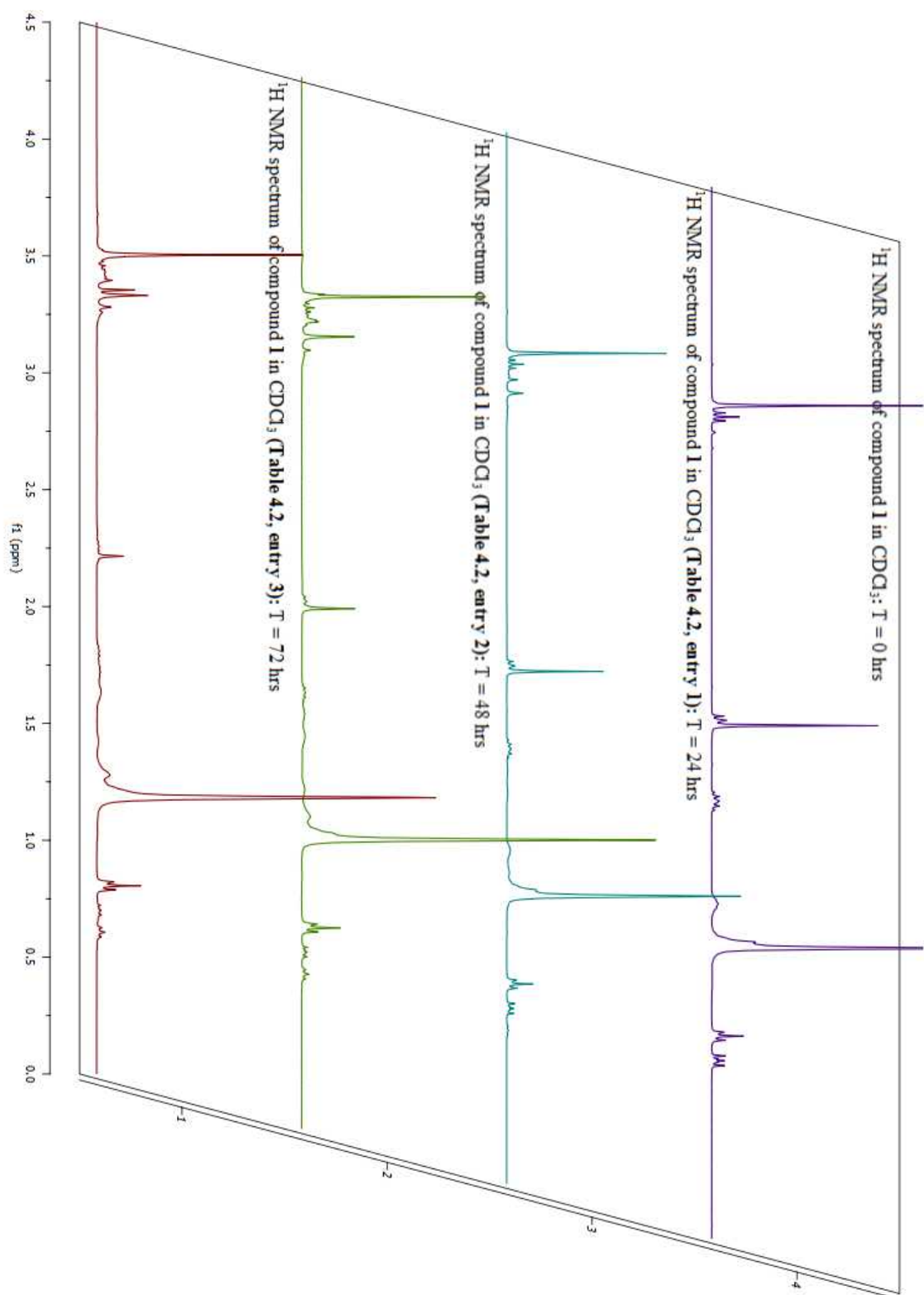


Figure A 17. ^1H stacked NMR spectra of compound 3 in CDCl_3 (Table 2.1, entry i-iii)

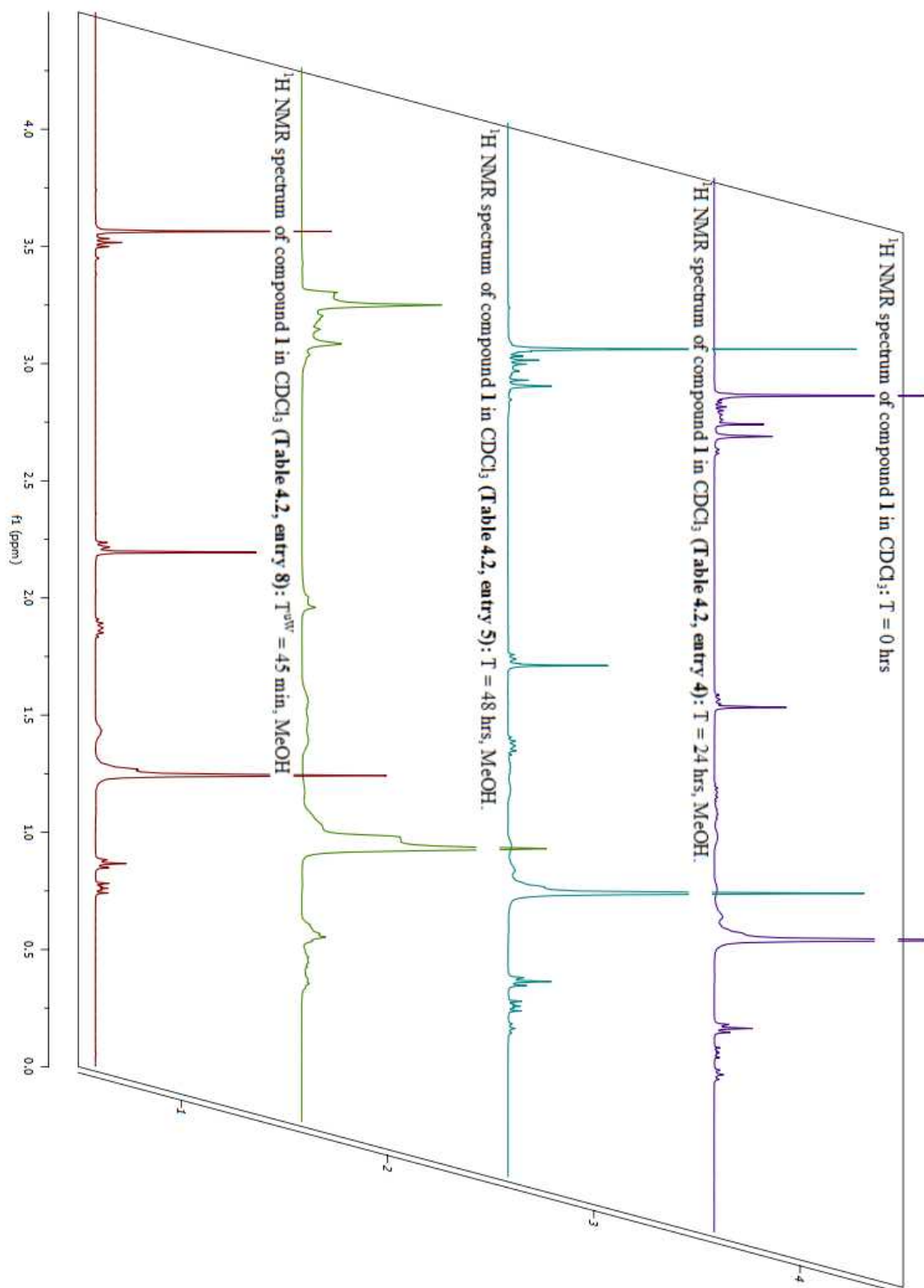


Figure A 18. ^1H stacked NMR spectra of compound **3** in CDCl_3 (Table 2.1, entry iv-v, viii)

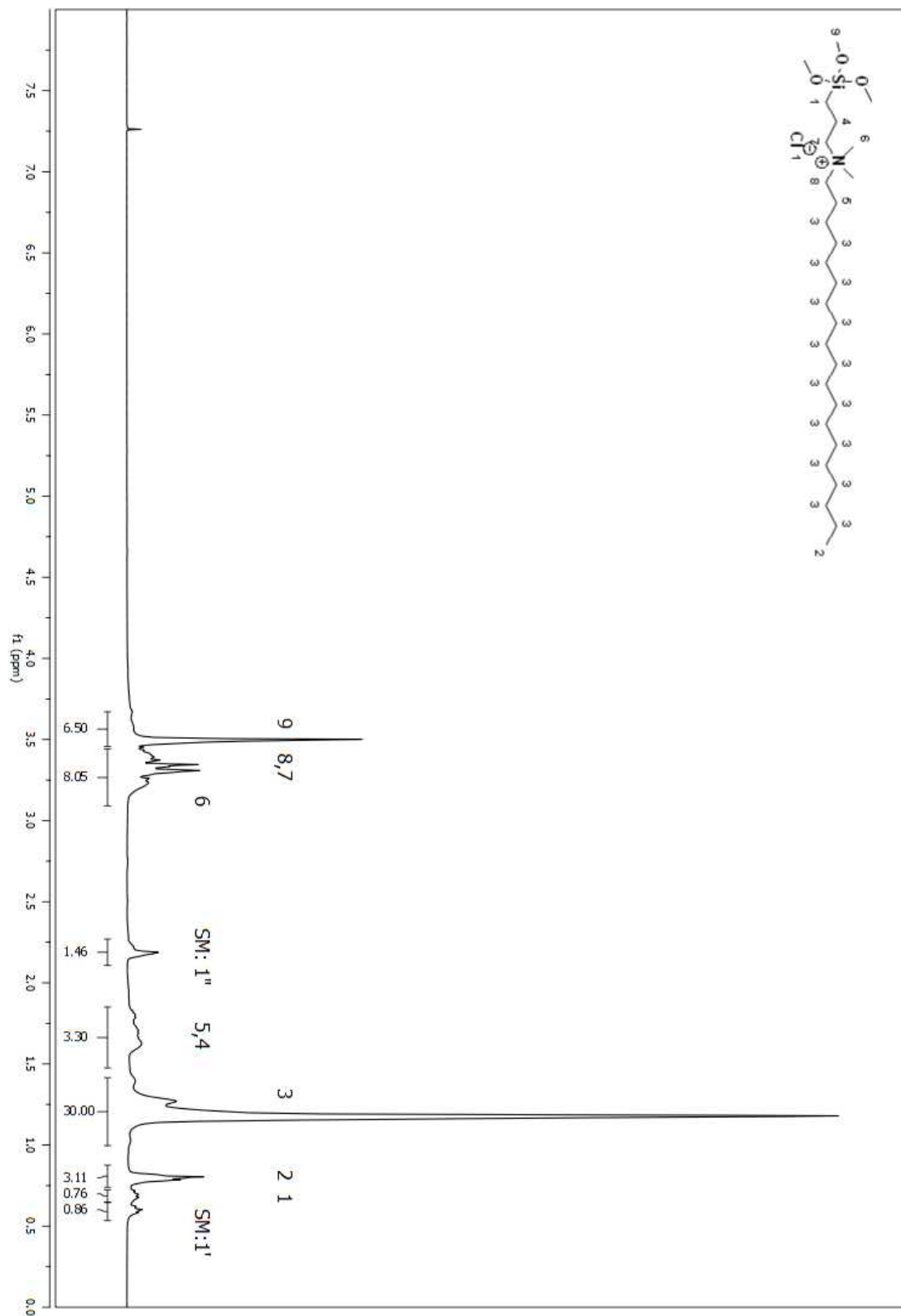


Figure A 19. ¹H NMR spectrum of compound **3** in CDCl₃ (Table 2.2, entry iii)

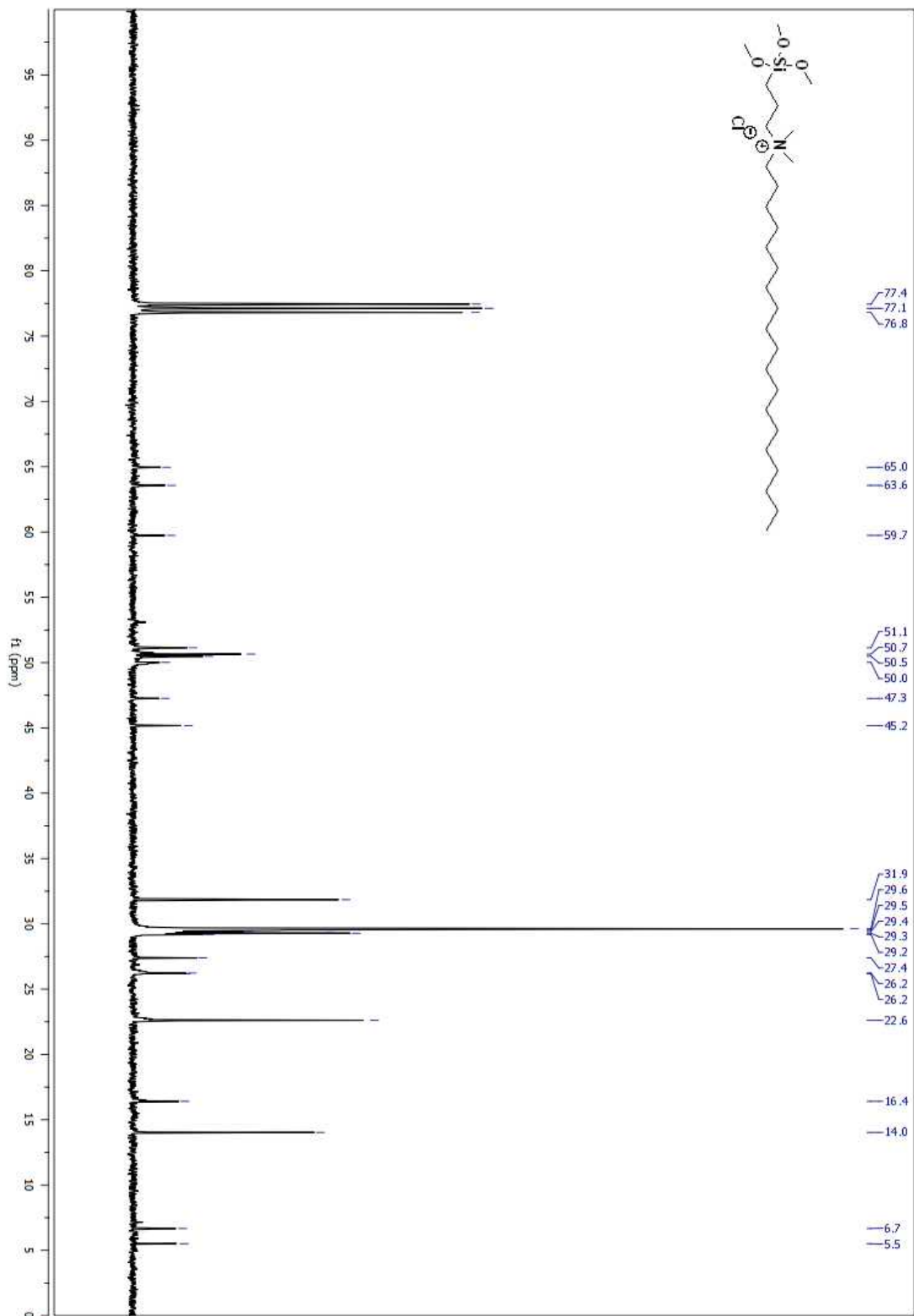


Figure A 20. ¹³C NMR spectrum of compound **3** in CDCl₃ (Table 2.2, entry iii)

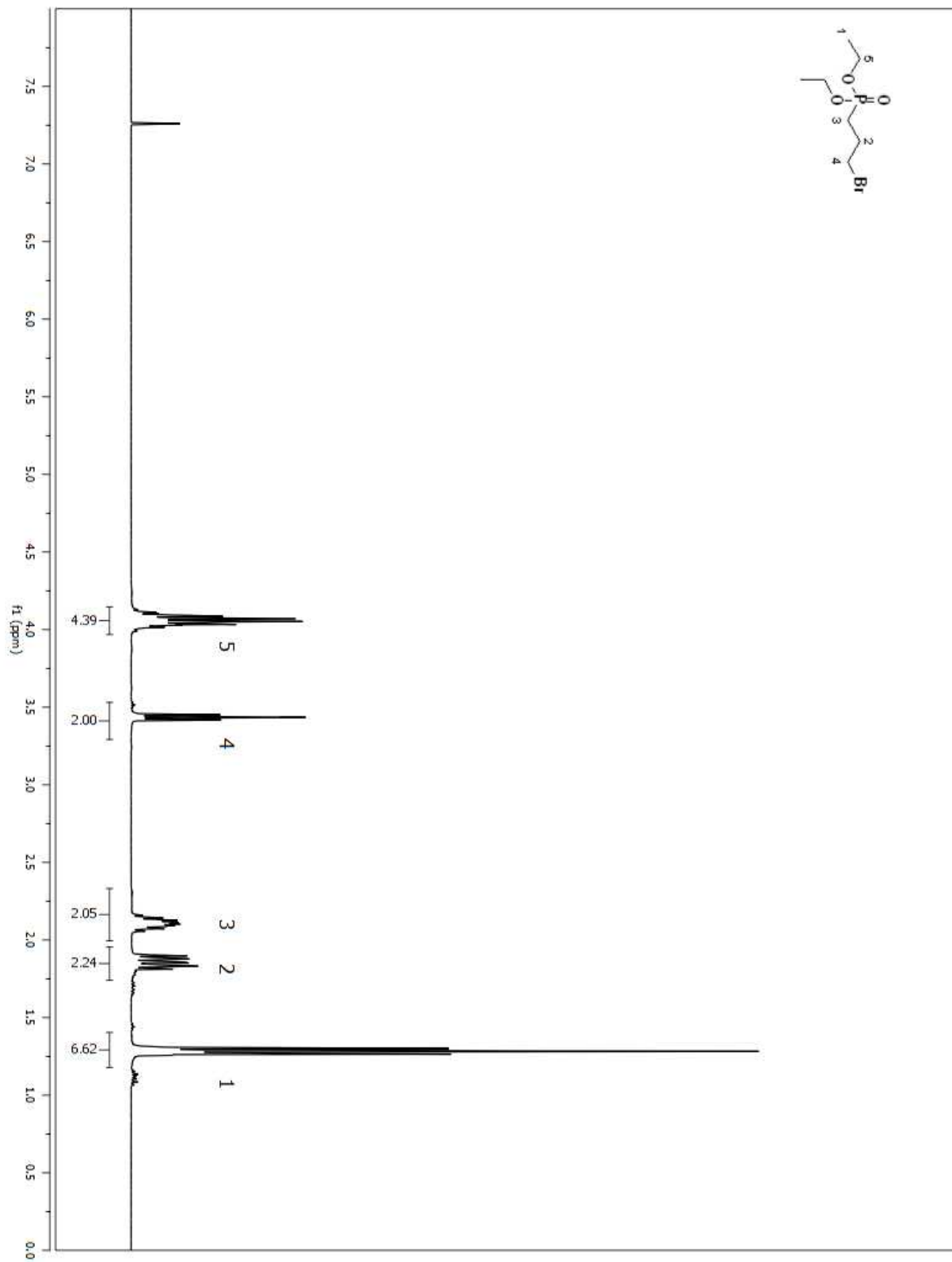


Figure A 21. ^1H NMR spectrum of compound **12** in CDCl_3 (Table 2.3, entry iii)

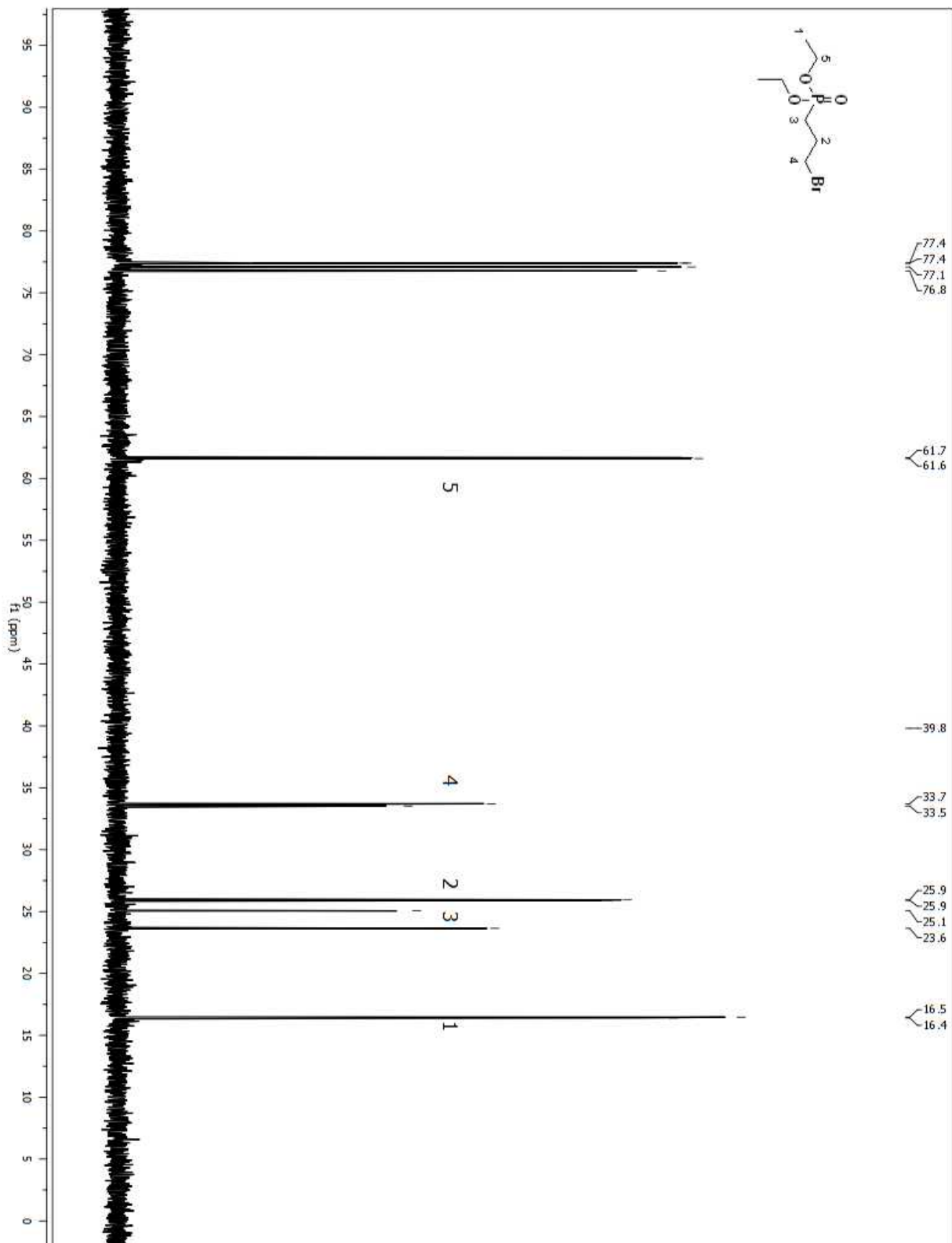


Figure A 22. ¹³C NMR spectrum of compound **12** in CDCl₃ (Table 2.3, entry iii)

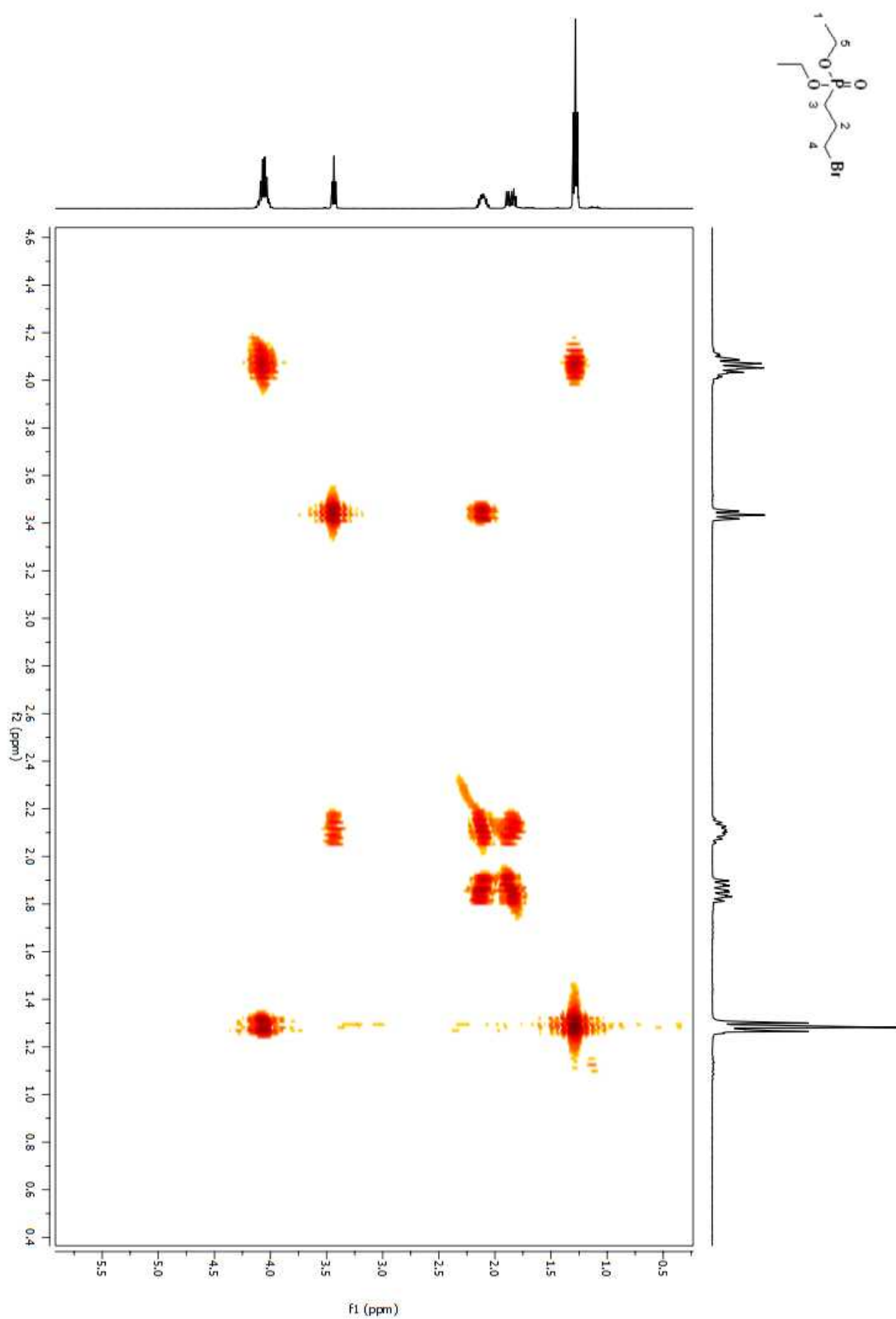


Figure A 23. COSY 2D NMR spectrum of compound **12** in CDCl₃ (Table 2.3, entry iii)

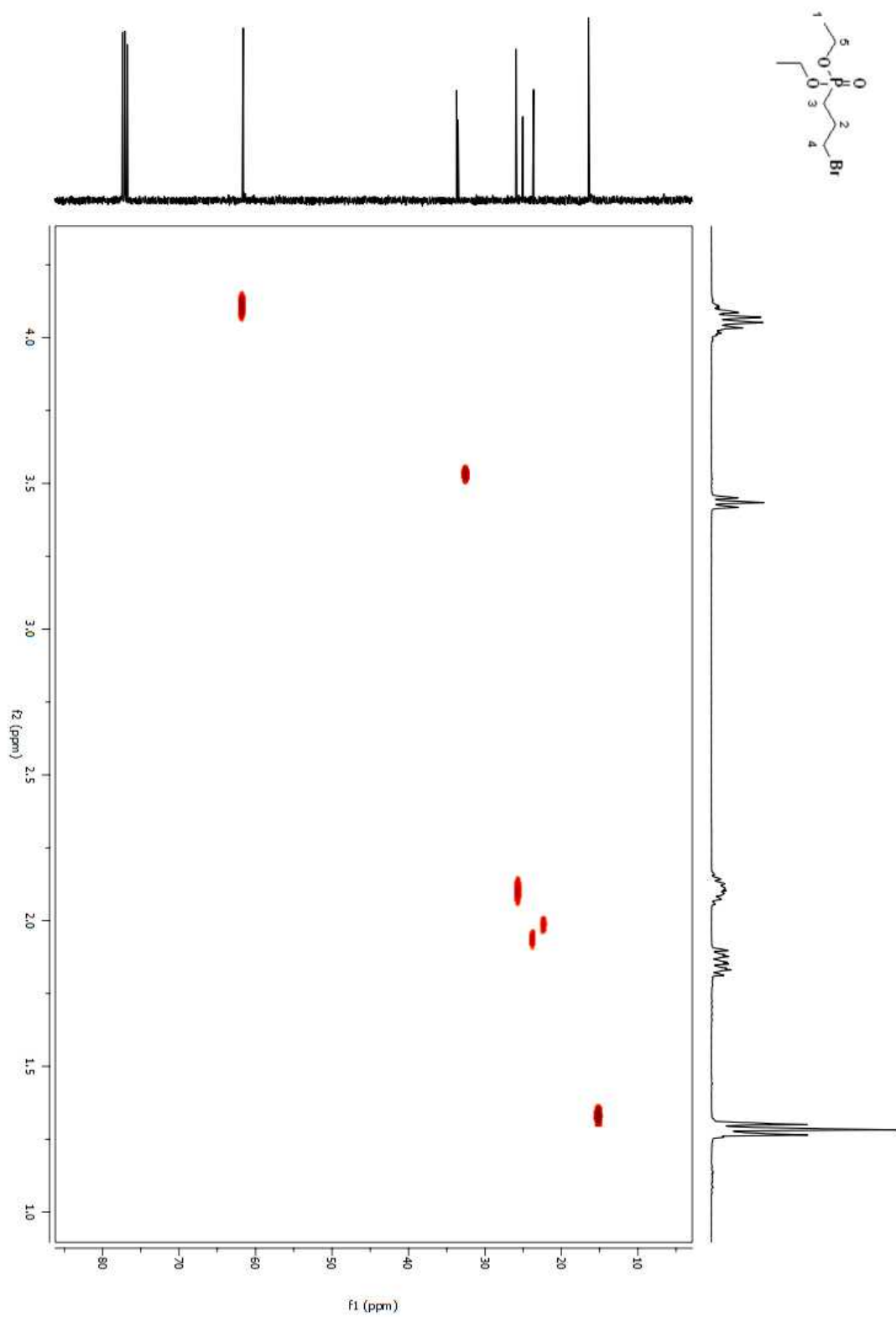


Figure A 24. HSQC 2D NMR spectrum of compound **12** in CDCl₃ (Table 2.3, entry iii)

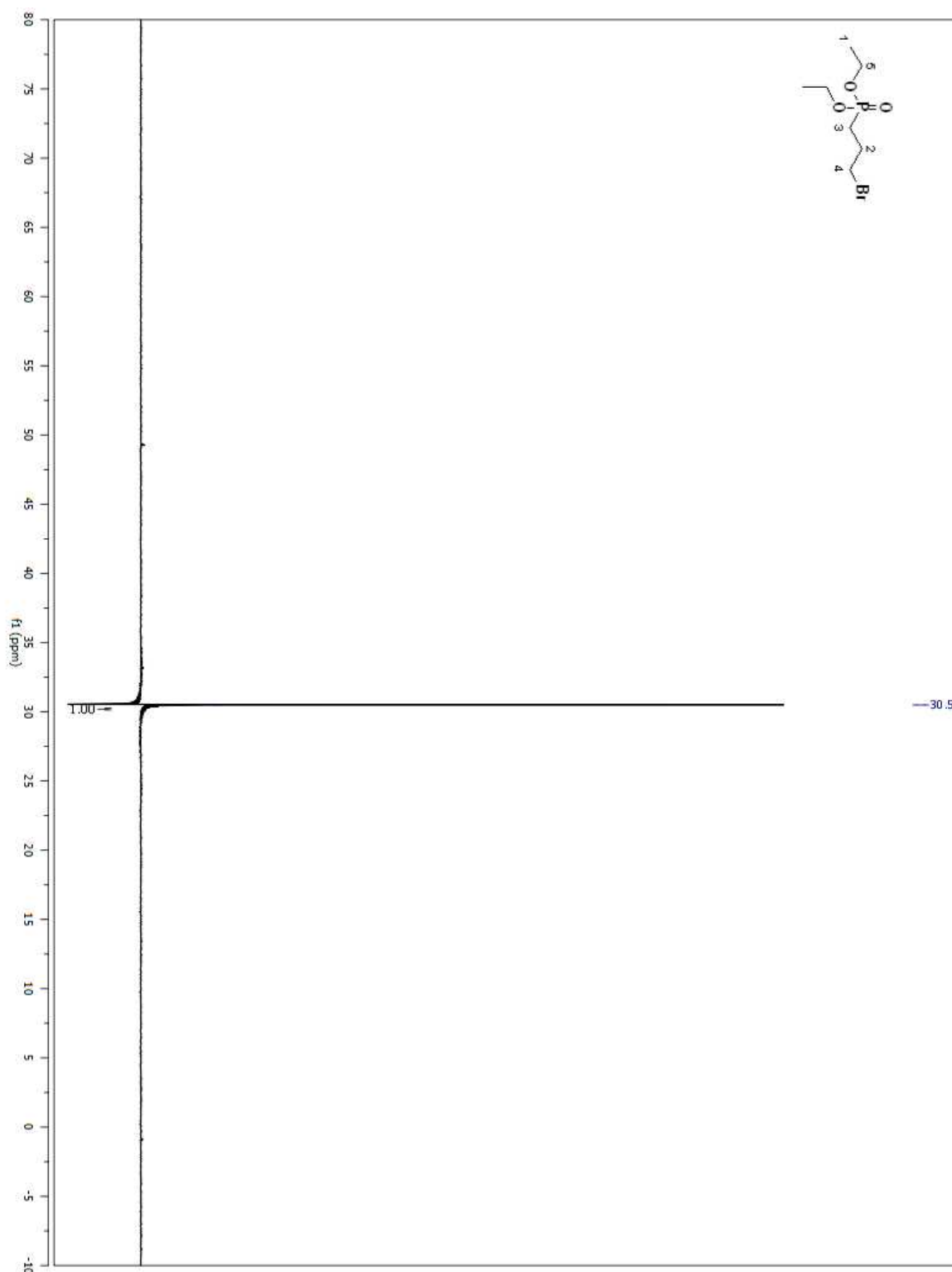


Figure A 25. ³¹P NMR spectrum of compound **12** in CDCl₃ (Table 2.3, entry iii)

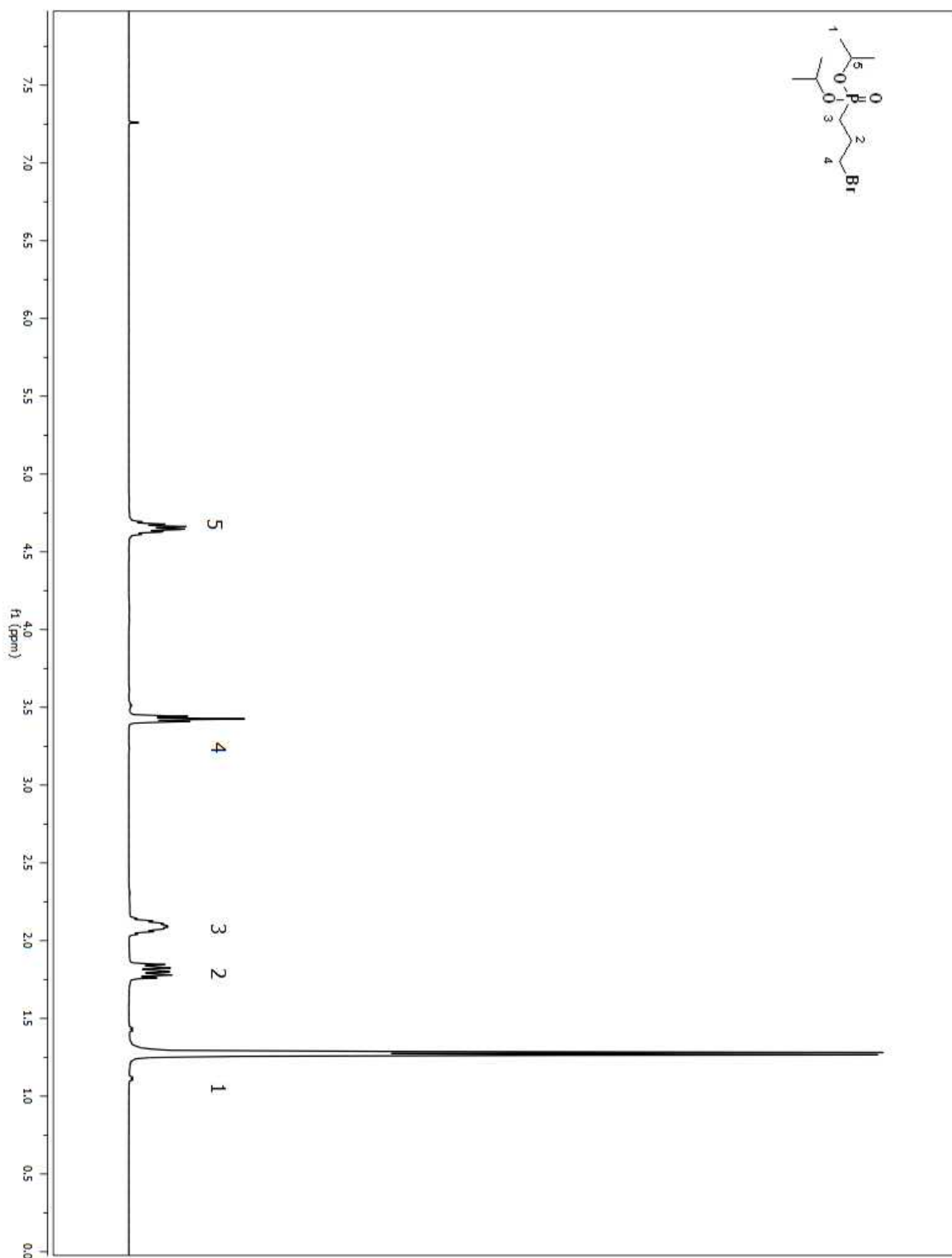


Figure A 26. ^1H NMR spectrum of compound **13** in CDCl_3 (Table 2.3, entry vii)

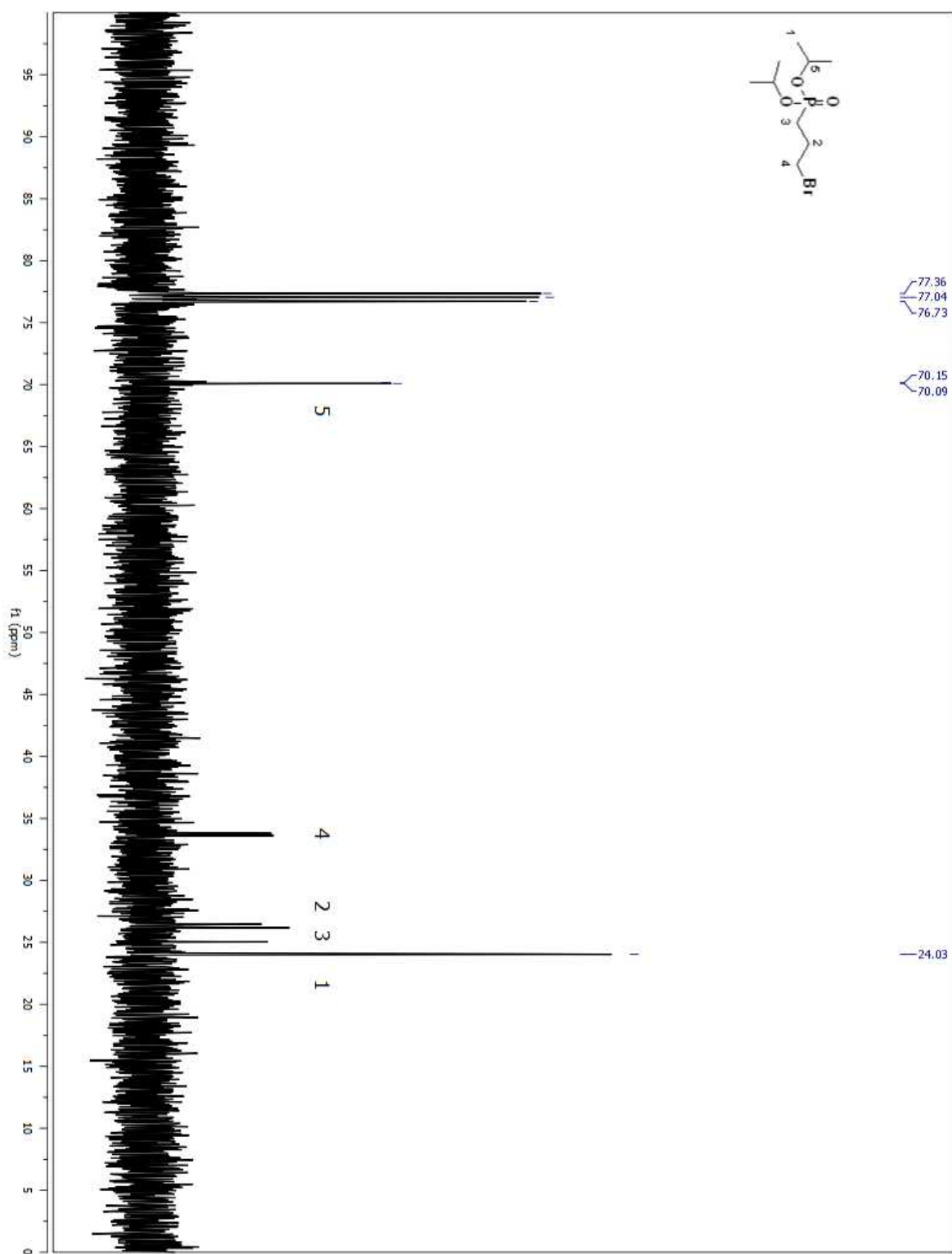


Figure A 27. ^{13}C NMR spectrum of compound **13** in CDCl_3 (Table 2.3, entry vii)

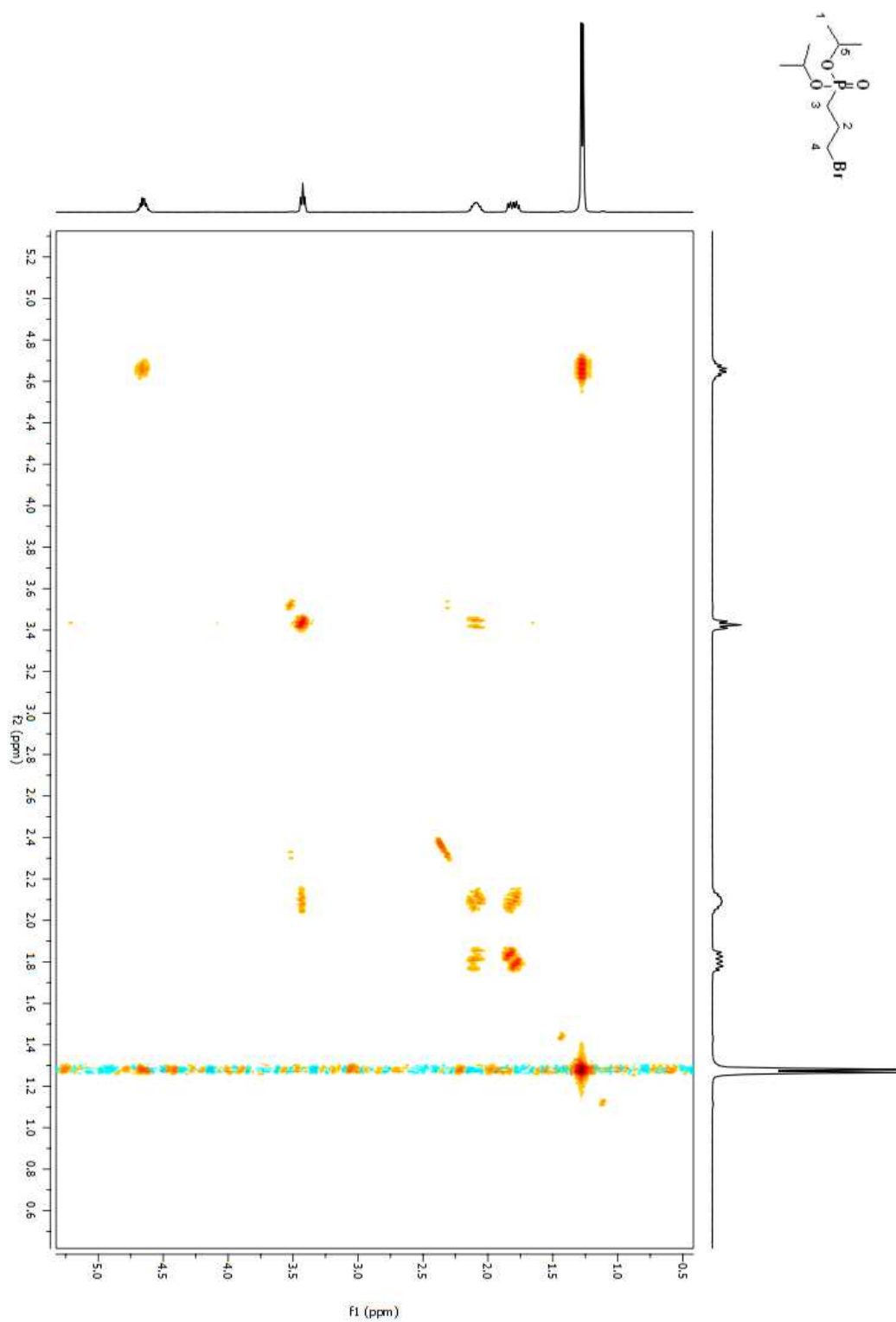


Figure A 28. COSY 2D NMR spectrum of compound **13** in CDCl₃ (Table 2.3, entry vii)

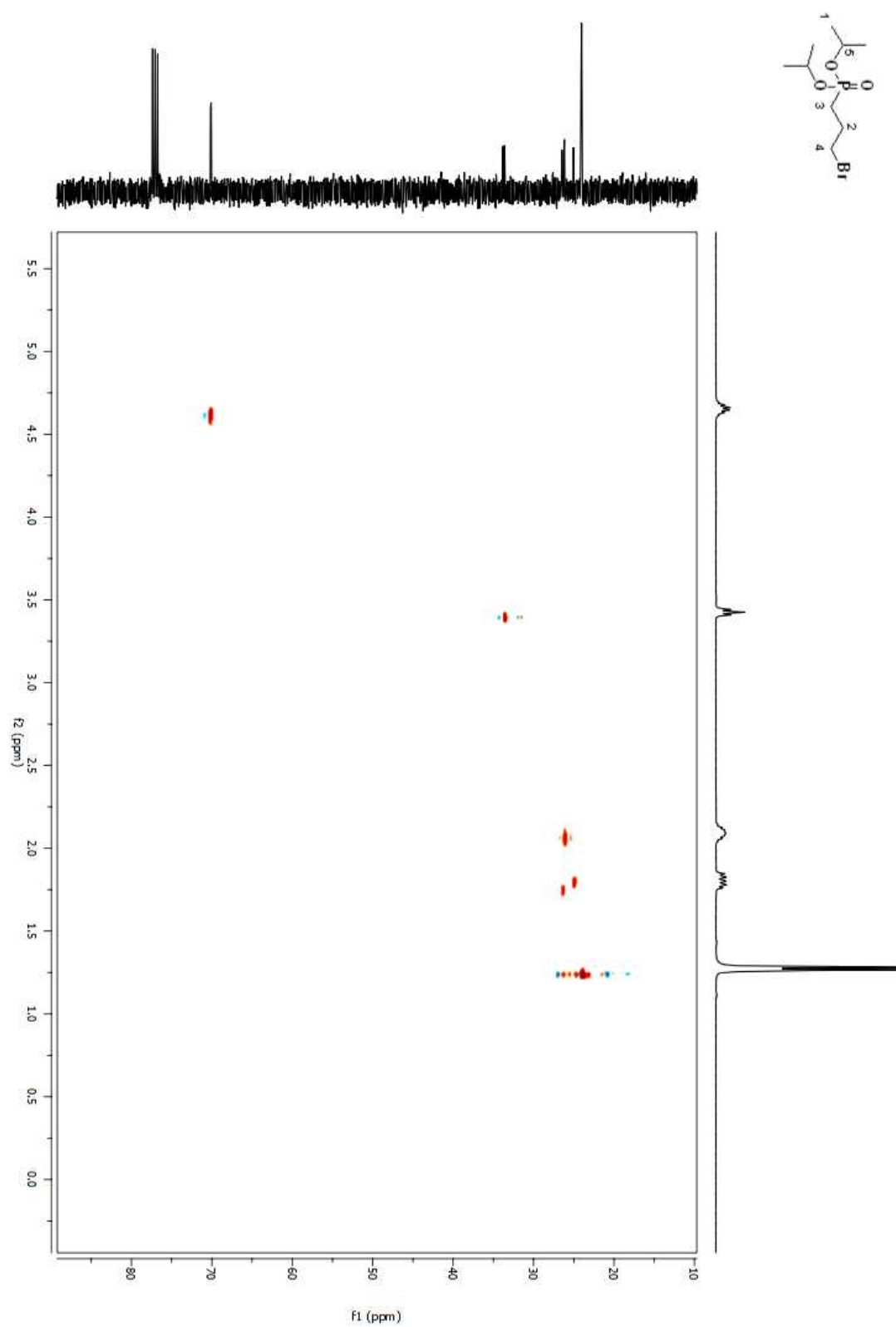


Figure A 29. HSQC 2D NMR spectrum of compound **13** in CDCl_3 (Table 2.3, entry vii)

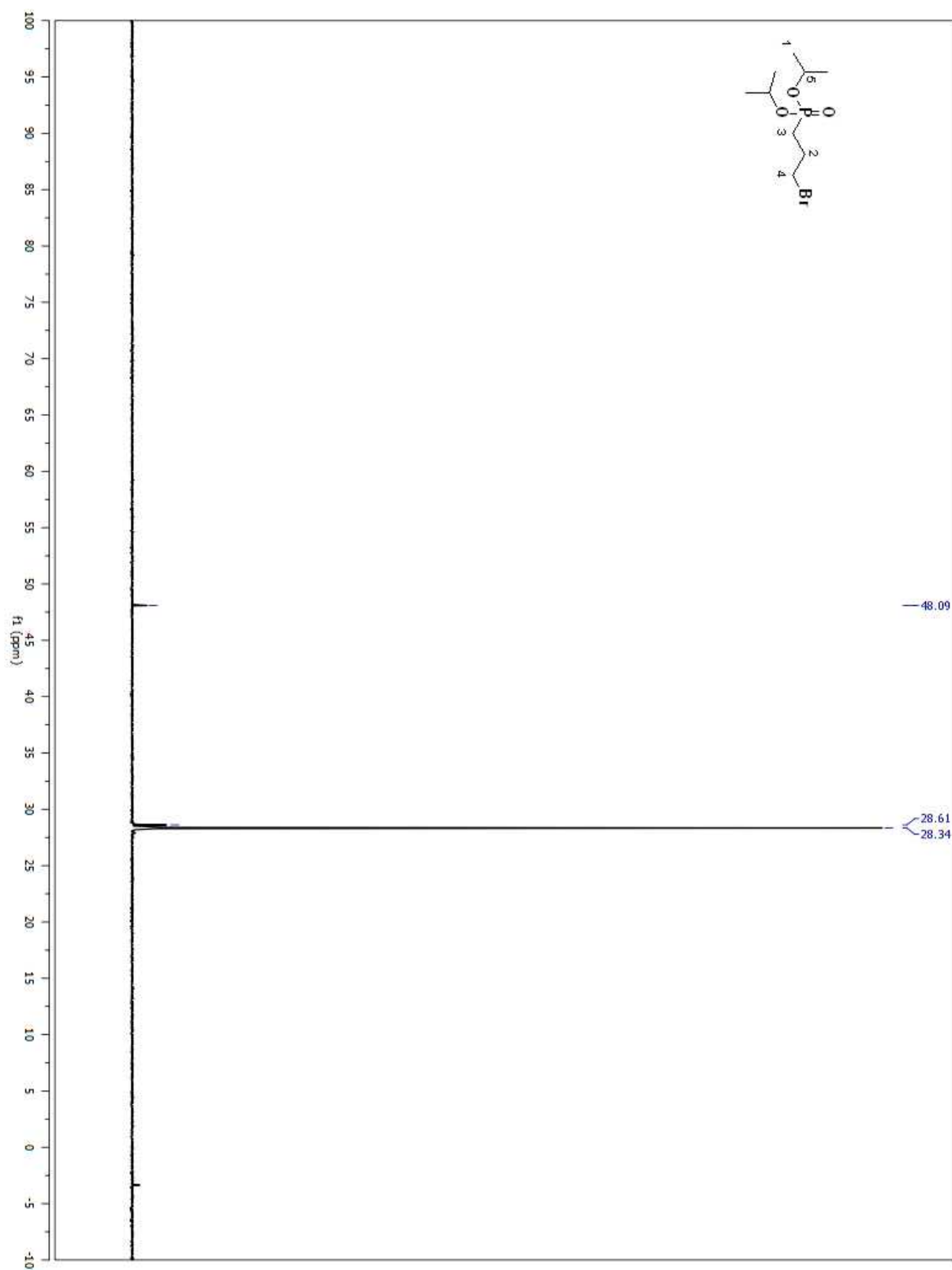


Figure A 30. ^{31}P NMR spectrum of compound **13** in CDCl_3 (Table 2.3, entry vii)

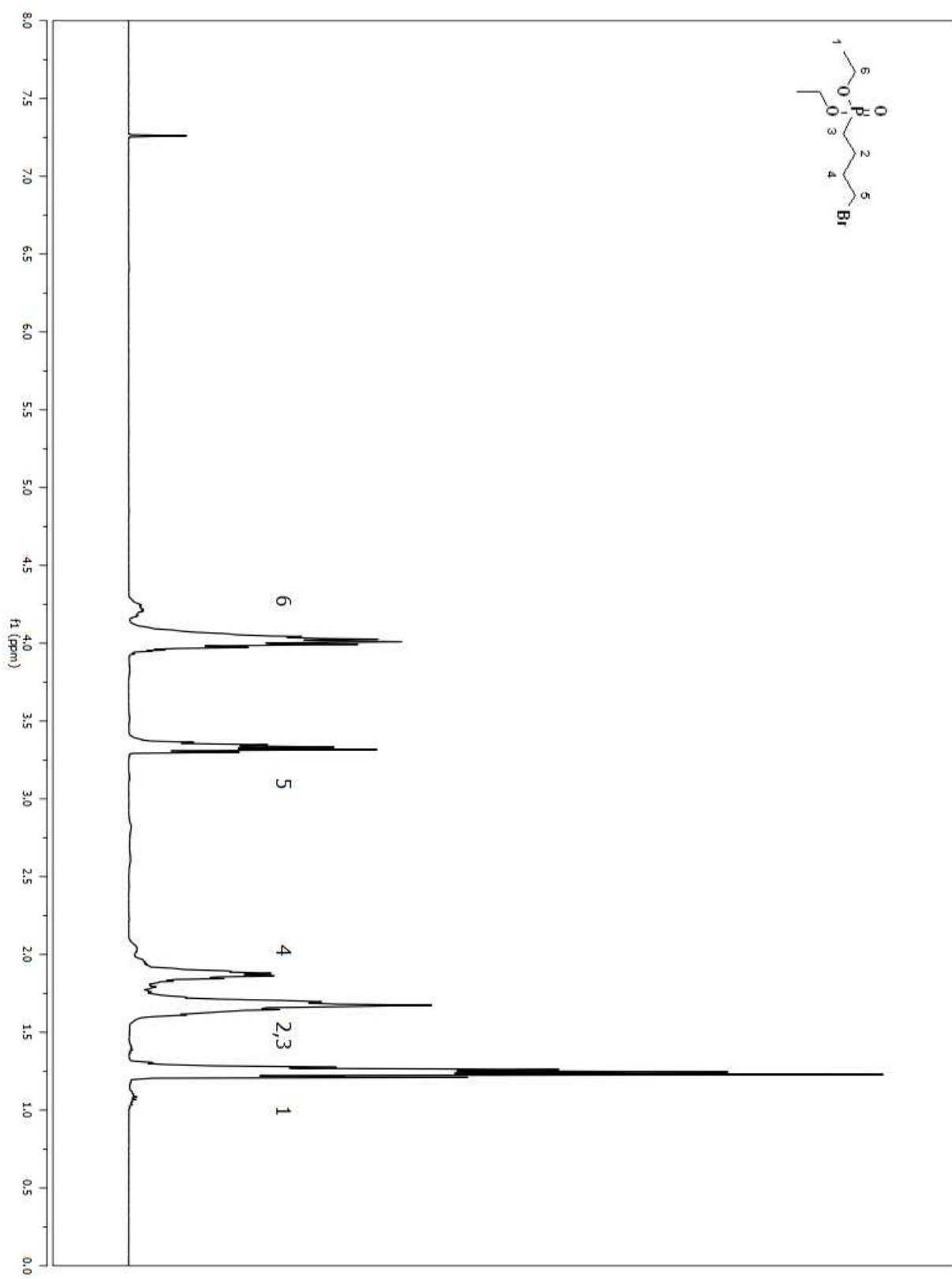


Figure A 31. ^1H NMR spectrum of compound **14** in CDCl_3 (Table 2.3, entry ix)

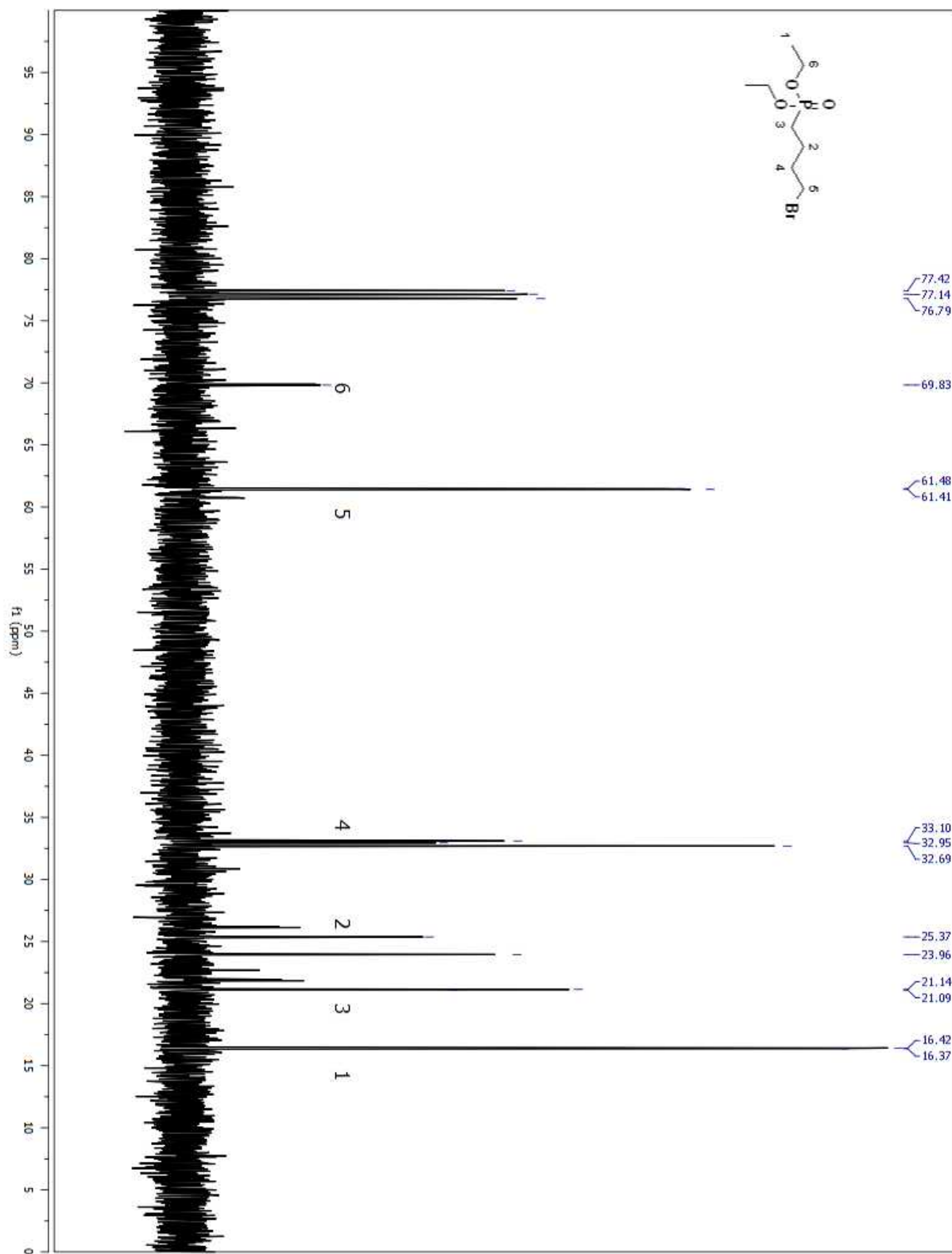


Figure A 32. ^{13}C NMR spectrum of compound **14** in CDCl_3 (Table 2.3, entry ix)

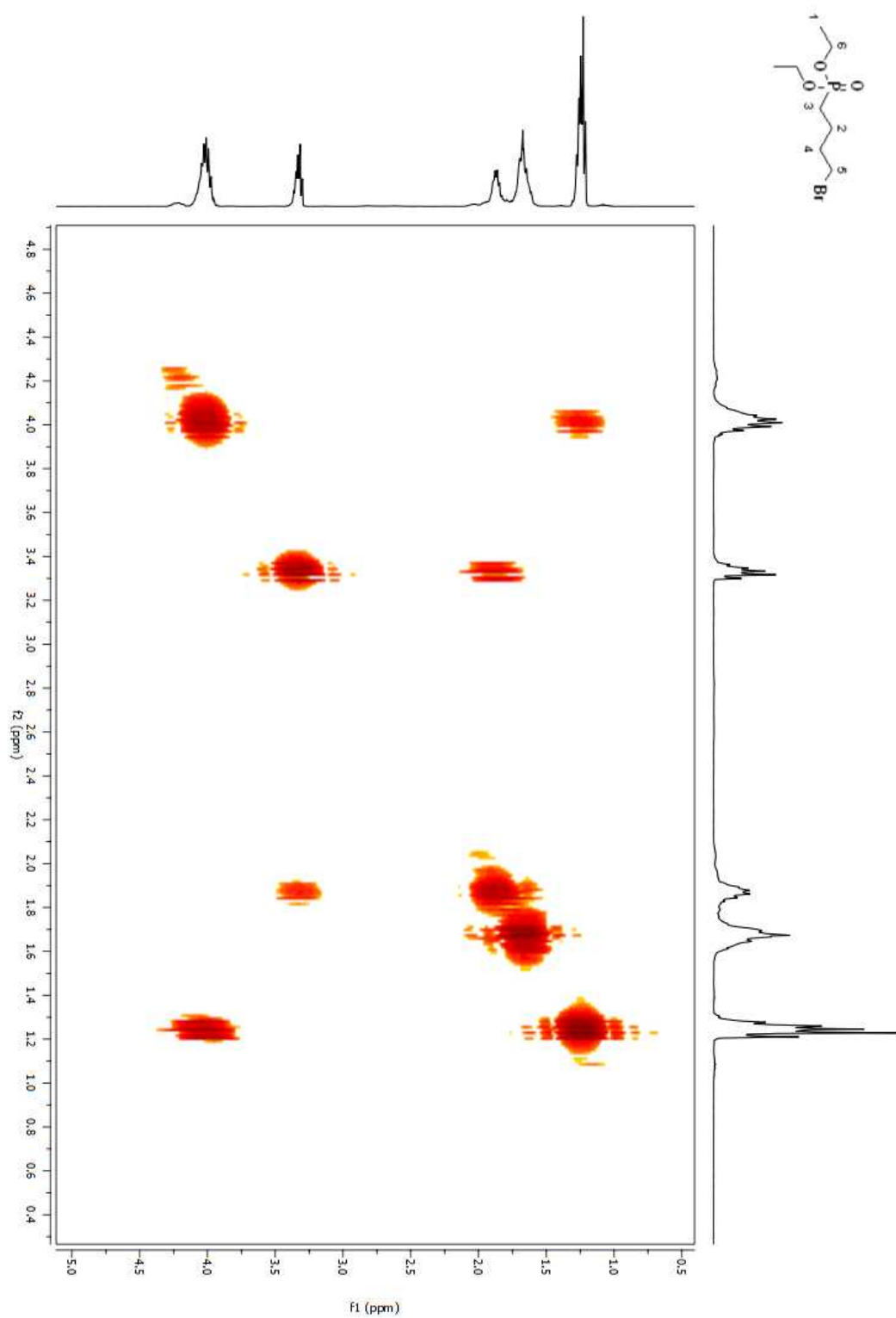


Figure A 33. COSY 2D NMR spectrum of compound **14** in CDCl_3 (Table 2.3, entry ix)

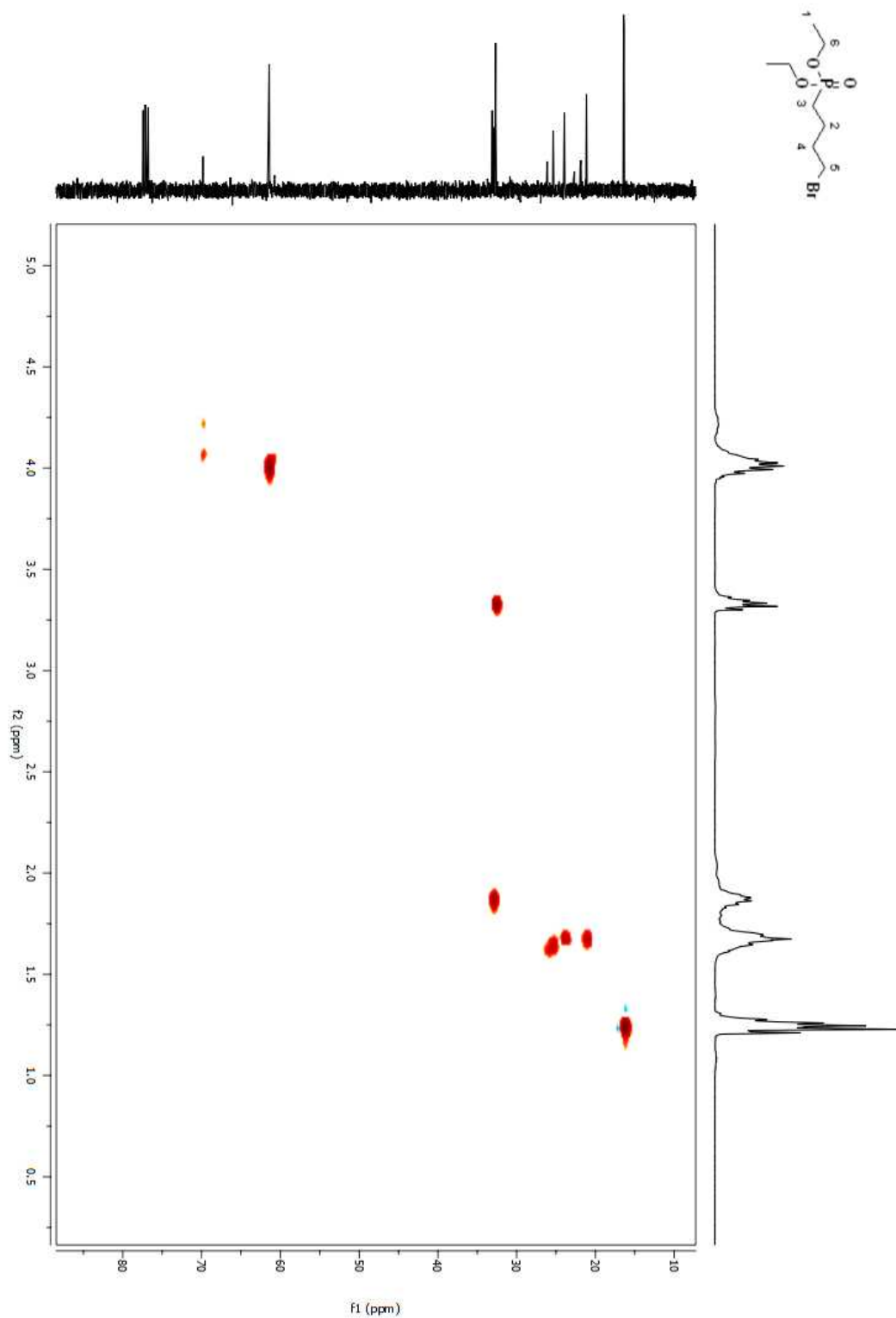


Figure A 34. HSQC 2D NMR spectrum of compound **14** in CDCl₃ (Table 2.3, entry ix)

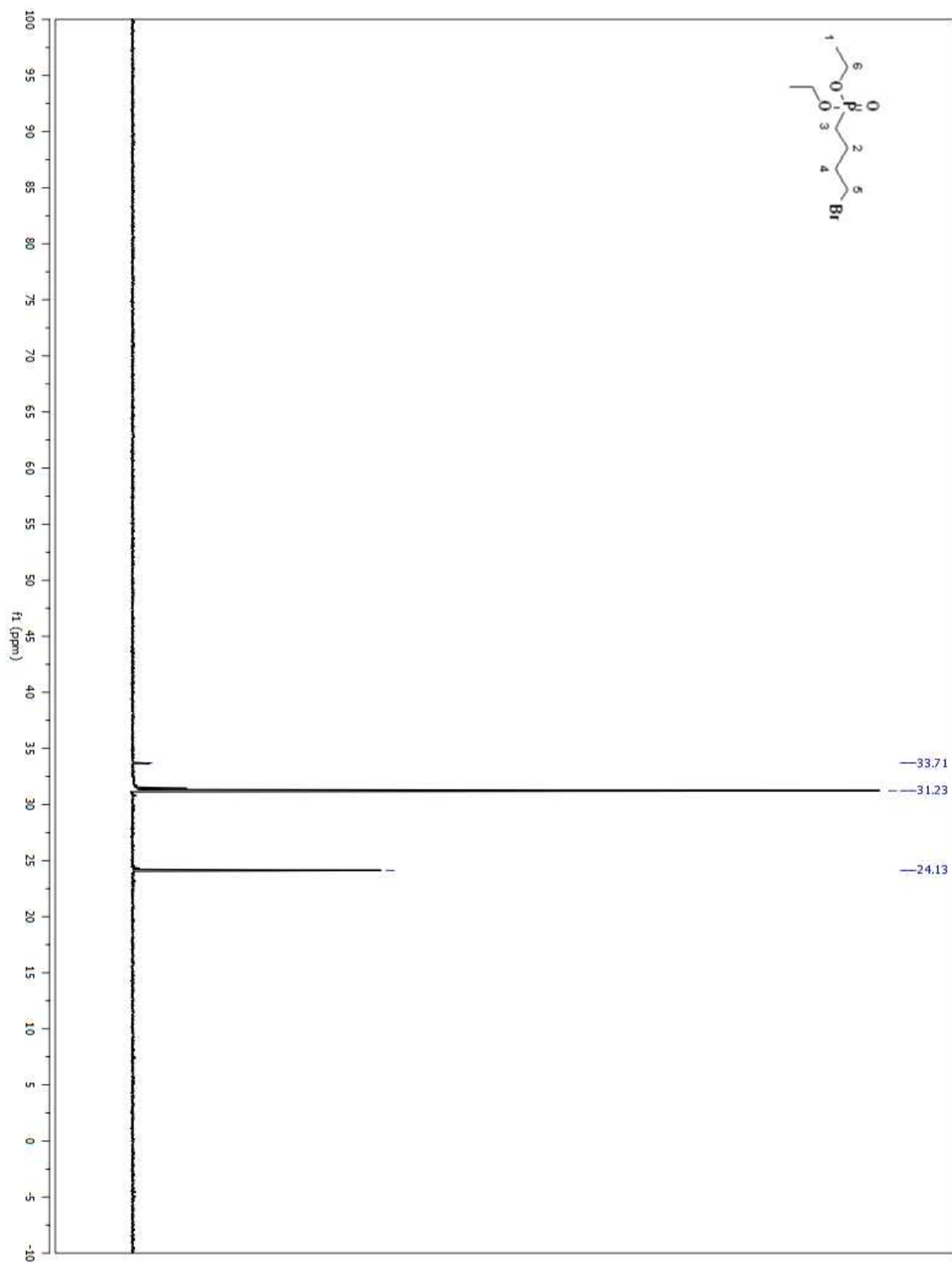


Figure A 35. ^{31}P NMR spectrum of compound **14** in CDCl_3 (Table 2.3, entry ix)

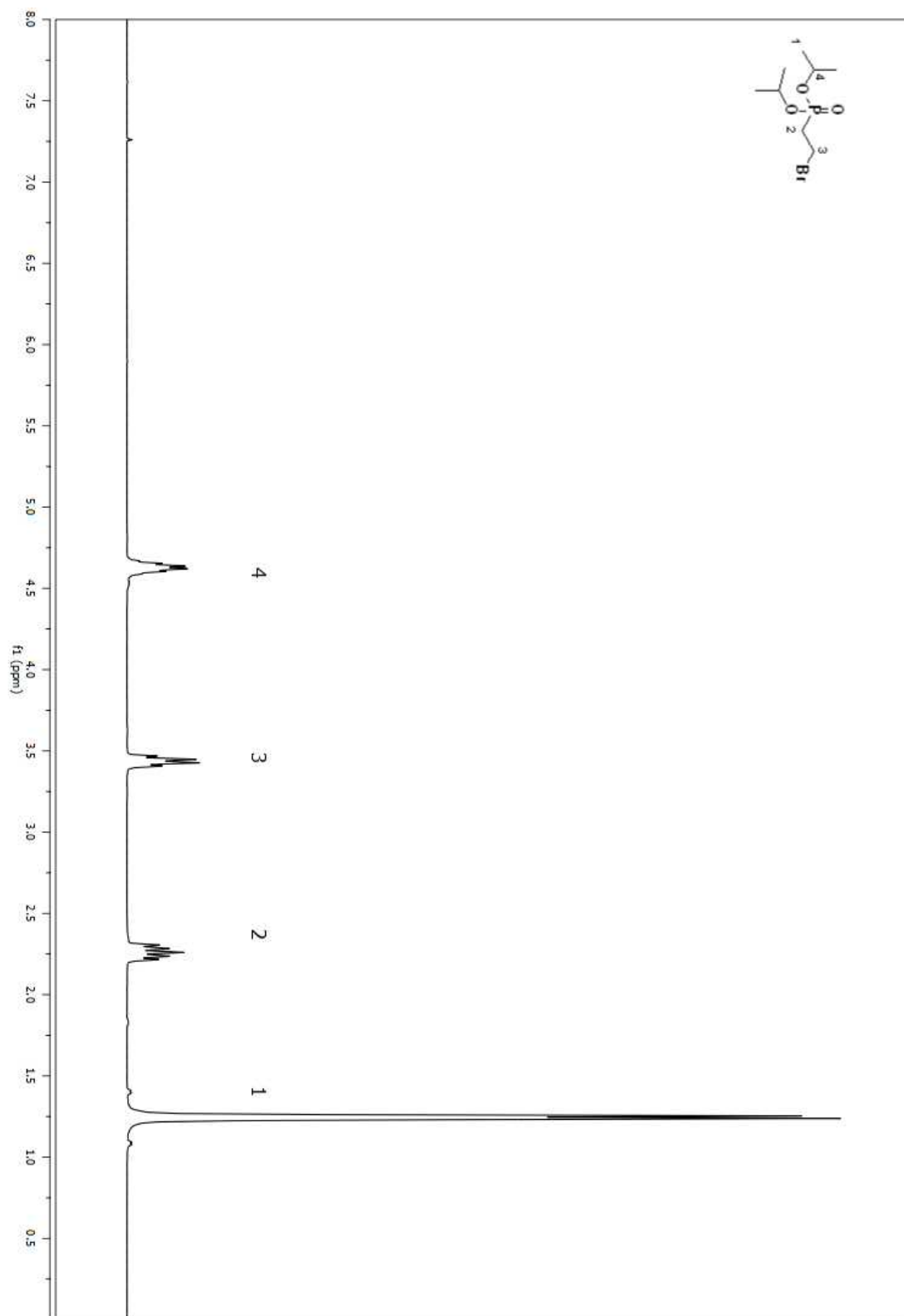


Figure A 36. ^1H NMR spectrum of compound **16** in CDCl_3 (Table 2.3, entry xv)

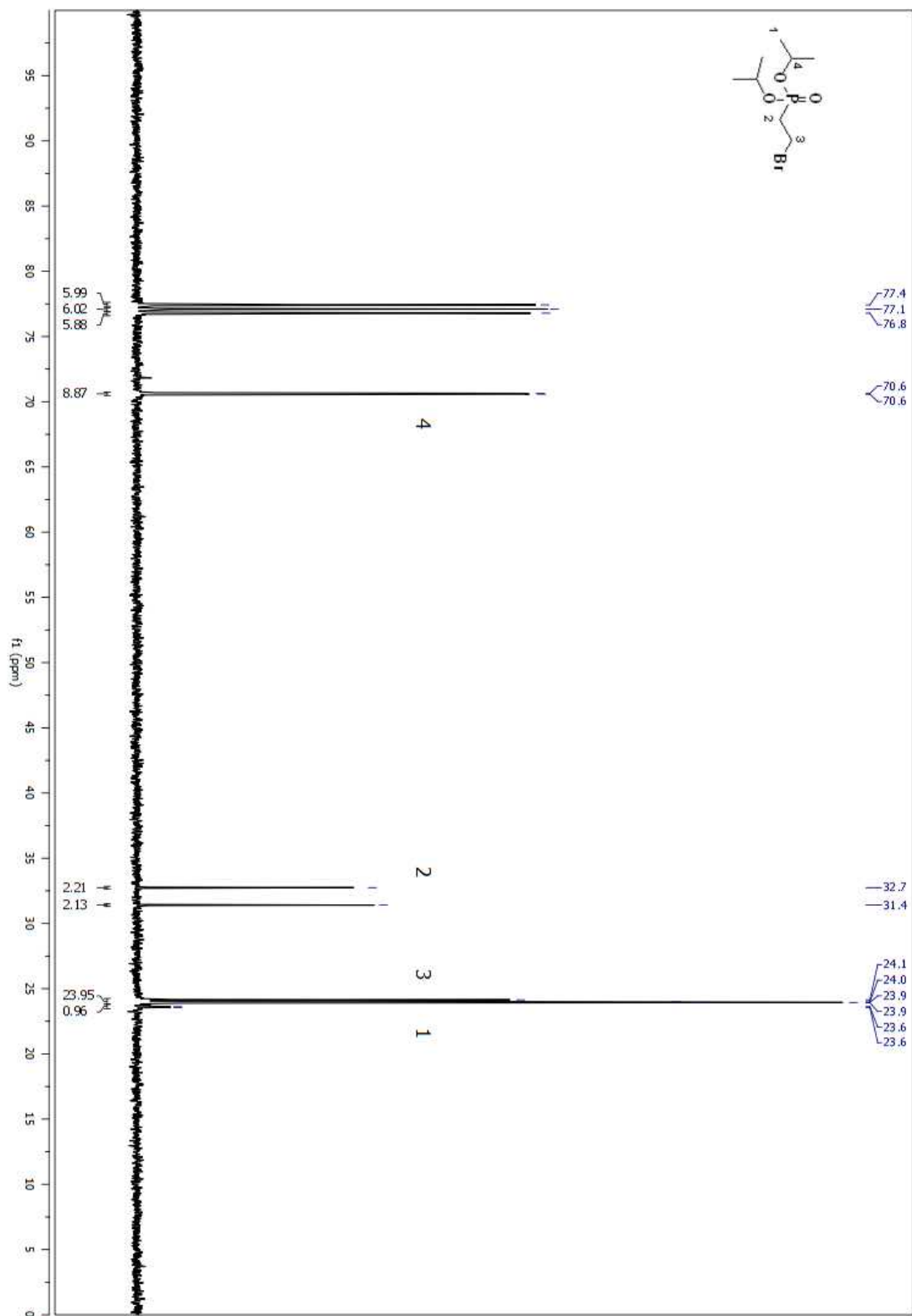


Figure A 37. ¹³C NMR spectrum of compound **16** in CDCl₃ (Table 2.3, entry xv)

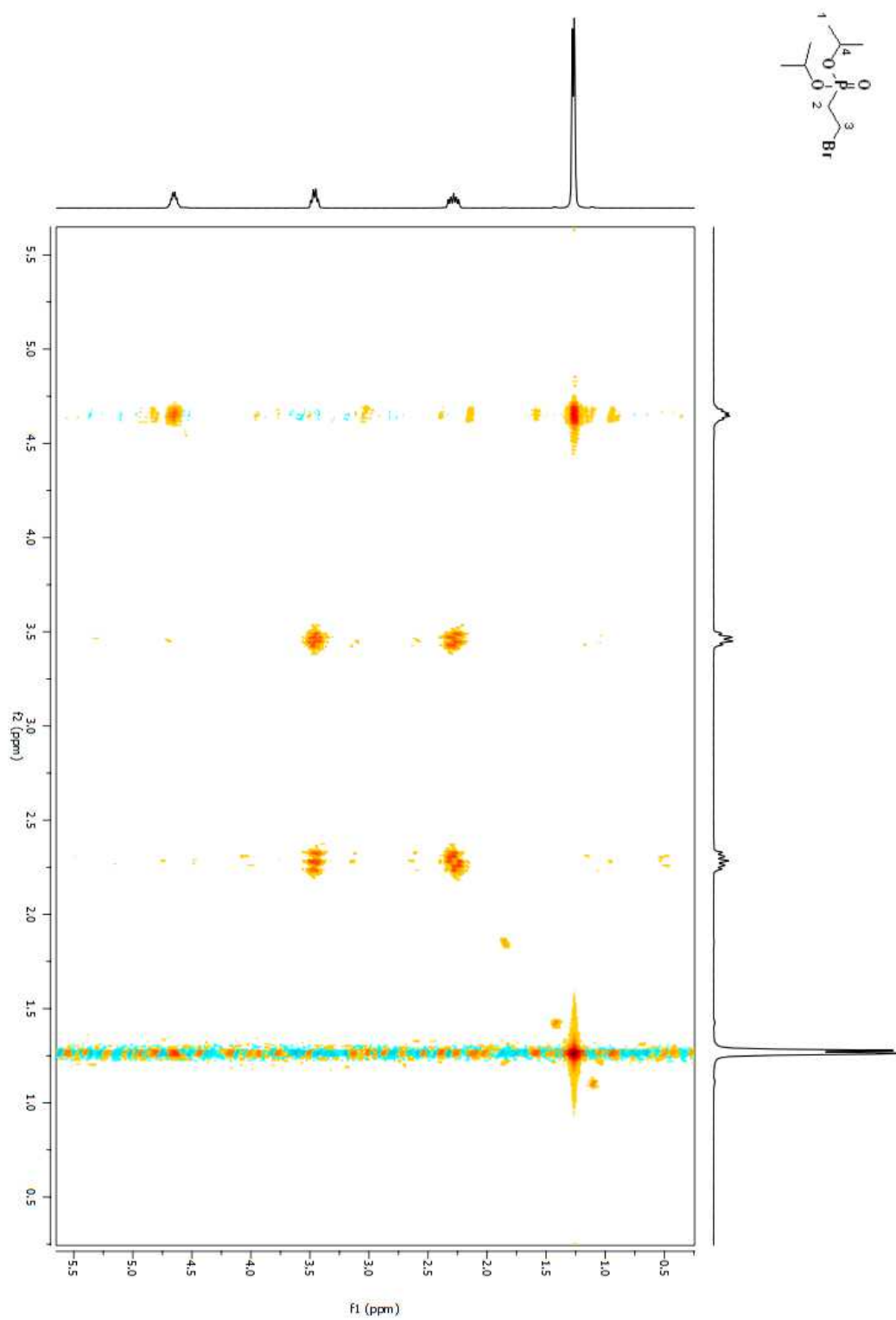


Figure A 38. COSY 2D NMR spectrum of compound **16** in CDCl₃ (Table 2.3, entry xv)

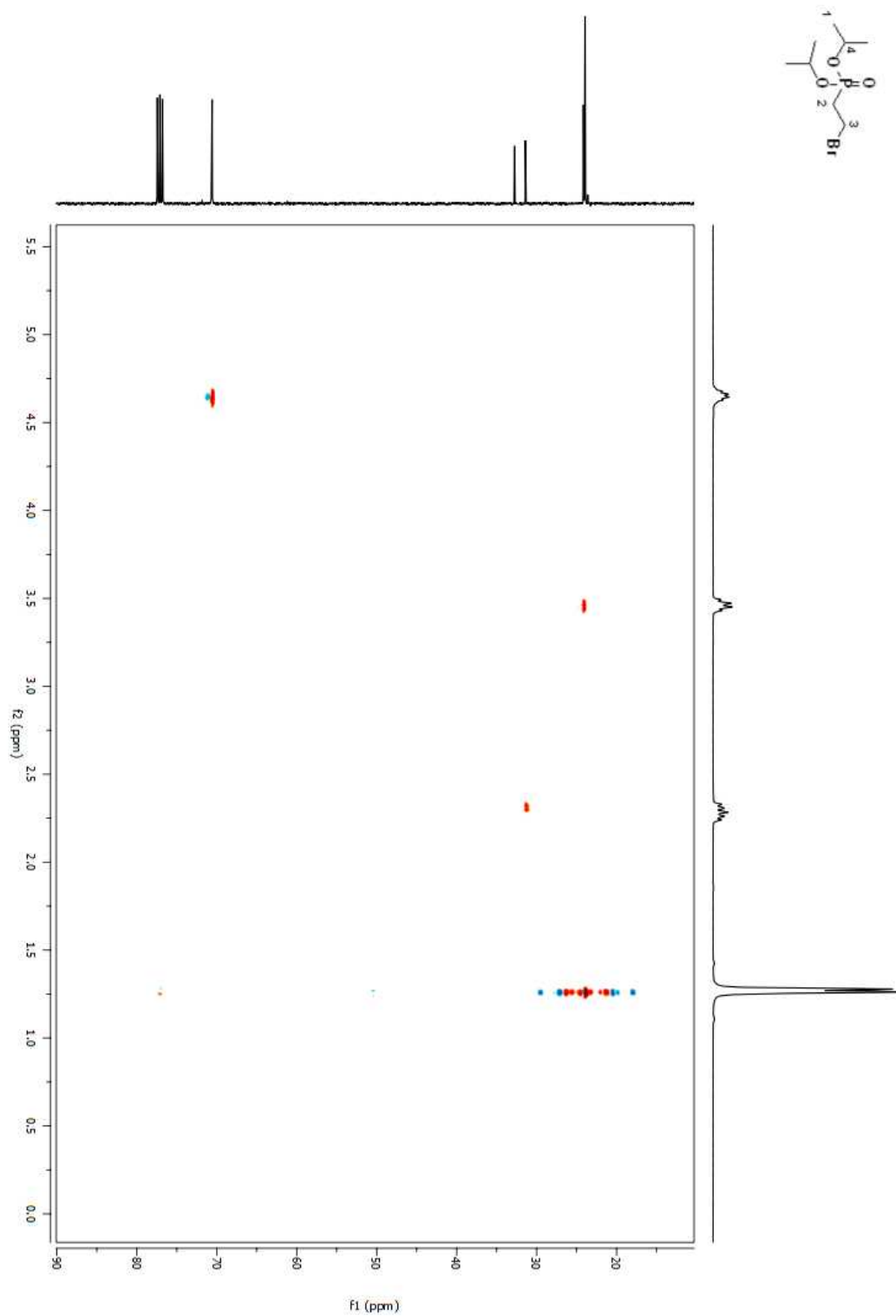


Figure A 39. HSQC 2D NMR spectrum of compound **16** in CDCl_3 (Table 2.3, entry xv)

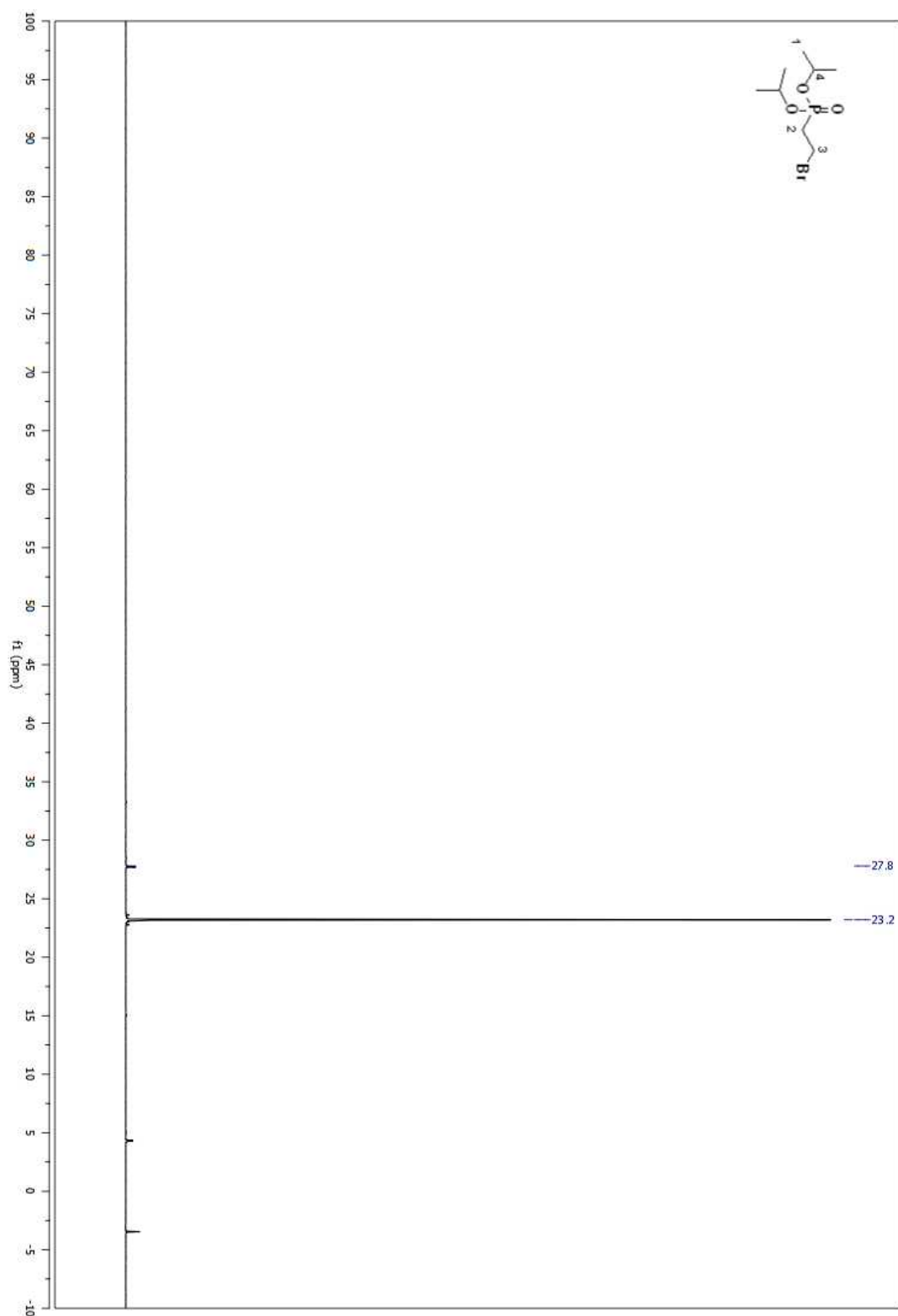


Figure A 40. ^{31}P NMR spectrum of compound **16** in CDCl_3 (Table 4.3, entry xv)

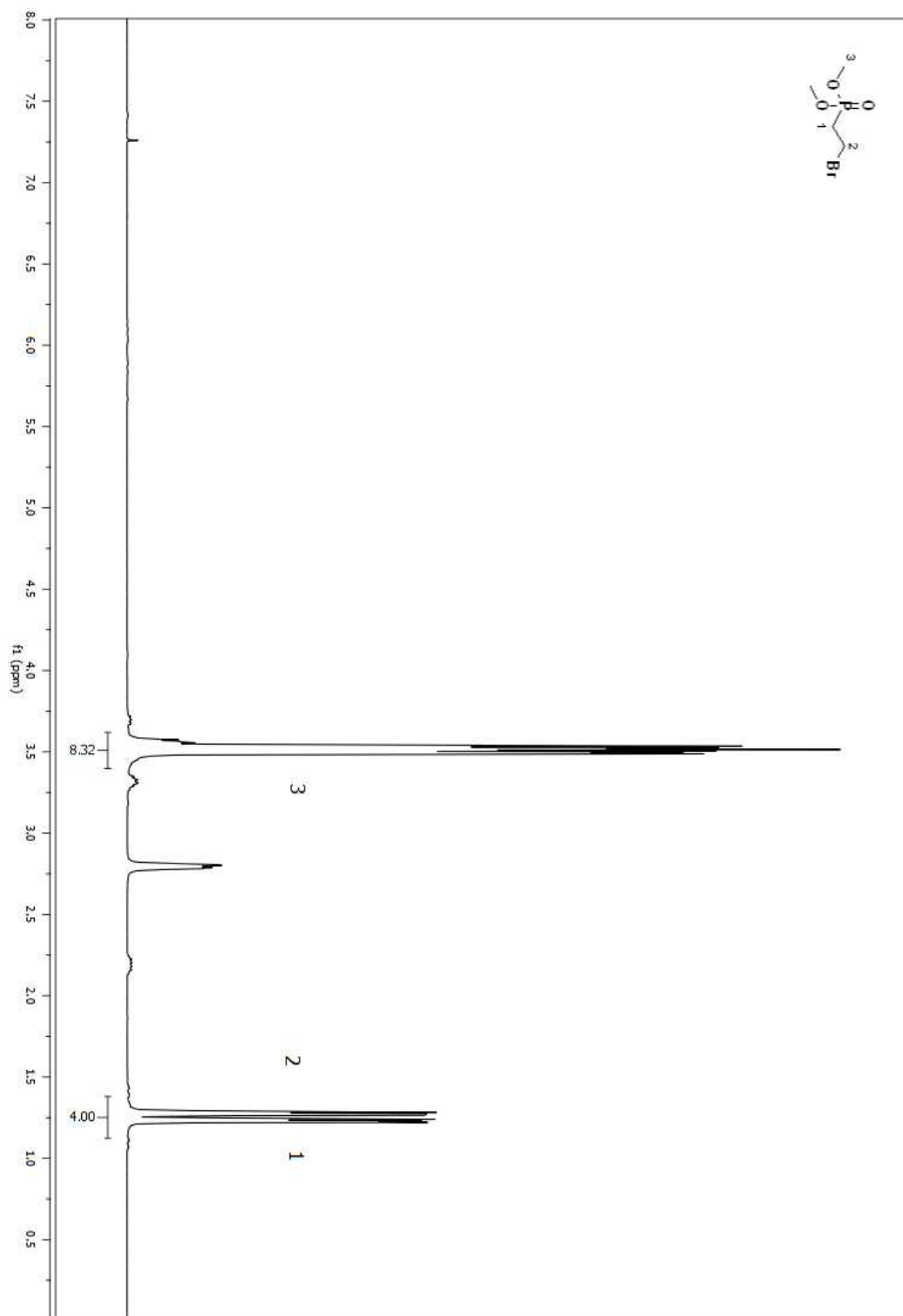


Figure A 41. ^1H NMR spectrum of compound **17** in CDCl_3 (Table 2.3, entry xvi)

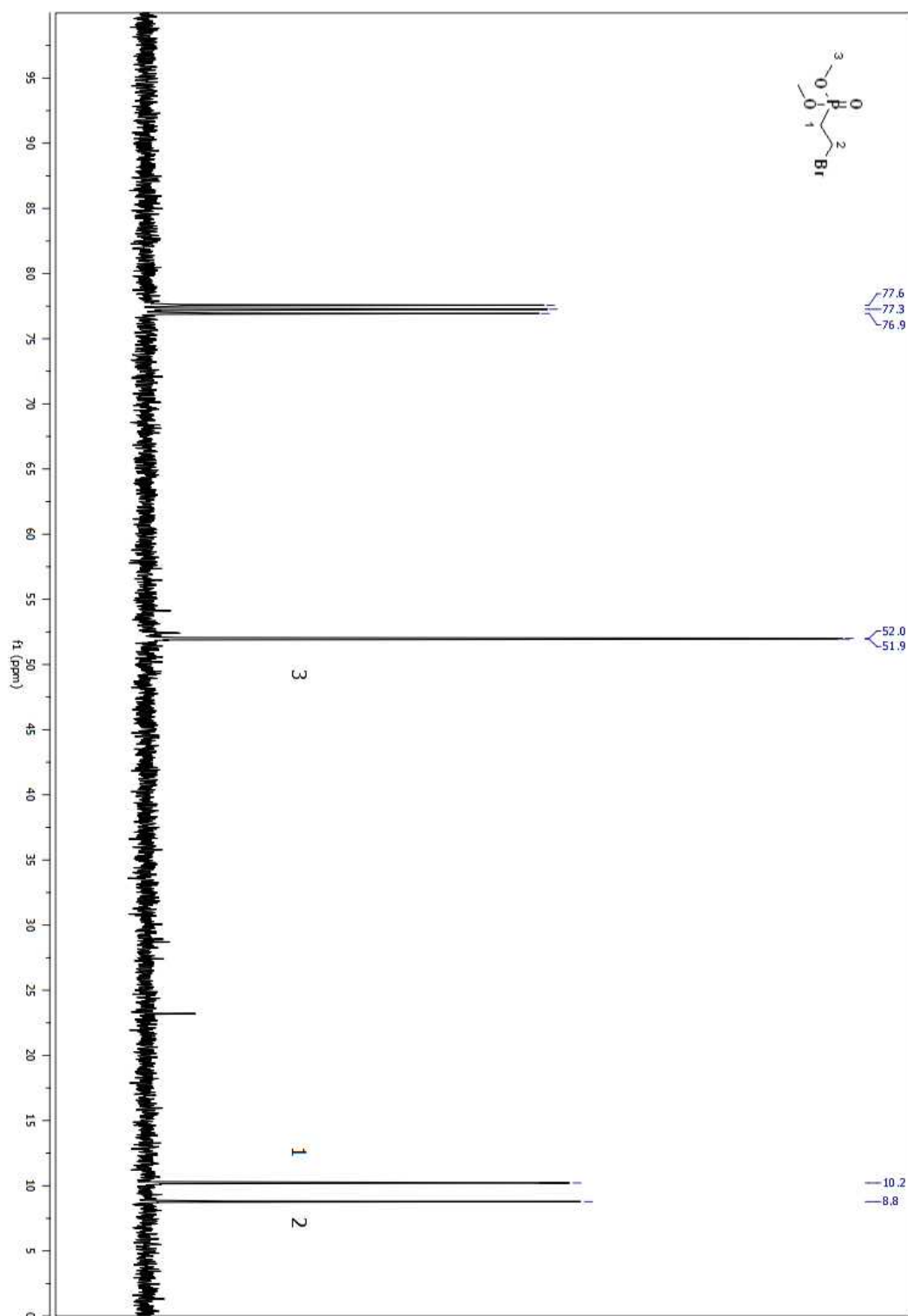


Figure A 42. ^{13}C NMR spectrum of compound **17** in CDCl_3 (Table 2.3, entry xvi)

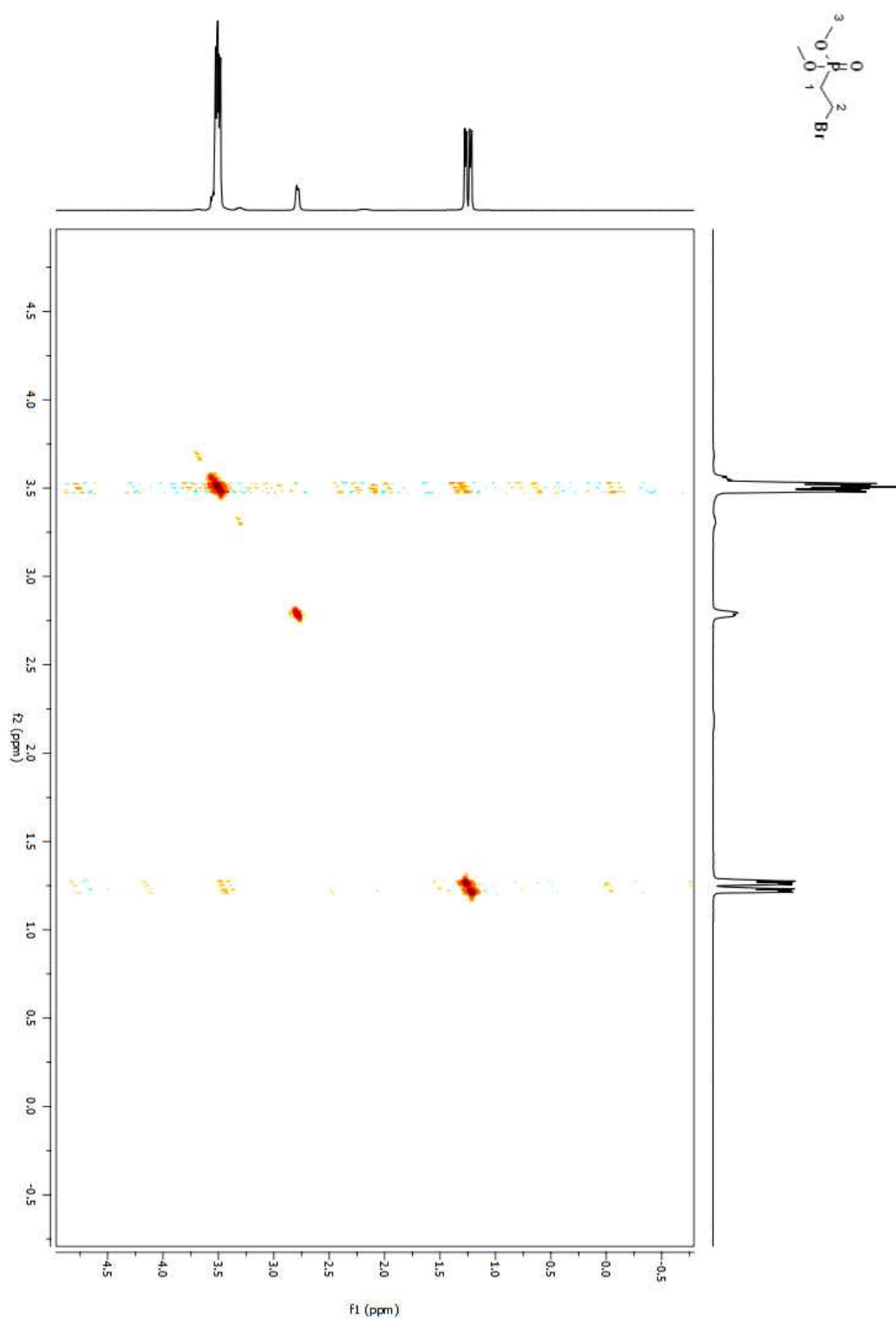


Figure A 43. COSY 2D NMR spectrum of compound **17** in CDCl_3 (Table 2.3, entry xvi)

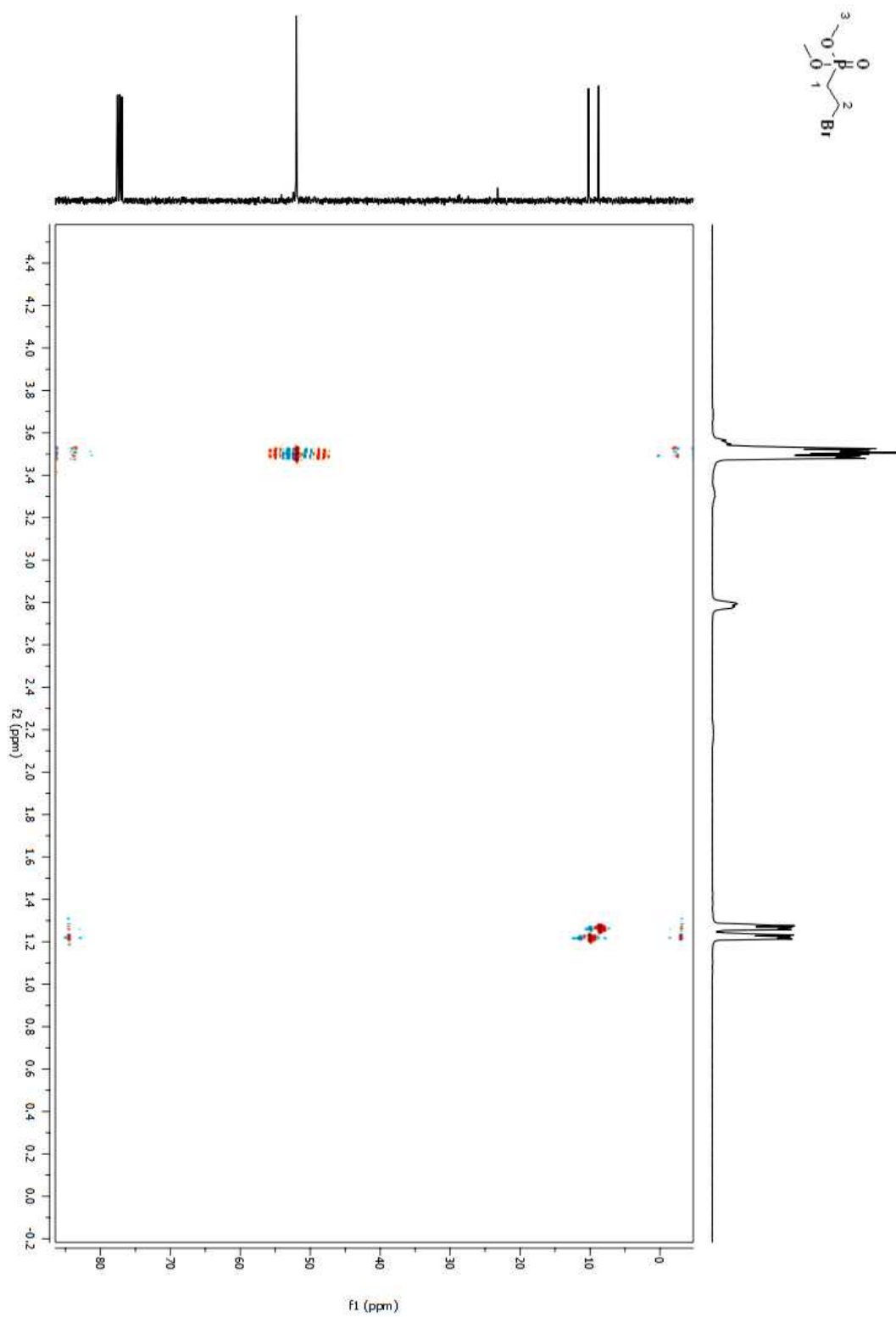


Figure A 44. HSQC 2D NMR spectrum of compound **17** in CDCl₃ (Table 2.3, entry xvi)

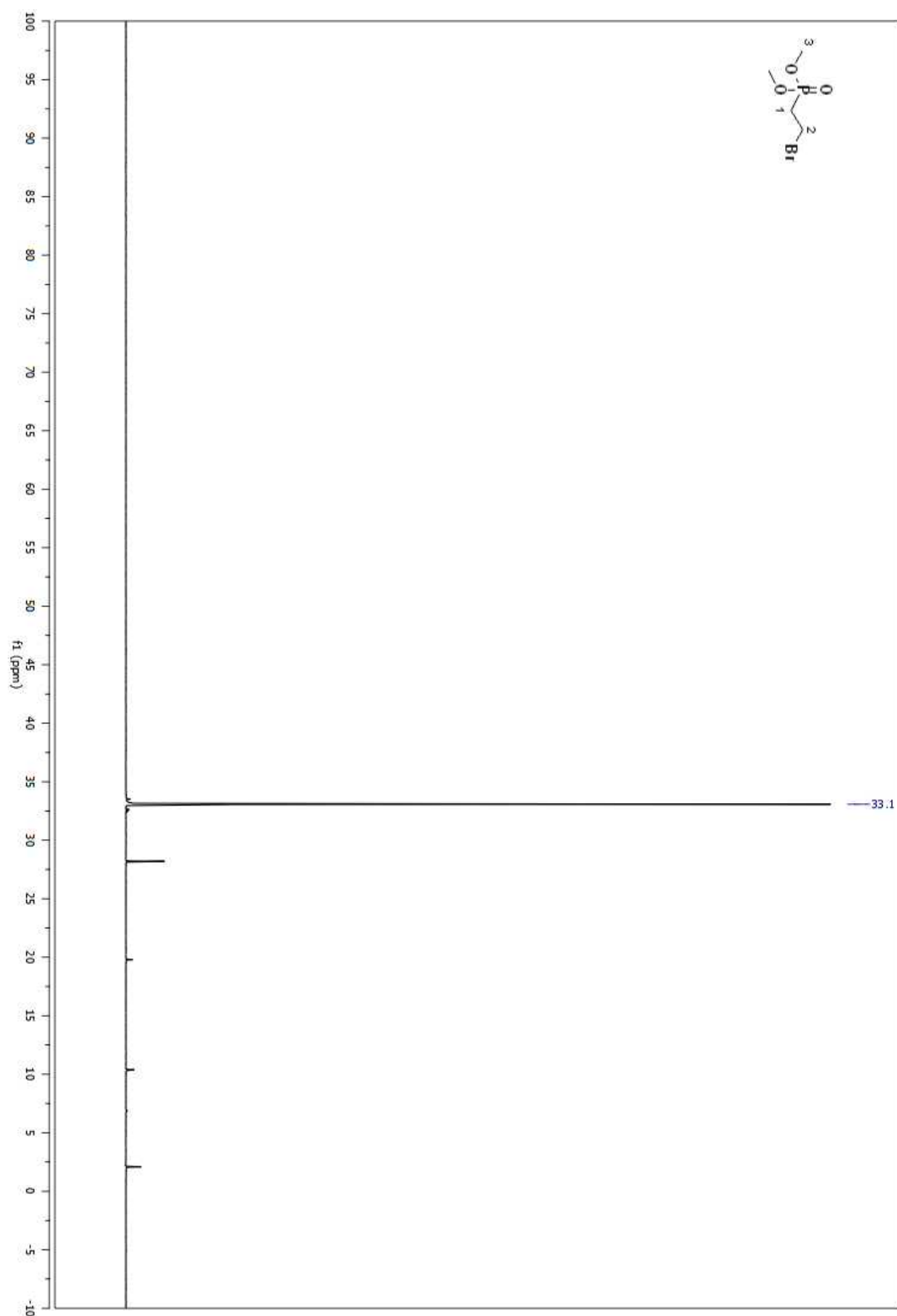


Figure A 45. ^{31}P NMR spectrum of compound **17** in CDCl_3 (Table 2.3, entry xvi)

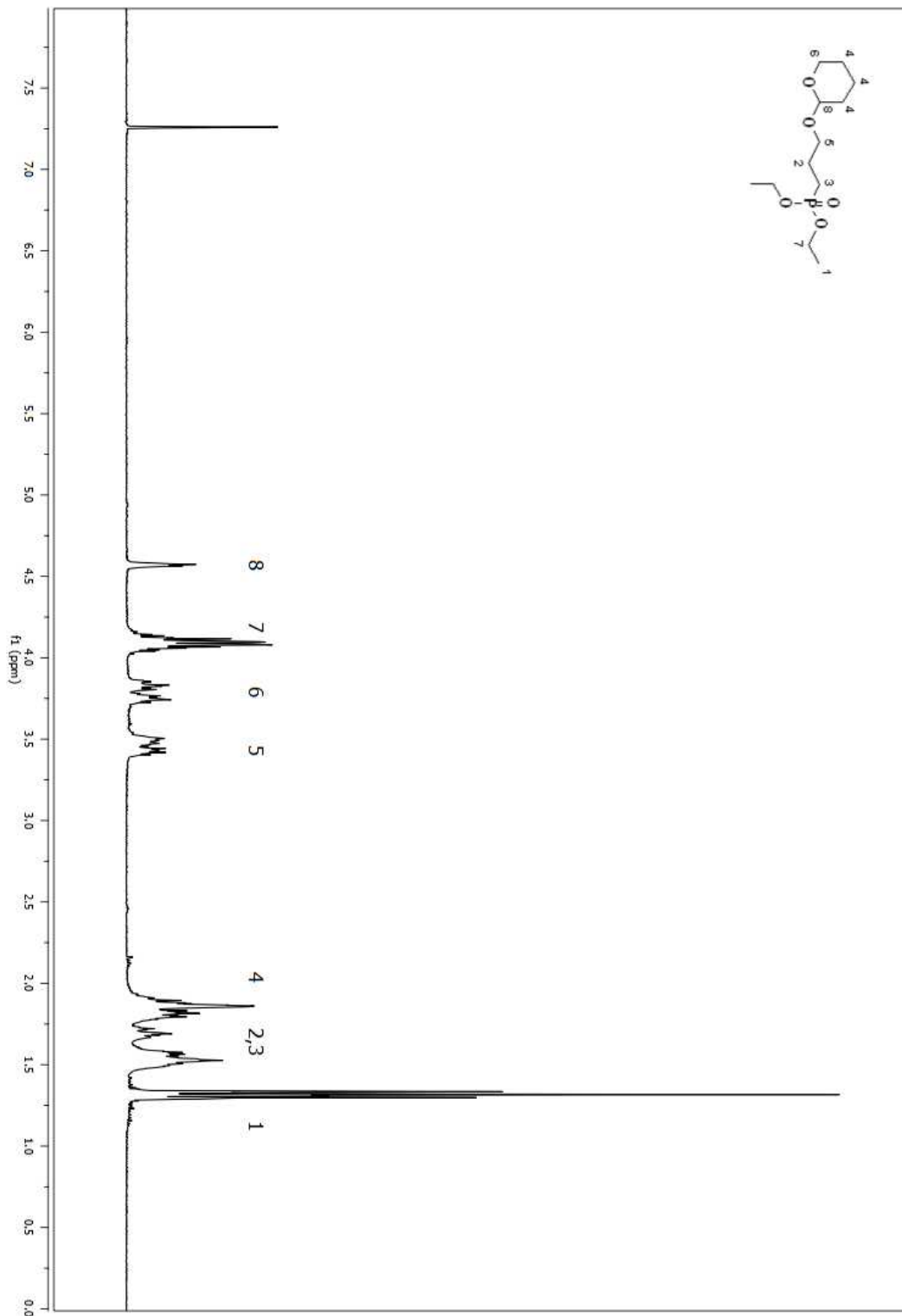


Figure A 46. ^1H NMR spectrum of compound **18** in CDCl_3 (Table 2.3, entry xvii)

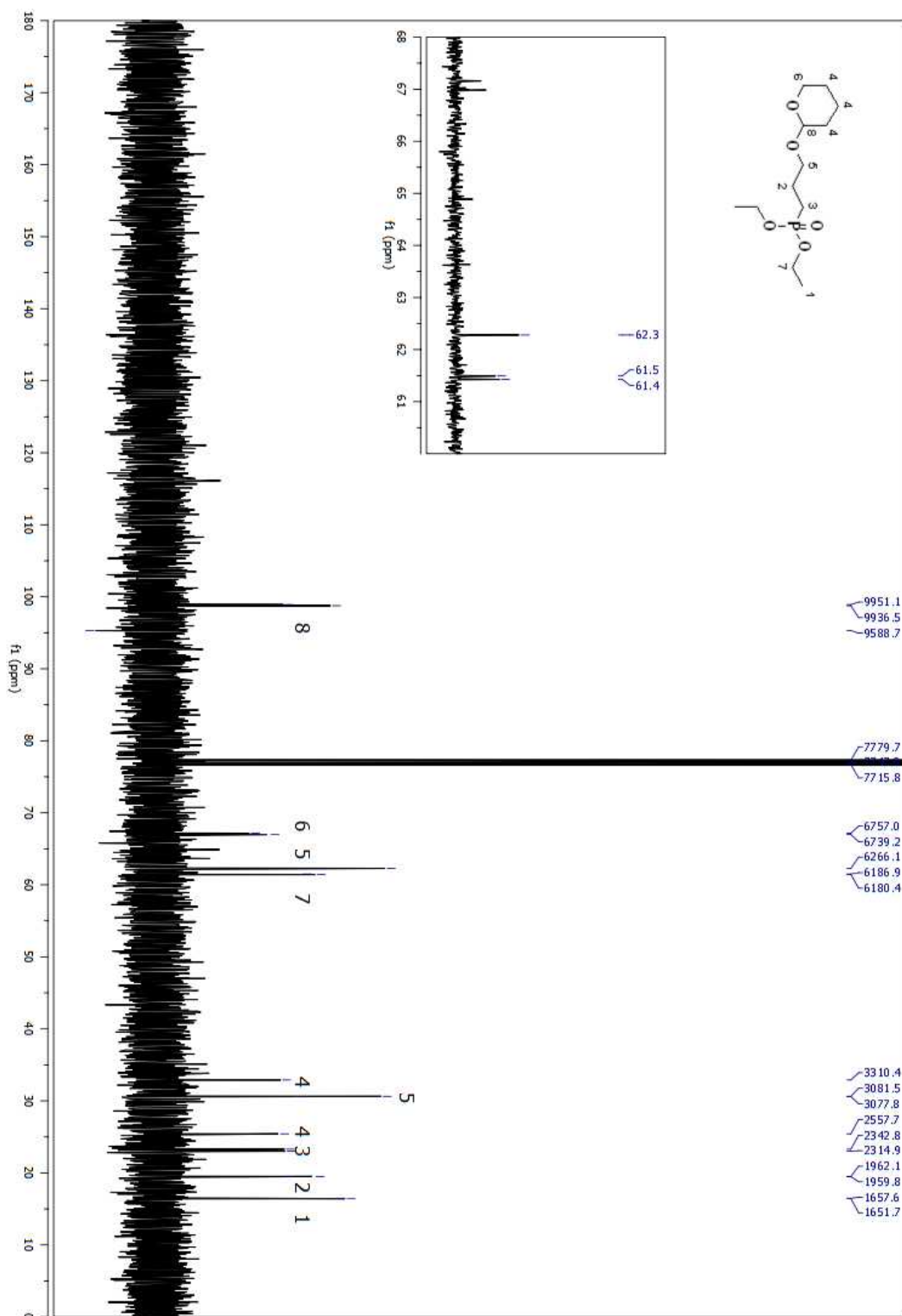


Figure A 47. ¹³C NMR spectrum of compound **18** in CDCl₃ (Table 2.3, entry xvii)

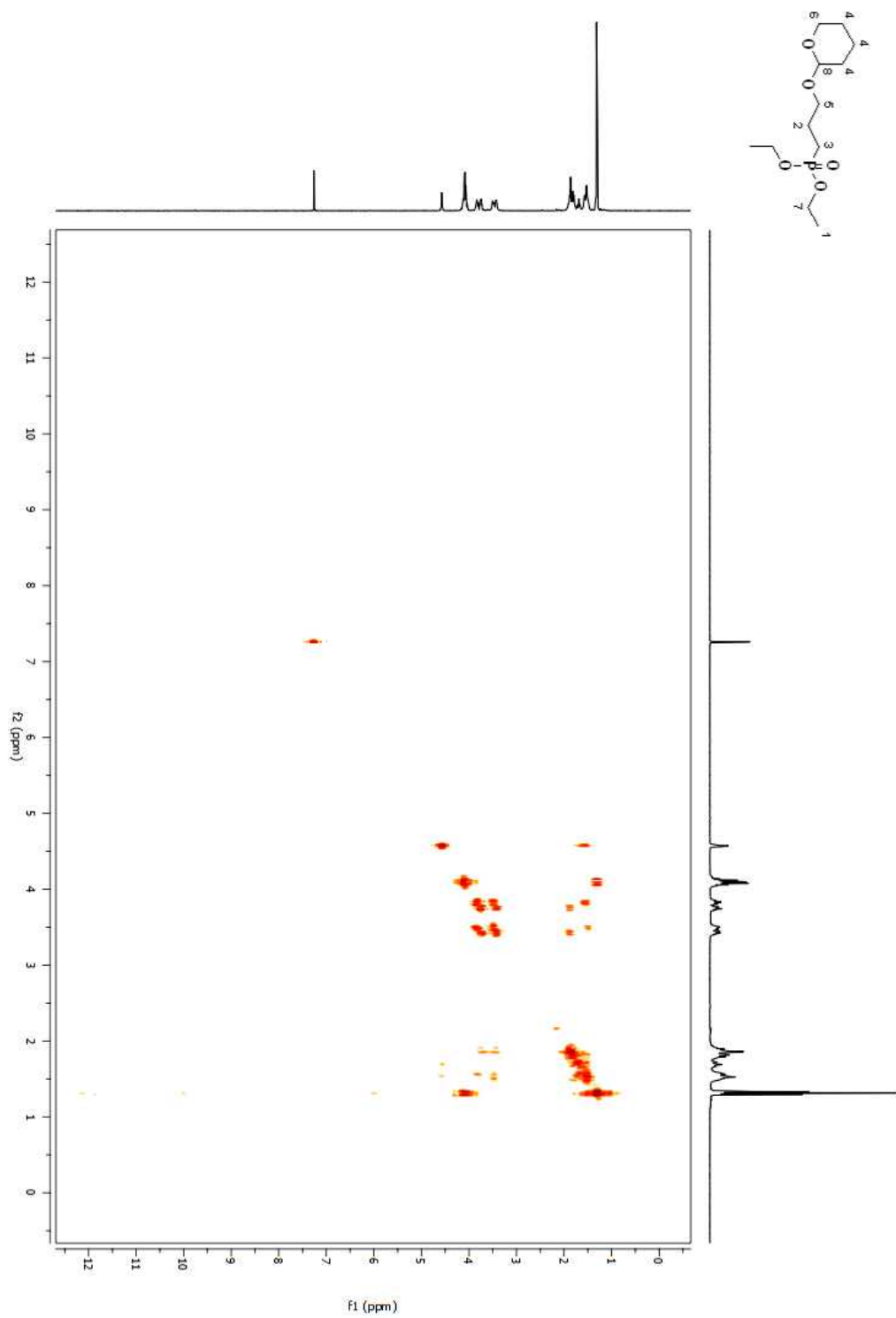


Figure A 48. COSY 2D NMR spectrum of compound **18** in CDCl₃ (Table 2.3, entry xvii)

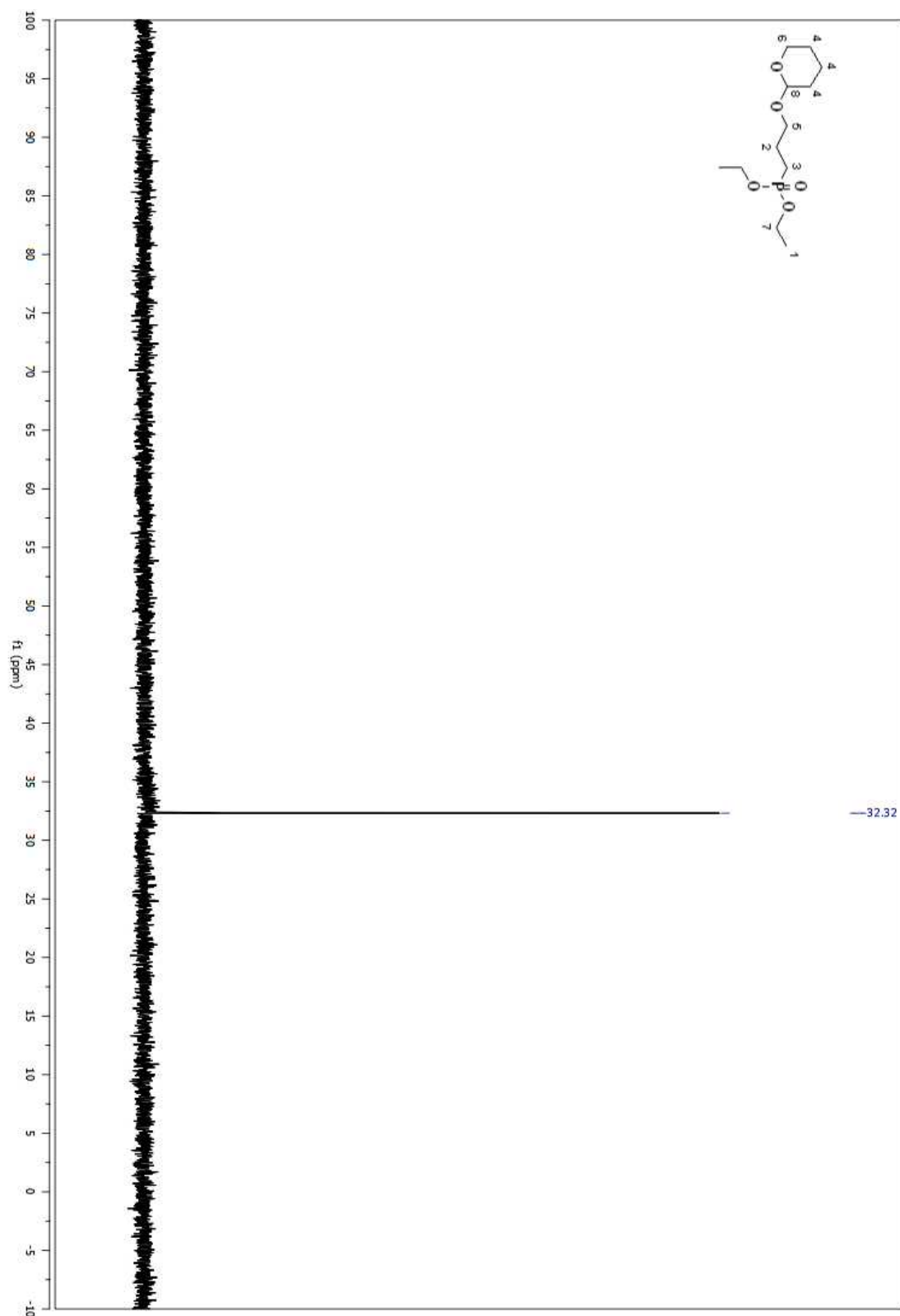


Figure A 49. ^{31}P NMR spectrum of compound **18** in CDCl_3 (Table 4.3, entry xvii)

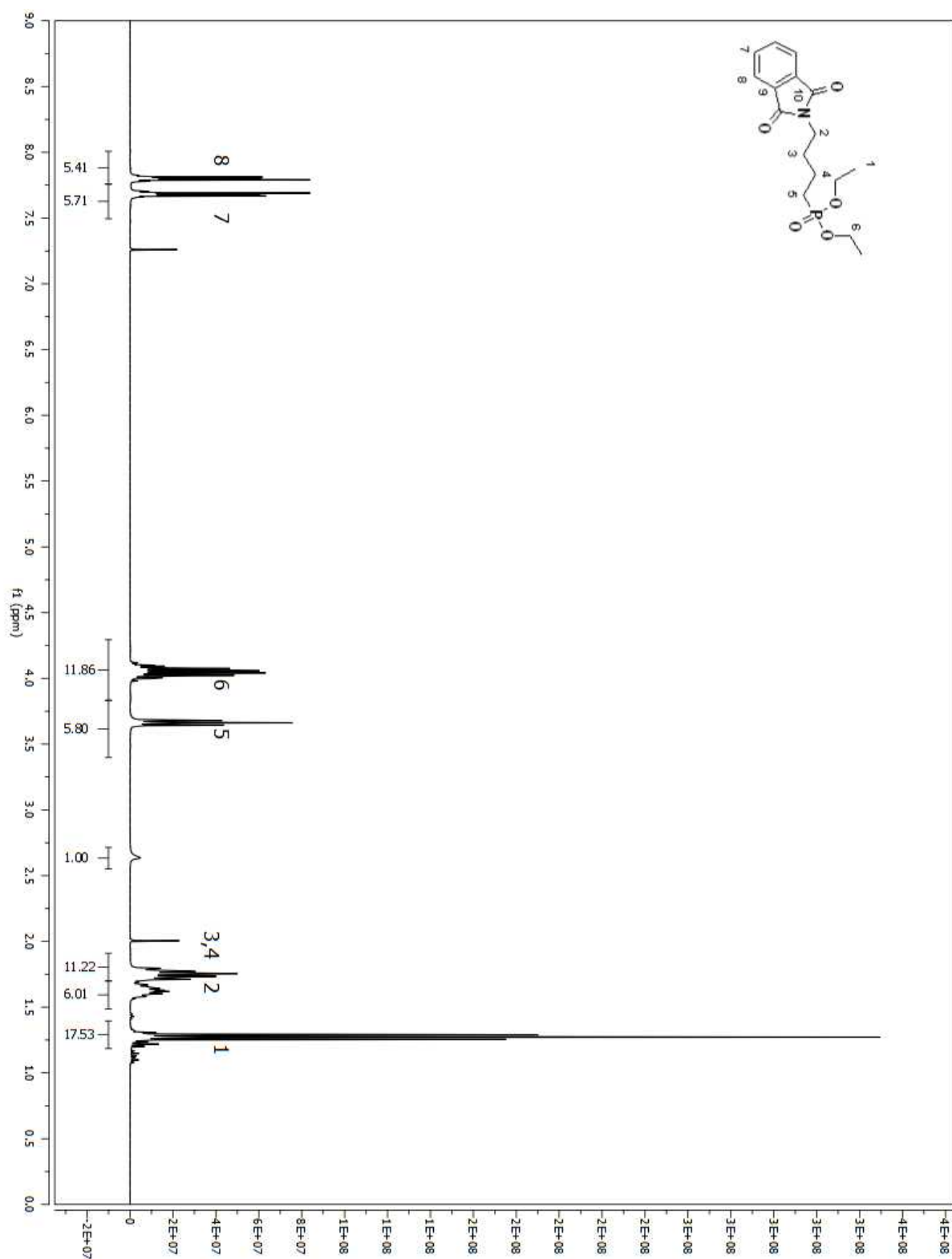


Figure A 50. ^1H NMR spectrum of compound **19** in CDCl_3 (Table 2.3, entry xviii)

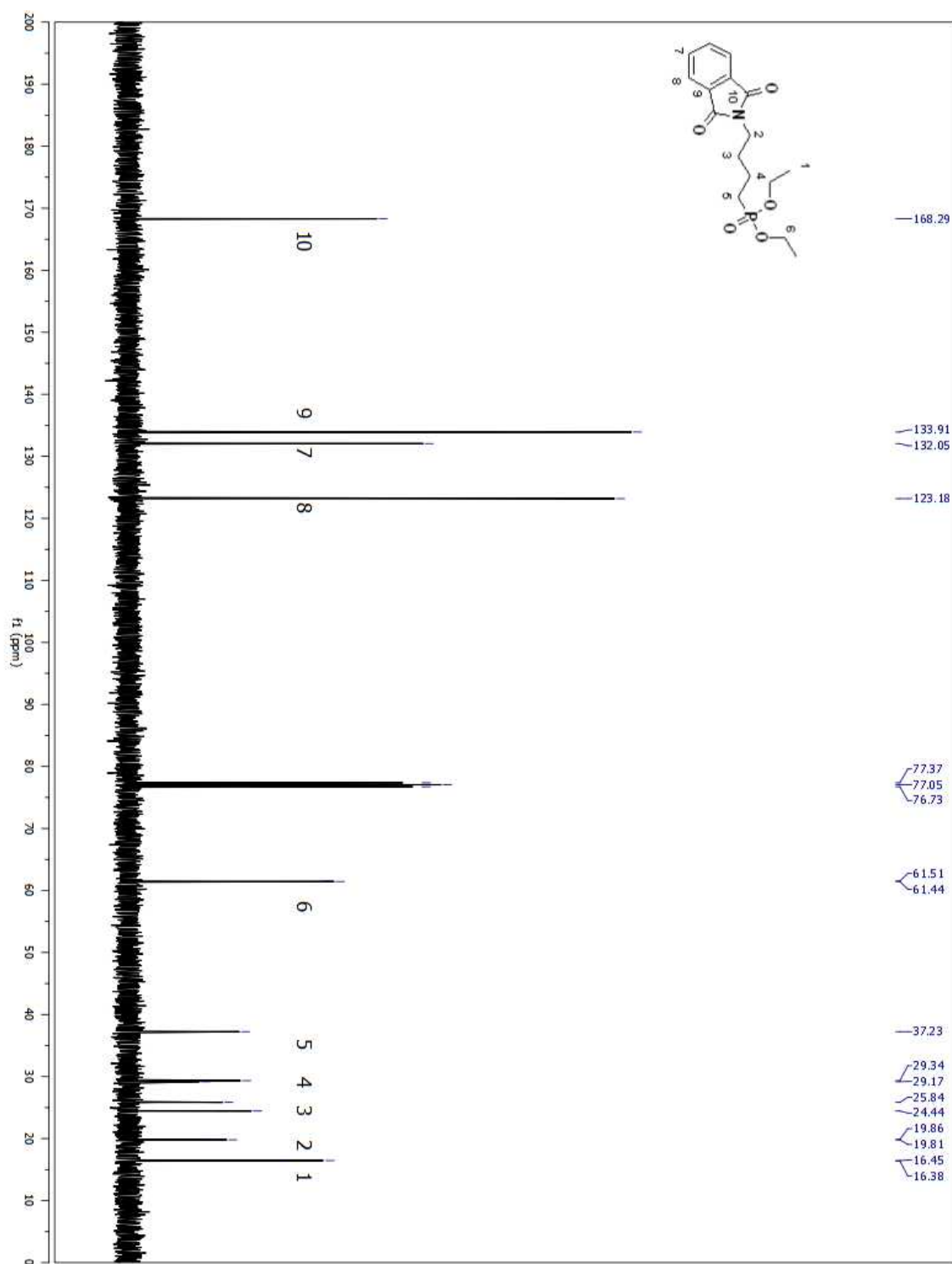


Figure A 51. ^{13}C NMR spectrum of compound **19** in CDCl_3 (Table 2.3, entry xviii)

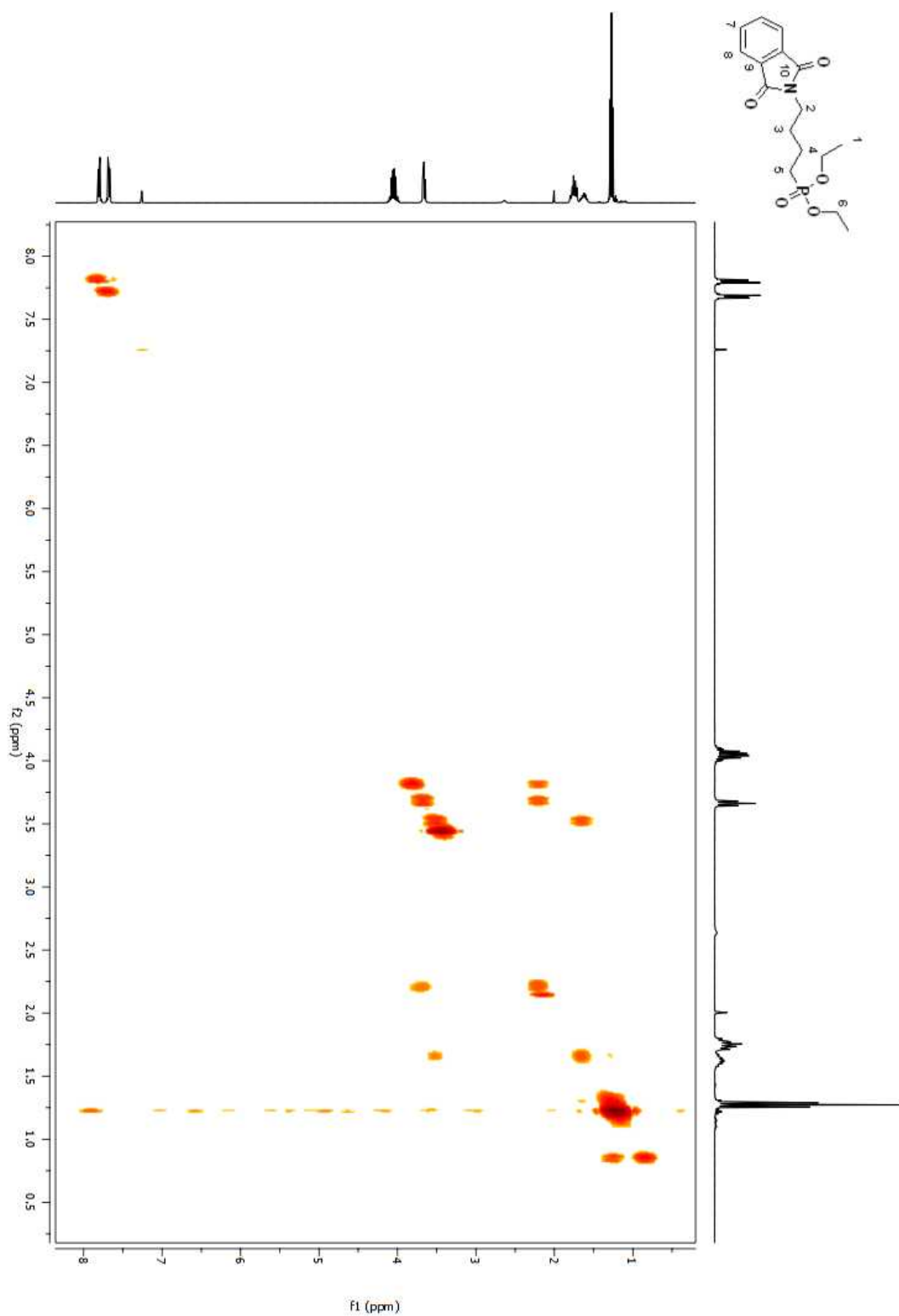


Figure A 52. COSY 2D NMR spectrum of compound **19** in CDCl₃ (Table 2.3, entry xviii)

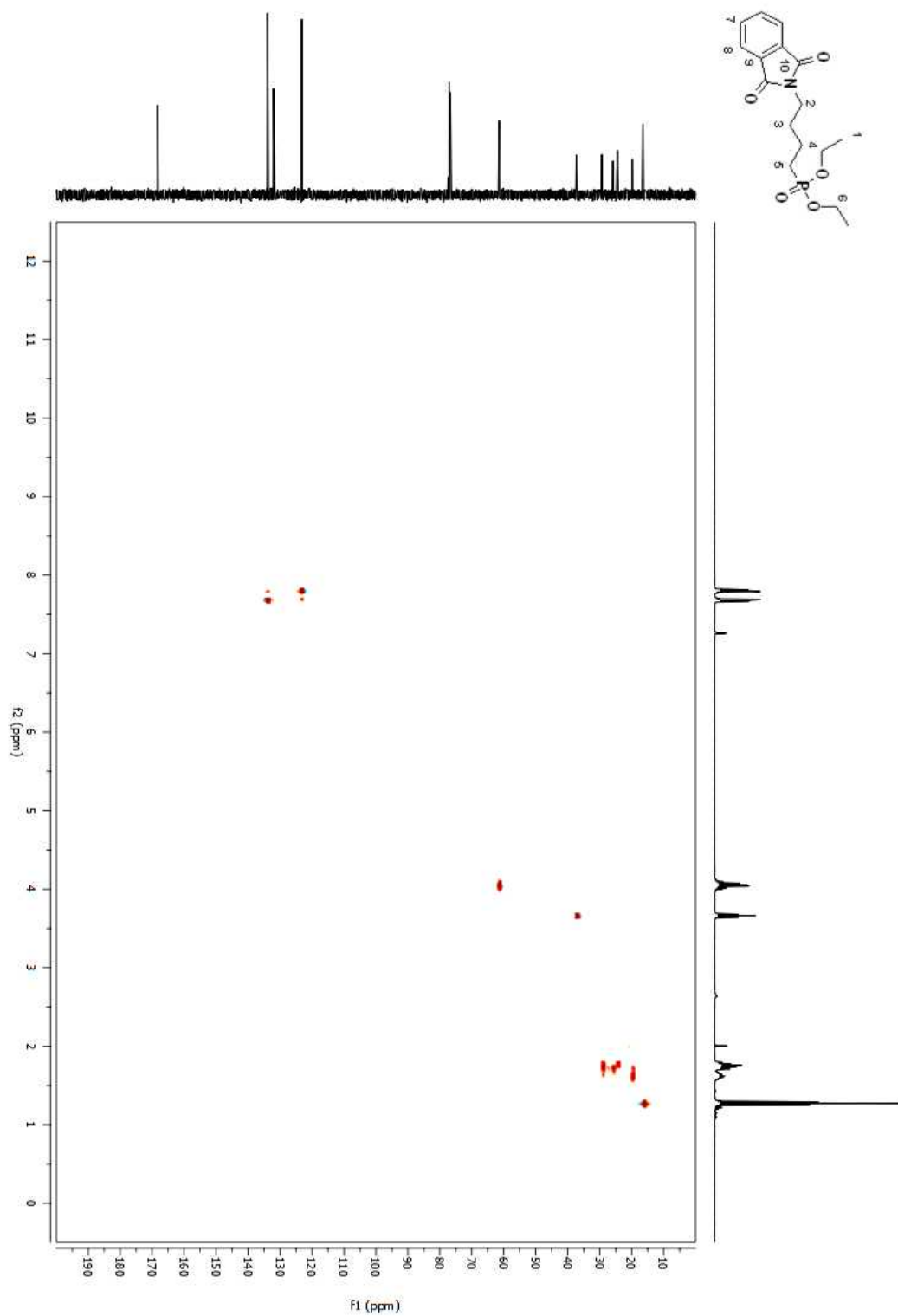


Figure A 53. HSQC 2D NMR spectrum of compound **19** in CDCl₃ (Table 2.3, entry xviii)

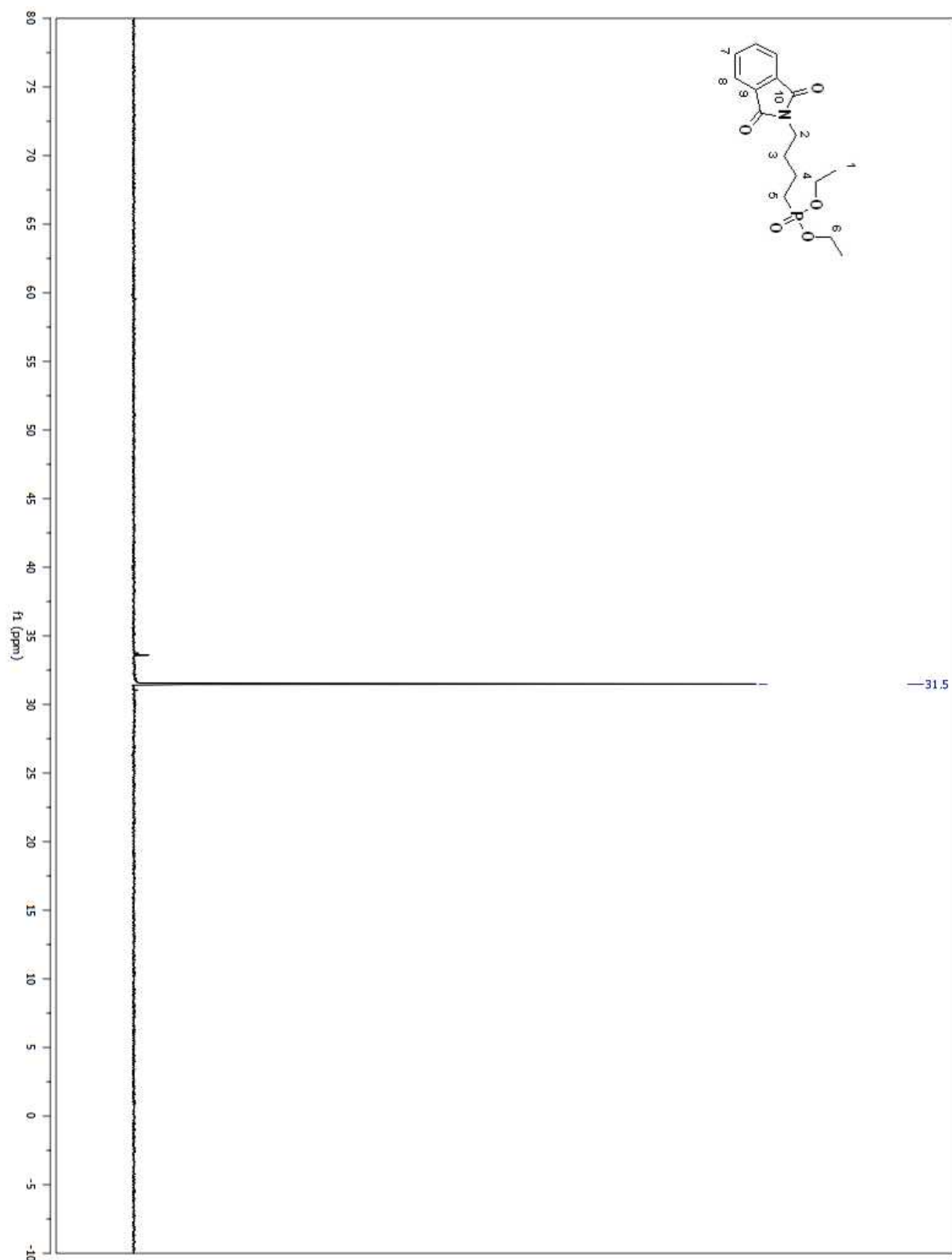


Figure A 54. ^{31}P NMR spectrum of compound **19** in CDCl_3 (Table 2.3, entry xviii)

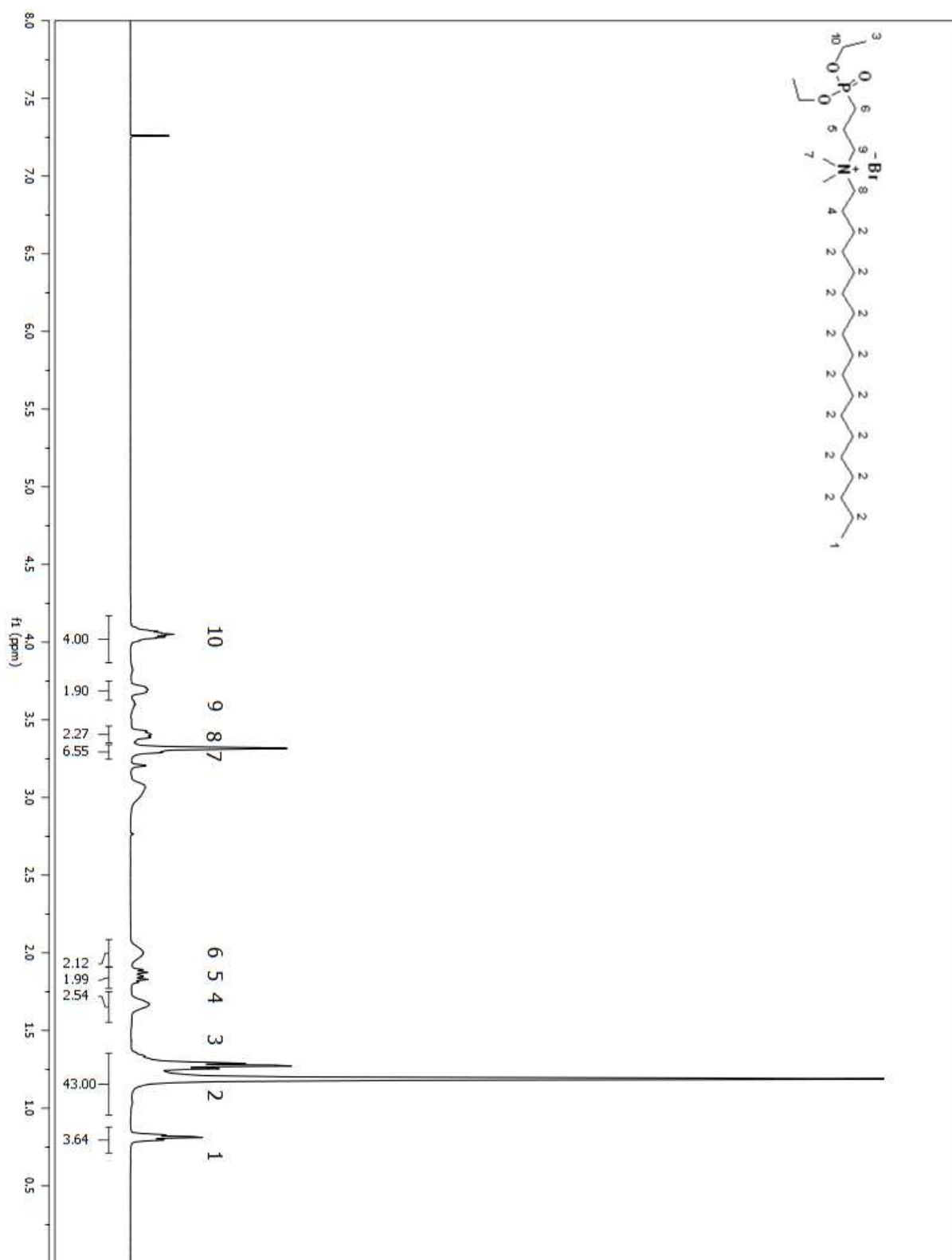


Figure A 55. ¹H NMR spectrum of compound **26** in CDCl₃ (Table 2.4, entry i)

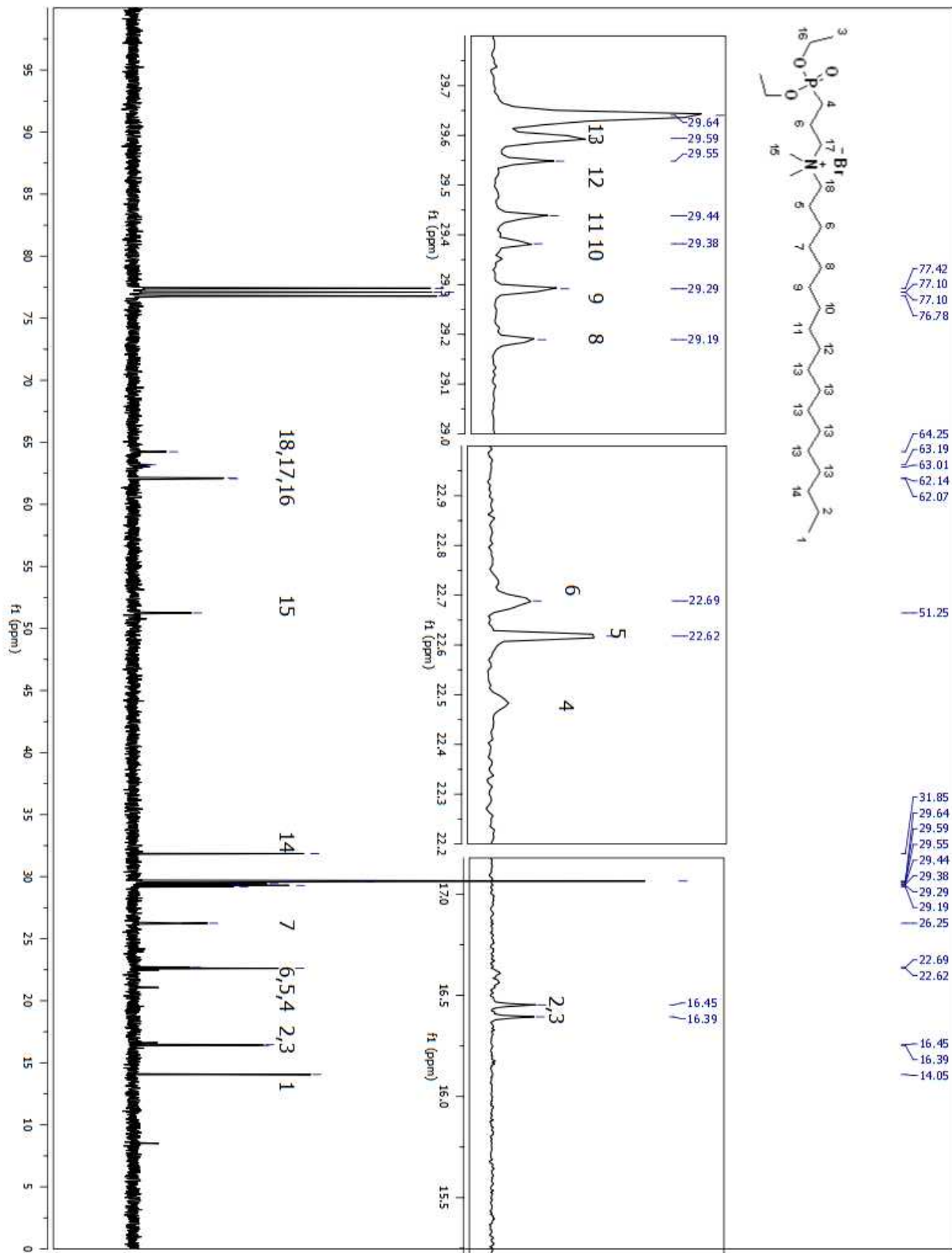


Figure A 56. ^{13}C NMR spectrum of compound **26** in CDCl₃ (Table 2.4, entry i)

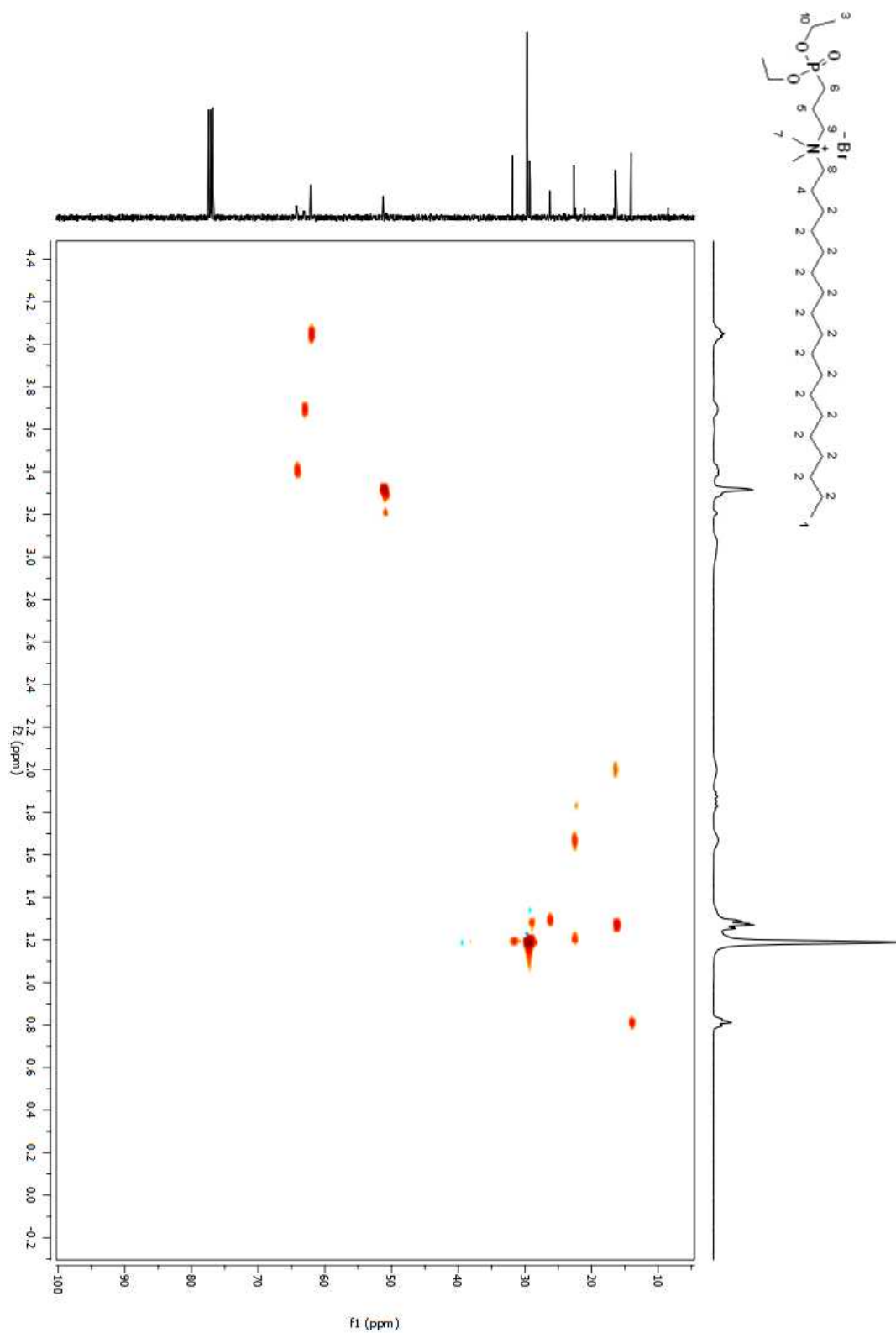


Figure A 58. HSQC 2D NMR spectrum of compound **26** in CDCl₃ (Table 2.4, entry i)

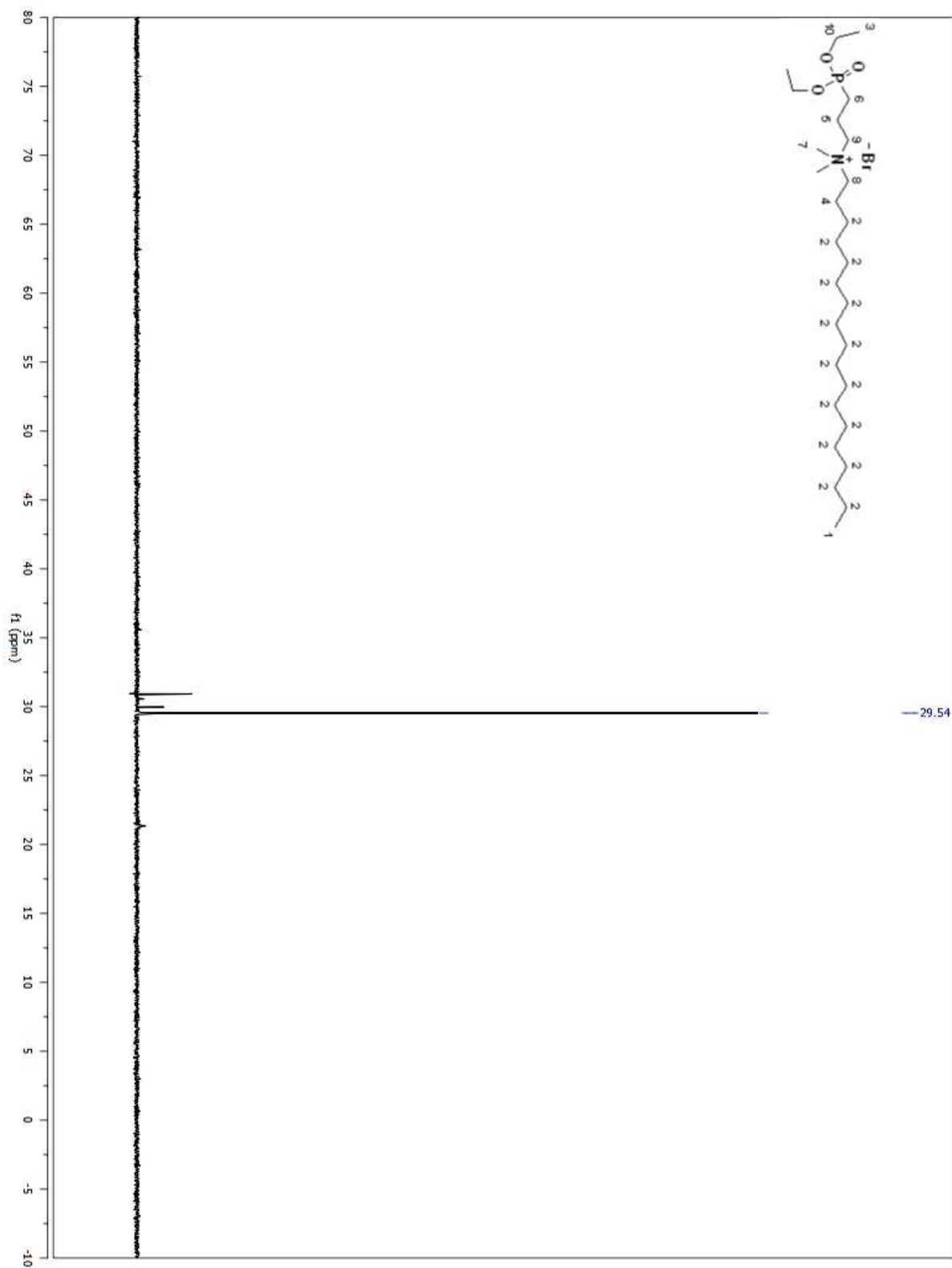


Figure A 59. ^{31}P NMR spectrum of compound **26** in CDCl_3 (Table 2.4, entry i)

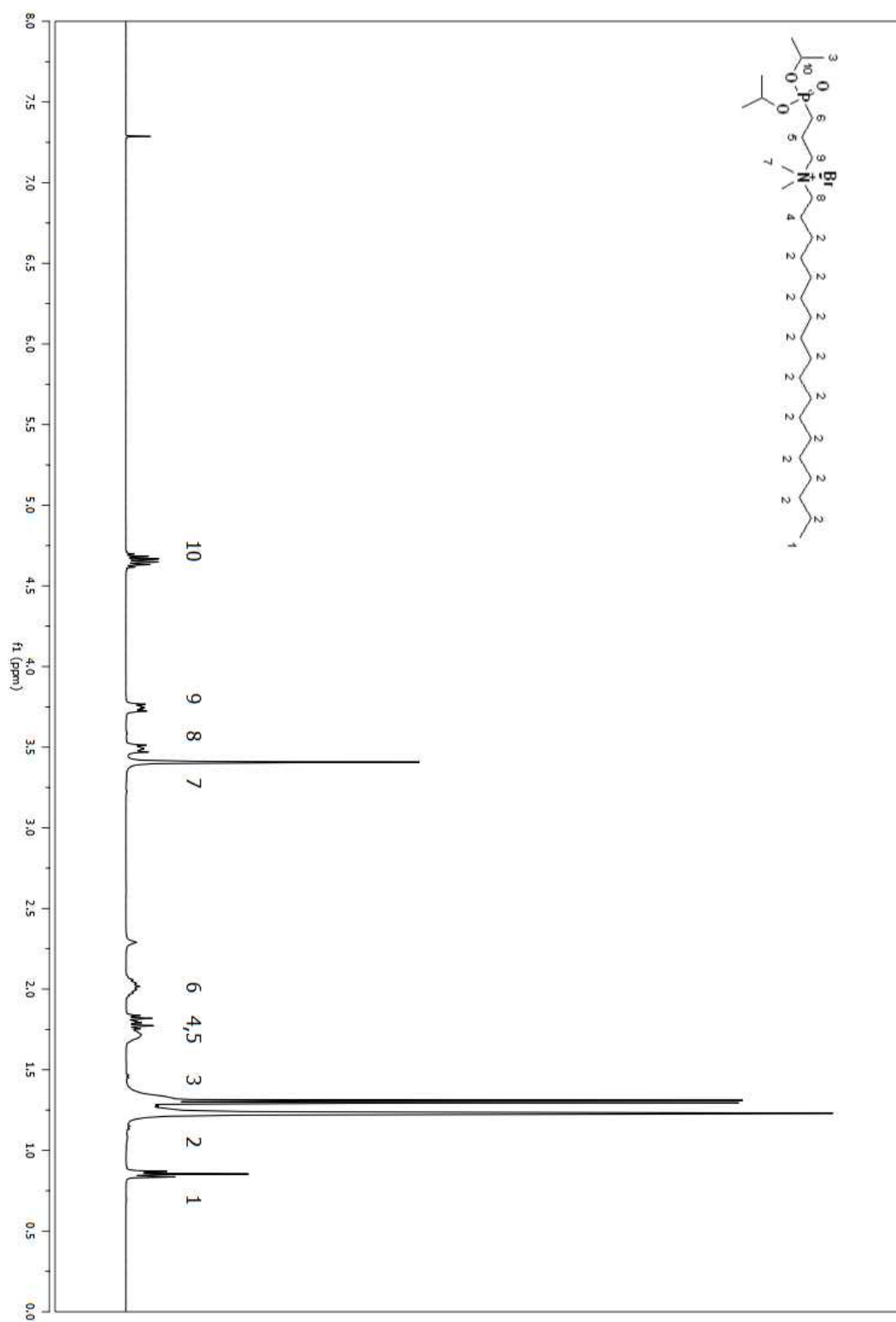


Figure A 60. ^1H NMR spectrum of compound **27** in CDCl_3 (Table 4.4, entry iv)

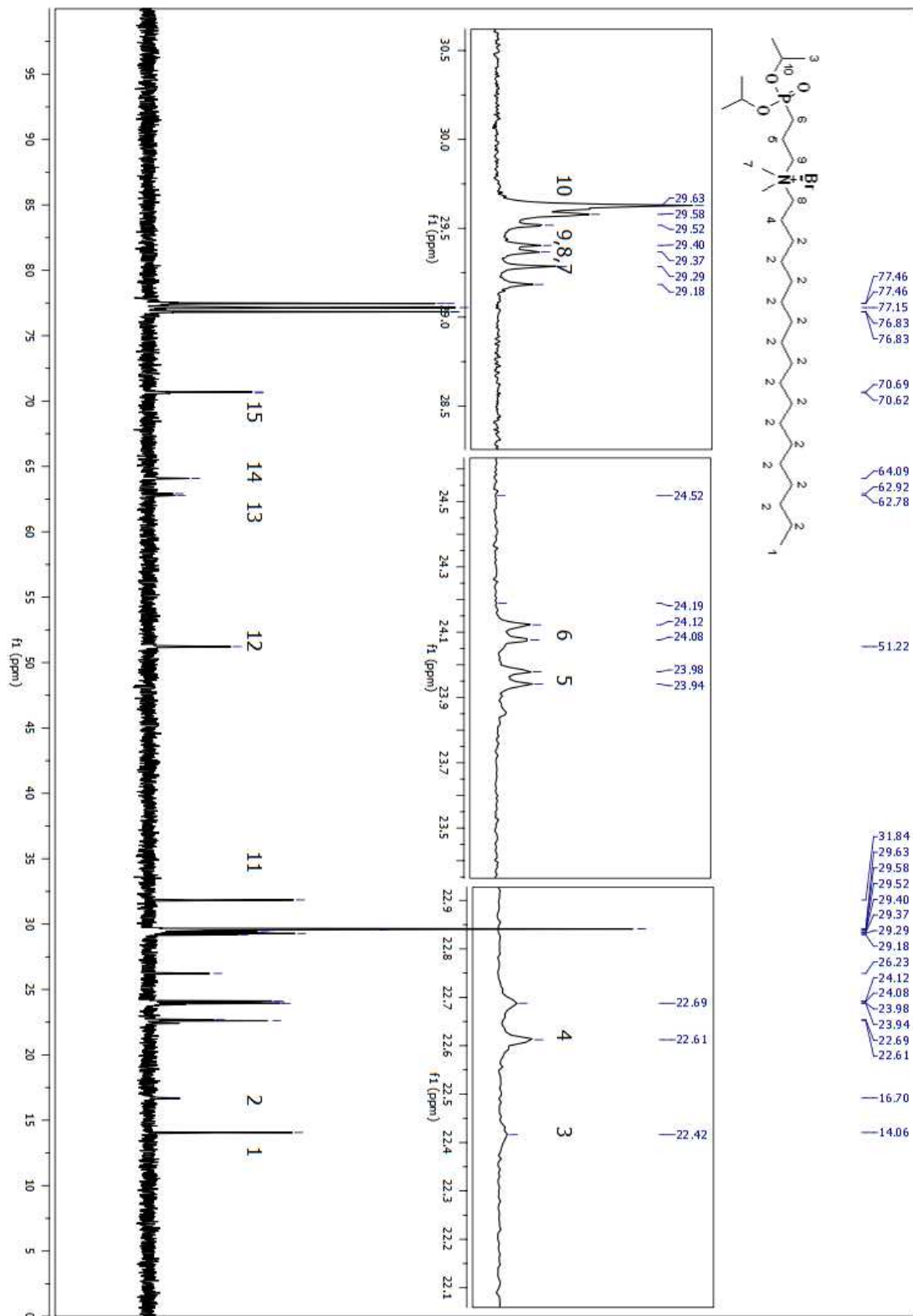


Figure A 61. ¹³C NMR spectrum of compound **27** in CDCl₃ (Table 2.4, entry iv)

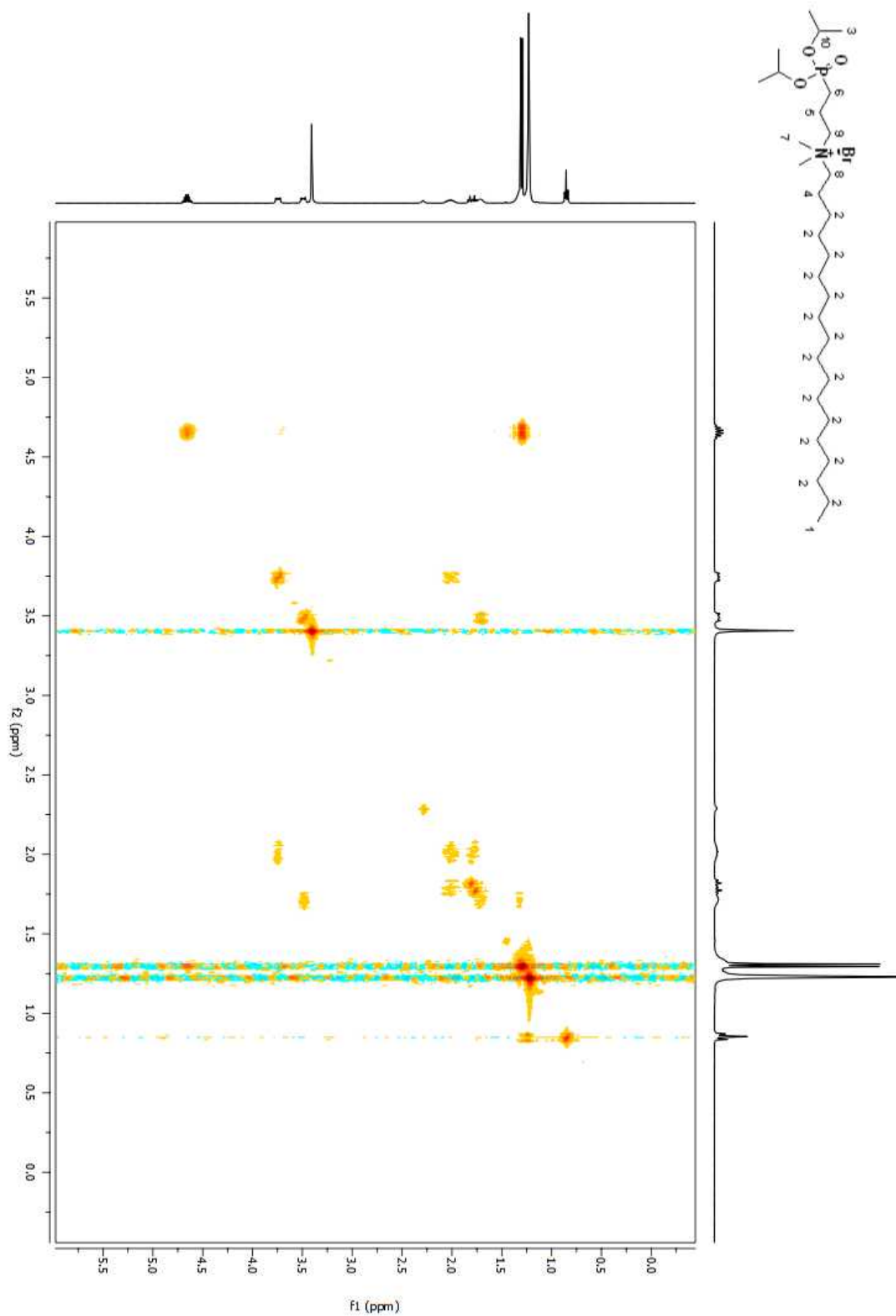


Figure A 62. COSY 2D NMR spectrum of compound **27** in CDCl_3 (Table 2.4, entry iv)

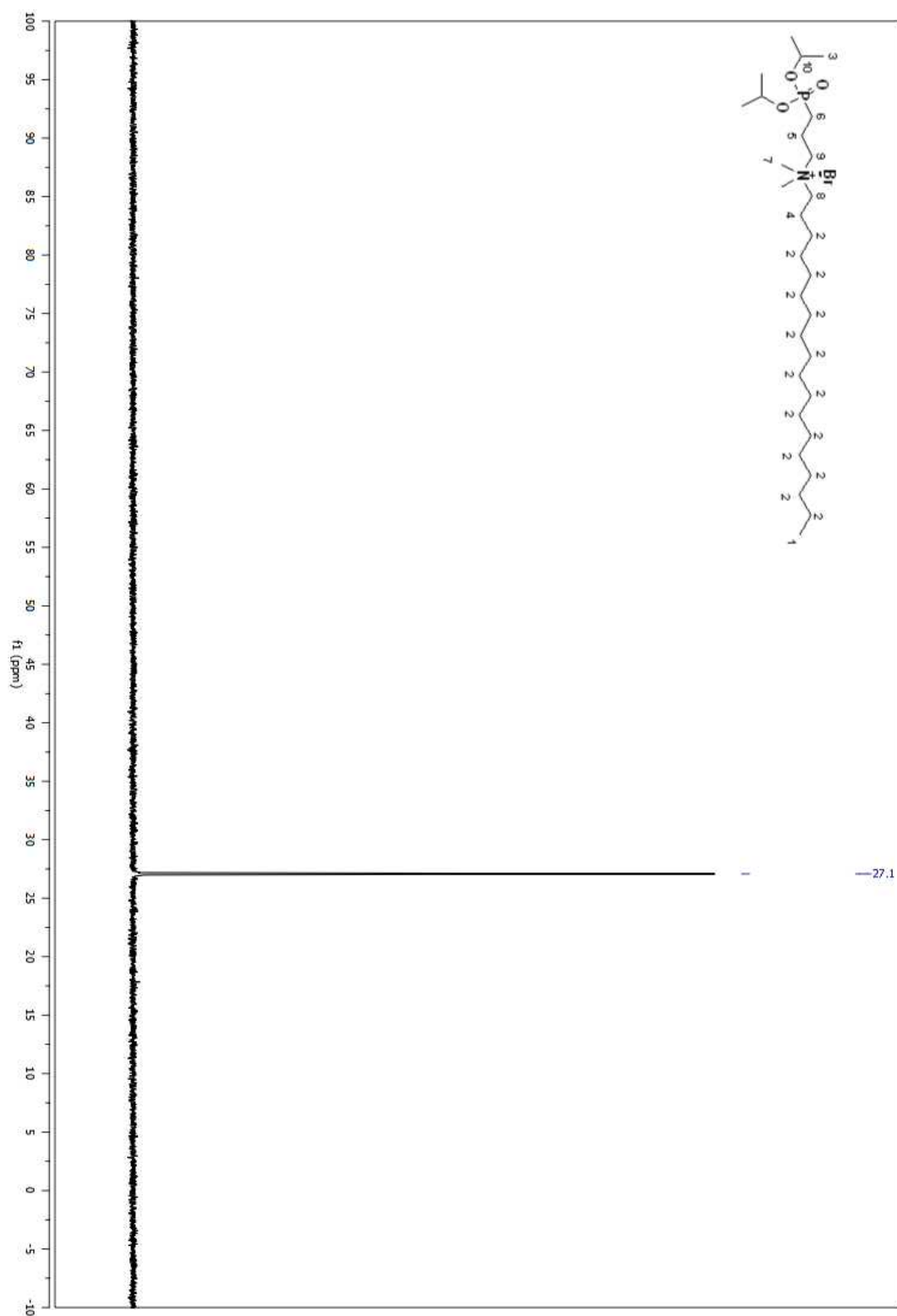


Figure A 63. ^{31}P NMR spectrum of compound **27** in CDCl_3 (Table 2.4, entry iv)

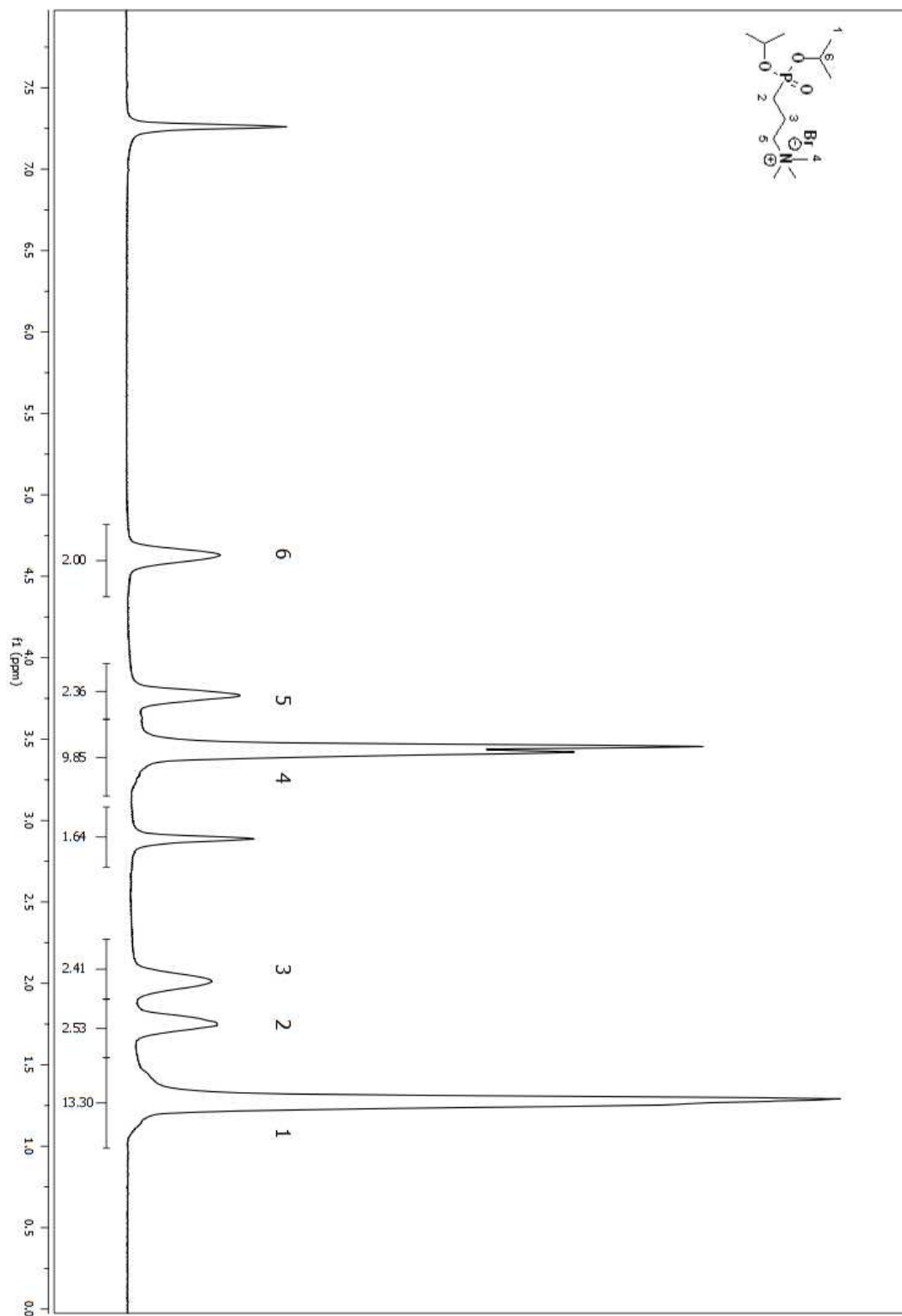


Figure A 64. ^1H NMR spectrum of compound **28** in CDCl_3 (Table 2.4, entry vii)

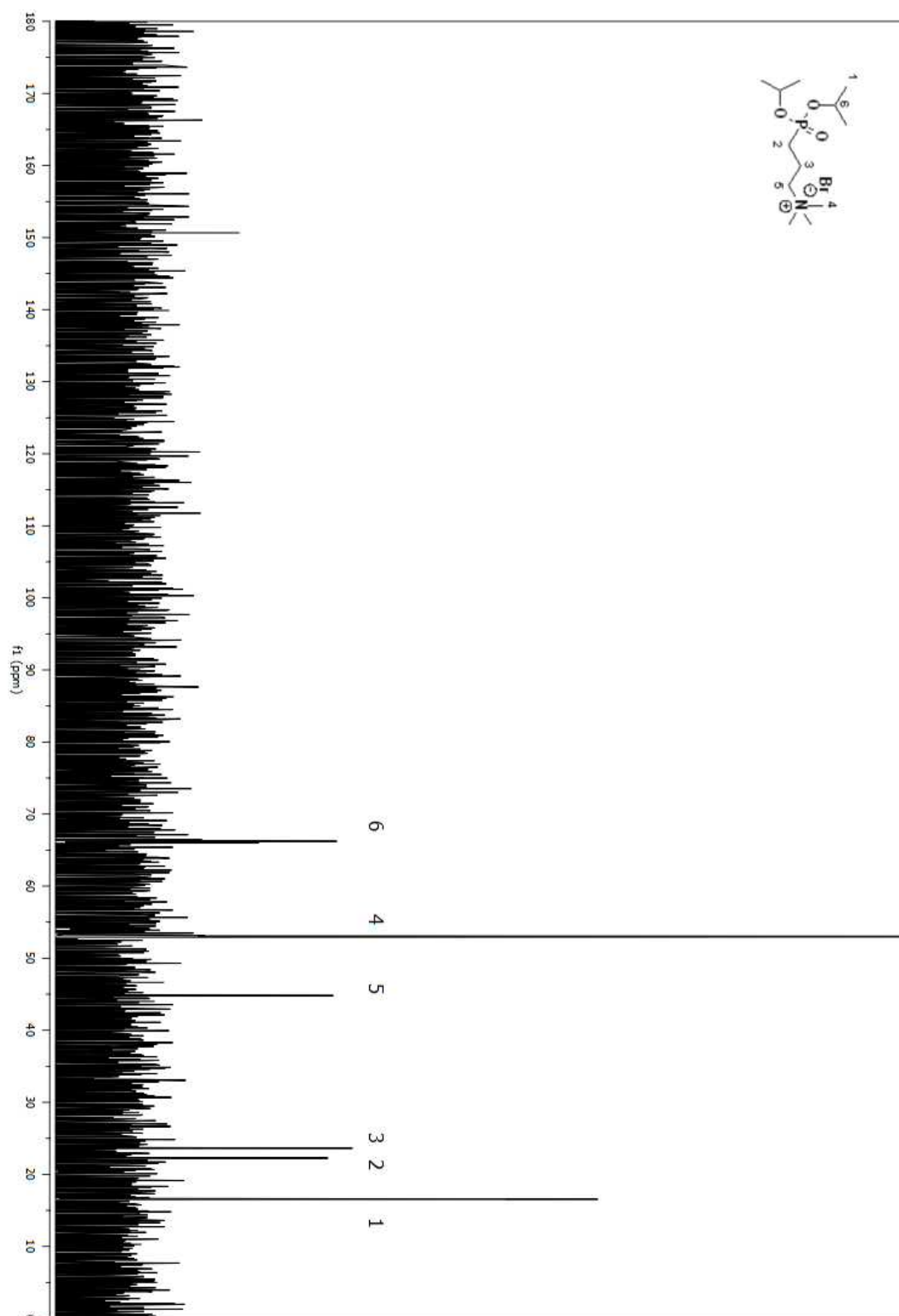


Figure A 65. ^{13}C NMR spectrum of compound **28** in CDCl_3 (Table 2.4, entry vii)

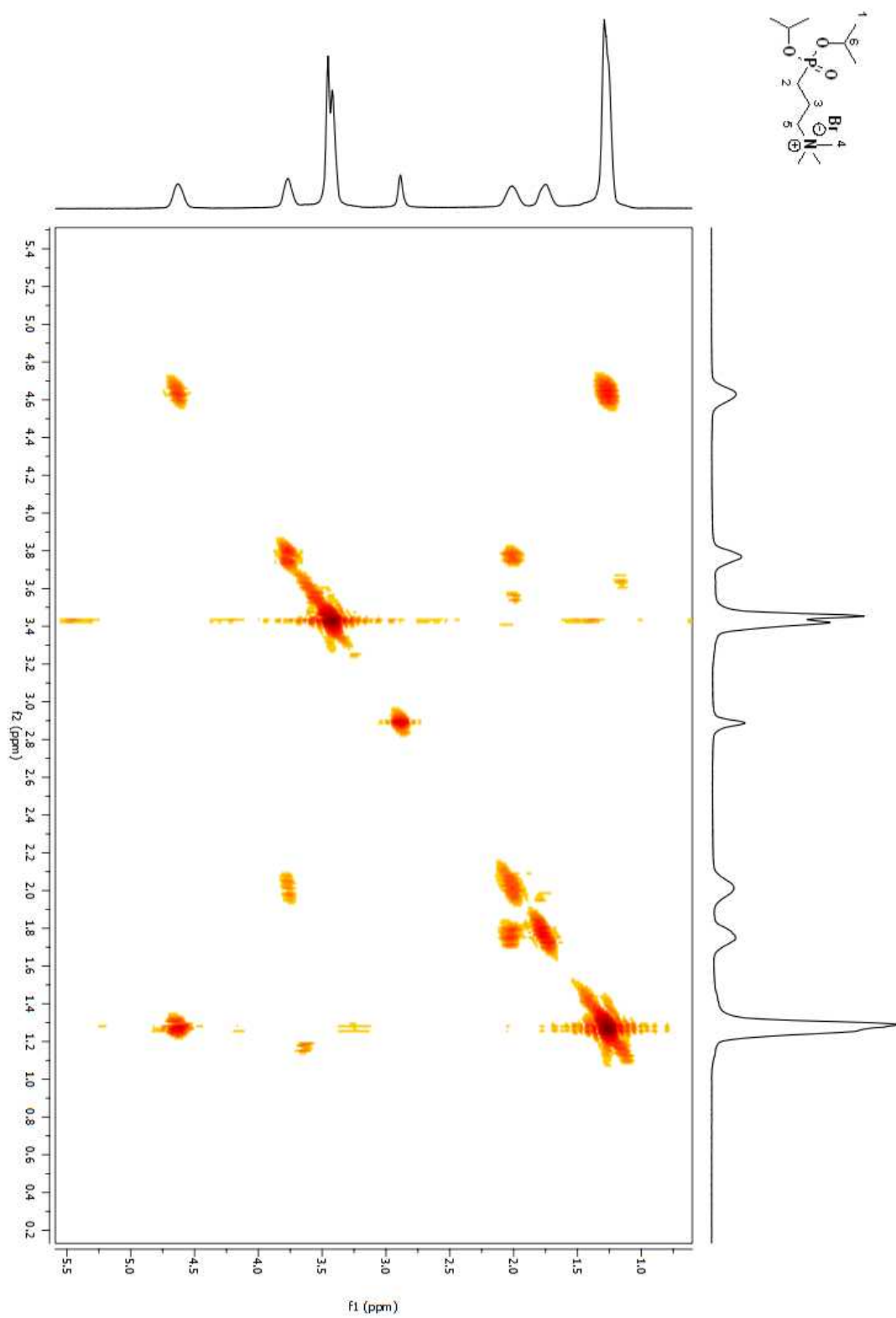


Figure A 66. COSY 2D NMR spectrum of compound **28** in CDCl₃ (Table 2.4, entry vii)

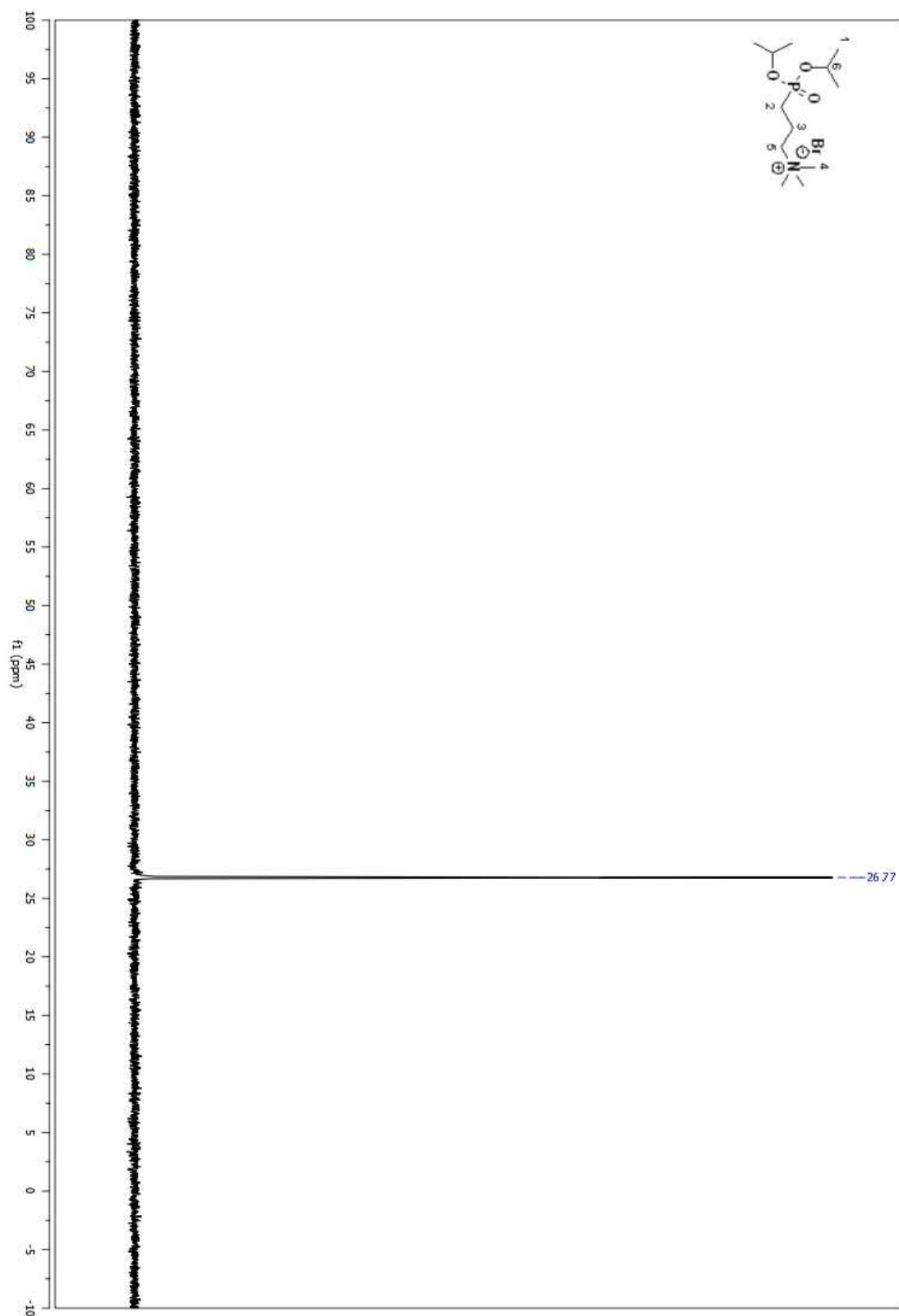


Figure A 67. ^{31}P NMR spectrum of compound **28** in CDCl_3 (Table 2.4, entry vii)

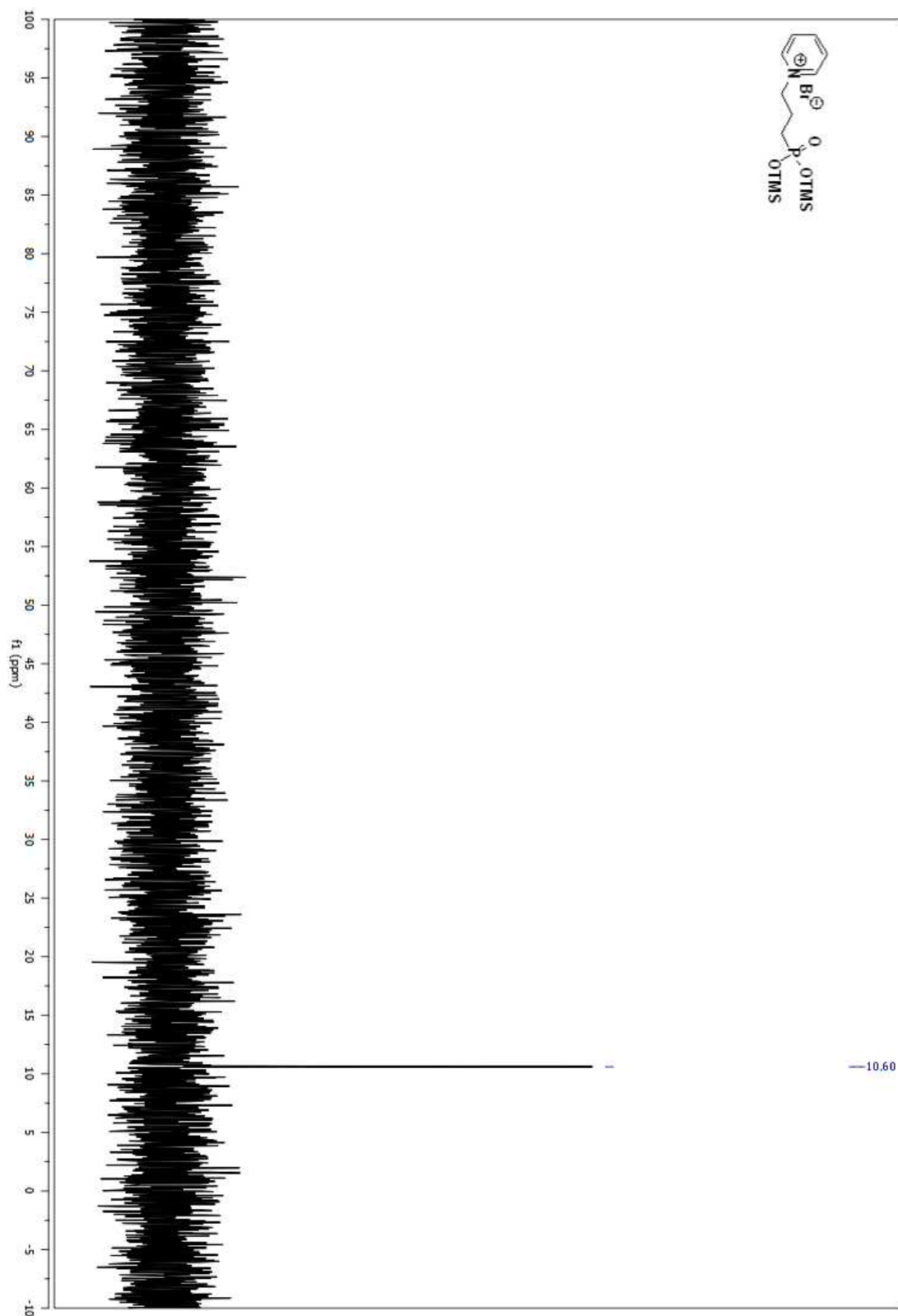


Figure A 68. ^{31}P NMR spectrum of compound **29** in CDCl_3 (Table 2.4, entry viii)

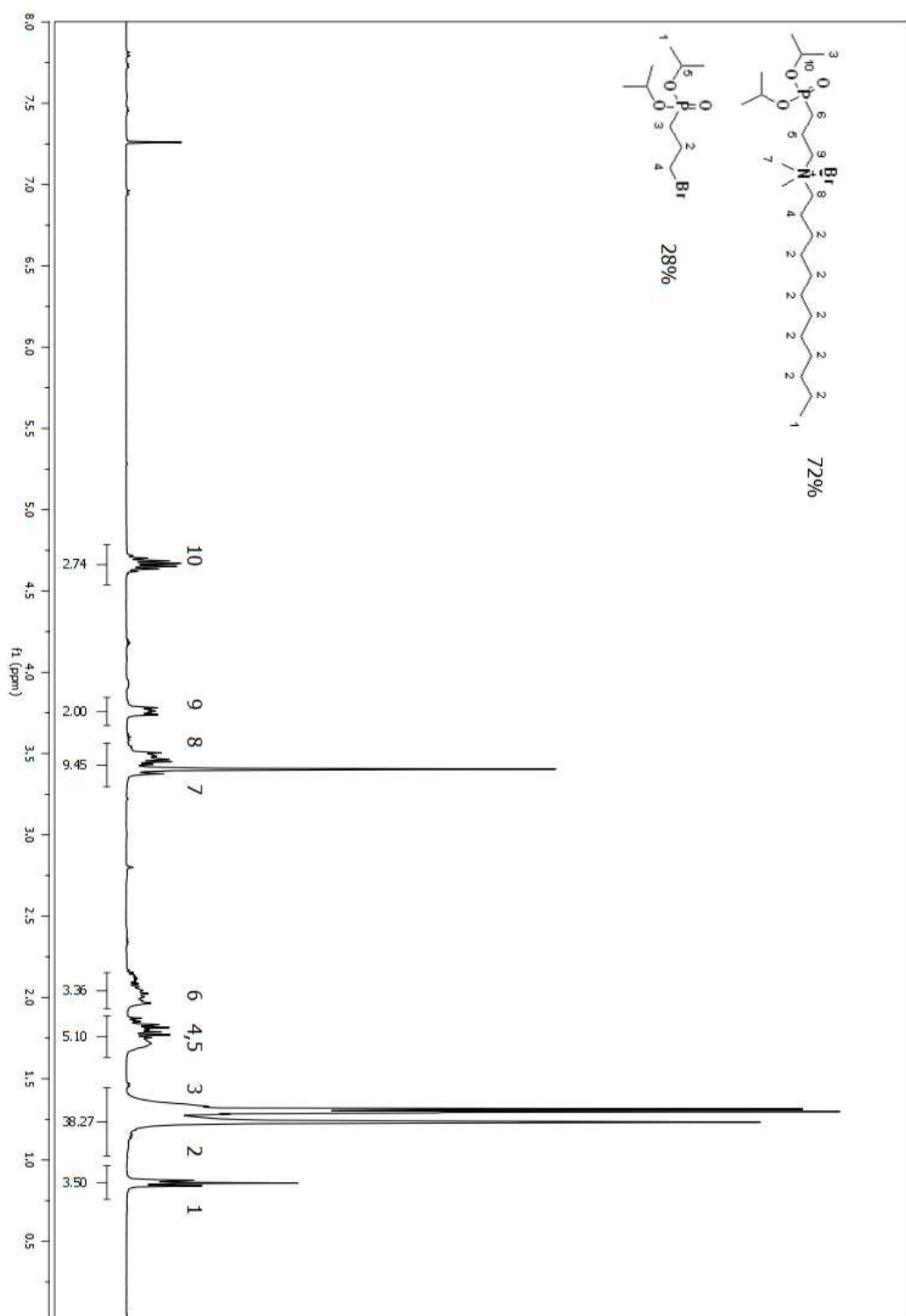


Figure A 69. ¹H NMR spectrum of compound **30** in CDCl₃ (Table 2.4, entry ix)

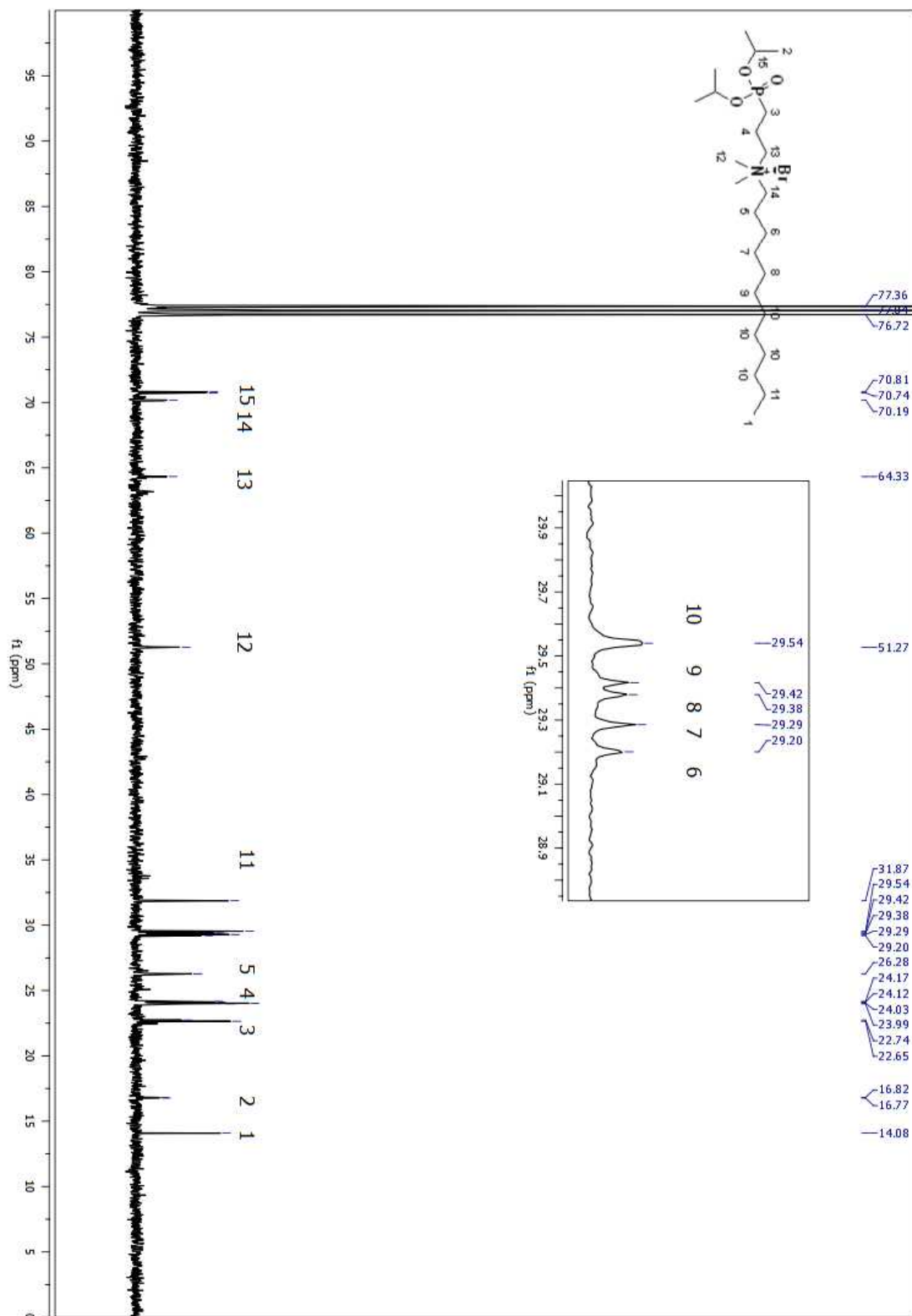


Figure A 70. ^{13}C NMR spectrum of compound **30** in CDCl_3 (Table 2.4, entry ix)

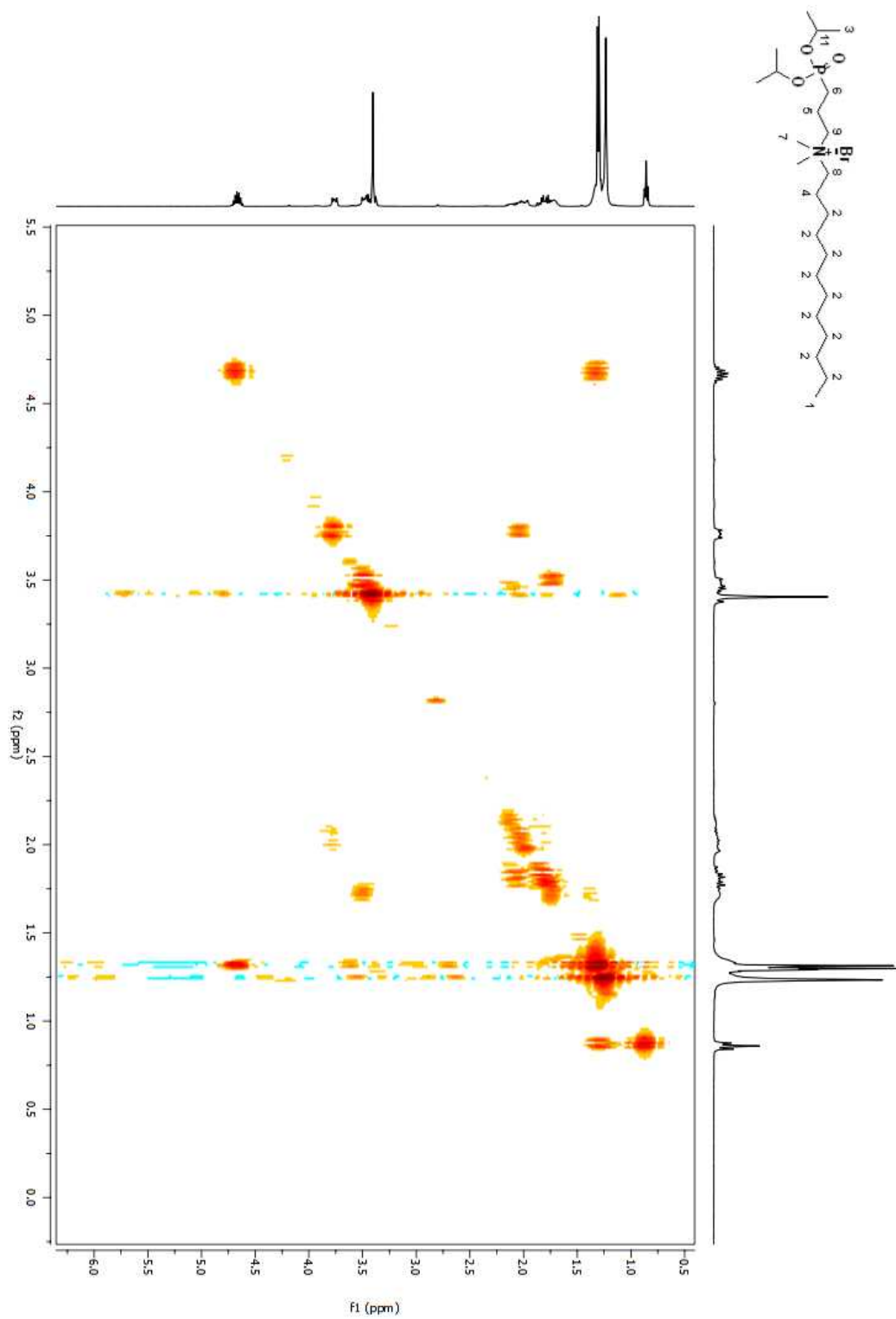


Figure A 71. COSY 2D NMR spectrum of compound **30** in CDCl₃ (Table 4.4, entry ix)

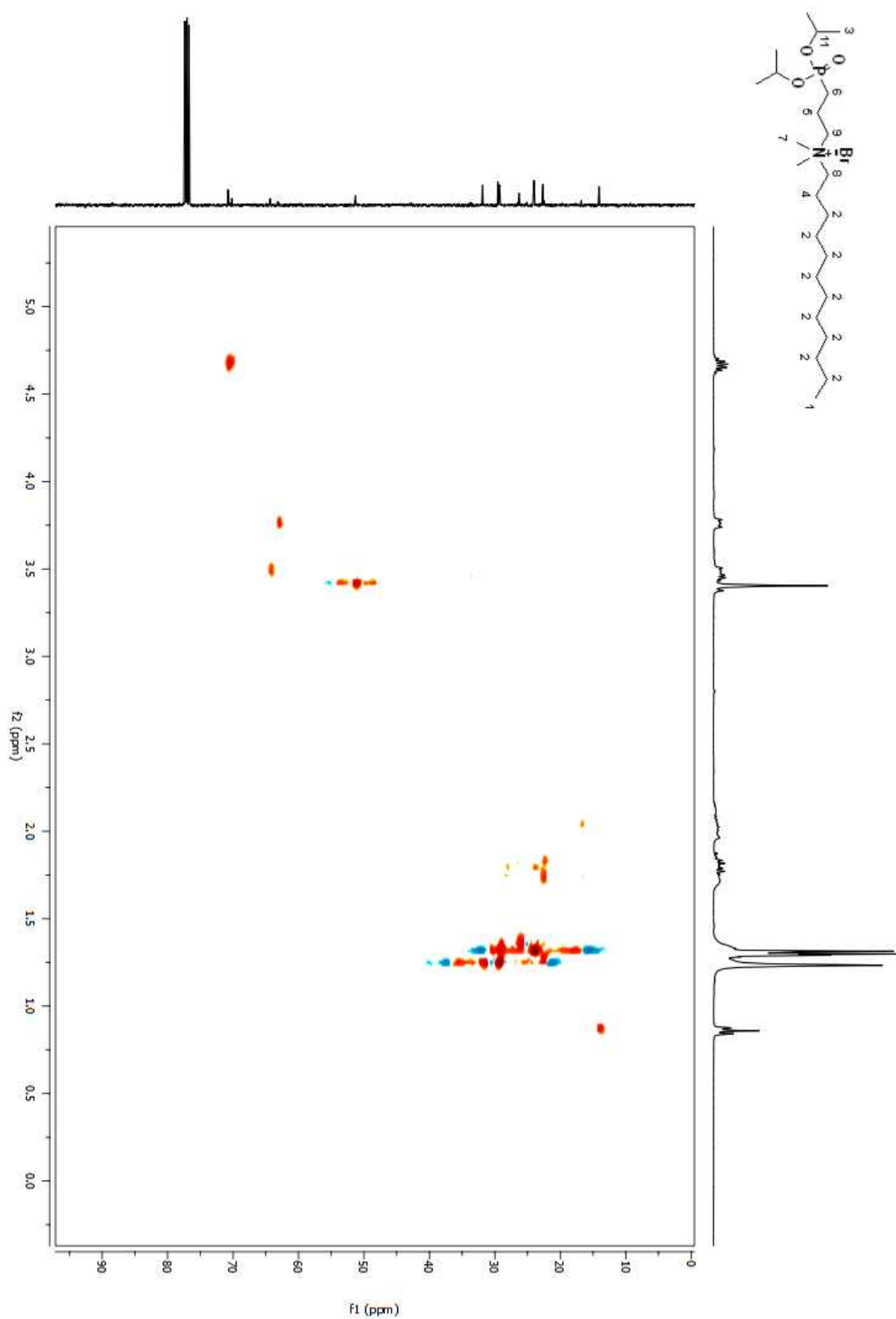


Figure A 72. HSQC 2D NMR spectrum of compound **30** in CDCl_3 (Table 2.4, entry ix)

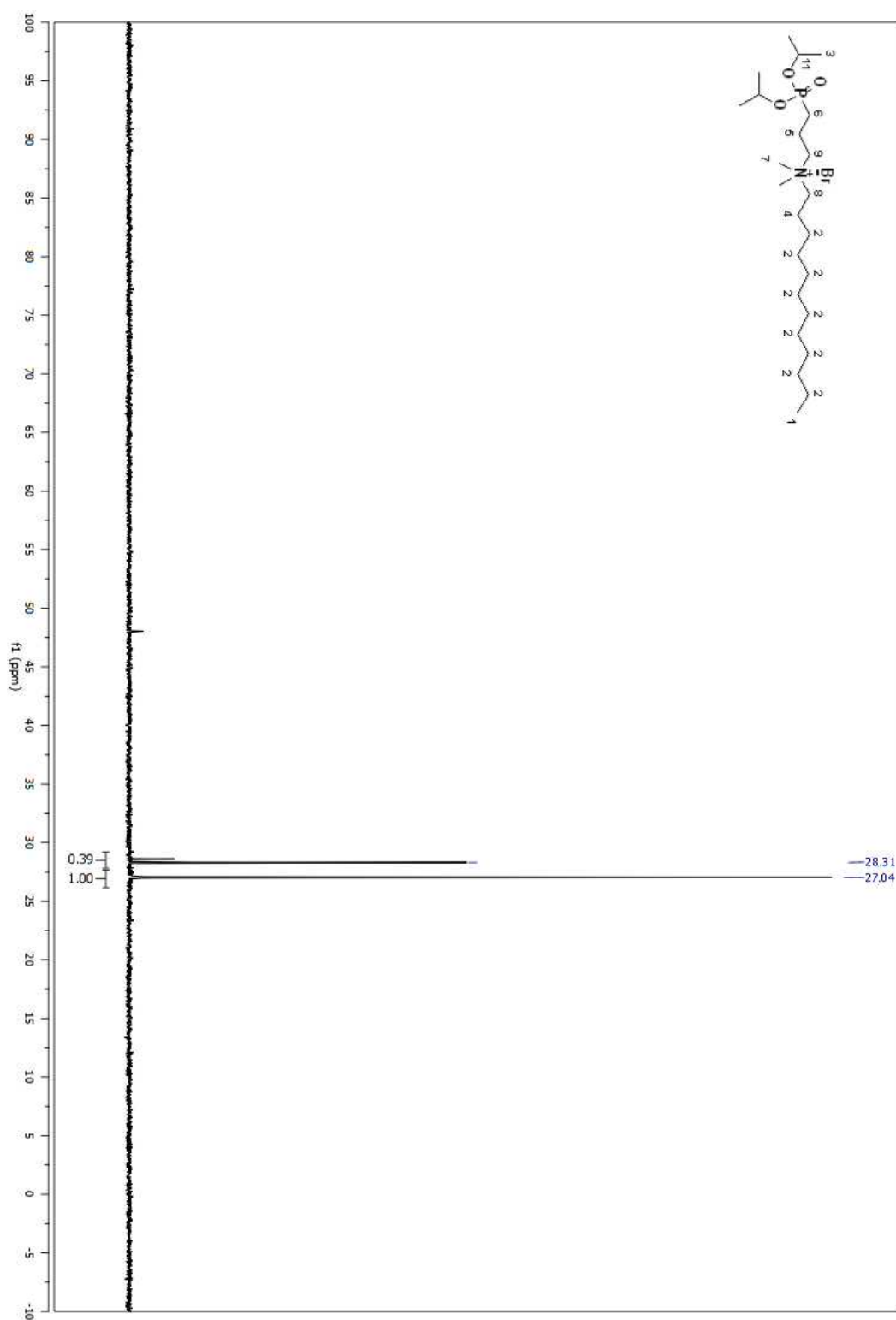


Figure A 73. ^{31}P NMR spectrum of compound **30** in CDCl_3 (Table 2.4, entry ix)

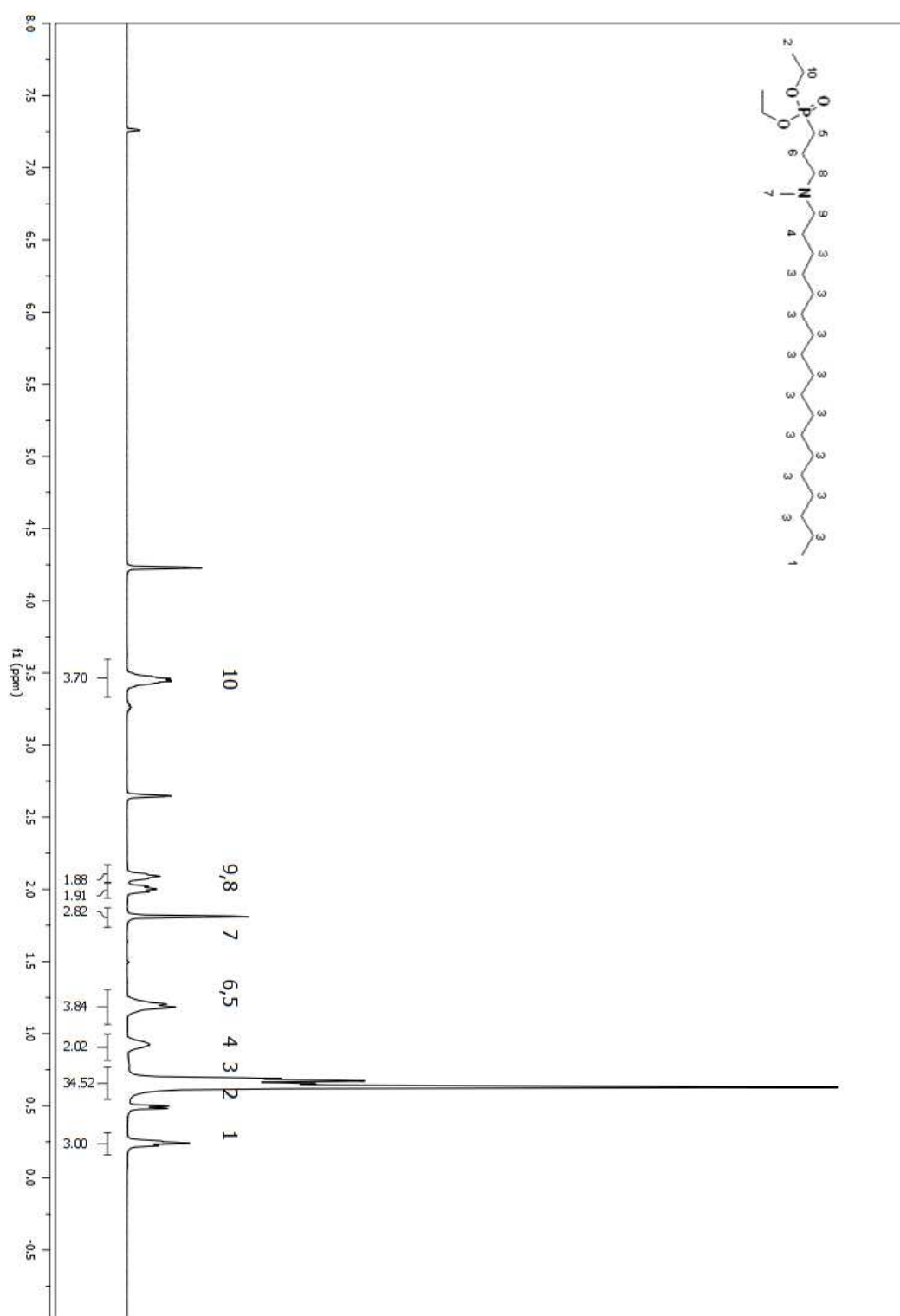


Figure A 74. ^1H NMR spectrum of compound **31** in CDCl₃ (Table 2.4, entry x)

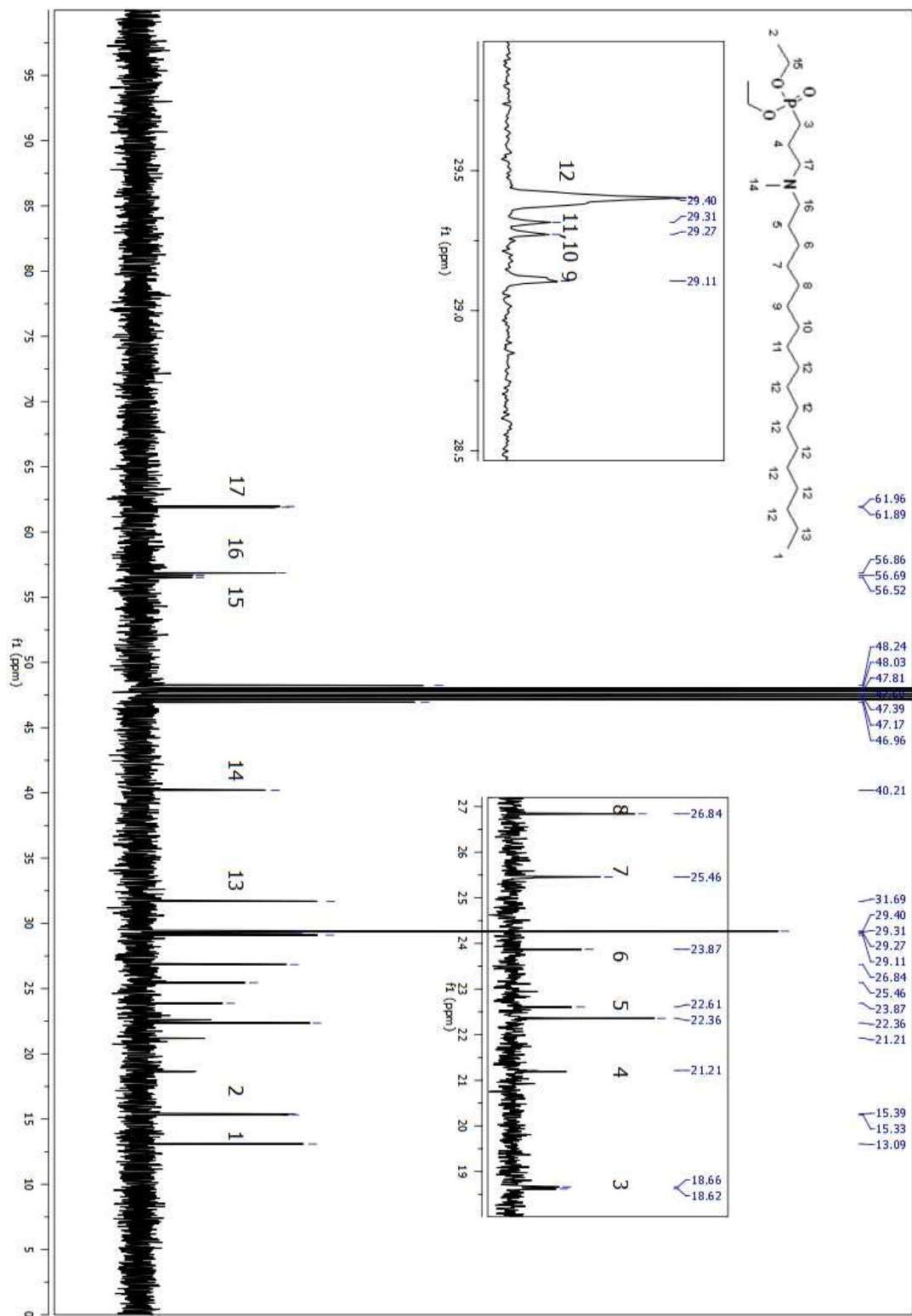


Figure A 75. ^{13}C NMR spectrum of compound **31** in CDCl_3 (Table 2.4, entry x)

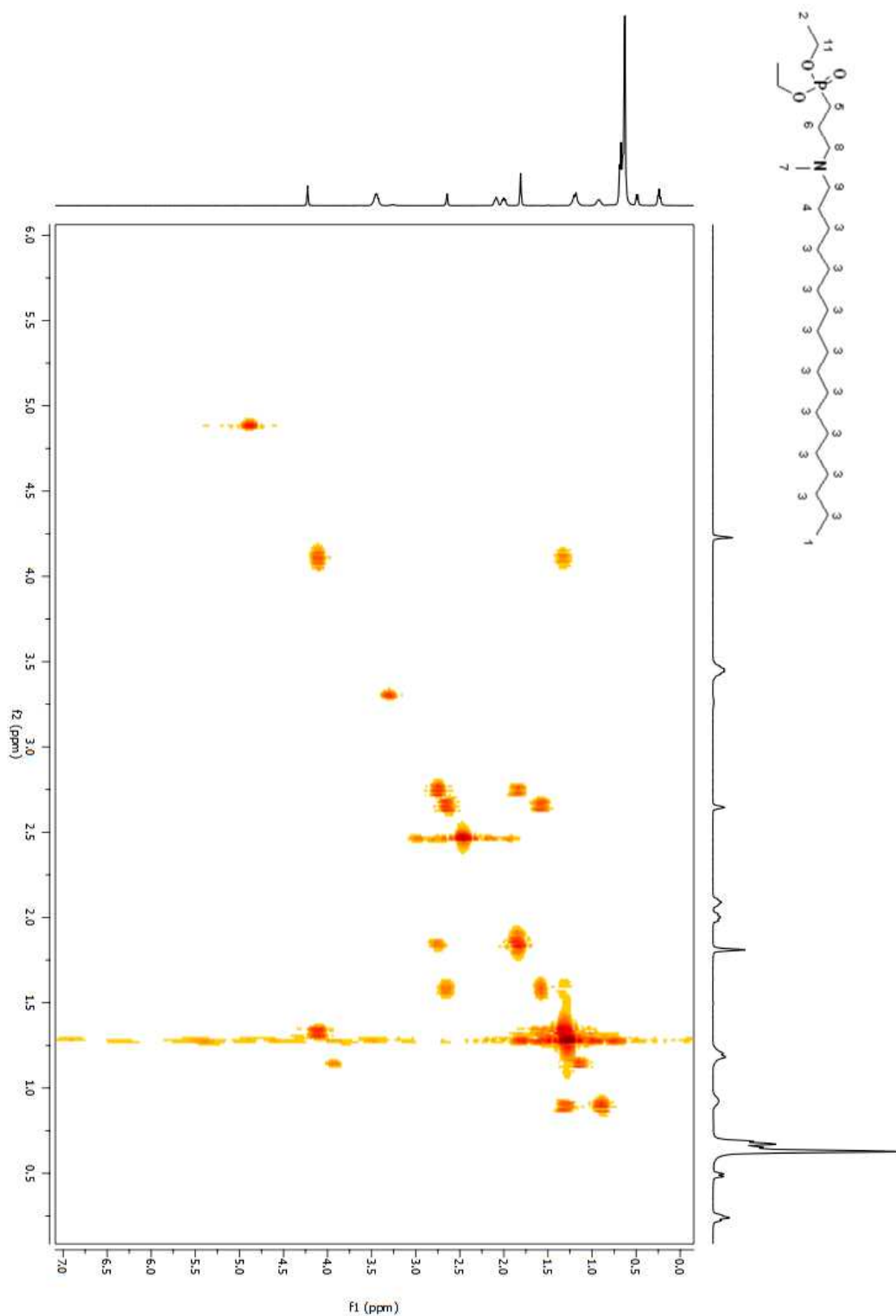


Figure A 76. COSY 2D NMR spectrum of compound **31** in CDCl₃ (Table 2.4, entry x)

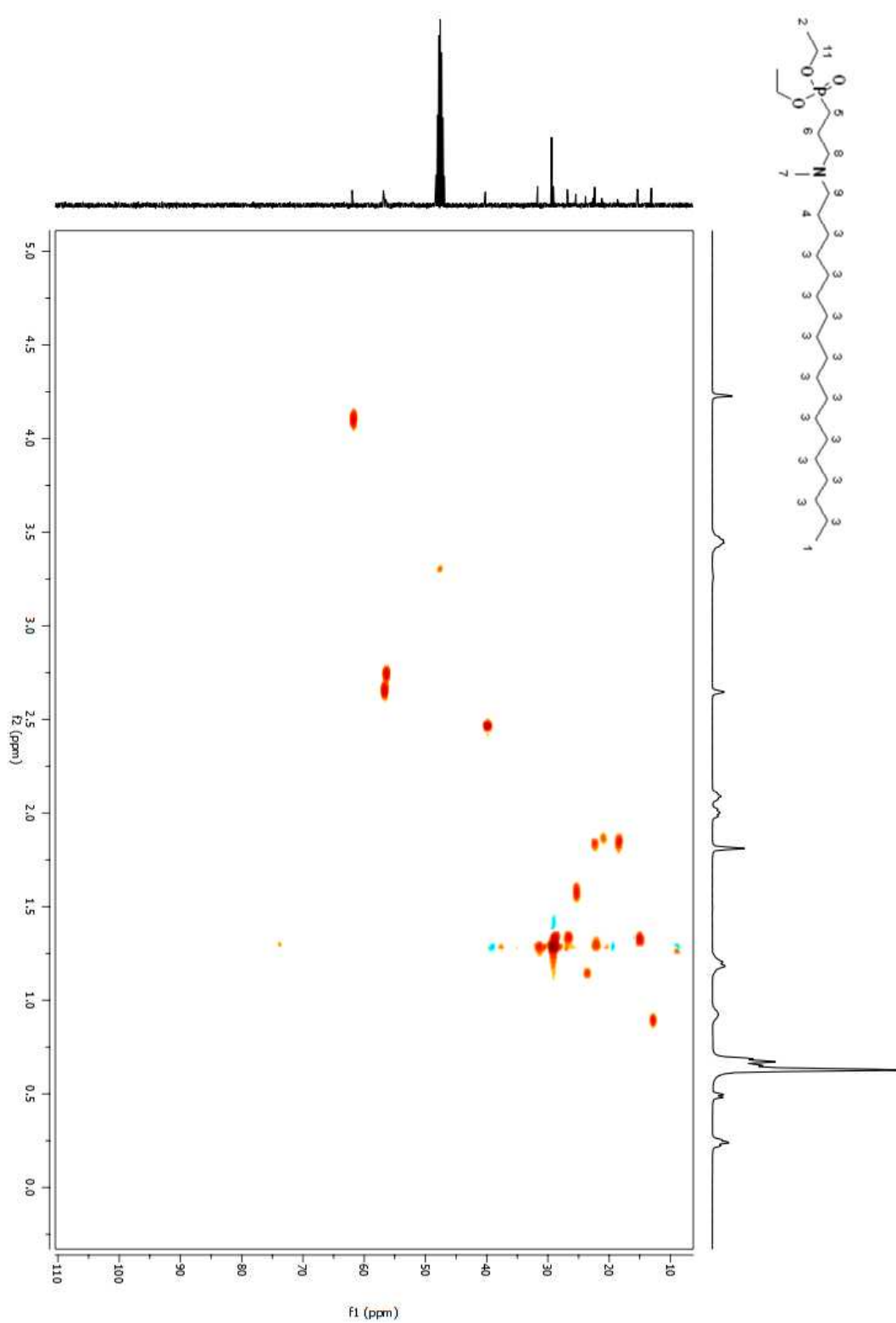


Figure A 77. HSQC 2D NMR spectrum of compound **31** in CDCl₃ (Table 4.4, entry x)

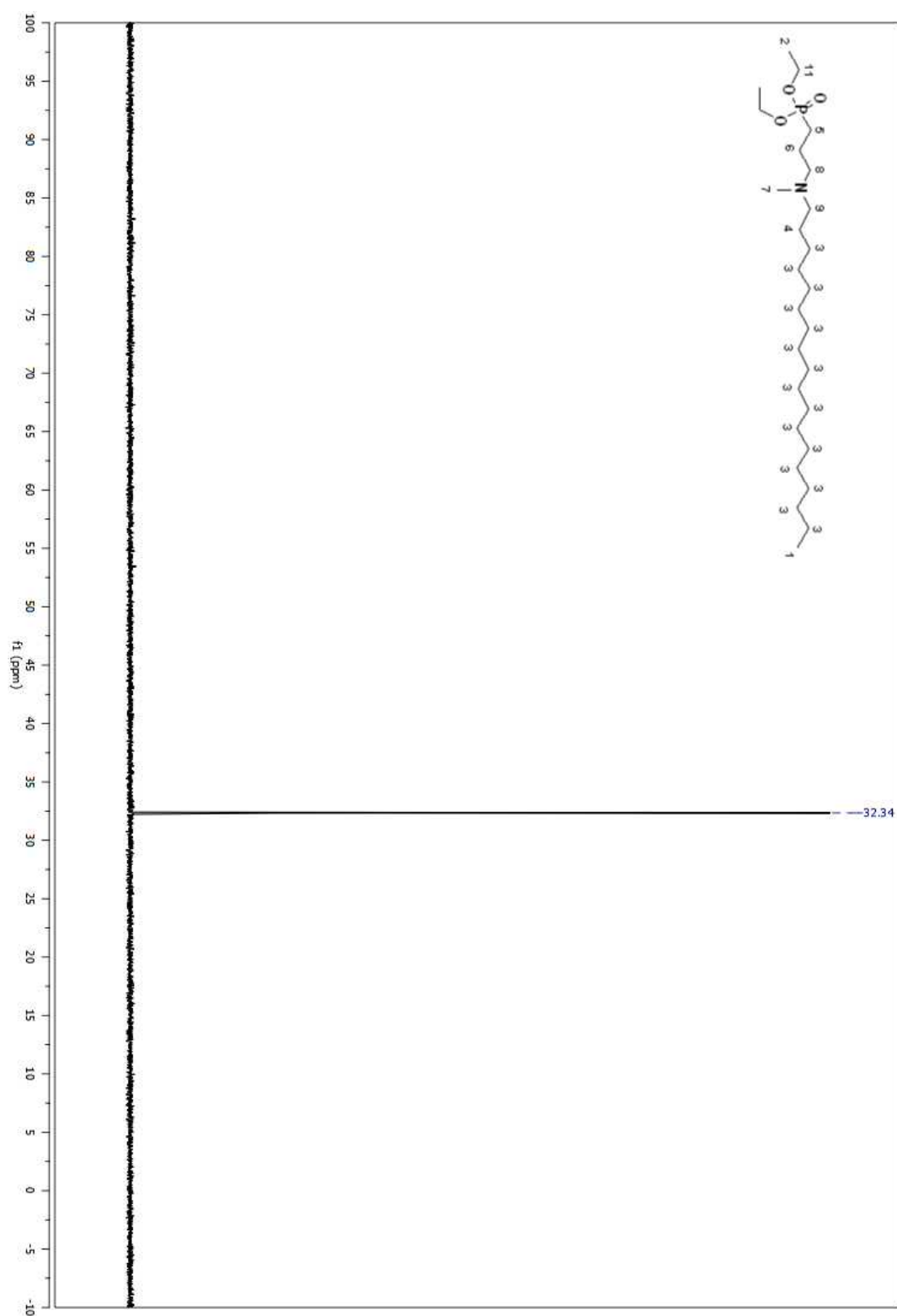


Figure A 78. ^{31}P NMR spectrum of compound **31** in CDCl_3 (Table 2.4, entry x)

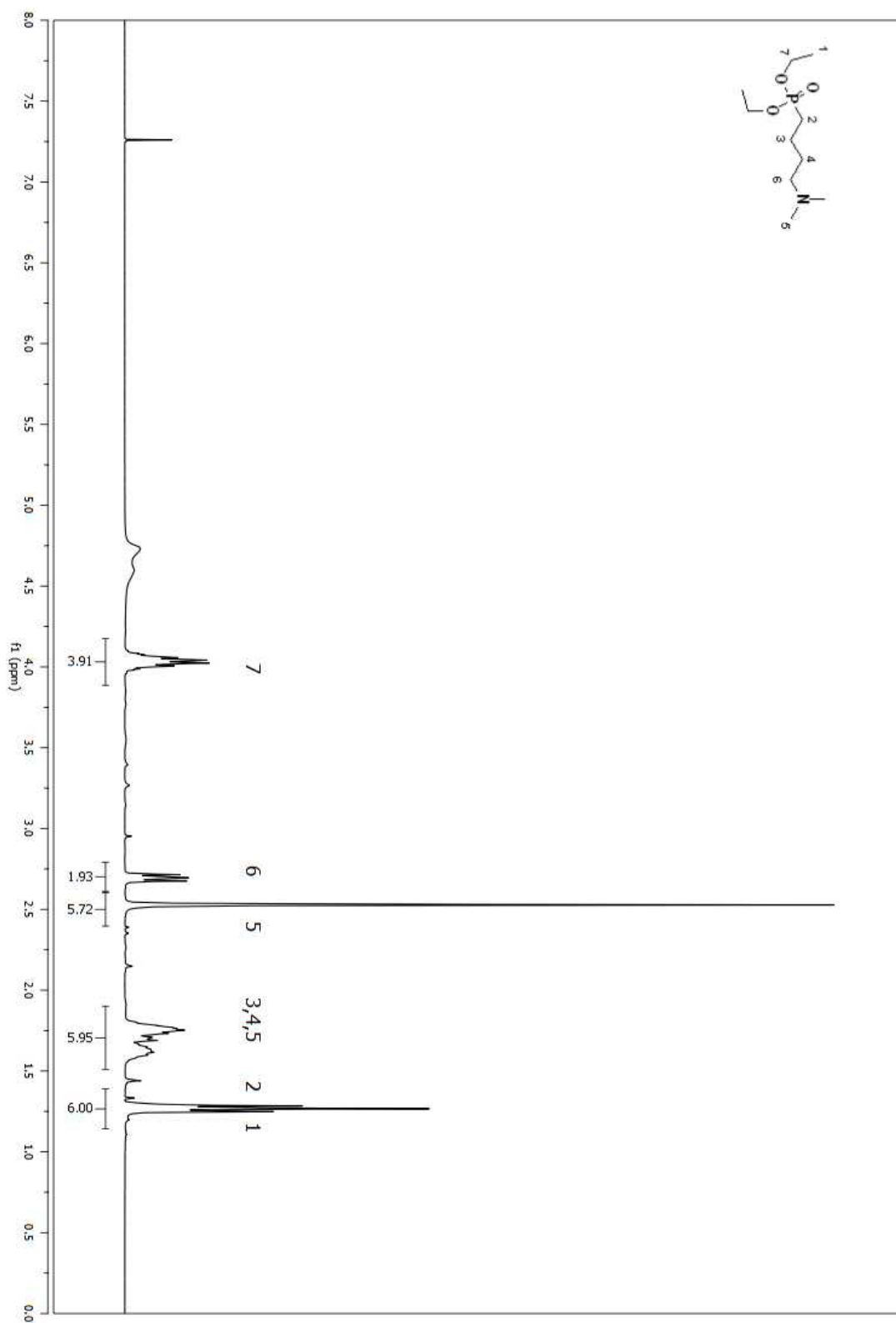


Figure A 79. ¹H NMR spectrum of compound **32** in CDCl₃ (Table 2.4, entry xi)

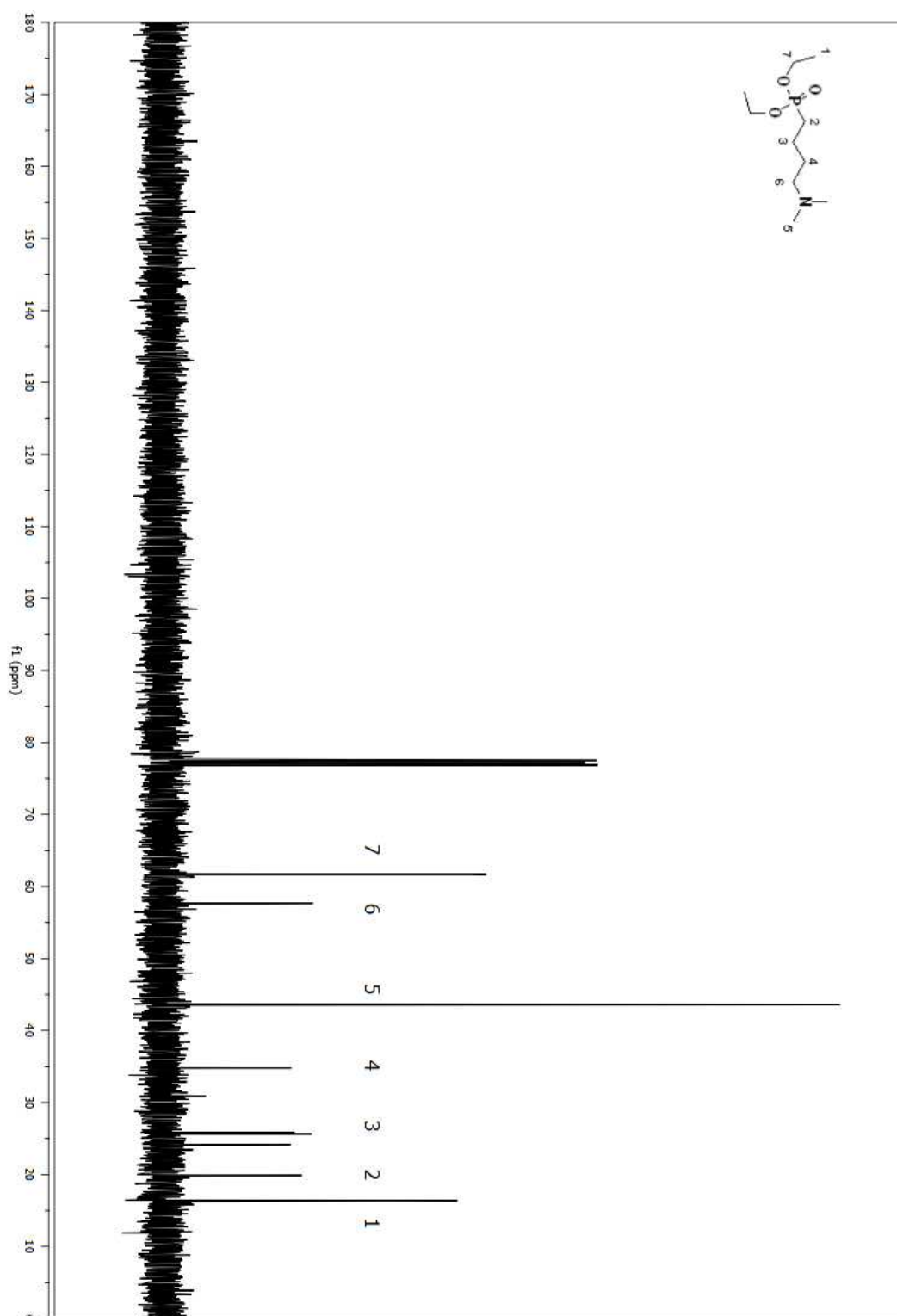


Figure A 80. ¹³C NMR spectrum of compound **32** in CDCl₃ (Table 2.4, entry xi)

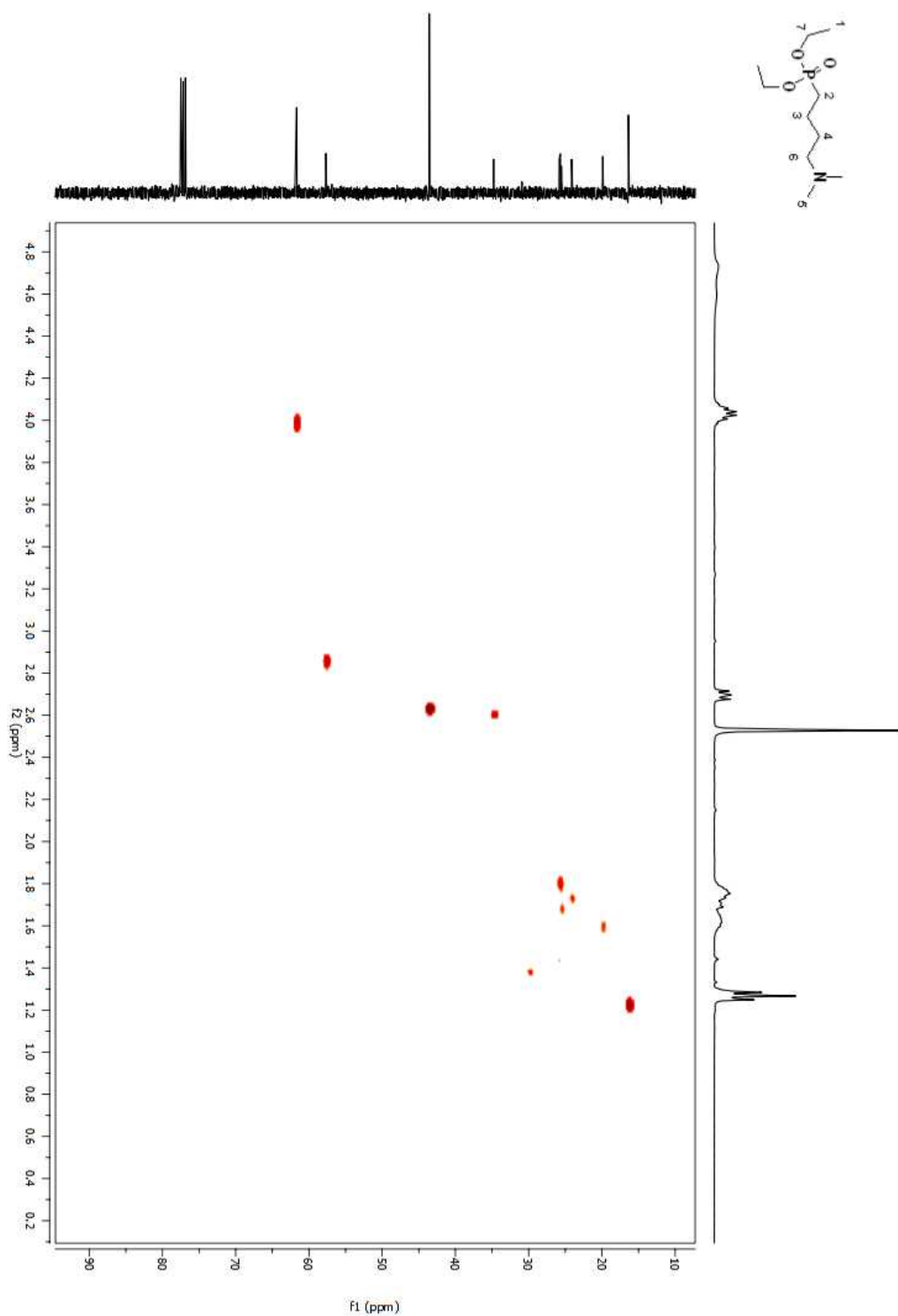


Figure A 81. HSQC 2D NMR spectrum of compound **32** in CDCl₃ (Table 2.4, entry xi)

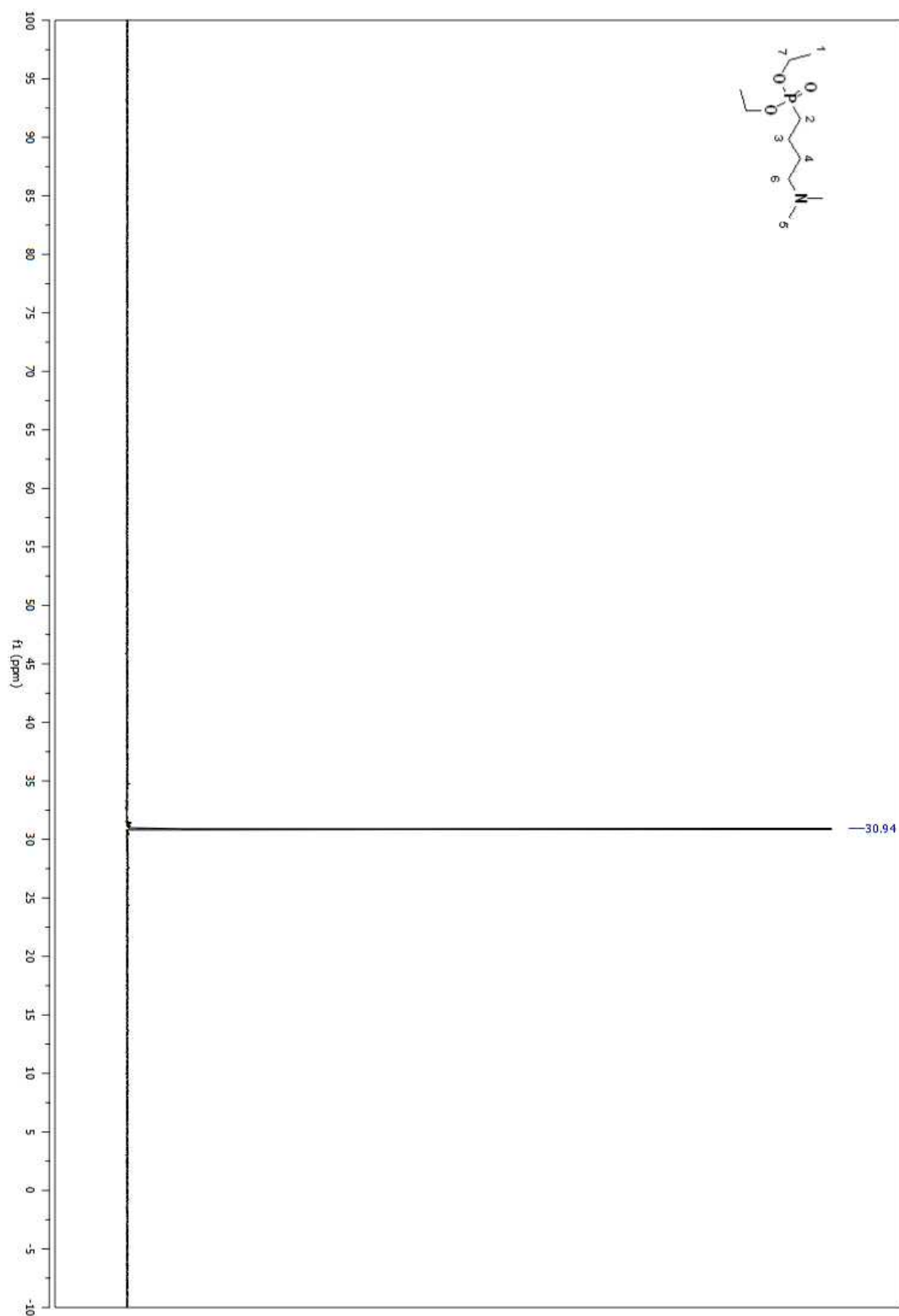


Figure A 82. ^{31}P NMR spectrum of compound **32** in CDCl_3 (Table 2.4, entry xi)

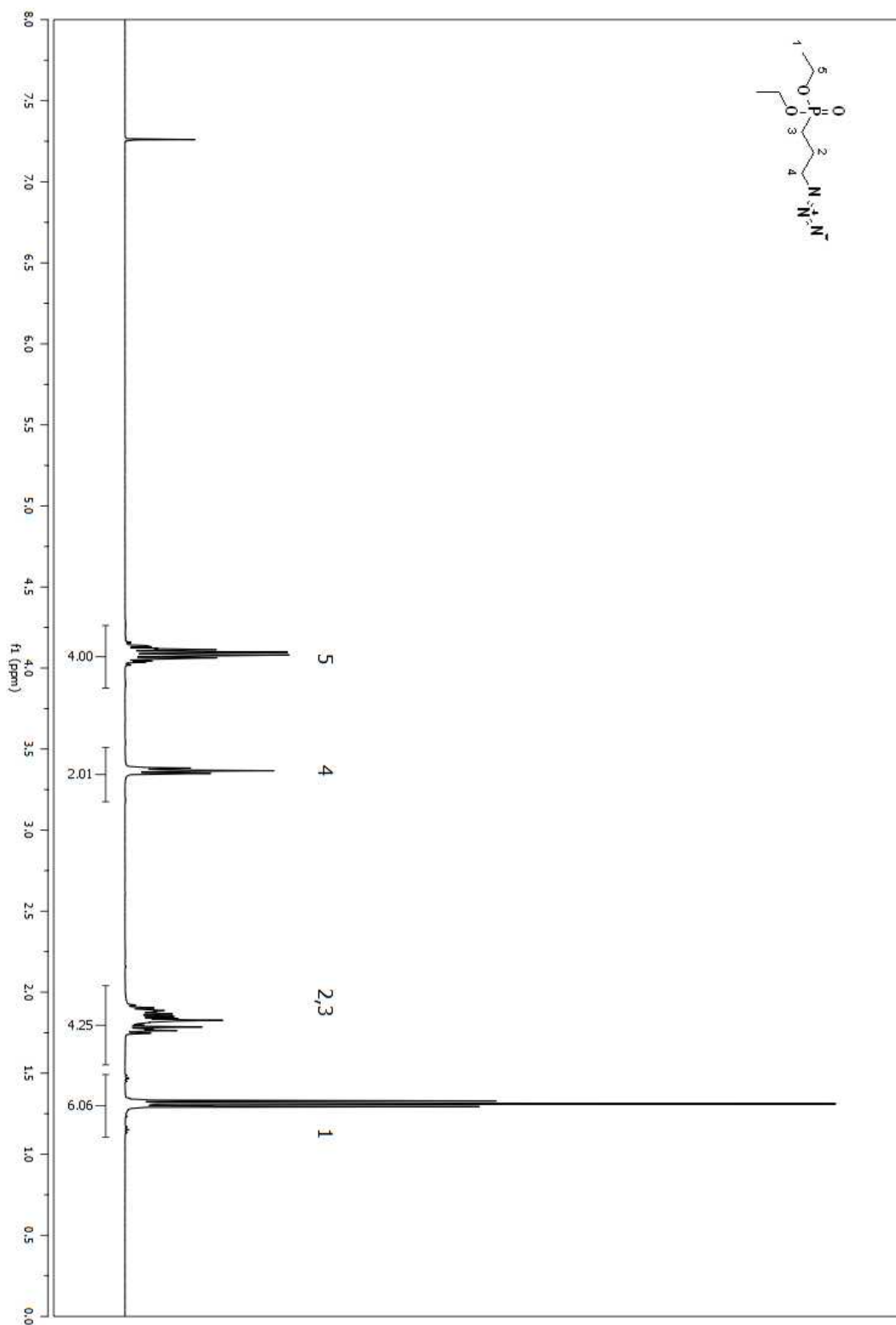


Figure A 83. ^1H NMR spectrum of compound **33** in CDCl_3 (Table 2.4, entry xii)

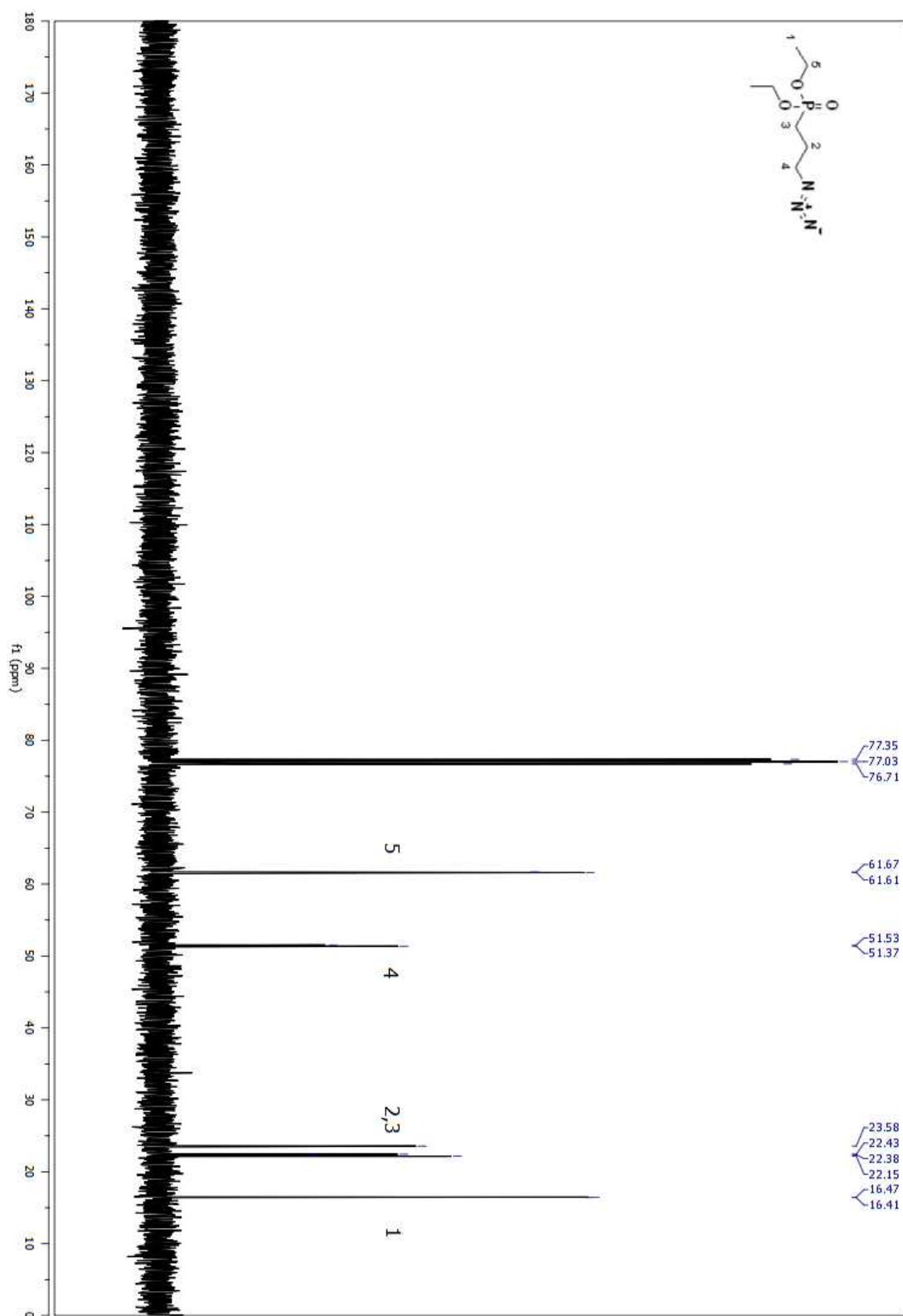


Figure A 84. ^{13}C NMR spectrum of compound **33** in CDCl_3 (Table 2.4, entry xii)

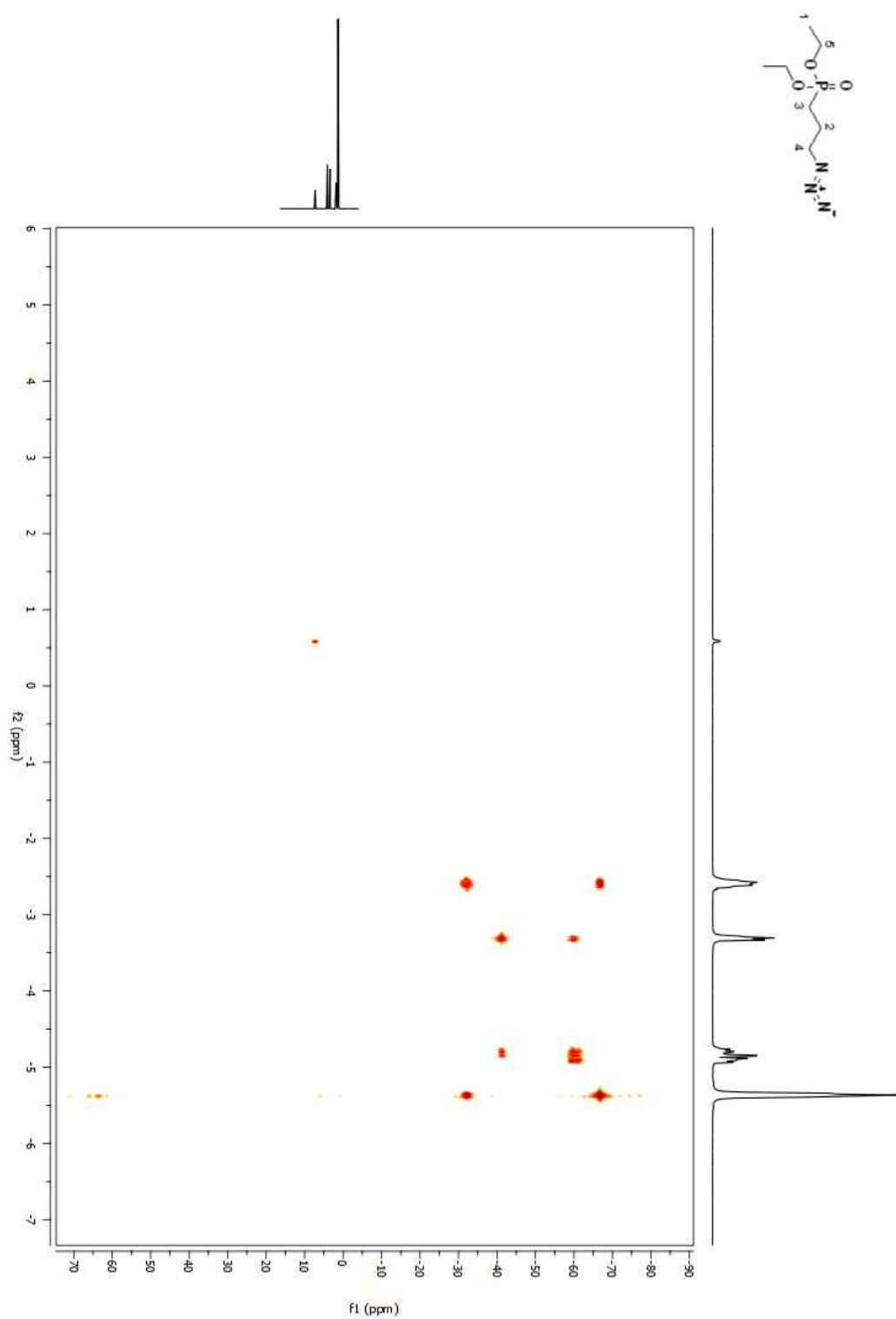


Figure A 85. COSY 2D NMR spectrum of compound **33** in CDCl_3 (Table 2.4, entry xii)

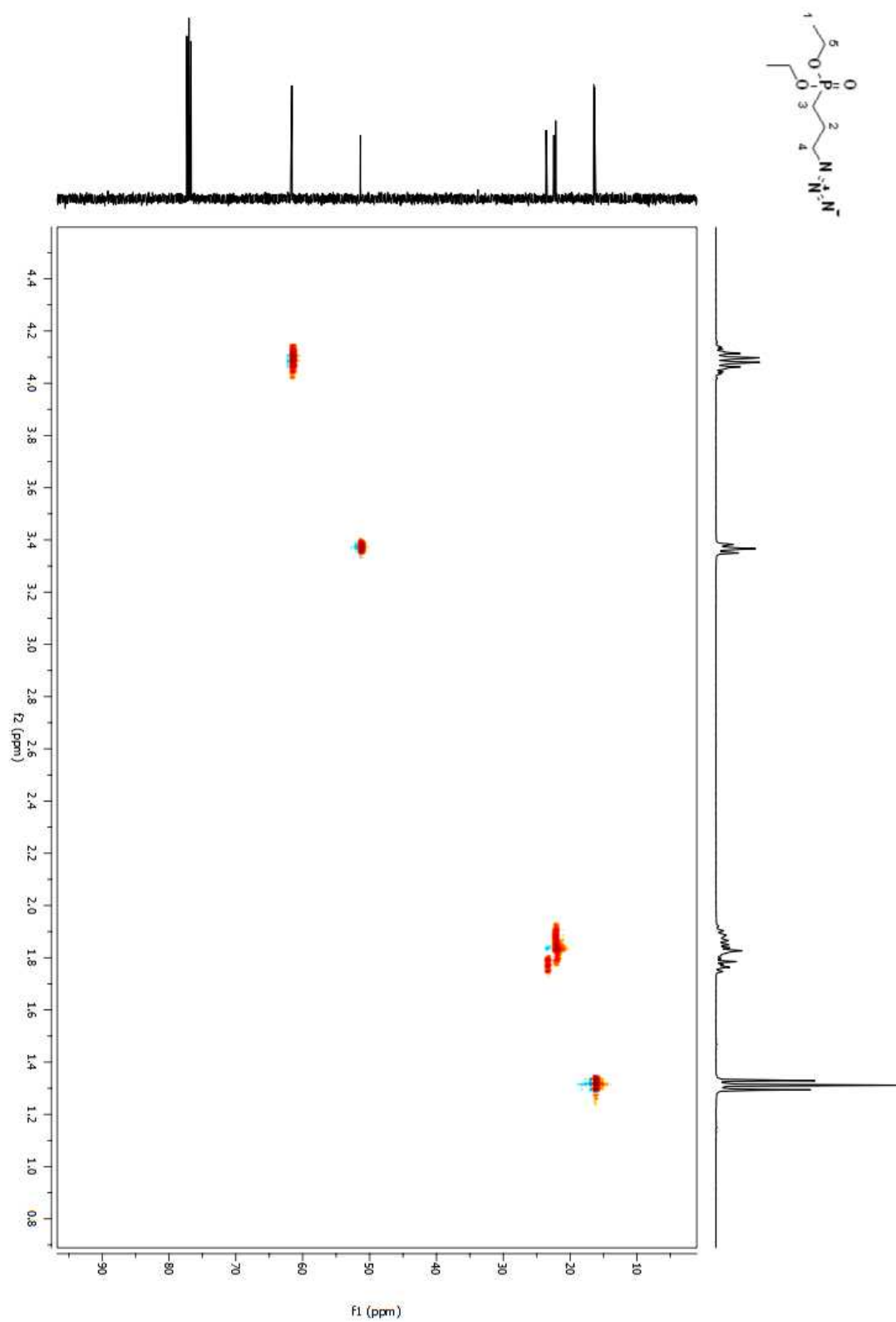


Figure A 86. HSQC 2D NMR spectrum of compound **33** in CDCl₃ (Table 2.4, entry xii)

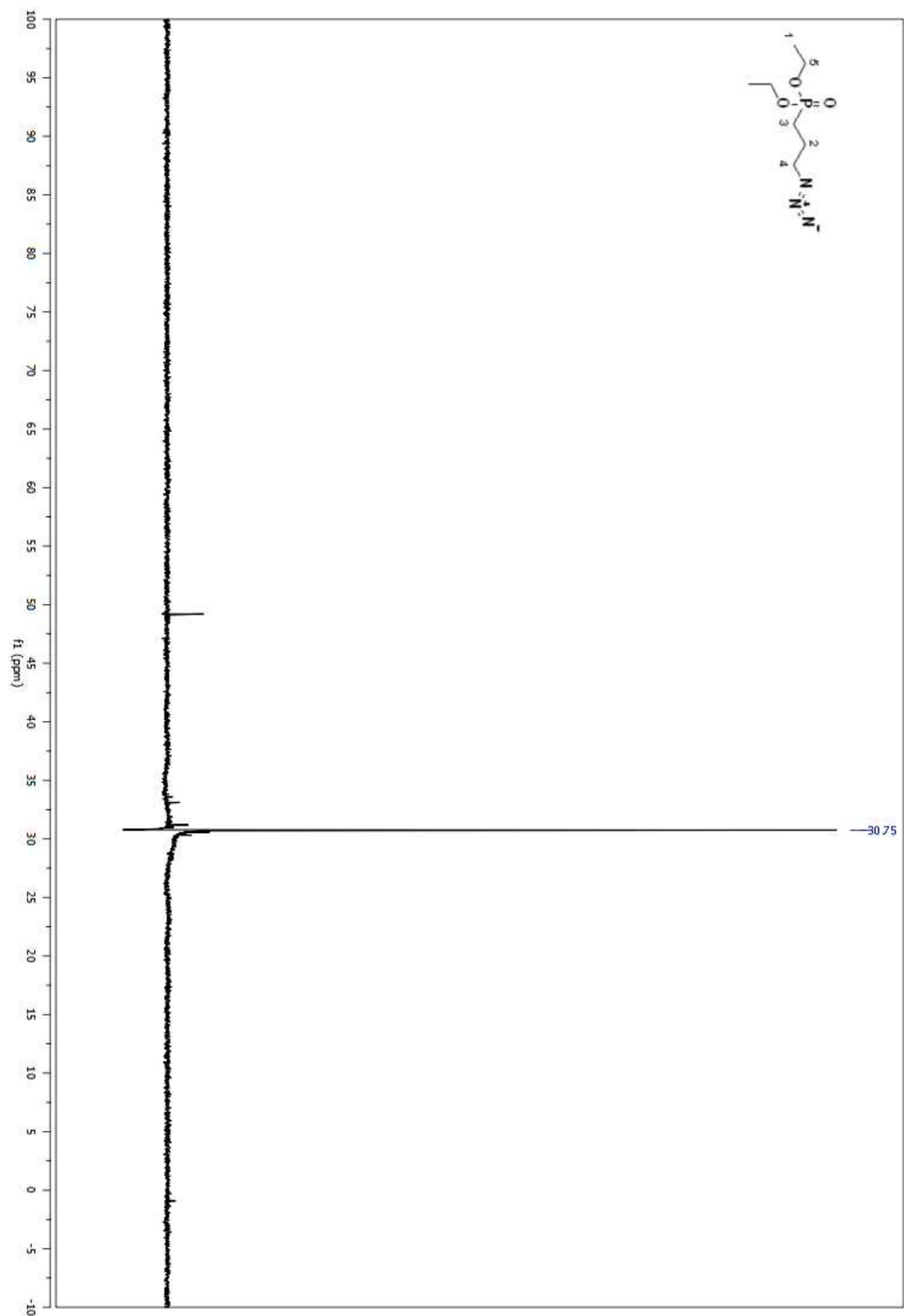


Figure A 87. ^{31}P NMR spectrum of compound **33** in CDCl_3 (Table 2.4, entry xii)

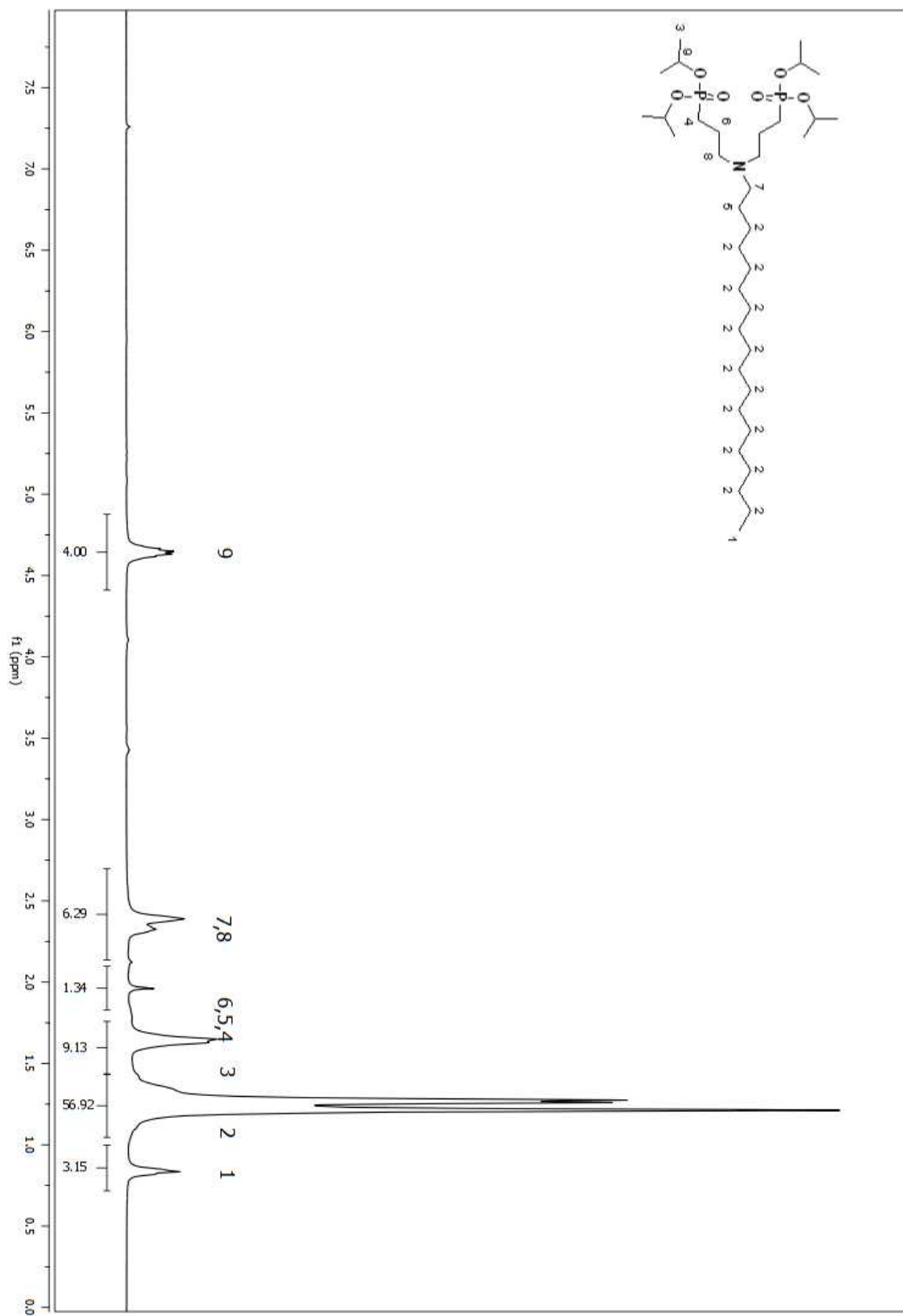
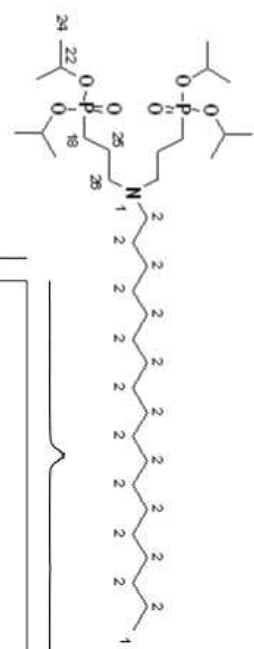


Figure A 88. ¹H NMR spectrum of compound **39** in CDCl₃



456

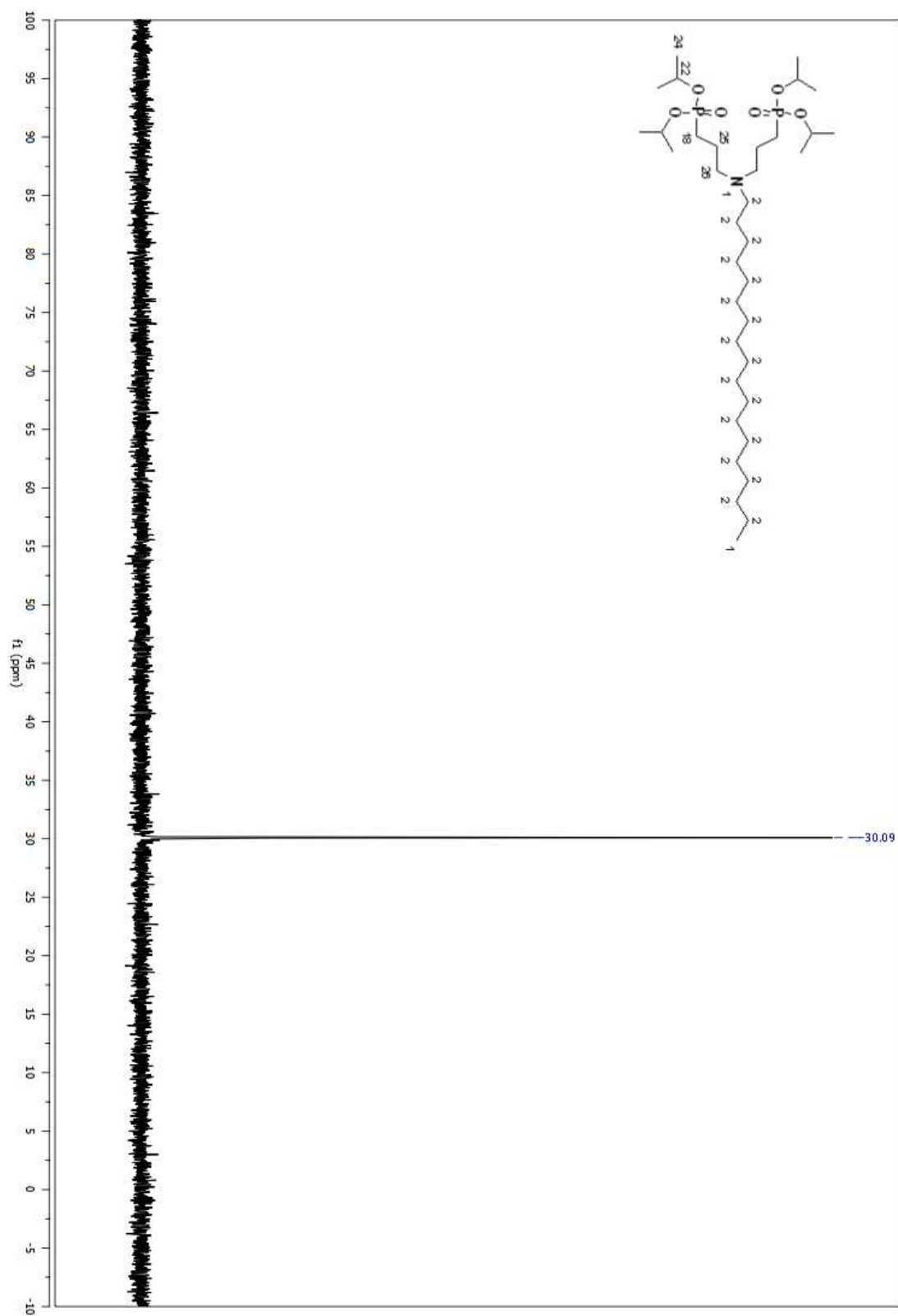


Figure A 90. ^{31}P NMR spectrum of compound **39** in CDCl_3

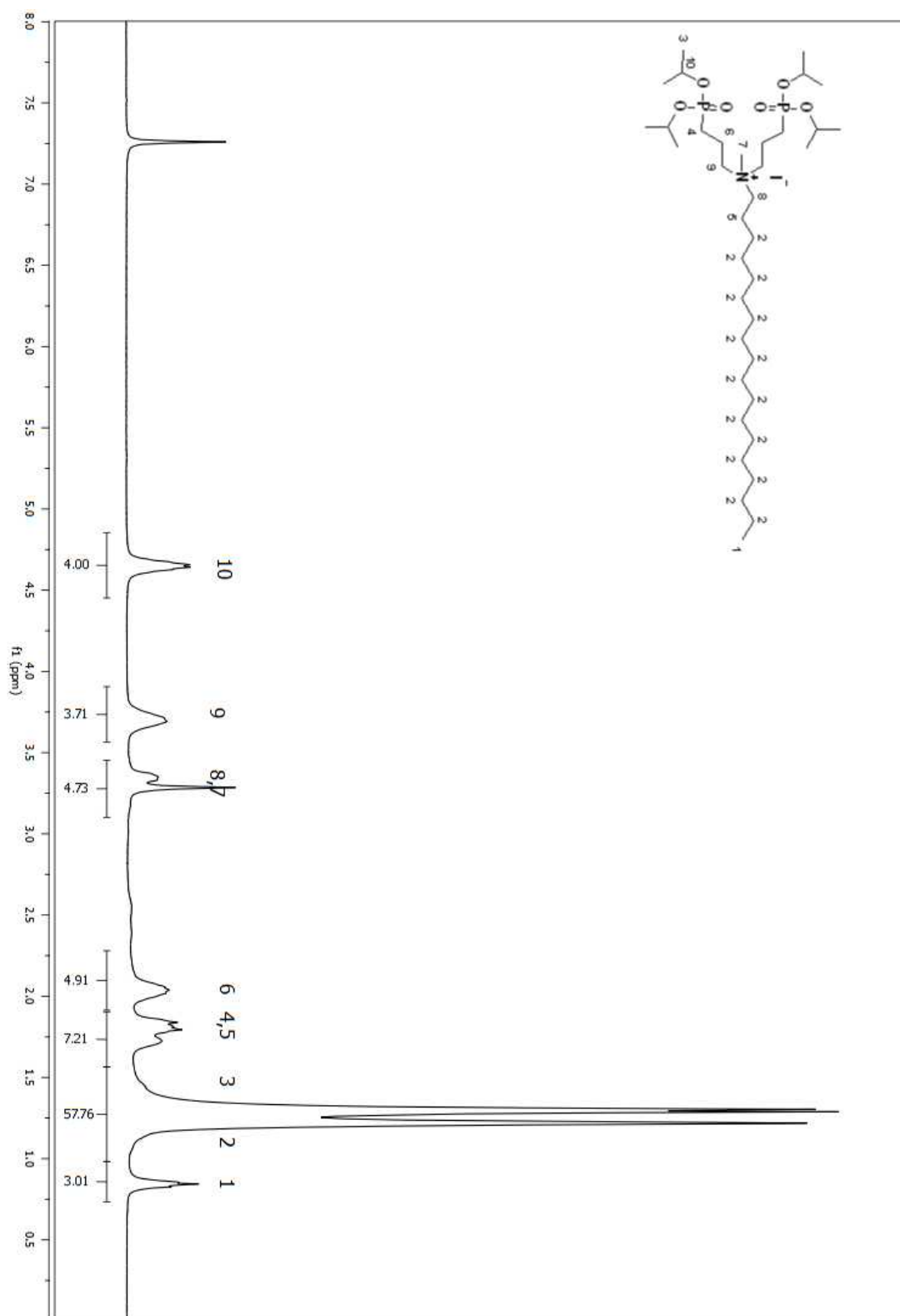
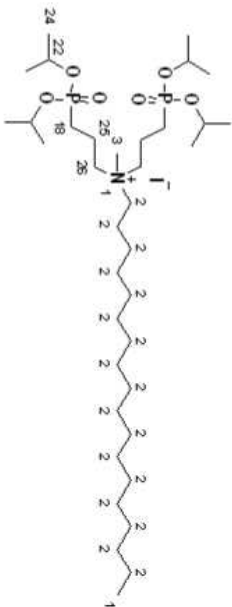


Figure A 91. ^1H NMR spectrum of compound **40** in CDCl_3



459

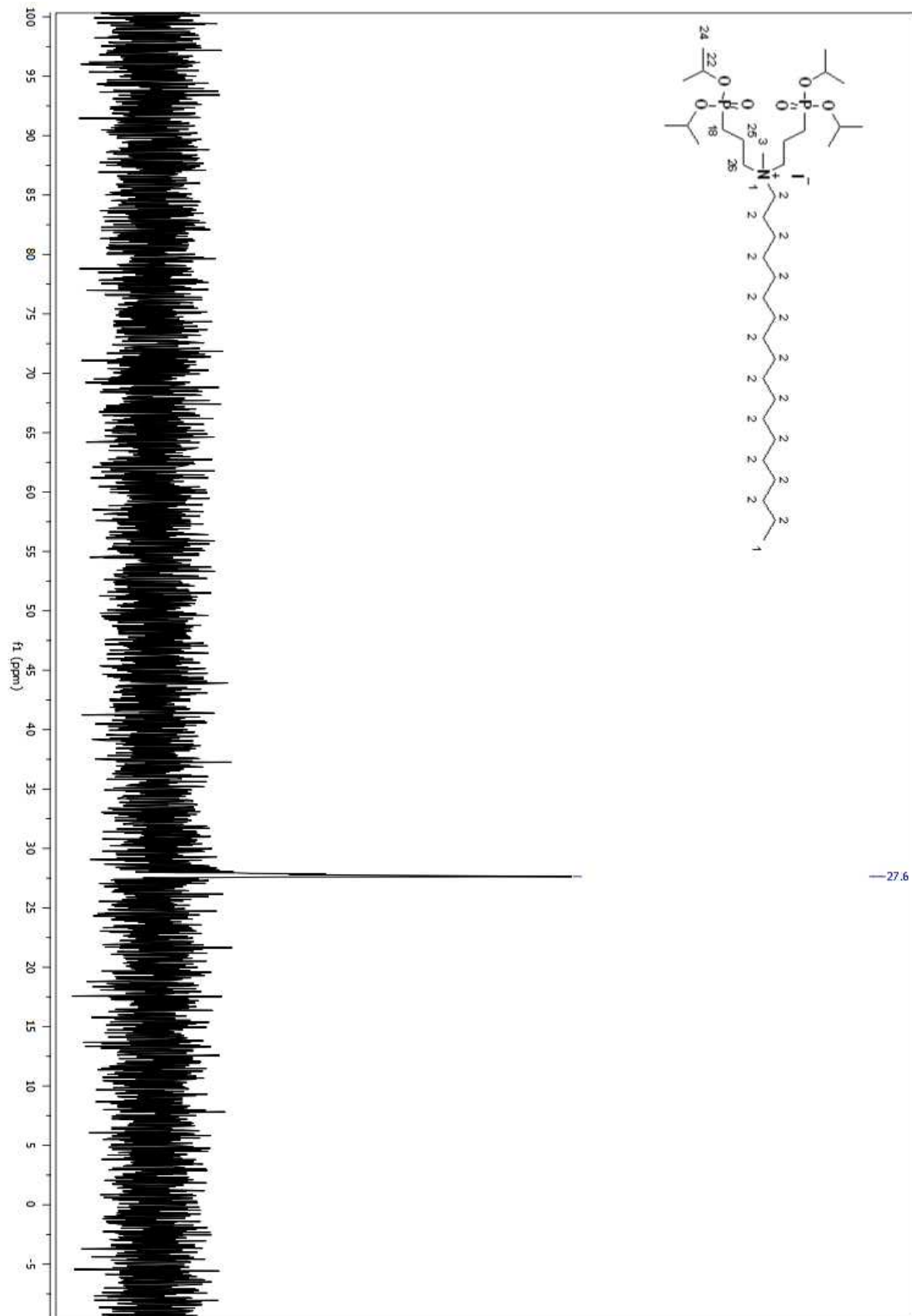


Figure A 93. ^{31}P NMR spectrum of compound **40** in CDCl_3 (AFTER COLUMN)

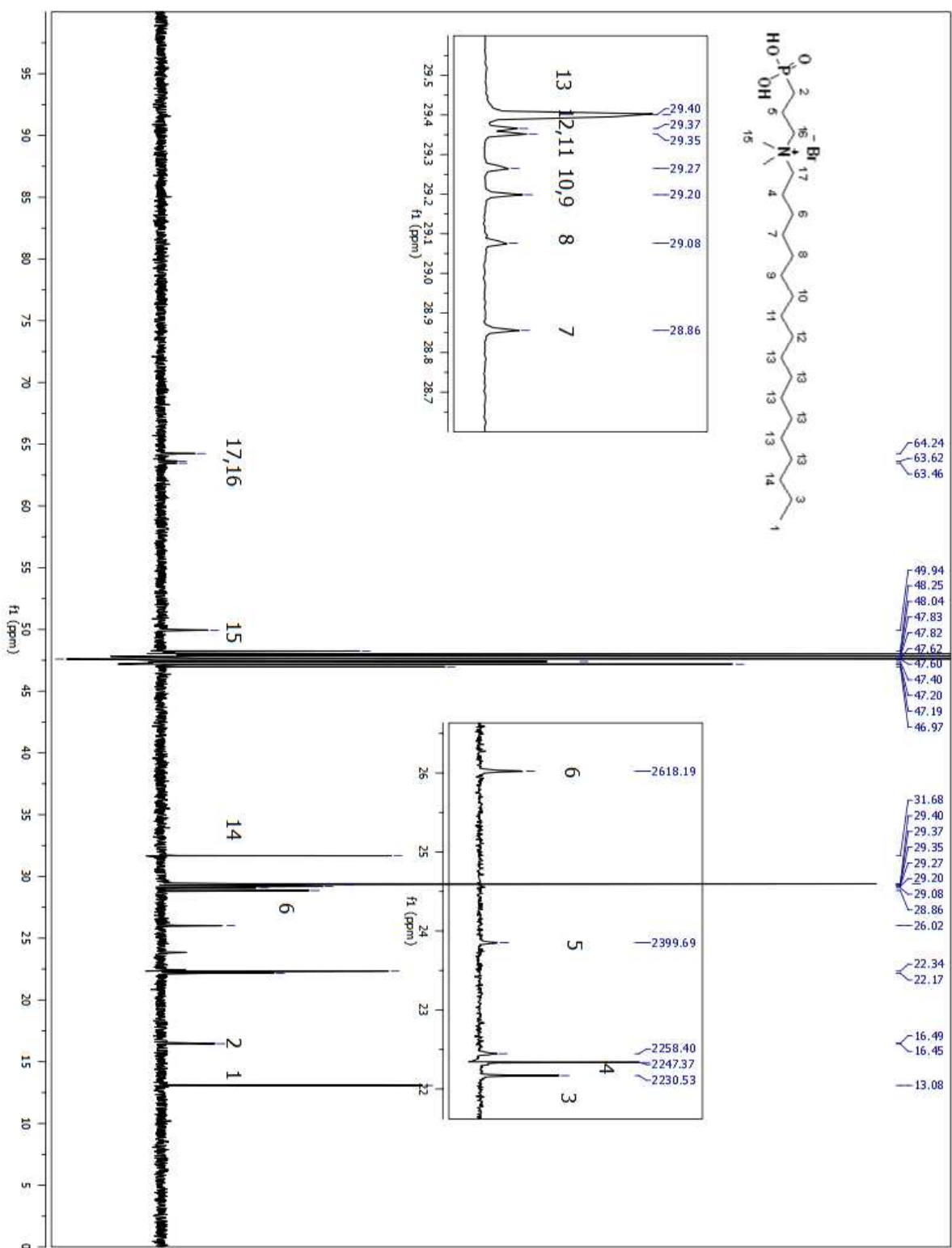


Figure A 95. ^{13}C NMR spectrum of compound **34** in MeOD (Table 2.5, entry i)

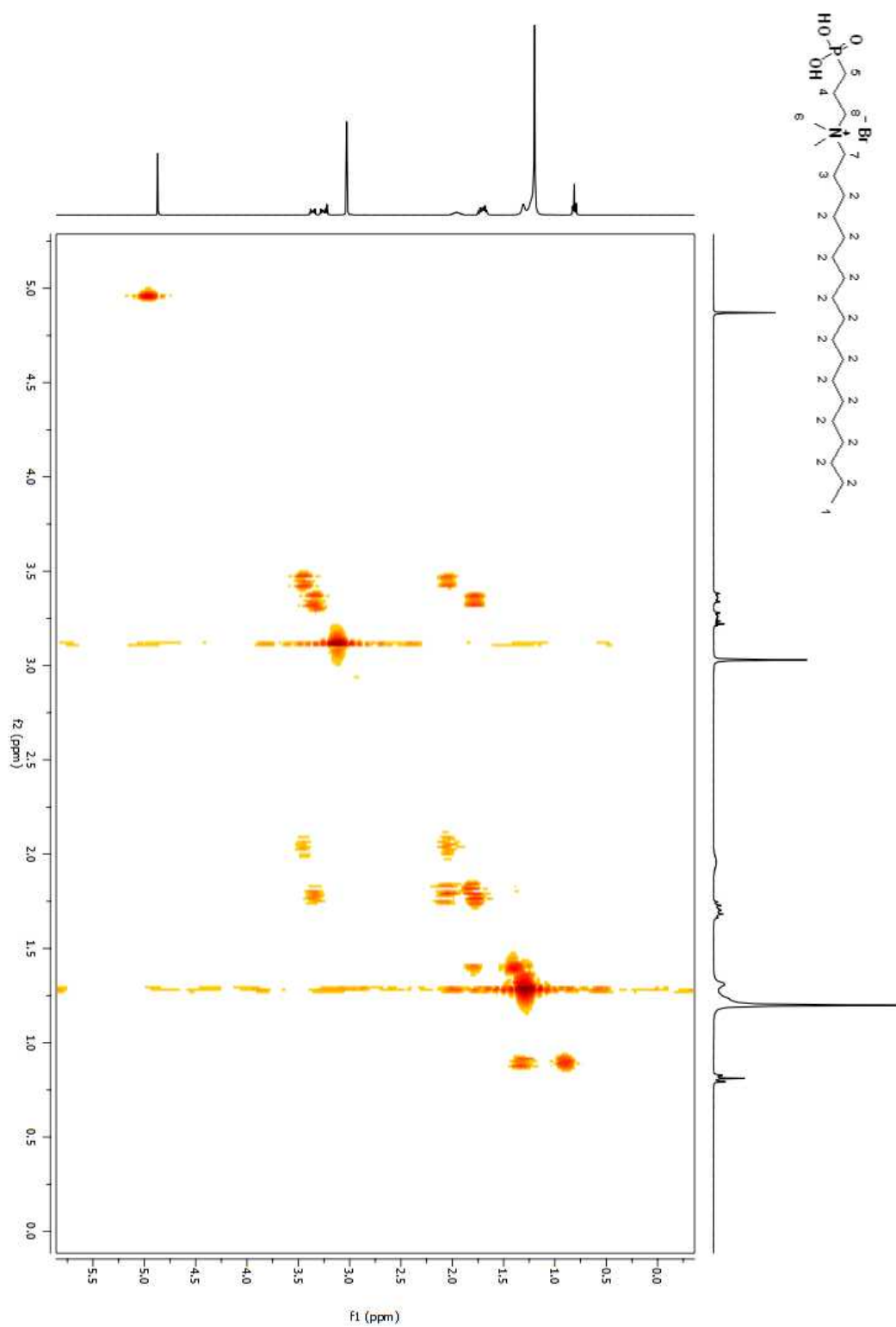


Figure A 96. ^1H NMR spectrum of compound **34** in MeOD (Table 2.5, entry i)

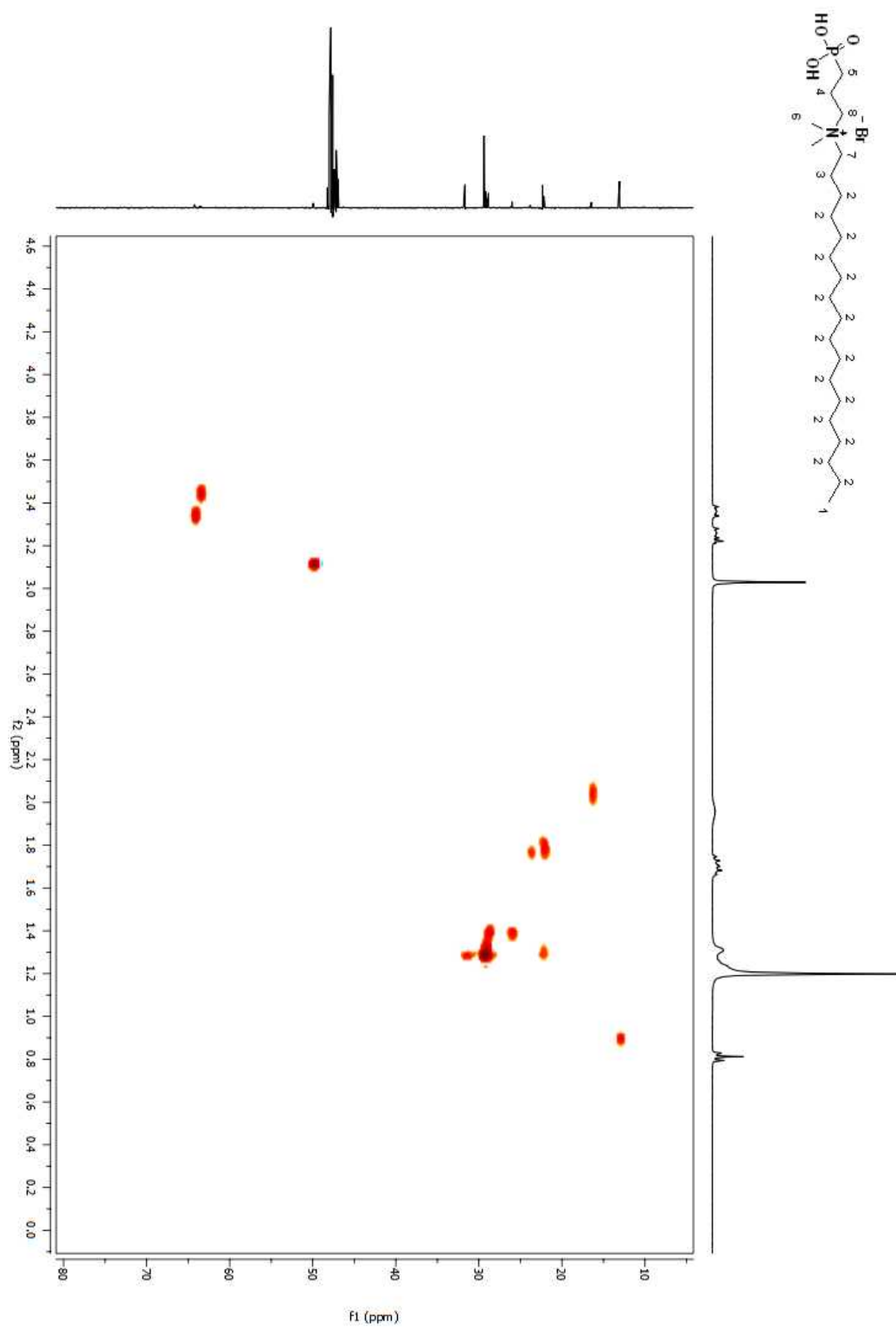


Figure A 97. ^1H NMR spectrum of compound **34** in MeOD (Table 2.5, entry i)

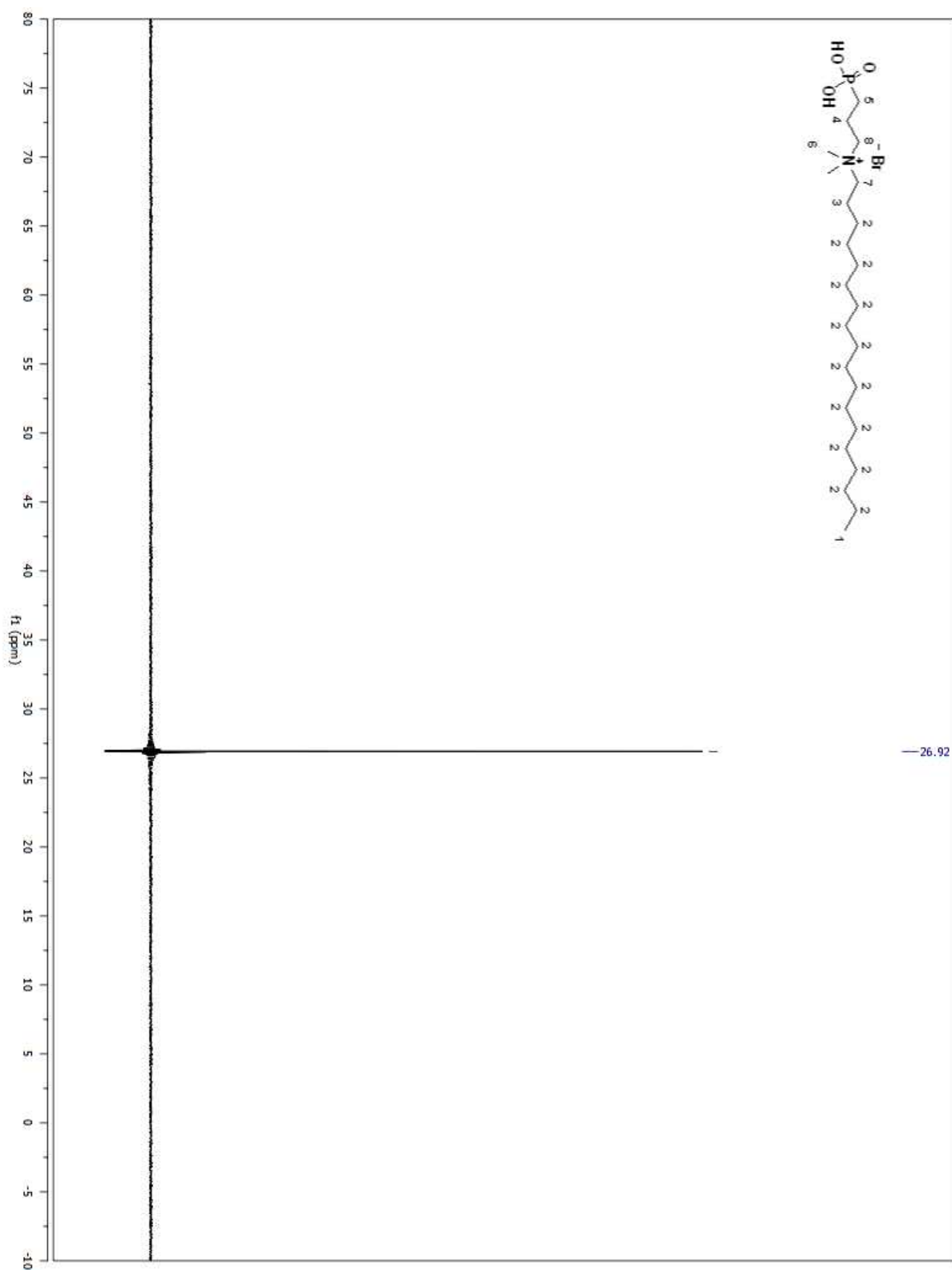


Figure A 98. ^{31}P NMR spectrum of compound **34** in MeOD (Table 2.5, entry i)

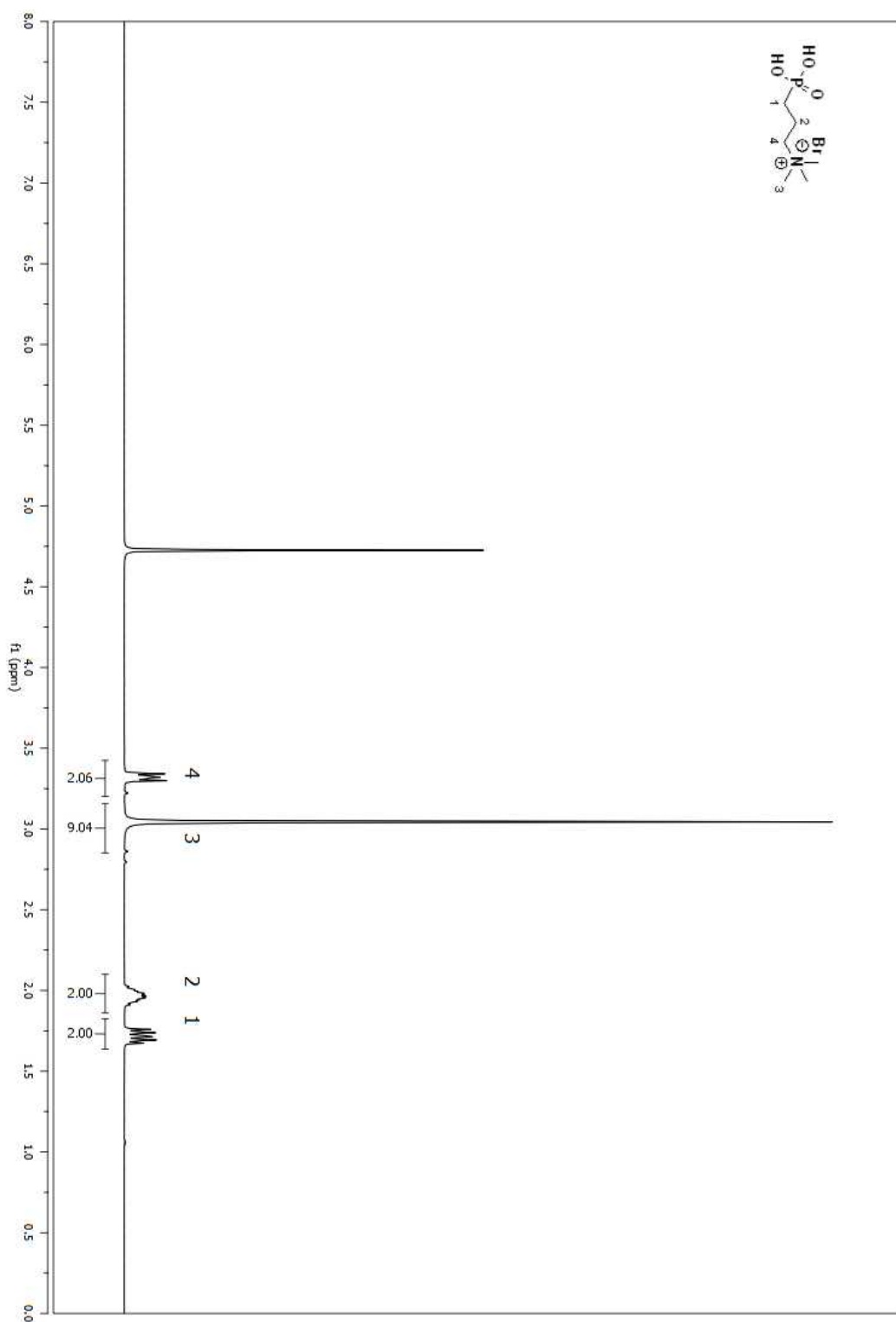


Figure A 99. ¹H NMR spectrum of compound **35** in D₂O (Table 4.5, entry ix)

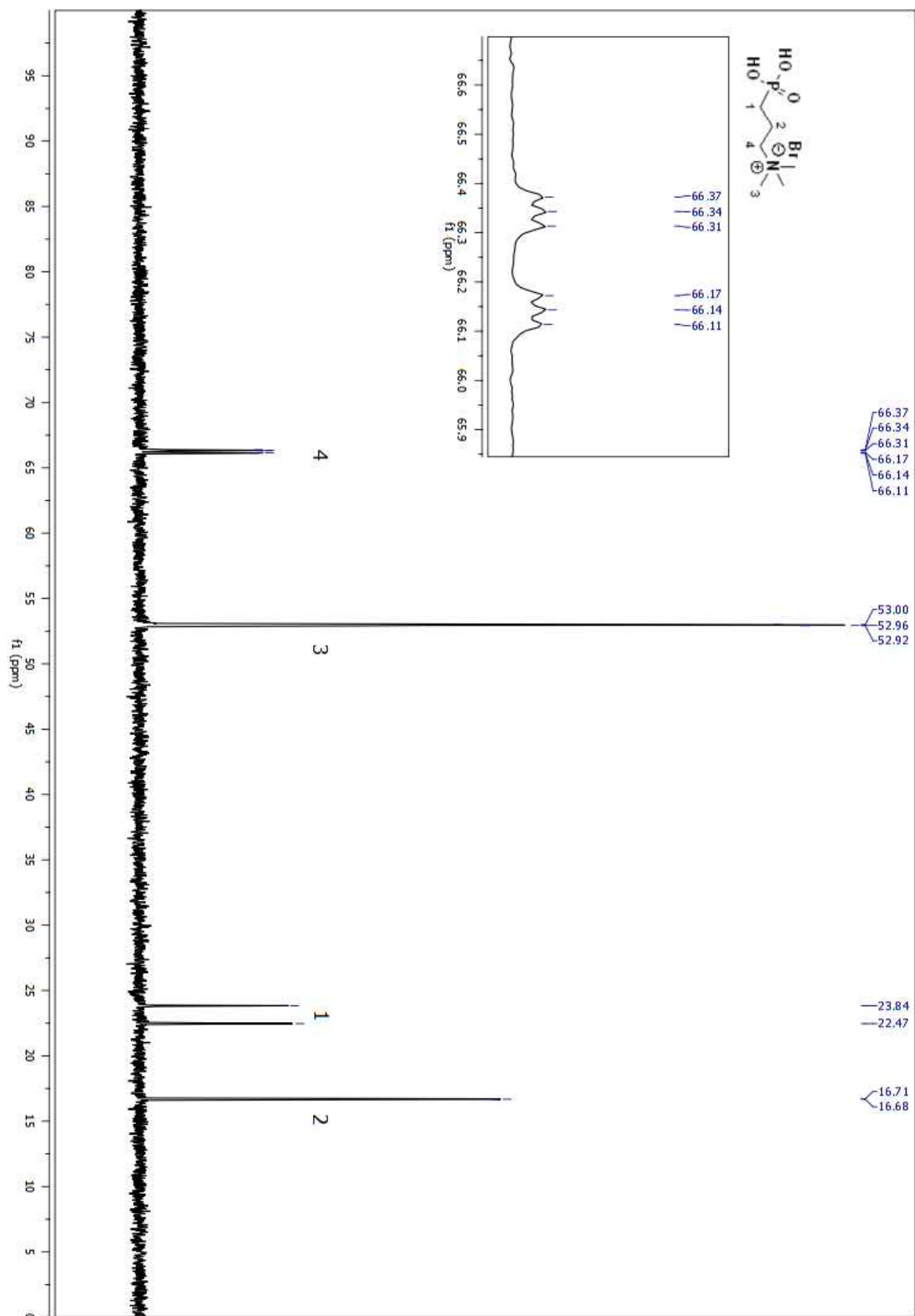


Figure A 100. ¹³C NMR spectrum of compound **35** in D₂O (Table 2.5, entry ix)

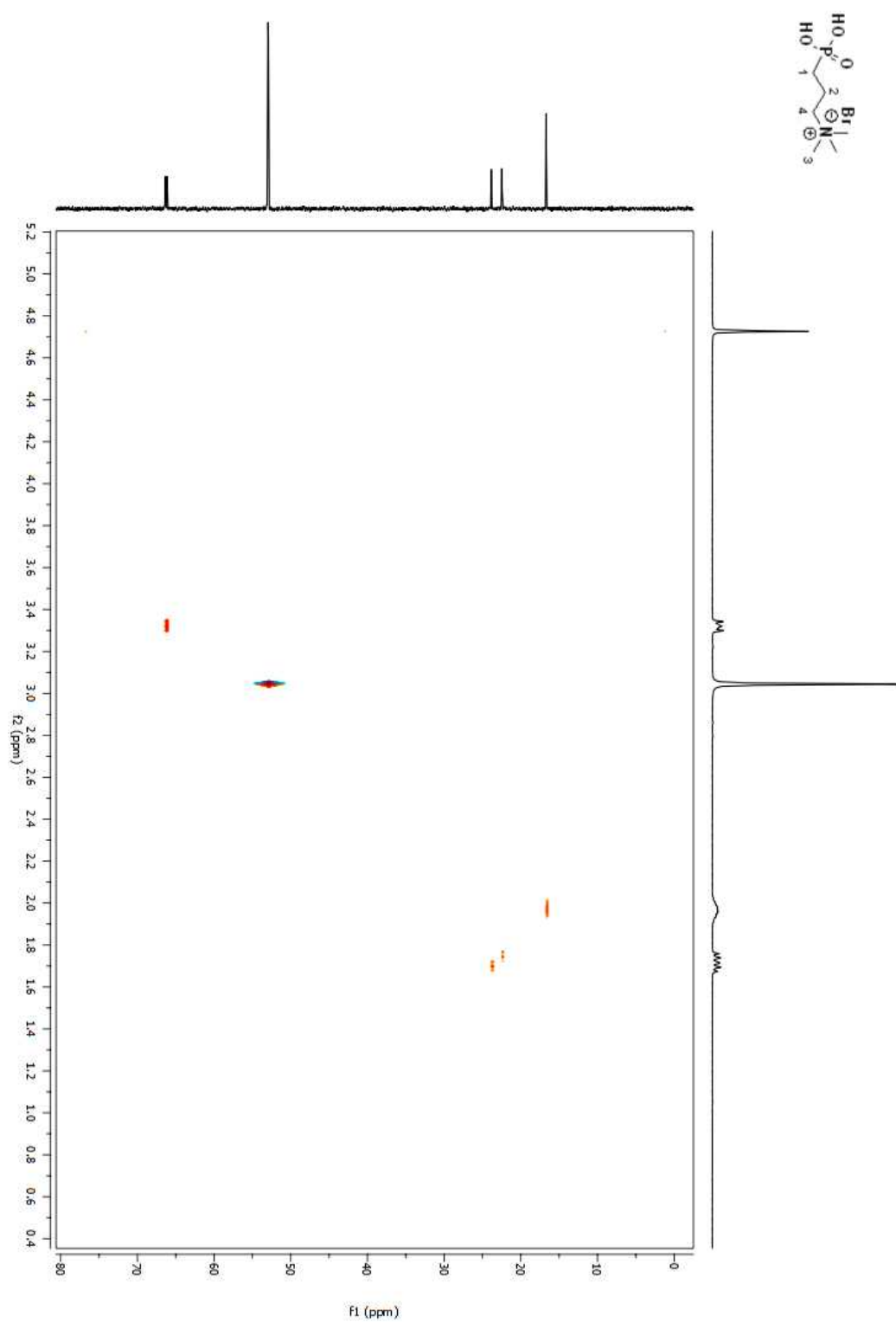


Figure A 101. HSQC spectrum of compound **35** in D₂O (Table 2.5, entry xi)

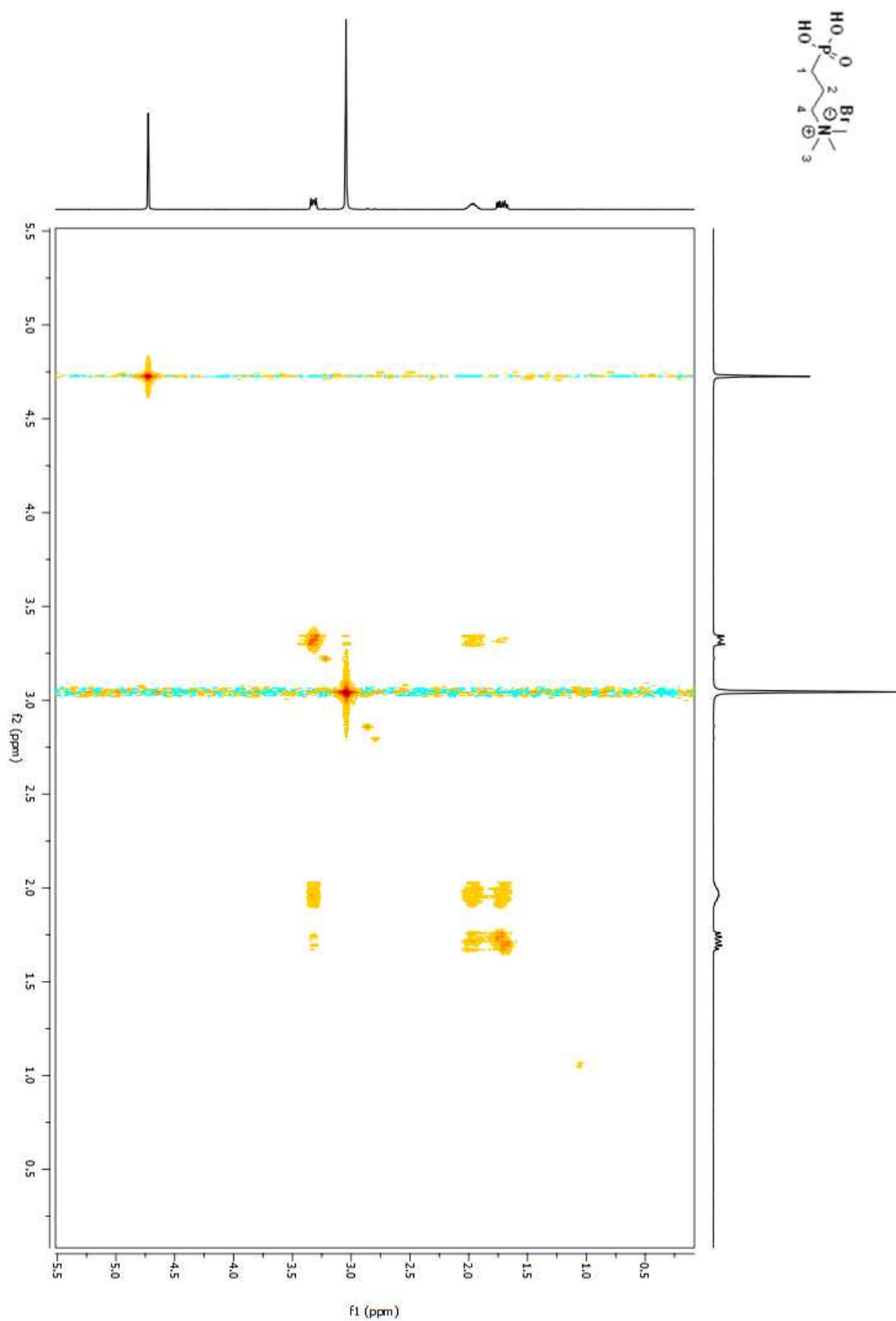


Figure A 102. COSY spectrum of compound **35** in D₂O (Table 2.5, entry ix)

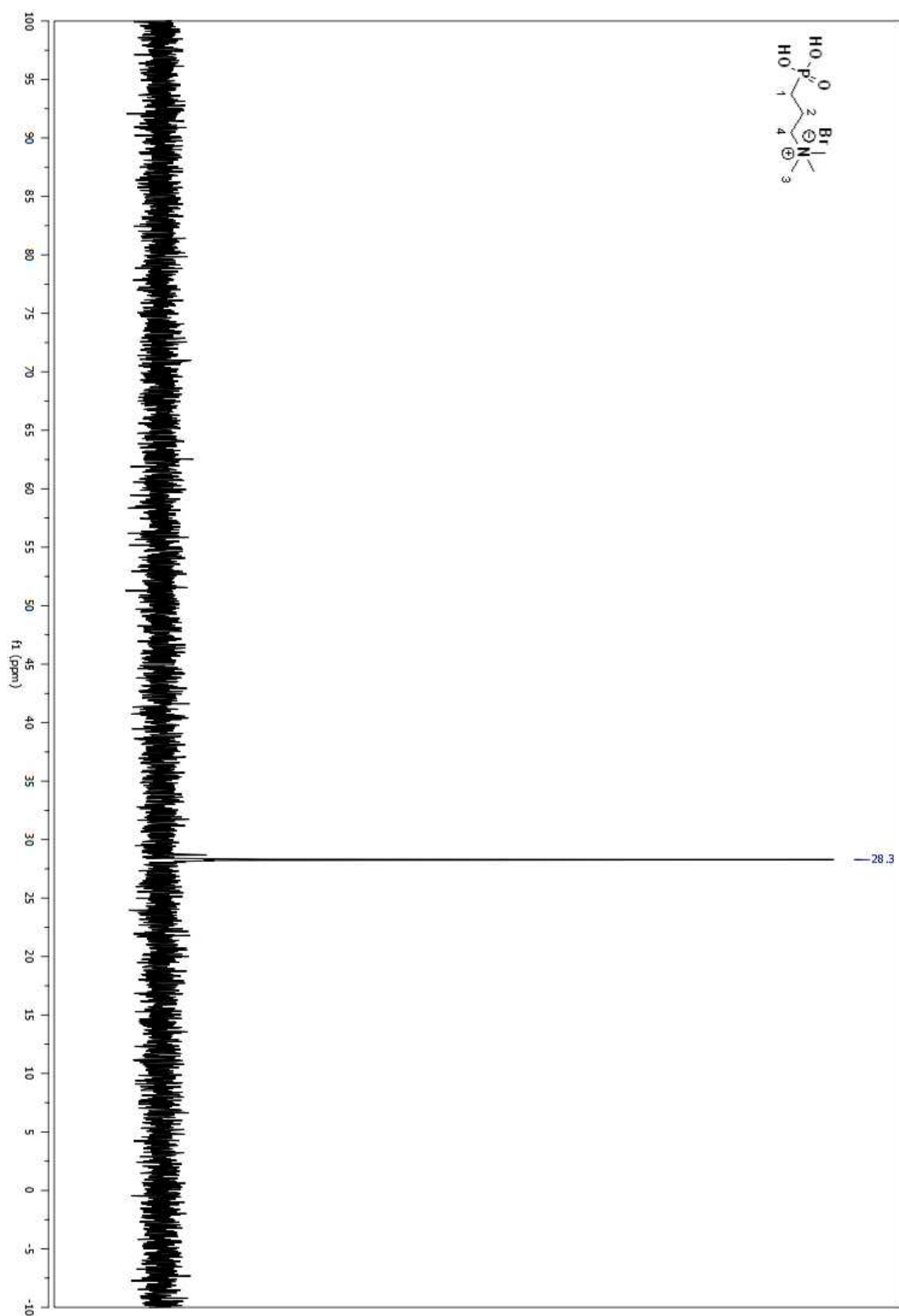


Figure A 103. ^{31}P spectrum of compound **35** in D_2O (Table 2.5, entry ix)

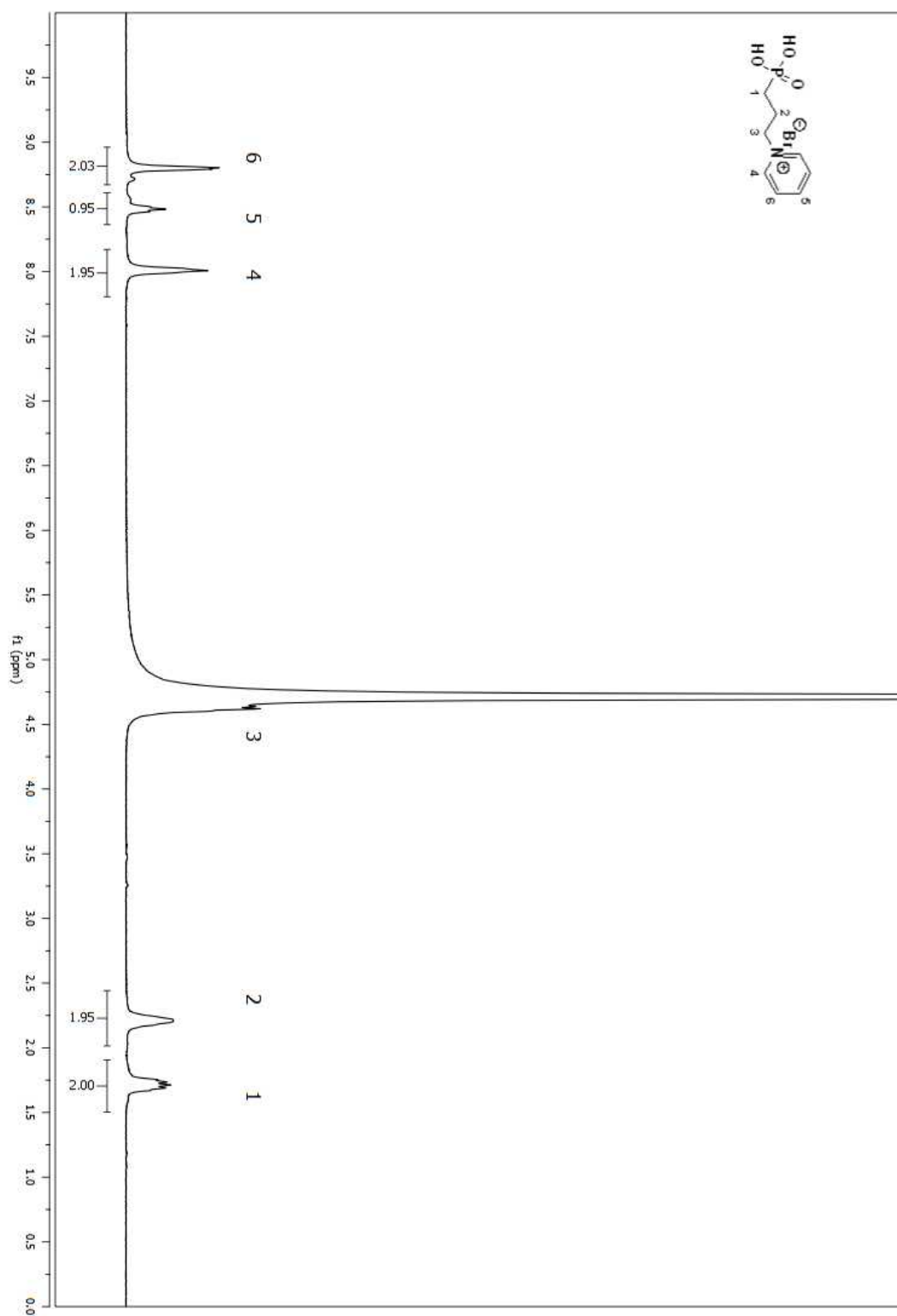


Figure A 104. ¹H NMR spectrum of compound **35** in D₂O (Table 2.5, entry ix)

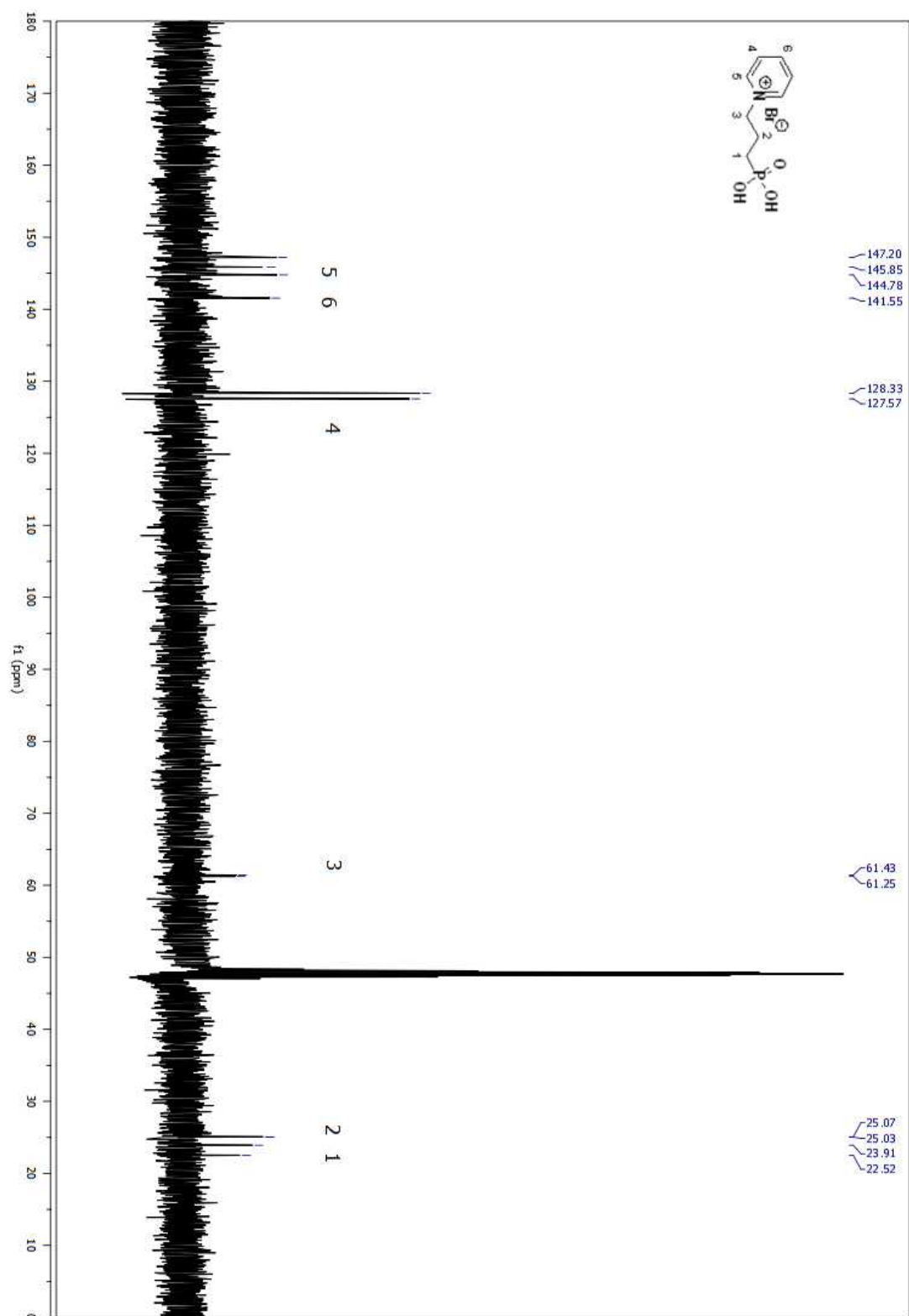


Figure A 105. ¹³C NMR spectrum of compound **36** in D₂O (Table 2.5, entry x)

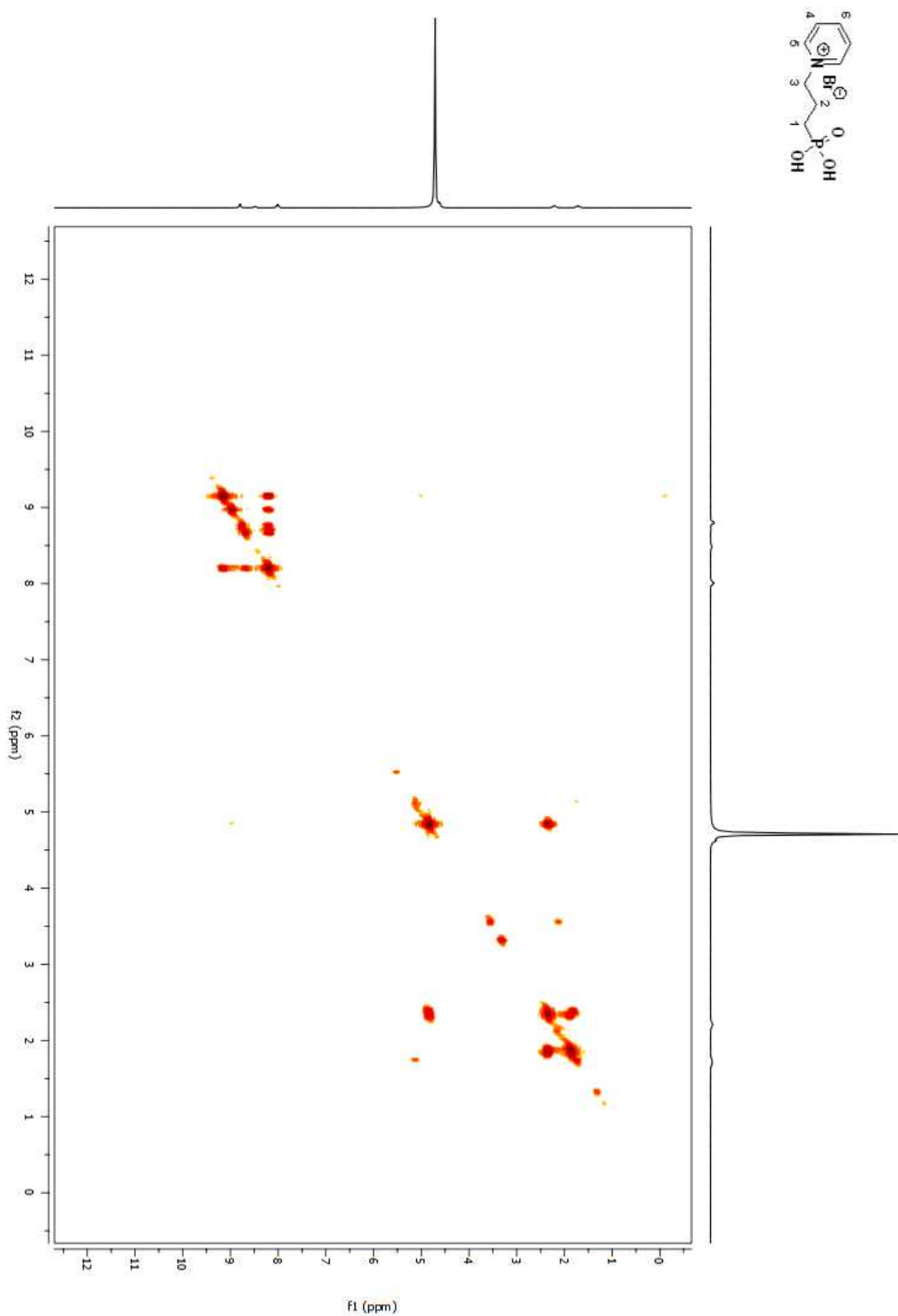


Figure A 106. ^1H NMR spectrum of compound **36** in D_2O (Table 2.5, entry x)

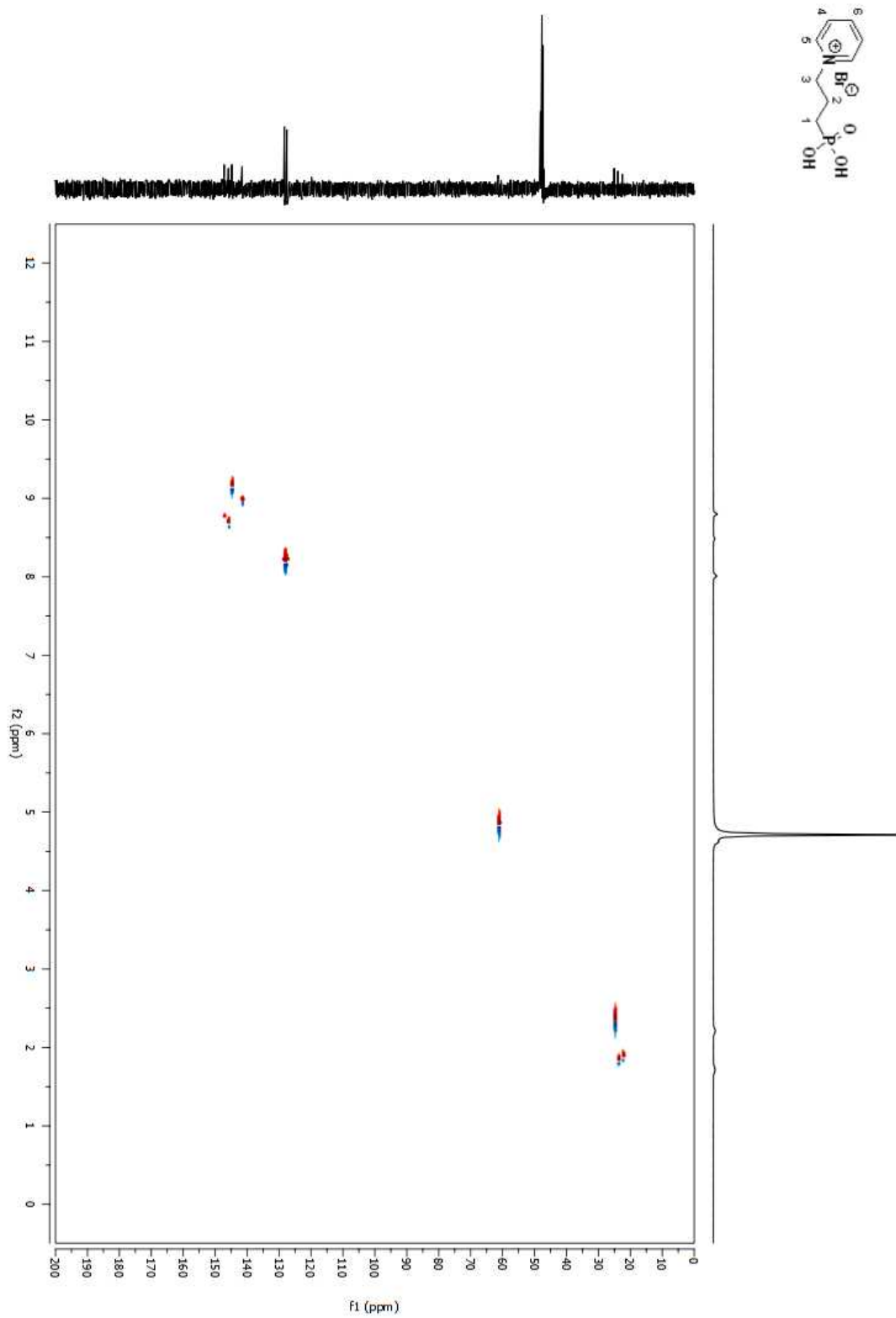


Figure A 107. HSQC NMR spectrum of compound **36** in D₂O (Table 2.5, entry x)

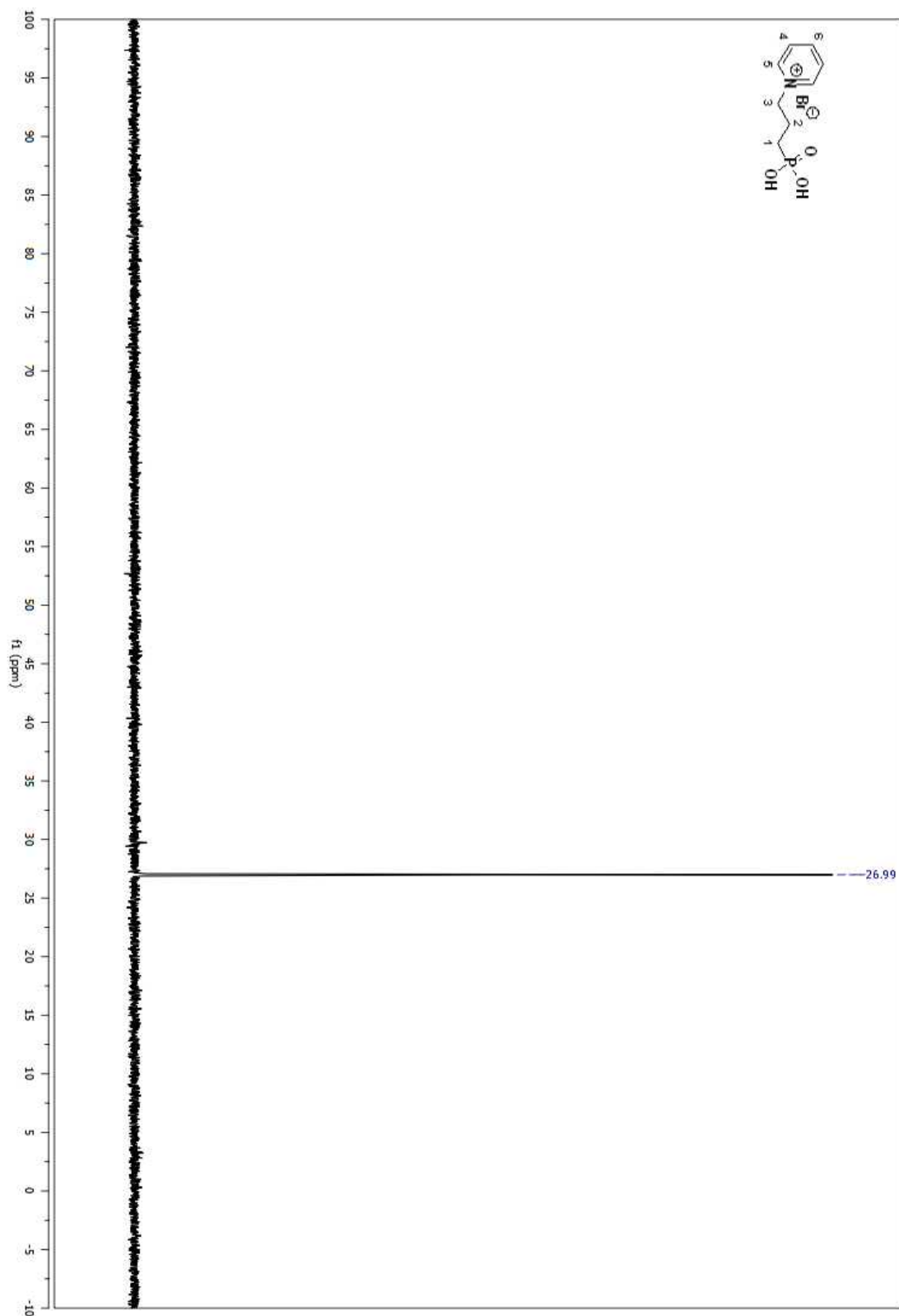


Figure A 108. ^{31}P NMR spectrum of compound **36** in D_2O (Table 2.5, entry x)

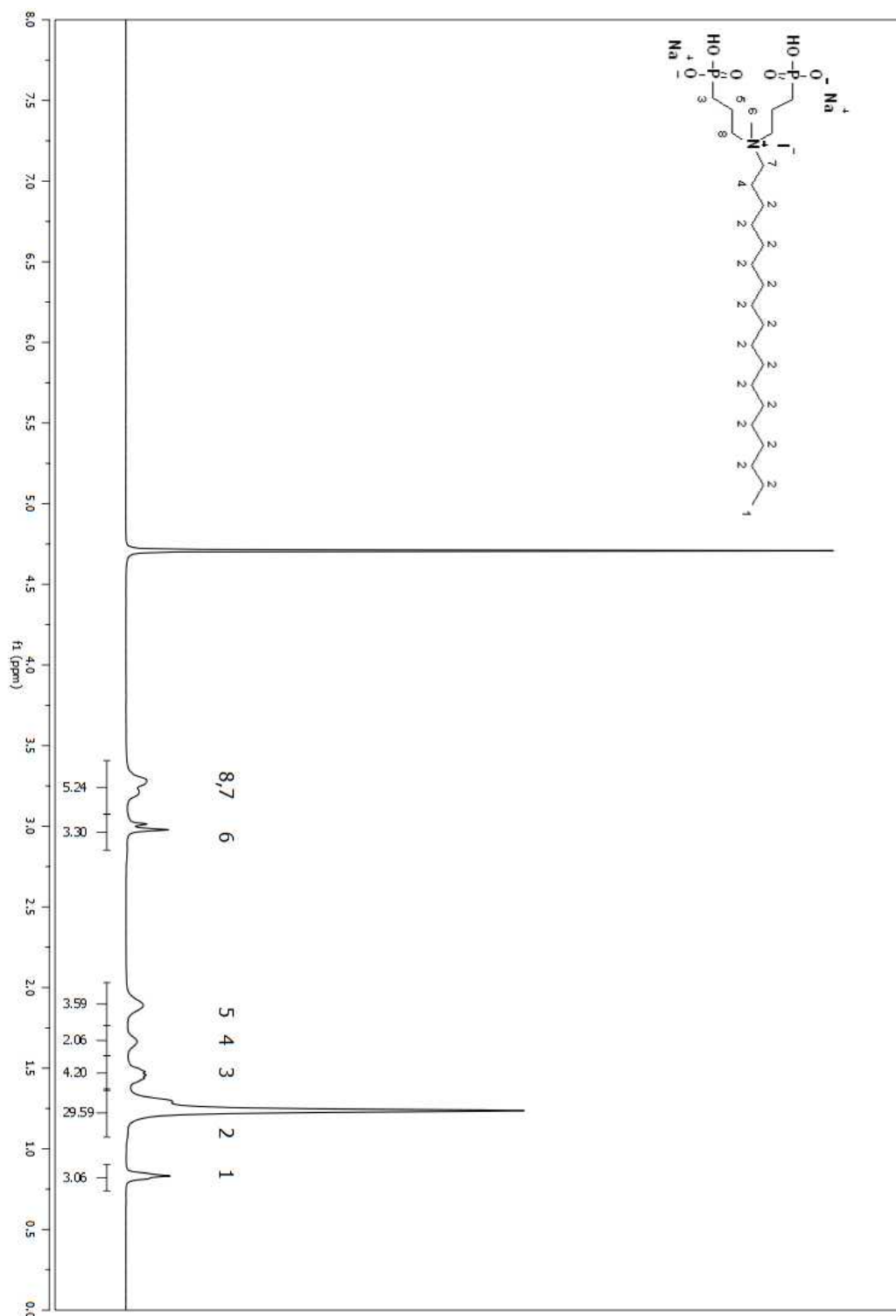


Figure A 109. ¹H NMR spectrum of compound **42** in D₂O.

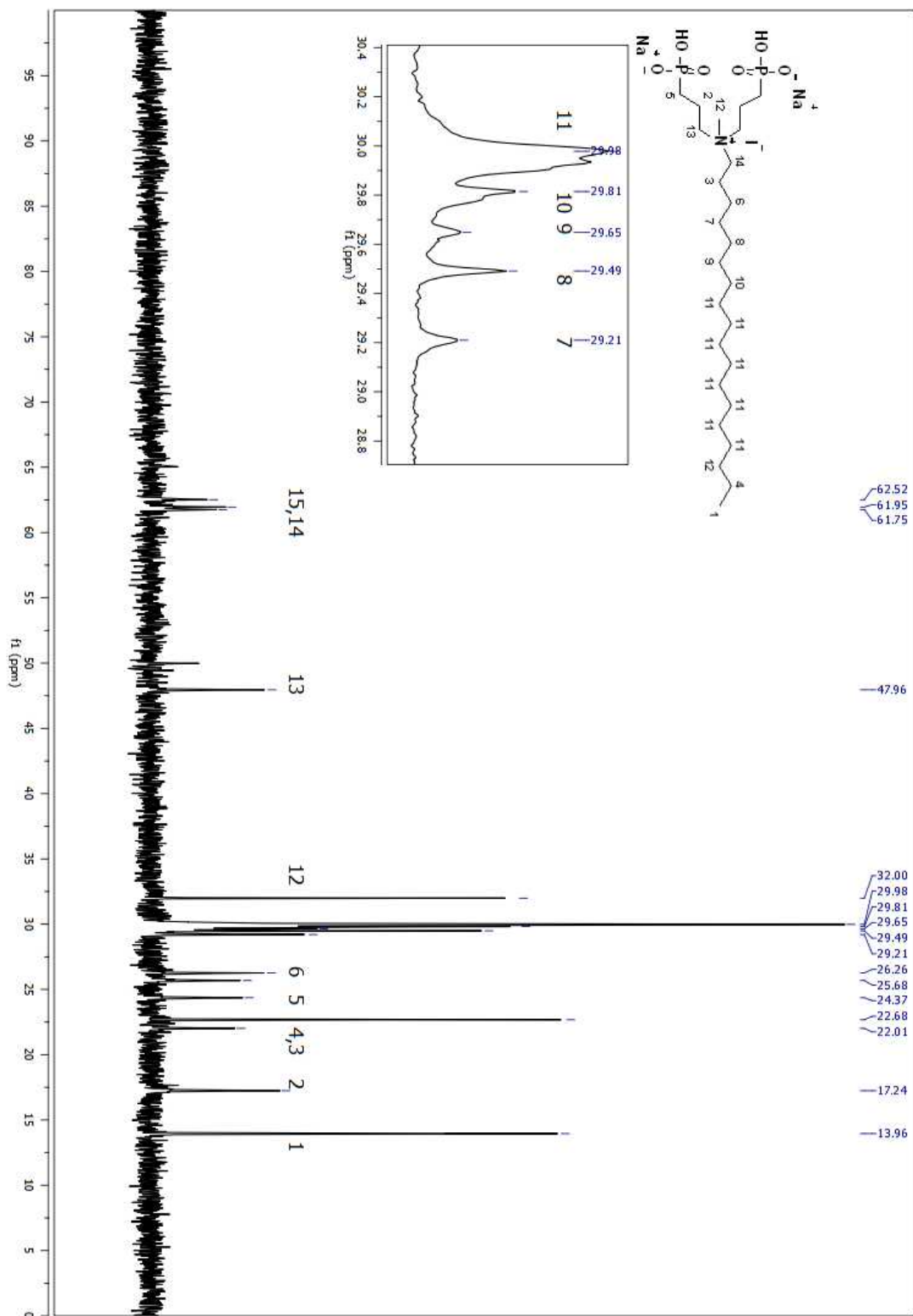


Figure A 110. ¹³C NMR spectrum of compound **42** in D₂O.

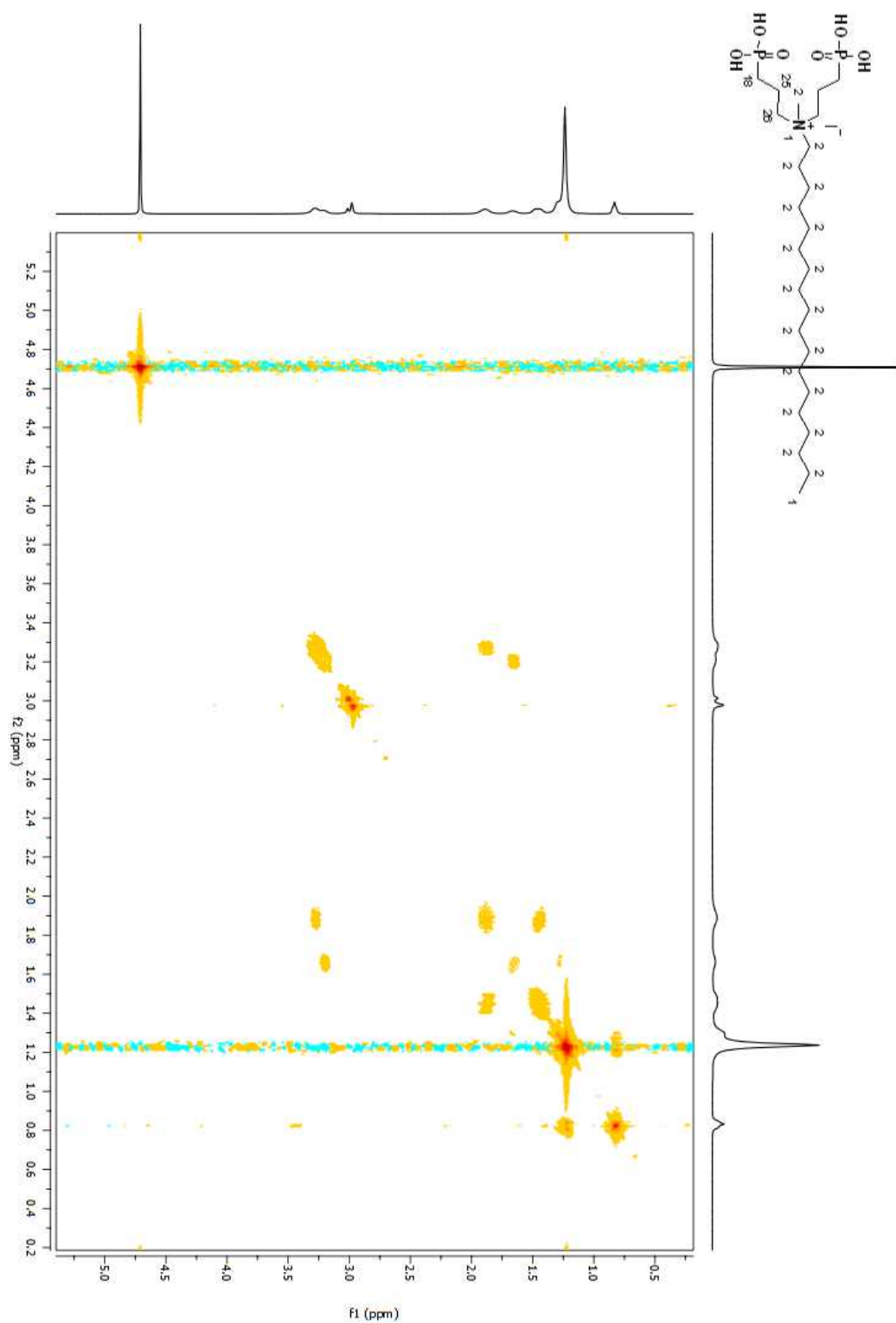


Figure A 111. COSY 2D NMR spectrum of compound **42** in D₂O.

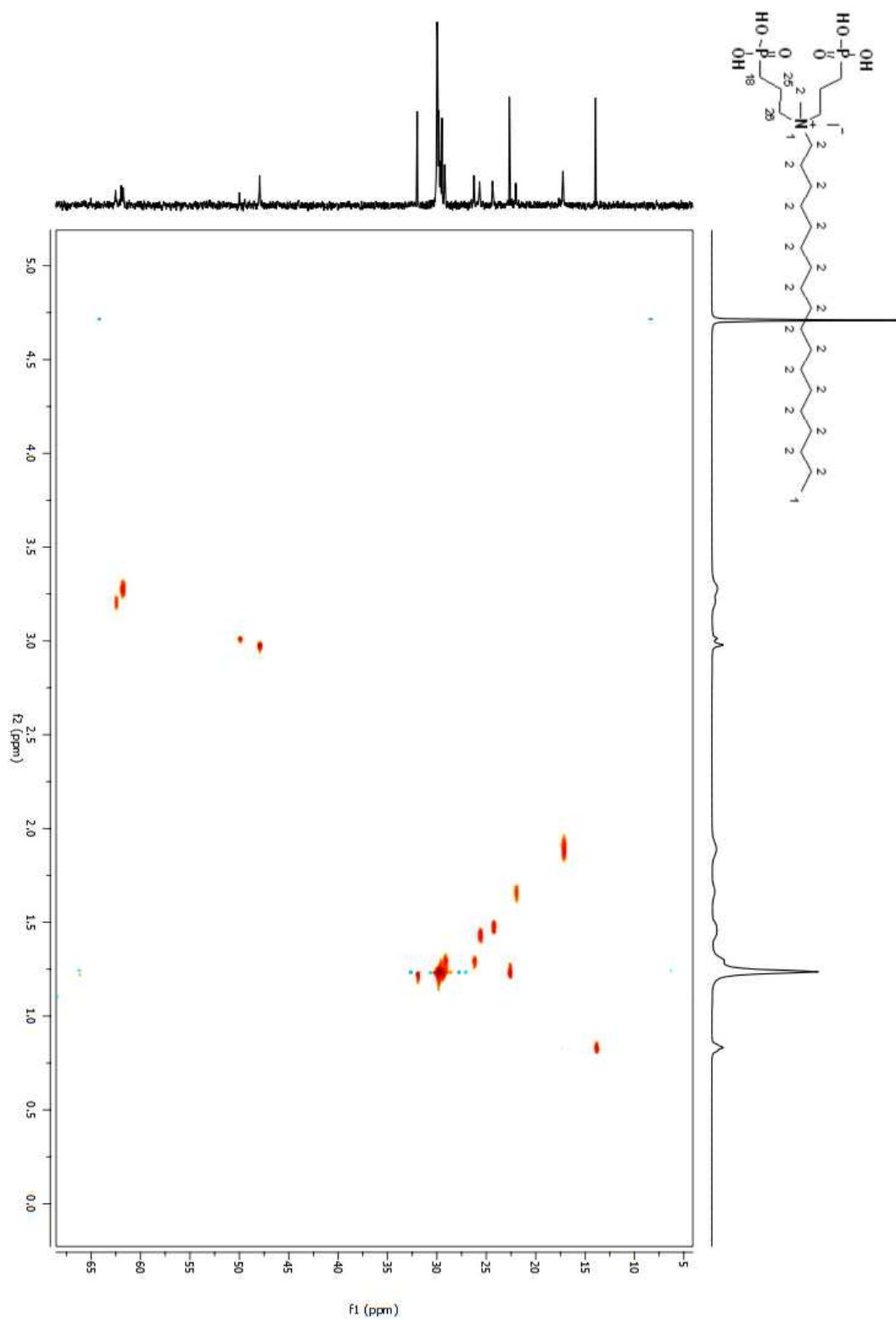


Figure A 112. HSQC 2D NMR spectrum of compound **42** in D₂O.

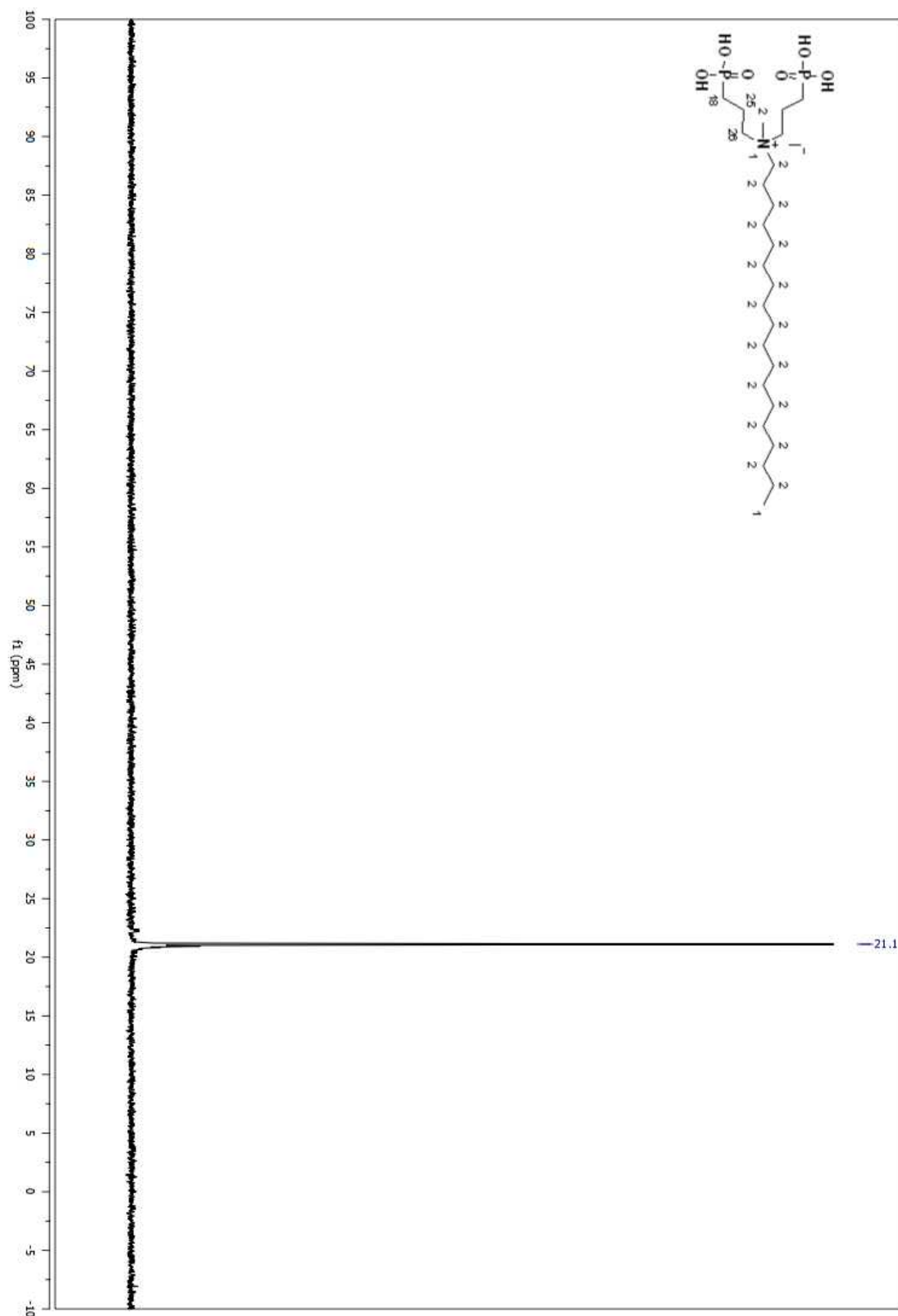


Figure A 113. ^{31}P NMR spectrum of compound **42** in D_2O .

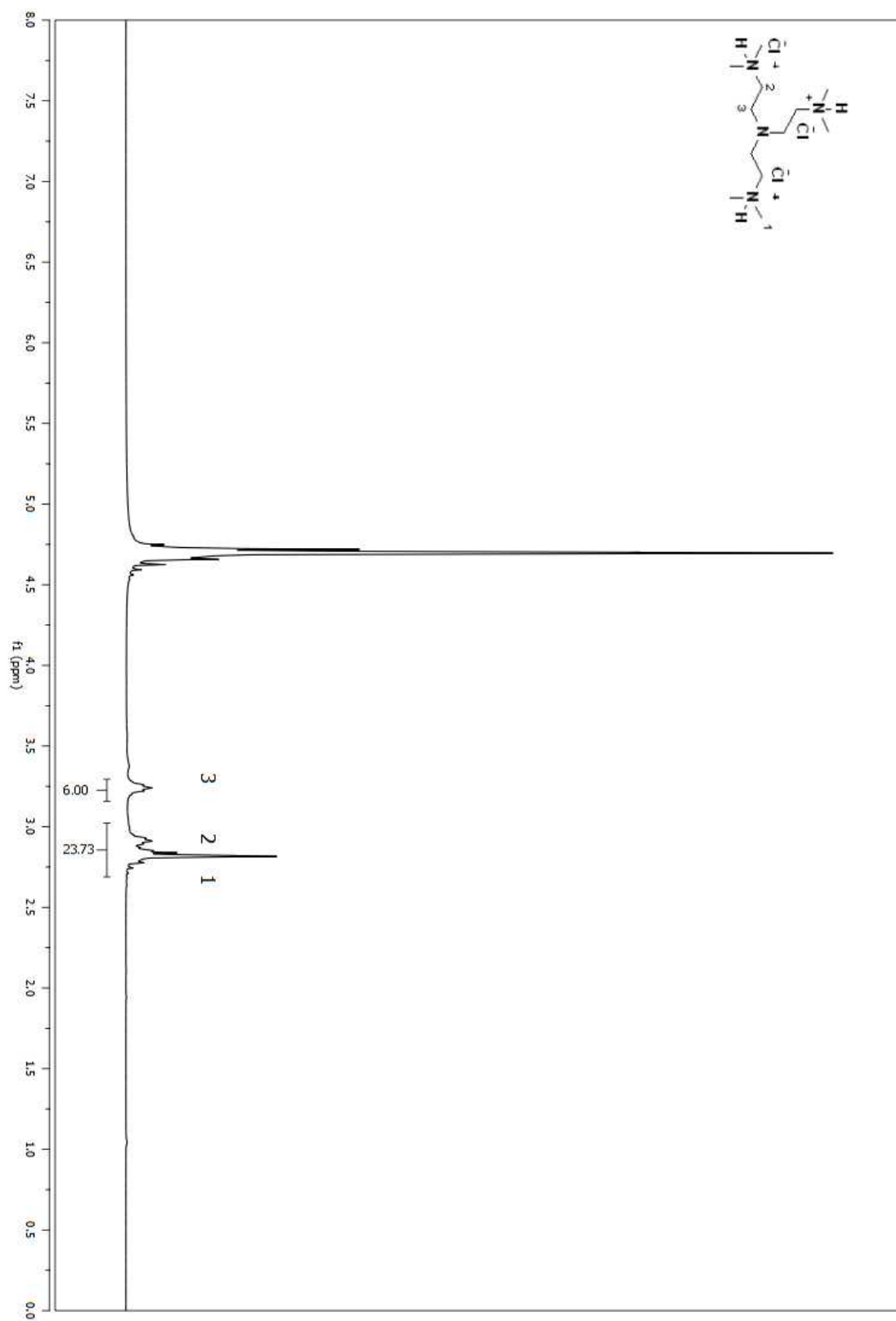


Figure A 114. ¹H NMR spectrum of compound **44** in D₂O.

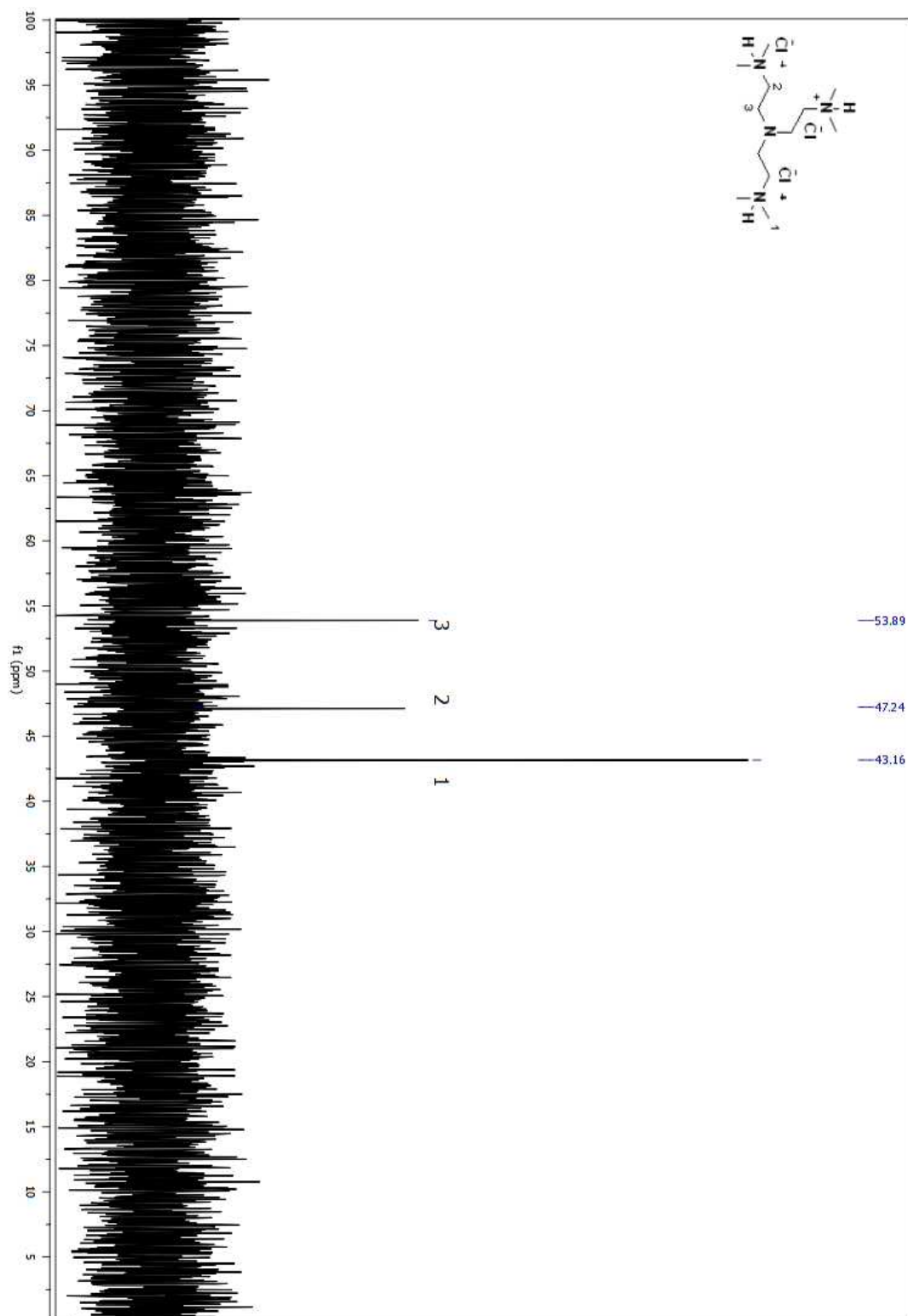


Figure A 115. ^{13}C NMR spectrum of compound **44** in D_2O .

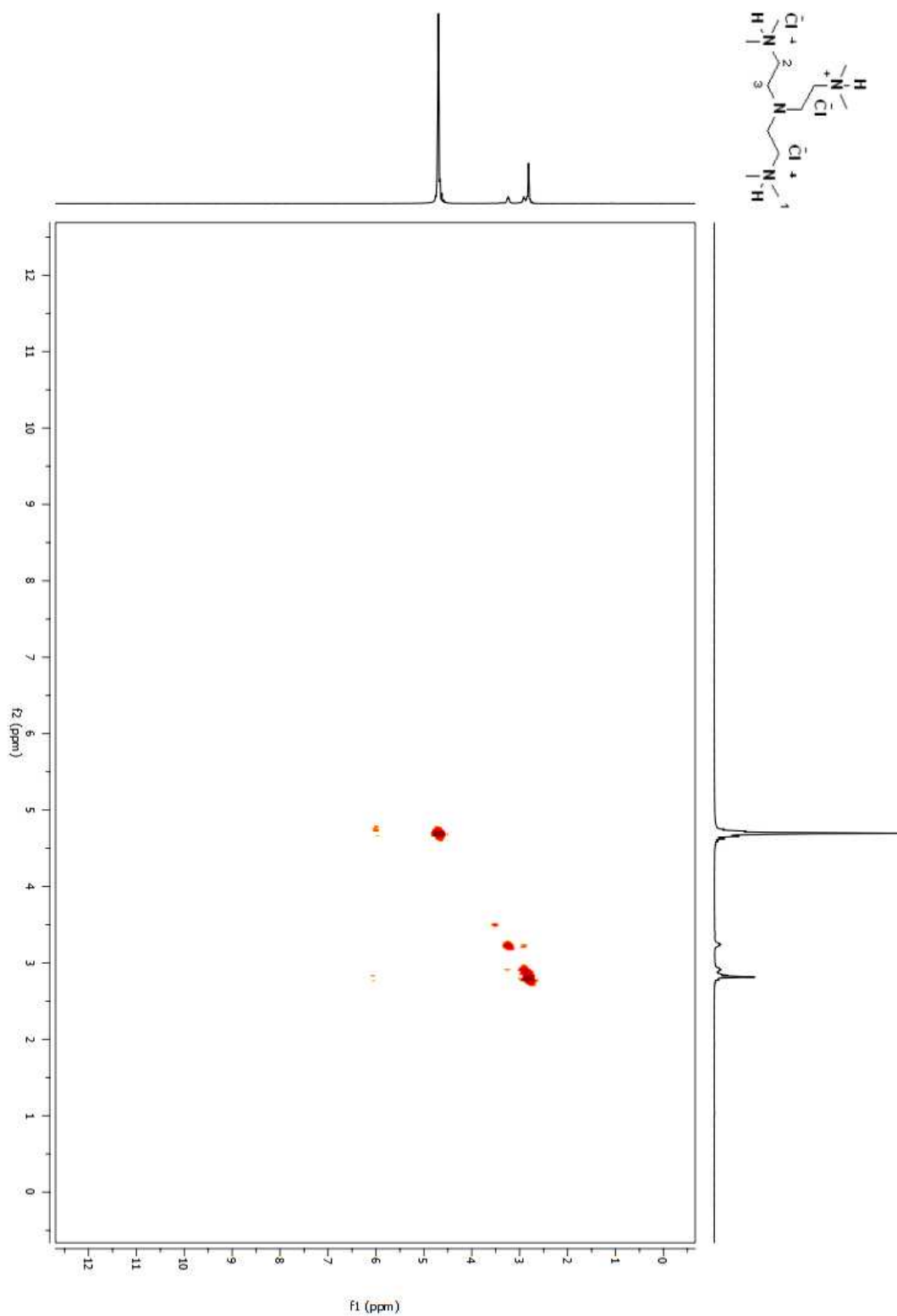


Figure A 116. COSY 2D NMR spectrum of compound **44** in D₂O.

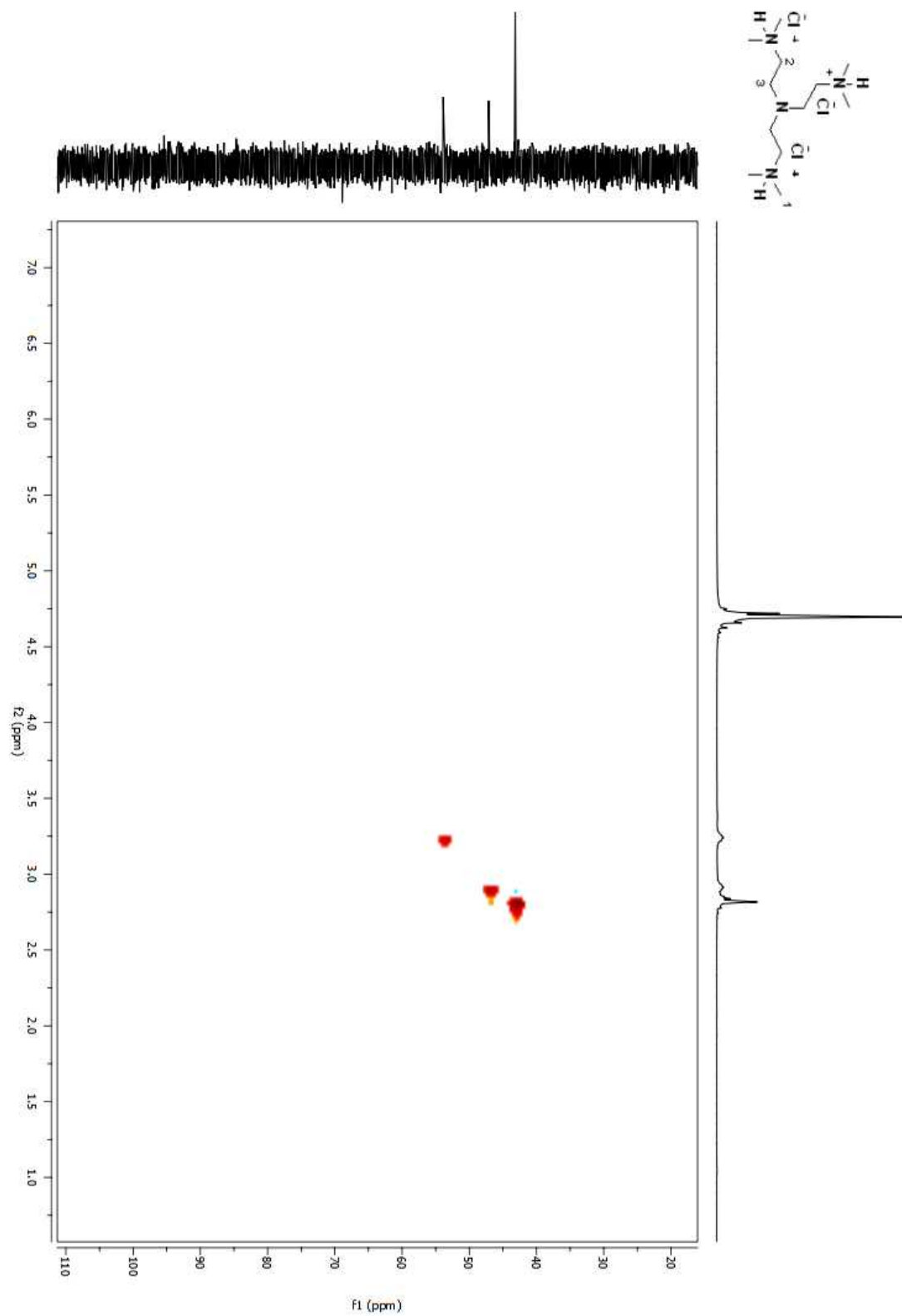


Figure A 117. HSQC 2D NMR spectrum of compound **44** in D₂O.

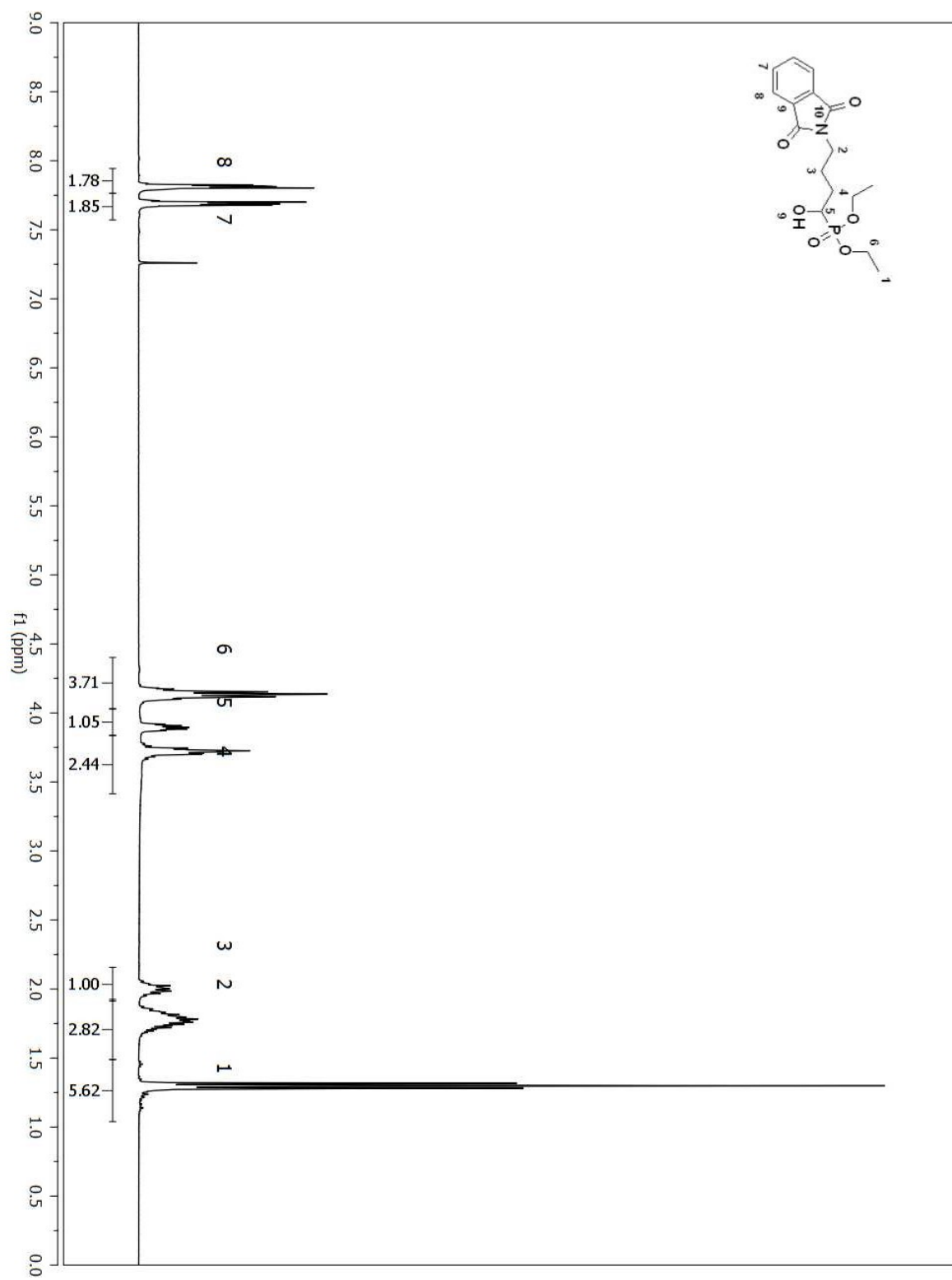


Figure A 118. ^1H NMR spectrum of compound (51) in CDCl_3 .

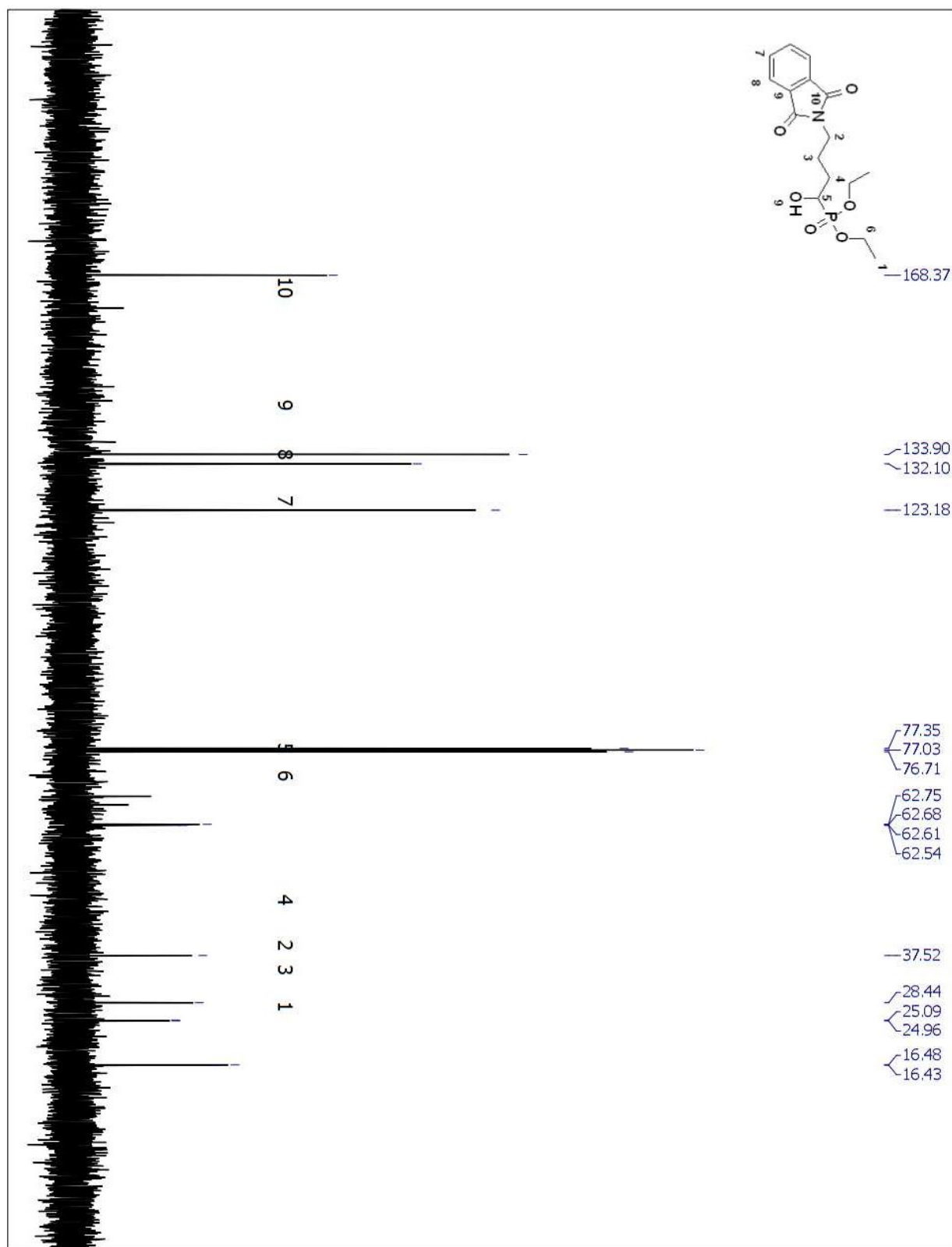


Figure A 119. ^{13}C NMR spectrum of compound (51) in CDCl_3 .

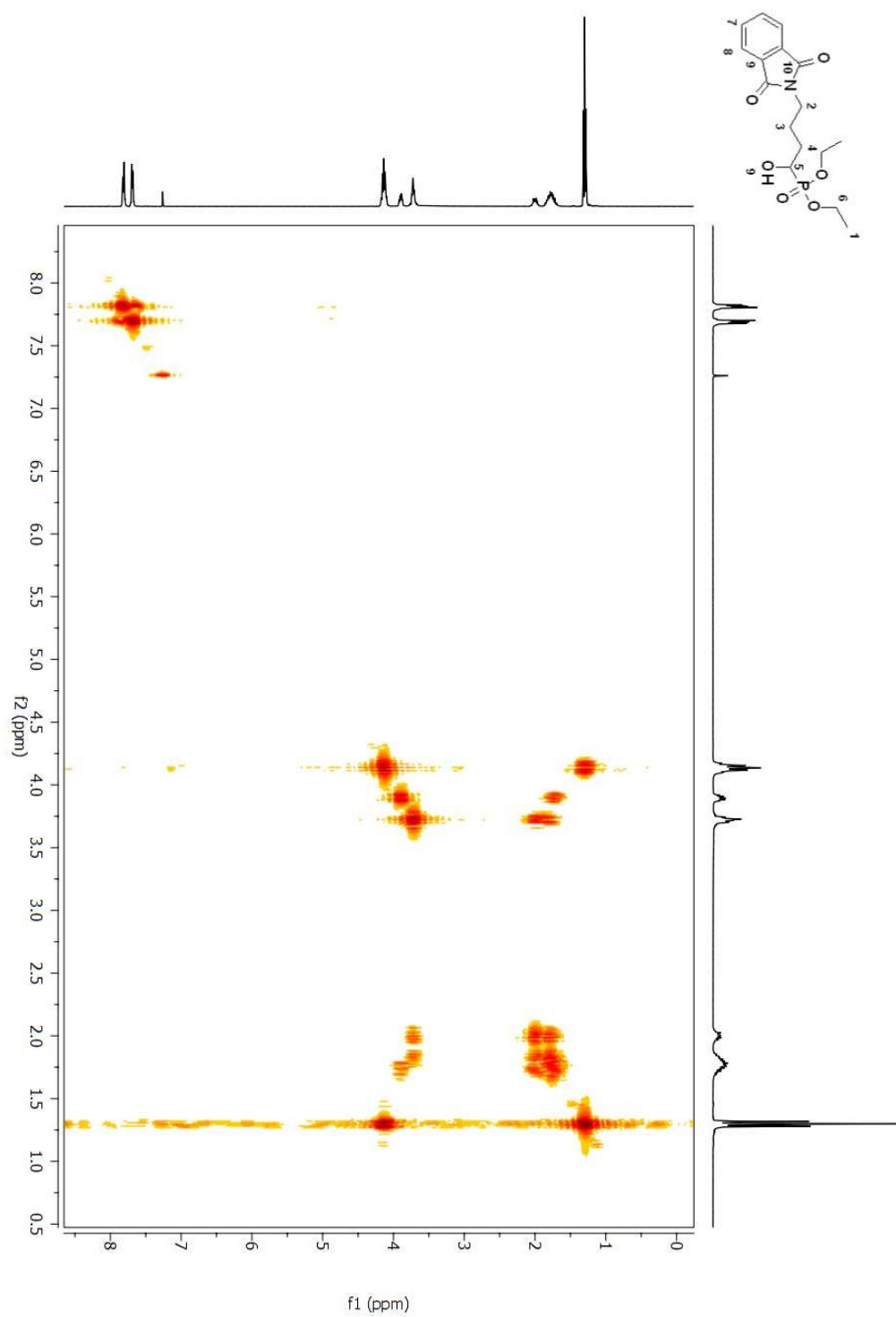


Figure A 120. COSY 2D NMR spectrum of compound (**51**) in CDCl₃.

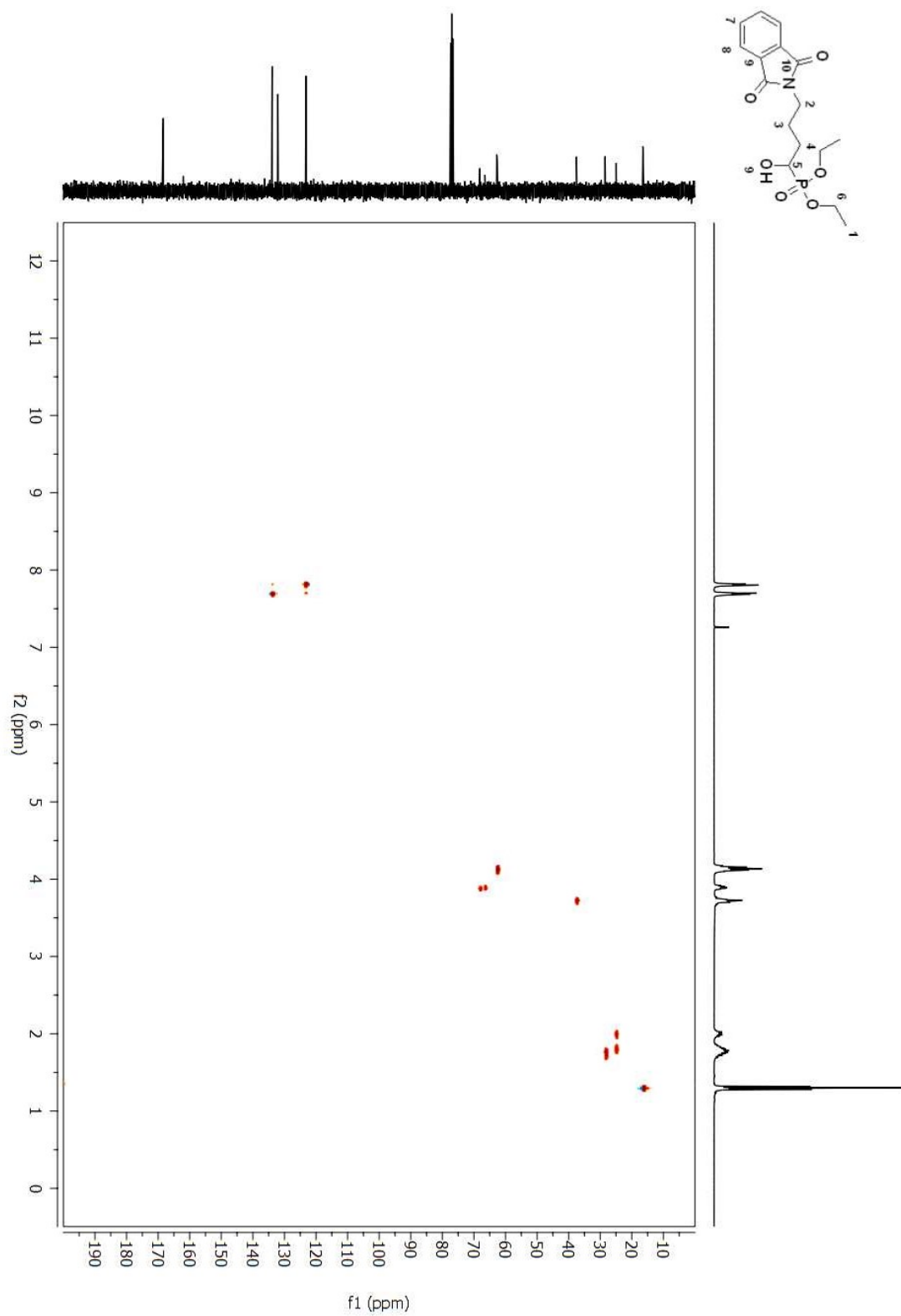


Figure A 121. HSQC 2D NMR spectrum of compound (**51**) in CDCl₃.

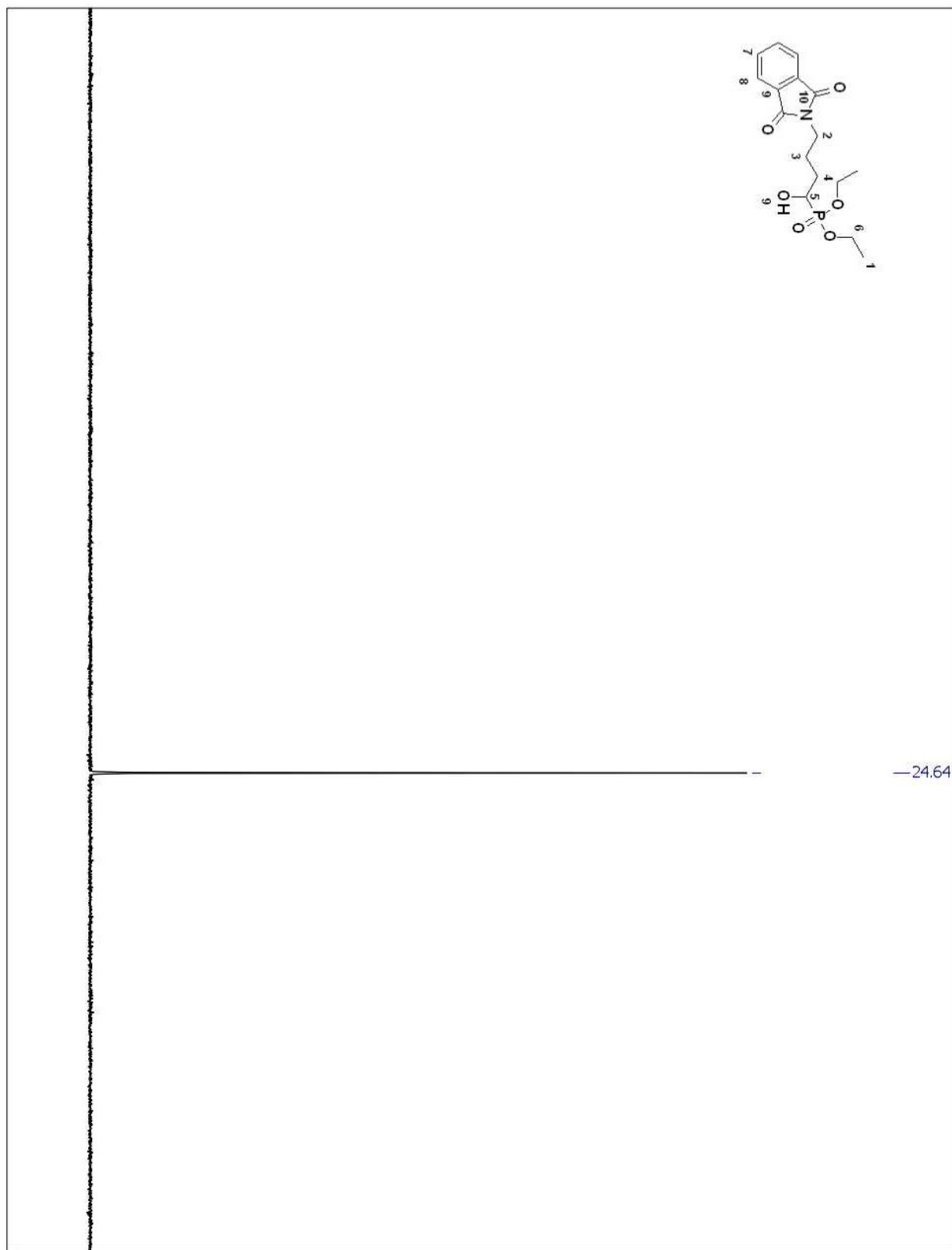
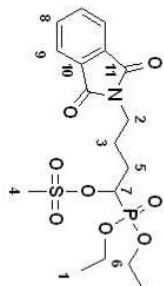


Figure A 122. ^{31}P NMR spectrum of compound (51) in CDCl_3 .



490

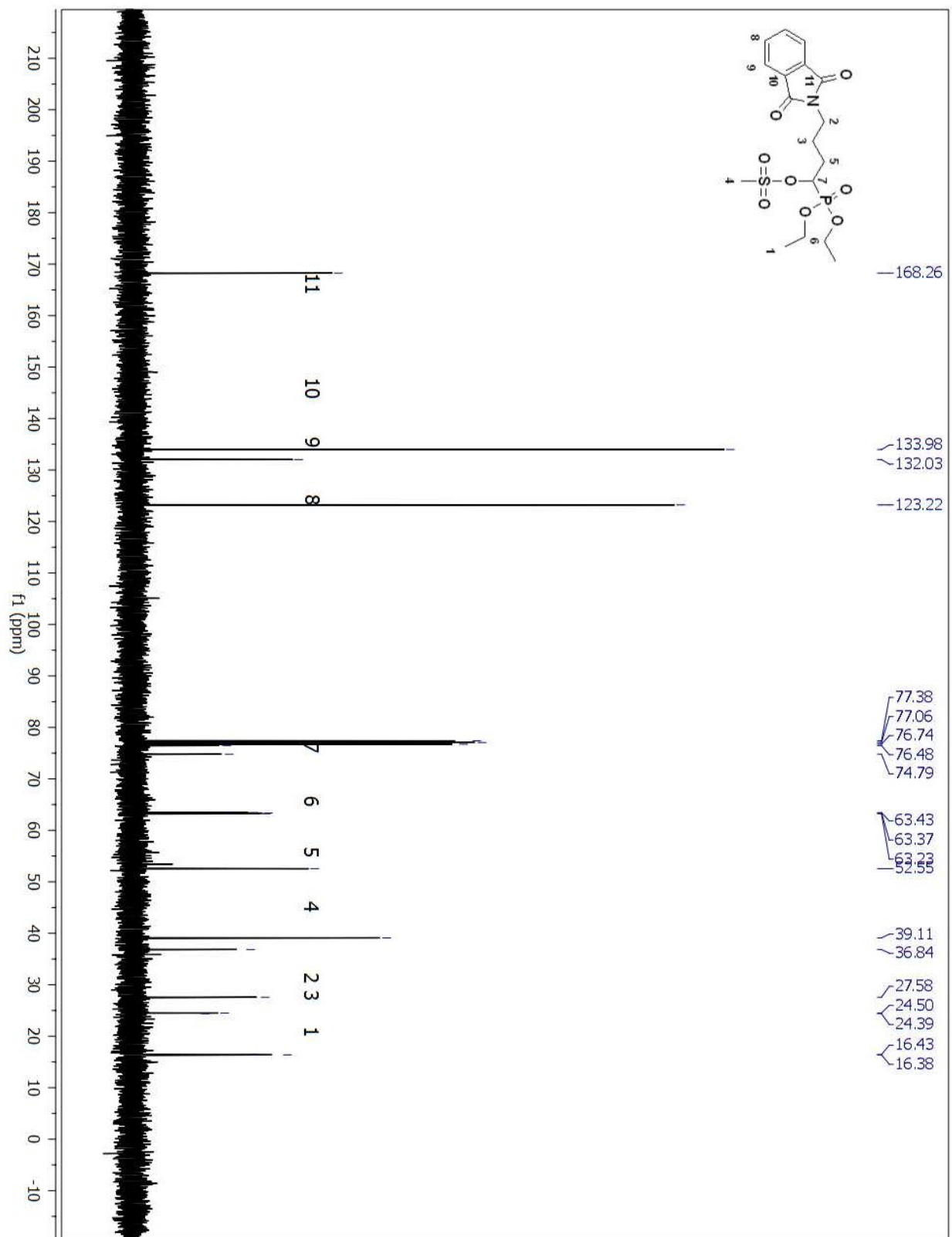


Figure A 124. ^{13}C NMR spectrum of compound (52) in CDCl_3 .

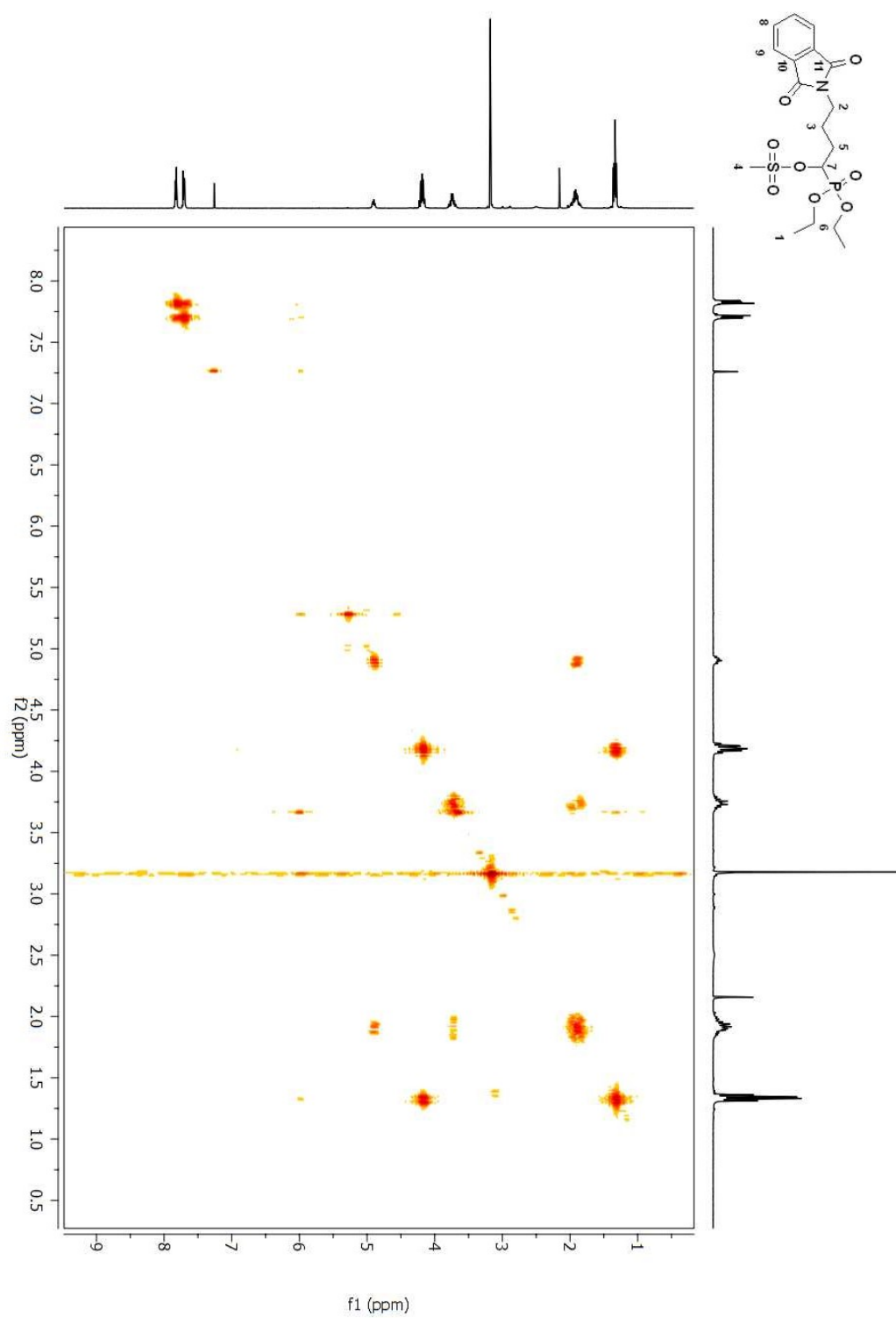


Figure A 125. COSY 2D NMR spectrum of compound (**52**) in CDCl₃.

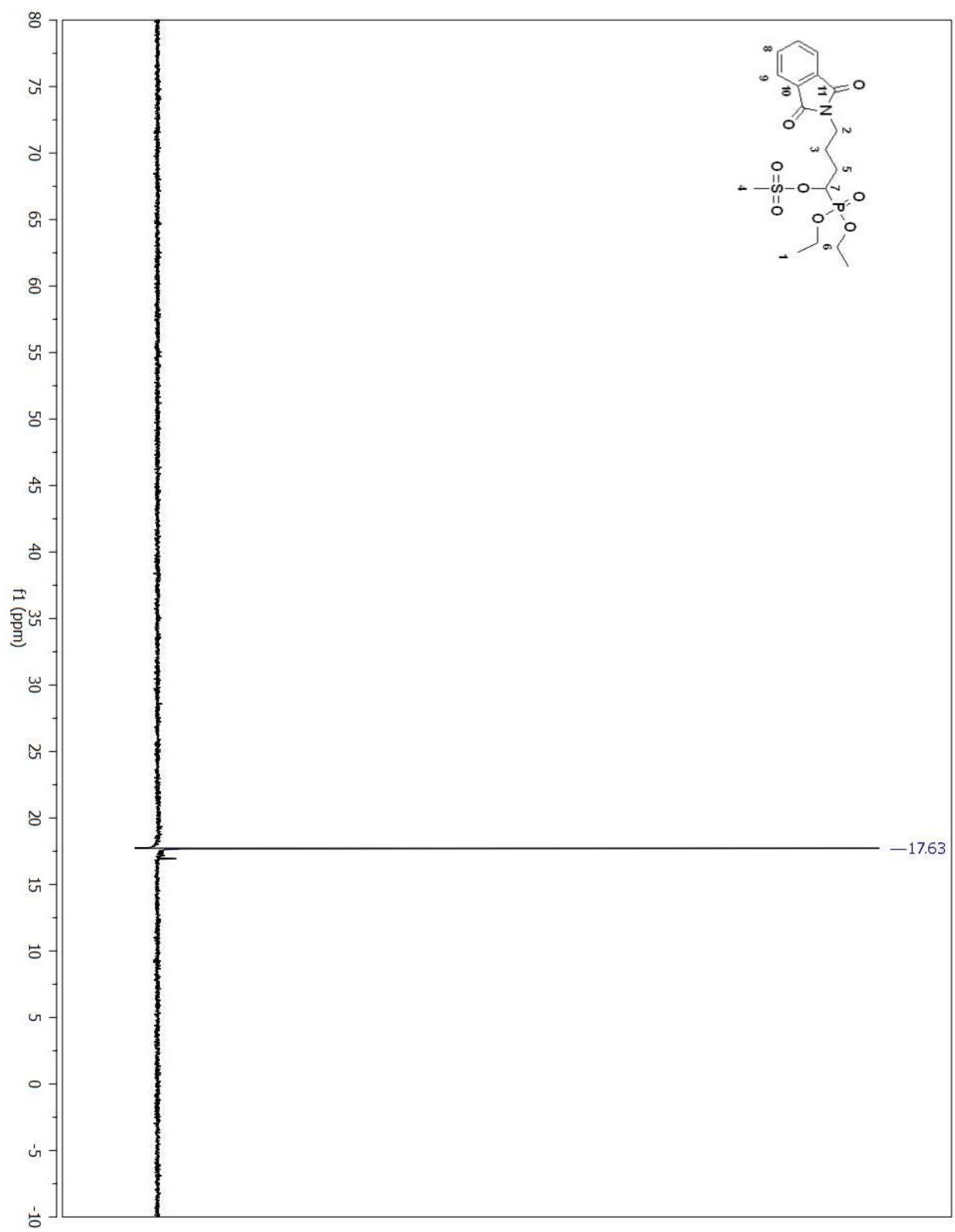


Figure A 126. ^{31}P NMR spectrum of compound (52) in CDCl_3 .

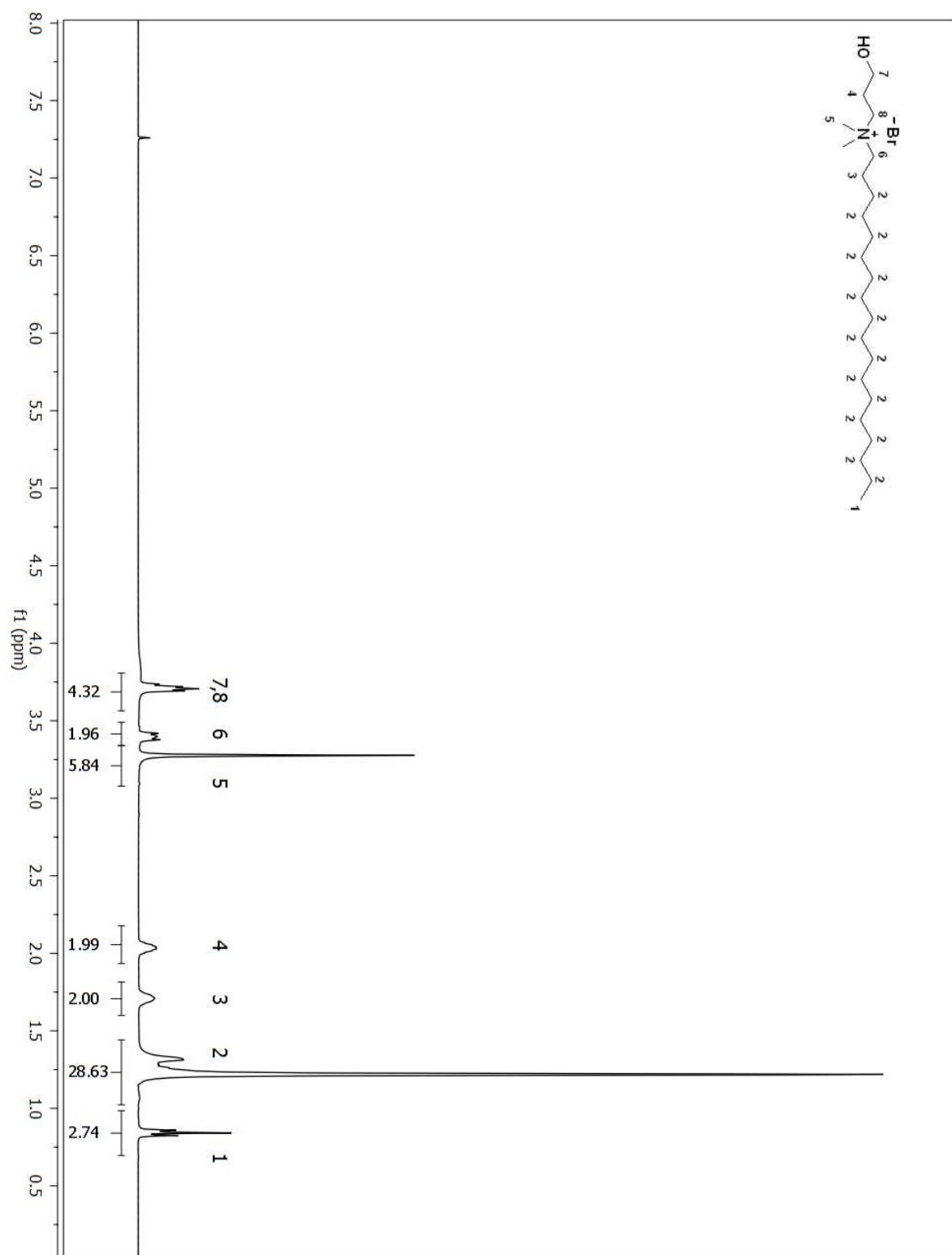


Figure A 127. ¹H NMR spectrum of compound (66) in CDCl₃.

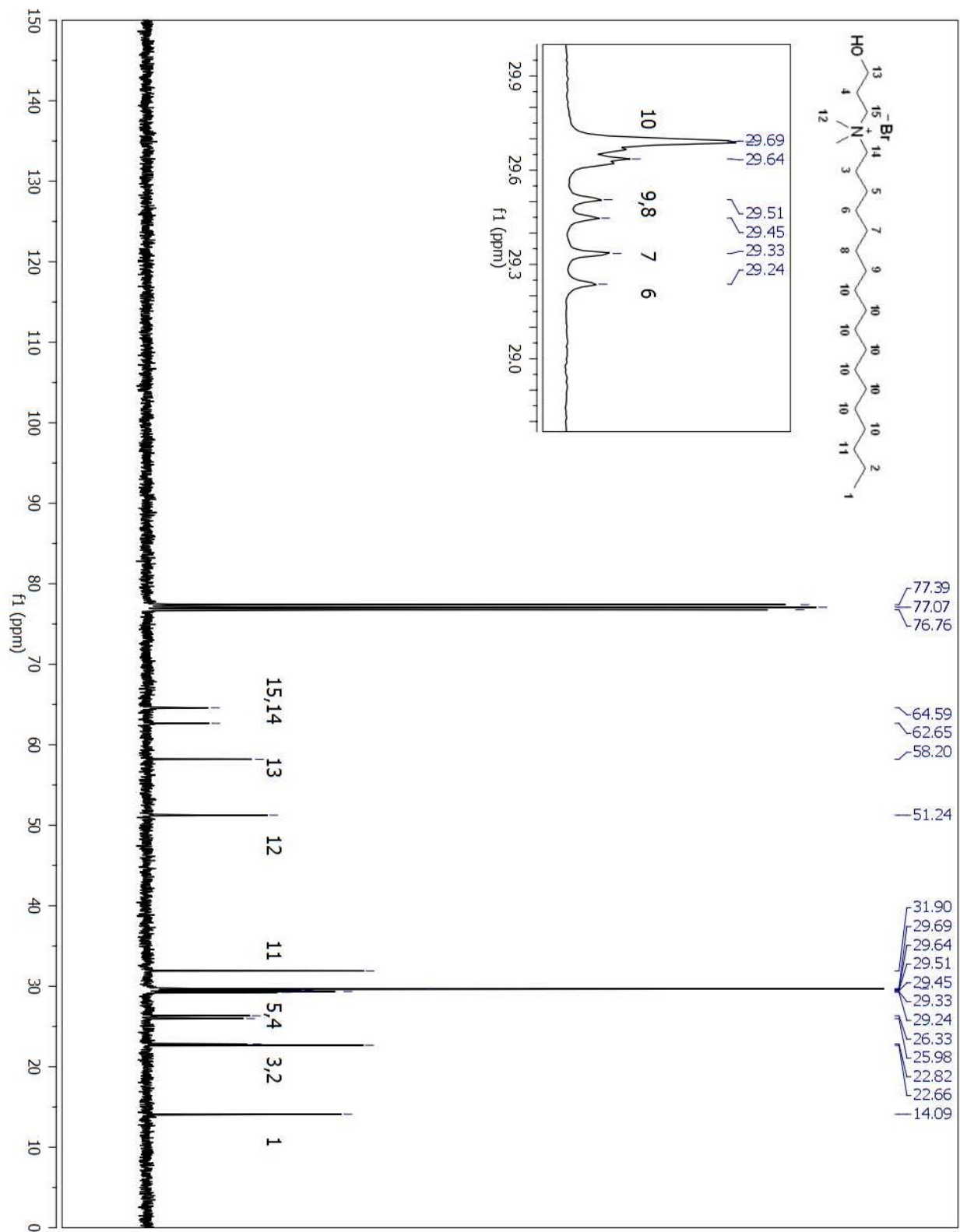


Figure A 128. ¹³C NMR spectrum of compound (66) in CDCl₃.
495

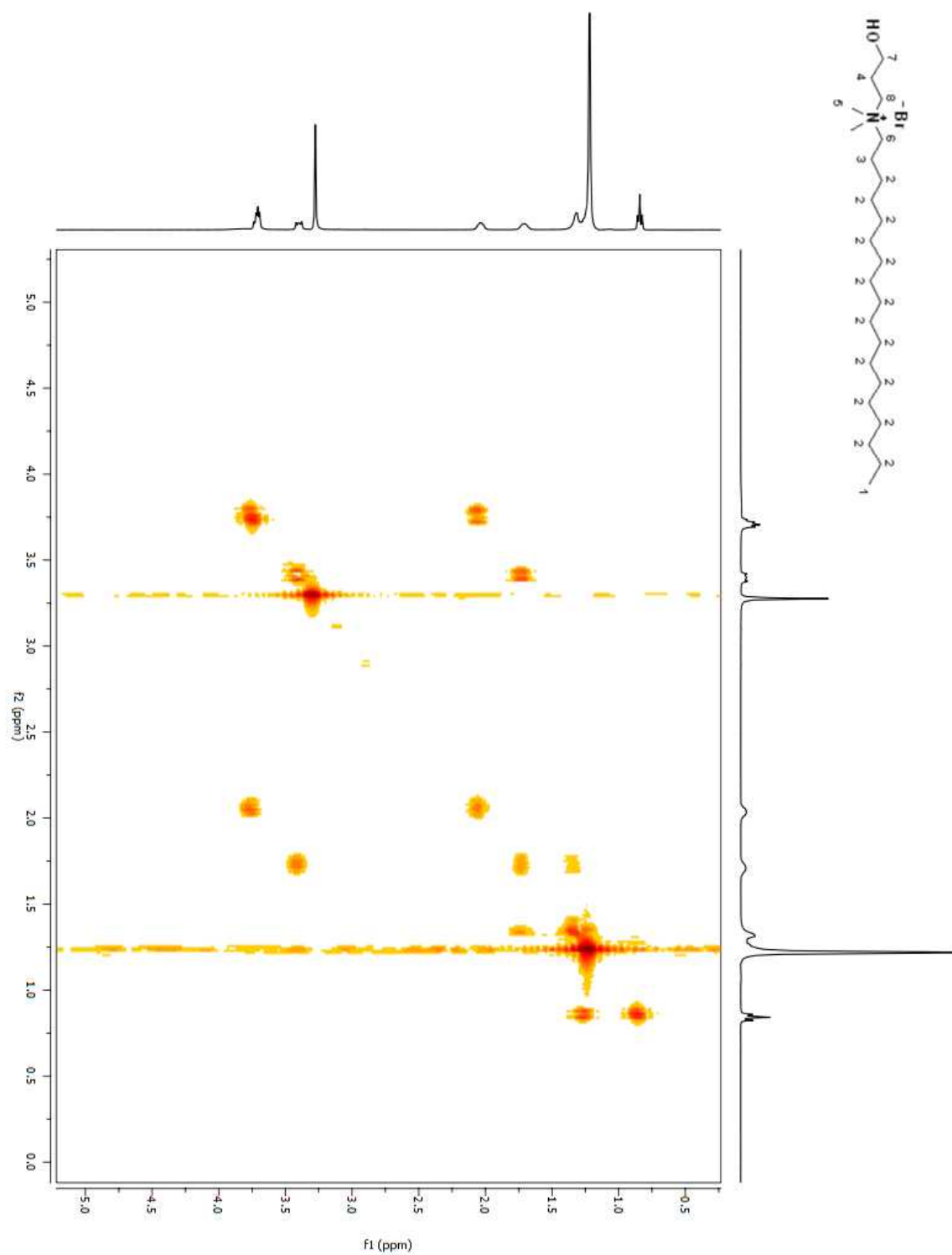
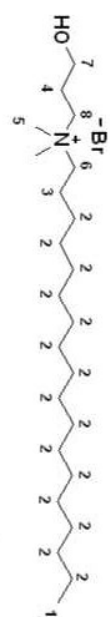


Figure A 129. COSY 2D NMR spectrum of compound (**66**) in CDCl_3 .



497

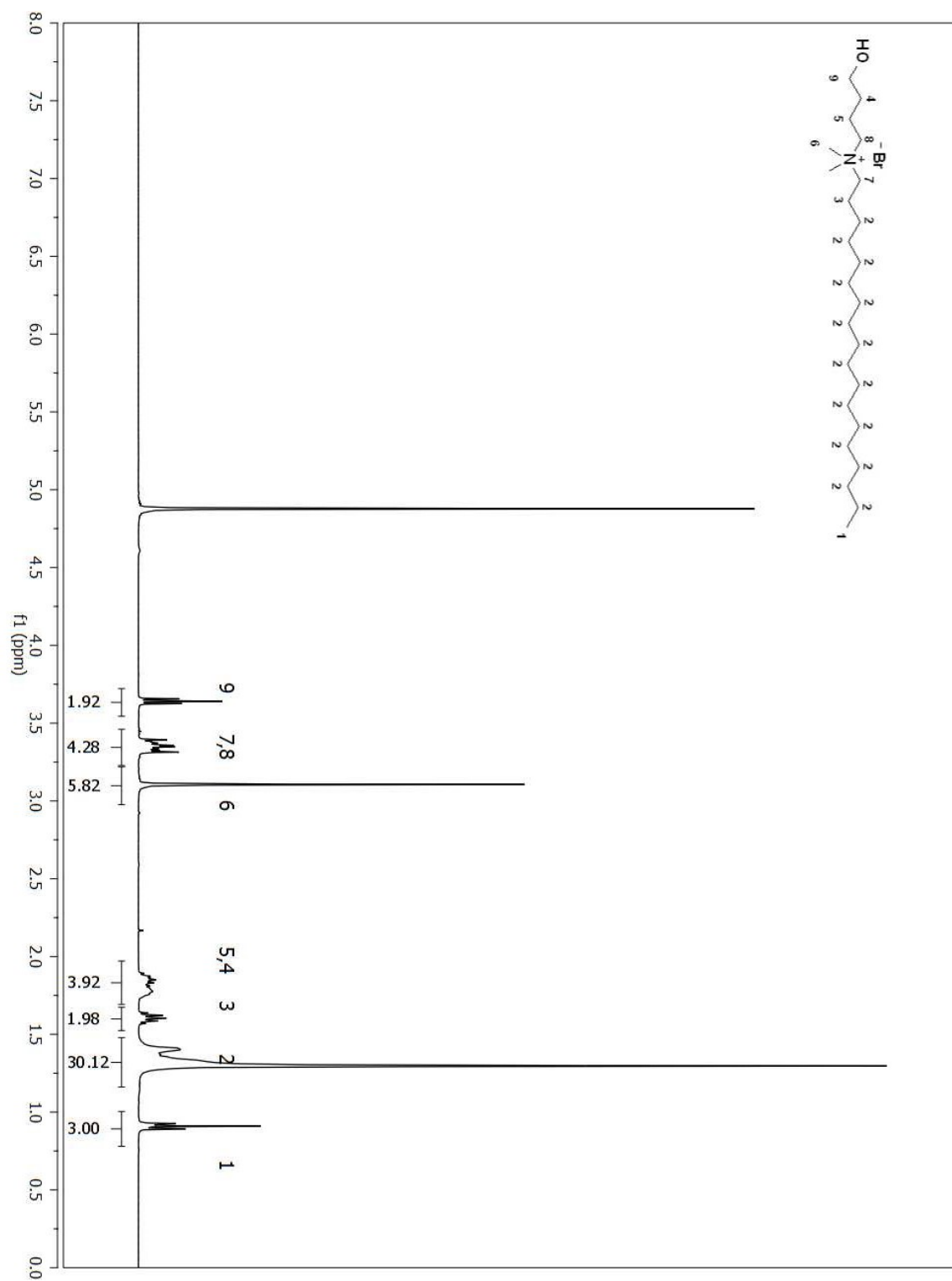


Figure A 131. ^1H NMR spectrum of compound (67) in MeOD .

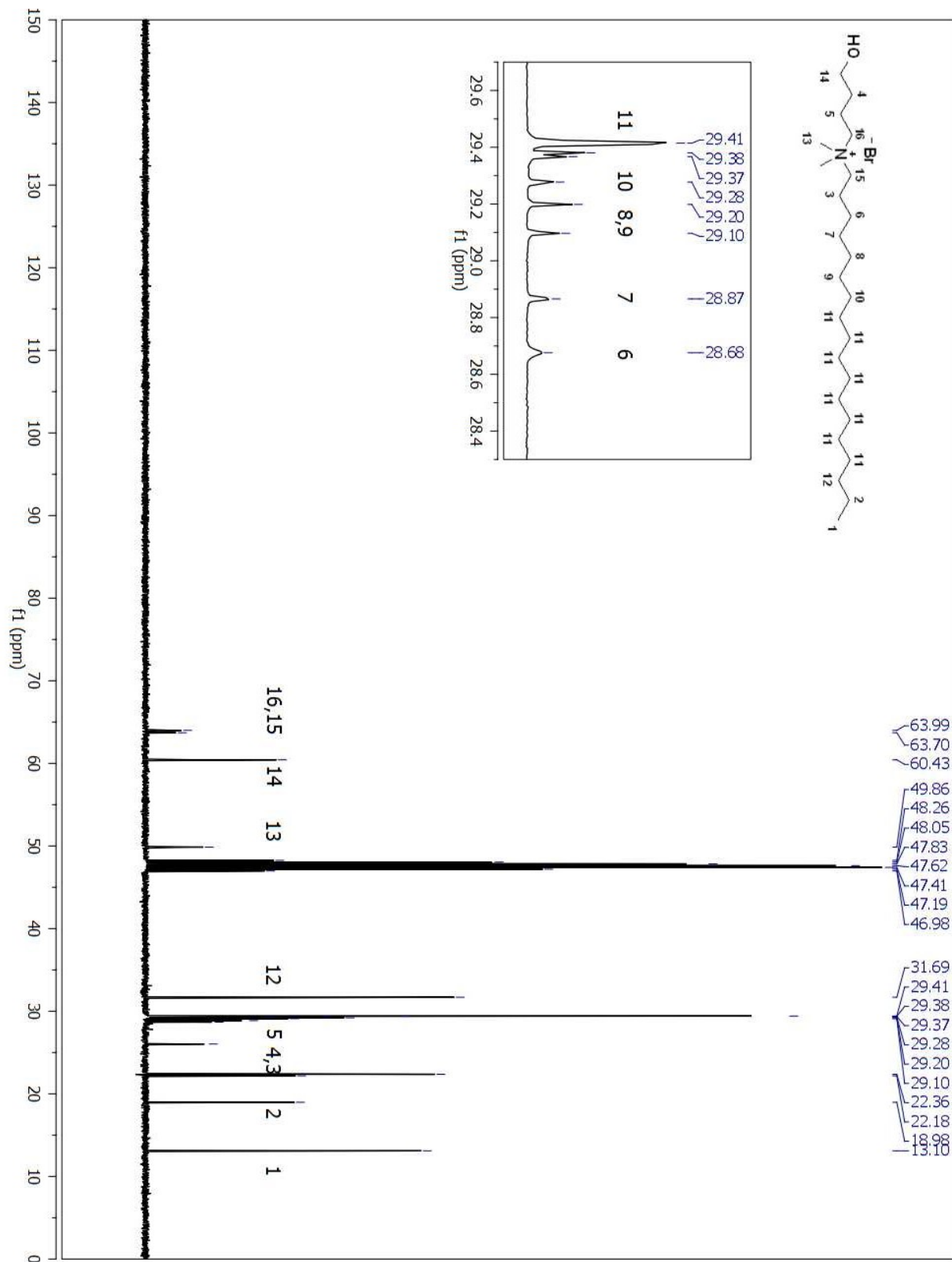


Figure A 132. ¹³C NMR spectrum of compound (67) in MeOD.

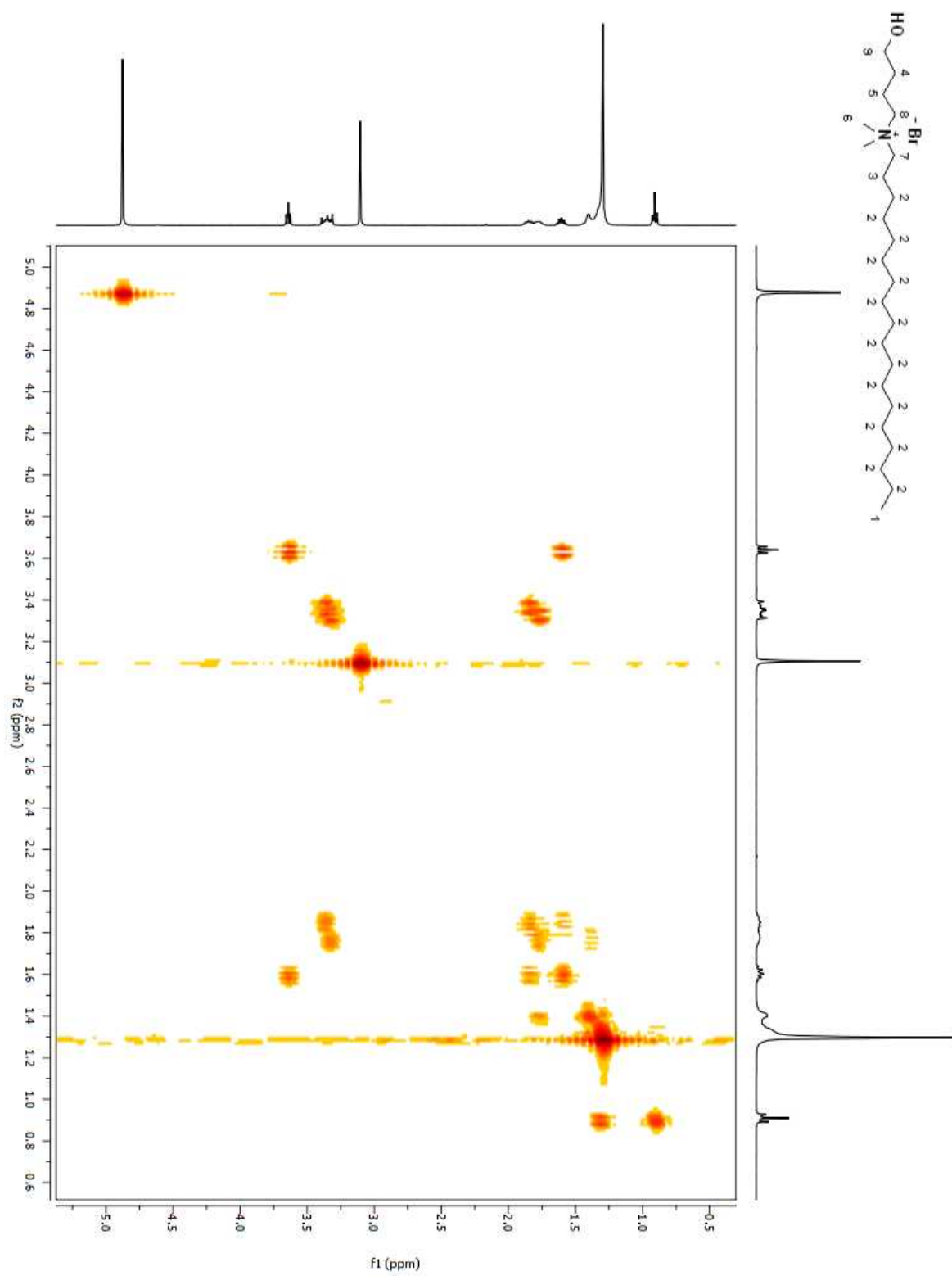


Figure A 133. COSY 2D NMR spectrum of compound (**67**) in MeOD.

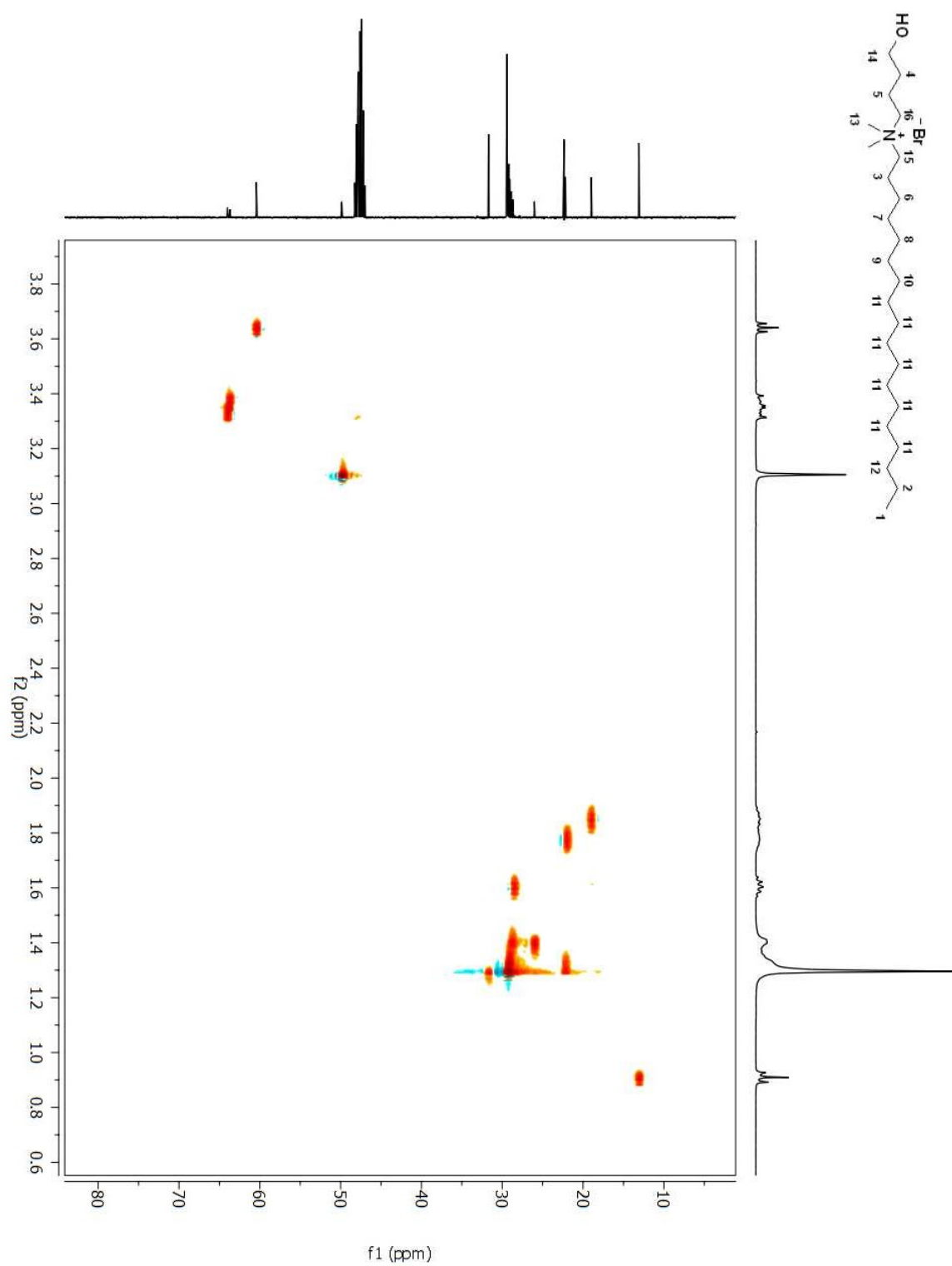


Figure A 134. HSQC 2D NMR spectrum of compound (**67**) in MeOD.

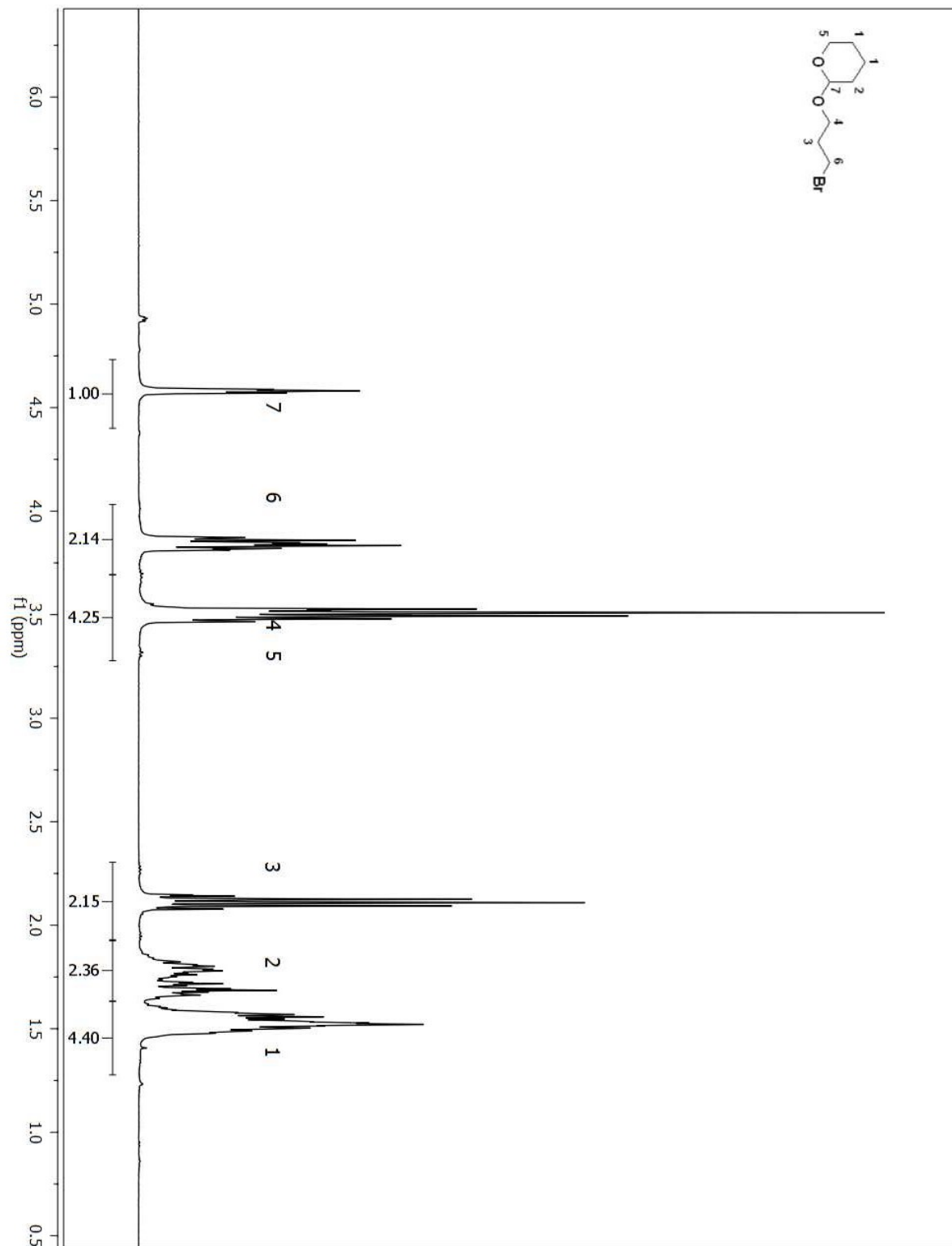


Figure A 135. ¹H NMR spectrum of compound (9) in CDCl₃.

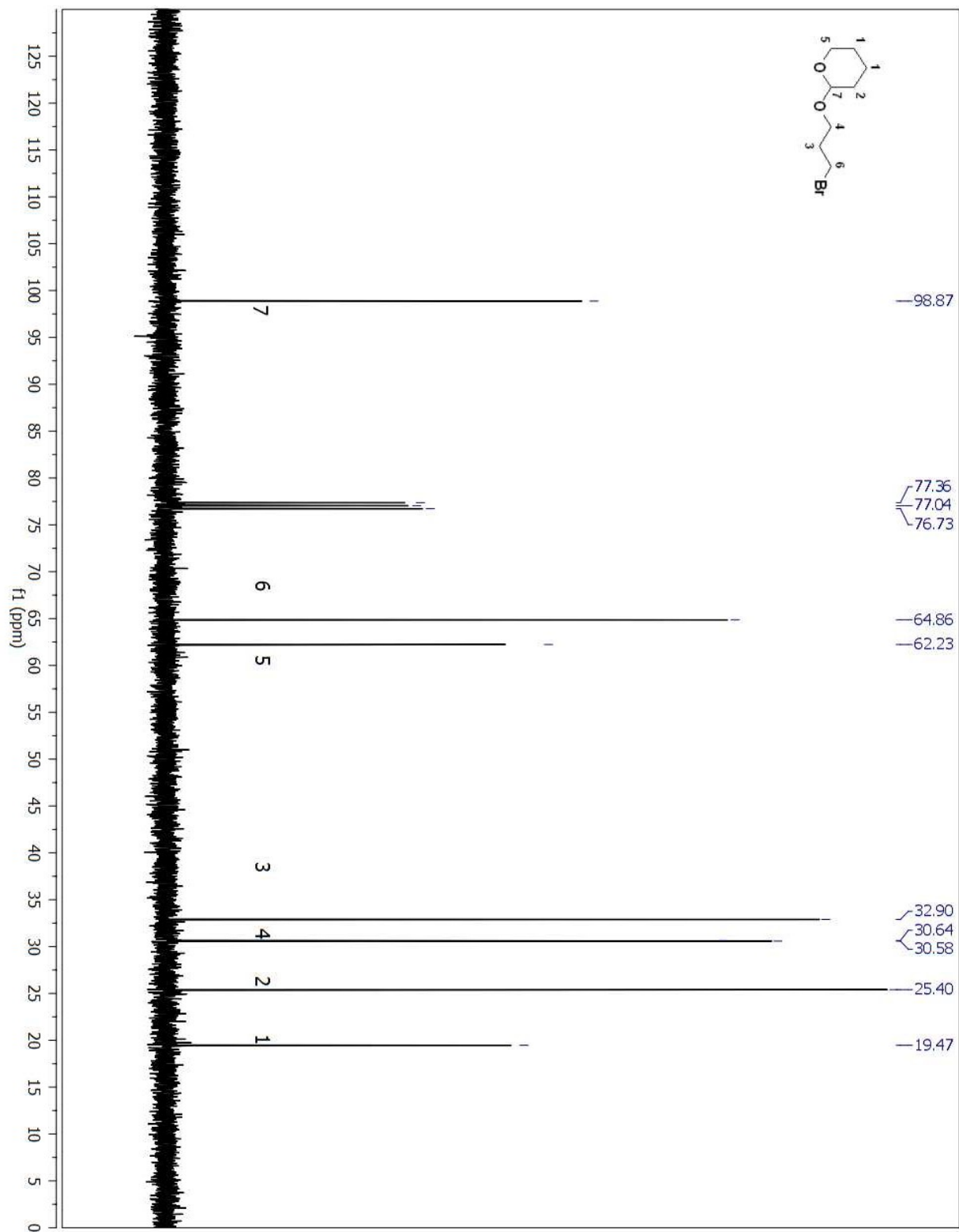


Figure A 136. ^{13}C NMR spectrum of compound (9) in CDCl_3 .

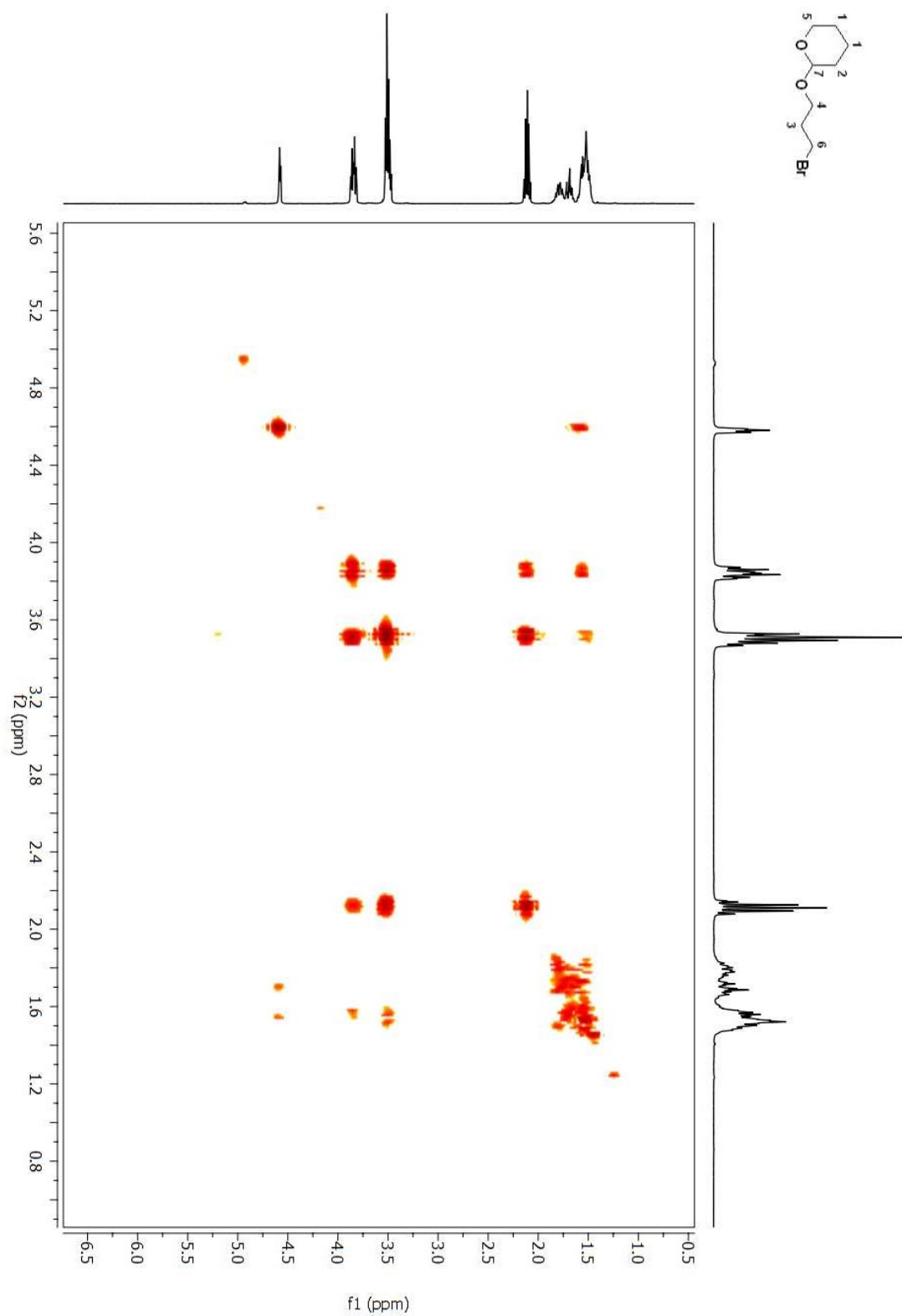


Figure A 137. COSY 2D NMR spectrum of compound (**9**) in CDCl₃.

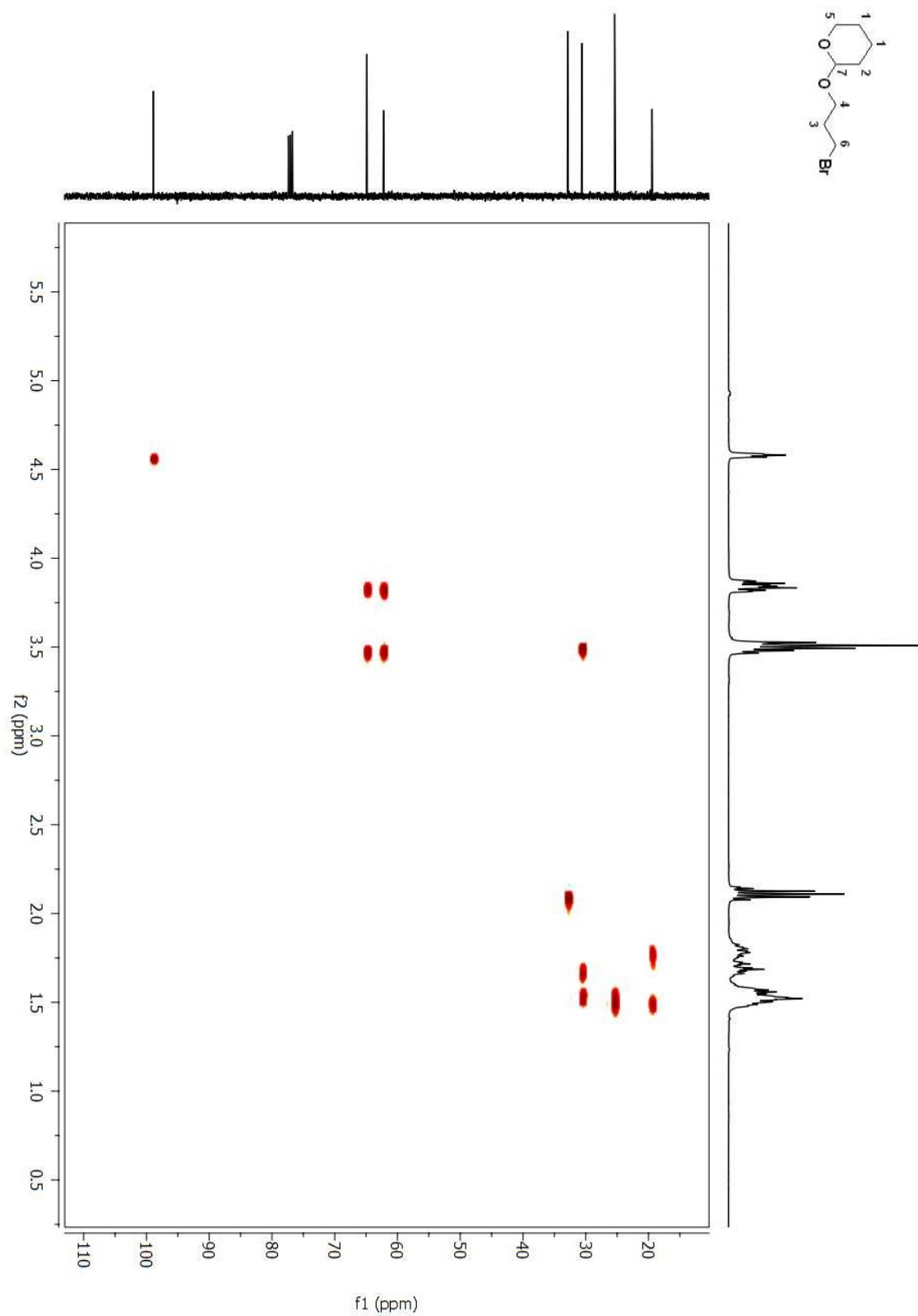


Figure A 138. HSQC 2D NMR spectrum of compound (9) in CDCl_3 .

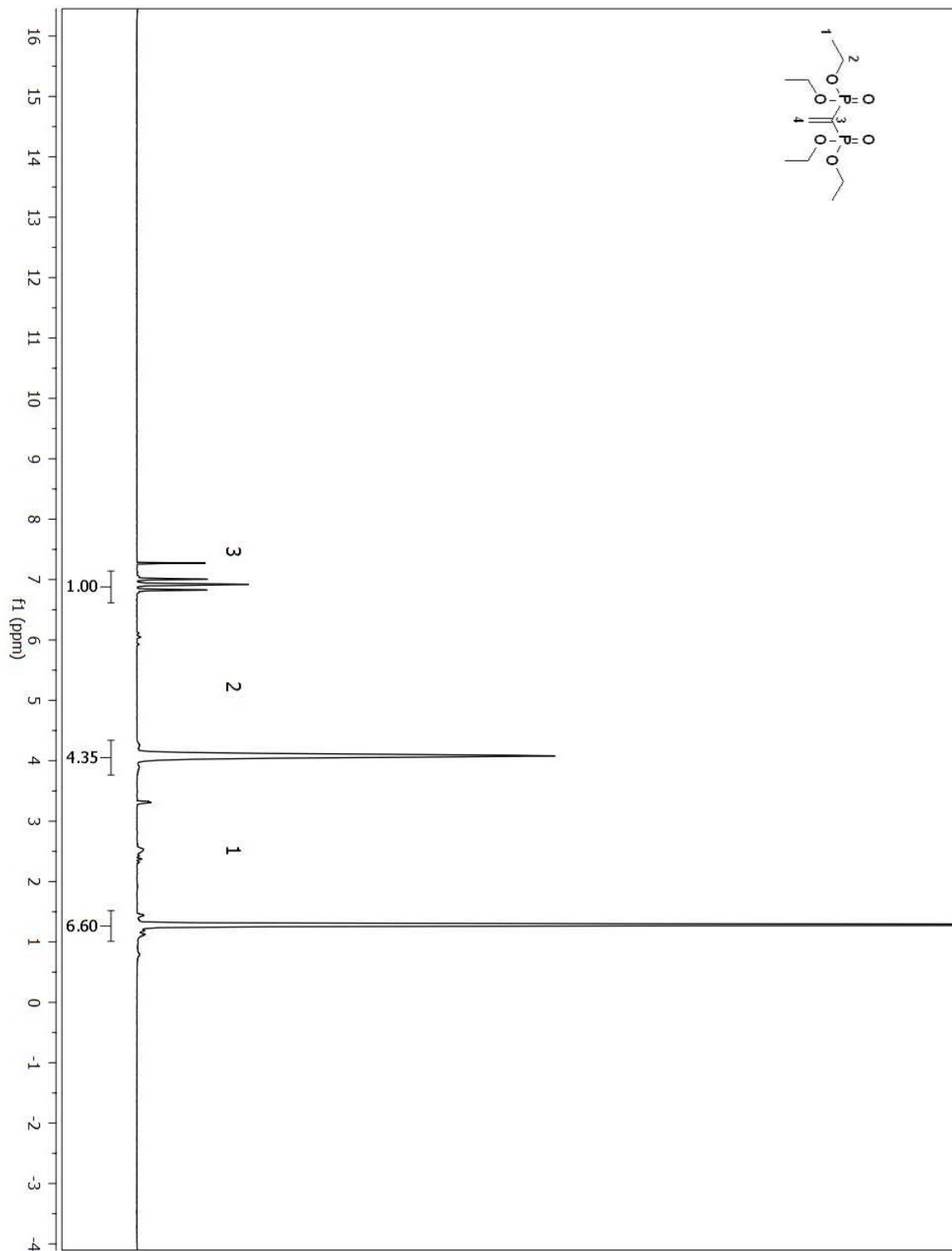


Figure A 139. ^1H NMR spectrum of compound (68) in CDCl_3 .

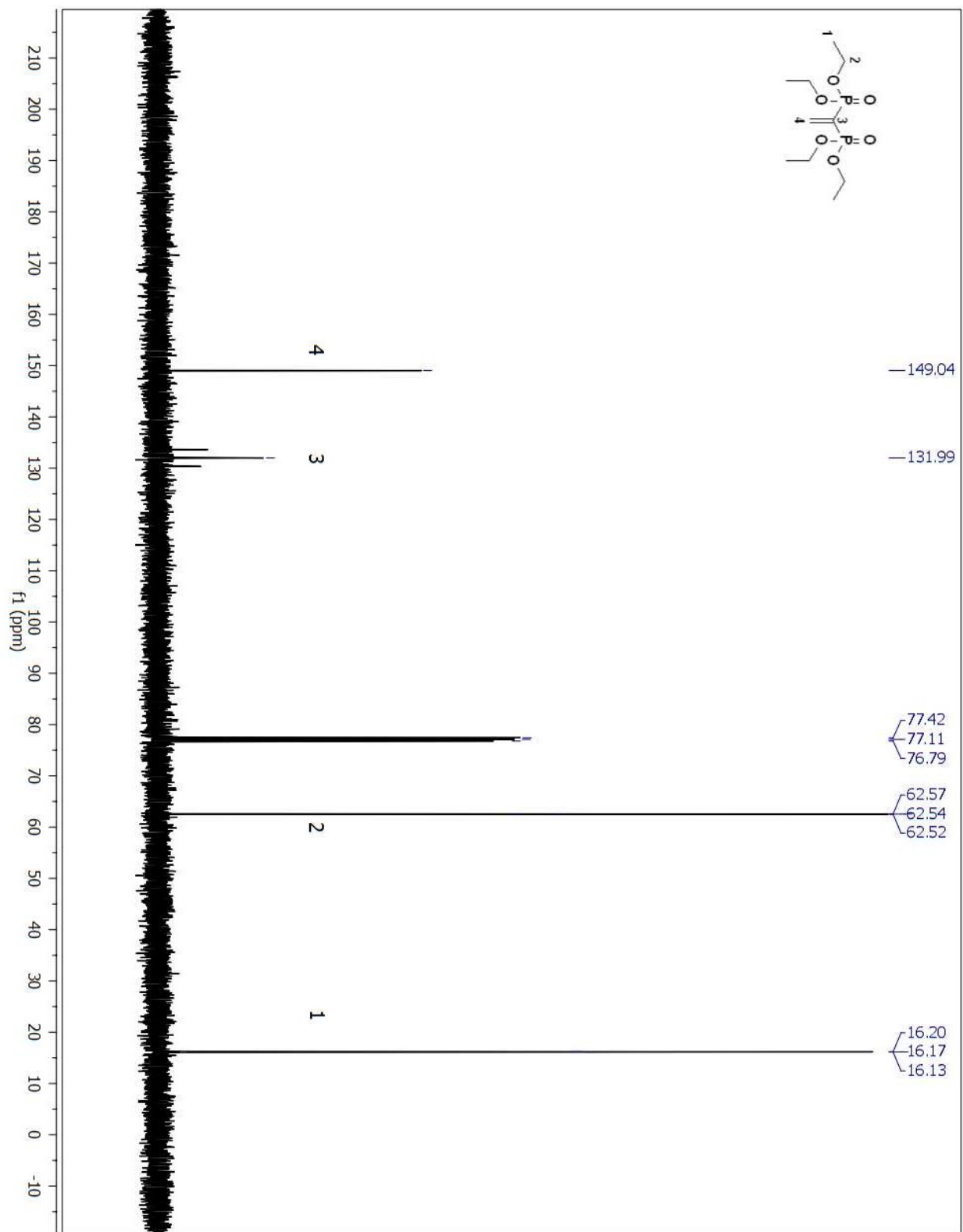


Figure A 140. ^{13}C NMR spectrum of compound (68) in CDCl_3 .

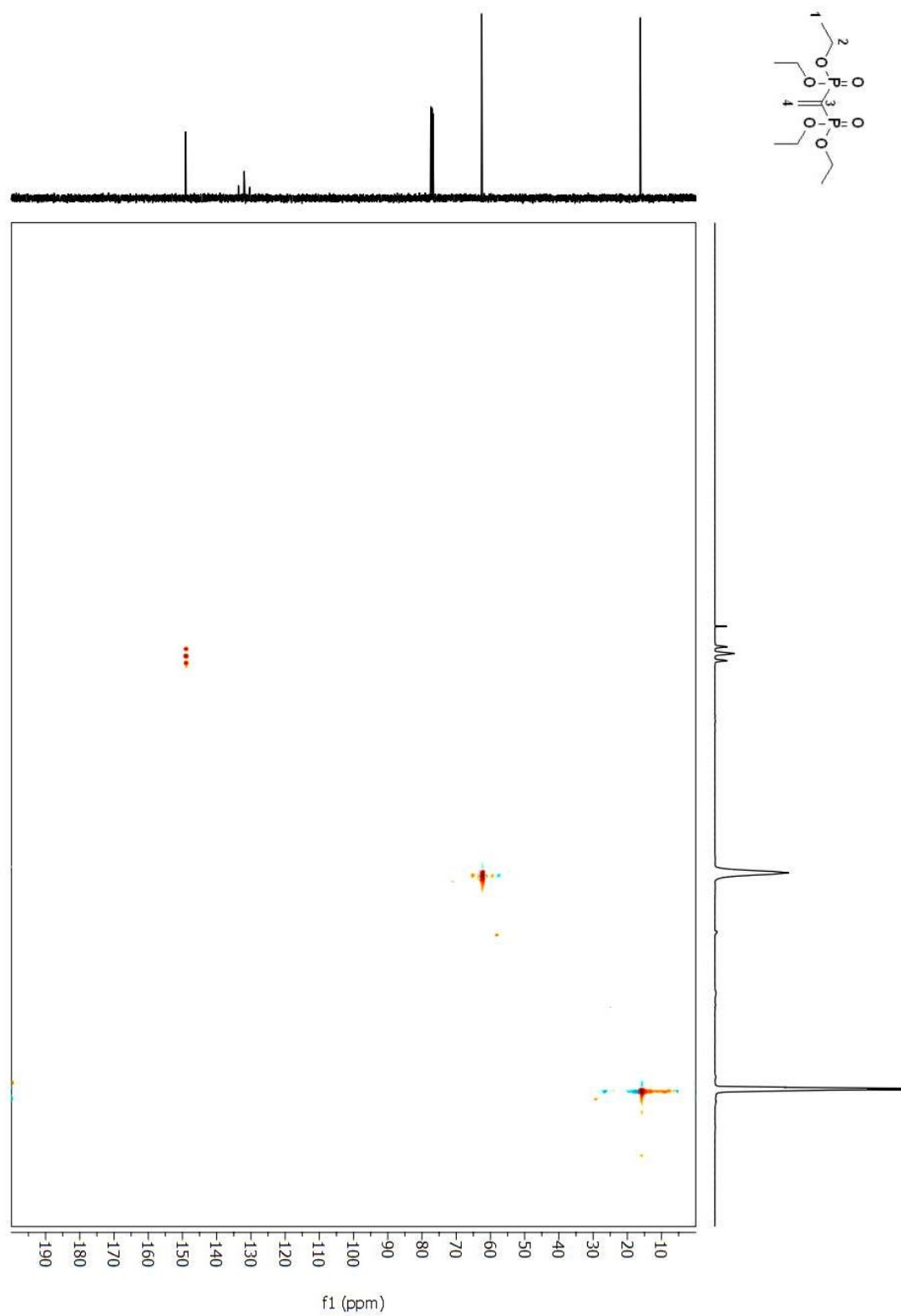


Figure A 141. HSQC 2D NMR spectrum of compound (**68**) in CDCl₃.

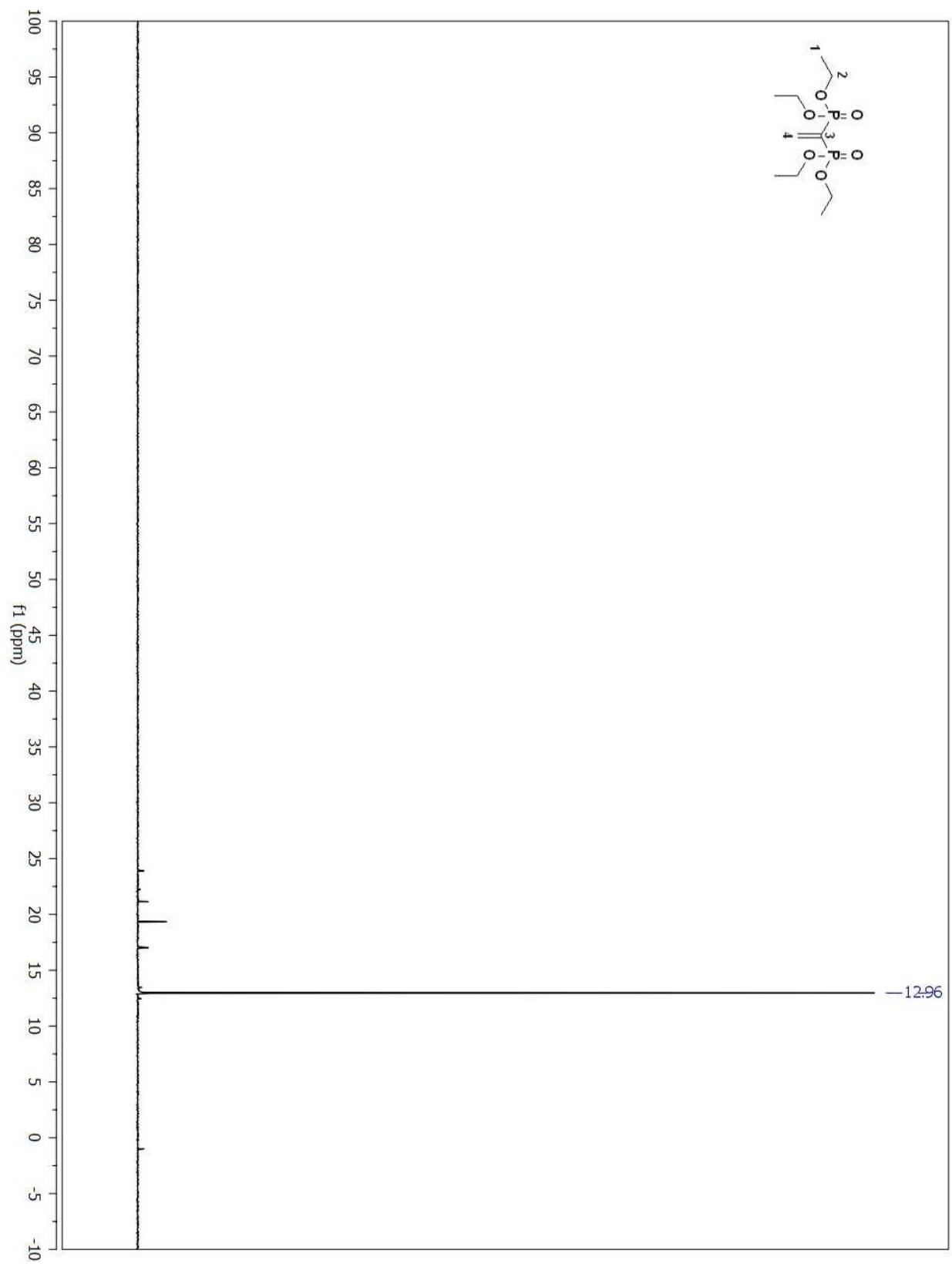


Figure A 142. ^{31}P NMR spectrum of compound (68) in CDCl_3 .

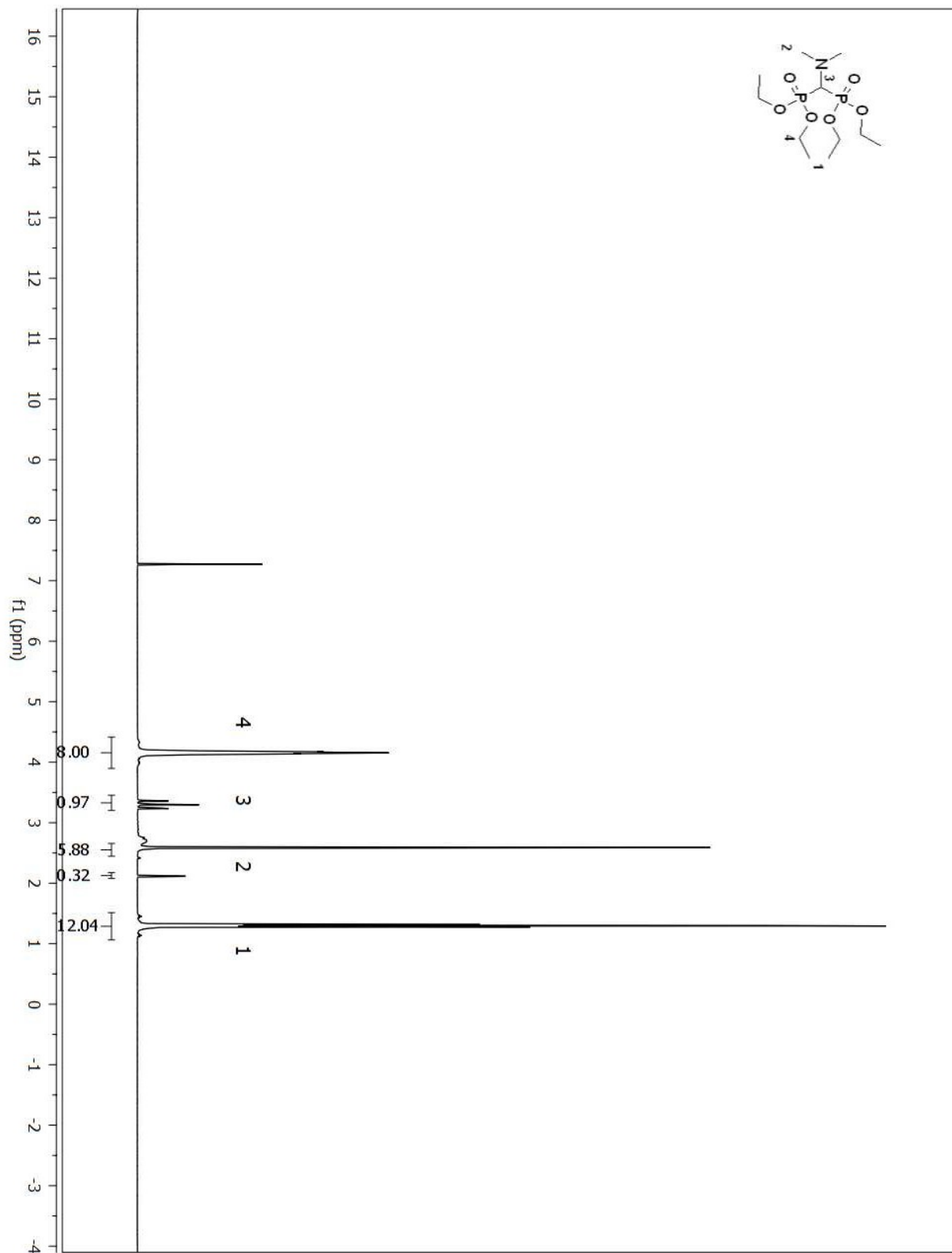


Figure A 143. ^1H NMR spectrum of compound (105) in CDCl_3 .

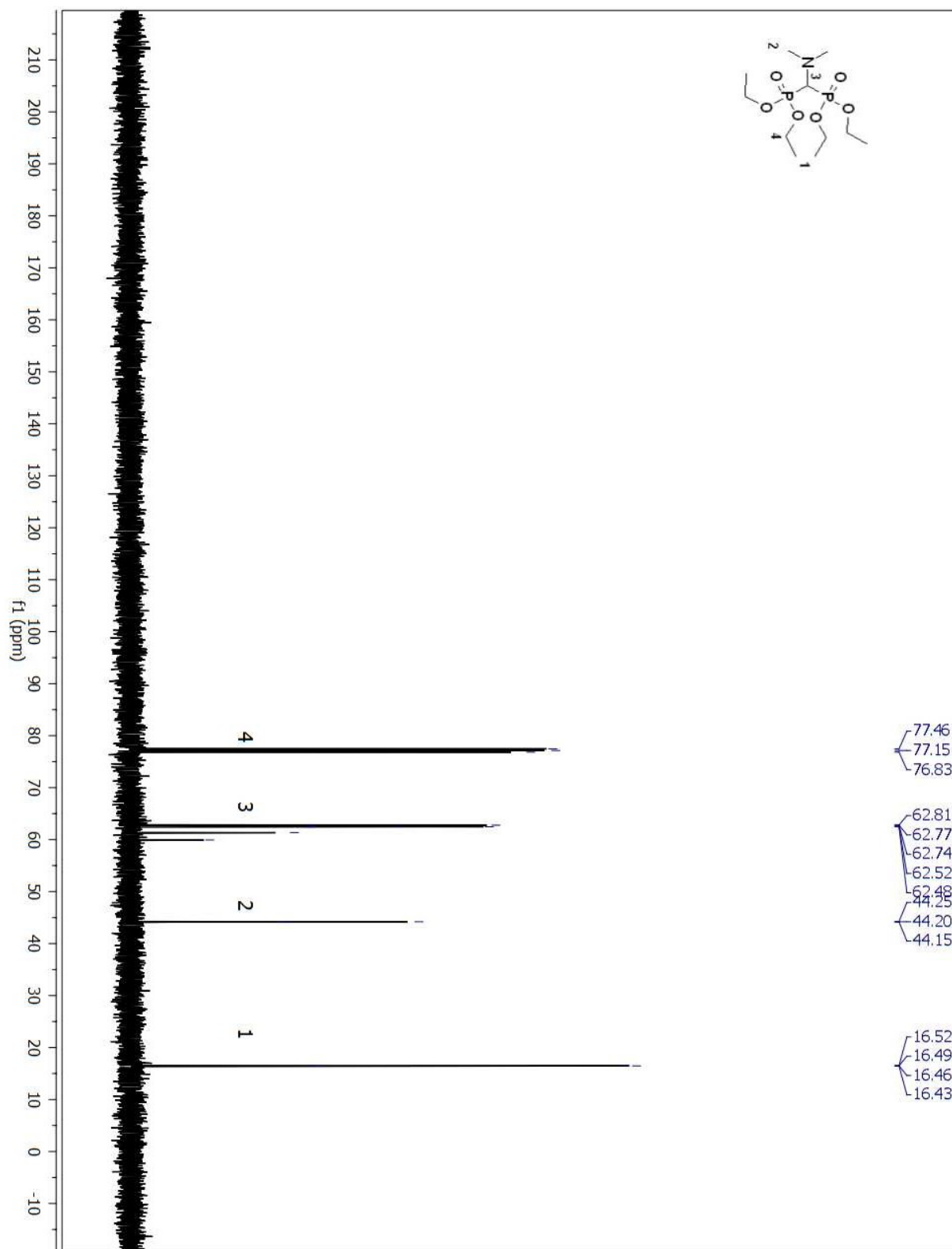


Figure A 144. ^{13}C NMR spectrum of compound (105) in CDCl_3 .

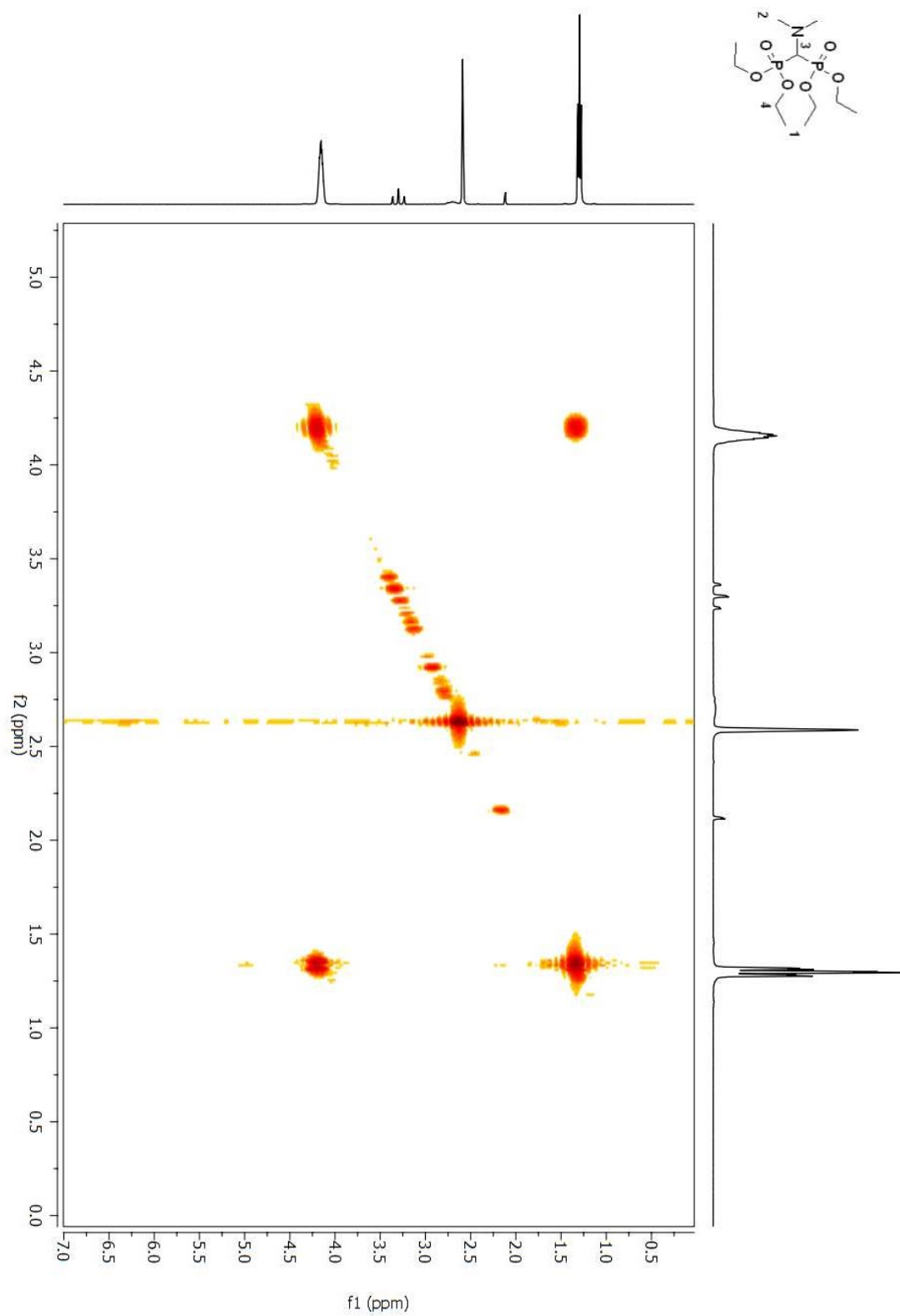


Figure A 145. COSY 2D NMR spectrum of compound (**105**) in CDCl_3 .

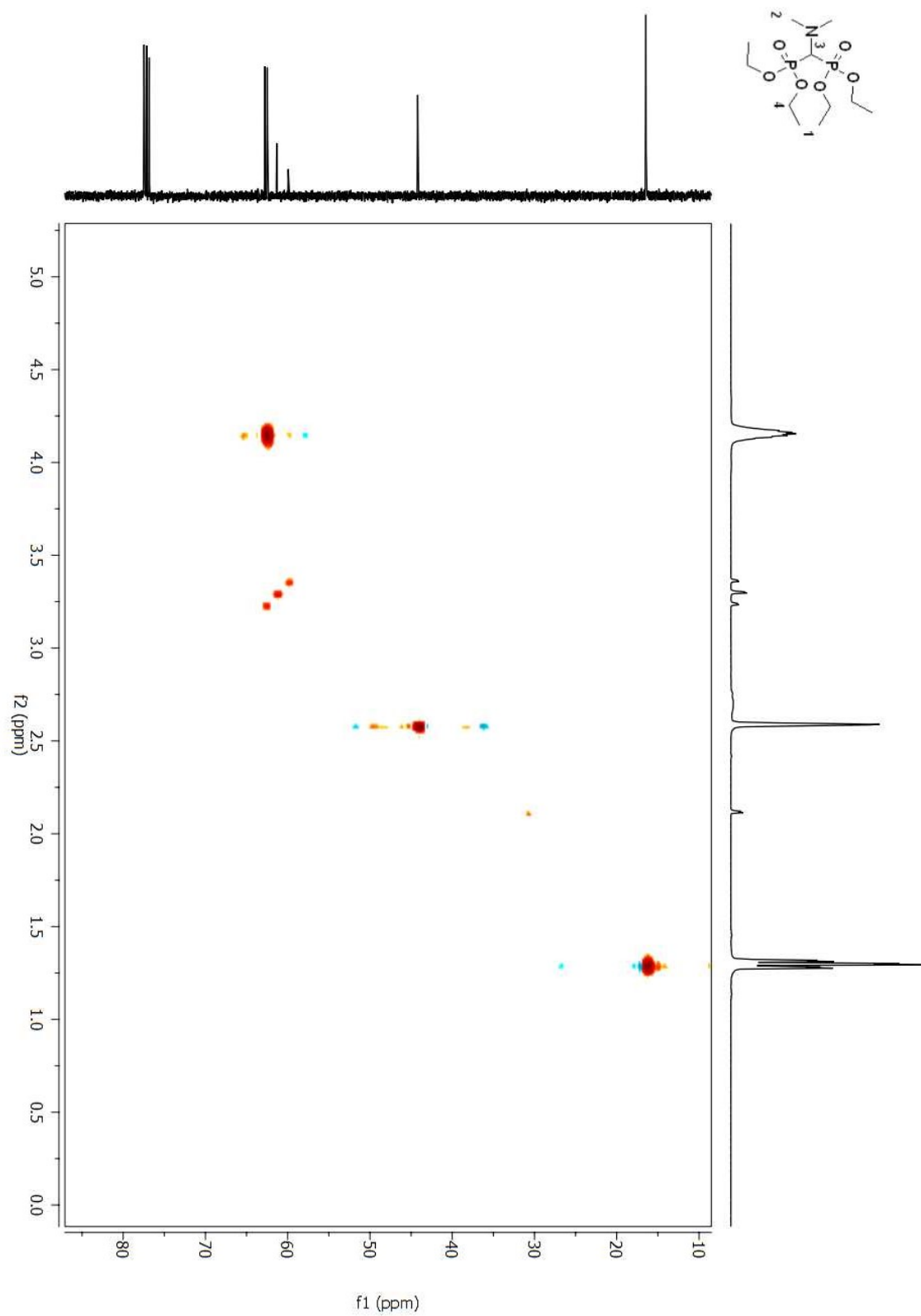


Figure A 146. HSQC 2D NMR spectrum of compound (**105**) in CDCl₃.

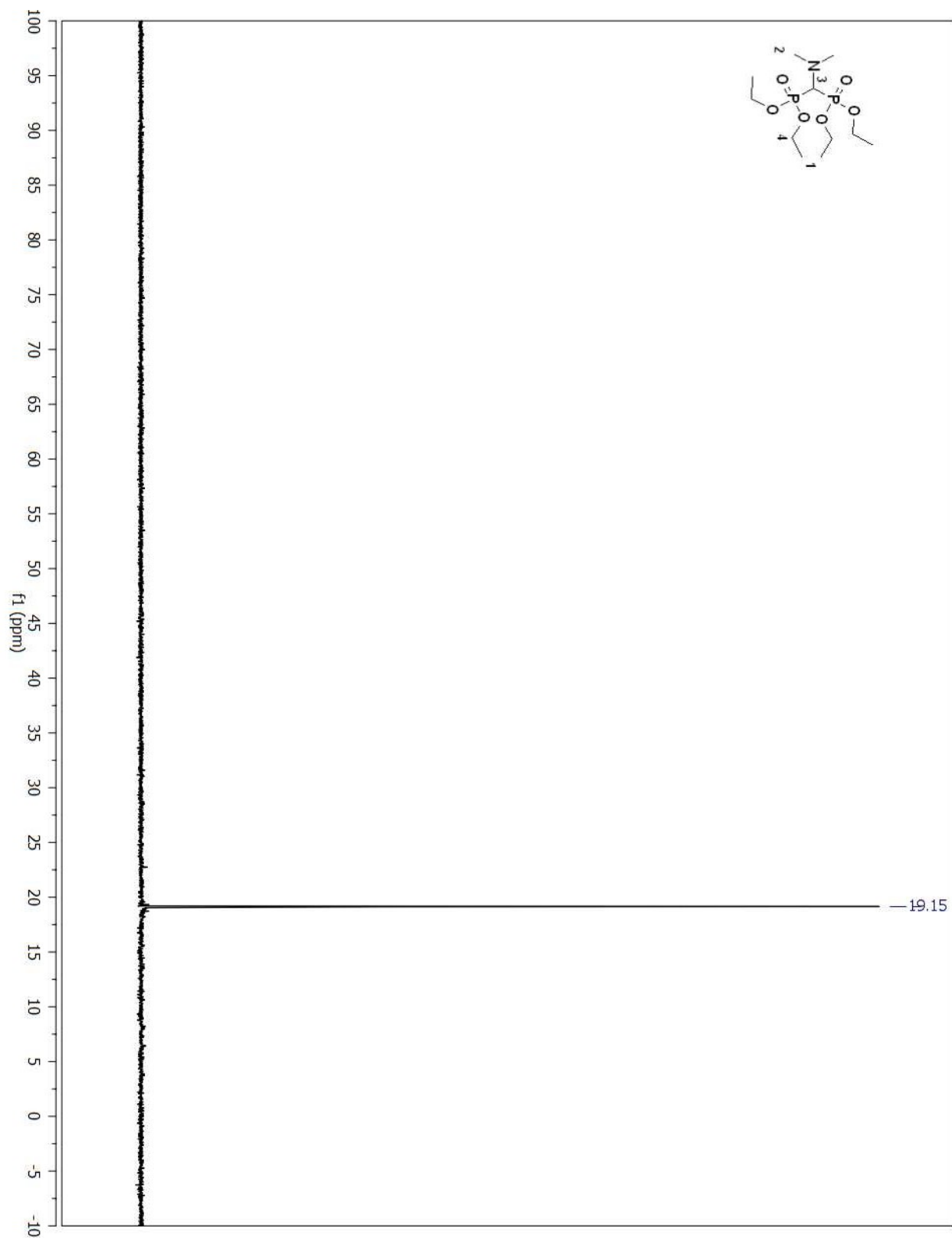


Figure A 147. ^{31}P NMR spectrum of compound (105) in CDCl_3 .
514

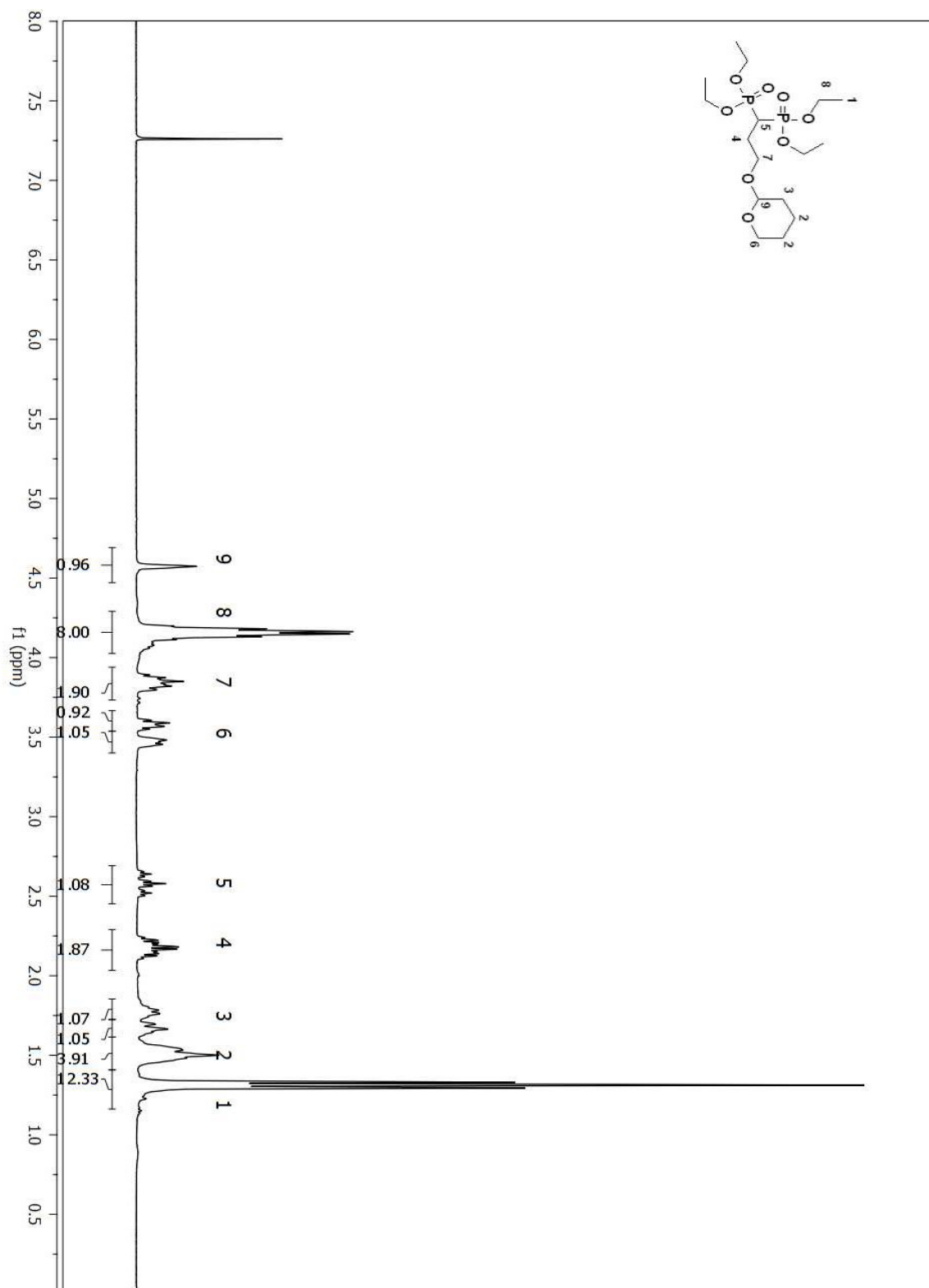


Figure A 148. ^1H NMR spectrum of compound (77) in CDCl_3 .
515

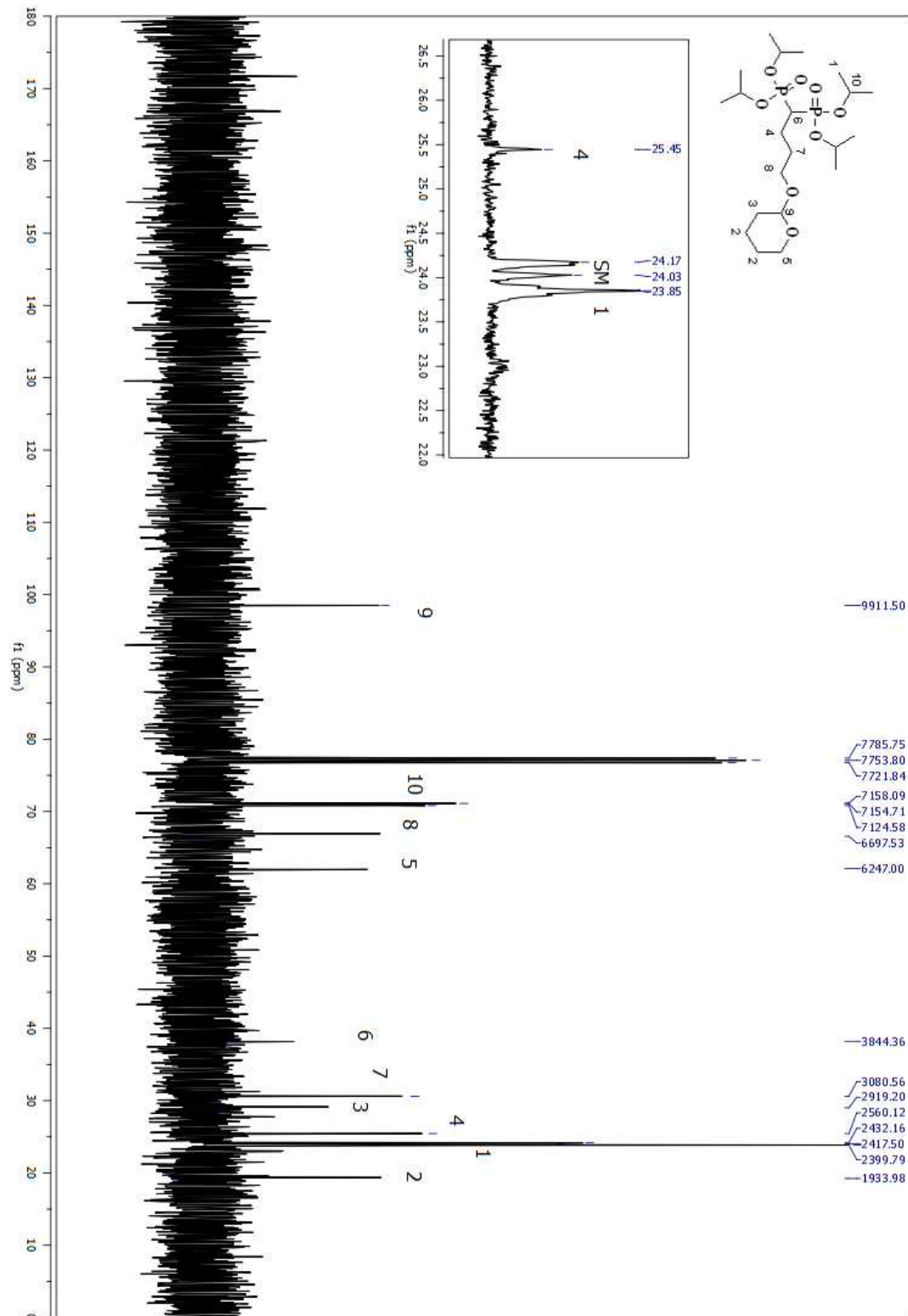


Figure A 149. ¹³C NMR spectrum of compound (77) in CDCl₃.

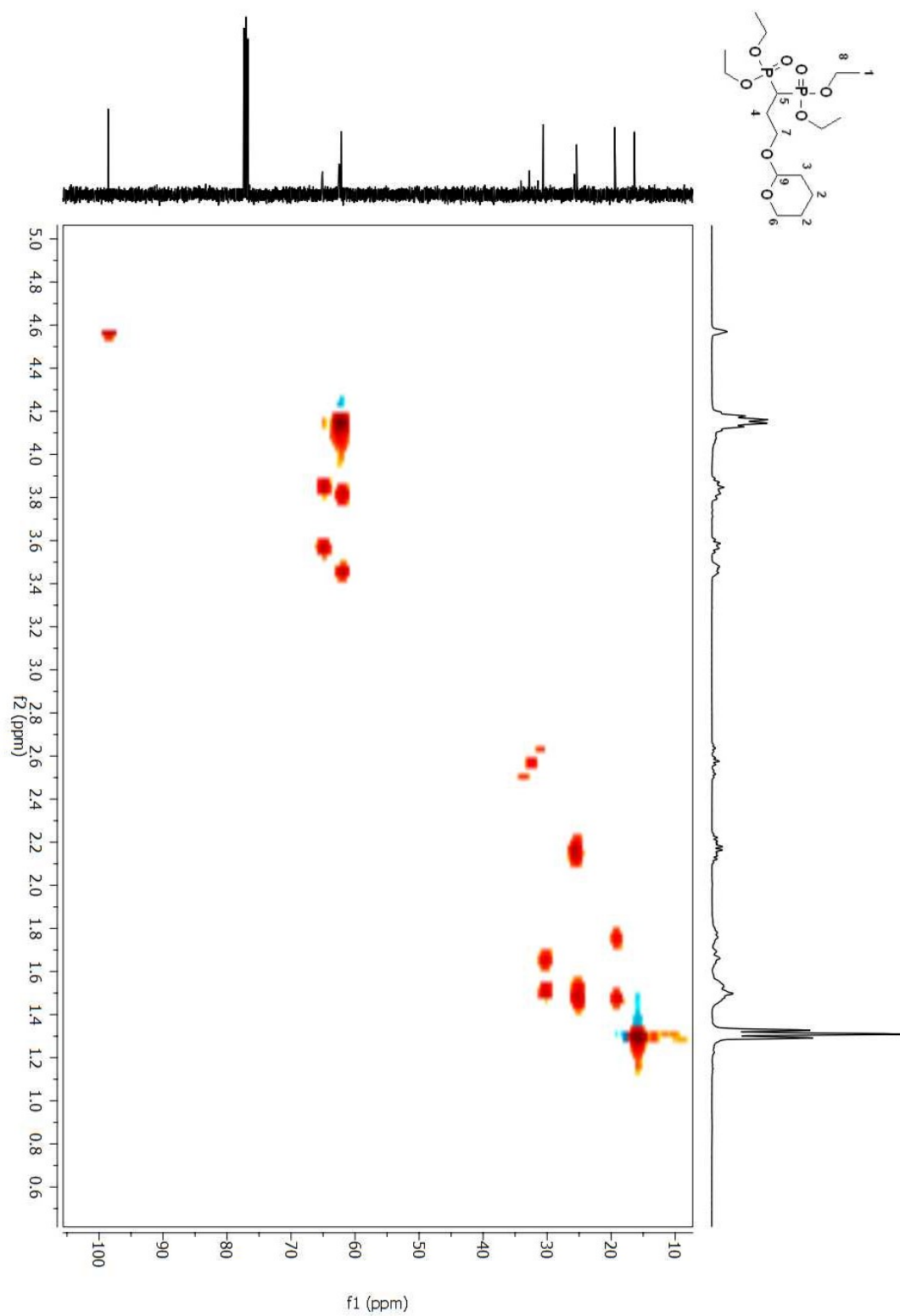


Figure A 150. HSQC 2D NMR spectrum of compound (**77**) in CDCl_3 .

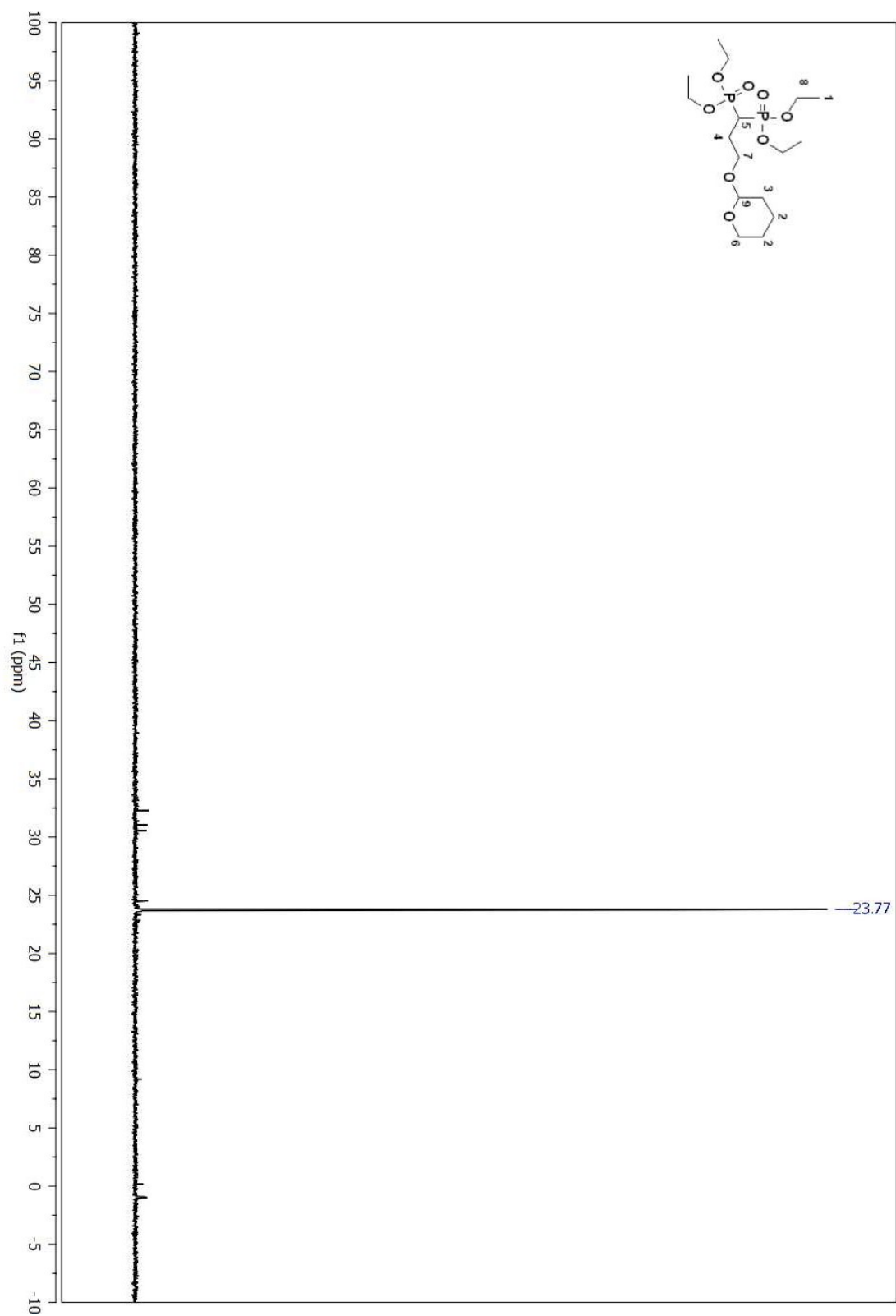


Figure A 151. ^{31}P NMR spectrum of compound (77) in CDCl_3 .

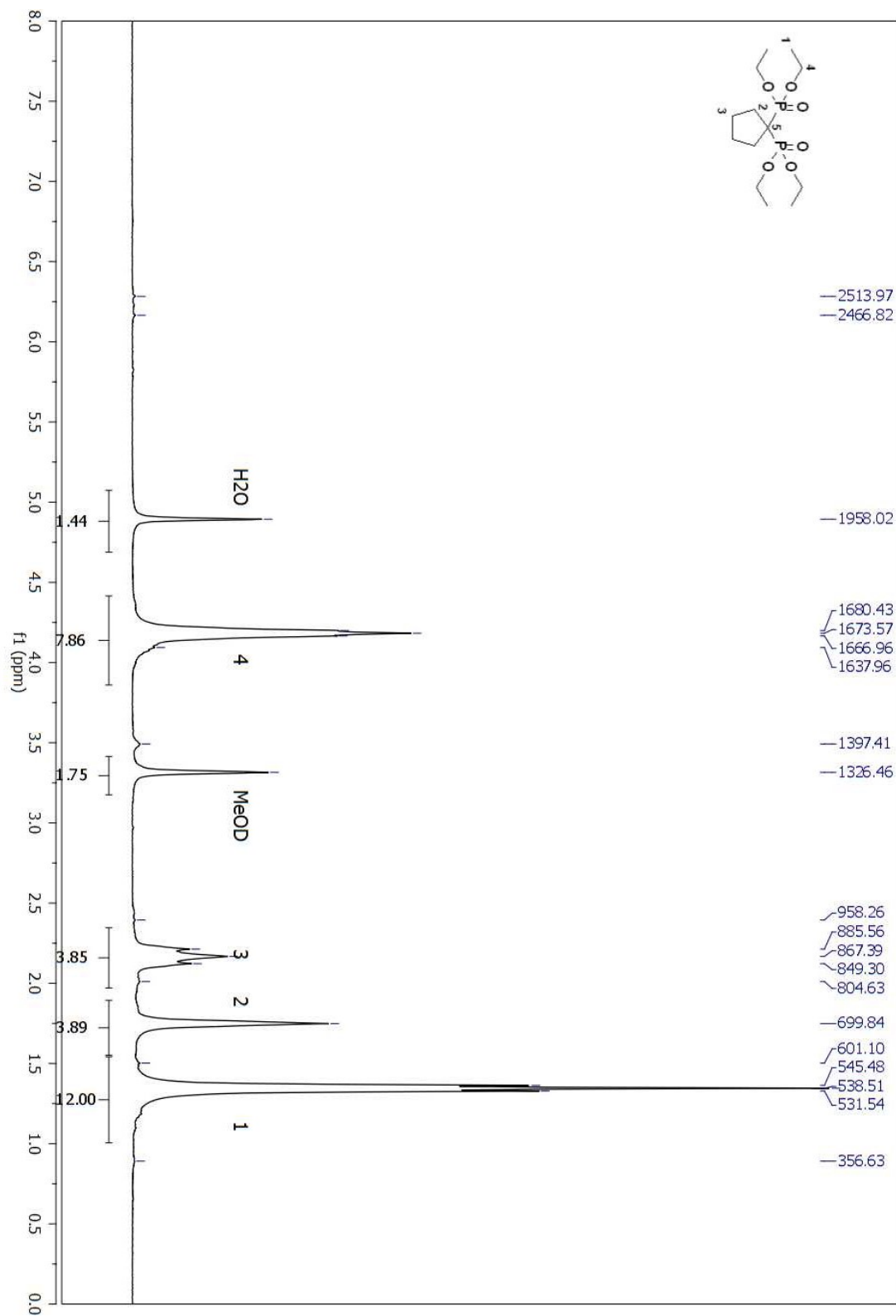


Figure A 152. ^1H NMR spectrum of compound (**97**) in MeOD.

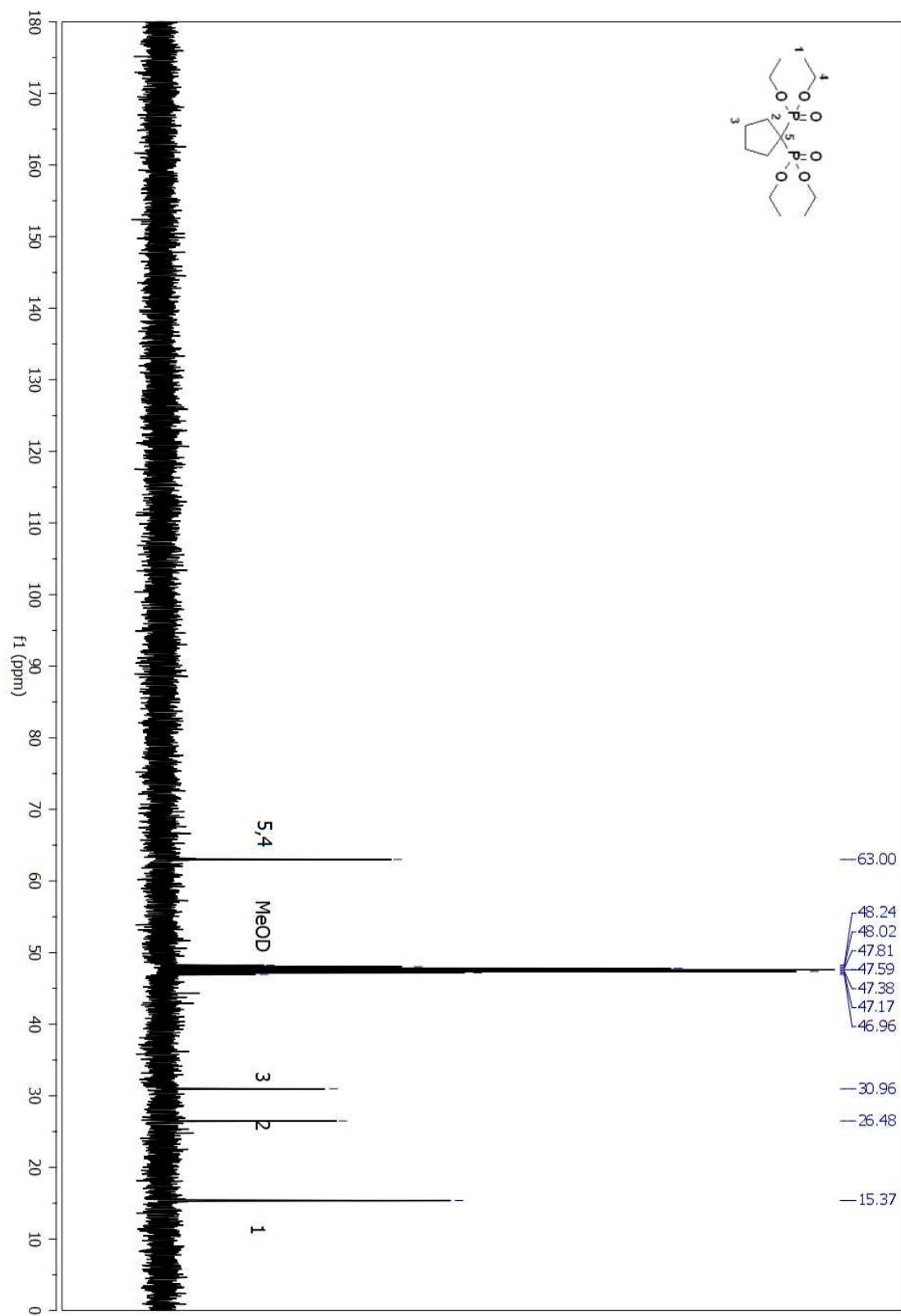


Figure A 153. ^{13}C NMR spectrum of compound (97) in MeOD.

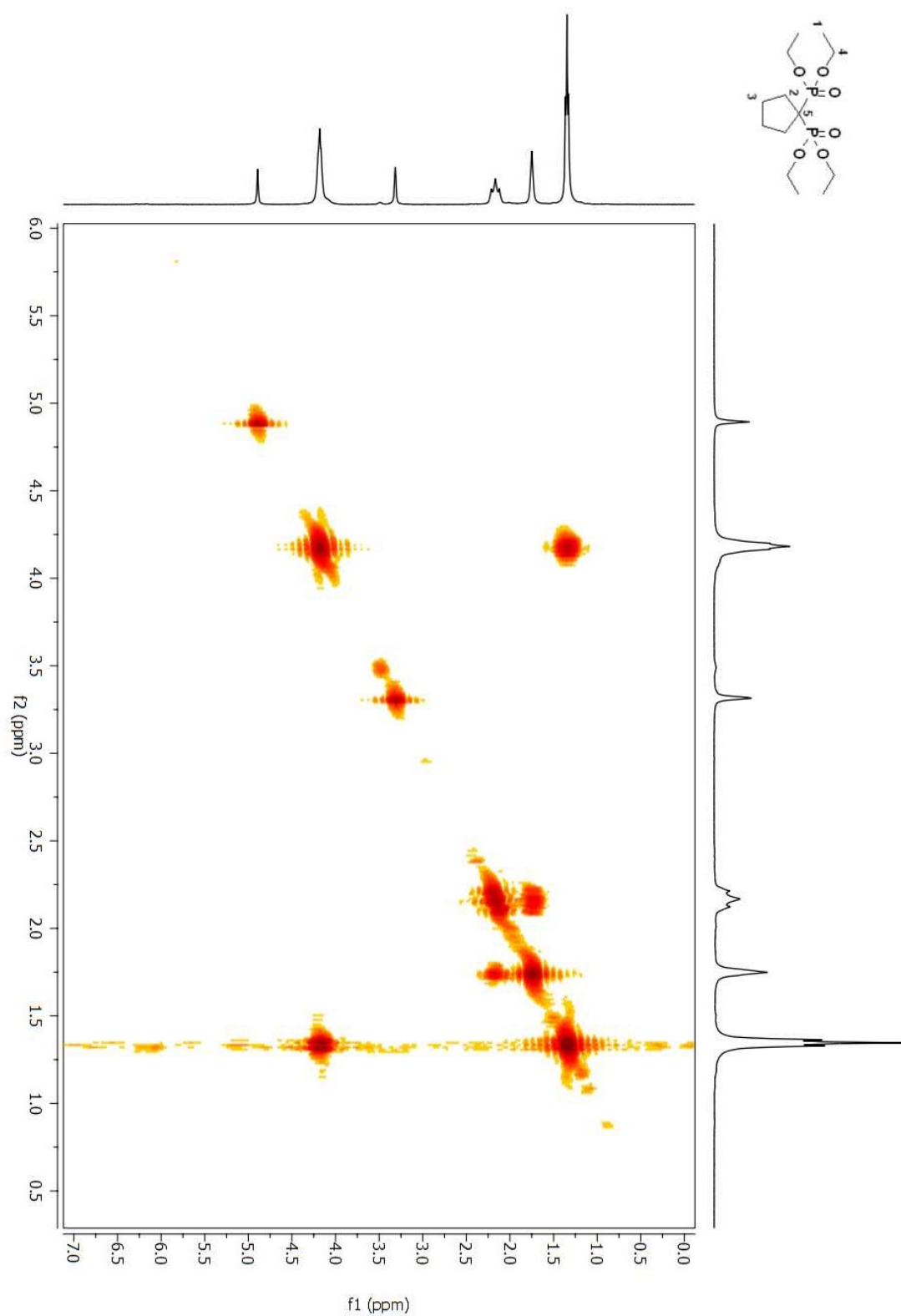


Figure A 154. COSY 2D NMR spectrum of compound (97) in MeOD.

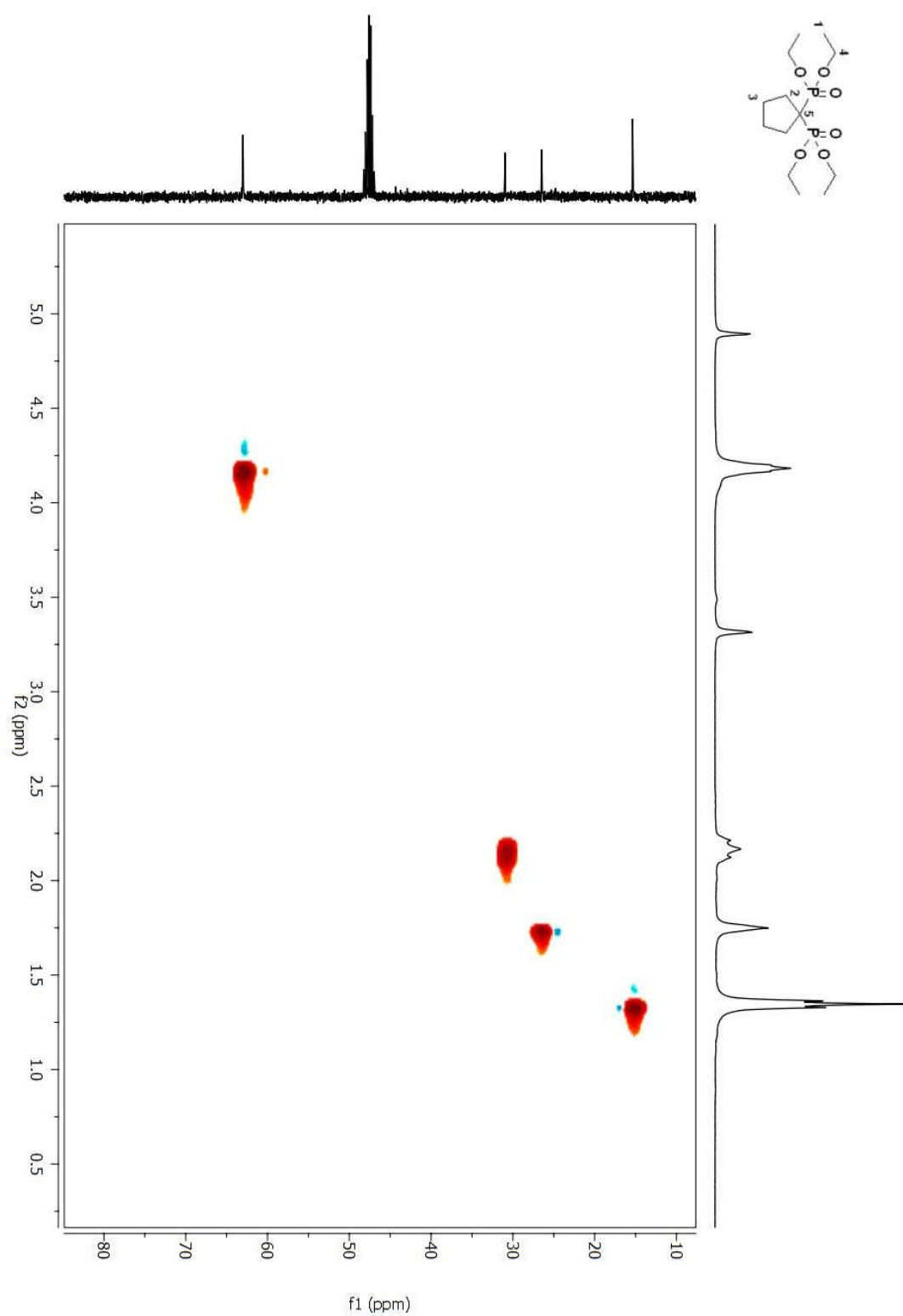


Figure A 155. HSQC 2D NMR spectrum of compound (**97**) in MeOD.

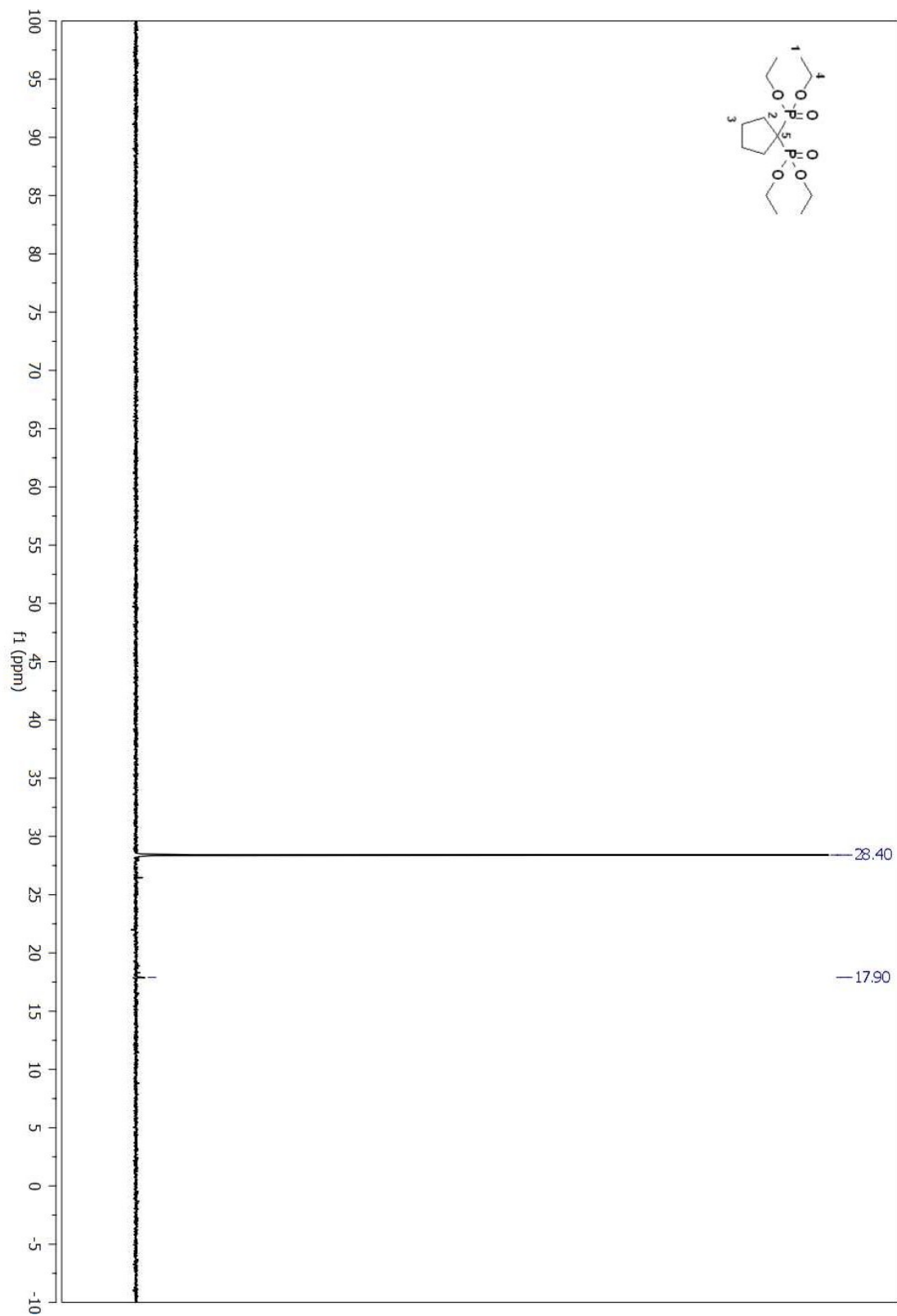


Figure A 156. ^{31}P NMR spectrum of compound (97) in MeOD .

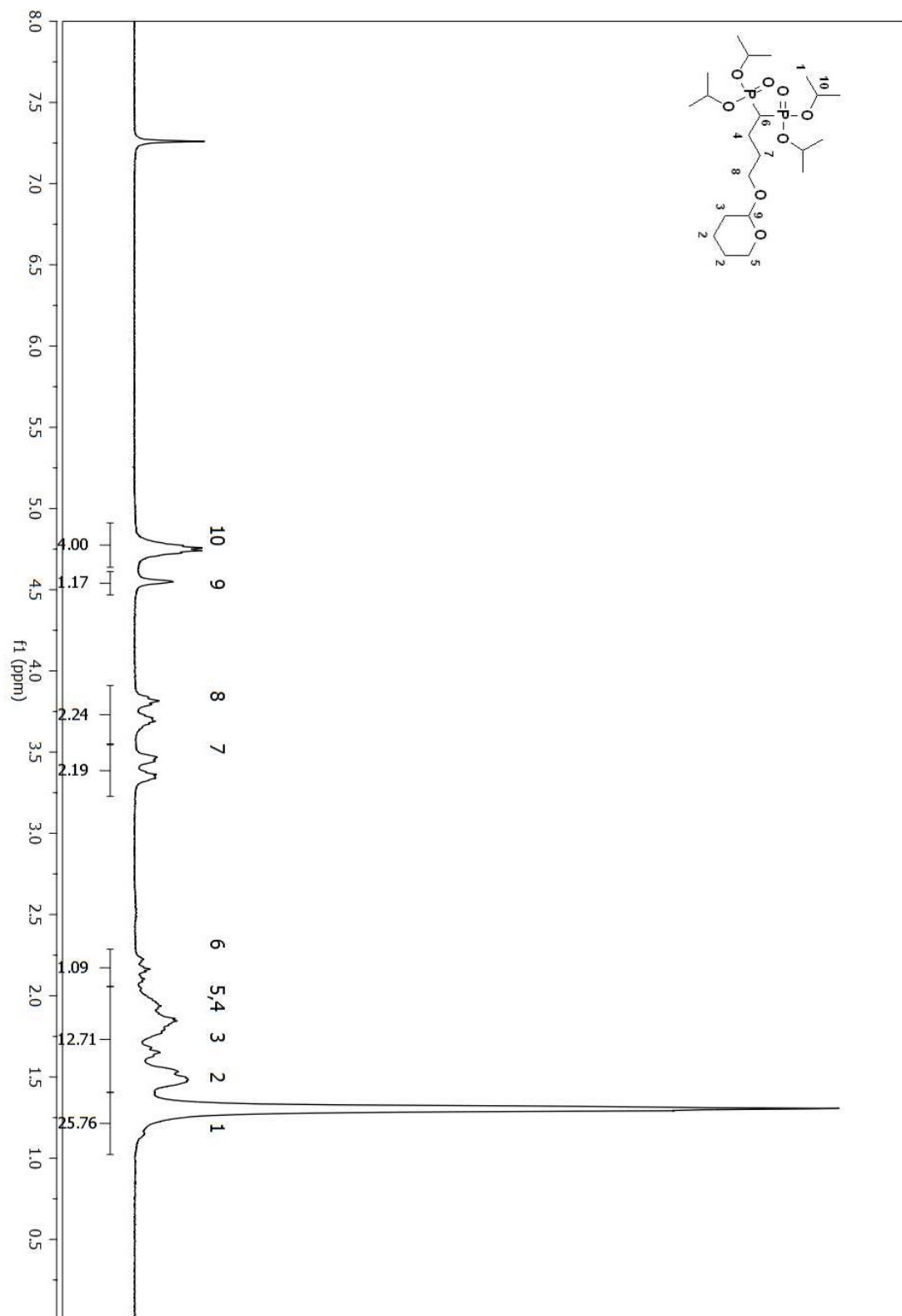


Figure A 157. ¹H NMR spectrum of compound (95) in CDCl₃.

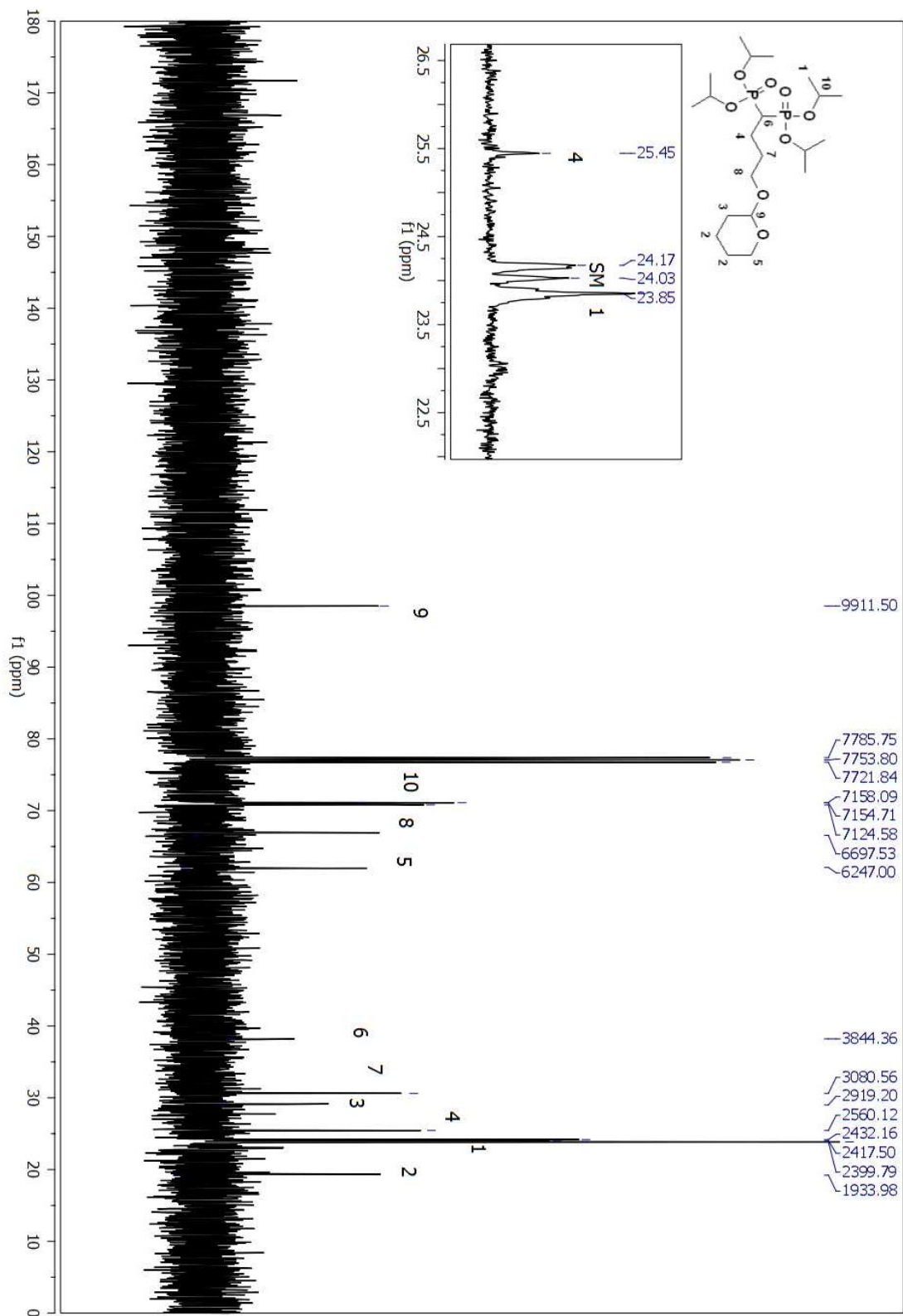


Figure A 158. ^{13}C NMR spectrum of compound (95) in CDCl_3 .

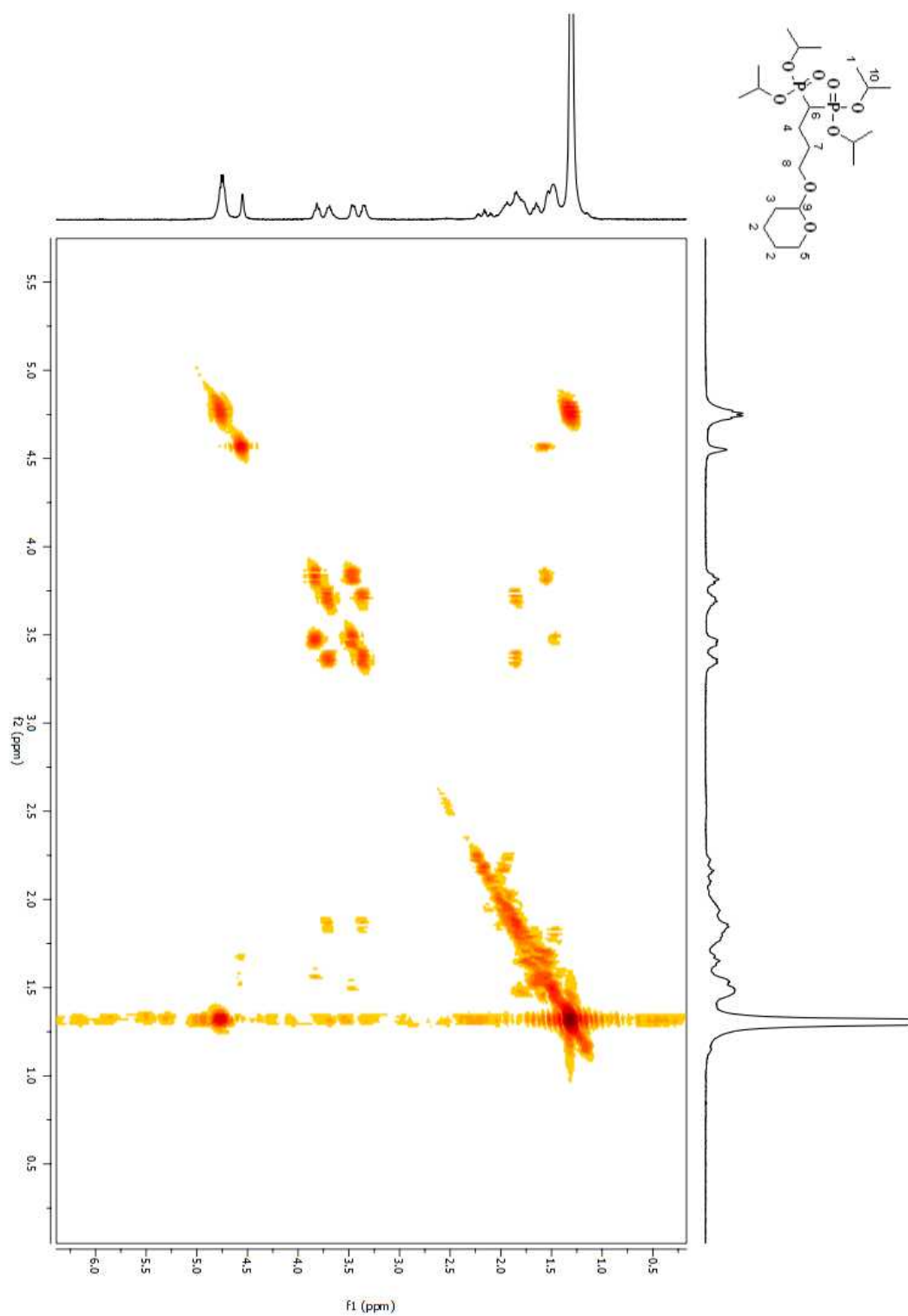


Figure A 159. COSY 2D NMR spectrum of compound (**95**) in CDCl_3 .

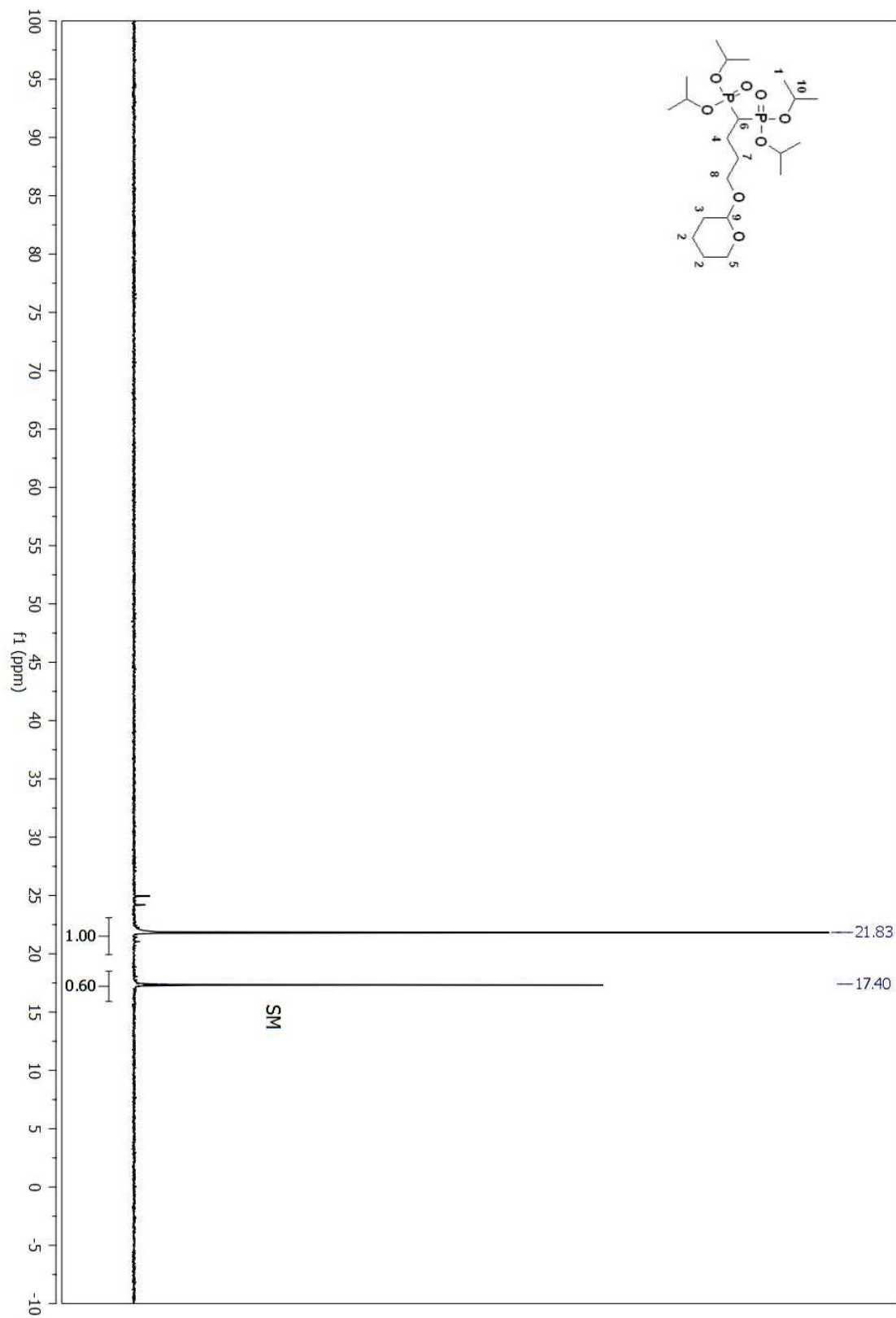


Figure A 160. ^{31}P NMR spectrum of compound (95) in CDCl_3 .

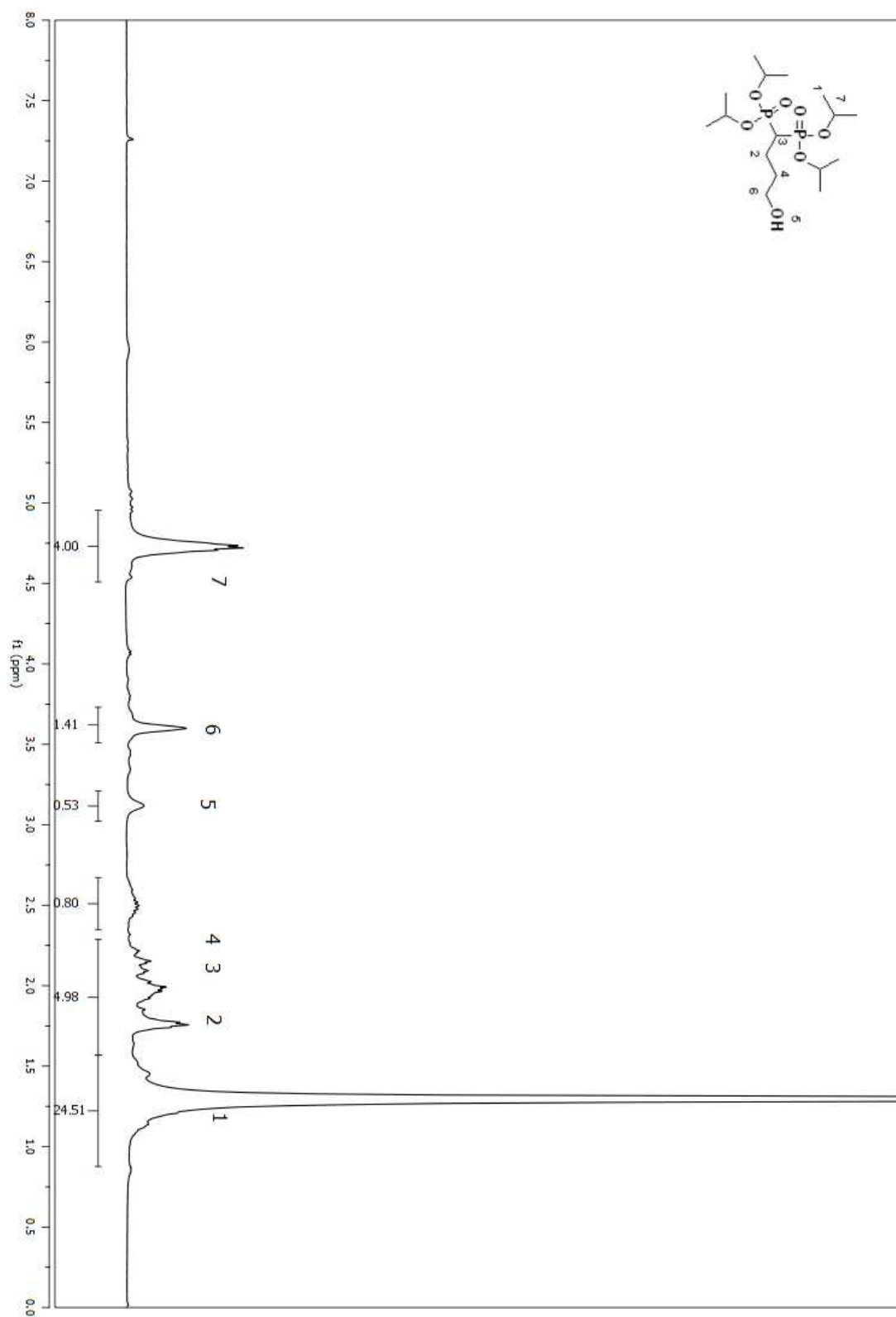


Figure A 161. ^1H NMR spectrum of compound (98) in CDCl_3 .

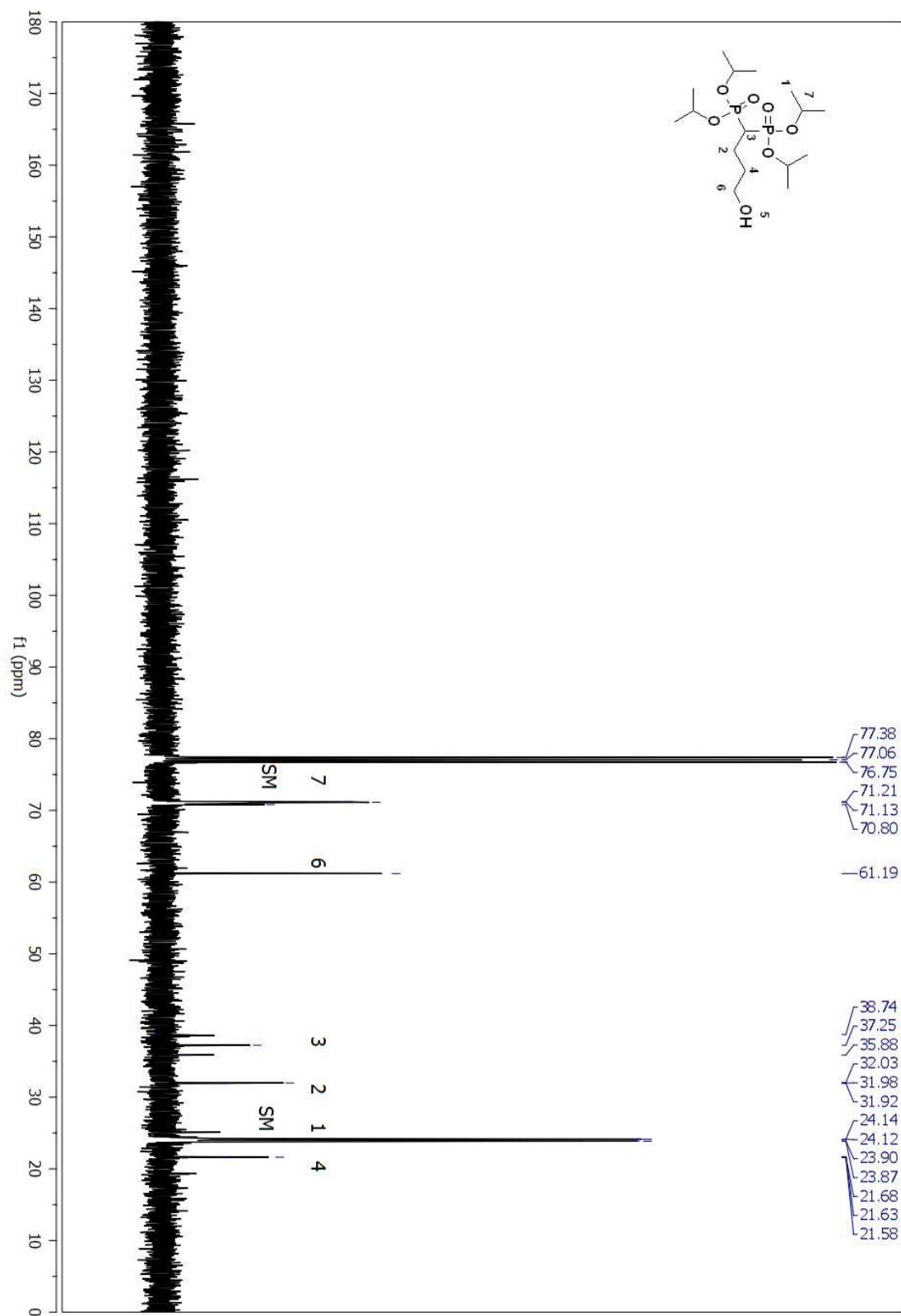


Figure A 162. ^{13}C NMR spectrum of compound (98) in CDCl_3 .

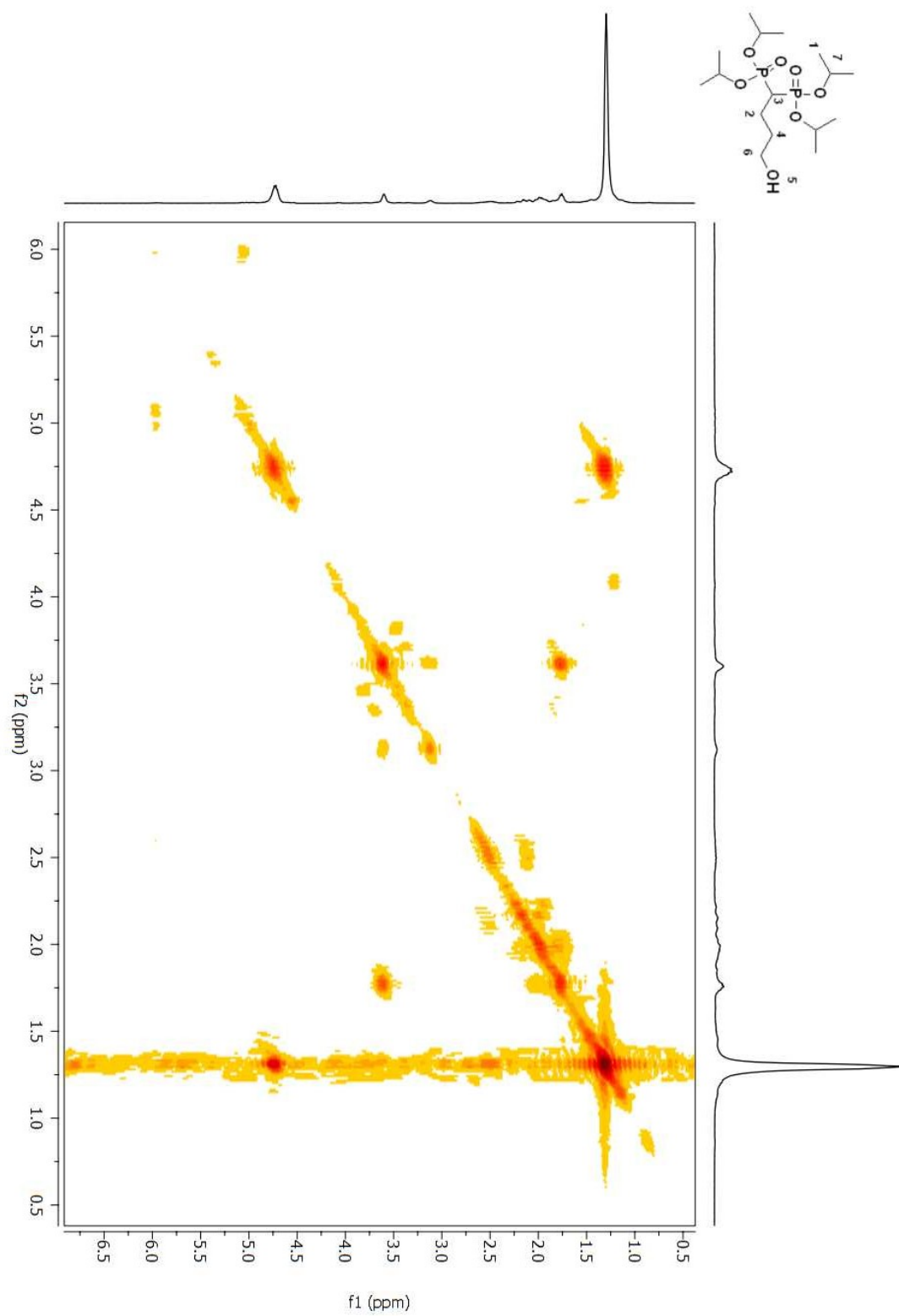


Figure A 163. COSY 2D NMR spectrum of compound (**98**) in CDCl_3 .

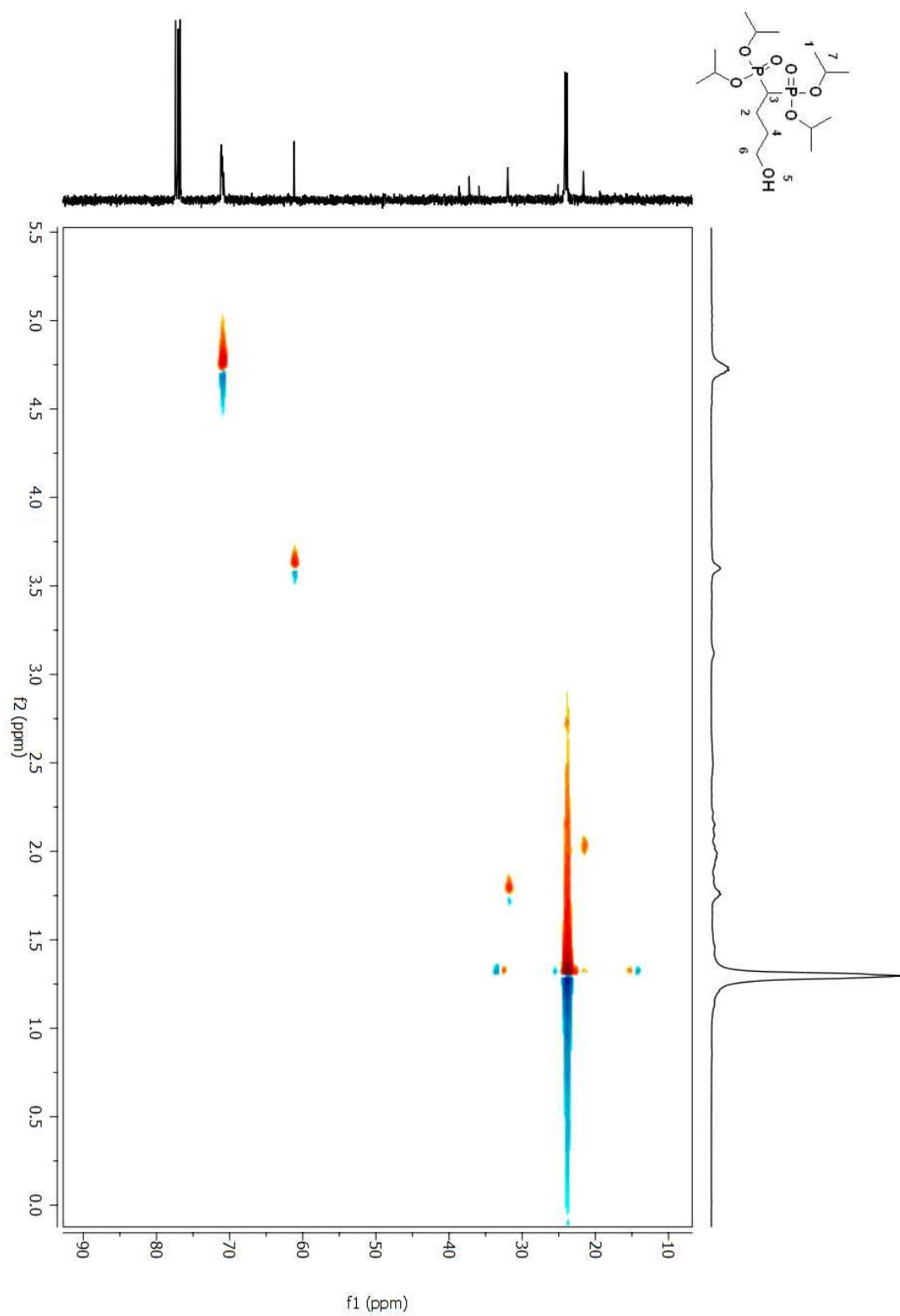


Figure A 164. HSQC 2D NMR spectrum of compound (**98**) in CDCl_3 .

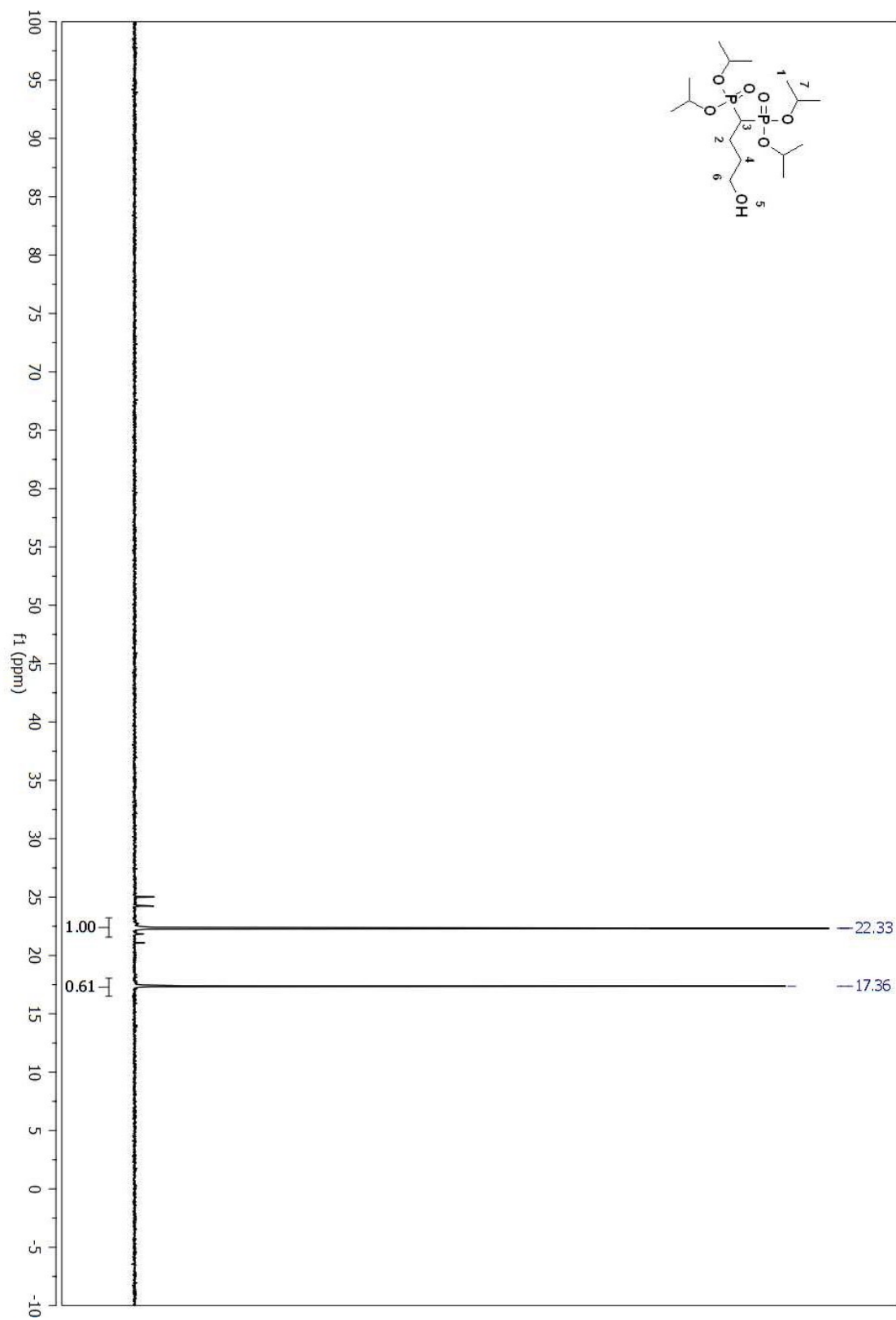


Figure A 165. ^{31}P NMR spectrum of compound (98) in CDCl_3 .

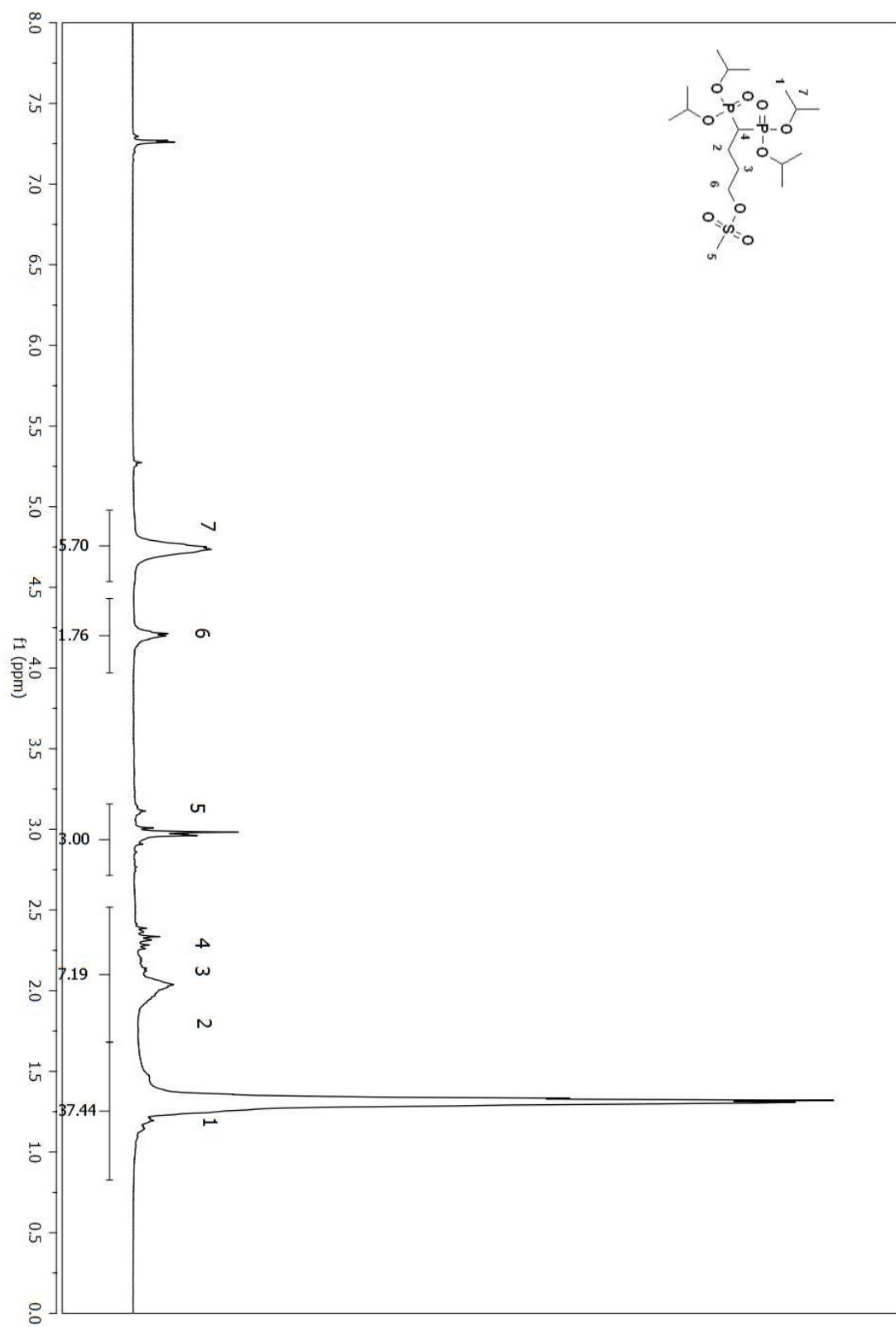


Figure A 166. ^1H NMR spectrum of compound (99) in CDCl_3 .

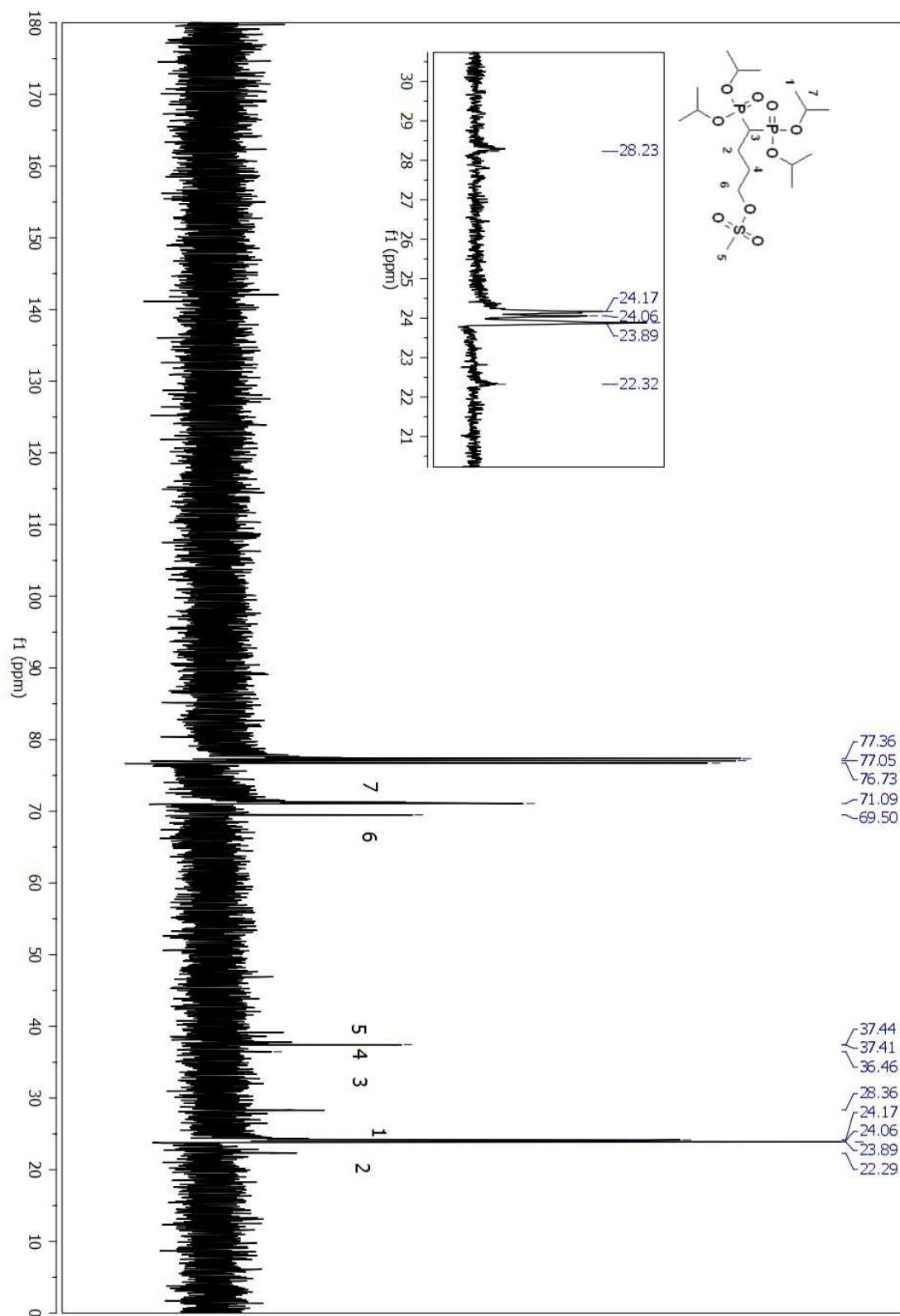


Figure A 167. ^{13}C NMR spectrum of compound (99) in CDCl_3 .

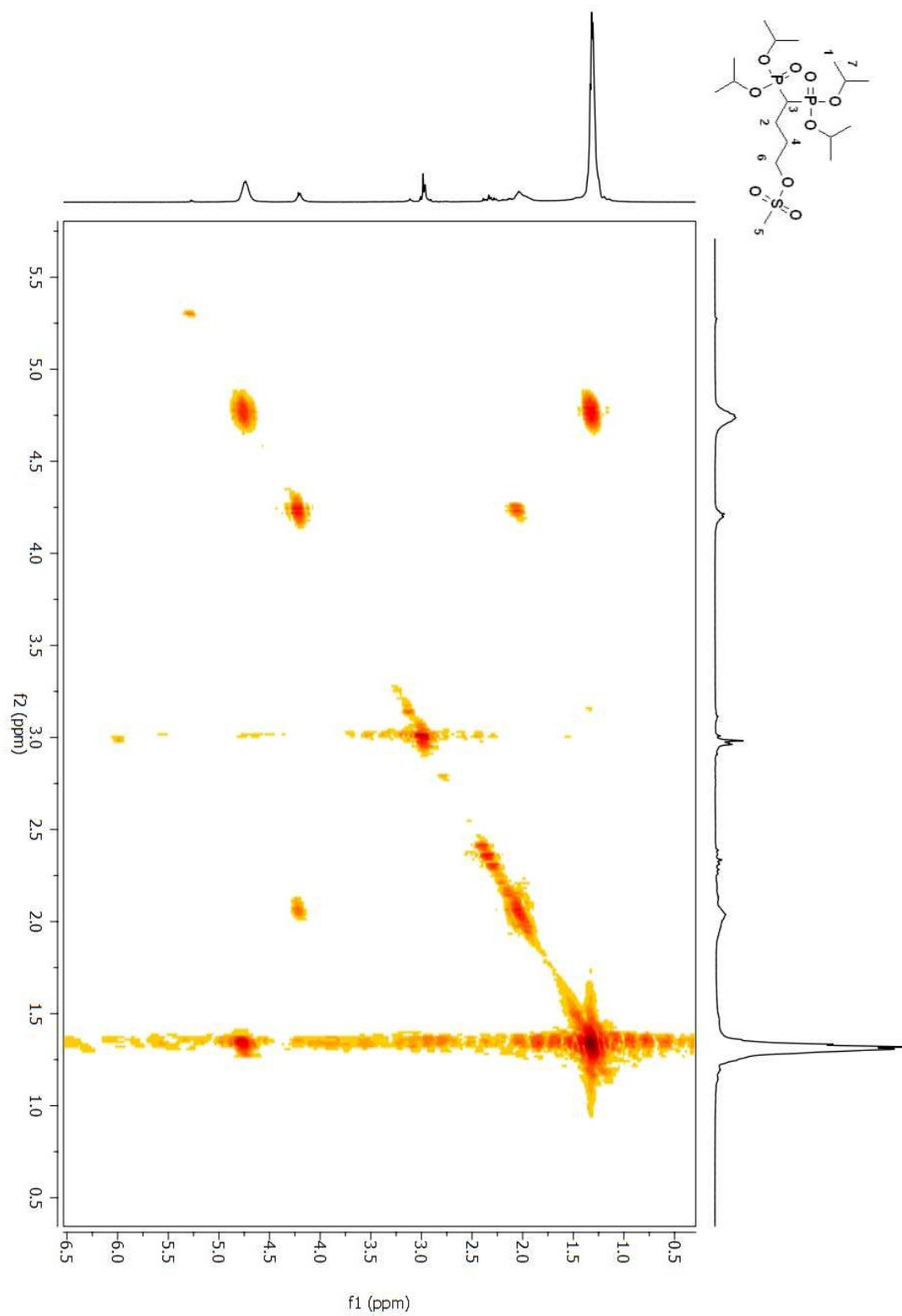


Figure A 168. COSY 2D NMR spectrum of compound (**99**) in CDCl₃.

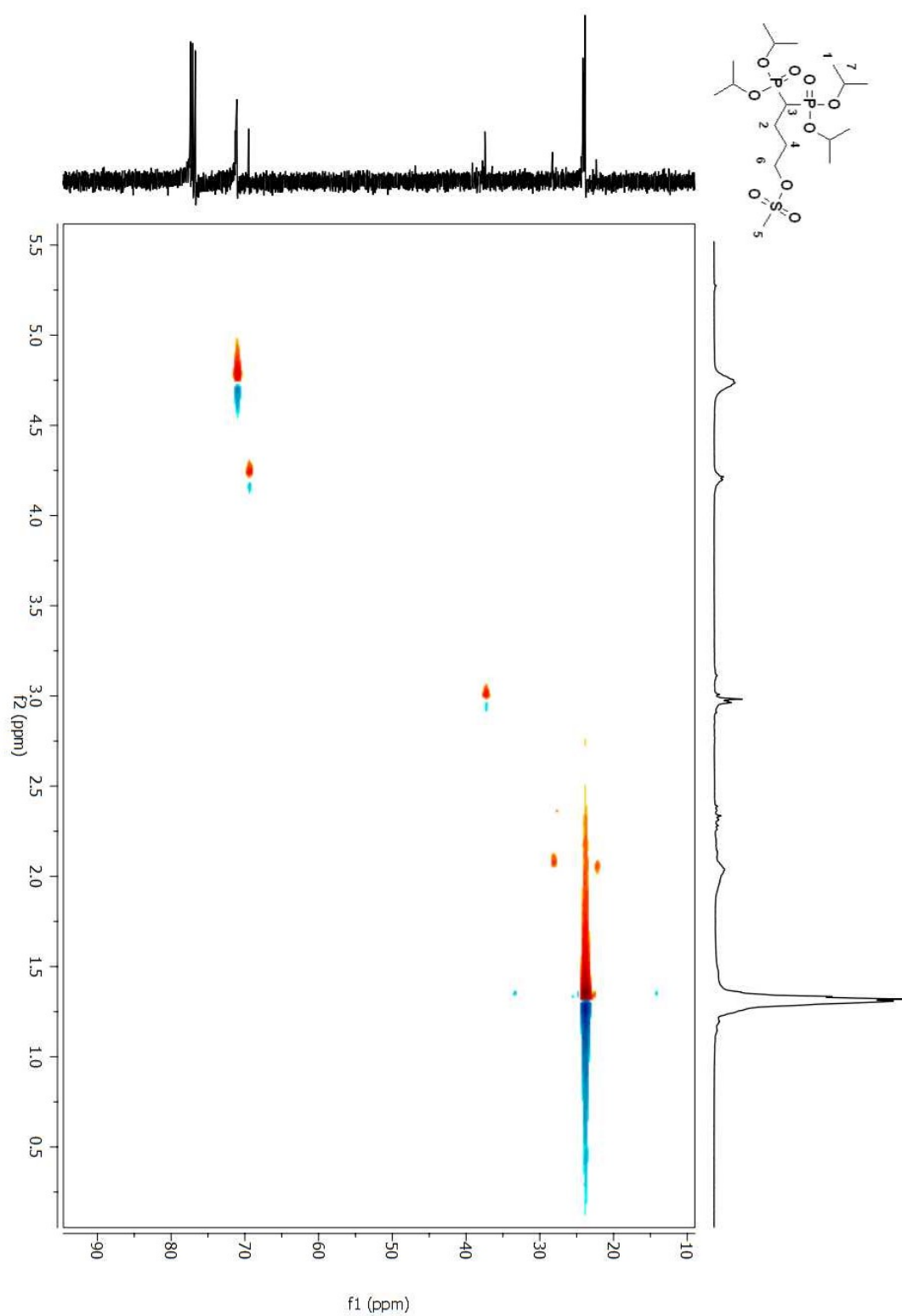


Figure A 169. HSQC 2D NMR spectrum of compound (**99**) in CDCl₃.

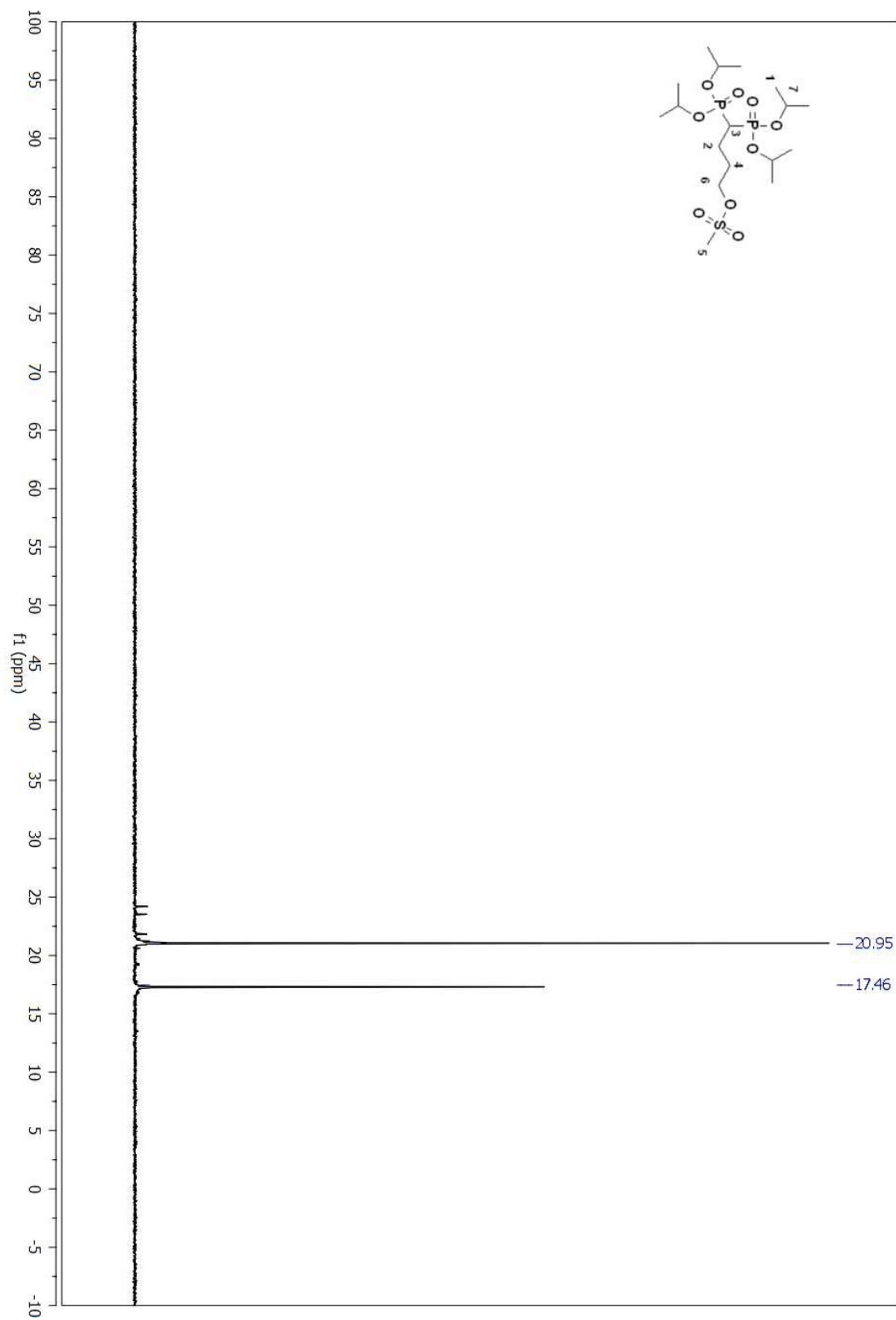


Figure A 170. ^{31}P NMR spectrum of compound (99) in CDCl_3 .

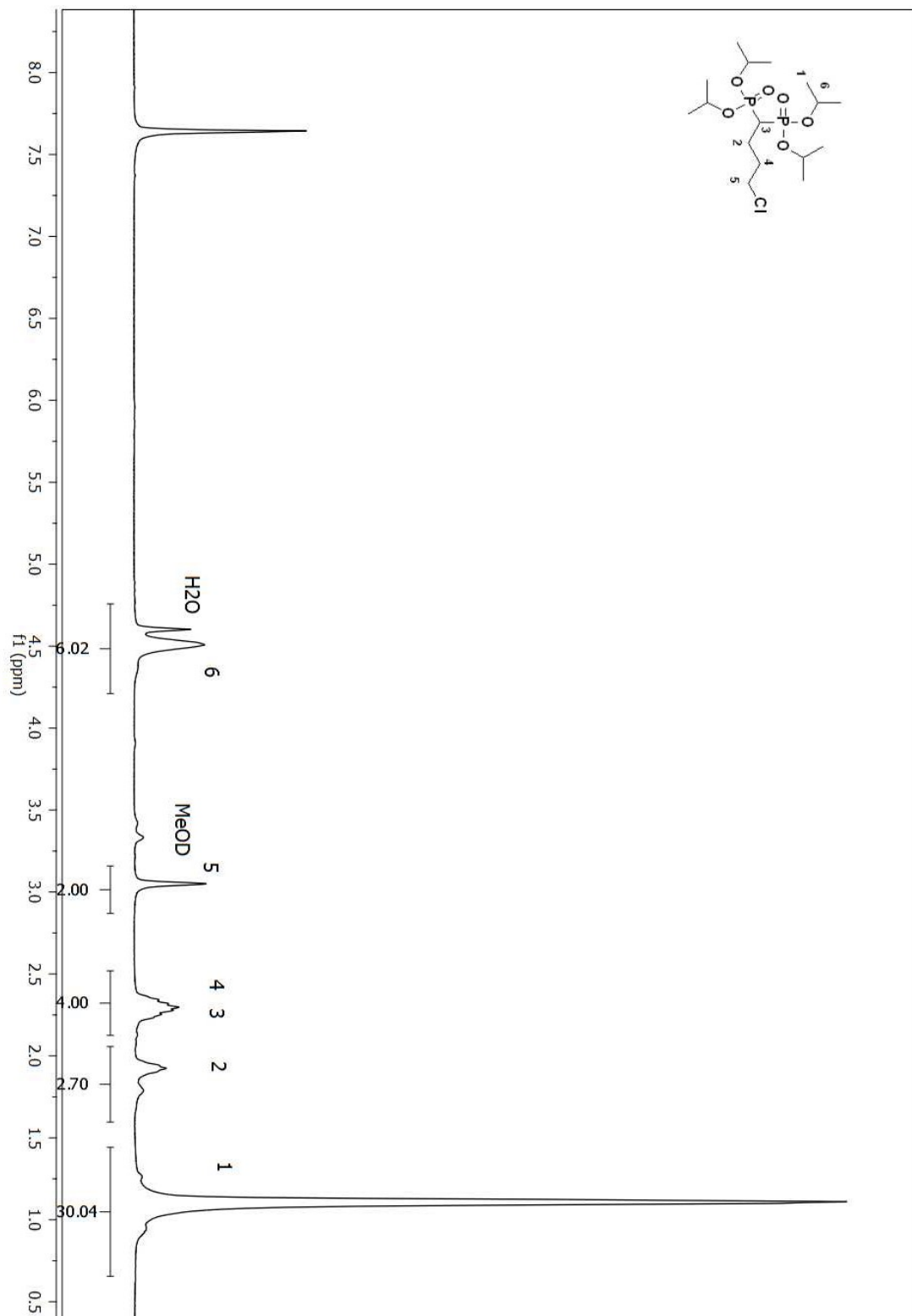


Figure A 171. ^1H NMR spectrum of compound (91) in MeOD .

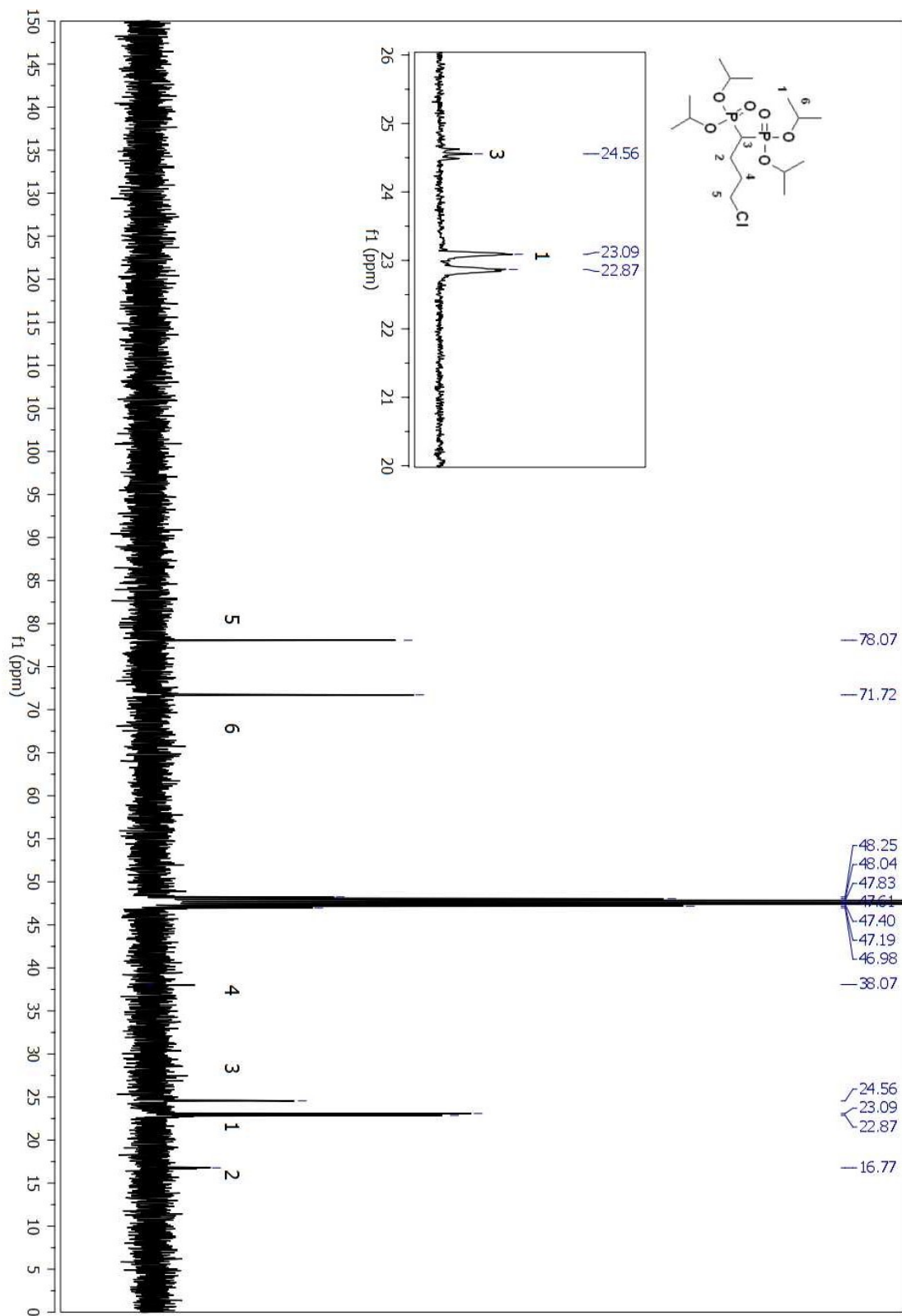


Figure A 172. ¹³C NMR spectrum of compound (91) in MeOD.

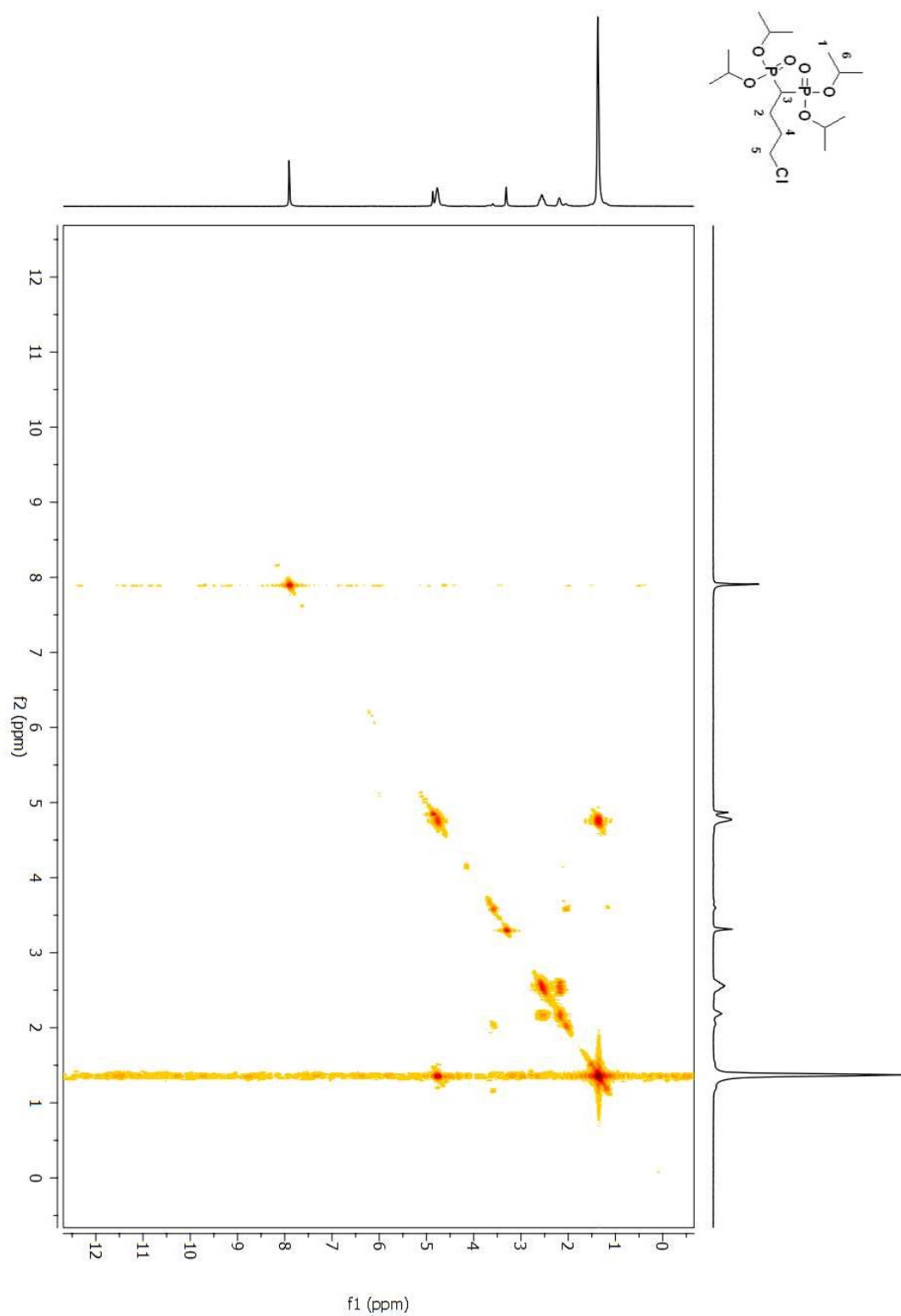


Figure A 173. COSY 2D NMR spectrum of compound (**91**) in MeOD.

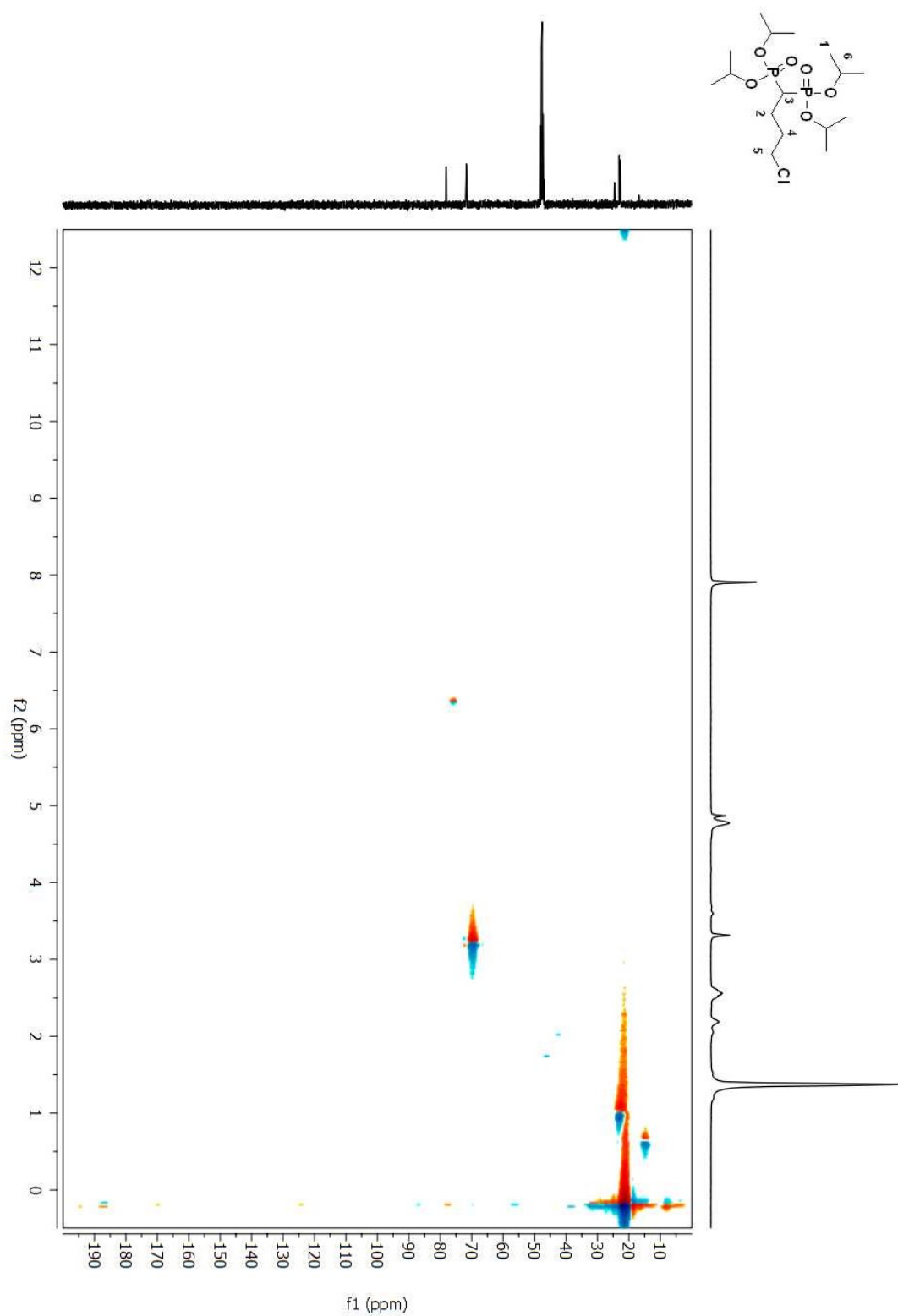


Figure A 174. HSQC 2D NMR spectrum of compound (**91**) in MeOD.

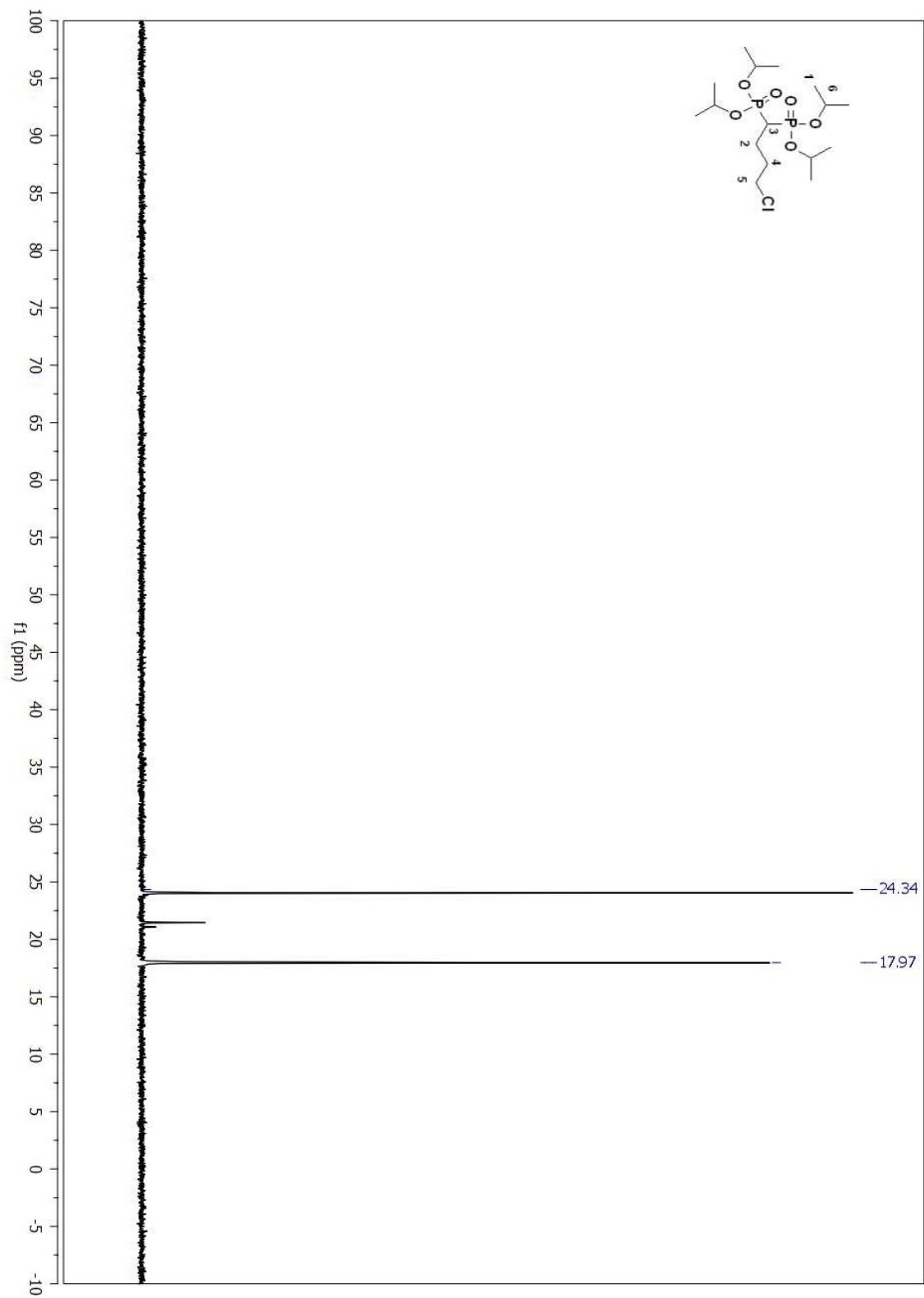


Figure A 175. ^{31}P NMR spectrum of compound (91) in MeOD. (CRUDE)

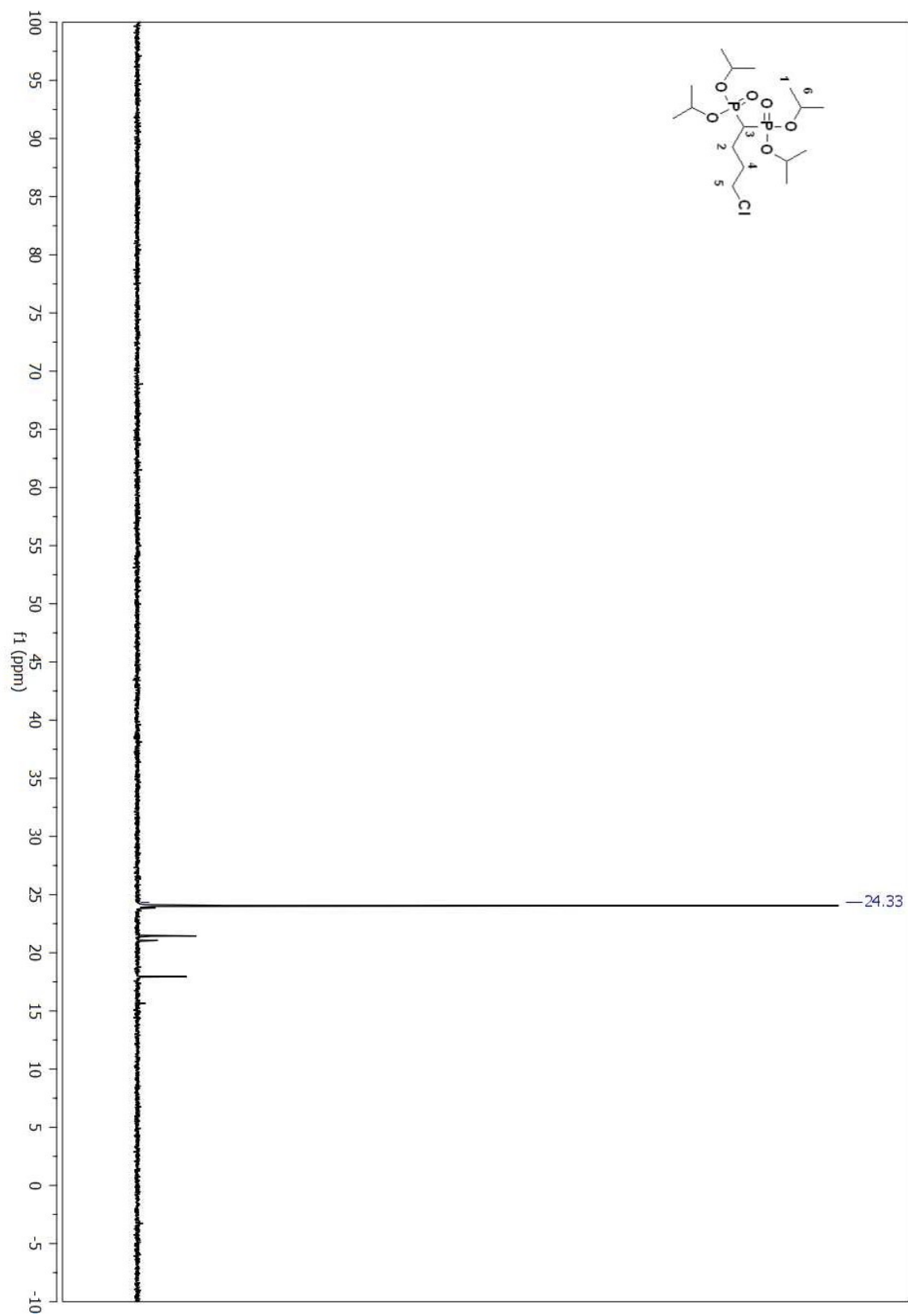


Figure A 176. ^{31}P NMR spectrum of compound (91) in MeOD . (COLUMNED FRACTION)

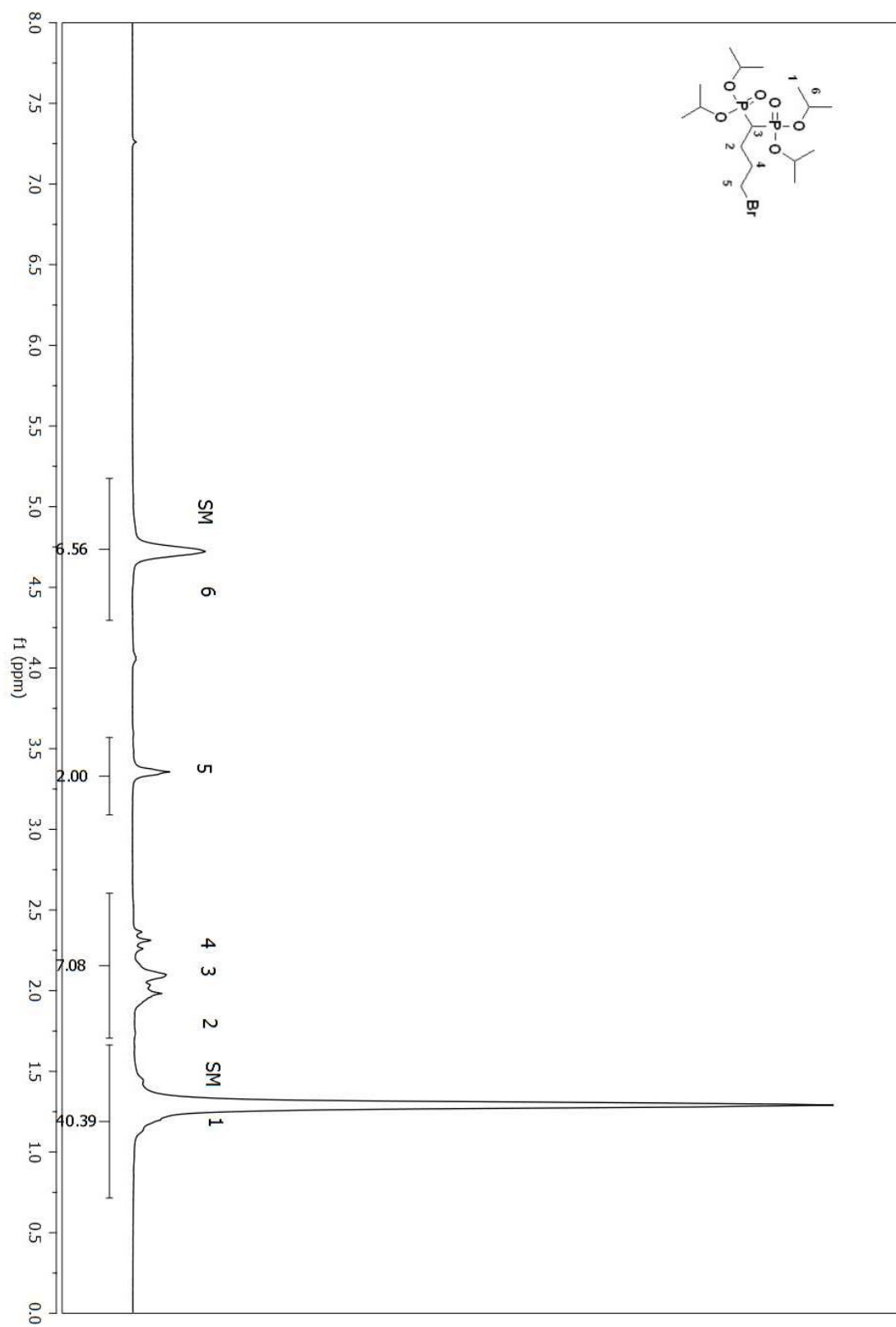


Figure A 177. ¹H NMR spectrum of compound (87) in CDCl₃.

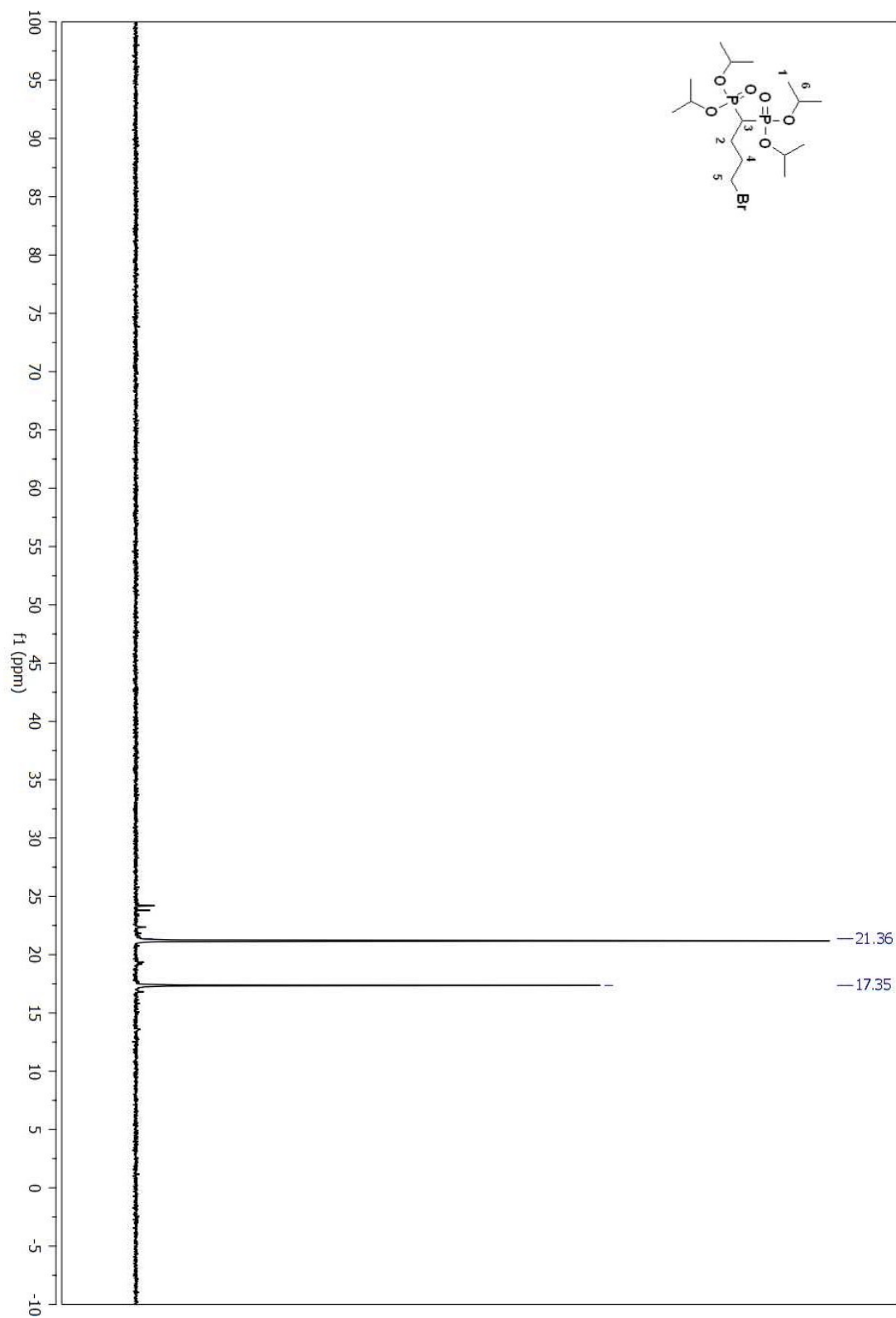


Figure A 178. ^{31}P NMR spectrum of compound (**87**) in CDCl_3 .

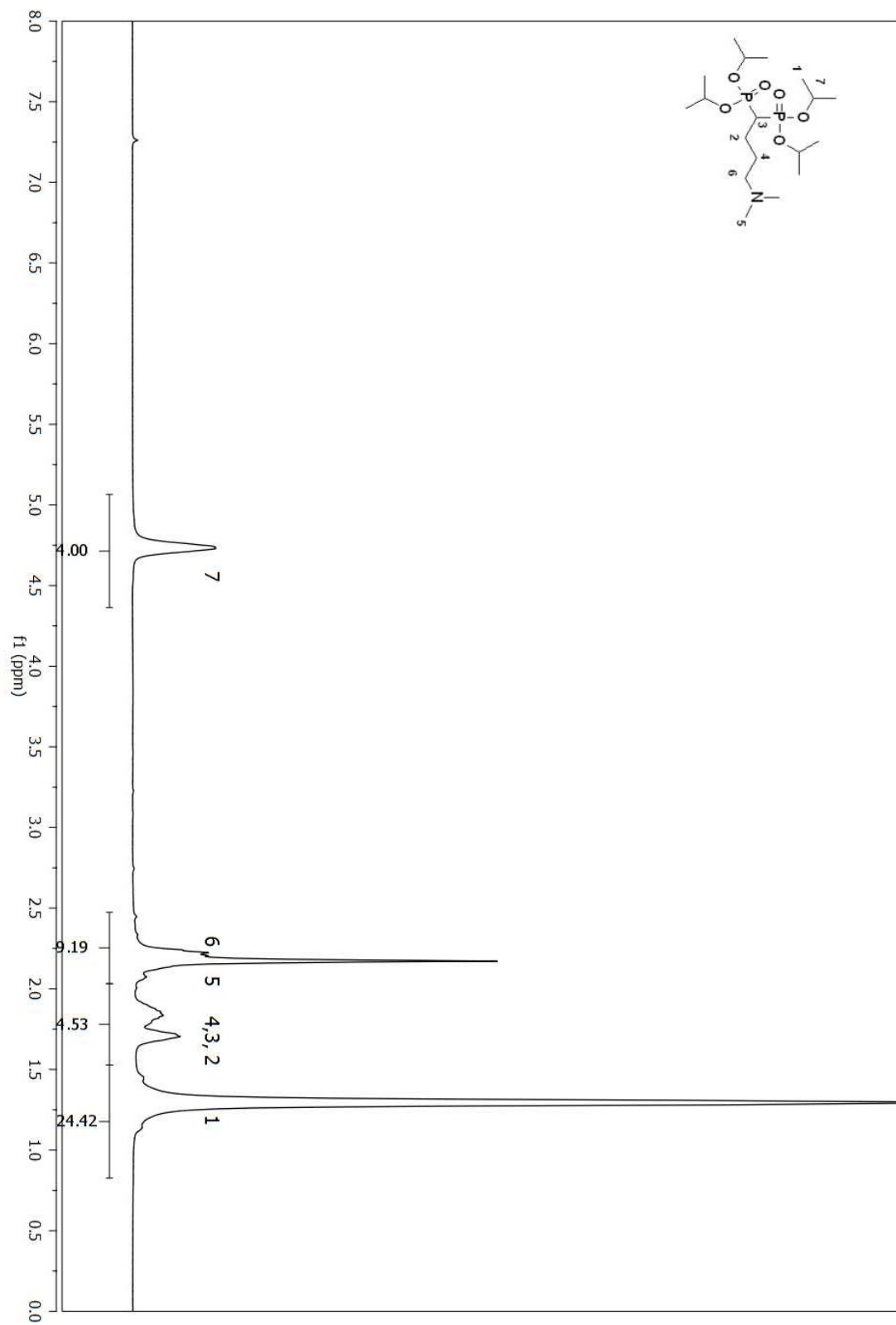


Figure A 179. ^1H NMR spectrum of compound (87) in CDCl_3 .

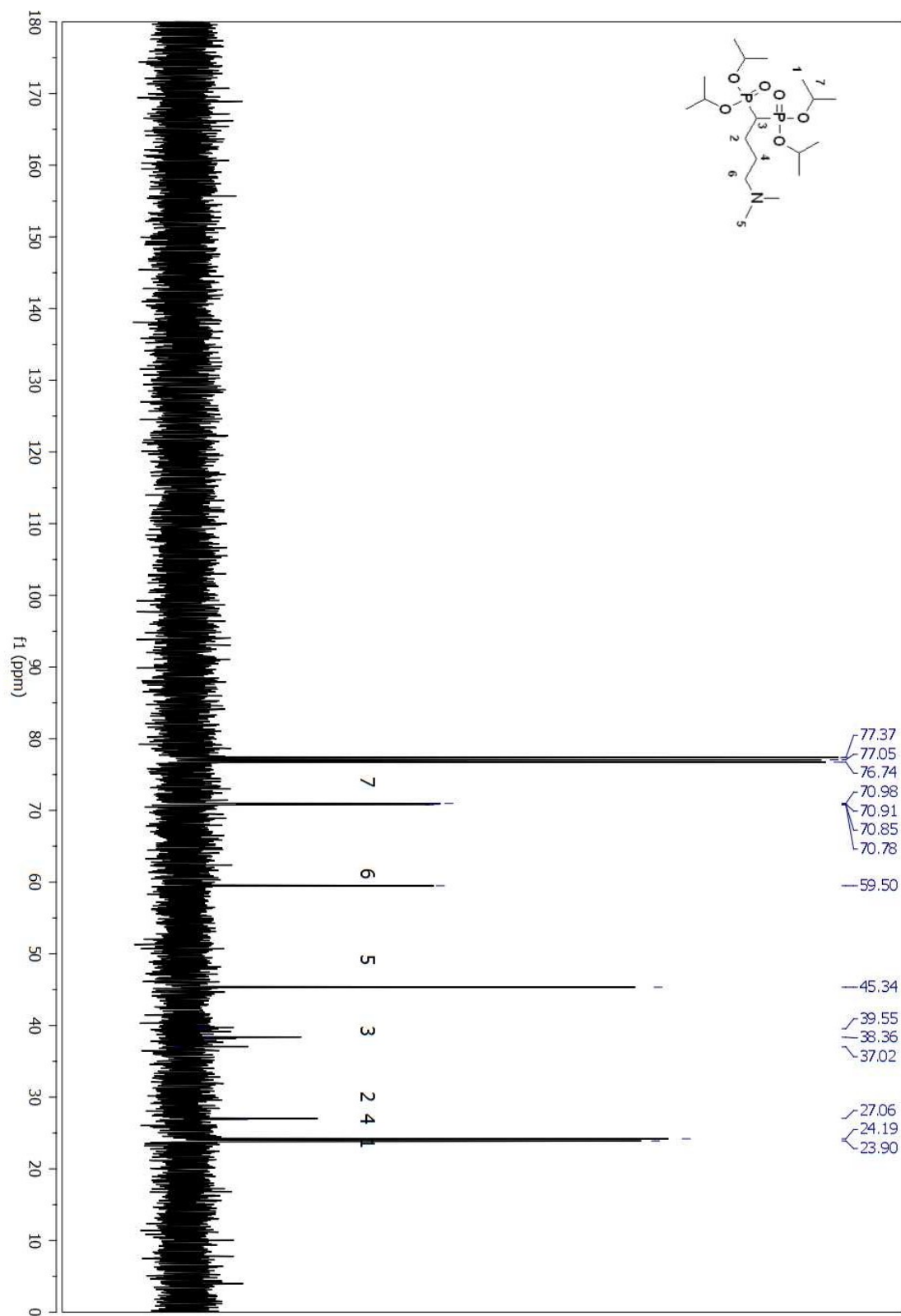


Figure A 180. ^{13}C NMR spectrum of compound (87) in CDCl_3 .

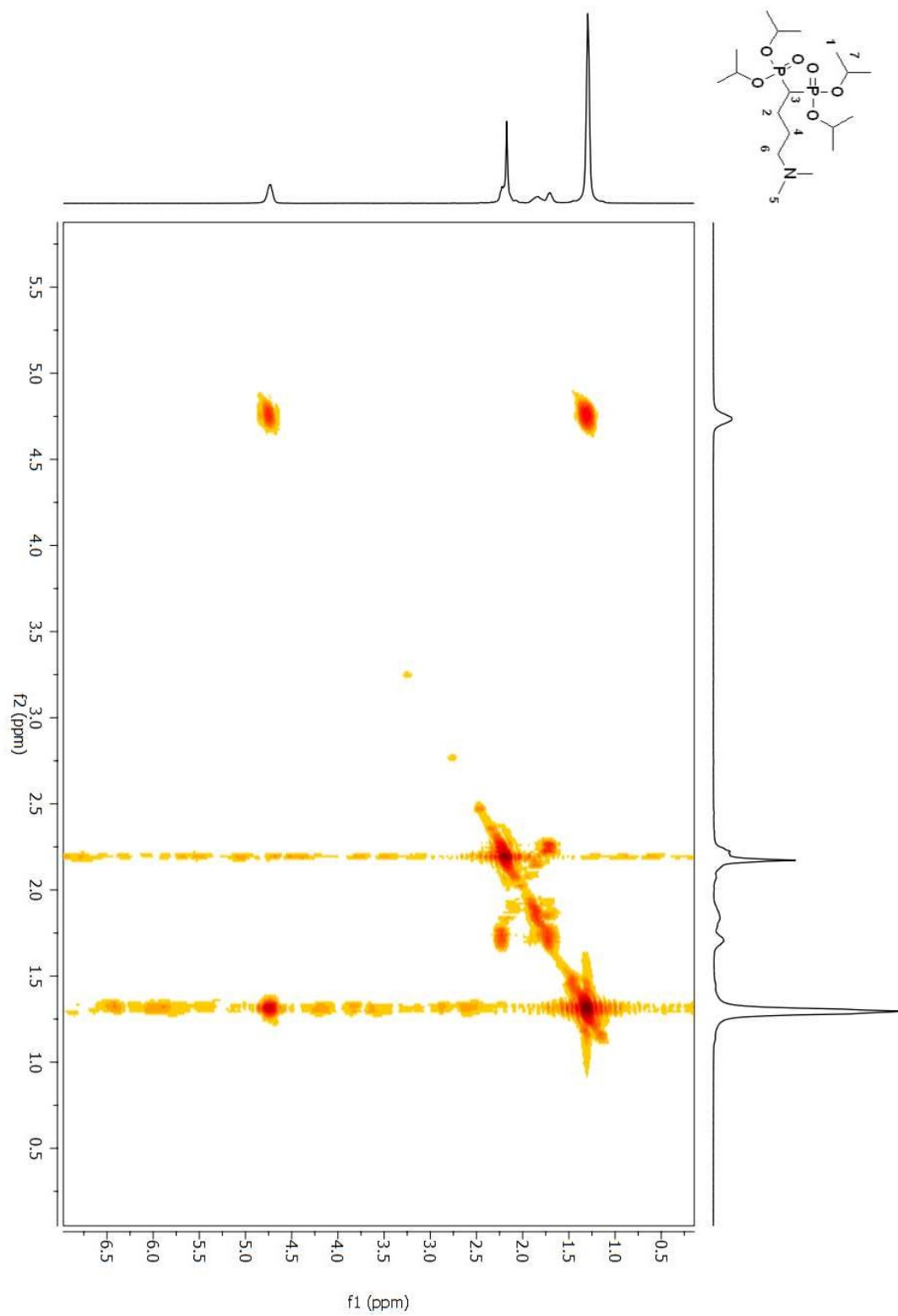


Figure A 181. COSY 2D NMR spectrum of compound (**96**) in CDCl₃.

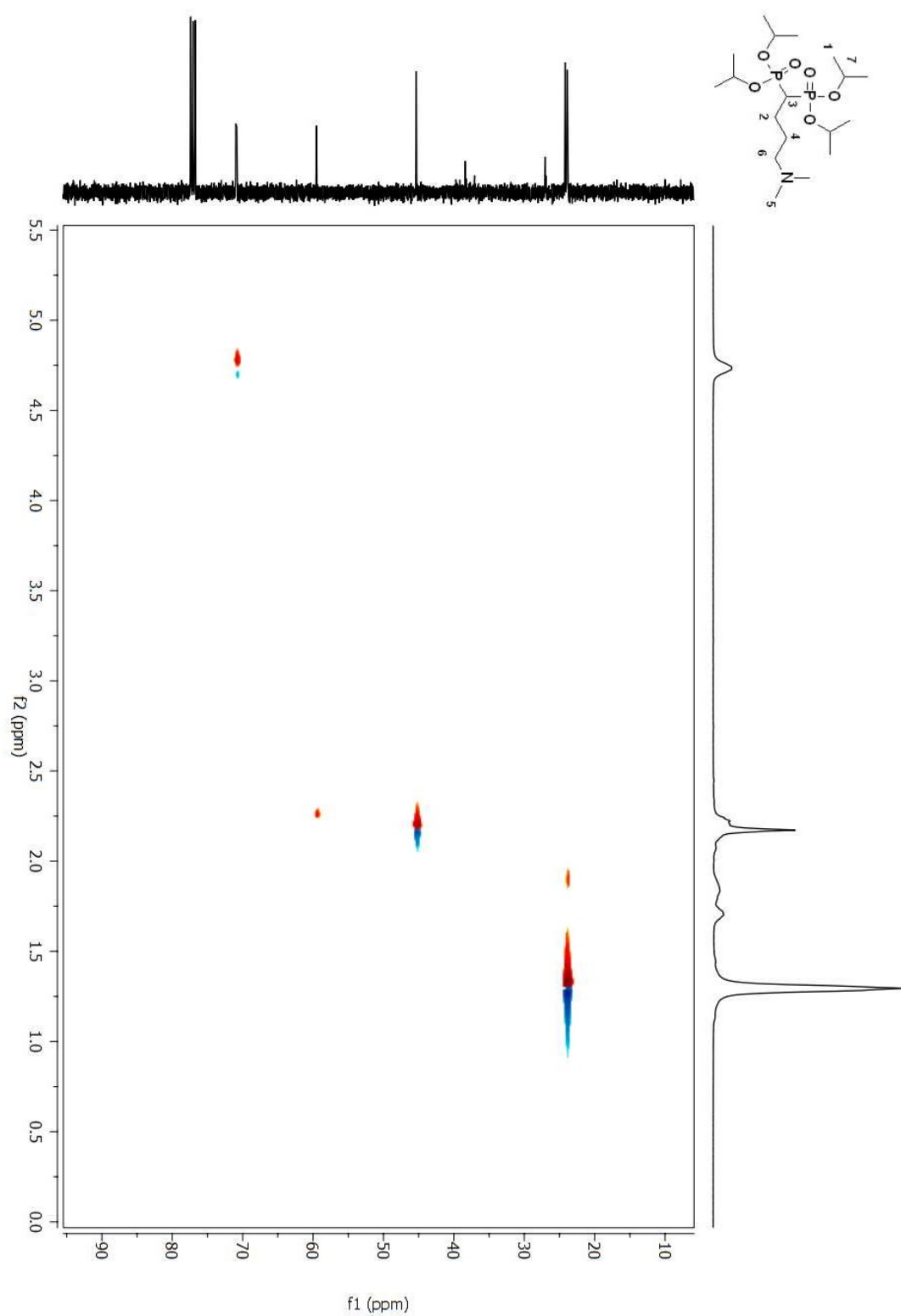


Figure A 182. HSQC 2D NMR spectrum of compound (**96**) in CDCl₃.

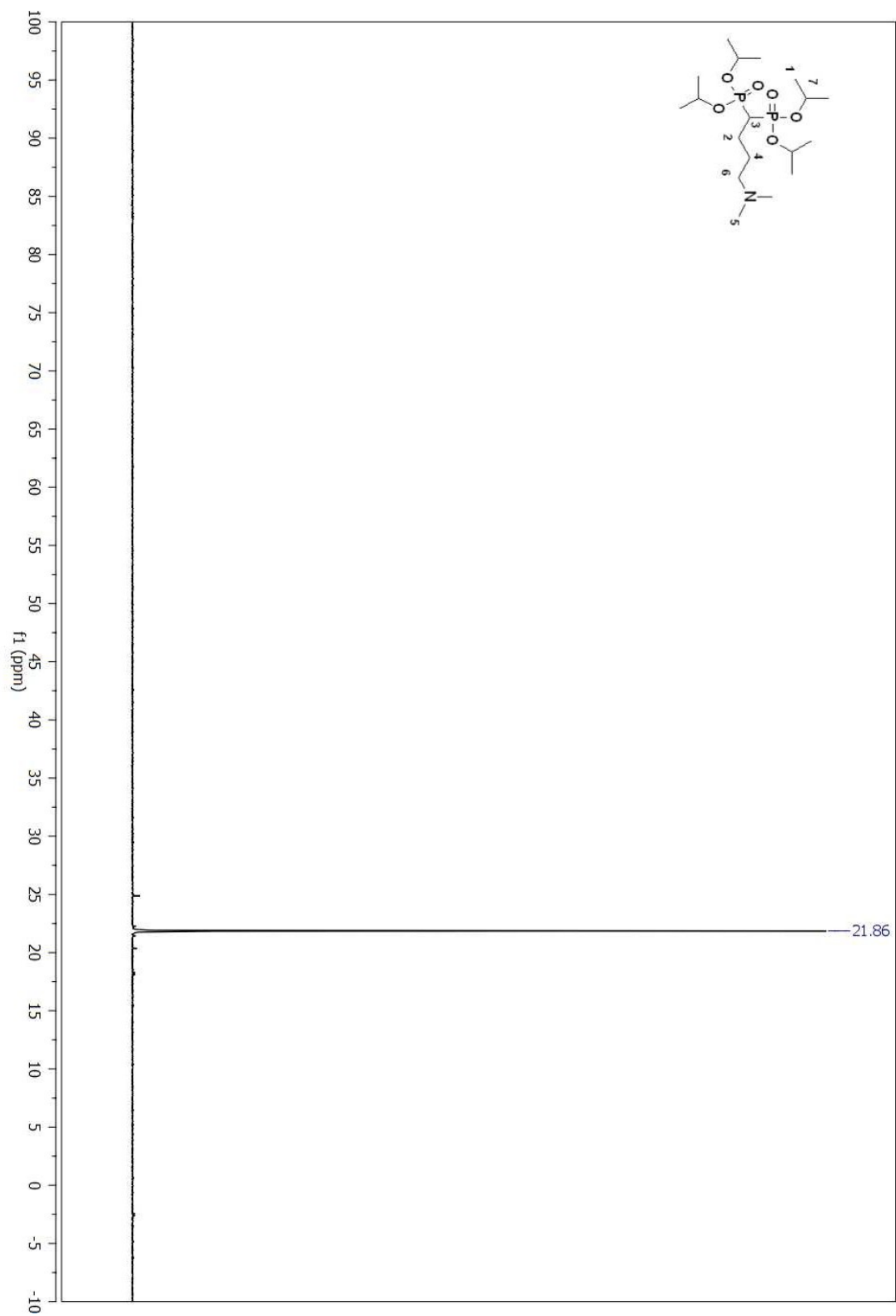


Figure A 183. ^{31}P NMR spectrum of compound (96) in CDCl_3 .

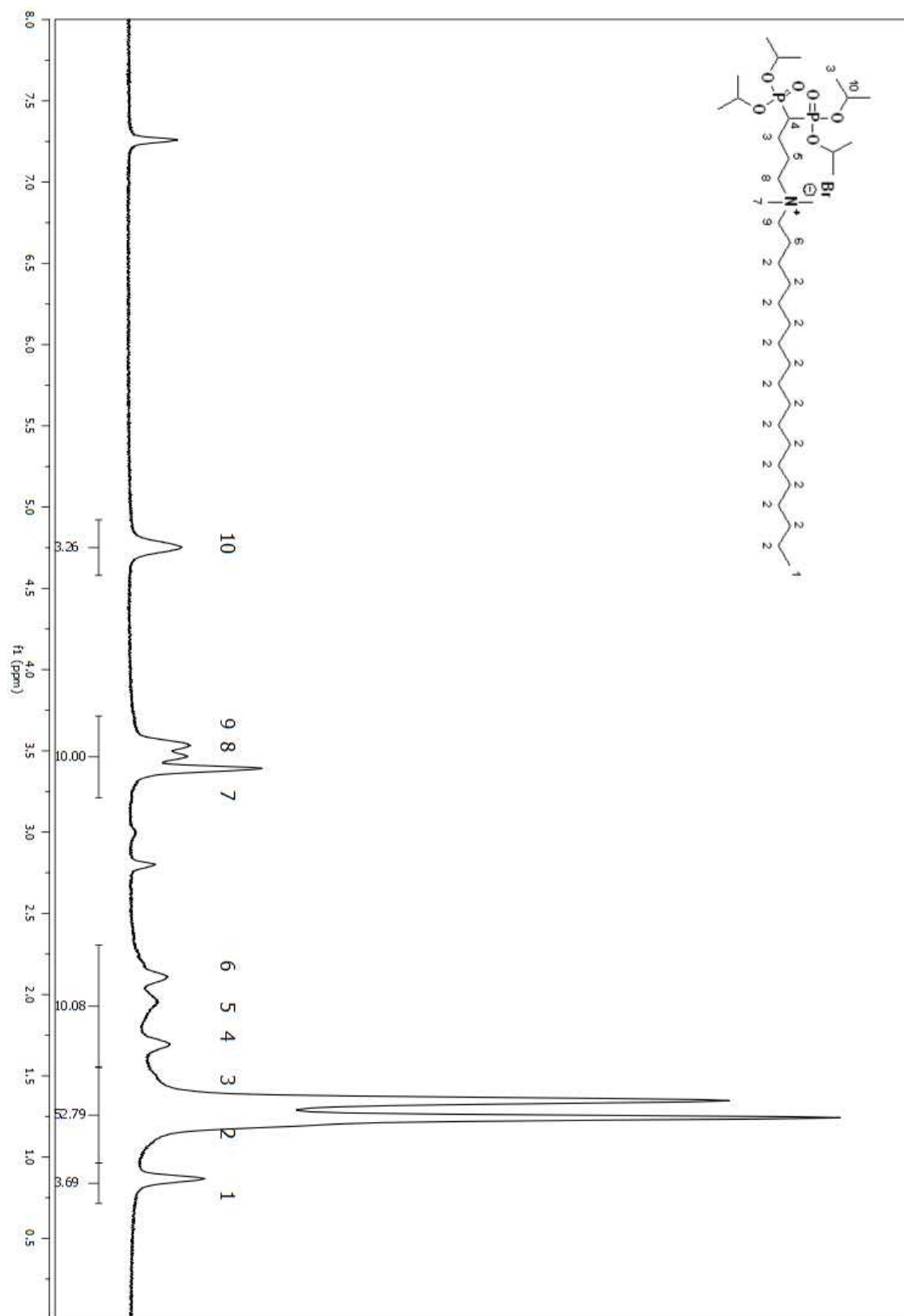


Figure A 184. ^1H NMR spectrum of compound (93) in CDCl_3 .

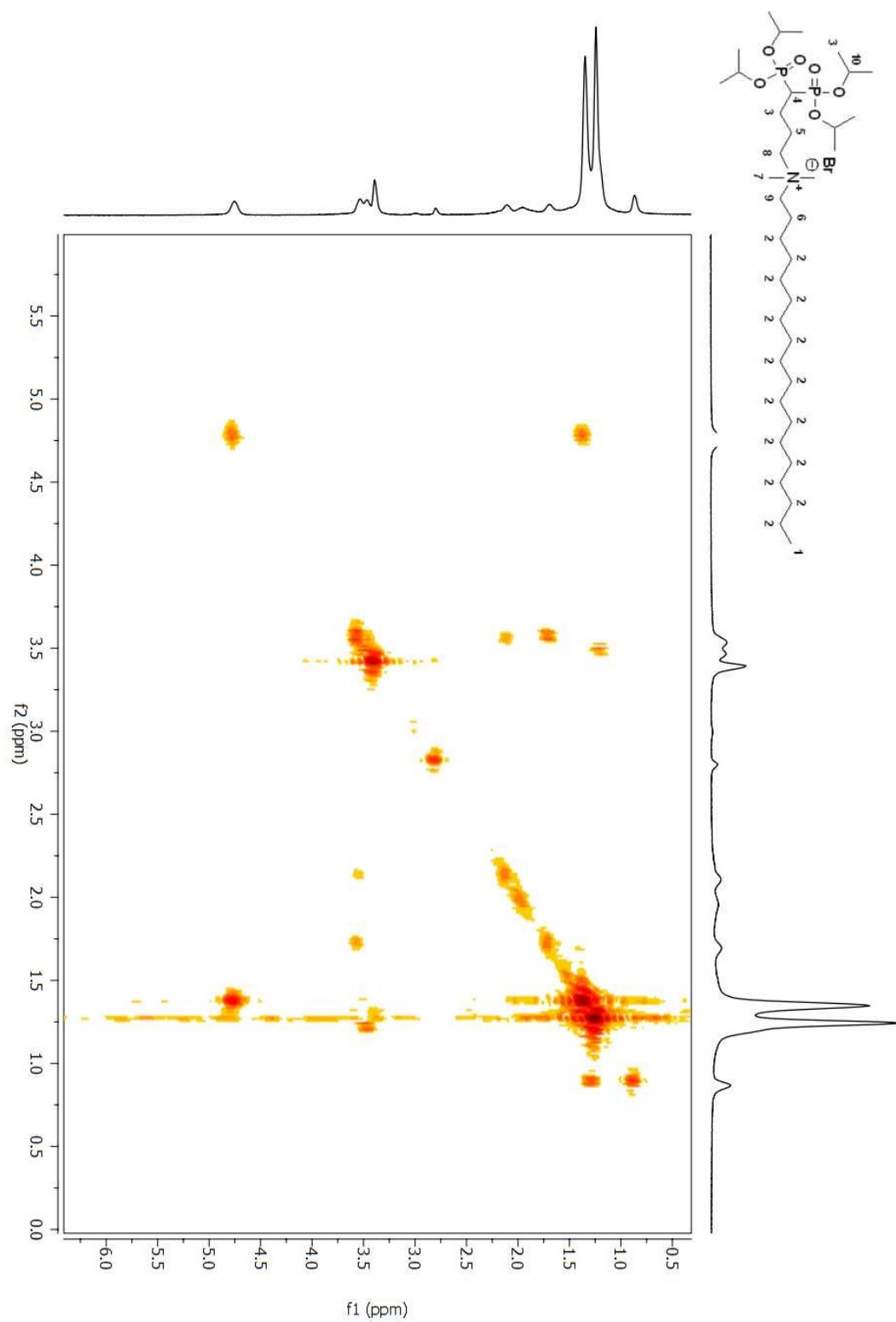


Figure A 185. COSY 2D NMR spectrum of compound (**93**) in CDCl_3 .

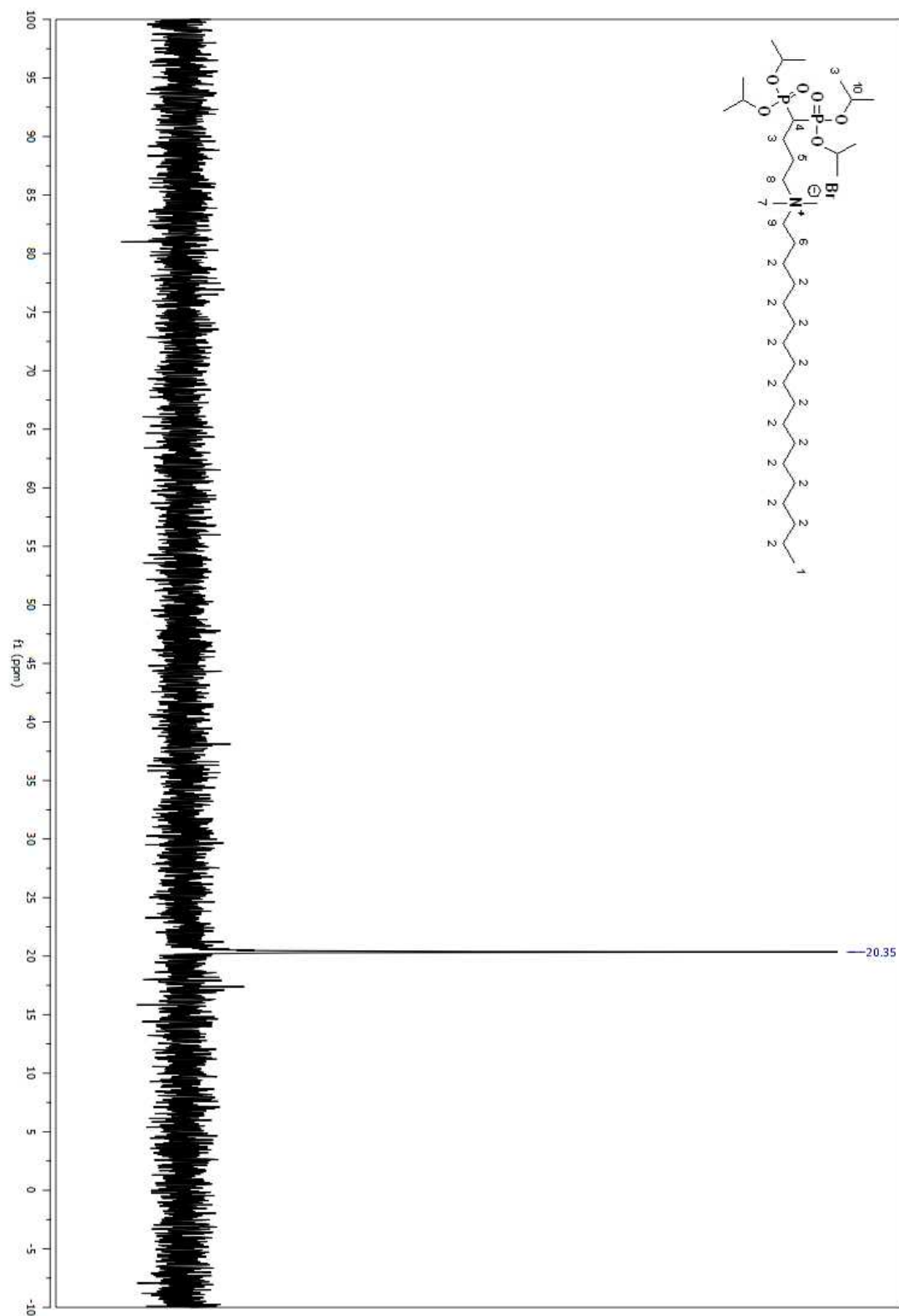


Figure A 187. ^{31}P NMR spectrum of compound (93) in CDCl_3 .

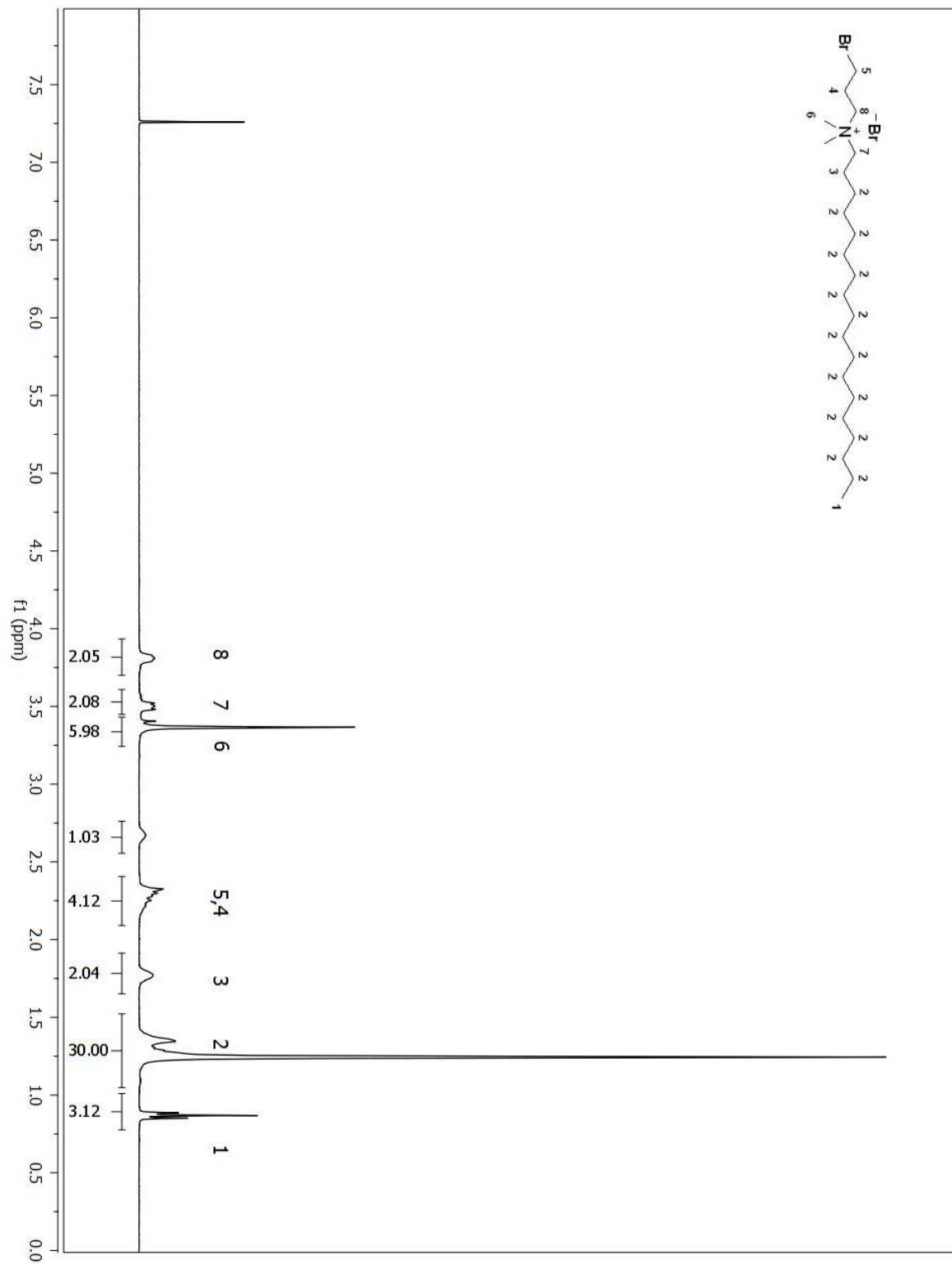


Figure A 188. ^1H NMR spectrum of compound (83) in CDCl_3 .

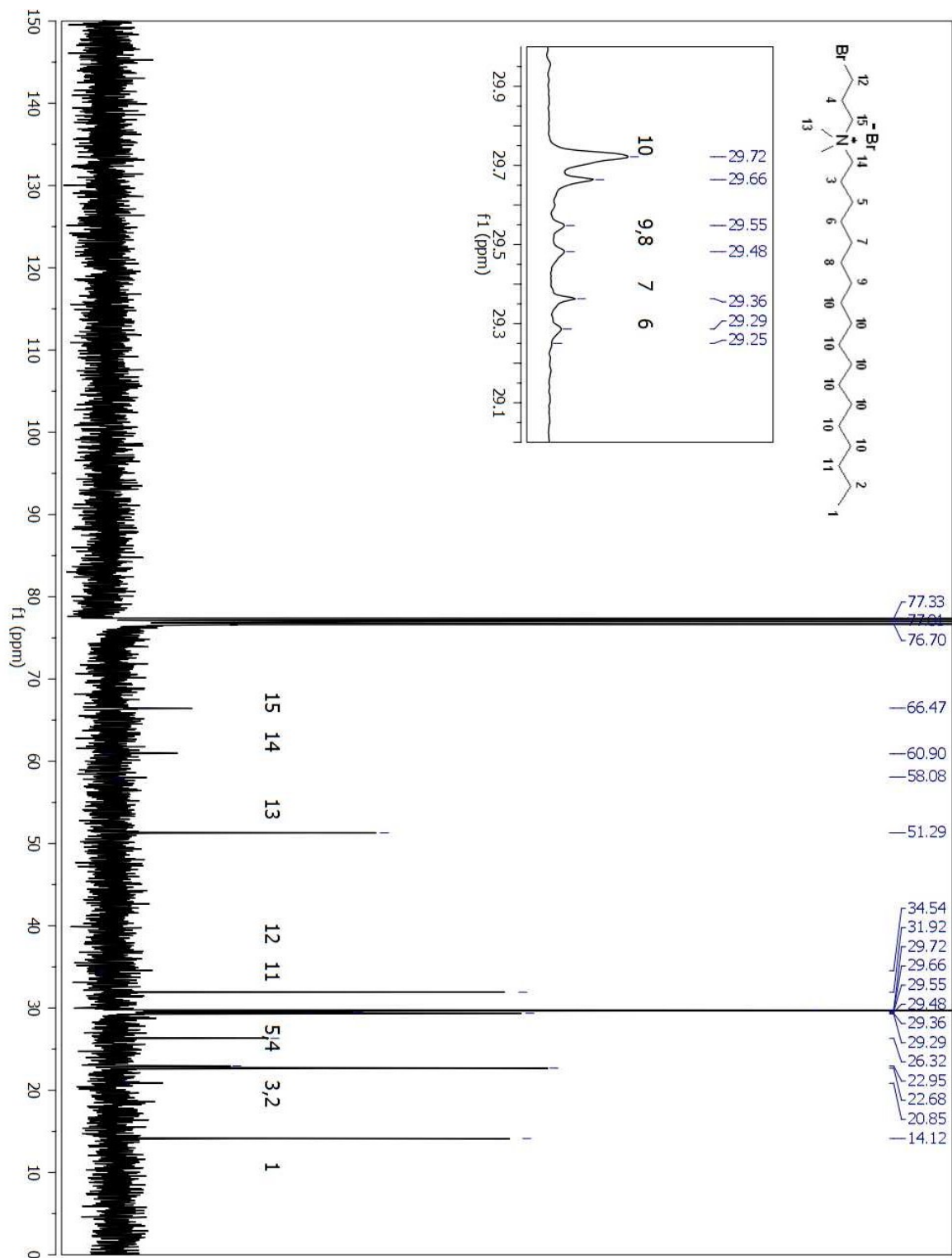


Figure A 189. ¹³C NMR spectrum of compound (83) in CDCl₃.

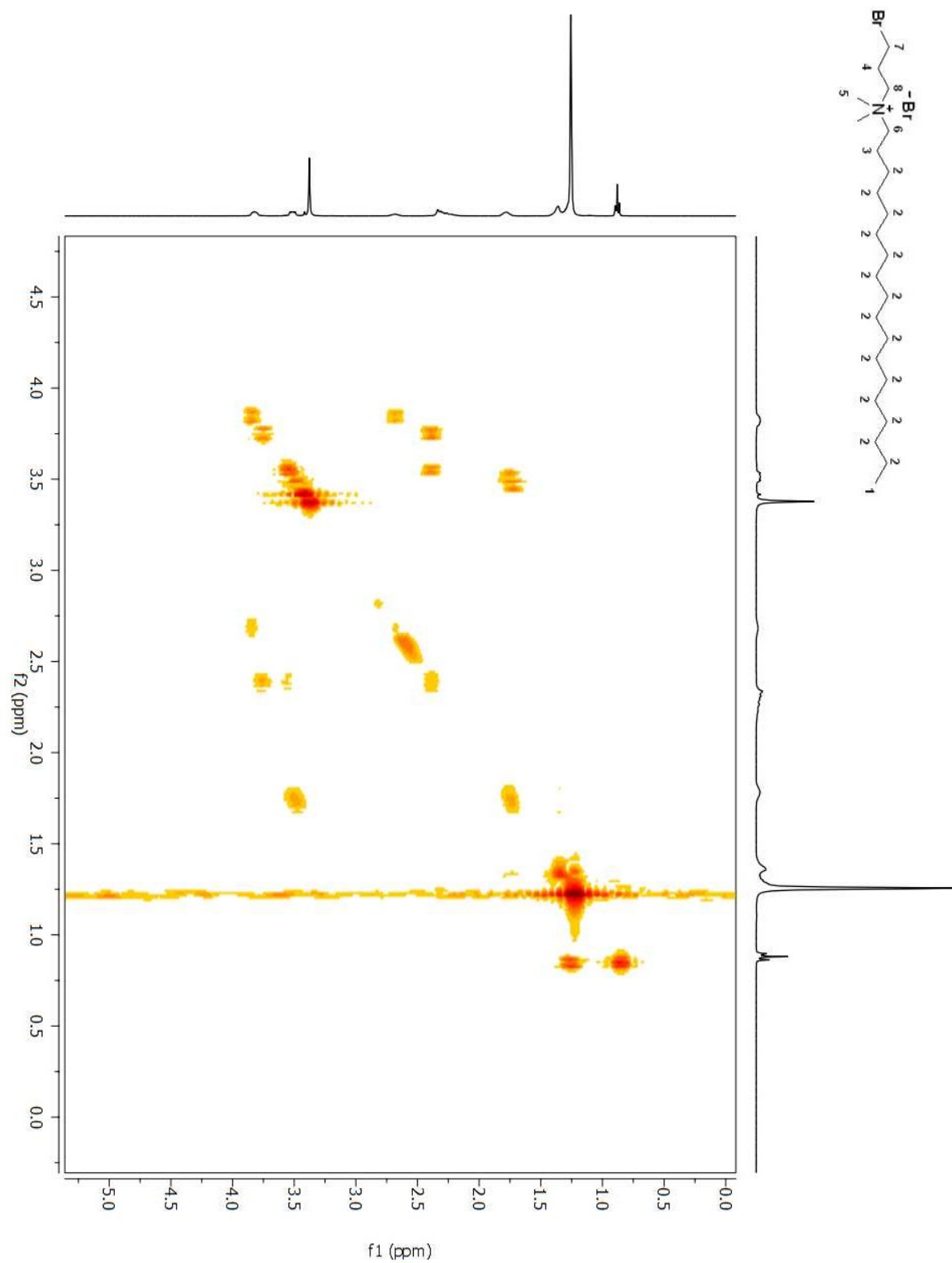


Figure A 190. COSY 2D NMR spectrum of compound (**83**) in CDCl₃.

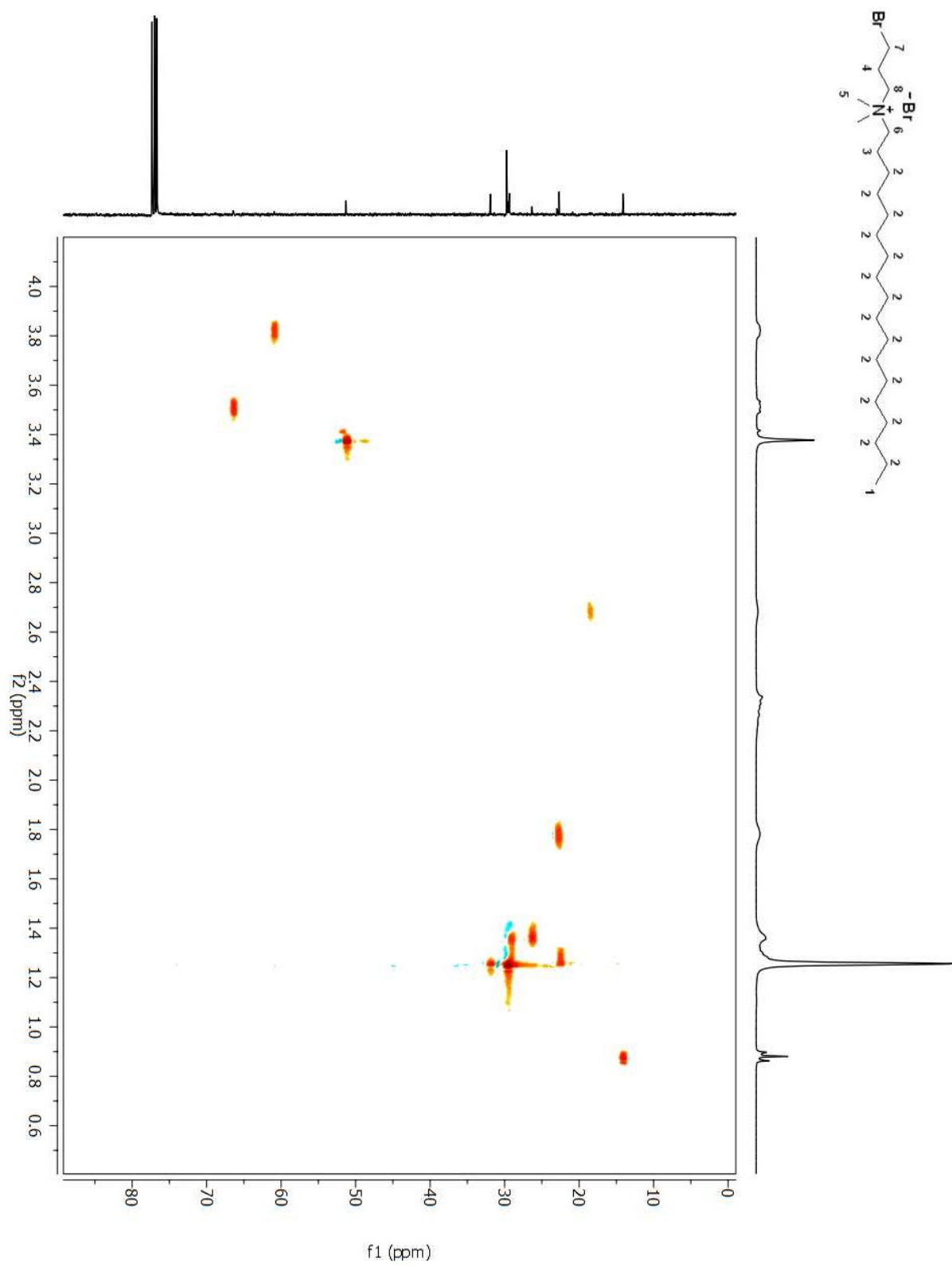


Figure A 191. HSQC 2D NMR spectrum of compound (**83**) in CDCl_3 .

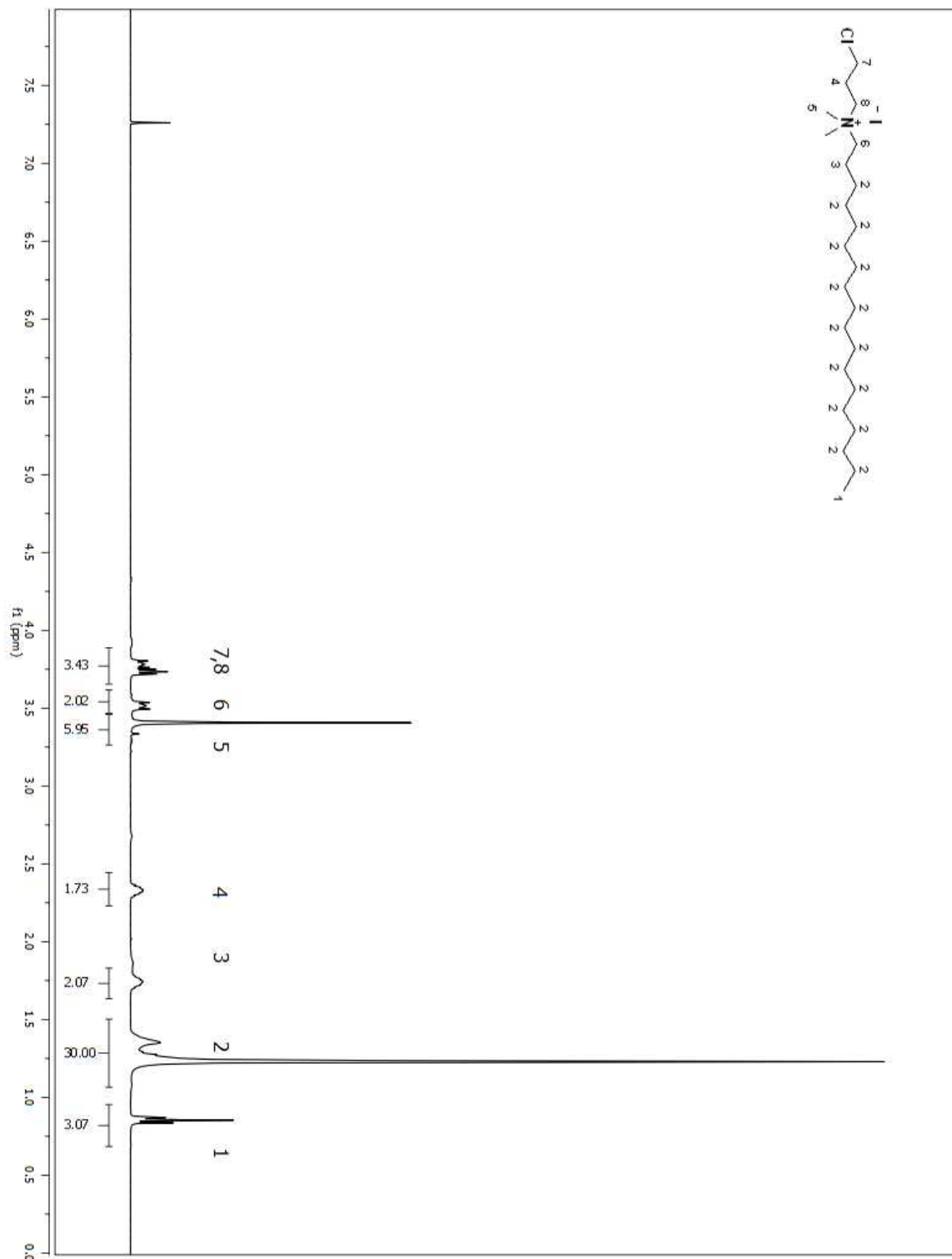


Figure A 192. ¹H NMR spectrum of compound (102) in CDCl₃.

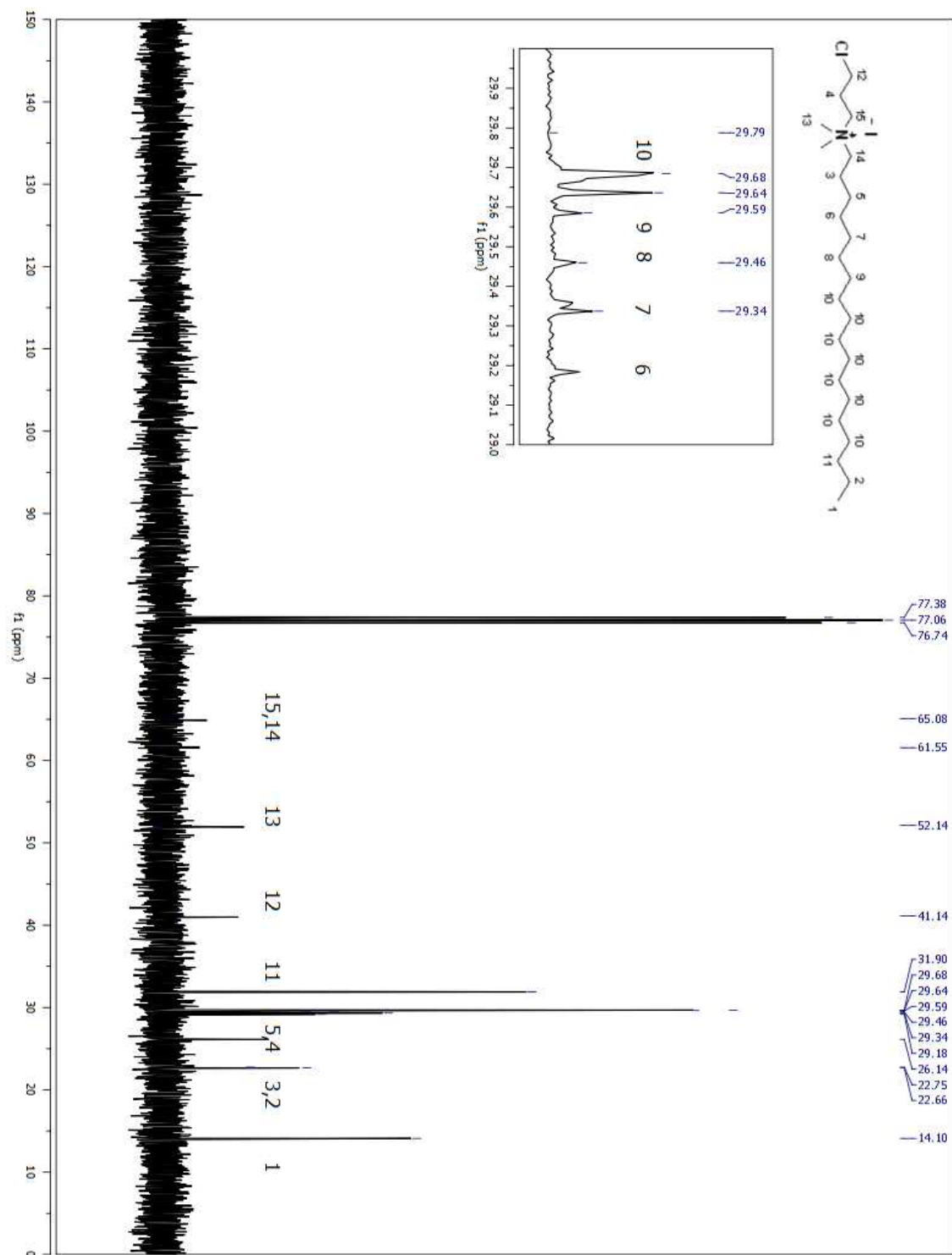


Figure A 193. ¹³C NMR spectrum of compound (102) in CDCl₃.

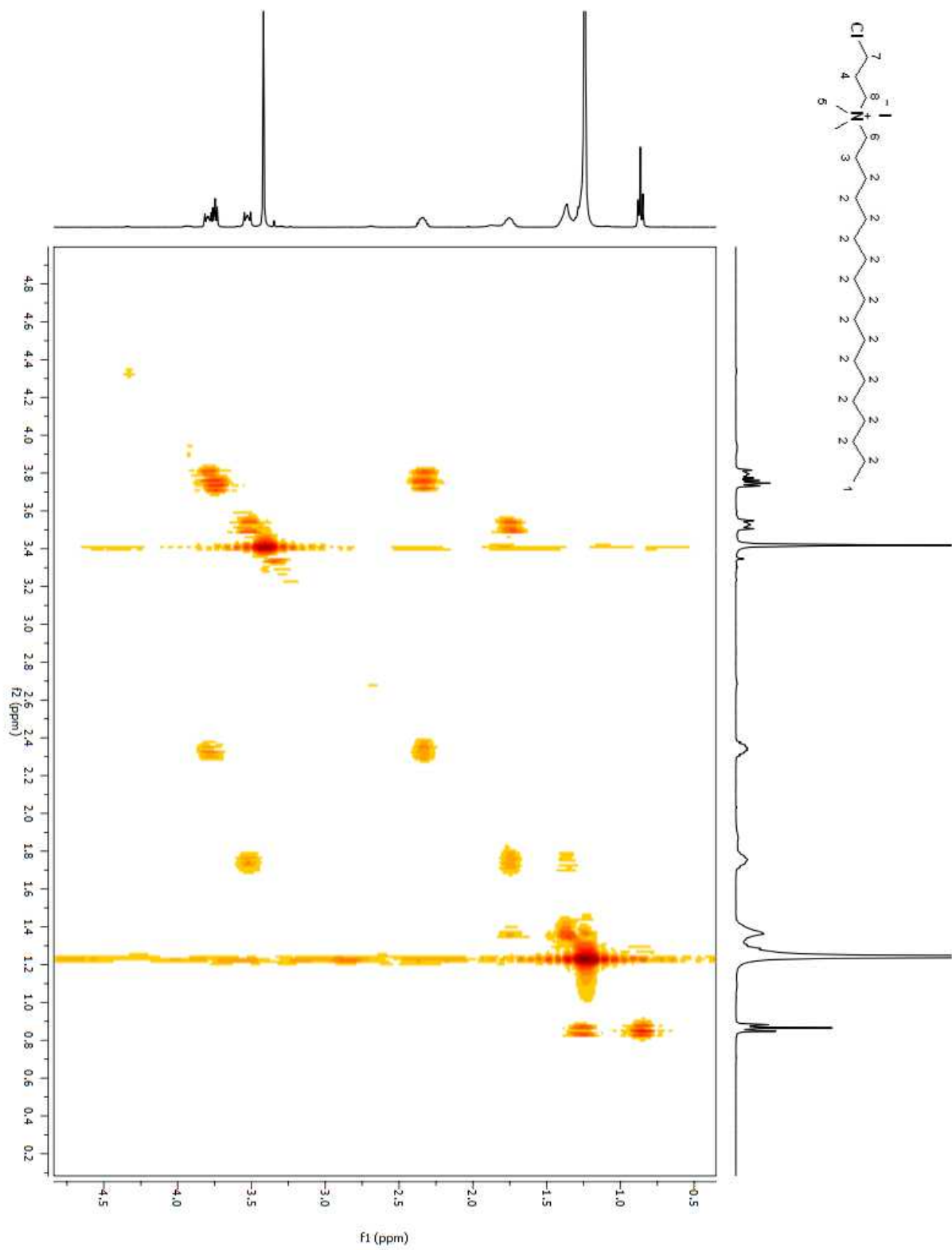


Figure A 194. COSY 2D NMR spectrum of compound (102) in CDCl₃.

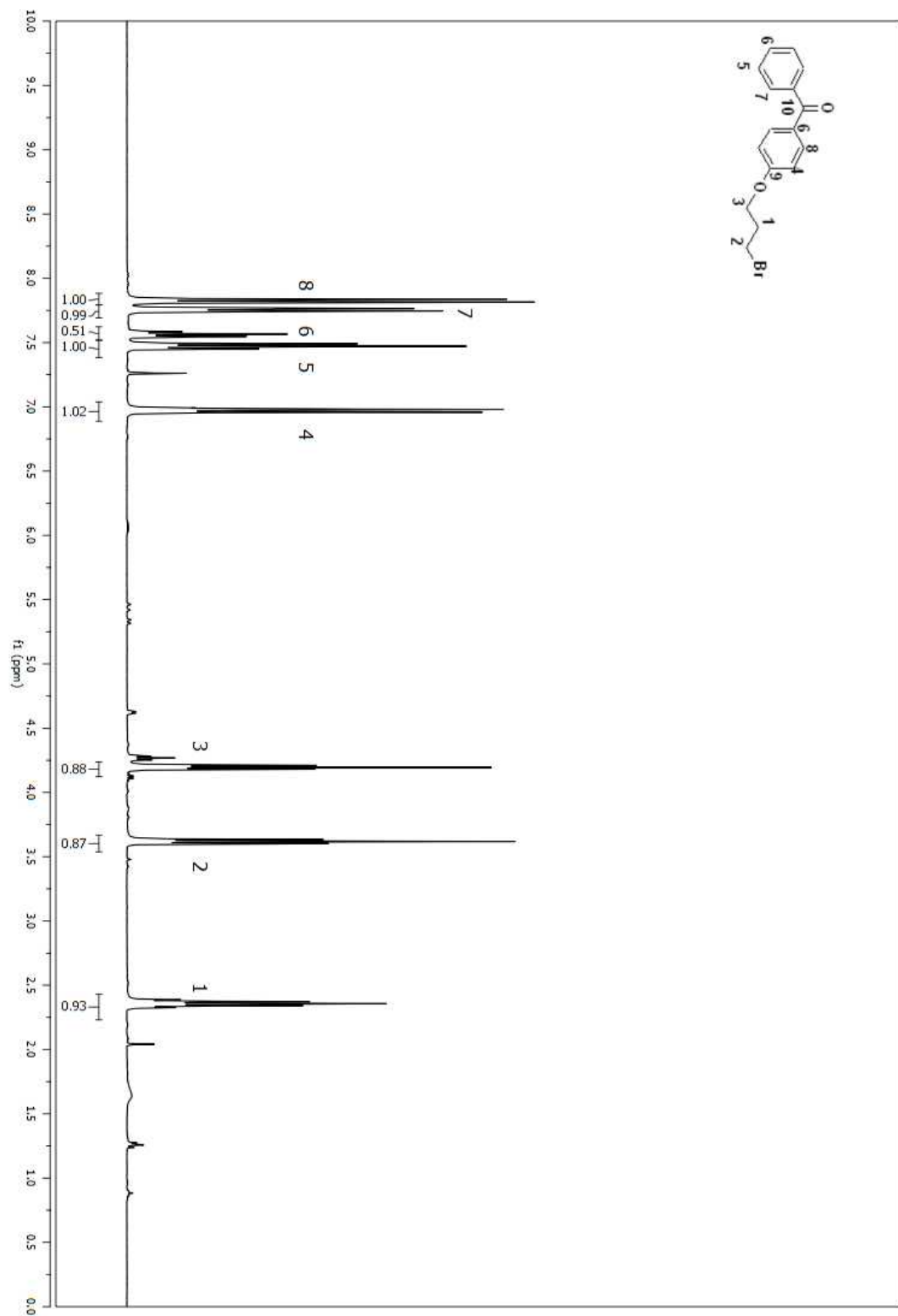


Figure A 196. ¹H NMR spectrum of compound (202) in CDCl₃.

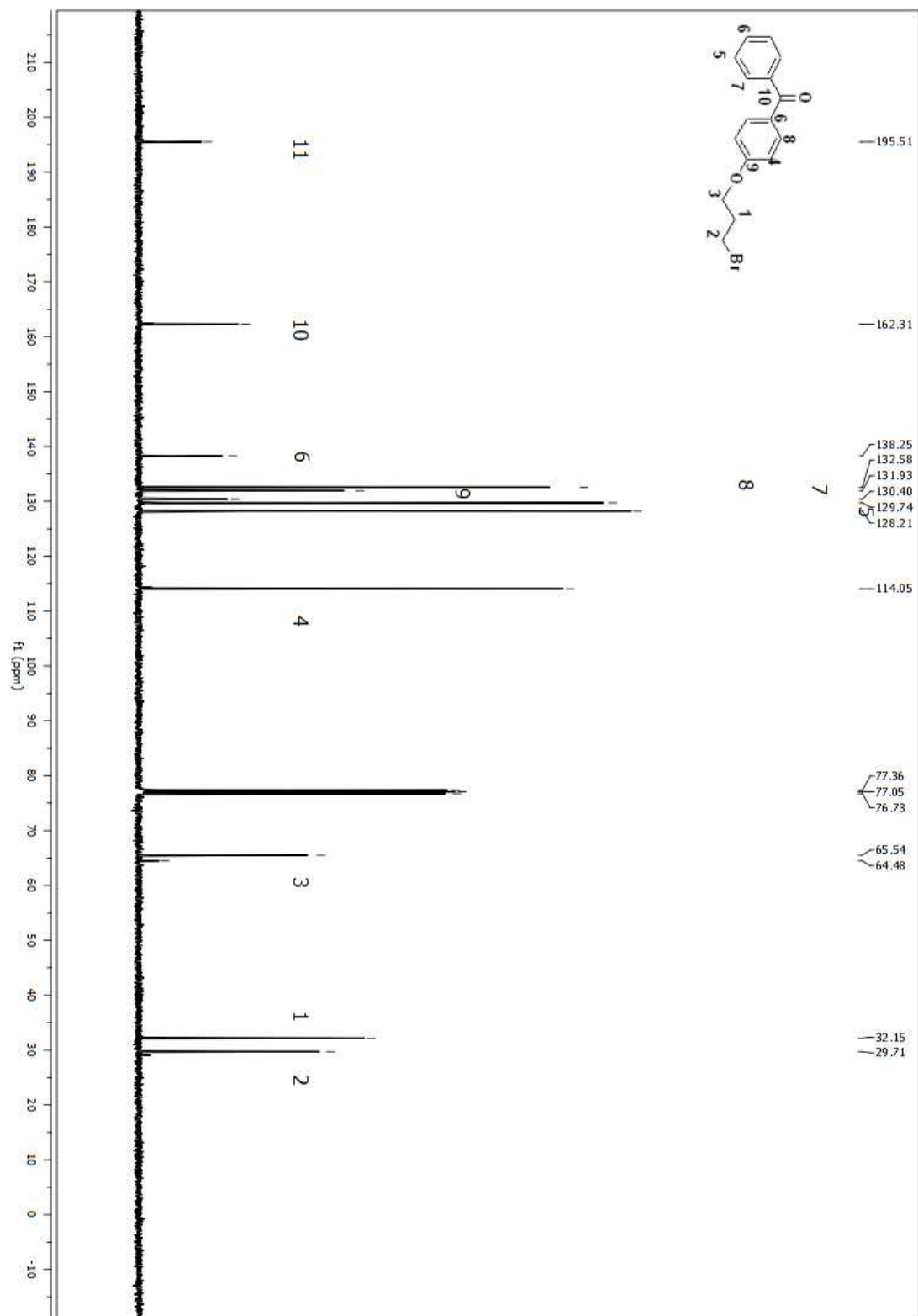


Figure A 197. ^{13}C NMR spectrum of compound (202) in CDCl₃.

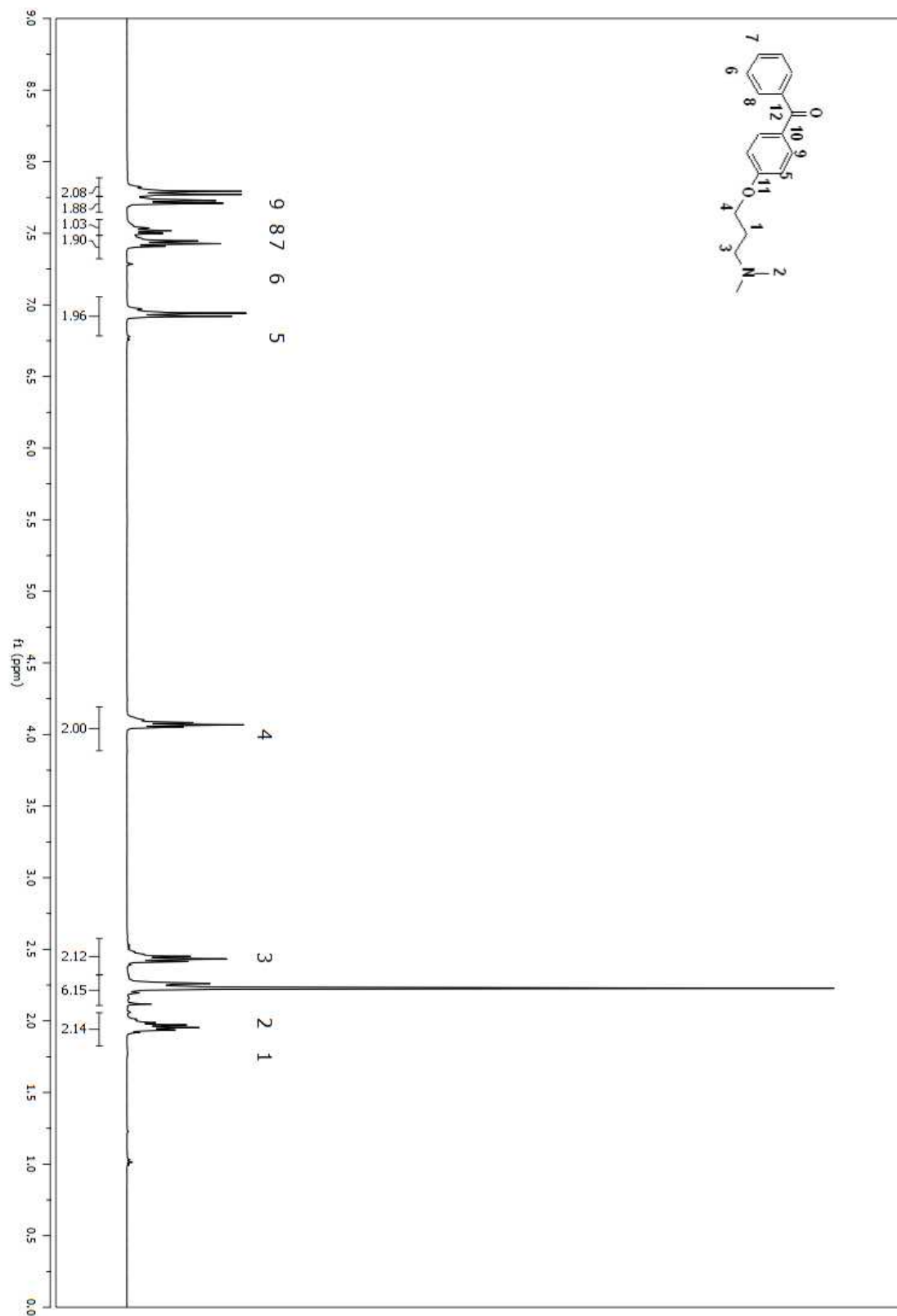


Figure A 198. ^1H NMR spectrum of compound (204) in CDCl₃.

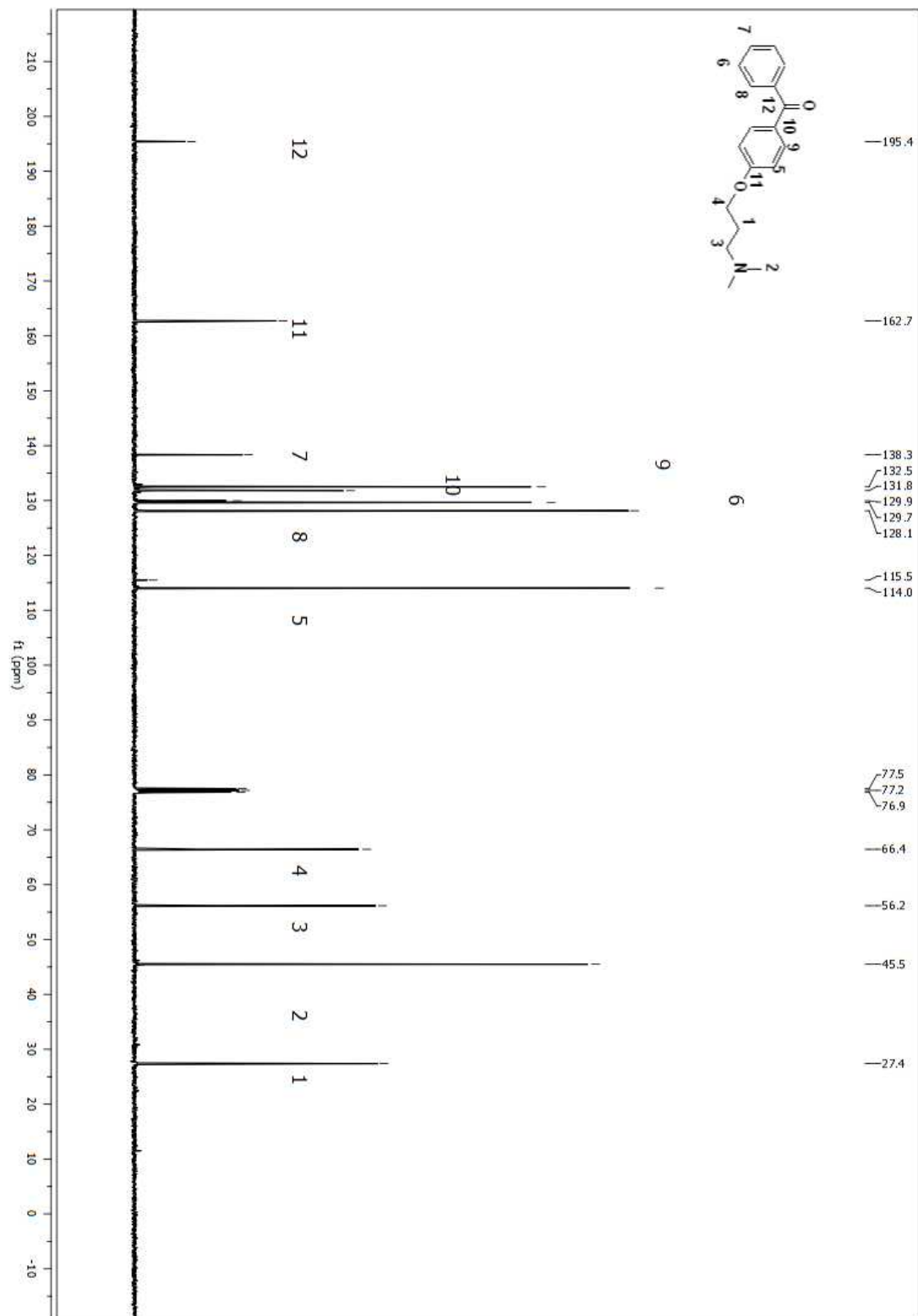


Figure A 199. ^{13}C NMR spectrum of compound (204) in CDCl_3 .

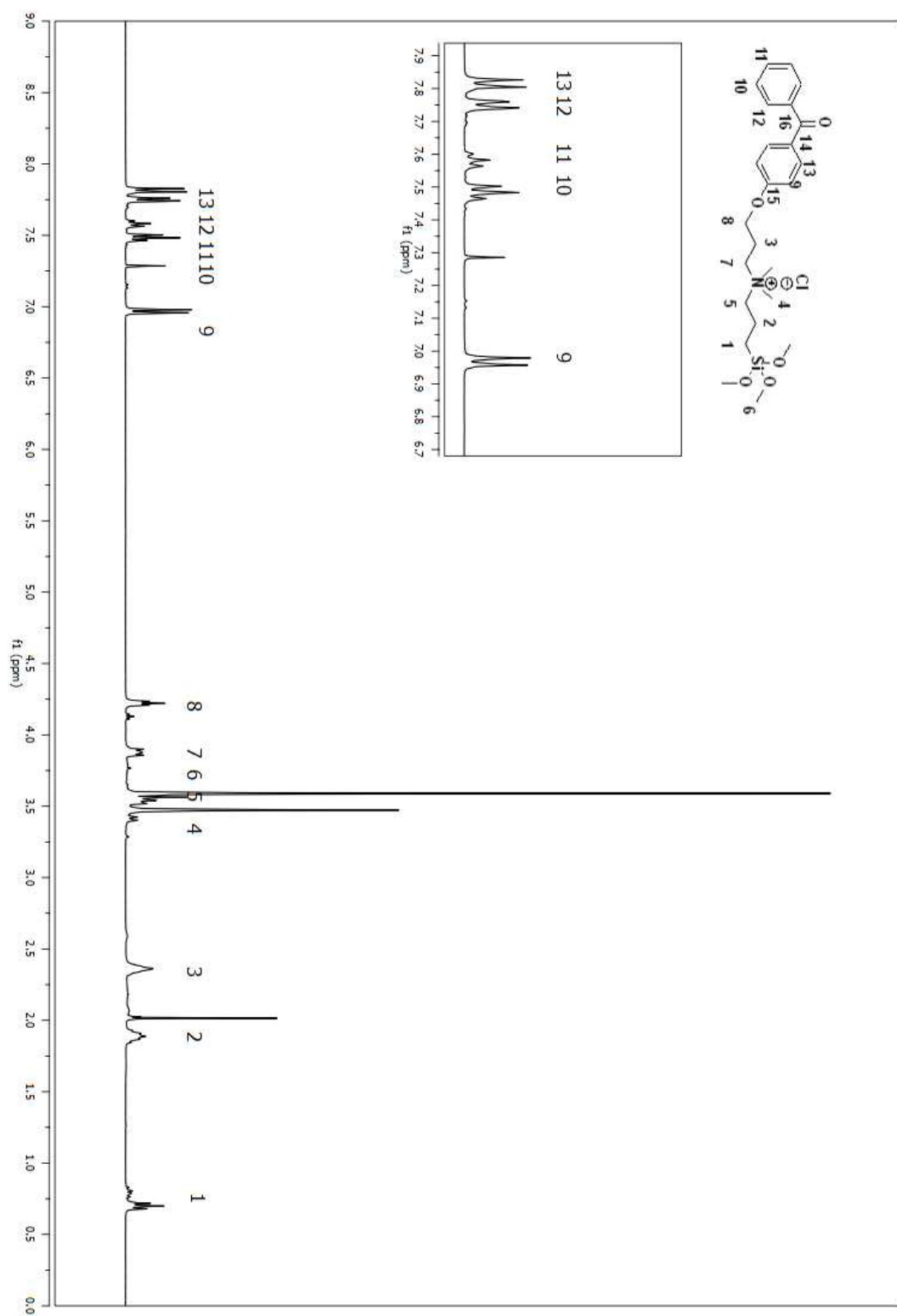


Figure A 200. ^1H NMR spectrum of compound (206) in CDCl_3 .

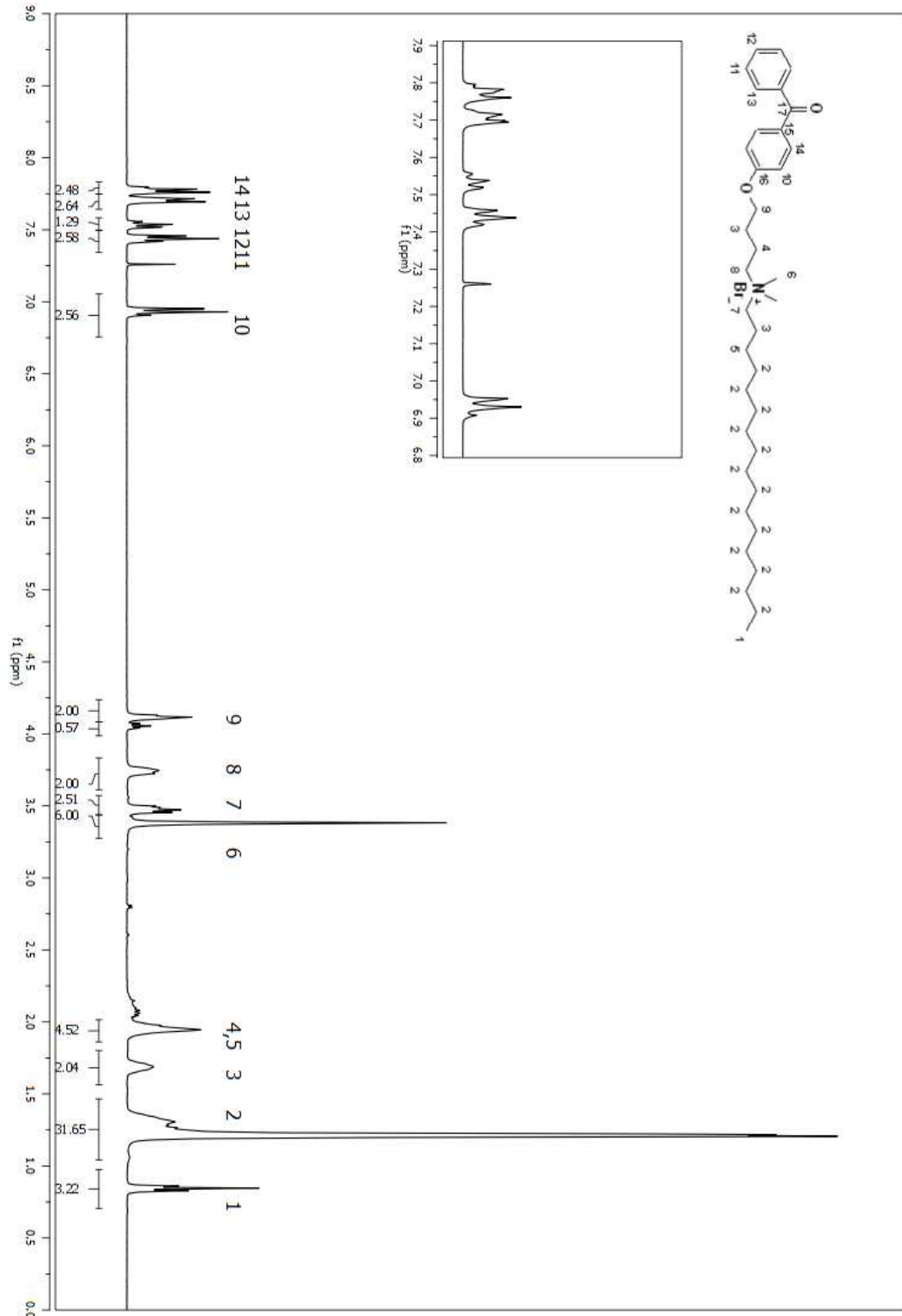


Figure A 202. ¹H NMR spectrum of compound (205) in CDCl₃.

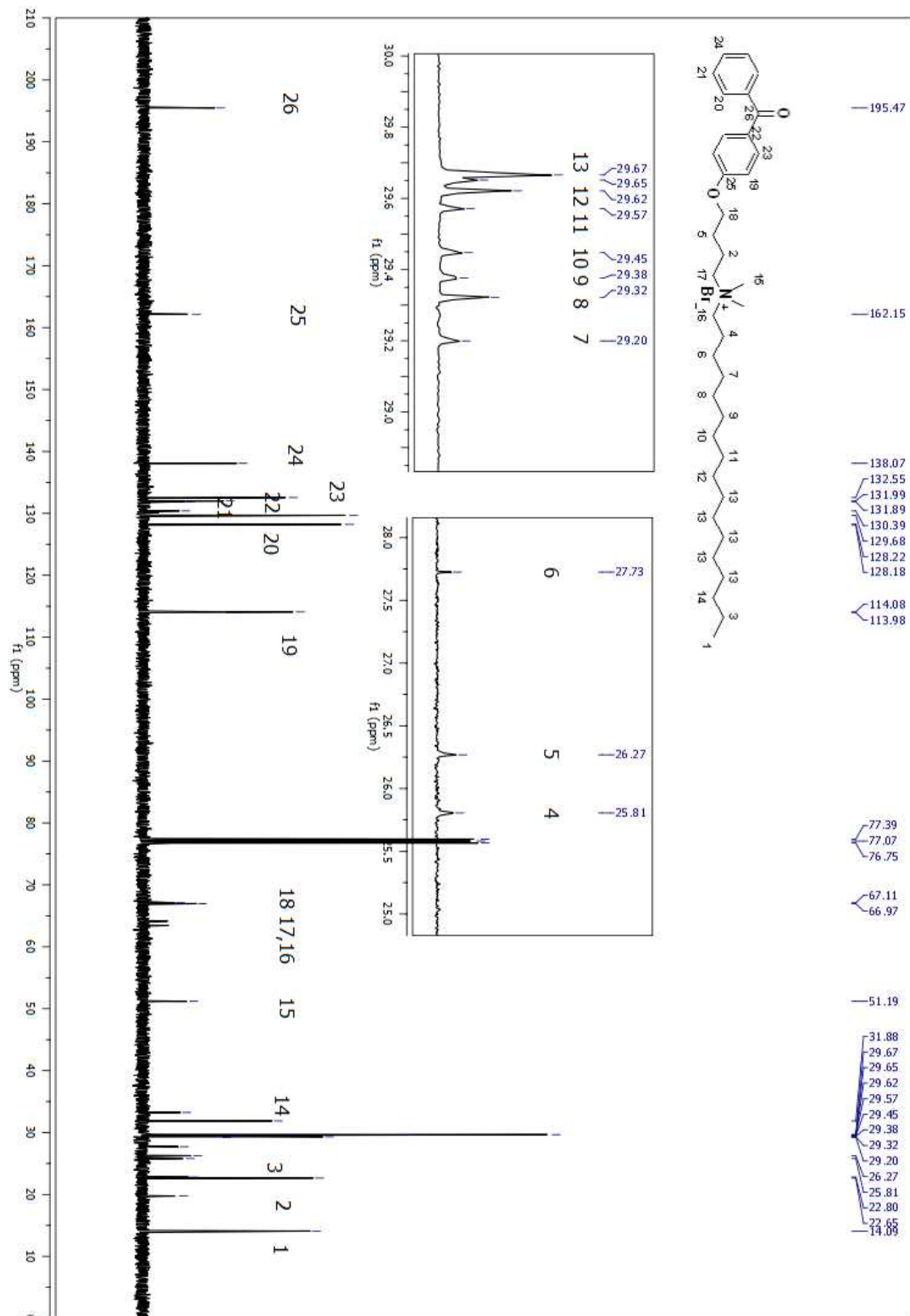


Figure A 203. ^{13}C NMR spectrum of compound (205) in CDCl_3 .

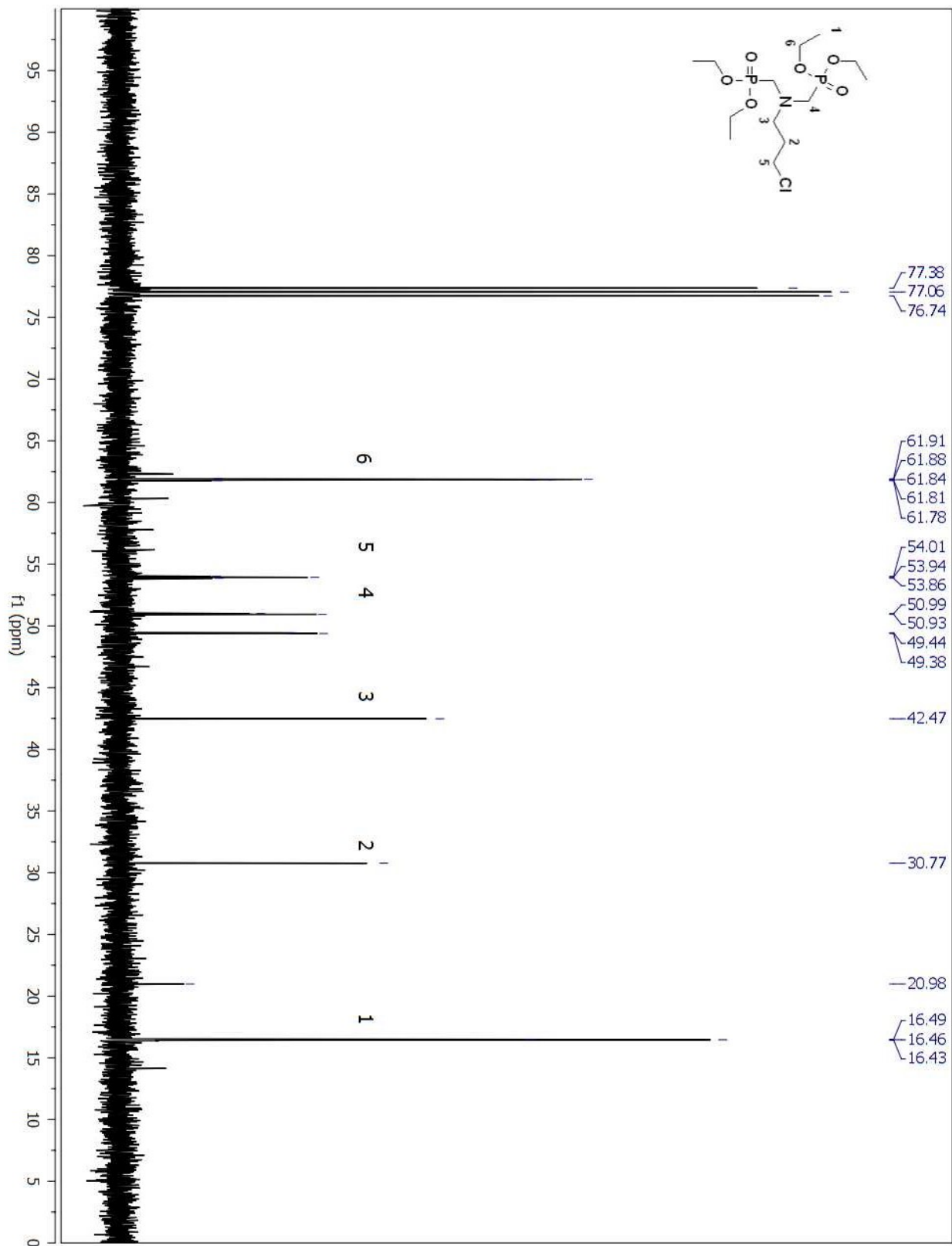


Figure A 204. ¹³C NMR spectrum of compound (114) in CDCl₃.

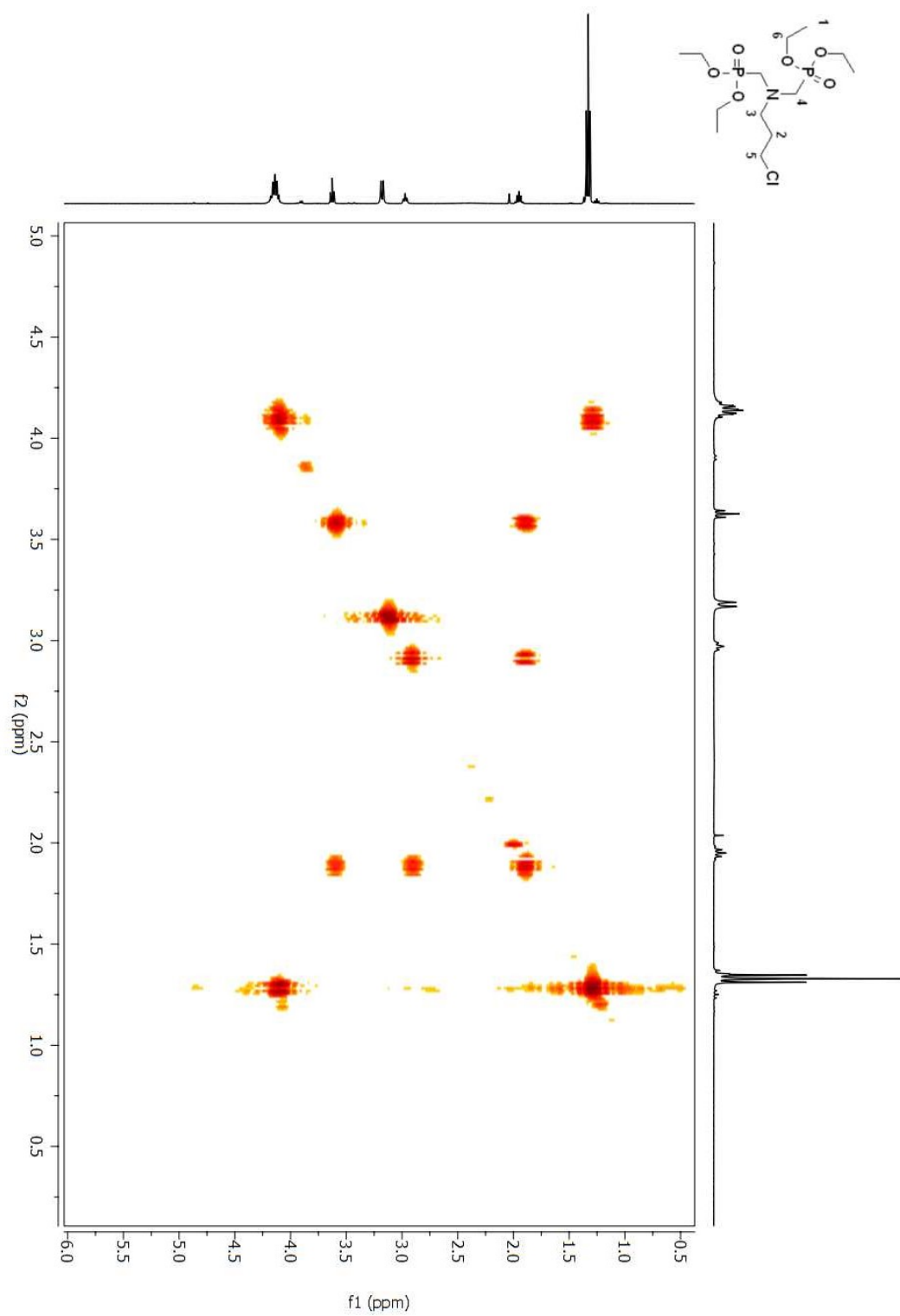


Figure A 205. COSY 2D NMR spectrum of compound (114) in CDCl₃.

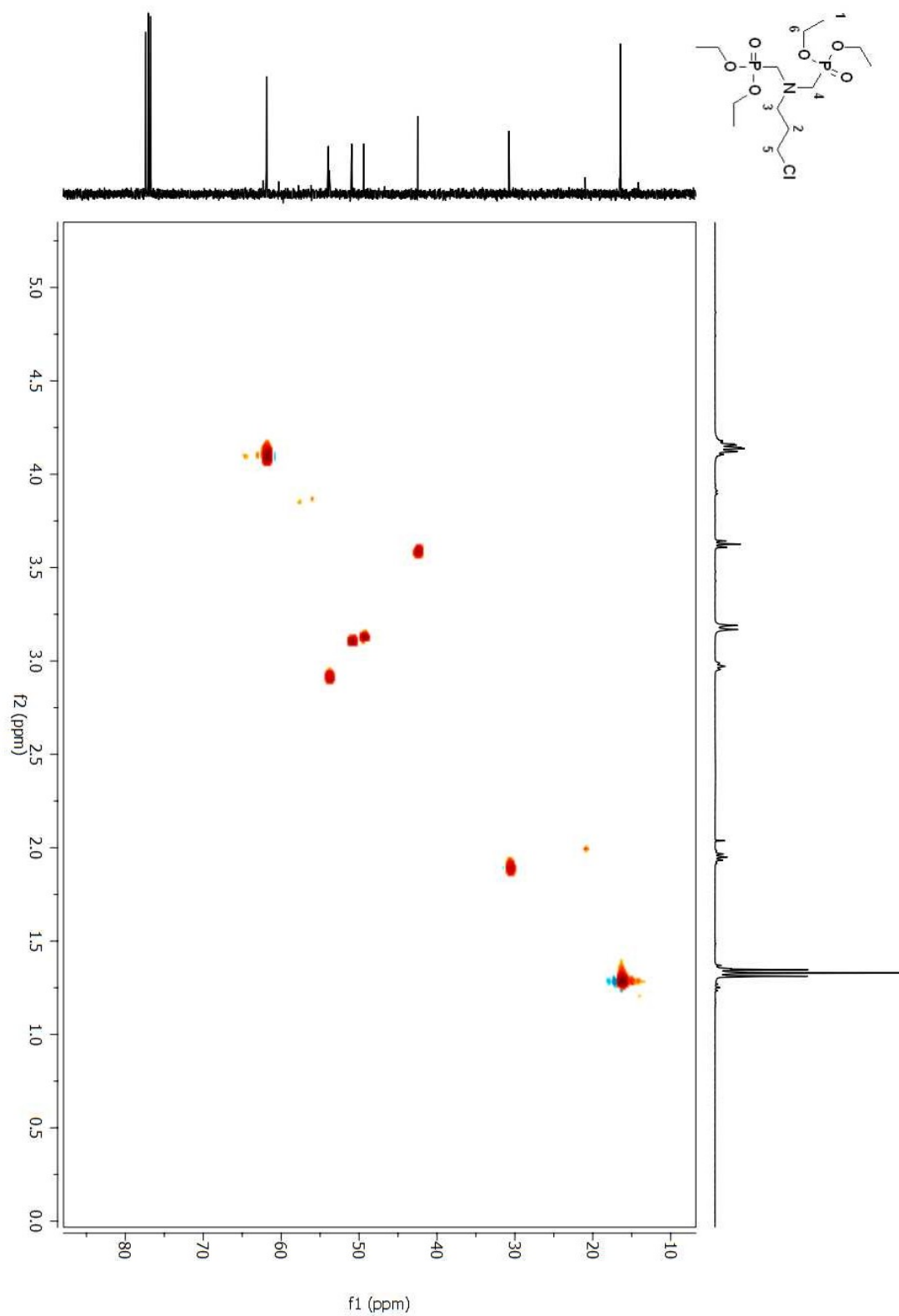


Figure A 206. HSQC 2D NMR spectrum of compound (114) in CDCl₃.

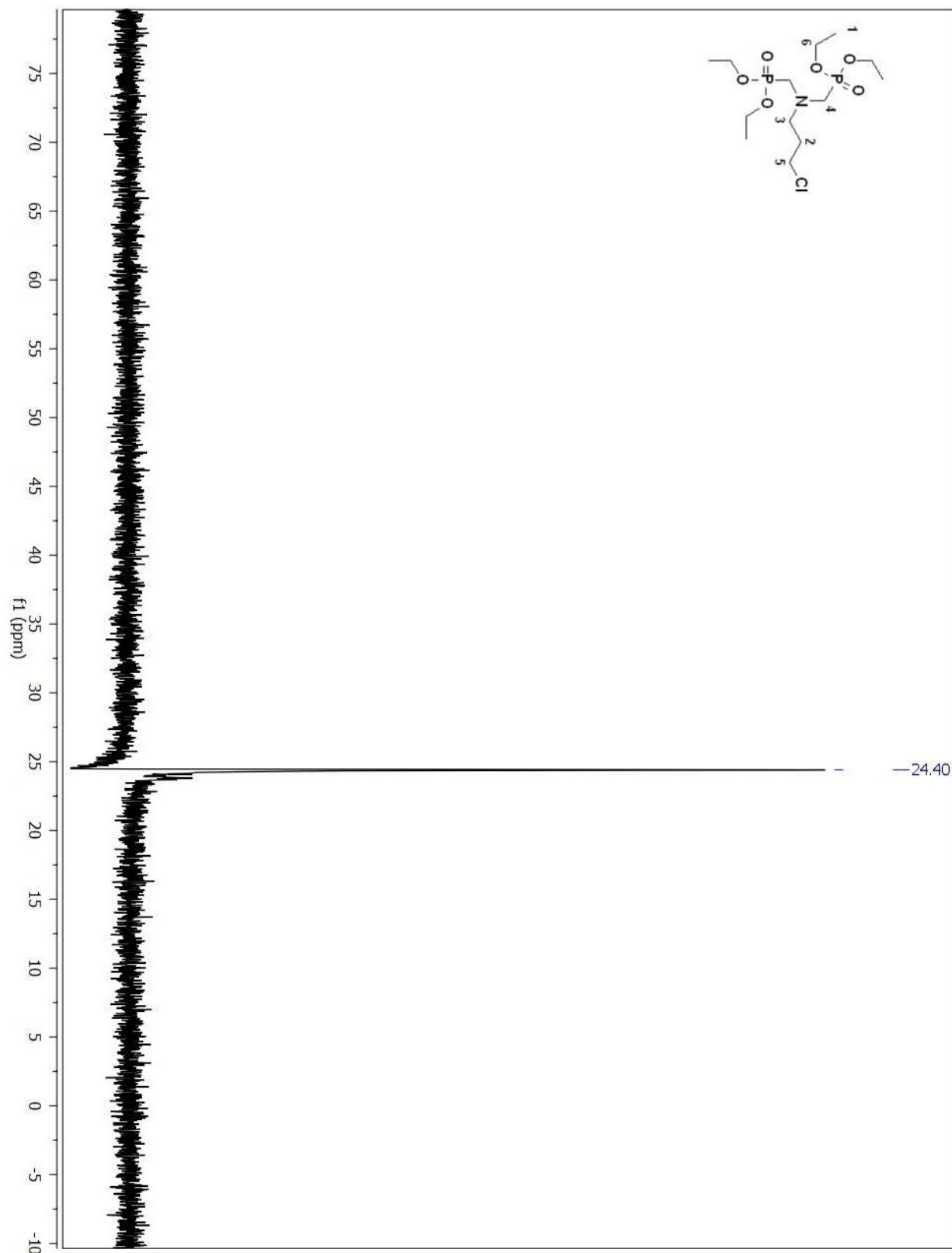


Figure A 207. ^{31}P NMR spectrum of compound (114) in CDCl_3 .

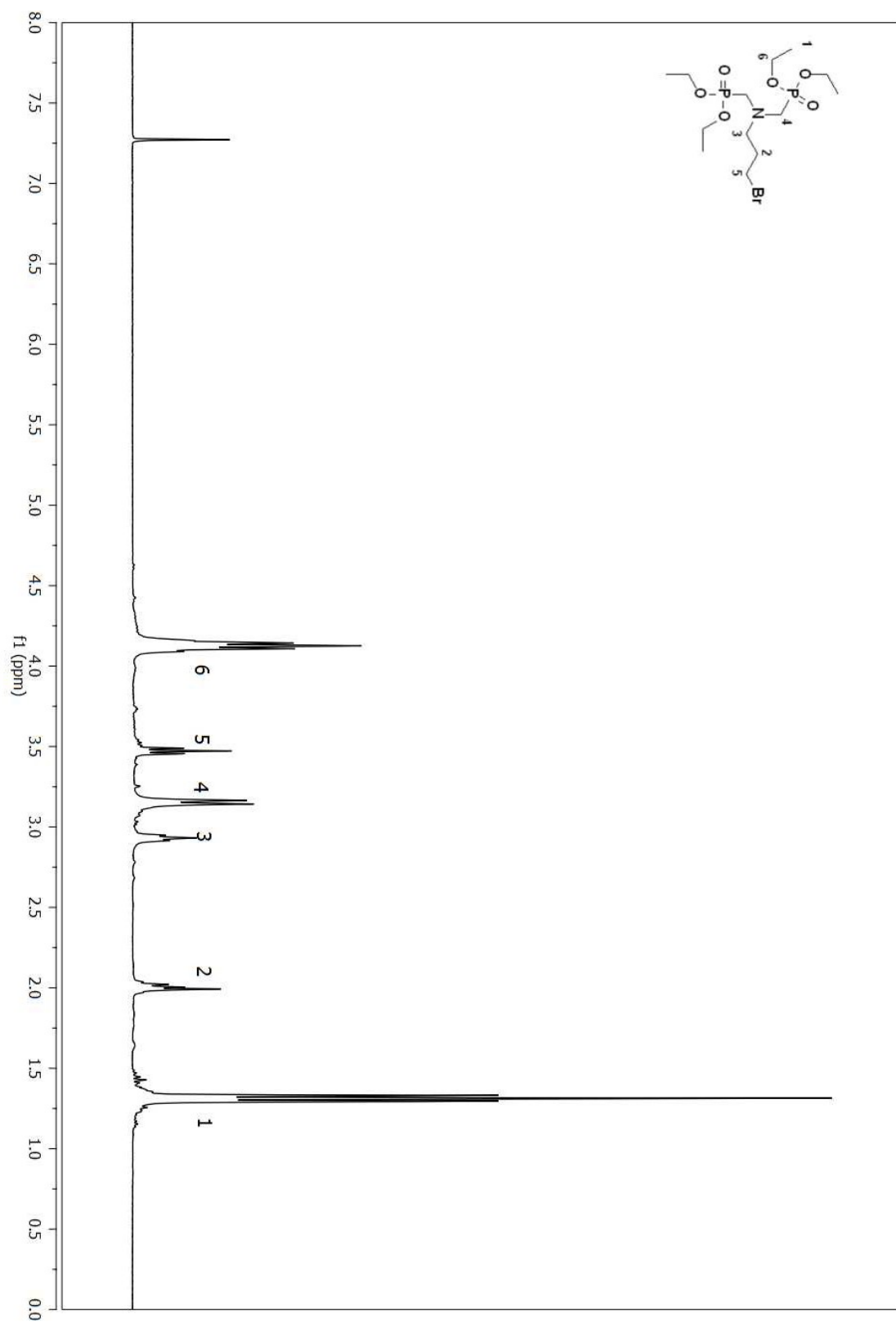


Figure A 208. ¹H NMR spectrum of compound (116) in CDCl₃.

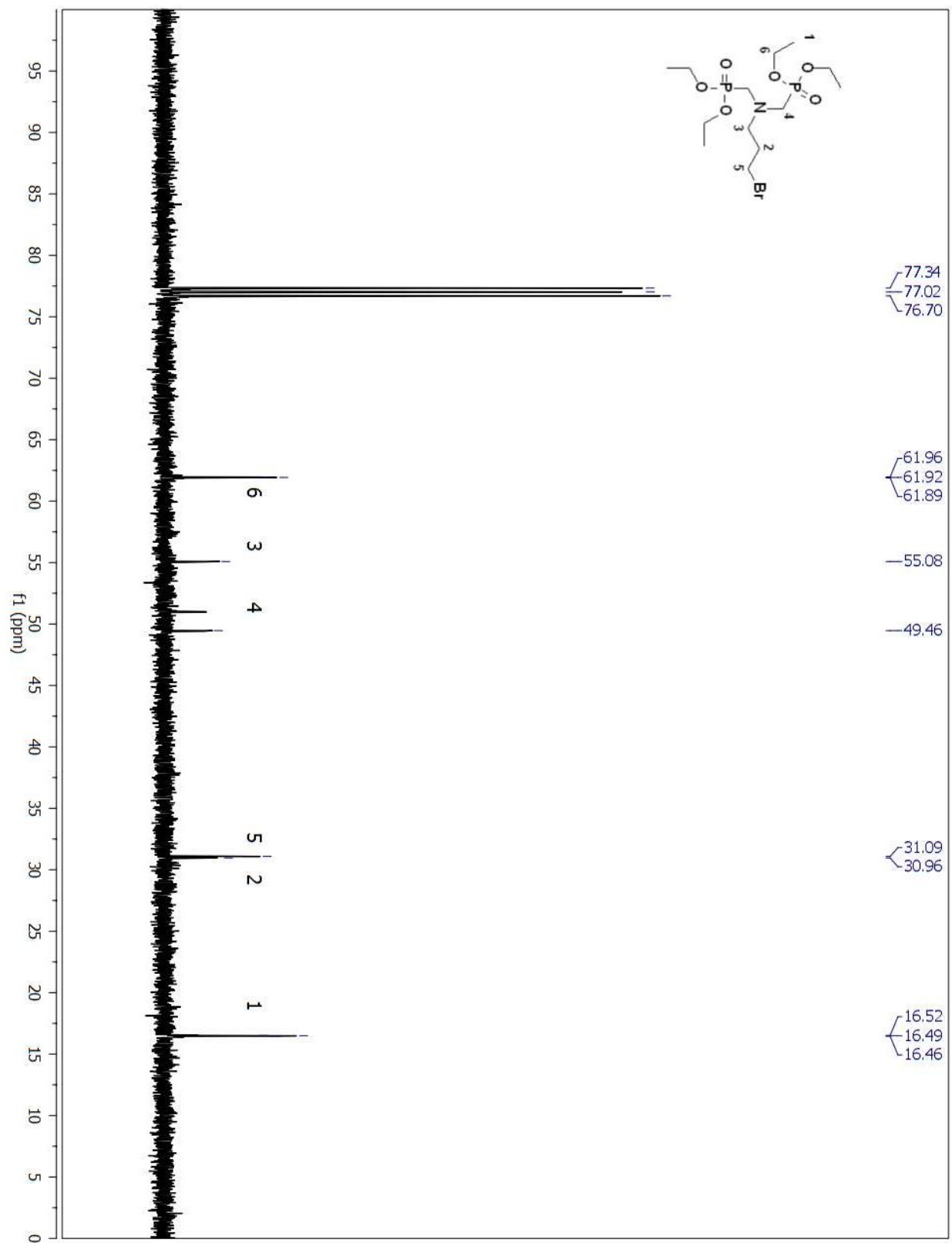


Figure A 209. ¹³C NMR spectrum of compound (116) in CDCl₃.

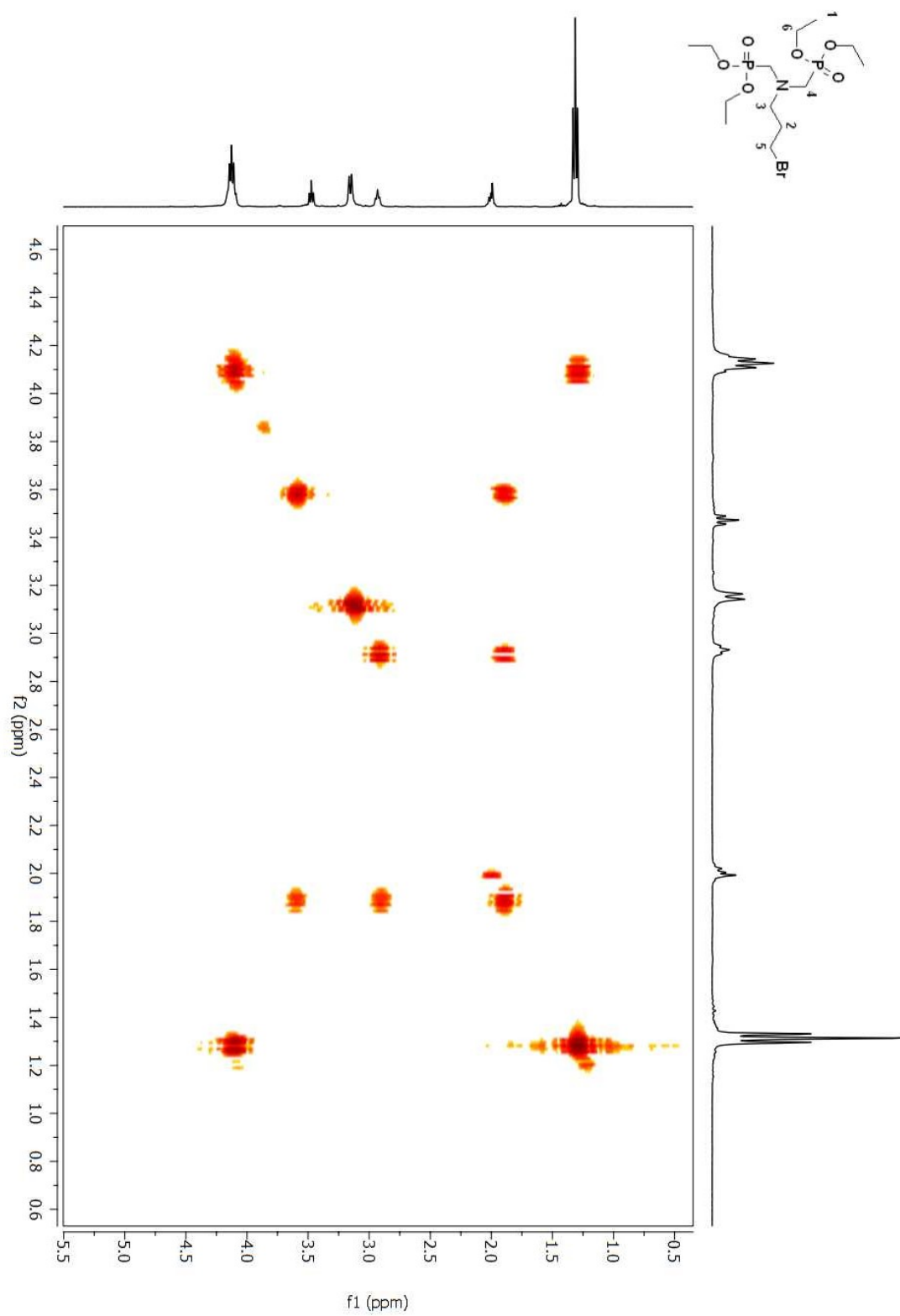


Figure A 210. COSY 2D NMR spectrum of compound (**116**) in CDCl_3 .

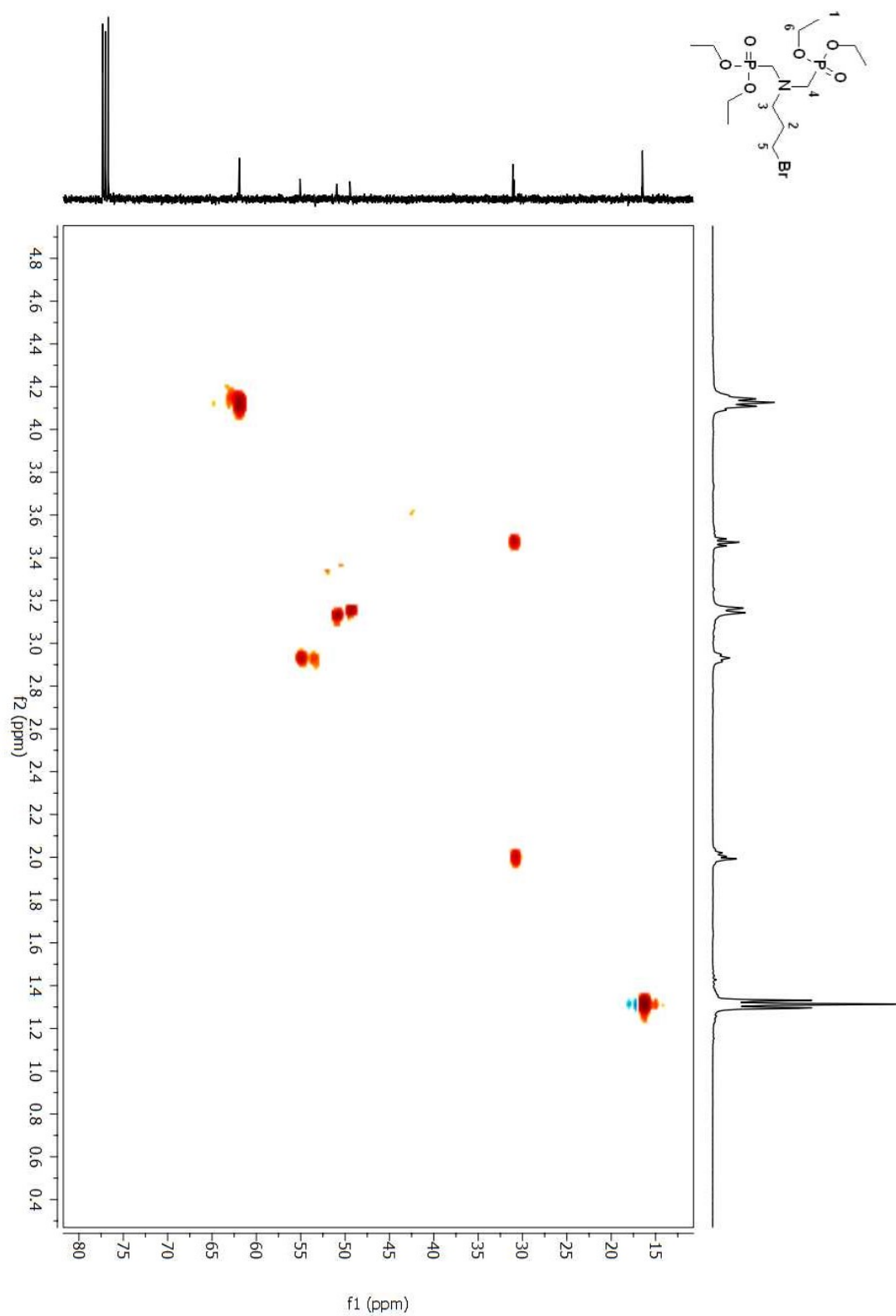


Figure A 211. HSQC 2D NMR spectrum of compound (**116**) in CDCl₃.

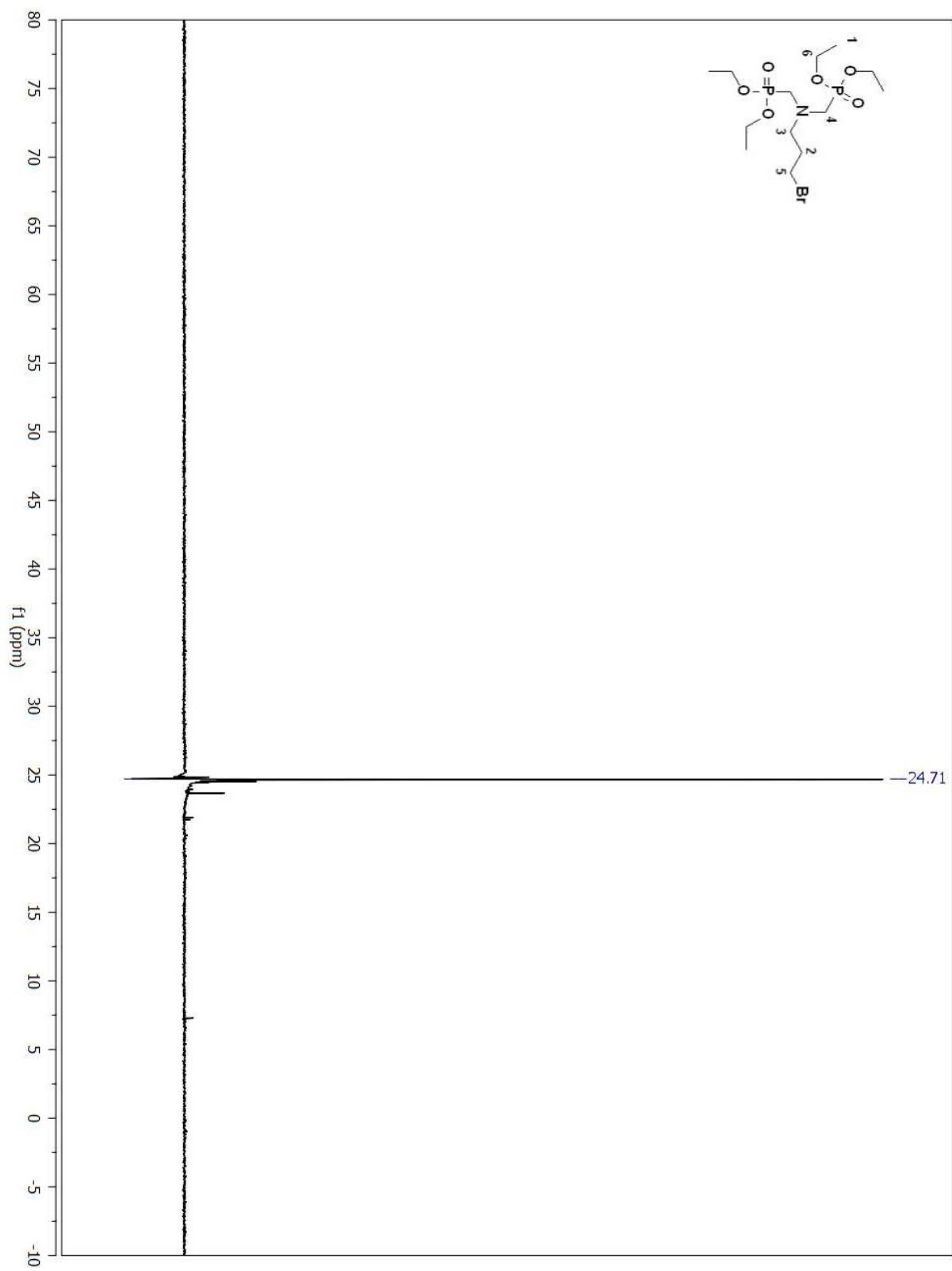


Figure A 212. ^{31}P NMR spectrum of compound (116) in CDCl_3 .

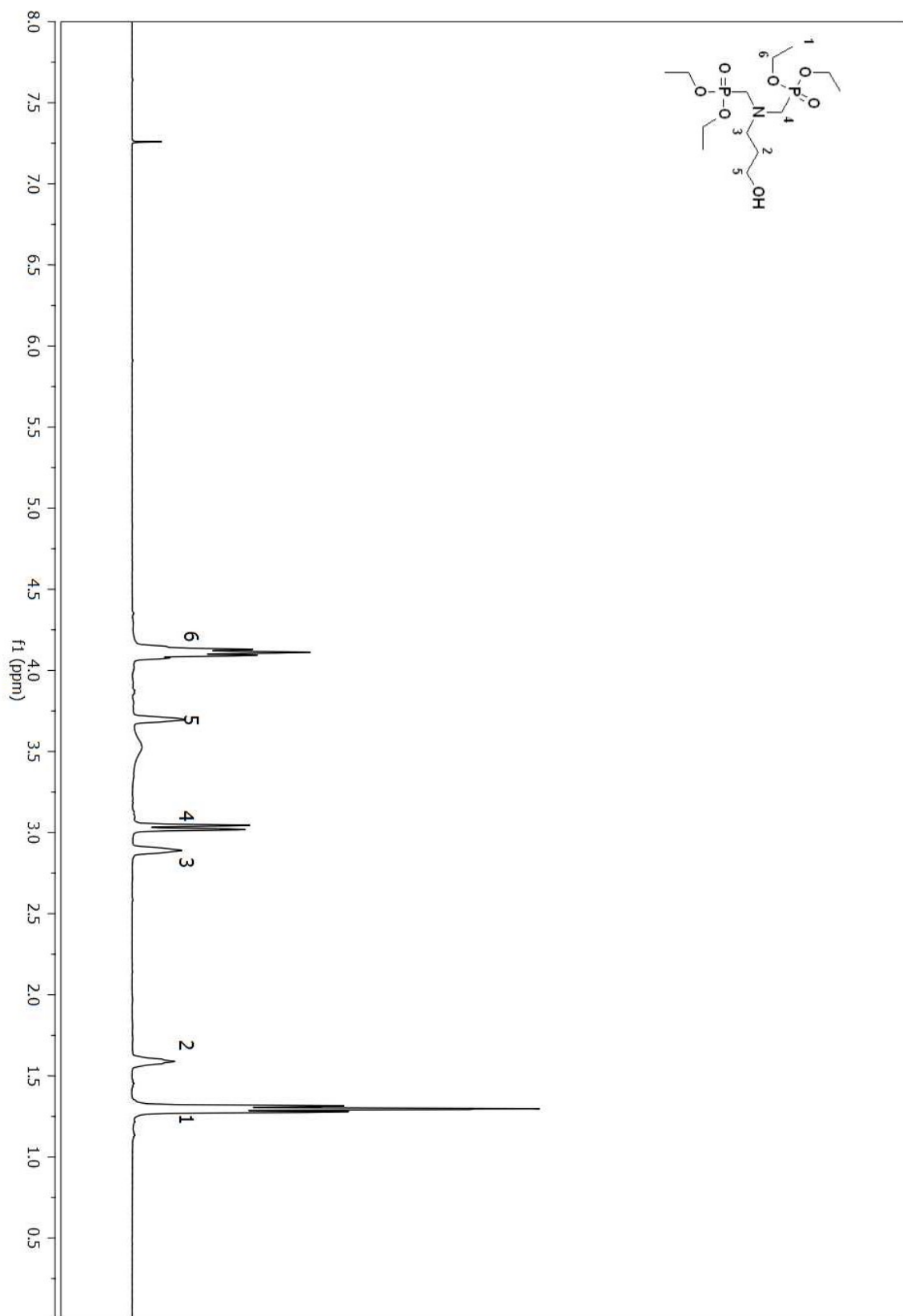


Figure A 213. ^1H NMR spectrum of compound (117) in CDCl_3 .

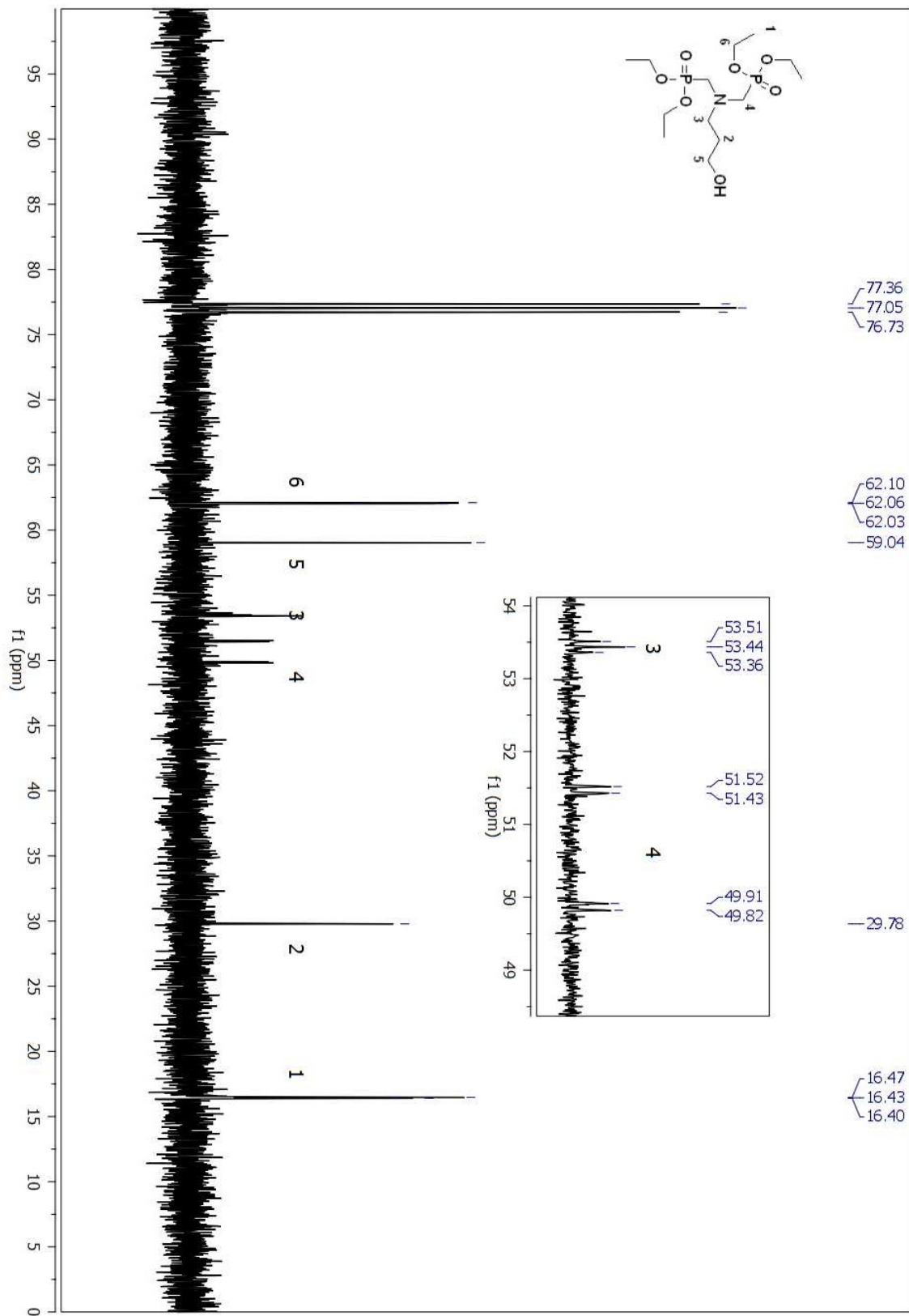


Figure A 214. ¹³C NMR spectrum of compound (117) in CDCl₃.

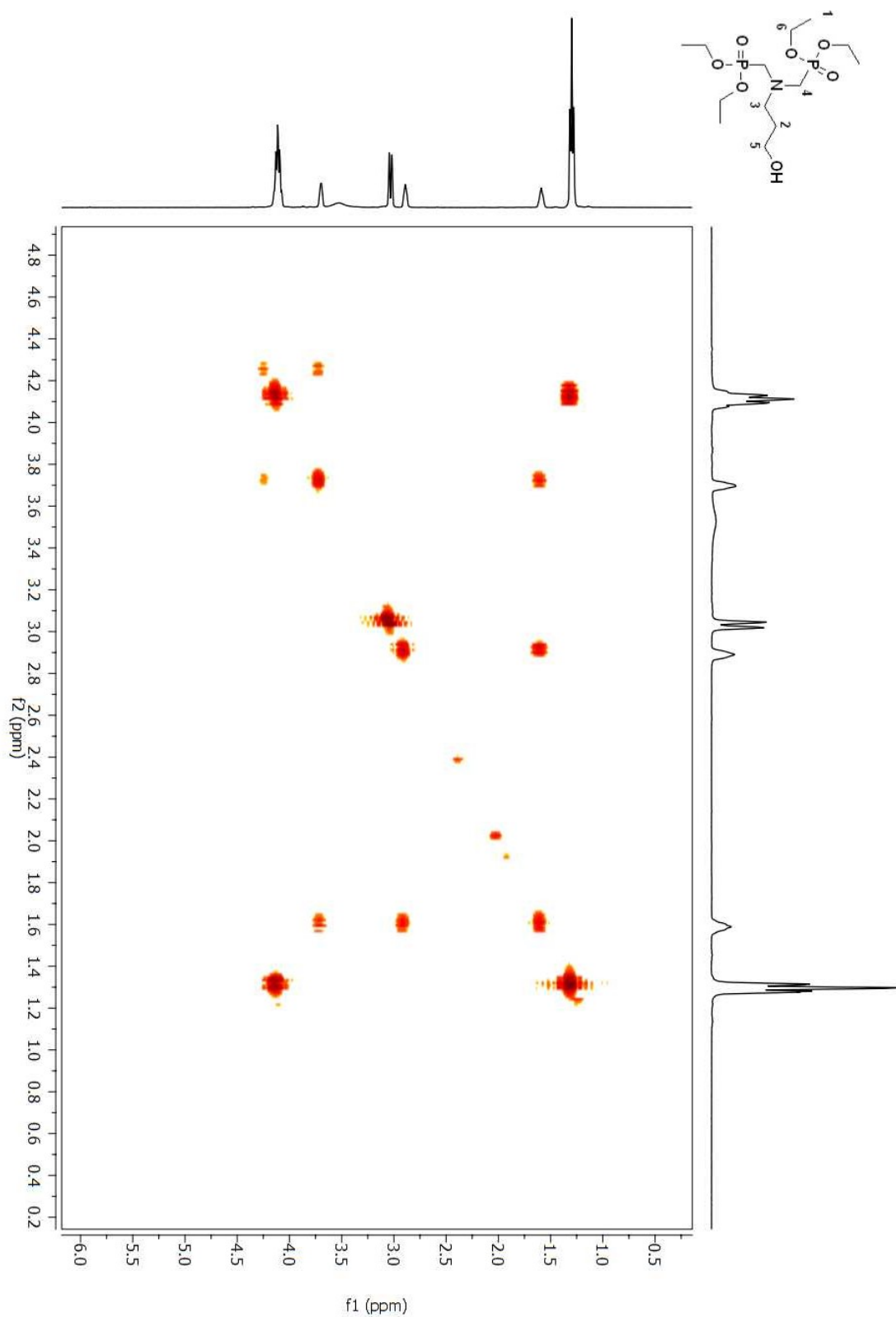


Figure A 215. COSY 2D NMR spectrum of compound (**117**) in CDCl_3 .

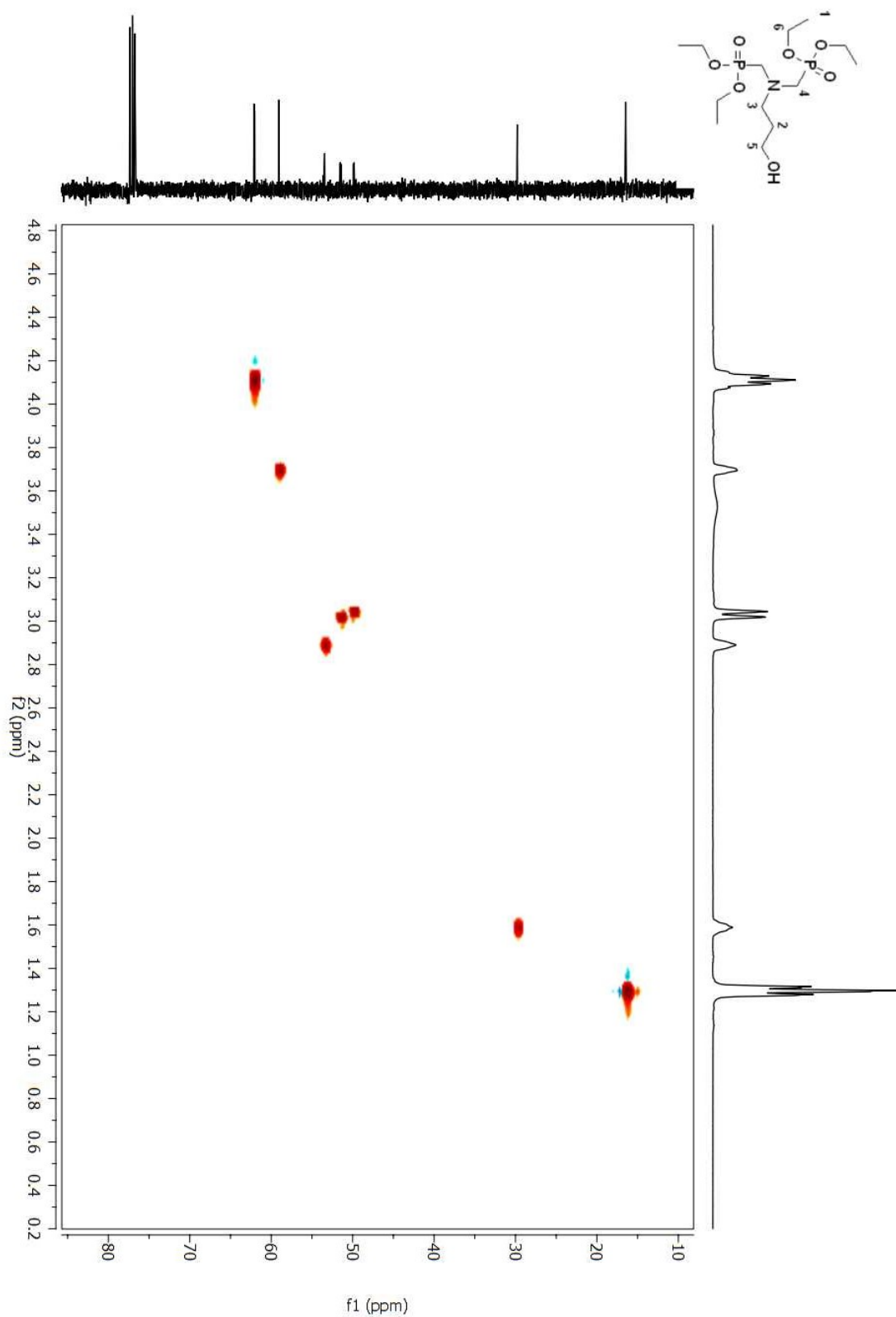


Figure A 216. HSQC 2D NMR spectrum of compound (117) in CDCl₃.

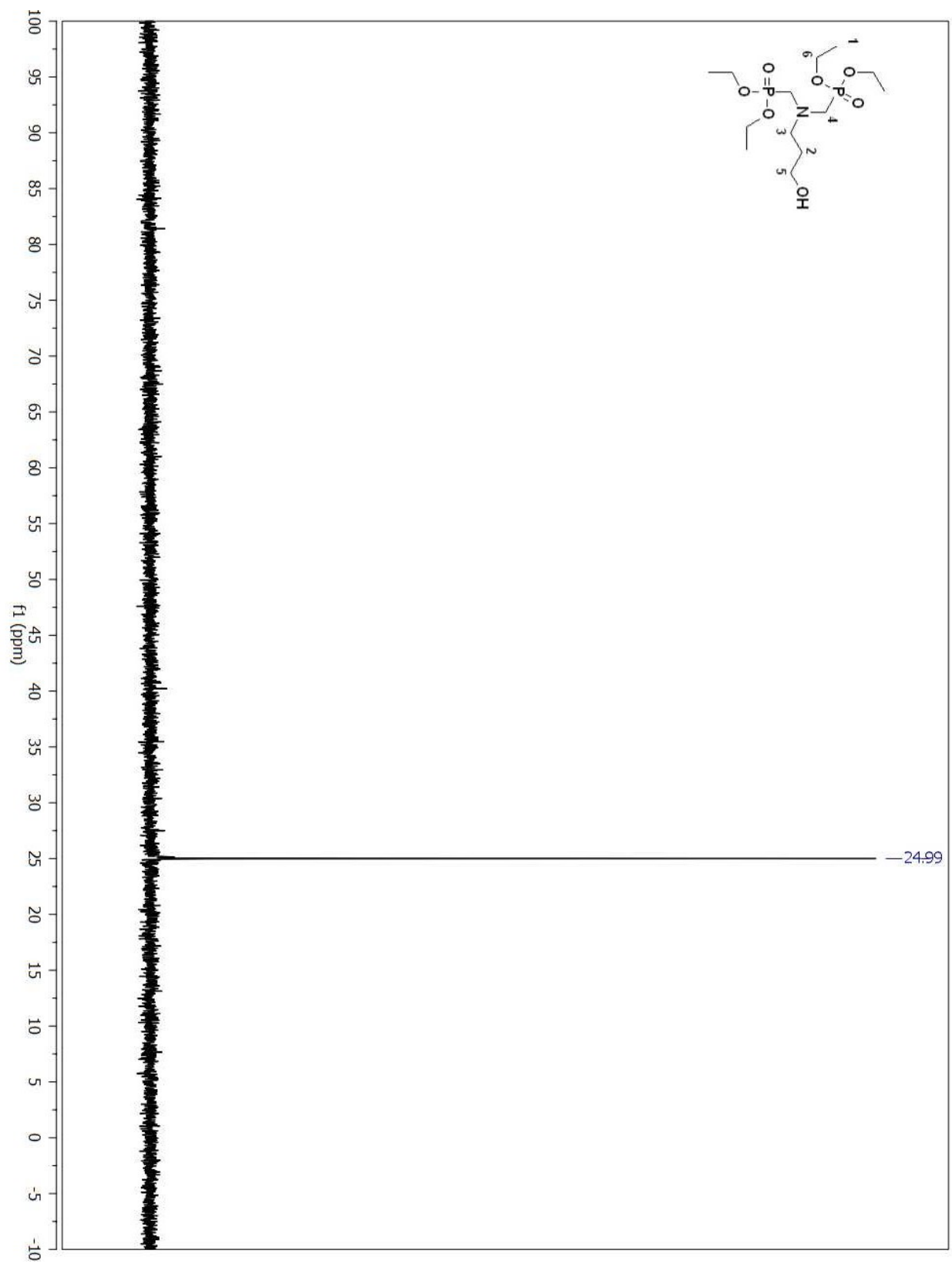
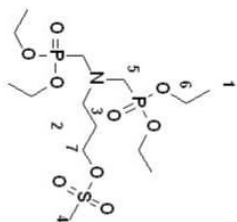


Figure A 217. ^{31}P NMR spectrum of compound (117) in CDCl_3 .



585

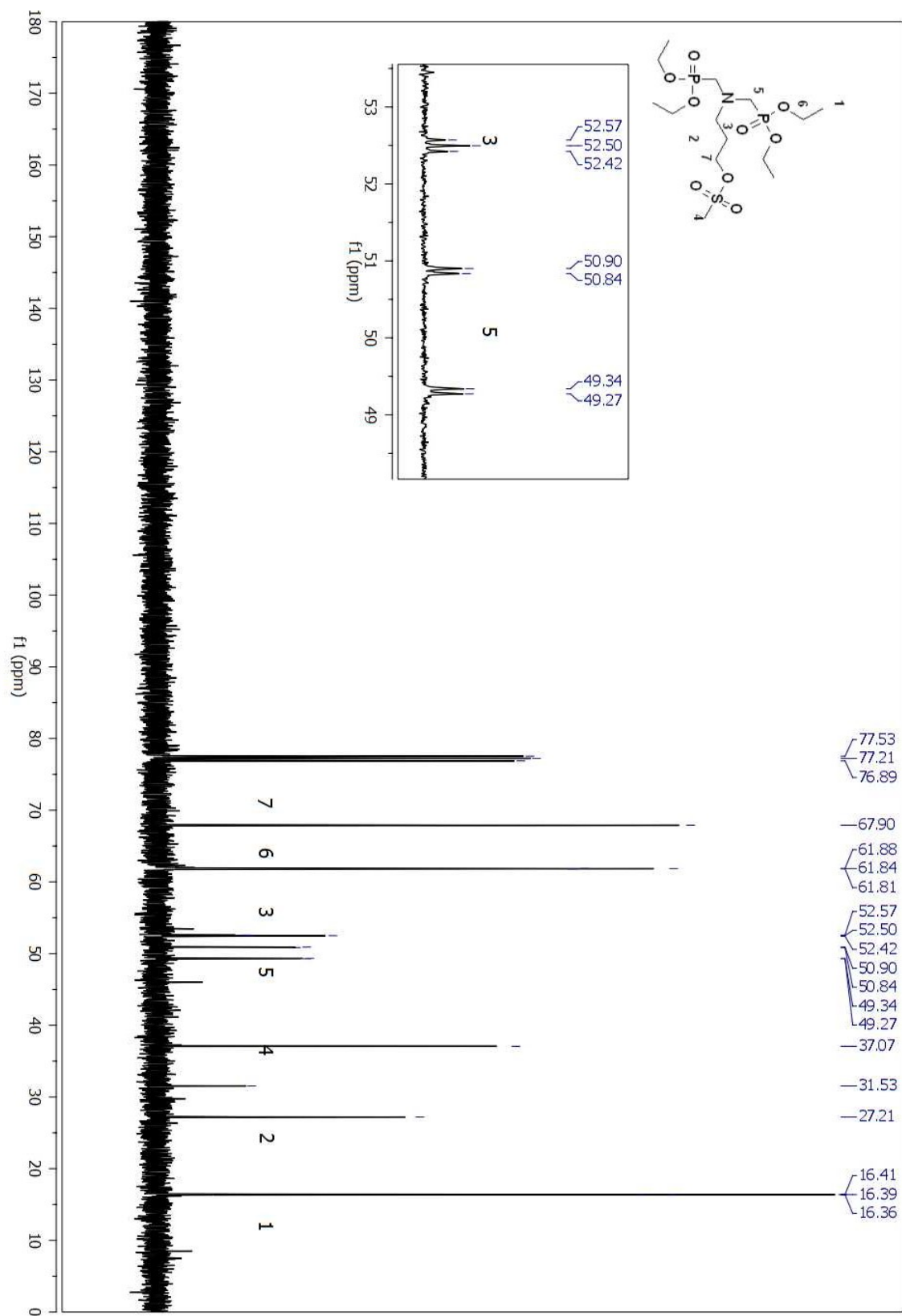


Figure A 219. ^{13}C NMR spectrum of compound (118) in CDCl₃.

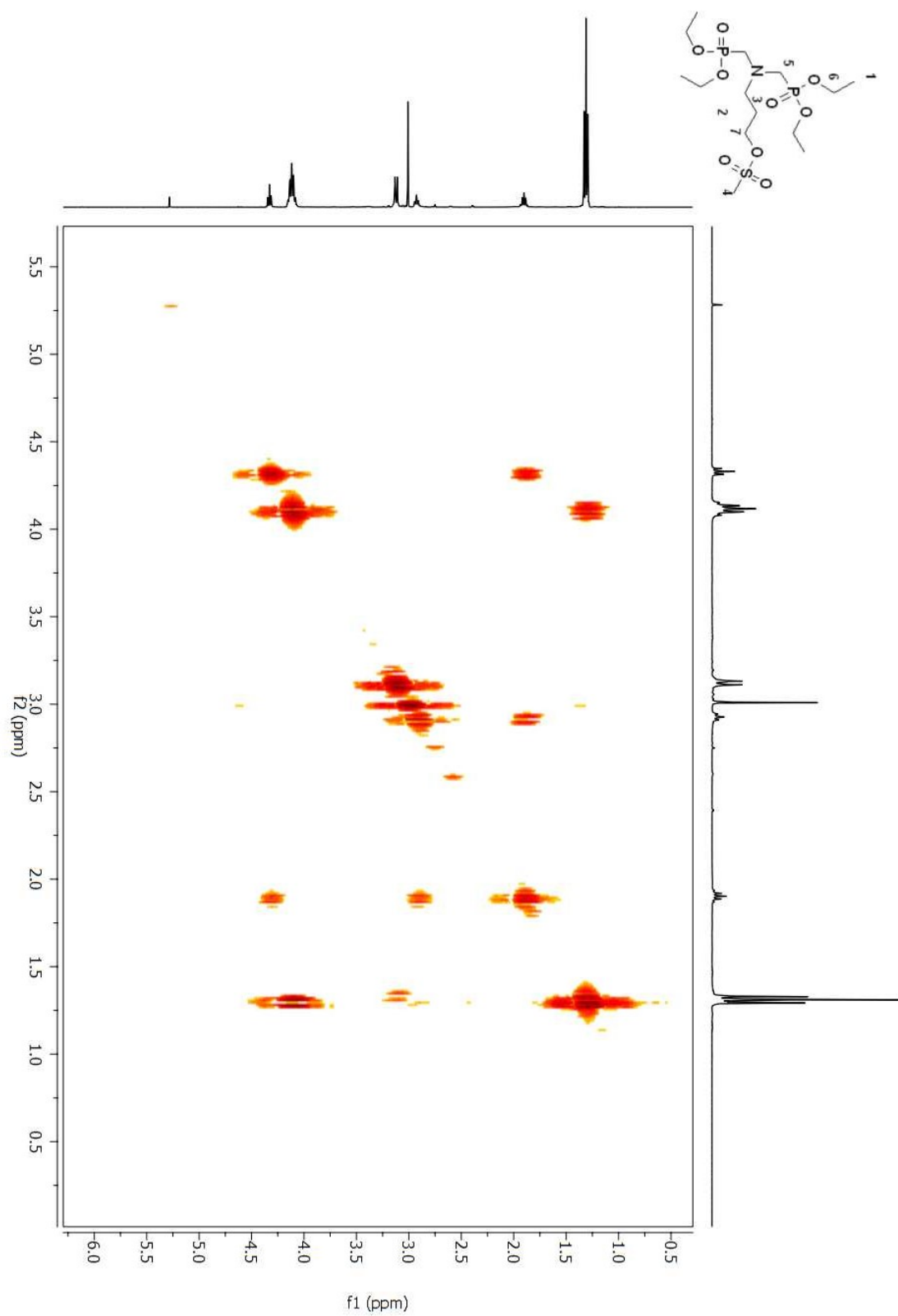


Figure A 220. COSY 2D NMR spectrum of compound (**118**) in CDCl₃.

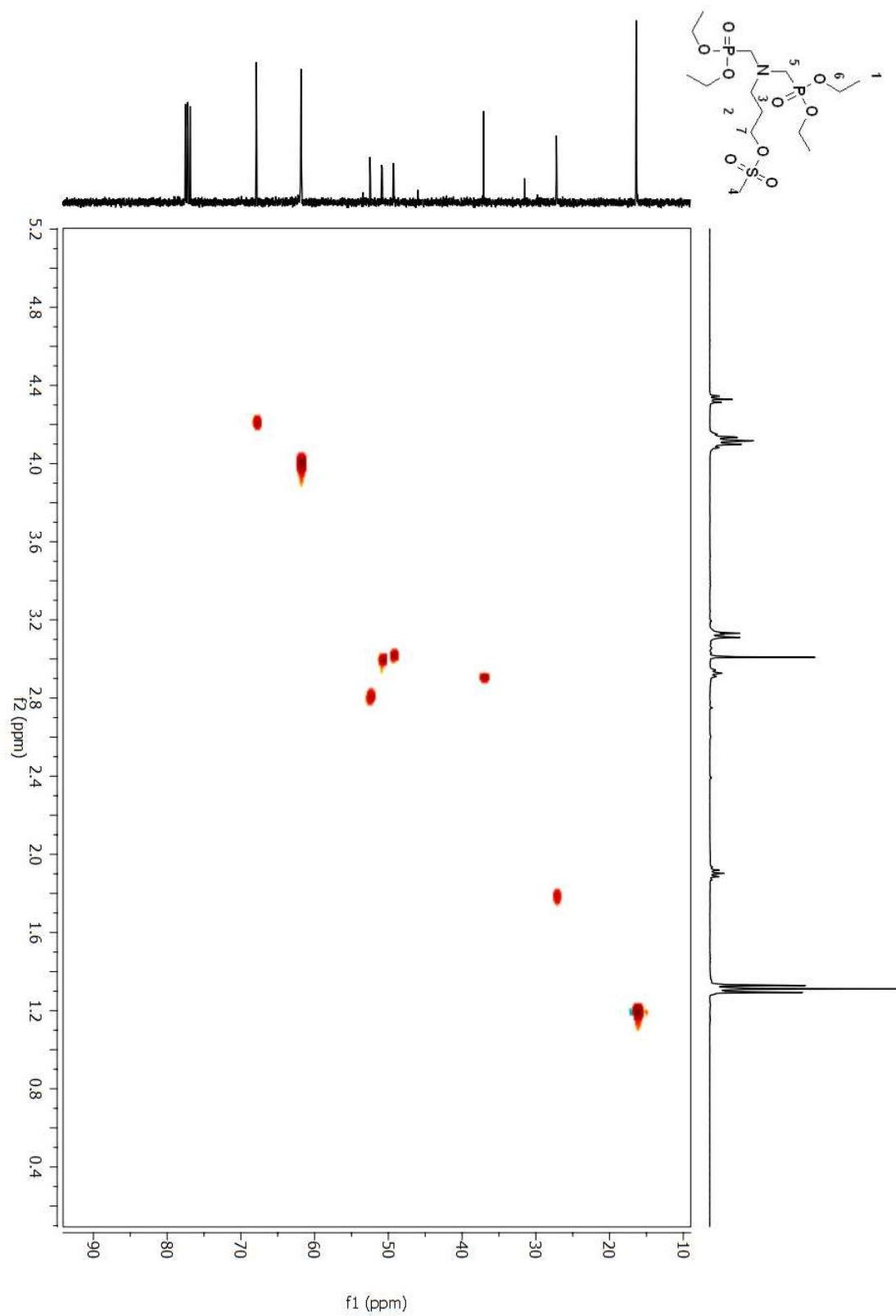


Figure A 221. HSQC 2D NMR spectrum of compound (**118**) in CDCl₃.

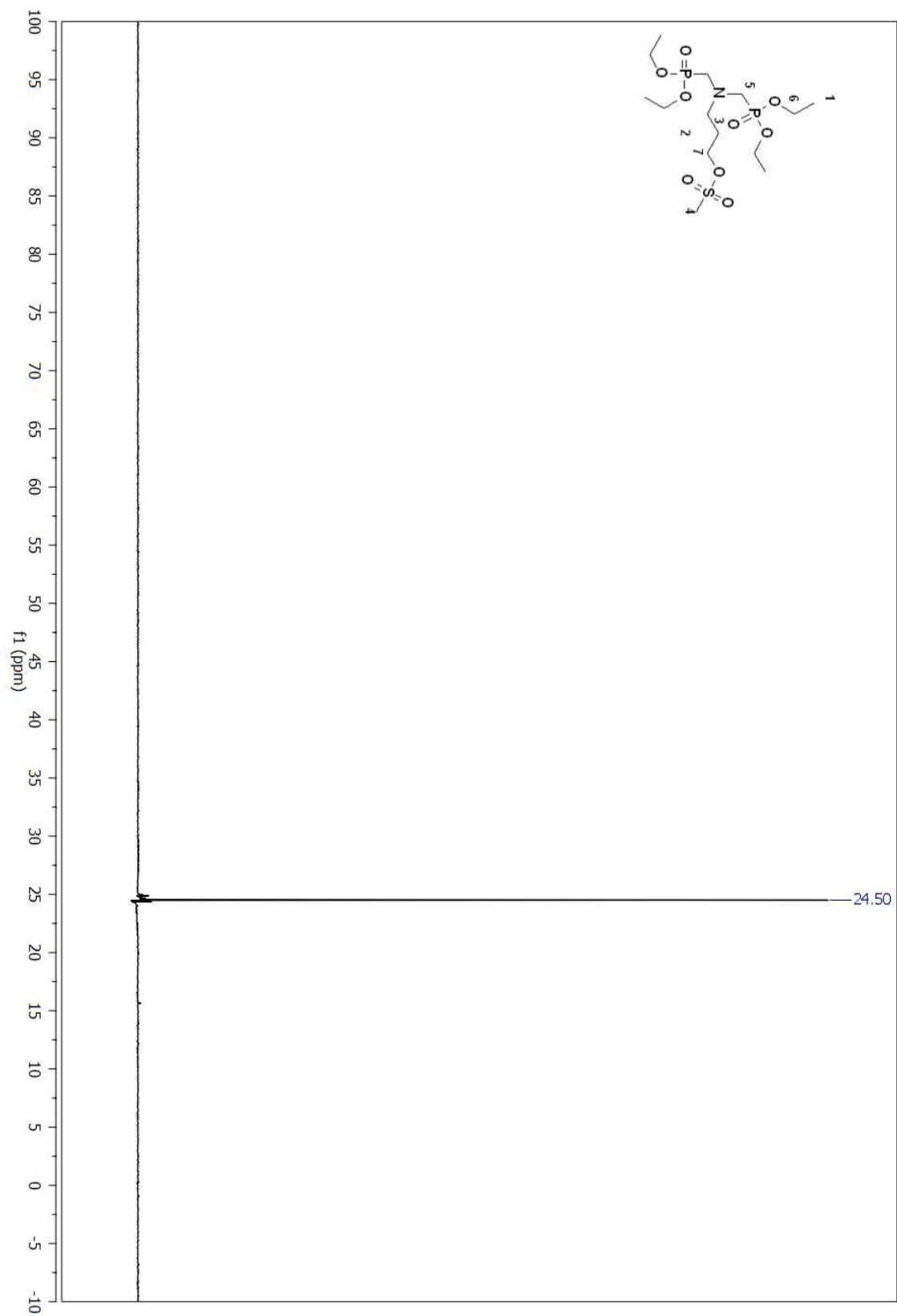


Figure A 222. ^{31}P NMR spectrum of compound (118) in CDCl_3 .

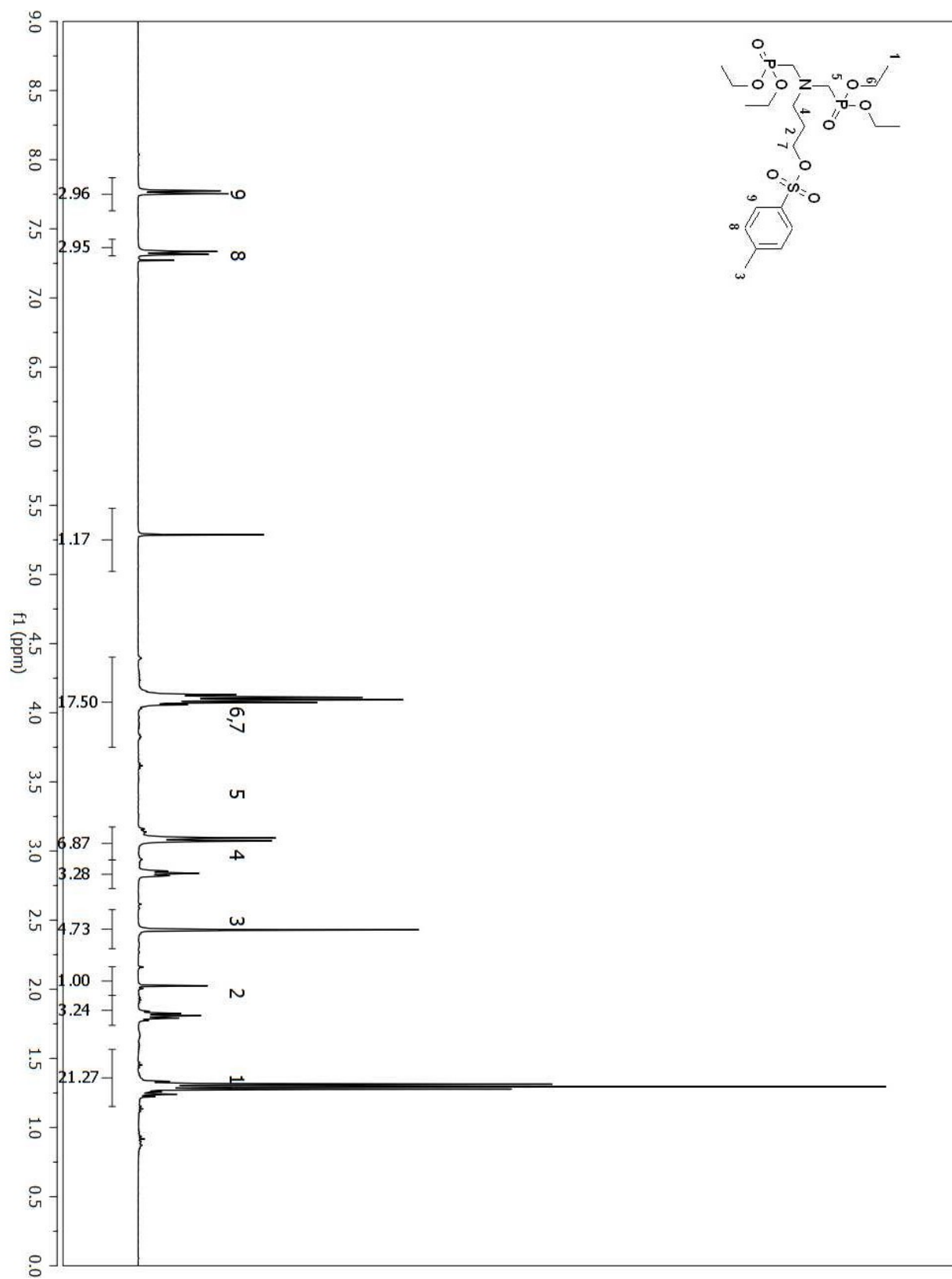


Figure A 223. ^1H NMR spectrum of compound (119) in CDCl_3 .

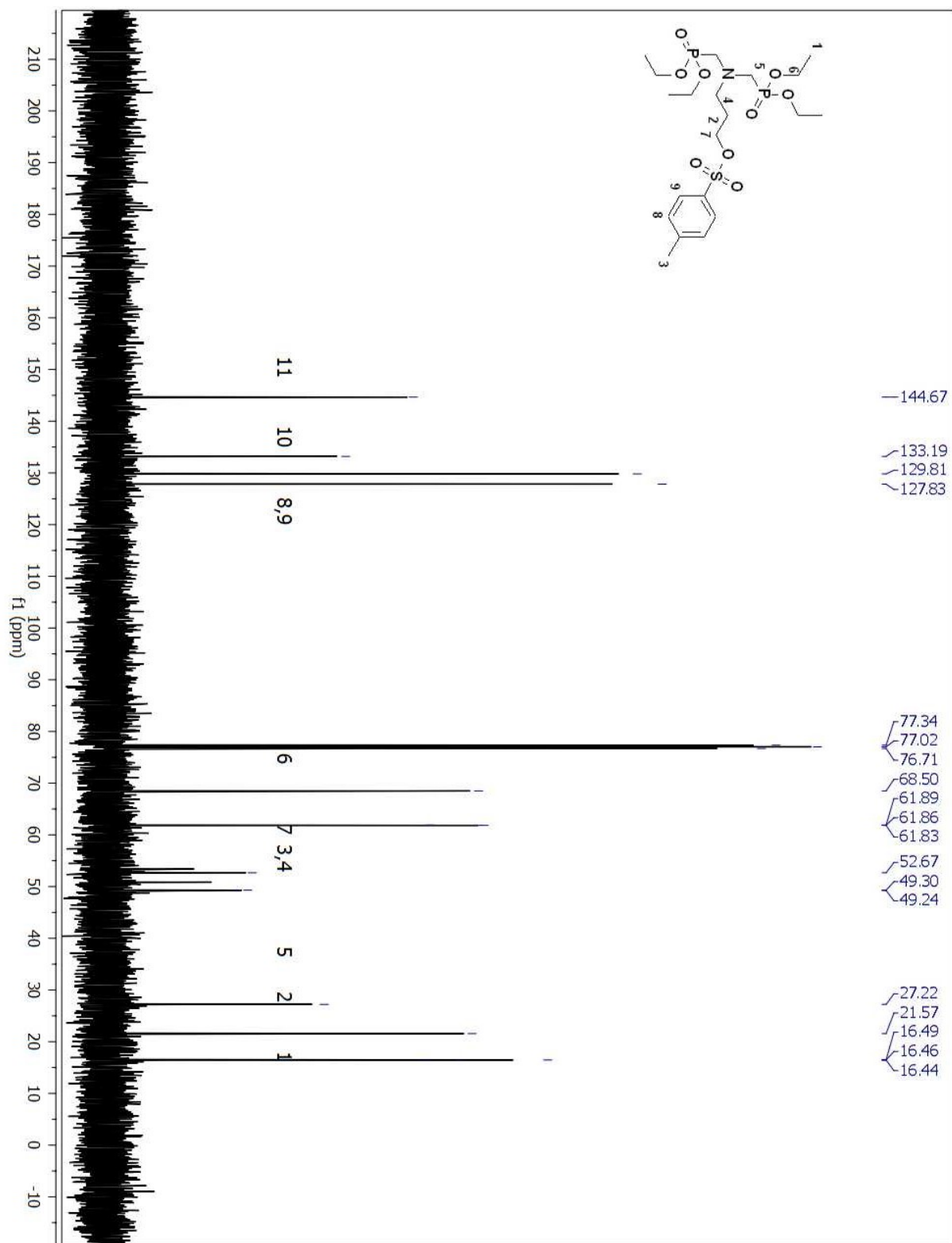


Figure A 224. ^{13}C NMR spectrum of compound (119) in CDCl_3 .
591

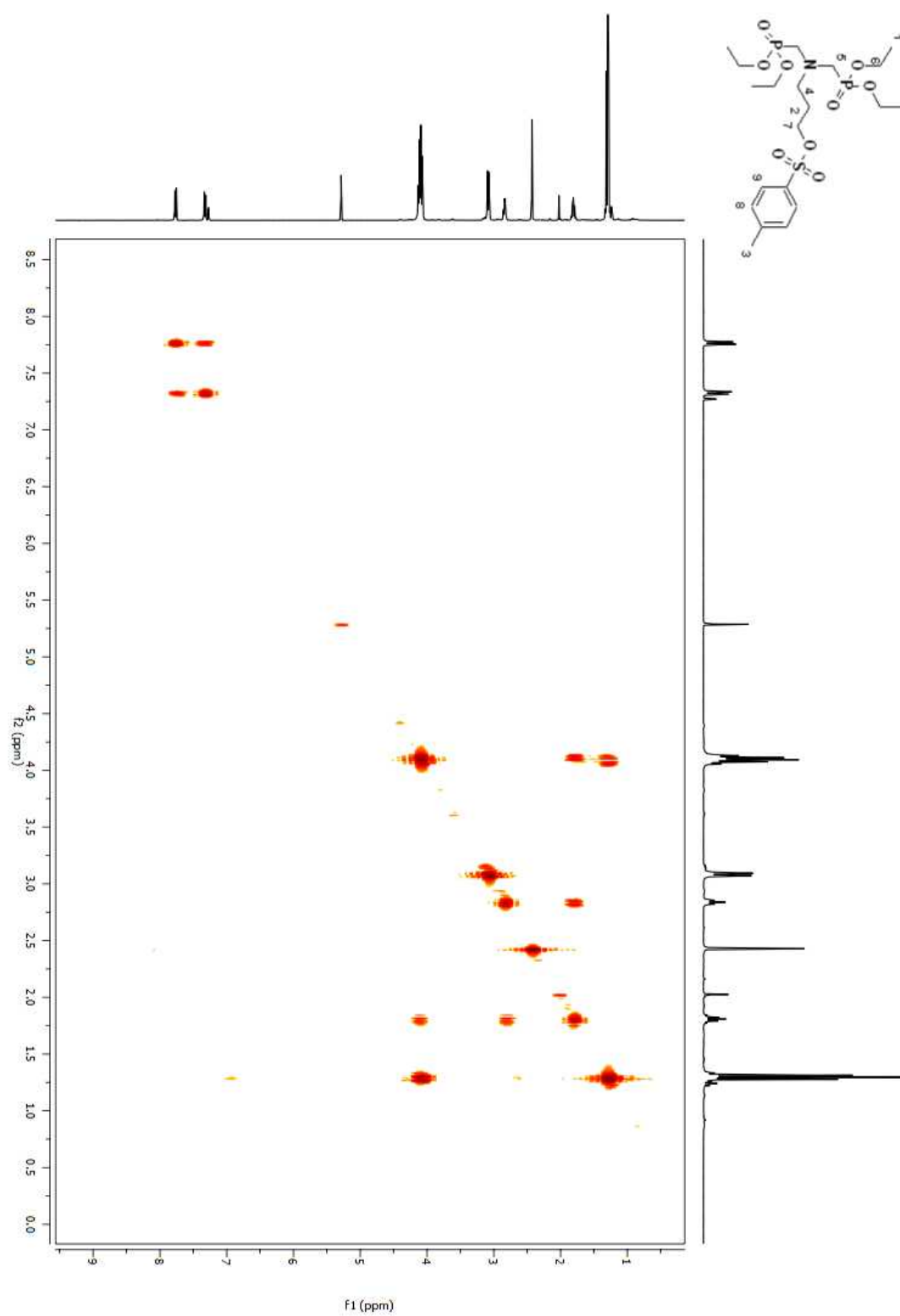


Figure A 225. COSY 2D NMR spectrum of compound (**119**) in CDCl₃.

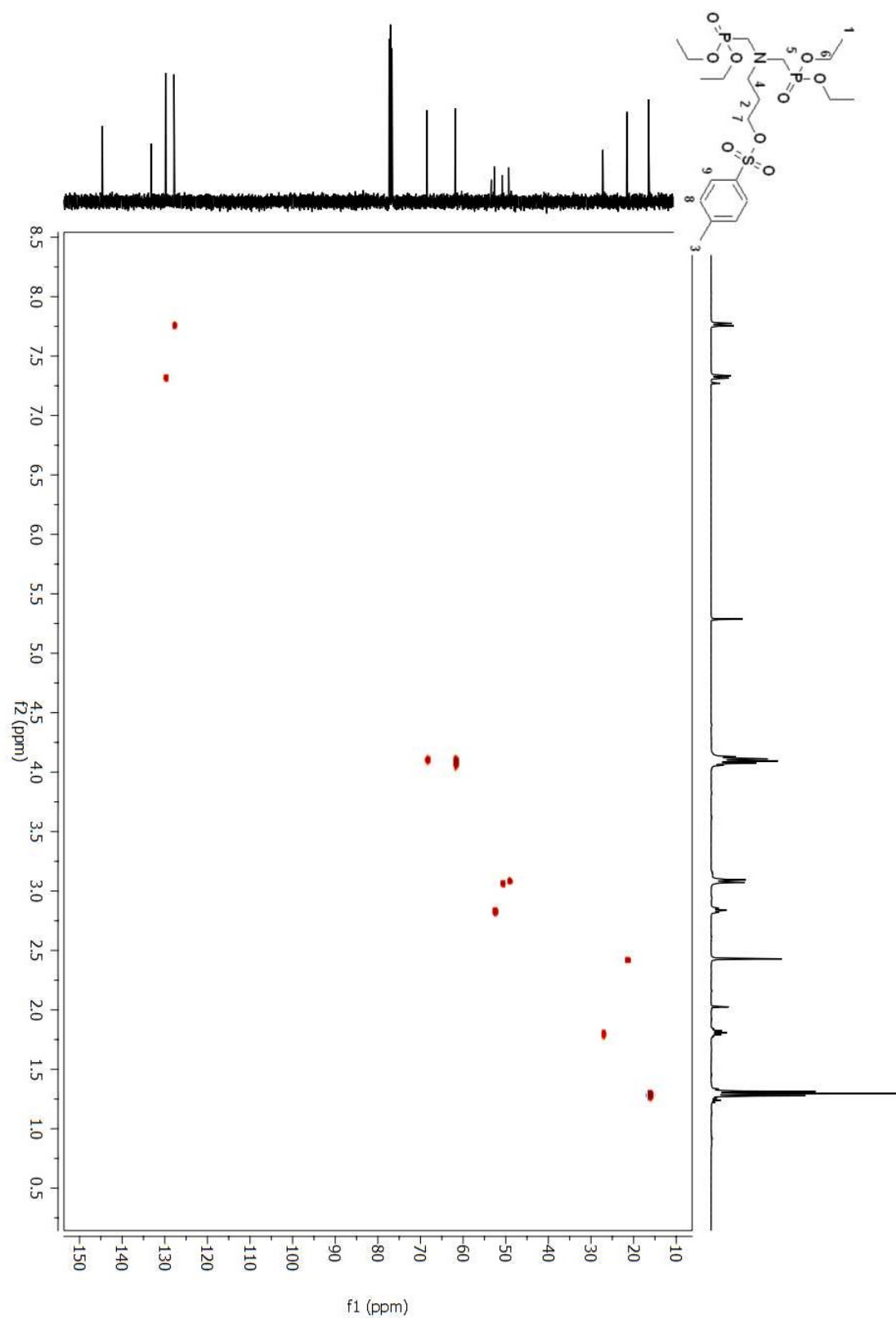


Figure A 226. HSQC 2D NMR spectrum of compound (119) in CDCl₃.

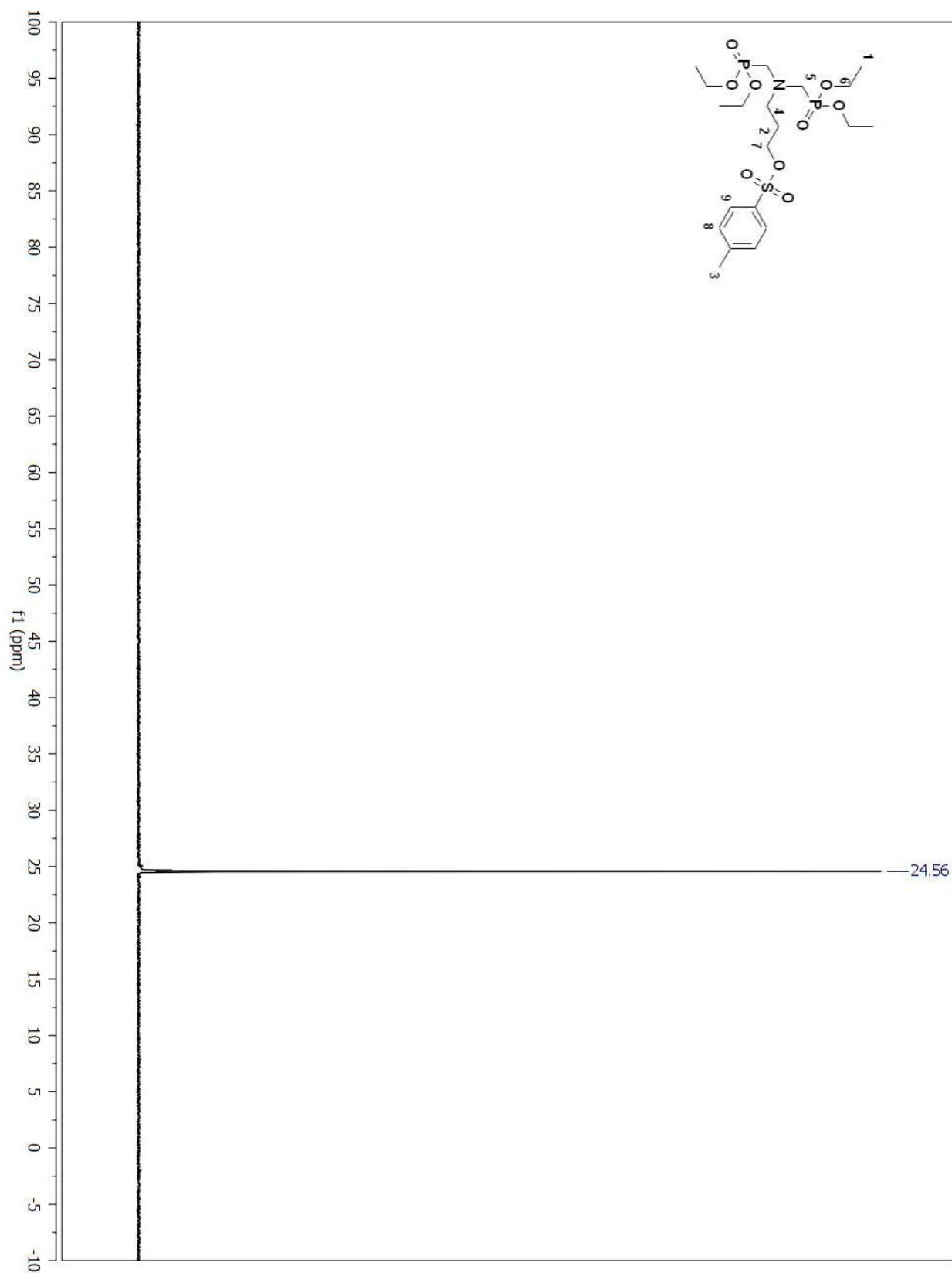


Figure A 227. ^{31}P NMR spectrum of compound (119) in CDCl_3 .

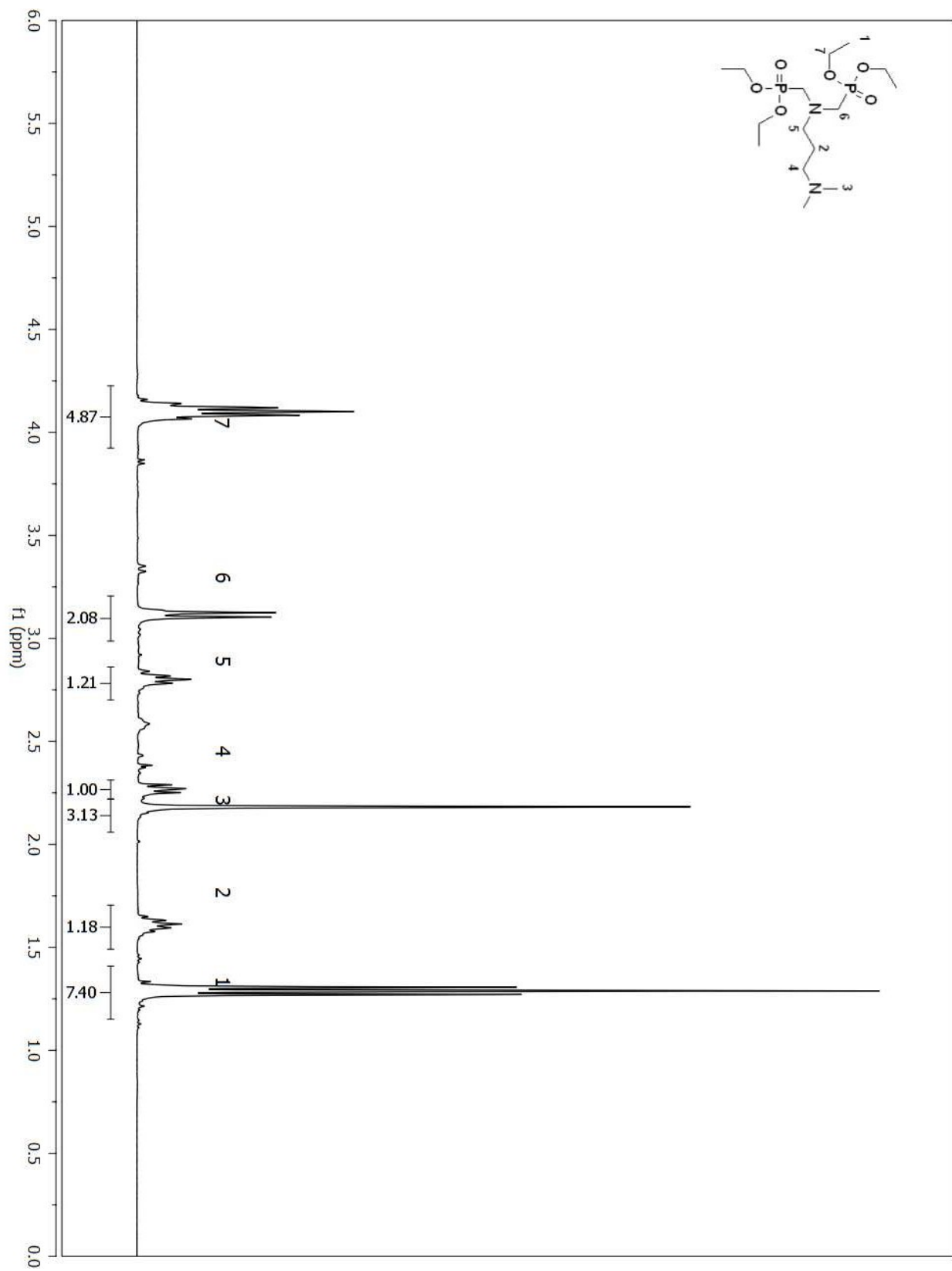


Figure A 228. ^1H NMR spectrum of compound (113) in CDCl_3 .

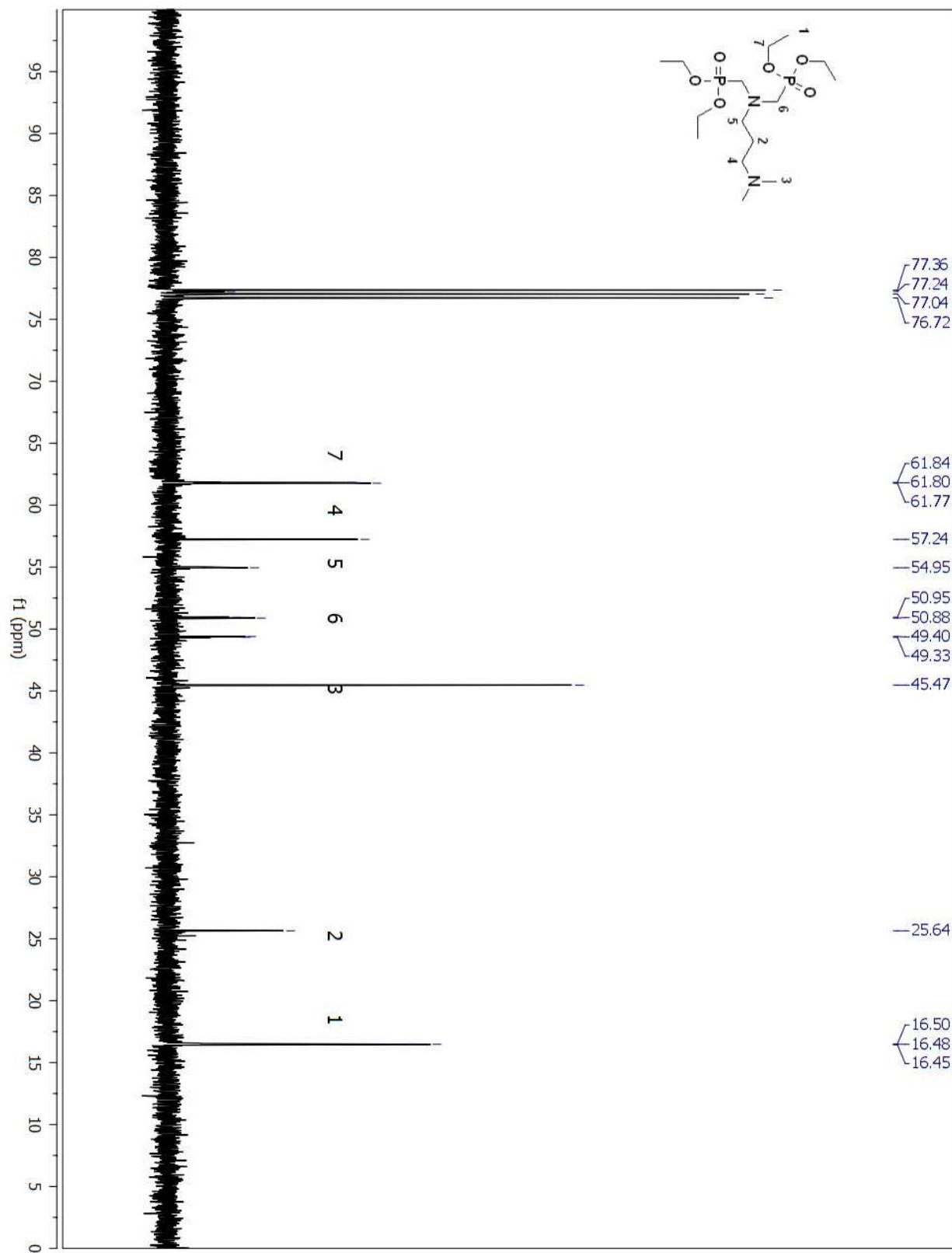


Figure A 229. ¹³C NMR spectrum of compound (113) in CDCl₃.

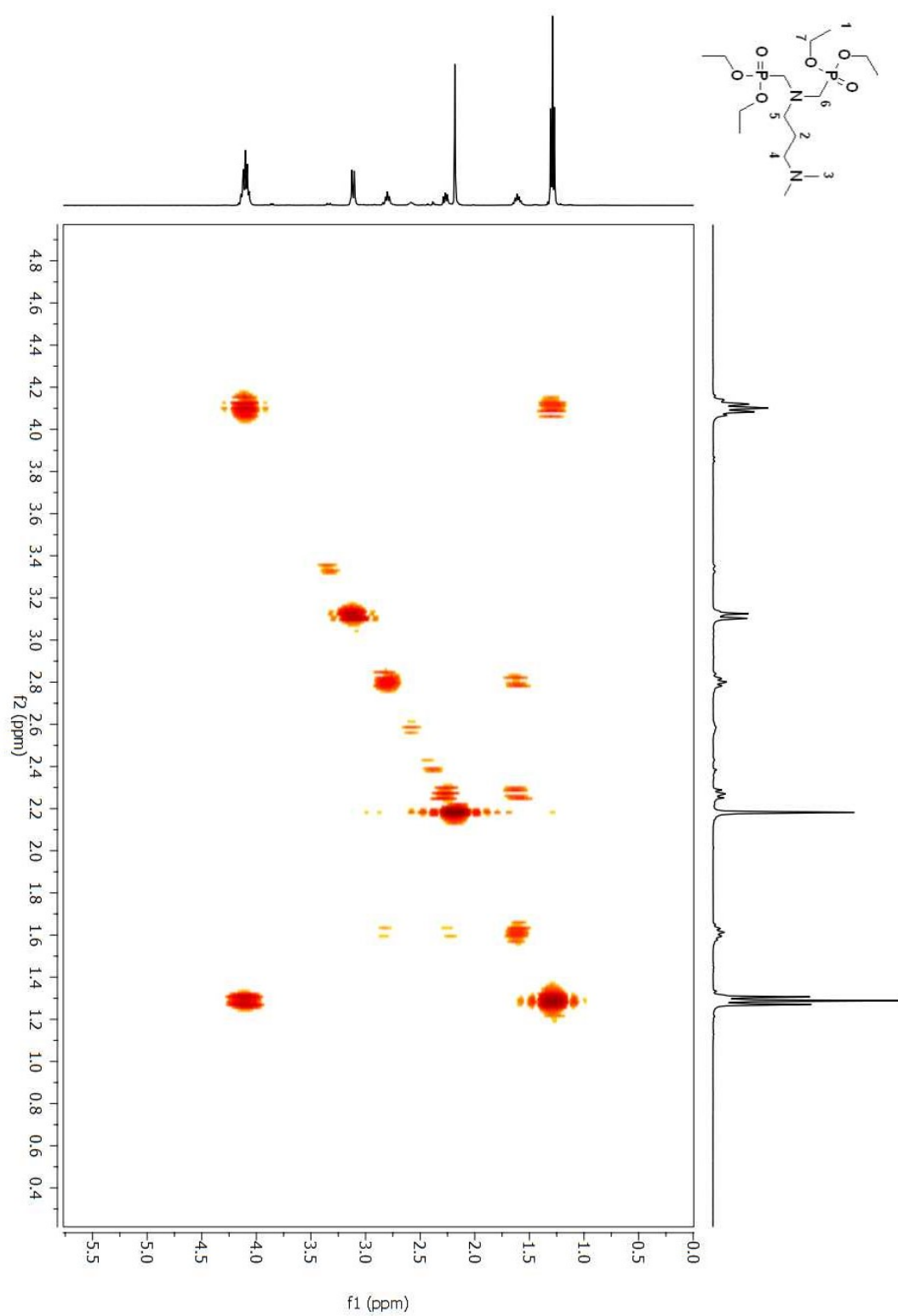


Figure A 230. COSY 2D NMR spectrum of compound (113) in CDCl_3 .

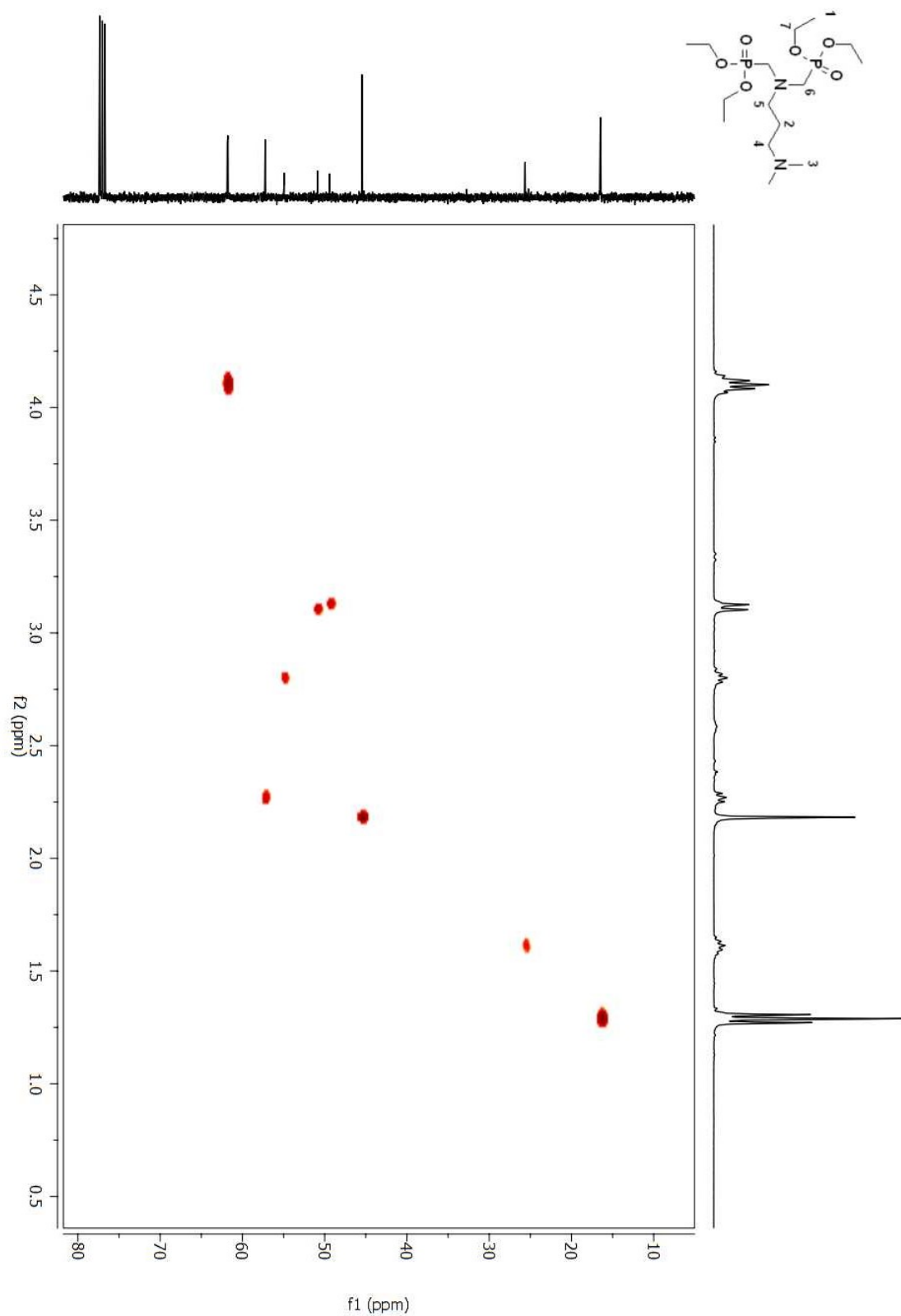


Figure A 231. HSQC 2D NMR spectrum of compound (113) in CDCl_3 .

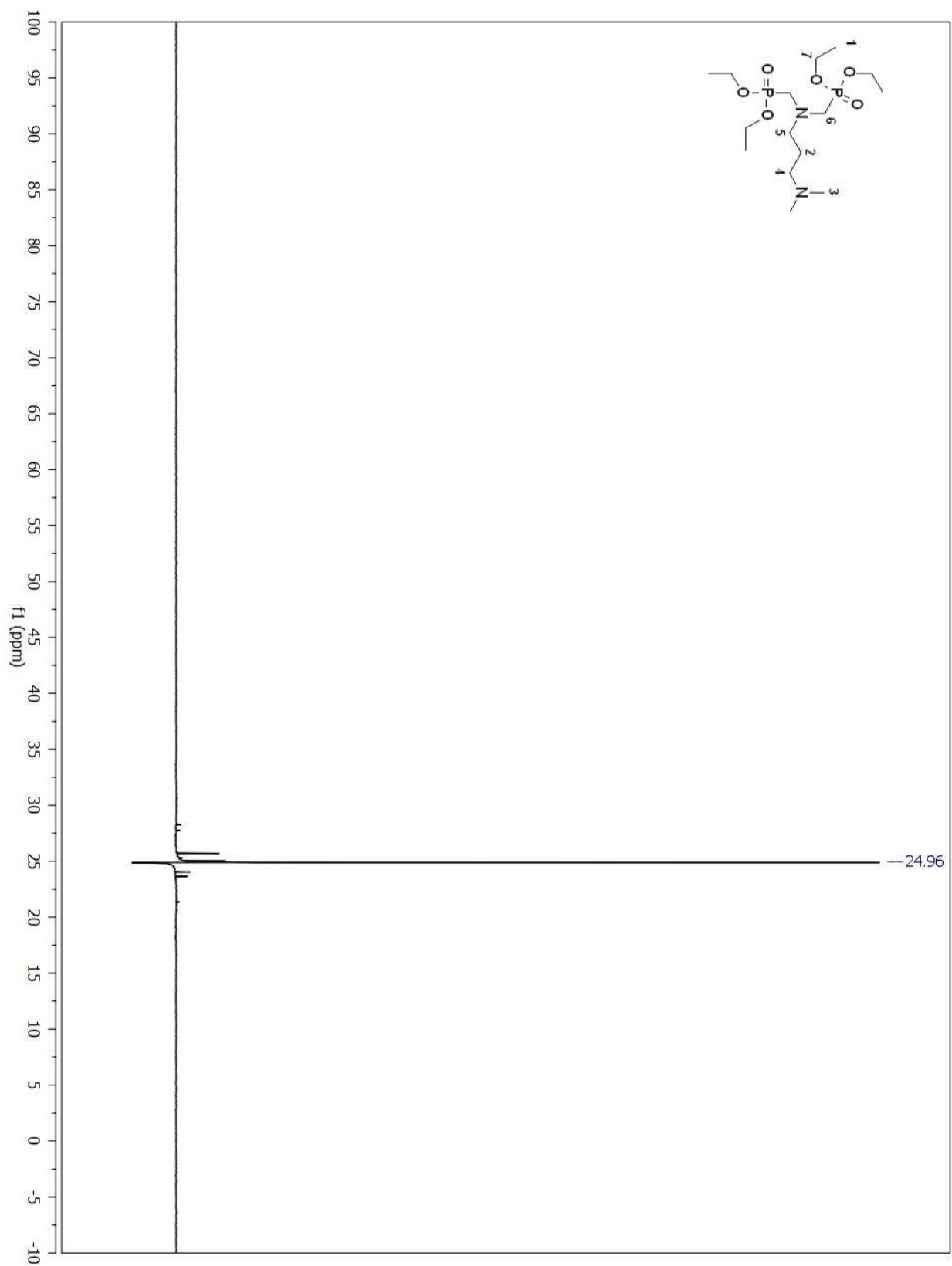


Figure A 232. ^{31}P NMR spectrum of compound (113) in CDCl_3 .

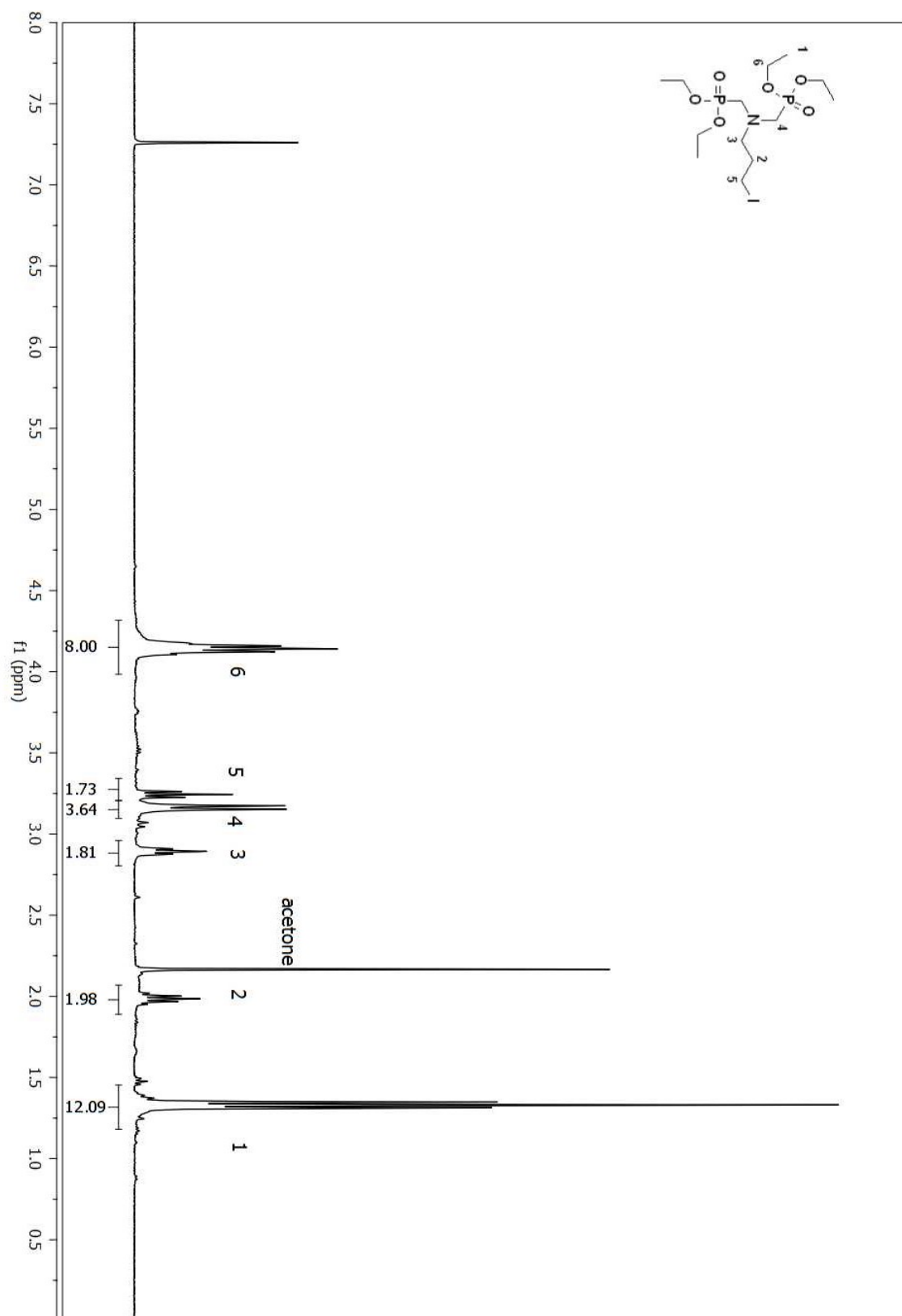


Figure A 233. ^1H NMR spectrum of compound (120) in CDCl_3 .

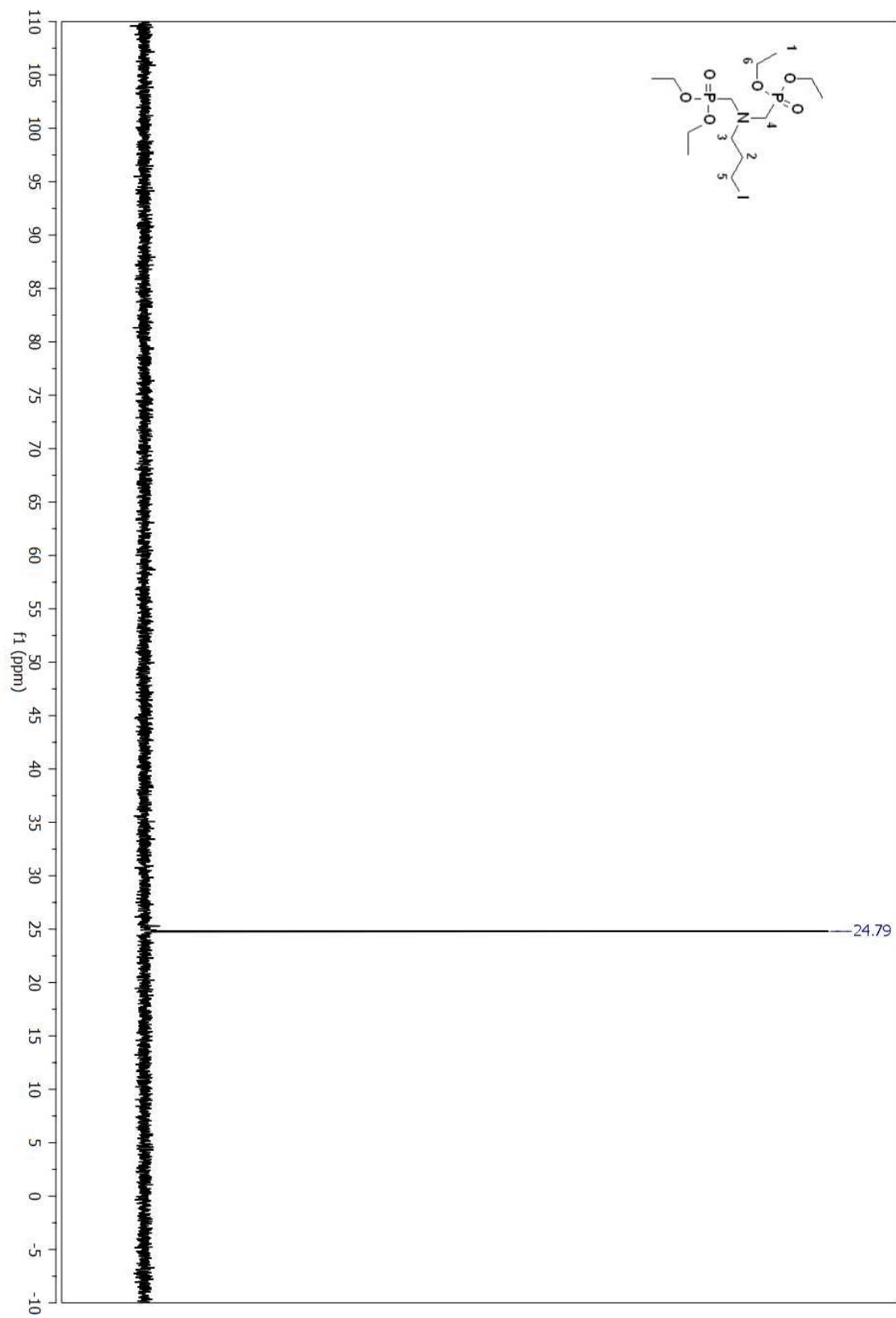


Figure A 234. ^{31}P NMR spectrum of compound (120) in CDCl_3 .

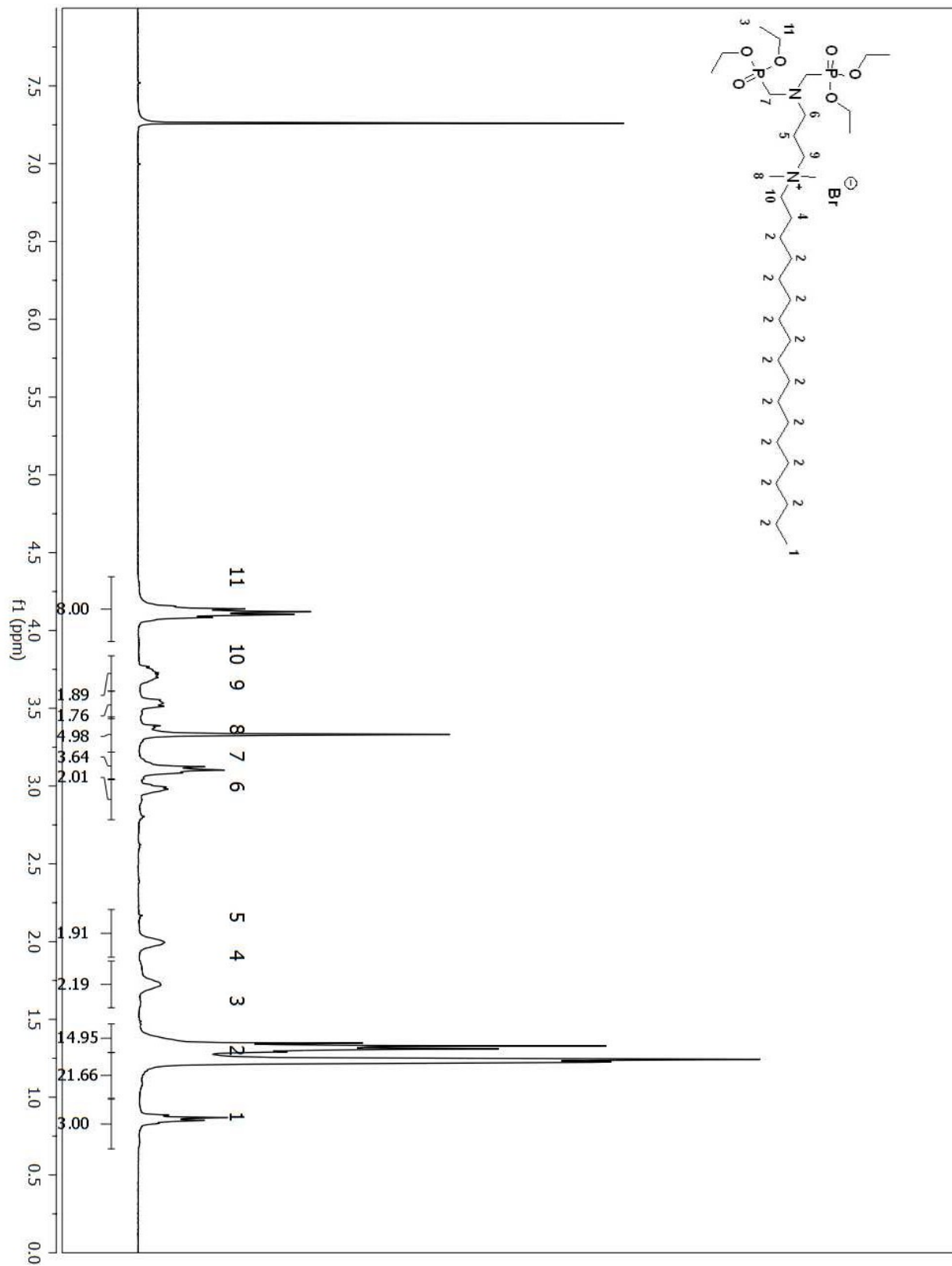


Figure A 235. ^1H NMR spectrum of compound (121) in CDCl_3 .

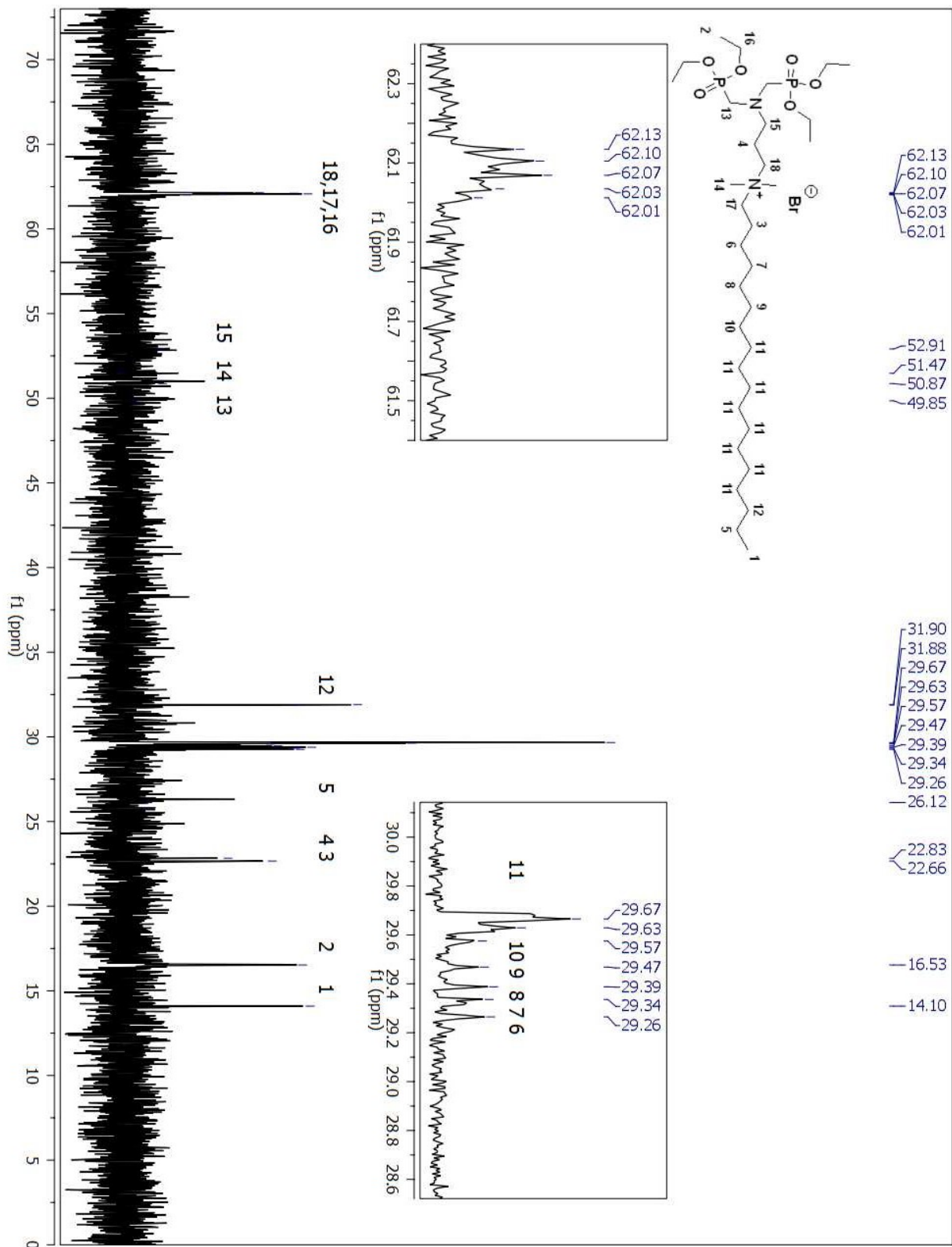


Figure A 236. ^{13}C NMR spectrum of compound (121) in CDCl_3 .

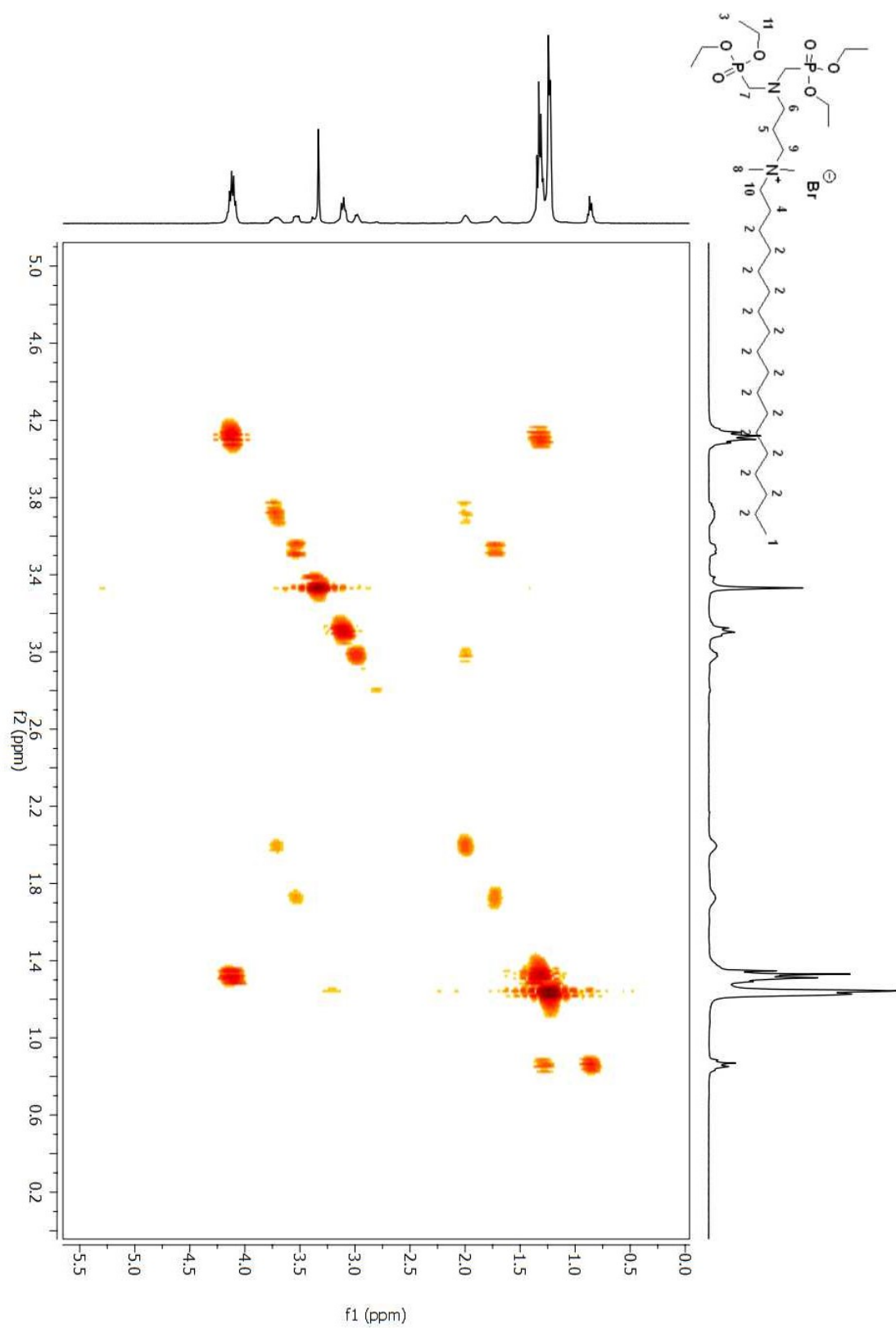


Figure A 237. COSY 2D NMR spectrum of compound (**121**) in CDCl₃.

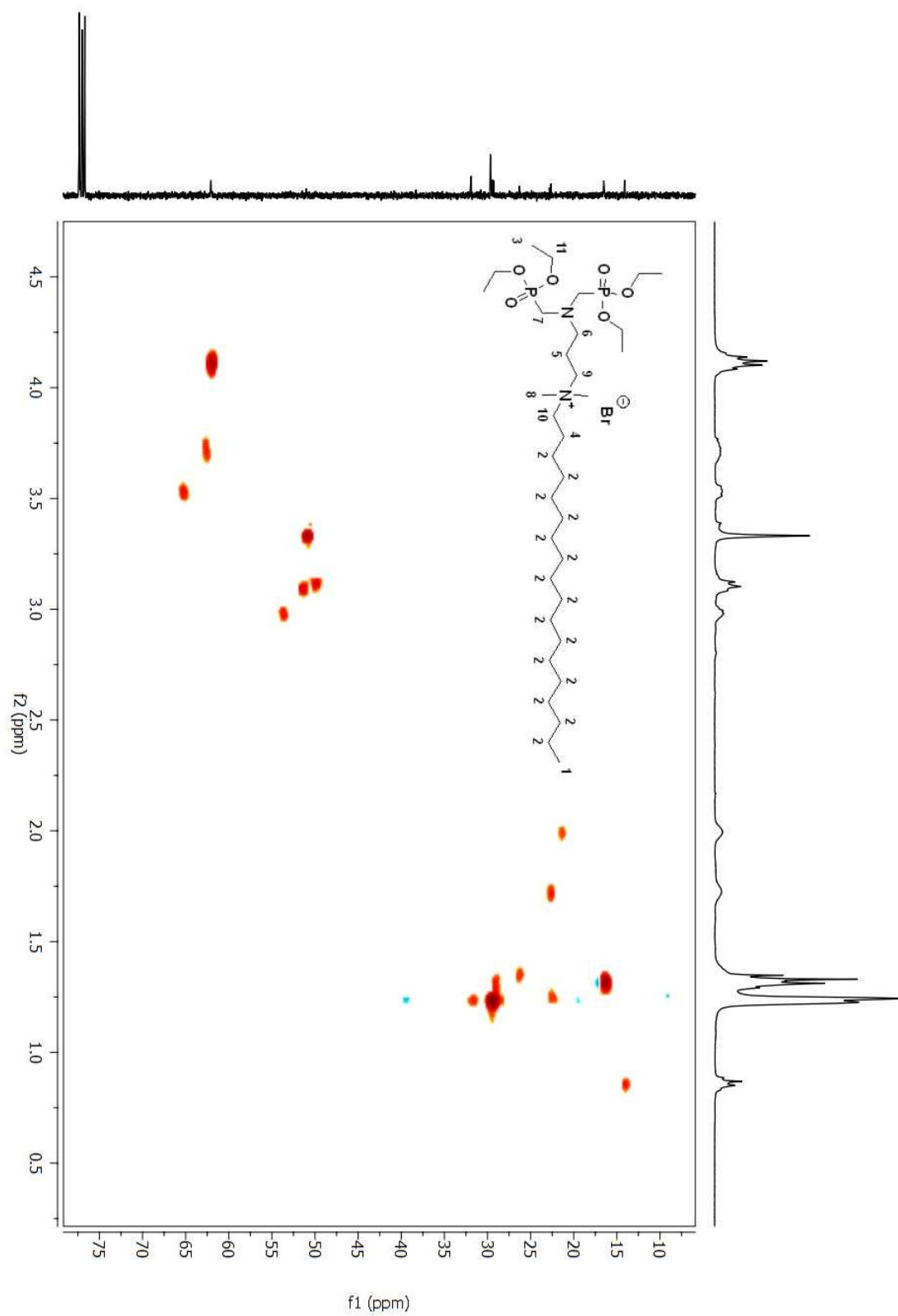


Figure A 238. HSQC 2D NMR spectrum of compound (**121**) in CDCl₃.
605

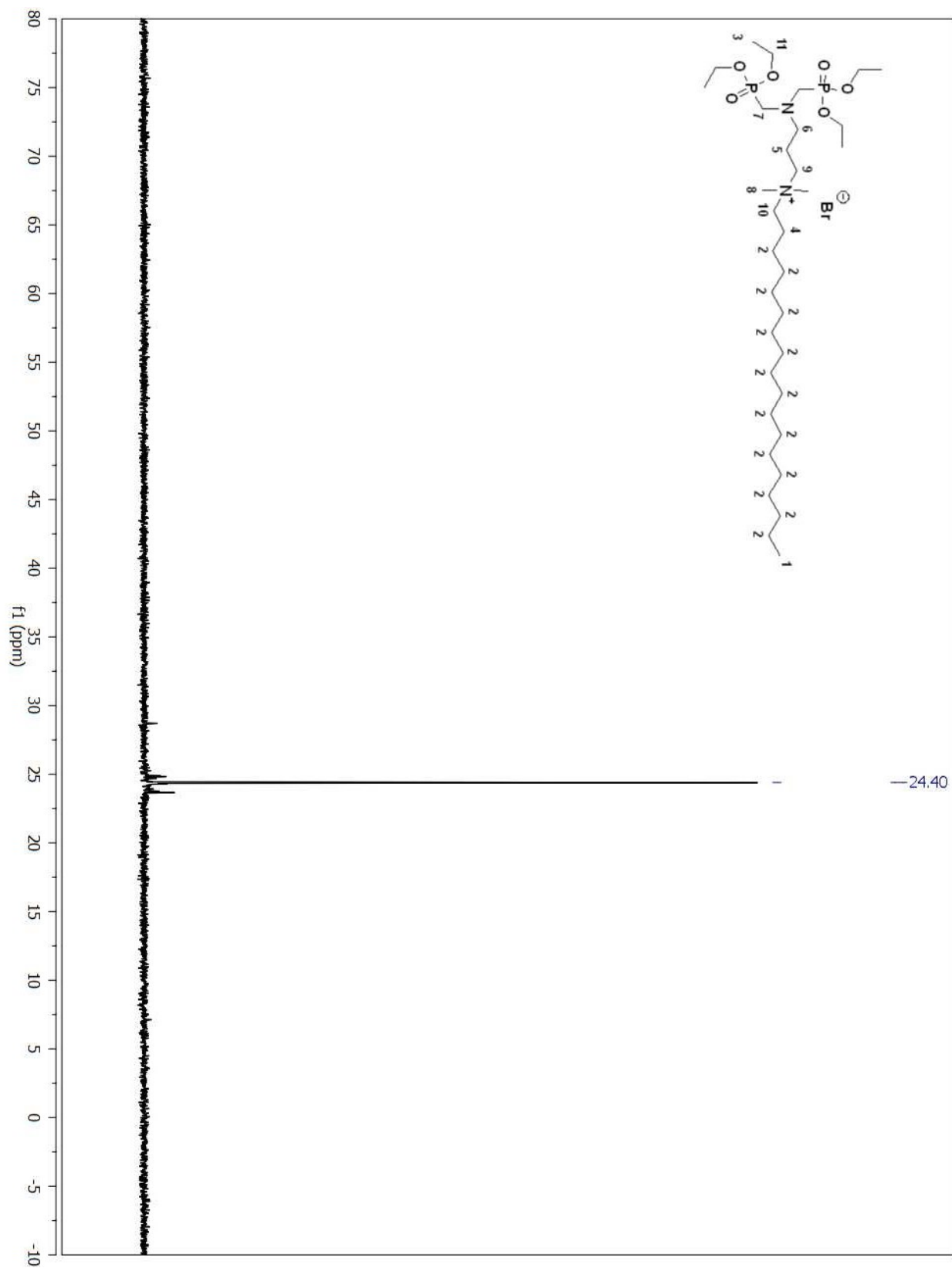


Figure A 239. ^{31}P NMR spectrum of compound (121) in CDCl_3 .

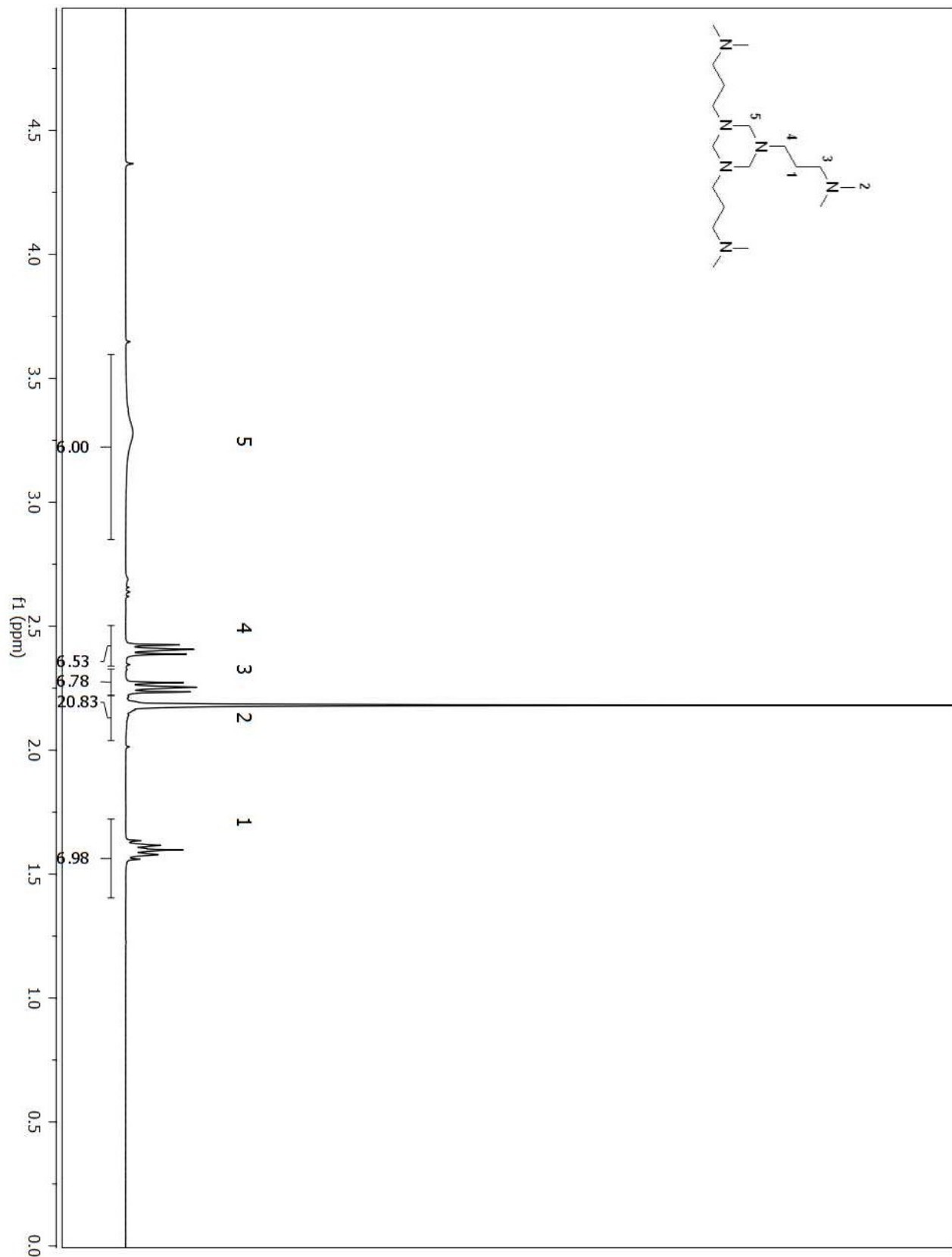


Figure A 240. ^1H NMR spectrum of compound (123) in CDCl_3 .
607

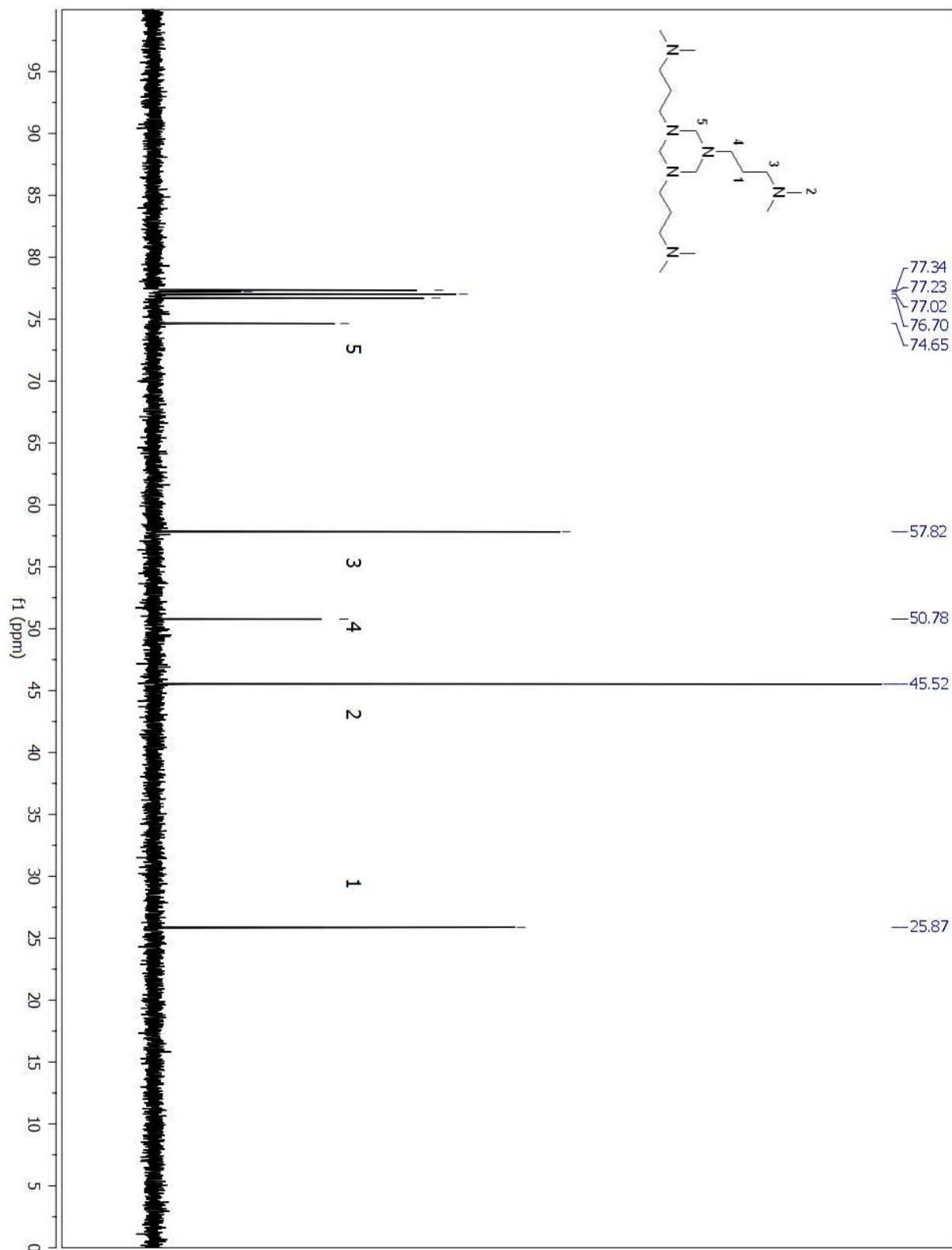


Figure A 241. ^{13}C NMR spectrum of compound (123) in CDCl_3 .

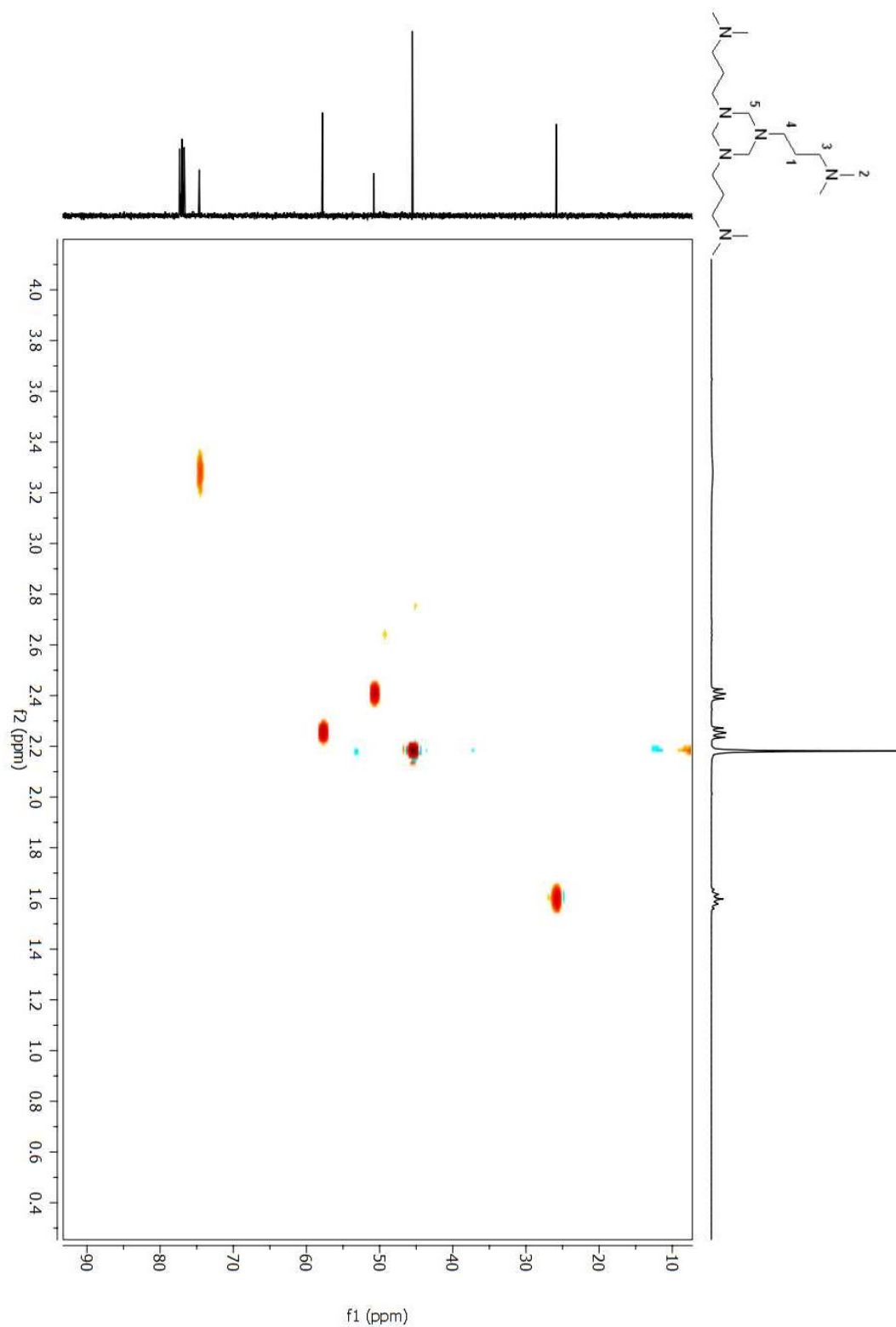


Figure A 242. HSQC 2D NMR spectrum of compound (**123**) in CDCl₃.

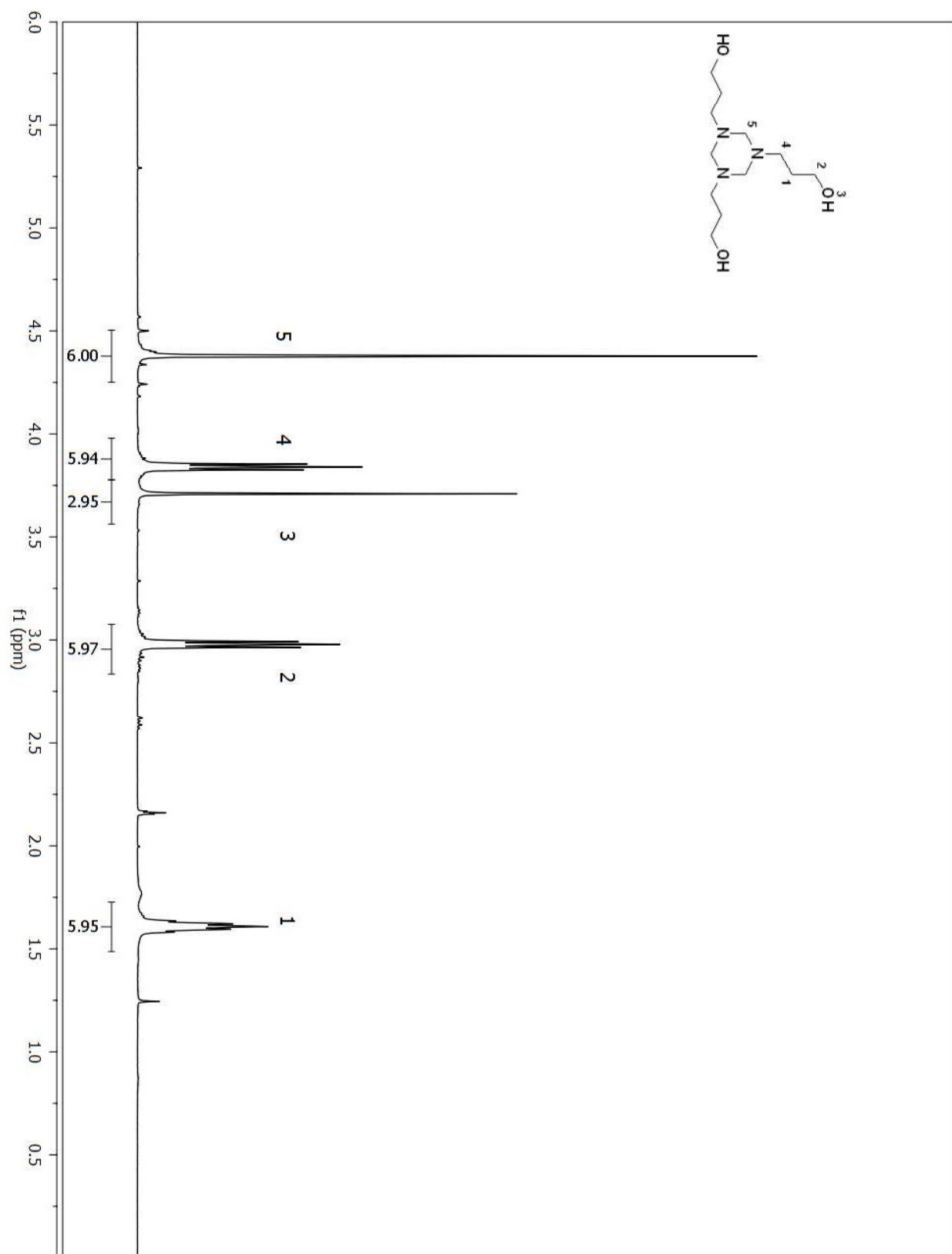


Figure A 243. ¹H NMR spectrum of compound (122) in CDCl₃.

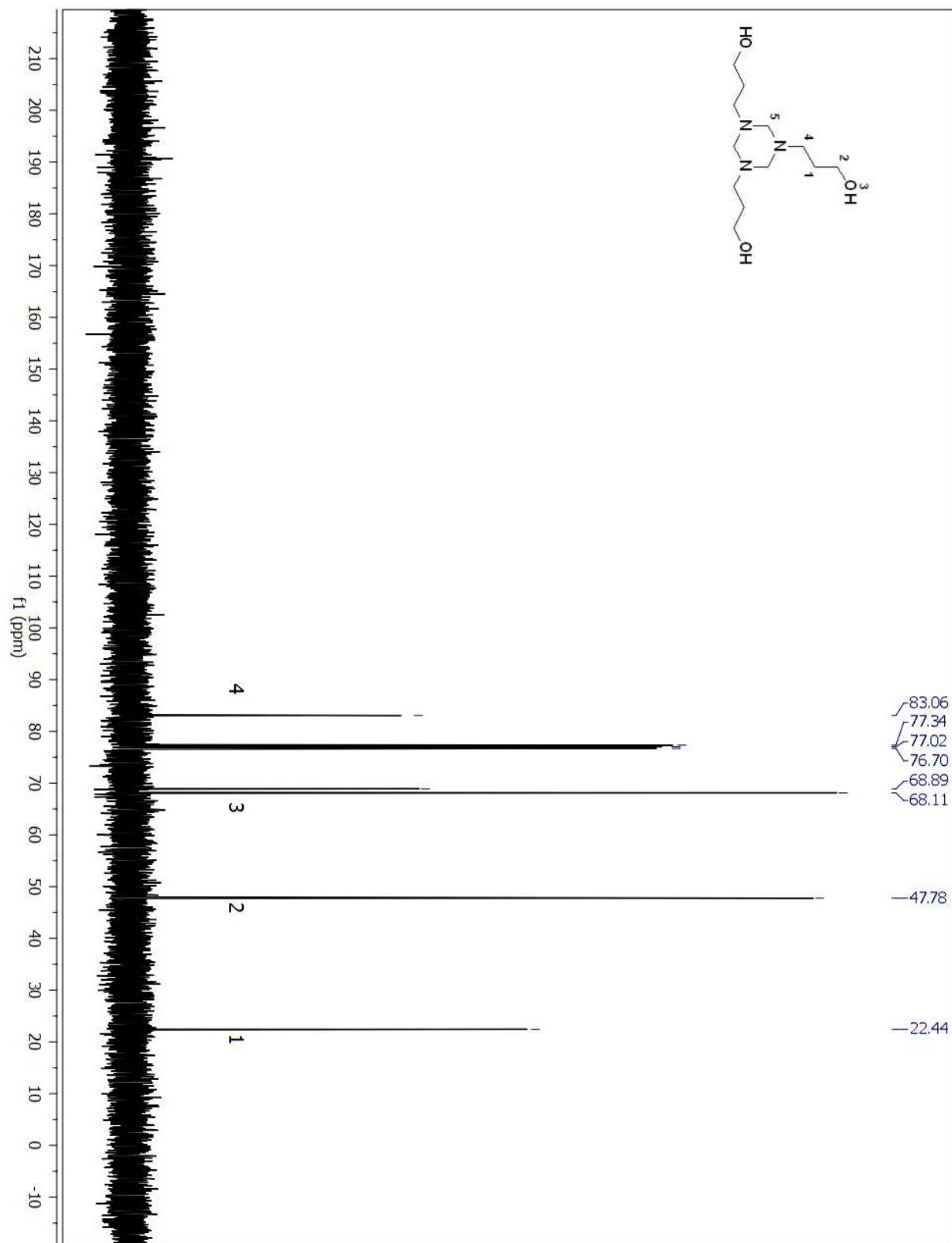


Figure A 244. ^{13}C NMR spectrum of compound (122) in CDCl_3 .

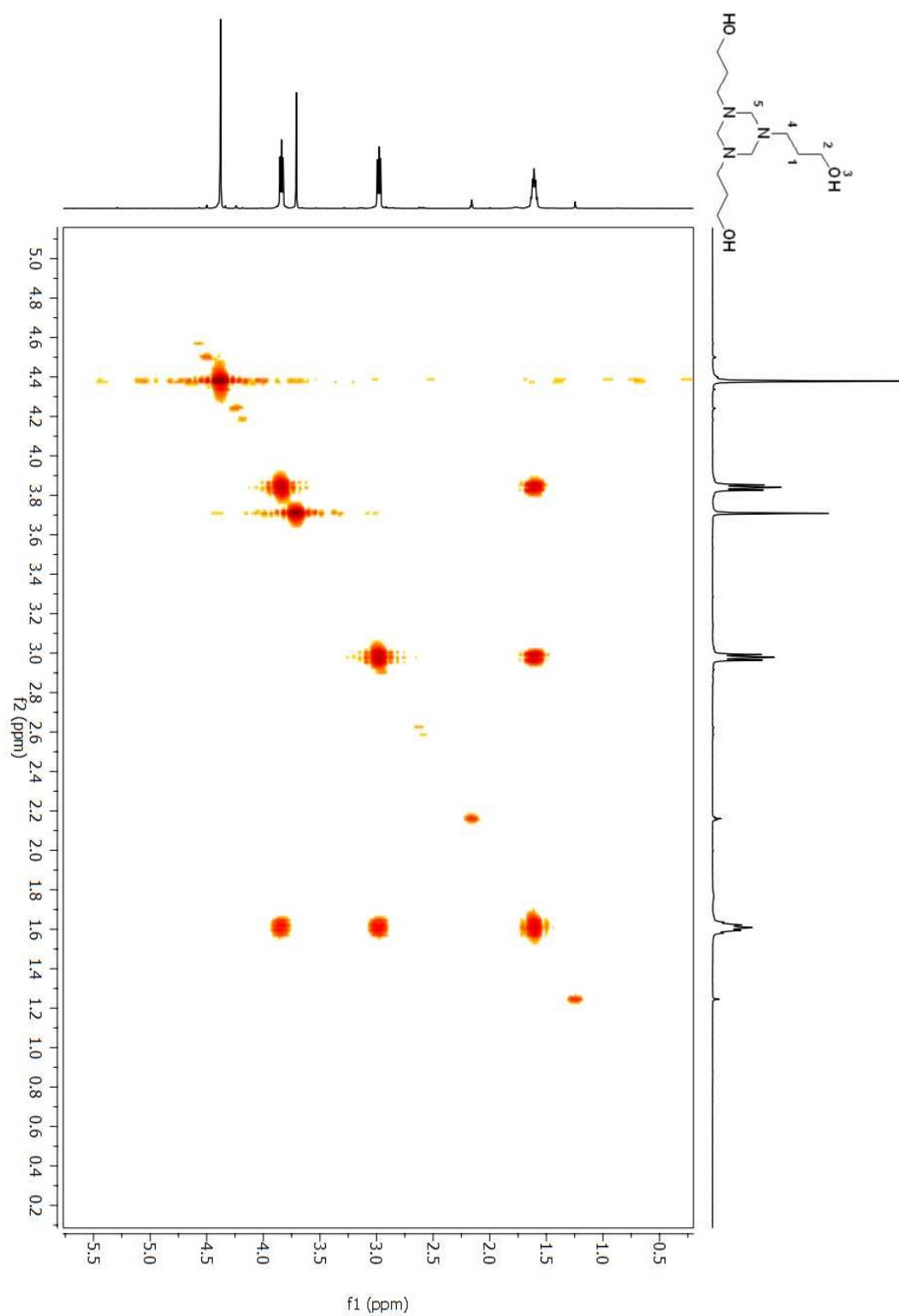


Figure A 245. COSY 2D NMR spectrum of compound (**122**) in CDCl₃.

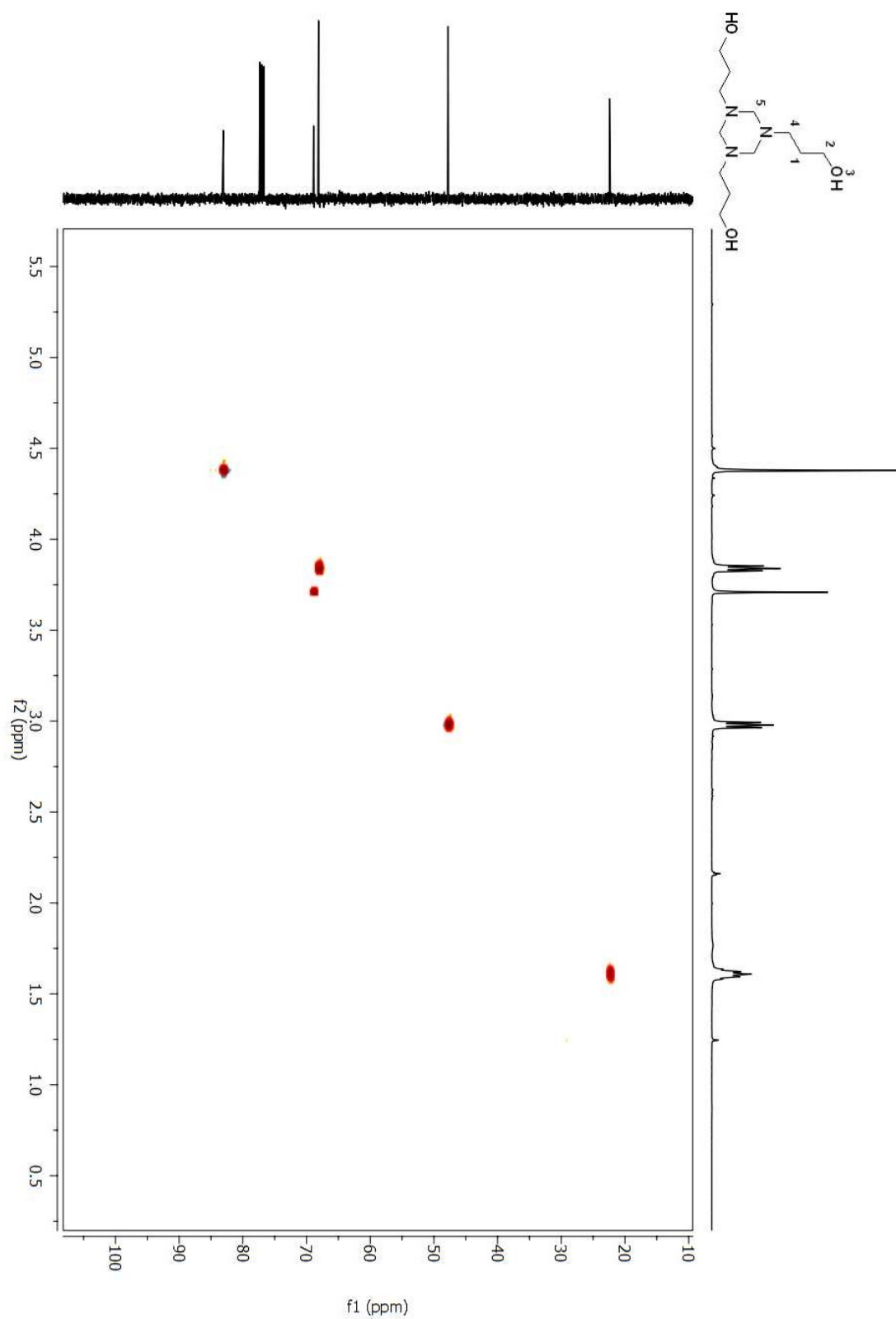


Figure A 246. HSQC 2D NMR spectrum of compound (**122**) in CDCl₃.

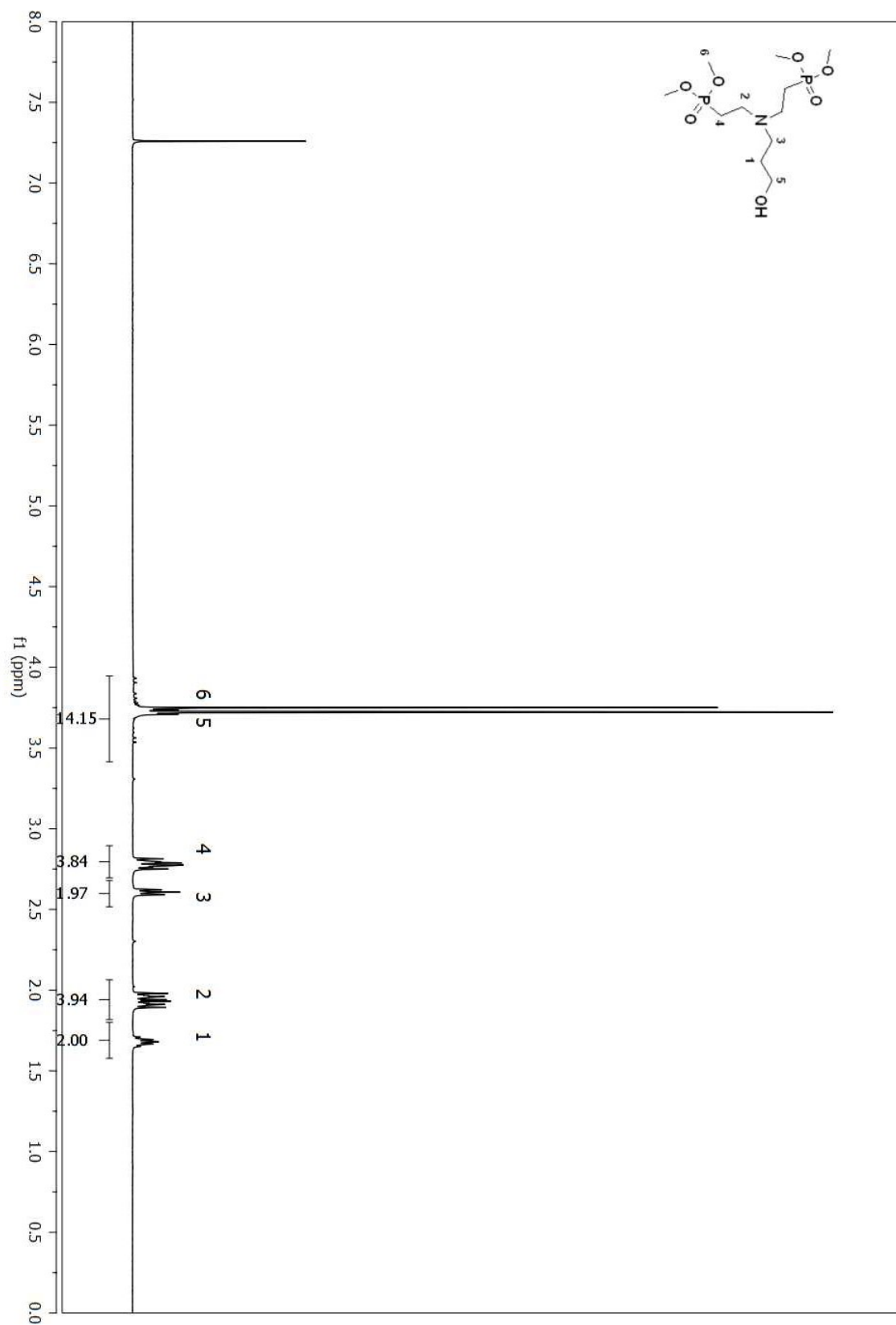


Figure A 247. ^1H NMR spectrum of compound (135) in CDCl_3 .

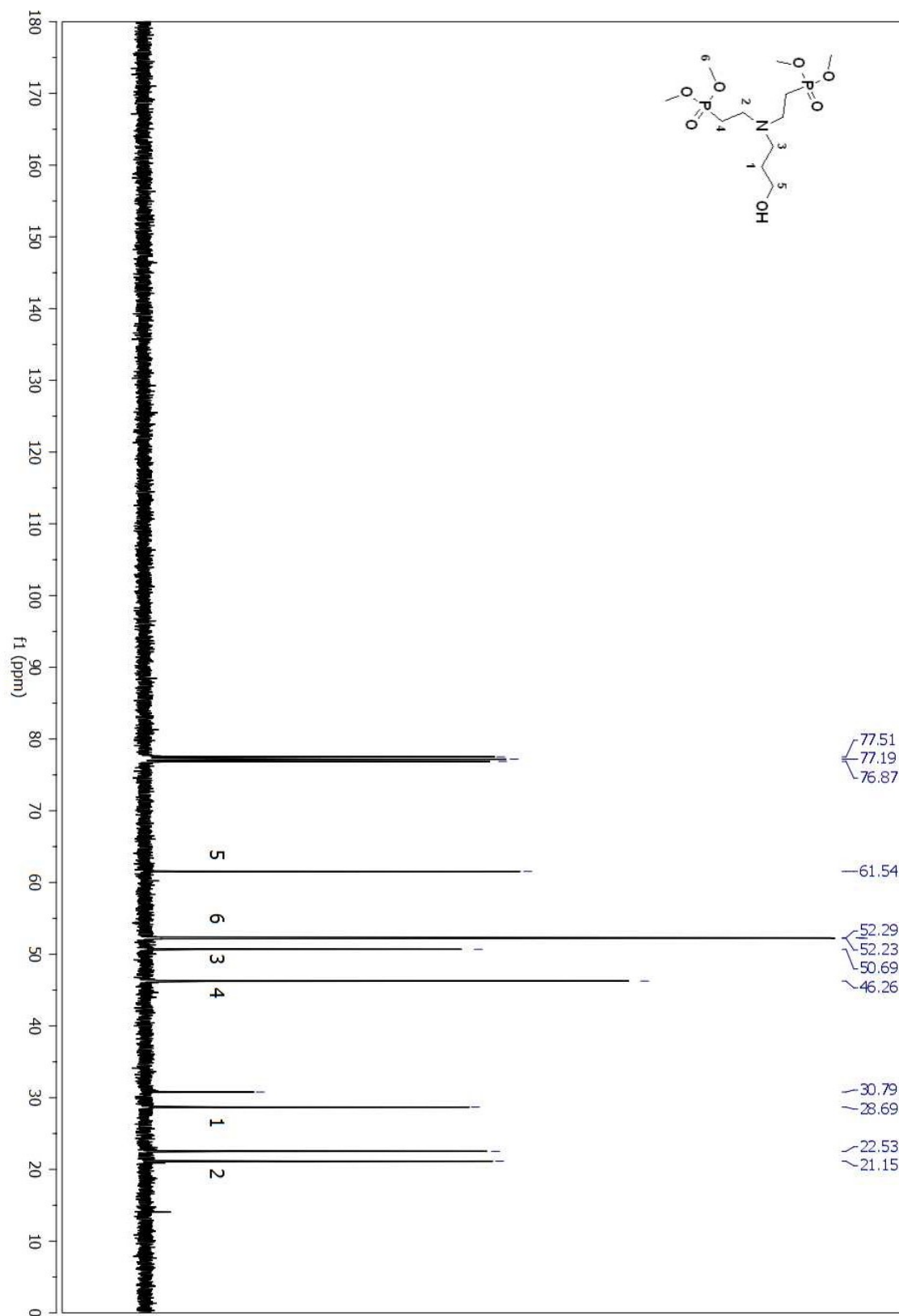


Figure A 248. ¹³C NMR spectrum of compound (135) in CDCl₃.

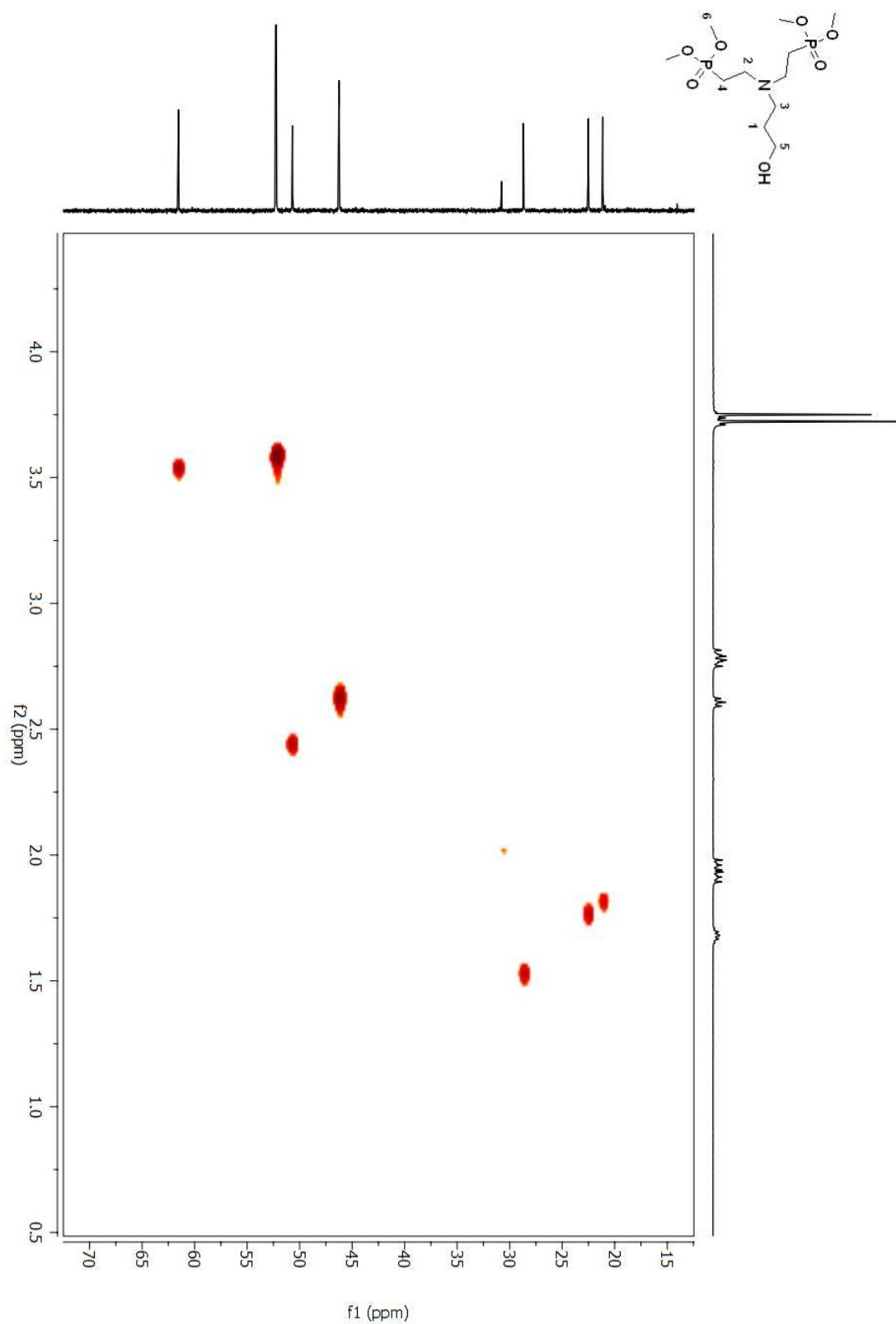


Figure A 249. HSQC 2D NMR spectrum of compound (135) in CDCl₃.

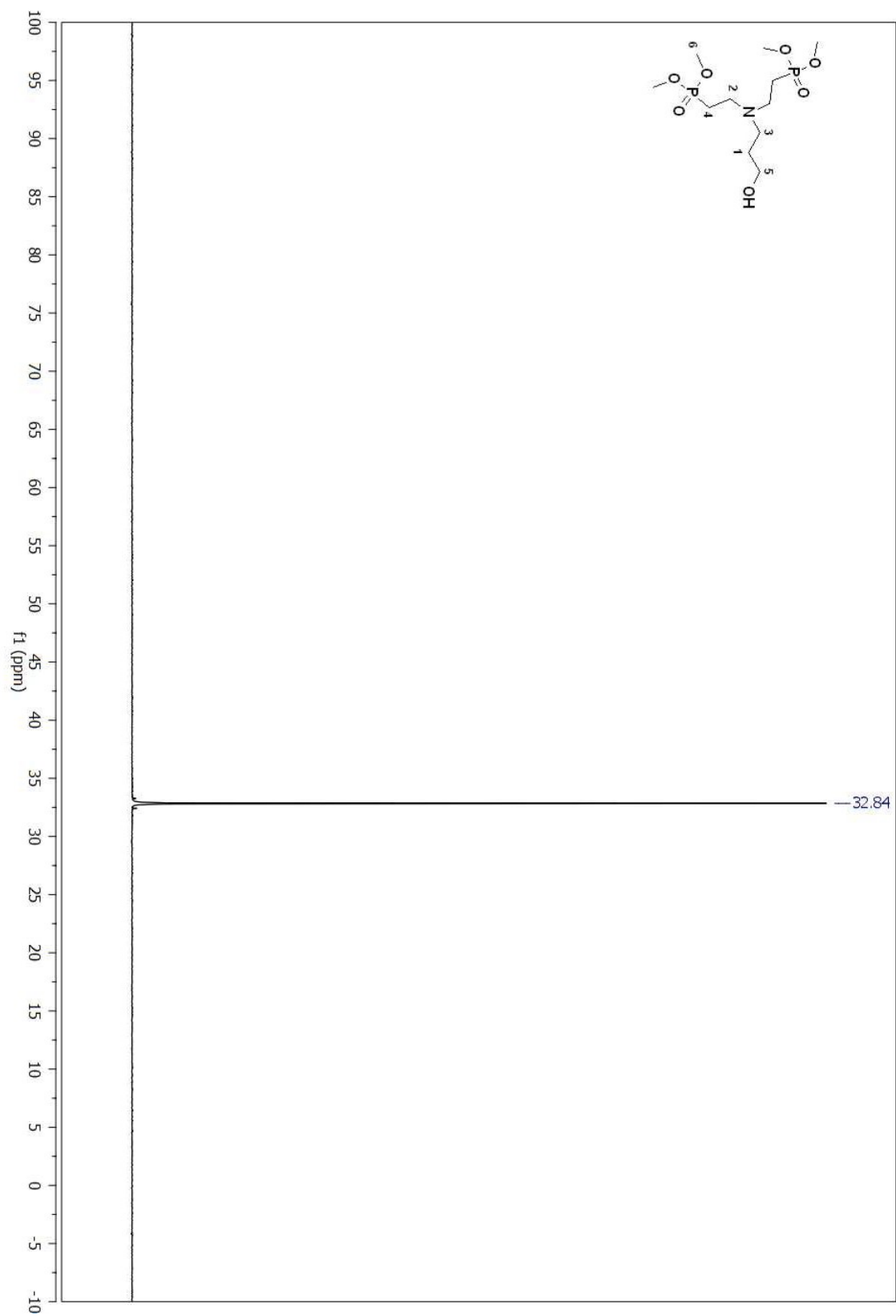


Figure A 250. ^{31}P NMR spectrum of compound (135) in CDCl_3 .

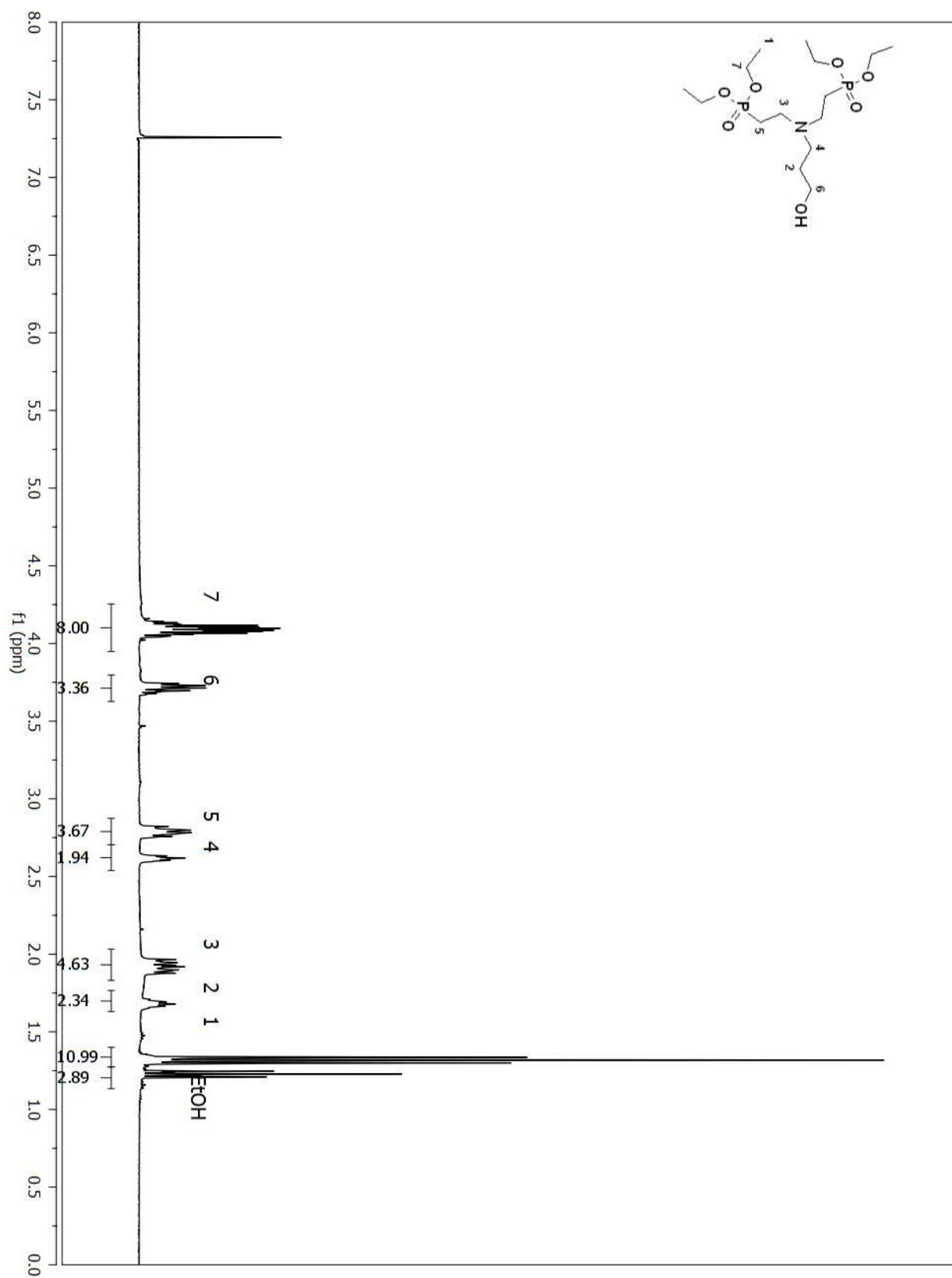


Figure A 251. ^1H NMR spectrum of compound (136) in CDCl_3 .

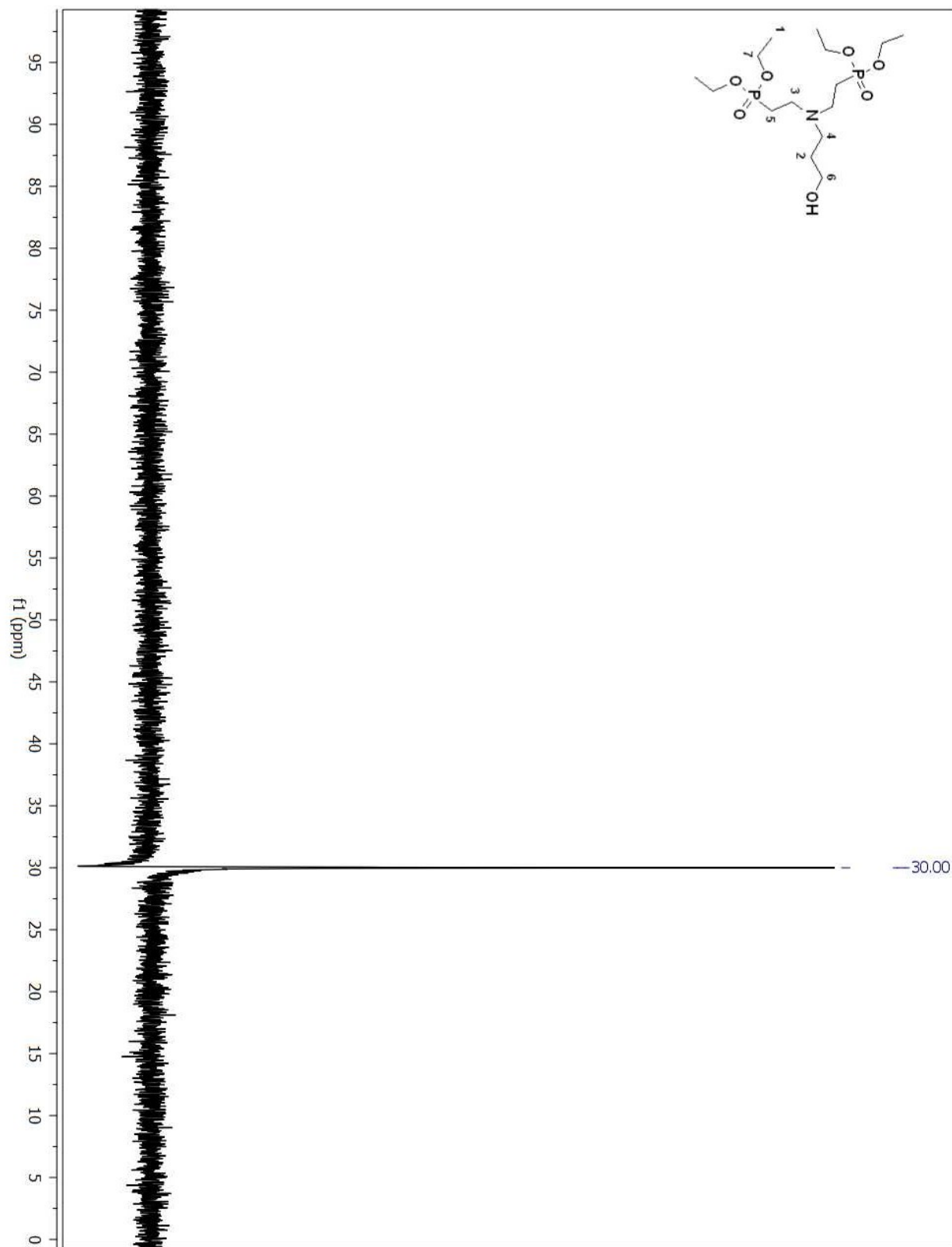


Figure A 252. ^{31}P NMR spectrum of compound (136) in CDCl_3 .

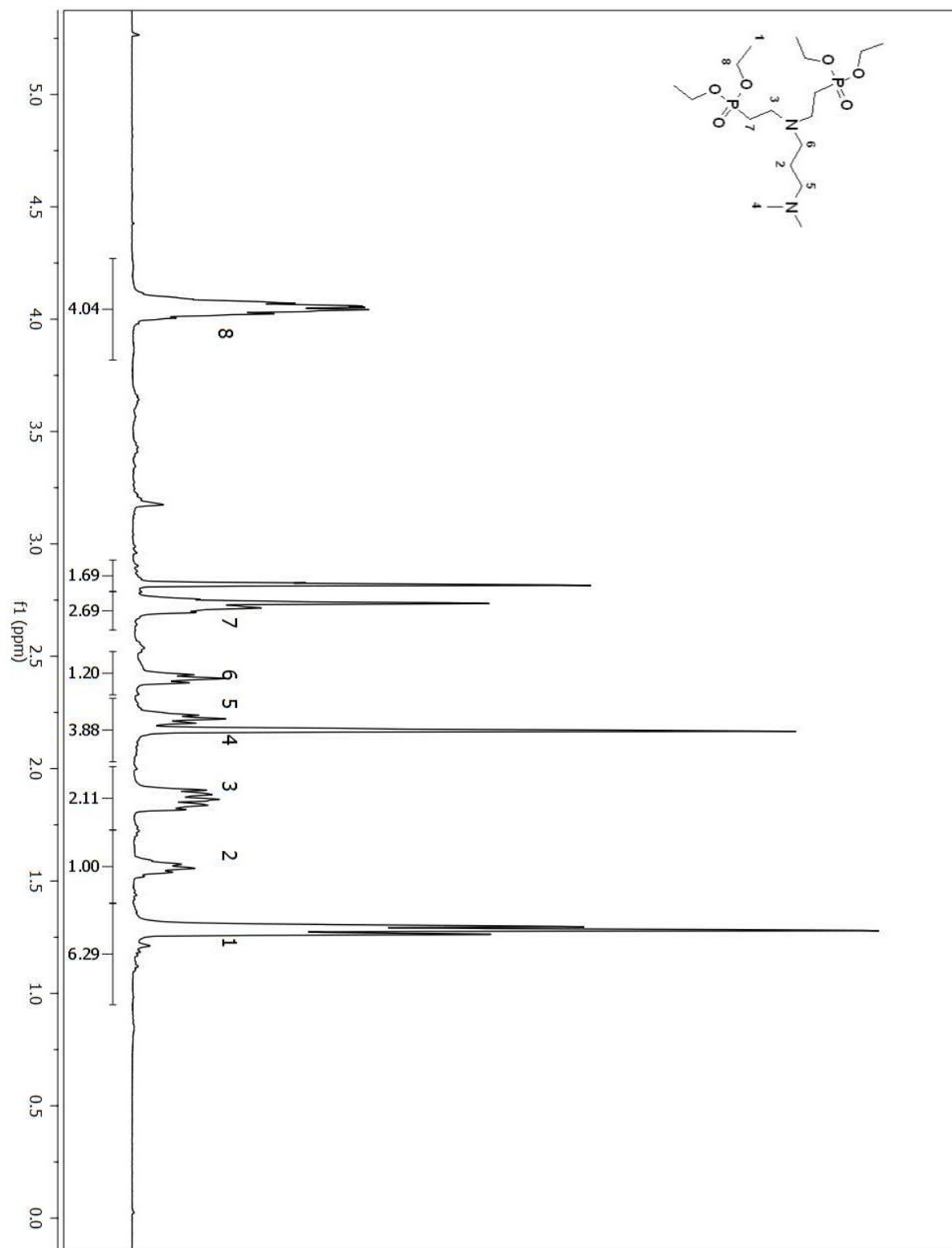


Figure A 253. ^1H NMR spectrum of compound (131) in CDCl_3 .
620

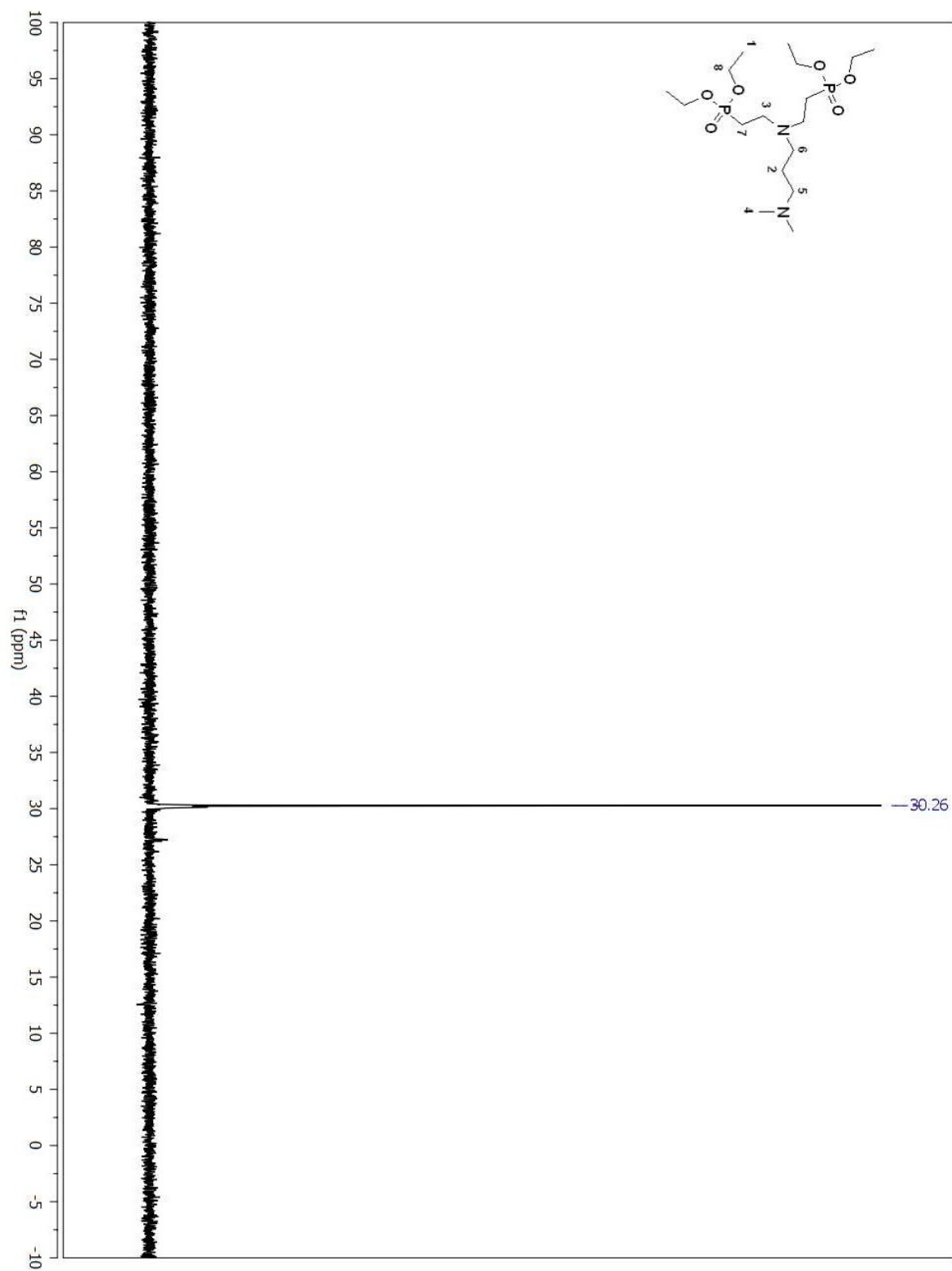


Figure A 254. ^{31}P NMR spectrum of compound (131) in CDCl_3 .

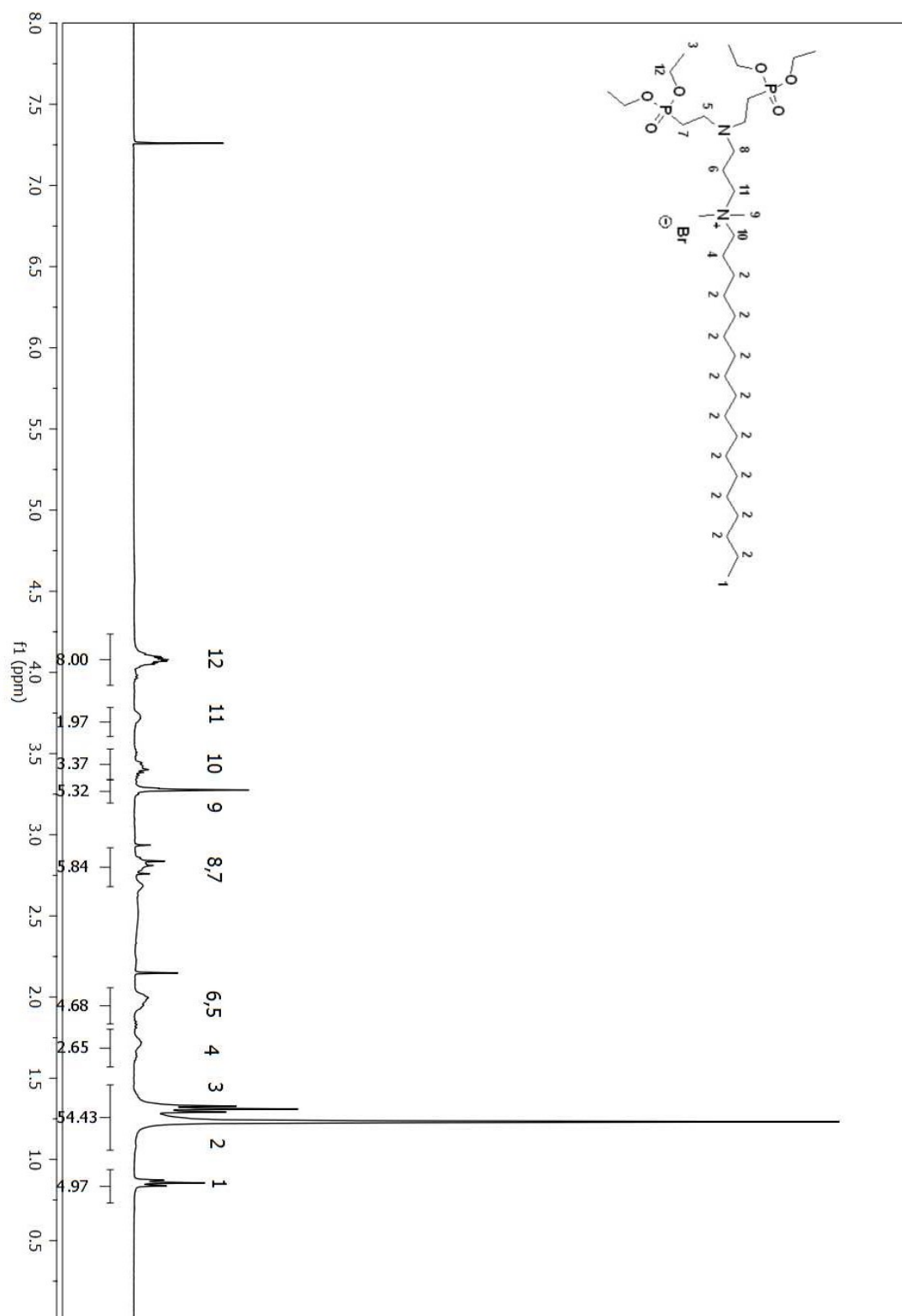


Figure A 255. ¹H NMR spectrum of compound (140) in CDCl₃.

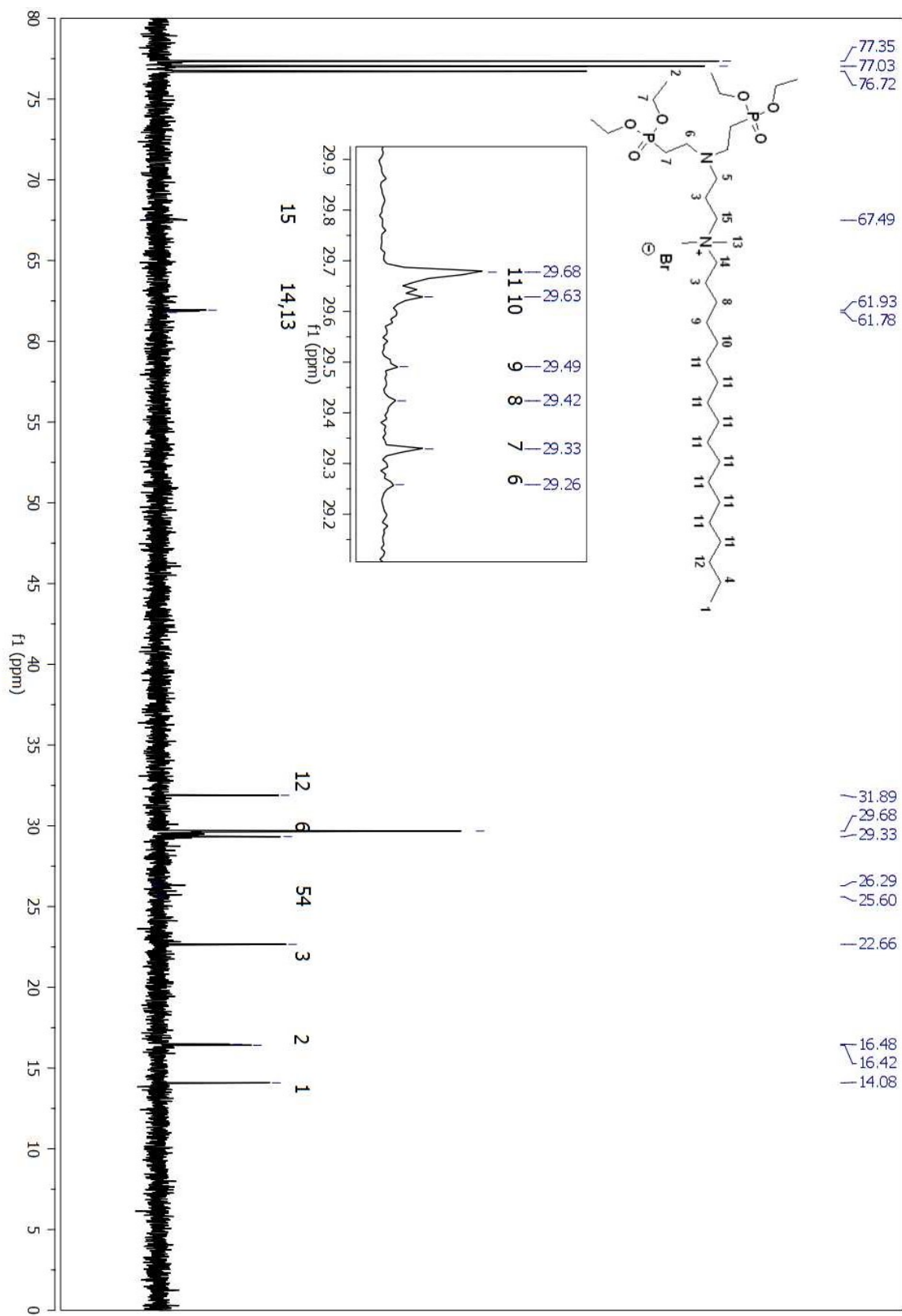
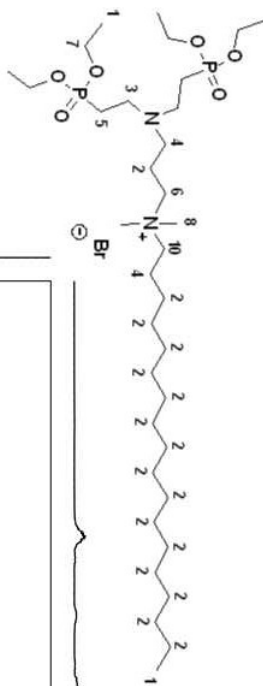


Figure A 256. ^{13}C NMR spectrum of compound (140) in CDCl_3 .



624

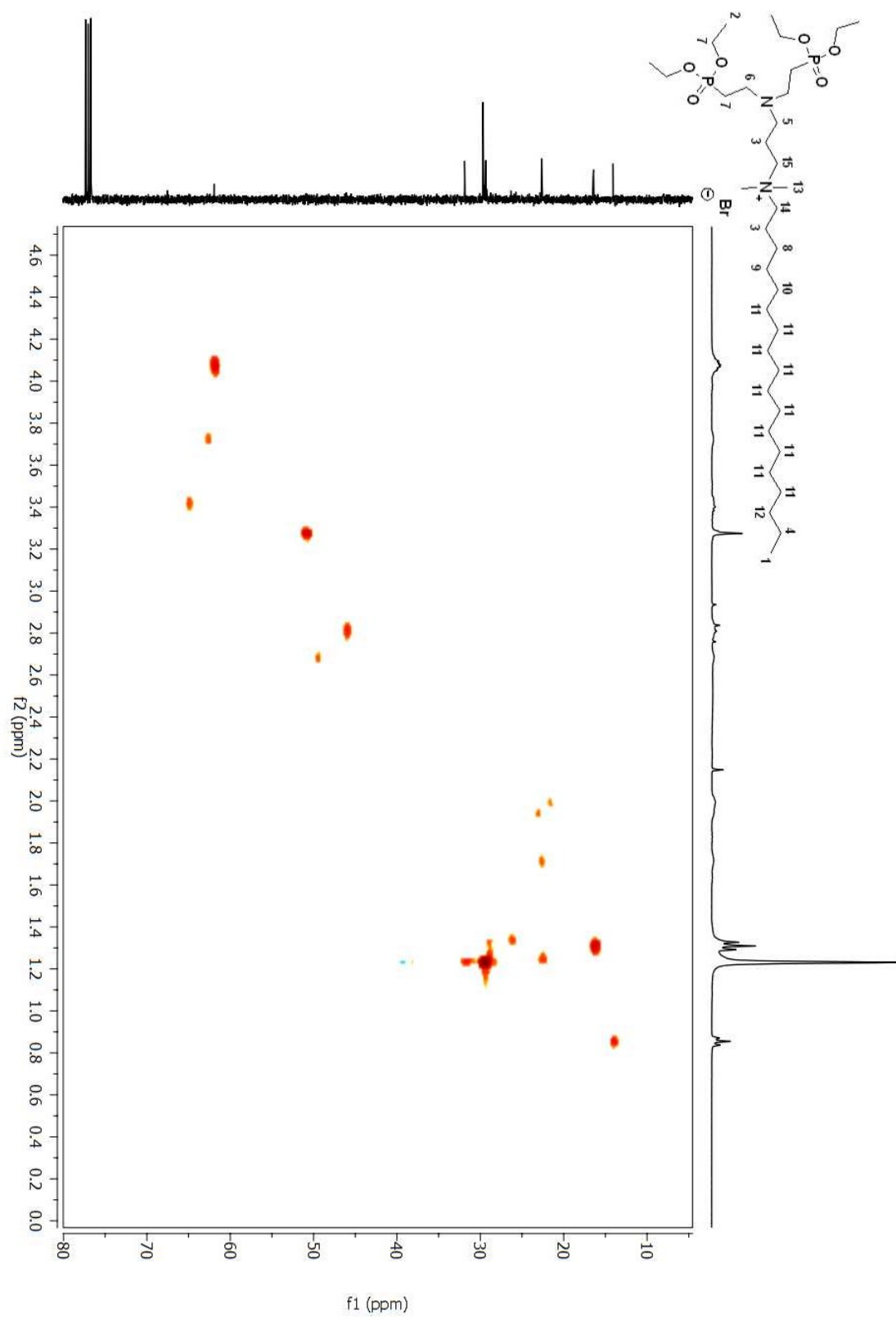


Figure A 258. HSQC 2D NMR spectrum of compound (**140**) in CDCl₃.

Figure A 259. ^1H NMR spectrum of compound (**153**) in CDCl_3 .

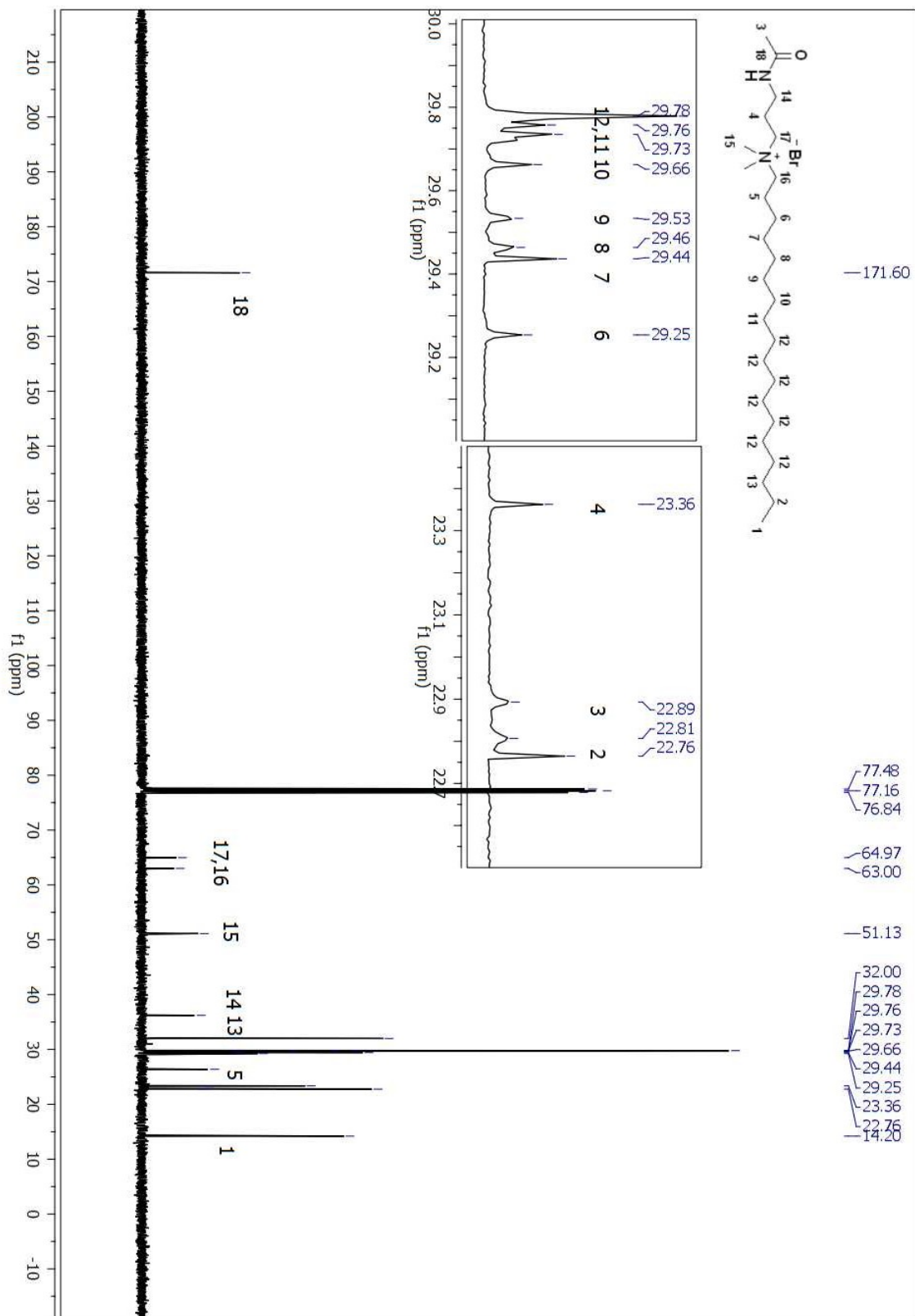


Figure A 260. ^{13}C NMR spectrum of compound (**153**) in CDCl_3 .

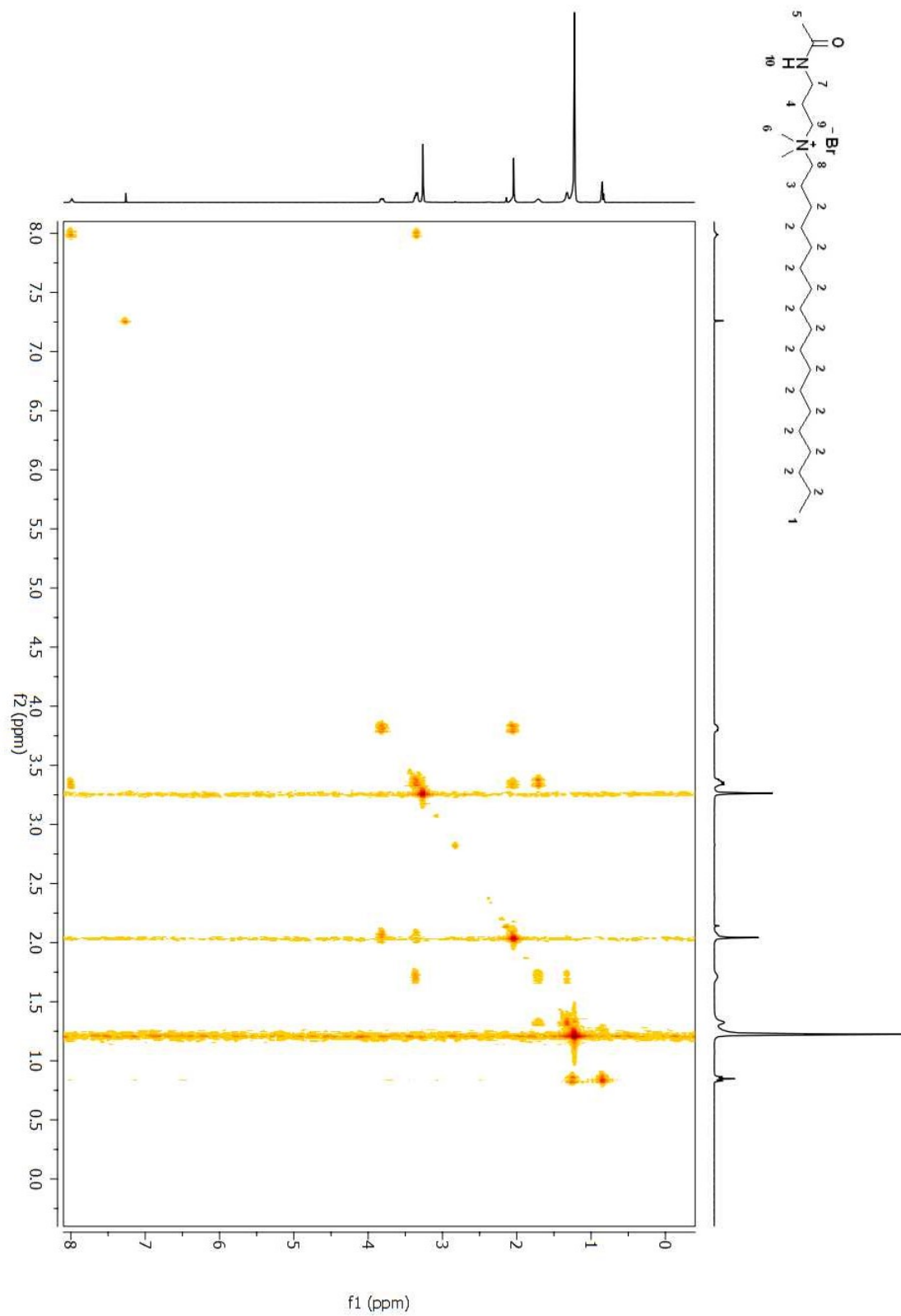


Figure A 261. ^{13}C NMR spectrum of compound (153) in CDCl_3 .

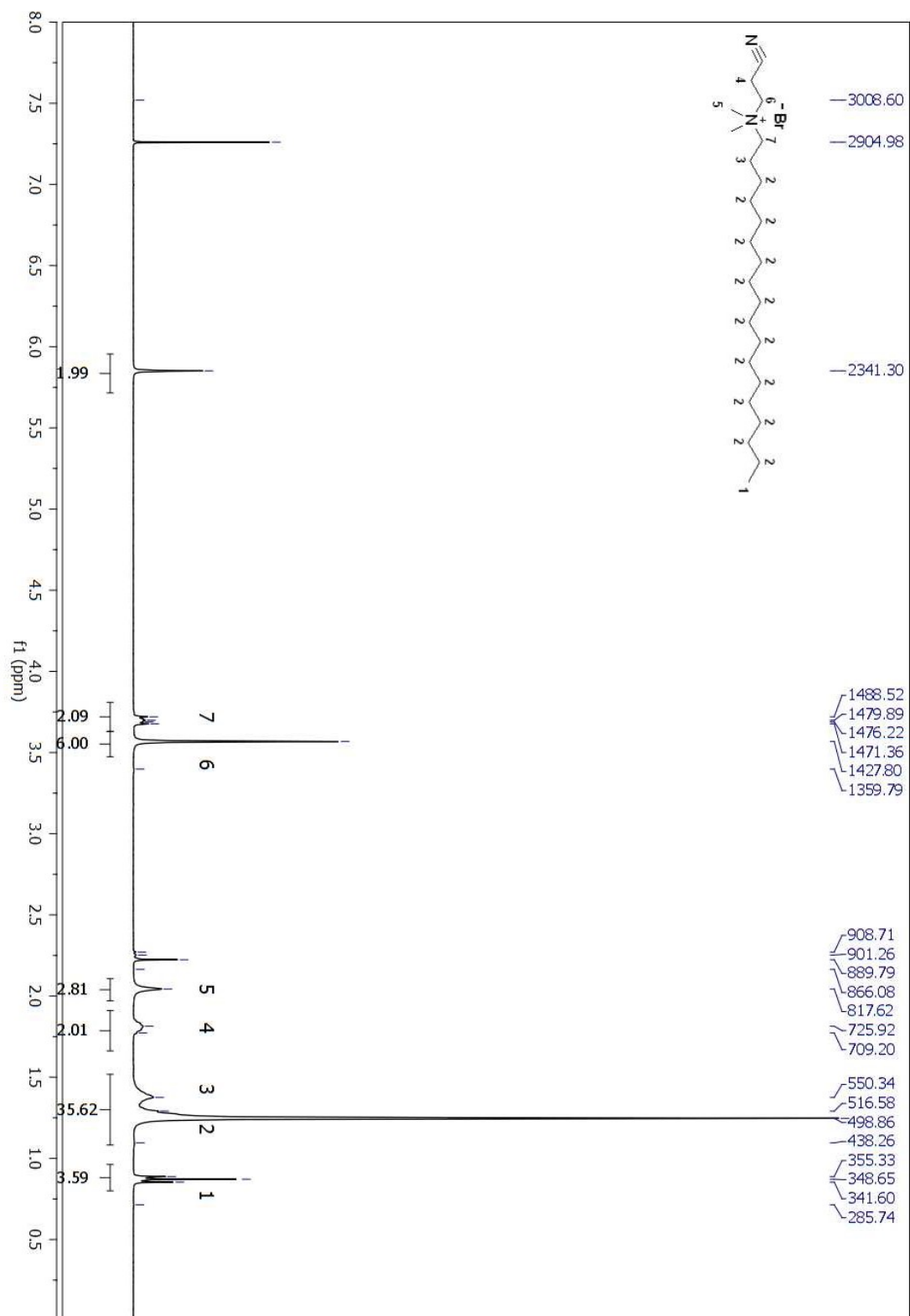


Figure A 262. ^1H NMR spectrum of compound (154) in CDCl_3 .

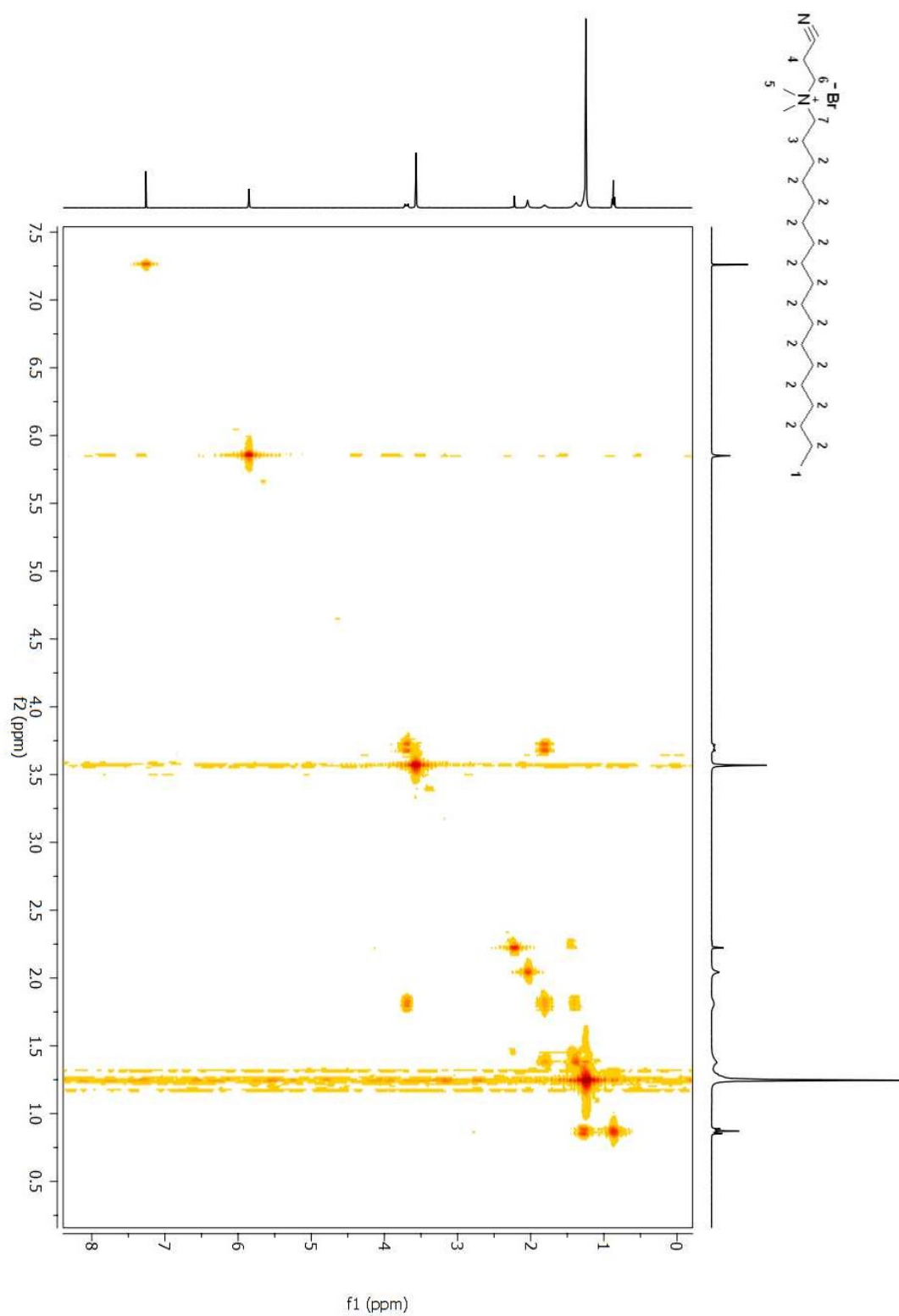


Figure A 263. COSY 2D NMR spectrum of compound (**154**) in CDCl_3 .

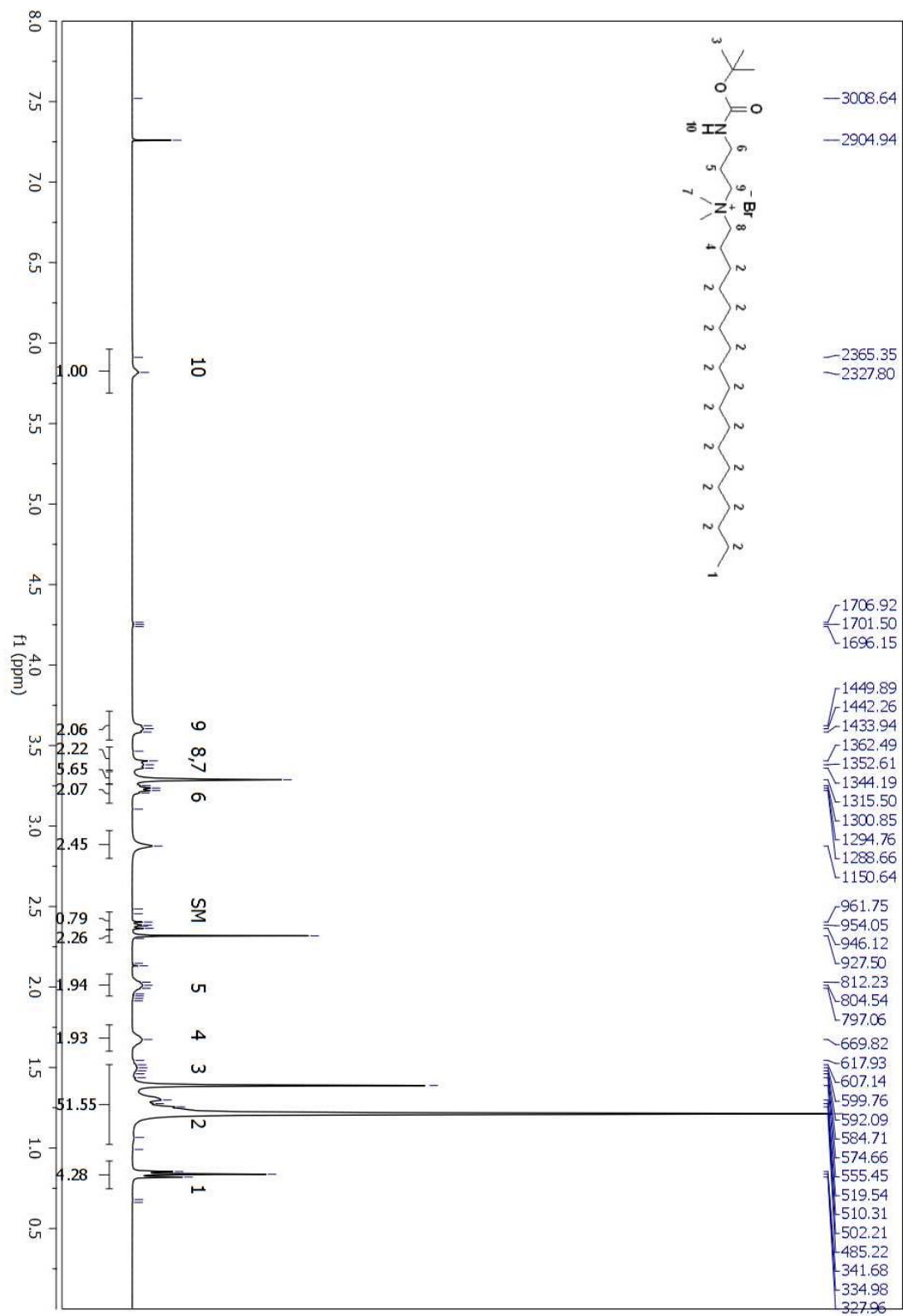


Figure A 264. ¹H NMR spectrum of compound (155) in CDCl₃.

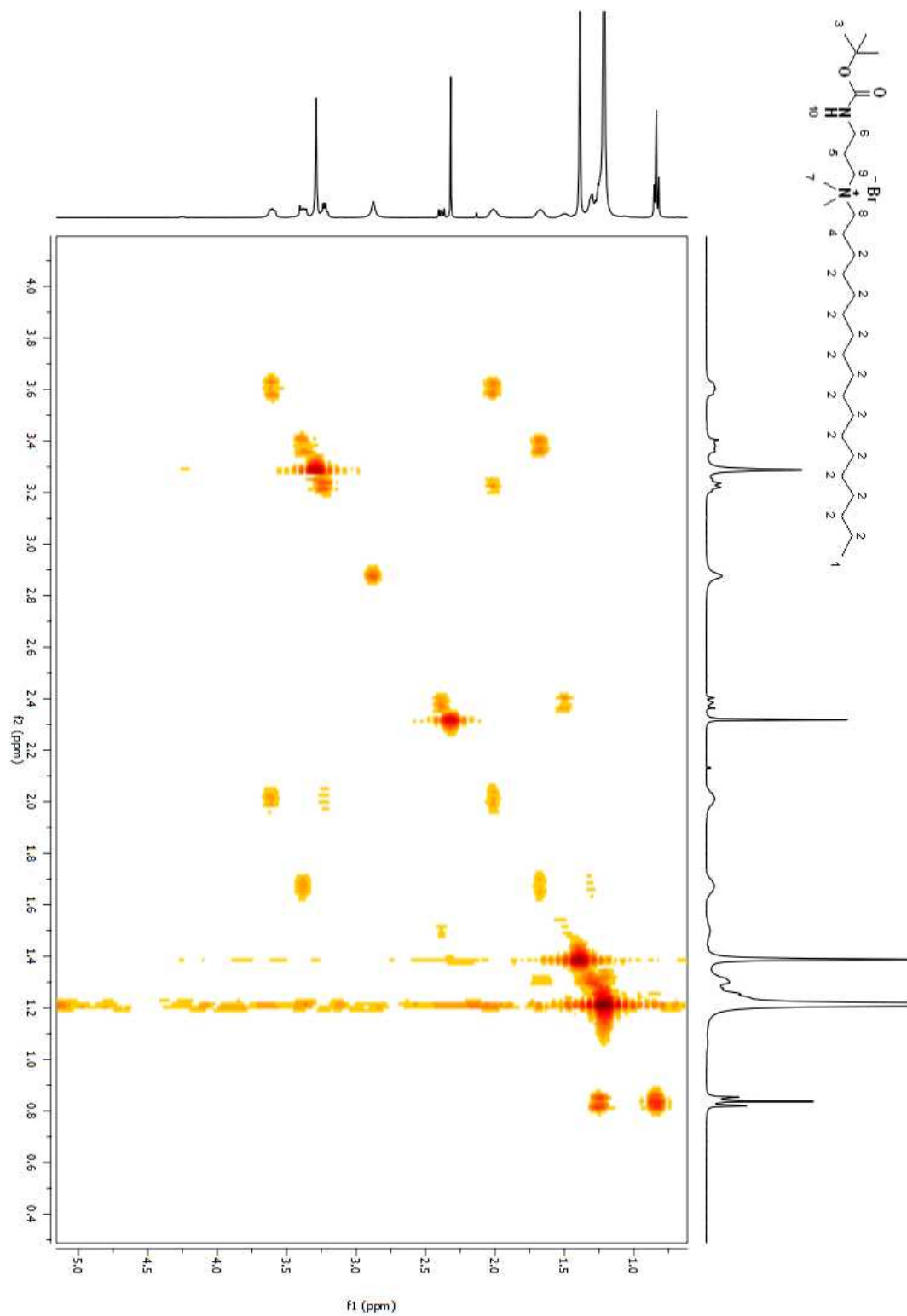
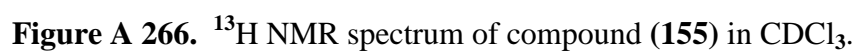


Figure A 265. COSY 2D NMR spectrum of compound (**155**) in CDCl₃.



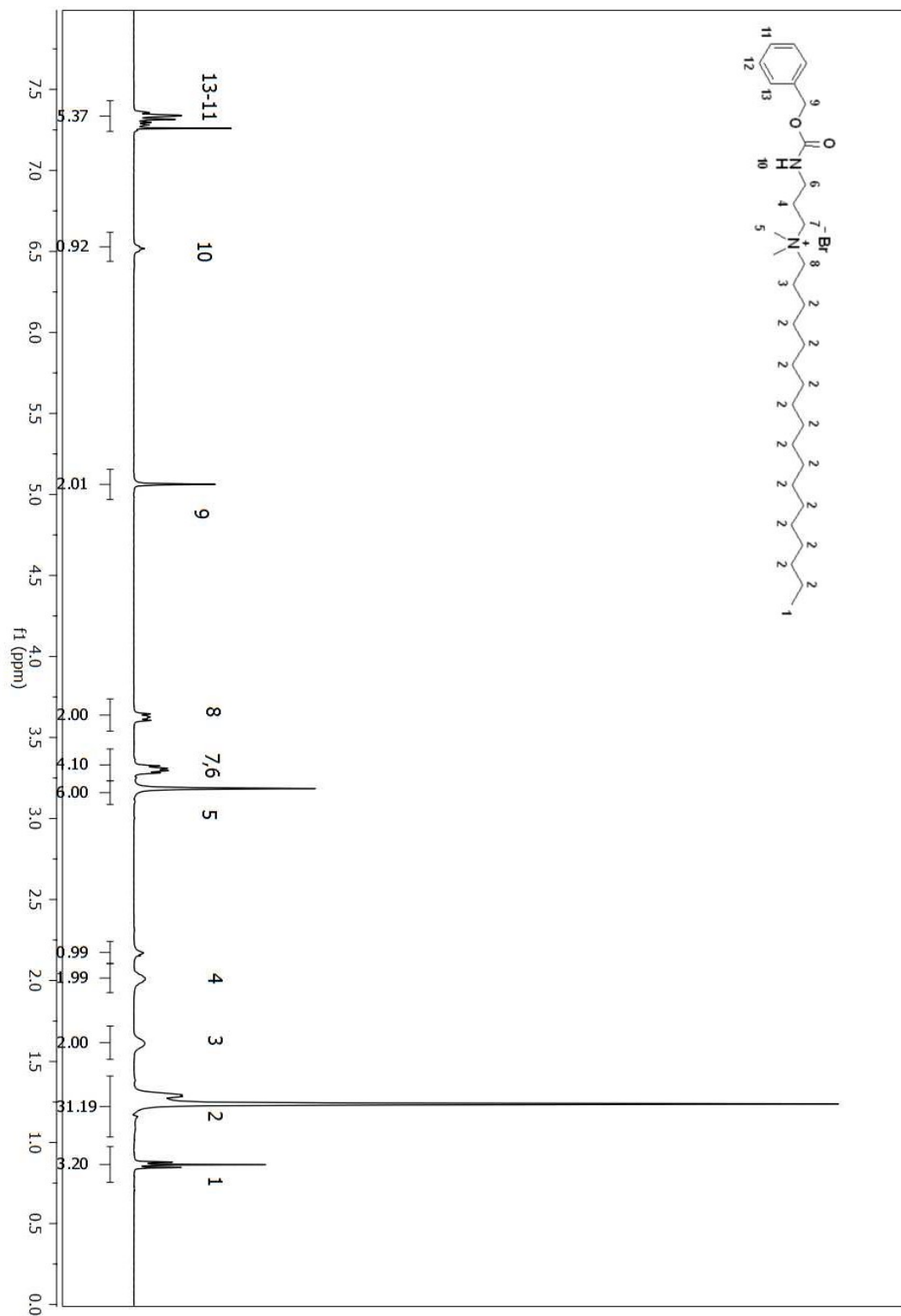


Figure A 267. ¹H NMR spectrum of compound (156) in CDCl₃.

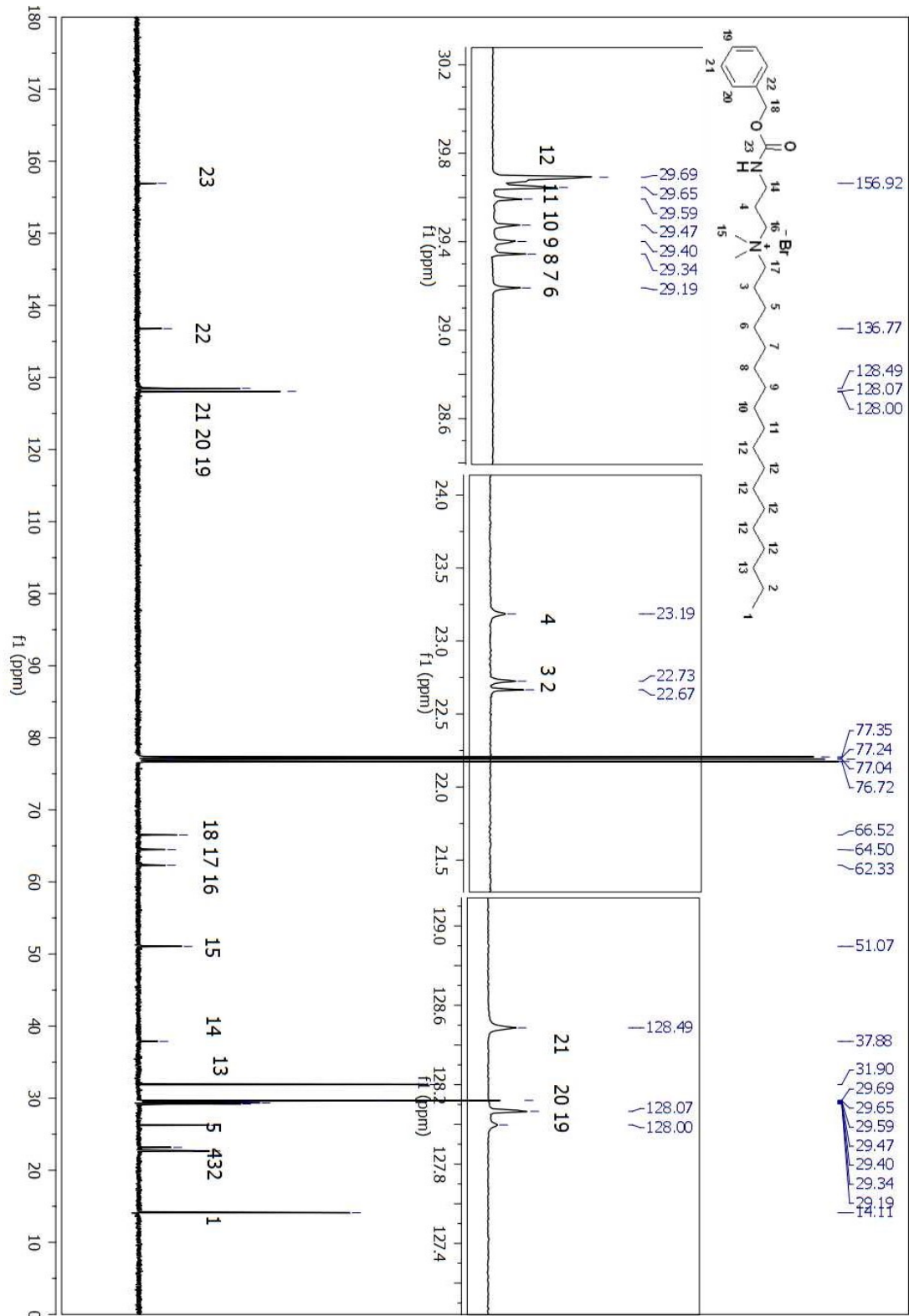


Figure A 268. ^{13}C NMR spectrum of compound (156) in CDCl_3 .

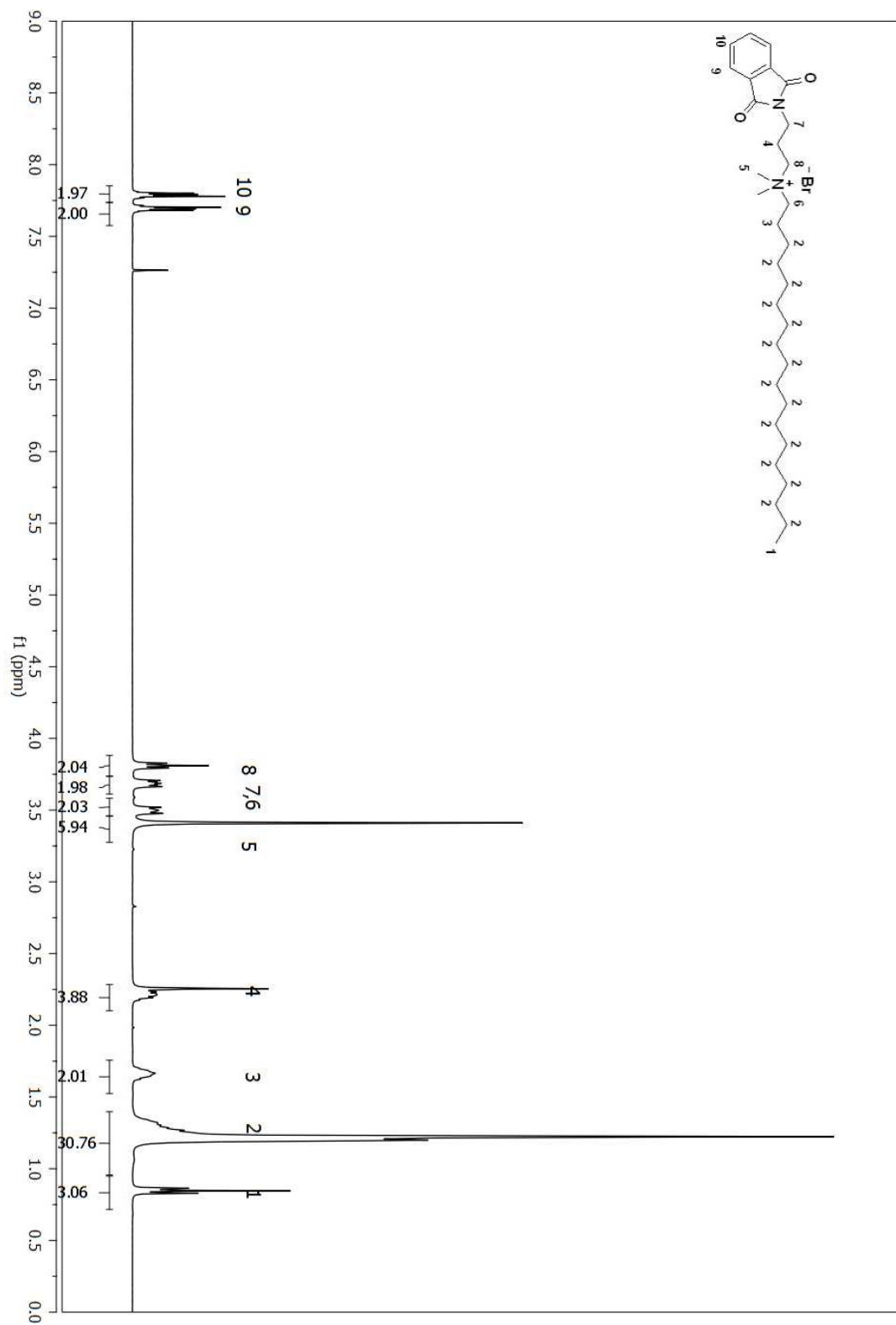


Figure A 269. ¹H NMR spectrum of compound (152) in CDCl₃.

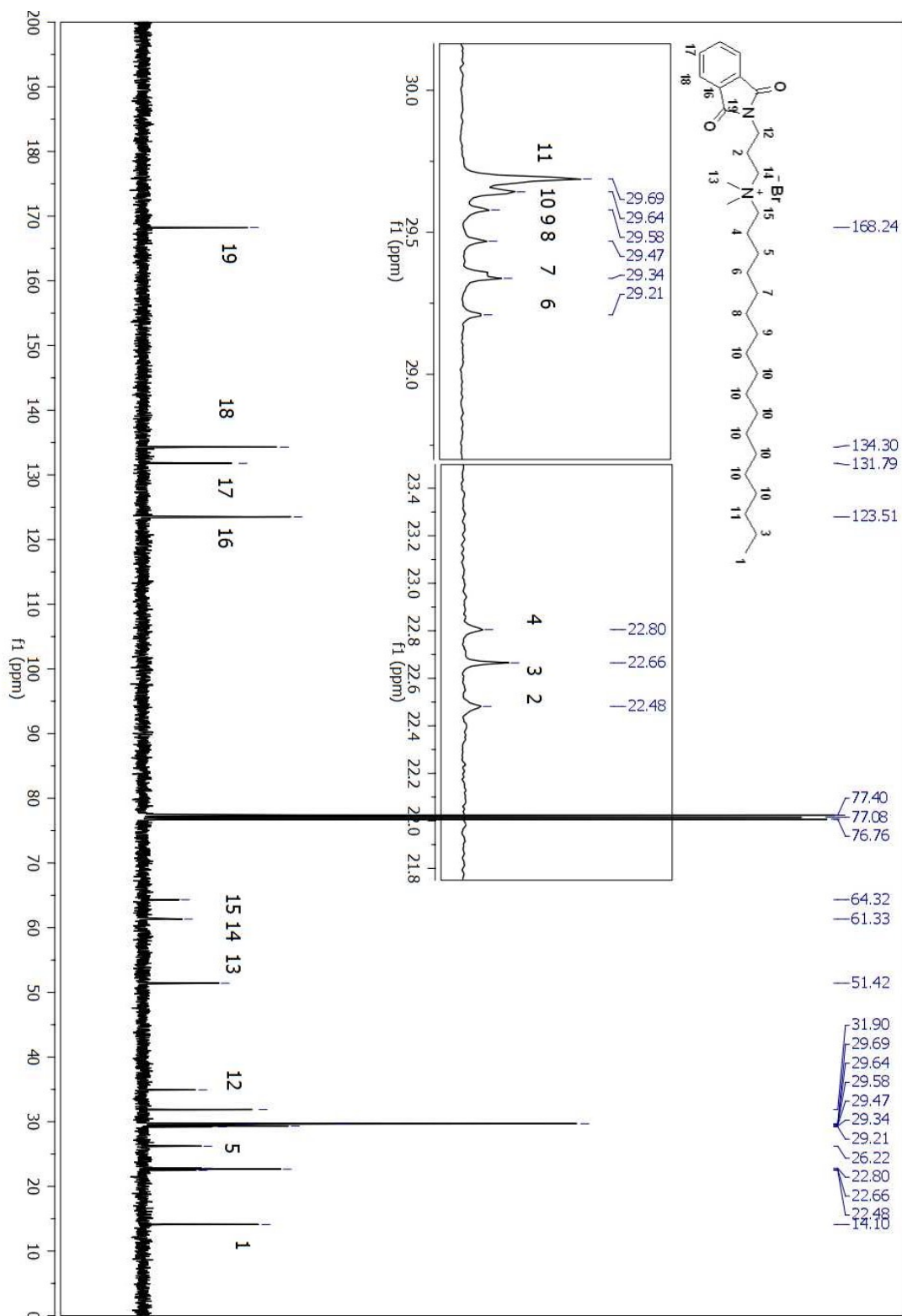


Figure A 270. ^{13}C NMR spectrum of compound (152) in CDCl_3 .

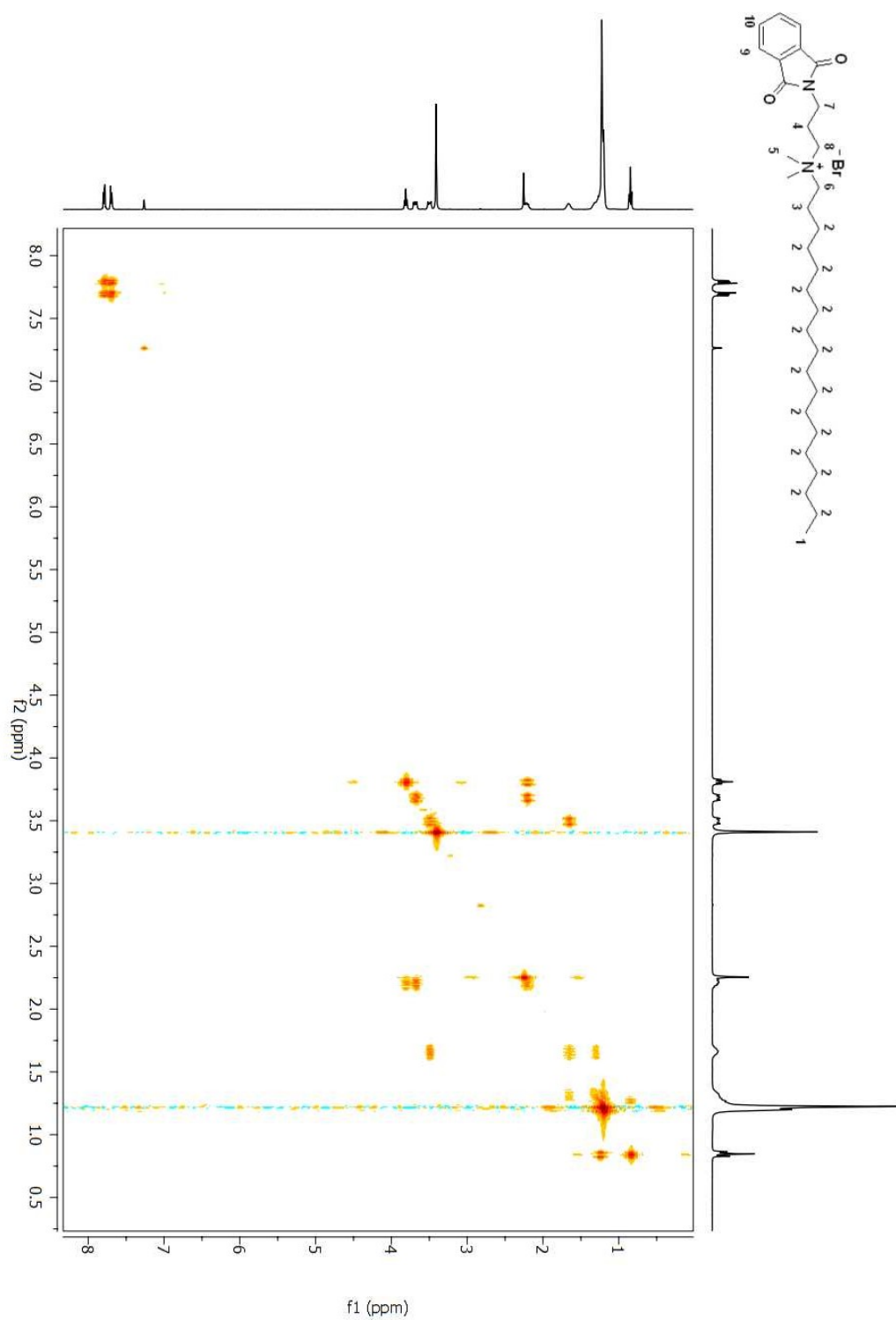


Figure A 271. COSY 2D NMR spectrum of compound (152) in CDCl₃.

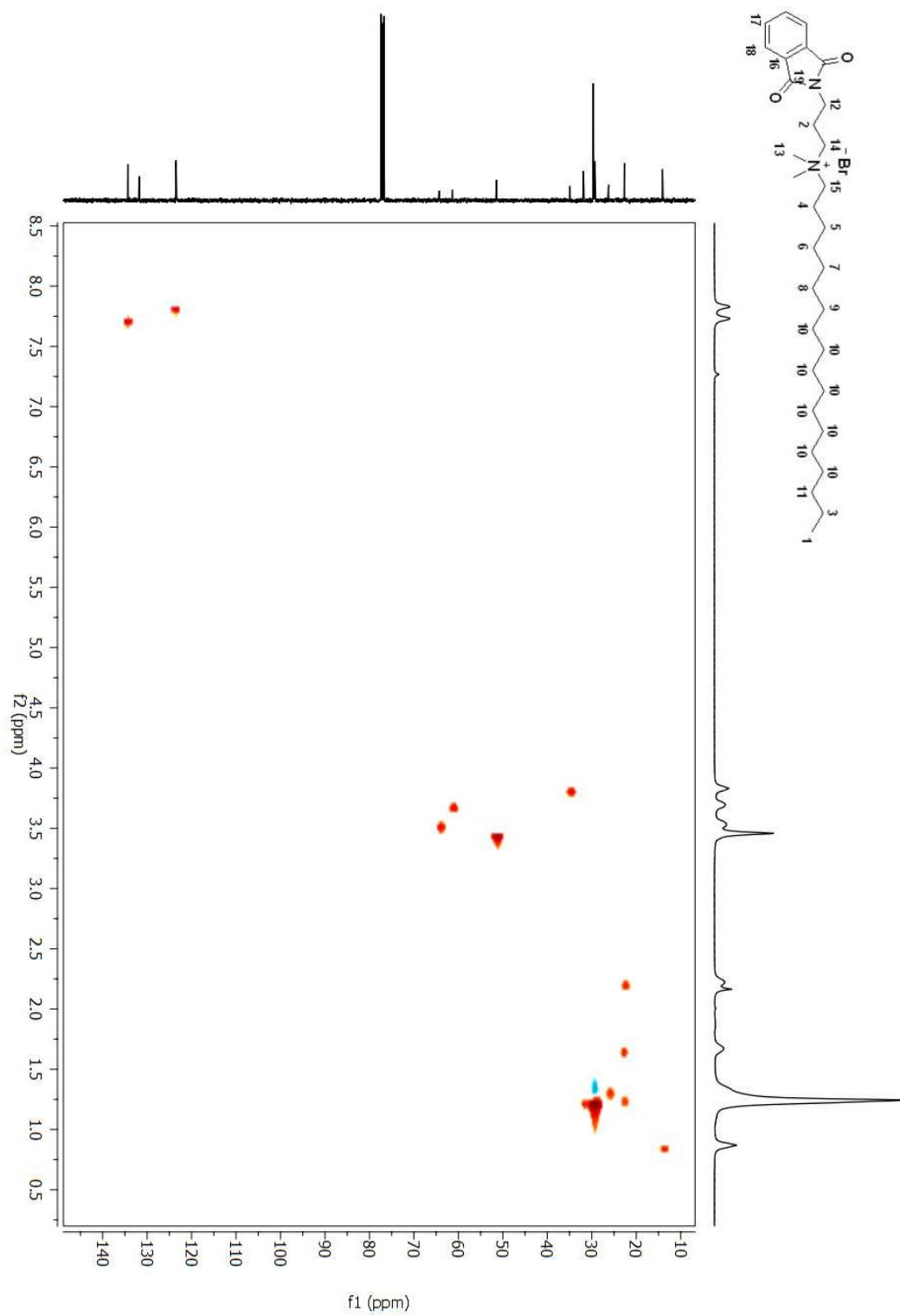


Figure A 272. HSQC 2D NMR spectrum of compound (152) in CDCl_3 .

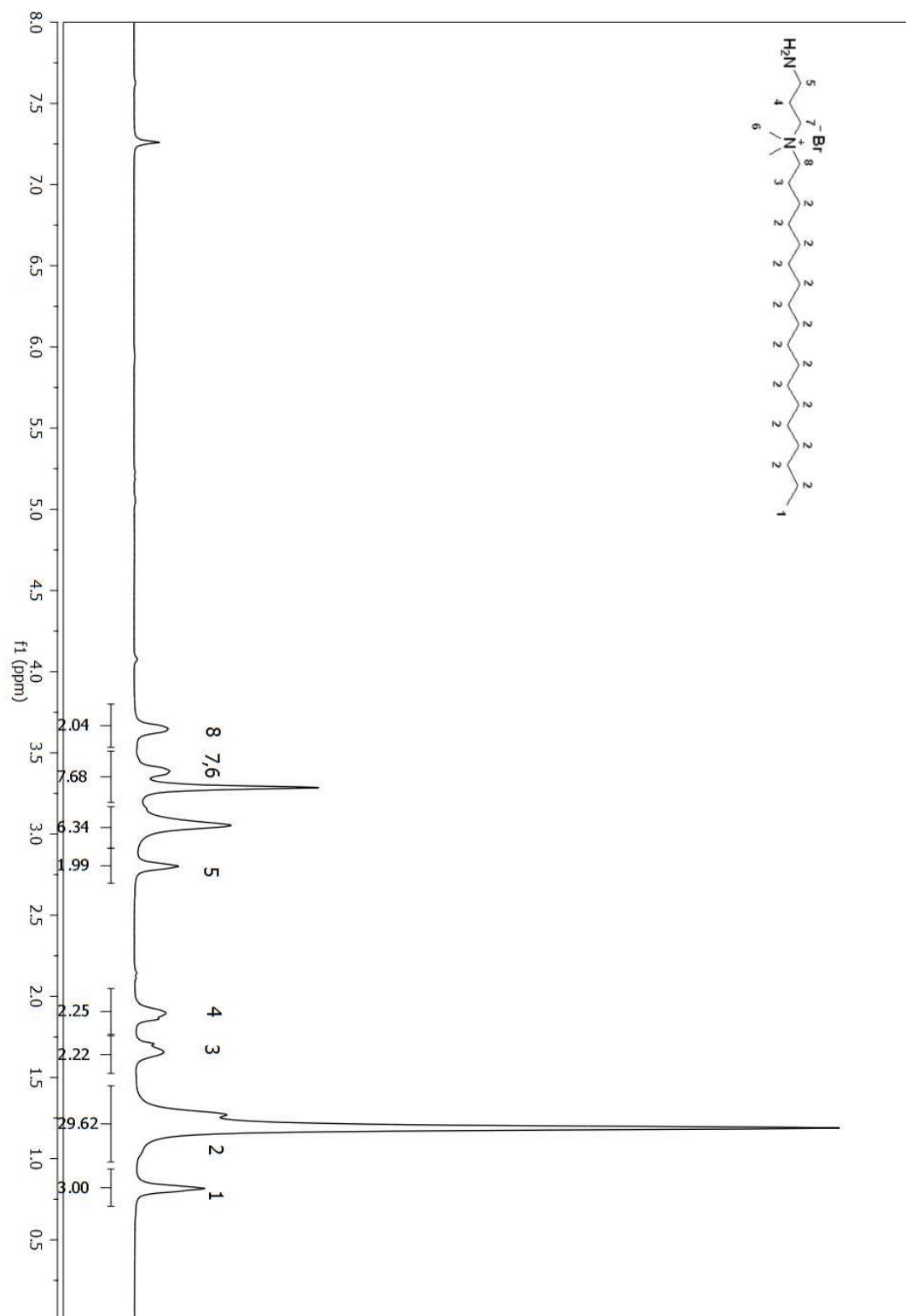


Figure A 273. ^1H NMR spectrum of compound (144) from (152) in CDCl_3 .

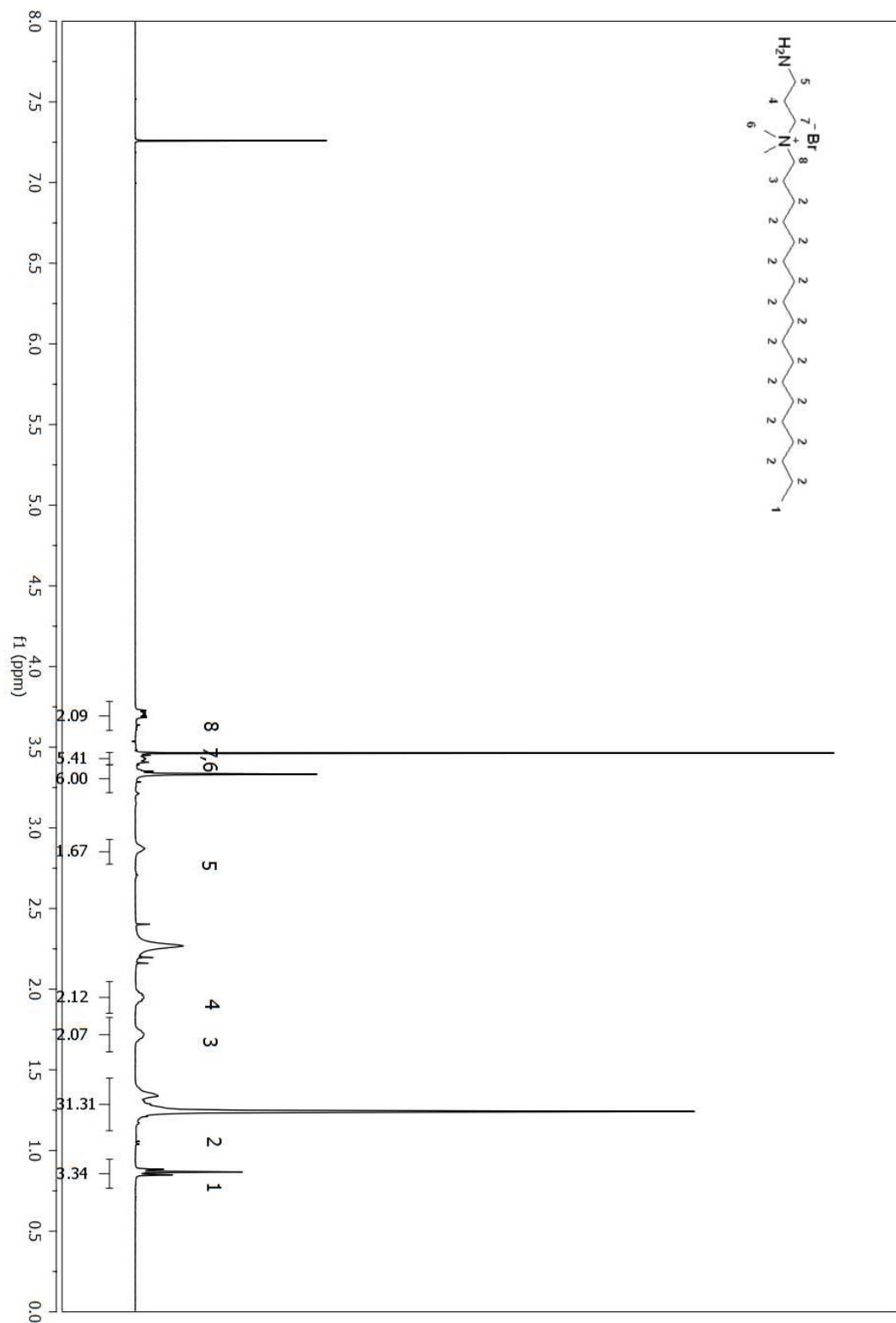


Figure A 274. ^1H NMR spectrum of compound (144) from (156) in CDCl_3 .

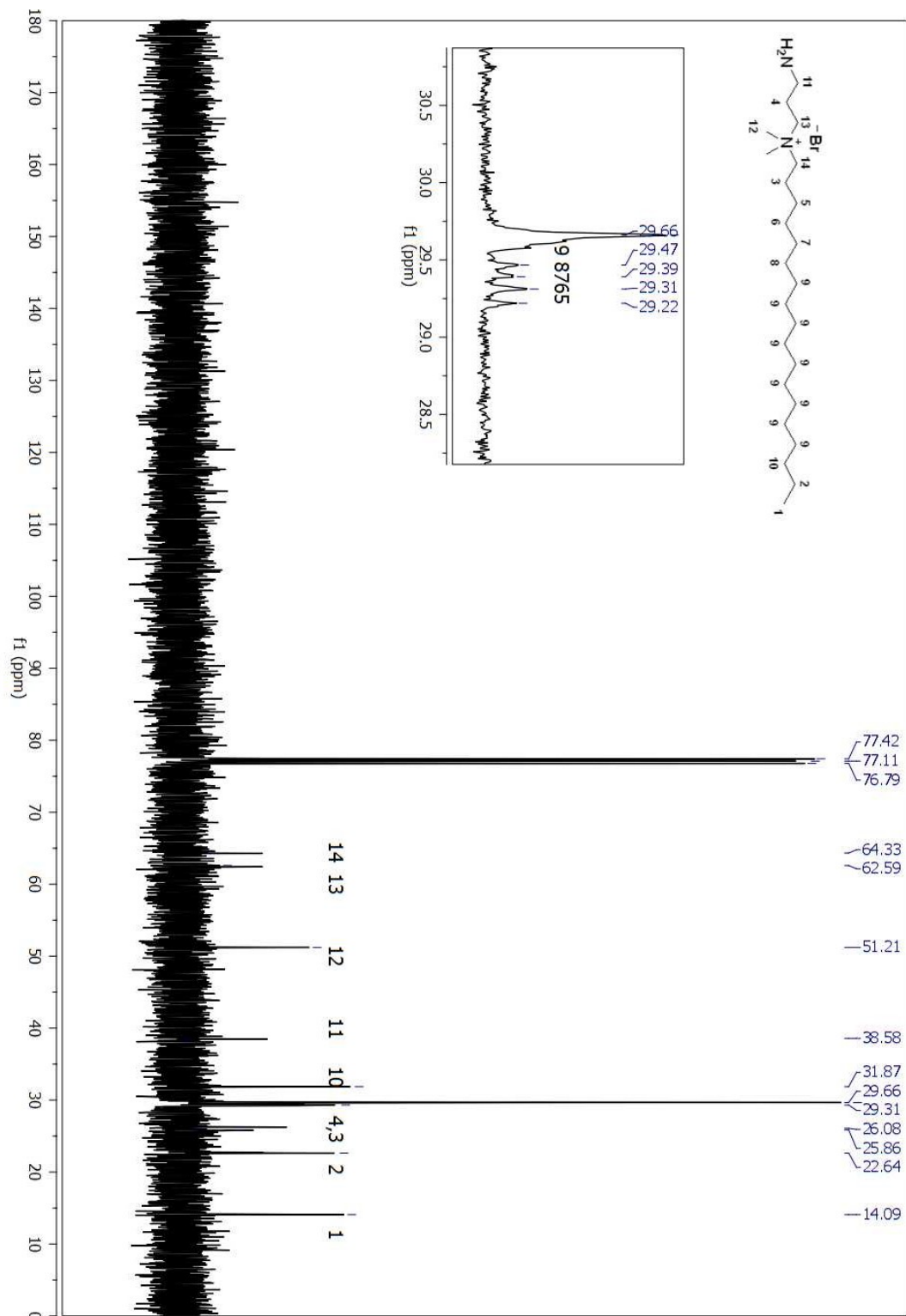


Figure A 275. ¹³C NMR spectrum of compound (144) from (152) in CDCl₃.

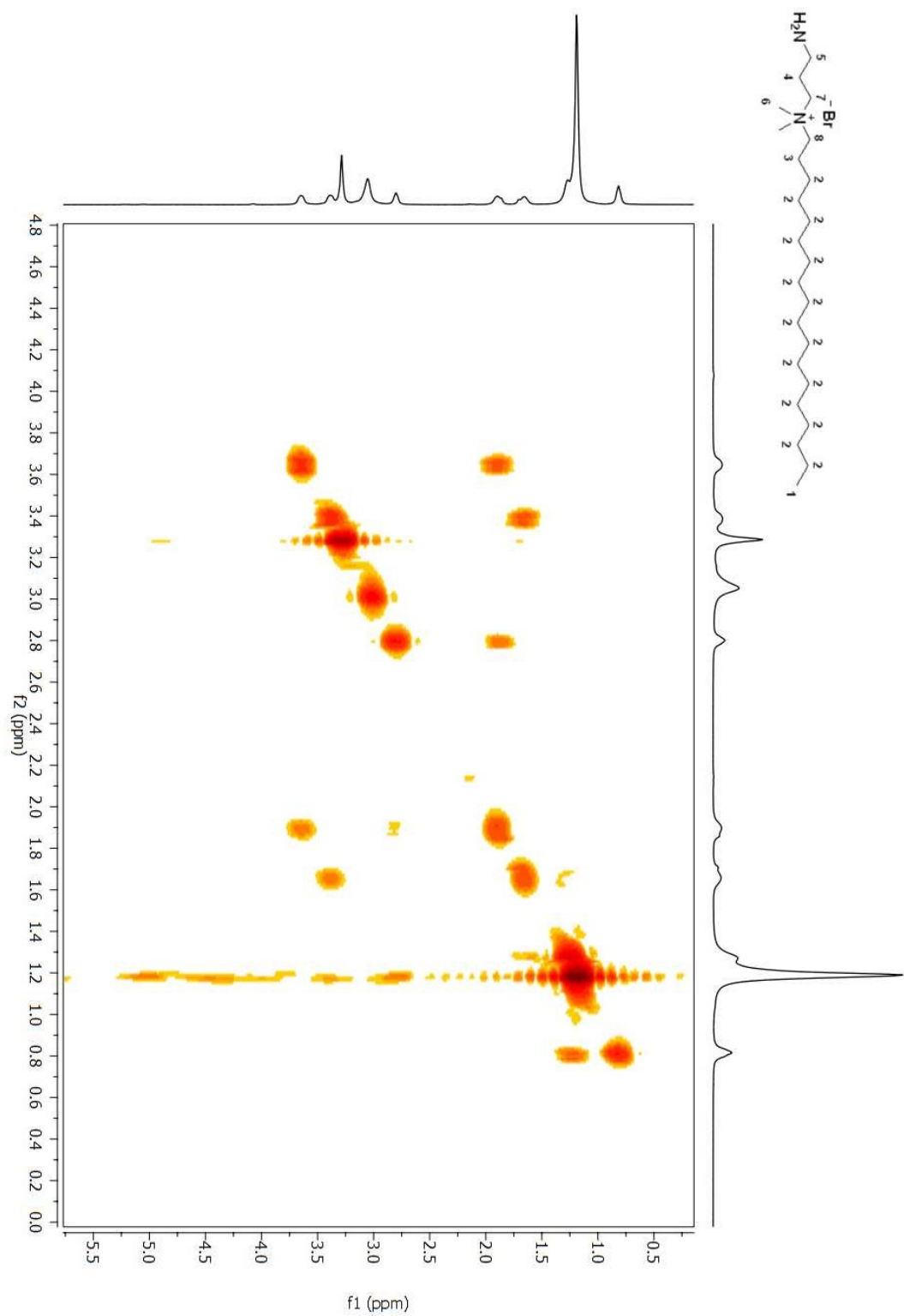


Figure A 276. COSY 2D NMR spectrum of compound (144) from (152) in CDCl₃.

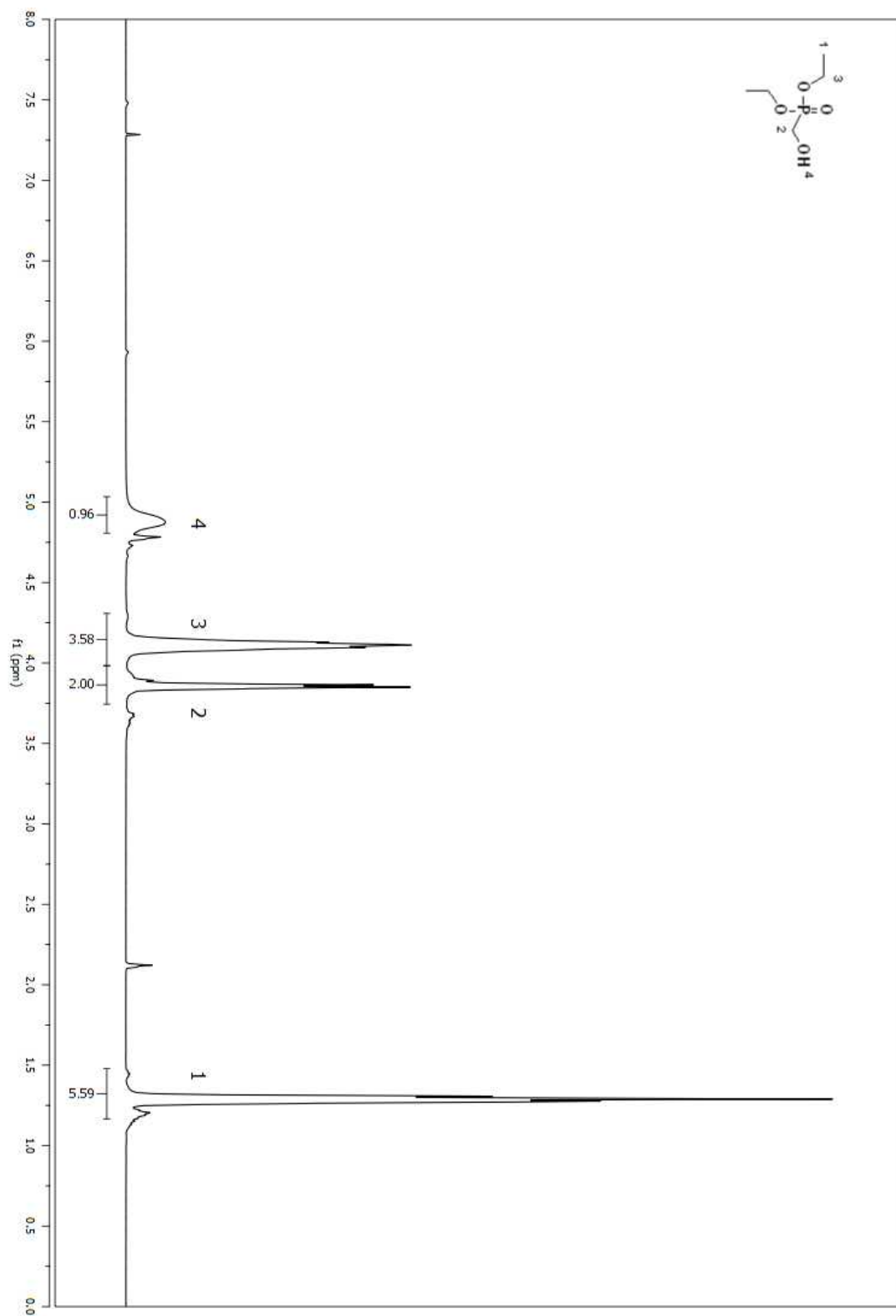


Figure A 278. ^1H NMR spectrum of compound (169) in CDCl_3 .

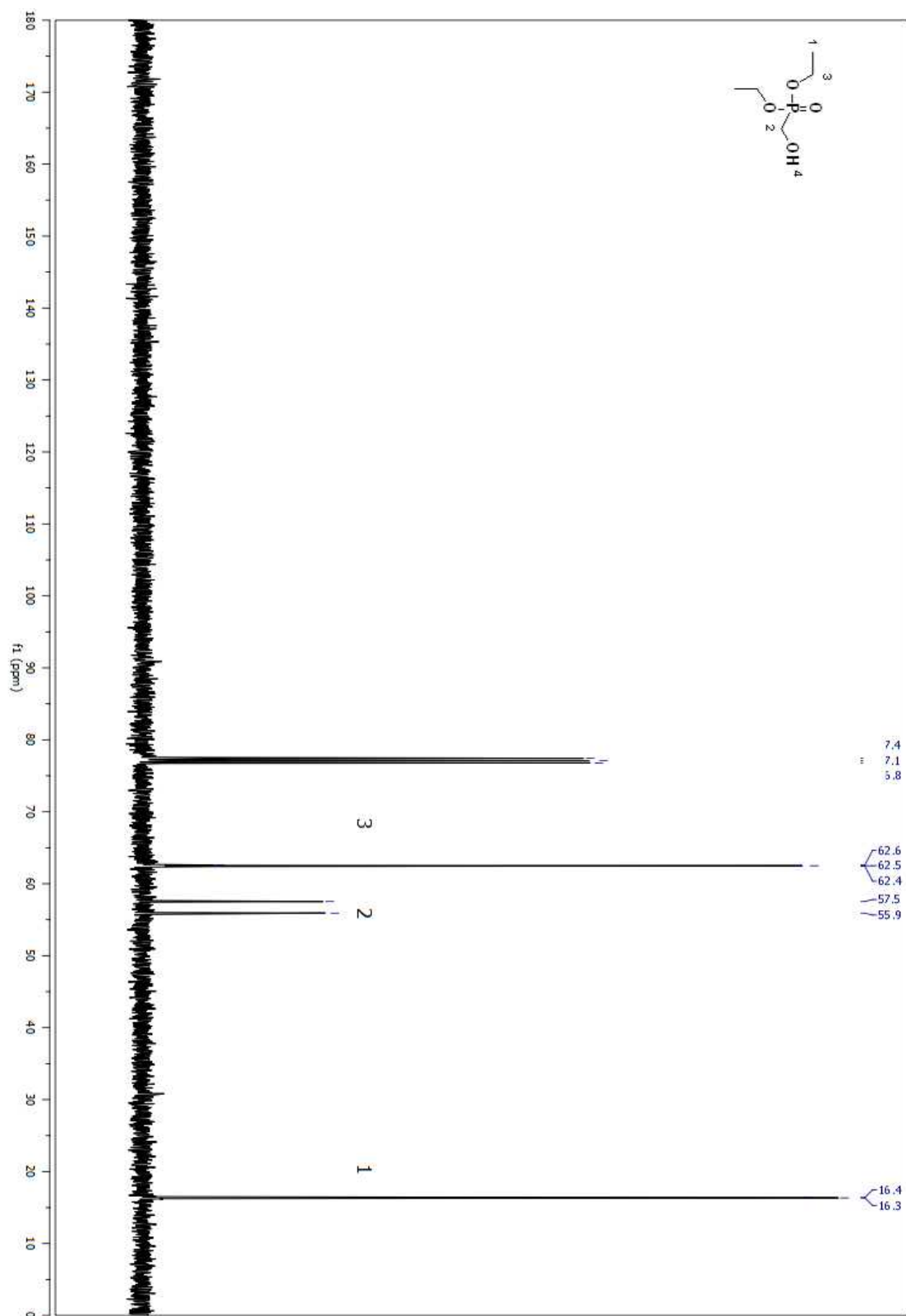


Figure A 279. ^{13}C NMR spectrum of compound (169) in CDCl_3 .

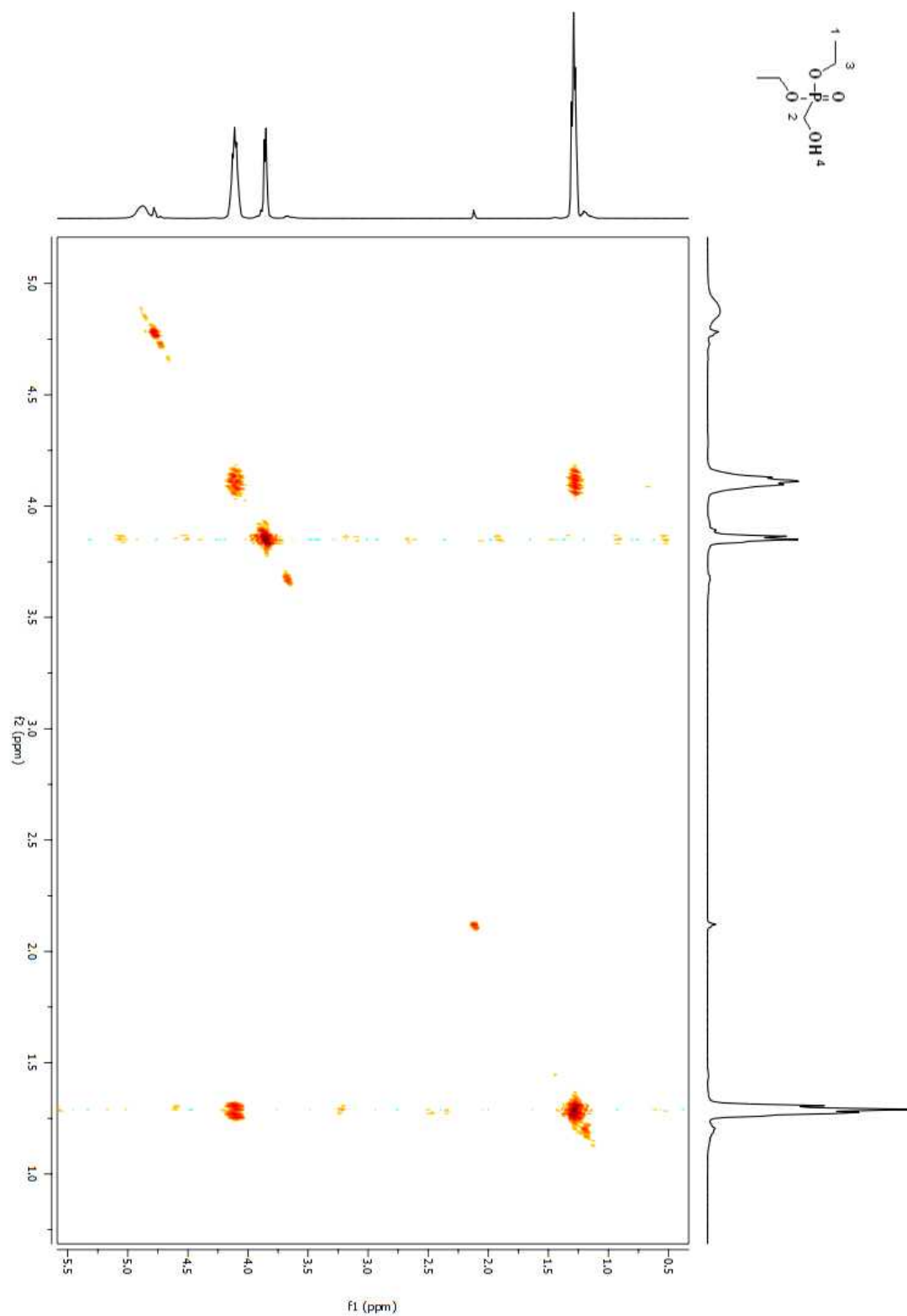


Figure A 280. COSY 2D NMR spectrum of compound (169) in CDCl₃.

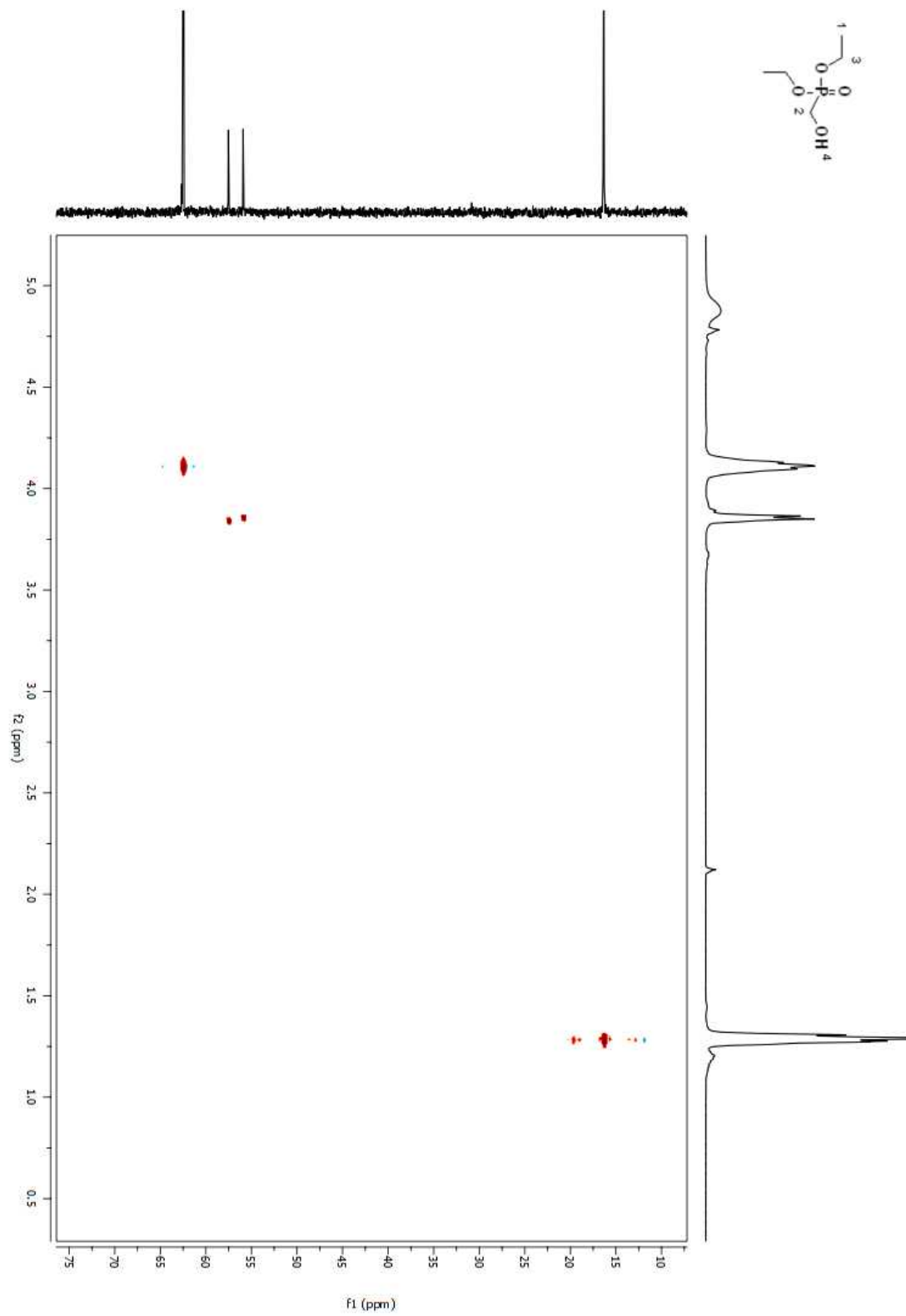


Figure A 281. HSQC 2D NMR spectrum of compound (**169**) in CDCl₃.

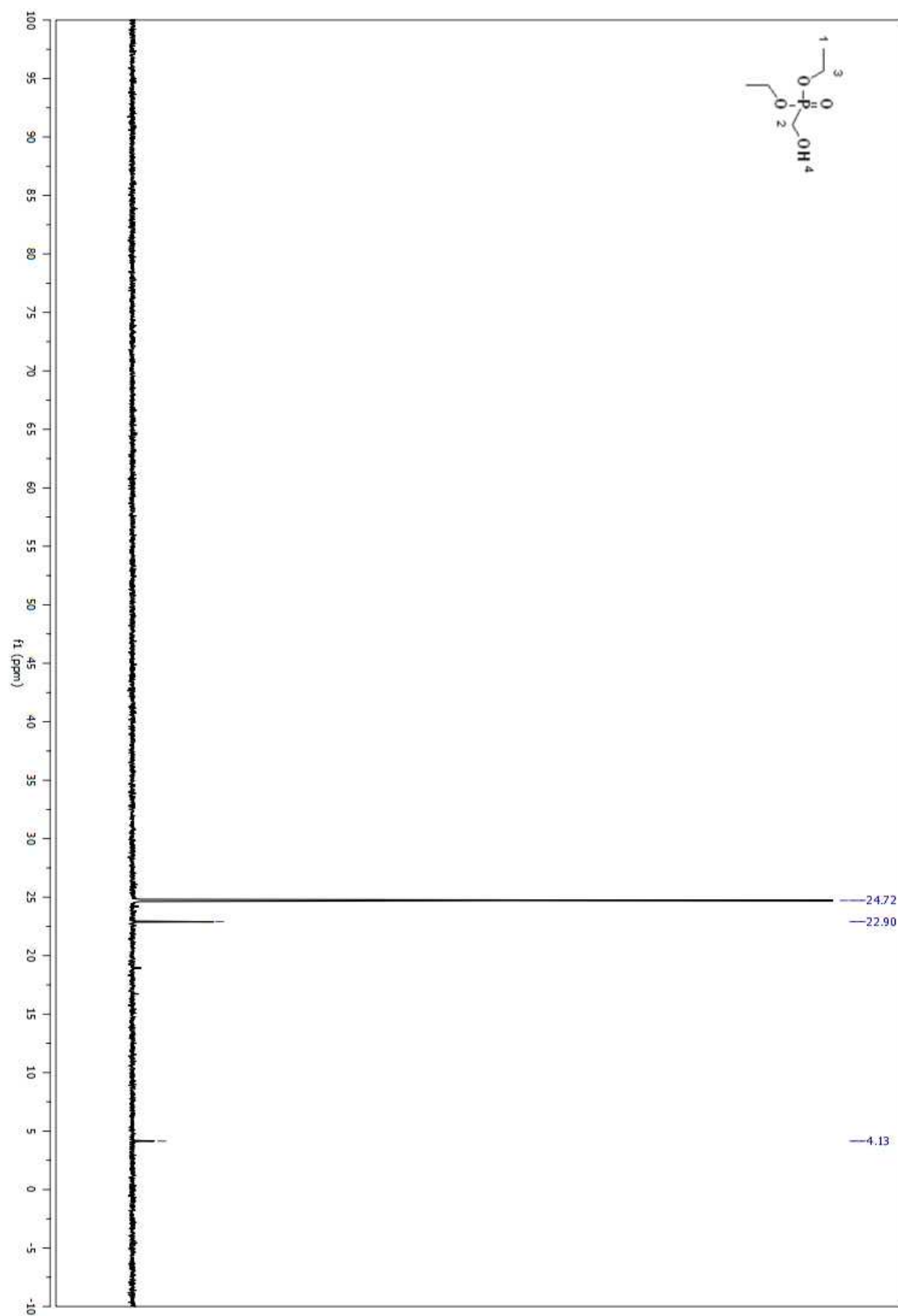


Figure A 282. ^{31}P NMR spectrum of compound (169) in CDCl_3 .

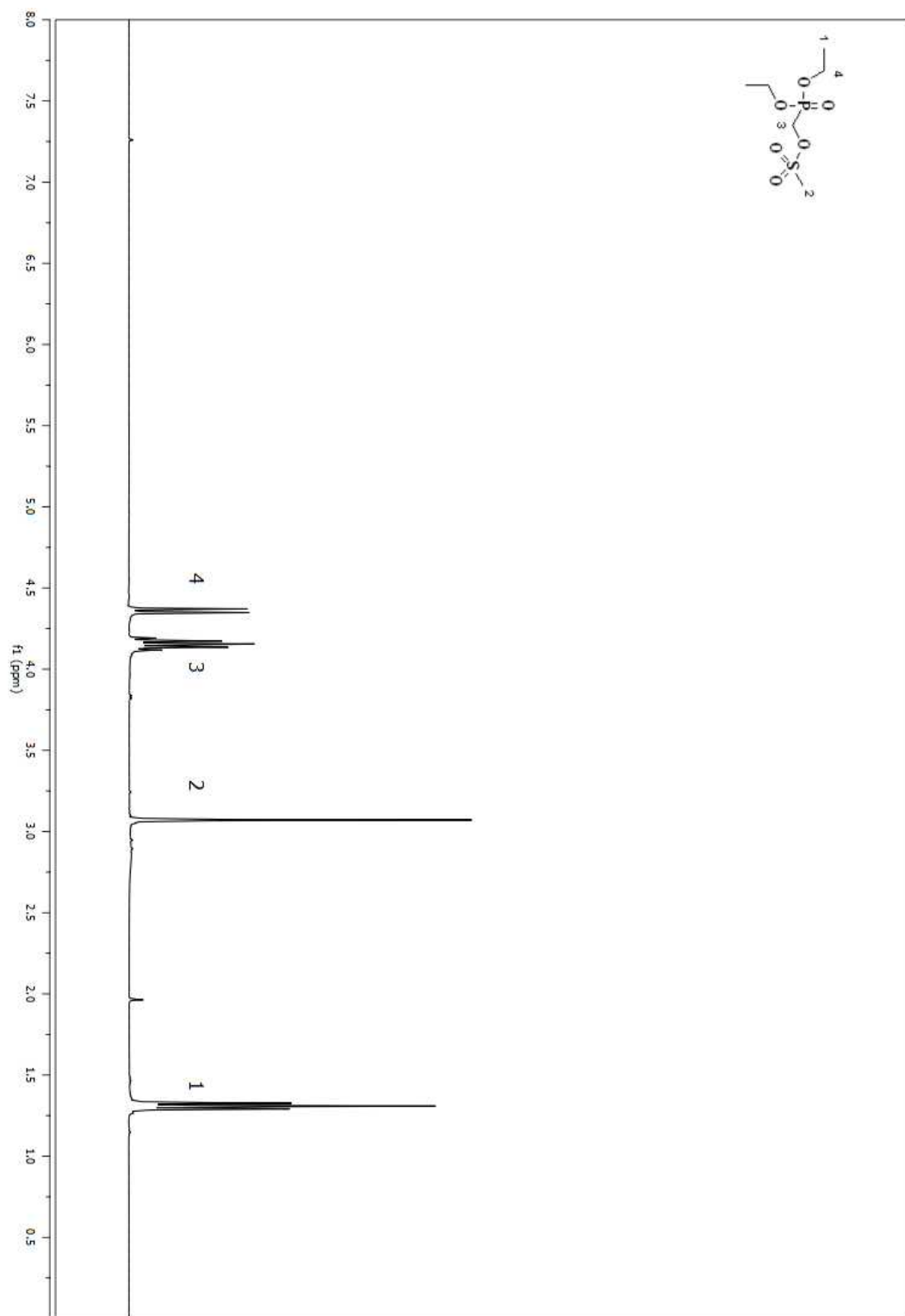


Figure A 283. ^1H NMR spectrum of compound (158) in CDCl_3 .

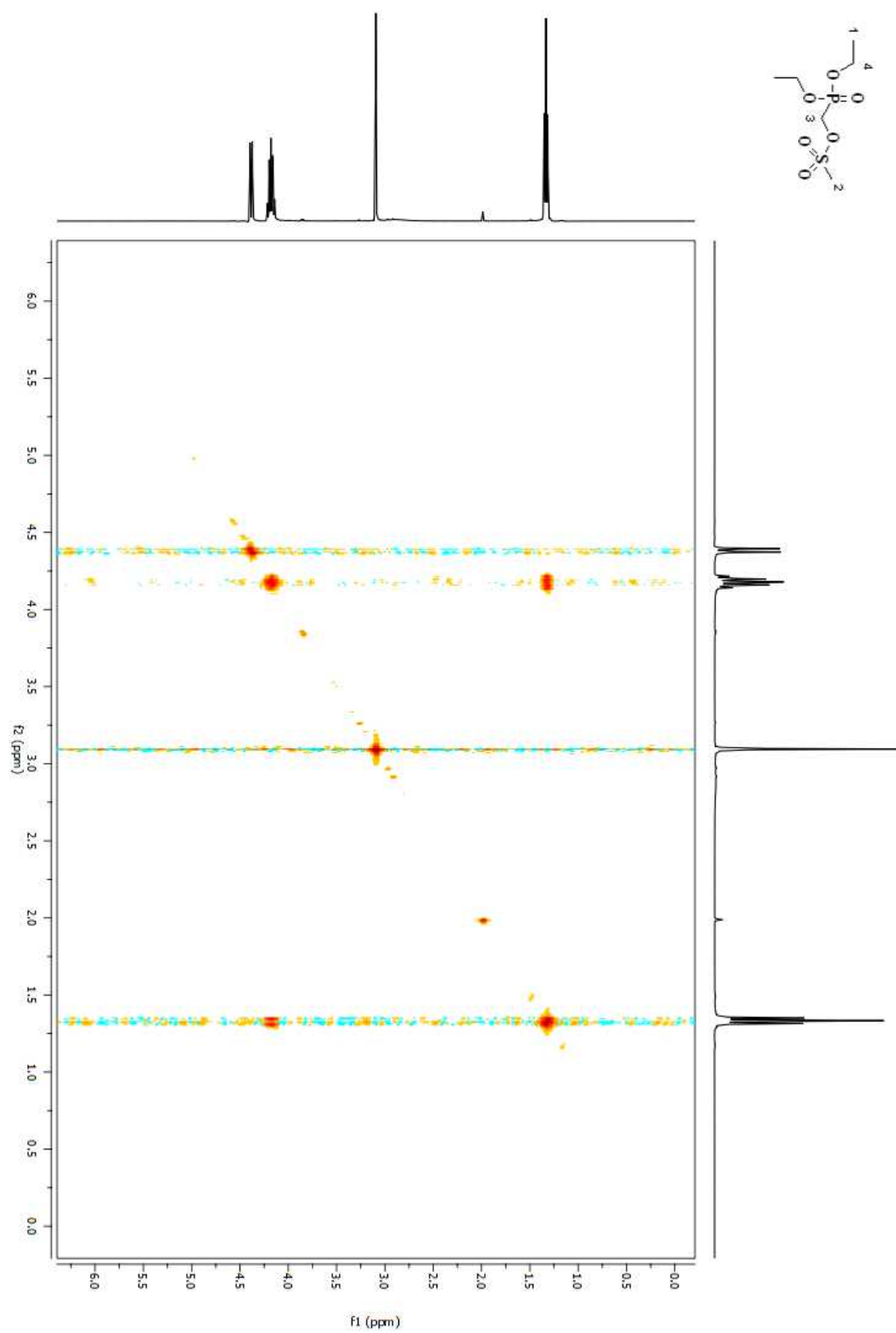


Figure A 285. COSY 2D NMR spectrum of compound (**158**) in CDCl_3 .

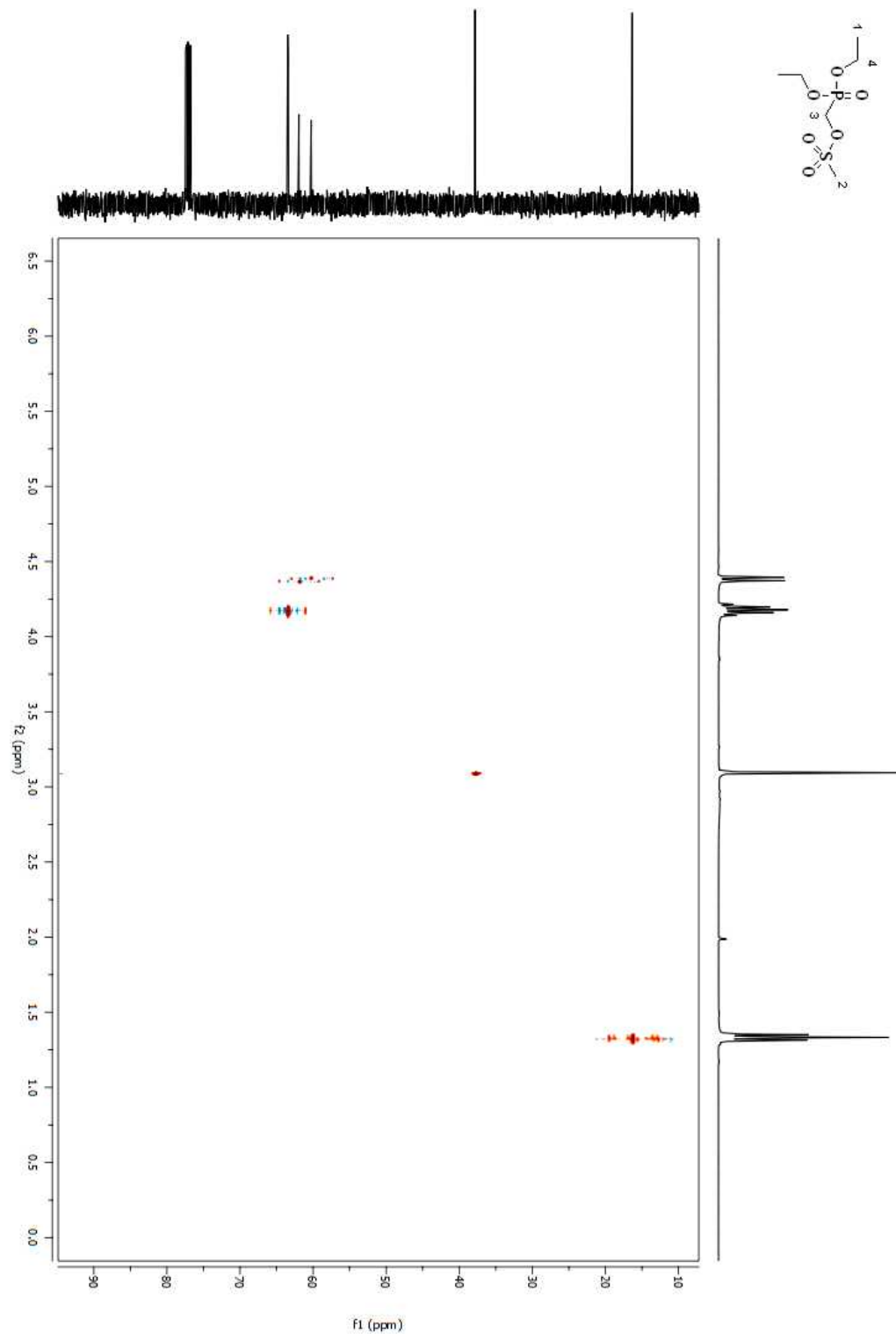


Figure A 286. HSQC 2D NMR spectrum of compound (**158**) in CDCl_3 .

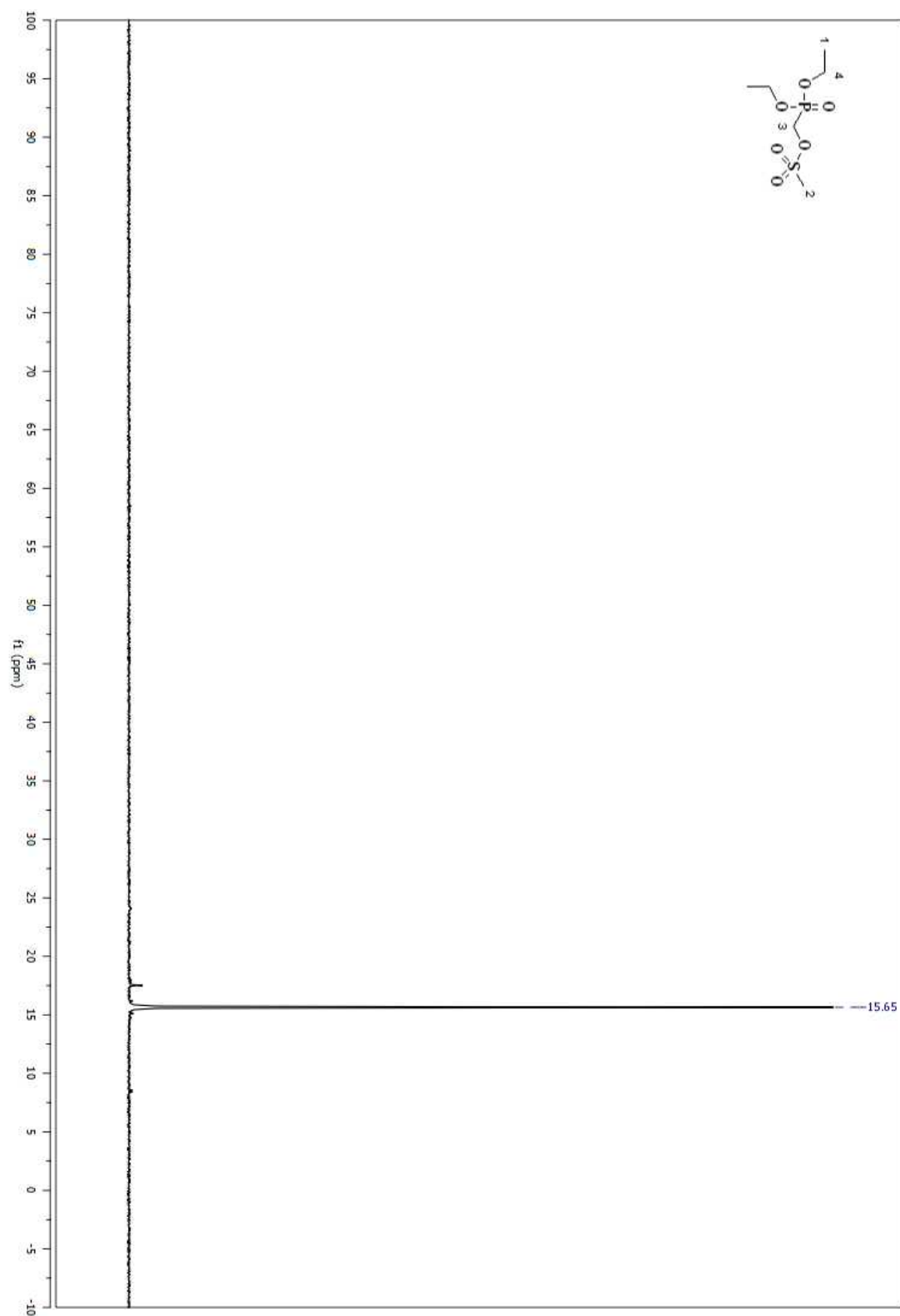


Figure A 287. ^{31}P NMR spectrum of compound (158) in CDCl_3 .

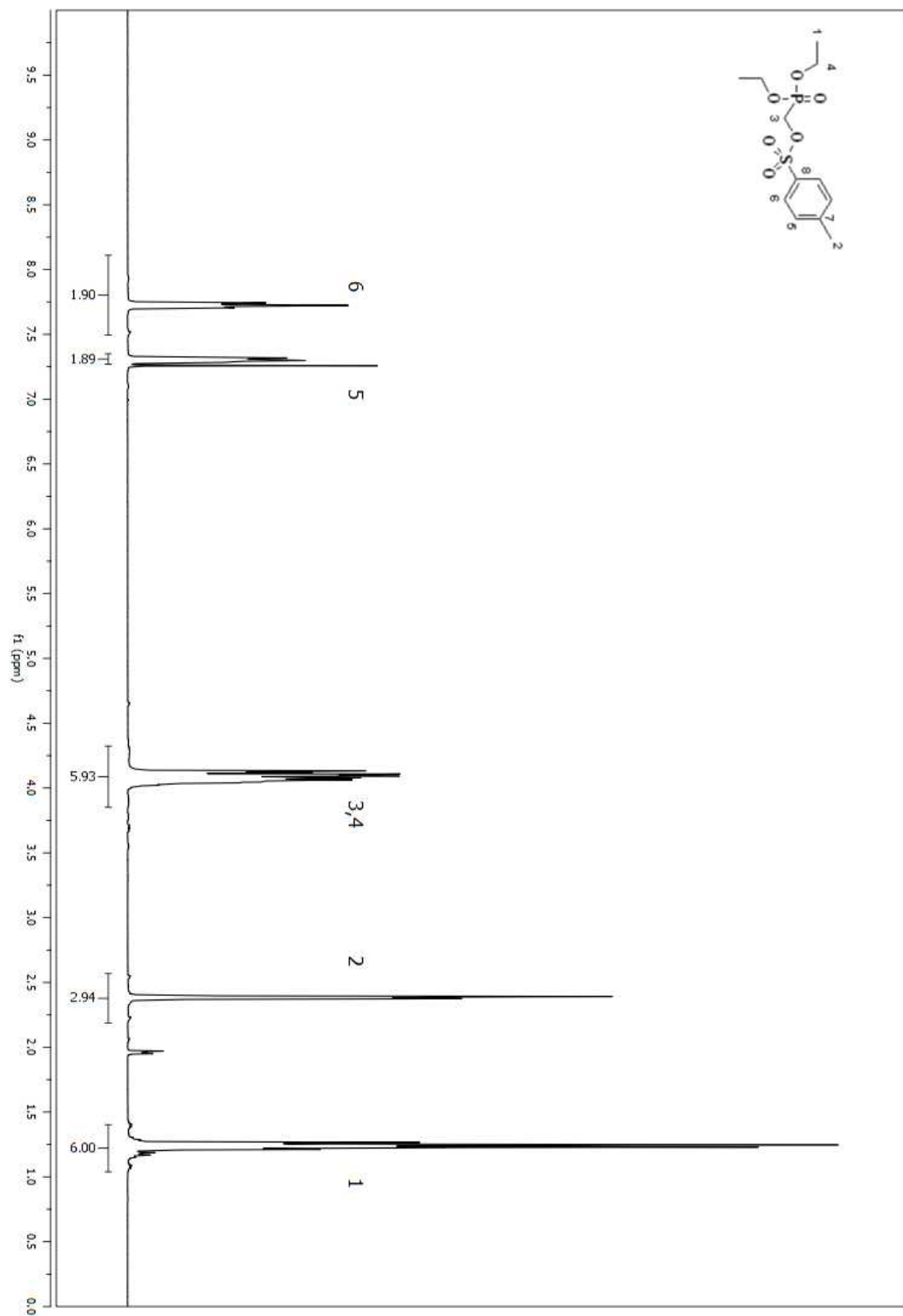


Figure A 288. ^1H NMR spectrum of compound (170) in CDCl_3 .

Figure A 289. ^{13}C NMR spectrum of compound (**170**) in CDCl_3 .

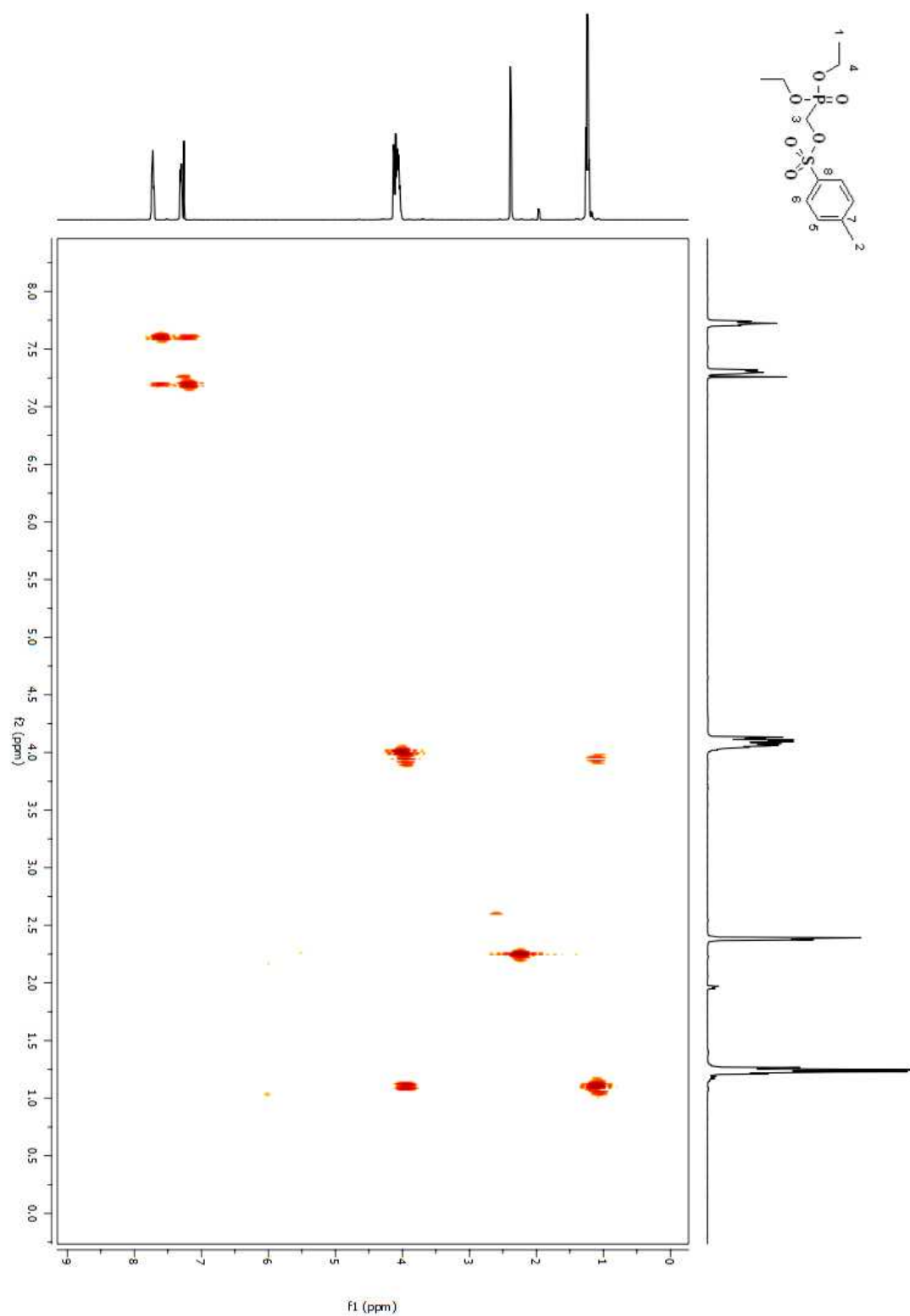


Figure A 290. COSY 2D NMR spectrum of compound (170) in CDCl₃.

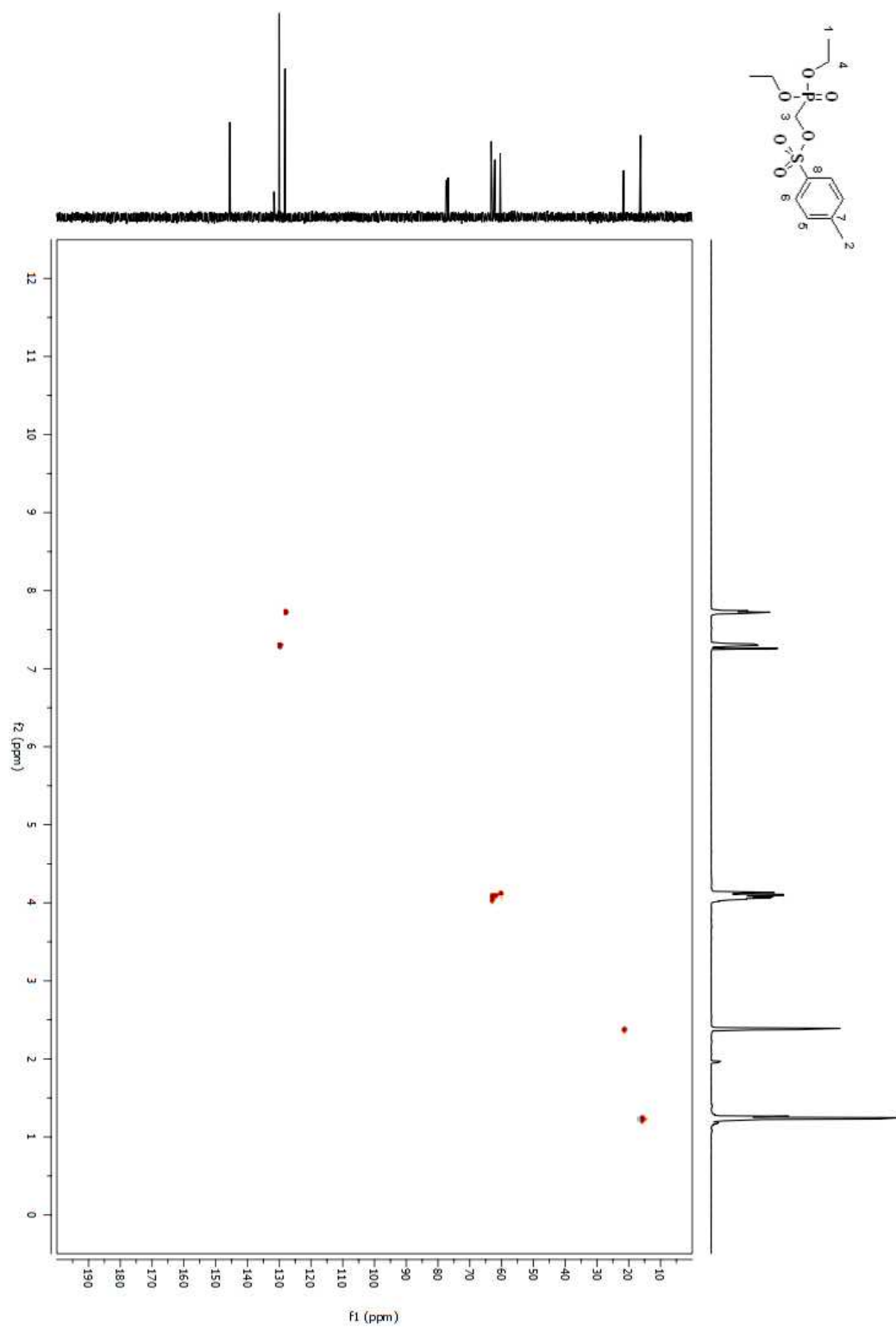


Figure A 291. HSQC 2D NMR spectrum of compound (170) in CDCl₃.

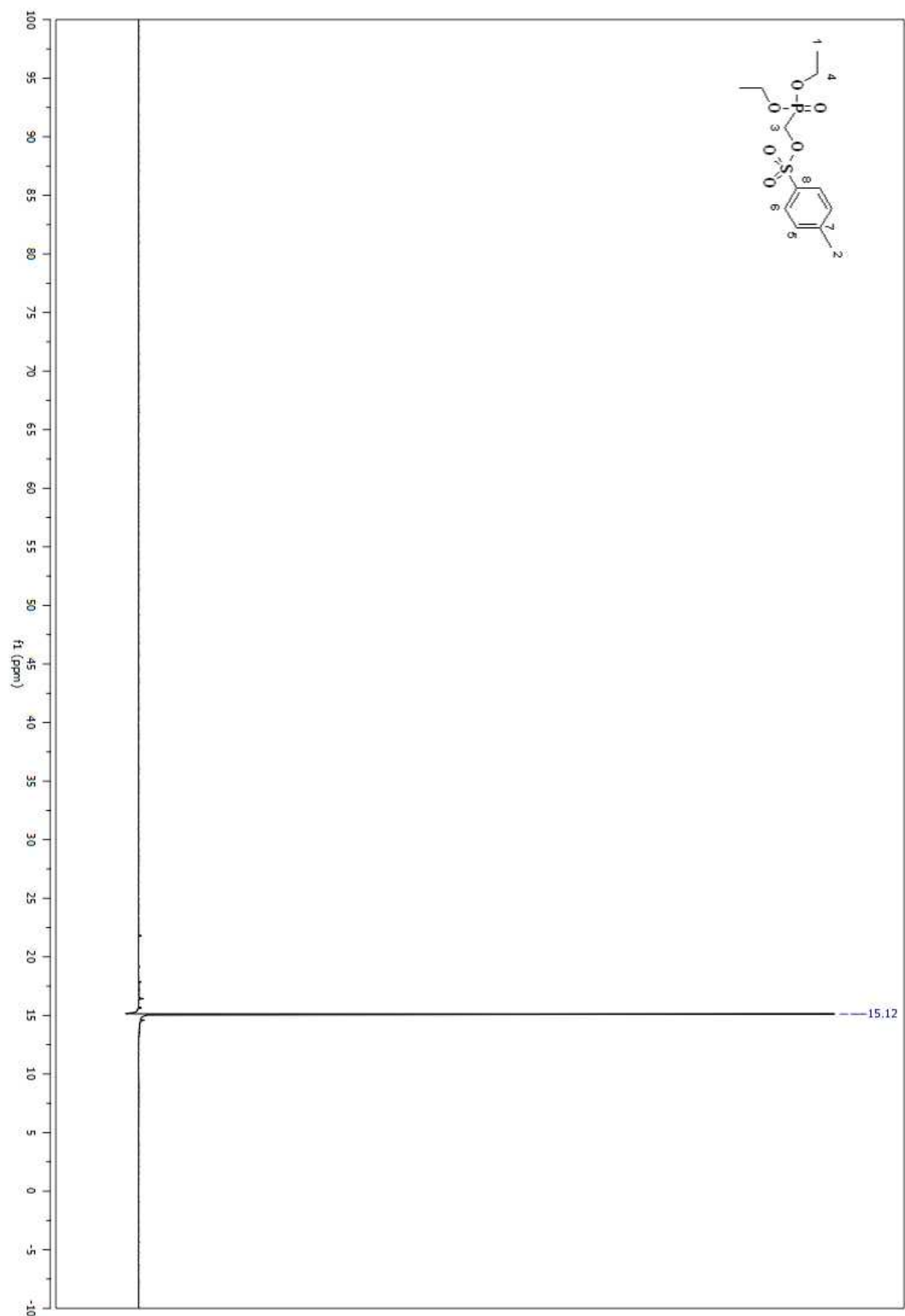


Figure A 292. ^{31}P NMR spectrum of compound (170) in CDCl_3 .

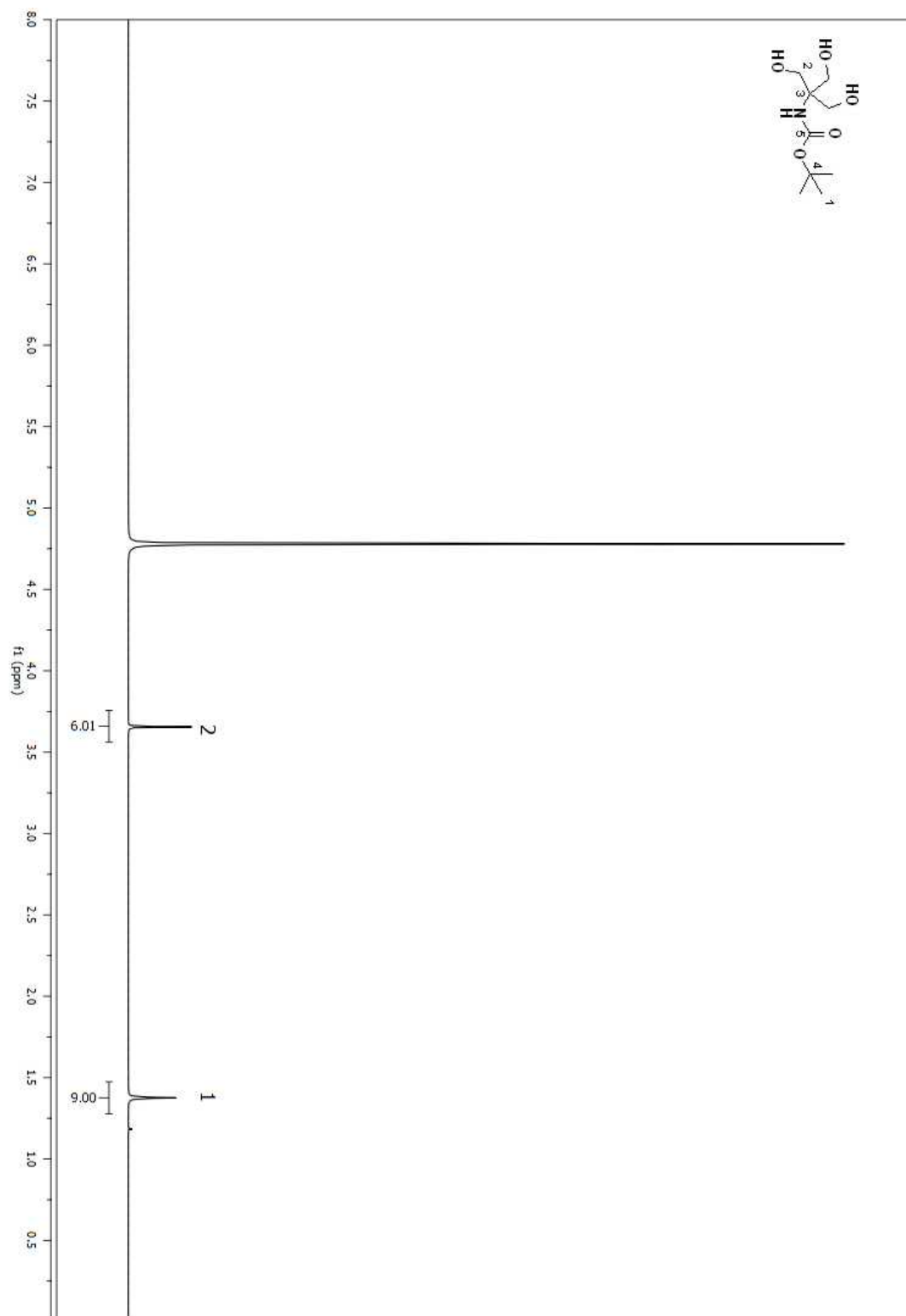


Figure A 293. ^1H NMR spectrum of compound (157) in D_2O .

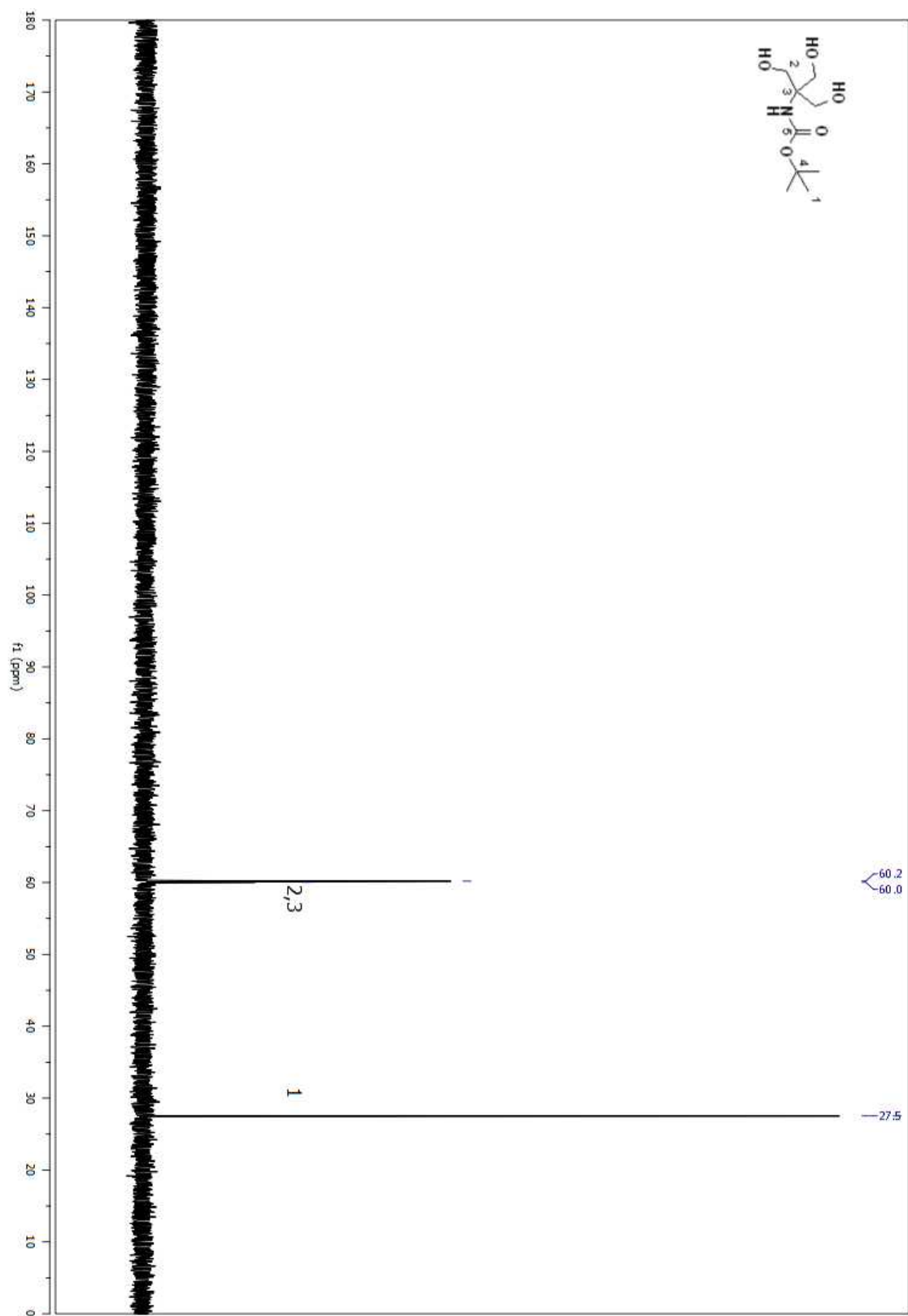


Figure A 294. ^{13}C NMR spectrum of compound (157) in D_2O .

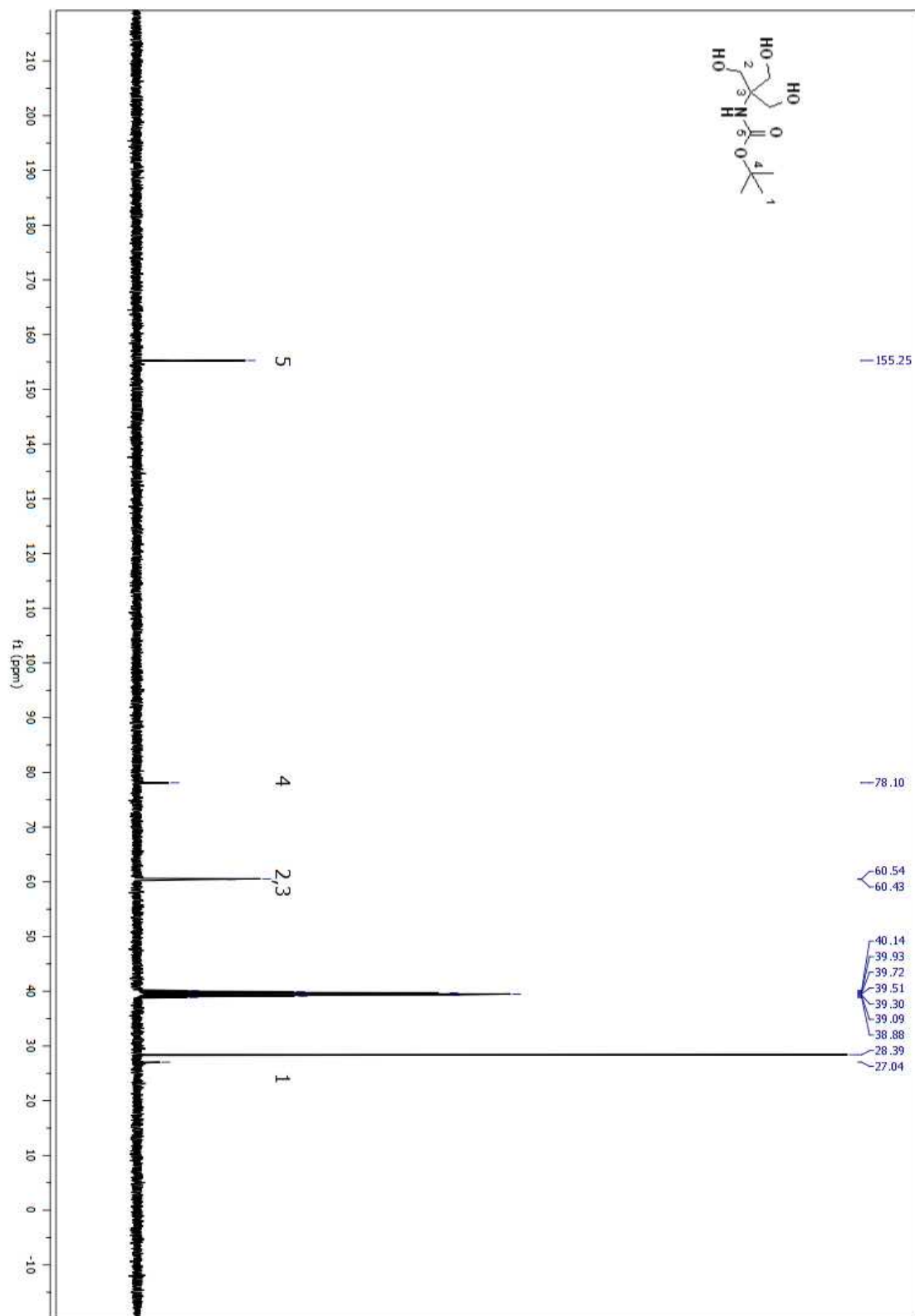


Figure A 295. ^{13}C NMR spectrum of compound (157) in DMSO- d_6 .

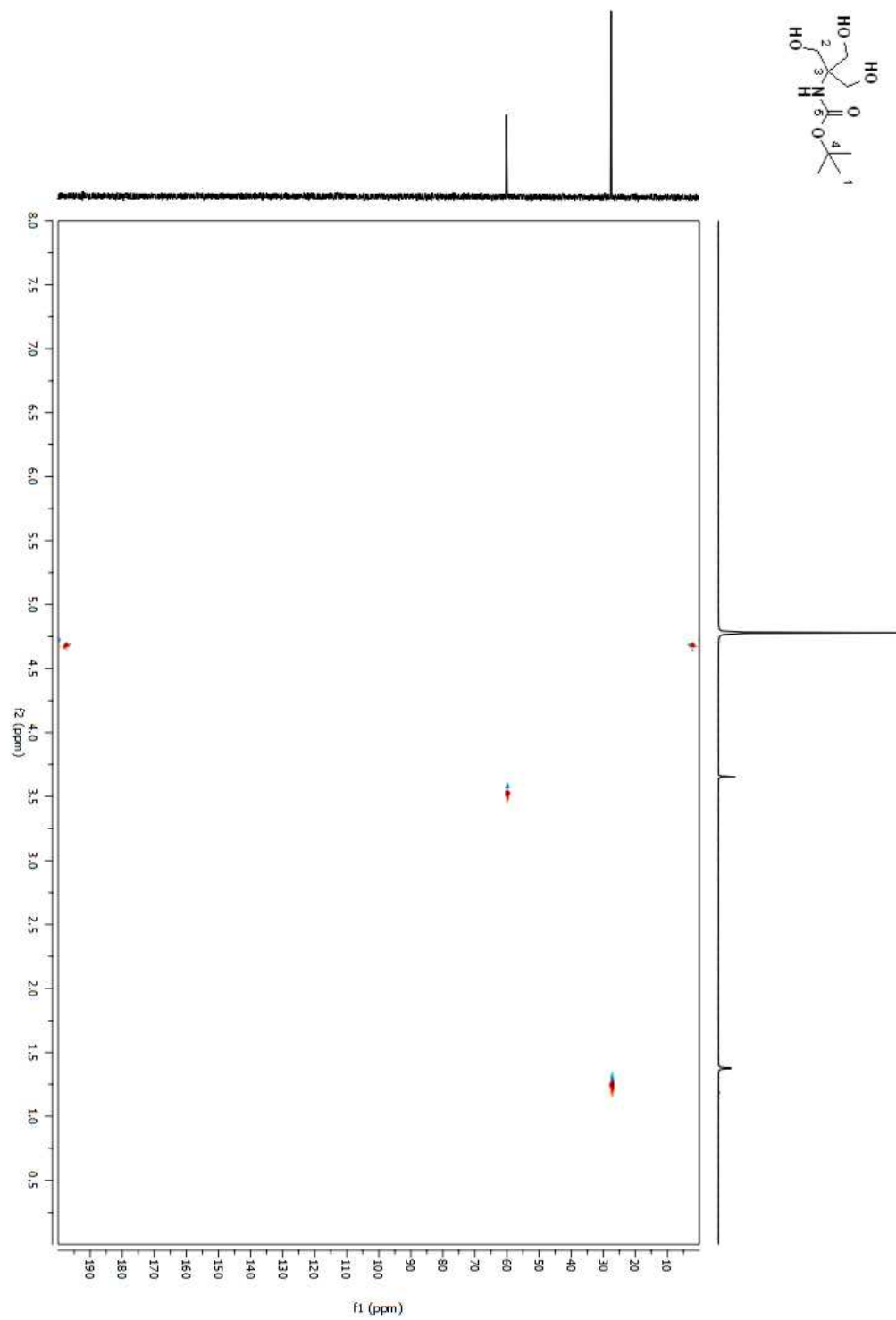


Figure A 296. HSQC 2D NMR spectrum of compound (157) in CDCl₃.

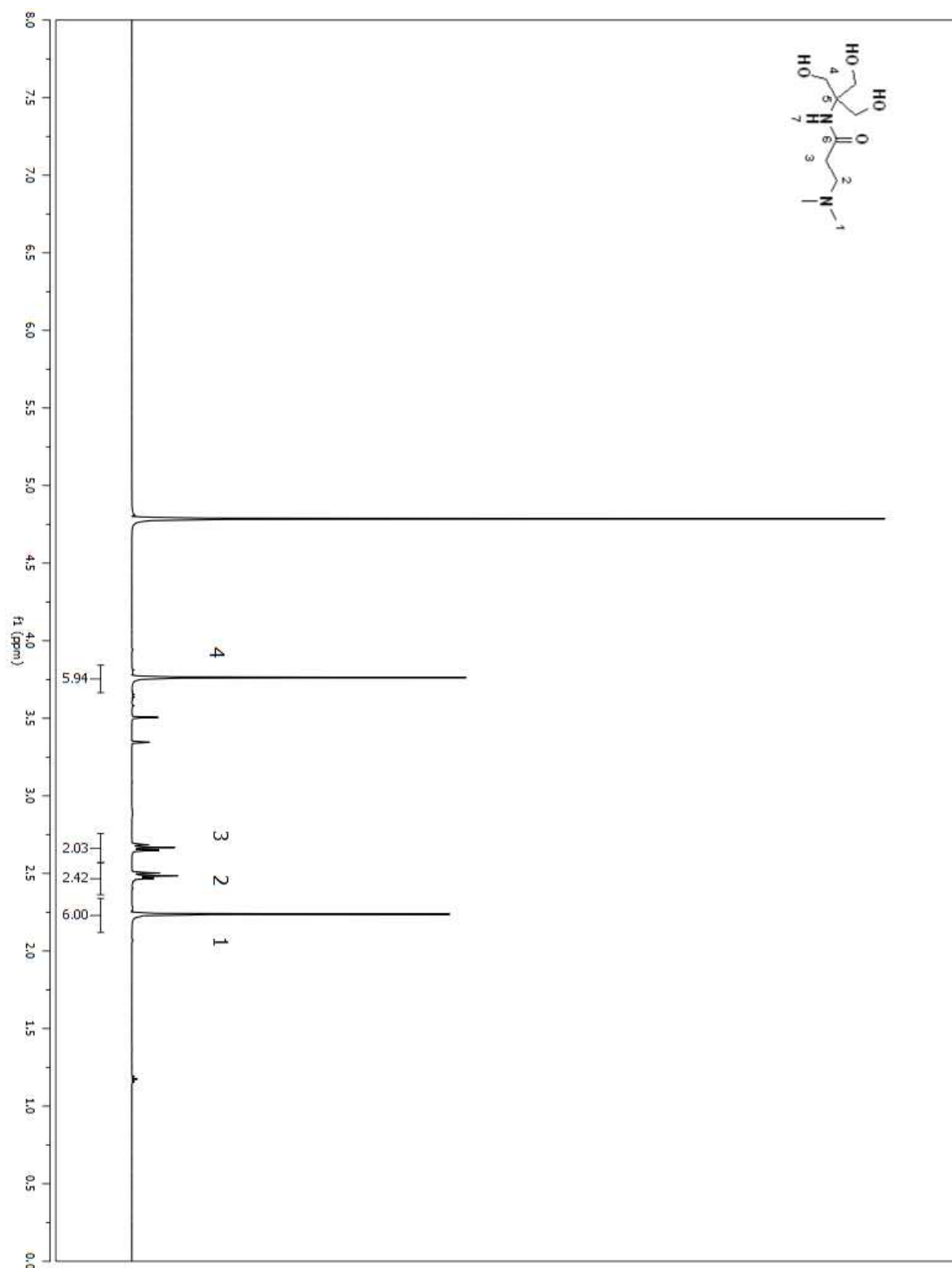


Figure A 297. ^1H NMR spectrum of compound (163) in D_2O .

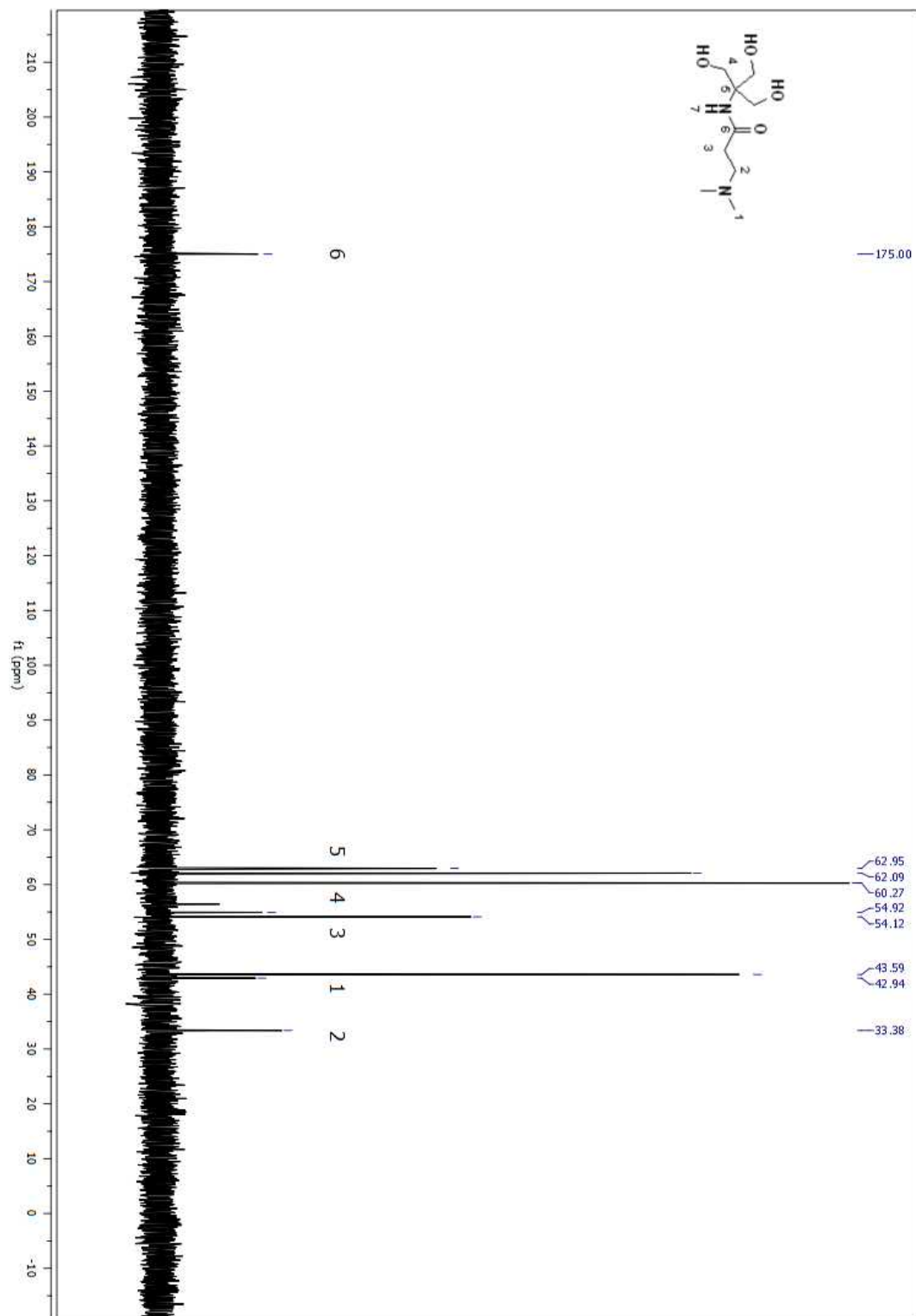


Figure A 298. ^{13}C NMR spectrum of compound (163) in D_2O .

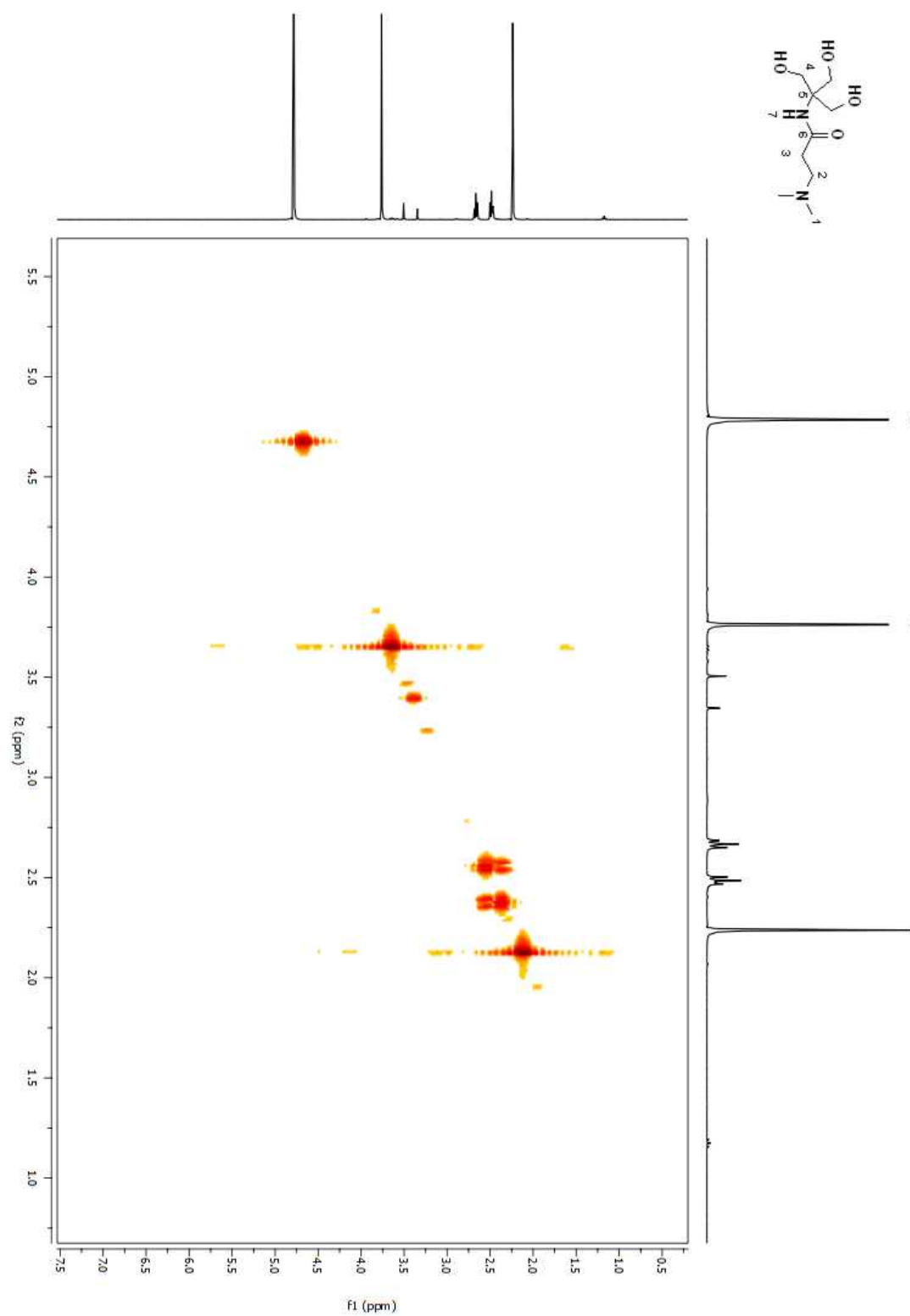


Figure A 299. COSY 2D NMR spectrum of compound (**163**) in CDCl₃.

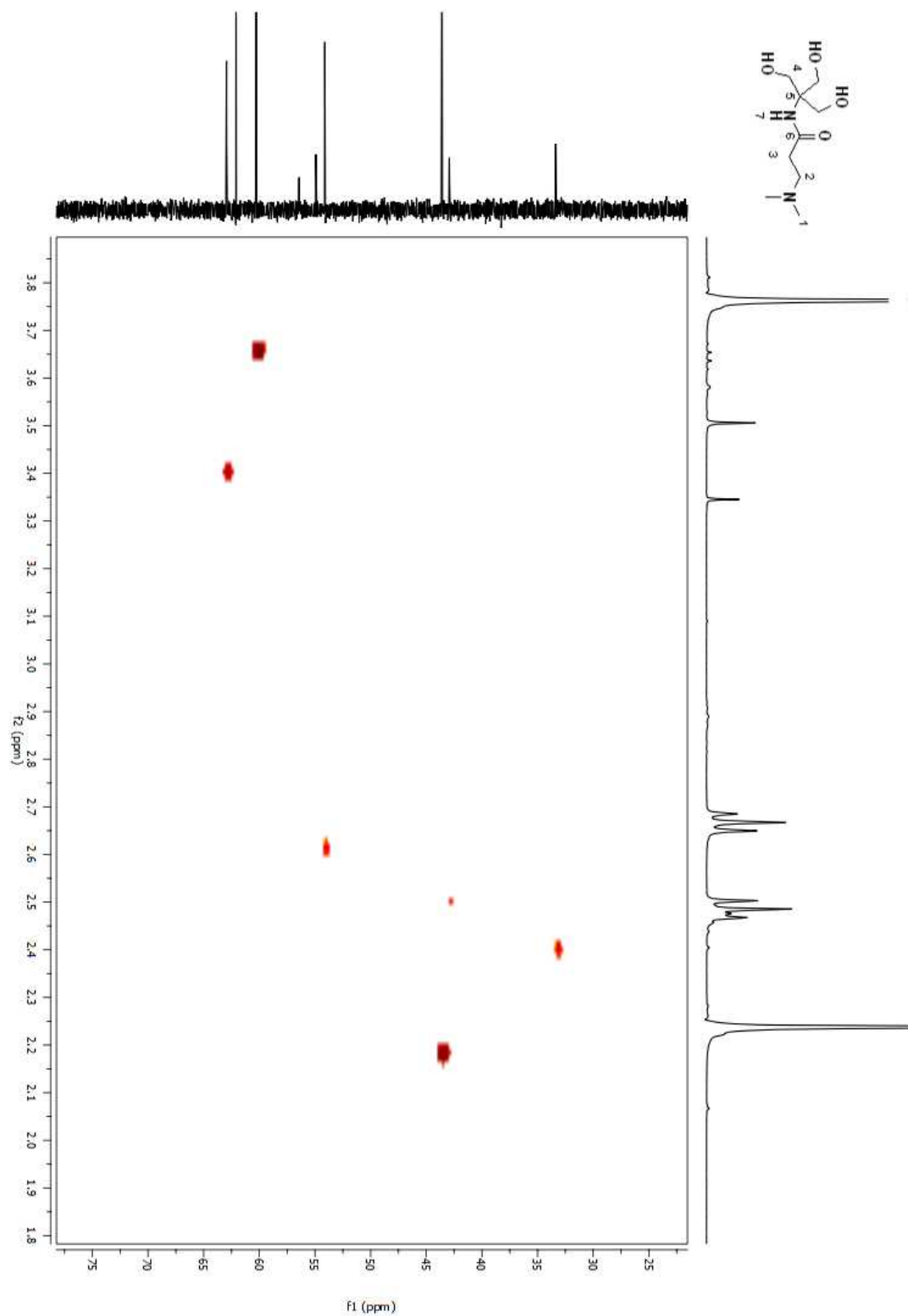


Figure A 300. HSQC 2D NMR spectrum of compound (**163**) in CDCl₃.

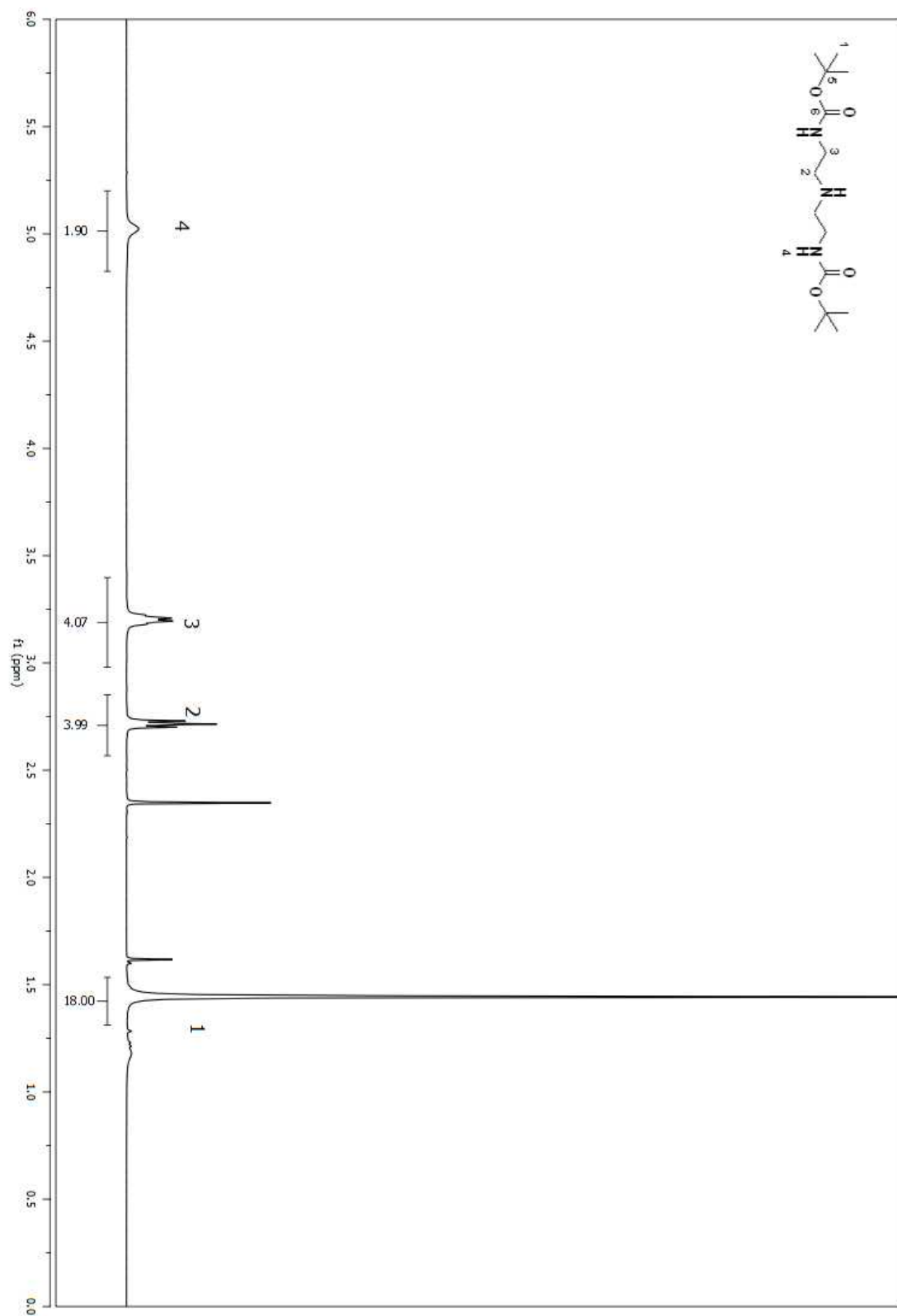


Figure A 301. ^1H NMR spectrum of compound (176) in CDCl_3 .

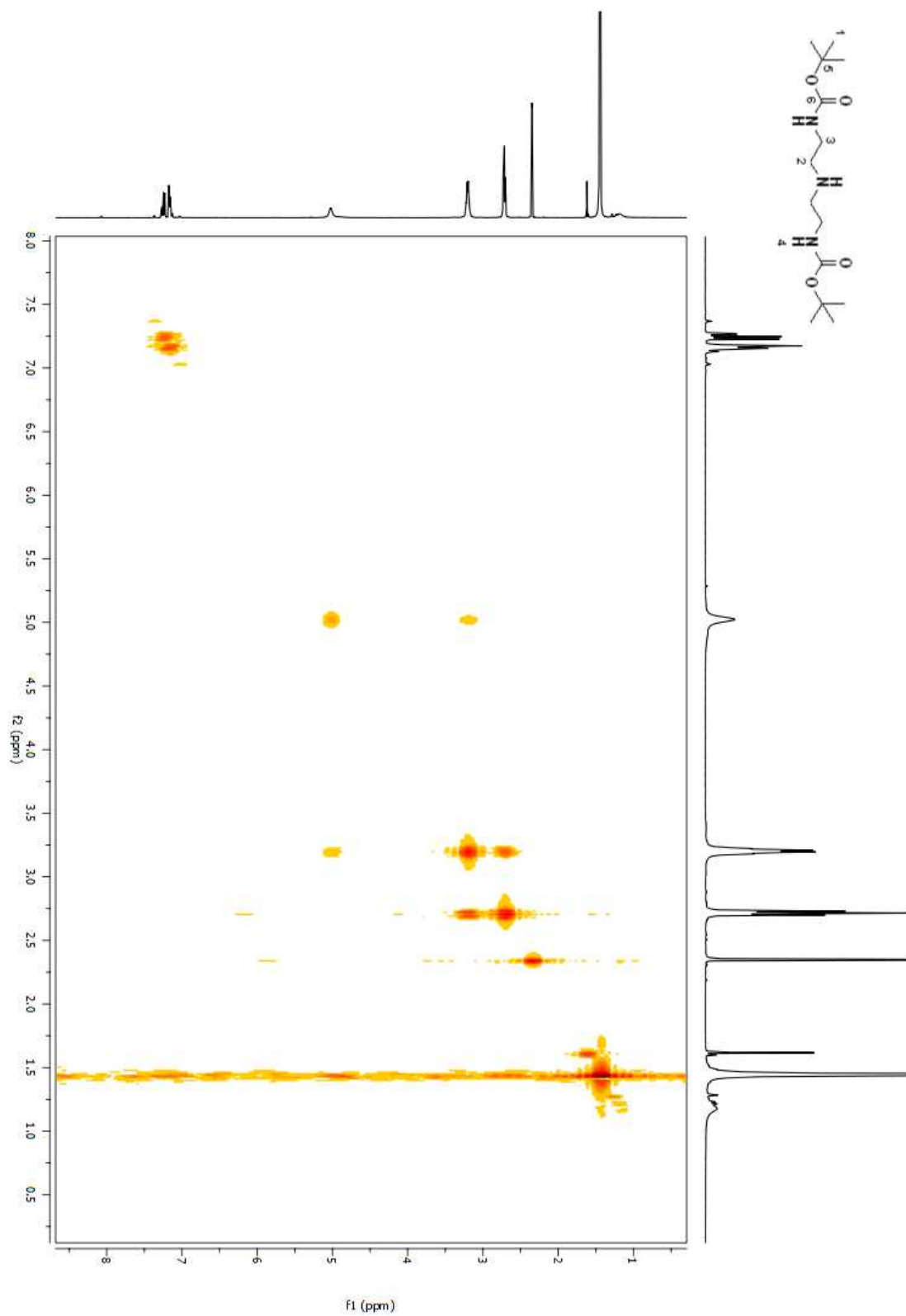


Figure A 302. COSY 2D NMR spectrum of compound (**176**) in CDCl₃.

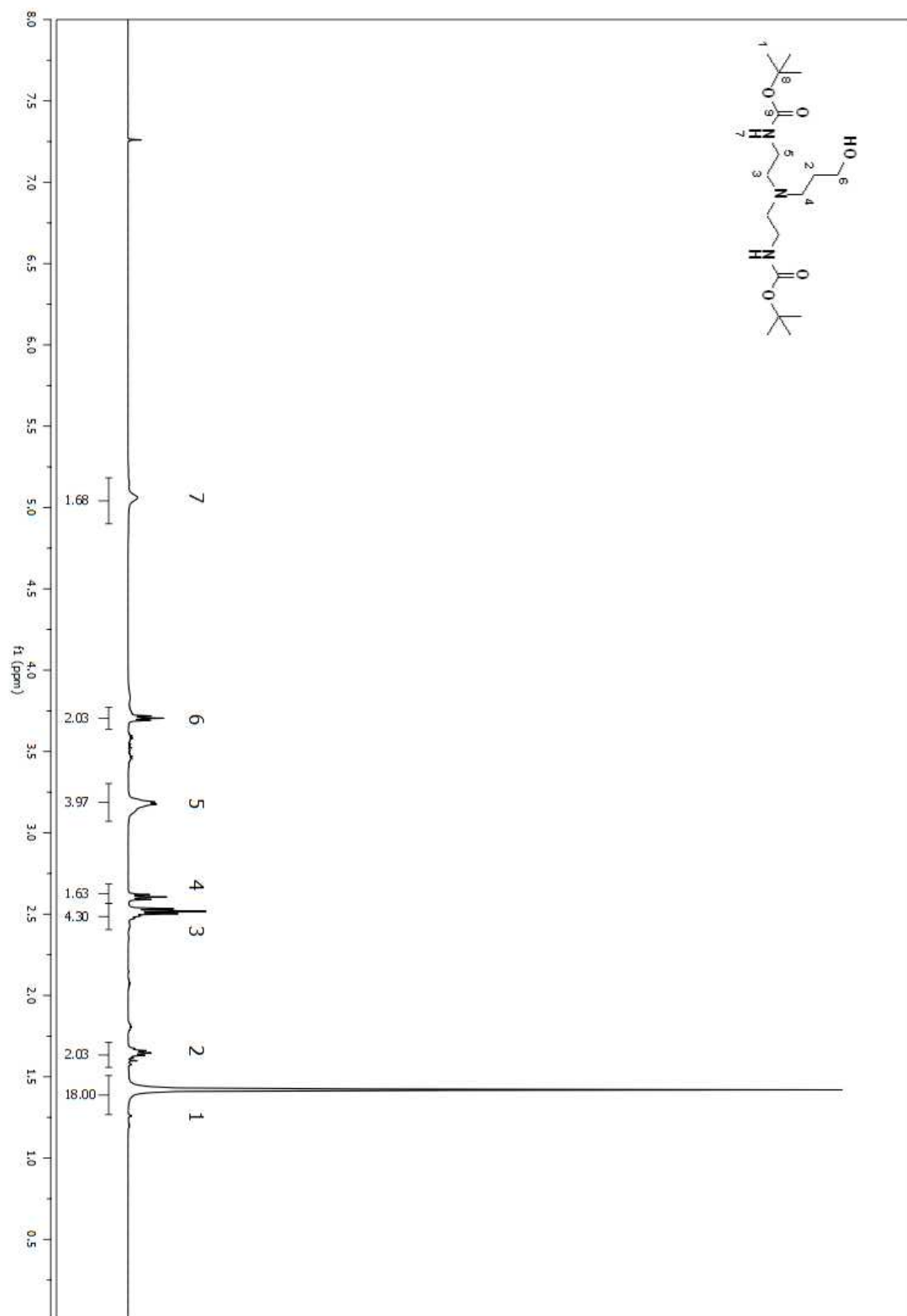


Figure A 303. ^1H NMR spectrum of compound (177) in CDCl_3 .

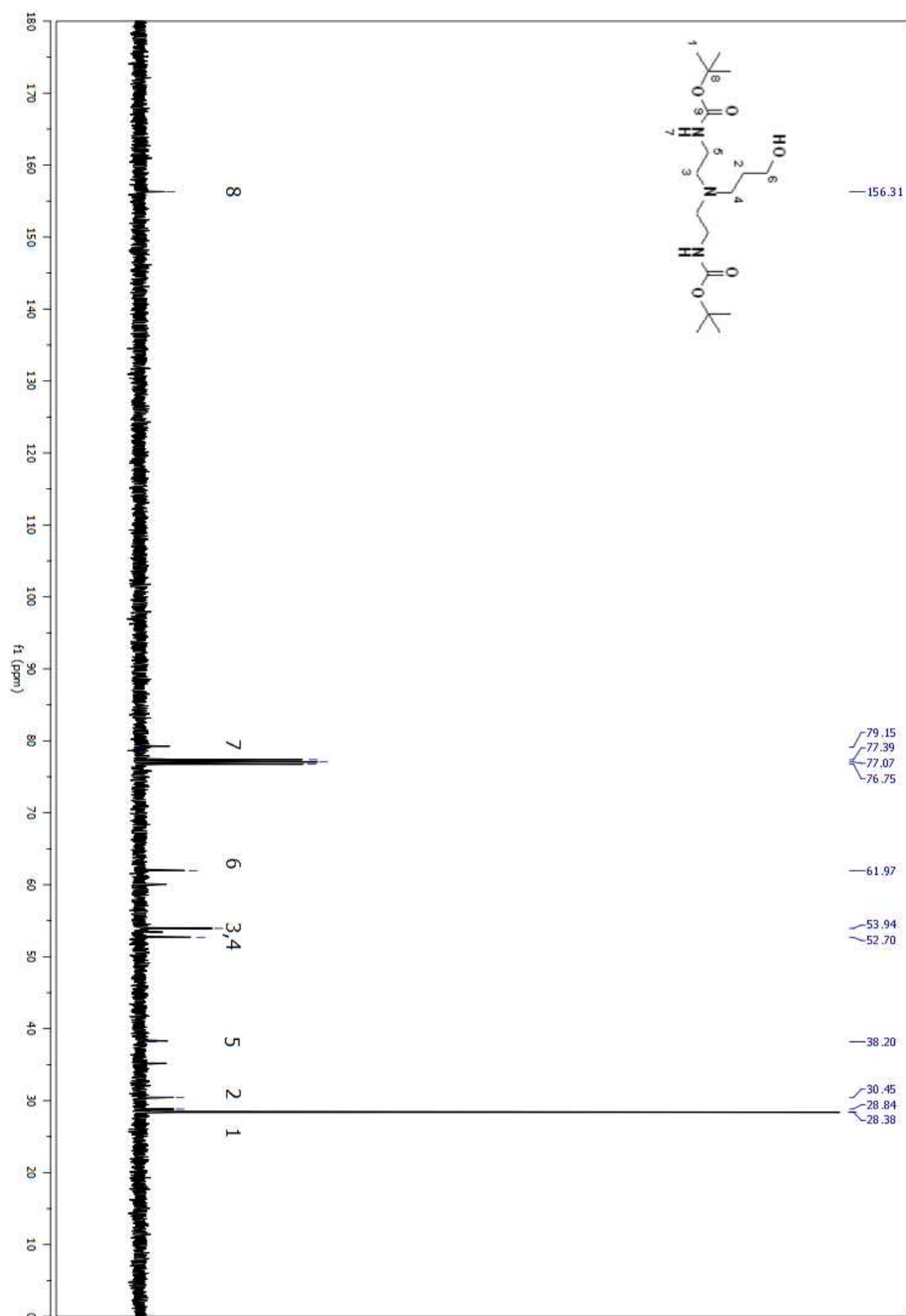


Figure A 304. ^{13}C NMR spectrum of compound (177) in CDCl_3 .

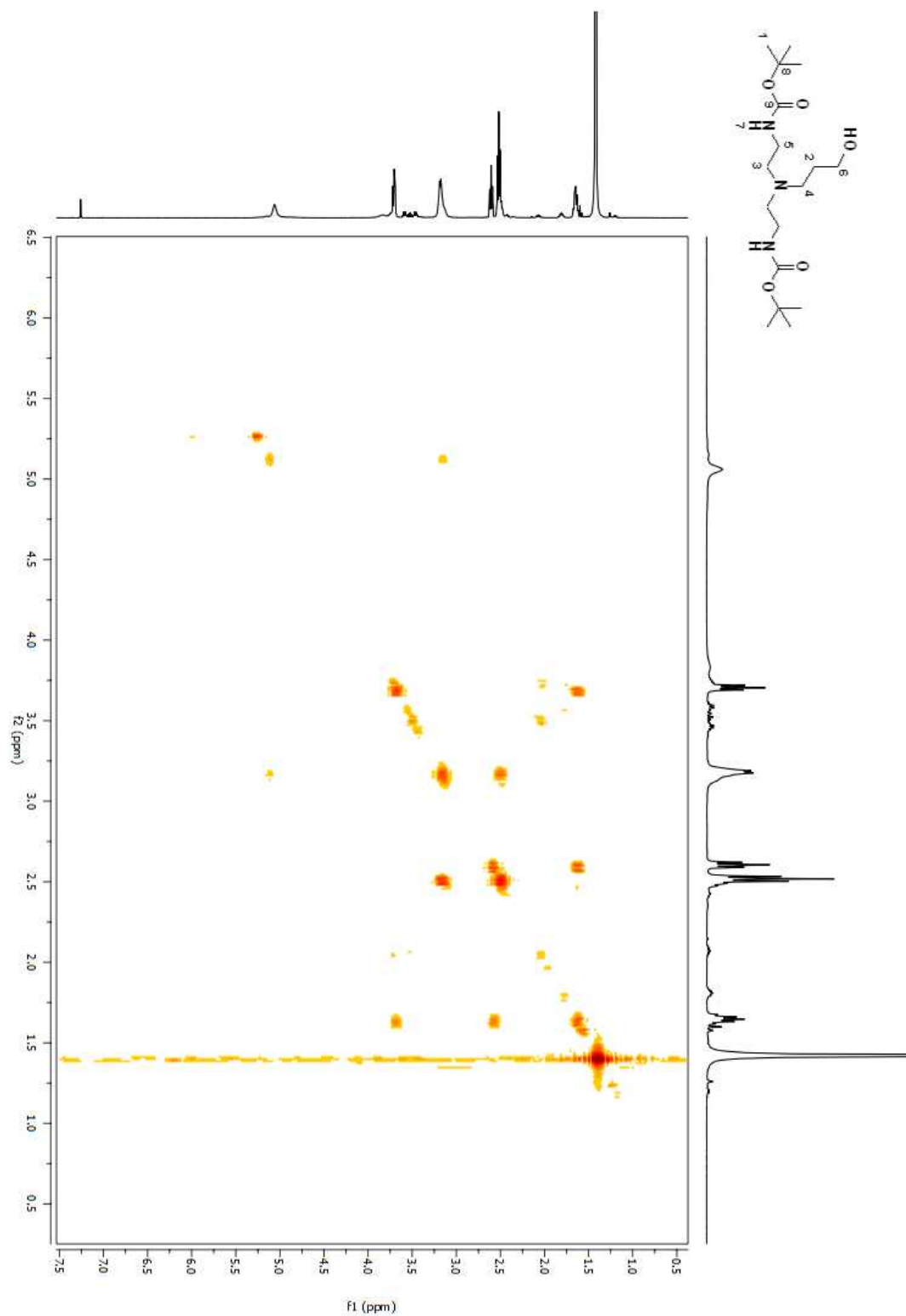


Figure A 305. COSY 2D NMR spectrum of compound (**177**) in CDCl_3 .

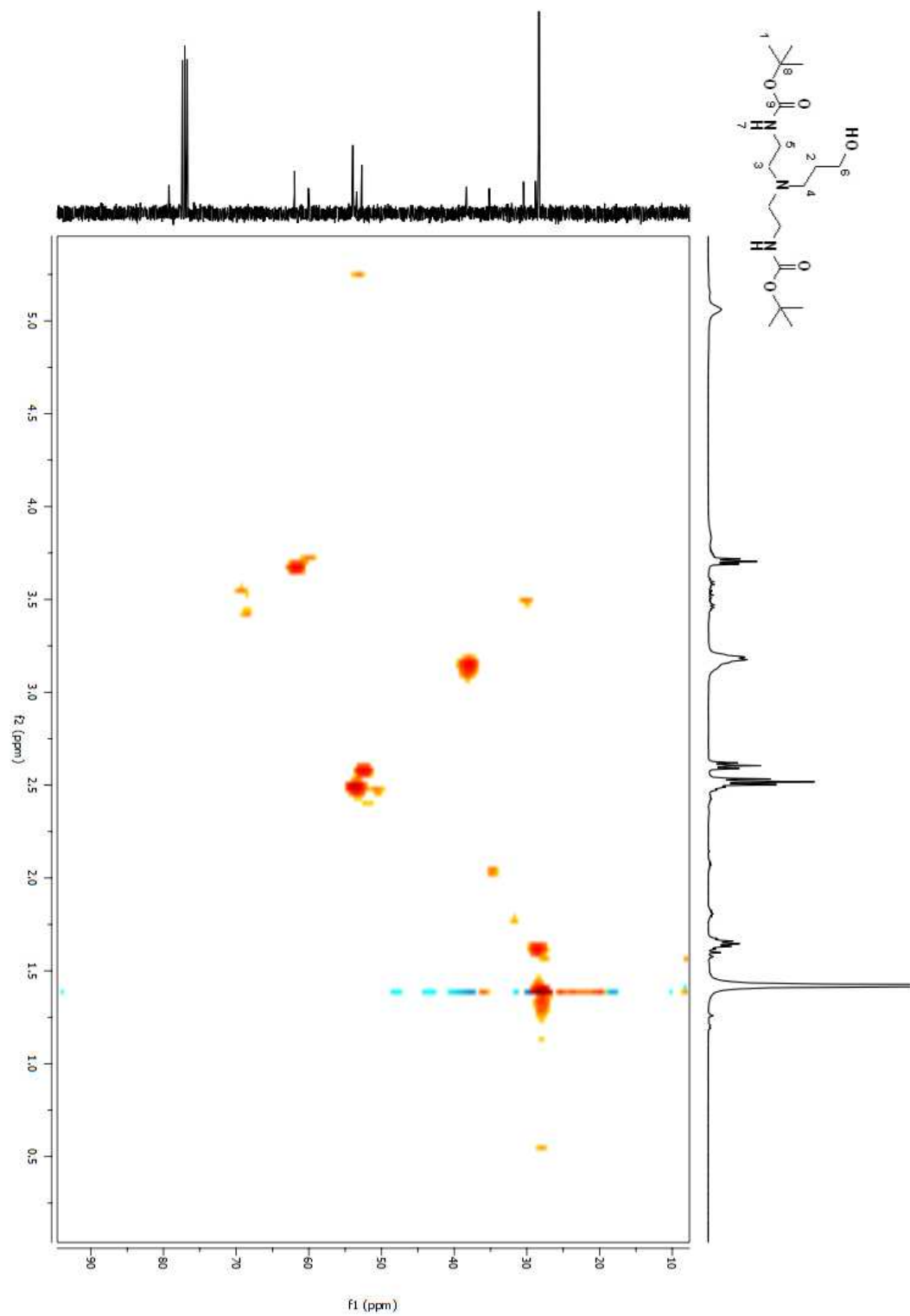


Figure A 306. HSQC 2D NMR spectrum of compound (177) in CDCl₃.

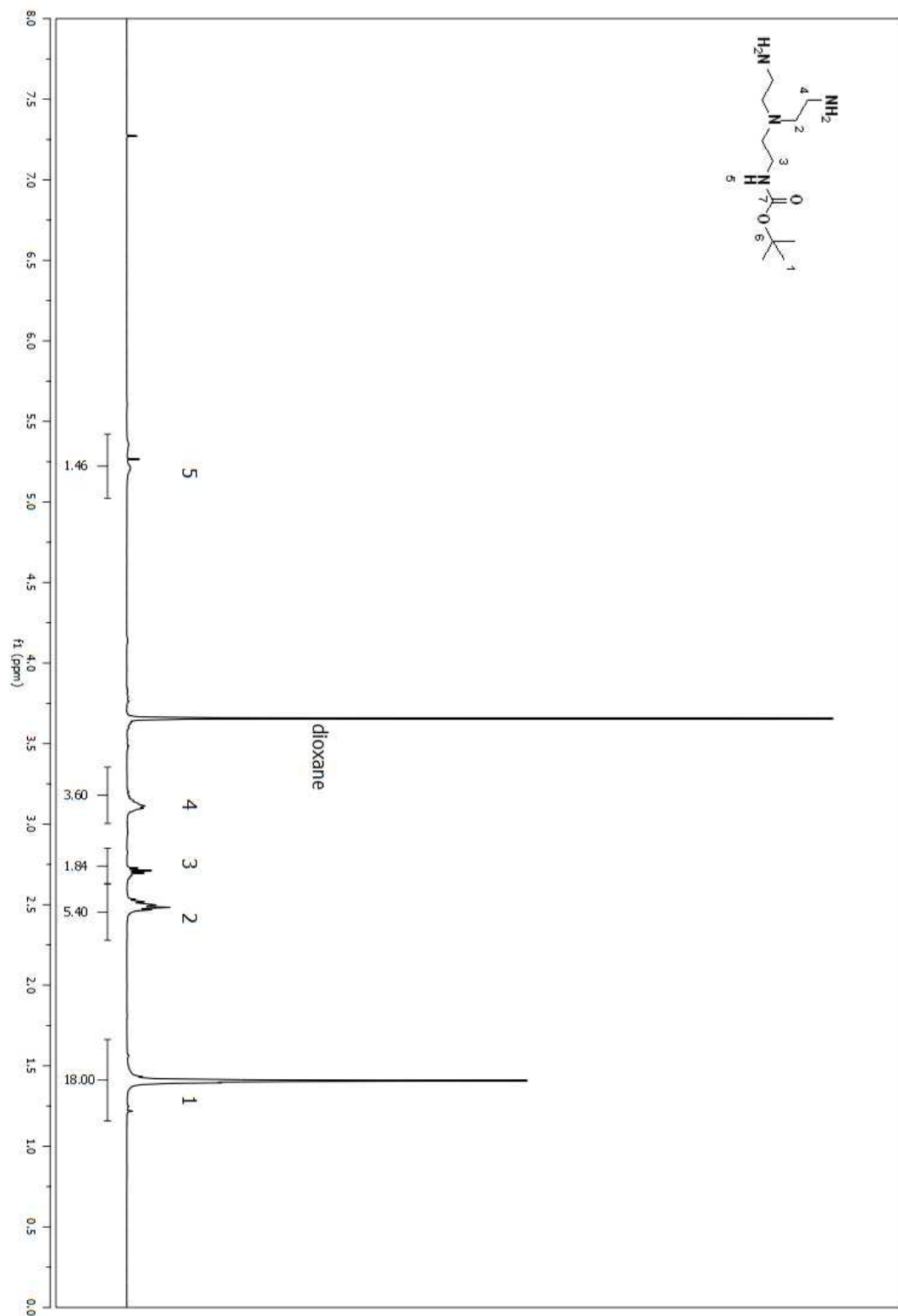


Figure A 307. ^1H NMR spectrum of compound (181) in CDCl_3 .

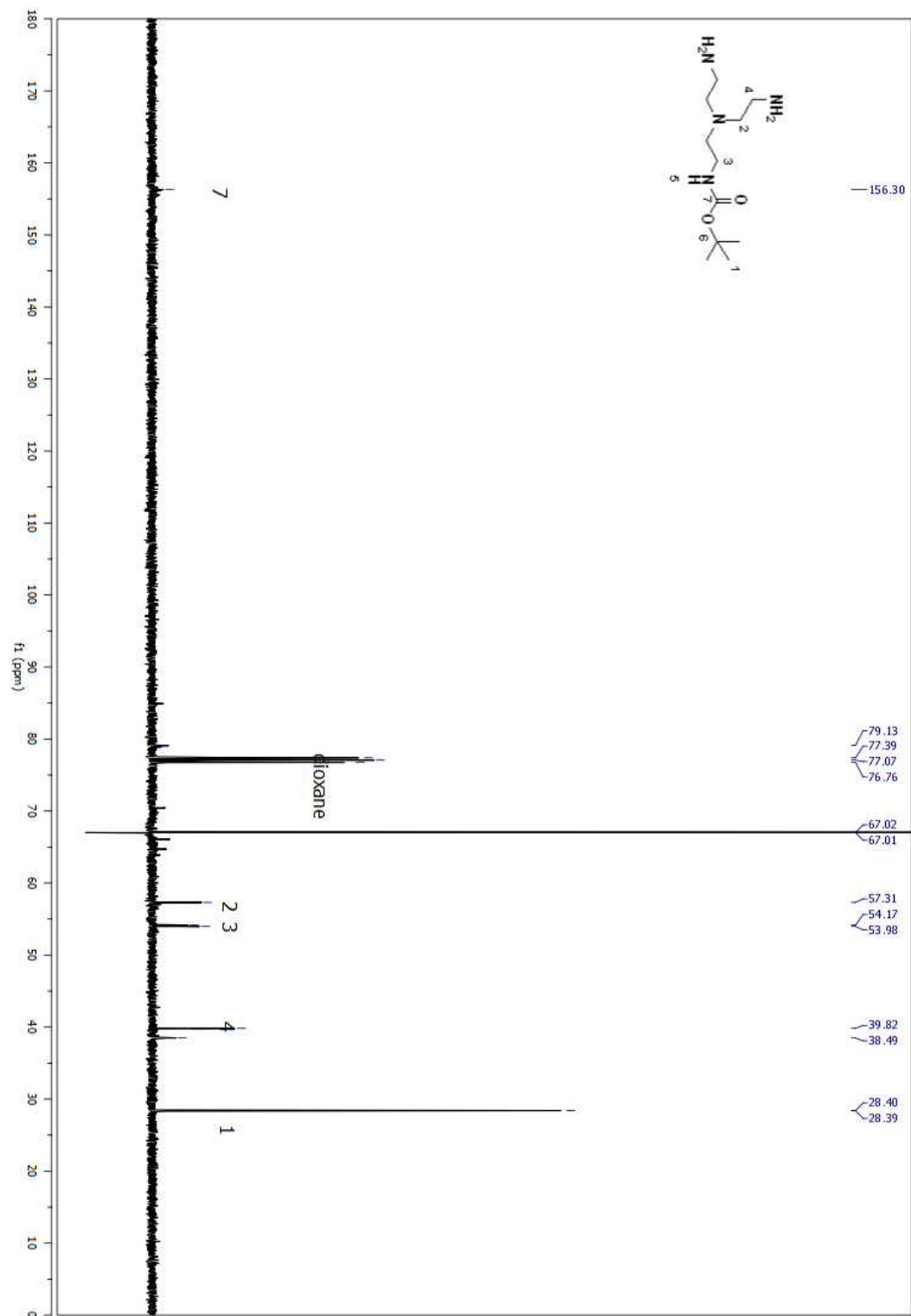


Figure A 308. ¹³C NMR spectrum of compound (181) in CDCl₃.

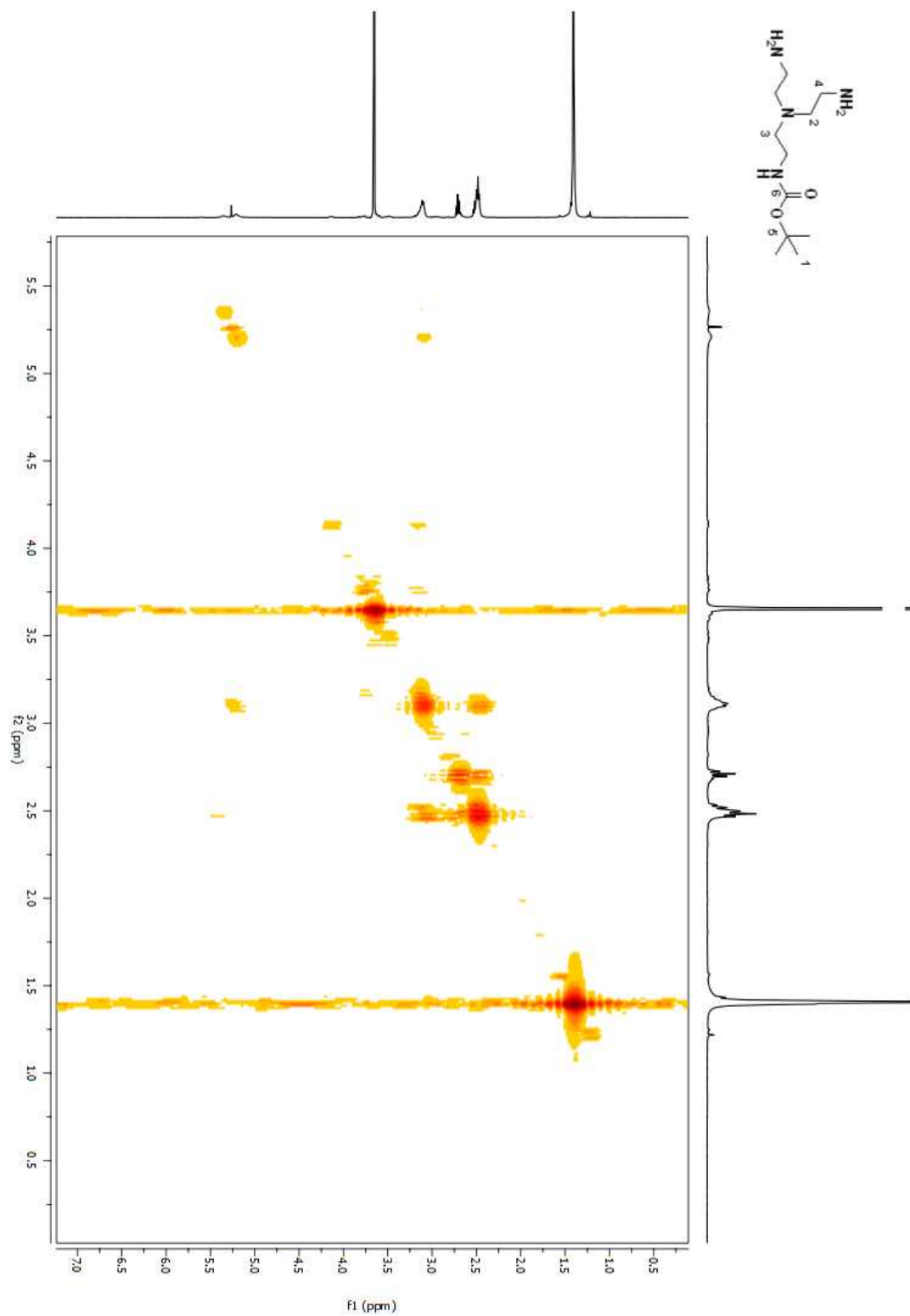


Figure A 309. COSY 2D NMR spectrum of compound (**181**) in CDCl₃.

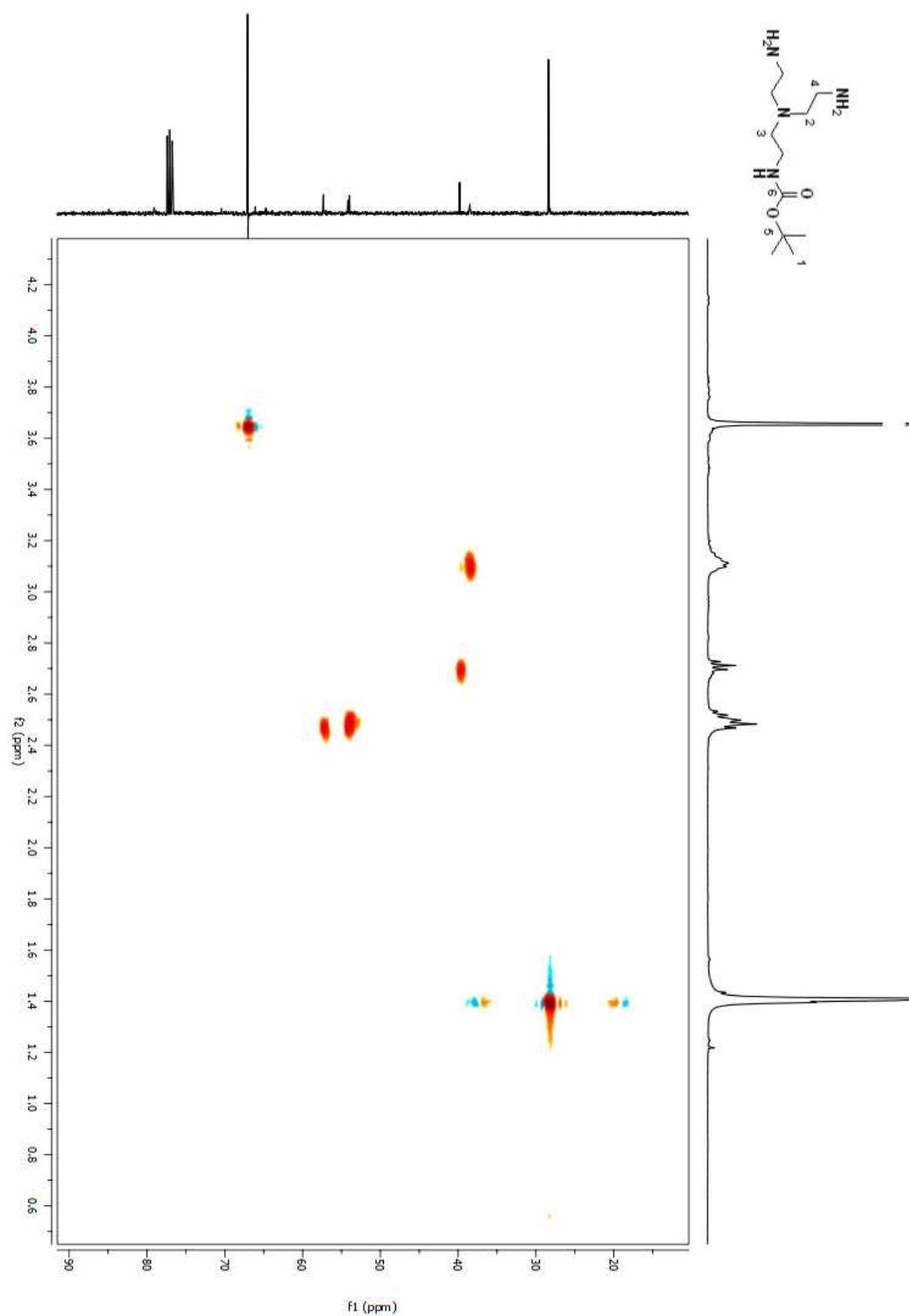


Figure A 310. HSQC 2D NMR spectrum of compound (**181**) in CDCl₃.

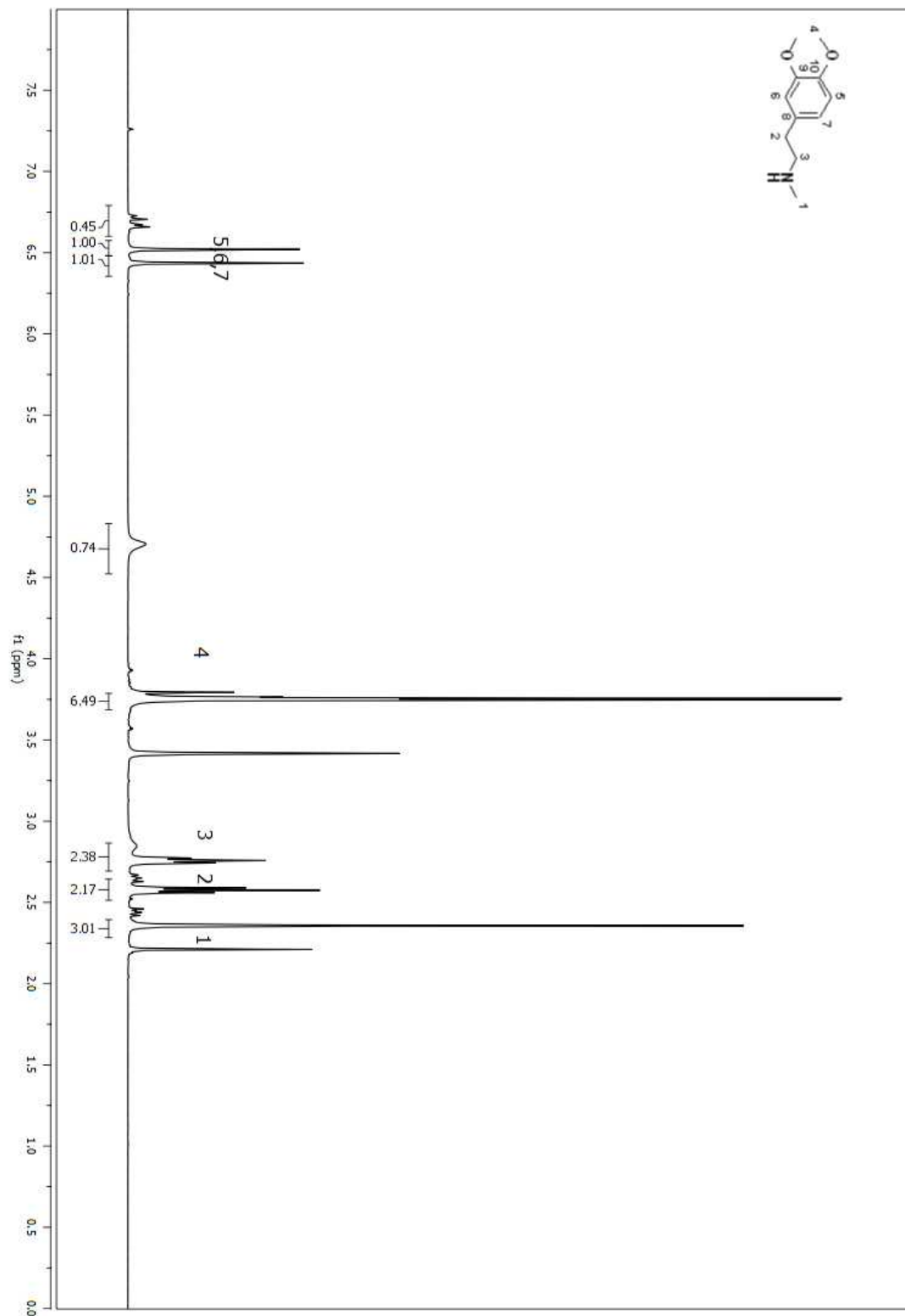


Figure A 311. ^1H NMR spectrum of compound (185) in CDCl_3 . (CRUDE)

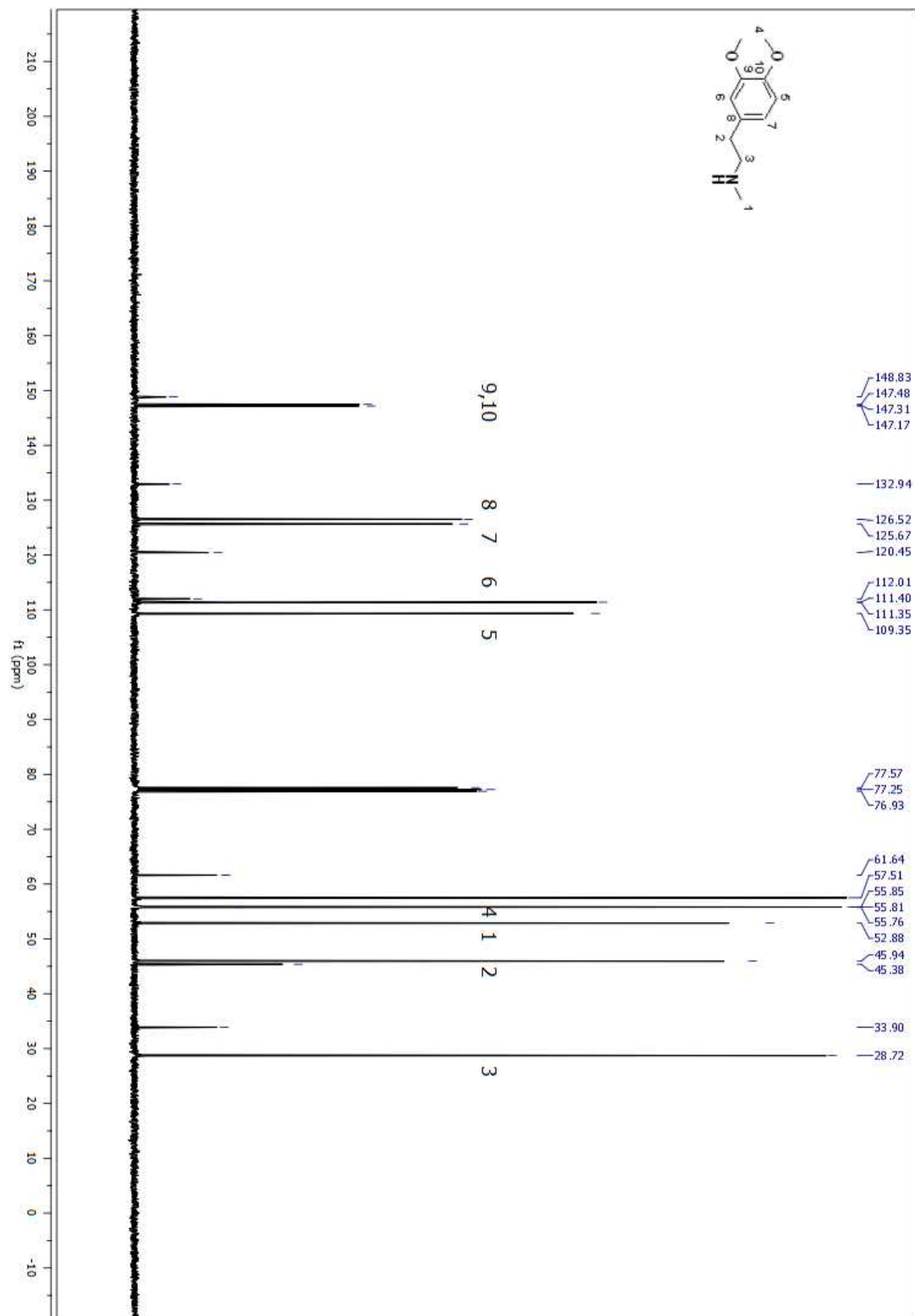


Figure A 312. ¹³C NMR spectrum of compound (185) in CDCl₃.(CRUDE)

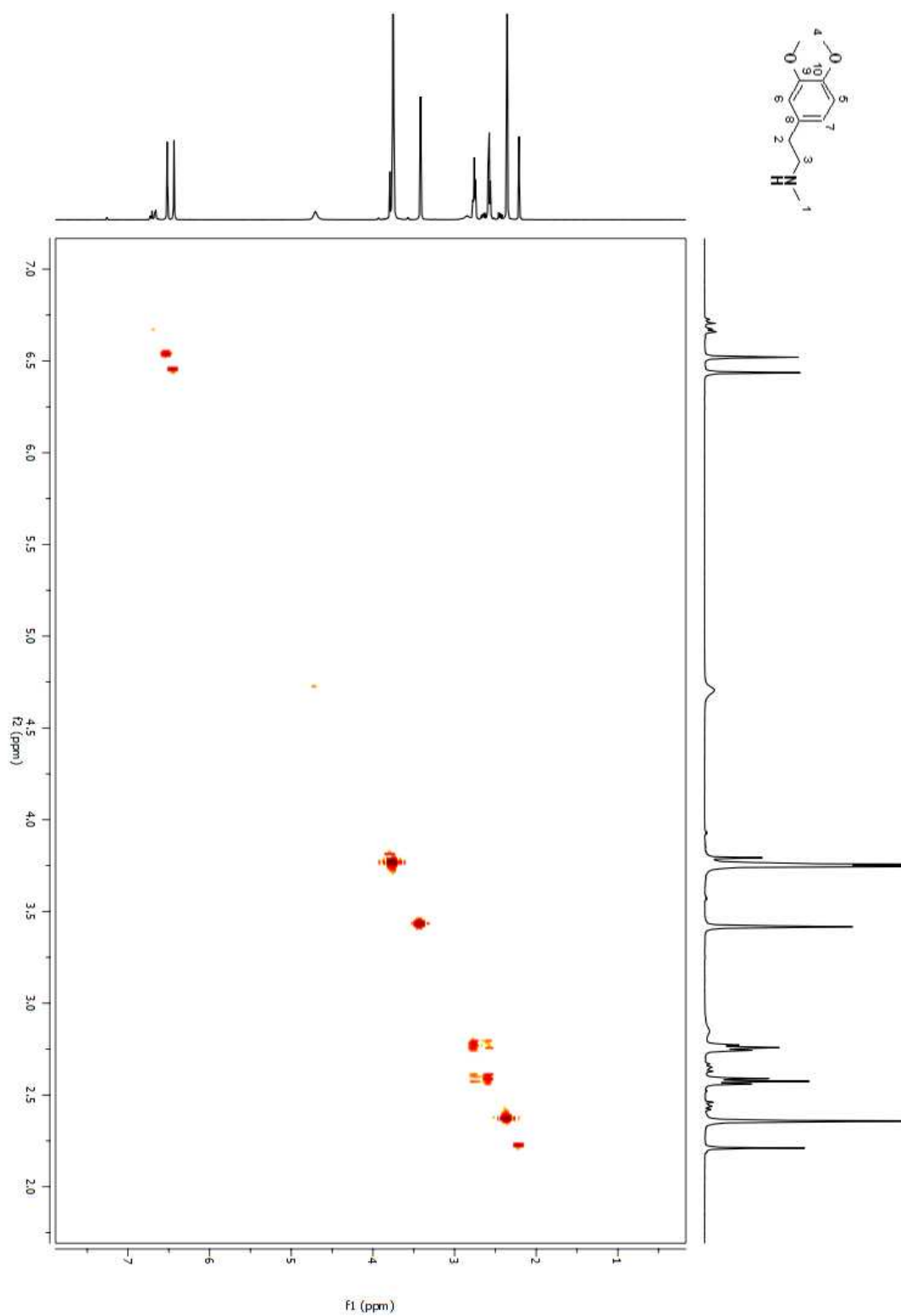


Figure A 313. COSY 2D NMR spectrum of compound (**185**) in CDCl₃.

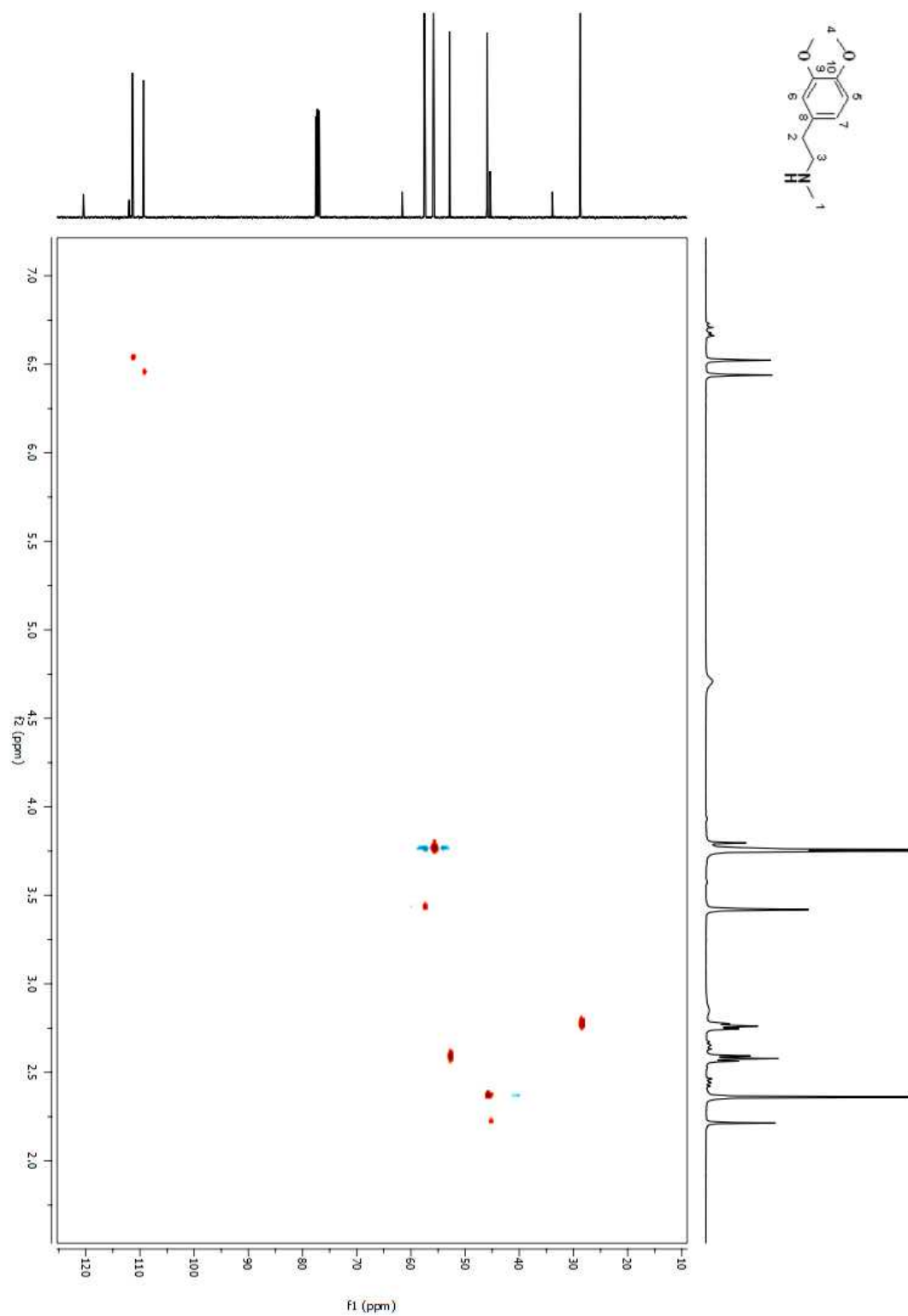


Figure A 314. HSQC 2D NMR spectrum of compound (**185**) in CDCl_3 .

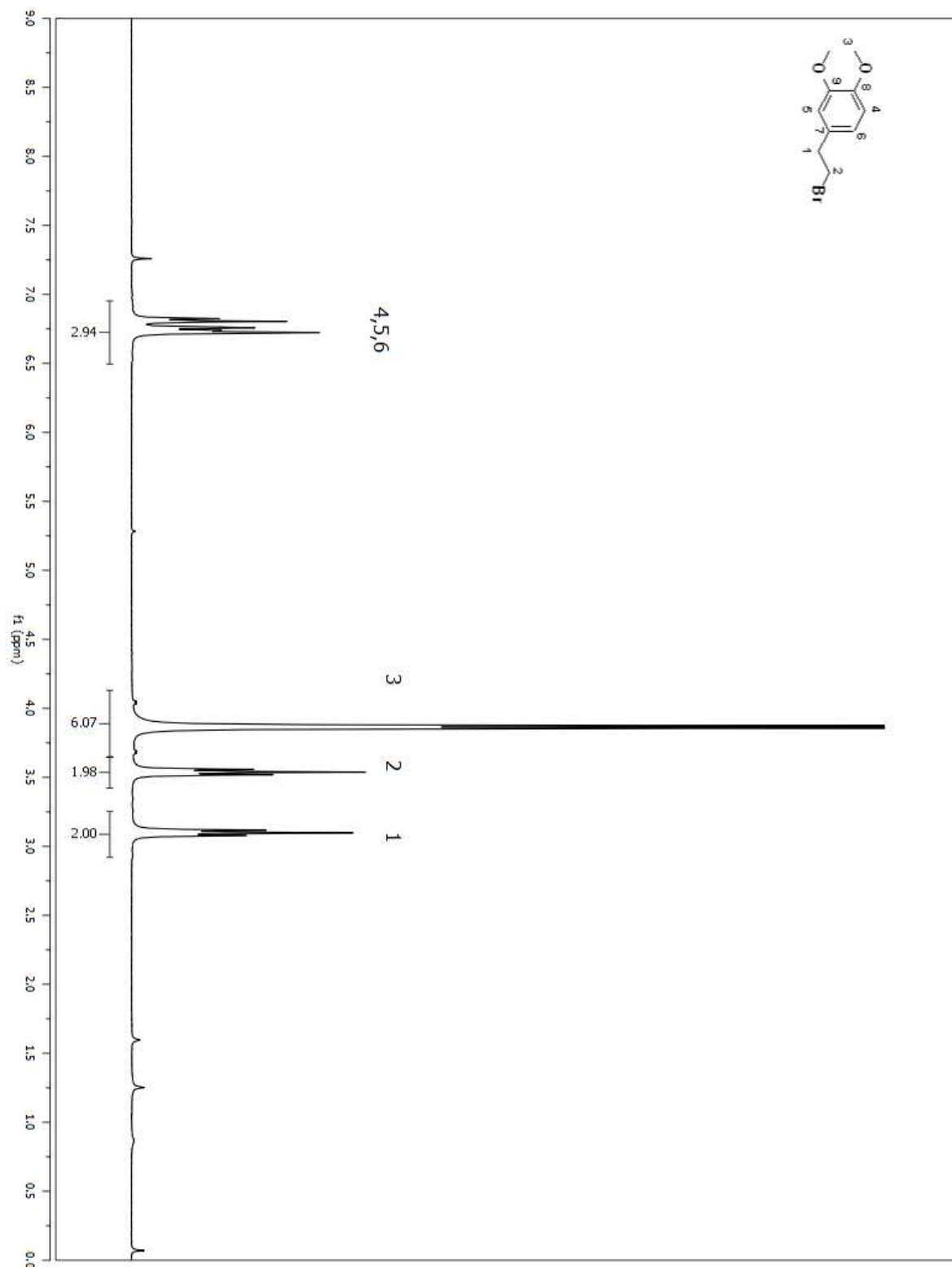


Figure A 315. ^1H NMR spectrum of compound (188) in CDCl_3 .

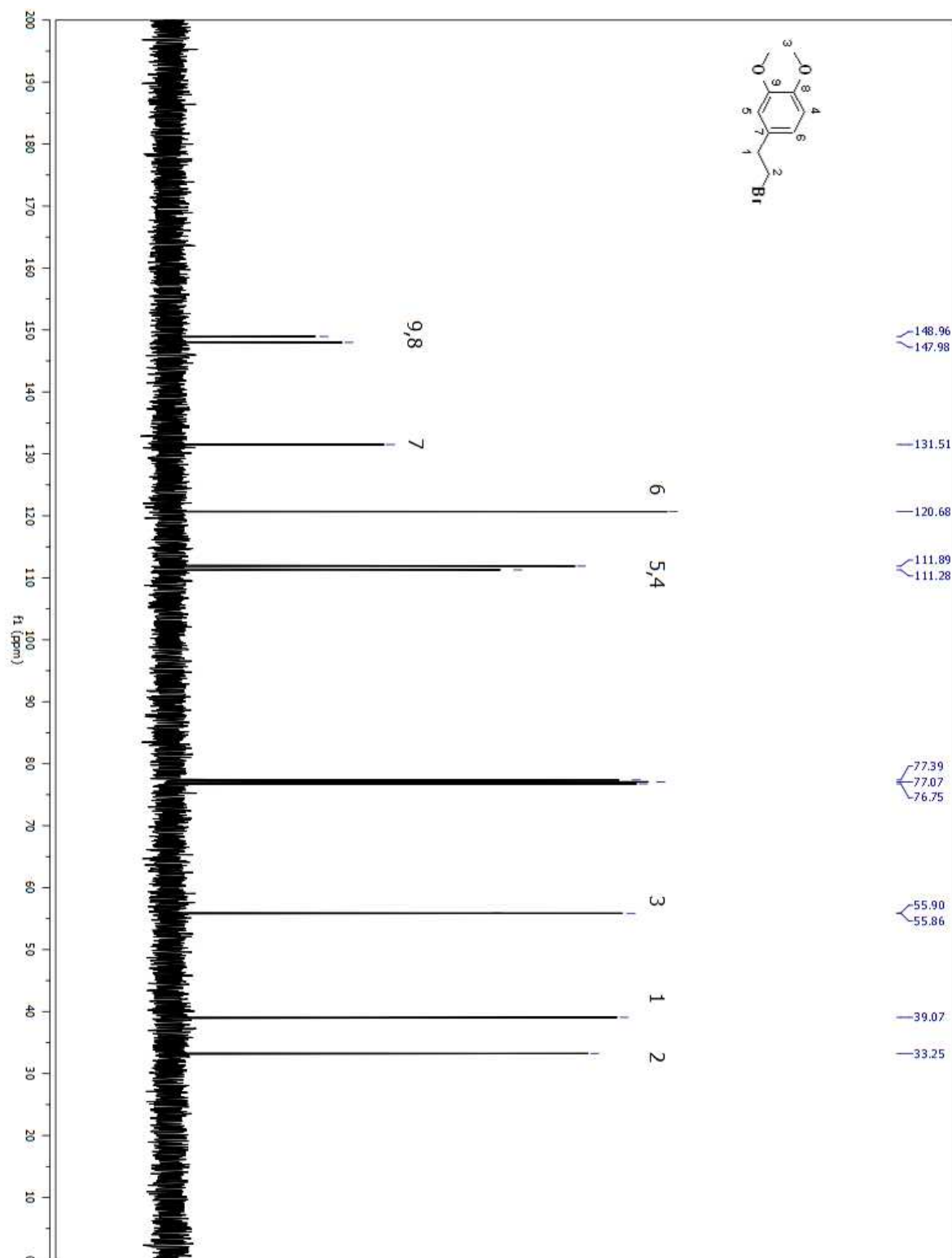


Figure A 316. ¹³C NMR spectrum of compound (188) in CDCl₃.

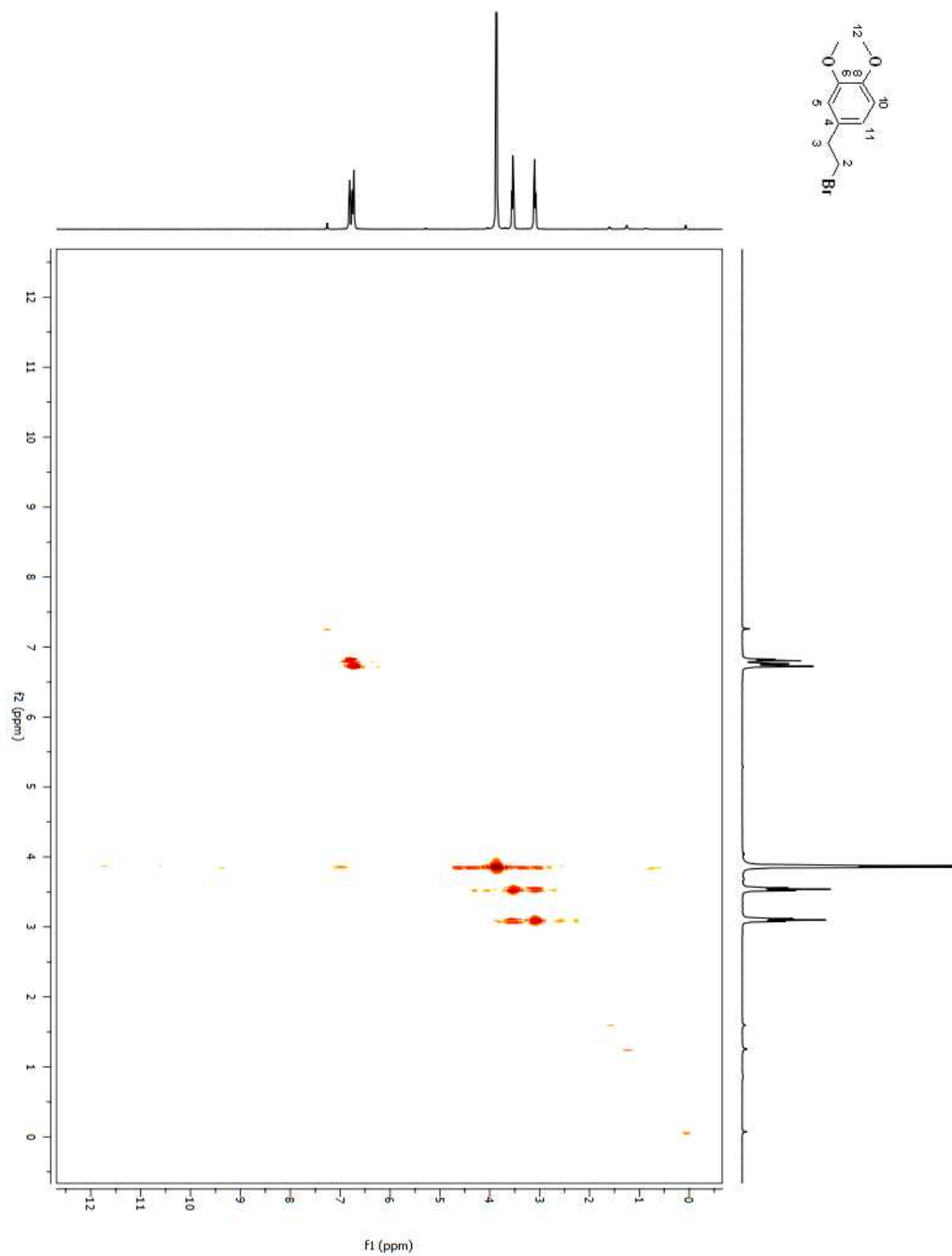


Figure A 317. COSY 2D NMR spectrum of compound (**188**) in CDCl₃.

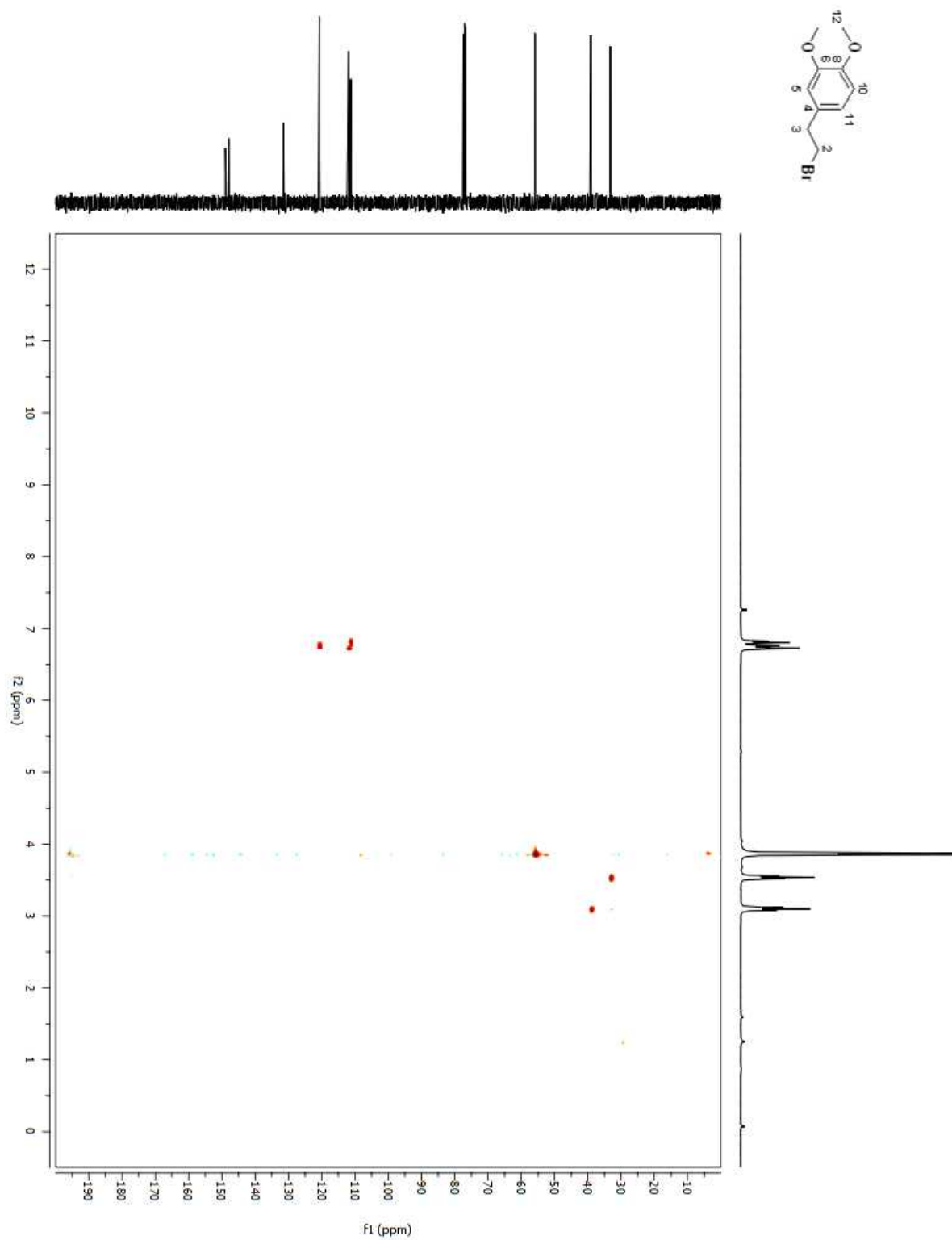


Figure A 318. HSQC 2D NMR spectrum of compound (**188**) in CDCl₃.

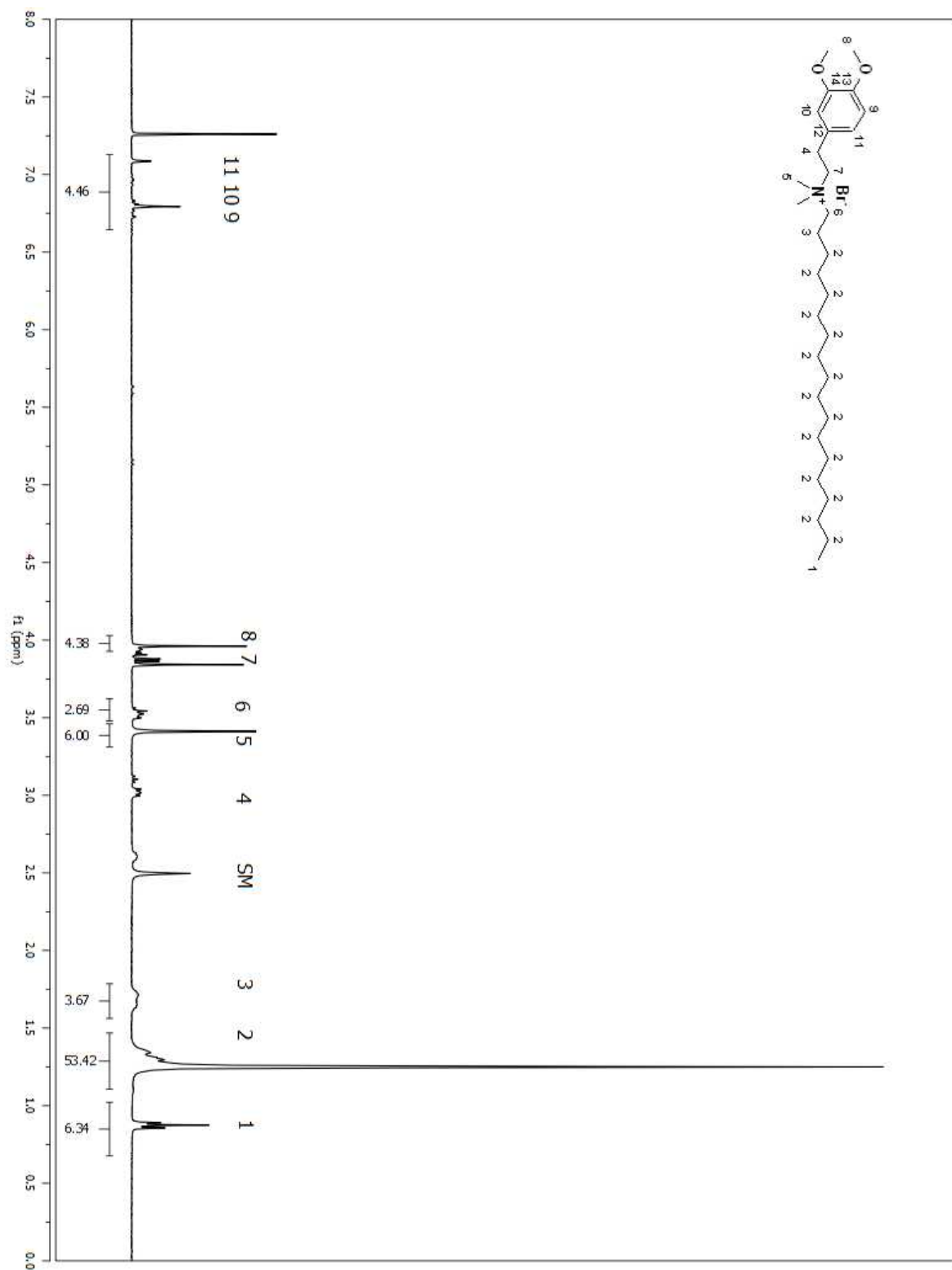


Figure A 319. ^1H NMR spectrum of compound (189) in CDCl_3 . (CRUDE)

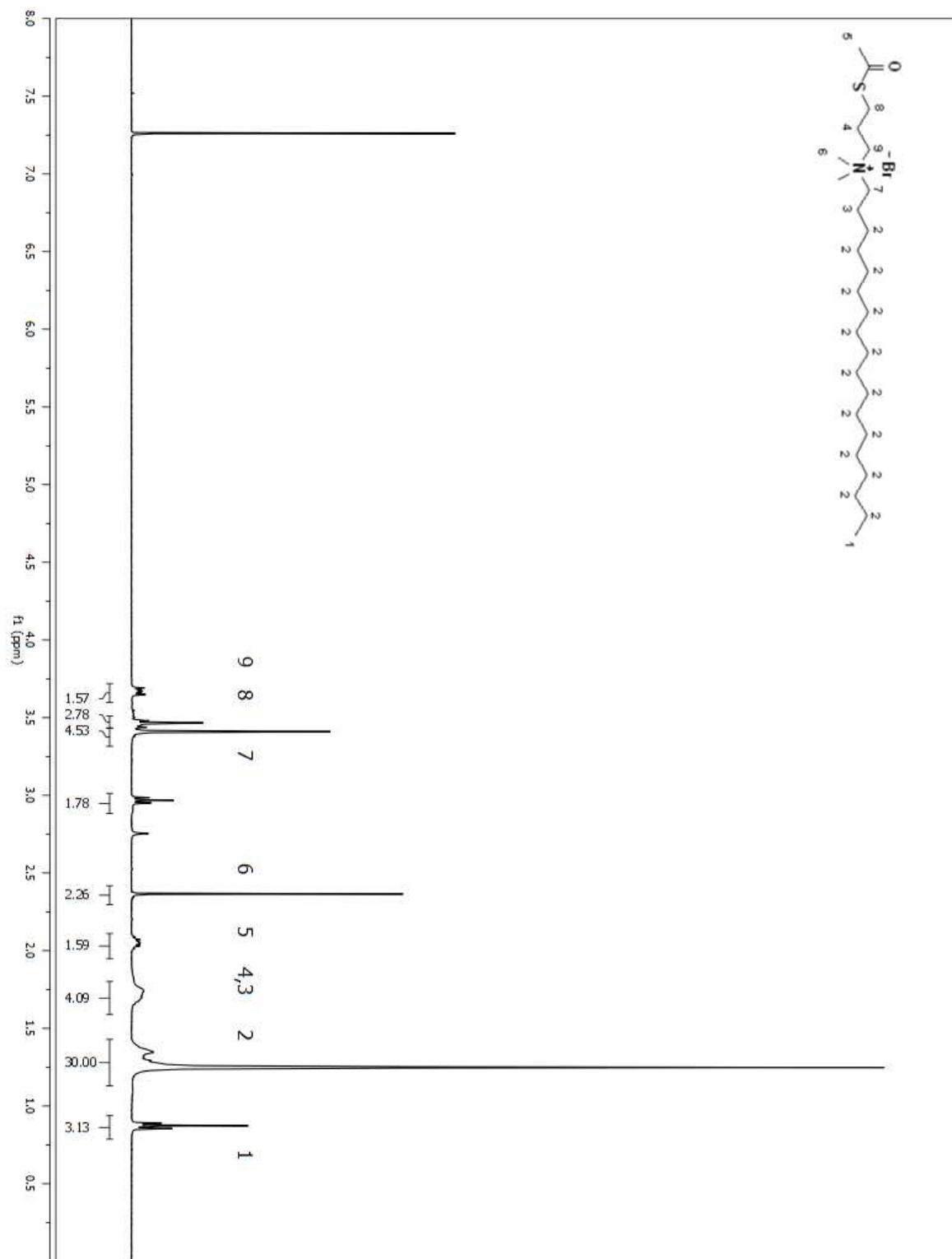


Figure A 320. ¹H NMR spectrum of compound (192) in CDCl₃.

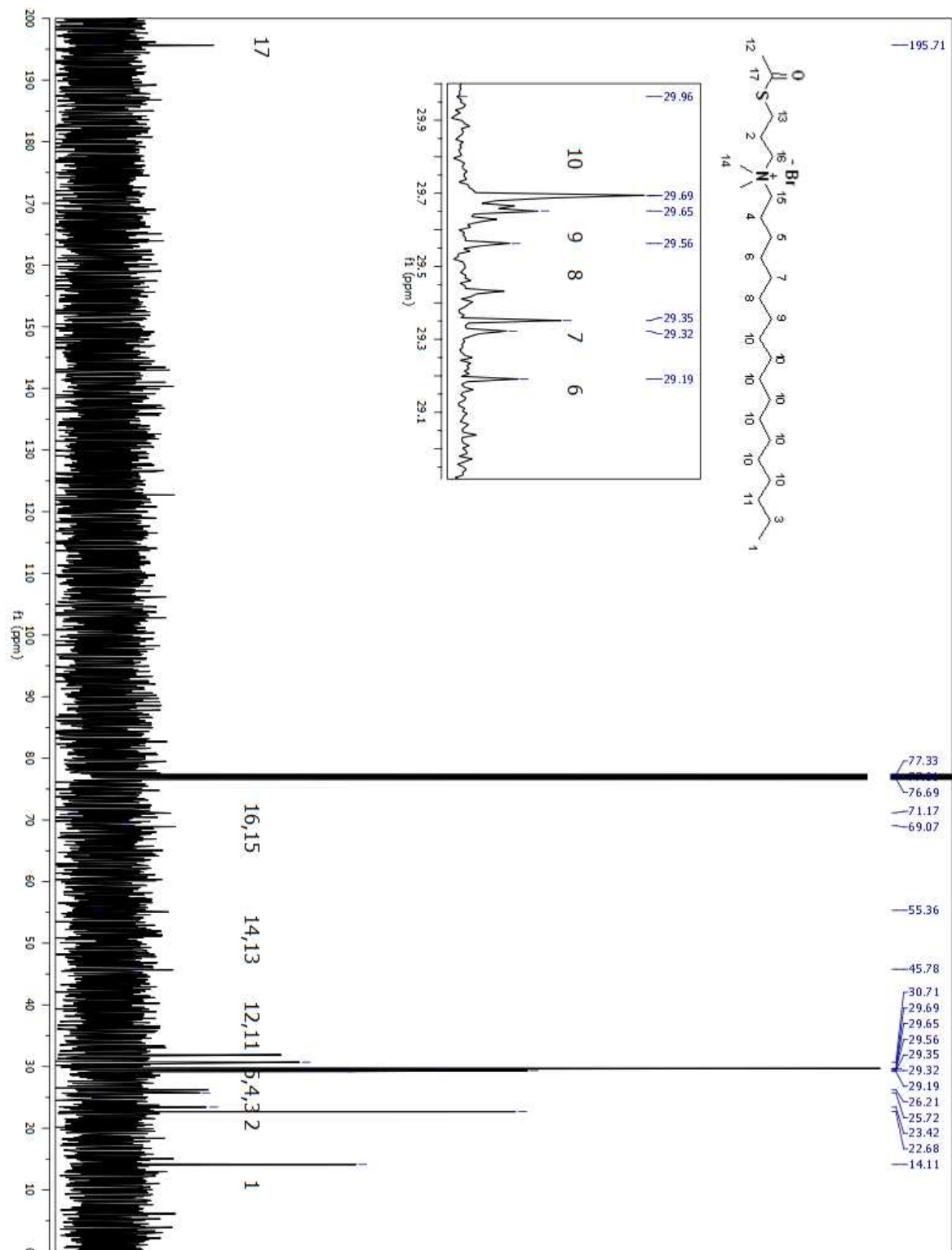


Figure A 321. ^{13}C NMR spectrum of compound (192) in CDCl_3 .

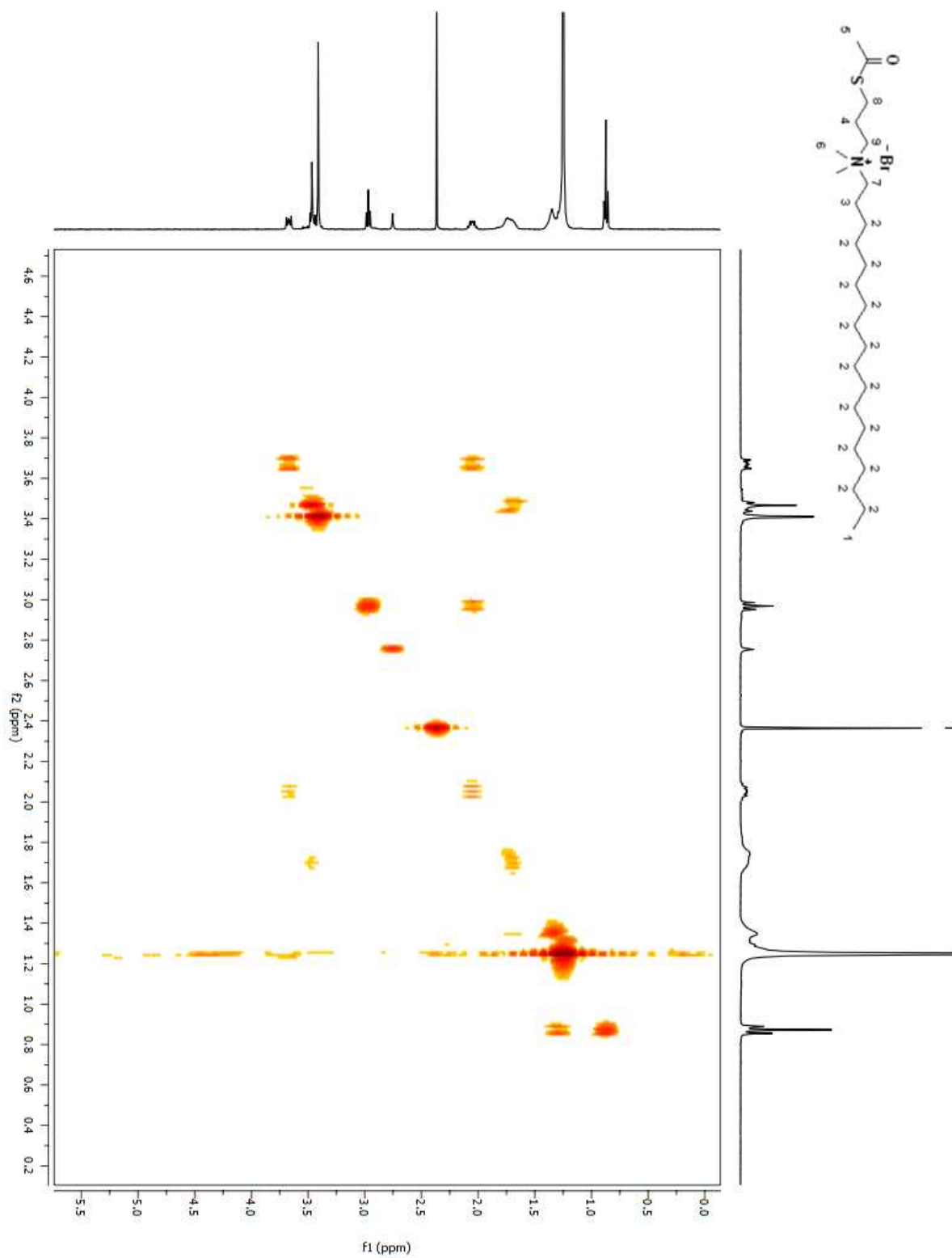


Figure A 322. COSY 2D NMR spectrum of compound (**192**) in CDCl₃.

Figure A 323. ^1H NMR spectrum of compound (**194**) in CDCl_3 .

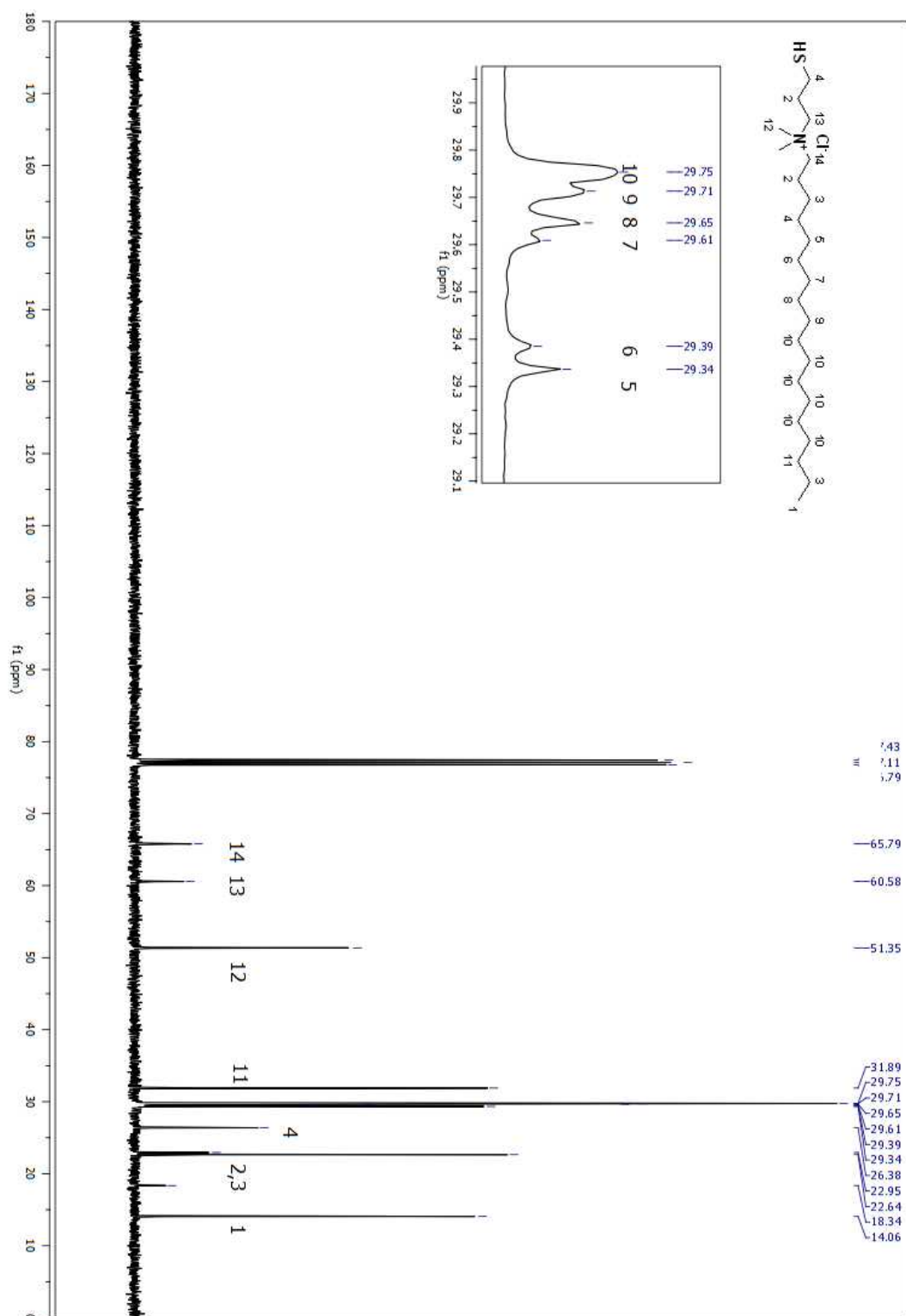


Figure A 324. ¹H NMR spectrum of compound (194) in CDCl₃.

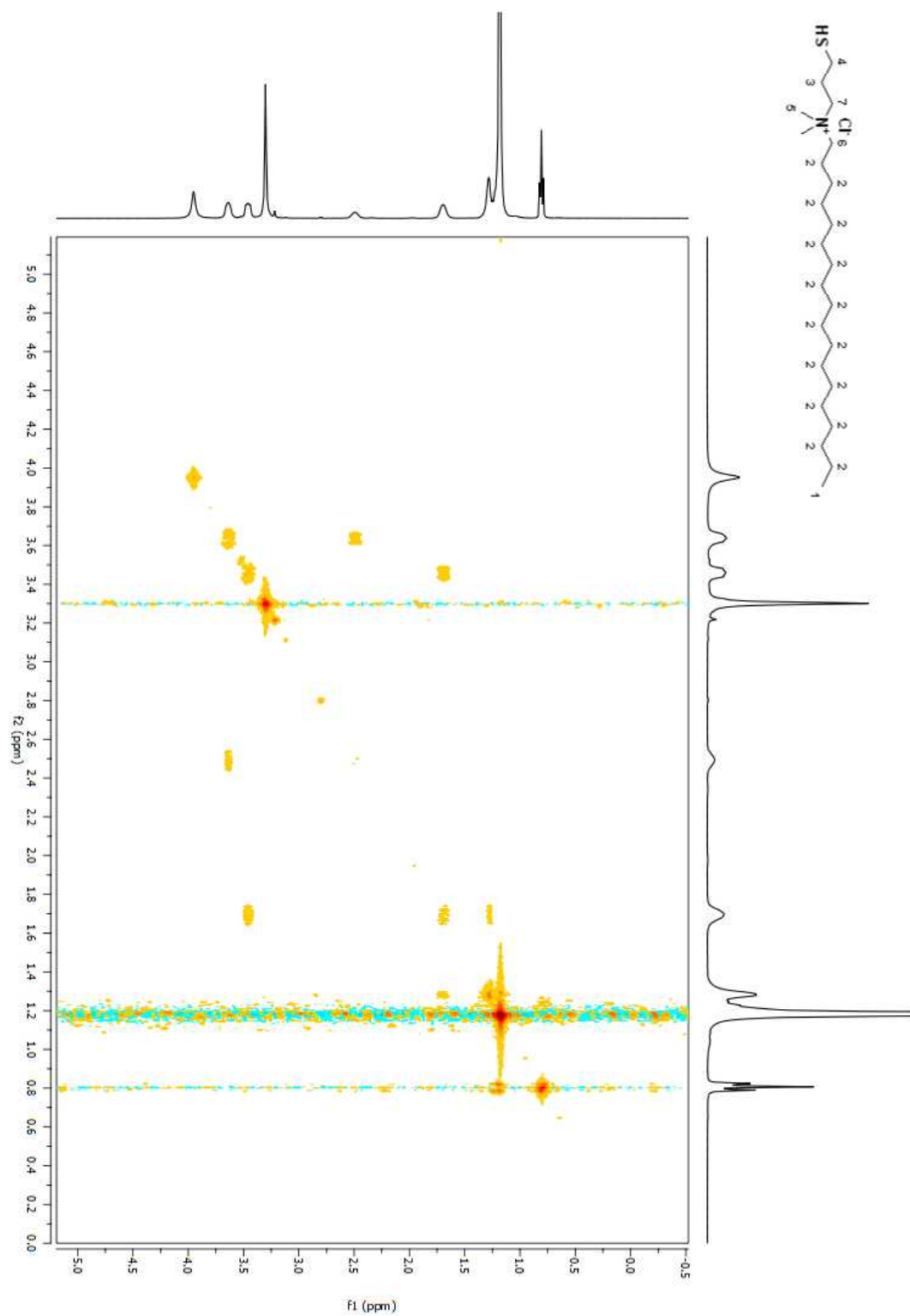


Figure A 325. COSY 2D NMR spectrum of compound (**194**) in CDCl₃.

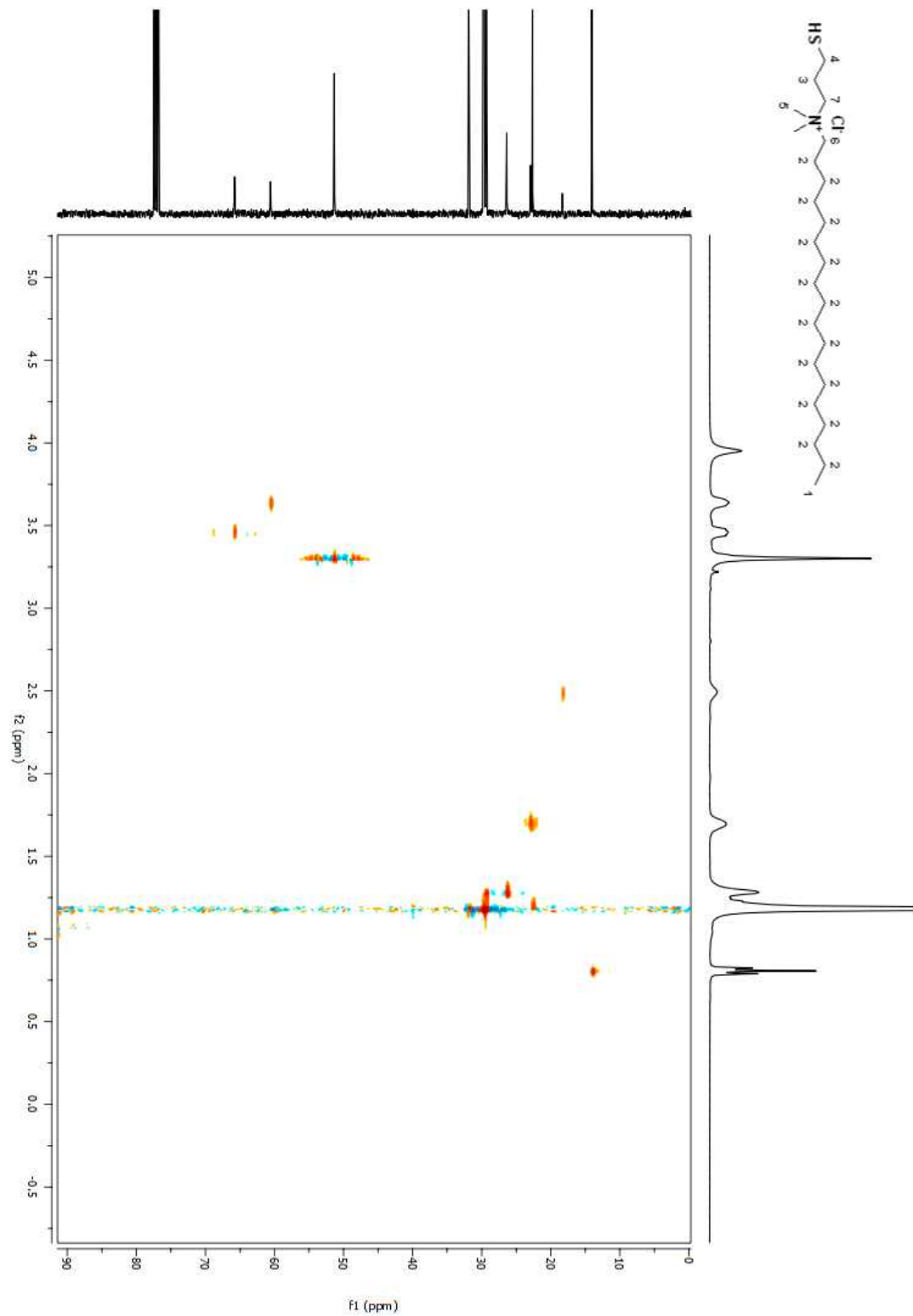


Figure A 326. HSQC 2D NMR spectrum of compound (194) in CDCl₃.

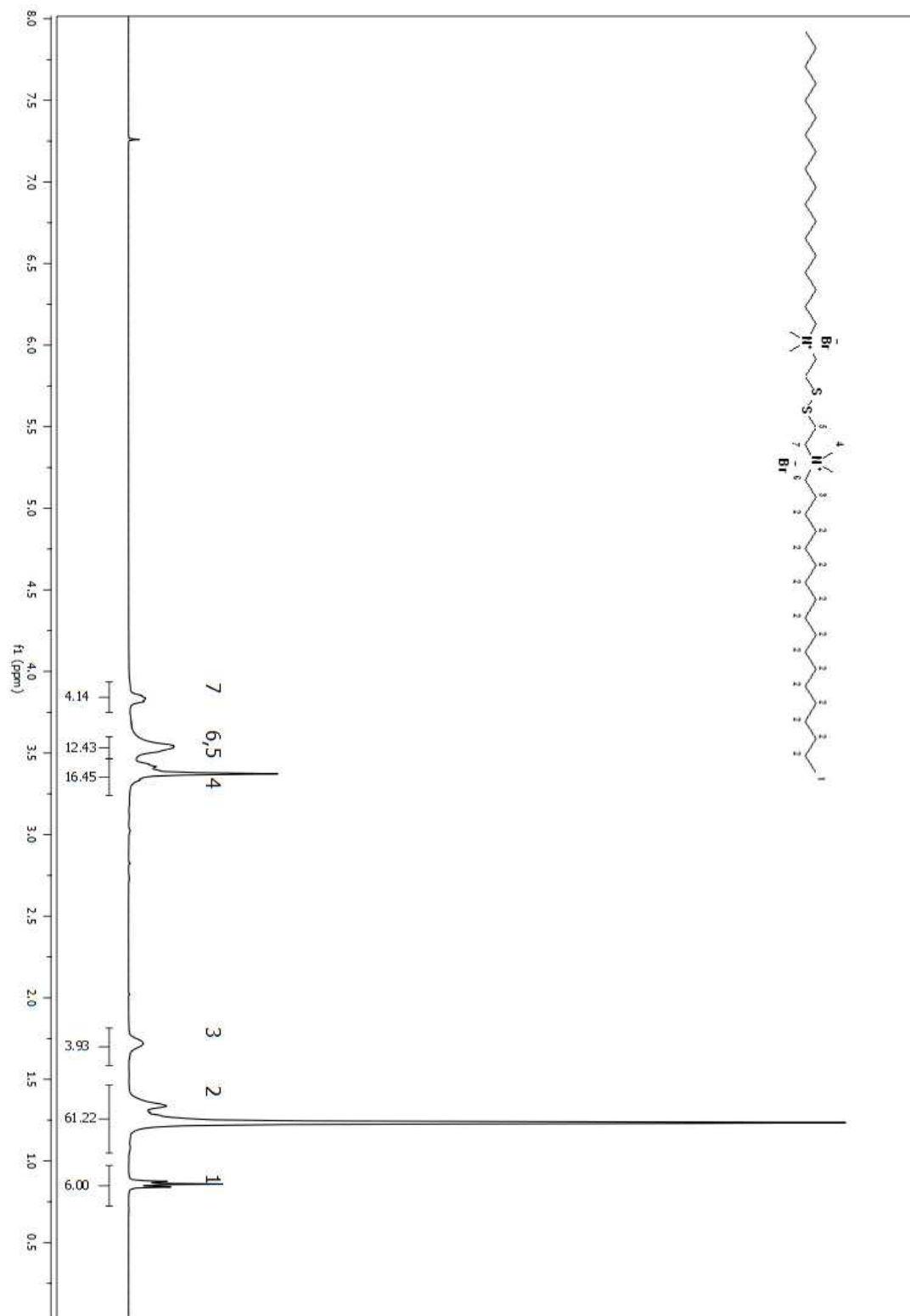


Figure A 327. ¹H NMR spectrum of compound (198) in CDCl₃.

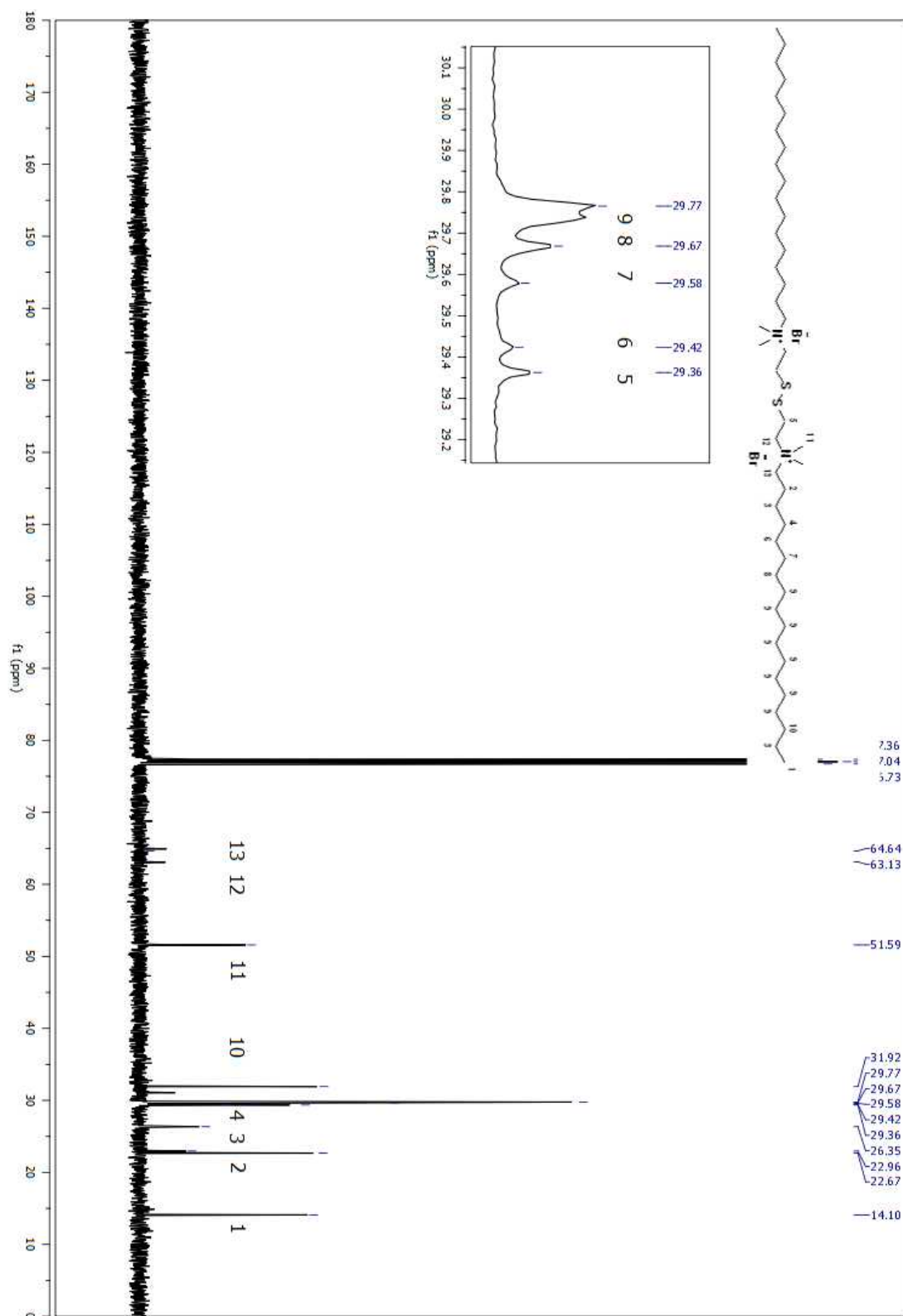


Figure A 328. ^{13}C NMR spectrum of compound (198) in CDCl_3 .

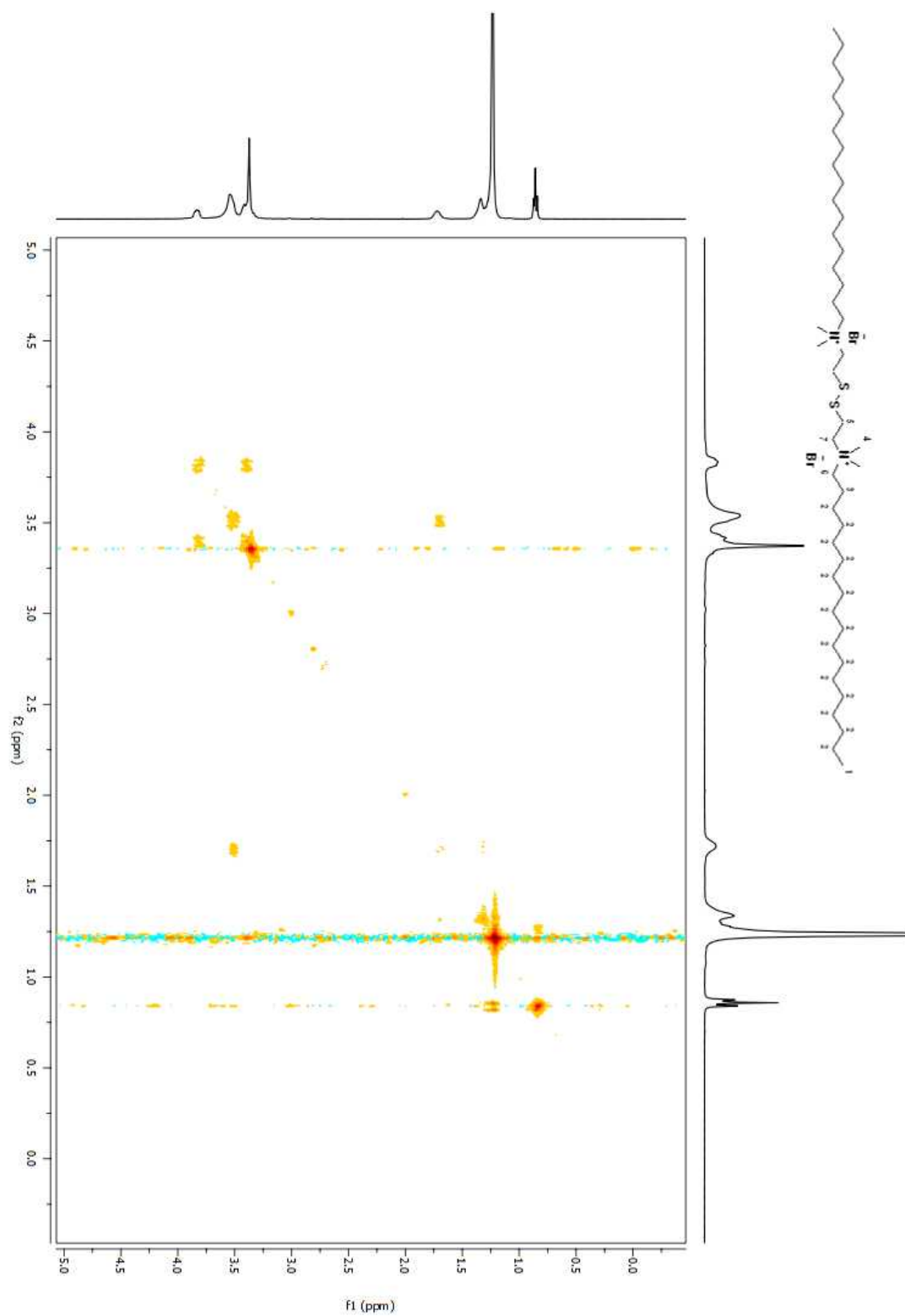


Figure A 329. COSY 2D NMR spectrum of compound (**198**) in CDCl₃.

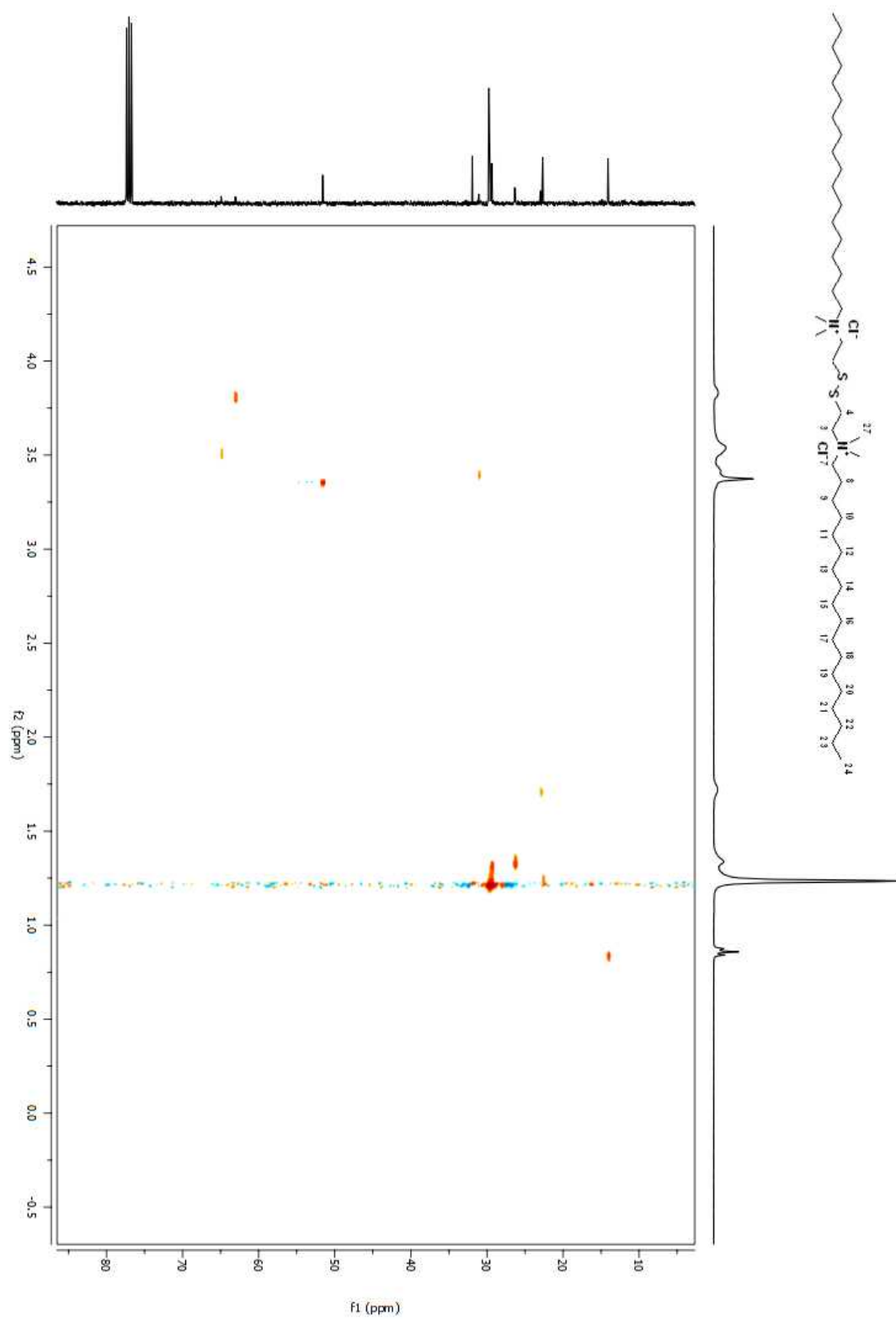


Figure A 330. HSQC 2D NMR spectrum of compound (**198**) in CDCl₃.

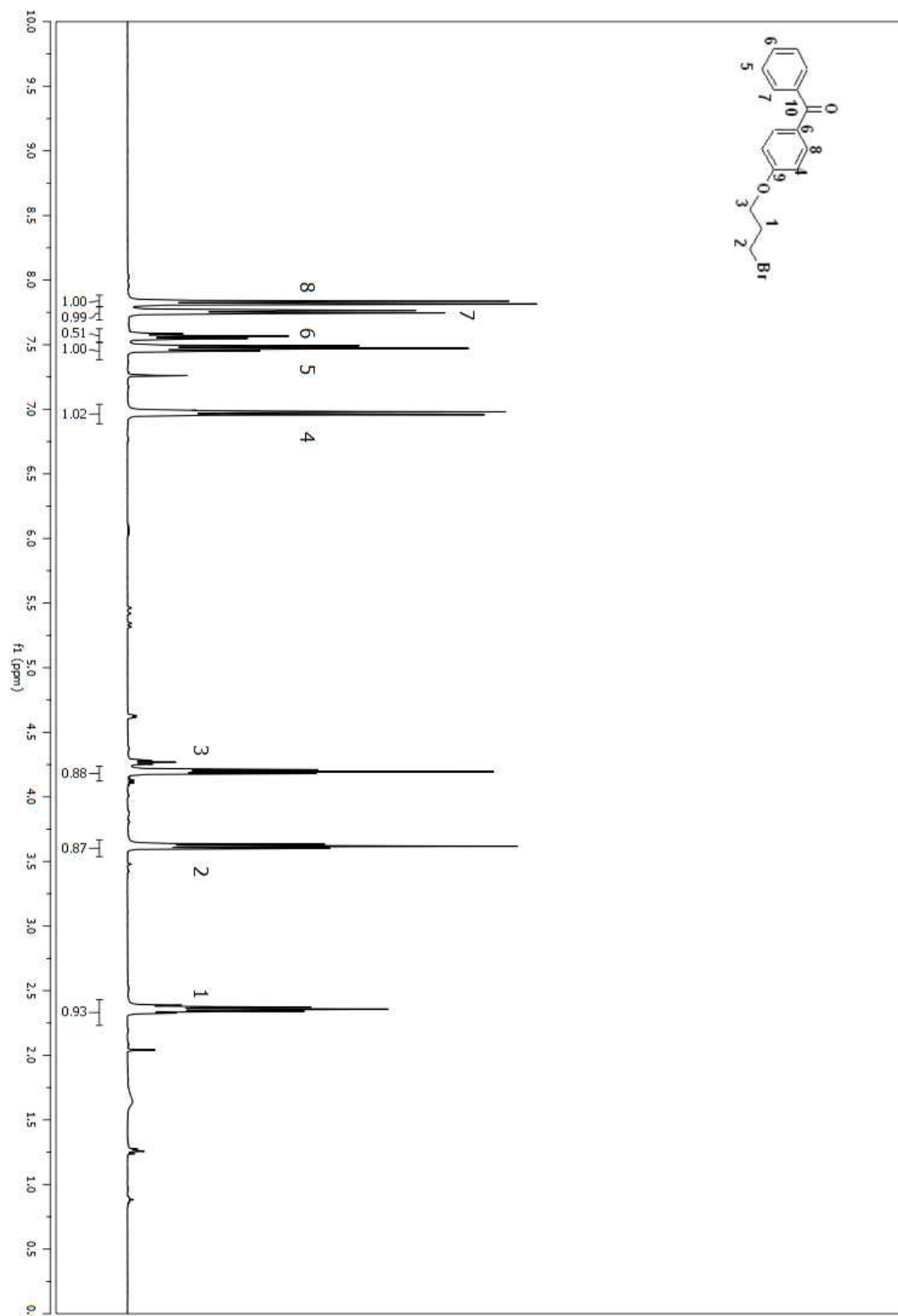


Figure A 331. ¹H NMR spectrum of compound (202) in CDCl₃.

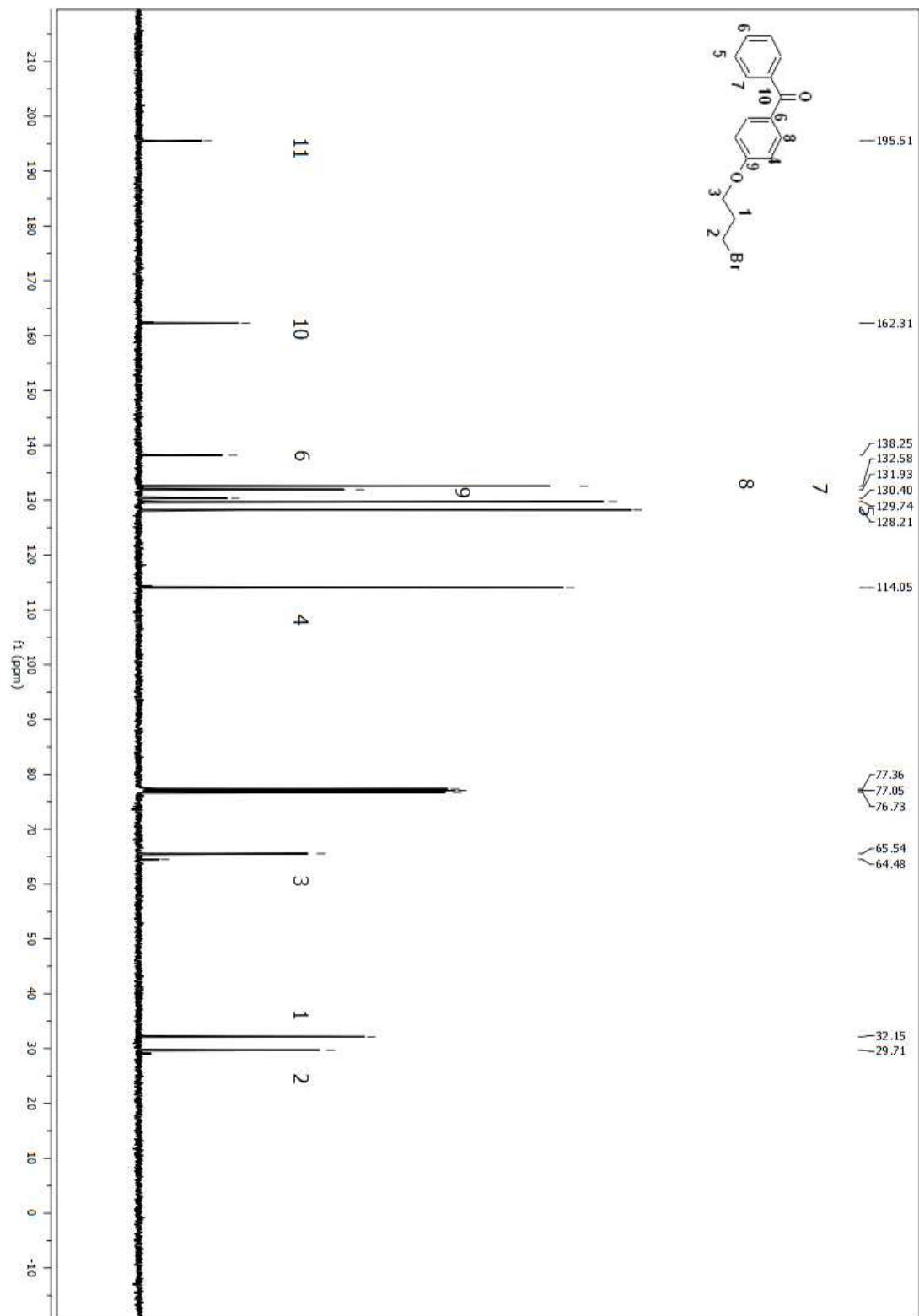


Figure A 332. ¹³C NMR spectrum of compound (202) in CDCl₃.

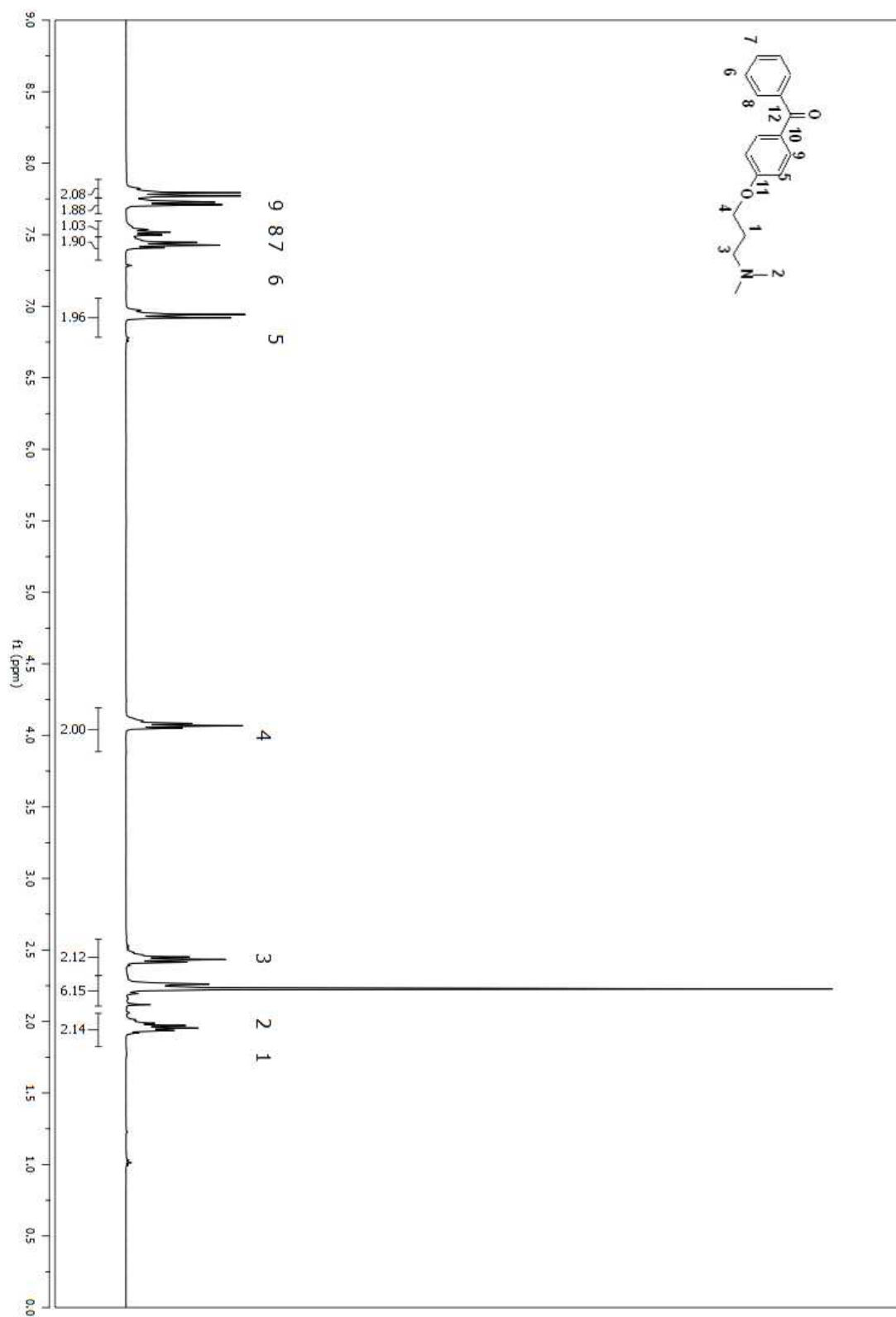


Figure A 333. ^1H NMR spectrum of compound (204) in CDCl_3 .

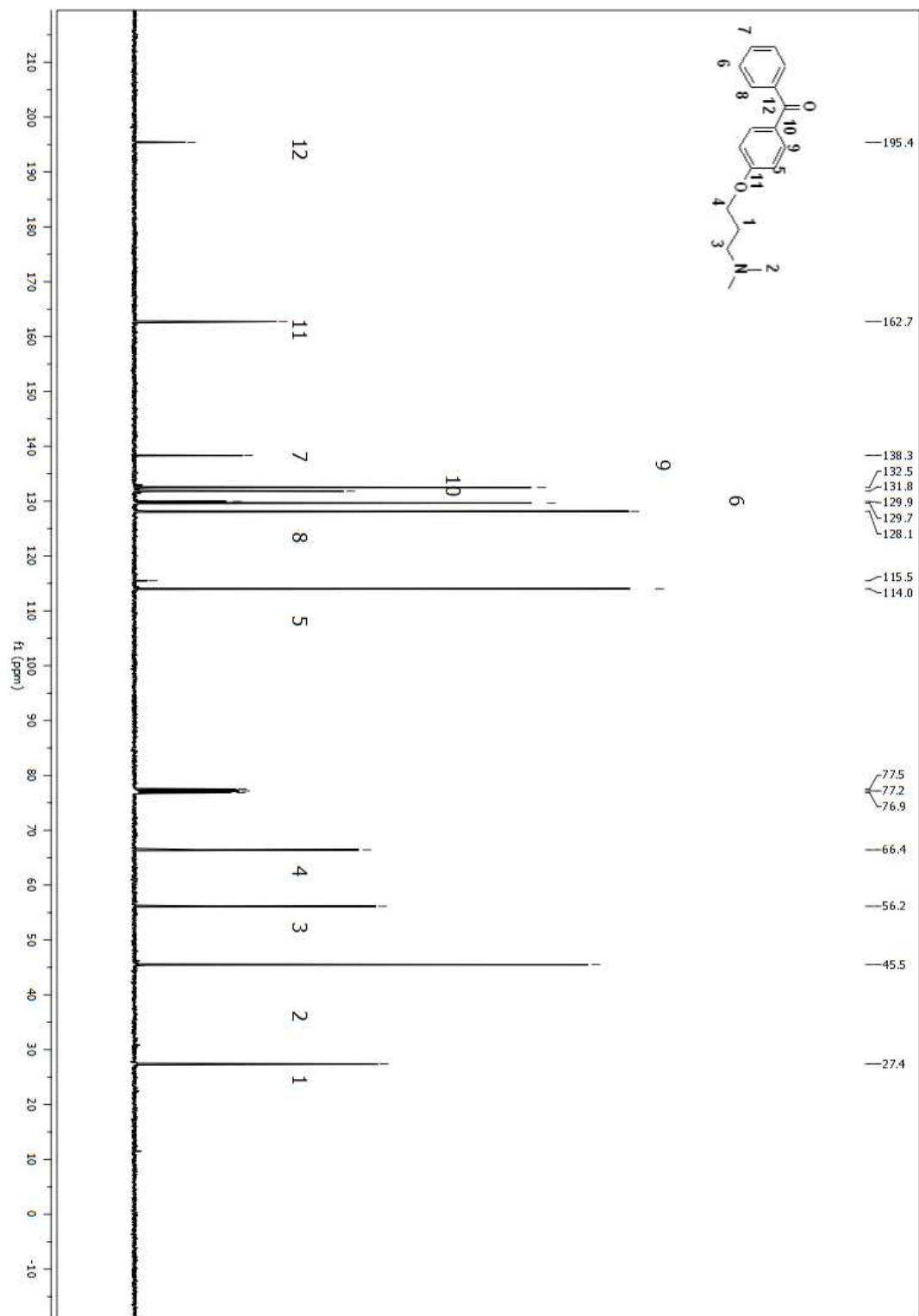


Figure A 334. ¹³C NMR spectrum of compound (204) in CDCl₃.

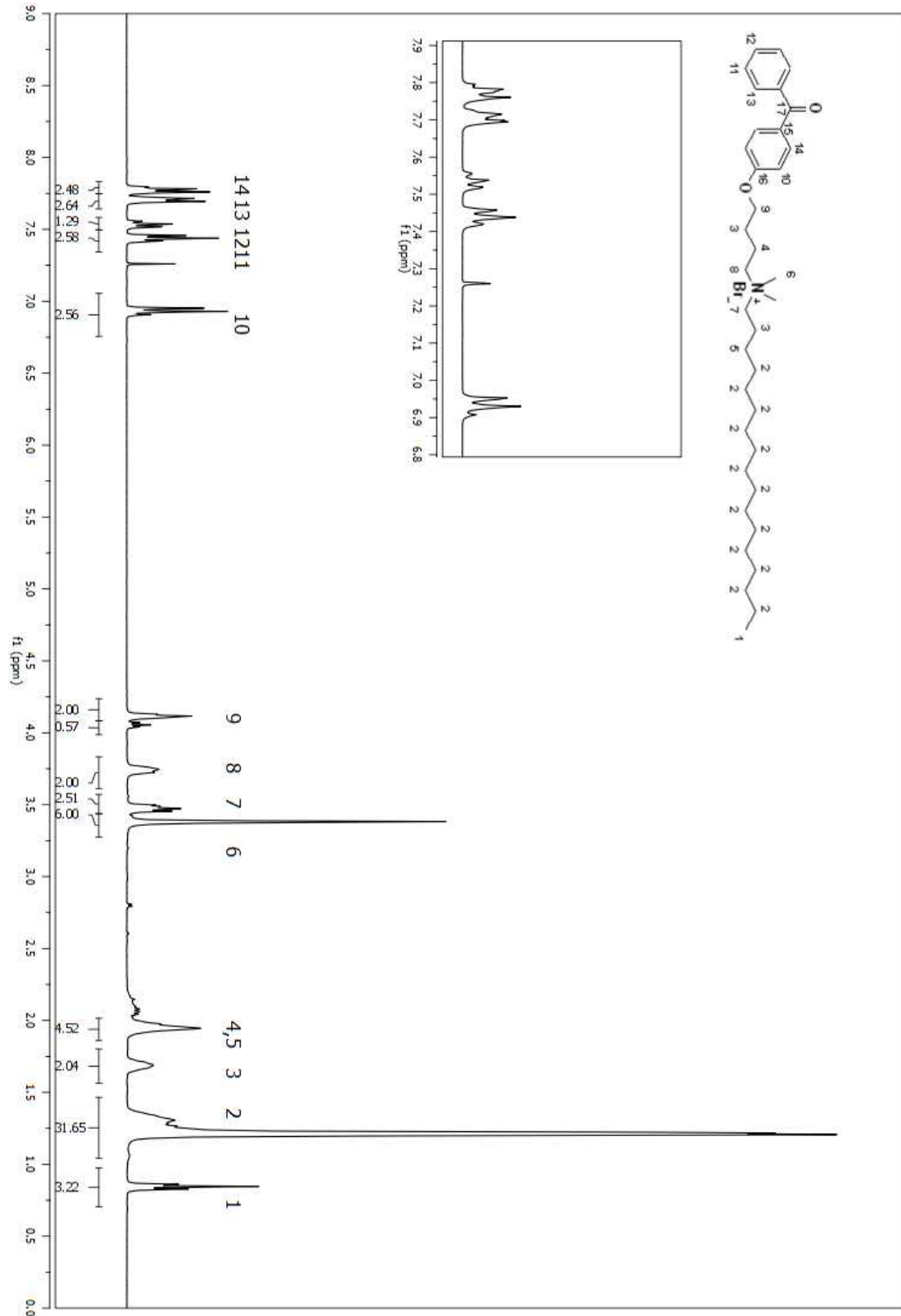


Figure A 335. ^1H NMR spectrum of compound (205) in CDCl_3 .

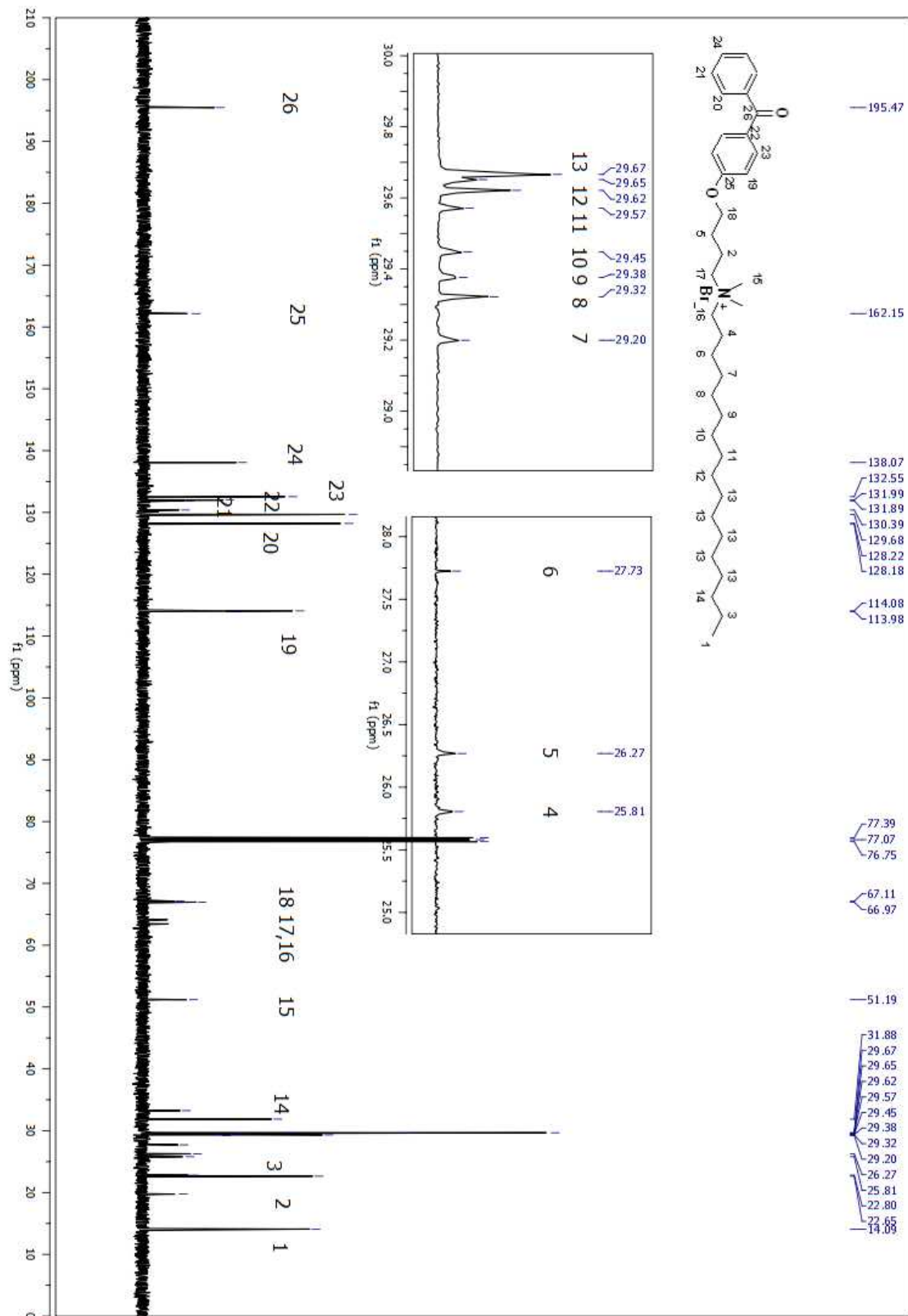


Figure A 336. ¹³C NMR spectrum of compound (205) in CDCl₃.

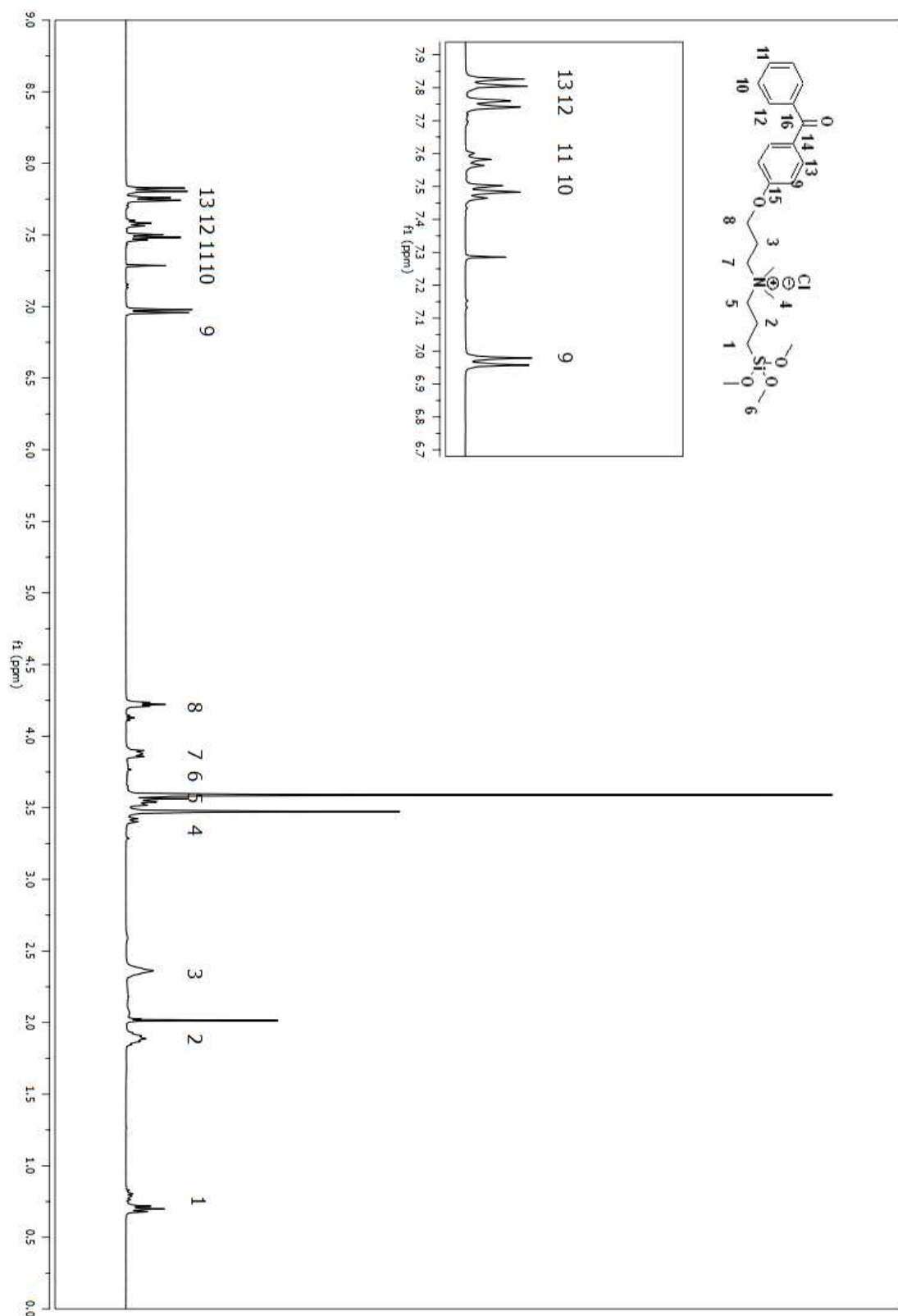


Figure A 337. ¹H NMR spectrum of compound (206) in CDCl₃.

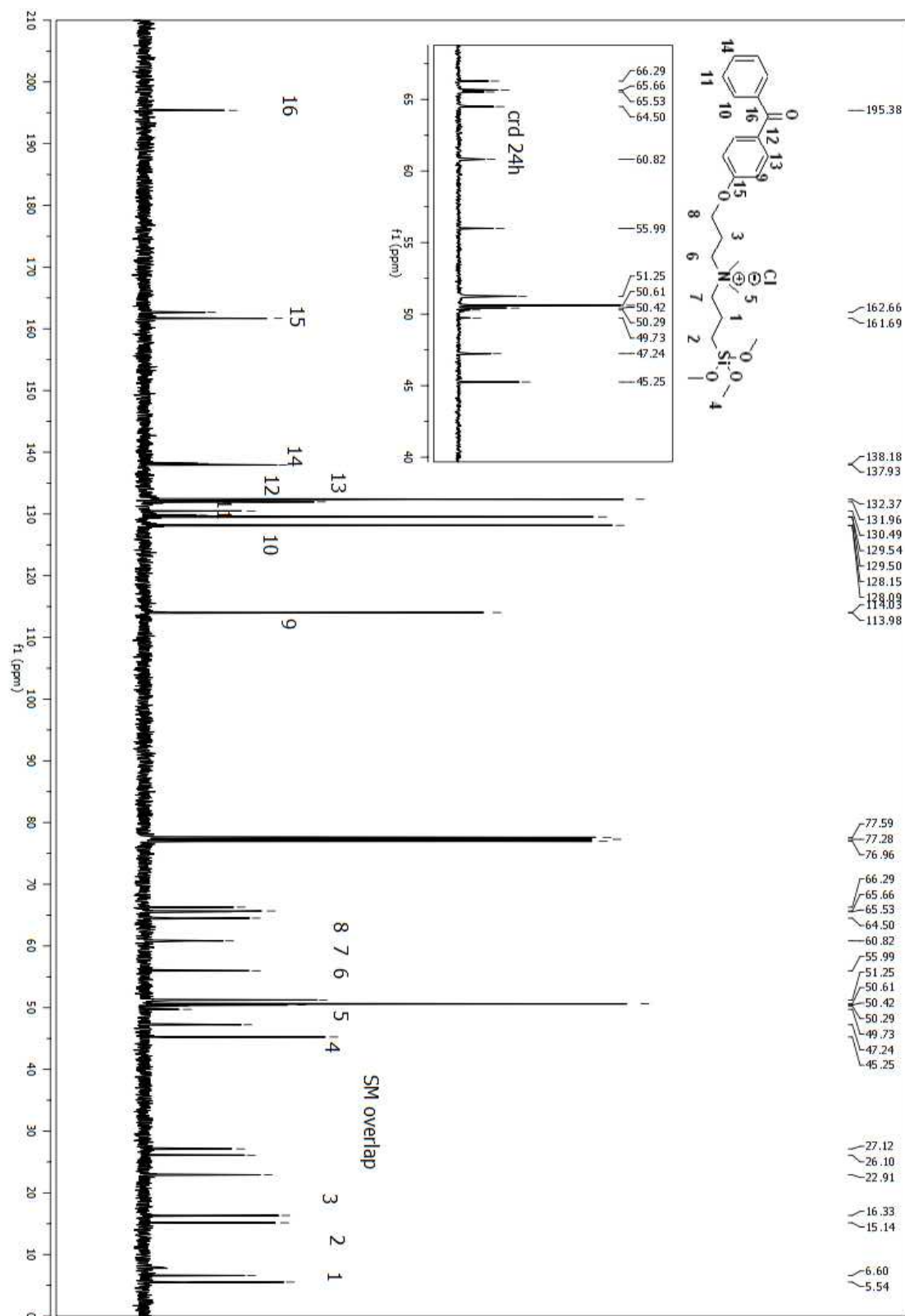


Figure A 338. ^{13}C NMR spectrum of compound (**206**) in CDCl_3 .

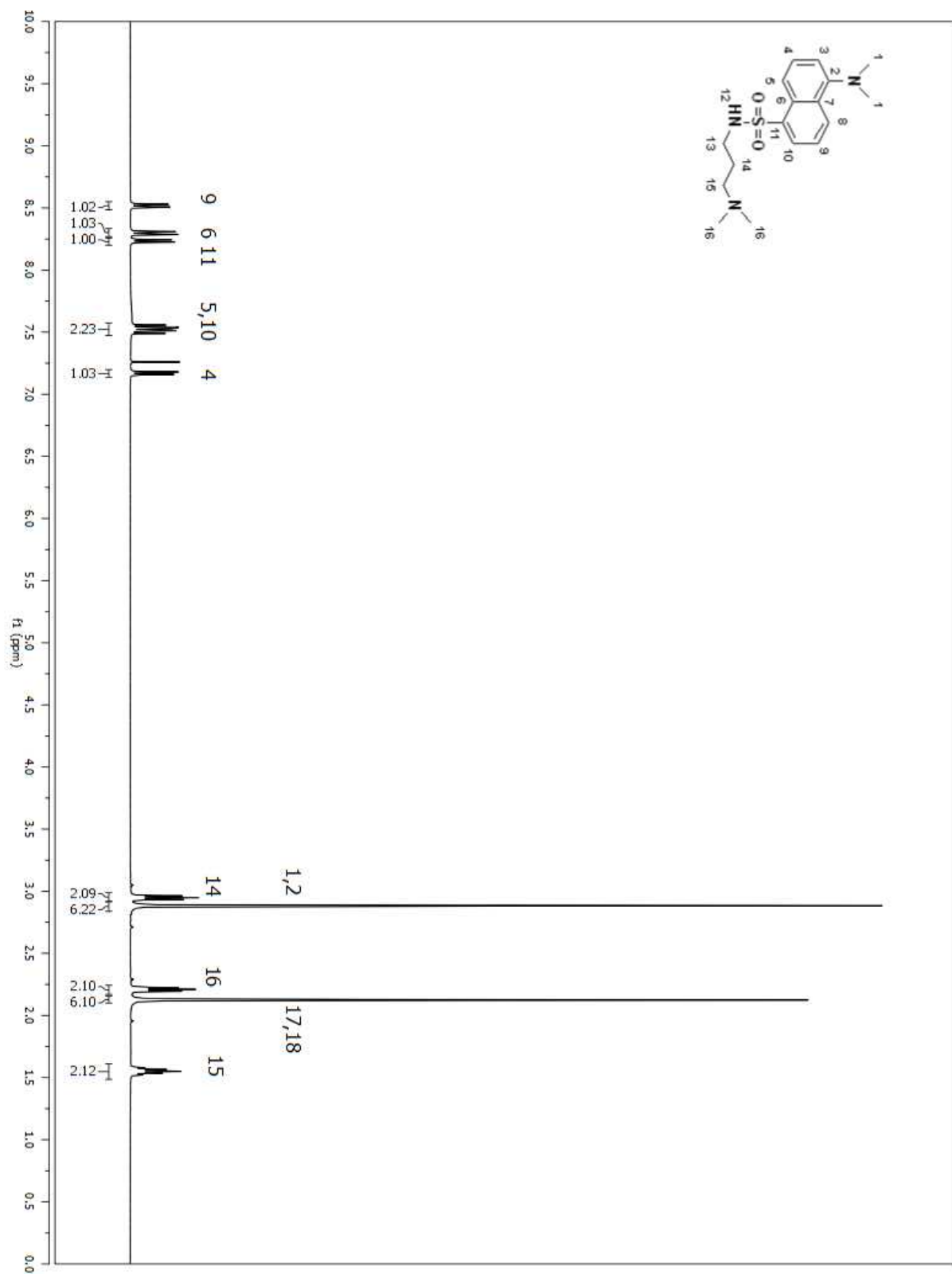


Figure A 339. ^1H NMR spectrum of compound (208) in CDCl₃.

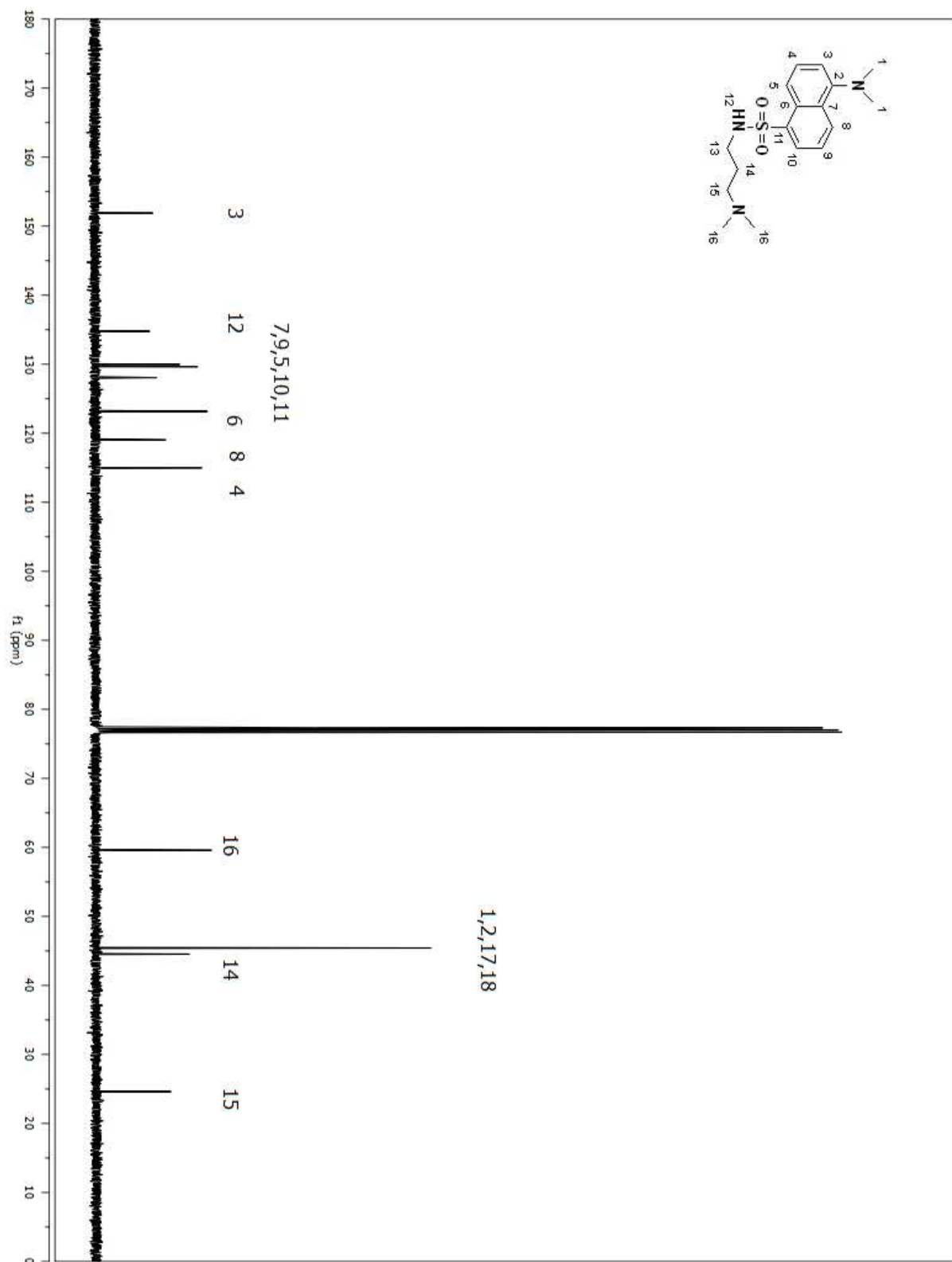


Figure A 340. ¹³C NMR spectrum of compound (208) in CDCl₃.

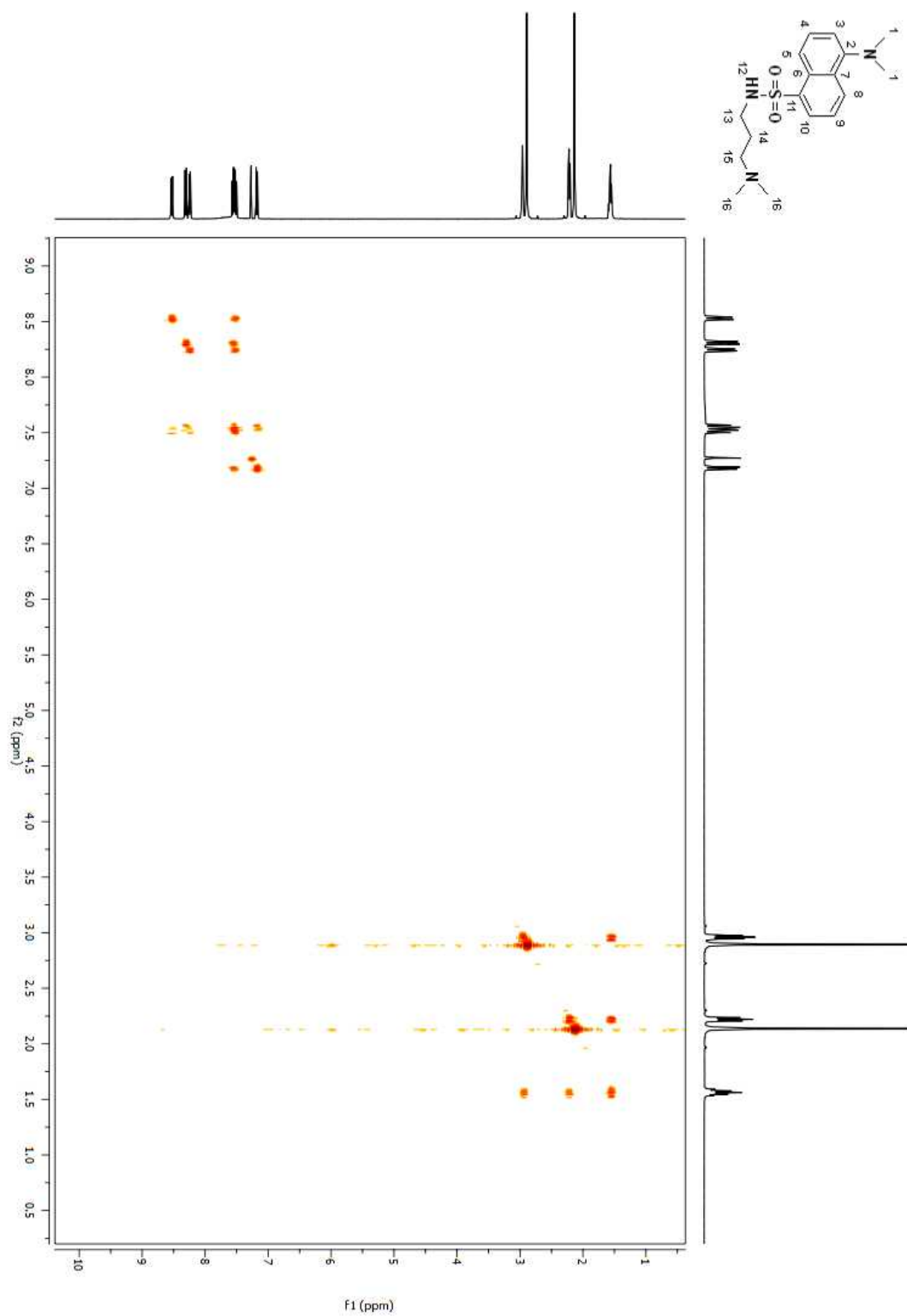


Figure A 341. COSY 2D NMR spectrum of compound (**208**) in CDCl_3 .

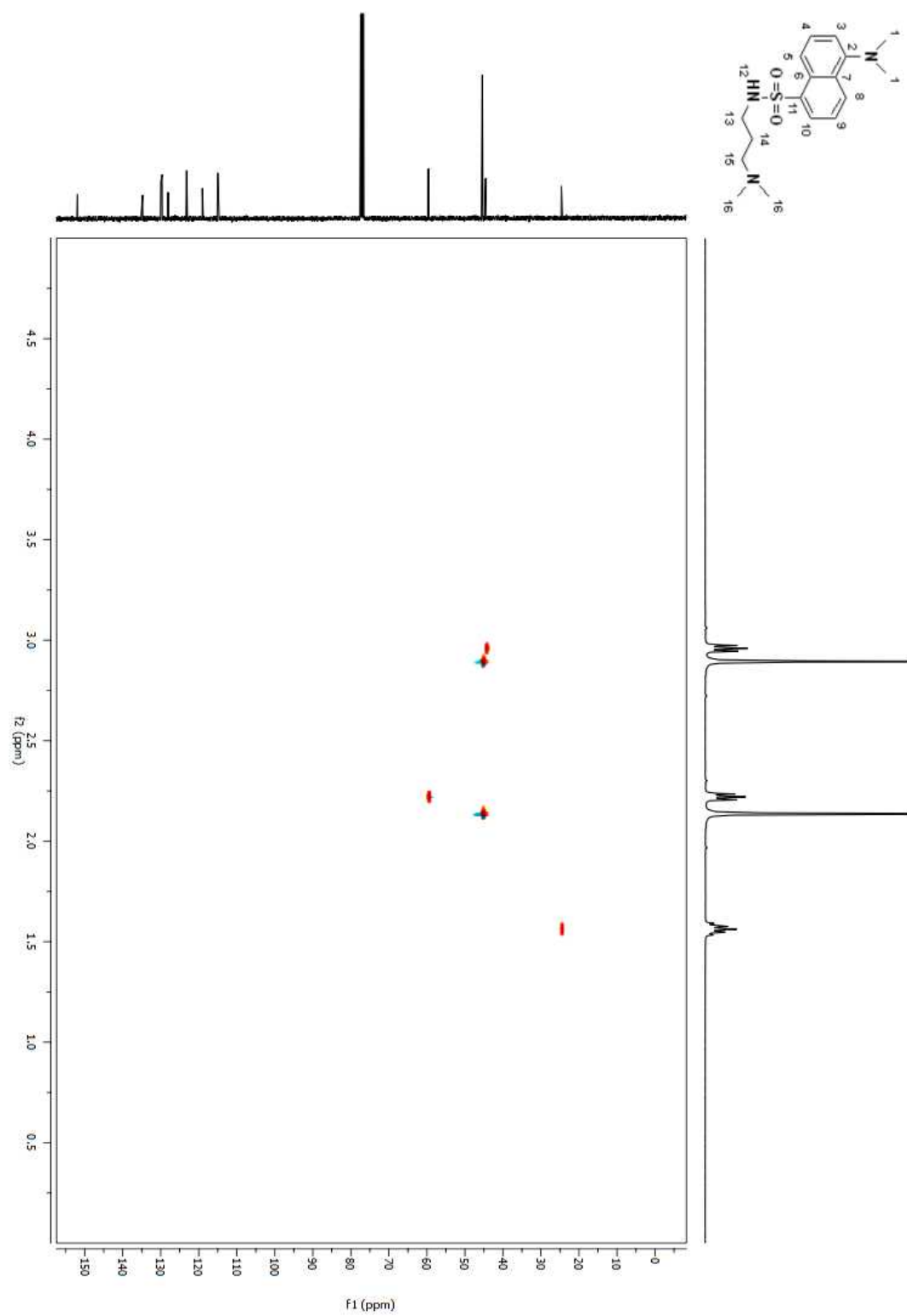


Figure A 342. HSQC 2D NMR spectrum of compound (**208**) in CDCl_3 .

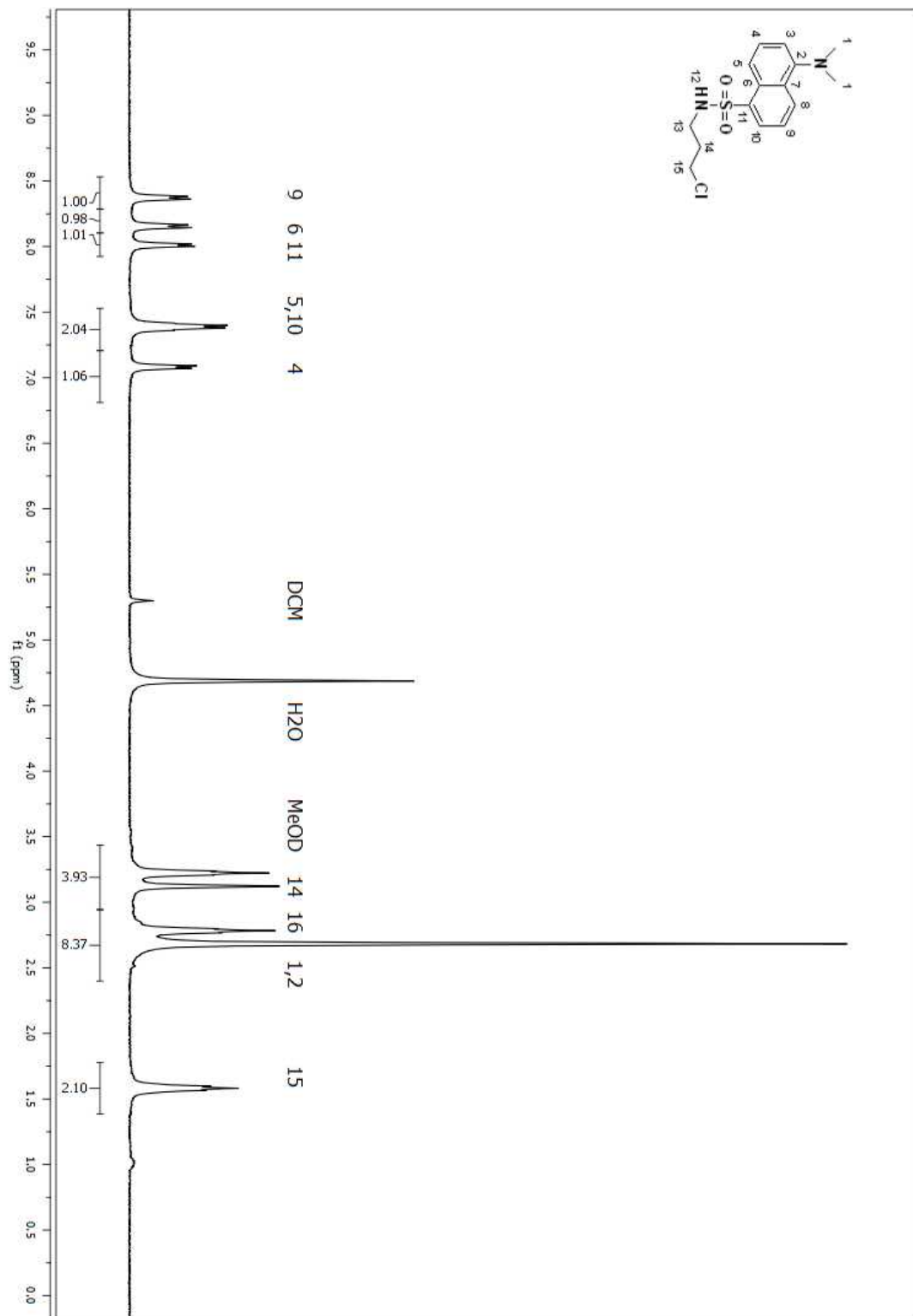


Figure A 343. ^1H NMR spectrum of compound (209) in MeOD.

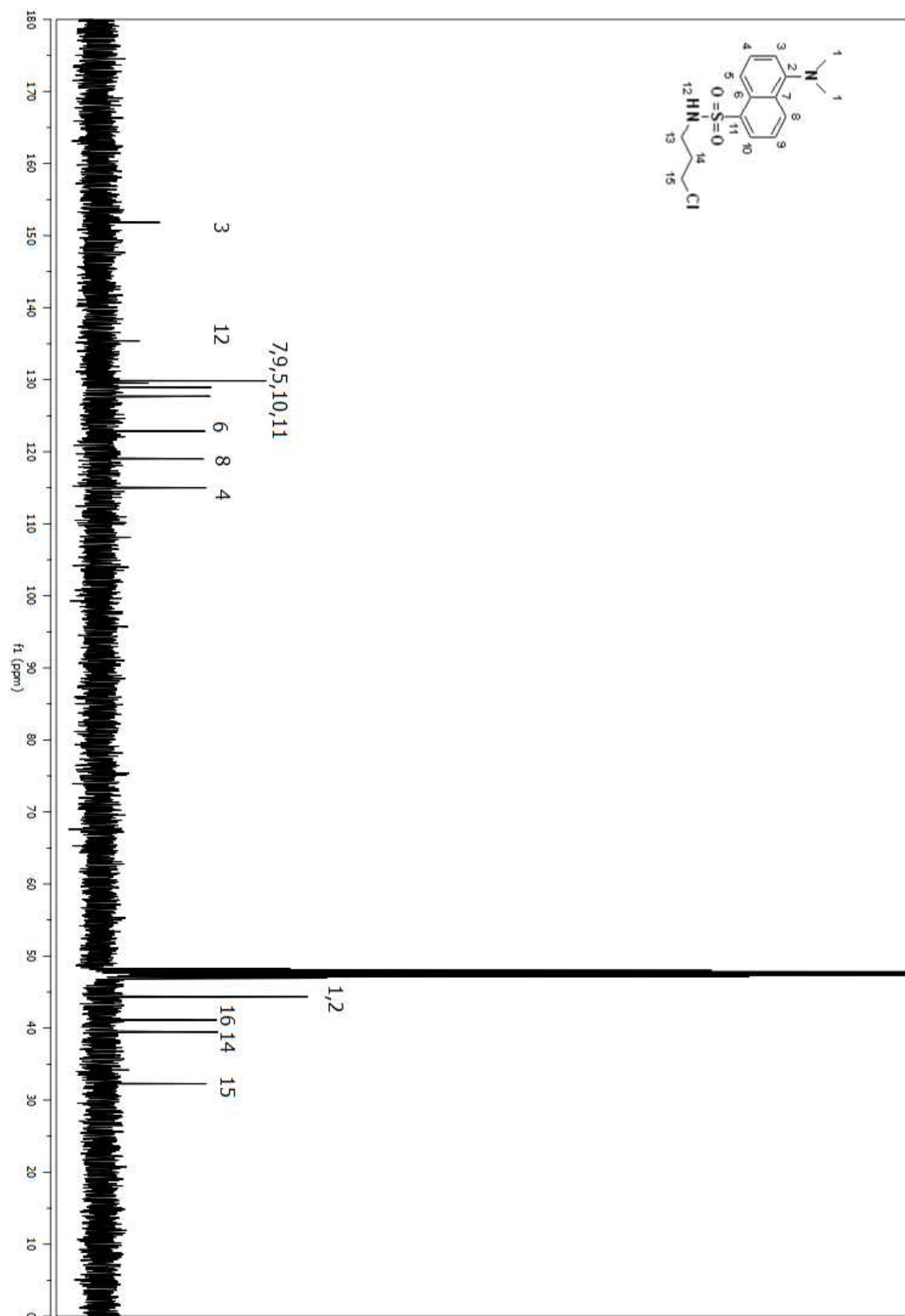


Figure A 344. ^{13}C NMR spectrum of compound (209) in MeOD .

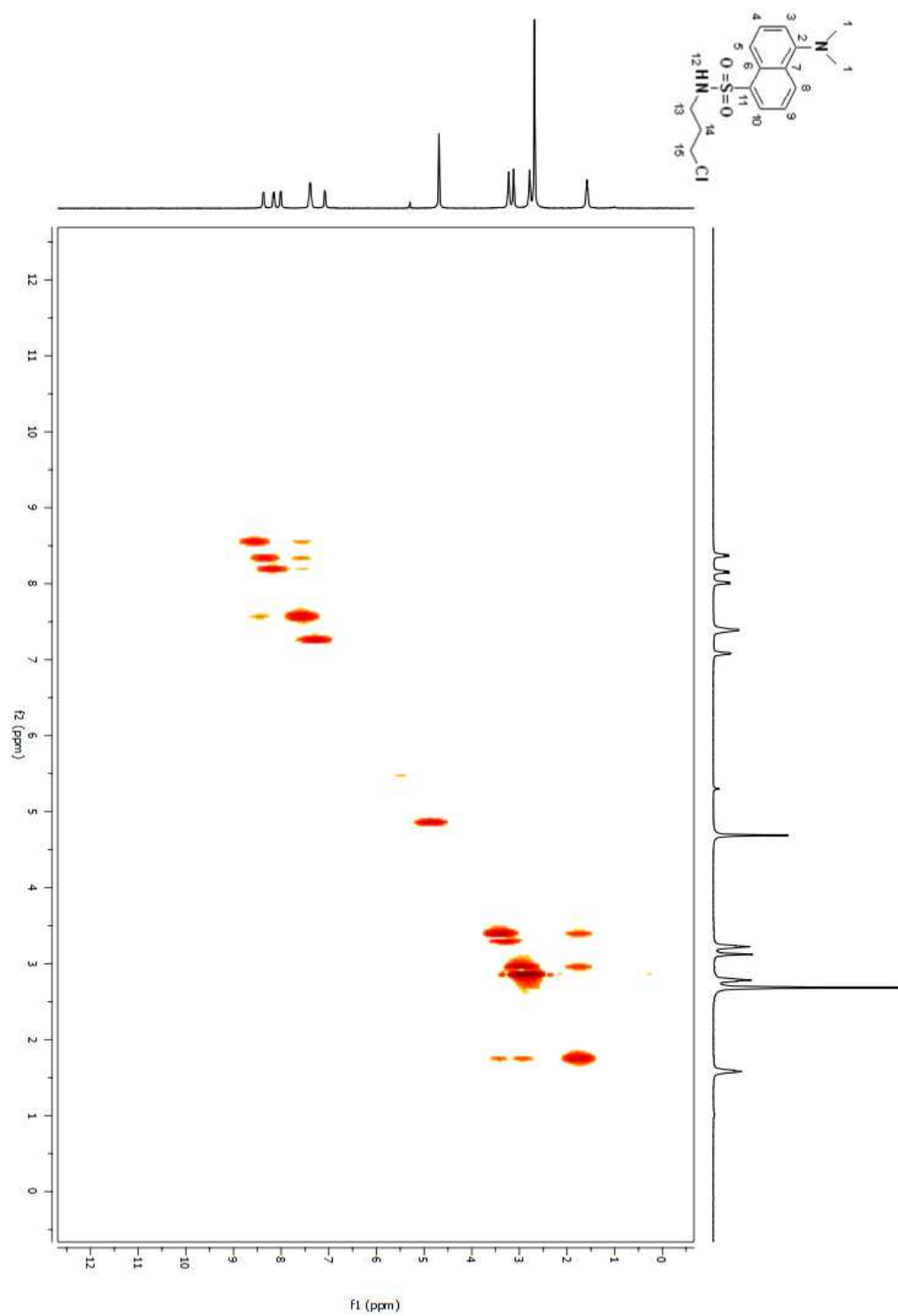


Figure A 345. COSY 2D NMR spectrum of compound (209) in MeOD.

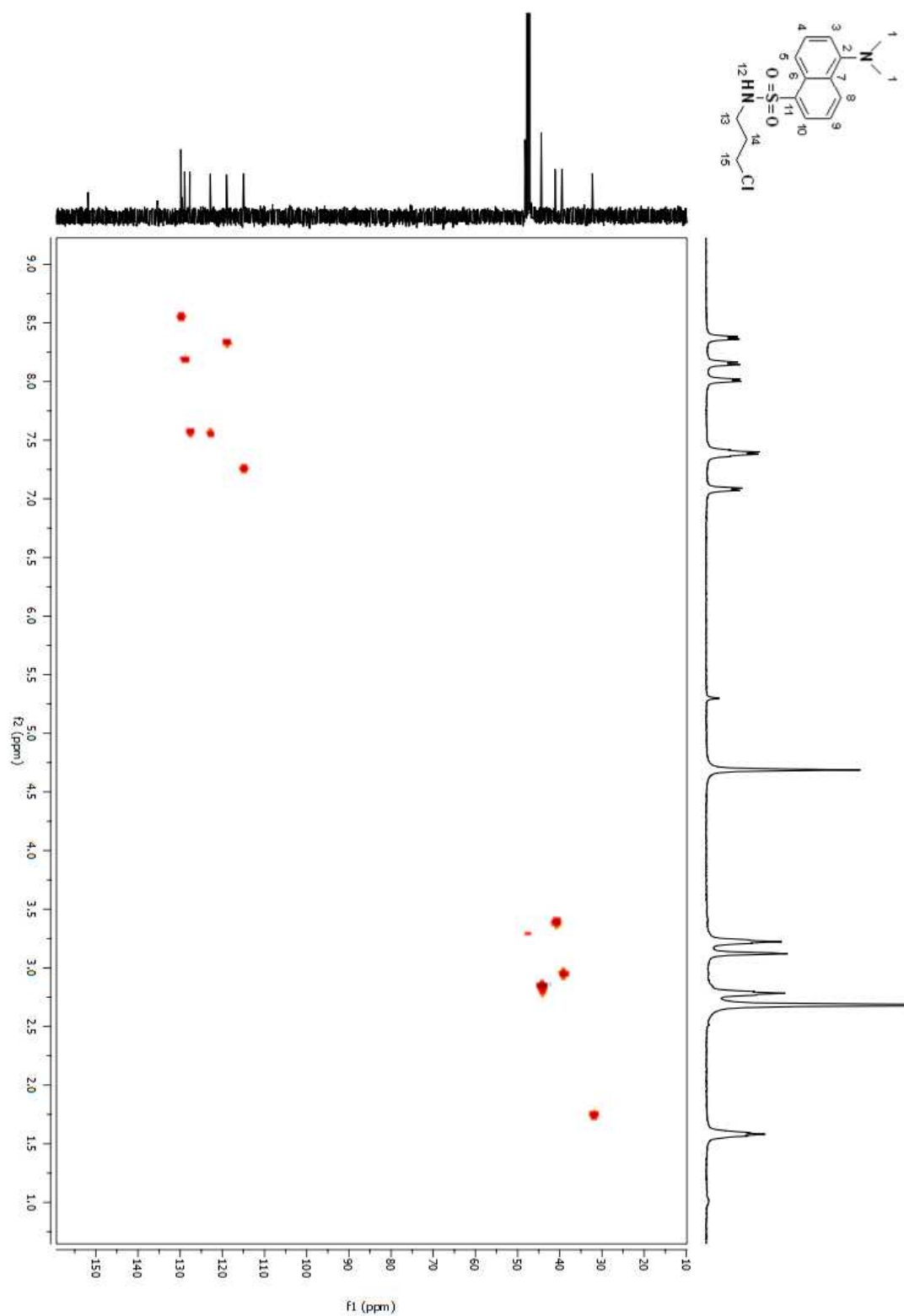


Figure A 346. HSQC 2D NMR spectrum of compound (209) in MeOD.

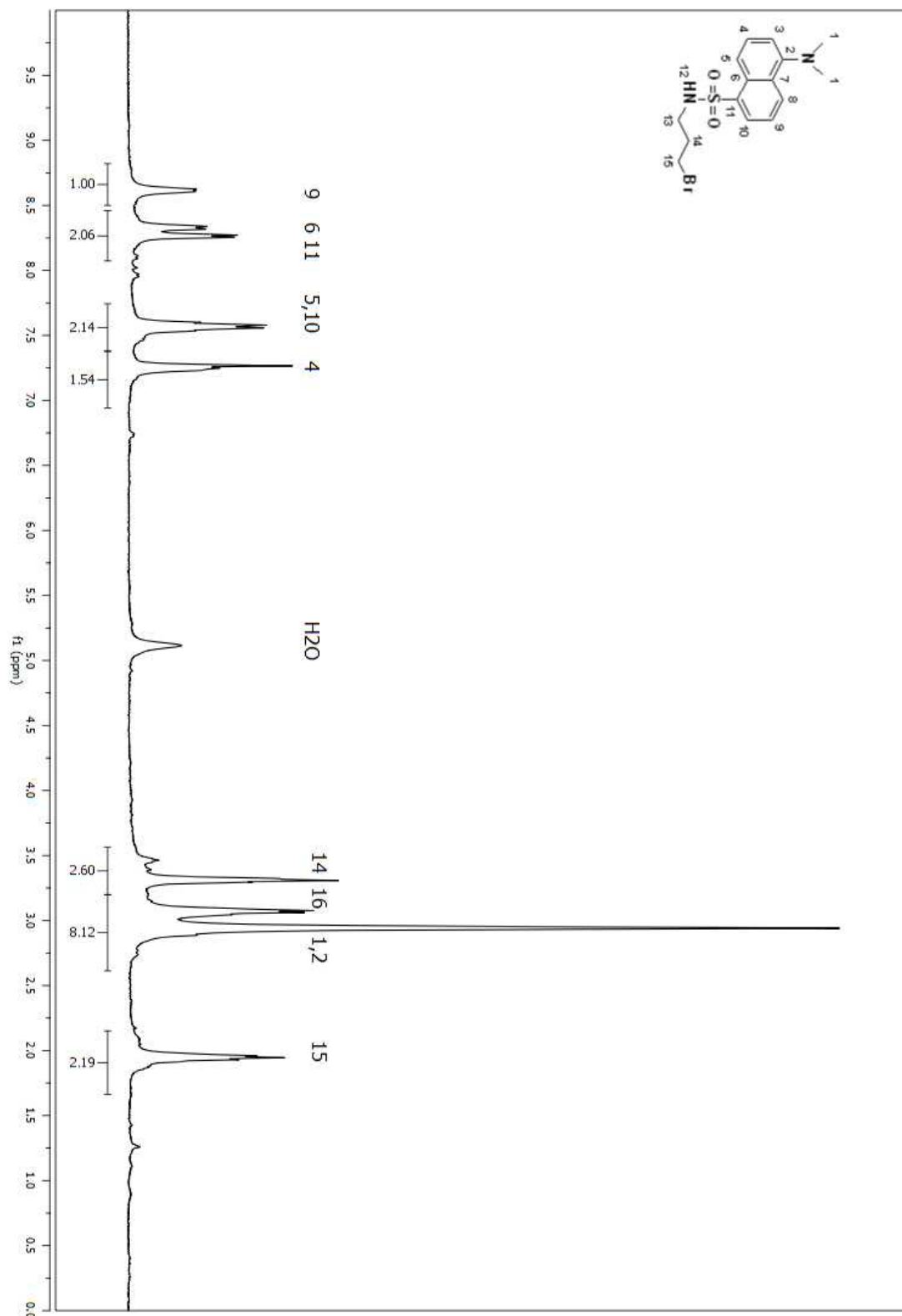


Figure A 347. ^1H NMR spectrum of compound (210) in MeOD.

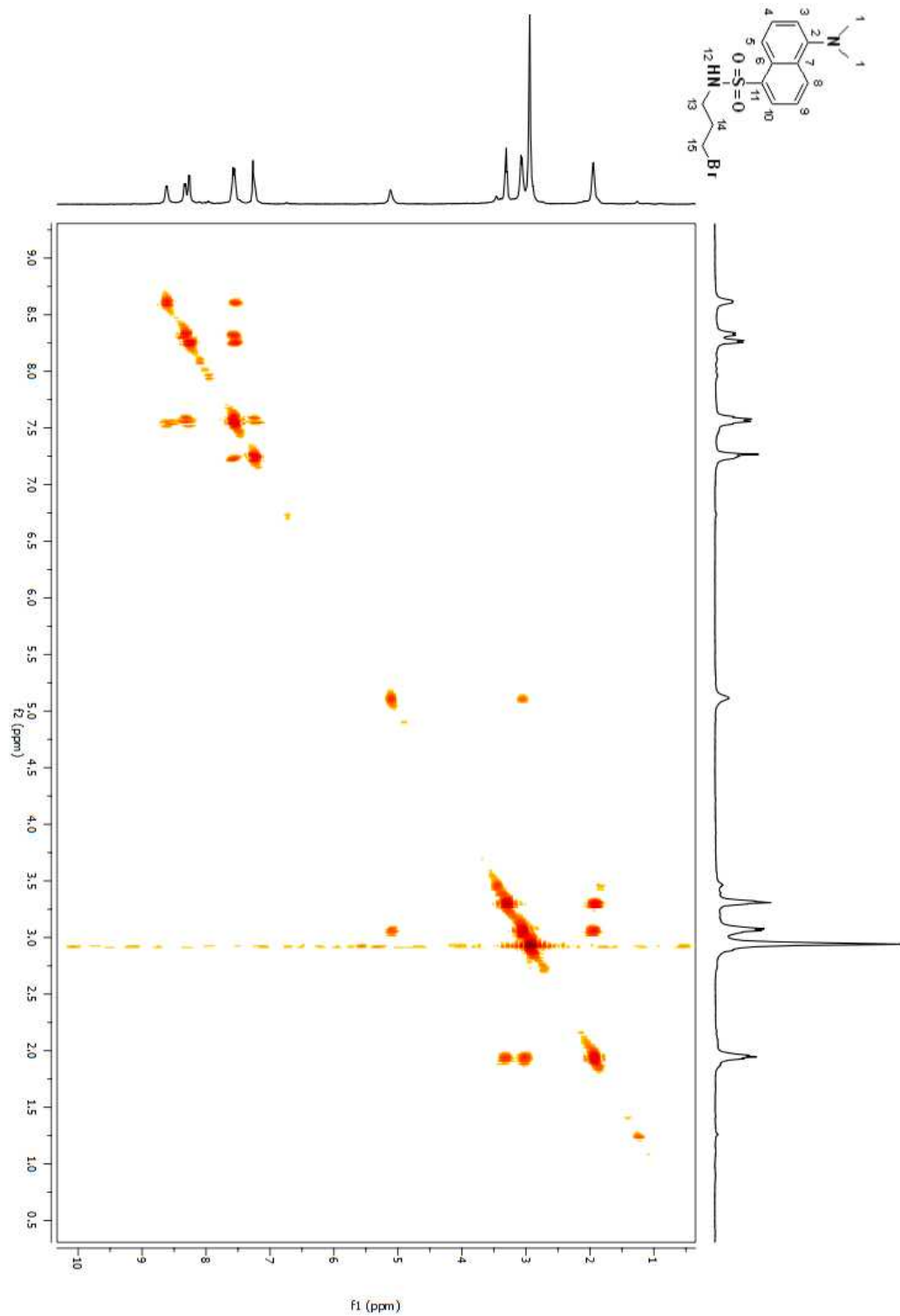


Figure A 348. COSY 2D NMR spectrum of compound (210) in MeOD.

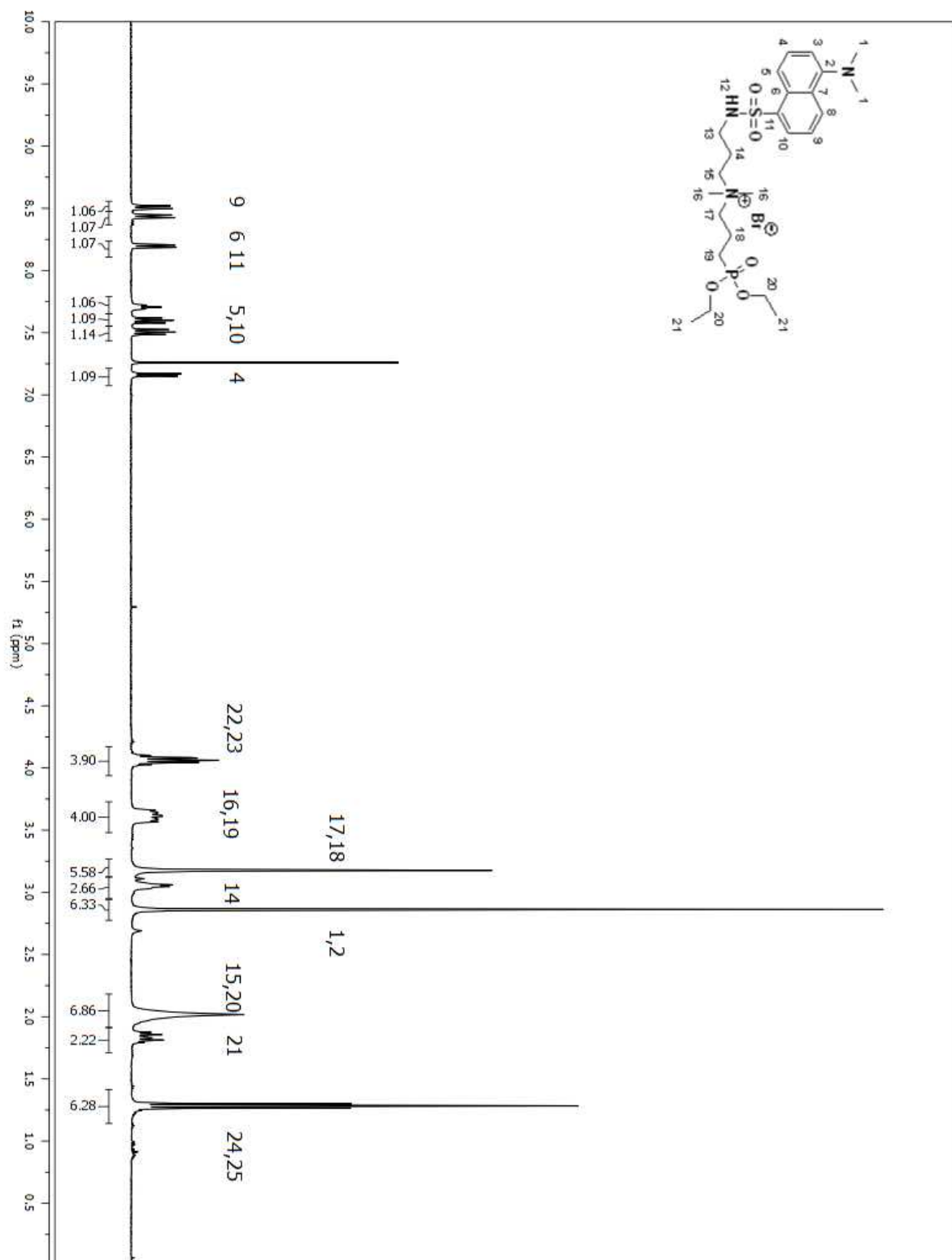


Figure A 349. ^1H NMR spectrum of compound (211) in CDCl_3 .

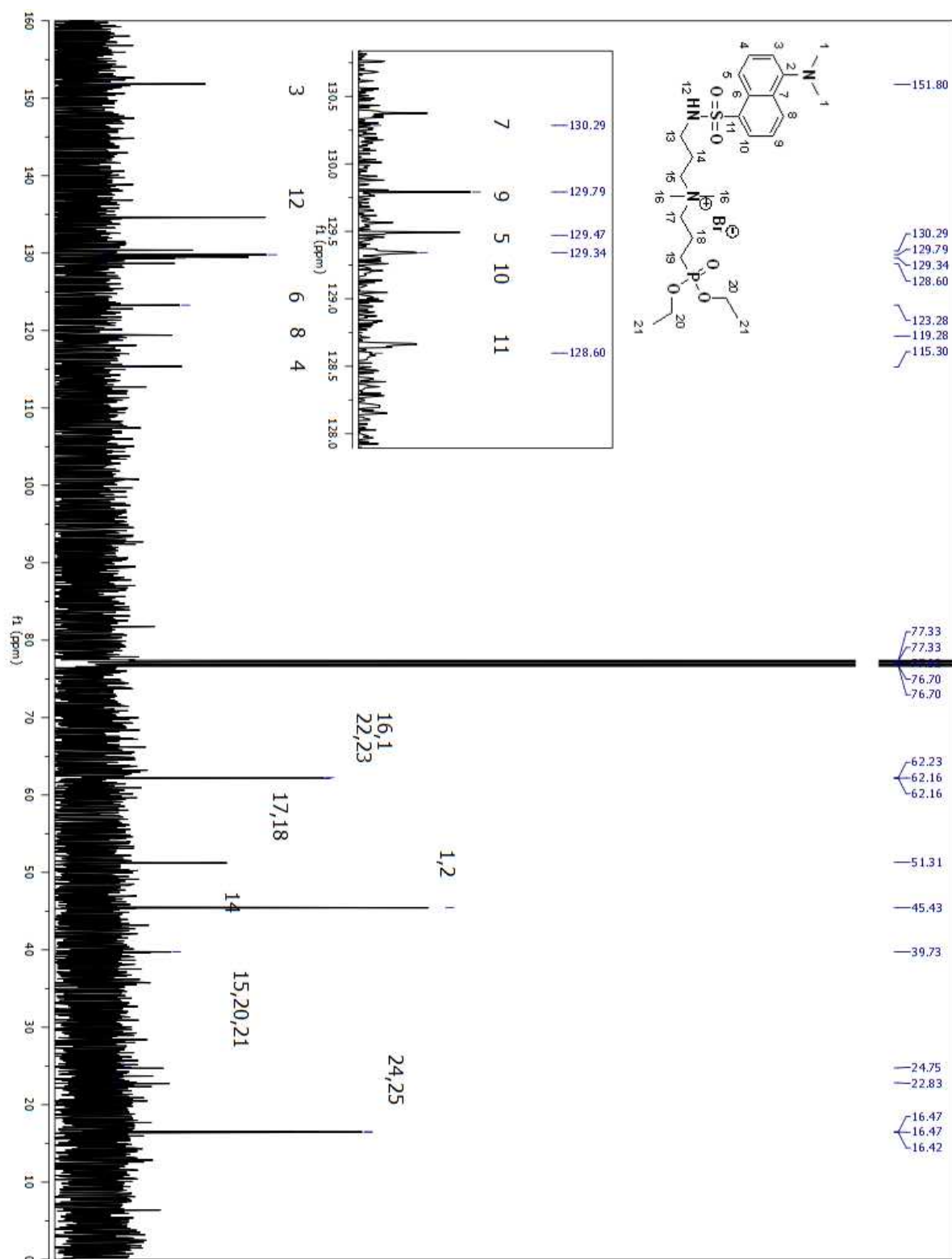


Figure A 350. ¹³C NMR spectrum of compound (**211**) in CDCl₃.

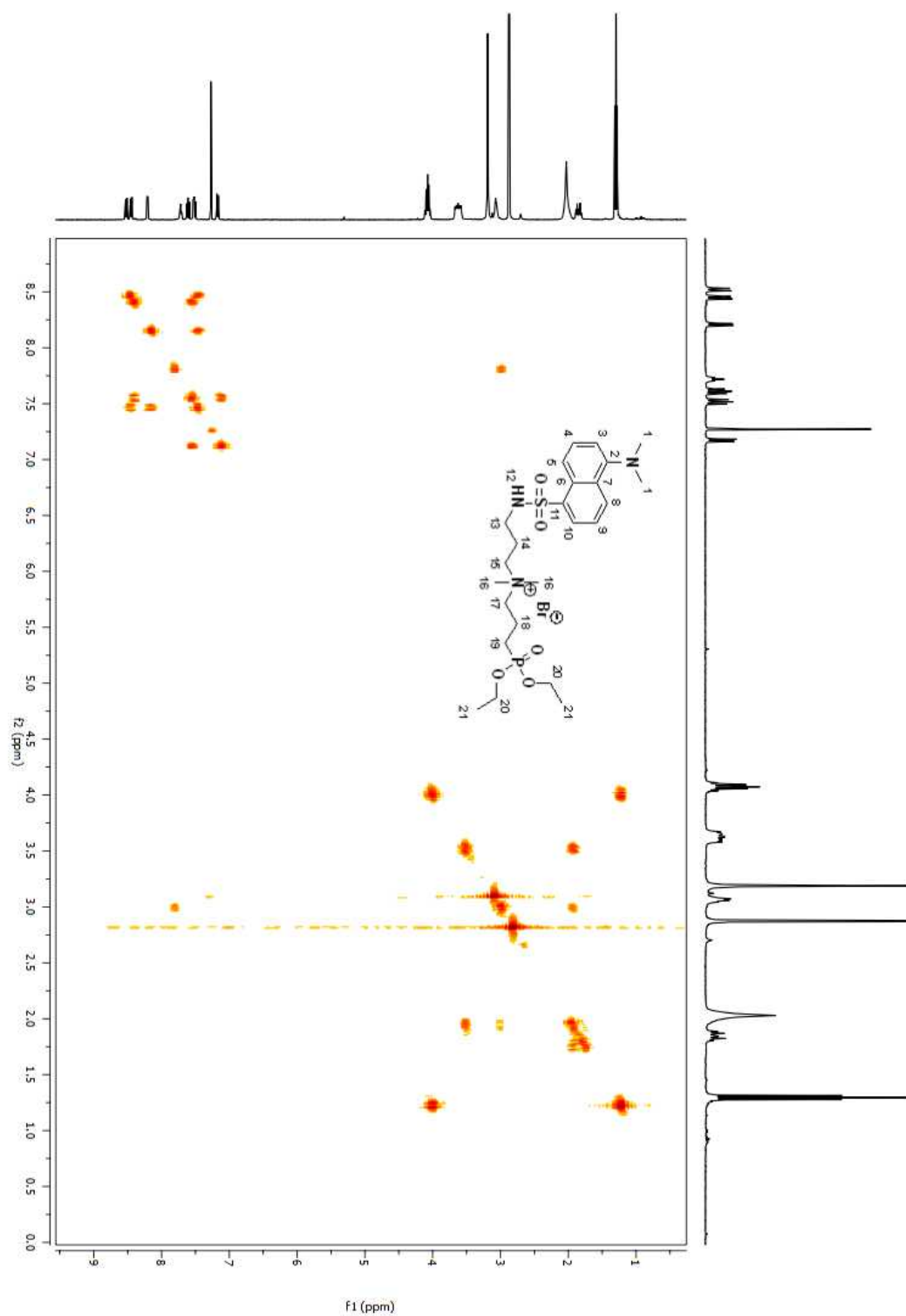


Figure A 351. COSY 2D NMR spectrum of compound (**211**) in CDCl_3 .

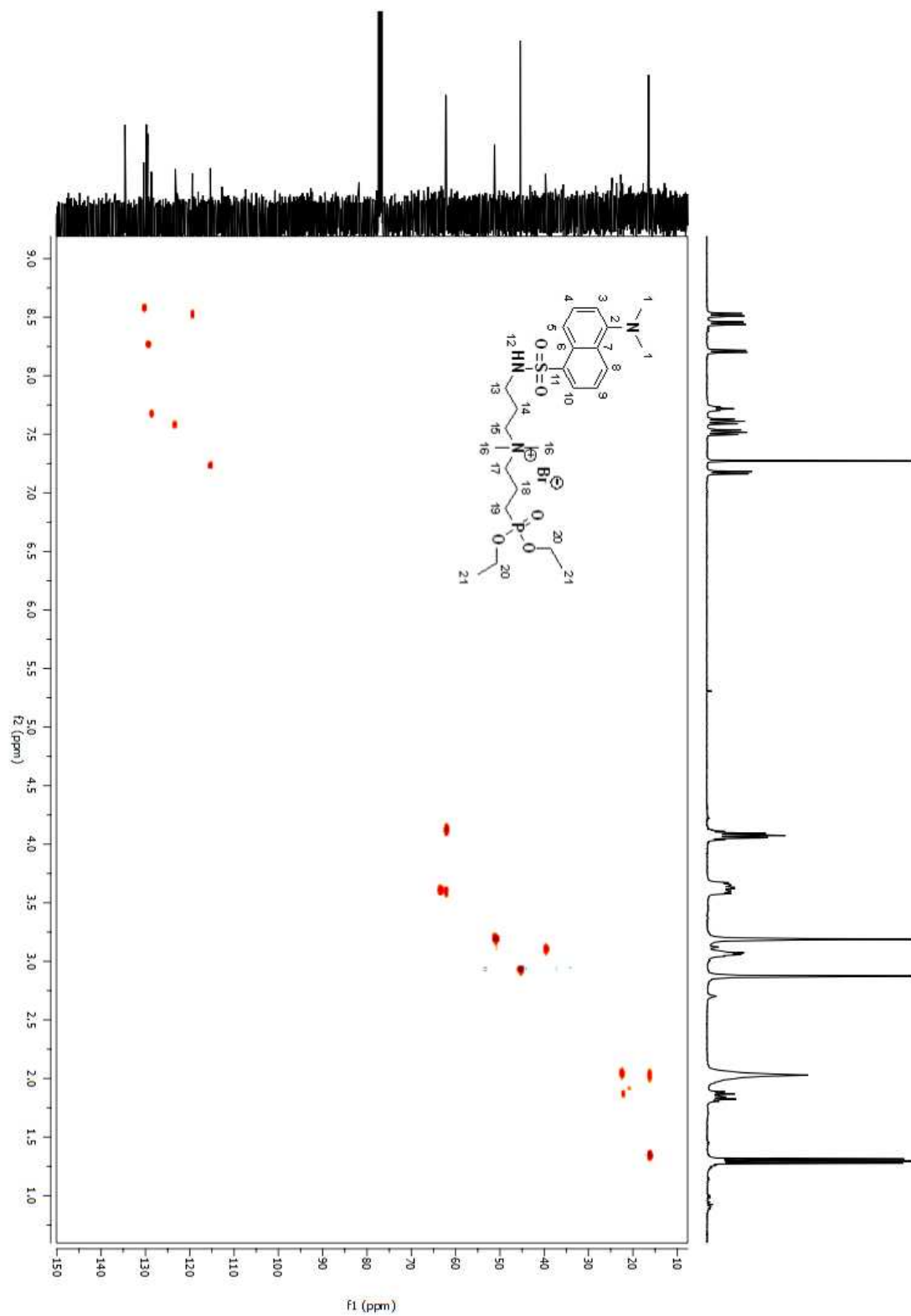


Figure A 352. HSQC 2D NMR spectrum of compound (**211**) in CDCl₃.

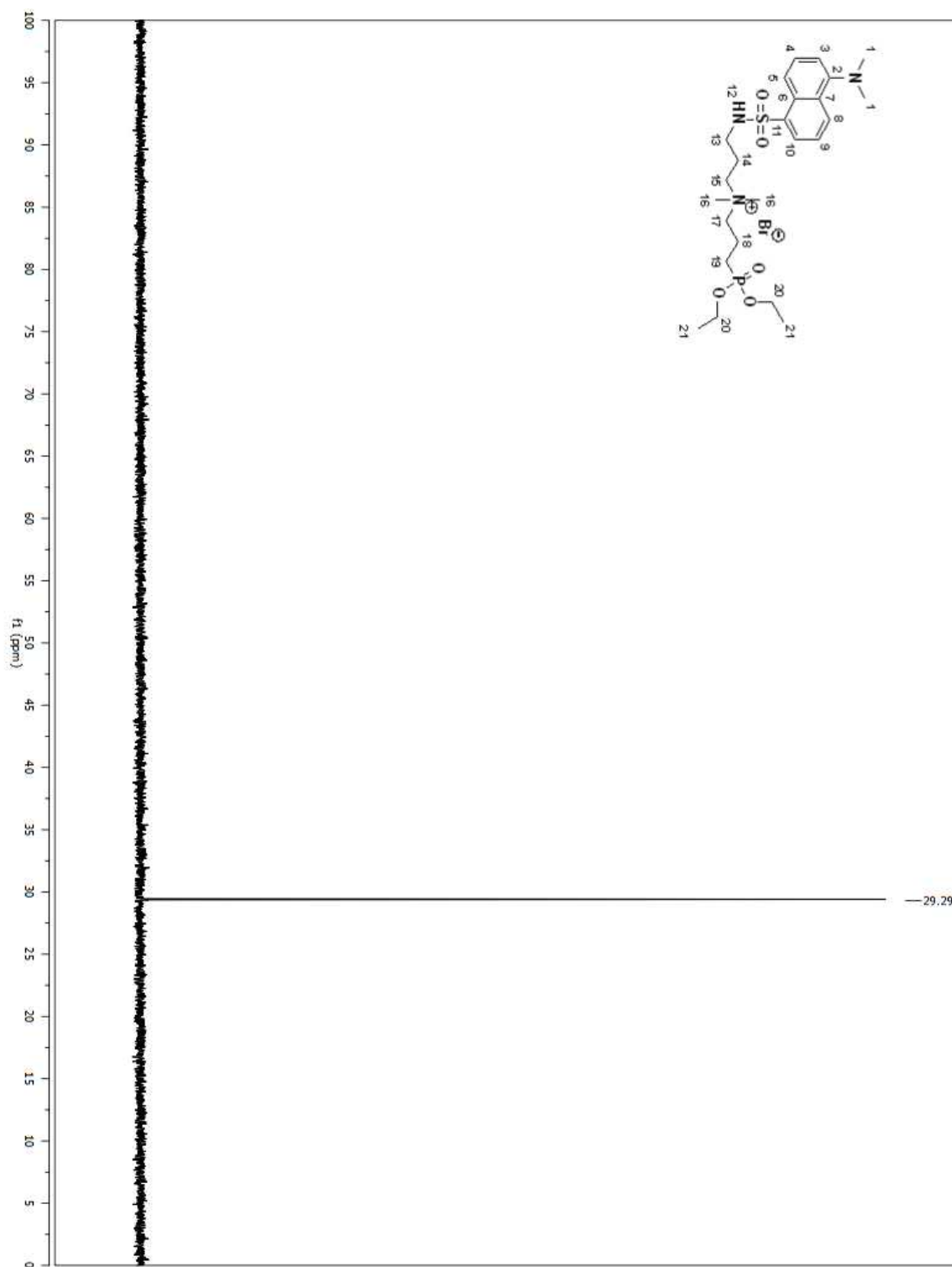


Figure A 353. ^{31}P NMR spectrum of compound (211) in CDCl_3 .

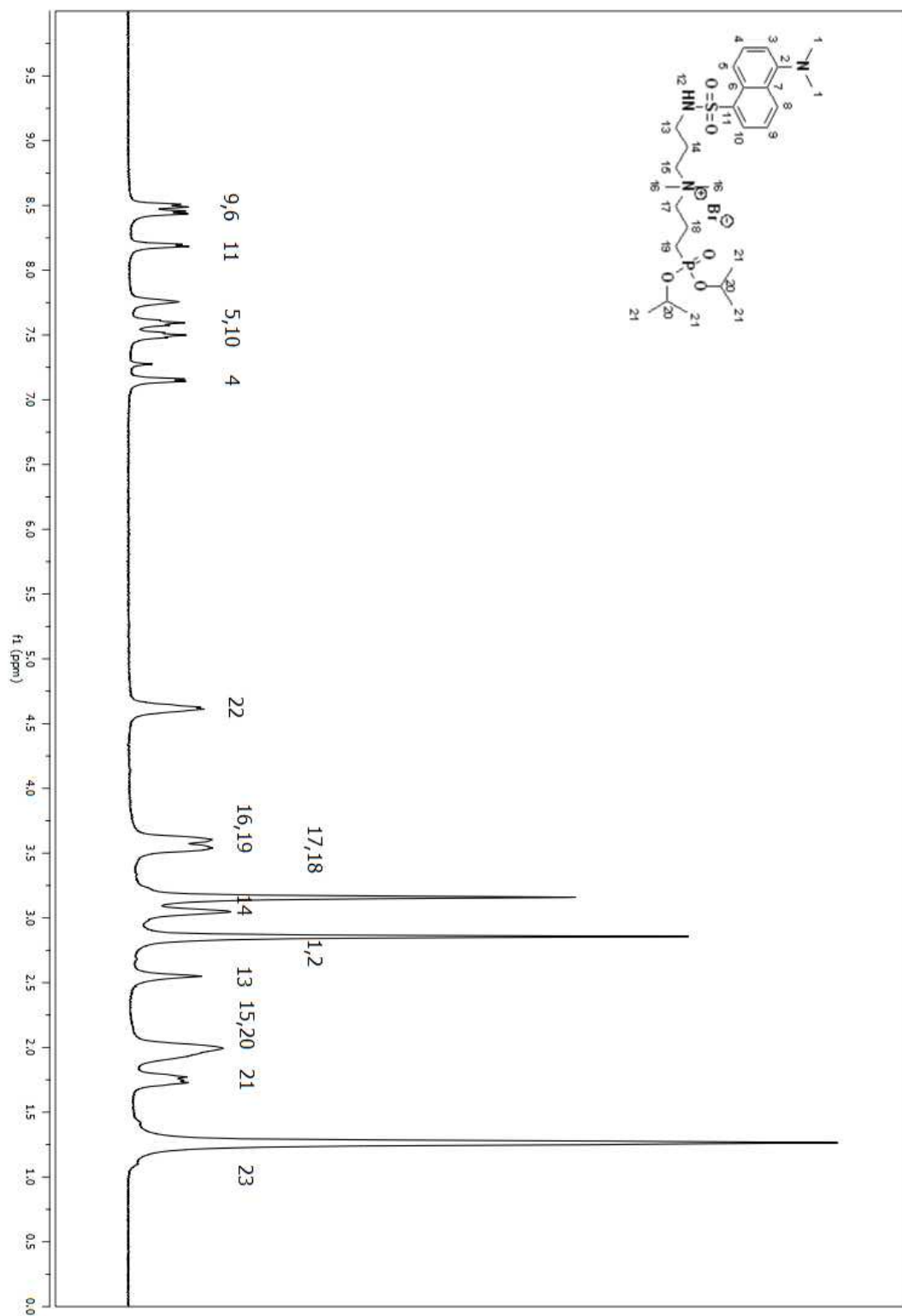


Figure A 354. ¹H NMR spectrum of compound (212) in CDCl₃.

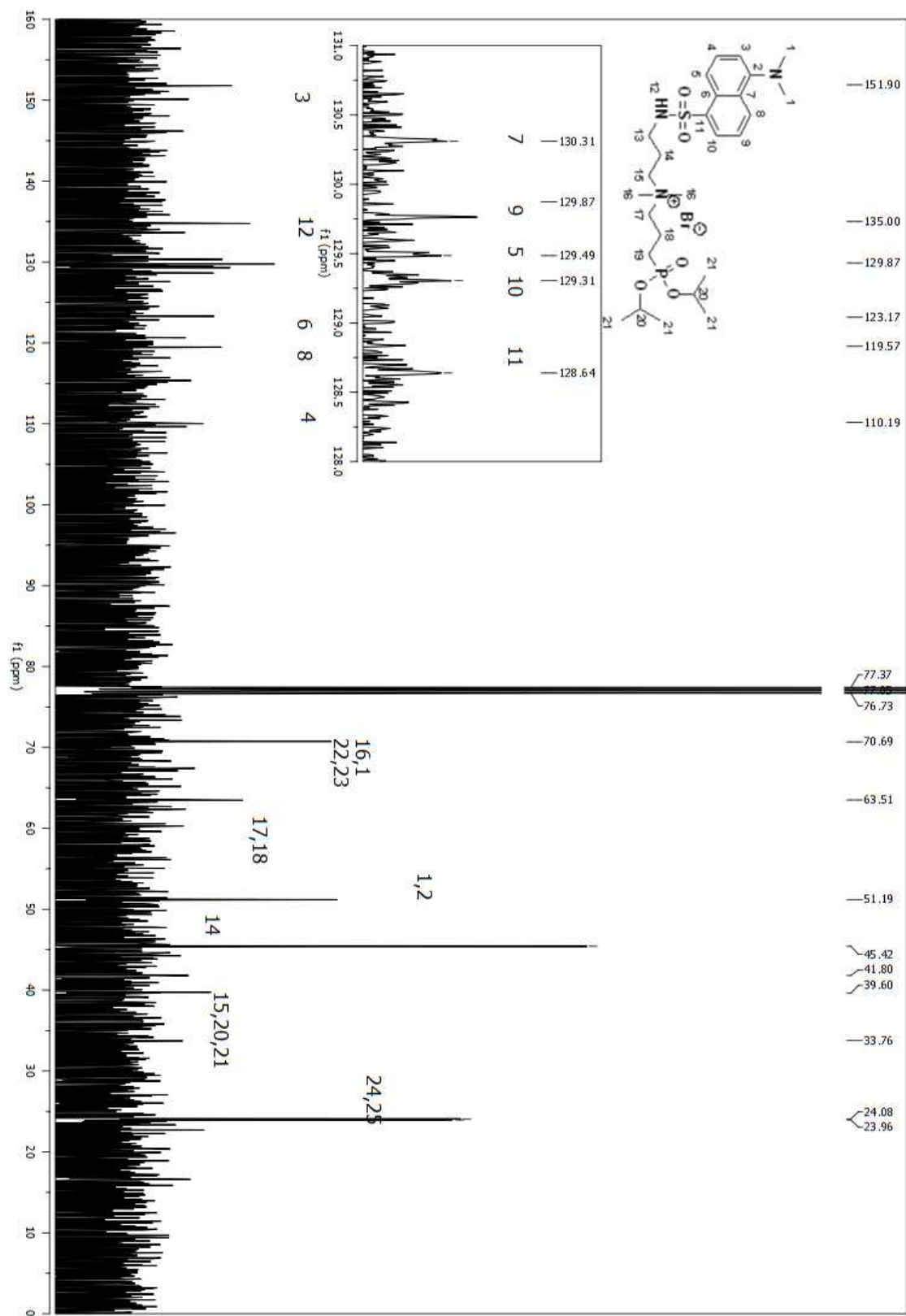


Figure A 355. ^{13}C NMR spectrum of compound (**212**) in CDCl_3 .

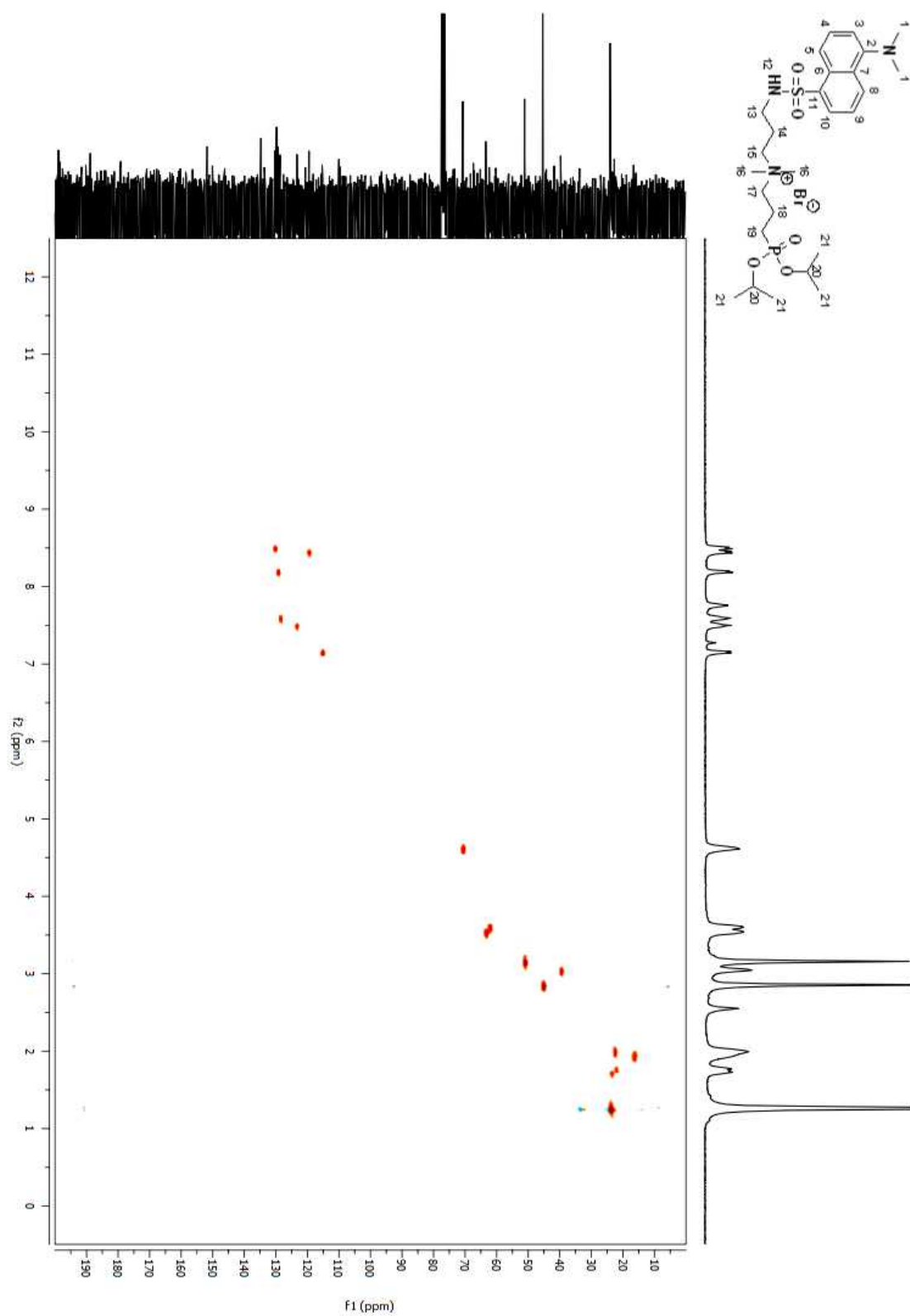


Figure A 356. HSQC 2D NMR spectrum of compound (212) in CDCl₃.

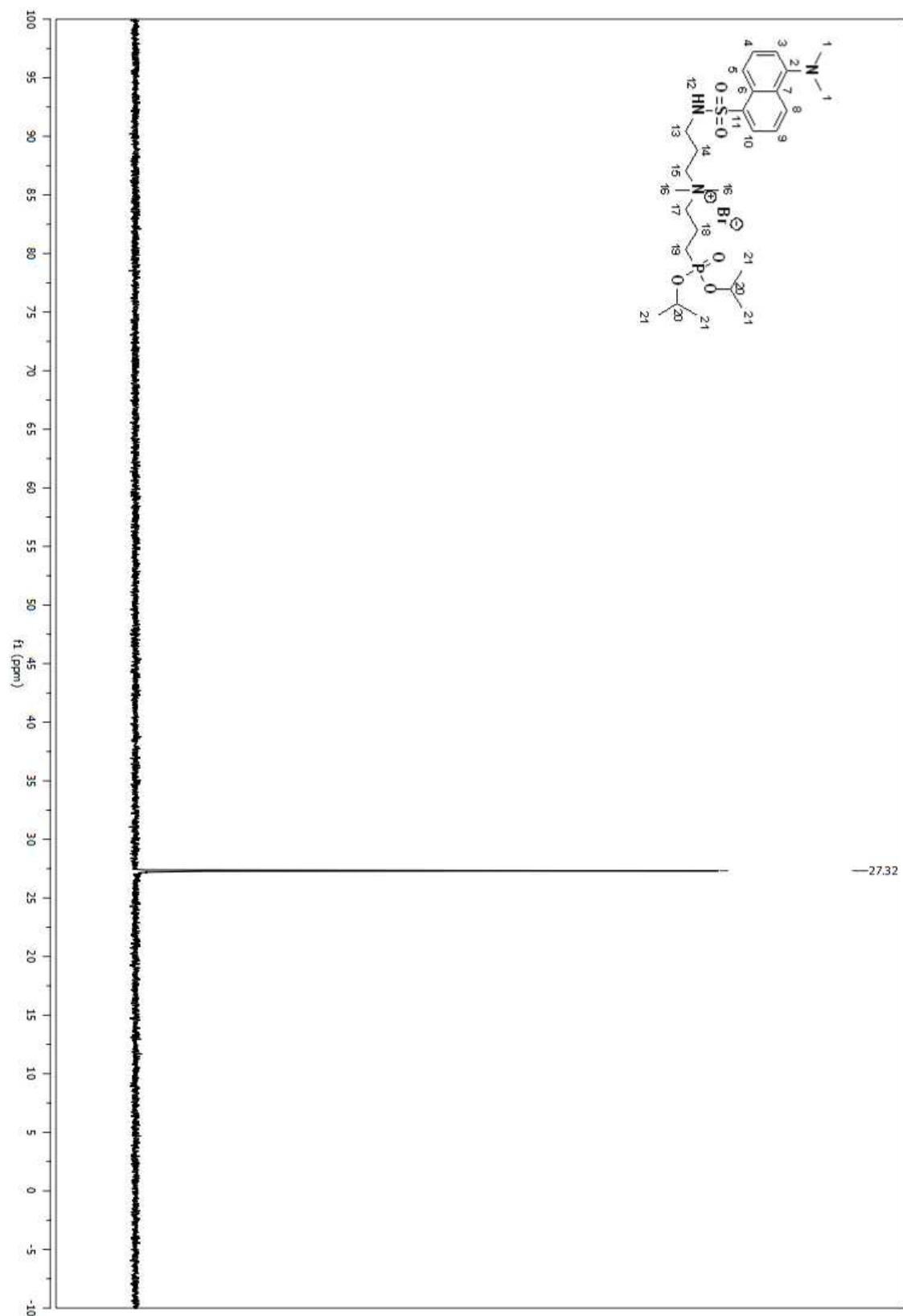


Figure A 357. ^{31}P NMR spectrum of compound (212) in CDCl_3 .
724

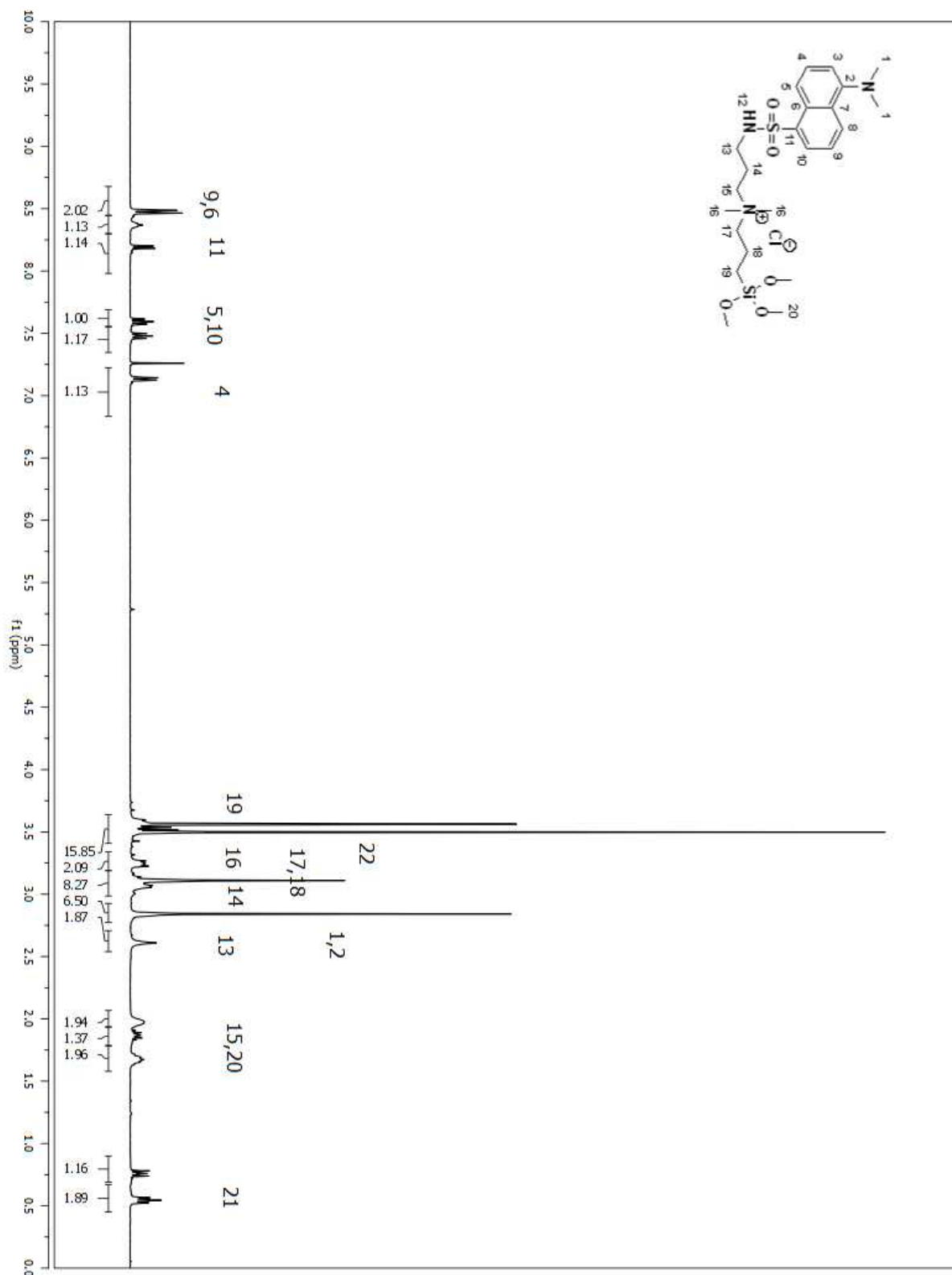


Figure A 358. ¹H NMR spectrum of compound (213) in CDCl₃.

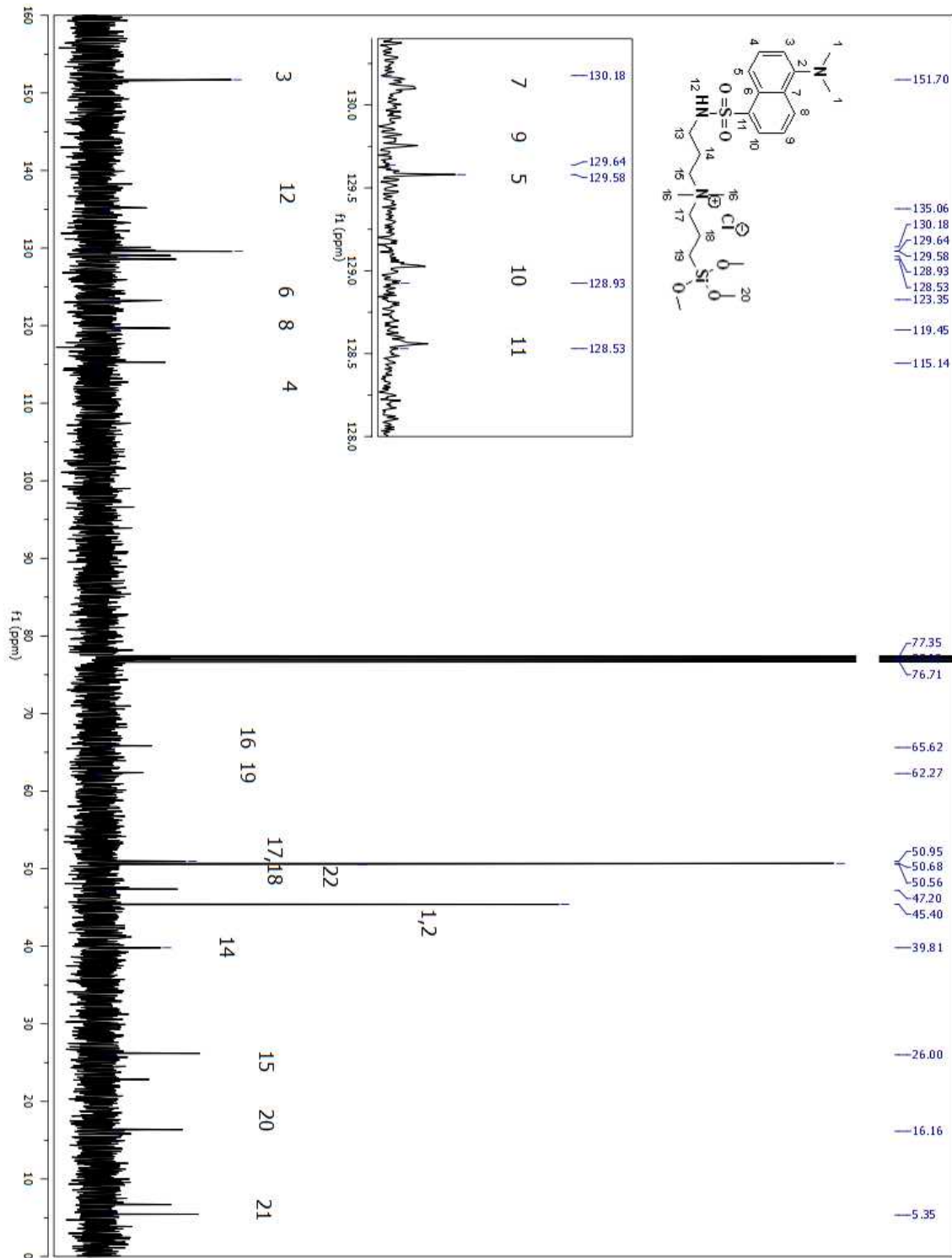


Figure A 359. ^{13}C NMR spectrum of compound (213) in CDCl_3 .

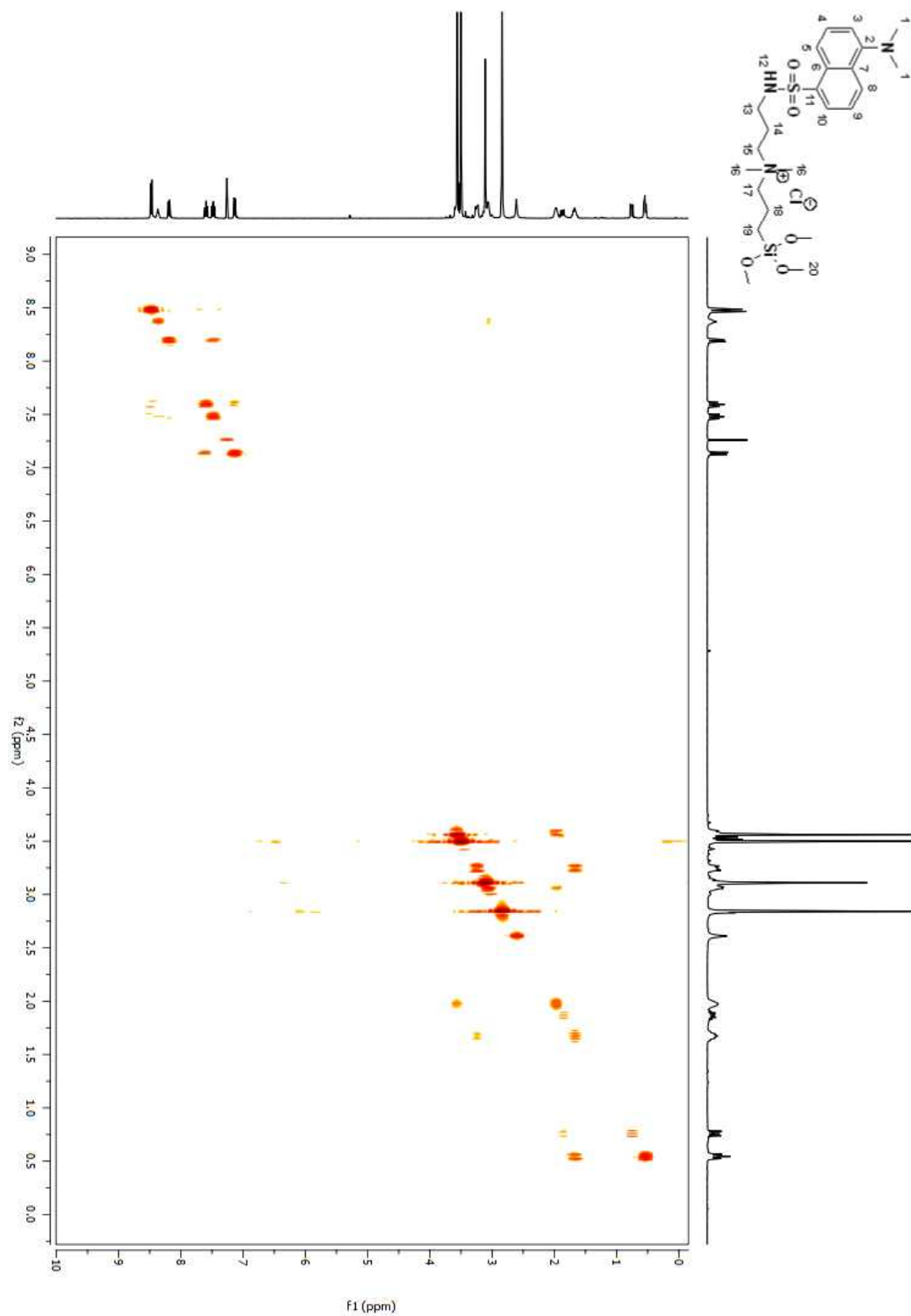


Figure A 360. COSY 2D NMR spectrum of compound (**213**) in CDCl_3 .

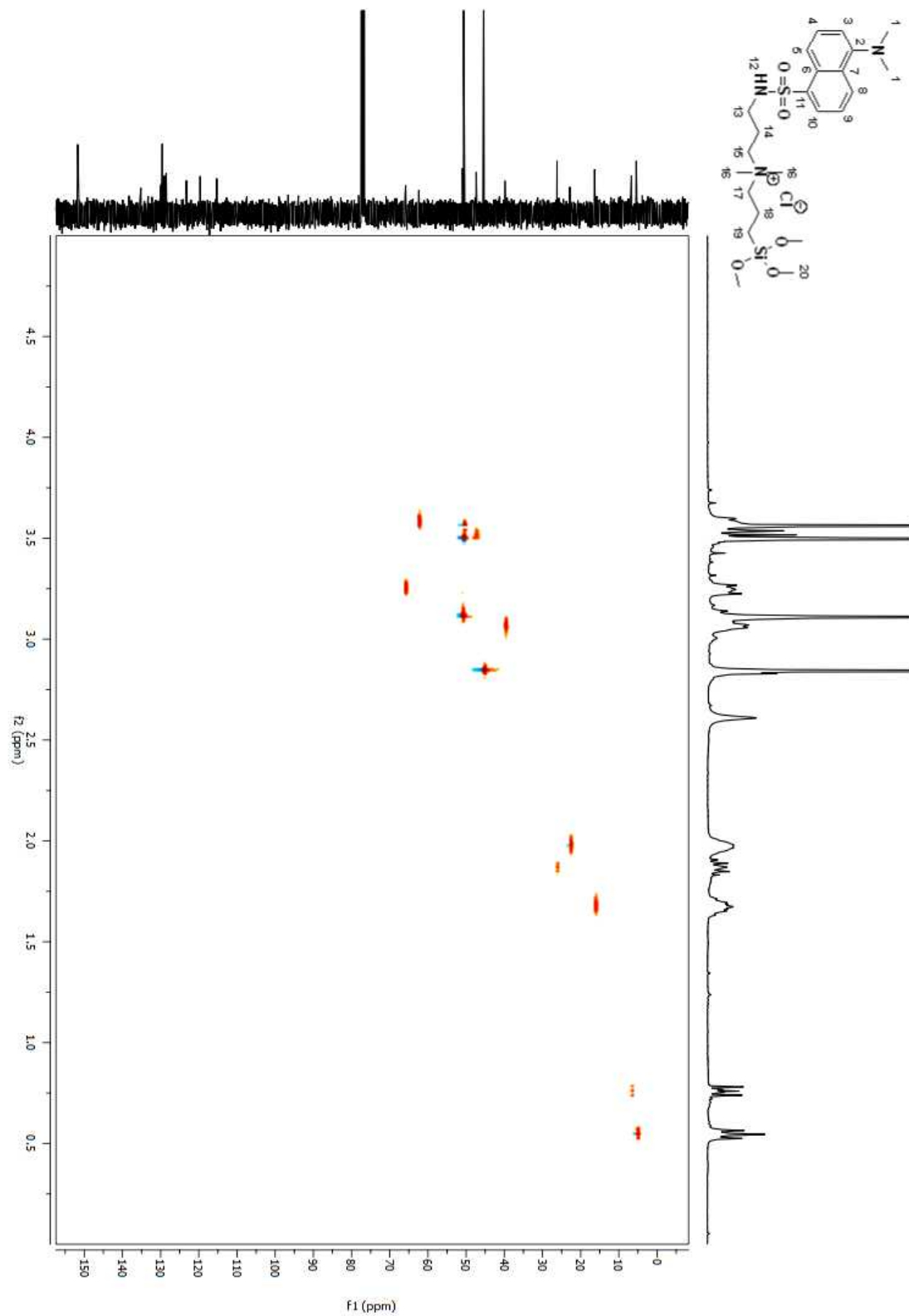


Figure A 361. HSQC 2D NMR spectrum of compound (213) in CDCl₃.

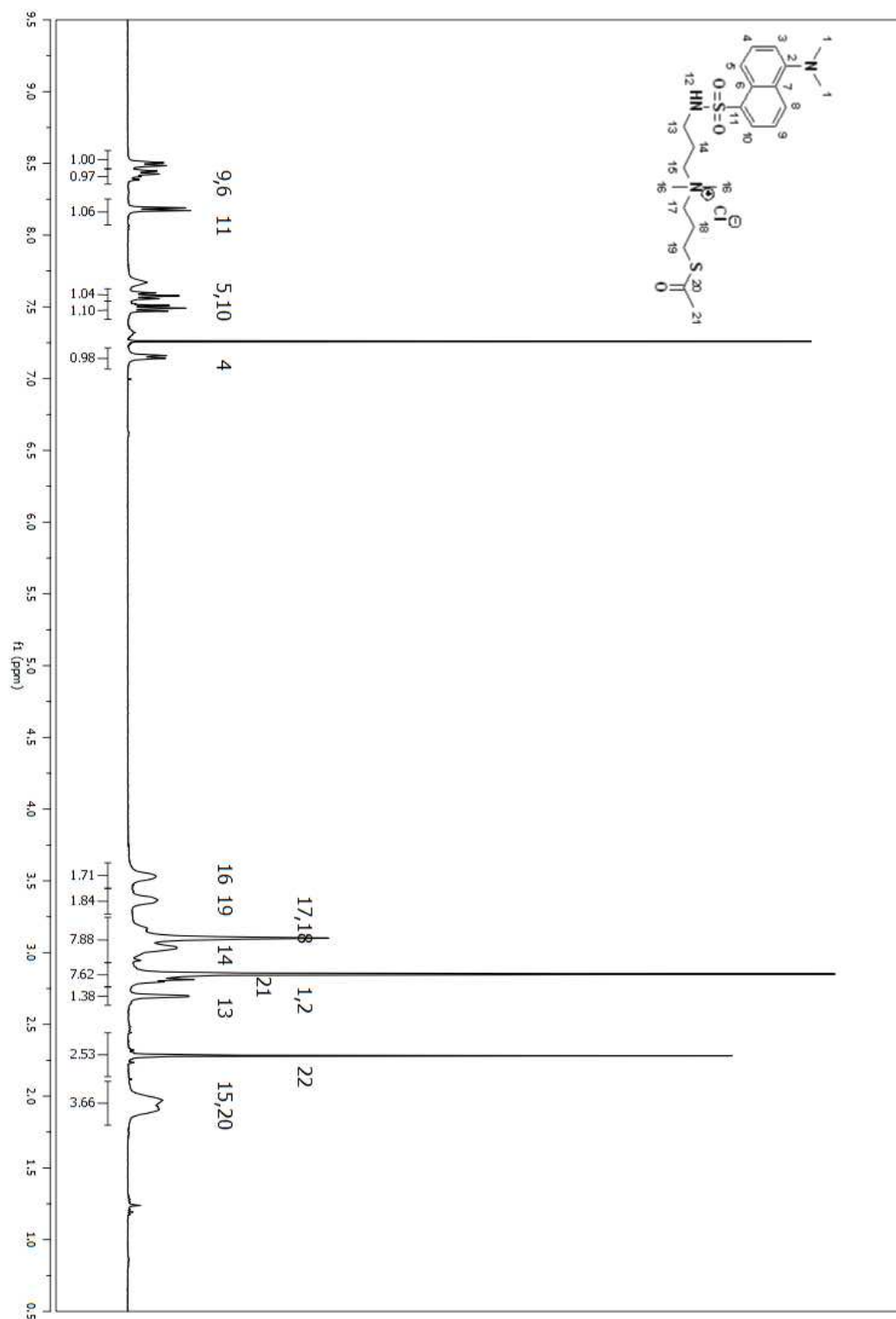


Figure A 362. ^1H NMR spectrum of compound (214) in CDCl_3 .

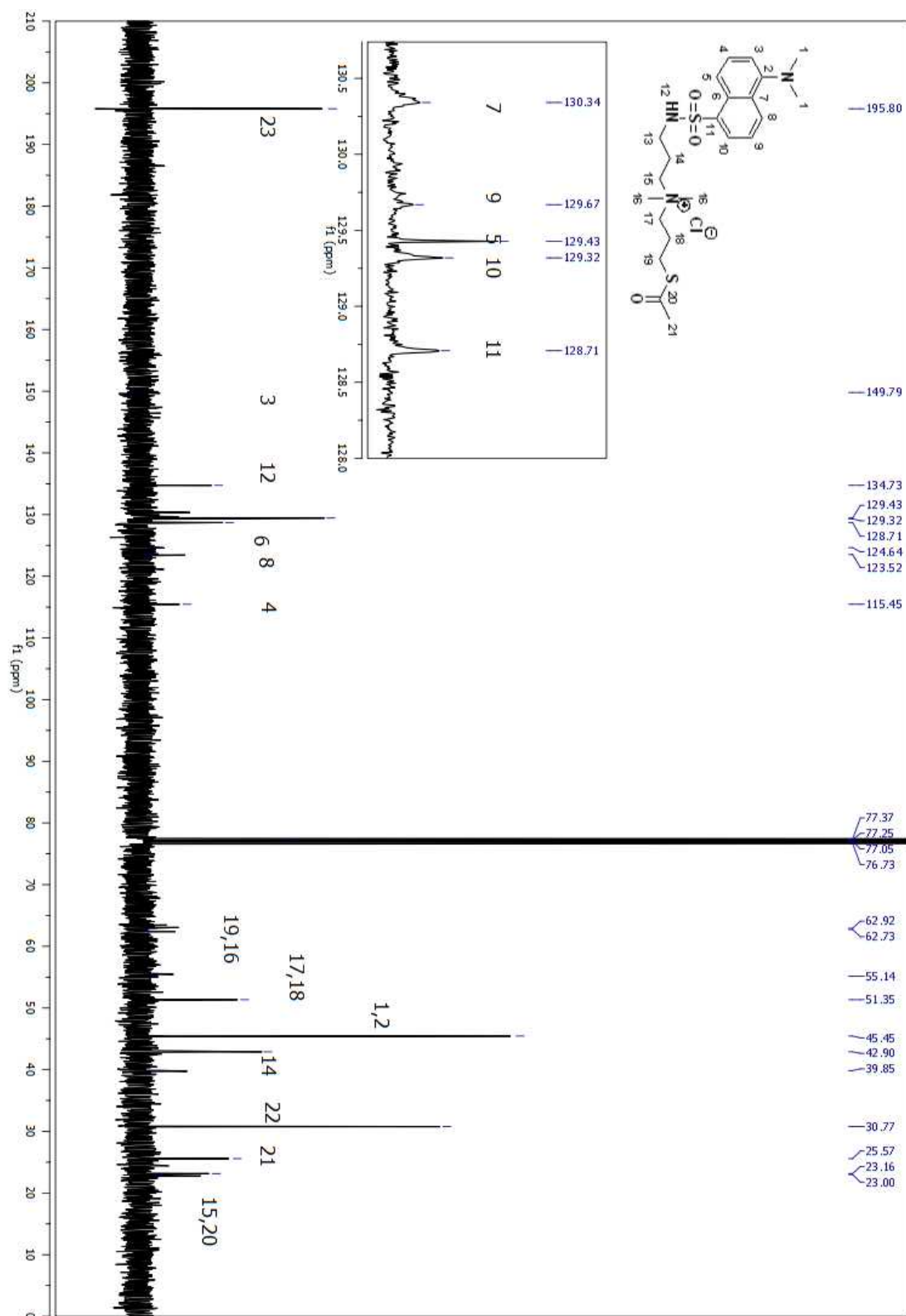


Figure A 363. ¹³C NMR spectrum of compound (214) in CDCl₃.

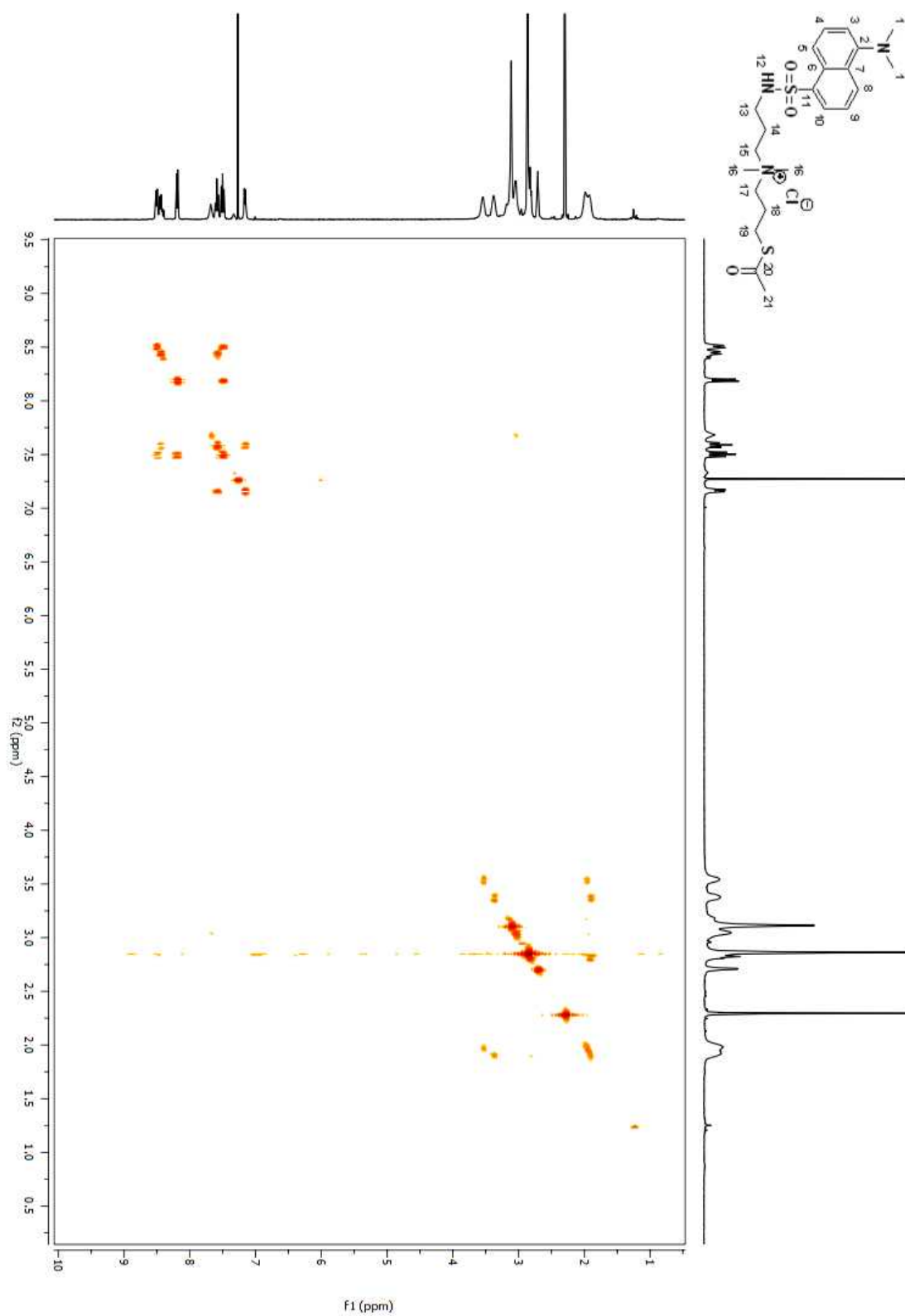


Figure A 364. COSY 2D NMR spectrum of compound (**214**) in CDCl₃.

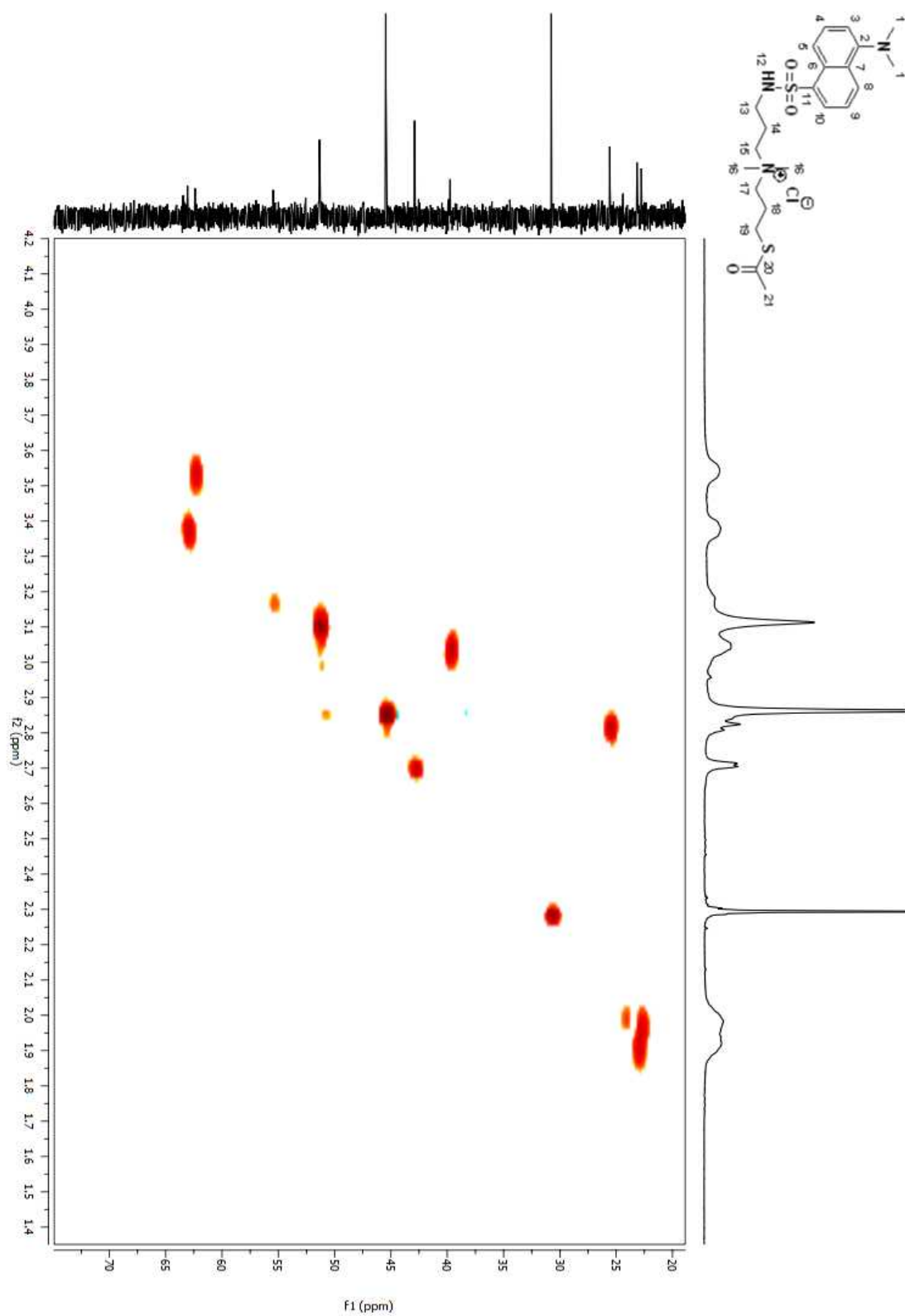


Figure A 365. HSQC 2D NMR spectrum of compound (**214**) in CDCl₃.

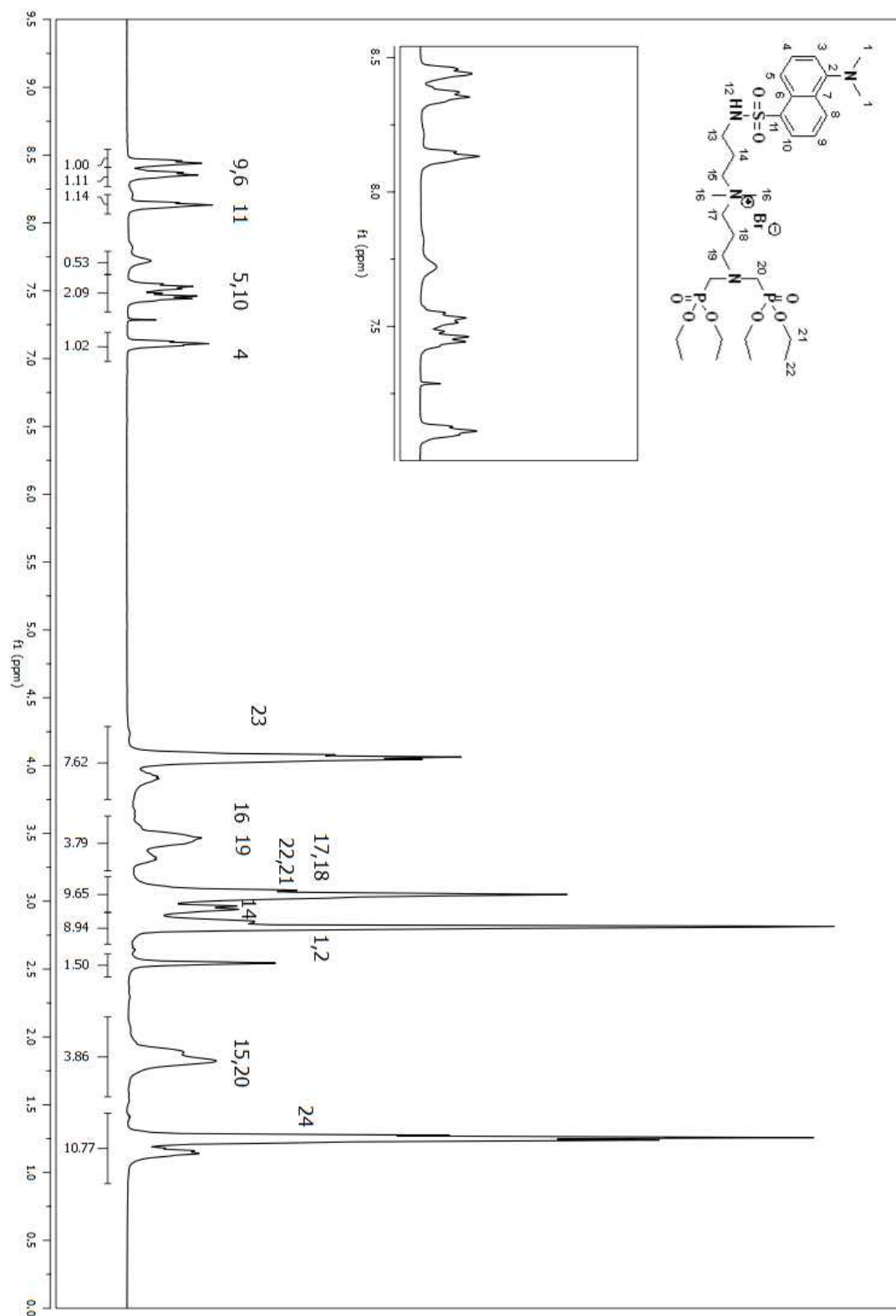


Figure A 366. ^1H NMR spectrum of compound (215) in CDCl_3 .

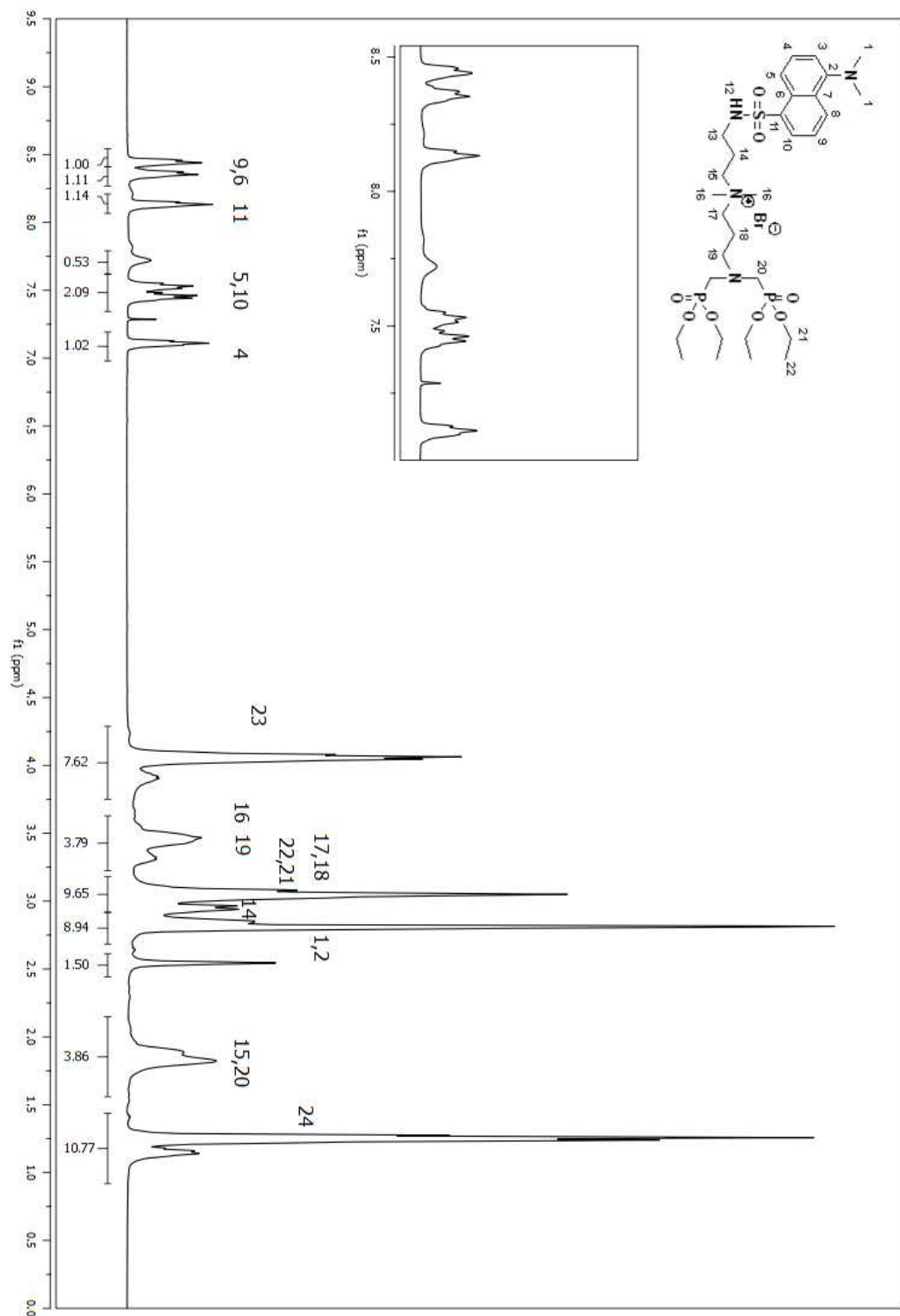


Figure A 367. ^{13}C NMR spectrum of compound (215) in CDCl_3 .

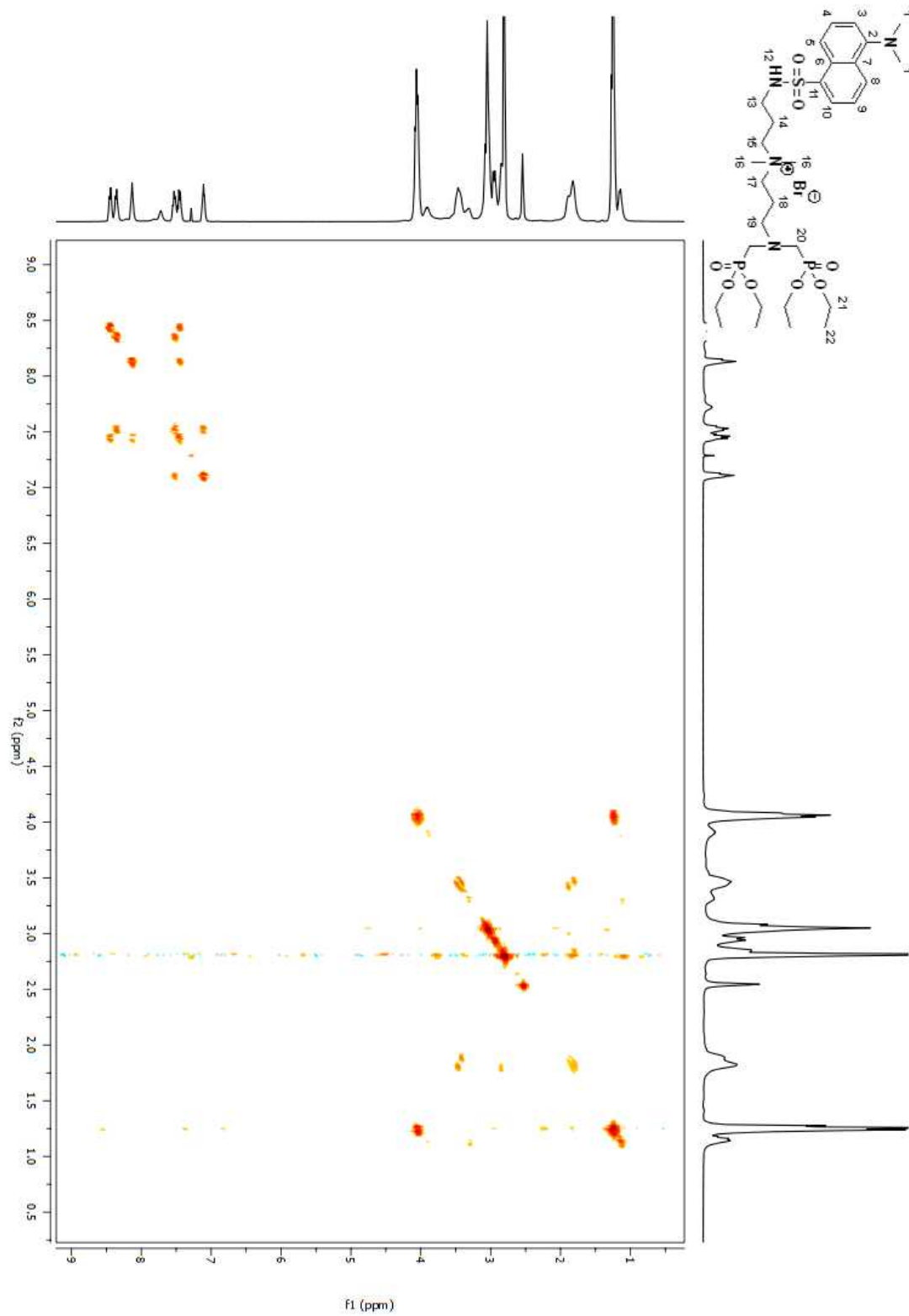


Figure A 368. COSY 2D NMR spectrum of compound (**215**) in CDCl₃.

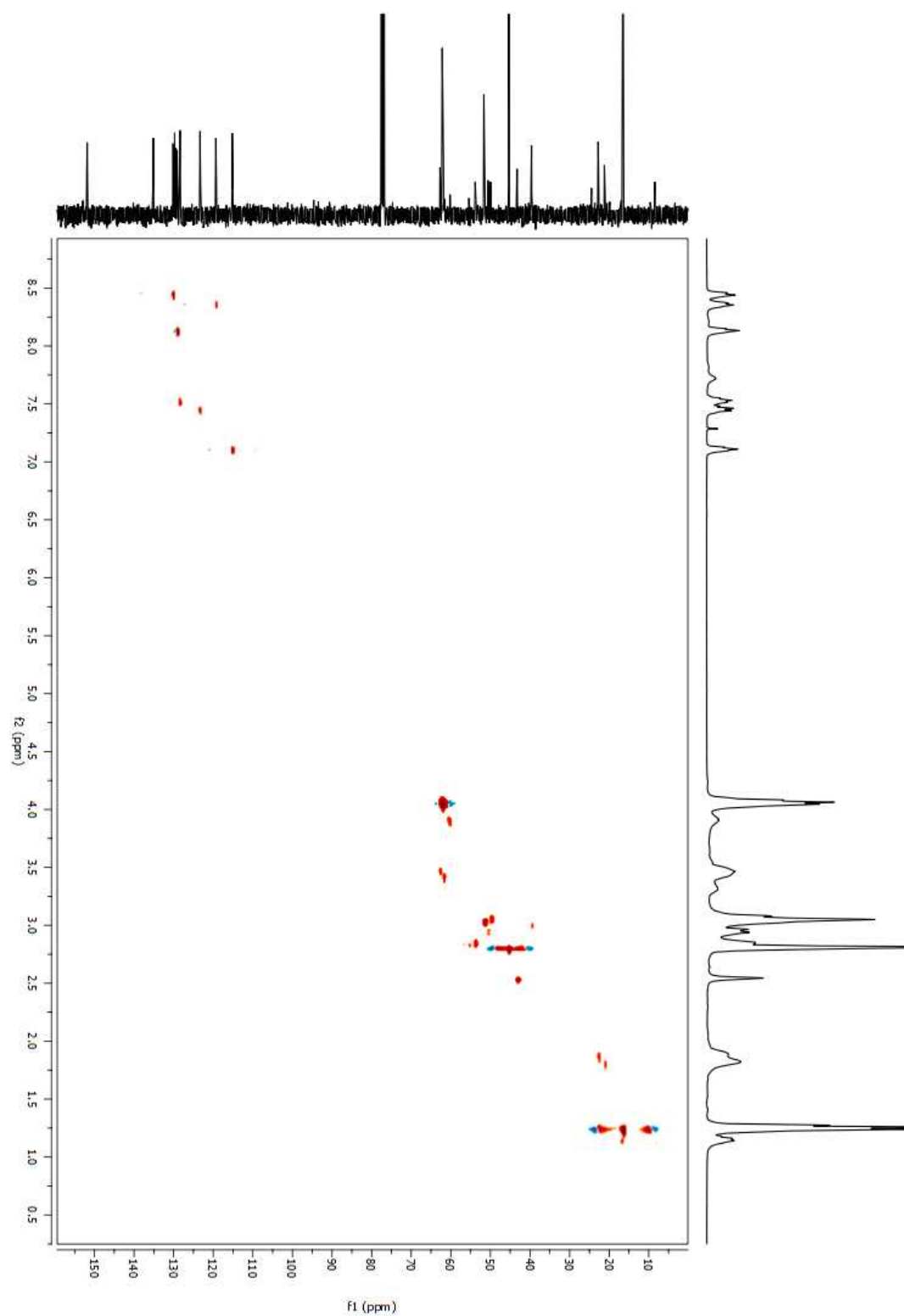


Figure A 369. HSQC 2D NMR spectrum of compound (215) in CDCl₃.

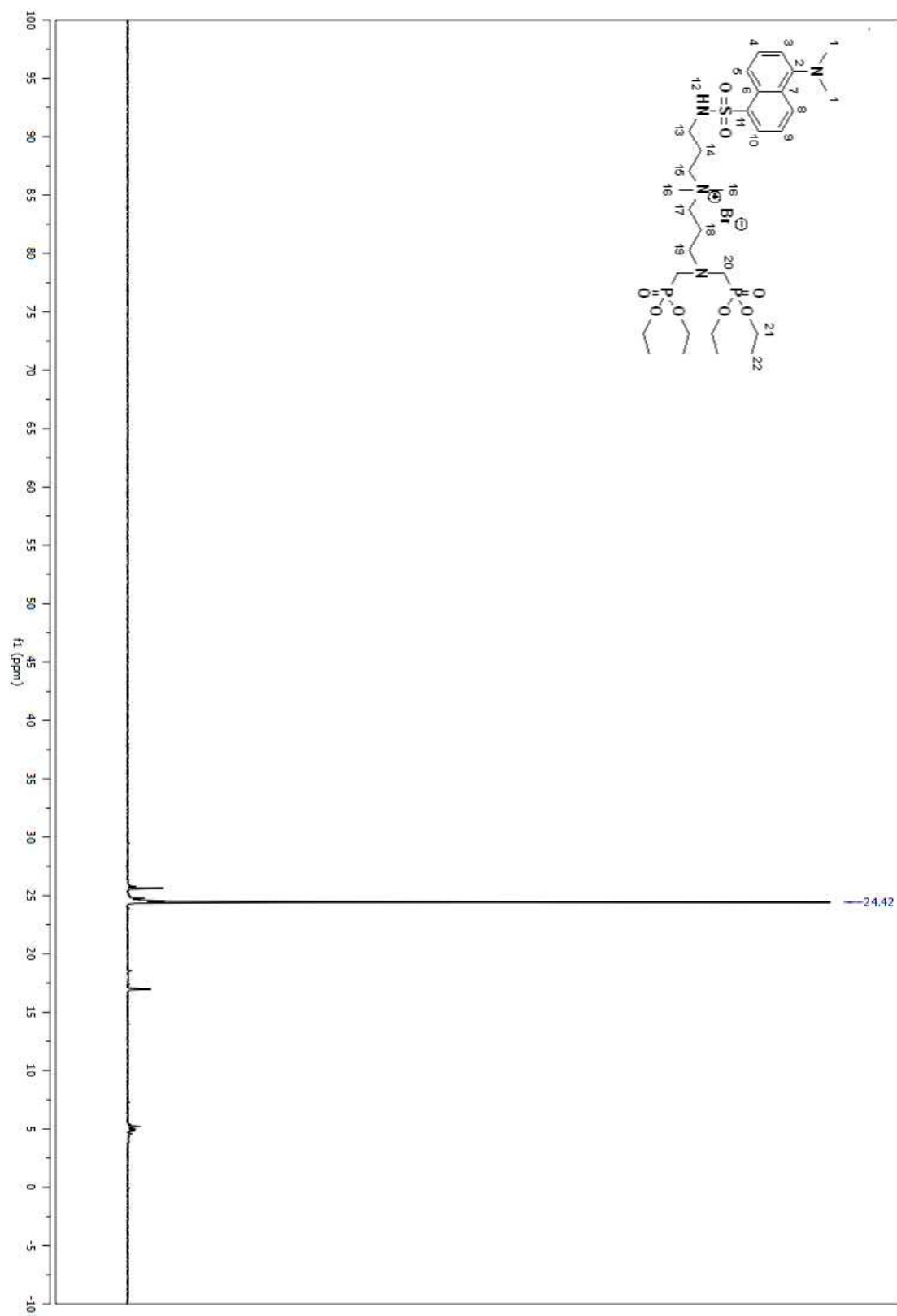


Figure A 370. ^{31}P NMR spectrum of compound (215) in CDCl_3

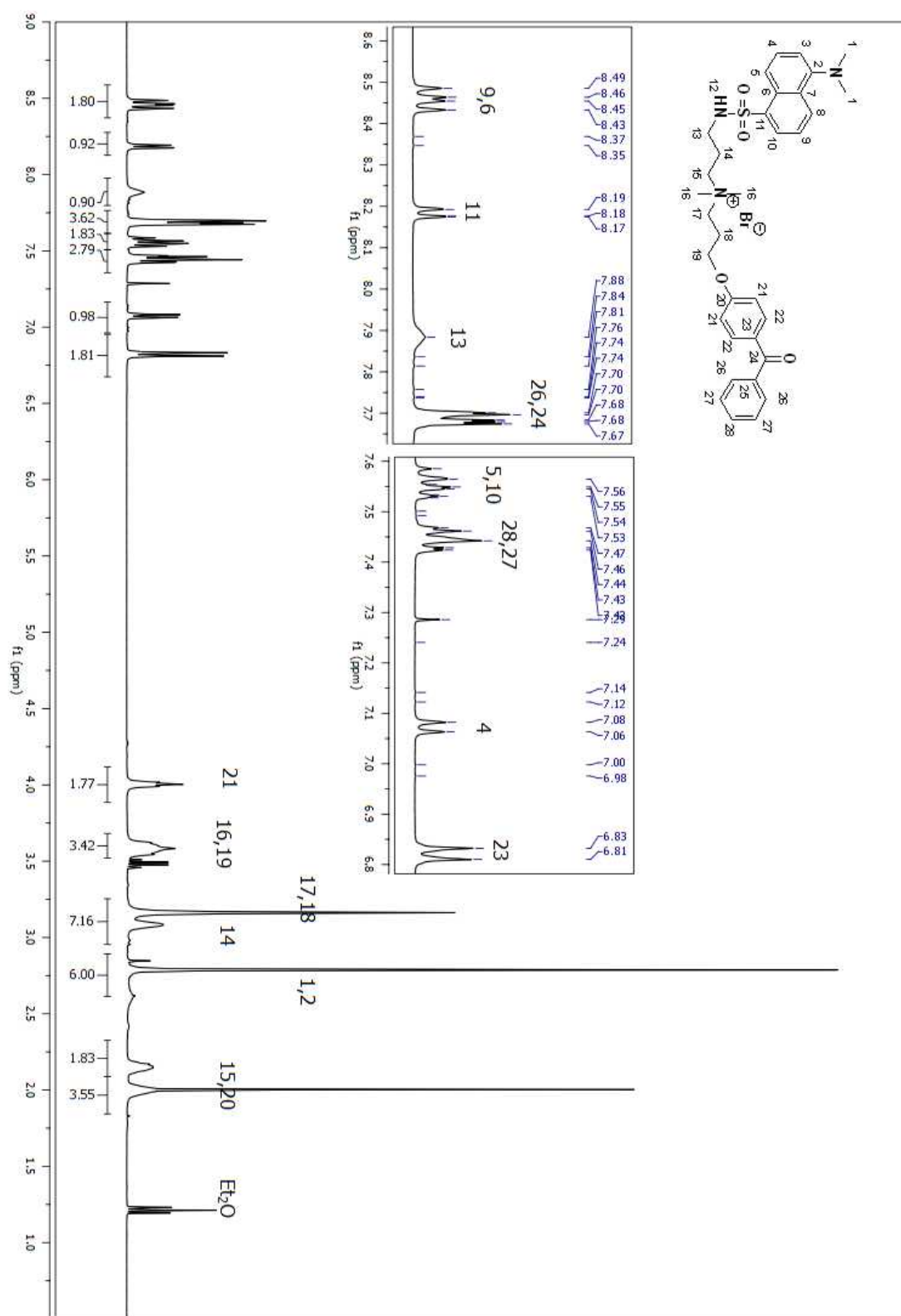


Figure A 371. ¹H NMR spectrum of compound (216) in CDCl₃.
738

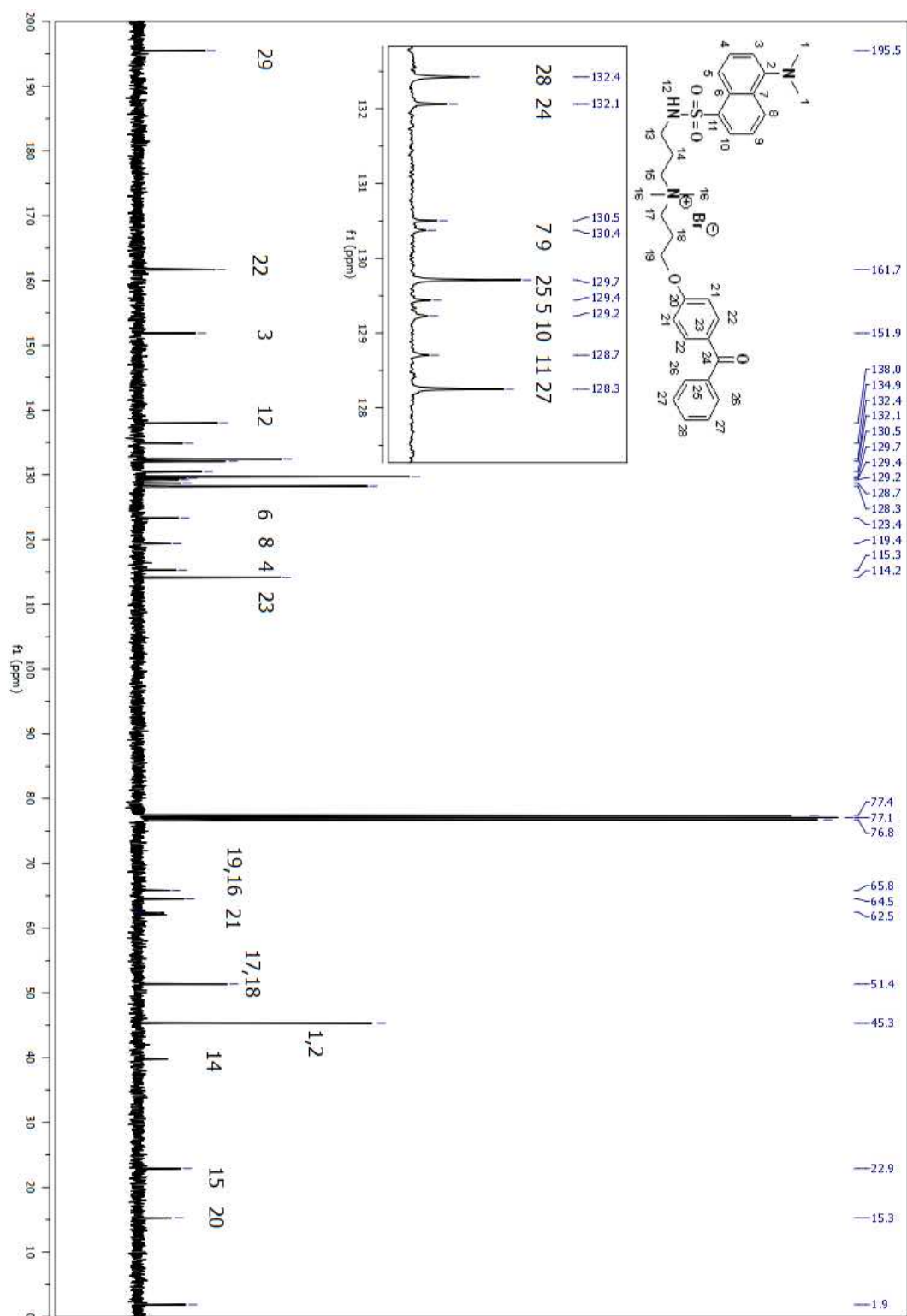


Figure A 372. ¹³C NMR spectrum of compound (**216**) in CDCl₃.

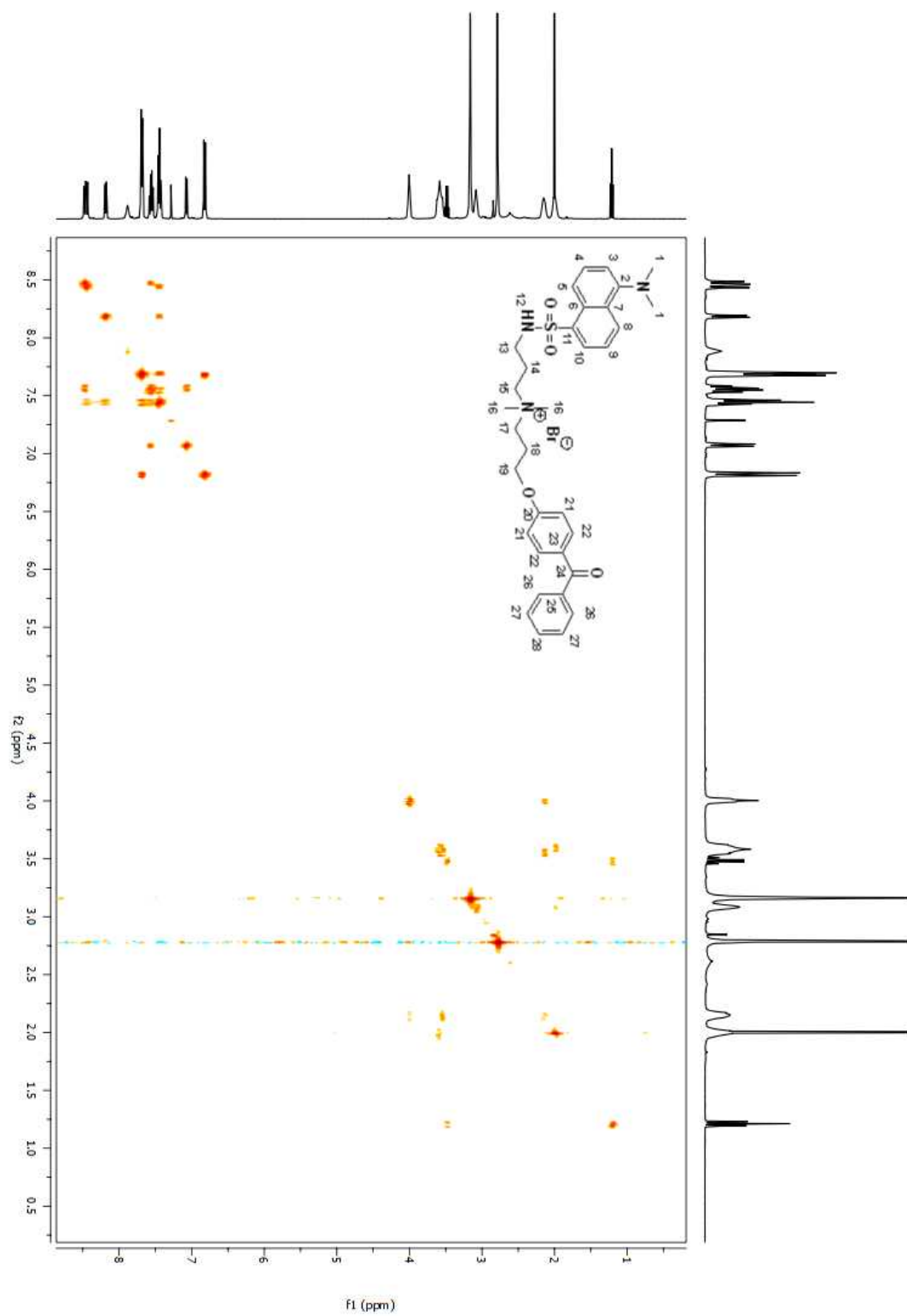


Figure A 373. COSY 2D NMR spectrum of compound **(216)** in CDCl₃.

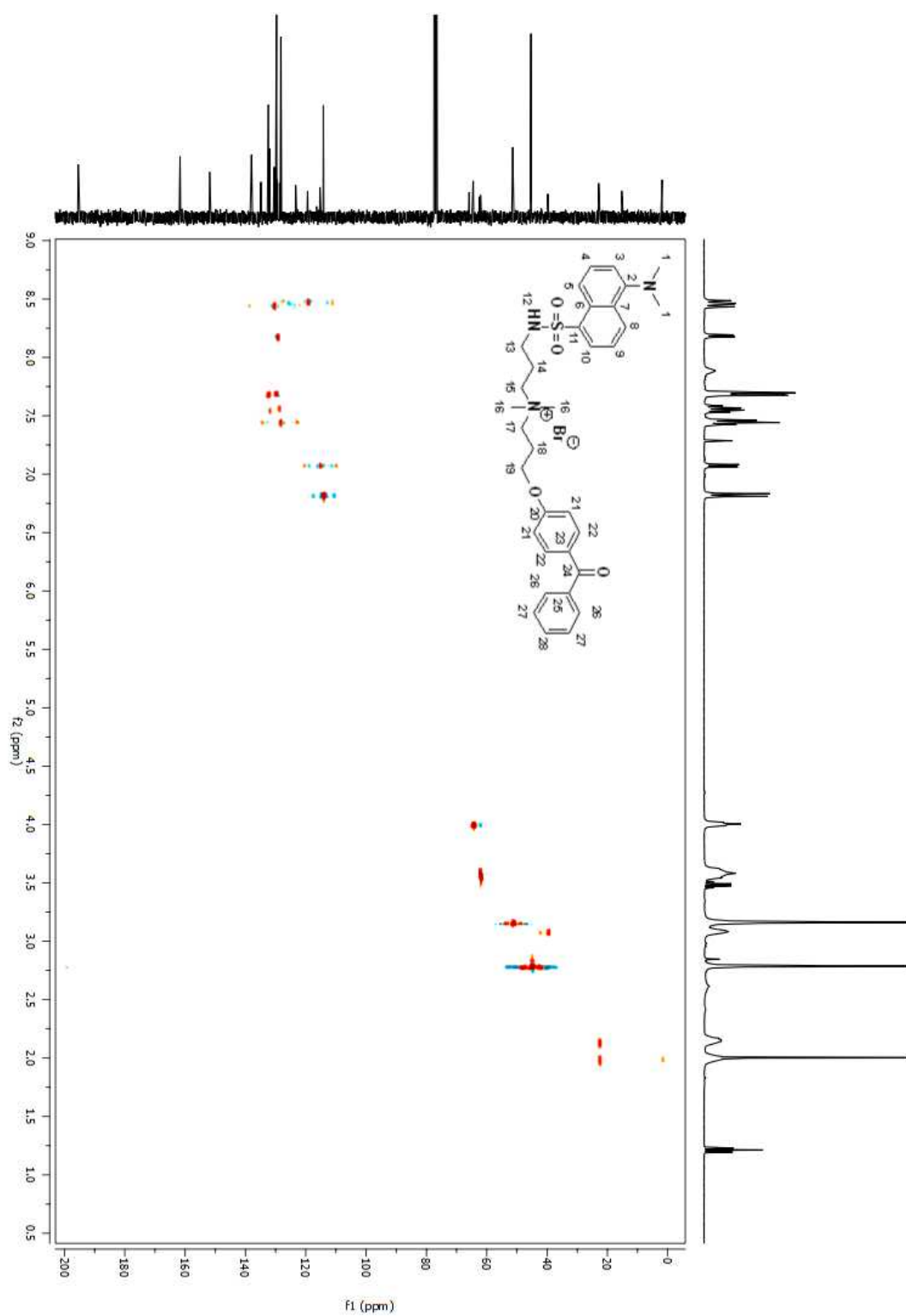


Figure A 374. HSQC 2D NMR spectrum of compound (216) in CDCl₃.

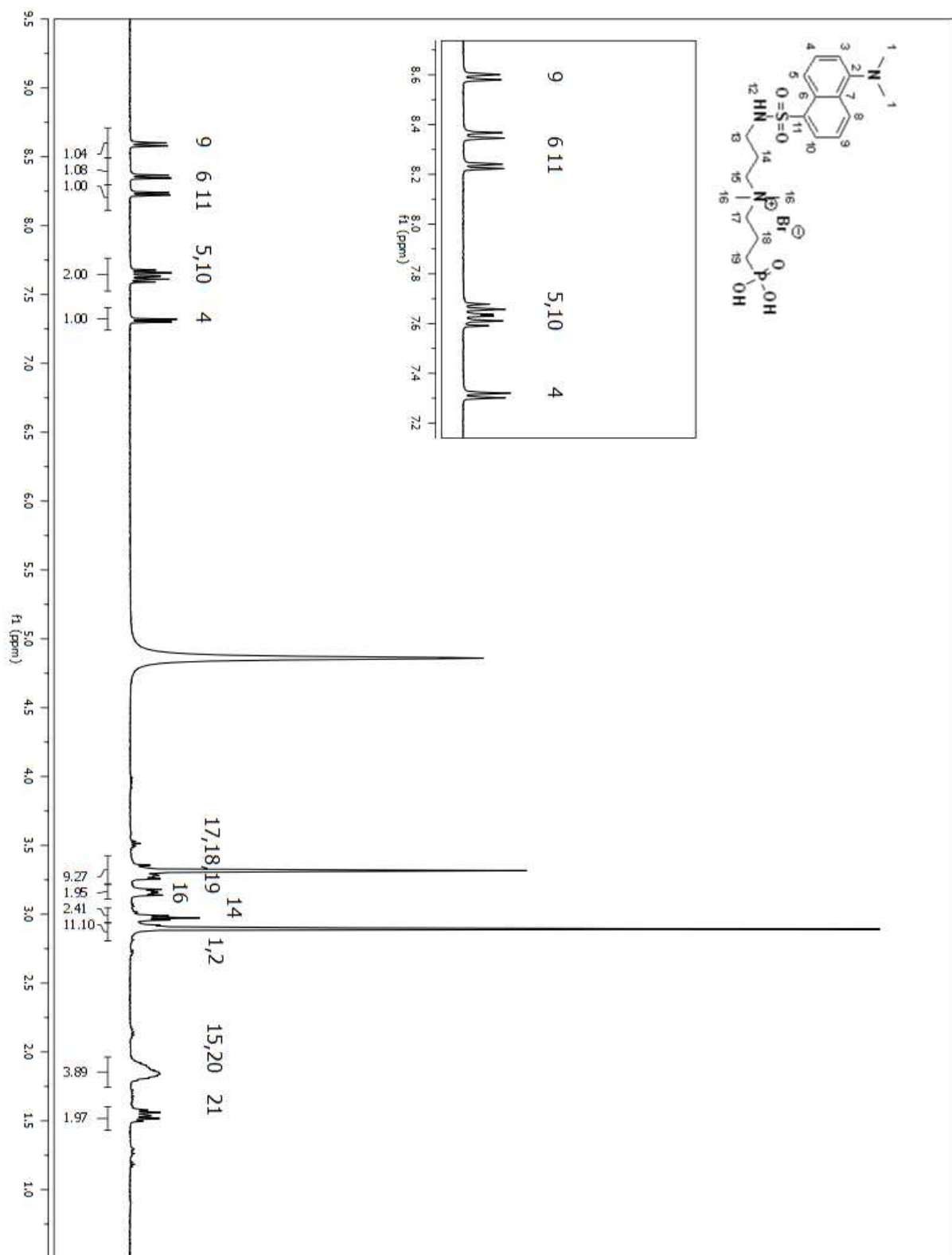


Figure A 375. ¹H NMR spectrum of compound (217) in D₂O.

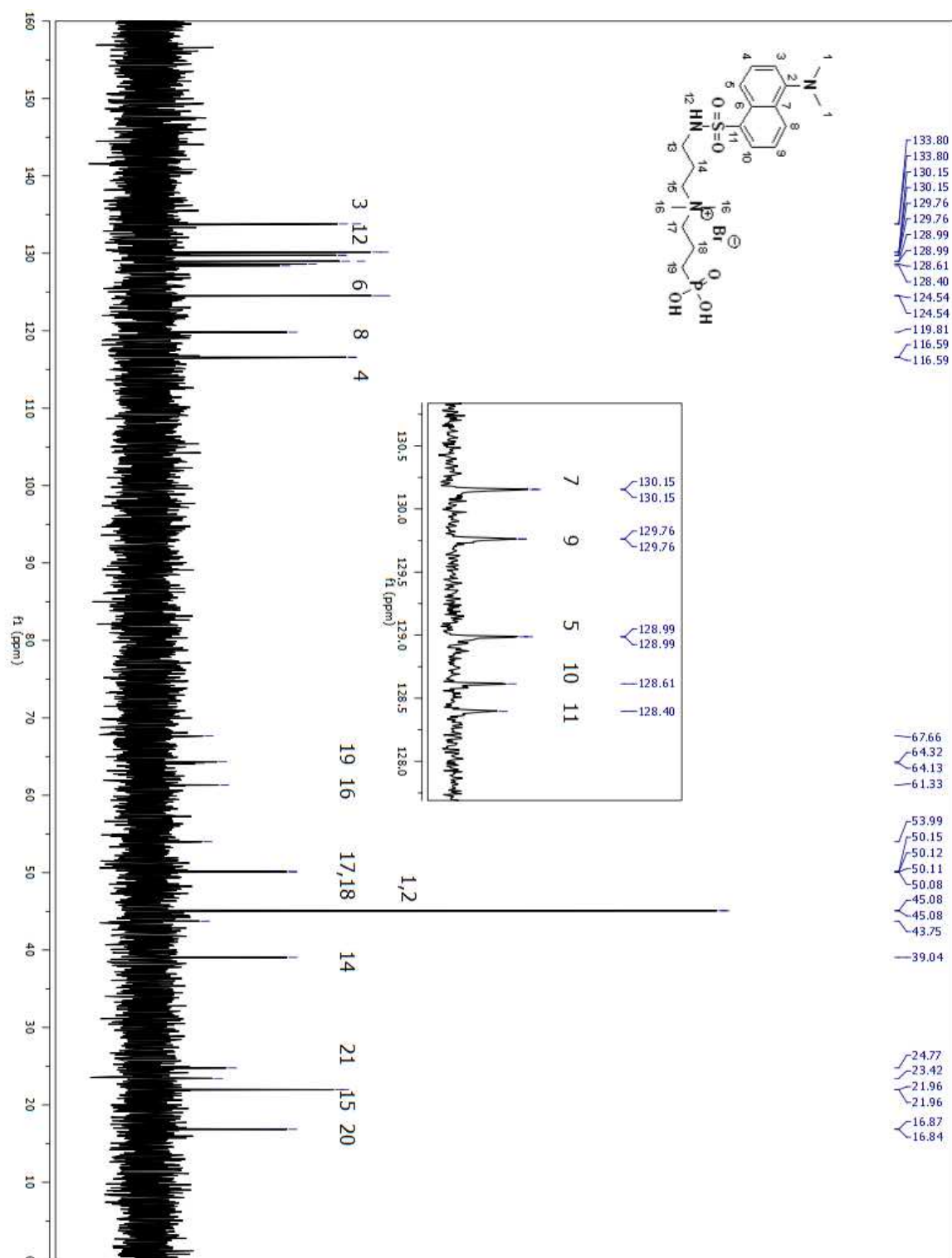


Figure A 376. ^{13}C NMR spectrum of compound (217) in D_2O .

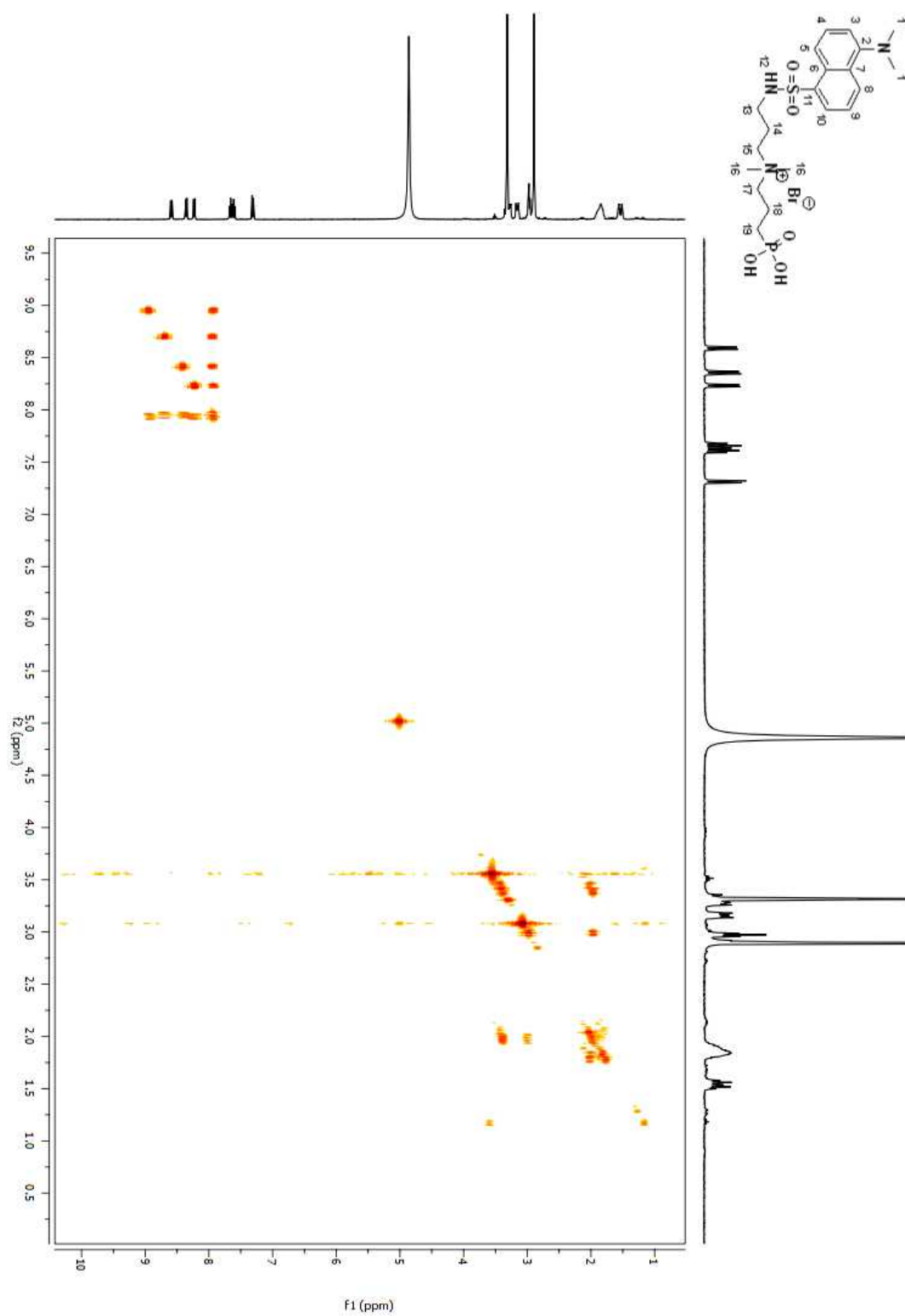


Figure A 377. COSY 2D NMR spectrum of compound (**217**) in D_2O .

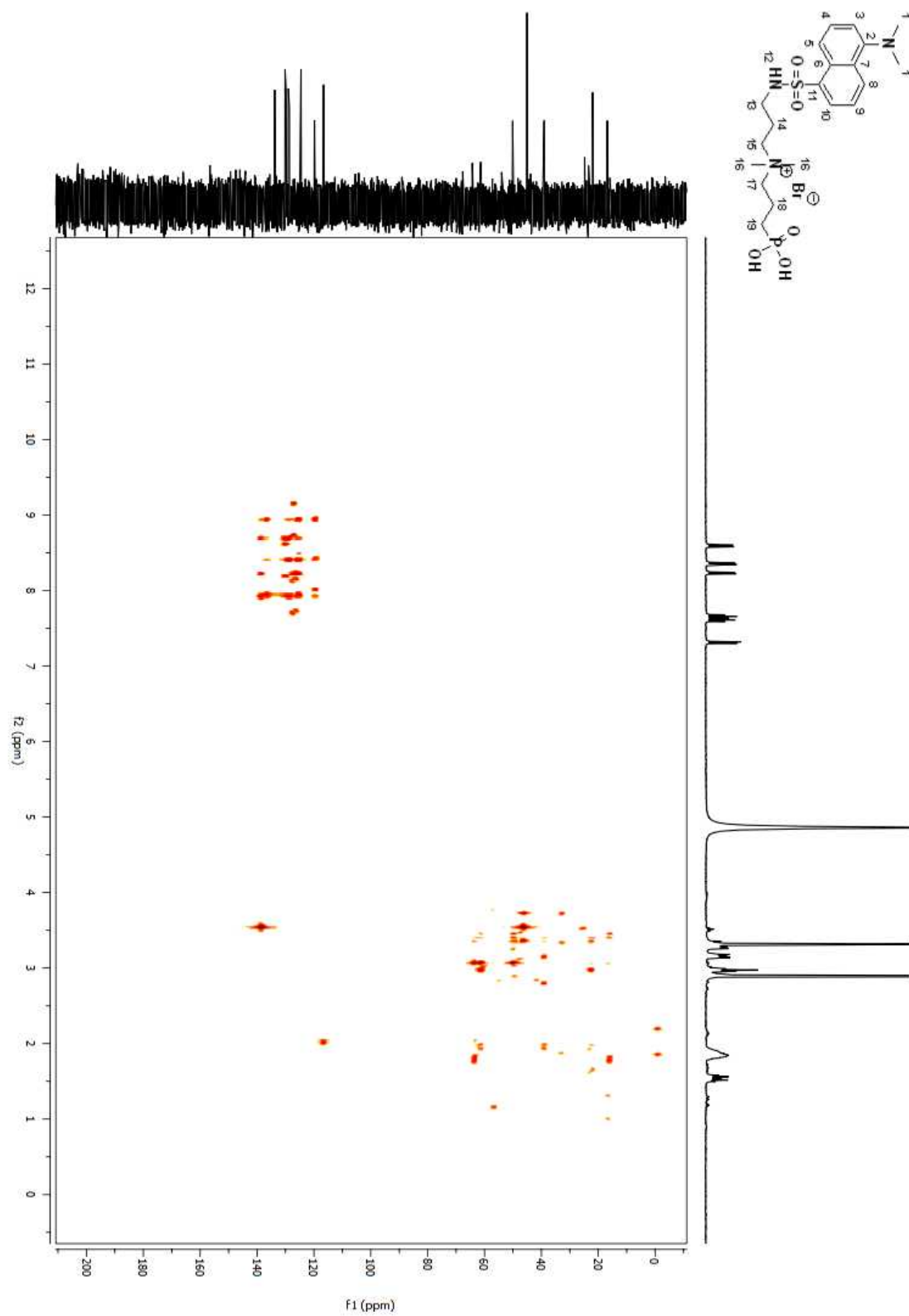


Figure A 378. HSQC 2D NMR spectrum of compound (**217**) in D₂O.

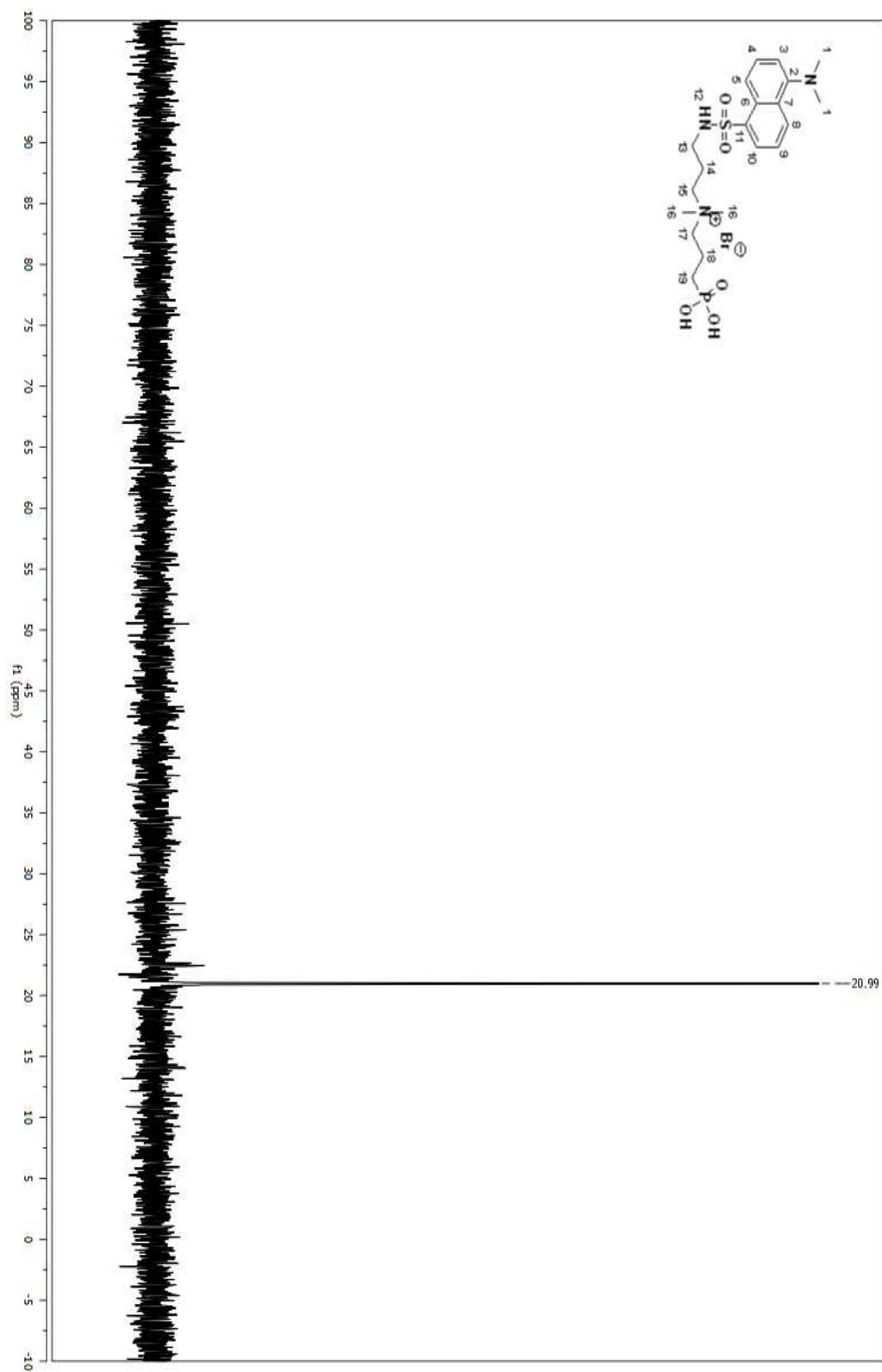


Figure A 379. ^{31}P NMR spectrum of compound in (217) D_2O .

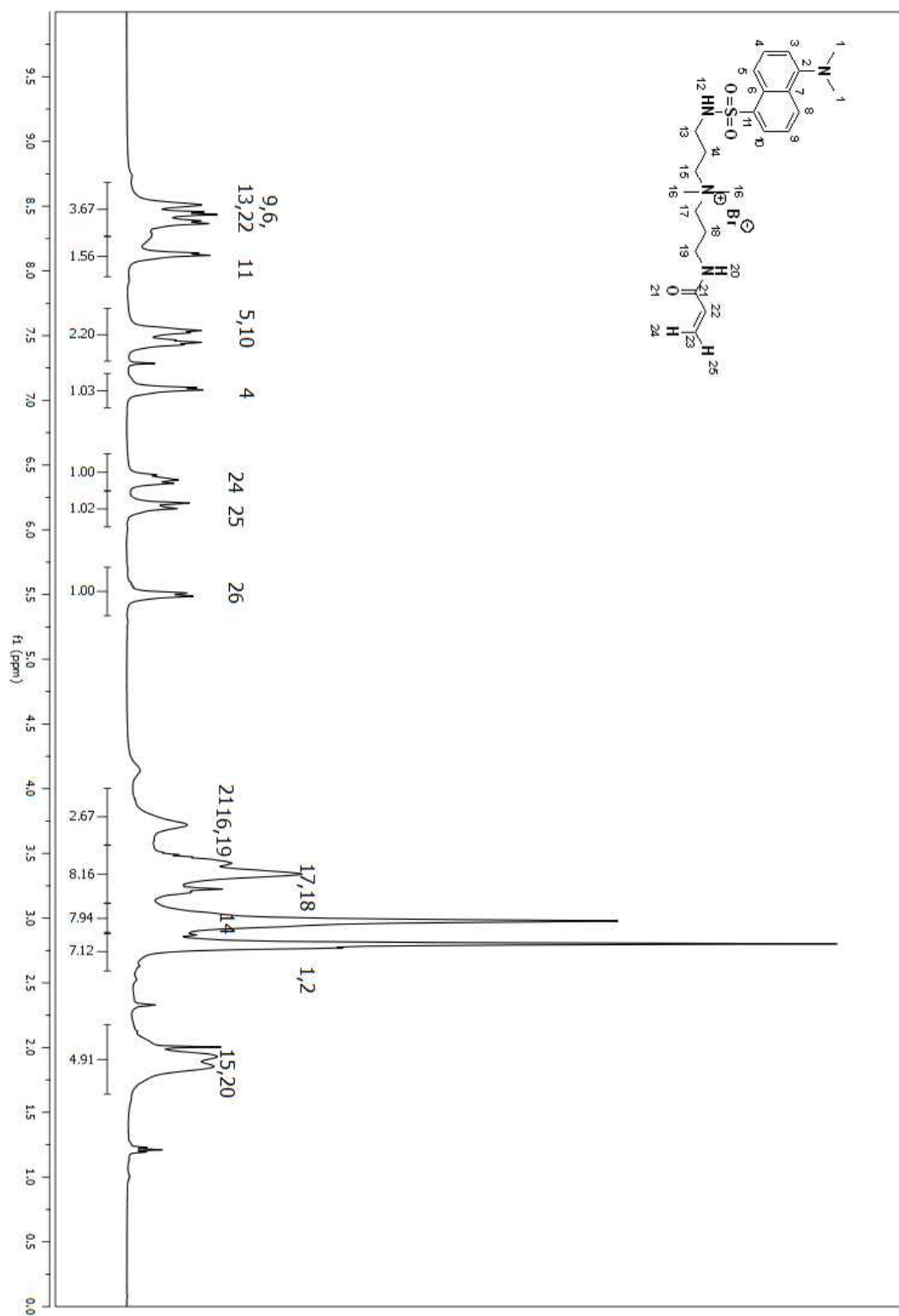


Figure A 380. ^1H NMR spectrum of compound (219) in CDCl_3 .

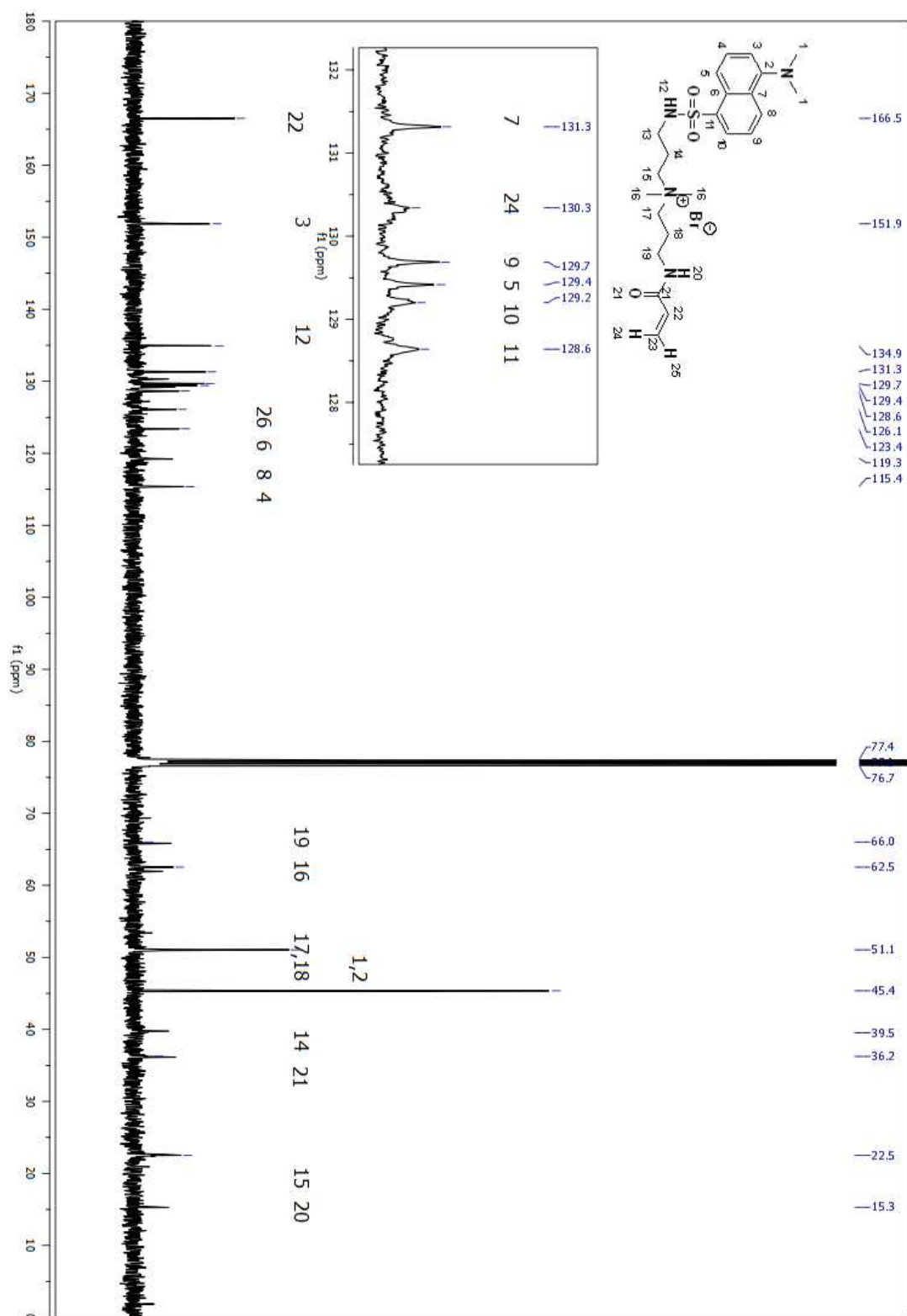


Figure A 381. ^{13}C NMR spectrum of compound (219) in CDCl_3 .

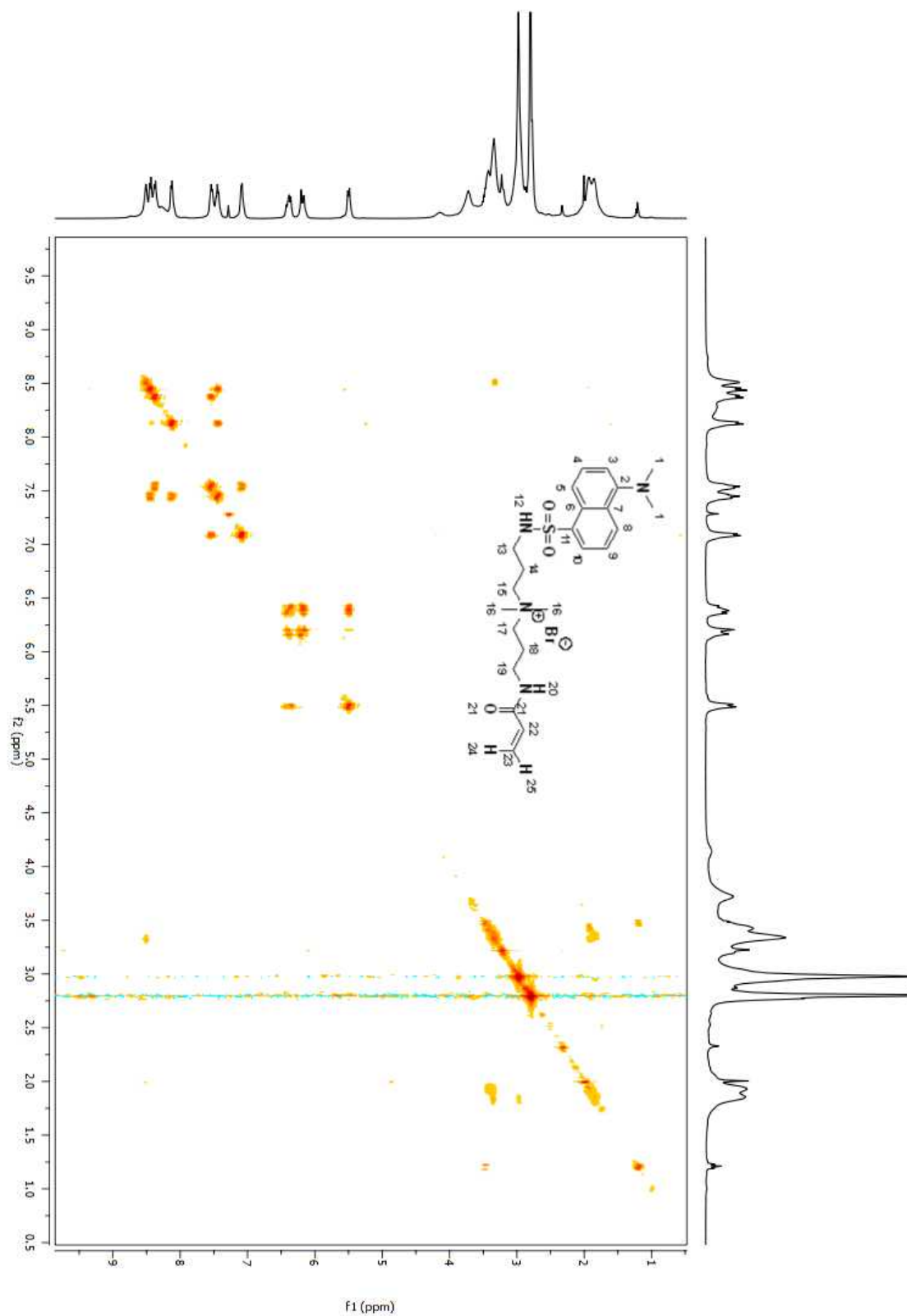


Figure A 382. COSY 2D NMR spectrum of compound (219) in CDCl₃.

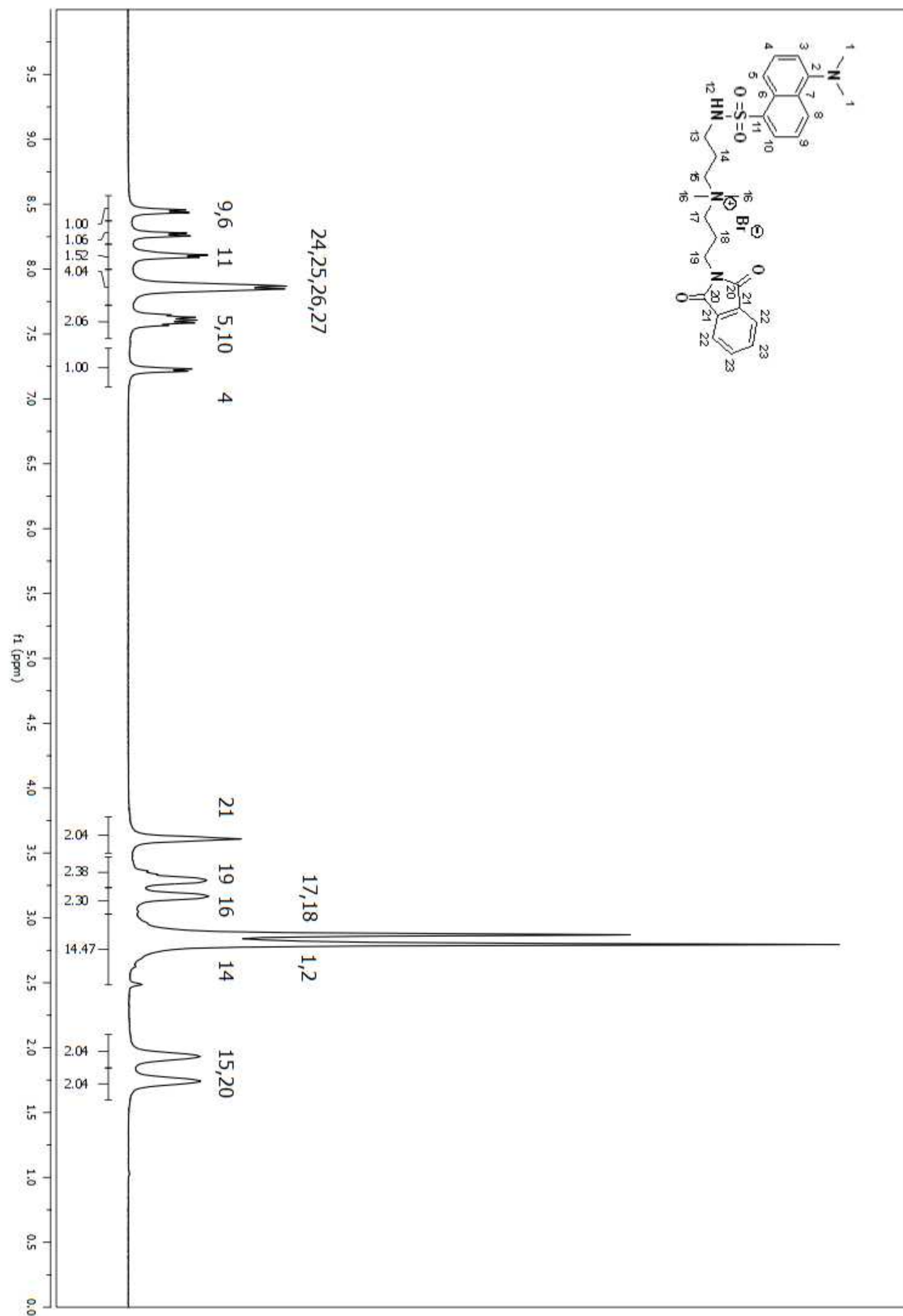


Figure A 383. ^1H NMR spectrum of compound (220) in DMSO-d_6 .
750

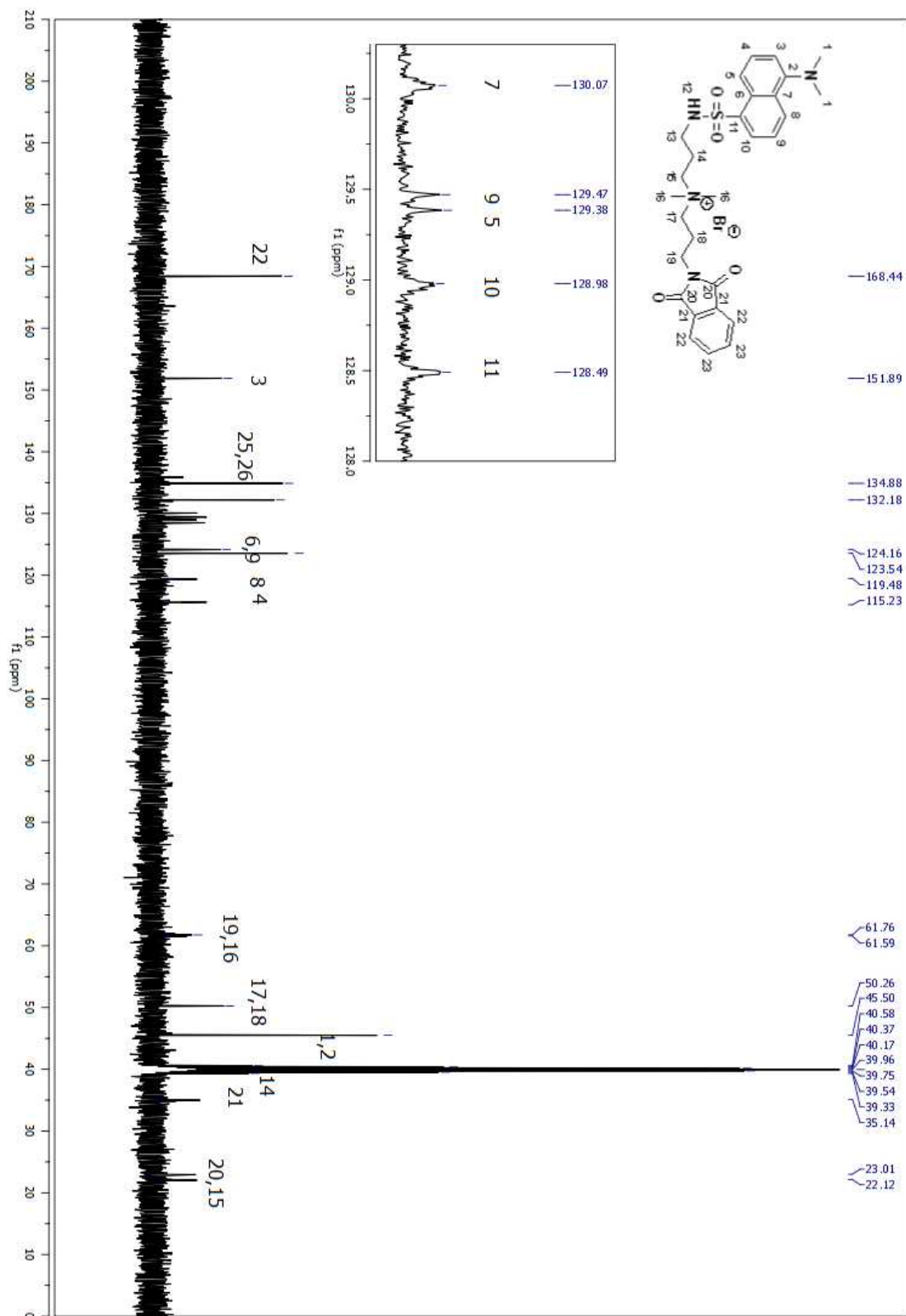


Figure A 384. ^{13}C NMR spectrum of compound (220) in DMSO- d_6 .

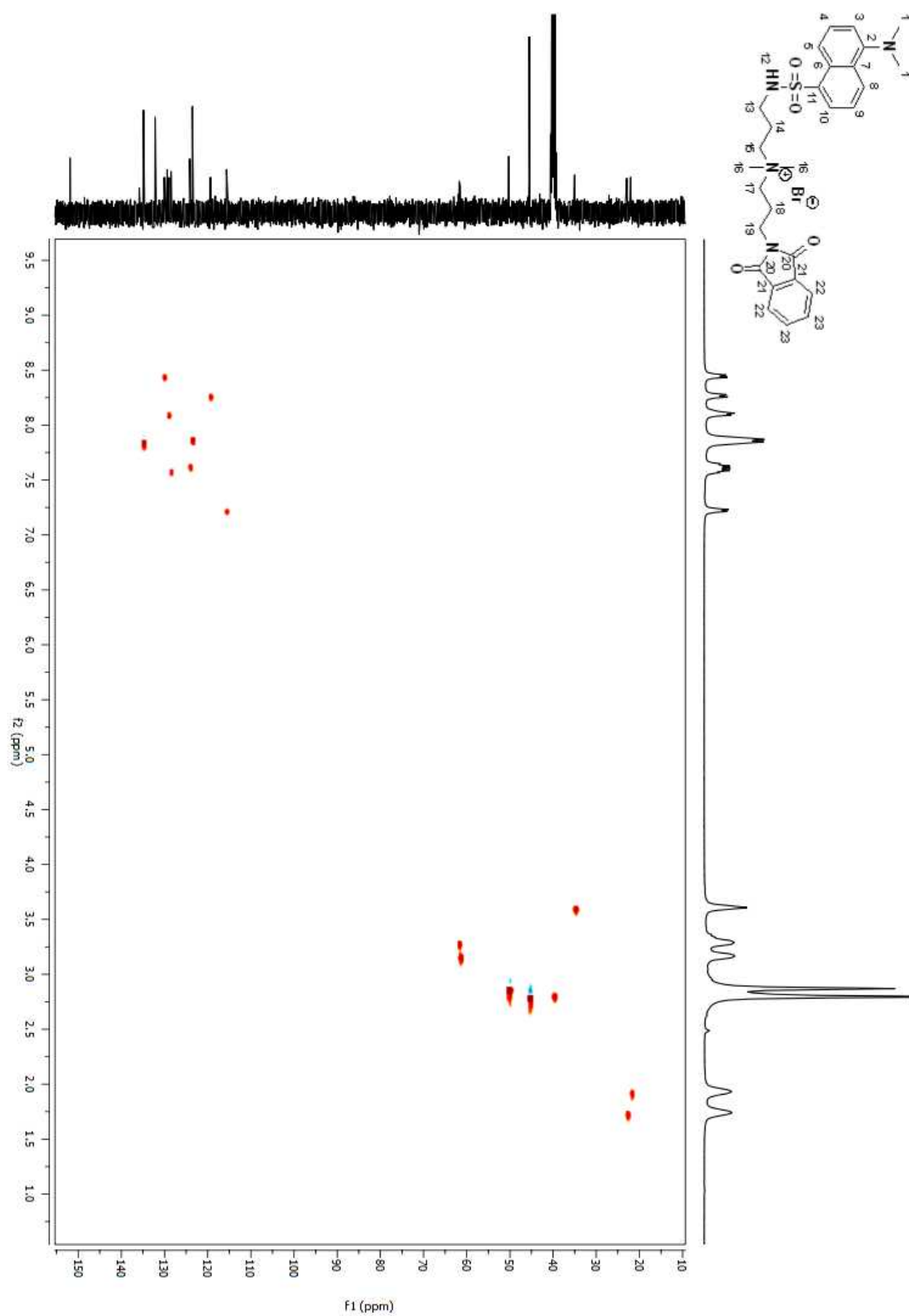


Figure A 385. HSQC 2D NMR spectrum of compound (220) in DMSO-d₆.

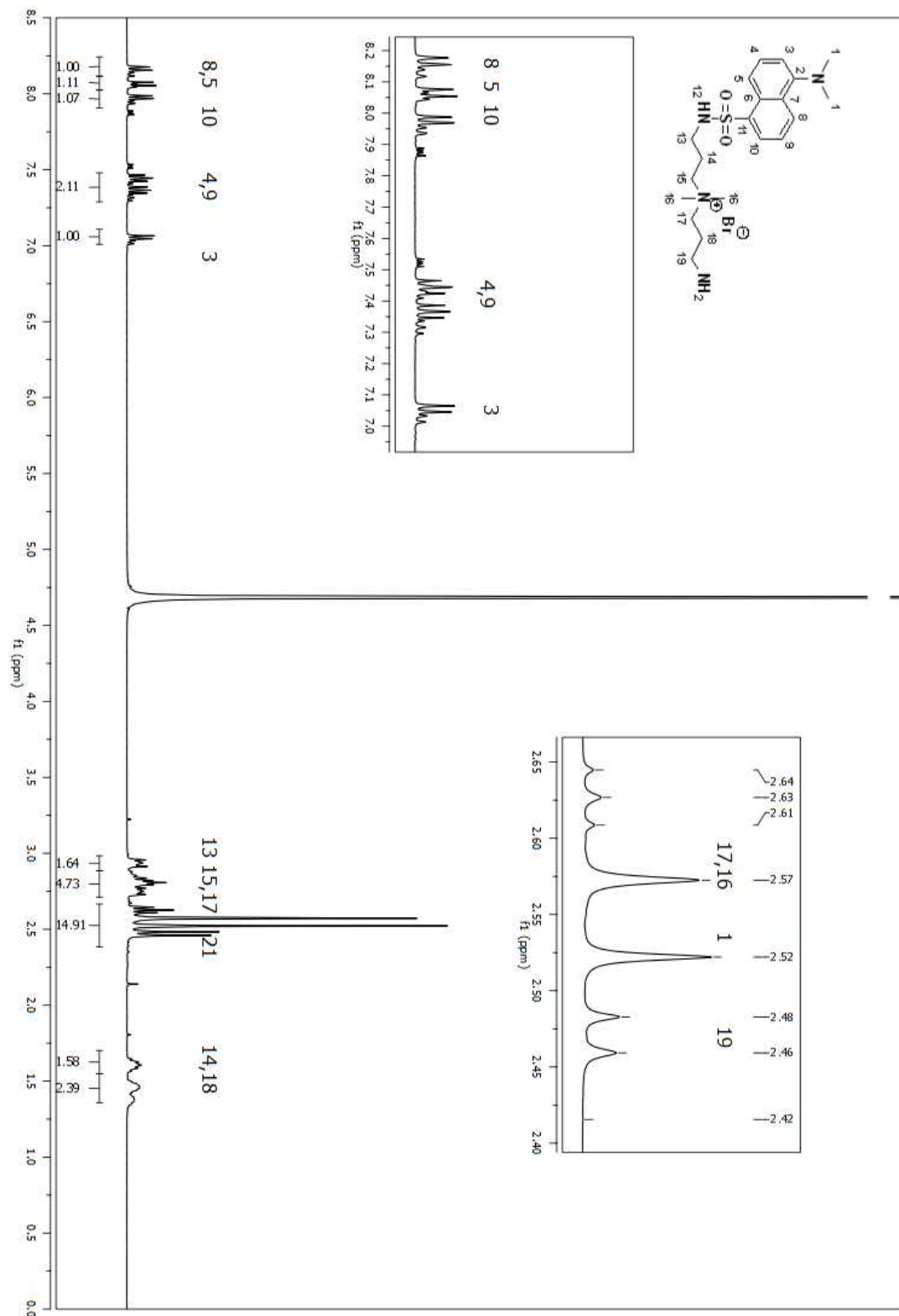


Figure A 386. ¹H NMR spectrum of compound (221) in D₂O.

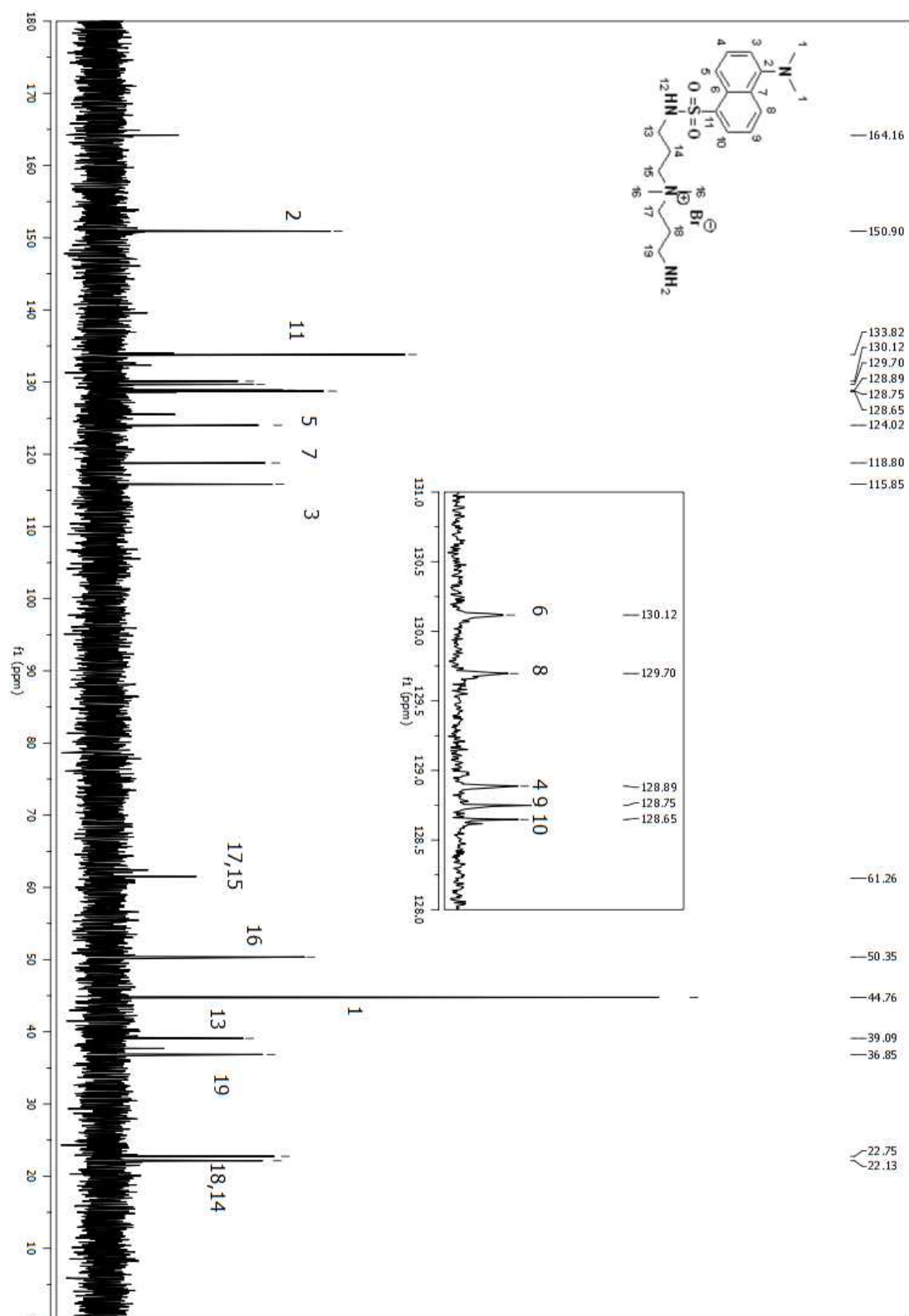


Figure A 387. ^{13}C NMR spectrum of compound (221) in D_2O .
754

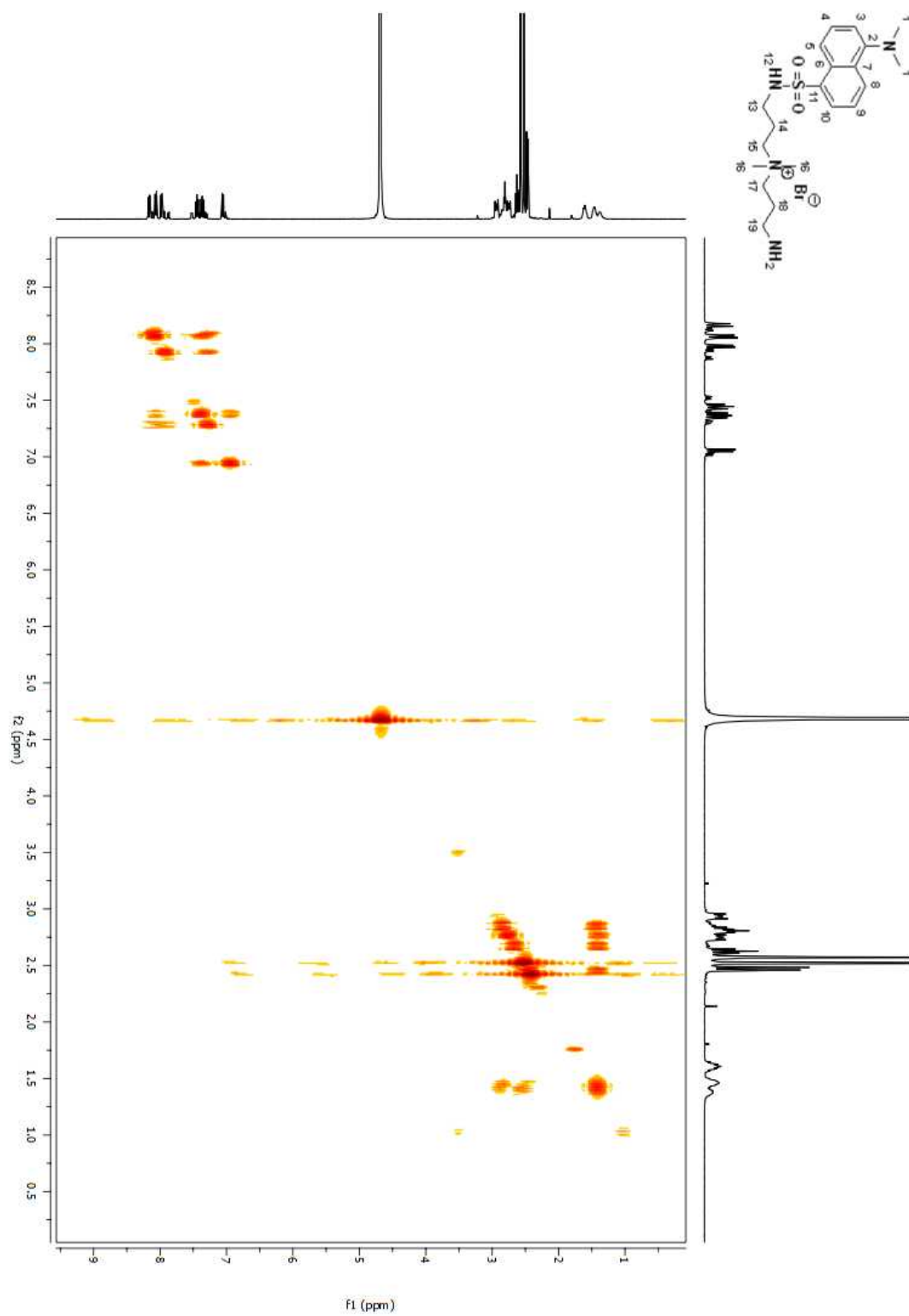


Figure A 388. COSY 2D NMR spectrum of compound (**221**) in D₂O.

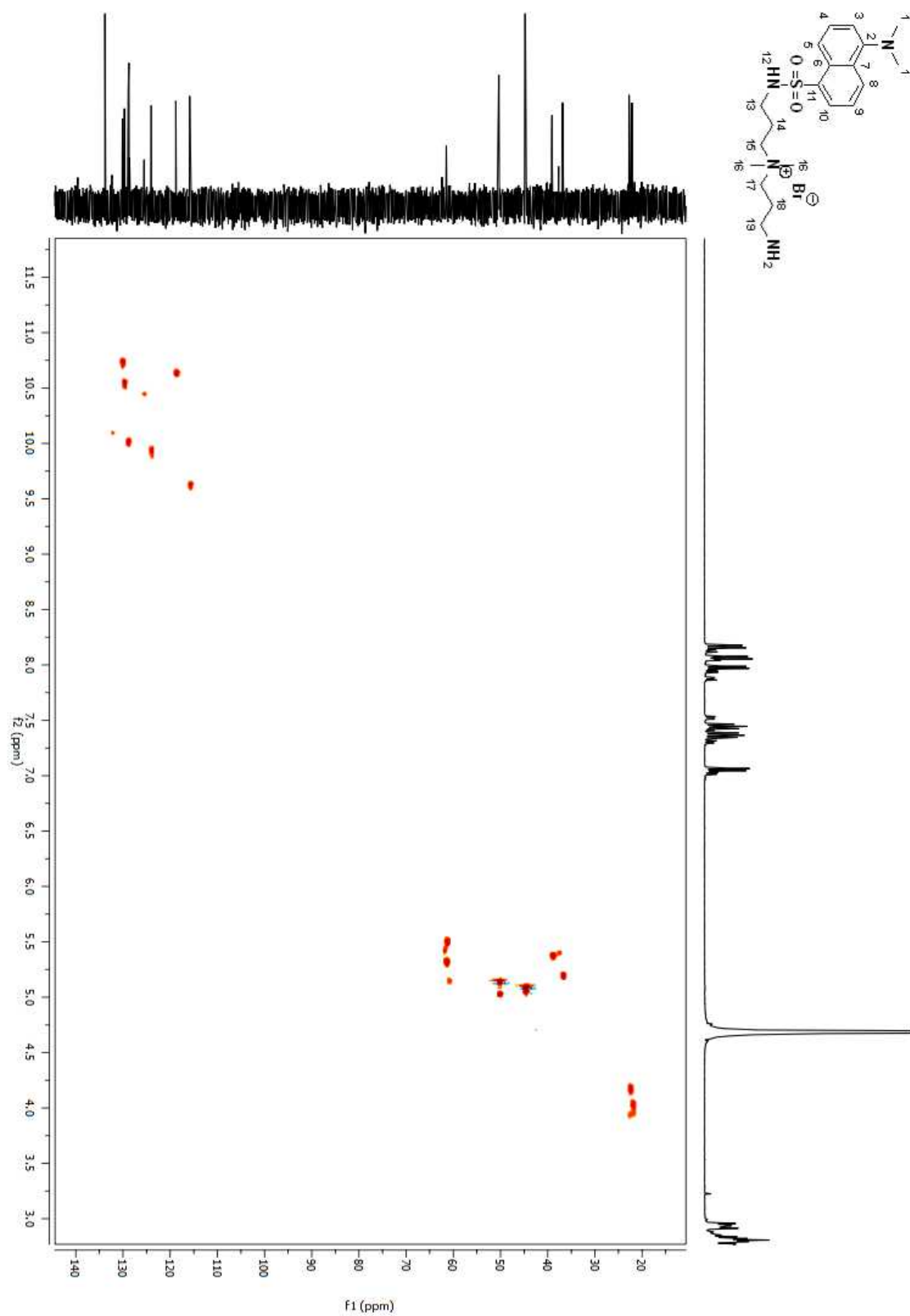


Figure A 389. HSQC 2D NMR spectrum of compound (221) in D₂O.

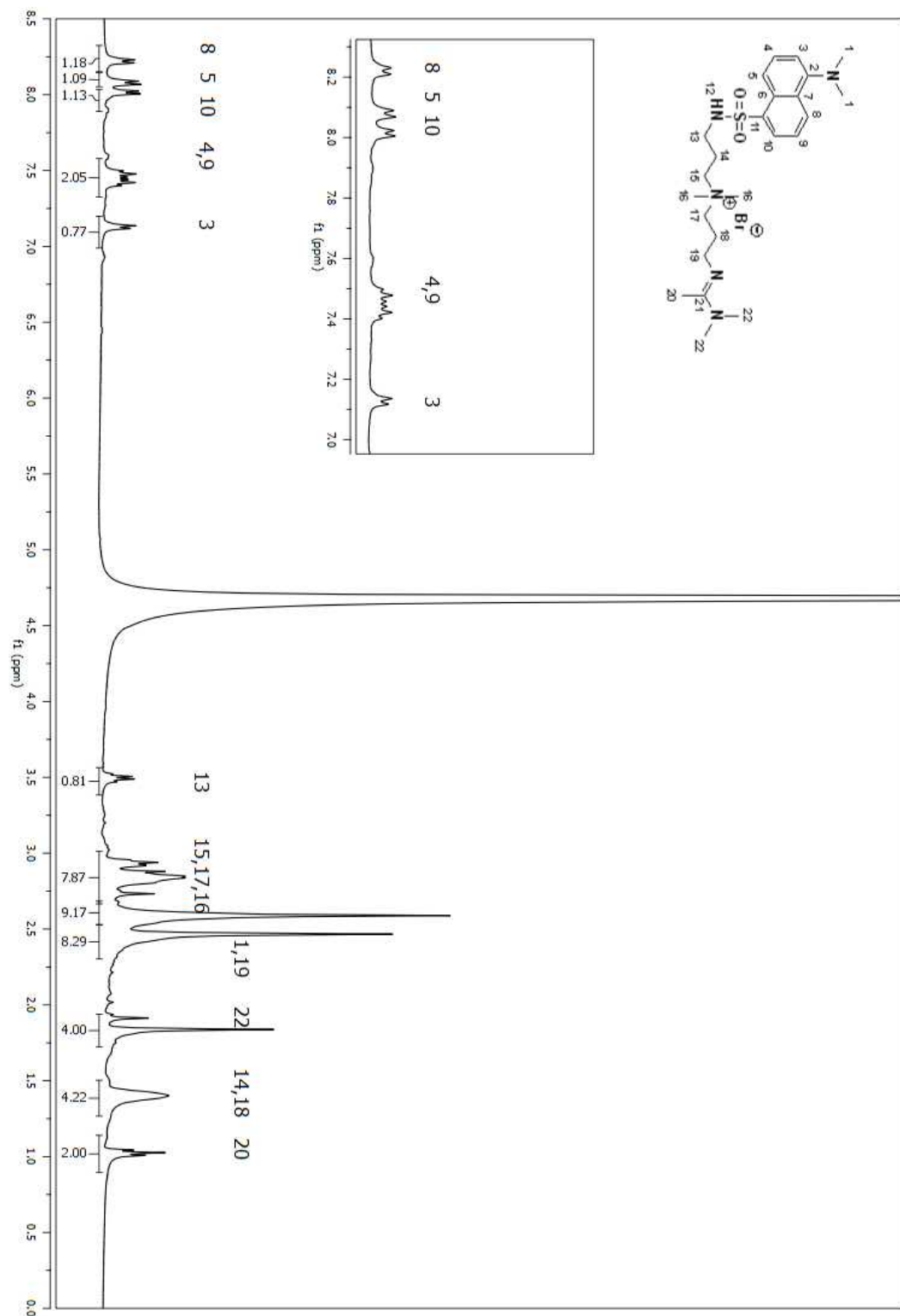


Figure A 390. ^1H NMR spectrum of compound (222) in D_2O .

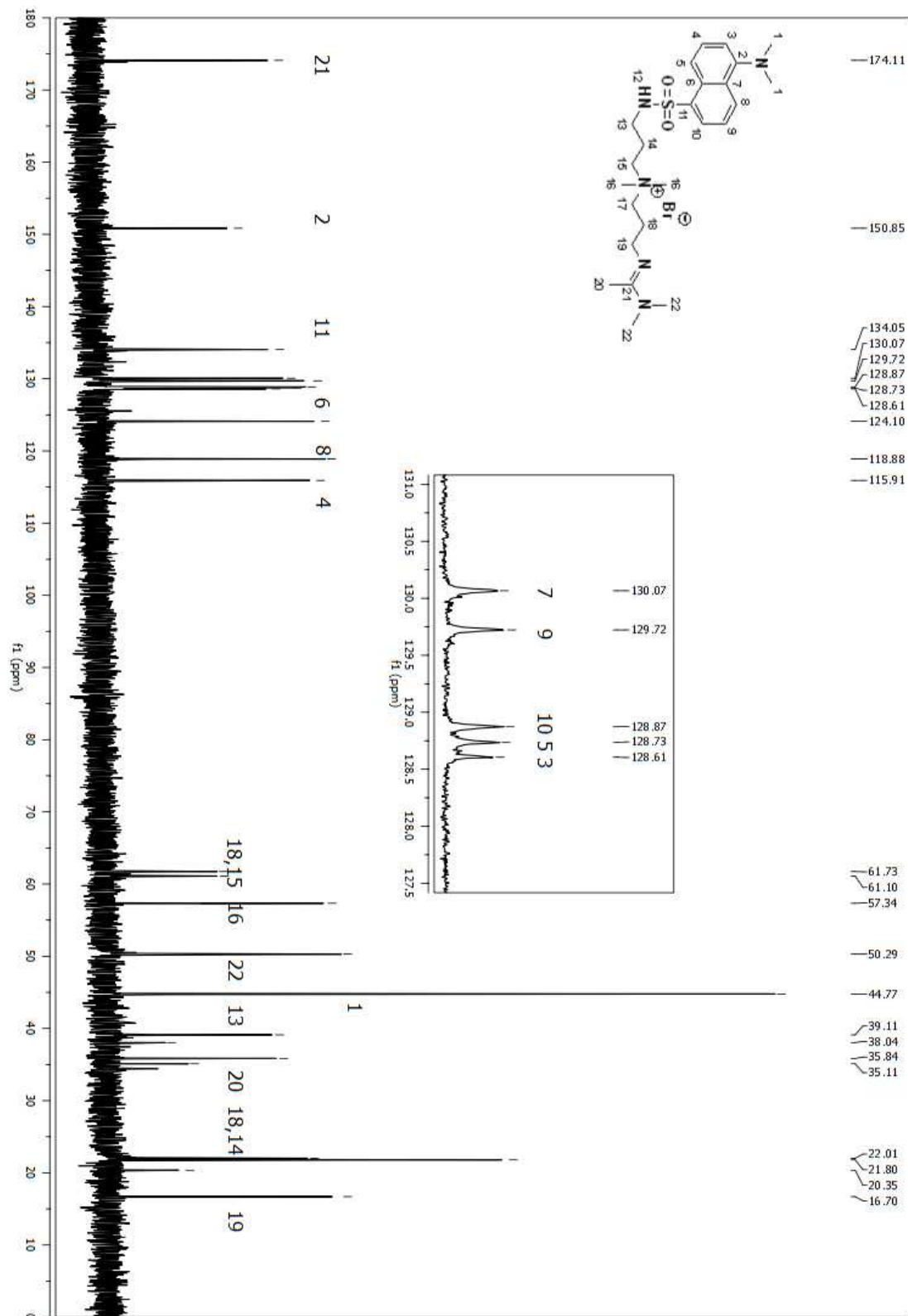


Figure A 391. ¹³C NMR spectrum of compound (222) in D₂O.

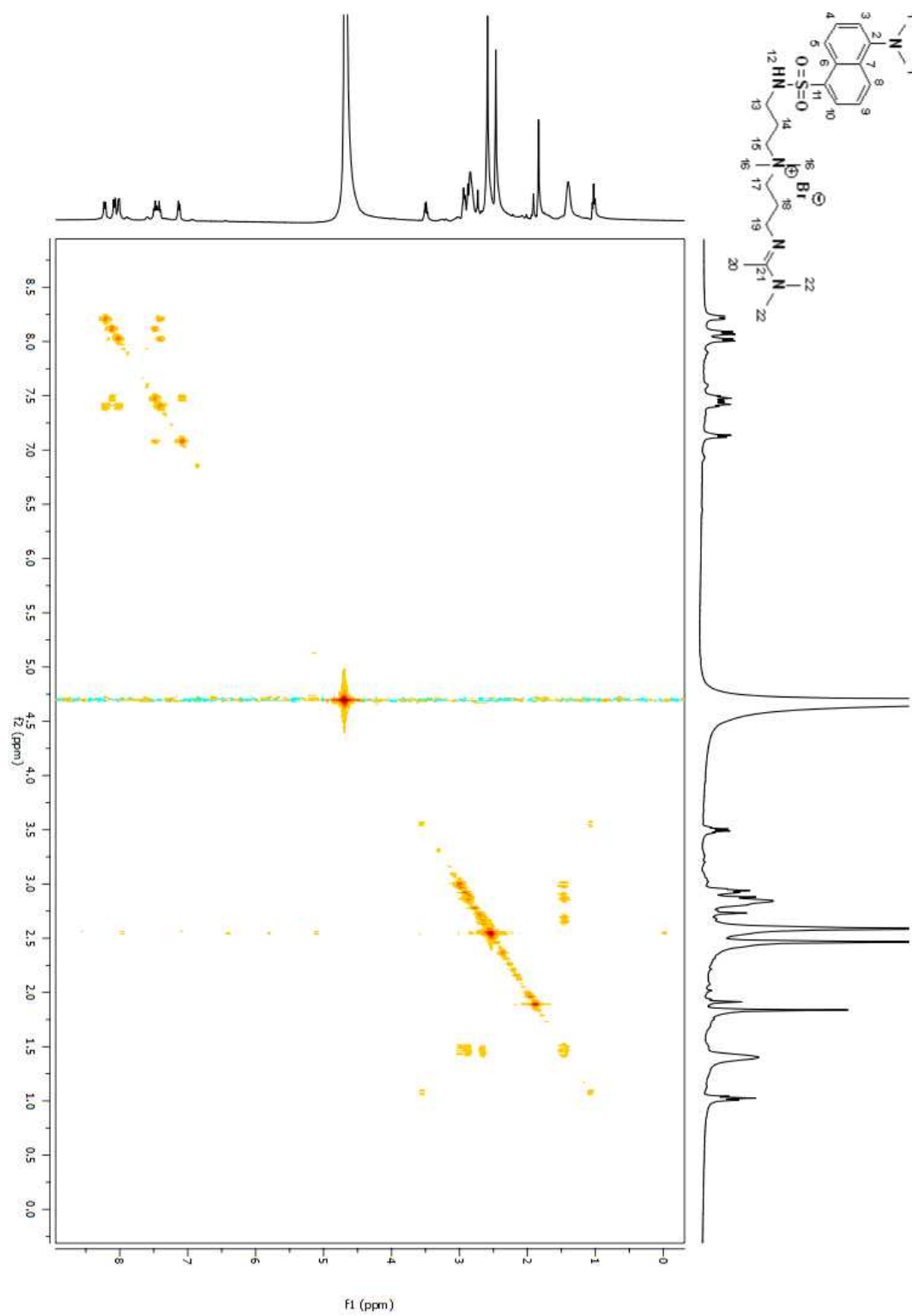


Figure A 392. COSY 2D NMR spectrum of compound (222) in D₂O.

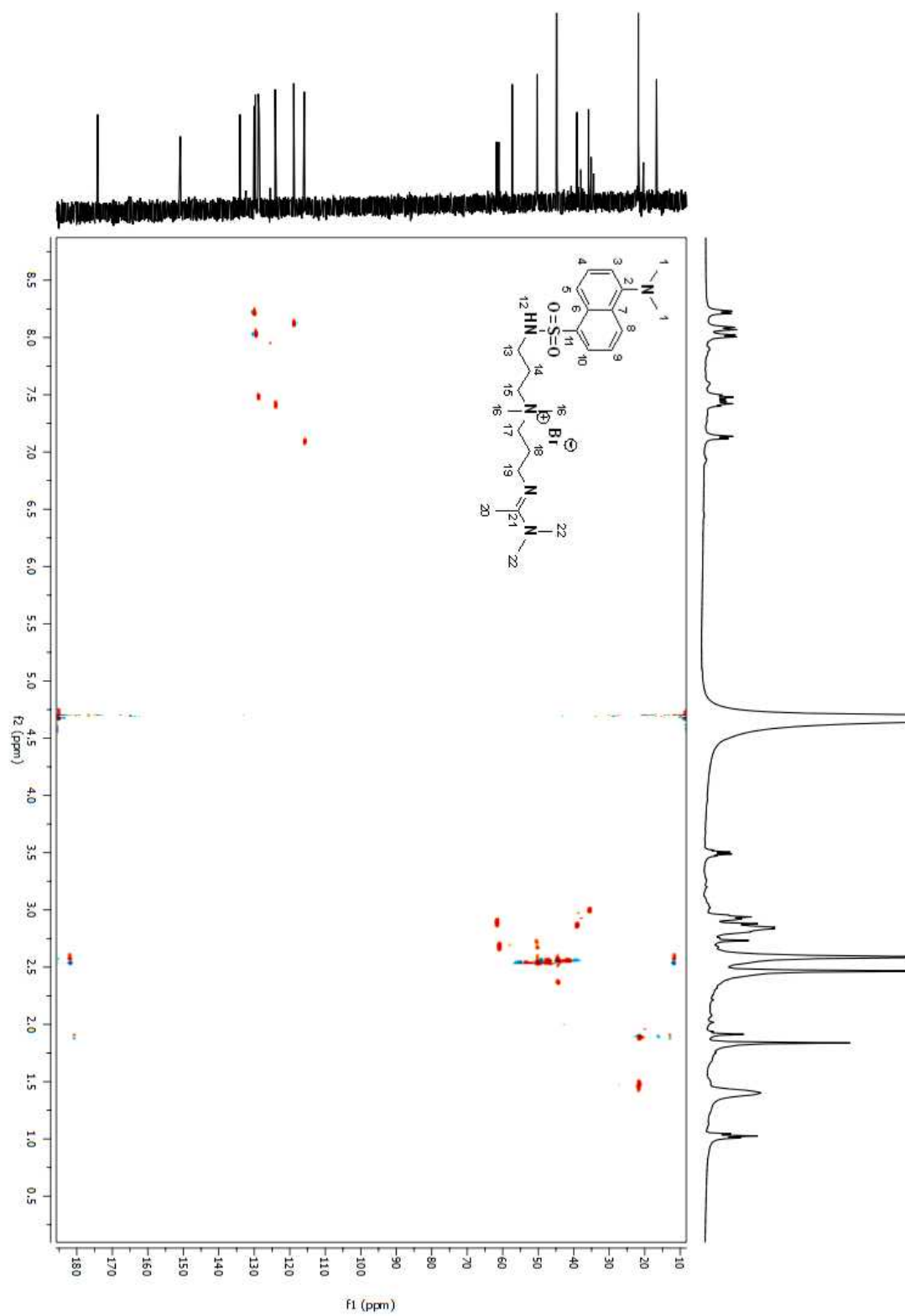


Figure A 393. HSQC 2D NMR spectrum of compound (222) in D₂O.

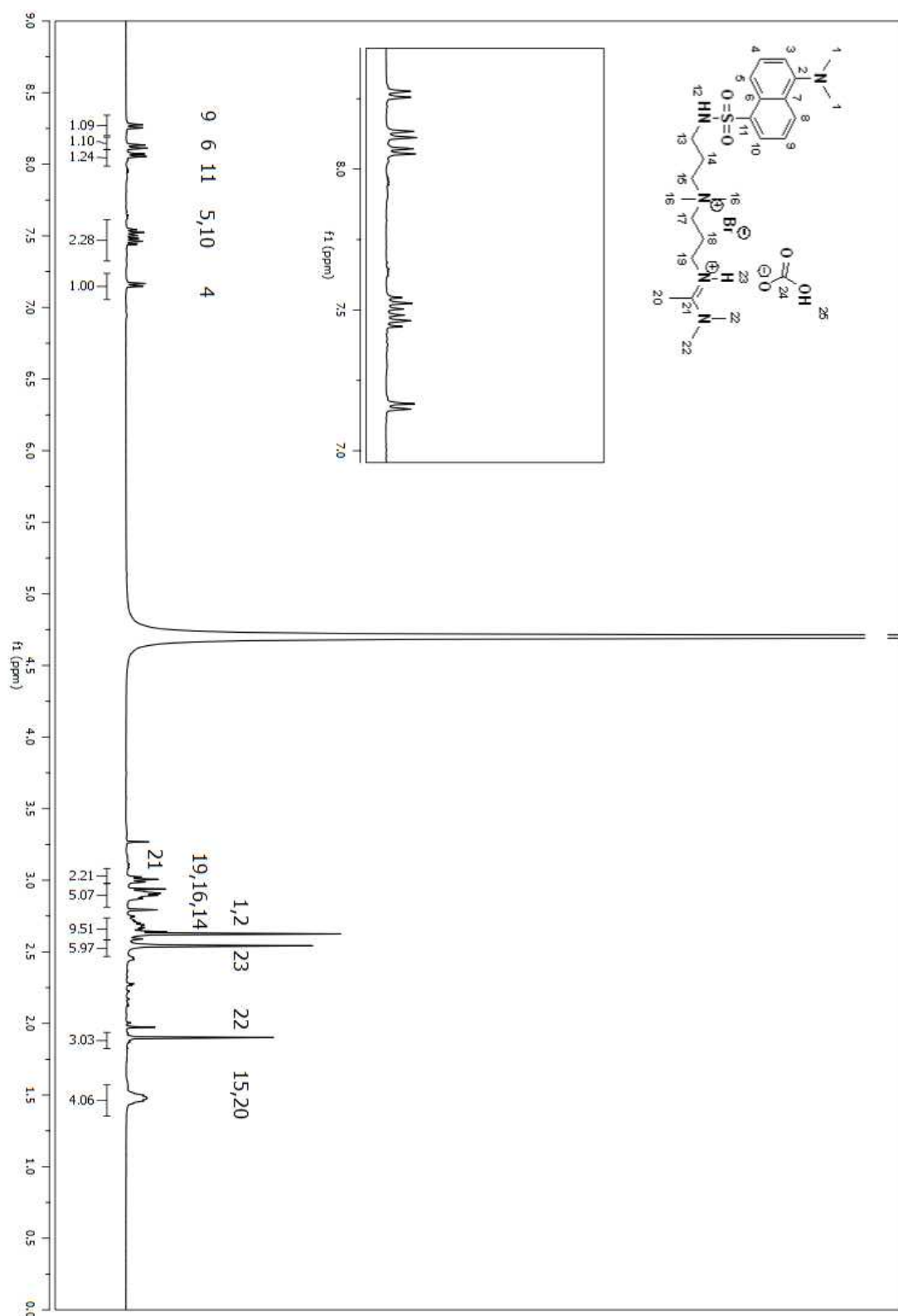


Figure A 394. ^1H NMR spectrum of compound (223) in D_2O .

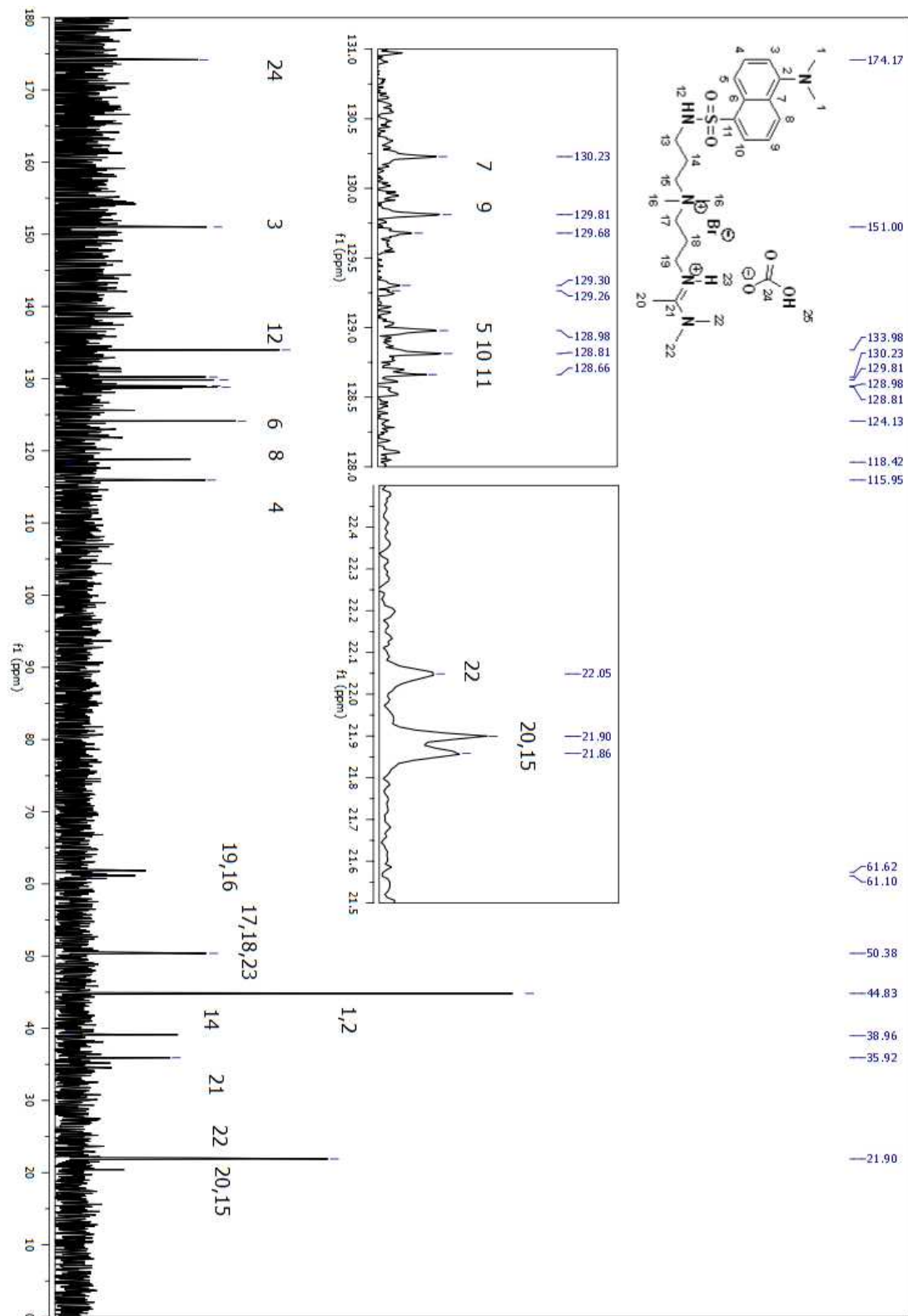


Figure A 395. ^{13}C NMR spectrum of compound (223) in D_2O .

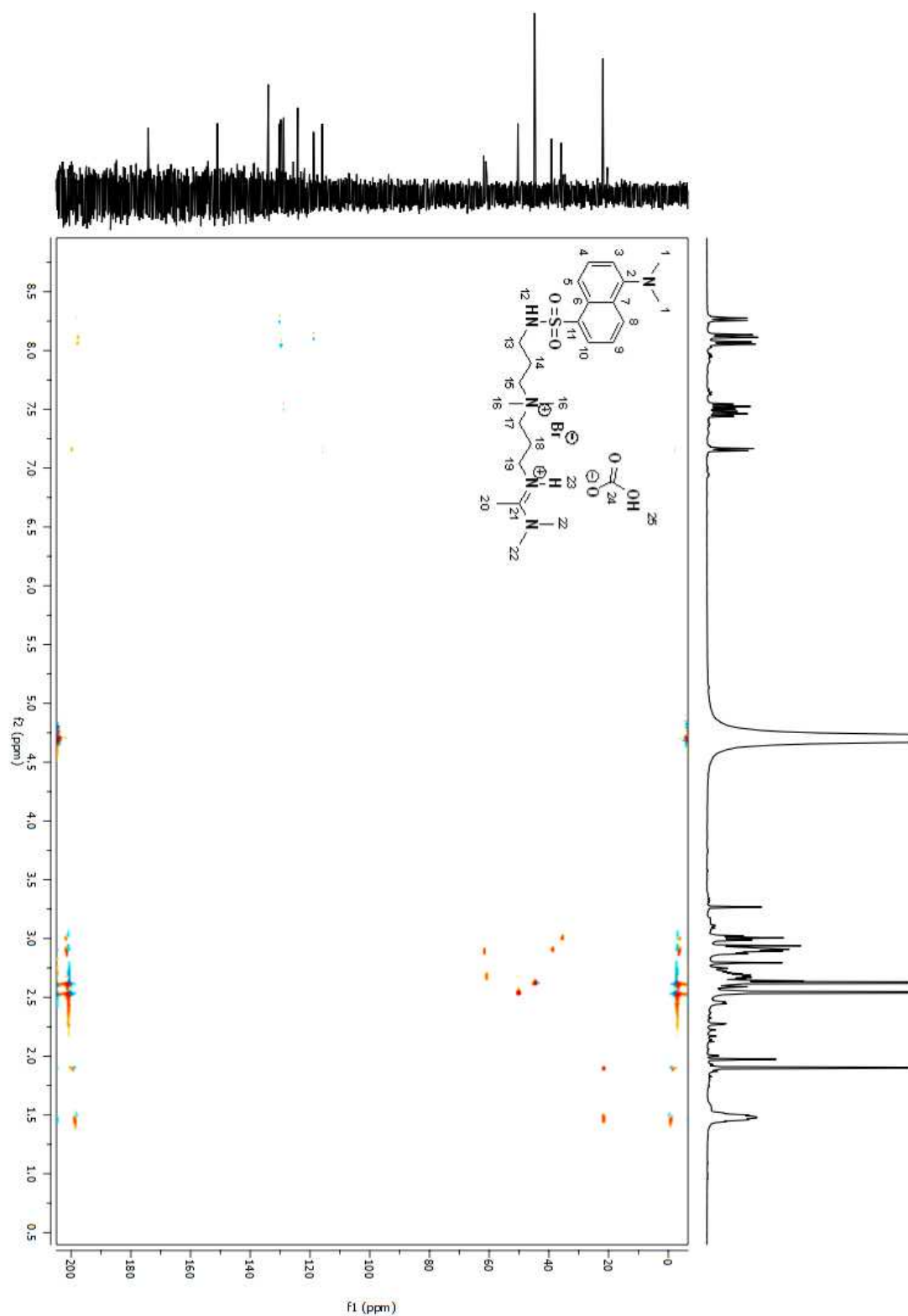


Figure A 396. HSQC 2D NMR spectrum of compound (223) in D₂O.

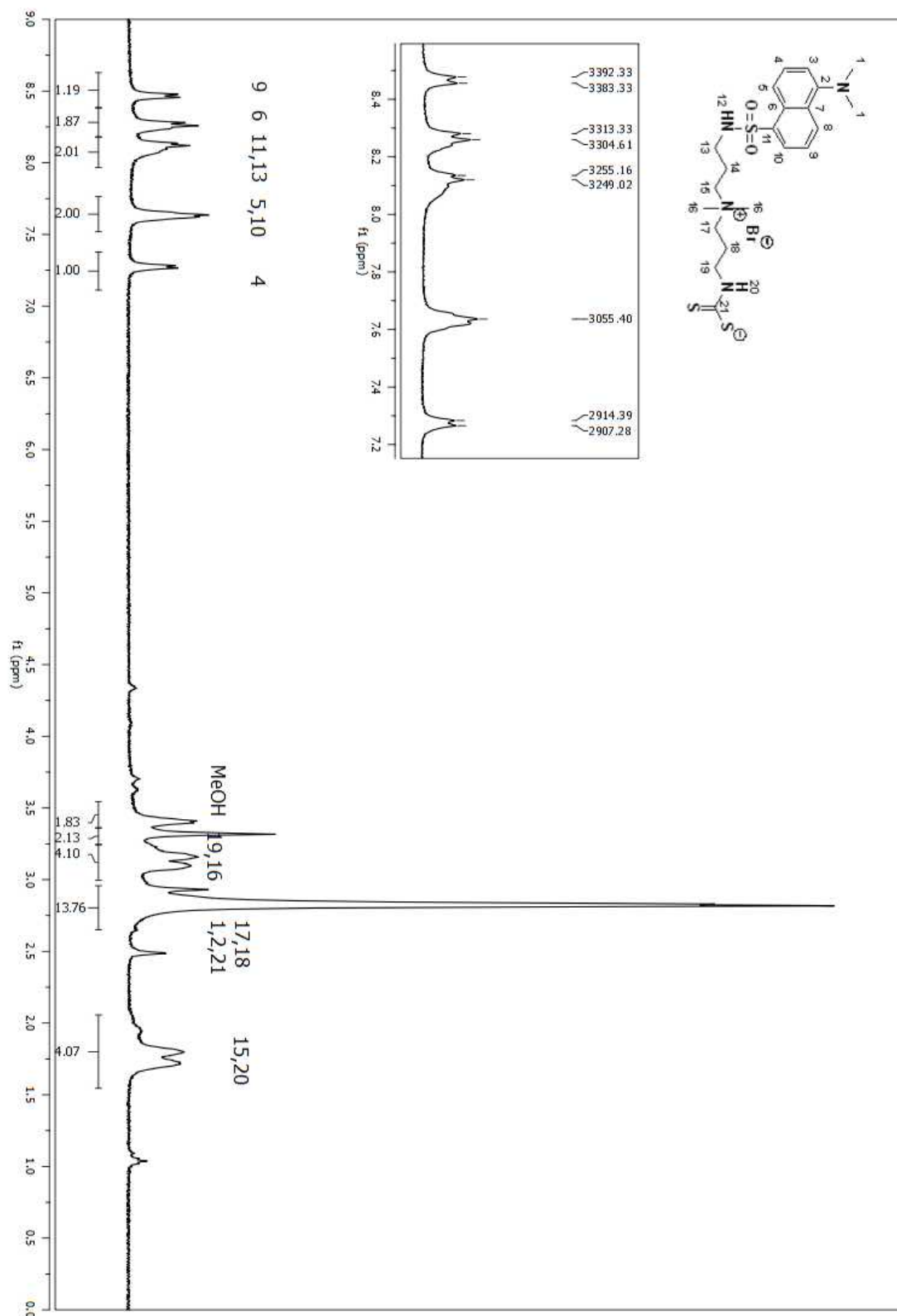


Figure A 397. ¹H NMR spectrum of compound (**225**) in DMSO-d₆.

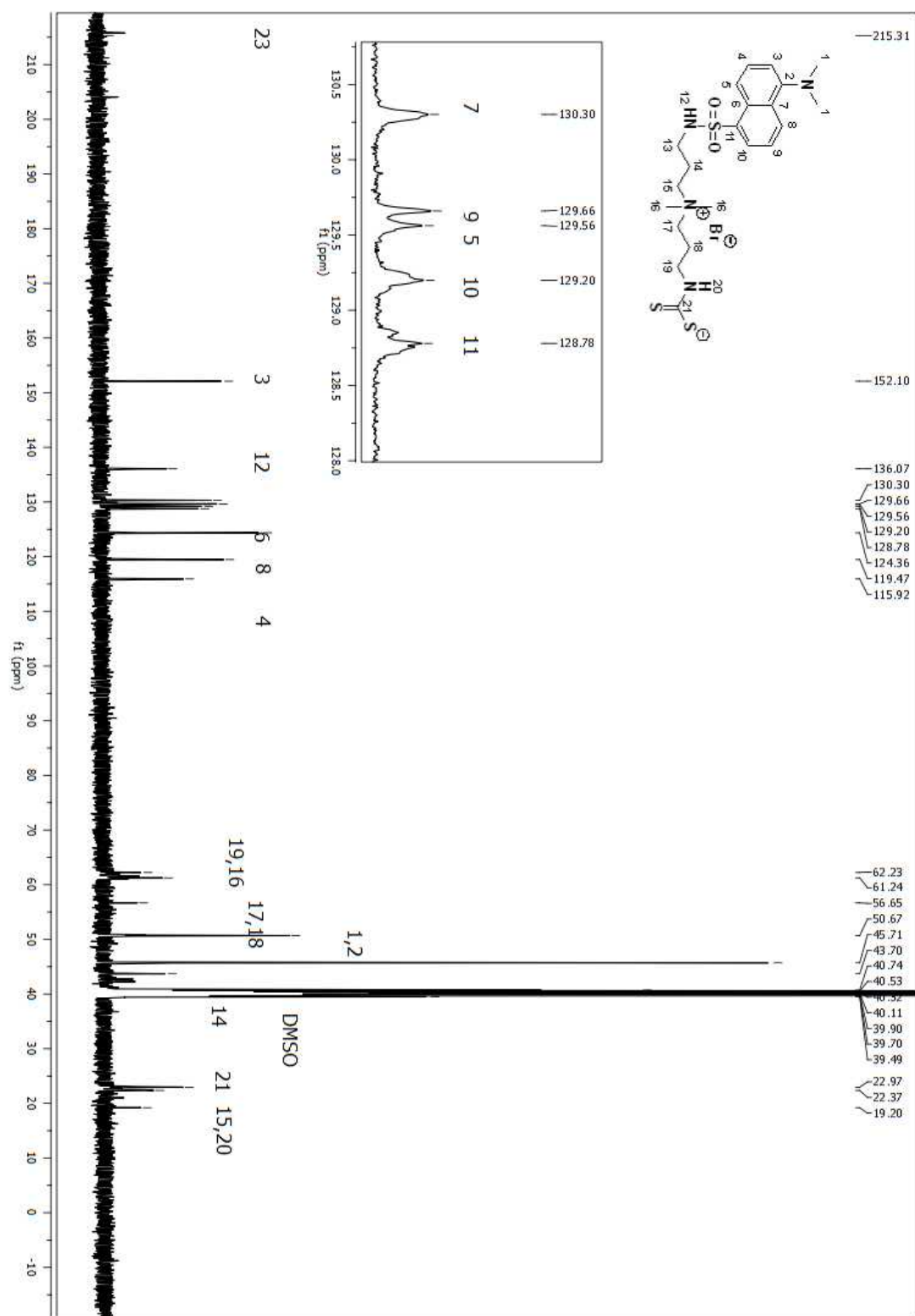


Figure A 398. ^{13}C NMR spectrum of compound (**225**) in DMSO- d_6 .

6.6 Appendix 1.3 – MS Spectra

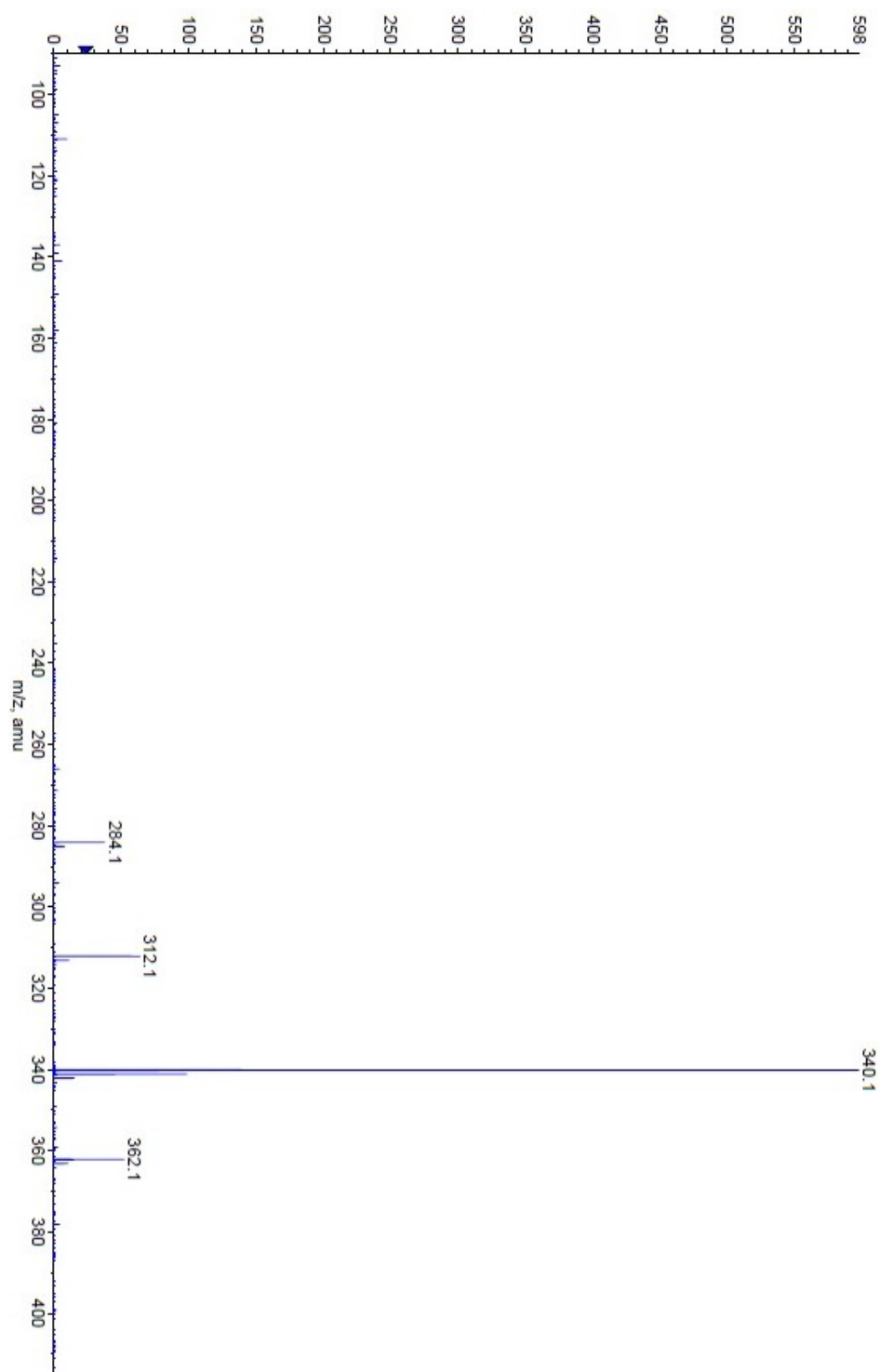


Figure A 399. ESI-TOF spectrum of compound **19**.

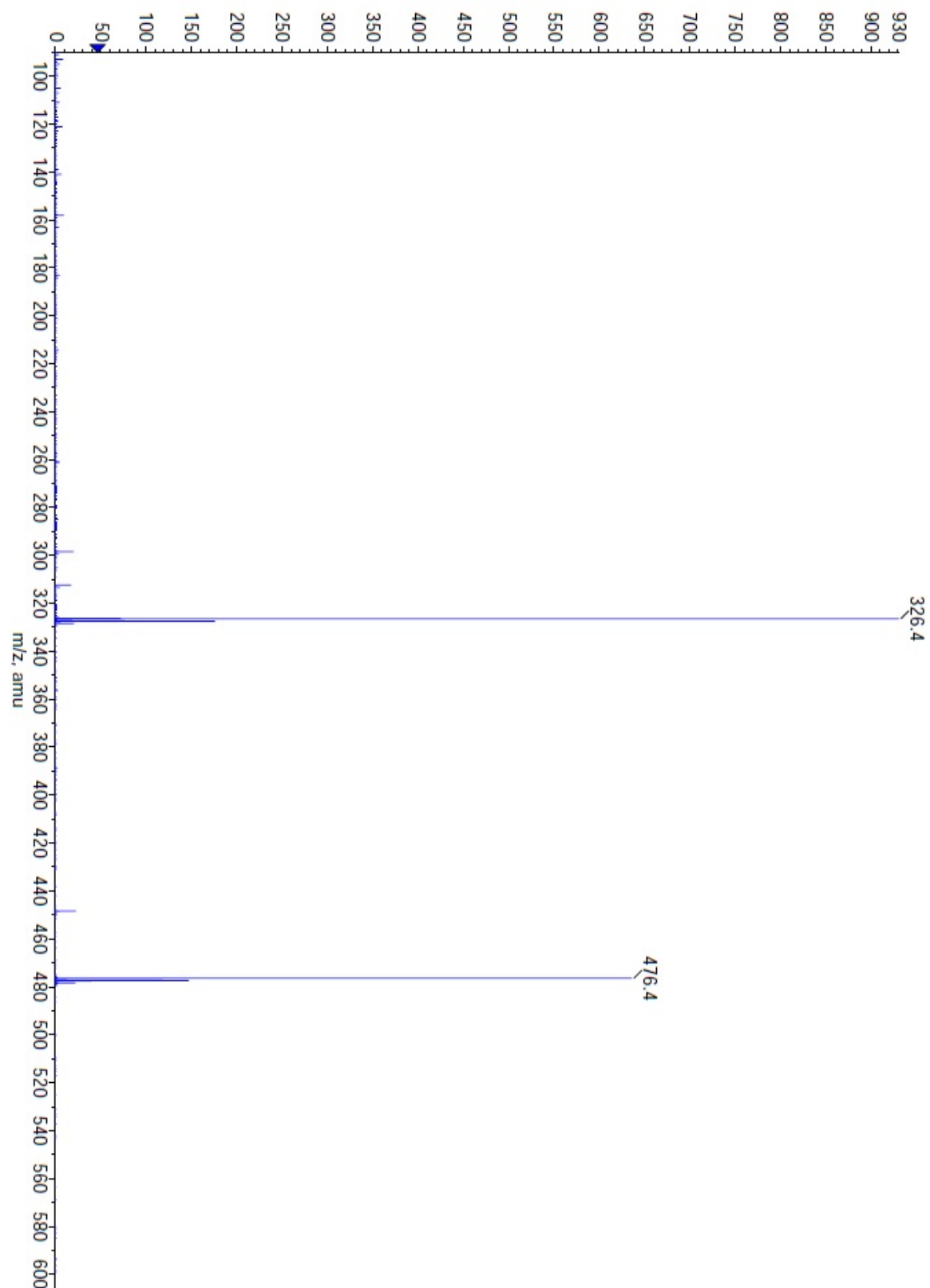


Figure A 400. ESI-TOF spectrum of compound **26**.

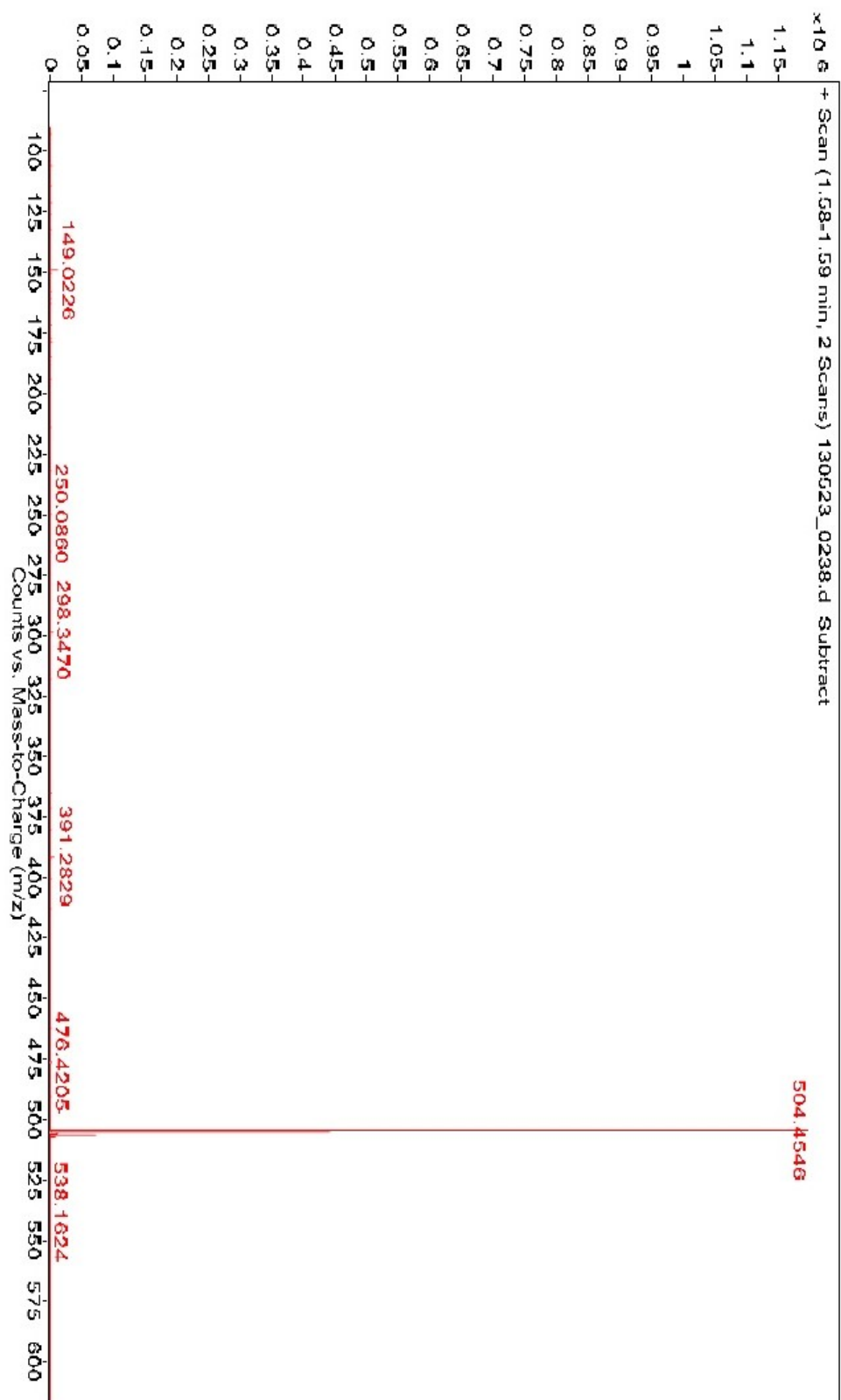


Figure A 401. HRMS ESI-TOF spectrum of compound **27**.

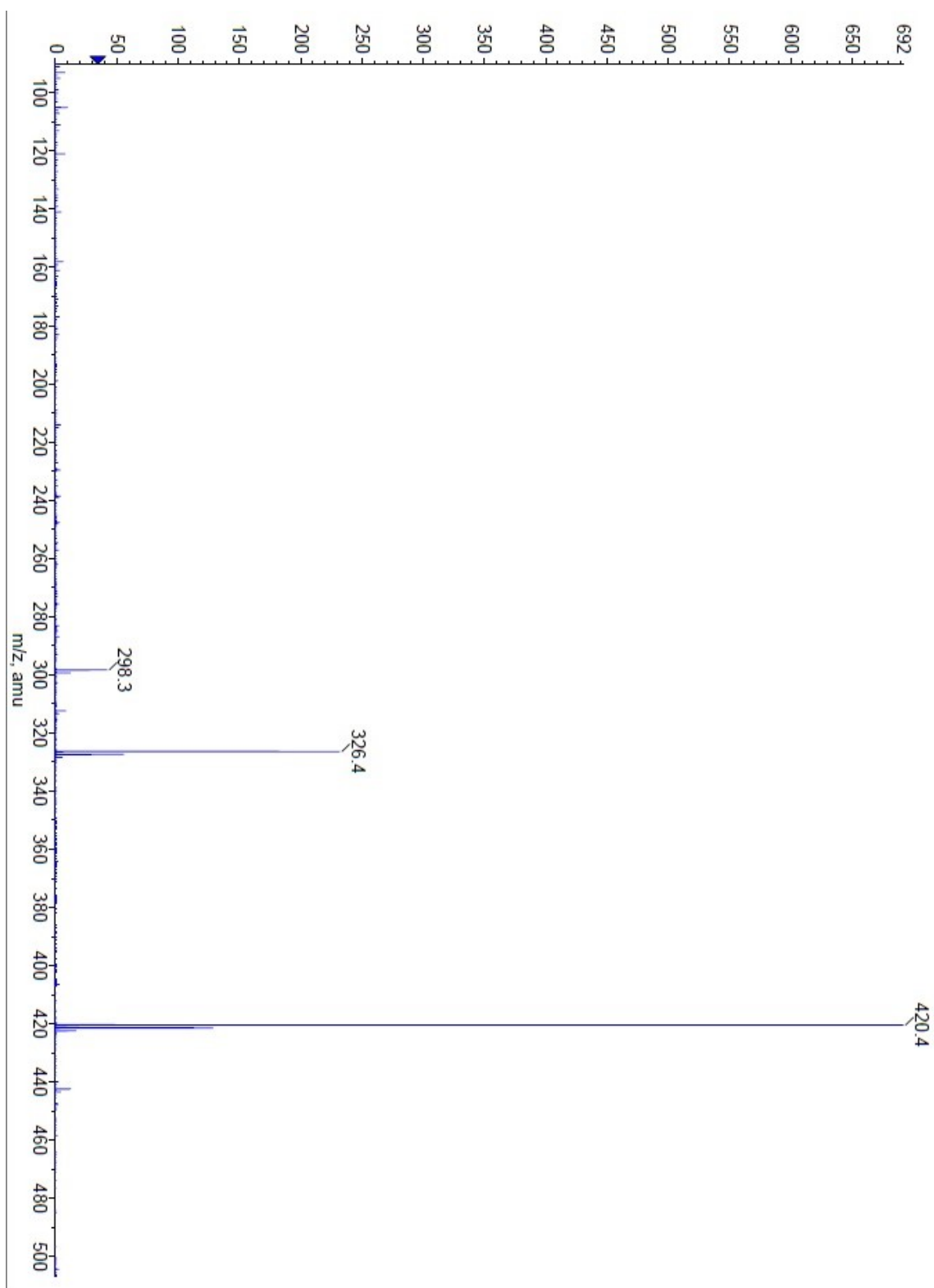


Figure A 402. ESI-TOF spectrum of compound **34**.
769

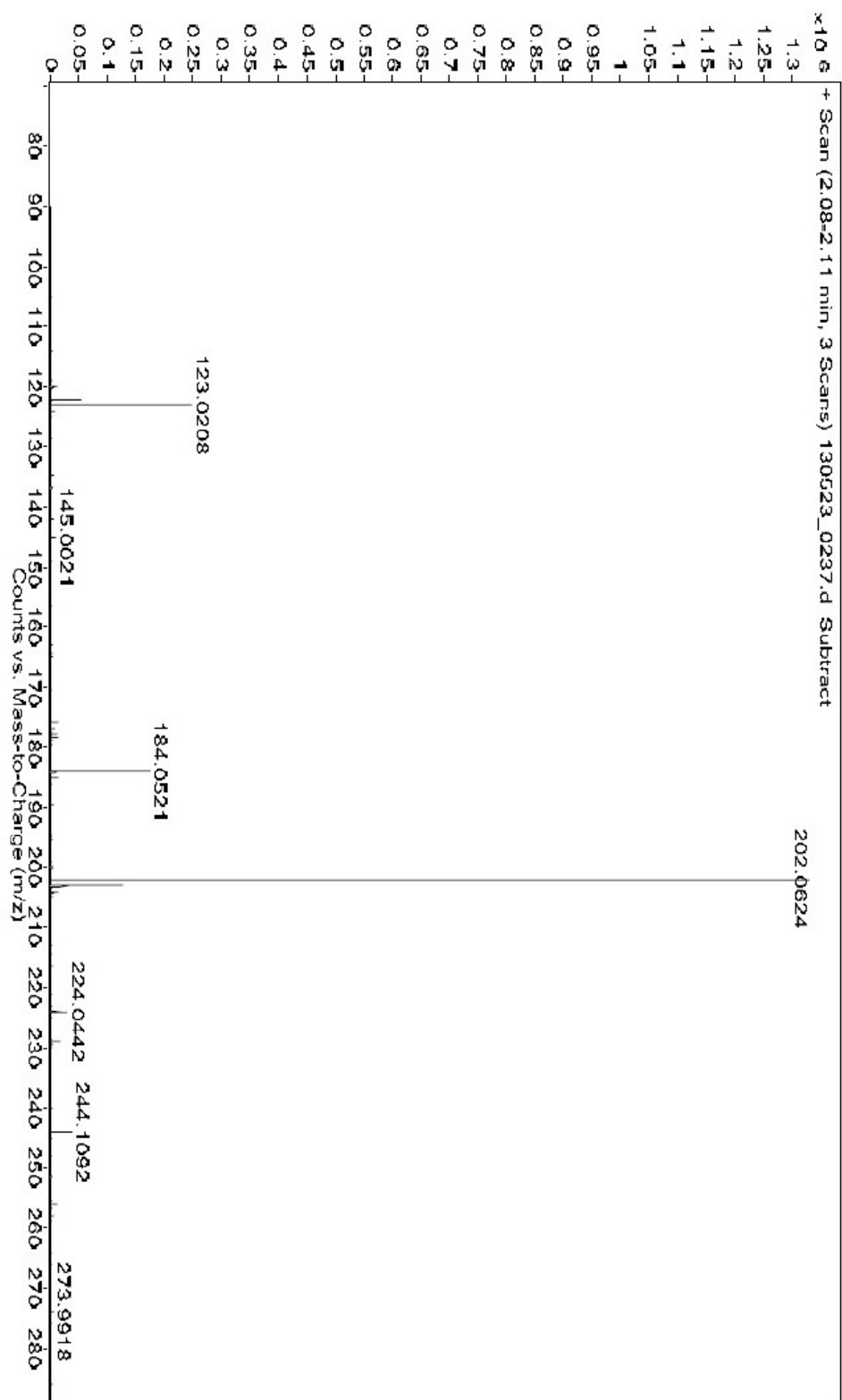


Figure A 403. HRMS ESI-TOF spectrum of compound **36**.

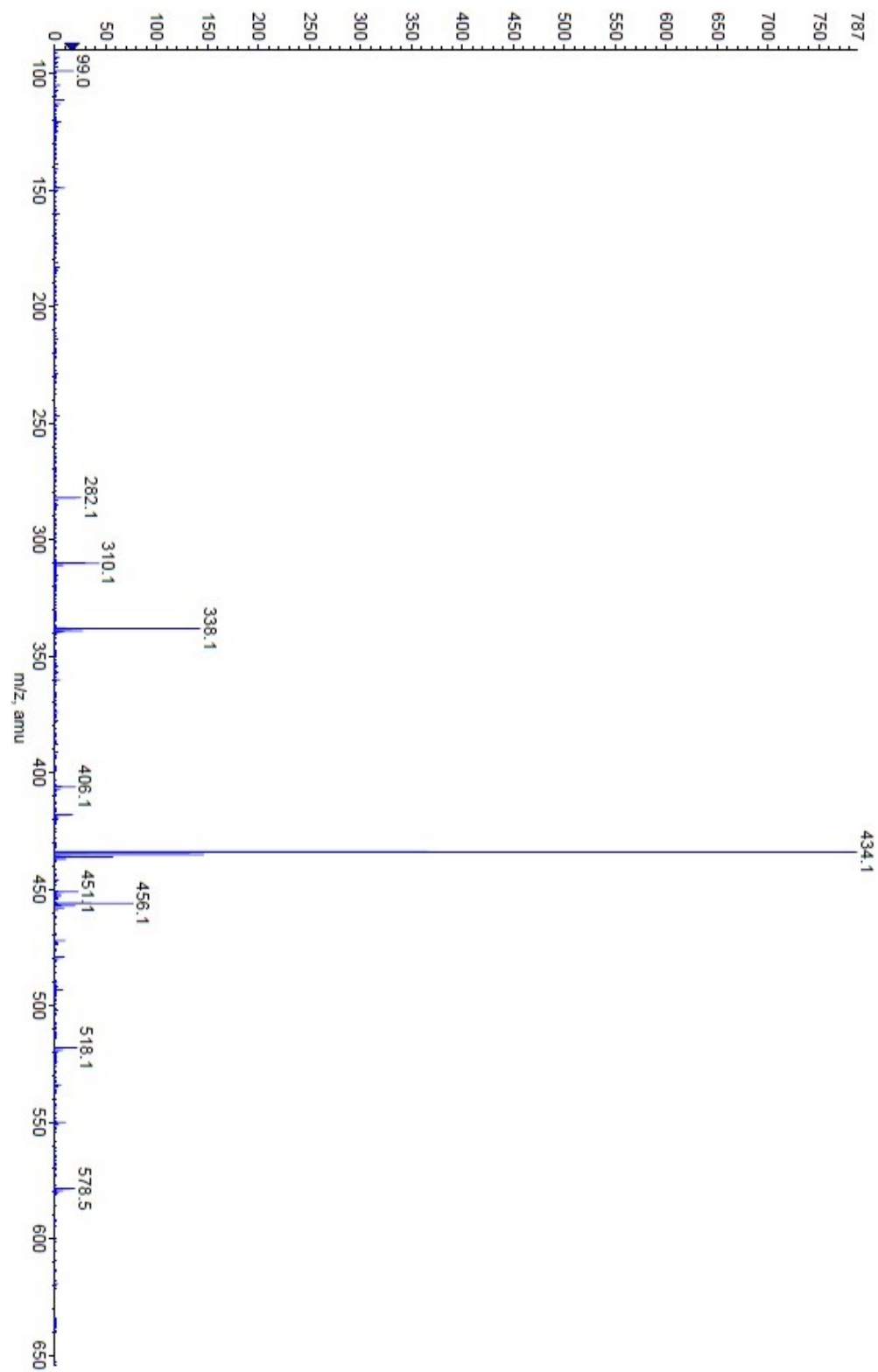


Figure A 404. ESI-TOF spectrum of compound **51**.

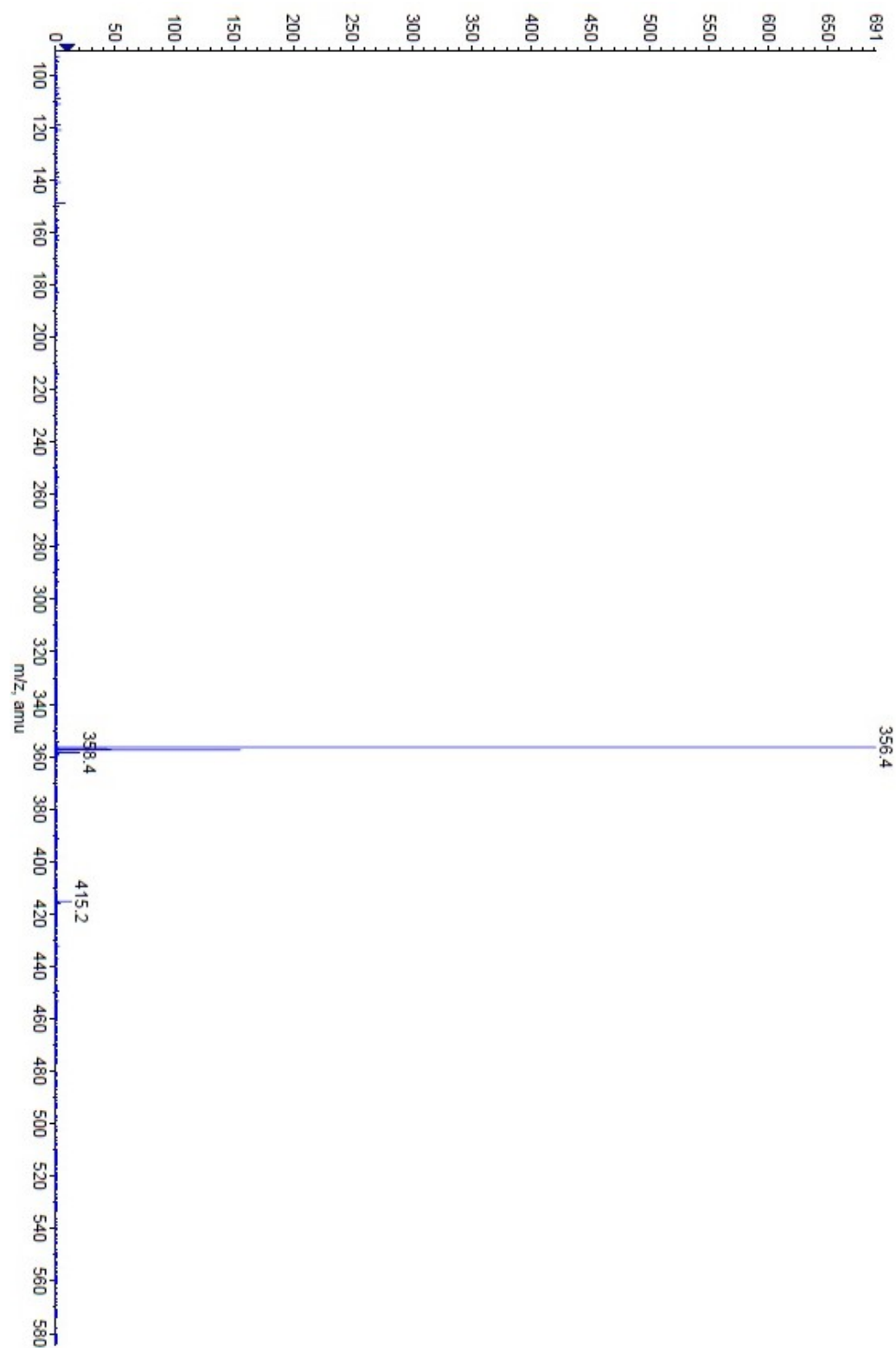


Figure A 405. ESI-TOF spectrum of compound **66**.

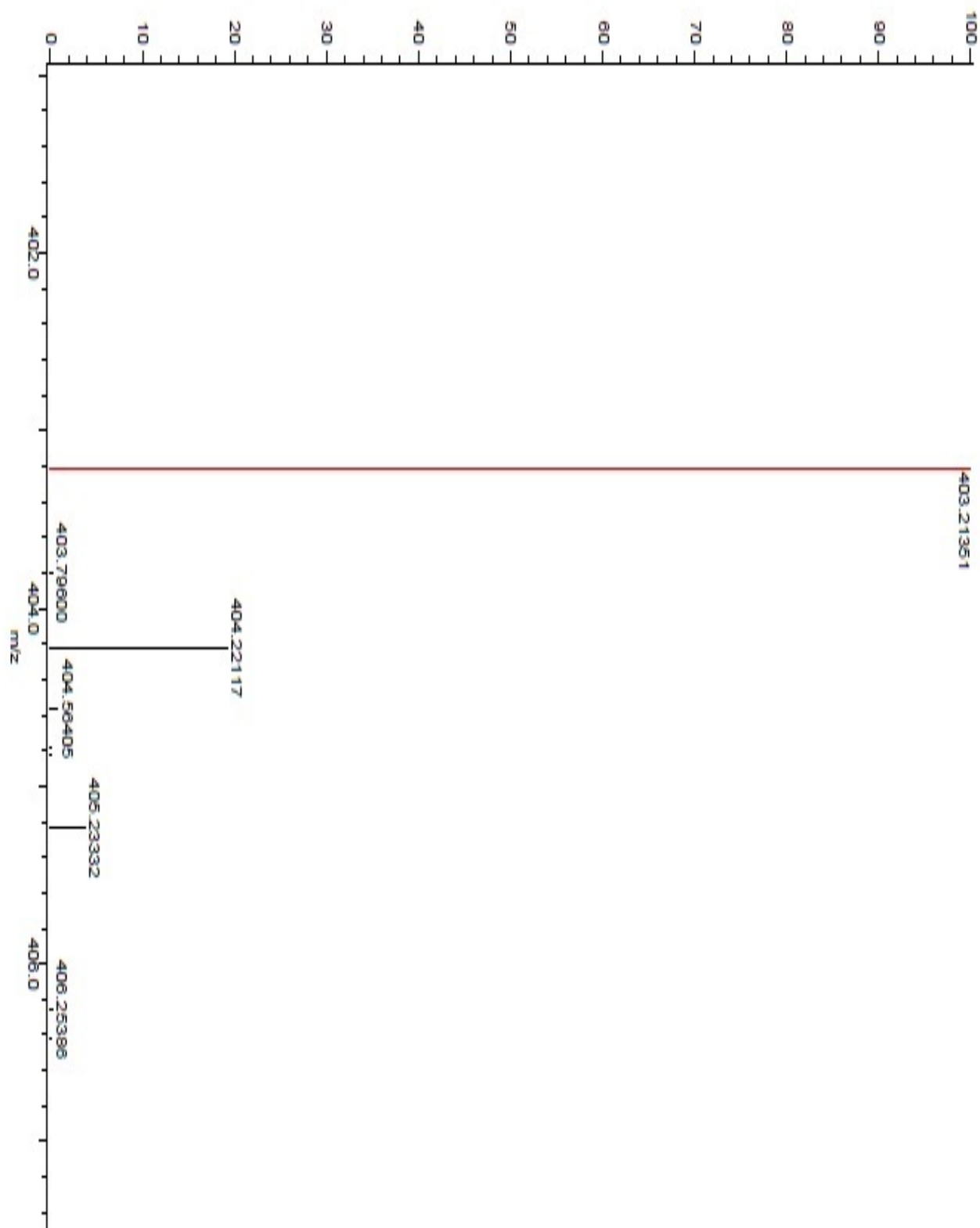


Figure A 406 .DART-HRMS spectrum of compound **113**.

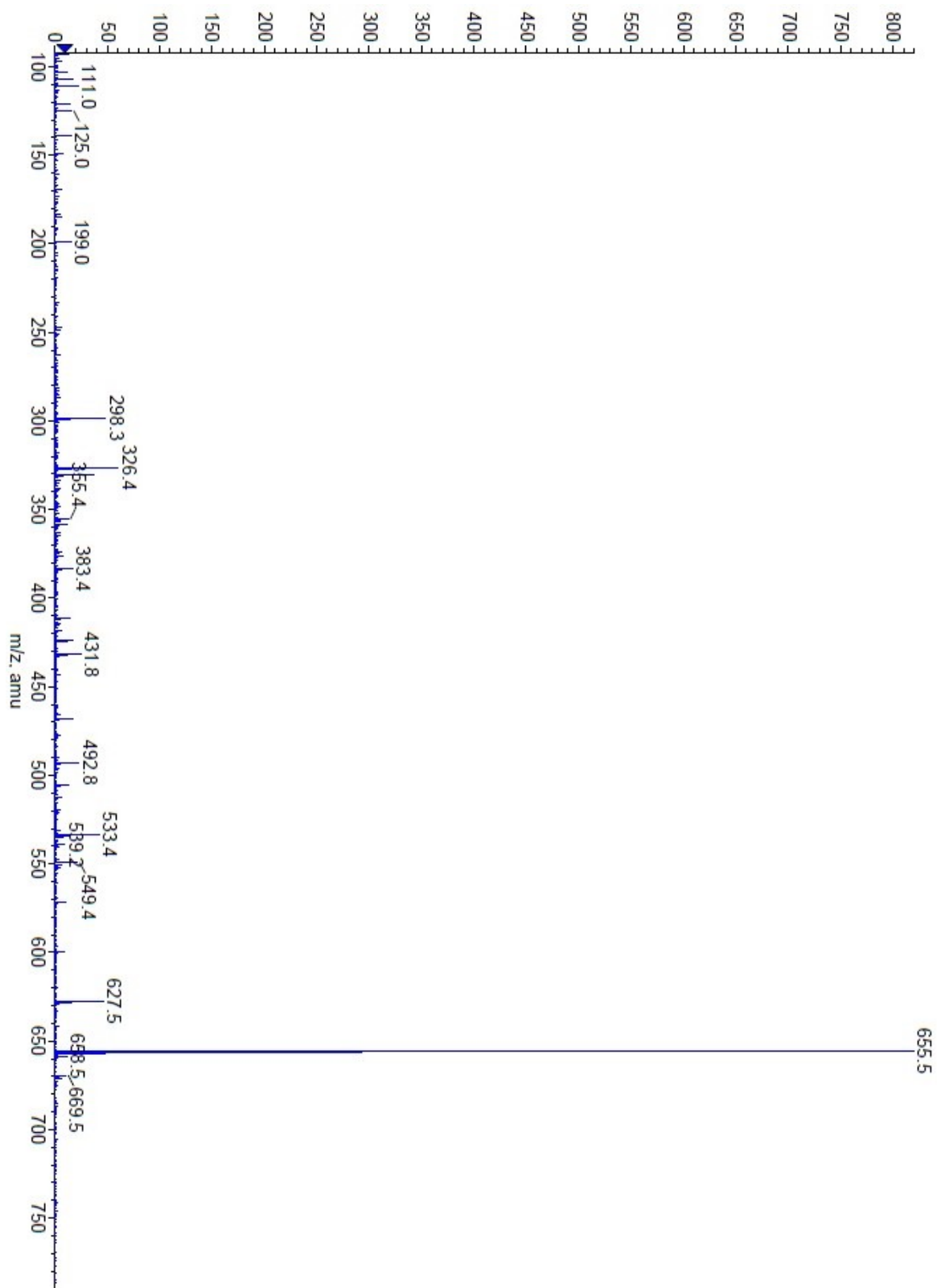


Figure A 407. ESI-TOF spectrum of compound **121**.

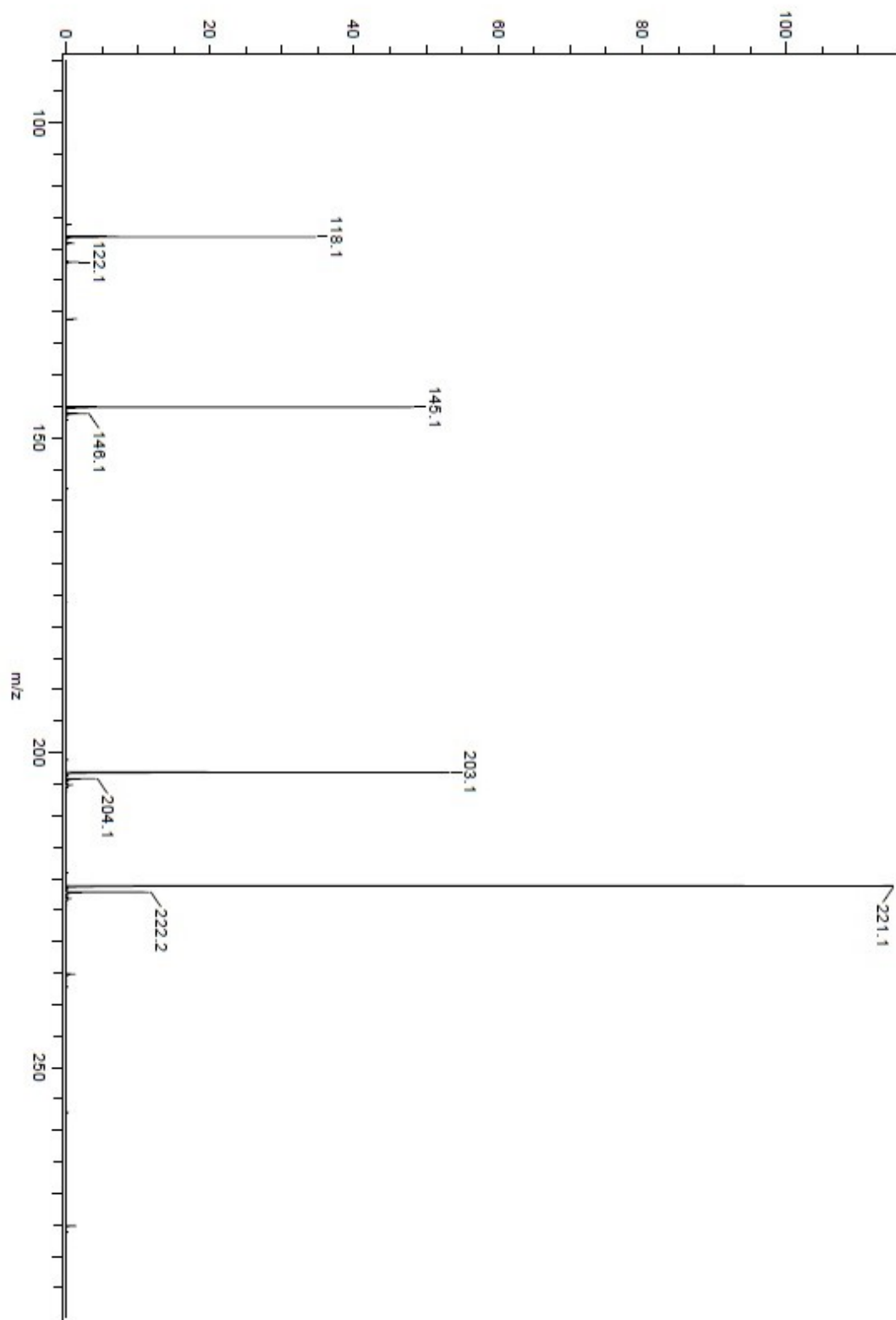


Figure A 408. DART spectrum of compound **163**.

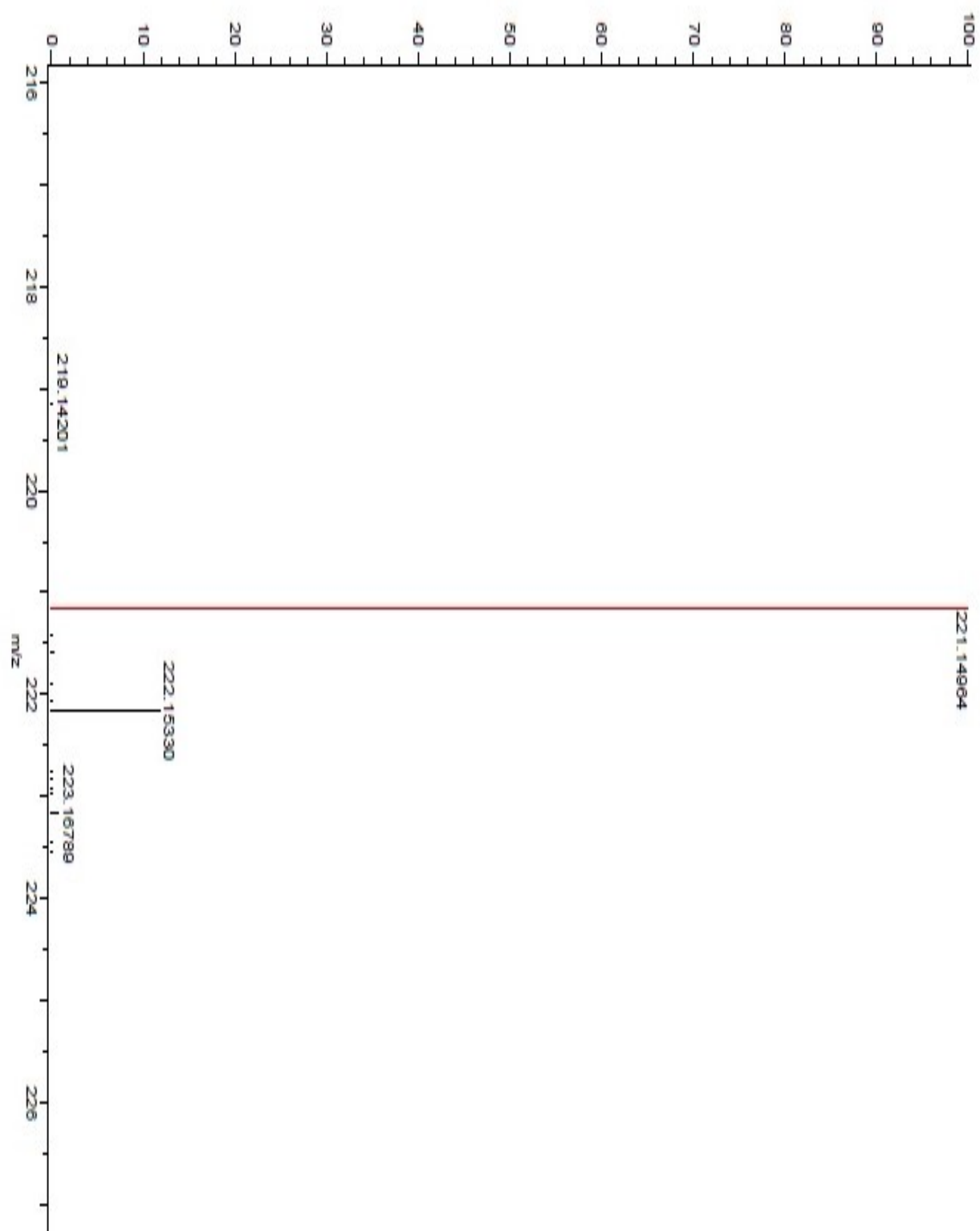


Figure A 409. HRMS-DART spectrum of compound **163**.

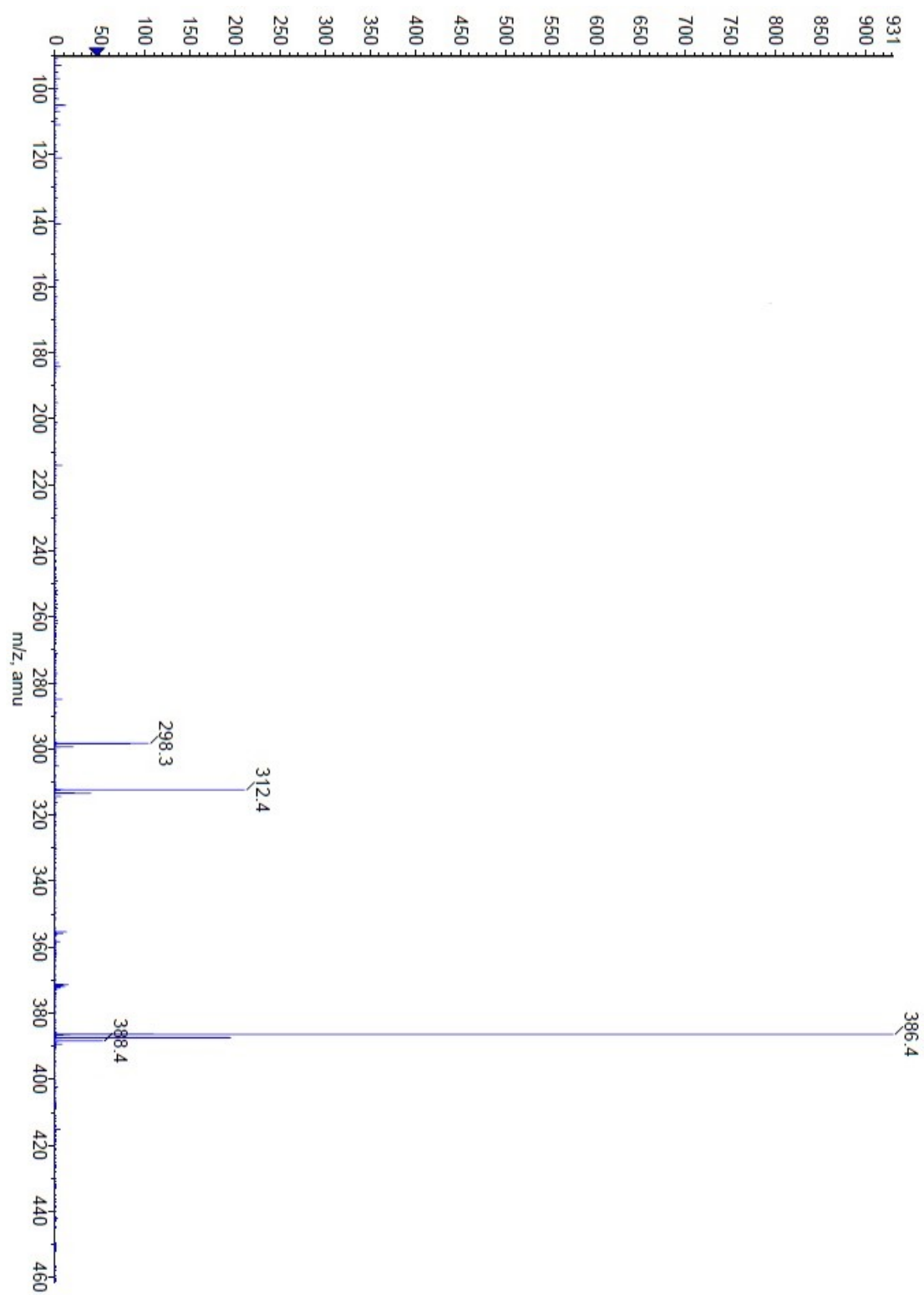


Figure A 410. ESI-TOF spectrum of compound **194**.

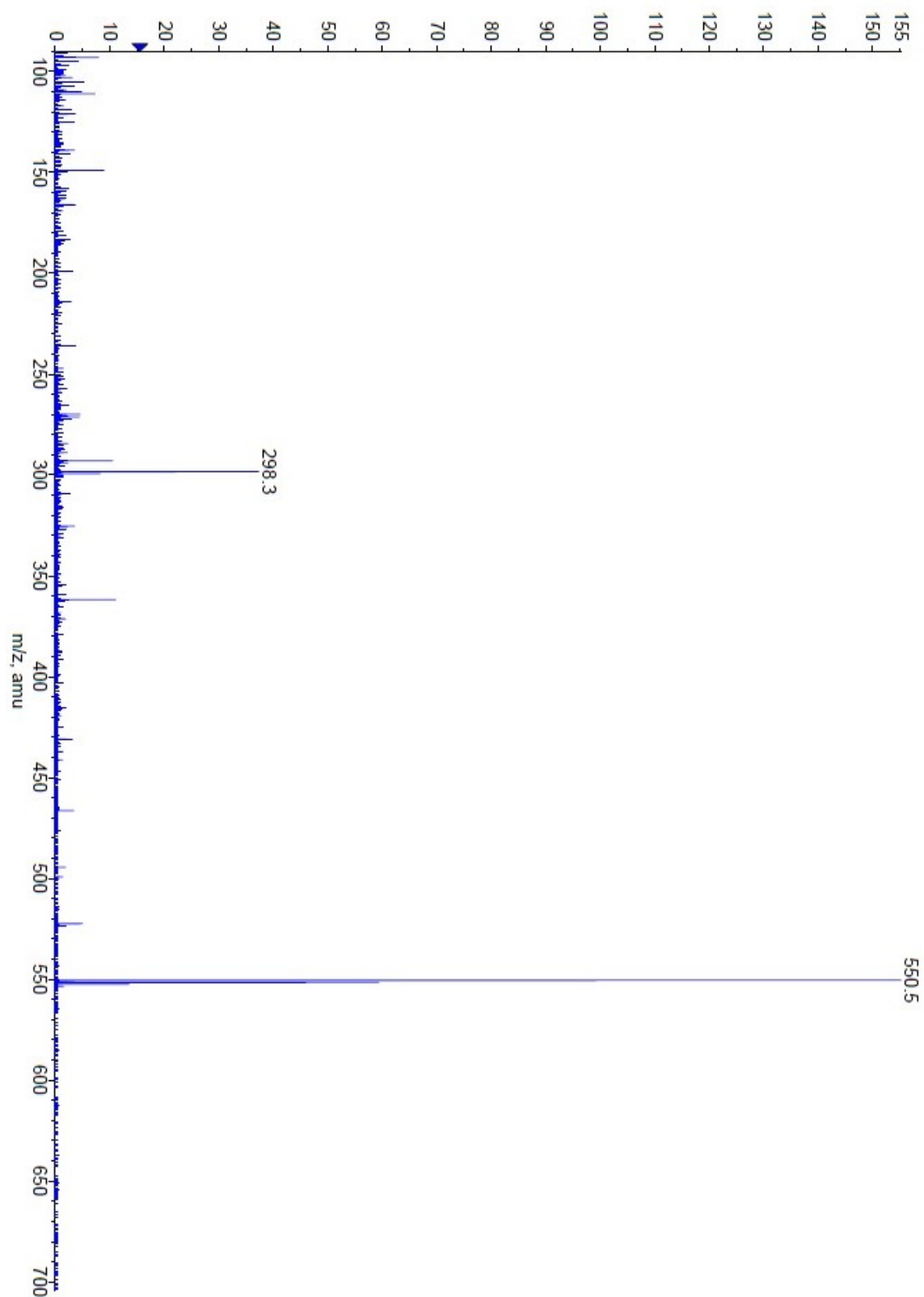


Figure A 411. ESI-TOF spectrum of compound **205**.

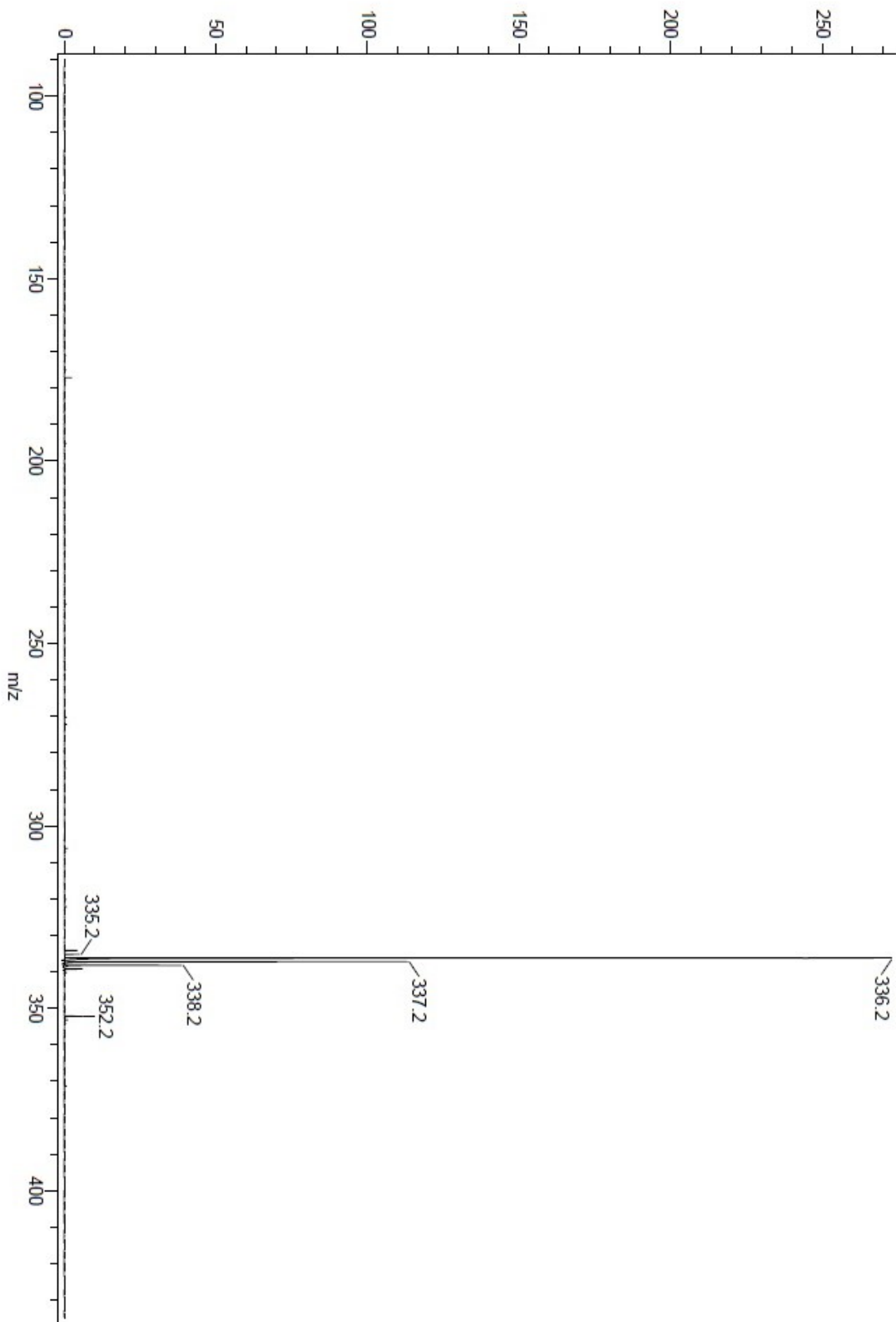


Figure A 412. DART spectrum of compound **208**.

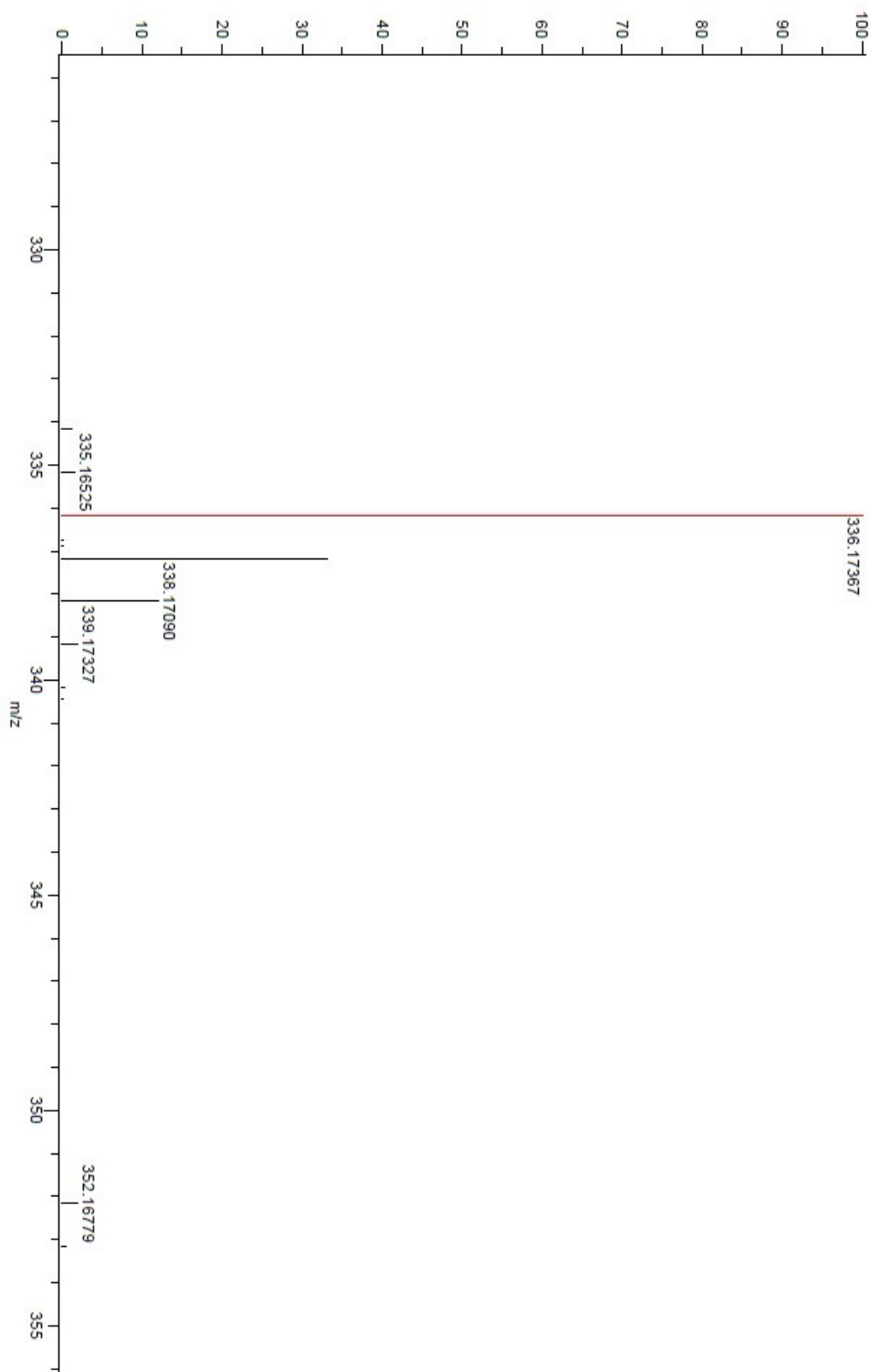


Figure A 413. HRMS-DART spectrum of compound **208**.

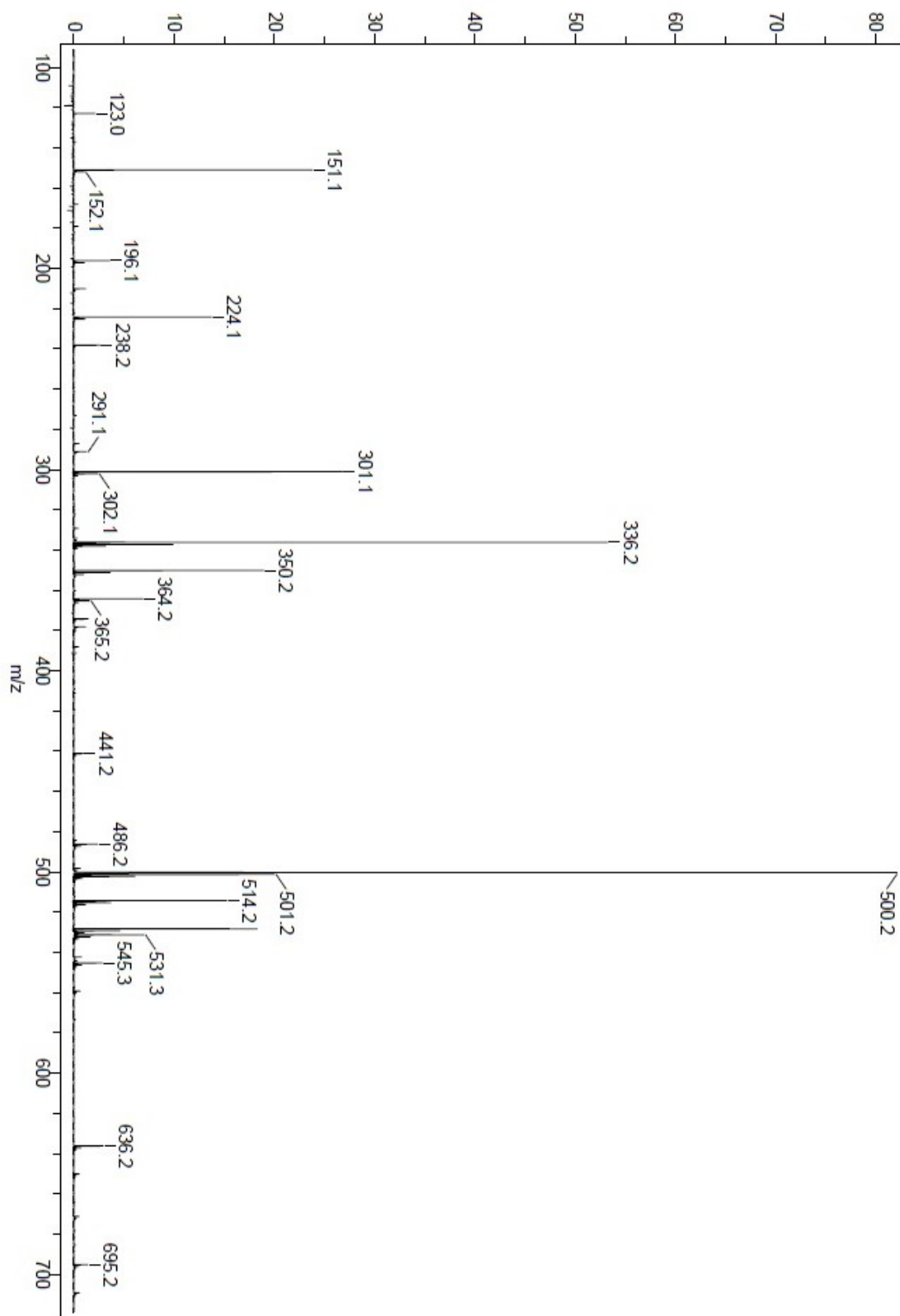


Figure A 414. DART spectrum of compound **211**.

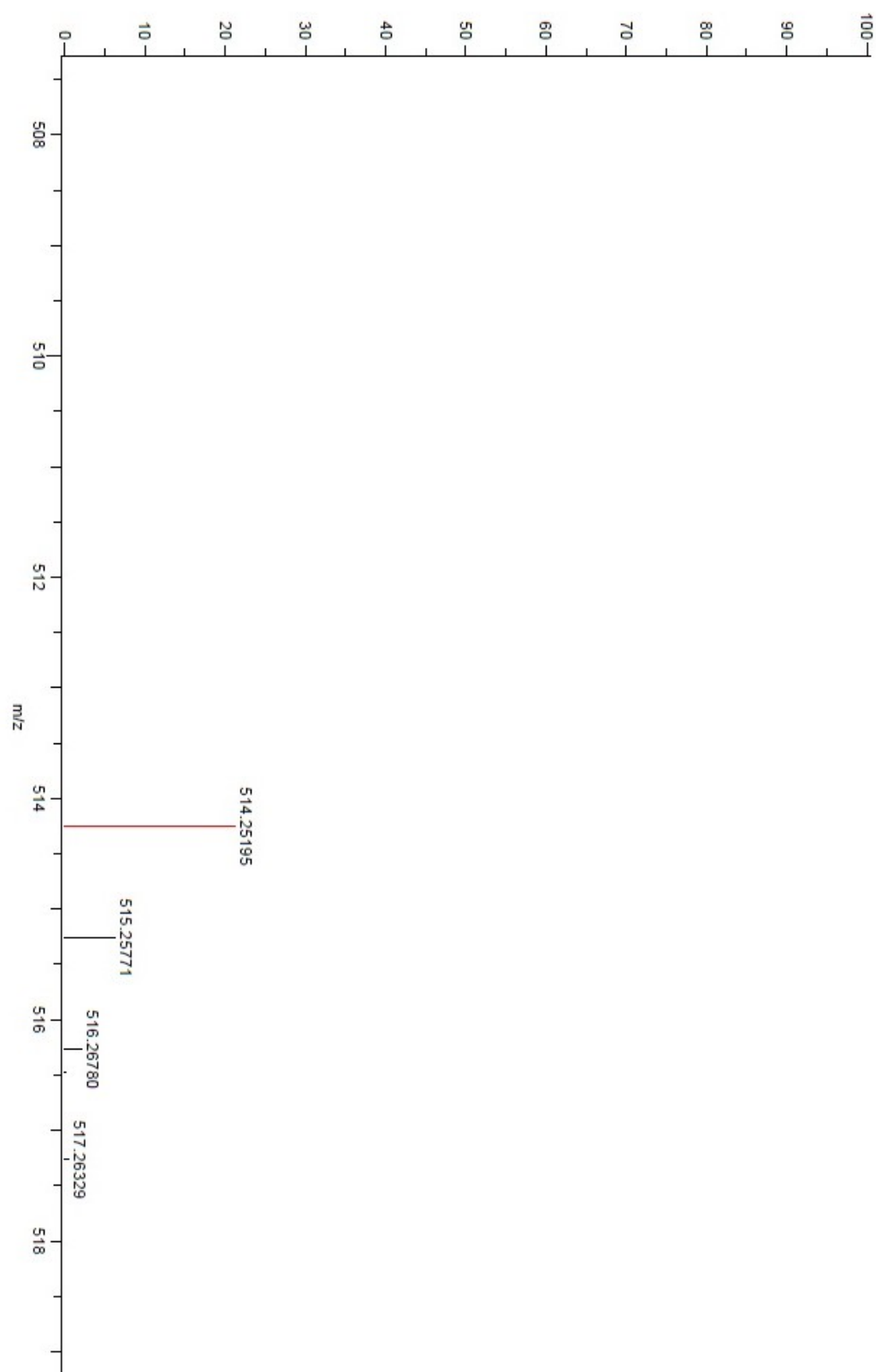


Figure A 415. HRMS-DART spectrum of compound **211**.

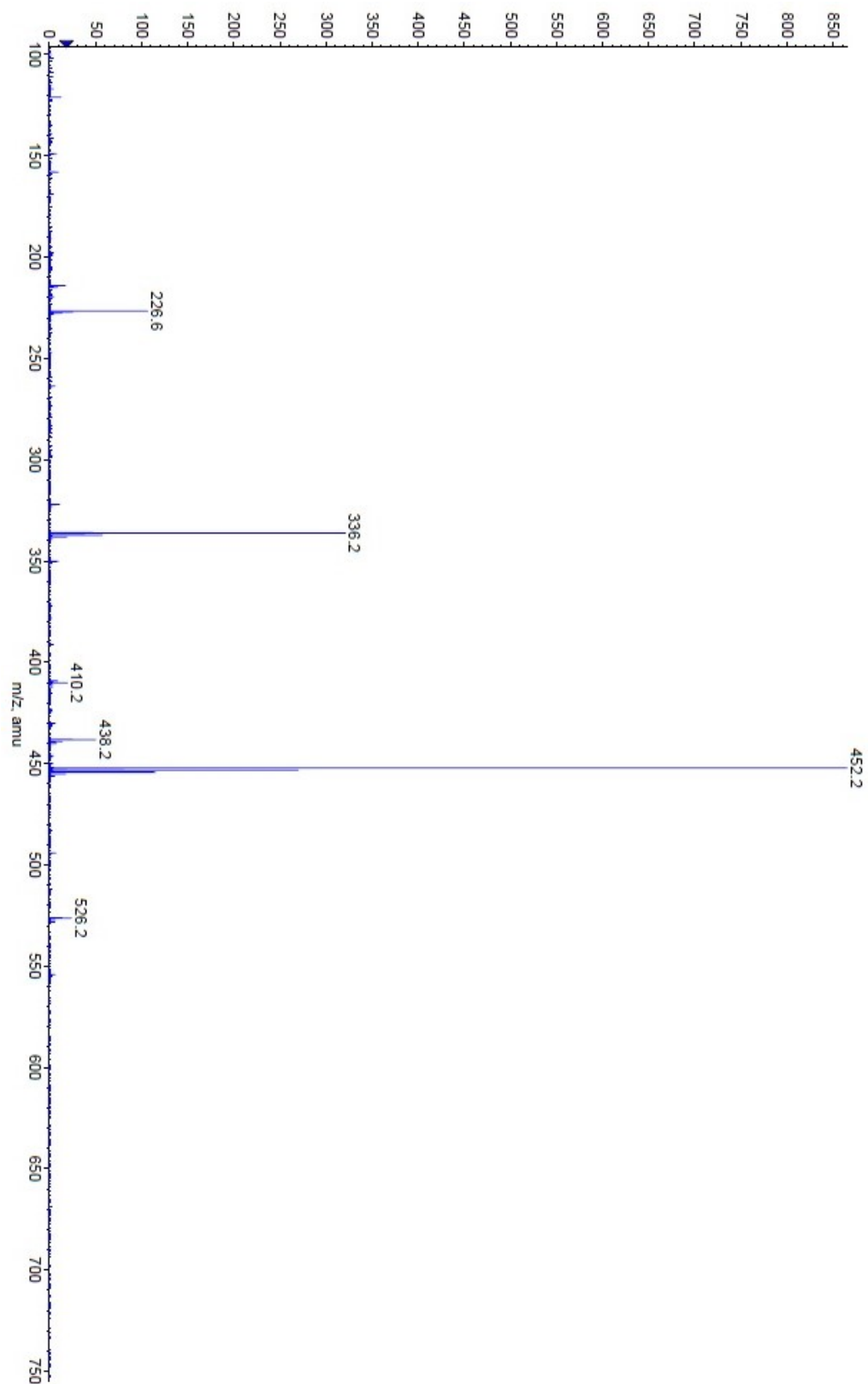


Figure A 416. ESI-TOF spectrum of compound **212**.

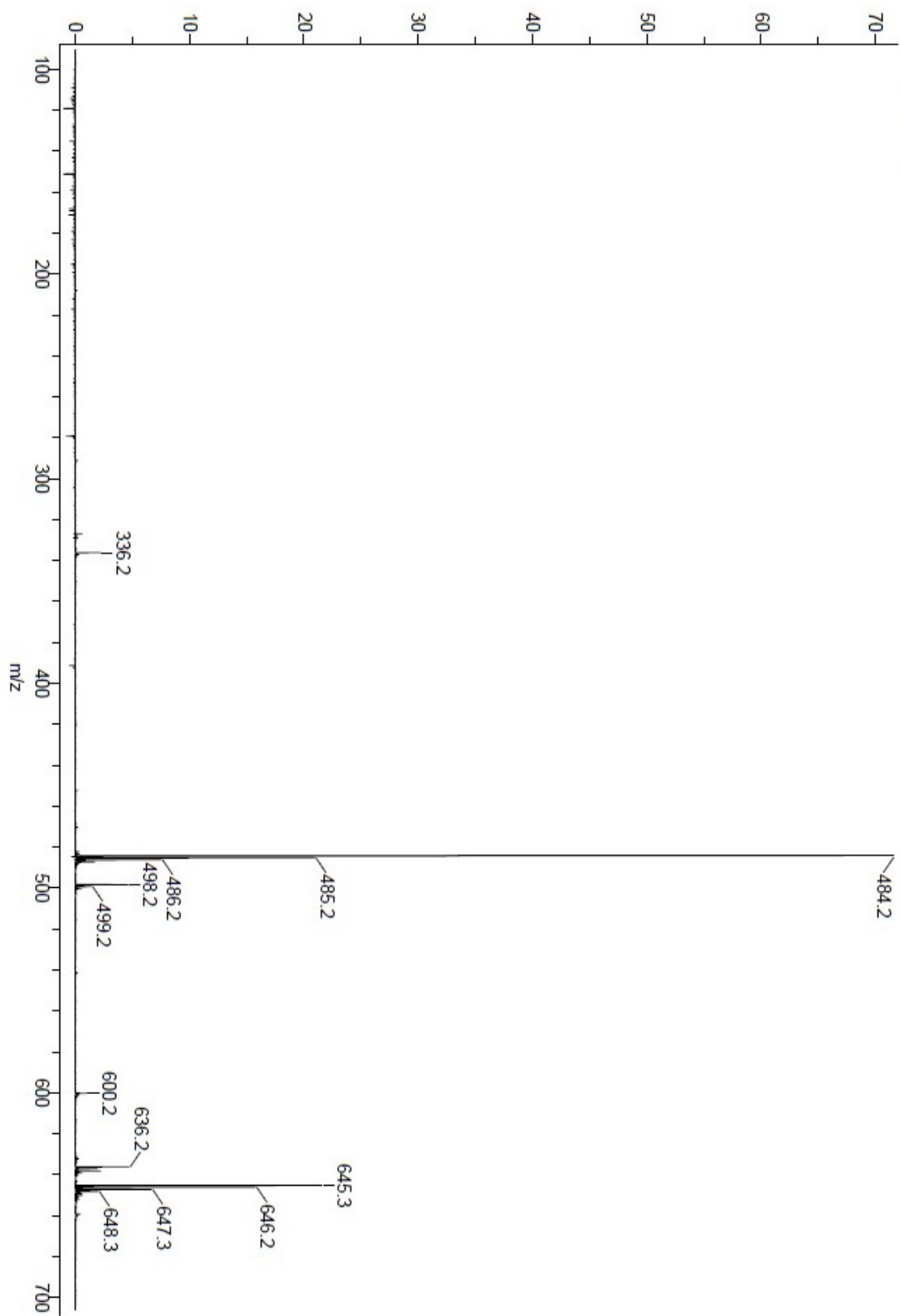


Figure A 417. HRMS-DART spectrum of compound **213**.

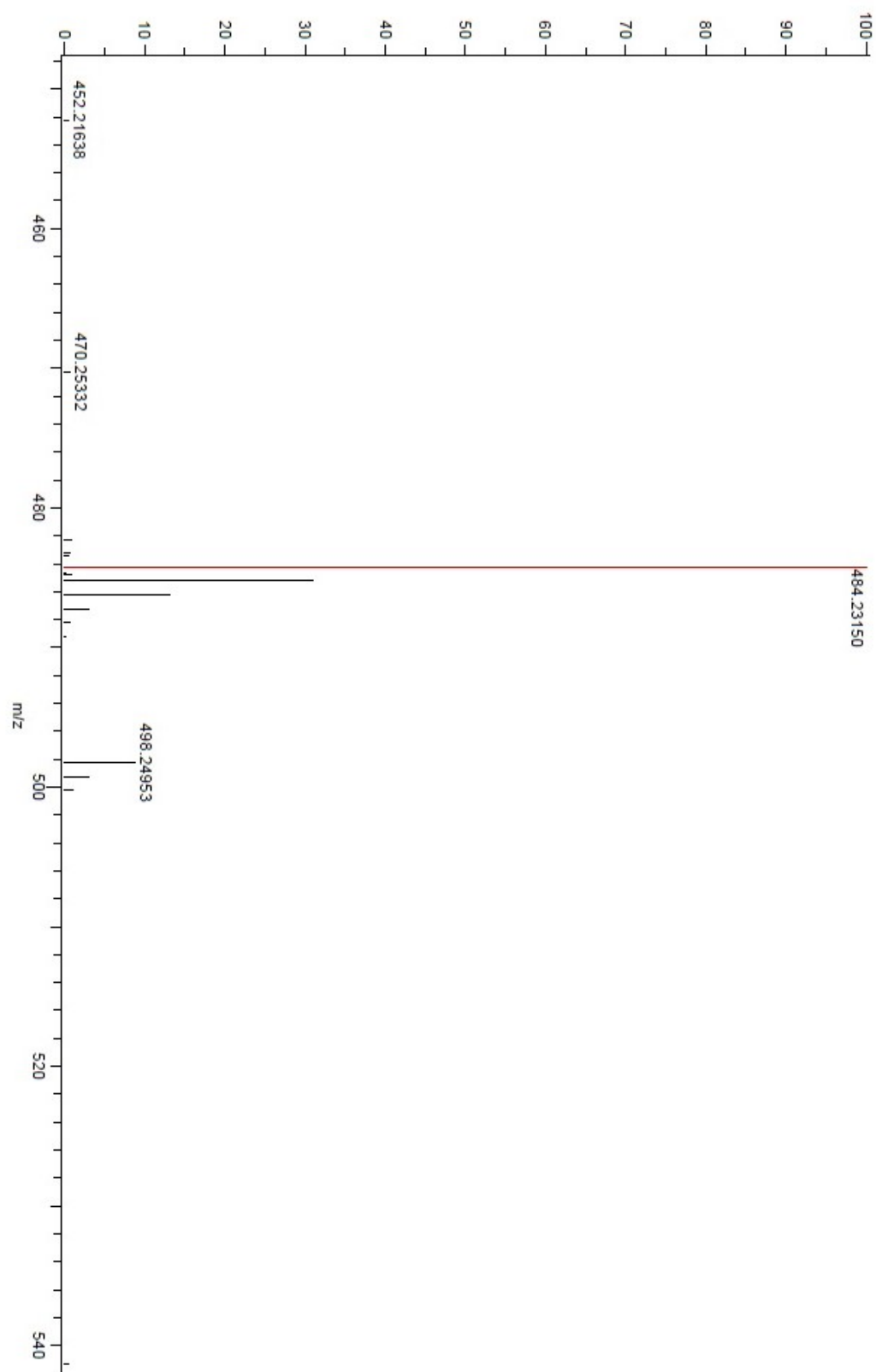


Figure A 418. HRMS-DART spectrum of compound **213**.

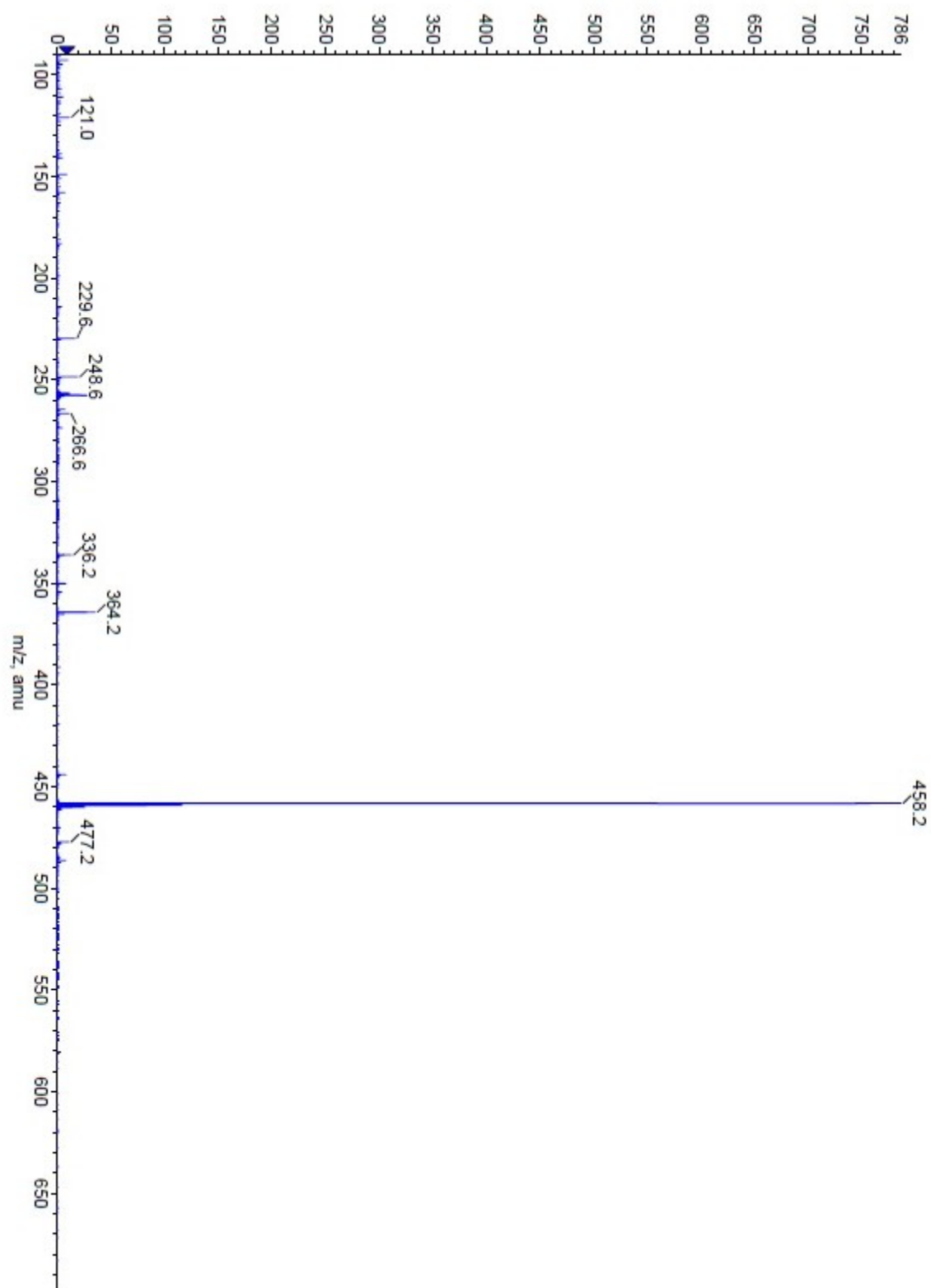


Figure A 419. ESI-TOF spectrum of compound **217**.

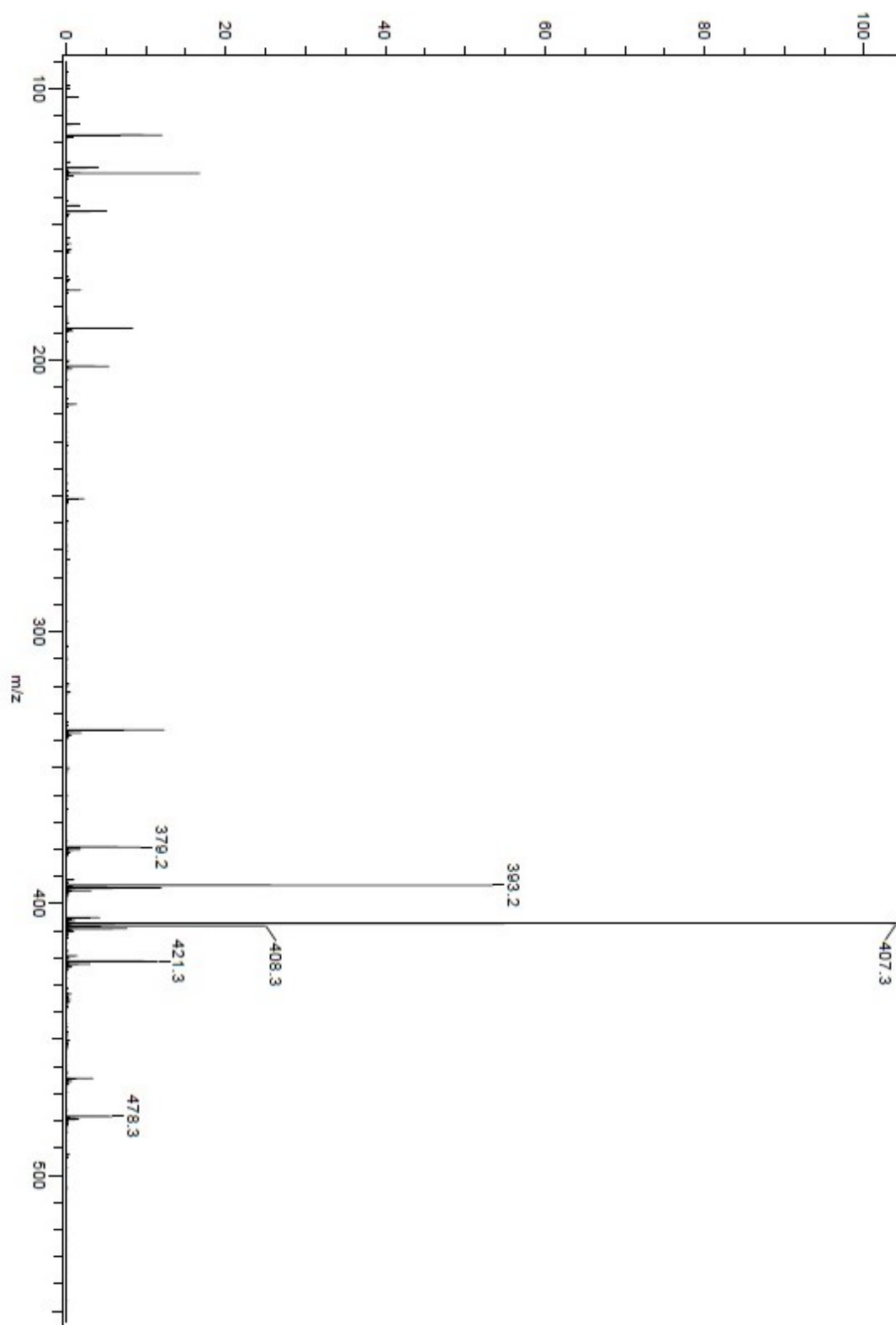


Figure A 420. DART spectrum of compound **221**.

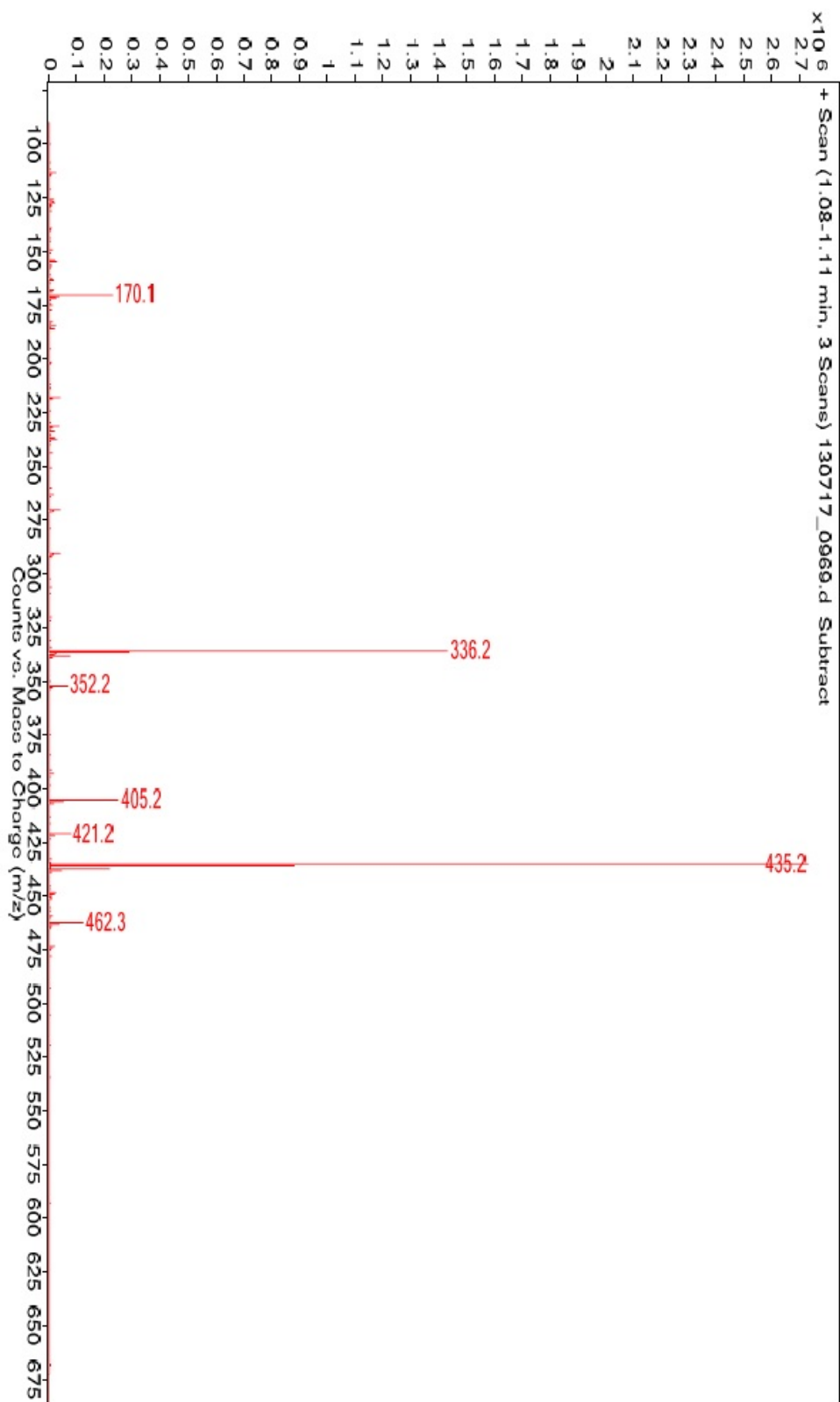


Figure A 421. ESI-TOF spectrum of compound **222**.

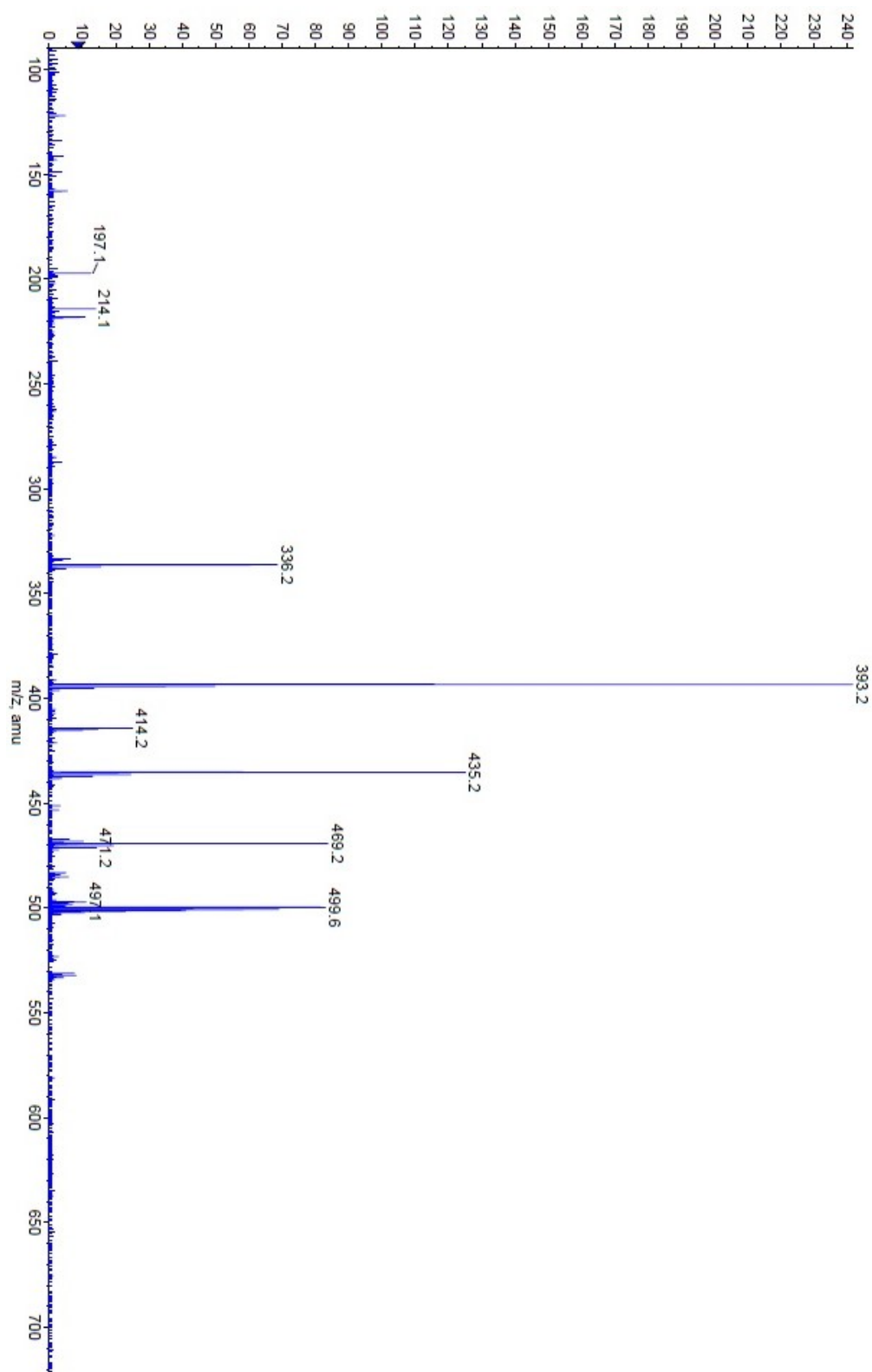


Figure A 422. ESI-TOF spectrum of compound **225**.

7.0 REFERENCES

1. **Grass, G., Rensing, C., and Solioz, M.** Metallic Copper as an Antimicrobial Surface. *Appl Environ. Microbiol.*, **77**, 1541-1547 (2011).
2. **Chen-Yu, J. H., Eberhardt, D. M., and Kincade, D. H.** Antibacterial and Laundering Properties of AMS and PHMB as Finishing Agents on Fabric for Health Care Workers' Uniforms. *Cloth. Text. Res. J.*, **25**, 258-272 (2007).
3. **Ferreira, L., and Zumbuehl, A.** Non-leaching surfaces capable of killing microorganisms on contact. *J. Mater. Chem.*, **19**, 7796-7806 (2009).
4. **McFee, R. B.** Nosocomial or Hospital-acquired Infections: An Overview. *Disease-a-Month* **55**, 422-438 (2009).
5. **World Health Organization.** Prevention of hospital-acquired infections. A practical guide. 2nd edition (2002). Retrieved August 10, 2013 from <http://www.who.int/csr/resources/publications/whodscsreph200212.pdf>.
6. **Klevens, R. M., Edwards, J. R., Richards, C. L., Horan, T. C., Gaynes, R. P., Pollock, D. A., and Cardo, D. M.** Estimating Health Care-Associated Infections and Deaths in U.S. Hospitals, 2002. *Public Health Rep.*, **122**, 160-166 (2007).
7. **Hetrick, E. M., and Schoenfisch, M. H.** Reducing implant-related infections: active release strategies. *Chem. Soc. Rev.*, **35**, 780-789 (2006).
8. **Kramer, A., Schwebke, I., and Kampf, G.** How long do nosocomial pathogens persist on inanimate surfaces? A systematic review. *BMC Infect. Dis.*, **6**, 1-8 (2006).
9. **Page, K., Wilson, M., and Parkin, I. P.** Antimicrobial surfaces and their potential in reducing the role of the inanimate environment in the incidence of hospital-acquired infections. *J. Mater. Chem.*, **19**, 3819-3831 (2009).
10. **Lichter, J. A., Van Vliet, K. J., and Rubner, M. F.** Design of Antibacterial Surfaces and Interfaces: Polyelectrolyte Multilayers as a Multifunctional Platform. *Macromolecules*, **42**, 8573-8586 (2009).
11. **Gao, Y., and Cranston, R.** Recent Advances in Antimicrobial Treatments of Textiles. *Text. Res. J.*, **78**, 60-72 (2008).
12. **Tiller, J. C.** Antimicrobial Surfaces. *Springer, Berlin / Heidelberg, Adv. Polym. Sci.*, **240**, 193-217 (2011).
13. **Siedenbiedel, F., and Tiller, J. C.** Antimicrobial Polymers in Solution and on Surfaces: Overview and Functional Principles. *Polymers*, **4**, 46-71 (2012).

14. **Denyer, S. P.** Mechanisms of action of biocides. *Inter. Biodeter.*, **26**, 89-100 (1990).
15. **Russell, A. D.** Introduction of biocides into clinical practice and the impact on antibiotic-resistant bacteria. *J. Appl. Microbiol.*, **92**, 121S-135S (2002).
16. **Perkins, J. J.** *Principles and Methods of Sterilization in Health Sciences* (2nd Ed.), 39-42, (1980).
17. **Sharma, V. K., Yngard, R. A., and Lin, Y.** Silver nanoparticles: Green synthesis and their antimicrobial activities. *Adv. Colloid Interface Sci.*, **145**, 83-96 (2009).
18. **Kugel, A., Stafslie, S., and Chisholm, B. J.** Antimicrobial coatings produced by “tethering” biocides to the coating matrix: A comprehensive review. *Prog. in Org. Coat.*, **72**, 222-252 (2011).
19. **Klibanov, A. M.** Permanently microbicidal materials coatings. *J. Mater. Chem.*, **17**, 2479-2482 (2007).
20. **Simonic, B., and Tomsic, B.** Structures of Novel Antimicrobial Agents for Textiles - A Review. *Text. Res. J.*, **80**, 1721-1737 (2010).
21. **Caillier, L., de Givenchy, E. T., Levy, R., Vandenberghe, Y., G ribaldi, S., and Guittard, F.** Synthesis and antimicrobial properties of polymerizable quaternary ammoniums. *Eur. J. Med. Chem.*, **44**, 3201-3208 (2009).
22. **Fristrup, C. J., Jankova, K., and Hvilsted, S.** Surface-initiated atom transfer radical polymerization-a technique to develop biofunctional coatings. *Sof. Mater.*, **5**, 4623-4634 (2009).
23. **Pahnke, J., and R  he, J.** Attachment of Polymer Films to Aluminium Surfaces by Photochemically Active Monolayers of Phosphonic Acids. *Macromol. Rapid. Commun.*, **25**, 1396-1401 (2004).
24. **Prucker, O., Naumann, C., Ruhe, J., Knoll, W., and Frank, C.** Photochemical attachment of polymer films to solid surfaces via monolayers of benzophenone derivatives, *J. Am. Chem. Soc.*, **121**, 8766-8770 (1999).
25. **Dhende, V. P., Samanta, S., Jones, D. M., Hardin, I. R., and Locklin, J.** One-Step Photochemical Synthesis of Permanent, Nonleaching, Ultrathin Antimicrobial Coatings for Textiles and Plastics. *ACS Appl. Mater. Interfaces.*, **3**, 2830-2837 (2011).
26. **Li, B., Franking, R., Landis, E. C., Kim, H., and Hamers, R. J.** Photochemical Grafting and Patterning of Biomolecular Layers onto TiO₂ Thin Films. *ACS Appl. Mater. Interfaces.*, **1**, 1013-1022 (2009).
27. **Ye, Q., Zhou, F., and Liu, W.** Bioinspired catecholic chemistry for surface modification. *Chem. Soc. Rev.*, **40**, 4244-4258 (2011).

28. **Barbey, R., Lavanant, L., Paripovic, D., Schuàwer, N., Sugnaux, C., Tugulu, S., and Klok, H. A.** Polymer Brushes via Surface-Initiated Controlled Radical Polymerization: Synthesis, Characterization, Properties, and Applications. *Chem. Rev.*, **109**, 5437-5527 (2009).
29. **Tew, N. W., and Madkour, A. E.** Towards self-sterilizing medical devices: controlling infection. *Polym. Inter.*, **57**, 6-10 (2008).
30. **Dong, H., Huan, J., Koepsel, R., Ye, P., Russell, A. J., and Matyjaszewski, K.** Recyclable Antibacterial Magnetic Nanoparticles Grafted with Quaternized Poly(2-(dimethylamino)ethyl methacrylate) Brushes. *Biomacromol.*, **12**, 1305-1311 (2011).
31. **Faure, E., Lecomte, P., Lenoir, S., Vreuls, C., Weerdt, Van De., Archambeau, C., Martial, J., Jerome, C., Duwez, A. S., and Detrembleur, C.** Sustainable and bio-inspired chemistry for robust antibacterial activity of stainless steel. *J. Mater. Chem.*, **21**, 7901-7904 (2011).
32. **Huang, J., Murata, H., Koepsel, R. R., Russell, A. J. and Matyjaszewski, K.** Antibacterial Polypropylene via Surface-Initiated Atom Transfer Radical Polymerization Biomacromolecules. *Biomacromol.*, **8**, 1396-1399 (2007).
33. **Sweat, D. P., Kim, M., Yu, X., and Gopalan, P.** A Single-Component Inimer Containing Cross-Linkable Ultrathin Polymer Coating for Dense Polymer Brush Growth. *Langmuir*, **29**, 3805-3812 (2013).
34. **Yang, Y., Hu, H., Li, Y., Wan, L., and Xu, Z.** Membrane surface with antibacterial property by grafting polycation. *J. Membr. Sci.*, **376**, 132-141 (2011).
35. **Isquith, A. J., and McCollum, C. J.** Surface kinetic test method for determining rate of kill by an antimicrobial solid. *Appl. Environ. Microbiol.*, **36**, 700-704 (1978).
36. **Speier, J. L., and Malek, J. R.** Destruction of microorganisms by contact with solid surfaces. *J. Colloid Interface Sci.*, **89**, 68-76 (1982).
37. **Plueddemann, E. P. and Revis, A.** Organosilicon quaternary ammonium antimicrobial compounds. *Dow Corning Corporation*, US 4866192 A (1988).
38. **Isquith, A. J., Abbott, E. A., and Walters, P. A.** Surface bonded antimicrobial activity of an organosilicon quaternary ammonium chloride. *Appl. Microbiol.*, **2**, 859-863 (1972).
39. **Pallavicini, P., Taglietti, A., Dacarro, G., Diaz-Fernandez, Y. A., Galli, M., Grisoli, P., Patrini, M., Santucci De Magistris, G., and Zanoni, R.** Self-assembled monolayers of silver nanoparticles firmly grafted on glass surfaces: Low Ag⁺ release for an efficient antibacterial activity. *J. Colloid. Inter. Sci.*, **350**, 110-116 (2010).
40. **Guido, K., Rutzinger, D., and Gallauner, T.** Synthesis of hexadentate hexahydro 1,3,5-triazine based ligands and their copper (I) complexes. *Mont. fuer Chem.*, **133**, 1157-1164 (2002).

41. **Gottesman, R., Shukla, S., Perkas, N., Solovyov, L. A., Nitzan, Y., and Gedanken, A.** Sonochemical Coating of Paper by Microbiocidal Silver Nanoparticles. *Langmuir*, **27**, 720-726 (2011).
42. **Huang, J., Koepsel, R. R., Murata, H., Wu, W., Lee, S.B., Kowalewski, T., Russell, A. J., Matyjaszewski, K.** Nonleaching Antibacterial Glass Surfaces via “Grafting Onto”: The Effect of the Number of Quaternary Ammonium Groups on Biocidal Activity. *Langmuir*, **24**, 6785-6795 (2008).
43. **Sambhy, V., Peterson, B. R., and Sen, A.** Multifunctional Silane Polymers for Persistent Surface Derivatization and Their Antimicrobial Properties. *Langmuir*, **24**, 7549-7558 (2008).
44. **Bouloussa, O., Rondelez, F. and Semetey, V.** A new, simple approach to confer permanent antimicrobial properties to hydroxylated surfaces by surface functionalization. *Chem. Commun.*, 951-953 (2008).
45. **Ohlhausen, H. G., and Ludwig, J. H.** Solvent-Free Organosilane Quaternary Ammonium Compositions, Method of Making and Use. *Resource Development, LLC*. US 20110271873 (2011).
46. **Aegis.** Microbeguard Technology, (2009). Retrieved May 10, 2011 from http://www.nwmoldprevention.com/downloads/microbe_guard_technology.pdf.
47. **Allred, G. D., and Liebeskind, L. S.** Water-stabilized organosilane compounds and methods for using the same. *Emory University*, US 5959014 A (1996).
48. **Isquith, A. J., Abbott, E. A., and Walters, P. A.** Algicidal activity of a surface-bonded organosilicon quaternary ammonium chloride. *Appl. Microbiol.*, **25**, 253-256 (1973).
49. **Nakagawa, Y., Hayashi, H., Tawaratani, T., Kourai, H., Horie, T., and Shibasaki, I.** Disinfection of Water with Quaternary Ammonium Salts Insolubilized on a Porous Glass Surface. *Appl. Environ. Microbiol.*, **47**, 513-518 (1984).
50. **Battice, D. R., and Hales, M. G.** A New Technology for Producing Stabilized Foams Having Antimicrobial Activity. *J. Cell. Plast.*, **21**, 332-337 (1985).
51. **Murray, P. R., Niles, A. C., and Heeren, R. L.** Microbial inhibition on hospital garments treated with Dow Corning 5700 antimicrobial agent. *J. Clin. Microbiol.*, **26**, 1884-1886 (1988).
52. **Gottenbos, B., van der Mei, H. C., Klatter, F., Nieuwenhuis, P., and Busscher, H. J.** In vitro and in vivo antimicrobial activity of covalently coupled quaternary ammonium silane coatings on silicone rubber. *Biomaterials*, **23**, 1417-1423 (2002).
53. **Abo El Ola, S. M., Kotek, R., White, W. C., Reeve, J. A., Hauser, P., and Kim, J. H.** Unusual polymerization of 3-(trimethoxysilyl)-propyldimethyloctadecyl ammonium chloride on PET substrates. *Polymer*, **45**, 3215-3225 (2004).

54. **Nikawa, H., Ishida, K., Hamada, T., Satoda, T., Murayama, T., Takemoto, T., Tamamoto, M., Tajima, H., Shimoe, S., Fujimoto, H., and Makihiro, S.** Immobilization of Octadecyl Ammonium Chloride on the Surface of Titanium and Its Effect on Microbial Colonization In Vitro. *Dent. Mater. J.*, **24**, 570-582 (2005).
55. **Osterhof, J. J., Buijssen, K. J., Busscher, H. J., van der Laan, B.F., and van der Mei, H. C.** Effects of quaternary ammonium silane coatings on mixed fungal and bacterial biofilms on tracheoesophageal shunt prostheses. *Appl. Environ. Microbiol.*, **72**, 3673-3677 (2006).
56. **Andresen, M., Stenstad, P., Møretør, T., Langsrud, S., Syverud, K., Johansson, L.S., and Stenius, P.** Nonleaching Antimicrobial Films Prepared from Surface-Modified Microfibrillated Cellulose. *Biomacromol.*, **8**, 2149-2155 (2007).
57. **Bouloussa, O., Rondelez, F. and Semetey, V.** A new, simple approach to confer permanent antimicrobial properties to hydroxylated surfaces by surface functionalization. *Chem. Commun.*, 951-953 (2008).
58. **Sambhy, V., Peterson, B. R., and Sen, A.** Multifunctional Silane Polymers for Persistent Surface Derivatization and Their Antimicrobial Properties. *Langmuir*, **24**, 7549-7558 (2008).
59. **Saif, M. J., Anwar, J. and Munawar, M. A.** A Novel Application of Quaternary Ammonium Compounds as Antibacterial Hybrid Coating on Glass Surfaces. *Langmuir*, **25**, 377-379 (2009).
60. **Köylü, D., Bilecen, K., Şahin, E., Duman, G., and Taralp, A.** Cotton gauze bearing non-diffusible quaternary ammonium salts and featuring anti-microbial activity: An example of single-use articles tailored to self-sterilize. Faculty of Engineering & Natural Sciences, Materials Science & Engineering Program, Sabanci University, Istanbul online poster (2010). Retrieved September 01, 2013 from <http://people.sabanciuniv.edu/taralp/presentations/ACS2003%20NewOrleansPoster%20Damla.pdf>
61. **Song, L., and Baney, R. H.** Antibacterial evaluation of cotton textile treated by trialkoxysilane compounds with antimicrobial moiety. *Text. Res. J.*, **81**, 504-511 (2011).
62. **Song, J., Kong, H. and Jang, J.** Bacterial adhesion inhibition of the quaternary ammonium functionalized silica nanoparticles. *Coll. Surf. B: Biointerfaces* **82**, 651-656 (2011).
63. **Green, J. D., Bickner, S., Carter, P. W., Fulghum, T., Luebke, M., Nordhaus, M. A., and Strathmann, S.** Antimicrobial testing for surface-immobilized agents with a surface-separated live–dead staining method. *Biotechnol. Bioeng.*, **108**, 231-236 (2011).
64. **Nanci, A., Wuest, J. D., Peru, L., Brunet, P., Sharma, V., Zalzal, S., McKee, M.D.** Chemical modification of titanium surfaces for covalent attachment of biological molecules. *J. Biomed. Mater. Res.*, **40**, 324-335 (1998).

65. **Gawalt, E. S., Avaltroni, M. J., Koch, N., and Schwartz, J.** Self-Assembly and Bonding of Alkanephosphonic Acids on the Native Oxide Surface of Titanium. *Langmuir*, **17**, 5736-5738 (2001).
66. **Jampala, S. N., Sarmadi, M., Somers, E. B., Wong, A. C. L., and Denes, F. S.** Plasma-Enhanced Synthesis of Bactericidal Quaternary Ammonium Thin Layers on Stainless Steel and Cellulose Surfaces. *Langmuir*, **24**, 8583-8591 (2008).
67. **Adden, N., Gamble, L. J., Castner, D. G., Hoffmann, A., Gross, G., and Menzel, H.** Phosphonic Acid Monolayers for Binding of Bioactive Molecules to Titanium Surfaces. *Langmuir*, **22**, 8197-8204 (2006).
68. **Raman, A., Dubey, M., Gouzman, I. and Gawalt, E. S.** Formation of Self-Assembled Monolayers of Alkylphosphonic Acid on the Native Oxide Surface of SS316L. *Langmuir*, **22**, 6469-6472 (2006).
69. **Schwartz, J., Avaltroni, M. J., Danahy, M. P., Silverman, B. M., Hanson, E. L., Schwarzbauer, J. E., Midwood, K. S., and Gawalt, E. S.** Cell attachment and spreading on metal implant materials. *Mat. Sci. Eng: C* **23**, 395-400 (2003).
70. **Mani, G., Johnson, D. M., Marton, D., Dougherty, V. L., Feldman, M. D., Patel, D., Ayon, A. A., and Agrawal, C. M.** Stability of Self-Assembled Monolayers on Titanium and Gold. *Langmuir*, **24**, 6774-6784 (2008).
71. **Vericat, C., Vela, M. E., Benitez, G., Carro, P., and Salvarezza, R. C.** Self-assembled monolayers of thiols and dithiols on gold: new challenges for a well-known system. *Chem. Soc. Rev.*, **39**, 1805-1834 (2010).
72. **Gawalt, E. S., Avaltroni, M. J., Koch, N., and Schwartz, J.** Self-Assembly and Bonding of Alkanephosphonic Acids on the Native Oxide Surface of Titanium. *Langmuir*, **17**, 5736-5738 (2001).
73. **Silverman, B. M., Wieghaus, K. A. and Schwartz, J.** Comparative Properties of Siloxane vs Phosphonate Monolayers on A Key Titanium Alloy. *Langmuir*, **21**, 225-228 (2005).
74. **Lecollinet, G., Delorme, N., Edely, M., Gibaud, A., Bardeau, J. F., Hindré, F., Boury, F., and Portet, D.** Self-Assembled Monolayers of Bisphosphonates: Influence of Side Chain Steric Hindrance. *Langmuir*, **25**, 7828-7835 (2009).
75. **Hanson, E. L., Schwartz, J., Nickel, B., Koch, N., and Danisman, M. F.** Bonding Self-Assembled, Compact Organophosphonate Monolayers to the Native Oxide Surface of Silicon. *J. Am. Chem. Soc.*, **125**, 16074-16080 (2003).
76. **Raman, A., Dubey, M., Gouzman, I., and Gawalt, E. S.** Formation of Self-Assembled Monolayers of Alkylphosphonic Acid on the Native Oxide Surface of SS316L. *Langmuir*, **22**, 6469-6472 (2006).

77. **Hoque, E., DeRose, J. A., Bhushan, B., and Mathieu, H. J.** Self-Assembled Monolayers on Aluminum and Copper Oxide Surfaces: Surface and Interface Characteristics, Nanotribological Properties, and Chemical Stability, *Nano. Sci. Tech.*, 235-281 (2008).
78. **Guerrero, G., Amalric, J., Mutin, P., Sotto, A., and Lavigne, J.** Inhibition de l'adhésion bactérienne et prévention de la formation d'un biofilm: utilisation de monocouches autoassemblées organiques sur des surfaces inorganiques. *Pathologie Biologie* **57**, 36-43 (2009).
79. **Mutin, P., Amalric, J., Guerrero, G., Ponche, J. P., and Lavigne, J.** Surface modification of titanium by Phosphonate monolayers Releasing Bactericidal Species. *European Cells and Materials* **21**, 63 (2011).
80. **Mutin, P. H, Guerrero, G., and Amalric, J. P.** Preparation of an inorganic substrate having antimicrobial properties. WO 2007080291 (2007).
81. **Amalric, J., Mutin, P. H., Guerrero, G., Ponche, A., Sotto, A., and Lavigne, J. P.** Phosphonate monolayers functionalized by silver thiolate species as antibacterial nanocoatings on titanium and stainless steel. *J. Mater. Chem.* **19**, 141-149 (2009).
82. **Denizot B., Hindre, F. and Portet, D.** Geminal bisphosphonates containing at least two quaternary ammonium functions in the backbone for coating of metallic and mineral surfaces for protection against biofilm formation and bacterial contamination. Brevet FR 2878248 (2006).
83. **Portet, D., LeCollinet, G., Hindre, F., Bejanin, S., Chappard, D., and Denizot, B.** Method of covering self-assembled metal or inorganic monolayer surfaces of gem-bisphosphonic compounds and uses thereof. Surfactis Technologies, Fr., WO2008017721 A3 (2008).
84. **Pfaffenroth, C., Winkel, A., Dempwolf, W., Gamble, L.J., Castner, D. G., Stiesch, Meike., and Menzel, H.** Self-Assembled Antimicrobial and Biocompatible Copolymer Films on Titanium. *Macromol. Biosci.*, **11**, 1515-1525 (2011).
85. **Chen, C. and Wickstrom, E.** Self-Protecting Bactericidal Titanium Alloy Surface Formed by Covalent Bonding of Daptomycin Bisphosphonates. *Bioconjug. Chem.*, **21**, 1978-1986 (2010).
86. **Dong, H., Huang, J., Koepsel, R., Ye, P., Russell, A. J., and Matyjaszewski, K.** Recyclable Antibacterial Magnetic Nanoparticles Grafted with Quaternized Poly(2-(dimethylamino)ethyl methacrylate) Brushes. *Biomacromol.*, **12**, 1305-1311 (2011).
87. **Kruszewski, K. M., Nistico, L., Longwell, M. J., Hynes, M. J., Maurer, J.A., Hall-Stoodley, L., and Gawalt, E. S.** Reducing *Staphylococcus aureus* biofilm formation on stainless steel 316L using functionalized self-assembled monolayers. *Mater. Sci. Eng., C: Mater. Biol. Applic.*, **33**, 2059-2069 (2013).

88. **Dalsin, J. L., Hu, B. H., Lee, B. P., and Messersmith, P. B.** Mussel Adhesive Protein Mimetic Polymers for the Preparation of Nonfouling Surfaces. *J. Amer. Chem. Soc.*, **125**, 4253-4258 (2003).
89. **Waite, J. H.** Surface chemistry: Mussel Power. *Nat. Mater.*, **7**, 8-9 (2008).
90. **Wach, J., Bonazzi, S. and Gademann, K.** Antimicrobial Surfaces through Natural Product Hybrids. *Angew. Chem. Int. Ed.*, **47**, 7123-7126 (2008).
91. **Yuan, S., Wan, D., L., Liang, B., Pehkonen, S. O., Ting, Y. P., Neoh, K. G., and Kang, E. T.** Lysozyme-Coupled Poly(poly(ethylene glycol) methacrylate)–Stainless Steel Hybrids and Their Antifouling and Antibacterial Surfaces. *Langmuir*, **27**, 2761-2774 (2011).
92. **Caro, A. Humblot, V., Meathivier, C., Minier, M., Salmain, M., and Pradier, C. M.** Grafting of Lysozyme and/or Poly(ethylene glycol) to Prevent Biofilm Growth on Stainless Steel Surfaces. *J. Phys. Chem. B.*, **113**, 2101-2109 (2009).
93. **Humblot, V., Yala, J. F., Thebault, P., Boukema, K., Hequet, A., Berjeaud, J. M., and Pradier, C. M.** The Antibacterial Activity of Magainin I Immobilized onto Mixed Thiols Self-Assembled Monolayers. *Biomaterials*, **30**, 3503-3512 (2009).
94. **Shalev, T., Gopin, A., Bauer., M., Stark, R., and Rahimipour., S.** Non-leaching antimicrobial surfaces through polydopamine bio-inspired coating of quaternary ammonium salts or an ultrashort antimicrobial lipopeptide. *J. Mater. Chem.*, **22**, 2026-2032 (2012).
95. **Appendini, P., and Hotchkiss, J. H.** Review of antimicrobial food packaging. *Innov. Food Sci. Emerg. Technol.*, **3**, 113-126 (2002).
96. **Muñoz-Bonilla, A., and Fernández-García, M.** Polymeric materials with antimicrobial activity. *Prog. Poly. Sci.*, **37**, 281-339 (2012).
97. **Kenawy, E., Worley, S. D. and Broughton, R.** The chemistry and applications of antimicrobial polymers: a state-of-the-art review. *Biomacromol.*, **8**, 1359-1384 (2007).
98. **Harney, M. B., Pant, R. R., Fulmer, P. A., and Wynne, J. H.** Surface Self-Concentrating Amphiphilic Quaternary Ammonium Biocides as Coating Additives. *ACS App. Mater. Inter.*, **1**, 39-41 (2009).
99. **Foucher, D., and Mocella, A.** Private Communication. Ryerson University, Toronto, Ontario (2013).
100. **Clarkson, N., and Evans, L. V.** Further studies investigating a potential non-leaching biocide using the marine fouling diatom *Amphora coffeaeformis*. *Biofouling*, **9**, 17-30 (1995).
101. **Majumdar, P., Crowley, E., Htet, M., Stafslie, S. J., Daniels, J., VanerWal, L., and Chisholm, B. J.** Combinatorial Materials Research Applied to the Development of New Surface

Coatings XV: An Investigation of Polysiloxane Anti-Fouling/Fouling-Release Coatings Containing Tethered Quaternary Ammonium Salt Groups. *ACS Combinat. Sci.*, **13**, 298-309 (2011).

102. **Yagci, M. B. Bolca, S. Heuts, J. P. A. and Ming. W.** Self-stratifying antimicrobial polyurethane coatings. *Prog. Org. Coat.*, **72**, 305-314 (2011).

103. **Stovicek, P.** Biocidal compositions based on polymers of dihydroxy quaternary ammonium salts. US 5084096 (1992).

104. **Waschinski, C., Zimmermann, J., Salz, U., Hutzler, R., Sadowski, G., and Tiller, J. C.** Design of Contact-Active Antimicrobial Acrylate-Based Materials Using Biocidal Macromers. *Adv. Mater.*, **20**, 104-108 (2008).

105. **Mocella, A.** UV Cured Benzophenone Terminated Quaternary Ammonium Antimicrobials for Plastics. 4th Year Undergraduate Thesis. Department of Chemistry and Biology, Ryerson University, Toronto, ON, 1-80 (2012).

106. **Yang, Y., Hu, H., Li, Y., Wan, L., and Xu, Z.** Membrane surface with antibacterial property by grafting polycation. *J. Membr. Sci.* **376**, 132-141 (2011).

107. **Griep-Raming, N., Karger, M., and Menzel, H.** Using Benzophenone-Functionalized Phosphonic Acid To Attach Thin Polymer Films to Titanium Surfaces. *Langmuir*, **20**, 11811-11814 (2004).

108. **Zou, P., Hartleb, W., and Lienkamp, K.** It takes walls and knights to defend a castle – synthesis of surface coatings from antimicrobial and antibiofouling polymers. *J. Mater. Chem.* **22**, 19579-19589 (2012).

109. **Hu, R., Li, G., Jiang, Y., Zhang, Y., Zou, J. J., Wang, L., and Zhang, X.** Silver–Zwitterion Organic–Inorganic Nanocomposite with Antimicrobial and Antiadhesive Capabilities. *Langmuir*, **29**, 3373-3779 (2013).

110. (i) **Cheng, G., Xue, H., Zhang, Z., Chen, S., and Jiang, S.** A Switchable Biocompatible Polymer Surface with Self-Sterilizing and Nonfouling Capabilities. *Angew. Chem. Int. Ed.* **47**, 8831-8834 (2008). (ii) **Cao, Z., Mi, L., Mendiola, J., Ella-Menye, J. R., Zhang, Lei., Xue, Hong., and Jiang, S.** Reversibly Switching the Function of a Surface between Attacking and Defending against Bacteria. *Angew. Chem. Int. Ed.*, **51**, 2602-2605 (2012). (iii) **Yu, Q., Cho, J., Shivapooja, P., Ista, L. K. and López, G. P.** Nanopatterned Smart Polymer Surfaces for Controlled Attachment, Killing, and Release of Bacteria. *ACS Appl. Mater. Interfaces.* XXX, XXX–XXX (2013).

111. **Gabriel, G., Maegerlein, J. A., Nelson, C. F., Dabkowski, J. M., Eren, T., Nüsslein, K., and Tew, G. N.** Comparison of Facially Amphiphilic versus Segregated Monomers in the Design of Antibacterial Copolymers. *Chem. Eur. J.* **15**, 433-439 (2009).

112. **Gong, S., Niu, L., Kemp, L. K., Yiu, C. K. Y., Ryou, H., Qi, Y., Blizzard, J. D., Nikonov, S., Brackett, M. G., Messer, R. L. W., Wu, C. D., Mao, J., Brister, L. B., Rueggeberg, F. A., Arola, D. D., Pashley, D. H., and Tay, F. R.** Quaternary ammonium silane-functionalized, methacrylate resin composition with antimicrobial activities and self-repair potential. *Acta Biomaterialia*, **8**, 3270-3282 (2012).
113. **Gilbert, P., and Moore, L. E.** Cationic antiseptics: diversity of action under a common apithet. *J Appl. Microbiol.*, **99**, 703-715 (2005).
114. **Jansen, A. C., Boucher, C. E., Coetse, E., Kock, J. L. F., vanWyk, P. W. J., Swart, H. C., and Bragg, R. R.** The influence of Didecyltrimethylammonium Chloride on the morphology and elemental composition of *Staphylococcus aureus* as determined by NanoSAM. *Sci. Res. Ess.*, **8**, 152-160 (2013).
115. **Hegstad, K., Langsrud, S., Lunestad, B. T., Scheie, A. A., Sunde, M. and Yazdankhah, S. P.** Does the wide use of quaternary ammonium compounds enhance the selection and spread of antimicrobial resistance and thus threaten our health? *Microb. Drug Resist.*, **16**, 91-94 (2010).
116. **Schaeufele, P.** Advances in Quaternary Ammonium Biocides. *J. Amer. Oil. Soc. Chem.*, **61**, 387 (1984).
117. **Iannou, C. J., Hanlon, G. W., and Denyer, S. P.** Action of disinfectant quaternary ammonium compounds against *Staphylococcus aureus*. *Antimicrob. Agents. Chemother.*, **51**, 296-306 (2007).
118. **Thebault, P., Taffin de Givency, E., Levy, R., Vandenberghe, Y., Guittard, F., and G ribaldi, S.** Preparation and antimicrobial behaviour of quaternary ammonium thiol derivatives able to be grafted on metal surfaces. *Eur.J.Med.Chem.*, **44**, 717-724 (2009).
119. **Russell, A. D.** Mechanism of antimicrobial action of antiseptics and disinfectants: An increasingly important area of investigation. *J.Antimicrob.Chemother.*, **49**, 597-599 (2002).
120. **McDonnell, G. A., and Russell D.** Antiseptics and Disinfectants: Activity, Action, and Resistance. *Clin. Microbiol. Rev.*, **12**, 147-179 (1999).
121. **Holdsworth, S.R., and Law, C.J.** The major facilitator superfamily transporter MdtM contributes to the intrinsic resistance of *Escherichia coli* to quaternary ammonium compounds. *J Antimicrob. Chemother.*, **68**, 831-839 (2013).
122. **Tabata, A., Nagamune, H., Maeda, T., Murakami, K., Miyake, Y., and Kourai, H.** Correlation between Resistance of *Pseudomonas aeruginosa* to Quaternary Ammonium Compounds and Expression of Outer Membrane Protein OprR. *Antimicrob. Agents Chemother.*, **47**, 2093-2099 (2003).

123. **Mangalappalli-Illathu, A. K., and Korber, D. R.** Adaptive Resistance and Differential Protein Expression of *Salmonella enterica* Serovar Enteritidis Biofilms Exposed to Benzalkonium Chloride. *Antimicrob. Agents Chemother.*, **50**, 3588-3596 (2006).
124. **Nonaka, T., Hua, L., Ogata, T., and Kurihara, S.** Synthesis of water-soluble thermosensitive polymers having phosphonium groups from methacryloyloxyethyl trialkyl phosphonium chlorides-N-isopropylacrylamide copolymers and their functions. *J. Appl. Polym. Sci.*, **87**, 386-393 (2003).
125. **Waschinski, C. J., Barnert, S., Theobald, A., Schubert, R., Kleinschmidt, F., Hoffmann, A., Saalwächter, K., and Tiller, J. C.** Insights in the Antibacterial Action of Poly(methyloxazoline)s with a Biocidal End Group and Varying Satellite Groups. *Biomacromol.*, **9**, 1764-1771 (2008).
126. **Lewis, K., and Klibanov, A. M.** Surpassing nature: rational design of sterile-surface materials. *Trends Biotechnol.*, **23**, 343-348 (2005).
127. **Tiller, J. C., Liao, C.J., Lewis, K., and Klibanov, A. M.** Designing surfaces that kill bacteria on contact. *PNAS.*, **98**, 5981-5985 (2001).
128. **Park, D., Wang, J., and Klibanov, A. M.** One-Step, Painting-Like Coating Procedures To Make Surfaces Highly and Permanently Bactericidal. *Biotechnol. Prog.*, **22**, 584-589 (2006).
129. **Lewis, K., and Klibanov, A. M.** Surpassing nature: rational design of sterile-surface materials. *Trends Biotechnol.*, **23**, 343-348.
130. **Murata, H., Koepsel, R. R., Matyjaszewski, K., and Russell, A. J.** Permanent, non-leaching antibacterial surfaces—2: How high density cationic surfaces kill bacterial cells. *Biomaterials*, **28**, 4870-4879 (2007).
131. **Kuegler, R., Bouloussa, O., and Rondelez, F.** Evidence of a charge-density threshold for optimum efficiency of biocidal cationic surfaces. *Microbiology Reading*, **151**, 1341-1348 (2005).
132. **Bieser, A. M., Thomann, Y., and Tiller, J. C.** Contact-Active Antimicrobial and Potentially Self-Polishing Coatings Based on Cellulose. *Macromol. Biosci.*, **11**, 111-121 (2011).
133. **Bieser, A. M., and Tiller, J. C.** Mechanistic Considerations on Contact-Active Antimicrobial Surfaces with Controlled Functional Group Densities. *Macromol. Biosci.*, **11**, 526-534 (2011).
134. **American Society for Testing and Materials.** Minimum Inhibitory Concentration (MIC) Determination. *Annual Book of ASTM Standards*, **1**, 1-10 (2002).
135. Antimicrobial Test laboratories. ISO 22196 Test for Antimicrobial Activity of Plastics. (2013). Retrieved June 10, 2013 from <http://www.antimicrobialtestlaboratories.com>.

136. **Green, J. D.** Science against microbial pathogens: communicating current research and technological advances. Méndez-Vilas Publishing, *FORMATEX Microbiology Series N° 3*, 578-585 (2011).
137. **Ronan, E.** Investigating Microbial Ecology at Solid-Air Interfaces. 4th Year Undergraduate Thesis. Department of Chemistry and Biology, Ryerson University, Toronto, ON, 1-89 (2011).
138. **Deng, H.** 4th Year Undergraduate Thesis. Department of Chemistry and Biology, Ryerson University, Toronto, ON, 1-78 (2013).
139. **Menschutkin, N.** Ueber die Einwirkung des Chloracetyls auf phosphorige Saure. *Ann. Chem. Pharm.*, **133**, 317-320 (1865).
140. **Stanger, K. J., Lee, J. J., and Smith, B. D.** Dramatic Acceleration of the Menschutkin Reaction and Distortion of Halide Leaving-Group Order. *J. Org. Chem.*, **72**, 9663 - 9668 (2007).
141. **Reinheimer, J. D., Harley, J. D., and Meyers, W. W.** Solvent Effects in the Menschutkin Reaction. *J. Org. Chem.*, **28**, 1575-1579 (1963).
142. **Smith, M.** March's advanced organic chemistry: reactions, mechanisms, and structure *Wiley-Interscience*, Hoboken, N.J., 525, (2007).
143. **Sommer, H. Z., Lipp, H. I., and Jackson, L. J.** Alkylation of amines. General exhaustive alkylation method for the synthesis of quaternary ammonium compounds. *J. Org. Chem.*, **36**, 824-828 (1971).
144. **Long, B., Nikitin, K., and Fitzmaurice, D.** Self-Assembly of a Tripodal Pseudorotaxane on the Surface of a Titanium Dioxide Nanoparticle. *J. Am. Chem. Soc.*, **125**, 5152-5160 (2003).
145. **Salvatore, R.** Synthesis of secondary amines. *Tetrahedron*, **57**, 7785-7811 (2001).
146. **Hayashi, Y., Fujiwara, T., Nagano, Y., and Teramura, K.** Preparation of tertiary amines having different substituents from quaternary 2-hydroxyethylammonium salts. *Yukagaku*, **36**, 409-412 (1987).
147. **Basu, B., Paul, S., and Nanda, A. K.** Highly selective *N*-Alkylation of amines promoted on silica: an efficient and recyclable surface. *Green Chem.*, **11**, 115-1120 (2009).
148. **Salvatore, R. N., Nagle, A. S., and Jung, K. W.** Cesium Effect: High Chemoselectivity in Direct *N*-Alkylation of Amines. *J. Org. Chem.*, **67**, 647-683 (2002).
149. **Ju, Y., and Varma, R. S.** Aqueous *N*-alkylation of amines using alkyl halides: direct generation of tertiary amines under microwave irradiation. *Green Chem.*, **6**, 219-221 (2004).

150. **Ju, Y., and Varma, R. S.** An efficient and simple aqueous *N*-heterocyclization of aniline derivatives: microwave-assisted synthesis of *N*-aryl azacycloalkanes. *Org. Lett.*, **7**, 2409-2411 (2005).
151. **Singh, C. B., Kavala, V., Samal, A. K., and Patel B. K.** Aqueous-Mediated *N*-Alkylation of Amines. *Eur. J. Org. Chem.*, **2007**, 1369-1377 (2007).
152. **Li, J. J., and Corey, E. J.** Name Reactions of Functional Group Transformations. *John Wiley and Sons*, USA, CH2, 86-92 (2007).
153. **Baxter, E. W., and Reitz, A. B.** Reductive aminations of carbonyl compounds with borohydride and borane reducing agents. *Org. React. (Hoboken, NJ, U. S.)* **59**, 101 (2002).
154. **Abdel-Magid, A. F., and Mehrman, S. J.** A Review on the Use of Sodium Triacetoxyborohydride in the Reductive Amination of Ketones and Aldehydes. *Org. Process Res. Dev.*, **10**, 971-1031 (2006).
155. **Abdel-Magid, A. F., and Maryanoff, C. A.** Use of sodium triacetoxyborohydride in reductive amination of ketones and aldehydes. *ACS Symp. Ser.*, **641**, 201-216 (1996).
156. **Lane, C. F.** Sodium cyanoborohydride, a highly selective reducing agent for organic functional groups. *Synthesis*, 135-46 (1975).
157. **Bhattacharyya, S.** Borohydride reductions in dichloromethane: a convenient, environmentally compatible procedure for the methylation of amines. *Synth. Commun.*, **25**, 2061-2069 (1995).
158. **Da Silva, R. A., Estevam, I. H. S., and Bieber, L. W.** Reductive methylation of primary and secondary amines and amino acids by aqueous formaldehyde and zinc. *Tetrahedron Lett.*, **48**, 7680-7682 (2007).
159. **Cope, A. C., Ciganek, E., Fleckenstein, L. J. and Meisinger, M. A. P.** Tertiary Amines from Methiodides and Lithium Aluminum Hydride. *J. Am. Chem. Soc.*, **82**, 4651-4655 (1960).
160. **Hutchins, R. O., Kandasamy, D., Dux, F., Maryanoff, C. A., Rotstein, D., Goldsmith, B., Burgoyne, W., Cistone, F., Dalessandro, J., and Puglis, J.** Nucleophilic borohydride: selective reductive displacement of halides, sulfonate esters, tertiary amines, and *N,N*-disulfonimides with borohydride reagents in polar aprotic solvents. *J. Org. Chem.*, **43**, 2259-67 (1978).
161. **Saurabh, S., Fadila, L., Moreau, J. P., Hurvois, J. L., Renaudde Weghe, T., and Hierry, R.** Synthesis of Alkaloids of *Galipea officinalis* by Alkylation of an α -Amino Nitrile. *Eur. J. Org. Chem.*, **2008**, 4622-4631 (2008).

162. **Yoshida, Y., Sakakura, Y., Aso, N., Okada, S., and Tanabe, Y.** Practical and efficient methods for sulfonylation of alcohols using Ts(Ms)Cl/Et₃N and catalytic Me₃N-HCl as combined base: promising alternative to traditional pyridine. *Tetrahedron*, **55**, 2183-2192 (1999).
163. **Olah, G. A., Gupta, B. G., Malhotra, R., and Narang, S. C.** Chlorotrimethylsilane/lithium bromide and hexamethyldisilane/pyridinium bromide perbromide: effective and selective reagents for the conversion of alkyl (cycloalkyl and aralkyl) alcohols into bromides. *J. Org. Chem.*, **45**, 1638-1639 (1980).
164. **Couture, G., Alaaeddine, A., Boschet, F., and Ameduri, B.** Polymeric materials as anion-exchange membranes for alkaline fuel cells. *Prog. Polym. Sci.*, **36**, 1521-1557 (2011).
165. **Cai, J. and Wathey, B.** A novel traceless solid phase tertiary amine synthesis based on Merrifield resin. *Tetrahedron Lett.*, **42**, 1383-1385 (2001).
166. **Grovenstein, E., Chandra, S., Collum, C. E., and Davis, W. E.** Carbanions. VIII. Products and mechanisms of reaction of allyl- and cyclopropyltrimethylammonium halides and of allyl chloride, alcohol, and p-tolyl sulfide with sodium in liquid ammonia. *J. Am. Chem. Soc.*, **88**, 1275-1289 (1966).
167. **Ho, T.S.** Dequaternization of ammonium salts by nucleophiles. *Synth. Commun.*, **3**, 99-100 (1972).
168. **Kametani, T., Kigasawa, K., Hiiragi, M., Wagatsuma, N., and Wakisaka, K.** Debenzylation of quaternary ammonium salts with thiophenol. *Tet. Lett.*, **8**, 635-638 (1969).
169. **Hutchins, R. O., Dux, and F. J.** Selective demethylation of quaternary salts with lithium propylmercaptide in hexamethylphosphoramide. *J. Org. Chem.*, **38**, 1961-1962 (1973).
170. **Ho, T. S.** Dealkylation of quaternary ammonium salts with 1,4-diazabicyclo[2.2.2]octane. *Synthesis*, **12**, 702 (1972).
171. **Bauera, B., Strathmannb, H., Effenbergerc, F.** Anion-exchange membranes with improved alkaline stability. *Desalination*, **79**, 125-144 (1992).
172. **Cope, A. C., Mehta, and A. S.** Mechanism of the Hofmann elimination reaction: an ylide intermediate in the pyrolysis of a highly branched quaternary hydroxide. *J. Amer. Chem. Soc.*, **85**, 1949-1952 (1963).
173. **William, E. W., and Manning, J. H.** Antimicrobial polyalcohols and their derivatives. CA1129851A1 (1982).
174. **Battaglini, G. T.** Assay of quaternary ammonium antimicrobial compounds by aqueous potentiometric titration. *J. Surfact. Deterg.*, **5**, 117-121 (2002).

175. **Jansson, S. O., Modin, R., and Schill, G.** Two-phase titration of organic ammonium ions with lauryl sulphate and methyl yellow as indicator. *Talanta*, **21**, 905-918 (1974).
176. **Bioshield Technologies.** Certification of Limits and Analytical Method for Enforcement of Limits for BST Protectant 50. 1-6 (1997).
177. **Mistry, K.** New Self-assembled Quaternary Ammonium Fluorescent Compounds. 4th Year Undergraduate Thesis. Department of Chemistry and Biology, Ryerson University, Toronto, ON, 1-37 (2011).
178. **Taffa, D., Kathiresan, M. and Walder, L.** Tuning the Hydrophilic, Hydrophobic, and Ion Exchange Properties of Mesoporous TiO₂. *Langmuir*, **25**, 5371-5379 (2009).
179. **Vermeulen, L. A., Fateen, R. Z. and Robinson, P. D.** Single Crystal Structure Determination of a New Zirconium *N*-Ethylpyridinium Phosphonate: Zr(O₃PCH₂CH₂NC₅H₅)(F⁻)₃. *Inorg. Chem.*, **41**, 2310-2312 (2002).
180. **Demmer, C. S., Krogsgaard-Larsen, N., and Bunch, L.** Review on Modern Advances of Chemical Methods for the Introduction of a Phosphonic Acid Group. *Chem. Rev.*, **111**, 7981-8006 (2011).
181. **Jansa, P., Baszczyński, Procházková, B., Dračinský, M., and Janeba, Z.** Microwave-assisted hydrolysis of phosphonate diesters: an efficient protocol for the preparation of phosphonic acids. *Green Chem.*, **14**, 2282-2288 (2012).
182. **Morita, J. Okamoto, Y., and Sakurai, H.** A convenient dealkylation of dialkyl phosphonates by chlorotrimethylsilane in the presence of sodium iodide. *Tet. Lett.*, **19**, 2523-2526 (1978).
183. **McKenna, C.** The facile dealkylation of phosphonic acid dialkyl esters by bromotrimethylsilane. *Tet. Lett.*, **18**, 155-158 (1977).
184. **Blackburn, G. M., and Ingleson, D.** The dealkylation of phosphate and phosphonate esters by iodotrimethylsilane: a mild and selective procedure. *J. Chem. Soc. Perkin Trans.*, **1**, 1150-1153 (1980).
185. **Chowdhury, S., Muni, N. J., Greenwood, N. P., Pepperberg, D. R. and Standaert, R. F.** Phosphonic acid analogs of GABA through reductive dealkylation of phosphonic diesters with lithium trialkylborohydrides. *Bioorg. Med. Chem. Lett.*, **17**, 3745-3748 (2007).
186. **Gauvry, N. M. J.** Dealkylation of dialkyl phosphonates with boron tribromide. *Synthesis*, **4**, 553-554 (2001).
187. **McKenna, C. E., and Schmidhauser, J.** Functional selectivity in phosphonate ester dealkylation with bromotrimethylsilane. *J. Chem. Soc. Chem. Commun.*, 739 (1979).

188. **Mortier, J., Gridnev, I. D., and Guenot, P.** Reactions of Phosphonates with Organohaloboranes: New Route to Molecular Borophosphonates. *Organometallics*, **19**, 4266-4275 (2000).
189. **Mortier, J.** Recent developments on the mechanism of the reaction of dialkyl phosphonates with haloboranes and their implications for synthesis. *Rec. Res. Develop. Org. Chem.*, **6**, 169-176 (2002).
190. **Erickson, J. G.** Phosphonoammonium compounds. US 2774786 19561218, General Mills Inc. (1956).
191. **Frederick, H.** Synthetic detergents. NL 79189 19551015 (1955).
192. **Germanaud, L., Brunel, S., Chevalier, Y., and Le Perchec, P.** Synthesis of neutral amphiphilic phosphobetaines with variable interionic distances. *Bull. Soc. Chim. Fra.*, **4**, 699-704 (1988).
193. **Fu, X. K., and Chen, W. S.** Synthesis of dimethyldodecylammonioethylphosphonic acid betaine. *Xinan Shifan Daxue Xuebao, Ziran Kexueban*, **27**, 61-63 (2002).
194. **Hüttinger, K. J. and Jung, M. F.** Kinetik der Synthese von Trialkyl[-3-(trimethoxysilyl)-propyl]-ammoniumchloriden und deren antimikrobielle Wirkung als fixierte Biozide. *Chem. Ingen. Tech.*, **61**, 258-259 (1989).
195. **Majumdar, P., Crowley, E., Htet, M., Stafslie, S. J., Daniels, J., VanderWal, L and Chisholm, B. J.** Combinatorial Materials Research Applied to the Development of New Surface Coatings XIII: An Investigation of Polysiloxane Antimicrobial Coatings Containing Tethered Quaternary Ammonium Salt Groups. *J. Comb. Chem.*, **11**, 1115-1127 (2009).
196. **Zhu, X. Yang, C., Chen, G., Wan, Y.** Microwave-assisted synthesis of siloxane quaternary ammonium salts. *Zhongshan Daxue Xuebao, Ziran Kexueban*, **48**, 56-59 (2009).
197. **Hüttinger, K. J., and Zeller, D.** Chemisch und verfahrenstechnisch optimierte, trägergebundene Desinfektionsmittel für die Wasserentkeimung mit Tiefenfiltern. *Chem. Ingen. Tech.*, **59**, 516-517 (1987).
198. **Ragulin, V. V.** ω -Haloalkylphosphoryl Compounds: Synthesis and Properties. *Russ. J. Gen. Chem.*, **82**, 1928-1937 (2012).
199. **Yoshimura, T., Kusano, T., Iwase, H., Shibayama, M., Ogawa, T., and Kurata, H.** Star-Shaped Trimeric Quaternary Ammonium Bromide Surfactants: Adsorption and Aggregation Properties. *Langmuir*, **28**, 9322-9331 (2012).
200. **Gourves, J. P., Couthon, H., and Sturtz, G. F.** Synthesis of 3,4-dihydro-2H-pyrido[1,2-b]isoindol-1-one and 3,4-dihydro-2H-pyrido[1,2-b]pyrrolidin-1-one functionalized at the C(6)

position by an intramolecular Horner-Wadsworth-Emmons reaction. *Eur. J. Org. Chem.*, **12**, 3489-3493 (1999).

201. **Smits, J. P., and Wiemer, D. F.** Synthesis and Reactivity of Alkyl-1,1,1-trisphosphonate Esters. *J. Org. Chem.*, **76**, 8807-8813 (2011).

202. **O'Boyle, N. M., Greene, L. M., Bergin, O., Fichet, J. B., McCabe, T., Lloyd, D. G., Zisterer, D. M., and Meegan, M. J.** Synthesis, evaluation and structural studies of antiproliferative tubulin-targeting azetidin-2-ones. *Bioorg. Med. Chem.*, **19**, 2306-2325 (2011).

203. **Zefirov, N. S., and Matveeva, E. D.** Catalytic Kabachnik-Fields reaction: new horizons for old reaction. *ARKIVOC Special Issue Reviews and Accounts* **1**, 1-17 (2008).

204. **Keglevich, G., Szekrényi, A., Szöllősy, A., and Drahos, L.** Synthesis of Bis(phosphonomethyl), Bis(phosphinatomethyl), and Bis(phosphinoxidomethyl)amines, as Well as Related Ring Bis(phosphine) Platinum Complexes. *Synth. Commun.*, **41**, 2265-2272 (2011).

205. **Tibhe, G. D., Reyes-González, M. A., Cativiela, C., and Ordóñez, M.** Microwave-assisted High Diastereoselective Synthesis of α -Aminophosphonates under Solvent and Catalyst Free-conditions. *J. Mex. Chem. Soc.*, **56**, 183-187 (2012).

206. **Ishikawa, S., Tajima, M. and Mochizuki, M.** Synthesis and properties of bifunctional chloroalkyl nitrosamines with an intercalating moiety. *Bioorg. Med. Chem.*, **12**, 3791-3796 (2004).

207. **Mutin, P. H., Guerrero, G. and Vioux, A. J.** Hybrid materials from organophosphorus coupling molecules. *Mater. Chem.*, **15**, 3761-3768 (2005).

208. **Matveeva, E., Petrovskii, P. V., and Odinets, I. L.** Efficient synthesis of racemic β -aminophosphonates via aza-Michael reaction in water. *Tet. Lett.*, **49**, 6129-6133 (2008).

209. **Tiasto, F.** Preparation of bisphosphonoamine ligands for the synthesis of technetium nitride complexes for radiodiagnostic imaging. PCT Int Appl. 2007083395 (2007).

210. **Wang, J., Liang, Y. L., and Qu, J.** Boiling water-catalyzed neutral and selective *N*-Boc deprotection. *Chem. Commun.*, 5144-5146 (2009).

211. **Simonyan, G. S., Arutyunyan, R. S., Beileryan, N. M. and Grigoryan, E. A.** Synthesis of New Surface-Active *N*²-Amino Amides, Agents for Fixation of Dyes on Cotton Fibers, from *N*-Tri(hydroxymethyl)methylacrylamide. *Russ. J. Appl. Chem.*, **76**, 258-260 (2003).

212. (i) **Borgman, R. J., McPhillips, J. J., and Stitzel, R. E.** Synthesis and Pharmacology of Centrally Acting Dopamine Derivatives and Analogs in Relation to Parkinson's Disease. *J. Med. Chem.*, **16**, 630-633 (1973). (ii) **Louafi, F., Hurvois, J., Chibani, A., and Roisnel, T.** Synthesis

of Tetrahydroisoquinoline Alkaloids via Anodic Cyanation as the Key Step. *J. Org. Chem.*, **75**, 5721-5724 (2010).

213. **Haslegrave, J. A., and Sullivan, D. S.** Nitrogen and sulfur-containing corrosion inhibitors. Exxon Chemical Patents Inc. (Linden, NJ). United States Patent 4673436 (1987).

214. **Asakawa, T., Shimizu, Y., Ozawa, T., Ohta, A., and Miyagishi, S.** Aqueous solution properties of disulfide linked gemini and cleaved monomeric thiol surfactants. *J. Oleo Sci.*, **57**, 243-249 (2008).

215. **Thebault, P., Taffin de Givenchy, E., Levy, R., Vandenberghe, Y., Guittard, F., and G ribaldi, S.** Contact-active microbicidal gold surfaces using immobilization of quaternary ammonium thiol derivatives. *Eur. J. Med. Chem.*, **44**, 4227-4234 (2009).

215. **Harjani, J. R., Liang, C., and Jessop, P. G.** A Synthesis of Acetamidines. *J. Org. Chem.*, **76**, 1683-1691 (2011).

216. **Allen, F. H., Kennard, O., Watson, D. G., Brammer, L. and Orpen, A. G.** Tables of Bond Lengths Determined by X-Ray and Neutron Diffraction. *J. Chem. Soc. Perkin. Trans.*, **2**, S1-S19 (1997).

217. **Andrews, J. M.** Determination of minimum inhibitory concentrations. *J. Antimicrob. Chemother.*, **48**, 5-16 (2001).

218. **Wang, X. Xue, Y., Wang, Y.** Preparation and application of organosilicon quaternary ammonium salt composition. *Faming Zhuanli Shenqing*, CN 102391299, A 20120328 (2012).

219. **Li, F., Shishkin, E., Mastro, M. A., Hite, J. K., Eddy, C. R., Edgar, J. H., and Ito, T.** Photopolymerization of Self-Assembled Monolayers of Diacetylenic Alkylphosphonic Acids on Group-III Nitride Substrates. *Langmuir*, **26**, 10725-10730 (2010).

220. **Baber, A., de Vries, J. G., Orpen, A. G., Pringle, P. G., and von der Luehe, K.** Allosteric effects in asymmetric hydrogenation catalysis. Asymmetric induction as a function of the substrate and the backbone flexibility of C1-symmetric diphosphines in rhodium-catalysed hydrogenations. *Dalton Trans.*, 4821-4828 (2006).

221. **Viorner, C., Pechy, P., Boegli, M., Aronsson, B. O., Descouts, P., and Gratzel, M.** Synthesis of new polyphosphonic acids. *Phos. Sul. Silic. Rel. Elem.*, **177**, 231-241 (2002).

223. **Villemin, D. Simeon, F. Decreus, H., and Jaffres, P. A.** Rapid and efficient Arbuzov reaction under microwave irradiation. *Phos. Sul. Silic. Rel. Elem.*, **133**, 209-213 (1998).

224. **Jansa, P. Holy, A. Dracinsky, M. Baszczynski, O. Cesnek, M., and Janeba, Z.** Efficient and green' microwave-assisted synthesis of haloalkylphosphonates via the Michaelis-Arbuzov reaction. *Green Chem.*, **13**, 882-888 (2011).

225. **Sun, L. J., Cao, J. Q., Ge, C. H., Zhang, X. D., Tong, J. and Ma, Y. C.** Synthesis and characterization of alkyl substituted dimethyl phosphonates. *Liaoning Daxue Xuebao, Ziran Kexueban*, **31**, 78-80 (2004).
226. **Voigt, M. Klaumunzer, M., Ebel, A., Werner, F., Yang, G., Marczak, R., Spiecker, E., Guldi, D. M., Hirsch, A., and Peukert, W.** Surface Functionalization of ZnO Nanorods with C60 Derivatives Carrying Phosphonic Acid Functionalities. *J. Phys. Chem. C*, **115**, 5561-5565 (2011).
227. **Hara, T., Durell, S. R., Myers, M. C., and Appella, D. H.** Probing the Structural Requirements of Peptoids That Inhibit HDM2-p53 Interactions. *J. Am. Chem. Soc.*, **128**, 1995-2004 (2006).
228. (i) **Chevalier, Y., Germanaud, L., Brunel, S., Storet, Y., Berthelon, B., LePerchec, P., and Gallot, B.** Zwitterionic amphiphiles: synthesis and physical properties. *Comun. Jorn. Com. Esp. Deterg.*, **18**, 231-245 (1987). (ii). **Brunet, S., Germanaud, L., Perchec, P., and Sillion, B.** Neutral phosphobetaines, their preparation, and their use in petroleum recovery. *Fr. Demande*, 2572078-A1 (1986).
229. **Tucker, S. A, K. and Garrell, R. L.** Simple Preparation and Application of TEMPO-Coated Fe₃O₄ Superparamagnetic Nanoparticles for Selective Oxidation of Alcohols. *Chem. A Eur. J.*, **16**, 12718-12726 (2010).
230. **Conibear, A. C., Lobb, K. A., and Kaye, P. T.** ³¹P NMR kinetic study of the tandem cleavage of phosphonate esters by bromotrimethylsilane. *Tetrahedron*, **66**, 8446-8449 (2010).
231. **Martinelli, M. J., and Pollack, S. R.** Encyclopedia of Reagent for Organic Synthesis. John Wiley and Sons Ltd, *Bromotrimethylsilane*, 1-21 (2001).
232. **Paleos, C. M., Arkas, M. and Skoulios, A.** Mesomorphic character of quaternary ammonium salts affected by secondary hydrogen bonding interactions. *Molecular Crystals and Liquid Crystals Science and Technology, Section A: Molecular Crystals and Liquid Crystals*, **309**, 237-250 (1998).
233. **Pinchuk, A. N., Rampy, M. A., Longino, M. A., Skinner, R. W. S., Gross, M. D., Weichert, J. P., and Counsell, R. E.** Synthesis and Structure-Activity Relationship Effects on the Tumor Avidity of Radioiodinated Phospholipid Ether Analogues. *J. Med. Chem.*, **49**, 2155-2165 (2006).
234. **Simoni, D. Gebbia, N., Invidiata, F. P., Eleopra, M., Marchetti, P., Rondanin, R., Baruchello, R., Provera, S. S., Marchioro, C., Tolomeo, M., Marinelli, L., Limongelli, V., Novellino, E., Kwaasi, A., Dunford, J., Buccheri, S., Caccamo, N., and Dieli, F.** Design, Synthesis, and Biological Evaluation of Novel Aminobisphosphonates Possessing an in Vivo Antitumor Activity Through a gammadelta-T Lymphocytes-Mediated Activation Mechanism. *J. Med. Chem.*, **51**, 6800-6807 (2008).

235. **Gourves, J. P., Couthon, H., and Sturtz, G.** A new efficient synthesis of ω -aminoalkylidene-1,1-bisphosphonate tetraethyl esters. *Phos. Sul. Silic. Rel. Elem.*, **132**, 219-229 (1998).
236. **Neidlein, R. E. T.** Substituted methylphosphonates as synthons for alicyclic α -functionalized phosphonates. *Monatshefte fuer Chemie.*, **123**, 1037-1043 (1992).
237. **Tanaka, K. S., Houghton, T. J., Kang, T., Dietrich, E., Delorme, D., Ferreira, S. S., Caron, L., Viens, F., Arhin, F. F., Sarmiento, I., Lehoux, D., Fadhil, I., Laquerre, K., Liu, J., Ostiguy, V., Poirier, H., Moeck, G., Parr, TR. Jr., and Rafai Far, A.** Bisphosphonated fluoroquinolone esters as osteotropic prodrugs for the prevention of osteomyelitis. *Bioorg. Med. Chem.*, **16**, 9217-9229 (2008).
238. **Delorme, D., Houghton, T., Lafontaine, Y., Tanaka, K., Dietrick, E., Kang, T., and Rafai, F. A.** Phosphonated oxazolidinones and uses thereof for the prevention and treatment of bone and joint infections and their preparation. WO 2007138381A2 (2007).
239. **Lehn, J. M., Blacker, J., and Jazwinski, J.** Preparation of 2,7-diazapyrenium dications for photochemical cleavage of nucleic acids. WO 1987-FR142, Compagnie Oris Industrie, Fr., (1987).
240. **Polomoscanik, S. C., Holmes-Farley, S. R., Petersen, J. S., Sacchiero, R. J., and Dhal, P. K.** Hydrophobically Modified Poly (Allylamine) Hydrogels Containing Internal Quaternary Ammonium Groups as Cholesterol Lowering Agents: Synthesis, Characterization, and Biological Studies . *J. Macromol. Sci., Part A: Pure Appl. Chem.*, **49**, 1011-1021 (2012).
241. **Cavero, E., Zablocka, M., Caminade, A., and Majoral, J. P.** Design of Bisphosphonate-Terminated Dendrimers. *Eur. J. Org. Chem.*, 2759-2767 (2010).
242. **Chougrani, K., Boutevin, B., David, G., Seabrook, S., and Loubat, C.** Acrylate based anticorrosion films using novel bis-phosphonic methacrylates. *J. Polym. Sci. Part A: Polym. Chem.*, **46**, 7972-7984 (2008).
243. **Chougrani, K., Boutevin, B., David, G., and Boutevin, G.** New *N,N*-amino-diphosphonate-containing methacrylic derivatives, their syntheses and radical copolymerizations with MMA. *Eur. Polym. J.*, **44**, 1771-1781 (2008).
244. **Gatlin, L. W.** Alkylaminoalkyl substituted triazine sulfide scavenger. US 20030089641, Clearwater International (2003).
245. **Kauffman, W. J.** Synthesis and characterization of *N,N',N''*-tris(dimethylaminopropyl) hexahydro-s-triazine and isolable intermediates. *J. Heterocyclic Chem.*, **12**, 409-11 (1975).
246. **Jasiński, M., Mlostoń, G., Mucha, P., Linden, A., and Heimgartner, H.** Synthesis of New Bis-Imidazole Derivatives. *Helvetica Chimica Acta.*, **90**, 1765-1780 (2007).

247. **Hu, N., Johnson, L. M., Pothayee, N., Pothayee, N., Lin, Y., Davis, R. M., and Riffle, J. S.** Synthesis of ammonium bisphosphonate monomers and polymers. *Polymer*, **54**, 3188-3197 (2013).
248. **Bhattacharya, S., and Snehalatha, K.** Synthesis and Esterolytic Chemistry of Some (Dialkylamino)pyridine-Functionalized Micellar Aggregates. Evidence of Catalytic Turnover. *Langmuir*, **11**, 4653-4660 (1995).
249. **Haldar, J., Venkateswarlu, Y., and Padma, A.** Cationic antibacterial vancomycin derivatives and compositions. WO 2013072838 A1 (2013).
250. **Romeo, R., Carnovale, C., Giofre, Salvatore V., Romeo, G., Macchi, B., Frezza, C., Marino-Merlo, F., Pistara, V., and Chiacchio, U.** Truncated phosphonated C-1'-branched *N,O*-nucleosides: A new class of antiviral agents. *Bioorg. Med. Chem.*, **20**, 3652-3657 (2012).
251. **Hunter, C. A., Misuraca, M. C. and Turega, S. M.** Dissection of Complex Molecular Recognition Interfaces. *J. Amer. Chem. Soc.*, **133**, 582-594 (2011).
252. **Kaplanek, R., Briza, T., Havlik, M., Martasek, P., and Kral, V.** Three-fold polyfluoro alkylated amines and isocyanates based on [tris(hydroxymethyl)amino]methane (TRIS). *J. Fluor. Chem.*, **128**, 179-183 (2007).
253. **Rannard, S. P., and Davis, N. J.** The Selective Reaction of Primary Amines with Carbonyl Imidazole Containing Compounds: Selective Amide and Carbamate Synthesis. *Org. Lett.*, **2**, 2117-2120 (2000).
254. **Acton, A. L., and Fante, C.** Janus PEG-Based Dendrimers for Use in Combination Therapy: Controlled Multi-Drug Loading and Sequential Release. *Biomacromol.*, **14**, 564-574 (2013).
255. **Babu, D. A., Manohar, C. S., and Visweswaran, V.** Synthesis, characterization and antimicrobial activity studies of 2-[[2-(3,4-dimethoxyphenyl) ethyl] methylamino]sulphonylnaphthalenes. *Asian J. Chem.*, **20**, 1411-1419 (2008).
256. **Shahane, S., Saurabh, S., Fadila, L., Moreau, J., Hurvois, J. P., Renaudde, J-L., and Thierry Roisnel, T.** Synthesis of alkaloids of *Galipea officinalis* by alkylation of an α -amino nitrile. *Eur. J. Org. Chem.*, **27**, 4622-4631 (2008).
257. **Top, S., Kaloun, E. B., Vessières, A., Laïos, I., Leclercq, G., and Jaouen, G.** The first titanocenyl dichloride moiety vectorised by a selective estrogen receptor modulator (SERM). Synthesis and preliminary biochemical behaviour. *J. Organomet. Chem.*, **643-644**, 350-356 (2002).
258. **Saettone C., Alderigi, B., Giannaccini, C., Anslemi, M., Rossetti, M., and Scotton, R.** Substantivity of sunscreens-preparation and evaluation of some quaternary ammonium benzophenone derivatives. *Int. J. Cosm. Sci.*, **10**, 99-109 (1988).

259. **Wang, X. and Schneider, H.** Binding of dansylamide derivatives to nucleotides and nucleic acids. *J. Chem. Soc. Perkin Trans.*, **2**, 1323-1328 (1998).
260. **Jacobsen, D. W.** Preparation of cryptofluorescent analogs of cobalamin coenzymes. *Methods Enzymol.*, **67**, 12-19 (1980).
261. **Simonin, J., Vernekar, S. K. V., Thompson, A. T., Hothersall, J. D., Connolly, C. N., Lummis, S. R. L., and Lochner, M.** High-affinity fluorescent ligands for the 5-HT₃ receptor. *Bioorg. Med. Chem. Lett.*, **22**, 1151-1155 (2012).